SECOND
INTERNATIONAL CONFERENCE ON

Nuclear Data for Reactors

CONFERENCE PROCEEDINGS
HELSINKI,
15-19 JUNE 1970

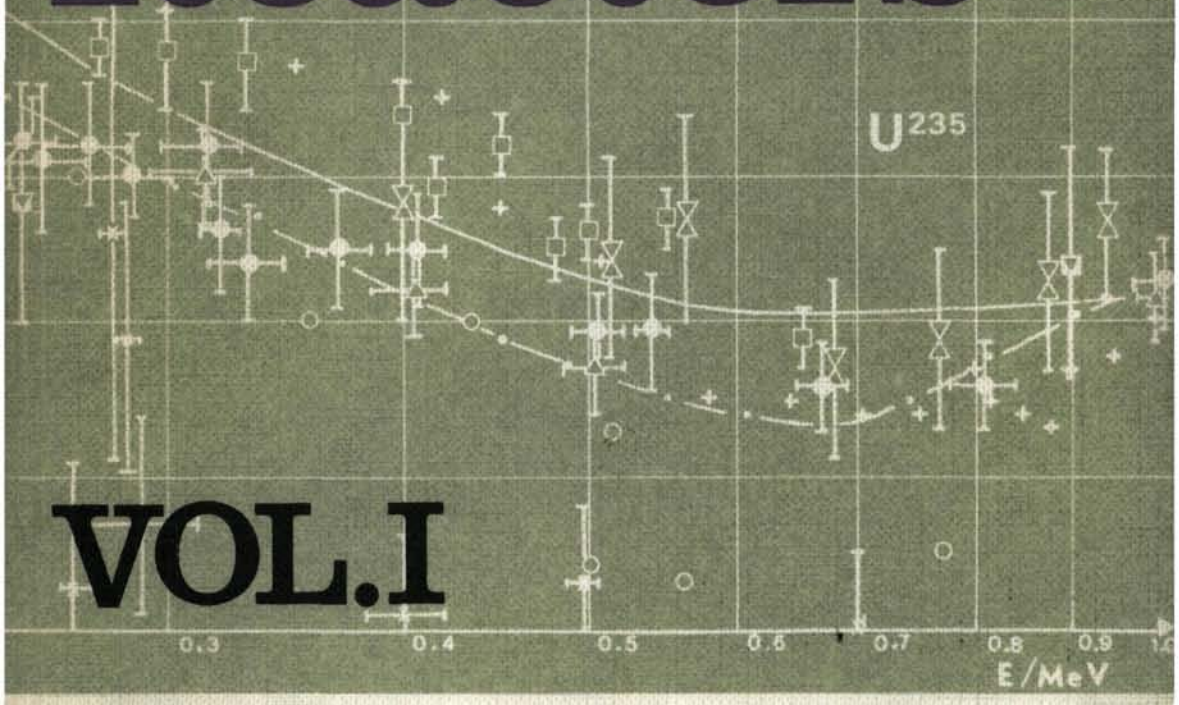

VOL. I

INTERNATIONAL ATOMIC ENERGY AGENCY, VIENNA, 1970

NUCLEAR DATA FOR REACTORS

VOL. I

The following States are Members of the International Atomic Energy Agency:

AFGHANISTAN
ALBANIA
ALGERIA
ARGENTINA
AUSTRALIA
AUSTRIA
BELGIUM
BOLIVIA
BRAZIL
BULGARIA
BURMA
BYELORUSSIAN SOVIET SOCIALIST REPUBLIC
CAMBODIA
CAMEROON
CANADA
CEYLON
CHILE
CHINA
COLOMBIA
CONGO, DEMOCRATIC REPUBLIC OF
COSTA RICA
CUBA
CYPRUS
CZECHOSLOVAK SOCIALIST REPUBLIC
DENMARK
DOMINICAN REPUBLIC
ECUADOR
EL SALVADOR
ETHIOPIA
FINLAND
FRANCE
GABON
GERMANY, FEDERAL REPUBLIC OF
GHANA
GREECE
GUATEMALA
HAITI
HOLY SEE
HUNGARY
ICELAND
INDIA
INDONESIA
IRAN
IRAQ
IRELAND
ISRAEL
ITALY
IVORY COAST
JAMAICA
JAPAN
JORDAN
KENYA
KOREA, REPUBLIC OF
KUWAIT
LEBANON
LIBERIA
LIBYAN ARAB REPUBLIC
LIECHTENSTEIN
LUXEMBOURG
MADAGASCAR
MALAYSIA
MALI
MEXICO
MONACO
MOROCCO
NETHERLANDS
NEW ZEALAND
NICARAGUA
NIGER
NIGERIA
NORWAY
PAKISTAN
PANAMA
PARAGUAY
PERU
PHILIPPINES
POLAND
PORTUGAL
ROMANIA
SAUDI ARABIA
SENEGAL
SIERRA LEONE
SINGAPORE
SOUTH AFRICA
SPAIN
SUDAN
SWEDEN
SWITZERLAND
SYRIAN ARAB REPUBLIC
THAILAND
TUNISIA
TURKEY
UGANDA
UKRAINIAN SOVIET SOCIALIST REPUBLIC
UNION OF SOVIET SOCIALIST REPUBLICS
UNITED ARAB REPUBLIC
UNITED KINGDOM OF GREAT BRITAIN AND NORTHERN IRELAND
UNITED STATES OF AMERICA
URUGUAY
VENEZUELA
VIET-NAM
YUGOSLAVIA
ZAMBIA

The Agency's Statute was approved on 23 October 1956 by the Conference on the Statute of the IAEA held at United Nations Headquarters, New York; it entered into force on 29 July 1957. The Headquarters of the Agency are situated in Vienna. Its principal objective is "to accelerate and enlarge the contribution of atomic energy to peace, health and prosperity throughout the world".

Printed by the IAEA in Austria
October 1970

PROCEEDINGS SERIES

NUCLEAR DATA FOR REACTORS

PROCEEDINGS OF THE
SECOND INTERNATIONAL CONFERENCE ON
NUCLEAR DATA FOR REACTORS
HELD BY THE
INTERNATIONAL ATOMIC ENERGY AGENCY
IN HELSINKI, 15 - 19 JUNE 1970

In two volumes

VOL. I

INTERNATIONAL ATOMIC ENERGY AGENCY
VIENNA, 1970

NUCLEAR DATA FOR REACTORS
IAEA, VIENNA 1970
STI/PUB/259

FOREWORD

The Second International Conference on Nuclear Data for Reactors, held in Helsinki at the invitation of the Finnish Government, was convened by the International Atomic Energy Agency from 15 to 19 June 1970. The Conference, held as a result of recommendations made by the International Nuclear Data Committee, was attended by 163 participants from 28 countries and four international organizations, and 21 invited and 98 contributed papers were presented.

This Conference was the second held by the IAEA on Nuclear Data for Reactors. Almost four years have elapsed since the first was held in Paris in 1966. During these years gratifying progress has been made by reactor, nuclear and evaluation physicists, whose collaboration has been greatly enhanced. As a result, many laboratories have concentrated their efforts on items of particular importance for reactor research and development, and many measurements are now available.

The main purpose of this Conference was to provide an opportunity to review results of recent basic neutron-physics investigations against a background need for basic information, especially concerning reactors.

The Conference itself, together with the preparatory meetings of IAEA experts in Studsvik on the status of $\alpha(^{239}\mathrm{Pu})$ and the $\bar{\nu}$-values for fissionable nuclei, showed an emphasis on the nuclear data aspects most important for nuclear technology.

Most contributors dealt with the measurement and analysis of neutron cross-sections. This extensive new cross-section information can be attributed to several factors, the most important being the development and systematic exploitation of high-intensity neutron sources, such as modern linear accelerators, modern cyclotrons and underground nuclear explosions, improvements in instrumentation and in sample preparation techniques, and other technical improvements.

Compared with the first IAEA Conference on Nuclear Data for Reactors this one has many more contributions on neutron data evaluation. Many papers are concerned with systematic evaluation of fission, capture and inelastic-scattering cross-sections of the most important fissile and fertile nuclei and of capture cross-sections of the main structural materials.

The vivid interest of the participants is clearly indicated by the extensive discussions, and pertinent problems still to be solved have been revealed, which constitute a challenge for the future.

The Agency wishes to thank the Finnish authorities as well as the authors and participants for their valuable contributions and the Chairmen of the individual sessions for their effort in organizing lively discussions.

EDITORIAL NOTE

The papers and discussions incorporated in the proceedings published by the International Atomic Energy Agency are edited by the Agency's editorial staff to the extent considered necessary for the reader's assistance. The views expressed and the general style adopted remain, however, the responsibility of the named authors or participants.

For the sake of speed of publication the present Proceedings have been printed by composition typing and photo-offset lithography. Within the limitations imposed by this method, every effort has been made to maintain a high editorial standard; in particular, the units and symbols employed are to the fullest practicable extent those standardized or recommended by the competent international scientific bodies.

The affiliations of authors are those given at the time of nomination.

The use in these Proceedings of particular designations of countries or territories does not imply any judgement by the Agency as to the legal status of such countries or territories, of their authorities and institutions or of the delimitation of their boundaries.

The mention of specific companies or of their products or brand-names does not imply any endorsement or recommendation on the part of the International Atomic Energy Agency.

CONTENTS OF VOL. I

GENERAL ASPECTS OF NEEDS AND USES FOR NUCLEAR DATA (Section I)

General status of nuclear data requirements (IAEA-CN-26/101).... 3
J.J. Schmidt
Implications of nuclear data uncertainties to reactor design (IAEA-CN-26/102)..... 17
P. Greebler, B.A. Hutchins and C.L. Cowan
Discussion 32
The importance of and needs for neutron nuclear data in astrophysics (IAEA-CN-26/103)..... 35
D.D. Clayton
Discussion 47
Ядерные данные для термоядерных реакторов (IAEA-CN-26/104)..... 49
Ю.Ф. Чернилин и Г.Б. Яньков
Nuclear cross-section requirements for fusion reactors (IAEA-CN-26/98)..... 67
V.S. Crocker, S. Blow and C.J.H. Watson
Discussion..... 91
Progress in understanding neutron interactions with nuclei (IAEA-CN-26/105)..... 93
J.E. Lynn
Discussion 112

CROSS-SECTIONS AND TECHNIQUES FOR HIGH-PRECISION NEUTRON NUCLEAR DATA MEASUREMENTS (Section II)

Precise 2200 m/s fission cross-sections of ^{239}Pu and ^{235}U (IAEA-CN-26/100)..... 117
A.J. Deruytter and W. Becker
Cross-sections and techniques for high-precision neutron nuclear data measurements (IAEA-CN-26/106)..... 127
A.J. Deruytter
Normalization of relative ^{235}U and ^{239}Pu fission cross-sections in the resonance region (IAEA-CN-26/106a)(abstract) 151
A.J. Deruytter, C. Wagemans and G. Penning
Low-energy neutron-scattering cross-section of ^{6}Li (IAEA-CN-26/25)..... 153
A. Asami and M.C. Moxon

A measurement of the ratio of the $^{6}Li(n,\alpha)$ and $^{10}B(n,\alpha)$ cross-sections from 10 eV to 80 keV and recommended values of the cross-sections up to 200 keV (IAEA-CN-26/26) 161
M.G. Sowerby, B.H. Patrick, C.A. Uttley and K.M. Diment
Discussion to Papers IAEA-CN-26/100, 106, 25, 26 175
Measurements of neutron elastic scattering from carbon in the energy region of 0.50 to 2.00 MeV (IAEA-CN-26/23) 177
N. Ahmed, M. Coppola and H.-H. Knitter
Analysis of the total cross-section of carbon from 70 eV to 1.5 MeV (IAEA-CN-26/24) 191
C.A. Uttley and K.M. Diment
Re-evaluation of gold shell transmission data at 24-keV neutron energy (IAEA-CN-26/8) 197
F.H. Fröhner
The temperature dependence of the average transmission of gold (IAEA-CN-26/10) 201
E. Schneider and F.H. Fröhner
Discussion to Papers IAEA-CN-26/8, 10 209
A neutron detector with a flat energy response for use in time-of-flight experiments (IAEA-CN-26/35) 211
M.S. Coates, G.J. Hunt and E.R. Rae
Discussion 218
Absolute neutron flux determination (IAEA-CN-26/9) 221
F. Käppeler and F.H. Fröhner
Discussion 227
Mesure absolue de la section efficace de fission de l'uranium-235 et du plutonium-239 entre 0.025 et 1 MeV (IAEA-CN-26/69) 229
I. Szabo, J.P. Marquette, E. Fort et J.L. Leroy
Développement des méthodes de mesure absolue des flux de neutrons rapides dans la gamme 10 keV à 1 MeV (IAEA-CN-26/70) 243
J.L. Leroy, J.L. Huet, I. Szabo et E. Fort
Section efficace de la réaction $^{6}Li(n,\alpha)T$ dans la gamme d'énergie comprise entre 100 keV et 500 keV 253
E. Fort
Discussion to Papers IAEA-CN-26/69, 70, 72 263

NUCLEAR DATA IN THE THERMAL RESONANCE ENERGY REGION; A > 220 (Section III)

Cross-sections of the heavy nuclei in the resonance region (IAEA-CN-26/107) 267
G.D. James
Discussion 286
Measurements of alpha and of fission cross-section ratios for ^{233}U, ^{235}U and ^{239}Pu at thermal energies (IAEA-CN-26/2) 287
M. Lounsbury, R.W. Durham and G.C. Hanna
Mesures des sections efficaces de l'uranium-233 pour les neutrons thermiques (IAEA-CN-26/97) 295
R. Vidal, M. Robin et C. Carniro da Silva
Discussion to Papers IAEA-CN-26/2, 97 305

Величина α для ^{239}Pu (IAEA-CN-26/127) 307
С. И. Сухоручкин
Discussion 311
Ratio of the capture and fission cross-sections of ^{239}Pu in the energy range 100 eV to 30 keV 315
M.G. Schomberg, M.G. Sowerby, D.A. Boyce, K.J. Murray and D.L. Sutton
^{235}U and ^{239}Pu capture-to-fission ratio (IAEA-CN-26/47) 331
J.B. Czirr and J.S. Lindsey
Измерение величины альфа для ^{235}U и ^{239}Pu (IAEA-CN-26/89) .. 339
Ф. Н. Беляев, К. Г. Игнатьев, С. И. Сухоручкин, С. П. Боровлев, В. В. Павлов, М. В. Полозов и А. Н. Солдатов
Измерения отношения сечений радиационного захвата и деления (α) для ^{235}U и ^{239}Pu в области энергий нейтронов ниже 30 кэв (IAEA-CN-26/124) 345
М. А. Куров, Ю. В. Рябов, Со Дон Сик, Н. Чиков, В. Н. Кононов, Е. Д. Полетаев, Ю. С. Ирокопец и Ю. Я. Стависский
Методика прямого измерения отношения сечения захвата к сечению деления (IAEA-CN-26/121) 357
Г. В. Мурадян, Т. А. Мостовая, В. И. Мостовой и Ю. Г. Щепкин
Observation of an isomeric level in ^{239}U by means of the ^{238}U(n,γ) ^{239}U reaction (IAEA-CN-26/36) 373
B.W. Thomas, J. Murray and E.R. Rae
High-energy γ-rays following neutron capture in ^{239}Pu and ^{235}U (IAEA-CN-26/42) 377
R.E. Chrien, O.A. Wasson, S. Dritsa, S. Bokharee and J.B. Garg
Discussion 386
Total neutron cross-section of ^{233}U from 0.7 eV to 320 eV (IAEA-CN-26/16) 387
W. Kolar, G. Carraro and G. Nastri
Neutron widths of ^{238}U from 60 eV to 5.7 keV (IAEA-CN-26/17) ... 403
G. Carraro and W. Kolar
Resonance parameters from neutron radiative capture in ^{238}U (IAEA-CN-26/18) 413
G. Rohr, H. Weigmann and J. Winter
Discussion to Papers IAEA-CN-26/17, 18 417
Fission-cross-section measurement of ^{233}U (IAEA-CN-26/19) 419
M.G. Cao, E. Migneco, J.P. Theobald and M. Merla
Neutron-induced fission cross-section of ^{241}Pu (IAEA-CN-26/95) 437
E. Migneco, J.P. Theobald and J.A. Wartena
Discussion to Papers IAEA-CN-26/16, 19, 95 447
Scattering cross-section of ^{235}U below 100 eV. Determination of Γ_n and J of resonances (IAEA-CN-26/20) 449
F. Poortmans, H. Ceulemans, E. Migneco and J.P. Theobald

The scattering cross-section of ^{235}U between 0.025 eV and 1 eV (IAEA-CN-26/21) 461
H. Ceulemans and F. Poortmans
Discussion to Papers IAEA-CN-26/20, 21 467
Mesure et analyse des sections efficaces de fission de l'uranium-235 et du plutonium-241 (IAEA-CN-26/60) 469
J. Blons, G. Debril, J. Fermandjian et A. Michaudon
Analyse simultanée de 5,7 à 160 eV des sections efficaces totale et de fission du plutonium-239 par un formalisme multiniveaux (IAEA-CN-26/61) 481
H. Derrien, J. Blons et A. Michaudon
Détermination du spin de résonances induites par des neutrons lents dans le plutonium-239 (IAEA-CN-26/62) 495
J. Trochon, H. Derrien, B. Lucas et A. Michaudon
Mesure à haute résolution et analyse de la section efficace de fission du plutonium-239 (IAEA-CN-26/63) 513
J. Blons, H. Derrien et A. Michaudon
Discussion to Papers IAEA-CN-26/60, 61, 62, 63 525
Fission and capture cross-sections of curium (IAEA-CN-26/45) ... 527
M.S. Moore, W.K. Brown, M.E. Ennis, R.R. Fullwood, G.A. Keyworth, J.H. McNally, F.B. Simpson, J.R. Berreth, R.D. Baybarz and M.C. Thompson
A simultaneous measurement of the fission, capture, scattering and total cross-sections of ^{239}Pu (IAEA-CN-26/46) 543
J.A. Farrell, G.F. Auchampaugh, M.S. Moore and P.A. Seeger
Discussion to Papers IAEA-CN-26/45, 46 551
Determination of resonance parameters of ^{240}Pu using a crystal spectrometer (IAEA-CN-26/48) 553
D.V.S. Ramakrishna and M.P. Navalkar
Discussion 557
Температурная зависимость структуры полного сечения урана-238 в области неразрешенных резонансов (IAEA-CN-26/85) 559
А.А. Ваньков, Ю.В. Григорьев, М.Н. Николаев, В.В. Филиппов, Б. Бемер, З. Коллатц и Л.Б. Пикельнер
Discussion 569
Evaluation dans le domaine des résonances pour les noyaux de nombre de masse superieur à 220 (IAEA-CN-26/108) 571
P. Ribon
Discussion 598

NUCLEAR DATA IN THE THERMAL AND RESONANCE ENERGY REGION: A < 220 (Section IV)

Нейтроноспектроскопическое исследование ядер с A < 220 в резонансной области энергий (IAEA-CN-26/109) 603
Г.В. Мурадян, Ю.Г. Щепкин и Ю.В. Адамчук

Total cross-sections of ^{45}Sc, ^{47}Ti, ^{49}Ti, ^{53}Cr, and ^{61}Ni in the keV-region (IAEA-CN-26/127) 619
M. Cho, F.H. Fröhner, M. Kazerouni, K.-N. Müller and G. Rohr
High-resolution measurements of radiative neutron-capture in ^{47}Ti, ^{56}Fe, ^{58}Ni, ^{60}Ni and ^{61}Ni between 7 and 200 keV (IAEA-CN-26/11) 633
A. Ernst, F.H. Fröhner and D. Kompe
Discussion 649
Нейтронные сечения изотопов-поглотителей используемых в атомных реакторах (IAEA-CN-26/87) 651
В.П. Вертебный, М.Ф. Власов, Н.Л. Гнидак, В.В. Колотый, А.Л. Кирилюк, Е.А. Павленко, М.В. Пасечник, В.Ф. Разбудей и А.Ф. Федорова
Discussion to Papers IAEA-CN-26/109, 87 667
Альфа-ширины нейтронных резонансов (IAEA-CN-26/125)..... 669
Ю.П. Попов, М. Пшитула, Р.Ф. Руми, М. Стэмпински, М. Флорек и В.И. Фурман
Measurements of neutron-resonance total cross-sections for fission product isotopes (IAEA-CN-26/14) 679
H.H. Jung, H.G. Priesmayer and H. Sulitze
The evaluation of fission product yields (IAEA-CN-26/3)..... 685
W.H. Walker
Redetermination of the thermal-neutron absorption cross-sections of gross fission products of ^{233}U, ^{235}U and ^{239}Pu (IAEA-CN-26/58) 703
A. Okazaki and E.K. Sokolowski
Neutron cross-section evaluation in the thermal and resonance energy range for nuclides of mass less than 220 (IAEA-CN-26/110) 721
J.S. Story
Chairmen of Sections and Secretariat of Conference 741

Section I

GENERAL ASPECTS OF NEEDS AND USES FOR NUCLEAR DATA

Chairman
R.F. TASCHEK (USA)

Invited Paper

GENERAL STATUS OF NUCLEAR DATA REQUIREMENTS

J.J. SCHMIDT
International Atomic Energy Agency,
Vienna

Abstract

GENERAL STATUS OF NUCLEAR DATA REQUIREMENTS.

After a brief historical survey of developments in the last few years in reactor physics and technology, nuclear data requirements and measurement techniques, this introductory paper deals with the present status of nuclear data requirements, with special reference to the papers printed in these Proceedings of the Second International Conference on Nuclear Data for Reactors. Subjects discussed in this paper include, e.g. the confidence level of important nuclear data, interpretation of fission resonances, ^{239}Pu resonances and α-values, the $\bar{\nu}$(^{252}Cf)standard, the energy dependence of $\bar{\nu}$, ^{235}U fast-neutron fission, ^{238}U fast-neutron capture, energy spectra of prompt fission neutrons. In addition, the paper deals with problems of compilation of experimental data and their detailed experimental characteristics,, a task undertaken by the four neutron data centres at Brookhaven, Obninsk, Saclay and Vienna.

1. INTRODUCTION

This conference is the Second IAEA Conference on Nuclear Data for Reactors. Almost four years have elapsed since the first Conference on the same subject in Paris in October 1966. Gratifying progress has been made in these four years. Reactor physicists have made great efforts towards more and more precise definitions of their nuclear data requirements and accuracy goals. The interaction between neutron nuclear physicists, evaluation physicists and reactor physicists has been enhanced substantially. As a consequence, nuclear data programs in many laboratories have become focussed on items of particular importance for reactor research and development, and many measurements are nowadays available on those items. A tendency is seen versus precision measurements and the development of more and more accurate methods to meet high-priority high-accuracy nuclear data requirements. The important role of nuclear data review and evaluation is more and more being acknowledged by the nuclear community owing to the necessity of reconciling conflicting experiments and establishing reliable nuclear data bases for nuclear technology. In parallel, integral experiments with critical facilities have become more and more refined and specific supplementary tools for establishing reliable nuclear data. All these interconnected developments are reflected by the topics and the attendance at this conference; together with the preparatory IAEA expert meetings in Studsvik on the status of α (^{239}Pu) and $\bar{\nu}$ for fissionable nuclei it displays indeed a clustering around the most important nuclear data aspects of nuclear technology.

These are all applied aspects of nuclear data. As one of the most important events of a fundamental nature in the last few years, Strutinsky

[1] has predicted the double-humped shape of the fission barrier for nuclei around A = 240. Since then, this prediction has been verified in many experiments; it has opened a new, very interesting field of experimental research, as has been demonstrated by the large number of contributions on this subject to the Second IAEA Symposium on the Physics and Chemistry of Fission [2] in August 1969. Neutron physicists were able to contribute greatly, in resonance experiments [3-6] and theory [7], to a deeper understanding of this phenomenon, since neutron resonances represent a unique tool for its investigation. More specifically, Strutinsky's detection turned out to be of basic importance for the understanding of the fission resonance properties of ^{239}Pu of the energy dependence of α (^{239}Pu) and of the Doppler effect of ^{239}Pu.

This prominent example should remind us that the field of neutron physics resembles a "Janus head" with two faces, one searching for applied, and the other one for fundamental goals. In fact, within the whole of nuclear physics, neutron physics and data play a singular role. On the one hand, because of their unhindered penetration into nuclei, neutrons serve as a unique means of investigating the properties of nuclear states at and above neutron binding energy. On the other hand, research in this field was enormously stimulated and encouraged by the physical and technical development of nuclear reactors. As the Janus head is only complete if we consider both faces together, it is not sufficient to just measure a nuclear parameter requested by a reactor physicist; we must also investigate and understand the physics behind it, in order to obtain a complete and more reliable picture. Both aspects have to be taken into account when the actual status of nuclear data requirements is to be reviewed.

2. HISTORY

2.1. Reactor development

A few remarks on the development of reactor physics and technology during the last ten years will shed some light on the present nuclear data requirements.

The fifties were characterized by the development of thermal reactors. In the beginning of the sixties, thermal light-water reactors became competitive with conventional electric power plants, starting with the well-known Oyster-Creek event in 1962. From this time onwards the data uncertainties still existing for the heaviest isotopes in the thermal energy range were no longer of economical importance in fuel cost estimates for thermal reactors [8, 9].

The sixties are characterized by the development of fast and intermediate reactors. Initially, in a number of laboratories trend studies were performed in which optimum characteristics in breeding, critical mass, burn-up and safety coefficients were sought as functions of changes in the composition of materials. Later on, these investigations gave rise to more thorough and realistic design studies of fast 300-MWe prototype reactors and large fast 1000-MWe power breeders. At present, a few prototype reactors are under construction. Power breeders of the 1000-MWe type are to be expected only for the second half of the seventies. On the reactor-physics side, this development is supported by extensive measurement programs in fast critical facilities in a number of laboratories.

2.2. Development of nuclear data needs

Compared with thermal reactors, the development of fast reactors opened a need for nuclear data in a much broader energy range and for a much greater variety of neutron nuclear reactions. In 1960, the knowledge of nuclear data was still very poor [10]. To illustrate this by a few typical examples: for important nuclei like ^{239}Pu only a small number of resonances was known, only few data on fast-neutron capture in reactor materials were available, and the knowledge of inelastic level excitation cross-sections was still very scarce. First compilations and evaluations of the available data helped in detecting the gaps in knowledge and in formulating data requirements.

The farther the development of fast reactors advanced from the initial trend studies into the region of actual design the more focussed and stringent became the data requirements. The increasing advent of high-speed big-storage computers simultaneously stimulated the development of sophisticated reactor-theory computer programs allowing very detailed prediction of reactor-physical properties. During the last few years, the errors due to defects in reactor theory have become smaller than the errors introduced by the uncertainties in important nuclear data. The design characteristics of fast reactors and critical facilities are very sensitive to any uncertainties in the nuclear data. Studies aimed at reducing these uncertainties have led to an increasing recognition of the fact that the capture, fission and scattering properties of the main fissile and fertile nuclei are mainly responsible for the neutronics behaviour and have also led to an increasingly precise determination of the accuracy goals for nuclear data of the important reactor materials.

2.3. Request lists for neutron data measurements

In meeting these nuclear data requirements the European American Nuclear Data Committee (EANDC) played a very important role. Since its formation in 1960, the EANDC recognized the needs for nuclear data and worked out procedures for meeting these needs within the OECD area. It began by compiling and issuing lists of requests for neutron nuclear data measurements from reactor and other applied nuclear physicists [11, 12]. These lists are being updated at almost yearly intervals. At each of its meetings, EANDC discusses the actual status of nuclear data measurements and requirements and issues recommendations on how to fulfill justified needs. Since 1968, the request lists are being prepared by a computerized system which allows for rapid updating (RENDA = Requests for Neutron Data Measurements [12]).

These request lists contain neutron nuclear data for which measurements are needed, for given materials in given energy ranges and specify the requirements in energy/angle resolution, accuracy and priority. A comments column is provided in which the requester's name and, in brief form, the status of the requested quantity are indicated.

2.4. Progress in measurement techniques

The EANDC request lists have, in fact, become important guidelines for applied neutron nuclear physics and data research. In particular, they

have helped, obviously among many other factors, in stimulating the development of improved techniques and equipment for nuclear data measurements to meet the increasing accuracy requirements. In the following, the progress in the last few years is illustrated by a few typical examples only:

1. High-intensity neutron sources have been developed, as e.g. modern linear accelerators (ORELA), modern cyclotrons and underground nuclear explosions. The nuclear-explosion technique allows measurements under minimum background conditions which makes it particularly suitable for cross-section measurements on radioactive nuclides and for the investigation of the cross-section behaviour in the valleys between resonances. The increasing importance of this technique is illustrated by the fact that at this conference, for the first time, a simultaneous measurement of total, fission, capture and scattering cross-sections, i.e. on ^{239}Pu between resonance energies and 1 MeV, is reported [15]. Modern linear accelerators and cyclotrons with fast-response detection equipment allow high-resolution resonance measurements for medium and heavy nuclei with the separation of up to a few 100 resonances [16, 17].

2. In the pursuit of absolute reaction cross-section measurements, the development of "flat" neutron detectors, whose efficiency as a function of neutron energy is close to constant, particularly for neutron-flux monitoring in the keV-range of neutron energies has found particular attention. Here we may mention the well-known grey detector developed by Pönitz [18] or the ^{10}B-vaseline sphere black detector constructed at Harwell [19].

3. Improved sample-preparation techniques together with the use of gas scintillation counters for fission fragment detection lately enable reliable absolute fission-rate measurements. By means of the electrospray procedure [20], it is possible to produce very thin fissile material samples of homogeneous thickness of the order of 100 μg/cm^2 and less. Because of the small thickness the actual fission rates per time unit are small, nearly all fission fragments can escape the sample, thus between 90 and 100% of the actual fission events can be detected. Furthermore, the small thickness considerably diminishes the slowing-down of the fission fragments in the sample, keeps the α-decay rate (e.g. in ^{239}Pu) and pile-up small, and, thus, allows a nearly quantitative separation of α and fission-fragment pulses. This has recently led to a considerable improvement of the reliability of fission cross-section ratio measurements [21, 22].

4. Improvements in the time-of-flight method with fast counting equipment have led to an increased energy resolution of the inelastically scattered neutrons, enable better separation of individual levels and of elastically and inelastically scattered neutrons and allow the measurements of inelastic excitation cross-sections for quite a number of levels per individual nuclide. The advent of Ge(Li)-detectors obviously led to a great improvement in the measurement of individual γ-ray excitation cross-sections. Both methods have become competitive to classical methods like Coulomb excitation, α-decay or charged-particle inelastic scattering in the investigation of nuclear level schemes.

3. PRESENT STATUS OF IMPORTANT NUCLEAR DATA REQUIREMENTS

We shall now turn to an outline of the present status of requirements for the more important nuclear data. The discussion of this item will be divided into two parts.

First, we shall quantitatively compare the accuracies requested with those achieved at present for some of the more important nuclear data of fissile and fertile nuclei.

Second, we shall qualitatively discuss the status of some of the outstanding nuclear data and related physics problems.

3.1. Confidence level of important nuclear data

From the progress in measurement techniques set forth in the preceding section, one might be tempted to conclude that a high confidence level in the knowledge of the important nuclear data has been reached. The opposite is true as is demonstrated by Table I. For important standard reactions and heavy-element cross-sections, we have listed here accuracy limits as requested in the last edition of the EANDC request list, briefly called RENDA 70 [12], and an estimate of the confidence level achieved by the combined measurements available at present.

It is immediately evident from this table that none of the accuracy requirements has been met, as yet. Clearly, cross-section-ratio measurements are easier to perform than absolute ones since they do not involve a determination of the neutron flux, but also for cross-section ratios – we listed here only one representative example – the accuracy goals have not been achieved.

In the next paper in these Proceedings, the meaningfulness of these accuracy goals for the heavy-element cross-sections [23] and of the consequences of the still existing data inaccuracies in terms of electric power cost uncertainties will be discussed. We should only like to make a few remarks on the confidence level.

The situation is probably not as bad as is suggested by the confidence level figures. First, it is important to note that in individual modern measurements better accuracies have been achieved which come close to the requested figures listed in column 4. Individual fission cross-section-ratio measurements reach accuracies between 2 and 3% [21, 22]. The recent measurements of the ^{238}U capture cross-section between 0.5 and 100 keV by Moxon [24] claim an accuracy of 3 - 6%. In individual measurements of energy-dependent or spontaneous $\bar{\nu}$ data often accuracies better than 1% are achieved. Secondly, the energy shapes of different cross-section measurements do in many cases well agree with each other, and the real discrepancy is in the absolute values.

However, often two series of measurements disagree by more than the respective measurement errors given by the authors. Since in modern measurements statistical errors are usually small, this suggests that in the individual measurements still unknown errors of a systematic nature exist which must be supposed to exceed by far the errors estimated by the author. We shall return to this question in Section 4. To remove these systematic errors particularly in relative measurements and to establish more reliable absolute cross-sections, it is certainly an important minimum requirement

TABLE I. PRESENT CONFIDENCE LEVEL OF IMPORTANT NUCLEAR DATA

Material	Quantity (*cross-section*)	Energy range	Accuracy requested (RENDA 70 [12]) (± %)	Confidence level achieved (± %)
^{3}He	n, p	10 KeV - 5 MeV	1 - 3	3 - 10 [29]
^{6}Li	n, α	10 KeV - 5 MeV	1 - 5	5 - 20 [29]
^{10}B	n, α	10 KeV - 1 MeV	1 - 5	3 - 10 [29, 30]
^{197}Au	capture	10 KeV - 3 MeV	1 - 5 (mostly)	5 - 15 [29, 31, 32]
^{235}U	*fission*	10 KeV - 1 MeV	1 - 3	$\lesssim$ 10
		1 - 5 MeV	1 - 3	5 - 10
^{235}U	$\bar{\nu}$	10 KeV - 3 MeV	1	$\lesssim$ 2
^{238}U	capture	10 KeV - 5 MeV	2 - 10	10
$^{239}Pu / ^{235}U$	fission ratio	10 KeV - 1 MeV	1 - 3	3 - 5
		1 - 5 MeV	1 - 3	5 - 10
^{239}Pu	fission	10 KeV - 1 MeV	1 - 3	10
		1 - 5 MeV	2 - 5	10 - 15
^{239}Pu	α	0.1 - 100 keV	3 - 5	10 - 20
^{239}Pu	$\bar{\nu}$	10 KeV - 4 MeV	0.5 - 1	2
^{235}U ^{239}Pu	$\bar{E}(\chi(E))$	$\geq$ thermal	2 - 5	10
^{252}Cf	$\bar{\nu}$ spontaneous	-	0.25 - 0.5	$\gtrsim$ 1

to check the normalizations and to improve the accuracy of the standard cross-sections used for normalization, particularly at higher keV and MeV energies.

3.2. Status of outstanding problems

I would now like to turn to a discussion of the status of some of the outstanding problems in neutron physics and nuclear data. The fact that all these items will be subject to extensive discussions during the Conference allows me to restrict myself to rather brief statements in each case and to draw simply the attention to these discussions.

3.2.1. Multilevel versus single-level interpretation of fission resonances

More and more resonance measurements on fissionable nuclei are being interpreted in terms of multilevel theories, the preferred formalisms being those of Reich and Moore [25] and F.T. Adler and D.B. Adler [26]. The preference of multilevel to single-level interpretation, particularly of resonance fission cross-sections, is suggested by the small number of fission channels available in resonance fission and the subsequent expectation of strong resonance-resonance interference. Multilevel fits to measured resonance fission cross-sections have been demonstrated to be superior to single-level fits. For Doppler-coefficient calculations, however, multilevel formulae do not seem to be so important. For example, Fischer [27] could achieve a reasonable agreement with ^{239}Pu Doppler-coefficient measurements [28], within the accuracies of the resonance parameters involved, by using recent single-level knowledge of the ^{239}Pu s-wave resonances.

3.2.2. ^{239}Pu resonances and α-values

Much progress has been made in the knowledge of ^{239}Pu s-wave resonance properties. In particular, from the extensive investigations with the Saclay linear accelerator [5, 16] resonances for energies of up to more than 600 eV are known. In particular, for a number of resonances the spin values have been determined, allowing an estimate of the strength functions for the two s-wave spin values. The distribution of the measured fission widths clearly shows a clustering around two largely different average values, which from the known spin values can be clearly inferred to belong to the 0^+ (large Γ_f) and 1^+ (small Γ_f) resonances, i.e. to above-threshold and sub-threshold fission, respectively. As just mentioned above, this improved knowledge enabled a much better calculational verification of measured ^{239}Pu Doppler coefficients [27]. Also the fluctuating behaviour of α as a function of the neutron energy observed below a few keV is now well understood as a consequence of sub-threshold fission in the 1^+ resonances proceeding via intermediate states in a double-humped fission barrier [33]. More experimental information is still needed on p-wave fission thresholds and widths for a better understanding of measured cross-sections in the "p-wave range" above 1 keV as well as for more reliable determinations of the (admittedly generally small) p-wave contribution to the ^{239}Pu Doppler coefficient.

More generally, the Strutinsky "model" of sub-threshold fission needs more practical exploitation for heavy nuclei with sub-threshold fission

regarding the energy dependence of average fission widths in regions of unresolved resonances. Also more theoretical work on the distribution of fission widths is needed.

The discrepancies between the different available α-measurements at low keV energies have not yet been solved satisfactorily. Thorough work on evaluating the various systematic errors involved in the measurements is still needed.

3.2.3. (^{252}Cf) standard

Many former and all present $\bar{\nu}$-measurements are done relative to $\bar{\nu}$ (^{252}Cf). The well-known discrepancy of about 2% between liquid scintillator measurements [34, 35] on the one hand, and both the $MnSO_4$-bath and boron-pile measurements [36-40] on the other hand has not yet been removed and is reflected in uncertainties of the same order of magnitude in measured relative $\bar{\nu}$-data when converted to absolute values. For the latest review of the $\bar{\nu}$ (^{252}Cf) situation we refer to the extensive work by Hanna et al. [41].

3.2.4. Energy dependence of $\bar{\nu}$

Several of the recent more detailed measurements of the energy dependence of $\bar{\nu}$ (review in Ref. [49]) show a structure below about 2 MeV, deviating from the generally assumed linear behaviour, being rather pronounced for ^{235}U [42-44, 46,47], and less pronounced for ^{239}Pu [42, 44-47] which could be related to similar variations in fission-fragment kinetic energies [47] and to saddle-point transition states of the fissioning compound nuclei involved [51]. Other authors [48, 50] actually find a much weaker structure in ^{235}U $\bar{\nu}$-values. It will, thus, be a particularly important future task, for experimentalists as well as for theorists, to obtain more reliable information on their existence, and on the expected size of such structure effects in $\bar{\nu}$ (E).

Regarding resonance $\bar{\nu}$-values in ^{235}U and ^{239}Pu, the discrepancy between the results of Weinstein et al. [52] and Ryabov [53] still exists and deserves further systematic experimental work. This is particularly important since it may turn out that an average of $\bar{\nu}$ taken over the resonance range which up to keV energies is generally assumed to be equal to the thermal value, actually differs from it. For a similar reason, it would be highly desirable to extend the very detailed recent measurements by Soleilhac et al. [42] on ^{235}U and ^{239}Pu further down below 200 keV. Also the current measurements of average $\bar{\nu}$-values in the neutron-energy spectrum of the Swedish fast zero-power reactor FRO by Condé and Widén [54] will contribute to an improved knowledge of $\bar{\nu}$-values for ^{235}U and ^{239}Pu in the lower keV energy range. Preliminary values are reported at this Conference [54].

3.2.5. ^{235}U fast-neutron fission

Recent high-resolution measurements of the ^{235}U fission cross-section for eV and keV neutron energies by Bowman et al. [55] and Patrick et al. [56] reveal a fluctuating cross-section structure, particularly also between 20 and 30 keV in which the normalization points for a number of ^{235}U fission cross-section measurements are located. The impact of this fluctuating

structure on the normalization of fission cross-section values at higher energies will certainly be subject to discussions at this Conference.

At higher energies the well-known discrepancies between White [57] and Pönitz (preliminary) [58], on the one hand, and between Allen, Ferguson [59] and Diven [60], and White [57], on the other hand, are still unsolved. The recent absolute measurements by Leroy et al. below 1 MeV to be reported at this Conference [61] essentially support White's data. Also Monte-Carlo K_{eff} calculations on small fast critical assemblies performed by Benzi et al. [62] appear to support White's data in contrast to Pönitz' preliminary data.

In view of the outstanding importance of the ^{235}U fission cross-section as basic standard in most fission and many capture cross-section measurements, an extensive concerted effort by nuclear experimentalists, compilers, evaluators, and reactor physicists is necessary in the future in order to solve the discrepancies mentioned. For a more thorough discussion of the present status we refer to the two review papers by Pönitz [31] and Davey [63] presented at this Conference.

3.2.6. ^{238}U fast-neutron capture

The well-known discrepancies between the available measurements [24, 64-69] will certainly be one of the main items of discussion at this Conference and, therefore, need not be stressed here. The new measurements to be reported at this Conference by Fricke et al. [32] will be of particular interest as they extend between 1 keV and 1 MeV and, thus, represent a bridge between the divergent data of Pönitz [67] and Barry [69].

In the energy range where the s- and p-waves are important, the still most controversial parameters are $\overline{\Gamma_\gamma}$ and the p-wave strength function (S_1), which are both needed in Doppler-coefficient calculations and in cross-section predictions in the unresolved resonance range. The $\overline{\Gamma_\gamma}$-values available vary from 19.1 MeV, the value obtained in the Los Alamos PETREL underground explosion experiment [70], to 24.8 MeV as obtained from synchrocyclotron and linear accelerator measurements (for review, see Ref. [71], chapter IV). S_1-values (in units of 10^{-4}) vary from 1.5 [70] to 2.5 [71]. In the PETREL experiment also a sort of regular fluctuations of the Γ_γ values as a function of resonance energy had been observed. More recent linear-accelerator capture measurements at Geel [72] do not reproduce this fluctuating behaviour; they also support the higher $\overline{\Gamma_\gamma}$ value. The recent capture cross-section measurements (see, e.g. Ref. [24]) seem to favour a lower S_1 value between 1.5 and 2.0 in better accord with – which is more appropriate for a strongly deformed nucleus such as ^{238}U – the deformed optical model [73] ($S_1 = 1.7$) than with spherical-optical-model predictions [71] which yield higher values ($S_1 = 3$).

3.2.7. Energy spectra of prompt fission neutrons

The well-known discrepancy between direct fission spectrum measurements for the main fissile nuclides (see, e.g. the review in Ref. [71], chapter VI) and the harder fission spectra inferred from unfolding integral activation measurements [74, 75] is still unsolved. New results on this subject are going to be reported at this Conference [76]. A clarification of this discrepancy would be helpful in understanding the 10% underestimate of

calculated fission-rate ratios like f (^{238}U)/(^{235}U) or f(^{238}U)/(^{239}Pu) compared to the results of integral measurements in fast critical assembly spectra [14, 77].

3.2.8. ^{238}U neutron inelastic scattering

The neutron inelastic scattering on ^{238}U actually provides the strongest slowing-down mechanism in fast reactors and is, thus, mainly responsible for the kind of neutron spectra occurring in fast reactors. The above-mentioned 10% underestimate of the fission-rate ratios due to using current evaluated data [78-80] might alternatively be due to an overestimate of the ^{238}U inelastic scattering, particularly in the 1-2 MeV energy range [77, 81]. Recent experiments performed at Argonne [82] seem to indicate that the total inelastic scattering cross-sections in the current evaluated data files around 1.5 MeV might be too high by about 10% (see, e.g. Ref. [31]).

3.2.9. (n, α) reaction in structural materials

The embrittlement and swelling of fuel canning materials by He-build-up due to the (n, α)-reaction have recently been recognized as a serious safety limitation of the achievable burn-up in fast reactors. The knowledge of cross-sections for this reaction in structural materials concerned like Fe or Ni is still very poor [83]. For ^{58}Ni, the main Ni isotope, up to a few years ago only one value, a fission-spectrum average measured by Schuman and Mewherter [85] in 1957 had been available. The value was rather small, 0.17 mb. At the last Washington Conference Weitman and Daverhög [84] reported a much larger experimental value for this quantity, i.e. 4.2 mb which would correspond to a much larger He-build-up in Ni containing fuel cannings than was assumed previously. In this respect, the careful statistical-theory studies by Eriksson [86] to be reported at this Conference deserve particular attention. It is strongly hoped that these theoretical studies will be supplemented, in future, by energy-dependent (n, α)-cross-section measurements.

3.2.10. Fast-neutron capture in structural materials

There are the well-known discrepancies particularly for Fe between lead-pile [87, 88] and linear-accelerator measurements [89] and also between calculated and directly measured infinite-dilution capture resonance integrals [71]. Recent capture measurements by Moxon [90] on natural Fe in the energy range of 0.02 - 200 eV revealed the existence of narrow resonances at low energies in the rare Fe isotopes which helped to reduce considerably the discrepancy between the non-1/V parts of the infinite-dilution resonance integral directly measured and those deduced from the linear-accelerator measurements. A number of interesting contributions to this subject is to be expected from this Conference (see, e.g. Refs [91, 92]).

3.2.11. Neutron elastic and inelastic scattering on medium and heavy nuclei

It is gratifying to notice that, in response to many data requests in the EANDC request lists, more and more systematic measurements of elastic-scattering angular distributions and of inelastic-scattering cross-sections

are performed and extended in the higher MeV-range. In particular, we refer here to recent Swedish work [93, 94]. These investigations do not only provide an improved experimental basis for systematic studies of optical-model parameters [93], but also help to satisfy the data requirements for more reliable shielding calculations [95, 96].

4. OUTLOOK

To summarize these remarks, we can say that, on the one hand, the microscopic-data and accuracy requirements of reactor physicists can be met to a fair degree by the techniques of measurement available at present. On the other hand, these accuracy targets have not yet been reached by the combined available data [13], which seems to be largely due to still unknown systematic errors in and deviations between different measurements. This fact does not always call for a new measurement or even the extensive development of an improved measurement technique, but more often for an increased effort by experimentalists and evaluators in understanding the source and magnitude of systematic errors in the existing measurements.

For this purpose, careful compilations of the experimental data concerned and of their detailed experimental characteristics are required. This is the task of the four neutron data centres at Brookhaven, Obninsk, Saclay, and Vienna. In a recent joint effort, the centres developed the so-called EXFOR system which provides a computer format for the coding and transmission of neutron data and auxiliary physics information between the centres. The routine transmission of data tapes in the exchange format will start on 1 July 1970. With increasing implementation of EXFOR an increasing access of experimentalists, evaluators and reactor physicists all over the world to the desired neutron data and physics information can be anticipated.

On the reactor physics side, specific integral experiments should be designed which could help to fix the absolute values of given microscopic cross-section shapes.

These few concluding remarks should show that only by increased concerted and coordinated efforts of nuclear physicists, compilers, evaluators and reactor physicists, the data accuracy goals of nuclear technology can be achieved. It is hoped that this Conference will see full and effective interaction between all those concerned with the pursuit of these goals.

REFERENCES

[1] STRUTINSKY, V.M., Nucl.Phys. A95 (1967) 420.
[2] Physics and Chemistry of Fission (Proc. 2nd Symp. Vienna, 1969) IAEA, Vienna (1969). Sessions C, D, and E.
[3] JAMES, G.D., RAE, E.R., Nucl.Phys. A118 (1968) 313.
[4] PAYA, D. et al., in Nuclear Data for Reactors (Proc.Conf. Paris, 1966) 2, IAEA, Vienna (1967).
[5] MICHAUDON, A., in Neutron Cross-Sections and Technology (Proc.Conf. Washington, 1968) 1 427.
[6] MIGNECO, E., THEOBALD, J.P., in Neutron Cross-Sections and Technology (Proc.Conf. Washington, 1968); 1 527; WEIGMANN, H., unpublished (1968).
[7] LYNN, J.E., in Physics and Chemistry of Fission (Proc. 2nd Symp. Vienna, 1969, IAEA, Vienna (1969) 249.
[8] KINCHIN, G.H., in Nuclear Data for Reactors (Proc.Conf. Paris, 1966) 2, IAEA, Vienna (1967) 13.
[9] FRENCH, R.J., in Neutron Cross-Sections and Technology (Proc.Conf. Washington, 1968) 1 259.

[10] SCHMIDT, J.J., in Physics of Fast and Intermediate Reactors (Proc.Symp.Vienna, 1961) 1, IAEA, Vienna (1962) 3.
[11] JOLY, R., PERRET, R.P., EANDC-13"U", 1961; JOLY, R., PERRET, R.P., EANDC-17"L", 1962; PERRET, R.P., SELBY, R.A., EANDC-25"L", 1963; EANDC-38"L", 1964; EANDC-43"U", 1965; EANDC-55"U", 1966.
[12] HÄUSSERMANN, W., SCHWARZ, S., "RENDA", EANDC-61"U", Jan.1968; SCHWARZ, S., HÄUSSERMANN, W., "RENDA", EANDC-78"AL", Dec.1968; "RENDA", EANDC-85"U", April 1970.
[13] GREEBLER, P., HUTCHINS, B.A., WOLFE, B., in Neutron Cross Sections and Technology (Proc.Conf. Washington, 1968) 1 291.
[14] KÜSTERS, H. et al., KFK-793 (EUR-3962e, EANDC(E)-113"U"), 1968; BROEDERS, C.H.M., KFK-939, 1969.
[15] FARRELL, J.A. et al., these Proceedings, paper CN-26/46.
[16] MICHAUDON, A., DERRIEN, H., et al., these Proceedings, papers CN-26/60, 61 and 62.
[17] CIERJACKS, S., these Proceedings, paper CN-26/113.
[18] PÖNITZ, W.P., Nucl.Instrum.Meth. 58 (1968) 39.
[19] RAE, E.R., private communication (1969).
[20] LAUER, K.F., VERDINGH, V., Nucl.Instrum.Meth. 21 (1963) 161; VERDINGH, V., LAUER, K.F., Nucl.Instrum Meth. 49 (1967) 179.
[21] PÖNITZ, W.P., Nucl. Sci.Eng., to be published, 1970; see also this Conference, paper CN-26/111.
[22] PFLETSCHINGER, E., KÄPPELER, F., Nucl.Sci.Engng to be published, 1970; see also Euratom Progress Report EANDC(E)-127"U", (1970) 54, 58.
[23] GREEBLER, P. et al., these Proceedings, paper CN-26/102.
[24] MOXON, M.C., AERE-R 6074, 1969.
[25] REICH, C.W., MOORE, M.S., Phys.Rev. 111 (1958) 929.
[26] ADLER, D.B., ADLER, F.T., ANL-6792, (1963) 695; in Neutron Cross-Section Technology (Proc.Conf. Washington, 1966) 2 873; in Neutron Cross-Sections and Technology (Proc.Conf.Washington, 1968) 2 967; final report Subcontract AEC-BNL-006977 (1966).
[27] FISCHER, E.A. et al., in Physics of Fast Reactor Operation and Design (BNES Conf.London, 1969) paper 1.11.
[28] FISCHER, E.A. et al., Nucl.Sci.Engng 25 (1966) 37.
[29] Nuclear Standards for Neutron Measurements (IAEA Panel Brussels, 1967); Technical Report IAEA-107 (1968).
[30] SOWERBY, M.G. et al., these Proceedings, paper CN-26/26.
[31] PÖNITZ, W.P., these Proceedings, paper CN-26/111.
[32] FRICKE, M.P. et al., these Proceedings, paper CN-26/43.
[33] SCHMIDT, J.J., Atomkernenergie 15 (1970) 26; see also KFK-966, 1969.
[34] ASPLUND-NILSSON, I. et al., Nucl.Sci.Engng 16 (1963) 124.
[35] HOPKINS, J.C., DIVEN, B.C., Nucl.Phys. 48 (1963) 433.
[36] COLVIN, D.W., SOWERBY, M.G., in Physics and Chemistry of Fission (Proc.Symp.Salzburg, 1965) 2 IAEA, Vienna (1966) 25.
[37] MOAT, A. et al., J.nucl.Energy, Parts A/B; Reactor Sci.Techn.15 (1961) 102.
[38] COLVIN, D.W. et al., in Nuclear Data for Reactors (Proc.Conf.Paris, 1966) 1, IAEA, Vienna (1967) 307.
[39] AXTON, E.J. et al., EANDC(UK)-110, 1969; private communication, 1969.
[40] De VOLPI, A., PORGES, K.G., private communication (1970).
[41] HANNA, G.C. et al., Atom.Energy Rev. 7 (1970) 3.
[42] SOLEILHAC, M. et al., these Proceedings, paper CN-26/67.
[43] MEADOWS, J.W., WHALEN, J.F., J.nucl.Energy 21 (1967) 157.
[44] SAVIN, M.V. et al., these Proceedings, paper CN-26/40.
[45] MATHER, D.S. et al., AWRE-0-42/70 (1970).
[46] NESTEROV, V.G. et al., these Proceedings, paper CN-26/74.
[47] VOROBEVA, V.G. et al., these Proceedings, paper CN-26/88.
[48] BOLDEMAN, J.W., WALSH, R.L., AAEC/TM 523 (1969).
[49] KONSHIN, V.A., MANERO, F., INDC(NDS)-19/N, to be published (1970).
[50] AJITANAND, N.N., BOLDEMAN, J.W., AAEC/TM 526 (1970).
[51] STRUTINSKY, V.M., PAVLINCHUK, V.A., in Physics and Chem. of Fission (Proc.Conf.Salzburg, 1965) IAEA, Vienna (1966) 127.
[52] WEINSTEIN, S. et al., in Physics and Chemistry of Fission (Proc.Conf. Vienna, 1969) IAEA, Vienna (1969) 477.

[53] RYABOV, Yu.V., in Physics and Chemistry of Fission (Proc.Conf.Vienna, 1969) IAEA, Vienna (1969) 486; see also JINR Dubna report D-3893, (1969) 88.
[54] CONDÉ, H., WIDÉN, L., these Proceedings, paper CN-26/59.
[55] BOWMAN, C.D. et al., these Proceedings, paper CN-26/41.
[56] PATRICK, B.H. et al., AERE-report (1970).
[57] WHITE, P.H., Reactor Sci.Techn. 19 (1965) 325.
[58] PÖNITZ, W.P., in Neutron Cross Sections and Technology (Proc.2nd Conf.Washington, 1968) 1, 503.
[59] ALLEN, W.D., FERGUSON, A.T.G., Proc.Phys.Soc. 70 (1957) 573.
[60] DIVEN, B.C., Phys.Rev. 105 (1951) 1350.
[61] LEROY, J.L. et al., these Proceedings, papers CN-26/69 and 70.
[62] BENZI, V. et al., these Proceedings, paper CN-26/49.
[63] DAVEY, W.G., these Proceedings, paper CN-26/112.
[64] MACKLIN, R.L. et al., WASH-1046, (1964) 88 90; ORNL-TM-761 (1964).
[65] MOXON, M.C., reported by FERGUSON, A.T.G., PATTENDEN, N.J., in ANL-6792, (1963) 11.
[66] MOXON, M.C., RAE, E.R., reported by RAE, E.R. et al., Geneva 3rd Conf. 1964, paper 167.
[67] PÖNITZ, W.P. et al., KFK-635 (EUR-3679e) (1967).
[68] MENLOVE, H.O., PÖNITZ, W.P., Nucl.Sci.Engng 33 (1968) 24.
[69] BARRY, J.F. et al., J.nucl.Engng, Pts.A/B, Reactor Sci.Techn. 18 (1964) 491.
[70] GLASS, N.W. et al., in Neutron Cross-Sections and Technology (Proc.2nd Conf. Washington, 1968) 1 573.
[71] SCHMIDT, J.J., KFK 120/part I(1966).
[72] ROHR, G. et al., these Proceedings, paper CN-26/18.
[73] BUCK, B., PEREY, F., Phys.Rev.Letts 8 (1962) 444.
[74] GRUNDL, J., Nucl.Sci.Engng 30 (1967) 39; Nucl.Sci.Engng 31 (1968) 191.
[75] FABRY, A., Nukleonik 10 (1967) 280.
[76] FABRY, A. et al., these Proceeding, paper CN-26/39.
[77] ROWLANDS, J.L., MacDOUGALL, J.D., in Physics of Fast Reactor Operation and Design, (BNES Conf.Lor London, 1969) paper 1.16; ROWLANDS, J.L., private communication (1969).
[78] LANGNER, I. et al., KFK 750 (1968).
[79] VASTEL, M., report HX-1/1375/CL RA-Fl-04 (1968).
[80] WITTKOPF, W.A. et al., ENDF-103 (BAW-316) (1967).
[81] KALLFELZ, J.M. et al., personal communication by PÖNITZ, W.P. (1969).
[82] SMITH, A.B., private communication (1969).
[83] MEYER, R., KFK-report, to be published (1970).
[84] WEITMAN, J., DAVERHÖG, N., in Neutron Cross-Sections and Technology (Proc.2nd Conf. Washington, 1968) 1 125.
[85] SCHUMAN, R.P., MEWHERTER, A.C., KAPL-1779 (1957).
[86] ISAKOV, A.I. et al., Zh.éksp.teor.Fiz. 38 (1960) 989; translated in Soviet Phys.JETP 11 (1960) 712.
[88] MITZEL, F., PLENDL, H.S., Nukleonik 6 (1964) 371.
[89] MOXON, M.C., in Study of Nuclear Structure with Neutrons (EANDC Conf.Antwerp, 1965) P/88.
[90] MOXON, M.C., RAE, E.R., private communication (1969).
[91] NISHIMURA, K. et al., these Proceedings, paper CN-26/28.
[92] MOXON, M.C. et al., these Proceedings, paper CN-26/32.
[93] HOLMQVIST, B., Arkiv Fysik 38 (1968) 403.
[94] HOLMQVIST, B., WIEDLING, T., in Neutron Cross-Sections and Technology (Proc.2nd.Conf. Washington, 1968) 2 845.
[95] GOLDSTEIN, H., in Nuclear Data for Reactors, (Proc.Conf.Paris, 1966) 1 39.
[96] GOLDSTEIN, H., in Neutron Cross-Sections and Technology (Proc.2nd.Conf. Washington, 1968) 1 37.

Invited Paper

IMPLICATIONS OF NUCLEAR DATA UNCERTAINTIES TO REACTOR DESIGN

P. GREEBLER, B.A. HUTCHINS, C.L. COWAN
General Electric Company,
Sunnyvale, Calif.,
United States of America

Abstract

IMPLICATIONS OF NUCLEAR DATA UNCERTAINTIES IN REACTOR DESIGN.

Uncertainties in nuclear data require significant allowances to be made in the design and the operating conditions of reactor cores and of shielded-reactor-plant and fuel-processing systems. These allowances result in direct cost increases due to overdesign of components and equipment and reduced core and fuel operating performance. Compromising the allowances for data uncertainties has indirect cost implications due to increased risks of failure to meet plant and fuel performance objectives, with warrantees involved in some cases, and to satisfy licensed safety requirements. Fast breeders are the most sensitive power reactors to the uncertainties in nuclear data over the neutron energy range of interest for fission reactors, and this paper focuses on the implications of the data uncertainties to design and operation of fast breeder reactors and fuel-processing systems. The current status of uncertainty in predicted physics parameters due to data uncertainties is reviewed and compared with the situation in 1966 and that projected for within the next two years due to anticipated data improvements. Implications of the uncertainties in the predicted physics parameters to design and operation are discussed for both a near-term prototype or demonstration breeder plant (~300 MW(e)) and a longer-term large (~1000 MW(e)) plant. Significant improvements in the nuclear data have been made during the past three years, the most important of these to fast power reactors being the ^{239}Pu alpha below 15 keV. The most important remaining specific data uncertainties are illustrated by their individual contributions to the computational uncertainty of selected physics parameters, and recommended priorities and accuracy requirements for improved data are presented.

1.0 INTRODUCTION

Nuclear data uncertainties influence the design and the operation of reactor systems for electrical power generation in the following ways:

1. Extra margins must be provided in the core design or more restrictive limits imposed on fuel performance objectives, with resultant cost penalty. This is to assure that, in the event of reasonably pessimistic data, fuel and other core materials do not exceed allowed temperatures, requirements for control and reactivity coefficients are satisfied, safety reactivity limits for potential reactivity-insertion mechanisms are not exceeded, and fuel performance meets warrantee requirements.
2. Shielding must be over-designed to allow for reasonably pessimistic shielding data, with associated costs incurred for the extra shielding material and the space required to accommodate the extra material. This involves not only radiation-damage protection for structural components in the reactor vessel and the primary coolant circuit and biological shielding for all personnel access areas within the plant environs, but also shielding of equipment used in the fabrication and the shipment of fuel utilizing recycled fissile material.
3. Planning of long-range fissile material requirements and, hence, fuel costs for all nuclear reactor systems must account for the uncertainties in the predicted fissile doubling times of breeder reactor systems associated with the nuclear data uncertainties.

These effects of data uncertainties will be reviewed and illustrated in this paper for fast breeder power reactor systems. The fast breeder was selected because 1) it is undergoing intensive development in many nations as the leading advanced reactor system, 2) it is the reactor type that is most affected by the nuclear data uncertainties over the energy range of interest to fission reactors, and 3) it does not have the benefit of considerable past operating experience which could lessen concern about the implications of nuclear data uncertainties.

The greater sensitivity of fast breeder reactor performance to data uncertainties has been indicated by studies reported on both thermal and fast reactors. Early fast reactor studies by Moorhead [1] and Greebler and Hutchins [2] pointed out the large uncertainties which existed in fast reactor computations due to data uncertainties. Comparison of papers by Kinchin [3] and Smith [4] in 1966 showed a factor of 3 to 5 difference in estimated accuracies of computed reactivity for thermal and fast reactors, in part due to having more operating experience with thermal reactors. Papers presented in 1967 and 1968 by French [5,6], Drake, et al [7], Craven and Perry [8] and Greebler, et al [9,10] indicated a fuel cost uncertainty for thermal and epi-thermal reactors of less than 0.05 mill/KW(e)h due to nuclear data uncertainties, compared to fast reactor uncertainties in the range of 0.15 to 0.25 mill/KW(e)h. Various aspects of the effects of data uncertainties on the physics of fast breeders have been investigated in recent years by Küsters, et al [11], Broeders [12], Schmidt [13], Barre and Ravier [14], Gandini, et al [15], and Kallfelz, et al [16]. These studies provide further evidence that present uncertainties in nuclear data have an important effect on fast reactor analysis and design. Data uncertainties important in shielding design have been discussed recently by Penny [17].

Uncertainties in the data associated with the principal fissile and fertile fuel isotopes in a fast breeder reactor, ^{239}Pu and ^{238}U, are the most important ones [2,4,10]. Until recently, the ^{239}Pu alpha below 15 keV was the most significant data uncertainty. The good agreement finally achieved in the ^{239}Pu alpha values below 15 keV measured in several laboratories worldwide [18,19,20] has considerably improved confidence in the nuclear data used for fast reactor calculations.

Although the most important data uncertainties remain those that relate directly to core and fuel performance, the uncertainties in the neutron removal cross section data most important to shielding calculations, especially steel isotopes and sodium, are becoming increasingly more significant as more detailed plant layouts are made for the several prototype or demonstration plants in the various national fast breeder programs. This significance has been accentuated in recent years by the recognition of the importance of the problem of neutron irradiation damage to structural materials [21,22]. Recent activity in the design of fabrication facilities and fuel shipping casks for fuel utilizing high-burnup plutonium has focused attention on the inadequacy of the cross section data pertaining to the production of the neutron-source isotopes that occur in high-burnup plutonium.

Sections 2.0 and 3.0 below deal with the uncertainties in predicted physics core parameters and in shielding requirements due to combined data uncertainties and the significance of such prediction uncertainty to reactor design operation. Section 4.0 considers important specific data uncertainties and their individual effects on predicted core and fuel performance parameters.

2.0 UNCERTAINTIES IN PREDICTED CORE PARAMETERS

Table I lists core compositions and geometries, and several physics parameters for two fast breeder reactors. One is for a 1000 MW(e) reactor which is intended here to be reasonably representative of the expected high

TABLE I. TYPICAL DESIGN PARAMETERS FOR EARLY 300 MW(e) AND MATURE 1000 MW(e) LIQUID METAL FAST BREEDER REACTOR CORES

Parameter	300 MW(e)[a]	1000 MW(e)[b]
Core Height/Diam. (metre)	0.76/2.0[c]	76/2.5[c]
Fuel (vol.% PuO_2-UO_2)	33	47
Steel/Sodium/BeO/B_4C (vol.%)	23/41/2/1	15/37/0/1
Core Fuel Burnup (MW(t)-d-t^{-1})	50 000	100 000
Core Avg. Fuel Linear Power (W/cm)	230	315
Core Peak-to-Avg. Power Density[d]	1.6	1.6
^{239}Pu + ^{241}Pu in Reactor (kg)	1050	2300
Breeding Ratio	1.2	1.4
Doubling Time (year)	30	8
Doppler Effect - Sodium In (T dk/dT)	-0.0060	-0.0060
Doppler Effect - Sodium Out (T dk/dT)	-0.0040	-0.0037
Total Sodium Void Reactivity ($)	0	2.2
Single-Element Sodium Void Reac. ($)	0.04	0.06
Total Shim Control Rod Reactivity ($)	15	7
Fluence at Core Center (nvt > 1 MeV)	2.5×10^{22}	7×10^{22}
in Spent Fuel Element (nvt Total)	2.5×10^{23}	7×10^{23}

(a) Parameters are listed for a first core at 25 000 MW(t)-d-t^{-1} average core fuel burnup halfway through a 6-month operating interval between refuelings. Plutonium isotopic composition in the fresh fuel, at.% 239/240/241/242, is 59/26/12/3, representative of plutonium discharged from a water reactor.

(b) Parameters are listed for an equilibrium fuel cycle with a 50 000 MW(t)-d-t^{-1} average core fuel burnup halfway through a one-year operating interval between refuelings. Plutonium isotopic composition in the fresh fuel, at.% 239/240/241/242, is 72/22/4/2, representative of plutonium recycled in a fast breeder system.

(c) Assume 0.4-metre blanket thicknesses with volumetric composition similar to the core for axial blankets; 50 vol.% fuel, 20 vol.% steel, and 30 vol.% sodium for radial blanket; depleted UO_2 for fresh blanket fuel.

(d) Includes radial power peaking for a two-zone core (higher Pu-to-U ratio in the outer zone), axial power peaking, and local power peaking due to control rod perturbations and variations in burnup between different fuel elements in the same region of the core.

core and fuel performance of mature fast breeder systems. The second is for a 300 MW(e) reactor intended here to be reasonably representative of a conservatively-designed first core in a prototype or demonstration breeder plant for near-term construction[1]. The conservative design may include factors such as large pitch-to-diameter ratio for fuel pins to reduce coolant pressure drop, large allowances for irradiation swelling of the fuel element structural material (steel), axial expansion voids in the fuel pins to accommodate fuel swelling, stringent requirements for primary and secondary control shutdown mechanisms with tight limits on the maximum reactivity

[1]The degree of conservatism is expected to differ considerably between the various worldwide design organizations, and some may design first cores intended for operation at conditions actually simulating the long-term fuel performance expected of the later large breeder plants.

worth of any single mechanism, stringent requirements for a minimum Doppler coefficient, and limits on reactivities associated with sodium voiding configurations. Conservatism of design in most of these areas tends to reduce the fuel volume fraction or to otherwise alter the core composition and geometry in such a manner as to reduce the fissile breeding ratio and increase the inventory of fissile material. These two reactor models will be used as examples to illustrate the implications of data uncertainties to reactor design and operation.

2.1 Current Prediction Uncertainties and Progress for Improvement

Table II indicates the current status of uncertainty in several important predicted physics parameters due to uncertainties in nuclear data. The uncertainty ranges in Table II are estimated to represent crudely a 90% confidence level that the actual value of the predicted parameter falls within the indicated range. The uncertainty ranges are approximately the same for the two reactors listed in Table I, but the implications of these uncertainties to design can be appreciably different for the two reactors, as discussed in Section 2.2.

The effects of current data uncertainties are compared in Table II with those of data uncertainties that existed in 1966[2] for several of the listed parameters. Goals for data improvement over a 5-year period, expressed in terms of uncertainties in calculated physics parameters, were recommended at the 1966 Washington, D.C. conference [2], and these are listed in Table II under "1971 Goals". Comparison of the current uncertainty ranges with those reported in the 1966 paper [2] shows that significant progress has been made in improvement of the data required for reactor core design. The most important data refinement was in the ^{239}Pu alpha below 15 keV [18,19, 20]. Several independent measurements of ^{238}U $\sigma(n,\gamma)$ [23,24,25] somewhat reduced the large uncertainties in this data. Also, there were a number of in-depth evaluations of fuel isotopic data [26,27,28,29] during this period which both reduced uncertainties and helped to identify discrepancies between absolute measurements based on different standards.

The "1971 Goals" for data accuracy recommended as a 5-year program objective in the 1966 paper [2] appear unlikely to be met--see Table II--if one simply extrapolates from the 1966 and the current uncertainties. However, the accelerated pace of important nuclear data measurements offers encouragement that the recommended "1971 Goals" will be met within the next two years. Current emphasis is being placed on refinement of the ^{238}U $\sigma(n,\gamma)$ data. The new ORELA Linac facility at Oak Ridge National Laboratory [30] is presently being used to measure this cross section, serving as an important example that supports such an optimistic view on the progress of nuclear data improvements.

Uncertainties due to inadequate computational models (e.g. limitations of computer codes) add to the uncertainties indicated in Table II due to inadequate data accuracy. It is estimated that the nuclear data uncertainties contribute most of the combined uncertainties due to methods and data in predicted fissile Pu inventory, breeding ratio, and neutron source level in recycled plutonium; more than half of the combined uncertainty in calculated Doppler coefficient, total sodium void reactivity, total control rod worth, and neutron flux and radiation level parameters related to plant shielding; and less than one-half of the combined uncertainty in power distribution. Thus, current data uncertainties contribute significantly to the uncertainties in predicted parameters that have a direct bearing on the economical and safety performance of fast breeder reactors.

[2]The year of the First International Conference on Nuclear Data Reactors, Paris, France, October 17-21, 1966, and of the First Conference on Neutron Cross Section Technology, Washington, D.C., March 22-24, 1966.

TABLE II. UNCERTAINTY RANGES IN PREDICTED PHYSICS PARAMETERS OF FAST BREEDER POWER REACTORS DUE TO NUCLEAR DATA UNCERTAINTIES

Parameters	Uncertainty Range		
	Present[a]	1966[b]	1971 Goals[b]
$^{239+241}$Pu Inventory in Reactor (±%)	8	10	3
Breeding Ratio (±)	0.10	0.13	0.05
Doppler Coefficient (±%)	20	30	10
Total Sodium Void Reactivity (±$)	2.0	2.3	1.5
Control Rod Reactivity Worth (±%)	15		
Peak-to-Avg. Core Power Density (±%)	5		
Total Neutron Flux at Reactor Vessel	1/3 to 3[c]		
^{24}Na Radiation Level in Secondary Coolant Circuit	1/10 to 10[c]		
Neutron Source Level of Recycled Pu	1/5 to 5		

(a) See Tables III, IV, and V for individual data contributions to uncertainties in predicted breeding ratio, fissile inventory, and fuel cost.

(b) "1966" uncertainties were estimated from the data uncertainty ranges of references [9,10]. These are essentially the same as the data uncertainties used for the 1966 Washington Conference paper [2], except the latter considered only data in the energy interval 0.1 to 100 keV. "1971 Goals" are consistent with Table 13 of reference [2]--as per the footnote of that table--with an additional correction to take into account the data uncertainties in $\bar{\nu}$ and for neutron energies above 100 keV. The additional corrections are based on the studies of sensitivity to data uncertainties reported in references [9,10], from which it is deduced that about two-thirds of the uncertainty in currently calculated physics parameters is associated with the neutron energy range 100 eV to 100 keV.

(c) Based on a ±20% uncertainty in removal cross sections.

2.2 Implications of Uncertainties in Predicted Core Physics Parameters

For the mature large fast breeder plants, the dominant consideration involving the uncertainties in nuclear data is the ultimate effect that these uncertainties will have on the fuel cycle parameters, fissile inventory and breeding ratio. These parameters largely determine the fissile doubling times which, in turn, effect not only the fuel cost of the breeder reactors, but also of thermal reactors that discharge plutonium which will be needed by new fast breeder reactors in a growing economy [31]. Current uncertainty in the doubling time potential of large fast breeder systems due to uncertain data contributes to the difficulty of predicting what the long-range balance will be between breeder and non-breeder reactors and the associated requirements for uranium, as well as the long-range fuel costs.

To illustrate the fuel cost influence of the data uncertainties, consider for the 1000 MW(e) reactor of Table I the ±0.1 uncertainty in the breeding ratio and the ±8% in the fissile plutonium inventory shown in

Table II as 90% confidence limits. These uncertainties result in a doubling time uncertainty range from 5.8 to 11.5 years and a ±0.13 mill/KW(e)h uncertainty in the fuel cost[3]. The 0.13 mill/KW(e)h fuel cost differential represents an uncertainty of about US $900,000 per year in operating cost for a single 1000 MW(e) plant. The uncertainty range in doubling time translates into a difference of about one million tons in cumulative U_3O_8 ore requirements over a 35-year period between 1985 and 2020 using one projective buildup of fast breeder electrical generating capacity [32].

The implications of nulcear data uncertainties to the design and operation of the near-term prototype or demonstration plants are more complex than for the case of the mature fast breeder plant discussed above. Because of their developmental status, the near-term breeder plants will have high capital and fuel processing costs. Hence, the differentials in the fuel cost associated with the data uncertainties will not have much impact toward making these plants economically competitive. Emphasis will be placed on assurance of reliability and safety, with many of the component and material operating limits not known nearly as well as they will be for the later mature breeder plants which will have the benefit of the earlier operating experience and of considerable additional information from continuing national breeder development programs. Performance goals will generally be modest, especially for a first core, compared with those for the mature large breeder plants to provide allowances for present uncertainties in thermal-hydraulic and mechanical characteristics, including factors such as irradiation-induced swelling of steel, thermal conductivity of fuel, material temperature limits, hydraulic pressure differentials, and behavior of coolant and fuel under transient conditions of varying severity for safety considerations, and taking into account also the uncertainties in the predicted physics parameters. There will, nevertheless, be some important performance goals and these will no doubt include a modest demonstration of breeding capability and of high fuel power density.

The core parameters of the illustrative 300 MW(e) reactor of Table I show such a compromise in performance goals to allow for the current status of technological uncertainties. The relatively low fuel volume fraction, compared with that of the mature 1000 MW(e) design, results mainly from the design changes made to allow for the uncertainties; and it appreciably reduces the breeding ratio and increases the fissile inventory. Uncertainties in the predicted amount of control required for burnup and for temperature changes between shutdown and full power operation, combined with uncertainties in predicted control rod strengths and a stringent limit imposed on the strength of a single control rod, significantly adds to the number of control rods required. This is one of the factors that contributes to the decrease in fuel volume fraction and, hence, in breeding ratio. In order to assure an adequate Doppler coefficient even in a voided core with fully-inserted shim control at the beginning of operation after a refueling (a coefficient that will limit the energy release sufficiently in a maximum hypothetical accident to assure integrity of the containment) taking into account also the uncertainty in the predicted Doppler coefficient, a small amount of moderating material, BeO, is included in the core composition of the 300 MW(e) reactor of Table I. This further decreases the breeding ratio. The predicted breeding ratio of 1.2 shown in Table I for the 300 MW(e) reactor provides a reasonable assurance of at least a 1.1 breeding ratio, and the possibility of one as high as 1.3 based on the uncertainty range indicated in Table II.

---

[3]These estimated doubling time and cost uncertainties assume a 30% out-of-pile fissile Pu inventory, a US $10/gm fissile Pu value, a 10%/yr interest rate on fuel, and an 80% plant load factor. These conditions, and especially the Pu value and the fuel interest rate, will vary considerably among different nations and with time.

The lower fuel linear power in the first core of the 300 MW(e) reactor, relative to the mature 1000 MW(e) reactor, which increases the fissile inventory, results from allowances for the uncertainties in the thermal properties of the fuel as well as the uncertainties in the predicted power distributions. It should be noted that critical assembly mockup experiments conducted in support of the design would reduce several of the uncertainties in the predicted parameters well below the ranges indicated in Table II, especially for fissile inventory and control rod worths. Running such a critical experimental program is in itself a significant cost factor, and some of the reactor design organizations may only have access to a critical facility for a final proof-test mockup, after many of the core design properties have already been finalized.

3.0 UNCERTAINTIES IN PREDICTED SHIELDING REQUIREMENTS AND RADIATION SOURCES

3.1 Plant Shielding

The factor of about a one-half decade uncertainty in the flux level at the reactor vessel is an example of the design allowances that must be made to adequately shield structural components in and near the reactor vessel against excessive irradiation-damage fluences. The extra thickness of the radial shield inside the vessel to accommodate the uncertainty is 12 cm, producing roughly an equal increase in the vessel radius. The approximately one-decade uncertainty in the activation of sodium in the secondary coolant circuit requires an additional 4 cm of B_4C shielding around the intermediate heat exchangers for a design in which the components of the primary coolant circuit are immersed in a sodium pool. Similar extra shielding allowances required throughout a 300 MW(e) size plant represents an increase in the capital cost of such a plant estimated to be in the order of one million dollars (for US construction). The uncertainties indicated in the shielding area examples listed in Table II may be high estimates in light of better agreement obtained between some calculations and benchmark experiments [33]. However, such experiments tend to have considerably simpler geometrical configurations and composition arrangements than those involved in a fast breeder plant, especially for the deep penetration paths. The uncertainties in shielding predictions indicated in Table II due to uncertainties in the nuclear data are very rough estimates since there has not been a systematic evaluation of all the shielding data uncertainties important to fast breeder systems, accompanied by a quantitative assessment of the effects of the combined uncertainties on predicted radiation levels at sensitive locations throughout such a plant.

Shielding data requirements for reactor design and operation include several important types [17]. Total cross sections and the angular distribution of elastic scattering cross sections are required in the keV and MeV energy range for deep penetration calculations. In addition, the level excitation for inelastic scattering is required to be able to predict neutron spectra accurately. Gamma rays produced by neutron capture and following inelastic scattering are also needed for shielding calculations. Differences between thermal neutron capture spectra and the resonance spectra have been found to be significant and indicate that the capture-gamma ray spectra should be known for all incident neutron energies.

3.2 Neutron Source Uncertainties in Fuel Processing

The factor of five uncertainty in the neutron source level of recycled plutonium--see Table II--contributes to the uncertainty in specifying shielding requirements for fuel fabrication and for shipment of spent fuel. Fabrication costs are sensitive to the requirements for neutron shielding

to the extent that such requirements influence the complexity of mechanization necessary for the various fabrication handling operations. Uncertainties in the nuclear data involved in the reactions leading to the buildup of ^{236}Pu and ^{238}Pu are the most important ones for improving the accuracy of the neutron source data used for shield design of fabrication plants [34]. Uncertainties in the nuclear data involved in the reactions leading to the buildup of ^{242}Cm and ^{244}Cm are the most important ones for improving the accuracy of neutron source data used for shielding design of spent fuel shipping casks [35]. (The latter is a problem not only for plutonium-fueled fast breeder systems, but also for uranium-fueled thermal reactors that discharge plutonium in fuel elements irradiated to high burnup.)

The principal reactions leading to the formation of ^{236}Pu, ^{238}Pu, ^{242}Cm, and ^{244}Cm are shown in Figure 1. Snyder [36] evaluated the requirements for data accuracy and indicated the status of the data uncertainties for thermal reactor systems. In plutonium-fueled, breeder reactors the buildup of ^{236}Pu and ^{238}Pu is almost entirely due to the sequence starting with the n,2n reaction in ^{238}U. The buildup of ^{242}Cm and ^{244}Cm follows from the irradiation and decay of the heavier plutonium isotopes and is, therefore, sensitive to the isotopic concentration of the fuel source. (Footnotes (a) and (b) of Table I show the considerably higher content of ^{241}Pu and ^{242}Pu in plutonium discharged from a water reactor relative to that discharged from a fast reactor.)

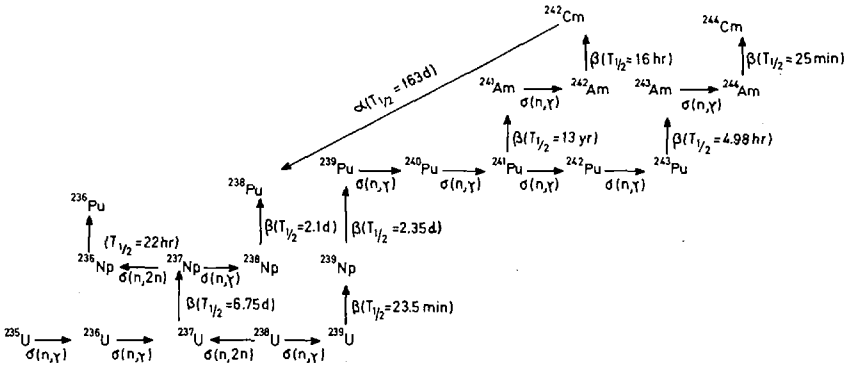

FIG. 1. Nuclear reaction sequences in Pu-U fuel for formation of neutron source isotopes.

The most crucial data uncertainties in the above reaction chains are the n,2n reaction for ^{238}U, and the reactions shown in Figure 1 for ^{237}Np, ^{241}Am, and ^{243}Am. Most of the data that is required for the determination of the neutron source isotopic concentrations are based upon nuclear model studies, integral measurements, and very few differential measurements at low energies.

Therefore, the present data uncertainties are very large and the estimated uncertainty in the neutron source level is about a factor of 5.

4.0 EFFECTS OF SPECIFIC DATA UNCERTAINTIES

4.1 Present Uncertainties and Recommended 5-Year Accuracy Goals - Economic Implications

Table III lists the effects of current data uncertainties in ^{239}Pu and ^{238}U on the predicted breeding ratio and fissile inventory of the 1000 MW(e) reactor of Table I. Similar effects of data uncertainties in the higher

TABLE III. EFFECTS OF ^{238}U AND ^{239}Pu UNCERTAINTIES ON PREDICTED VALUES OF BREEDING RATIO AND FISSILE Pu INVENTORY

Data Uncertainty	Incident Neutron Energy	Uncertainty Range (±%)[a]	Breeding Ratio (±)	Fissile Pu Inventory (±%)
^{238}U $\sigma(n,\gamma)$	1 to 100 keV	10	0.060[b]	2.5[b]
	> 100 keV	10	0.015[b]	0.6[b]
^{238}U $\sigma(n,n')$	0.1 to 1 MeV	15	0.005	0.3
	> 1 MeV	20	0.015	1.0
^{238}U $\sigma(n,f)$	> 1 MeV	6	0.010	0.7
^{238}U $\bar{\nu}$	> 1 MeV	3	0.005	0.5
^{239}Pu $\sigma(n,f)$	0.1 to 20 keV	10	0.003	1.5
	20 to 300 keV	10	0.015	5.5
	> 300 keV	6	0.004	1.5
^{239}Pu $\sigma(n,\gamma)$	0.2 to 20 keV	20	0.020	1.0
	20 to 80 keV	20	0.015	0.8
	> 80 keV	20	0.002	0.1
^{239}Pu $\bar{\nu}$	> 0.1 keV	2	0.040	3.0
^{239}Pu $\overline{E\chi(E)}$	> 0.1 keV	10	0.025	2.0
^{239}Pu $\sigma(n,n')$	> 10 keV	40	0.005	0.3

(a) The uncertainty range listed as a single value for the indicated energy range is intended to represent an effective average for roughly 90% confidence limits, taking into consideration the energy dependence of the reaction rates of interest and of the uncertainty in measured data within each indicated energy range.

(b) Uncertainties in the $\sigma(n,\gamma)$ of ^{238}U, and of other fertile isotopes such as ^{240}Pu, have opposite fuel cost effects on breeding ratio and fissile inventory. For example, a higher ^{238}U $\sigma(n,\gamma)$ increases both the breeding ratio and the fissile inventory. However, the effect on the breeding ratio is the dominant one for both fuel cost and fissile doubling time. For all the other data uncertainties listed in Tables III and IV, the corresponding uncertainties in the breeding ratio and the fissile inventory occur in a consistent direction insofar as their effects on fuel cost and doubling time are concerned.

plutonium isotopes, fission products, sodium, and steel are listed in Table IV. Uncertainty ranges for the 300 MW(e) reactor would be roughly the same as those listed in Tables III and IV for the 1000 MW(e) reactor. Tables III and IV also indicate the estimated magnitude of each of the data uncertainties corresponding to a 90% confidence limit. Table V shows a recommended goal for accuracy of the data in each case, such accuracy to be achieved before 1975 when it is expected that there will be considerable design activity on behalf of actual large breeder plants (~1000 MW(e)) to be constructed for operation sometime in the 1980 decade.

TABLE IV. EFFECTS OF UNCERTAINTIES IN FISSION AND RADIATIVE CAPTURE CROSS SECTIONS OF HIGHER Pu ISOTOPES, FISSION PRODUCTS, SODIUM AND STEEL ON PREDICTED VALUES OF BREEDING RATIO AND FISSILE Pu INVENTORY

Data Uncertainty	Incident Neutron Energy	Uncertainty Range (±%)[a]	Breeding Ratio (±)	Fissile Pu Inventory (±%)
^{240}Pu $\sigma(n,\gamma)$	0.1 to 100 keV	30	0.005[b]	0.3[b]
	> 100 keV	40	0.001[b]	0.1[b]
^{240}Pu $\sigma(n,f)$	1 to 300 keV	30	0.003	0.2
	> 300 keV	15	0.003	0.2
^{241}Pu $\sigma(n,f)$	>0.1 keV	25	0.003	1.0
^{241}Pu $\sigma(n,\gamma)$	>0.1 keV	40	0.002	0.1
Fission Products $\sigma(n,\gamma)$	>0.1 keV	40	0.030	2.0
Sodium $\sigma(n,\gamma)$	0.1 to 10 keV	30	0.003	0.2
	> 10 keV	50	0.001	∿0
Steel $\sigma(n,\gamma)$	<0.1 MeV	25	0.025	1.0
	>0.1 MeV	35	0.010	0.5
Steel $\sigma(n,n')$	>0.8 MeV	15	0.005	0.3

(a) See footnote (a) of Table III.

(b) See footnote (b) of Table III.

Fuel cost uncertainty is much more sensitive to the uncertainties in breeding ratio than to those in fissile Pu inventory. A rough estimate of 0.01 mill/KW(e)h change in fuel cost for each 0.01 change in breeding ratio is appropriate for the fuel cost assumptions listed in footnote (3). A fuel cost change of -.004 mill/KW(e)h for each 1% change in fissile Pu inventory is a similar rough estimate for the same cost assumptions[4]. It is seen that the ^{238}U $\sigma(n,\gamma)$ uncertainty below 100 keV has the largest single effect on breeding ratio uncertainty. The fissile Pu inventory is most affected by the uncertainty in ^{239}Pu $\sigma(n,f)$ between 20 and 300 keV. The uncertainties in ^{239}Pu alpha, $\bar{\nu}$, and average energy of fission spectrum neutrons $E_\chi(E)$, in ^{238}U $\sigma(n,n')$ and $\sigma(n,f)$, in ^{240}Pu $\sigma(n,\gamma)$ and $\sigma(n,f)$, in ^{241}Pu $\sigma(n,f)$, and in $\sigma(n,\gamma)$ of steel and of fission products also have significant effects on the accuracy of predicted physics parameters for a fast breeder reactor.

Table V indicates the present data uncertainty ranges for estimated 90% confidence limits and recommended targets for improvement of data accuracy in the next five years. Fuel cost uncertainties associated with the present and the target data uncertainties are also listed in the table. It is seen

[4]Doubling time for the 1000 MW(e) reactor of Table I changes approximately in accordance with the relationship: δ(years) = 8.5 [.01 δ(fissile inventory) -2.5 δ(breeding ratio)] for small changes in fissile inventory and breeding ratio.

TABLE V. CURRENT DATA UNCERTAINTIES AND RECOMMENDED ACCURACY GOALS FOR 1975

Data Type and Incident Neutron Energy Range	Uncertainty (±%)[a]		Cost Uncertainty (±mill/KW(e)h)[b]	
	Present[c]	1975 Goal	Present	1975 Goal
^{238}U σ(n,γ) 100 eV to 1 MeV	10	2	0.065	0.013
^{238}U σ(n,f) 1 to 10 MeV	6	3	0.013	0.006
^{238}U σ(n,n') 100 keV to 10 MeV	20	5	0.025	0.008
^{239}Pu σ(n,γ) 0.1 to 500 keV	20	3	0.045	0.007
^{239}Pu σ(n,f) 0.1 keV to 10 MeV	10	2	0.034	0.007
^{239}Pu $\bar{\nu}$ >0.1 keV	2	0.5	0.050	0.013
^{239}Pu $\overline{E\chi(E)}$ >0.1 keV	10	2	0.033	0.006
^{240}Pu σ(n,f) >1 keV	20	10	0.008	0.004
^{240}Pu σ(n,γ) 0.1 keV to 1 MeV	30	10	0.004	0.001
^{241}Pu σ(n,f) >0.1 keV	25	10	0.007	0.003
Fiss. Prod. σ(n,γ) >0.1 keV	40	10	0.038	0.010
Fe,Ni,Cr σ(n,γ) >0.1 keV	30	10	0.041	0.010
Combined Data Uncertainties			0.13 [d]	0.03 [d]

(a) Each independently listed data uncertainty is assumed to be correlated over the entire energy range indicated.
(b) For 1000 MW(e) reactor based on cost assumptions stated in footnote (3) of text and estimated 90% confidence limits in data uncertainties.
(c) Corresponds to values listed in Tables III and IV for estimated 90% confidence limits.
(d) Statistical combination assuming separately listed data uncertainties are not correlated. (The assumptions regarding correlation of data uncertainties stated in footnotes (a) and (d) are respectively too pessimistic and too optimistic, and the combination hopefully gives a reasonably correct correlation effect.)

that high precision, 3% or less uncertainty for 90% confidence limits, is required in much of the ^{238}U and ^{239}Pu data to lower the cost uncertainty associated with each type of data to the order of 0.01 mill/KW(e)h. The $\bar{\nu}$ uncertainty for ^{239}Pu should be reduced below 0.5%. On the other hand, uncertainties of the order of 10% (for 90% confidence limits) are acceptable for the data of other fuel isotopes and core structural materials for similar cost uncertainty. The target data accuracy gives a combined fuel cost uncertainty of 0.03 mill/KW(e)h, compared with the present estimated uncertainty of 0.13 mill/KW(e)h due to combined nuclear data uncertainties. It is apparent that to achieve such a target accuracy in the next five years, intensive effort will have to be focused on obtaining high precision measurements of the important ^{238}U and ^{239}Pu data.

4.2 Sources for Estimation of Specific Data Uncertainties

Data uncertainty ranges which were determined for a paper presented at the 1968 Conference on Neutron Cross Section Technology [10] were used as the bases for the present estimated uncertainties. Data measurements made since 1967 and described below have been used to modify those ranges where appropriate. Comprehensive data evaluations have also contributed to reductions in uncertainties.

The ^{239}Pu alpha value below 20 keV ranks as the nuclear quantity which has shown the greatest improvement in accuracy since 1968. The improvement is due to the measurements of Gwin, et al [18], Czirr and Lindsey [19] and recent results from the U.K. [20]. An analysis of single level statistical resonance parameters by Evatt and Hutchins [37] has indicated that a single set of parameters produces good agreement between the computed values and measured data.

Fission cross section measurements for ^{239}Pu have been reported by James and Patrick [27], Shunk, et al [38], Gwin, et al [18], Gilboy and Knoll [39], Ryabov, et al [40], White and Warner [41], and Letho [42]. Most of these measurements have been reported as the ratio $^{239}Pu\ \sigma(n,f)/^{235}U\ \sigma(n,f)$. Davey [26], Hart [28], and Green, et al [43] have used this ratio in attempts to arrive at consistent normalization between ^{239}Pu and ^{235}U fission cross section measurements.

Considerable attention has been given to the measurement of $^{238}U\ \sigma(n,\gamma)$, particularly between 1 and 500 keV. Reported measurements include the data of Moxon [23], and Menlove and Poenitz [24], both lower than the earlier measurements of Macklin, et al [44]. Petrel bomb results at lower energies have been reported by Glass, et al [25]. An in-depth review of $^{238}U\ \sigma(n,\gamma)$ data made by Davey [29] indicates the basic disagreement which exists between "absolute" measurements.

The $^{238}U\ \sigma(n,n')$ uncertainty is based on the recent preliminary results of A.B. Smith [45] and the earlier results by Barnard, et al [46].

Uncertainty ranges for the fission cross section of ^{238}U, ^{240}Pu and ^{241}Pu are nearly the same as given in 1968. Measurements have been reported by Stein, et al [47], White and Warner [41], and Byers, et al [48], but have not been instrumental in reducing the cross section uncertainties.

The stainless steel $\sigma(n,\gamma)$ uncertainty was decreased principally due to high resolution measurements of the total and scattering cross sections by Barnard, et al [49], Cierjacks, et al [50], and Carlson, et al [51].

The uncertainty in the thermal value of $\bar{\nu}$ has decreased but the energy dependence up to 500 keV remains relatively large due to measurements by Meadows [52] and Kuzentsov [53] for ^{235}U. Uncertainties in the fission neutron spectra have been slightly increased due to foil measurements by Grundl [54] and McElroy [55] which indicate a harder spectrum for ^{235}U.

Propagation of errors in this study is based upon the condition that the data errors are only correlated for a single quantity over the energy ranges indicated in Tables III and IV. Also, the effects that resonance parameters, as such, have on the reactor parameters have not been studied, although it is believed that this effect is of less importance.

Finally, the values chosen for the 1975 measurement goals given in Table V may appear to be too optimistic. There are two reasons why these goals may be realizable in the next 5 years and an optimistic attitude can be justified. First, the measurement programs at many facilities are focusing more directly on the needs of the reactor industry, and the scientists involved are applying their expertise in the evaluation of data. Second, basic differences between "absolute" measurements are being identified [29]. This provides the real possibility that a number of measurement differences will be understood and eliminated in the next 5 years. Elimination of these differences in absolute measurements is the main key to achievement of the tight measurement goals listed in Table V.

REFERENCES

1. MOORHEAD, T.P., "The Effects of Errors in Cross Section Data on Calculations for a Large Dilute Fast Reactor", Conference on Physics of Fast and Intermediate Reactors, II, IAEA, Vienna (1962).

2. GREEBLER, P., HUTCHINS, B.A., "User Requirements for Cross Sections in the Energy Range from 100 eV to 100 keV", Conference on Neutron Cross Section Technology, Washington, D.C., March 22-24 (1966).

3. KINCHIN, G.H., "Nuclear Data Requirements for Thermal Reactor Design and Operation", Conference on Nuclear Data for Reactors, Paris, October 17-21 (1966).

4. SMITH, R.D., "Nuclear Data Requirements for Fast Reactor Design and Operation", Conference on Nuclear Data for Reactors, Paris, October 17-21 (1966).

5. FRENCH, R.J., "Use of Neutron Data in Thermal Reactor Power Plant Design", 1967 Winter Meeting of American Nuclear Society, Chicago, November 5-9 (1967).

6. FRENCH, R.J., "Use of Neutron Data in Thermal Reactor Power Plant Design", Conference on Neutron Cross Section Technology, Washington, D.C., March 4-7 (1968).

7. DRAKE, M.K., STEWART, H.B., TAYLOR, R.C., "The Effects of Cross Section Uncertainties in the HTGR", 1967 Winter Meeting of American Nuclear Society, Chicago, November 5-9 (1967).

8. CRAVEN, C.W., Jr., PERRY, A.M., "Sensitivity of Molten-Salt Breeder Reactor Economics to Uncertainties in Basic Nuclear Data", 1967 Winter Meeting of American Nuclear Society, Chicago, November 5-9 (1967).

9. GREEBLER, P., "Sensitivity of Fast Reactor Economics to Uncertainties in Nuclear Data", 1967 Winter Meeting of American Nuclear Society, Chicago, November 5-9 (1967).

10. GREEBLER, P., HUTCHINS, B.A., WOLFE, B., "Significance of Neutron Data to Fast Reactor Power Plant Design", Conference on Neutron Cross Section Technology, Washington, D.C., March 4-7 (1968).

11. KÜSTERS, H., SCHMIDT, J.J., BROEDERS, C.H.M., EISEMANN, E., METZENROTH, M., SCHROETER, K.E., THIEM, D., "Analysis of Fast Critical Assemblies and Large Fast Power Reactors with Group Constant Sets Recently Evaluated at Karlsruhe", KFK 793, Kernforschungszentrum, Karlsruhe, November (1968).

12. BROEDERS, C.H.M., "The Influence of Nuclear Data Uncertainties on Properties of Critical Assemblies", KFK 939, Kernforschungszentrum, Karlsruhe, January (1969).

13. SCHMIDT, J.J., "Current State of Physical Knowledge of the Most Important Reactor Data", KFK 966, Kernforschungszentrum, Karlsruhe, April (1969).

14. BARRE, J.Y., RAVIER, J., "Inaccuracies in the Characteristic Parameters of a Fast Power Reactor Due to the Prevailing Uncertainties in the Basic Neutron Data", Symposium on Fast Reactor Physics, Karlsruhe, October 30-November 3 (1967).

15. GANDINI, A., SALVATORES, M., DAL BANO, I., "Sensitivity Study of Fast Reactors Using Generalized Perturbation Techniques", Symposium on Fast Reactor Physics, Karlsruhe, October 30-November 3 (1967).

16. KALLFELZ, J.M., ZOLOTAR, B.A., SEHGAL, B.R., "Modifications to Fissile Element Cross Sections, and their Influence on Calculated Fast Reactor Parameters", Personal Communication, W.B. Loewenstein to P. Greebler, Argonne National Laboratory, December (1969).

17. PENNY, S.K., "The Thrust of Cross Section Data Requirements for Reactor Shielding Calculations", 1969 Winter Meeting of American Nuclear Society, San Francisco, November 30-December 4 (1969).

18. GWIN, R., WESTON, L.W., deSAUSSURE, G., INGLE, R.W., TODD, J.H., GILLESPIE, F.E., HOCKENBURY, R.W., BLOCK, R.C., "Measurements of the Neutron Fission and Absorption Cross Section of ^{239}Pu Over the Energy Region 0.02 to 30 keV", Oak Ridge National Laboratory, October 7 (1969).

19. CZIRR, J.B., LINDSEY, J.S., "A Measurement of the Capture to Fission Ratios for Pu-239", UCRL-72080, Lawrence Radiation Laboratory, Livermore, California, November (1969).

20. SOWERBY, M.G. and SCHOMBERG, M.G., private communication from M.G. Schomberg, of U.K., to R. Gwin, of ORNL. Values reported on Figure 4 of Reference 18.

21. CAWTHORNE, C., FULTON, E.J., "Voids in Irradiated Stainless Steel", Nature, Vol. 216, p. 575, November 11 (1967).

22. LAURITZEN, T., WOLFF, U.E., WITHOP, A., "Swelling of Anstenitic Stainless Steels", GEAP-13536, General Electric Co. (to be published).

23. MOXON, M.C., "The Measurement of Average Neutron Capture Cross Sections in the Mass Region Above 100", Thesis Presented for Degree of M.Sc. to London University, Unpublished (1968).

24. MENLOVE, H.O. and POENITZ, W.P., "Absolute Radiative Capture Cross Section for Fast Neutrons in ^{238}U", Nuc. Sci. & Engng., 33, 24 (1968).

25. GLASS, N.W., SCHELBERG, A.D., TATRO, L.D., WARREN, J.H., "^{238}U Neutron Capture Results from Bomb Source Neutrons", Conference on Neutron Cross Section Technology, Washington, D.C., March 4-7 (1968).

26. DAVEY, W.G., "Selected Cross Sections for ^{232}Th, ^{233}U, ^{234}U, ^{235}U, ^{236}U, ^{237}Np, ^{238}U, ^{239}Pu, ^{240}Pu, ^{241}Pu and ^{242}Pu", Nuclear Science and Engineering, 32, p. 35-45, April (1968).

27. JAMES, G.D., PATRICK, B.H., "Evaluation of the ^{239}Pu Fission Cross Section in the Energy Range 1 keV to 100 keV", AERE-M2065 (Amended), AERE Harwell, October (1968).

28. HART, W., "Revised Fission Cross Section Evaluations for the Energy Range 1 keV to 15 MeV", AHSB(S)R169, AERE Risley, (1969).

29. DAVEY, W.G., "An Analysis of the Capture Cross Section of ^{238}U Between 1 keV and 15 MeV", Nuc. Sci. & Engng., 39, 337-360, March (1970).

30. PERING, N.C., LEWIS, T.A., "Performance of 140 MeV High Current Short Pulse Linac at ORNL", Proc. of Particle Accelerator Conference, Washington, D.C., March 5-7 (1969).

31. MURPHY, P.M., "The Influence of Plutonium on the Design of Advanced Reactors", Twelfth Annual Meeting of American Nuclear Society, Denver, Colorado, June 20-23 (1966).

32. DIETRICH, R.J., "Uranium Requirements for Nuclear Power", Nuclear News, Vol. 10, No. 9, September (1967).

33. CRAMER, S.N., CAIN, V.R., STRAKER, E.A., "Monte Carlo Graphite Benchmark Calculations Using S_n Adjoint Biasing", 1969 Winter Meeting of the American Nuclear Society, San Francisco, November 30-December 4 (1969).

34. ZIMMERMANN, H., "Dose Rate of Reprocessed Na-1 Breeder Fuel", EURFNR-385, Kernforschungszentrum, Karlsruhe, July (1967).

35. BAILEY, H.S., EVATT, R.N., RUIZ, C.P., GYOREY, G.L., "Neutron Shielding Problems in High Burnup Thermal Reactor Fuel Shipping", 1969 Winter Meeting of American Nuclear Society, San Francisco, November 30-December 4 (1969).

36. SNYDER, T.M., "Future Cross Section Needs of the Nuclear Power Industry", Conference on Neutron Cross Section Technology, Washington, D.C., March 22-24 (1966).

37. EVATT, R.N., HUTCHINS, B.A., "Derivation of ^{239}Pu Resonance Parameters from Correlation of Experimental Data", 1969 Annual Meeting of American Nuclear Society, Seattle, June (1969).

38. SHUNK, E.R., BROWN, W.K., LaBAUVE, R., "Fission Cross Sections from Petrel", LA-3586, Los Alamos Scientific Laboratory, December (1966).

39. GILBOY, W.B. and KNOLL, G., "The Fission Cross Sections of Some Plutonium Isotopes in the Neutron Energy Range 5 to 150 keV", KFK 450, Kernforschungszentrum, Karlsruhe (1966).

40. RYABOV, Y.V., et al, "Measurement of the Radiative Capture and Fission Cross Section Ratios for ^{235}U and ^{239}Pu in Resonance-Neutron Energy Region", Atomnaya Energiya, 24, 4 (1968).

41. WHITE, P.H. and WARNER, G.P., "The Fission Cross Sections of ^{233}U, ^{234}U, ^{236}U, ^{238}U and ^{237}Np, ^{239}Pu, ^{240}Pu, ^{241}Pu, Relative to that of ^{235}U for Neutrons in the Energy Range 1 to 14 MeV", Journal of Nuclear Energy, 21, 671 (1967).

42. LEHTO, W.K., "Fission Cross Section Ratio Measurements of ^{239}Pu and ^{233}U to ^{235}U from 0.24 to 24 keV", Nuclear Science and Engineering, 39, 361-367, March (1970).

43. GREENE, N.M., LUCIUS, J.L., CRAVEN, C.W., Jr., "An Evaluation and Compilation of the Fission and Capture Cross Sections of ^{239}Pu in the Energy Range 25 keV - 15 MeV", ORNL-TM-2797, Oak Ridge National Laboratory, January (1970).

44. MACKLIN, R.L., PASMA, P.J., GIBBONS, J.H., "Resonance Neutron Capture and Transmission in Sulphur, Iron and Lead", Phys. Rev., 136, B695 (1964).

45. SMITH, A.B., Argonne National Laboratory, Personal communication, B.A. Zolotar, of ANL, with B.A. Hutchins, of GE, November (1969).

46. BARNARD, E., FERGUSON, A.T.G., McMURRAY, W.R., van HEERDEN, I.J., "Scattering of Fast Neutrons by ^{238}U", International Conference on Study of Nuclear Structure with Neutrons, Antwert, EANDC-50-S, P/26 (1965).

47. STEIN, W.E., SMITH, R.K., SMITH, H.L., "Relative Fission Cross Sections of ^{236}U, ^{238}U, ^{237}Np, and ^{238}U", Conference on Neutron Cross Section Technology, Washington, D.C., March 4-7 (1968).

48. BYERS, D.H., et al, "Fission Cross Sections from Petrel", LA-3586, Los Alamos Scientific Laboratory (1966).

49. BARNARD, E., DeVILLIERS, J.A.M., ENGELBRECHT, C.A., REITMAN, D., SMITH, A.B., "High Resolution Fast Neutron Cross Section of Iron", PEL 180, Pelindaba, Pretoria, July (1968).

50. CIERJACKS, S., FONTI, P., KOPSCH, D., KROPP, L., NEBE, J., UNSELD, H., "High Resolution Total Neutron Cross Sections Between 0.5 - 30 MeV", KFK 1000, Kernforschungszentrum, Karlsruhe, June (1968).

51. CARLSON, A.D., CERBONE, R.J., WILLOUGHBY, D.F., "Measurement of Neutron Penetration Standards. Volumn III. High Resolution Measurements of the Total Neutron Cross Sections of Nitrogen and Iron", GA-9149 (Vol. 2), Gulf General Atomic, Inc., March 27 (1969).

52. MEADOWS, J.W., WHALEN, J.F., "Energy Dependence of $\bar{\nu}_p$ for Neutron-Induced Fission of ^{235}U Below 1.0 MeV", Journal of Nuclear Energy, 21, p. 157, February (1967).

53. KUZNETSOV, V.F., SMIRENKIN, G.N., "The Average Number of Neutrons in the Fission of ^{233}U and ^{235}U by 0.08 - 1 MeV Neutrons", Atomnaya Energiya, 22, p. 401, May (1967).

54. GRUNDL, J.A., "A Study of Fission Neutron Spectra with High Energy Activation Detectors, Part II: Fission Spectra", Nuclear Science and Engineering, 31, 191-206, February (1968).

55. McELROY, W.N., "Implications of Recent Fission-Averaged Cross Section Measurements", Nuclear Science and Engineering, 36, 109-113, April (1969).

DISCUSSION

J. Y. BARRE: Could you indicate what solution was used for obtaining the variation in critical mass? Depending on which solution is chosen - i. e. variation of enrichment before fabrication of the fuel or variation of shape after fabrication - the consequence as far as critical mass is concerned may be a difference by a factor of about 5 for the 300 MW(e) plant and of an even higher factor for the 1000 MW(e) plant.

B. A. HUTCHINS: The dimensions of fast power reactors are determined by a combination of physics and engineering considerations. Thus, because of reactivity considerations, it is not normal to have the capability of changing the core shape or size after fabrication. In our study the sensitivity of the fissile inventory was determined by varying the enrichment through the use of successive reactor neutronics calculations. I agree that if the vari-

ation had been made on the core radius the sensitivity would have been much higher, but this is not a practical approach for power reactors.

C. G. CAMPBELL: Fast reactors benefit from much shorter fuel dwelling times than thermal reactors. Some errors in prediction can be corrected by fuel enrichment changes in the second fuel charge and therefore do not persist for long in the operational life of the reactors. Has this operational flexibility of fast reactors been taken into account in arriving at the cost penalties of data uncertainties?

B. A. HUTCHINS: It was recognized in our study that certain operational flexibilities would be possible in the second and subsequent cores and that these could be used to overcome detrimental results in the first core. In the case of the 300 MW(e) plant the bulk of the cost penalties came from design defects which cannot be overcome in an economical way after initial start-up. An example of such a defect is an excessive volume fraction in the core for control. As far as the 1000 MW(e) plant is concerned, we are interested in making an evaluation right now of a future fast-reactor economy. Presumably, we will have a good knowledge by that time of the reactor parameters being considered here, and designs will have been optimized from that knowledge. Since we were not looking at the start-up cycles of a specific prototype reactor, we did not have to consider contingencies in the design which could later be modified as the characteristics of the reactor became known.

H. W. KÜSTERS: You mentioned a breeding-ratio uncertainty of 0.1. I think this is rather optimistic because I remember an evaluation made by Dr. Baker of the United Kingdom in which there is a spread in breeding gain from about 0.2 to 0.5. This evaluation was made after the British Nuclear Energy Society (BNES) Conference in London. Could you say something about this?

I would also like to make a comment on your accuracy goals for 1971 and 1975 for the prediction of 1000 MW(e) breeders. Personally, I do not think that any such plants will be operating before the eighties. It is to be hoped that the data uncertainties relating to large reactors will have been reduced by that time.

B. A. HUTCHINS: First of all, our 0.1 uncertainty gives a spread of 0.2, which is close to Dr. Baker's figure. You may remember that I quoted an uncertainty range of 1.1 to 1.3 for the 300 MW(e) plant. Perhaps this should have been more clearly indicated on the slides. To make an evaluative comparison with Dr. Baker's results would require that we know what type of reactor plant he considered, whether his uncertainties were one sigma or more, like our own 90% confidence limits, and what nuclear-data uncertainties he used. I have not made this comparison.

Your comment on the target date for precise measurements is well taken. We were considering 1000 MW(e) plants for the 1980s or beyond and I would not care to speculate on a more specific date. However, we need precise design data well before the plants start operating. We also need them for evaluations of the future reactor economy.

Invited Paper

THE IMPORTANCE OF AND NEEDS FOR NEUTRON NUCLEAR DATA IN ASTROPHYSICS

D.D. CLAYTON
Rice University, Houston, Texas,
United States of America

Abstract

THE IMPORTANCE OF AND NEEDS FOR NEUTRON NUCLEAR DATA IN ASTROPHYSICS.

Neutron nuclear data are of unique importance to astrophysics because many of the naturally occurring nuclei owe their origin to neutron reactions and because, unlike many charged-particle reactions, neutron cross-sections can be measured even at very low neutron energy. An enumeration of important neutron cross-sections within the context of the present state of the theory of nucleosynthesis will be provided. It will also be shown that certain dynamic details of exploding stars may be discuvered by measurements of neutron cross-sections.

The role of neutron reactions in the astrophysical questions of the origins of the nuclei of the chemical elements is especially interesting. The past two years have shown ever more convincingly that reactions among charged particles play the major role in the nucleosynthesis of the elements between and including carbon ($Z = 6$) and nickel ($Z = 28$). The nuclear evidence shows clearly that these elements are overwhelmingly due to stellar explosions in which the primary fuels for the charged-particle fusion reactions in stars burn furiously for times of order seconds at the time the stars explode. Arnett and Clayton [1] have recently reviewed these arguments and the nuclear evidence in their favour. Of immediate interest to us is the fact that reactions liberating and consuming free neutrons during these fusion epochs control many of the fine details of the burning process with the result that important features of the final abundance patterns reflect the rates of many interesting neutron reactions. I shall outline many of those reactions in this paper.

Charged-particle reactions are not effective in the syhthesis of elements heavier than those in the immediate abundance peak centred on iron for a simple reason: the temperature of the nuclear gas would have to be so great for charged particles to overcome the Coulomb barrier that effectively inhibits their interaction that heavy nuclei in such an environment would suffer photodisintegration at a greater rate than the fusion reactions. By statistical-mechanical arguments alone one sees that in such circumstances the nucleons will be distributed among those states in which they are most tightly bound. Because the binding energy per nucleon decreases for nuclei increasingly more massive than iron, high-temperature events have the sense of breaking down heavier nuclei into iron nuclei. What is needed, therefore, for the synthesis of the more massive nuclei is a flux of free neutrons in thermal environs not sufficiently

hot to break down those nuclei. Roughly speaking, this requires temperatures less than about 3×10^9°K. In such circumstances a successive chain of radiative neutron-capture reactions is capable of generating the heavy nuclei from lighter seed nuclei. These neutron-capture chains provide a wealth of astrophysical questions for the neutron physicist. The chains are basically of two types:

(1) In a weak flux operating for long times the capture rate is so slow that nuclei unstable against beta decay have sufficient time to decay to a stable daughter before the next neutron is captured – the so-called s-process.

(2) In an intense neutron flux the captures are more rapid than beta decay rates and very neutron-rich nuclei are formed – the so-called r-process. The general features of these processes are clearly discussed by Clayton [2] in his textbook on nucleosynthesis. I shall outline many of the specific reaction data needs for those processes.

1. CLASSES OF NEUTRON THERMONUCLEAR REACTIONS

A wide variety of reactions involving neutrons assume importance in the astrophysical problem. The identification of these reactions is by no means fixed, but changes as our understanding of the astrophysical environment and its composition changes. Nonetheless, there are certain types of common reactions, each with their own special considerations, for which experimental data are required. I would now like to outline certain features of these common classes, using specific reactions as examples.

1.1. Radiative neutron capture

A variety of techniques have been used for the measurement of radiative neutron capture cross-sections at neutron energies, primarily between 1 and 100 keV, for which these reactions are most important in stars. The best of these techniques has been the prompt detection of the gamma rays following a time-of-flight analysis of the neutron energy. This technique is well reviewed by Allen, Gibbons, and Macklin [3], who also review the s-process, which is the clearest application of radiative capture to astrophysics.

Free neutrons in a star undergo many elastic scatterings before they are captured. Their energy states may therefore be regarded as populated in accord with thermal principles. Since the neutron gas is non-degenerate in those environs where the value of the cross-section plays an important role, the fraction of the free neutrons having velocity v in the interval dv is Maxwellian:

$$\phi(v)\,dv = \frac{4}{\sqrt{\pi}} \left(\frac{v}{v_T}\right)^2 \exp\left[-\left(\frac{v}{v_T}\right)^2\right] \frac{dv}{v_T} \qquad (1)$$

where $v_T = (2kT/M_n)^{\frac{1}{2}}$ is the average thermal velocity at temperature T. Since the interesting range of stellar temperatures is of order 10^8 to

10^9 °K and since kT = 8.6×10^{-8} TkeV, we see that the capture cross-sections are of interest for neutron energies throughout the range $0 < E_n < 1$ MeV, although the greatest interest lies in the smaller interval $1 < E_n < 100$ keV. Since the velocities are statistical the average capture rate is determined by a Maxwellian averaged cross-section:

$$\langle \sigma \rangle \equiv \langle \sigma v \rangle / v_T = \frac{1}{v_T} \int_0^\infty \sigma(v)\, v\, \phi(v)\, dv \qquad (2)$$

What is required, in principle, is the energy-dependent cross-section $\sigma(v)$, which may then be thermally averaged. The average cross-section contains contributions from the (terrestrial) thermal region, from the individual resonance region, and from the higher-energy region of continuous strength. The contributions from the 1/v thermal tail at lowest energies and from isolated narrow resonances is easily shown to be

$$\langle \sigma \rangle = \sigma_{th} \left(\frac{25.3 \times 10^{-6}}{kT} \right)^{\frac{1}{2}} + \frac{2}{\sqrt{\pi}} \sum_r A_c(r) \frac{E_r}{(kT)^2} \exp\left(-\frac{E_r}{kT} \right) \qquad (3)$$

where $\sigma_{th} = \sigma(25.3 \times 10^{-6}$ keV) is the value of the terrestrial thermal cross-section and $A_c(r) = 2\pi^2 \lambda\!\!\!^{-2} g_J (\Gamma_n \Gamma_\gamma / \Gamma)$ is the integrated capture area of the r-th narrow resonance located at energy E_r. To this must be added the higher-energy continuous cross-section.

In the case of heavy nuclei having non-magic neutron numbers it generally happens that the cross-section in the tens of keV region is relatively large, but that individual resonances are not resolved. Such cross-sections are generally characterized by s-and-p-wave strength functions. The thermally averaged cross-sections for those smoothly decreasing cross-sections are virtually equal to value of the cross-section at $E_n = kT$; for example, the value of $\langle \sigma \rangle$ for ^{181}Ta (n, γ) ^{182}Ta for kT = 30 keV is equal to the value of σ for the same reaction measured at E_n = 30 keV with typical not-too-fine resolution [4]. Ratios of cross-sections of two such nuclei tend to be nearly independent of the temperature.

1.2. Neutron-liberating reactions

Since free neutrons are quickly absorbed in a star the free-neutron density would vanish (in ordinary non-degenerate stars) were it not for the operation of reactions liberating new neutrons.

For these reactions the initial channel contains two charged particles. The important cross-sections are those exothermic (or slightly endothermic) neutron-liberating reactions of light nuclei which may be expected to occur in stars at temperatures low enough that photoneutron reactions have not yet become significant. The major reactions having these properties are ^{13}C (α, n) ^{16}O, ^{17}O (α, n)^{20}Ne, ^{18}O (α, n) ^{21}Ne, ^{21}Ne (α, n) ^{24}Mg, ^{22}Ne (α, n) ^{25}Mg, ^{12}C (^{12}C, n) ^{23}Mg, and ^{16}O (^{16}O, n) ^{31}S, and they probably account for virtually all of the sources of neutrons for the s-process. Since the incident particles are changed and the temperature low, these reactions are strongly inhibited by the Coulomb barrier. The particles

responsible for most of the reaction rate are those near the "most effective" stellar energy

$$E_0 = 0.122\,[Z_1^2\,Z_2^2\,A(T/10^9)^2]^{1/3} \qquad (4)$$

which is a compromise between the Coulomb penetration factor and the fact that the Maxwellian distribution is steeply falling in its high energy tail [5]. For example, near $T = 3 \times 10^8$ °K most of the reaction rate of the ^{13}C (α, n) ^{16}O reaction occurs at energies between 400 and 500 keV although the value of kT is only about 26 keV. For experiments of this type the major problem is that of measuring the cross-section to the lowest bombarding energy for which it is measurable and extrapolating, if necessary, down to the range of effective stellar energies. Davids [6] presents a good discussion of his study of the ^{13}C (α, n) ^{16}O reaction in which he measured the energy dependence of the cross-section down to about 475 keV and presented a reliable exptrapolation to lower energies. As far as neutron technique is concerned one must simply understand well the efficiency with which the liberated neutrons are being detected. Reeves [7] has presented an interesting evaluation of these stellar neutron sources. Some of these reactions, notably ^{18}O (α, n) ^{21}Ne and ^{12}C $(^{12}C, n)$ ^{23}Mg are sufficiently endothermic that one is interested in their cross-sections near threshold.

1.3. (n, p) and (p, n) competition with beta decay

Beta decays are of special importance in nuclear astrophysics because they allow the changing of protons into neutrons and vice versa with a resultant net effect on the composition of the gas. All beta decays are potentially in competition with either (p, n) or (n, p) reactions which do not alter the relative numbers of protons and neutrons in the gas. In most stars burning in hydrostatic equilibrium the beta-decay life-times are generally short compared with the life-time against nuclear interaction with a nucleon in the gas, but in the explosive burning stages the reverse tends to be true. Since our understanding of the circumstances of nuclear burning is still somewhat uncertain, a quantitative estimate of the competition is desirable, and more measurements are needed. An interesting feature of these competitions is that, because the final nucleus is stable in the beta decay, the corresponding nucleon-exchange reaction must normally be measured by performing the inverse reaction if one wishes to deal with stable target nuclei. Consider the example of the reaction ^{18}F (n, p) ^{18}O which is in competition with ^{18}F (β^+, ν) ^{18}O in explosive hydrogen burning where ^{18}F is created by the reaction ^{14}N (α, γ) ^{18}F. The rate of ^{18}F (β^+, ν) ^{18}O is known, but the rate of ^{18}F (n, p) ^{18}O is unknown and essentially unmeasureable since substantial targets of ^{18}F cannot be easily assembled. The quantum principle of reciprocity allows one to measure the cross-section by measuring that of the inverse reaction ^{18}O (p, n) ^{18}F. Since the thermal neutron energies in the stellar interior are adequate to cause the exothermic ^{18}F (n, p) ^{18}O reaction, the reverse reaction is of interest at proton energies of tens to hundreds of keV above the threshold. Other reactions of interest for the same reasons are ^{13}N (n, p) ^{13}C, ^{21}Na (n, p) ^{21}Ne, ^{22}Na (n, p) ^{22}Ne, ^{23}Mg (n, p) ^{23}Na, ^{25}Al (n, p) ^{25}Mg, and

^{26}Al (n, p) ^{26}Mg. It is not difficult to show from the reciprocity condition that the cross-section for the reaction 1 + 2 → 3 + 4 + Q averaged over the thermal velocities of 1 and 2 is related to the cross-section for the reaction 3 + 4 → 1 + 2 - Q averaged over the thermal velocities of 3 and 4 by the relation

$$\langle \sigma v \rangle_{34 \to 12} = \langle \sigma v \rangle_{12 \to 34} \left(\frac{M_1 M_2}{M_3 M_4} \right)^{3/2} \frac{(2J_1+1)\,(2J_2+1)}{(2J_3+1)\,(2J_4+1)} \exp\left(-\frac{Q}{kT} \right) \qquad (5)$$

Thus, measurement of $\langle \sigma v \rangle_{12 \to 34}$ yields immediately the thermal average of the desired inverse reaction[1]. An analogous experiment involving a neutron beam is the ^{24}Mg (n, p) ^{24}Na reaction, whose cross-section is needed to know the competition of the ^{24}Na (p, n) ^{24}Mg reaction with the ^{24}Na (β^-, $\bar{\nu}$) ^{24}Mg decay. This reaction limits the neutron enrichment of the gas during carbon burning at constant temperature [8]. The neutron energies of interest in this (n, p) case are the sum of the threshold energy plus the most effective energy E_0 for the interaction of a proton with sodium at temperature T, as given in Eq. (4).

By exactly similar reasoning one can calculate many photoneutron reaction rates of interest averaged over the Planck spectrum at temperature T if the inverse (n, γ) rate has been determined for the thermal distribution of neutron velocities. One has for γ + 3 → n + 2

$$\langle \lambda_\gamma \rangle = \langle \sigma v \rangle_{n2 \to 3\gamma} \left(\frac{M_n kT}{2\pi\hbar^2} \right)^{3/2} \frac{2G_2}{G_3} \exp\left(-\frac{Q_{n2 \to 3\gamma}}{kT} \right) \qquad (6)$$

where M_n is the reduced neutron mass with 2, and G is the nuclear partition function $G = \sum_i (2J_i + 1) \exp(-E_i/kT)$. Photoneutron cross-sections find their primary application in the question of the formation of the most proton-rich isotopes of the heavy elements by a combination of (γ, n) and (p, γ) reactions, the so-called p-process [9, 10].

2. THE s-PROCESS

If the neutron flux is sufficiently weak that beta decays occur (when energetically possible) before a second neutron is captured, the capture flow to increasing atomic weight follows a unique path in the Z, A plane along the valley of beta stability. The beta decays can then be eliminated from the differential equations for the abundances, which become simply

$$\frac{dN_A(t)}{dt} = \langle \sigma v \rangle_{A-1}\, n_n N_{A-1} - \langle \sigma v \rangle_A\, n_n N_A \qquad (7)$$

where $\langle \sigma v \rangle_A$ is the thermal average of σ_A (n, γ)v and N_A is that isobar of atomic weight A lying on the unique s-process path. The properties of these equations have been studied in several papers [9, 11, 13, 2, 3] to which the reader is referred. The distribution σN as a function of A is a

[1] The equation as written is correct for inverse reactions involving the ground states only [23].

smooth curve showing steep decreases where the cross-sections are smallest. The most dramatic tests of the correctness of the idea, however, are found in a small range of atomic weight, where one obtains the approximation

$$\sigma_A N_A \approx \sigma_{A+1} N_{A+1} \tag{8}$$

since the time derivative in Eq. (7) is adjusted by the process to be a small difference between two large and nearly equal terms. The greatest difficulty in checking this equation against nature, other than the difficulty of actually measuring the (n,γ) cross-sections, lies in the fact that, in general, the abundance of a stable heavy nucleus of atomic weight A is only partially due to the s-process. In addition, the decay of neutron-rich progenitors (the r-process) contributes also to the abundance. To test the correlation implied by Eq. (8) requires that we compare nearby s-process nuclei whose entire abundance is due to the s-process, which will be possible only if there exist more neutron-rich stable isobars of the same atomic weight. These isobars will shield the s-process nucleus from production by the decay of neutron-rich nuclei in the manner shown in Fig. 1, where ^{148}Nd and ^{150}Nd shield ^{148}Sm and ^{150}Sm from production by neutron-rich matter. Since the s-process path flows through Sm, the s-process idea suggests that σN for the other isotopes on the path be greater than that value. The experimental results listed in Table I confirm dramatically the correctness of that interpretation. The studies of Macklin and Gibbons have confirmed the s-process idea in several other elements as well [14].

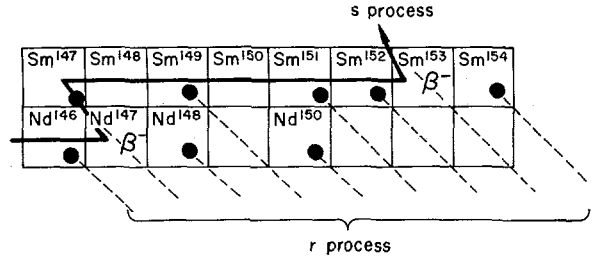

FIG. 1. The s-process path through the isotopes of samarium is shown as a heavy solid line. The r-process yield from the decay of neutron-rich nuclei contributes to the abundances of those nuclei containing the solid dots. Two of the isotopes of Sm lying on the s-path, ^{148}Sm and ^{150}Sm, are shielded from the r-process by ^{148}Nd and ^{150}Nd.

The large-scale structure of the curve σN_s versus A also follows the general expectations of the s-process theory by decreasing monotonically from iron to lead with the major decreases occurring at the magic neutron numbers N = 50 and N = 82. Allen et al. [3] have provided the latest analysis of this general s-process correlation, and they find that although the present correlation is very good some of its features remain somewhat puzzling. Only continued improvement in the measurements of element abundances by geochemists and of the (n,γ) cross-sections by neutron physicists can clarify further the correctness of our ideas. For the time being, the s-process seems to work rather well.

TABLE I. σN FOR SAMARIUM ISOTOPES [14]

Nucleus	Process	σ (30 keV (mb))	N (abundance)	σN
Sm 144	p	150 ± 70	0.031	5 ± 2
147	r + s	1170 ± 190	0.150	175 ± 28
148	s-only	257 ± 50	0.112	28.9 ± 5.6
149	r + s	1620 ± 280	0.138	224 ± 39
150	s-only	370 ± 72	0.074	27.4 ± 5.3
152	r + s	410 ± 70	0.267	110 ± 19
154	r	325 ± 60	0.227	74 ± 14

Probably the most profound and fascinating of the s-process applications is to the question of cosmochronology and the age of the elements. The simplest and most important task of neutron physics is the measurement of the (n, γ) cross-sections of two isotopes of osmium, ^{186}Os and ^{187}Os. This measurement will determine what fraction of ^{187}Os is due to the decay of long-lived ^{187}Re [15], which will in turn provide a measure of the age of the ^{187}Re. This measurement is extremely important for cosmology because a ^{187}Re age as great as the Hubble time is not compatible with some cosmological models of a big-bang evolving universe, and the ^{187}Re decay is our best tool for measuring the time of the beginning of nucleosynthesis. Like most problems in nature, this one is made more spicy by the possibility that ^{187}Re decays faster in stars than on earth, in which case the rhenium deposited on the lunar surface by the solar wind will be depleted in ^{187}Re [16].

Another interesting set of neutron cross-sections for cosmochronology is to be found in the element lead [15]. The abundances of $^{206,207,108}Pb$ received contributions from the decay of thorium and uranium in addition to the usual s-and-r-process contributions. To estimate the amount of cosmoradiogenic decay requires careful measurements of the neutron-capture cross-sections of those lead nuclei. Clayton [17, 18] carefully detailed the issues and requirements for a satisfactory understanding of the Pb abundances, and although the cross-sections did not at that time seem to nicely fit the requirements, current measurements seem more favourable [3].

There is another exciting problem which can only be settled by measurements of (n, γ) cross-sections; namely, what fraction of matter in the interstellar medium must be recycled through weak neutron fluxes in stars (low-exposure s-processes). The best way of answering this important question for astrophysics is by measuring the neutron-capture cross-sections of the isotopes of titanium, chromium, iron, nickel, and copper, especially $^{48,49,50}Ti$, $^{52,53,54}Cr$, $^{56,57,58}Fe$, and $^{58,60,61,62,64}Ni$. The situation is as follows. Calculations of the explosive ejection from stars of burning zones of carbon, oxygen, and silicon can now be seen to quantitatively reproduce the abundances of almost every nucleus between A = 20 and A = 62. This evidence has just been reviewed by Arnett and Clayton [1]. The fascinating thing is that the neutron-rich isotopes ^{50}Ti,

^{54}Cr, and ^{58}Fe are not produced in such explosions, and seem, therefore, to have been produced from the more abundant isotopes of those elements by weak s-processes. It is easy enough to hypothesize such an explanation but it is much harder to make it work, especially since it depends on nuclear neutron cross-sections that can be measured. Peters, Fowler, and Clayton [19] have shown that a solution will be difficult unless the key cross-sections have the proper relative values, and even then, very definite features of weak s-process remixing will have to be satisfied. It should perhaps also provide the neutron physicist some satisfaction to realize that measurements he can make can confirm, limit, or perhaps destroy an entire picture of the origin of the elements. Just a few years ago, for example, it was widely held that ^{58}Fe was due to a thermodynamic equilibrium which established the abundances of the iron isotopes. If the cross-sections do not fit the s-process theory, we may again be forced back to that picture, which would seriously demolish the entire point of view reviewed by Arnett and Clayton [1].

Another very interesting cross-section for the s-process is that of ^{142}Nd. Clayton and Perrone [20] have recently shown that σN for ^{142}Nd may lie above the expected s-process curve because of the alpha decay of thermally excited states of ^{144}Nd during the s-process. It will be astrophysically very interesting to ascertain whether this σN product is in fact anomalously large. If it is, a thermometer for the s-process results;

TABLE II. IMPORTANT (n, γ) CROSS-SECTIONS FOR s-PROCESS

Element	Isotopes	Element	Isotopes
Ti	48, 49, 50	Sn	116, 117, 118, 119, 120
Cr	52, 53, 54	Te	122, 123, 124
Fe	56, 57, 58	Xe	128, 130
Co	59	Ba	134, 135, 136, 137, 138
Ni	58, 60, 61, 62, 64	La	139
Cu	63, 65	Ce	140
Zn	64, 66, 67, 68	Pr	141
Ga	69, 71	Nd	142
Ge	70	Sm	148, 150
Se	76	Gd	154
Kr	80, 82, 83, 84, 86	Dy	160
Sr	86, 87, 88	Hf	176
Y	89	Os	186, 187
Zr	90, 91, 92, 94	Pt	192
Mo	96	Hg	198
Ru	99, 100	Pb	204, 206, 207, 208
Pd	104	Bi	209
Cd	110		

if it is not, the temperature must, for a given neutron flux, be smaller than a prescribed limiting value.

In Table II we have listed those nuclei whose (n, γ) cross-sections seem to me to be the most important for the s-process theory. Some of these cross-sections have been measured, and the reader is referred to the review of Allen et al. [3] and their bibliography for the status of the measurements. In presenting the most interesting nuclei for the s-process in Table II we do not imply that the other nuclei on the s-path have useless cross-sections. Indeed, all nuclei on the path have cross-sections of interest because more complete measurements allow the establishment of a systematics for neutron cross-sections, as in Figs 8 and 9 of Allen et al. [3] and because knowledge of the capture cross-section of a nucleus due to both r-and s-processes allows the required r-process yield to be determined by subtraction [12].

3. CARBON BURNING

The thermonuclear combustion of carbon, both at constant temperature [8] and explosively [1, 21], involves a large number of neutron reactions with subtle but observable consequences. The applications are of three types:

(a) Which cross-sections control the free neutron density?
(b) Which cross-sections control the total neutron-to-proton ratio of the gas?
(c) Which cross-sections control, at least partially, the final abundances of key nuclei?

The primary neutron liberating reactions are the ^{12}C (^{12}C, n) ^{23}Mg branch of the $^{12}C + ^{12}C$ reaction and the (α, n) reactions on ^{13}C, ^{17}O, and ^{21}Ne. Those last three nuclei are formed when protons, liberated initially by ^{12}C (^{12}C, p) ^{23}Na are captured by ^{12}C, ^{16}O, and ^{20}Ne and followed by a (β^+, ν) emission. For a given rate of neutron liberation, the free neutron density is determined by the rate of absorption of the neutrons. This rate is determined by the (n, γ) cross-sections of all the major nuclear constituents that coexist in the gas during the burning; e.g. ^{12}C, ^{16}O, ^{20}Ne, ^{23}Na, $^{24,25,26}Mg$, ^{27}Al, etc. We require the (n, γ) cross-sections for temperatures of 1 to 2×10^9 °K, which involves neutron energies from tens of keV to roughly 1 MeV – a large experimental task indeed.

The final abundances in carbon burning depend upon the number of excess neutrons per nucleon in the gas, a number of the order 10^{-3}. This neutron excess is controlled by beta decays and by charged-particle reactions which, if competitive, quench the beta decays. A single major example should suffice. In their study of carbon burning at constant temperature Arnett and Truran [8] found that the formation of several positron emitters, notably ^{13}N, ^{18}F, $^{21,22}Na$, ^{23}Mg, and $^{25,26}Al$, results in a gradual increase in the neutron excess during carbon burning. This increase is terminated by an equal rate of conversion of neutrons to protons associated with the formation of the negaton emitter ^{24}Na. The limiting value of the neutron excess is set by the rate of the ^{24}Na (β^-, $\bar{\nu}$) ^{24}Mg reaction, which is in turn controlled by two neutron reactions: the reaction

^{23}Na(n, γ) ^{24}Na is primarily responsible for the formation of ^{24}Na, and the reaction ^{24}Na (p, n) ^{24}Mg competes, if the temperature is high enough, with the positron decay. Because the 15 hour half-life of ^{24}Na is too short for preparation of ^{24}Na targets, the latter reaction would require study of the inverse ^{24}Mg (n, p) ^{24}Na reaction at neutron energies near 6 MeV, a difficult task indeed with outgoing proton energies of only 1 to 2 MeV. But the issues here are quite important, and this particular example illustrates again the way in which difficult neutron physics in the laboratory can yield answers capable of great influence on our conception of the origin of the elements.

Finally, we note that there are many neutron reactions that control or strongly influence the final abundances of certain nuclei in carbon burning. Some are quite obviously important; for example the ^{24}Mg (n, γ) ^{25}Mg (n, γ) ^{26}Mg (n, γ) ^{27}Mg reactions contribute to the determination of the final isotopic composition of magnesium. Other effects are more subtle; for example the origins of relatively rare ^{36}S, which Arnett and Clayton [1] report as not being produced by the primary reaction network in any thermonuclear explosions. From the study of Howard, Woosley, Arnett, and Clayton [22] they attribute ^{36}S to reactions during explosive carbon burning on seed amounts of ^{36}A present in its natural fractional abundance, 2×10^{-4} parts by mass, at the time the carbon ignites. The ^{36}S appears to result from the sequence ^{36}A (n, p) ^{36}Cl (n, p) ^{36}S, with considerably smaller contributions from ^{35}S (n, γ) ^{36}S and ^{39}A (n, α) ^{36}S. In the early stages of the burning the rate of ^{36}A (n, p) ^{36}Cl (n, p) ^{36}S is such that the entire flow goes to ^{36}S. As the free proton density increases, the reaction ^{36}A (n, p) ^{36}Cl is reversed and some of the ^{36}A is restored by ^{36}Cl (p, n) ^{36}A. As the rate of formation of ^{36}S decreases due to this flow reversal, the rate of ^{36}S (p, γ) ^{37}Cl causes a decrease in the abundance of ^{36}S by almost an order of magnitude before freezeout. Several rare neutron-rich isotopes, namely ^{36}S, ^{40}A, ^{40}K, ^{46,48}Ca, ^{50}Ti, ^{50}V, and ^{64}Ni, seem to owe their origins to similar neutron induced reactions on traces of seed nuclei [22, 1].

One of the most interesting aspects of the creation of these rare nuclei from reactions on seed nuclei is that measurements of the neutron cross-sections can reveal thermal properties of the explosive carbon burning and expansion. Considering for example the synthesis of ^{36}S once again we see that the ^{36}S abundance cannot be numerically accounted for unless the temperature and time scale of the expansion are consistent with the measured cross-sections of the reactions responsible for ^{36}S. I think we shall see dynamic features of the explosion revealed by the demand that it produce these nuclei in the proper amounts.

Table III contains a listing of the large number of neutron reactions whose cross-sections at temperatures from 1 to 2×10^9 °K are needed for these quantitative analyses of carbon burning. Many of the reactions would require study of the inverse reactions. The relevant energies for such studies are stellar thermal for neutron induced reactions and the most effective stellar energy E_0 for charged-particle reactions. In a study of the reverse reaction the incident particle energies of interest should be selected accordingly. Many of these reactions would be quite difficult to perform, a situation common in astrophysics. I can do no better than quote from the study [23] of the United States National Academy

TABLE III. NEUTRON REACTIONS IMPORTANT DURING CARBON BURNING

^{12}C (^{12}C, n) ^{23}Mg	^{28}Si (n, γ) ^{29}Si	^{37}Cl (n, p) ^{35}S
^{12}C (n, γ) ^{13}C	^{29}Si (n, γ) ^{30}Si	^{36}A (n, γ) ^{37}A
^{13}C (n, γ) ^{14}C	^{29}Si (α, n) ^{32}S	^{36}A (n, α) ^{33}S
^{13}C (α, n) ^{16}O	^{30}Si (n, γ) ^{31}Si	^{36}A (n, p) ^{36}Cl
^{13}N (n, p) ^{13}C	^{32}S (n, γ) ^{33}S	^{37}A (n, α) ^{34}S
^{14}N (n, γ) ^{15}N	^{33}S (n, α) ^{30}Si	^{37}A (n, p) ^{37}Cl
^{16}O (n, γ) ^{17}O	^{33}S (n, p) ^{33}P	^{37}A (n, γ) ^{38}A
^{17}O (n, γ) ^{18}O	^{33}S (n, γ) ^{34}S	^{38}A (n, γ) ^{39}A
^{17}O (α, n) ^{20}Ne	^{34}S (n, γ) ^{35}S	^{39}A (n, γ) ^{40}A
^{18}O (n, γ) ^{19}O	^{35}Cl (n, p) ^{35}S	^{39}A (n, α) ^{36}S
^{18}O (γ, n) ^{21}Ne	^{35}Cl (n, γ) ^{36}Cl	^{40}A (n, γ) ^{41}A
^{18}F (n, p) ^{18}O	^{36}Cl (n, p) ^{36}S	^{39}K (n, p) ^{39}A
^{20}Ne (n, γ) ^{21}Ne	^{36}Cl (n, γ) ^{37}Cl	^{39}K (n, γ) ^{40}K
^{21}Ne (n, γ) ^{22}Ne		^{40}K (n, p) ^{40}A
^{22}Ne (n, γ) ^{23}Ne		^{40}K (n, γ) ^{41}K
^{22}Ne (α, n) ^{25}Mg		^{41}K (n, γ) ^{42}K
^{21}Na (n, p) ^{21}Ne		^{42}K (n, γ) ^{43}K
^{22}Na (n, p) ^{22}Ne		^{40}Ca (n, γ) ^{41}Ca
^{23}Na (n, p) ^{24}Na		^{40}Ca (n, α) ^{37}S
^{24}Na (p, n) ^{24}Mg		^{40}Ca (n, p) ^{40}K
^{23}Mg (n, p) ^{23}Na		^{41}Ca (n, γ) ^{42}Ca
^{24}Mg (n, γ) ^{25}Mg		^{41}Ca (n, α) ^{38}A
^{25}Mg (n, γ) ^{26}Mg		^{41}Ca (n, p) ^{41}K
^{25}Mg (α, n) ^{28}Si		^{42}Ca (n, γ) ^{43}Ca
^{26}Mg (n, γ) ^{27}Mg		^{43}Ca (n, γ) ^{44}Ca
^{26}Mg (α, n) ^{29}Si		^{44}Ca (n, γ) ^{45}Ca
^{25}Al (n, p) ^{25}Mg		^{45}Ca (n, γ) ^{46}Ca
^{26}Al (n, p) ^{26}Mg		^{46}Ca (n, γ) ^{47}Ca
^{27}Al (n, γ) ^{28}Al		^{48}Ca (n, γ) ^{49}Ca

of Sciences, which is recommended to the reader interested in experiments of this type:

> A potential investigator in laboratory nuclear astrophysics should confront squarely the nature of the problem he is to encounter. The desired cross-sections are among the smallest measured in the low-energy nuclear laboratory. Long integration times and careful attention to background counts are common necessities. From a purely nuclear point of view, moreover, the reactions studied are often of comparatively little interest. The intellectual stimulation is more often to be found in wresting from nature a hard-won number that she herself has presumably used and in evaluating its astrophysical consequences. An investigator not sharing this interest will be little amused by his task.

4. THE r-PROCESS

If the neutron density is sufficiently great ($n_n > 10^{18}$) that neutron-capture life-times are shorter than beta decay life-times, multiple capture will occur rapidly until it is stopped by photoejection of neutrons. The

photoneutron reaction becomes increasingly more important for increasingly neutron-rich isotopes because of the gradual (except at neutron magic shell closures) decrease of the neutron-separation energy. The abundances produced are proportional to the time the flow must wait when further captures are completely inhibited until beta decay occurs. As a result, the r-process abundances show no correlation with neutron-capture cross-sections, but rather with the beta-decay life-times of extremely neutron-rich nuclei at the waiting point [9, 12, 2]. The key need from neutron physics is a compelling set of nuclear systematics that will allow contruction of a good semi-empirical mass formula yielding the neutron separation energies of very neutron-rich nuclei. Leading efforts along these lines are due to Seeger [24, 12, 25, 26] and to Cameron and Elkin [27]. The reader is referred to those papers for this technical problem. For the neutron physicist the most useful experimental information will probably come from a better understanding of fission and the masses of the neutron-rich fragments and from the formation and stability of very heavy nuclei through multiple neutron capture in the intense flux of thermonuclear devices. The reader is referred to the review by Bell [28] of nucleosynthesis in bombs for this last point.

I have attempted to outline the large amount of neutron nuclear data needed by the nuclear astrophysicist. I find it both gratifying and challenging that the origins of our material being can be probed by the countless interactions of that complex and elusive thing, the neutron. I should like to thank Professor W.D. Arnett for his help in the preparation of many of the ideas expressed in this paper. This research was supported by the Air Force Office of Scientific Research, United States Air Force, under grant AFOSR 68-1363.

REFERENCES

[1] ARNETT, W.D., CLAYTON, D.D., Nature, to be published in summer 1970.
[2] CLAYTON, D.D., Principles of Stellar Evolution and Nucleosynthesis, Chap 7, McGraw-Hill Book Company, New York (1968).
[3] ALLEN, B.J., GIBBONS, J.H., MACKLIN, R.L., "Nucleosynthesis and neutron-capture cross-sections", to be published in Advances in Nuclear Physics.
[4] MACKLIN, R.L., GIBBONS, J.H., Rev. mod. Phys. 37 (1965) 166.
[5] See Chapter 4 of Ref. [2] for a clear introductory discussion of thermonuclear reaction rates between charged particles.
[6] DAVIDS, C.N., Astrophys. J. 151 (1966) 775.
[7] REEVES, H., Astrophys. J. 146 (1966) 447.
[8] ARNETT, W.D., TRURAN, J.W., Astrophys. J. 157 (1969) 339.
[9] BURBIDGE, E.M., BURBIDGE, G.R., FOWLER, W.A., HOYLE, F., Rev. mod. Phys. 29 (1957) 547.
[10] ITO, K., Progr. theor. Phys. 26 (1961) 990.
[11] CLAYTON, D.D., FOWLER, W.A., HULL, T.E., ZIMMERMAN, B.A., Ann. Phys. 12 (1961) 331.
[12] SEEGER, P.A., FOWLER, W.A., CLAYTON, D.D., Astrophys. J. Suppl. 97 (1965) 121.
[13] CLAYTON, D.D. "Distribution of neutron-source strengths for the s-process" in Nucleosynthesis (ARNETT, W.D., HANSEN, C.J., TRURAN, J.W., CAMERON, A.G.W., Eds) Gordon and Breach, New York (1968) 225.
[14] MACKLIN, R.L., GIBBONS, J.H., Astrophys. J. 149 (1967) 577.
[15] CLAYTON, D.D., Astrophys. J. 139 (1964) 637.
[16] CLAYTON, D.D., Nature 224 (1969) 56.
[17] CLAYTON, D.D., "Nucleosynthesis of the isotopes of lead" in Origin and Distribution of the Elements (Ahrens, L.H., Ed.), Pergamon Press, New York (1968) 63.
[18] CLAYTON, D.D., RASSBACH, M., Astrophys. J. 148 (1967) 69.

[19] PETERS, J., FOWLER, W.A., CLAYTON, D.D., in preparation for Astrophys. J.
[20] CLAYTON, D.D., PERRONE, F., Astrophys. J. in preparation.
[21] ARNETT, W.D., Astrophys. J. 157 (1970) 1369.
[22] HOWARD, W.M., WOOSLEY, S.E., ARNETT, W.D., CLAYTON, D.D., Astrophys. J., in preparation.
[23] New Uses for Low-Energy Accelerators (prepared by an Ad Hoc Panel of the National Academy of Sciences, FOWLER, W.A., chairman) National Academy of Sciences, Washington, D.C. (1968).
[24] SEEGER, P.A., Nucl. Phys. 25 (1961) 1.
[25] SEEGER, P.A., Arkiv f. Phys. 36 Nr. 57 (1967) 495.
[26] SEEGER, P.A., "A model based mass law and a table of binding energies", Los Alamos Scientific Laboratory Report LA-3751 (1967).
[27] CAMERON, A.G.W., ELKIN, R.M., Can. J. Phys. 43 (1965) 1288.
[28] BELL, G.I., Rev. mod. Phys. 39 (1967) 59.

DISCUSSION

A. PRINCE: Since there are several ranges of uncertainty in the binding energies of capture cross-sections for many of these isotopes, what type of accuracy do you attribute to your predictions?

D. D. CLAYTON: We always attempt to use measured nuclear data in the calculations. Naturally, when the nuclear data do not exist, we try to estimate the answer and thus we use cross-sections inferred from nuclear systematics. The binding energies are much better known, except for the case of the neutron-rich matter synthesized by the r-process. I believe that the systematics are good enough for us to infer that the general picture is very nearly correct, but many of the interesting details and conclusions for astrophysics depend on the numerical value of specific cross-sections and in such cases we try to get measurements of the cross-section.

F. RUSTICHELLI: My question concerns a particular neutron quantity, the electrical neutron charge. There is a certain line of speculation which explains the expansion of the universe by assuming an electrical neutron charge Q_n different from zero, the value of which is found to be of the same order of magnitude as the present experimental limit $Q_n \leqq \sim 10^{-18} Q_e$, where Q_e is the electron charge.

Could you make any comments on this subject and, in particular, on the usefulness, from the astrophysics point of view, of continuing the efforts to increase the precision of neutron-charge measurements?

D. D. CLAYTON: History shows that each new surprise in physics has implications for our understanding of cosmology; however, I do not see what the immediate relevance of a small neutron charge would be. Certainly, the theory of thermonuclear reactions would be unaffected. I also doubt that macroscopic bodies would develop a new charge, because they are formed when matter is in a highly conducting state. Thus, a charge of 10^{-18}e for the neutron would imply that every 10^{18} neutrons are accompanied by one electron to maintain the electric neutrality of bulk matter. At nuclear densities such as those found in a neutron star, nuclear matter consists primarily of neutrons plus an electron density having a Fermi energy just high enough to inhibit the neutron decay. In the usual theory the proton density will then equal the electron density. If the neutron has a small charge this latter equality will be weakly violated with no results of immediate importance, as far as I can see. And lastly, there are many reasons which lead me to think that the expansion of the universe is not connected with the fact that it may possess a net charge per unit mass.

ЯДЕРНЫЕ ДАННЫЕ ДЛЯ ТЕРМОЯДЕРНЫХ РЕАКТОРОВ

Ю. Ф. ЧЕРНИЛИН, Г. Б. ЯНЬКОВ
Институт атомной энергии им. И. В. Курчатова,
Москва,
Союз Советских Социалистических Республик

Abstract — Аннотация

NUCLEAR DATA FOR THERMONUCLEAR REACTORS.

On the basis of a consideration of the principles governing a thermonuclear reactor, the problem of nuclear data needed for its construction is discussed. An analysis of the nuclear data published up to 1969 inclusively is given for the three main materials to be used in a thermonuclear reactor: ^{6}Li, ^{7}Li, Nb. The requirements to be met by nuclear data for these reactors are considered in the concluding section of the paper.

ЯДЕРНЫЕ ДАННЫЕ ДЛЯ ТЕРМОЯДЕРНЫХ РЕАКТОРОВ.

На основе рассмотрения принципиальной схемы термоядерного реактора обсуждается вопрос о ядерных данных, необходимых для его создания. Приводится анализ ядерных данных, опубликованных до 1969 года включительно, для трех основных материалов, которые предполагается использовать в термоядерном реакторе: ^{6}Li, ^{7}Li, Nb. Потребности в ядерных данных для этих реакторов рассматриваются в заключительной части доклада.

I. ВВЕДЕНИЕ

Научно-исследовательские программы всех стран по осуществлению контролируемого термоядерного синтеза [1,2] направлены, в основном, на получение устойчивой плазмы и, в конечном итоге, на практическое получение термоядерной энергии.

Для современного мира, с его быстрым ростом народонаселения и быстрым ростом индустриализации, проблема использования управляемой реакции синтеза для производства энергии стала рассматриваться не просто как проблема возможного метода получения энергии, а как один из основных путей дальнейшего прогресса энергетики в целом. Данная конференция не является тем местом, где следует обсуждать проблему энергетических потребностей и путей их удовлетворения. Однако можно отметить, что существует очень много серьезных аргументов, говорящих в пользу возможного применения термоядерной энергии. Среди этих аргументов – такие, как экономические преимущества, практическая неограниченность запасов топлива и, кроме того, относительно малая величина радиоактивных отходов (в 10^{6} раз меньшая, чем для атомных электростанций), что в настоящее время является одним из самых главных критериев применимости того или иного метода производства энергии.

Несмотря на то что до настоящего времени в исследованиях, проводимых в области физики плазмы, окончательный успех еще не достигнут, т. е. не получена плазма необходимых параметров (плотность, время удержания, температура), позволяющая "поджечь" управляемую термоядерную реакцию, прогресс в плазменных исследованиях, достигнутый за последние годы, существенно повысил интерес к инженерно-технологическим и экономическим аспектам термоядерной энергетики. Это обстоятельство

поставило на повестку дня вопрос о рассмотрении инженерных характеристик возможных моделей термоядерных реакторов.

Первая международная конференция, посвященная инженерным аспектам термоядерной энергетики (Калем, Великобритания, сентябрь 1969 г.), фактически провела анализ основных проблем создания термоядерной энергетики, исходя из современного положения в исследованиях по физике плазмы и в смежных областях. Из трудов этой конференции можно сделать вывод (и это подчеркивалось на самой конференции ее участниками), что помимо задач, связанных непосредственно с решением главной проблемы – создание устойчивой плазмы необходимых параметров, имеется целый ряд важнейших проблем, непосредственно не связанных с главной проблемой, без решения которых, однако, невозможно создать термоядерную энергетику. Среди этого перечня "вспомогательных" проблем проблема ядерных данных является одной из наиболее общих и важных. Так же как при создании реакторов деления, знание ядерных микроконстант позволило рассчитать реактор и на основе расчета создать саму установку, так и в случае термоядерного реактора этот процесс неизбежен. Одной из задач данного доклада является желание привлечь внимание широкого круга экспериментаторов к измерению ядерных данных, необходимых для создания термоядерного реактора.

Для конкретного и наглядного описания характера нейтронно-ядерных взаимодействий, происходящих в термоядерном реакторе, рассмотрим их на основе возможной схемы такой установки.

В данной работе считается, что главная физическая проблема – получение устойчивой плазмы – может быть решена, и этот вопрос не обсуждается.

II. СХЕМА ТЕРМОЯДЕРНОГО РЕАКТОРА

В таблице 1 приведены четыре типа реакций синтеза, которые могут быть в принципе использованы для целей термоядерной энергетики [3].

В настоящее время еще трудно сказать, какая из указанных в таблице 1 реакций окажется основной в термоядерной станции будущего. Исходя из необходимого уровня энергии плазмы и величины ядерных сечений заряженных частиц, наиболее легко осуществимой реакцией является: $D + T \rightarrow {}^4He + n$. Около 80% всей энергии этой реакции выделяется в виде кинетической энергии нейтронов, которая должна быть реализована путем их замедления и поглощения. Полная энергия, высвобождаемая в одном акте синтеза, значительно увеличивается при поглощении нейтрона, за счет его энергии связи. Если принять, что медленные нейтроны в основном поглощаются литием-6, тогда полная эффективная теплота становится равной:

$$Q'_{дт} = Q_{дт} + 4{,}8 \text{ Мэв} = 22{,}4 \text{ Мэв}.$$

Существует достаточно большое число возможных схем термоядерных реакторов, основанных на использовании реакции DT [4-6]. Поскольку принципиальный характер нейтронно-ядерных взаимодействий не зависит от конструктивных особенностей реактора, то для данного рассмотрения эти различия не играют существенной роли. Не касаясь вопросов обоснования целесообразности той или иной схемы термоядерного реактора, остановимся на одной из возможных.

ТАБЛИЦА 1. ТИПЫ РЕАКЦИЙ СИНТЕЗА

№ пп.	Тип реакции	Энергия в Мэв		
		заряженные частицы	нейтроны	радиация
1	$D + T \longrightarrow {}^4He + n$	3,37 (19%)	14,1 (80%)	0,13 (1%)
2	$D + D \xrightarrow{50\%} {}^3He + n$; $D + D \xrightarrow{50\%} T + p$	1,2 (33%)	1,2 (33%)	1,2 (33%)
3	$D + {}^3He \longrightarrow {}^4He + p$	14,4 (79%)	0	3,9 (21%)
4	$D + {}^6Li \xrightarrow{\sim 50\%} {}^7Be + n$; $\xrightarrow{\sim 30\%} Li + p$; $\xrightarrow{20\%} {}^4He + {}^4He$	-9,2 (-147%)	3 (47%)	13,4 (200%)

ПРИМЕЧАНИЯ: 1. Распределение энергии реакции синтеза (Мэв) дано приближенно.
2. В скобках указаны доли в % от общей величины энергии реакции.

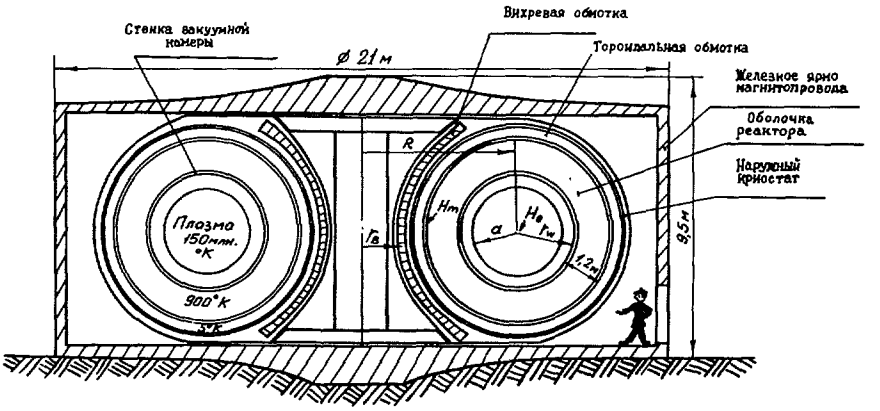

Рис. 1. Реактор-токамак с мощностью 2 млн. квт (эл).

На рис. 1 показана схема реактора, основанная на модели тороидальной замкнутой ловушки типа Токамак [7,8]. Размеры и расположение составляющих оболочки реактора взяты из работы [7] и носят ориентировочный характер. Предполагается, что реактор сжигает равнокомпонентную смесь дейтерия и трития, и почти вся высвободившаяся энергия, определяемая "термоядерными" нейтронами, преобразуется в тепловую энергию в оболочке, окружающей вакуумную камеру плазмы. Основные процессы взаимодействия нейтронов с веществом сосредоточены в этой оболочке, называемой зоной воспроизводства. Будем считать, что эта зона воспроизводства простирается от стенки вакуумной камеры до зоны расположения сверхпроводящих магнитных катушек, удерживающих плазму.

Исходя из того, что практически все нейтронно-ядерные взаимодействия происходят внутри зоны, будем считать, что наши интересы ограничены только этой областью.

Зона воспроизводства, которую часто называют оболочкой термоядерного реактора, предназначена для выполнения следующих функций:

а) преобразования кинетической энергии "термоядерных" нейтронов в тепловую энергию и отвода этой энергии с помощью теплоносителей в силовую установку;

б) регенерации трития для поддержания термоядерной реакции, по крайней мере, с той же скоростью, с какой выгорает тритий. Эта регенерация может быть осуществлена с помощью реакций:

$$^{7}\mathrm{Li}(n, n', ^{4}\mathrm{He})\mathrm{T}$$
$$^{6}\mathrm{Li}(n, ^{4}\mathrm{He})\mathrm{T}$$

в) так как на каждый "сгоревший" атом трития вылетает только один нейтрон, потребуется размножение нейтронов, которое может быть осуществлено за счет реакций типа (n, 2n);

г) и, наконец, оболочка должна обеспечить защиту сверхпроводящих катушек от нейтронного и γ-облучения.

Важнейшими техническими характеристиками термоядерного реактора являются его полная тепловая мощность P_T и размеры. Исходя из условий самоподдержания реакции синтеза (критерий Лоусона)[9], из условия устойчивости плазмы в замкнутых системах [10], а также из допустимых прочностных характеристик материалов и критического значения магнитных полей, создаваемых сверхпроводящими катушками [11], минимальная тепловая мощность термоядерного реактора Токамак оценивается в несколько гигаватт [7]. При таких уровнях мощности поток термоядерных нейтронов на стенке вакуумной камеры составит примерно 10^{15} н/см^2·сек [12].

III. МАТЕРИАЛЫ ДЛЯ ТЕРМОЯДЕРНОГО РЕАКТОРА

Как и в случае реакторов деления, выбор материалов для создания оболочки термоядерного реактора определяется не только технологическими характеристиками, такими, как механическая прочность, теплопроводность, коррозионная и радиационная стойкость и т. д., но также их ядерно-физическими характеристиками и, в частности, величинами различных нейтронно-ядерных сечений. Поскольку создание термоядерного реактора находится только в начальной стадии, следует иметь в виду, что по мере углубления и расширения наших знаний требования к материалам будут меняться, т. е. материалы, которые по современным представлениям являются наиболее подходящими, завтра могут быть отодвинуты на второй план.

Кратко рассмотрим условия, в которых должны работать материалы в термоядерном реакторе, и требования, которым они должны удовлетворять.

1. Стенка вакуумной камеры

Приблизительно четвертая часть кинетической энергии "термоядерных" нейтронов и вся энергия тормозного и циклотронного излучений из плазмы поглощаются в стенке. По расчетам [13] температура стенки

вакуумной камеры составит около 1000°С. Так как стенка находится в области очень высоких потоков нейтронов достаточно широкого интервала энергий, то используемый материал должен иметь малое сечение захвата. Кроме того, желательно, чтобы материал стенки допускал размножение нейтронов по реакции (n, 2n). Таким требованиям, по-видимому, могут удовлетворять ниобий [14] или молибден [15]. Пока что довольно трудно отдать предпочтение какому-либо из этих материалов.

2. Воспроизводство трития

Выше отмечалось, что воспроизводство одной из составляющих топлива термоядерного реактора – трития – может происходить за счет реакций с литием.

Реакция $^{7}Li(n,n'^{4}He)T$ протекает только на быстрых нейтронах (порог реакции 2,8 Мэв [16]), и к тому же образование ядра трития не сопровождается исчезновением нейтрона, который и дальше может участвовать в процессах, поэтому эффективное использование этой реакции очень важно. Поскольку жидкометаллический литий (температура плавления ~ 179°С) может также применяться в качестве теплоносителя, то его использование для охлаждения стенки вакуумной камеры, где спектр нейтронов наиболее "жесткий", является очень эффективным.

Максимальное сечение реакции $^{6}Li(n,^{4}He)T$ имеет место при тепловой энергии нейтронов (σ = 946 барн), поэтому область воспроизводства трития за счет использования этой реакции должна располагаться после области замедления нейтронов.

3. Теплоноситель

Эффективность охлаждения стенки вакуумной камеры, а также отвод тепла от замедлителя имеют очень важное значение. В качестве материала теплоносителя, как отмечалось, может рассматриваться в первую очередь расплавленный литий или его соли, например $2LiF - BeF_2$ [17]. Главная трудность в применении жидкометаллического теплоносителя состоит в наличии высоких потерь при прокачке его поперек магнитных силовых линий. В работе [15] рассматривались также такие материалы, как расплавленный свинец, органические жидкости, вода и ряд других материалов. Однако их применение гораздо менее эффективно (а иногда невозможно) в сравнении с использованием жидкометаллического лития или его солей.

4. Размножители нейтронов

Как показали расчеты [18], необходимая величина воспроизводства трития может быть получена и без применения дополнительных размножителей нейтронов, а только за счет (n,2n) – реакций на конструкционных материалах (например, Nb) и на ^{7}Li за счет реакций (n, n', T). Однако расчеты сделаны с рядом допущений и не отражают реальной конструкции термоядерного реактора, и поэтому в окончательном варианте реактора может оказаться, что потребуются дополнительные размножители нейтронов. Наиболее эффективным размножителем нейтронов, помимо делящихся материалов, является Be, но высокая стоимость и недостаточная радиационная стойкость ограничивают его применение в термоядерном ре-

акторе. Размножение нейтронов может быть осуществлено также за счет реакций (n, 2n) на тяжелых элементах, таких, например, как Pb и Bi. Окончательные выводы по этому вопросу еще предстоит сделать.

5. Замедлитель нейтронов

Так как в замедлителе поглощается половина всей энергии нейтронов [15], разумный и обоснованный выбор материалов очень важен. Из физических, конструктивных и экономических соображений важно, чтобы толщина зоны воспроизводства, а следовательно, области замедления, была минимальной. Поэтому очень заманчивыми являются материалы с высокой замедляющей способностью, т. е. с высоким содержанием водорода или дейтерия, такие, например, как дейтерид лития (LiD) или гидрид циркония. Однако, ввиду того что температура замедлителя достаточно высока, а также по целому ряду технологических причин, применение таких материалов очень ограничено. Наиболее вероятным материалом замедлителя является графит.

6. Защита катушек

Выбор материалов для защиты сверхпроводящих магнитных катушек термоядерного реактора определяется главным образом спектрами нейтронов и γ-лучей в оболочке и ограниченностью толщины защитного слоя. Эти требования существенно ограничивают диапазон материалов, которые могут быть использованы для этой цели. Предполагается [15], что в защитном слое будут использованы такие материалы, как свинец, вода, бор.

IV. ЯДЕРНЫЕ ДАННЫЕ ДЛЯ ТЕРМОЯДЕРНЫХ РЕАКТОРОВ

1. Назначение ядерных данных

Из вышеприведенного краткого перечисления можно видеть, что уже сейчас спектр материалов, которые предполагается использовать при создании термоядерного реактора, достаточно велик: ^{6}Li, ^{7}Li, Be, B, C, O, F, Nb, Mo, Pb, Bi и др. Ясно, что выбор материалов не может быть сделан без достаточного знания нейтронно-ядерных характеристик применяемых материалов. Помимо задачи выбора материалов для термоядерного реактора, знание ядерных данных необходимо для решения целого ряда других задач, среди которых наиболее важными являются:

1. Выполнение всех нейтронно-физических расчетов и расчетов ядерного нагрева зоны воспроизводства, куда включаются воспроизводство трития, производство энергии и все другие связанные с этим задачи.

2. Обеспечение радиационной стойкости материалов, если учесть высокие потоки нейтронов, вылетающих из плазмы (10^{15} н/см^2·сек). При начальной энергии нейтронов $E_{нач.} = 14{,}1$ Мэв на величину и характер радиационных нарушений будут существенно влиять не только эффекты упругого рассеяния (как это имеет место в реакторах деления), но и неупругие взаимодействия. Поэтому знание таких сечений, как (n,p), (n,α), (n,2n) и др. [19], очень важно при оценках радиационной стойкости.

3. Расчет радиационной защиты сверхпроводящих катушек термоядерного реактора, для чего необходимо знание сечений взаимодействия нейтронов. Для случая защиты термоядерного реактора расчет осложняется тем фактом, что большая часть γ-лучей, генерируемых в оболочке, явля-

ется результатом неупругих столкновений быстрых нейтронов, для которых, как известно, очень мало экспериментальных данных.

В настоящее время вопрос о создании проектов термоядерных реакторов находится в начальной стадии, т.е. в той стадии, когда делаются некоторые предварительные физические, теплотехнические, инженерные и другие расчеты, на основе которых можно делать предположения в отношении осуществимости проектов и их экономической конкурентоспособности. Поэтому для выполнения подобных расчетов вопрос о точности ядерных данных еще не стоит очень остро. Однако, как известно, каждый этап разработки требует дополнительных уточнений уже ранее измерявшихся констант или информации по константам, ранее не измерявшимся.

2. Обзор ядерных данных

Для удобства рассмотрения всей задачи разделим область энергии "термоядерных" нейтронов на две: одна область – от тепловых значений до энергий порядка ~ 5 Мэв, другая – от ~ 5 до 14 Мэв.

Можно считать, что первая область является традиционной для реакторов деления, и количество накопленных ядерных данных позволяет достаточно удовлетворительно выполнить необходимые расчеты термоядерных реакторов, связанных с этой областью энергии нейтронов.

Вторая область (5-14 Мэв) характеризуется гораздо меньшим количеством экспериментальной информации, особенно в интервале энергий 8-13 Мэв. Это положение легко объяснимо. Эффекты взаимодействия нейтронов этой области энергий не играют существенной роли для реакторов деления. В большинстве случаев этими данными пренебрегают. Отсюда и потребность в ядерных данных этой области энергий была очень ограничена. Возникновение проблемы создания термоядерных реакторов заставляет по-новому взглянуть на получение ядерных данных этого интервала энергий.

Как отмечалось, перечень материалов, предполагающихся к использованию для термоядерного реактора, уже достаточно широк. В рамках одного доклада практически не представляется возможным провести детальный анализ всех имеющихся ядерных данных для всех упомянутых выше материалов. Поэтому в качестве примера ограничимся детальным рассмотрением сечений взаимодействия трех наиболее важных элементов: лития-6, лития-7 и ниобия.

а) Полные сечения для изотопов лития

Измерения полных сечений по пропусканию образца являются наиболее простыми нейтронными измерениями. Однако получение значений полных сечений с точностью 1% и с хорошим энергетическим разрешением около 0,5% и выше требует соблюдения ряда условий. Использование мощных источников нейтронов в сочетании с методикой времени пролета [20] дает, по-видимому, наиболее точные в настоящее время значения полных сечений.

На рис. 2 и 3 приведены полные сечения для ^{6}Li и ^{7}Li, данные взяты из работ [27-31,42]. Авторами работы [28] выполнена большая серия измерений полных сечений при 240 различных значениях энергий нейтронов от 3 до 15 Мэв со статистической точностью от 0,6 до 2% и разрешением

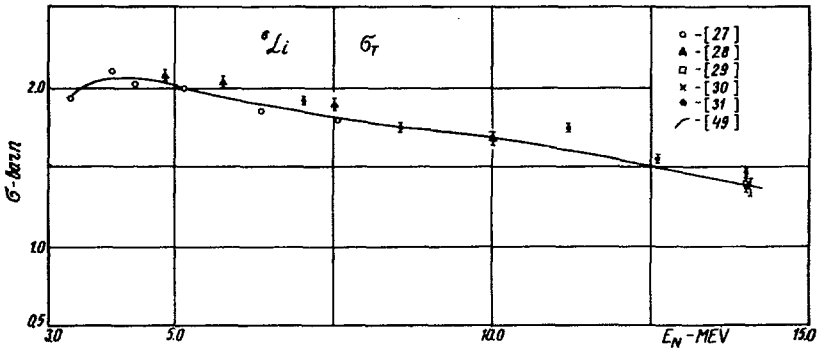

Рис. 2. Полные сечения для ^{6}Li.

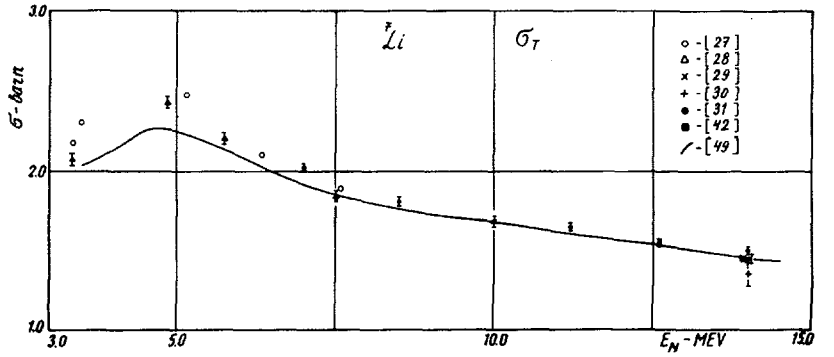

Рис. 3. Полные сечения для ^{7}Li.

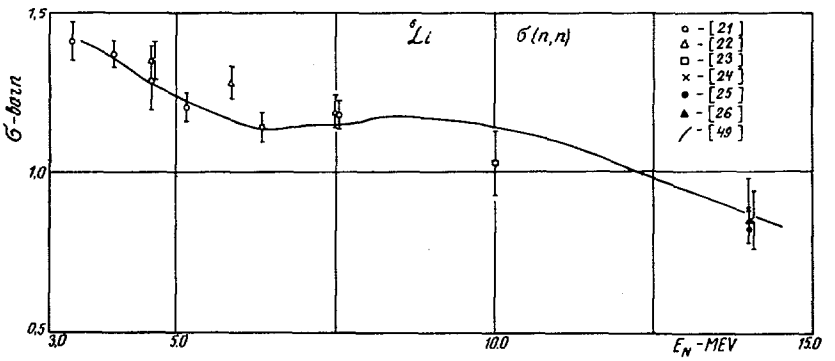

Рис. 4. Сечение упругого рассеяния нейтронов для ^{6}Li.

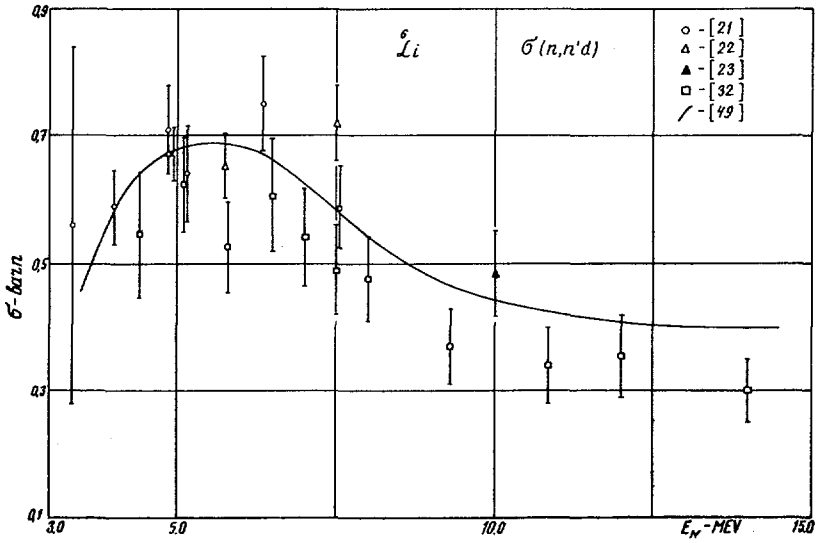

Рис. 5. Сечение реакции $^6Li(n,n'\alpha)^4He$.

по энергии от 2,5 до 11,5% в указанном интервале. Некоторые из этих величин, обозначенные зачерненными треугольниками, приведены на рис. 2 и 3. Сплошные кривые проведены по оцененным данным [49].

б) Парциальные сечения для лития-6

Процесс упругого рассеяния для изотопов лития составляет большую часть полного сечения. На рис. 4 представлено сечение упругого рассеяния нейтронов для ^6Li. Приведенные данные взяты из работ [21-26]. Сплошная линия соответствует оцененным данным [49]. Полные сечения рассеяния получены интегрированием измеренных дифференциальных сечений рассеяния. Точность отдельных значений сечения колеблется в пределах от 3 до 10%. Хотя в обсуждаемой энергетической области экспериментальных данных мало, по данным работы [22] полное сечение рассеяния для этого изотопа удовлетворительно описывается прямой линией.

Неупругое рассеяние нейтронов на изотопах лития характеризуется как дискретными группами нейтронов, соответствующими узким возбужденным состоянием ядра-мишени, так и непрерывным спектром, получающимся по ряду причин, например при распаде на три частицы. Даже в случае, когда конечные продукты реакций одни и те же, форма этого спектра зависит от способа протекания реакции. Рассматривая литий как один из основных элементов в термоядерном реакторе, важно знать, какие реакции и в какой степени ответственны за наблюдаемый спектр рассеянных нейтронов и как вклады различных реакций меняются в зависимости от энергии падающих нейтронов. В настоящее время в этом вопросе полной ясности нет.

На рис. 5 приведено сечение реакции $^6Li(n,n',\alpha)^4He$, данные взяты из работ [21,22,23,32]. Сплошная кривая на этом графике соответствует оцененным данным [49]. Хотя точность отдельных значений составляет

около 10%, разброс точек заметно больше. Наблюдается систематическое расхождение экспериментальных данных, полученных при измерениях нейтронных спектров [21,22,23], и данных, полученных путем регистрации заряженных частиц в фотоэмульсии, содержащей ^{6}Li [32]. Для понимания и устранения ошибок в значениях сечения реакции ^{6}Li(n,n',d)^{4}He, которая определяет второй по величине процесс взаимодействия нейтронов с ^{6}Li, требуются дополнительные измерения во всей рассматриваемой области энергий.

Реакция (n, 2n) на ^{6}Li, имеющая энергетический порог при 6,2 Мэв, изучалась только при двух значениях энергий нейтронов: при 10,2 Мэв величина сечения $\sigma = 33 \pm 15$ мбарн [38] и при 14 Мэв величина сечения $\sigma = 70 \pm 6$ мбарн [38]; 50 ± 10 мбарн [37] и $78{,}1 \pm 4{,}1$ мбарн [39].

С точки зрения воспроизводства одной из компонент топлива термоядерного реактора – трития очень важную роль играют реакции типа (n, T). На рис. 6 приведены данные реакции ^{6}Li(n, T)^{4}He, взятые из работ [27, 33-37,48]. Сплошная кривая соответствует данным работы [49]. Как видно из представленного графика, результаты различных авторов хорошо согласуются между собой. Однако в интервале энергий от 8 до 12 Мэв экспериментальные данные отсутствуют вообще.

Реакция ^{6}Li(n,p)^{6}He, имеющая порог при 3,1 Мэв, достаточно хорошо изучена в интервале энергий от пороговой до 9 Мэв, а также при энергиях 14 Мэв [36,40,41,50]; сечение ее сравнительно невелико.

В силу того что возбужденные уровни ^{6}Li нестабильны по отношению к распаду на частицы, γ-излучение при неупругом рассеянии нейтронов на ^{6}Li почти отсутствует. Источником его является только распад с уровней, запрещенных к развалу на частицы, например по изотопическому спину. γ-излучение с такого уровня (3,56 Мэв) изучалось [50] только в области энергий 4,1-7 Мэв.

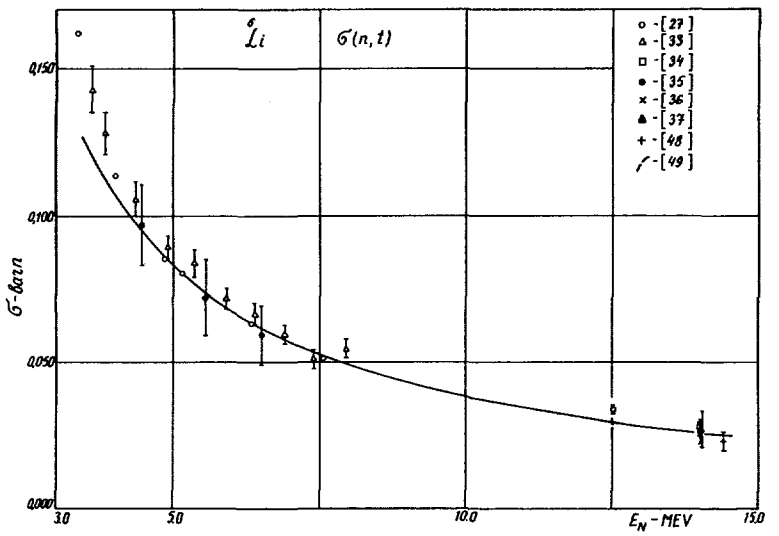

Рис. 6. Данные реакции ^{6}Li(n,T)^{4}He.

в) Парциальные сечения для лития-7

Сумма сечений упругого рассеяния и неупругого рассеяния на уровень 0,478 Мэв для ^{7}Li приведена на рис. 7, данные взяты из работ [21-26]. Сплошная линия соответствует данным работы [49]. Полные сечения рассеяния получены интегрированием измеренных дифференциальных сечений. Как видно из данных рис. 7, в интервале энергий от 3 до 14 Мэв имеется всего 9 значений энергий нейтронов, где проводились измерения, а в интервале 8-13 Мэв всего одна экспериментальная точка. При таком количестве экспериментальных данных трудно описать детальный ход сечения рассеяния в зависимости от энергии нейтронов, особенно имея в виду широкий, четко наблюдаемый максимум в сечениях в области 4,3 Мэв.

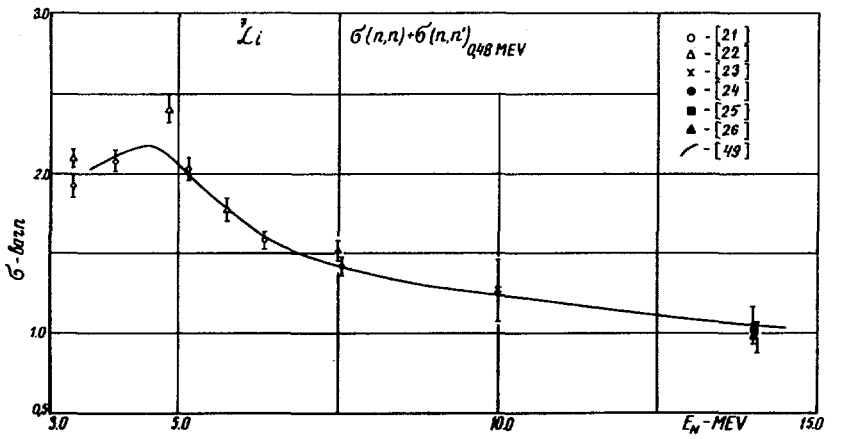

Рис. 7. Сумма сечений упругого и неупругого рассеяний на уровень 0,478 Мэв для ^{7}Li.

Основным процессом неупругого рассеяния нейтронов на ^{7}Li является реакция с образованием трития – главный источник воспроизводства трития на быстрых нейтронах. На рис. 8 приводится зависимость сечения реакции ^{7}Li(n,n',T)^{4}He от энергии нейтронов в интервале 3,5-15 Мэв [21,22,23,32,44,45,47]. Сплошная линия соответствует данным работы [49]. Учитывая важность данной реакции для термоядерного реактора, разброс отдельных значений сечения является слишком большим, а в интервале энергии примерно 10,7-13,5 Мэв, как и для большинства процессов, экспериментальные точки вообще отсутствуют. Кроме того, нет полной ясности о вкладах различных путей протекания данной реакции в нейтронный спектр [51], а также о доле прямых процессов по сравнению с компаунд-ядром. Все это затрудняет интерпретацию экспериментальных данных и получение надежных энергетических и угловых характеристик указанной реакции.

Первое возбужденное состояние ^{7}Li(0,478 Мэв) распадается с испусканием γ-излучения. Видимо, этот распад является практически единственным источником γ-излучения, возникающим при взаимодействии нейтронов с ядром ^{7}Li, но его доля сравнительно велика. На рис. 9 приведено сечение неупругого рассеяния нейтронов ^{7}Li(n,n',γ)^{7}Li на уровень

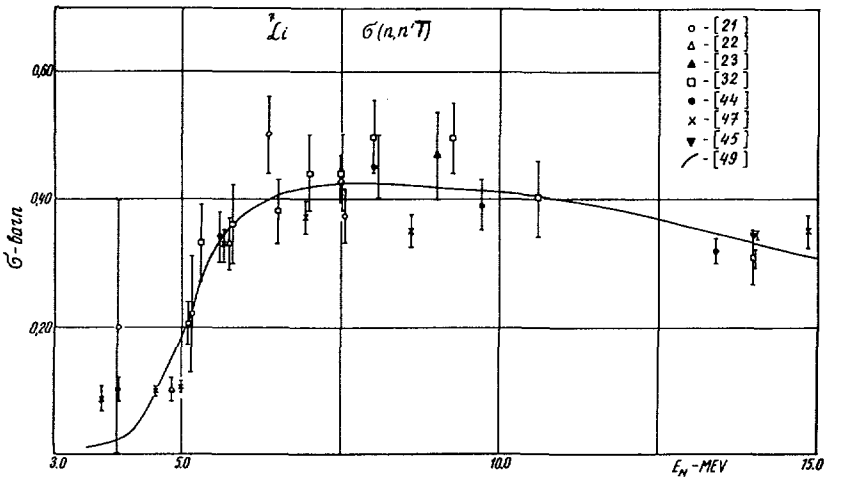

Рис. 8. Зависимость сечения реакции $^{7}Li(n,n',T)^{4}He$ от энергии нейтронов.

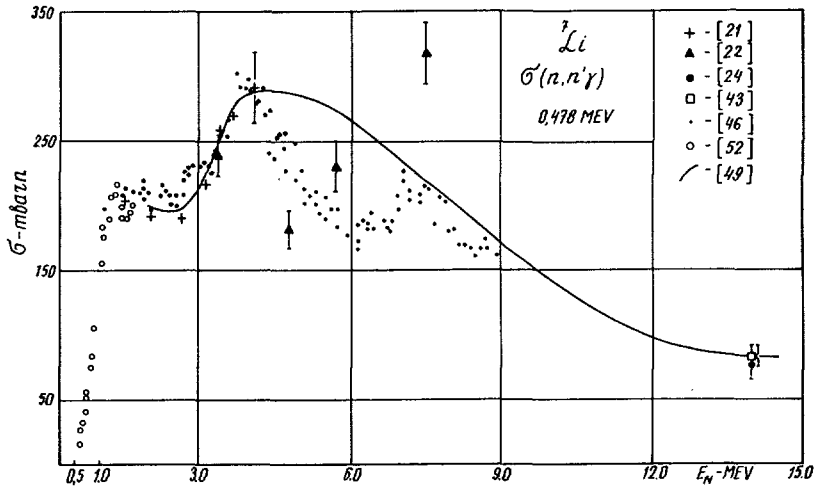

Рис. 9. Сечение неупругого рассеяния нейтронов $^{7}Li(n,n'\gamma)^{7}Li$ на уровень 0,478 Мэв, измеренное в основном по γ-излучению.

0,478 Мэв, измеренное в основном по γ-излучению. Данные взяты из работ [21,22,24,43,46,52]. Сплошная кривая проведена по оцененным данным работы [49]. Обращает на себя внимание расхождение экспериментальных данных в работах [22] и [46], особенно при энергии нейтронов 7,5 Мэв.

Сечение процесса (n, 2n) на ^{7}Li измерялось при двух значениях энергии нейтронов: при 10,2 Мэв $\sigma = 27 \pm 15$ мбарн [38] и при 14 Мэв $\sigma = 56 \pm 5$ мбарн [38] и 49,7 ± 3,2 мбарн [39]. В то же время, по данным работы [49], сечение этой реакции составляет 10 мбарн и 22 мбарн, для указанных энергий соответственно.

Другие реакции на ^{7}Li, как например, (n, 3n) и (n,d), имеют незначительные сечения [39,40,41] и здесь не рассматриваются.

г) Полное сечение для ниобия

На рис. 10 представлено полное сечение для ниобия, данные взяты из работ [29,53,54]. Сплошная кривая проведена согласно данным [55]. Экспериментальные данные, полученные как раньше, так и в последнее время [54,56], хорошо согласуются между собой. Кроме того, детальный анализ экспериментальных данных и сравнение их с теоретическими значениями, выполненное в работе [28], показали также хорошее согласие. В частности, для Nb экспериментальные и теоретические значения [57] согласуются в пределах 3%.

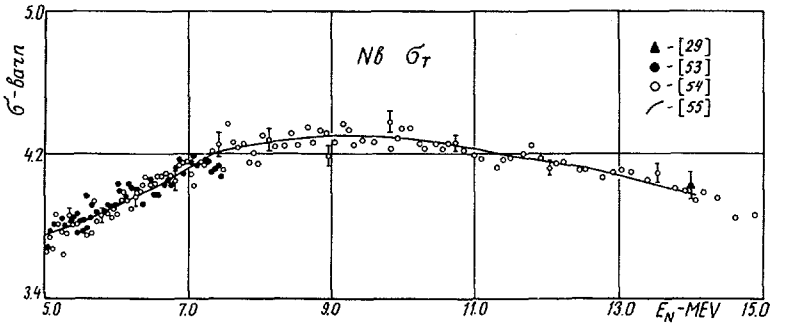

Рис. 10. Полное сечение для ниобия.

д) Парциальные сечения для ниобия

Экспериментальных данных по парциальным сечениям для ниобия гораздо меньше, чем для изотопов лития. На рис. 11 приведены значения сечения упругого рассеяния нейтронов для ниобия, данные взяты из работ [58,59,60,61]. Сплошная кривая проведена по данным работы [55]. Значения сечений при энергии нейтронов 5 Мэв и 14 Мэв получены нами путем интегрирования дифференциальных сечений рассеяния, приведенных в работах [59,61].

На рис. 12 показаны значения эффективного сечения неупругих взаимодействий, данные взяты из работ [58,60,61,62]. Сплошная и пунктирная линии проведены согласно [55]. Пунктирная линия соответствует рекомендованным значениям сечения неупругого рассеяния. В интервале энергий 4-6 Мэв сечение неупругого рассеяния практически совпадает с сечением неупругого взаимодействия, так как сечение радиационного захвата нейтронов убывает с ростом энергии и здесь уже мало (1,5-3 мбарна), а сечение процесса (n,p) хотя и растет, но еще невелико. Непрерывный спектр неупруго-рассеянных нейтронов является в основном испарительным [60,62,63], хотя уже при энергии первичных нейтронов 5-7 Мэв прямое взаимодействие играет заметную роль [62] и составляет 5-7% от сечения неупругого рассеяния. В работе [64] приведены рекомендованные спектры неупруго-рассеянных нейтронов для ниобия в интервале начальных энергий от 0,5 до 15 Мэв. Спектры получены как результат обработки и интерполяции всех экспериментальных данных по неупругому рассеянию, опубликованных до 1967 г. Метод интерполяции, оценки и компактного представления данных по неупругому рассеянию нейтронов приводится в работе [65].

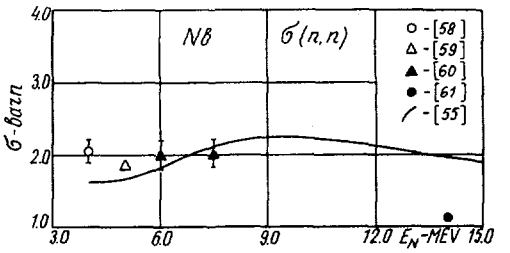

Рис. 11. Значения сечения упругого рассеяния нейтронов для ниобия.

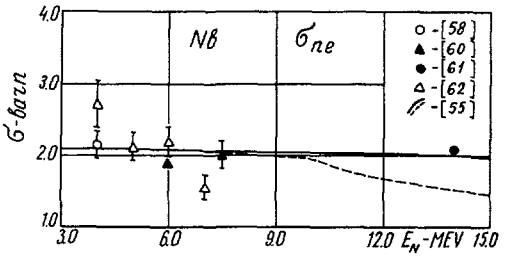

Рис. 12. Значения эффективного сечения неупругих взаимодействий.

Общим для описания сечений упругого и неупругого рассеяния нейтронов на ниобии является невозможность сравнения экспериментальных данных, полученных в различных лабораториях, из-за их малочисленности (в интервале энергий 8-13 Мэв экспериментальных данных нет).

При энергиях нейтронов 10-15 Мэв разность между сечением неупругих взаимодействий и сечением неупругого рассеяния определяется в основном эффективным сечением процесса (n, 2n). Зависимость сечения реакции (n, 2n) от энергии приведена на рис. 13, данные взяты из работ [66-70]. Сплошная кривая проведена согласно рекомендованным данным [55]. Следует отметить, что расхождение отдельных значений сечения реакции (n, 2n) при 14-15 Мэв гораздо больше величин погрешностей, указанных авторами.

Накопление гелия в ниобии под действием нейтронов обусловлено несколькими процессами [68,70-74]. Величина сечения этого процесса при энергии 14,5 Мэв составляет около 17-18 мбарн. На рис. 14 приведены значения сечения для одного из процессов, другие характеризуются меньшими величинами сечений.

Реакция (n,p) при энергии 14 Мэв имеет величину сечения 22 ± 8 мбарн [75]. Вероятность радиационного захвата в ниобии при энергии 14 Мэв незначительна [68].

Суммируя проведенное рассмотрение ядерных данных для трех элементов, можно сделать следующие выводы:

1. Для области энергий нейтронов 5-15 Мэв ядерных данных существенно меньше, чем в области более низких энергий. Для большинства процессов экспериментальные данные концентрируются в интервале энергий 5-8 Мэв и около 14 Мэв, а в интервале энергий 8-13 Мэв для ряда процессов в лучшем случае имеются одна-две экспериментальные точки.

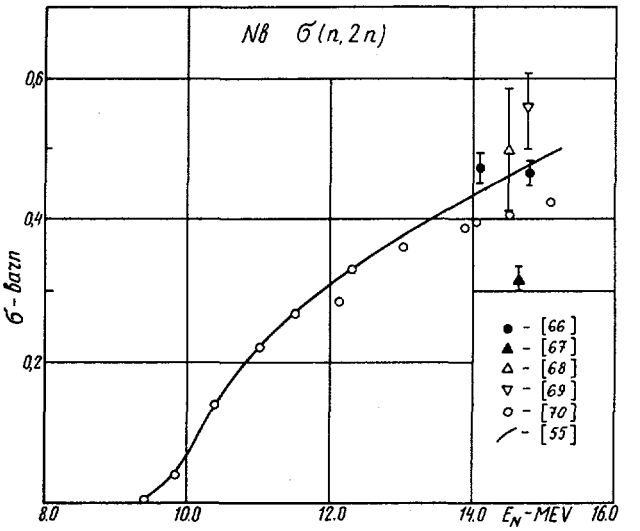

Рис. 13. Зависимость сечения реакции (n,2n) от энергии.

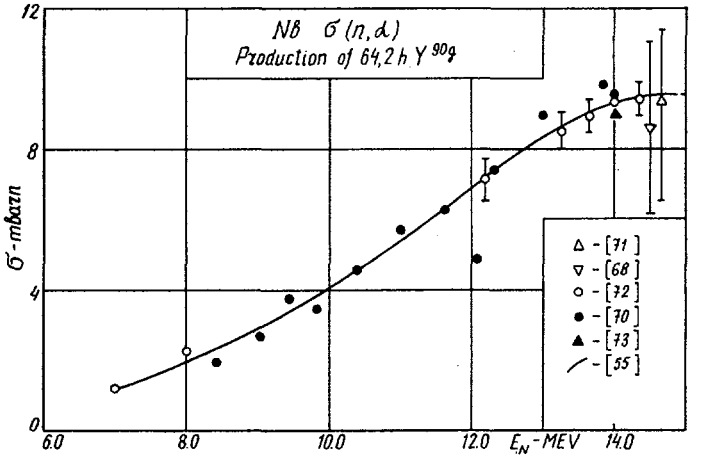

Рис.14. Значения сечения для одного из процессов, обусловливающих накопление гелия в ниобии под действием нейтронов.

2. Там, где есть несколько экспериментальных точек и возможно сравнение, в ряде случаев имеет место расхождение данных, выходящее за пределы погрешностей измерений, указываемых авторами.

3. Для некоторых процессов оцененные рекомендованные значения сечений заметно отличаются от измеренных величин.

При этом необходимо подчеркнуть, что среди элементов, представляющих интерес для термоядерных реакторов, изотопы лития изучены лучше других; для других элементов, например ниобия, экспериментальных данных уже значительно меньше.

3. Потребности в ядерных данных

С ростом энергии нейтронов число каналов, по которым могут идти реакции взаимодействия нейтронов с ядрами, существенно увеличивается. При этом необходимо подчеркнуть, что появляется много реакций, в результате которых испускаются заряженные частицы.

Поскольку энергия "термоядерных" нейтронов значительно выше средней энергии нейтронов спектра деления, число возможных каналов реакций в этом случае будет существенно выше. Таким образом, становится достаточно очевидным, что для удовлетворения потребностей расчета термоядерных реакторов предстоит изучить существенно больше ядерных взаимодействий, чем это имеет место для реакторов деления.

Помимо общего замечания о потребности в ядерных данных для термоядерных реакторов, кажется целесообразным остановиться подробнее на двух типах ядерных данных, которые играют значительно более важную роль в термоядерных реакторах, чем в случае реакторов деления.

1. Как отмечалось (см. табл. 1), при использовании D + T – реакции 80% всей энергии, создаваемой термоядерным реактором, определяется энергией "термоядерных" нейтронов, которая должна быть преобразована в тепловую энергию в оболочке, окружающей вакуумную камеру. Ввиду этого вопрос об энерговыделении в оболочке за счет замедления и захвата нейтронов становится существенно более важным, чем в случае реакторов деления.

Общее энерговыделение в оболочке термоядерного реактора создается за счет следующих процессов:

а) торможения заряженных частиц, получающихся в результате различных реакций взаимодействия с нейтронами;

б) торможения ядер отдачи, образующихся при упругом и неупругом рассеянии нейтронов;

в) ионизационного замедления β-частиц при распаде нестабильных продуктов реакций;

г) поглощения вторичных γ-лучей.

Все вышеперечисленные процессы, за исключением поглощения γ-лучей, на данном этапе развития термоядерных реакторов могут быть достаточно удовлетворительно рассчитаны на основе имеющейся информации. Несколько иначе обстоит дело с расчетом энерговыделения, определяемого поглощением вторичных γ-лучей, которое составляет примерно половину общего энерговыделения в оболочке реактора.

Спектры γ-излучения, получающиеся при захвате тепловых нейтронов, подробно изучены [76], однако большая часть γ-лучей, образующихся в оболочке реактора, обязана неупругим взаимодействиям быстрых нейтронов, а спектры γ-лучей, обязанные этим процессам, изучались мало.

2. Другой важный для термоядерных реакторов раздел, где ощущается недостаток экспериментальной информации по ядерным данным, – это угловые распределения вторичных нейтронов.

Для реакторов деления вопросы, связанные с анизотропией нейтронов, в общем не играют определяющей роли, исключая отдельные случаи, например небольшие реакторы на быстрых нейтронах с толстым отражателем – бланкетом, расчеты защиты реакторов и т. п.

В случае термоядерных реакторов дело обстоит несколько иначе. Поскольку толщина оболочки термоядерного реактора должна быть сде-

лана предельно малой и начальная энергия быстрых нейтронов достаточно велика, анизотропия рассеяния вторичных нейтронов имеет важное значение. Поэтому данные по измерениям угловых распределений вторичных нейтронов очень важны при выполнении нейтронно-физических расчетов оболочки термоядерного реактора.

V. ЗАКЛЮЧЕНИЕ

В данной работе была сделана попытка показать, что ядерные взаимодействия в энергетической области, определяемой "термоядерными" нейтронами, еще мало изучены, и тем самым привлечь внимание экспериментаторов к измерению ядерных сечений, которые необходимы для создания термоядерной энергетики термоядерных реакторов.

В то время как для реакторов деления основная задача заключается в увеличении точности уже имеющихся ядерных данных [77,78,79], для термоядерных реакторов – еще предстоит заполнять "белые пятна".

Мы выражаем надежду, что экспериментальные трудности, которые придется преодолеть исследователям при получении ядерных данных для термоядерных реакторов, будут вознаграждены успешным решением важнейшей проблемы века.

ЛИТЕРАТУРА

[1] АРЦИМОВИЧ, Л. А., УФН 91 март-апрель (1967).
[2] ADAMS, J.B., Proc.Phys.Soc. 89 594, part 2 (Oct. 1966).
[3] HILTON, J.L., IEEE Trans. Nucl. Sci. 16 4 (Aug.1969).
[4] ROSE, D.J., USAEC Report ORNL-TM-2204, May 1968.
[5] SPITZER, L. et al., USAEC Report NYO-6047, Princeton University, 1954.
[6] CHRISTOFILOS, N.C. et al., USAEC Report TID-7558, Suppl.1, 1960.
[7] ГОЛОВИН, И.Н. и др. О возможности создания реактора Токамак. Отчет ИАЭ им. И.В. Курчатова (ИАЭ-1937). Москва, 1969 г. Доклад на конференции по термоядерным реакторам (Калем, Англия, сентябрь 1969 г.).
[8] HUBERT, P., Thermonuclear Future of the TOKAMAK Magnetic Confinement Device. Доклад на конференции по термоядерным реакторам (Калем, Англия, сентябрь 1969 г.).
[9] LOWSON, J.D., Proc.Phys.Soc. 70 4458, pt.1 (Jan.1957).
[10] ШАФРАНОВ, В.Д., ЖЭТФ 33 (1957) 710.
[11] АЛЕКСЕЕВСКИЙ, Н.Е. и др., ЖЭТФ 9 (1969) 1.
[12] MILLS, R., Some Engineering Problems of Thermonuclear Reactors, MATT-548,1967.
[13] FRAAS, A.P., Conceptual Design of a Fusion Paver Plant. Доклад на конференции по термоядерным реакторам (Калем, Англия, сентябрь 1969 г.).
[14] STEINER, D., Neutronics Calculations and Cost Estimates for Fusion Reactor Blanket Assemblies, USAEC Report ORNL-TM-2360 (1968).
[15] HOMEYER, W.G., Thermal and Chemical Aspects of the Thermonuclear Blanket Problem, M.I.T. Technical Report 435 (1965).
[16] Second Edition BNL-325, vol.1.
[17] The ORNL Thermonuclear Program, USAEC Report ORNL-2457, 1958.
[18] BELOW, S, CROCKER, V., WADE, B., Neutronics Calculations for Blanket Assemblies of a Fusion Reactor. Доклад на конференции по термоядерным реакторам (Калем, Англия, сентябрь 1969 г.).
[19] ROBINSON, M.T., The Energy Dependence of Neutron Radiation Damage in Solids. Доклад на конференции по термоядерным реакторам (Калем,Англия,сентябрь 1969 г.).
[20] CEIRACKS, S. et al., Rev. Scient.Instrum. 39 (1968) 1279.
[21] BATCHELOR, R., TOWLE, J.H., Nucl.Phys. 47 (1963) 385.
[22] HOPKINS, J.C. et al., Nucl.Phys. A107 (1968) 139.
[23] COOKSON, J.A., DANDY, D., Nucl.Phys. A 91 (1967) 273.
[24] ARMSTRONG, A.H. et al., Nucl.Phys. 52 (1964) 505.
[25] WONG, C. et al., Nucl.Phys. 33 (1962) 680.

[26] MERCHEZ, F. et al., Proc.Conf. (Paris, 17-21 Oct.1961), IAEA, Vienna, 1(1967)393.
[27] HUGHES, D.J., SCHWARTZ, R.B., BNL 325, 2nd Edn (1958).
[28] GLASGOW, D.W., FOSTER, D.G., Phys.Rev.Lett. 22 (1969) 139.
[29] CONN et al., Phys.Rev. 88 (1952) 562.
[30] KATSOUROV et al., Sov.J.atom.Energ.Suppl. 5 (1958) 67.
[31] BRATENAHL, A. et al., Phys. Rev. 110 (1958) 921.
[32] ROSEN, L., STEWART, L., Phys. Rev. 126 (1962) 1150.
[33] MURRAY, R.B., SCHMITT, H.W., Phys. Rev. 115 (1959) 1707.
[34] KERN, B.D., KREGER, W.E., Phys. Rev. 112 (1958) 926.
[35] RIBE, F.L., Phys. Rev. 103 (1956) 741.
[36] FRYE, G.M., Jr., Phys.Rev. 93 (1954) 1086.
[37] МИХАЙЛИНА, К.М. и др., В сб. "Нейтронная физика". М., 1961, стр. 249.
[38] ASHBY, V.J. et al., Phys. Rev. 129 (1963) 1771.
[39] MATHER, D.S., PAIN, L.F., AWRE Report N O-47/69.
[40] BARRY, J.F., J. nucl. Energy, A/B 17 (1963) 273.
[41] BATTAT, M.E., RIBE, F.L., Phys. Rev. 89 (1953) 80.
[42] COOK, C.F., BONNER, T.W., Phys. Rev. 94 (1954) 651.
[43] BENVENISTE, J. et al., Nucl.Phys. 38 (1962) 300.
[44] WYMAN, M.E., THORPE, M.M., LA-2235 (1958).
[45] BENJAMIN et al., AWRE-NR/A-2/62, 1962.
[46] PRESSER, G., BASS, R., Proc. Int. Conf., Antwerpen, Belgium (July 1965) 35 (North-Holland Publ. Co, Amsterdam, 1966), p.508.
[47] BROWN, F. et al., J.nucl. Energy, A/B 17 (1963) 137.
[48] RENDIC, D., PAIC, G., Proc.2nd Conf.Nucl.React.Light Nuclei and Nucl.Str. (1967, Rossendorf) Dresden, 1967, p.143.
[49] The U.K.A.E.A. Nuclear Data Library Fib.1968.
[50] PRESSER, G. et al., Nucl.Phys. A131 (1969) 679.
[51] VOLKOVIC, V., Nucl.Phys. 60 (1964) 581.
[52] FREEMAN, J.F. et al., Phil.Mag. 46 (1955) 17.
[53] CARLSON, A.D., Bull. Am. Phys. Soc. 11 (1966) 29.
[54] FOSTER, D.G., GLOSGOW, D.W., Priv.Comm.(1965); GOLDERG, M.D. et al., BNL-325 Second Ed.Suppl. N2 (1966).
[55] ALLEN, M.S., DRAKE, M.K., GA-8133 (1967).
[56] CARLSON, A.D., BARSCHALL, H.H., Phys.Rev. 158 (1967) 1142.
[57] PERRY, F., BUCK, B, Nucl.Phys. 32 (1962) 353.
[58] ГОРЛОВ, Г.В. и др., ЯФ 6 (1967) 910.
[59] BUCCINO, S.G., Z. Phys. 196 (1966) 103.
[60] HOPKINS, C.J., DRAKE, D.M., Nucl.Sci. Engng 36 (1969) 275.
[61] WESTERN, G.T., Conf. on Neutr.Cr.Sect. and Tech.Proc., Wash. 2 (1966) 675.
[62] THOMSON, D.B., Phys.Rev. 129 (1963) 1649.
[63] САЛЬНИКОВ, О.А. и др., Англо-советский семинар "Ядерные константы для расчета реакторов". Дубна, 1968, ACC-68/6.
[64] ПОПОВ, В.И. и др., Бюллетень информационного центра по ядерным данным. Вып.4. М., Атомиздат, 1967, стр. 169.
[65] ПОПОВ, В.И. и др., Англо-советский семинар "Ядерные константы для расчета реакторов", Дубна, 1968, ACC-68/11.
[66] PIEDER, R., MUNZER, H., Proc.Int.Conf., Antwerpen, Belgium (July 1965)123, (North-Holland Publ. Co, Amsterdam) 1966, p.547.
[67] STROHAL, P. et al., Nucl.Phys. 30 (1962) 49.
[68] BRAMLITT, E.T., FINK, R.W., J. inorg.nucl.Chem. 24 (1962) 132; Phys. Rev. 131 (1963) 2649.
[69] ГЛАГОЛЕВ, В.Л., ЯМПОЛЬСКИЙ, П.А., ЖЭТФ 40 (1961) 743.
[70] TEWES, H.A. et al., Priv.Comm. (1960); GOLDBERG, M.D. et al., BNL-325, Second. Ed.Suppl., N2 (1966).
[71] KULISIC, P. et al., Nucl.Phys. 54 (1964) 17.
[72] BAYHURST, B.P., PRESTWOOD, R.J., J. inorg.nucl.Chem. 23 (1961) 173.
[73] BLOSSER, H.G. et al., Phys.Rev. 110 (1958) 531.
[74] ALFORD, W.L. et al., Phys.Rev. 123 (1961) 1365.
[75] VERBINSKI, V.V. et al., Phys.Rev. 108 (1957) 779.
[76] ГРОШЕВ, Л.В., БАРТОЛОМЬЮ, Г.А. и др., Ядерные данные. В сб. "Результ.измер. гамма-излучен. возн. при захв. тепл. нейтр.". ч.I-III, М., Атомиздат, 1970.
[77] УСАЧЕВ, Л.Н., Доклад CN-23/130 на Конференции по ядерным данным. (Париж, октябрь 1966 г.).
[78] KINCHIN, G.H., Paper CN-23/117 at Nuclear Data Conference (Paris, Oct.1966).
[79] SMITH, R.D., Paper CN-23/52 at Nuclear Data Conference (Paris, Oct.1966).

NUCLEAR CROSS-SECTION REQUIREMENTS FOR FUSION REACTORS

V.S. CROCKER, S. BLOW
UKAEA, Research Group,
Culham Laboratory,
Abingdon, Berks,
and
C.J.H. WATSON
UKAEA, Research Group,
AERE, Harwell,
Didcot, Berks,
United Kingdom

Abstract

NUCLEAR CROSS-SECTION REQUIREMENTS FOR FUSION REACTORS

1. The paper considers nuclear cross-section requirements for the plasma and the surrounding blanket.

2. Both toroidal and open-ended (e.g. mirror) confinement systems are considered. From the permissible plasma pressure it appears that the former are limited to temperatures up to 100 keV (energy equivalent), whilst for open-ended machines the temperature limit appears to be as high as 1 MeV.

Taking into account

i) the various forms of energy loss from the plasma;

ii) economic considerations related to magnetic-field winding costs

a relationship is derived for selecting possible thermonuclear reactions. In general, it excludes reactions with $Z > 10$, and all reaction with cross-sections less than a millibarn at energies less than 10 MeV. The number of 'interesting' reactions remaining is surprisingly large, and a table of data on reactions for Z up to 3 is given. A literature search has revealed the cross-section data to be poor for many of these reactions.

3. Since the neutronic design of fusion reactors is still at a very early stage, a model blanket design is used to illustrate the importance of nuclear cross-sections in various blanket problems. The blanket is designed around a fusion system using the D-T reaction which emits 14.1 MeV neutrons. The accuracy of the nuclear cross-sections and their effect on the neutron spectra, tritium breeding, heat generation, radiation damage and radioactivity, are commented on.

The main fields in which there is a shortage of data are:

a) non-elastic cross-sections in the range 1 MeV to 14 MeV (e.g. (n, 2n) in niobium and molybdenum);

b) secondary neutron spectra from elastic, inelastic and (n, 2n) scattering;

c) gamma-ray spectra from non-elastic events (mainly inelastic scattering and radiative capture).

1. INTRODUCTION

The controlled release of nuclear fusion energy under thermonuclear conditions has been a gleam in the eye of nuclear physicists since the early years of this century. However, large scale research programmes on practical means of achieving controlled thermonuclear reactions are a post-war phenomenon, with the major effort dating only from the late 1950s, and progress has been very uneven, with smooth advances punctuated by disappointments and setbacks. Even today it is possible to regard controlled fusion research as something directed towards a distant goal with a quite uncertain outcome. However, opinion has recently swung towards the view that the prototype fusion reactor will be constructed during this century, and some very preliminary attempts have been made to produce self-consistent and technically plausible fusion reactor designs. Accounts of this work can be found in the proceedings of the International Conference on Fusion Reactors, held at Culham in September 1969.

The reactor designs which have been produced so far fall into about six groups, each based upon a different thermonuclear plasma confinement concept. It is likely that during the next few years each of the countries involved in this research will have to make some hard technological decisions and concentrate its efforts on one (or at most a very few) system concepts. It is in this context that accurate nuclear cross-sections may come to play a crucially important role. In spite of the various features which distinguish these rival concepts, there are a number of features which are common to all the current fusion reactor systems. These features are schematically represented in Fig.1 (due to Carruthers et al 1967). There is an inner core of confined plasma, at a temperature in the range 10 keV-1 MeV. The nuclear fuels present in the plasma are still open to debate, with the various isotopes of hydrogen, helium and lithium (at least) as possible contenders, although a 50:50 deuterium-tritium mixture has hitherto been preferred. In almost every case, however, at least one of the reactions occurring in the plasma releases neutrons. Consequently, a feature of every reactor which has been considered seriously so far is a "neutron blanket" surrounding the plasma, in which the neutrons are captured, normally after some neutron multiplication, and their energy recovered as heat. In addition, if the plasma contains isotopes not readily available in nature (e.g. T, ^{3}He), these have to be bred in the blanket (e.g. by (n,t) reactions). The precise spectrum and flux of neutrons entering the blanket depend on the design: however for orientation, a typical D-T reactor with an "economic" overall heat flux out of the plasma of 1·3 KW/cm^2 has an incident current of 7 10^{14} neutrons cm^{-2} sec^{-1} of 14 MeV neutrons. Because of back-scattering in the lithium coolant channels the flux in the first wall is 2·8 x 10^{15} neutrons cm^{-2}s^{-1}. This is comparable with the flux in the Dounreay Fast Reactor (D.F.R.), and in Fig.3 we give spectra taken from the fusion reactor First wall, from the D.F.R. core (flux of 2·5 x 10^{15} n cm^{-2} s^{-1}) and the D.F.R. inner breeder region (flux 1·5 x 10^{15} n cm^{-2} s^{-1}). The histograms represent absolute flux values over the appropriate energy interval. In spite of the comparability of the fluxes, the point to emphasise is that the 14 MeV peak in the fusion spectrum means that non-elastic processes are much more significant than in a fission reactor - even for fast fission designs. Finally, surrounding the neutron blanket are the windings used to produce the magnetic field which confines the plasma. In most designs, for economic reasons, these windings are superconducting, and there is therefore a upper limit to the incident neutron flux and the nuclear heating in them.

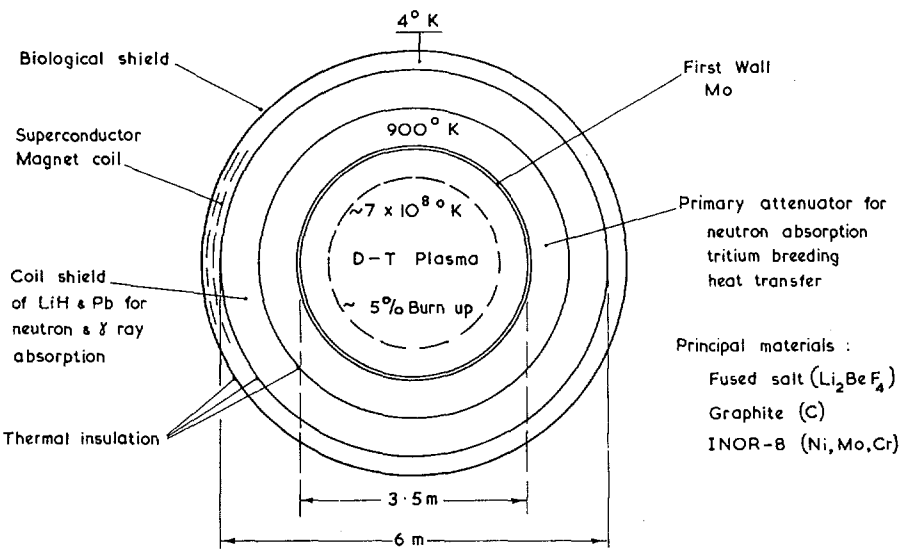

FIG.1. Conceptual design cross-section of D-T reactor-blanket after Homeyer (1965).

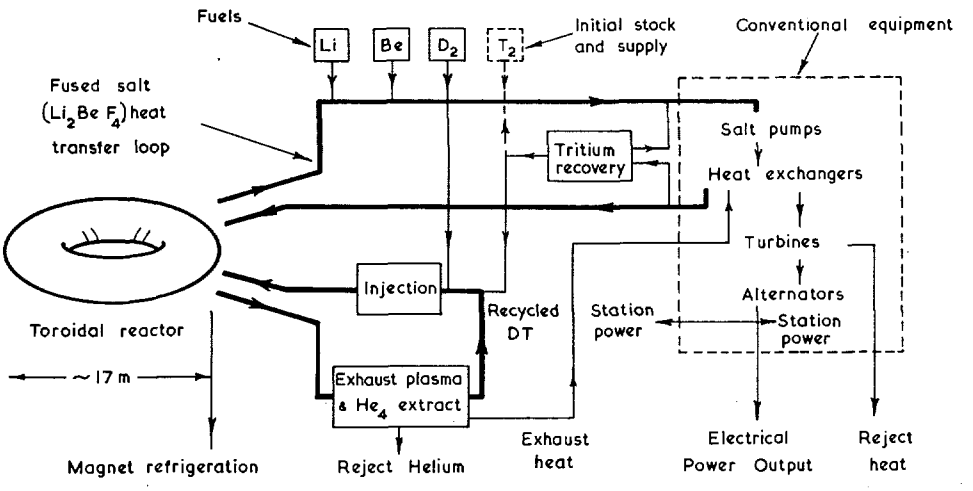

FIG. 2. Functional diagram of D-T fusion-reactor generating station.

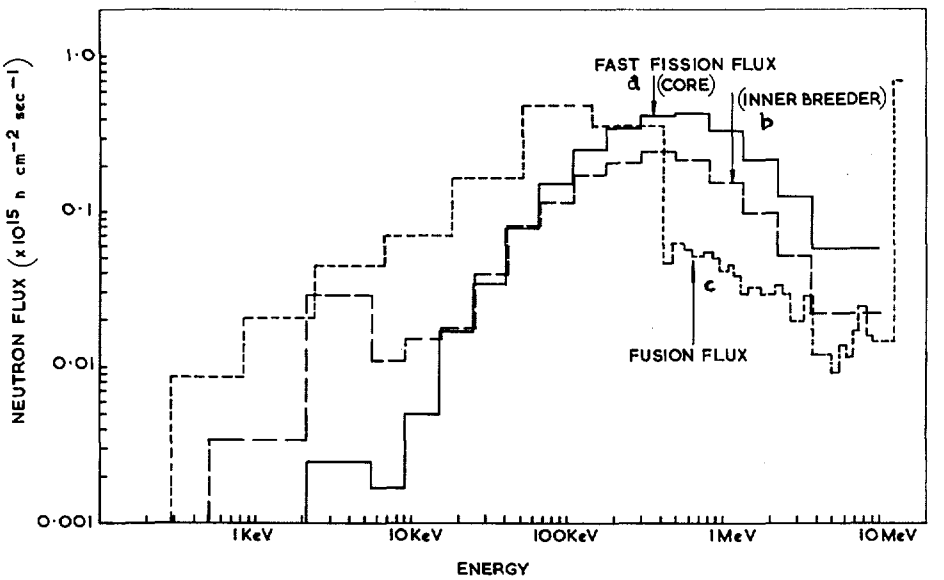

FIG. 3. Neutron-flux values in various energy groups in (a) Dounreay fast-reactor core; (b) D.F.R. inner breeder; (c) fusion reactor model first wall.
Total Flux in (a) = 2.5×10^{15} n cm^{-2} s^{-1}.
(b) = 1.5×10^{15} n cm^{-2} s^{-1}
(c) = 2.77×10^{15} n cm^{-2} s^{-1}

The structure which has just been described, which we might call the "nuclear boiler", is integrated into a power station in the manner indicated in the functional diagram shown in Fig.2 (due to Carruthers et al), in which a system using the basic reaction cycle, $T(d,n)^4He$ in the plasma + $^6Li(n,t)^4He$, $^7Li(n,nt')^4He$ in the blanket has been assumed. Although this is by no means the only possible cycle, it has been investigated in more detail than any other, because of a number of attractive features. The deuterium-tritium fusion reaction has the advantage of having the largest known fusion cross-section (5 barns), reaching its maximum at an energy (107 keV) which is four times lower than any other fusion resonance. Deuterium exists as 0·0153% of the hydrogen in sea-water, so the supply is effectively limitless. Tritium is radioactive and not naturally found and must therefore be bred in the neutron blanket. Lithium, the other fuel material, is likewise abundant (to about the same degree as uranium), and the two lithium reactions are the only ones which appear to offer real hope of tritium regeneration.

Of the features which distinguish the various fusion reactor concepts, only three require discussion: (i) the temperature of operation, (ii) the location of the windings used to produce the confining magnetic field and (iii) the means used to heat the plasma.

(i) The temperature of operation

This is crucial because if it is less than about 100 keV then only the D-T reaction can be considered, all others having a cross-section at least two orders of magnitude smaller. However, by 400 keV a number of alternative reactions are becoming of interest, and by 1 MeV a wide range of possibilities needs to be considered. In reactor concepts based on confinement in a toroidal magnetic field, it appears at present that plasma physics restrictions on the permissible plasma pressure effectively exclude operation at temperatures exceeding 100 keV; in "open-ended" machines, such as the mirror machine or the Astron however, the plasma is typically created by injecting high energy particles into the confinement system, and although temperatures as high as 1 MeV raise formidable technological problems, it is difficult to exclude them at the present stage, and the current design trend is towards higher temperature operation. A further feature to be considered in these machines is the comparatively long time (say of order 1 second) which it takes for a high energy charged reaction product to come into thermal equilibrium with the plasma. It is therefore necessary to take into account the possibility of nuclear reactions in the multi-MeV range during this "slowing down" period.

(ii) Location of the magnet windings

There is one reactor concept - the theta-pinch - in which the plasma is created in a series of fast pulses of the magnetic field. In such a system the windings have to be inside the blanket in order to allow a sufficiently rapid rise time for the magnetic field, and they have to have simultaneously a sufficiently low electrical resistivity and acceptable neutronic properties. One material system which has been investigated (Bell et al.1969) in this context is a copper-zirconium coil backed by molybdenum hoops. The difficulties raised by this approach are formidable, and are not considered in this paper.

(iii) Plasma heating

This has cross-section implications only if the apparatus used to heat the plasma is situated inside the blanket. One possibility which is being considered for toroidal systems is a radio-frequency heating system, requiring electrically insulated coils inside the blanket. The neutronic properties of both the conducting and insulating components of this system have still to be investigated.

2. THERMONUCLEAR CROSS-SECTIONS

In standard reference works on controlled fusion research, the reactions normally mentioned are $T(d,n)^4He$, $D(d,n)^3He$, $D(d,p)T$ and $^3He(d,p)^4He$. However, as has been noted, recent developments in at least two potential fusion reactor concepts - the mirror machine and the Astron - have been in the direction of substantially higher working temperatures, with particle injection at energies measured in hundreds of keV or even MeV, and a number of plasma physicists (notably McNally and Post) have

pointed out advantages in considering reactions other than these four. The question therefore arises whether there exist criteria by which one can determine in advance whether a given reaction is of potential interest in fusion research. The answer appears to be that there are, and that they arise because (i) it must be possible to sustain the plasma temperature in spite of various energy loss processes and (ii) the reactor must generate power in an economically competitive manner. These considerations restrict the number of "interesting" reactions as follows.

(i) The principal causes of energy loss from a confined thermonuclear plasma are particle loss, heat conduction, synchrotron radiation and bremsstrahlung radiation. Each of the first three can in principle be reduced indefinitely, though it is no easy matter to reduce all three at once. The bremsstrahlung loss is essentially irreducible since a laboratory plasma is virtually transparent to it, and it cannot be reflected back into the plasma, so its energy can only be recovered by passing it through a thermal cycle with (at most) 50% efficiency. Thus it is essential that P_{th}, the net thermonuclear power released (including the energy resulting from neutron induced reactions in the blanket) should be of the same order as the bremsstrahlung power radiated P_b. Now

$$P_{th} = 4\ 10^{-14}\ n^2\ \overline{\sigma v}\ Q_t \text{ watts/cm}^3$$

and

$$P_b = 1{\cdot}7\ 10^{-29}\ n^2\ \zeta\ \overline{Z^2}\ \sqrt{T_e} \text{ watts/cm}^3$$

where n is the plasma density (in particles/cm^3), $\overline{\sigma v}$ the mean reaction rate parameter in cm^3/sec., Q_t the net energy yield per fusion reaction in MeV (including that of consequential neutron or disintegration reactions), $\overline{Z^2}$ the mean square ionic charge (in atomic units), T_e the electron temperature in MeV and ζ a relativistic correction factor (of order unity unless $T_e \gtrsim 5$ MeV), so at the very least we must have

$$\overline{\sigma v} \gtrsim 4{\cdot}2\ 10^{-16}\ \zeta\ \overline{Z^2}\ \sqrt{T_e}\ /Q_t \qquad (1)$$

(ii) The economic criterion arises from a combination of an upper limit on the permissible plasma pressure, taken below as about 2000 atmospheres, and a lower limit on the permissible thermonuclear power density, shown to be about 1 watt/cm^3. The plasma pressure limit results from the fact that above a certain field strength, the cost of providing the magnetic field which confines the plasma rises very rapidly. At moderate field strengths (e.g. ~ 100 KGauss) the cost scales roughly as B^2 and as the surface area of the plasma: at sufficiently high field strengths however, as one approaches the absolute limit set by the strength of the materials used to withstand the magnetic forces, the cost rises more rapidly than this. Since the thermonuclear power output scales as the square of the plasma pressure (which must of course be less than the magnetic pressure $B^2/8\pi$), the reactor designer has a clear incentive to increase the plasma pressure until the steeply rising magnet cost ensures that there is no further decrease in the magnet cost per unit of power output. At the present time, this limit is encountered around 150KGauss: however it is to some extent a function of the state of magnet technology, and for present purposes we have taken it as 220KGauss (2000 atmospheres) to allow for plausible developments in this technology.

The power density limit is due to the fact that there is an upper limit to the plasma radius (again largely dictated by magnet costs) and a lower limit to the power flux through the plasma surface, due to the need to keep the capital cost of the magnet per unit of power output at an acceptable level. The maximum practicable plasma radius is of order 10 meters, since (as Rose has shown) for magnets of larger radius the cost of the structural material used to withstand the hoop stresses in the windings becomes dominant. The minimum power flux through the first wall turns out (magnet costs being what they are) to be essentially equal to the maximum flux permitted by thermal stress and/or radiation damage considerations - about 1 KWatt/cm^2. Thus the minimum power density is of order 1 watt/cm^3.

Combining these two limits, a reaction is "interesting" if

$$\overline{\sigma v} \gtrsim 1{\cdot}6\ 10^{-17}\ (T_e+T_i)^2/Q_t \qquad (2)$$

where T_e and T_i are the electron and ion temperatures in MeV. Only a limited significance should be attached to the numerical factor in (2), which varies inversely as the square of the maximum pressure which is regarded as economically and technologically feasible.

The quantity T_e appearing in the criteria (1) and (2) above should strictly be determined by means of an energy balance calculation, in which the energy transferred from the ions to the electrons is equated to the energy radiated by the electrons as bremsstrahlung and synchrotron radiation plus the energy which they carry off when they eventually escape from the plasma confinement system. This balance depends on the ion energy distribution and hence on the cross-sections for the thermonuclear reactions which heat the ions, and this dependence is rather sensitive: in the calculations of Petravic et al, for example, a change amounting to only a factor of two in the fusion cross-section taken essentially reversed the verdict of Fowler and Rankin on the feasibility of a mirror reactor based on the $T(d,n)^4He$ reaction. Fortunately, however, it is not necessary for present purposes to perform such a calculation, since it is possible to state with sufficient precision the temperature T_e which it must yield if the fusion reaction concerned is to be of interest. This is because the synchrotron radiation rises rapidly with T_e, becoming dominant for $T_e \gtrsim 100$ keV (see for example Mills (1969)), whereas the cooling of the ions by the electrons increases as $(T_i-T_e)/T_e^{3/2}$ and (for $T_i \gtrsim 1$ MeV) becomes unacceptable if $T_e \ll 100$ keV. Thus reactions which require ion temperatures $T_i \gtrsim 1$ MeV are of interest only if it is possible to run the reactor in such a way that the electron temperature is close to 100 keV.

It remains an open question whether one could design a fusion reactor in which the temperature ratio T_i/T_e was as high as this argument requires ($\gtrsim 10$). The calculations of Petravic et al mentioned above showed that a ratio of the order of 5 is possible, and this figure might be increased in a system in which the fusion reactions released a larger fraction of their energy as charged particle energy. Reliable calculations on this point will be made possible by more accurate cross-section data. However, on the assumption that electron temperatures of order 100 keV are feasible, we can set $T_e = 0{\cdot}1$ in (1), obtaining

$$\overline{\sigma v} \gtrsim 1{\cdot}4\ 10^{-16}\ \overline{Z^2}\ /Q_t$$

a condition which is seen to be more stringent than (2) except at very high ion temperatures. We can rewrite (1) as

$$\sigma \gtrsim 100\ \overline{Z^2}\ (m/T_i)^{\frac{1}{2}}/Q_t \text{ mbarns} \qquad (3)$$

where m is the reduced mass for the reaction in atomic units and $1 \lesssim T_i \lesssim 10$ MeV, and in this form it provides a useful rule-of-thumb for selecting reactions of interest. It excludes most if not all thermonuclear reactions in which Z is greater than about 10 and all reactions in which σ is less than one millibarn at energies less than 10 MeV. The number of reactions which remain is however surprisingly large.

We present here some preliminary results, relating to charged species with $Z \leqslant 3$, of an extensive literature search for information on the cross-sections of thermonuclear reactions satisfying the criterion (3) in the range 0–10 MeV. The reactions which meet this requirement are listed in table 1, together with their Q values, the known or suspected reaction channels, the maximum value of σ(for $\varepsilon < 10$ MeV) and the energy at which it occurs. The symbol > in this table indicates that the maximum lies at a higher energy than the maximum at which data are available, and ~ indicates an order of magnitude figure in cases where there is substantial disagreement in the literature. In Figs.4–13 we show compilations of the cross-section measurements for each of these reactions. The energy scale is logarithmic running from 10 keV to 10 MeV in each case; the cross-section scale is linear, and marked in millibarns. The name given is that of the first author of the publication from which it was derived. For the most part these are uncritical compilations, with no data adjustments apart from those sanctioned by the authors concerned, though un-normalised yield curves have been normalised to the work of other authors. In a few cases the cross-sections have been renormalised in the light of subsequent and more accurate determinations of absolute cross-sections, or to ensure a standard definition of the cross-section (e.g. in the reaction $^6Li(d,\alpha)^4He$, which disintegrates one lithium nucleus and produces two alpha particles). When only differential cross-sections at a single angle were available, total cross-sections were derived by assuming isotropic angular distributions.

This rather crude procedure was made necessary by the paucity of the data available for many of these reactions. A more detailed account of this data, together with a full bibliography, will be published shortly as a separate report (Dance & Watson CLM-BIB 9): the papers cited here cover only the most directly relevant publications.

It will be seen from Figs.4–13 that the state of knowledge of the "interesting" charged particle reaction cross-sections is by no means uniformly satisfactory. The data on the D-D and D-T reactions sets a standard which is hardly approached by any other reaction. For several reactions – notably

TABLE I. REACTIONS SATISFYING CRITERION (3)

Reaction	Q value (MeV)	σ_{max}(mb)	ε_{max}(MeV)	Sources
D(p,np)P	−2.2	>400	>5.5	Henkel
D(d,n)^{3}He	3.27	105	1.9	Blair, Brolley
D(d,p)T	4.03	90	2.0	Blair, Brolley
T(p,n)^{3}He	−0.76	500	3.0	Taschek, Willard
T(d,np)T	−2.2	>700	>6.0	Henkel, Smith
T(d,2n)^{3}He	−3.0	?>1200	>6.5	
T(d,n)^{4}He	17.6	5000	0.108	Arnold, Balabanov, Conner Poppe
T(t,n)^{5}He(n)^{4}He	11.4	>100	>1.8	Agnew, Allen, Govorov, Leland
T(t,2n)^{4}He				
T(t,n)^{5}He*(n)^{4}He		?>1200	>2.4	
^{3}He(d,np)^{3}He	−2.2	>70	>1.0	Henkel
^{3}He(d,p)^{4}He	18.4	700	0.4	Bonner, Kunz, Yarnell
^{3}He(t,d)^{4}He	14.3	~50	~1.0	Almquist Barry Kuhn Youn
^{3}He(t,p)^{5}He(n)^{4}He	11.3+1.0			
^{3}He(t,np)^{4}He	12.1			
^{3}He(t,n)^{5}Li(p)^{4}He	10.3+1.8			
^{3}He(^{3}He,p)^{5}Li(p)^{4}He	11.0+1.8	>30	>0.8	Good
^{3}He(^{3}He,2p)^{4}He	12.8			
^{4}He(d,np)^{4}He	−2.2	>240	>6	Henkel
^{6}Li(p,^{3}He)^{4}He	4.02	~200	1.8	Bashkin, Jeronymo Marion
^{6}Li(d,n)^{3}He+^{4}He	1.72	~>600	>5.0	Baggett Slattery Whaling
^{6}Li(d,n)^{7}Be(e_k)^{7}Li 43 day	3.34			
^{6}Li(d,p)^{7}Li	5.02	100	1.2	Nickell, Whaling
^{6}Li(d,p')^{7}Li*(γ)^{7}Li	4.54+0.45			
^{6}Li(d,t)^{5}Li(p)^{4}He	0.9+1.6	>300	>4.0	Macklin
^{6}Li(d,α)^{4}He	22.4	30	3.7	Jeronymo, Mani, Meyer, Whaling
^{6}Li(t,d)^{7}Li	0.995	>320	>2.1	Pepper, Serov, Valter
^{6}Li(t,d')^{7}Li*(γ)^{7}Li	0.509+0.45			
^{6}Li(t,p)^{8}Li(e_-)2α	0.800			
^{6}Li(t,n)^{8}Be* or 2^{4}He	16.0			
^{6}Li(^{3}He,p)^{8}Be(α)^{4}He	16.8	30	~5	Schiffer
^{6}Li(^{3}He,p)^{8}Be*(αγ)^{4}He	13.9+2.9	>60	>5	Schiffer
^{7}Li(p,n)^{7}Be	−1.63	>800	>7	Blaser, Taschek
^{7}Li(p,α)^{4}He	17.5	65	3	Heydenburg, Jeronymo, Mani, Taschek
^{7}Li(d,n)^{8}Be(α)^{4}He	15.0	>1000	>5	Baggett, Bennett, Slattery
^{7}Li(d,p)^{8}Li(e_-)^{8}Be(α)^{4}He	−0.26+16.0	?160	3	Bennett, Bashkin, Baggett
^{7}Li(d,t)^{6}Li	−0.995	>150	>4	Macklin
^{7}Li(t,2nα)^{4}He	8.88	>1300	>2.1	Crews, Serov, Valter
^{7}Li(t,n)^{9}Be	10.52			
^{7}Li(t,2n)^{8}Be(α)^{4}He	8.83			
^{7}Li(t,2nα)^{4}He	8.85			
^{7}Li(t,nα)^{5}He(n)^{4}He	8.08+1.0			
^{7}Li(t,α)^{6}He,^{6}He*	9.83	>40	>1.8	Holmgren
^{7}Li(^{3}He,n)^{9}B(p)^{8}Be(α)^{4}He	9.3+0.3	>600	>1.4	Allen, Moak, Serov
^{7}Li(^{3}He,np)^{8}Be(α)^{4}He	9.5+0.1			
^{7}Li(^{3}He,p)^{9}Be	11.2			
^{7}Li(^{3}He,d)^{8}Be(α)^{4}He	11.7+0.1			

Note: The Q values have been taken from the source quoted when given. Missing values were supplied from Maples et al. UCRL 16964. Discrepancies of up to 0.3 MeV can be detected.

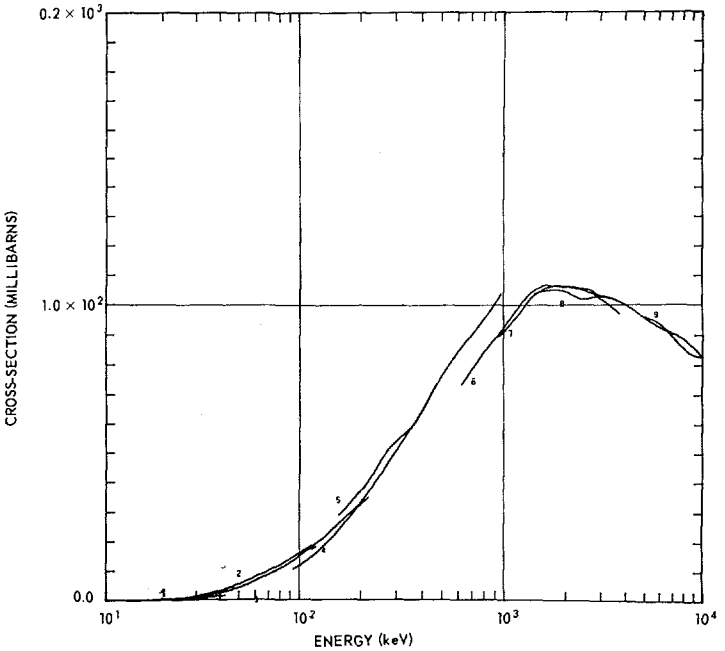

FIG. 4. D(d, n) ^{3}He. Arnold[3], Blair[7], Brolley[8], Davidenko[2], Eliot[1], Ganeev[4], Hunter[6], Preston[5] and Thornton[9].

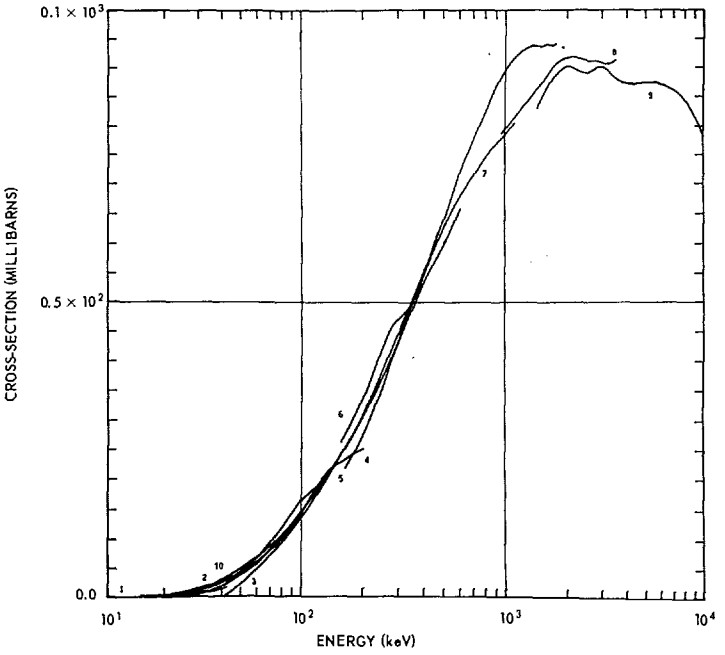

FIG. 5. D(d, p) T. Arnold[1], Balabanov[4], Blair[8], Brolley[9], Cook[10], Eliot[2], Ganeev[7], Preston[6], Volkov[5] and Wenzel[3].

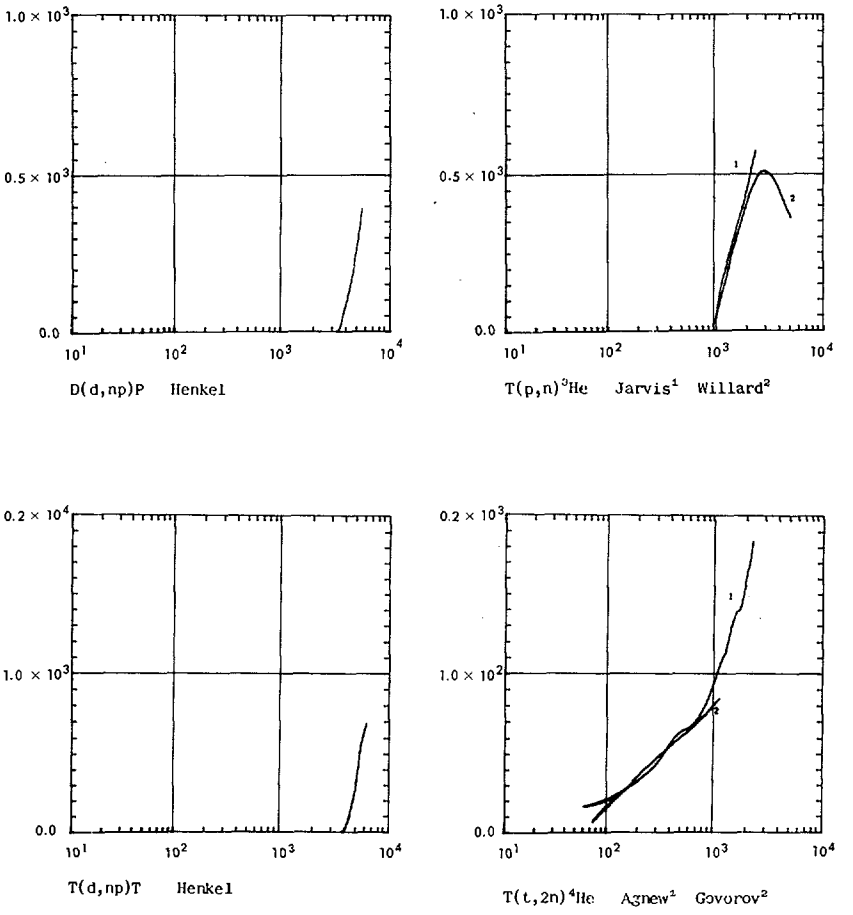

FIG.6. Reactions involving D and T.

the ^{3}He–^{3}He, $^{4}He(d,np)^{4}He$, $^{6}Li(d,t)$, $^{6}Li(^{3}He)$, $^{7}Li(p,n)$, $^{7}Li(d,t)$, $^{7}Li(^{3}He)$ reactions, we have only found one absolute measurement of the cross-section in the relevant energy range, and for several more reactions no measurement extends up the energy scale as far as the first cross-section maximum. When a number of overlapping measurements exist, the disagreement often lies outside the stated experimental error (when it is stated). These disagreements are particularly marked in the T-T ^{3}He-T, ^{6}Li-P, $^{6}Li(d,n\alpha)$, $^{6}Li(t,n)$, $^{7}Li(d,p)$ reactions. The branching ratios are in many cases unknown, or known only at one energy.

It is difficult at this stage to give a clear list of priorities for the cross-section requirements in this area. The $^{6}Li(p,^{3}He)^{4}He$ and $^{6}Li(^{3}He,p)^{8}Be$ reactions are of particular interest in that they are apparently the only one leading to exclusively charged particle reaction products, raising the tempting possibility of a fusion reactor without a neutron blanket. The ^{3}He–D, ^{7}Li–D, ^{7}Li–T and ^{7}Li–^{3}He reactions have attractively high cross-sections. (The problem of breeding ^{3}He

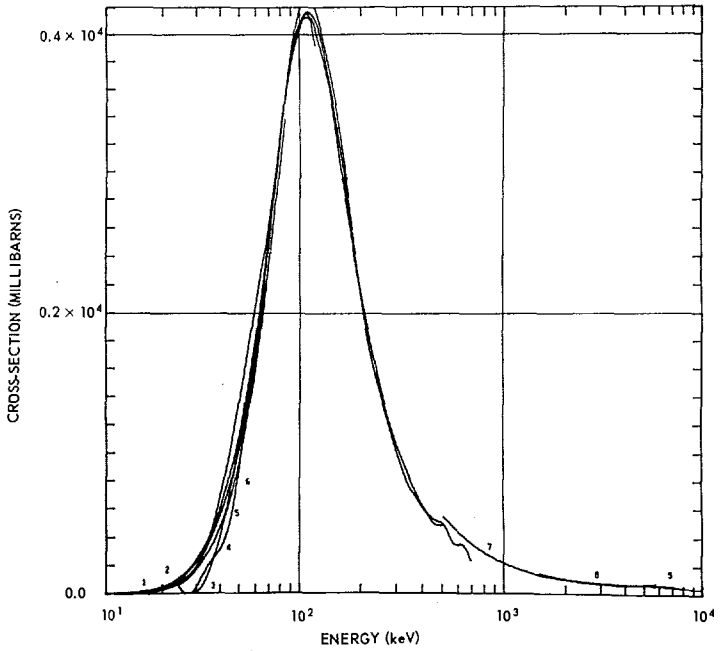

FIG. 7. T(d, n) ^{4}He. Argo[6], Arnold[1], Balabanov[4], Bame[7], Bretscher[5], Conner[3], Cook[2], Galonsky[8] and Stewart[9].

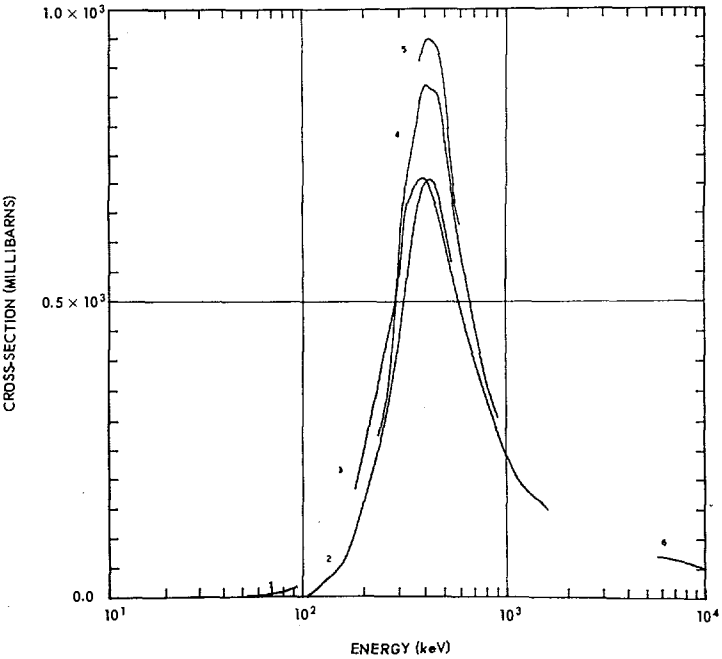

FIG. 8. ^{3}He (d, p) ^{4}He. Arnold[1], Bonner[3], Frier[5], Kunz[2], Stewart[6] and Yarnell[4].

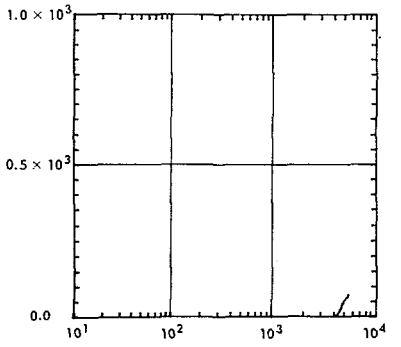

$^3He(d,np)^3He$ Henkel

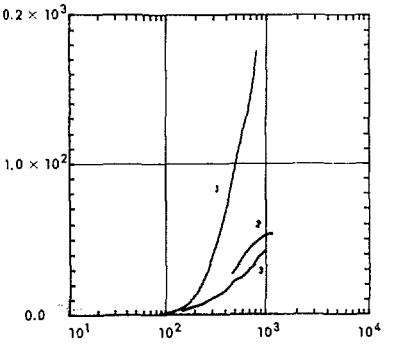

$^3He(t,np)^4He$ and $^3He(t,d)^4He$
Kuhn[3] Moak[4] Youn[2]

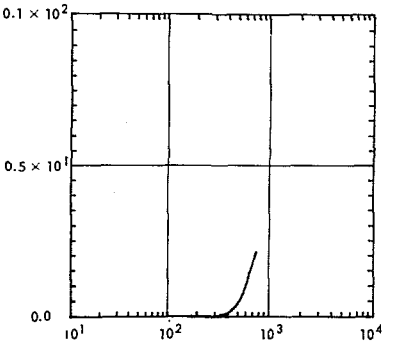

$^3He(^3He,2p)^4He$ Good

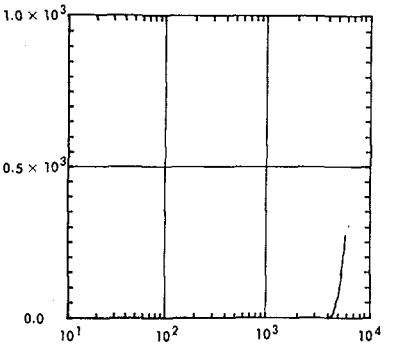

$^4He(d,np)^4He$ Henkel

FIG. 9. Helium reactions.

has been discussed by for example Post (1969) and is not obviously insuperable). The accuracy required is not enormously high; ± 10% for the principal reaction channel in each case would probably suffice, and would certainly be a substantial improvement on the existing situation. As regards elements with Z > 3: it is our intention to extend the survey to higher Z numbers, but without any great expectation of return, since with increasing Z the difficulty of maintaining the necessary ratio of ion to electron temperatures becomes much more severe, as does the net particle loss rate from the confinement system. However, a reaction with a large resonance cross-section below about 1 MeV might be of interest.

Finally, it should be remarked that we have considered only fusion and stripping reactions: however inelastic scattering cross-sections and elastic scattering cross-sections which are substantially different from the Rutherford limit are also relevant to the energy exchange between species in the plasma, and hence to the effective overall reaction rate.

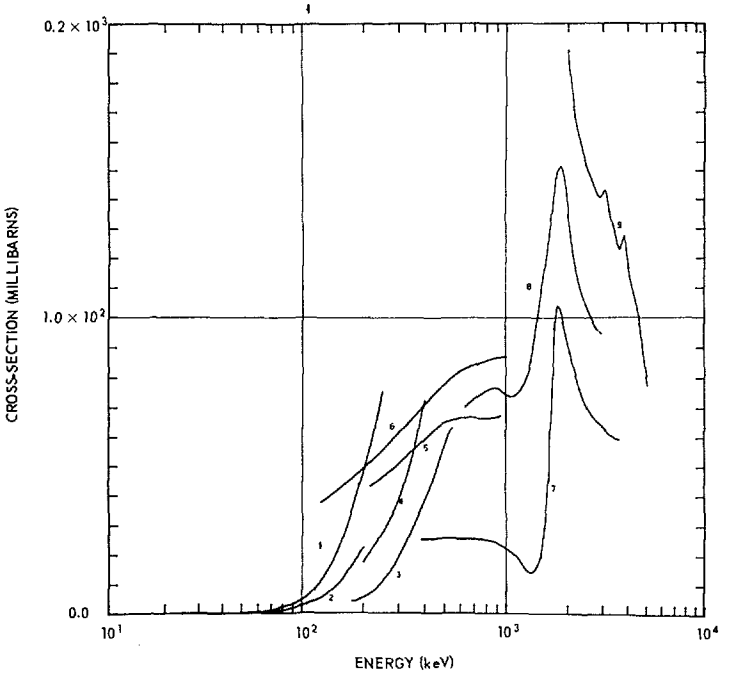

FIG.10. ^{6}Li(p, ^{3}He) ^{4}He. Bashkin[7], Beaumevieille[3], Bertrand[6], Bowersox[4], Burcham[5], Gemeinhardt[2], Jeronymo[9], Marion[8] and Sawoyer[1].

3. NEUTRON BLANKET CALCULATIONS

(i) Introduction

In this section the cross-section data required for the design of the neutron blanket surrounding a fusion plasma are considered. Since the design of fusion reactors is still at a very early stage, it is not possible to predict with any degree of confidence what materials will be used in the construction of a viable reactor, although there are certain general requirements which a blanket must satisfy (see Impink (1965) Chapter II). We shall therefore restrict attention here to one particular class of blankets for which detailed neutronic calculations have been performed, which is illustrative of the cross-section requirements that arise. It is assumed that the plasma reaction is the D-T reaction, producing 14 MeV neutrons, and that the functions of the blanket are to regenerate the tritium by means of the reaction scheme described in the introduction, to extract the neutron energy as heat, and to provide a stable engineering structure.

(ii) Blanket Model

To illustrate the importance of neutron cross-sections in various blanket problems, and to put the discussion on a quantitative basis, a model has been chosen which includes structure, reflector and (for illustrative purposes) two different coolants. This is shown in Fig.14, Test Case 7. The radius of the first wall, the containment wall, is 1·5 m. It is of cellular construction, fabricated of either niobium or molybdenum. It is cooled by a fused salt LiF(66%) + BeF_2(34%), normally written as Li_2BeF_4 and known as 'Flibe'. This region is then followed by a coolant plus structure region, which for the purposes of this paper consists of Flibe and Lithium with some structural

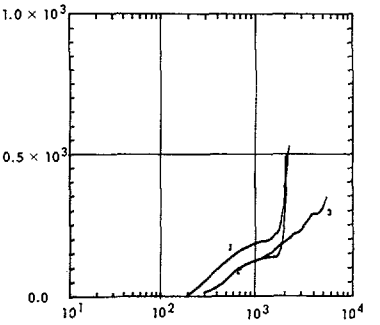

^{6}Li(d,nα)^{3}He Baggett[1] Slattery[3] Whaling[2]

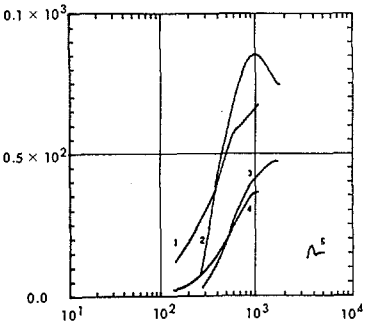

^{6}Li(d,p)^{7}Li Bertrand[1] Whaling[3]
^{6}Li(d,p')^{7}Li* Bertrand[2] Meyer[5] Whaling[4]

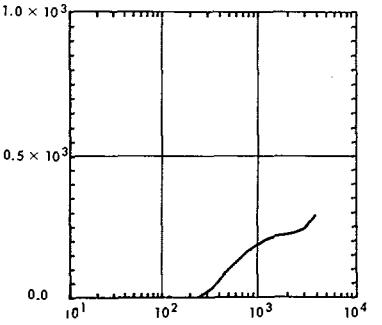

^{6}Li(d,t)^{5}Li Macklin

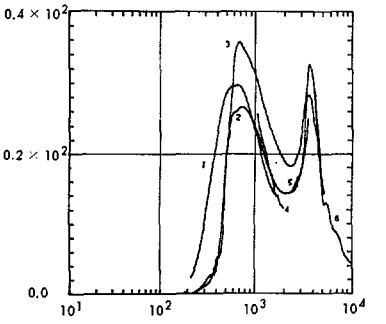

^{6}Li(d,α)^{4}He Bruno[4] Heydenburg[3] Jeronymo[2] Mani[6] Whaling[1]

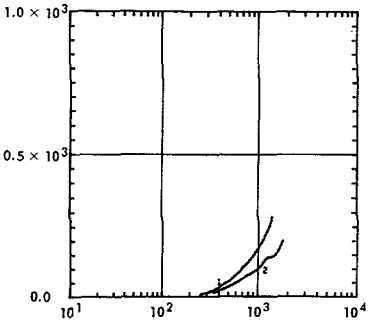

^{6}Li(t,n)^{8}Be Serov[1] Valter[2]

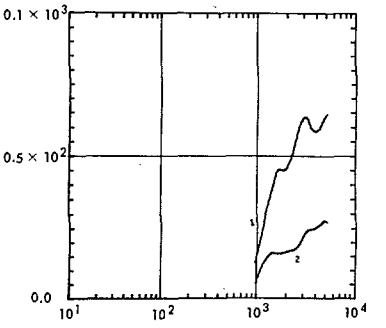

^{6}Li(^{3}He,p')^{8}Be* Schiffer[1]
^{6}Li(^{3}He,p)^{8}Be Schiffer[2]

FIG. 11. ^{6}Li reactions.

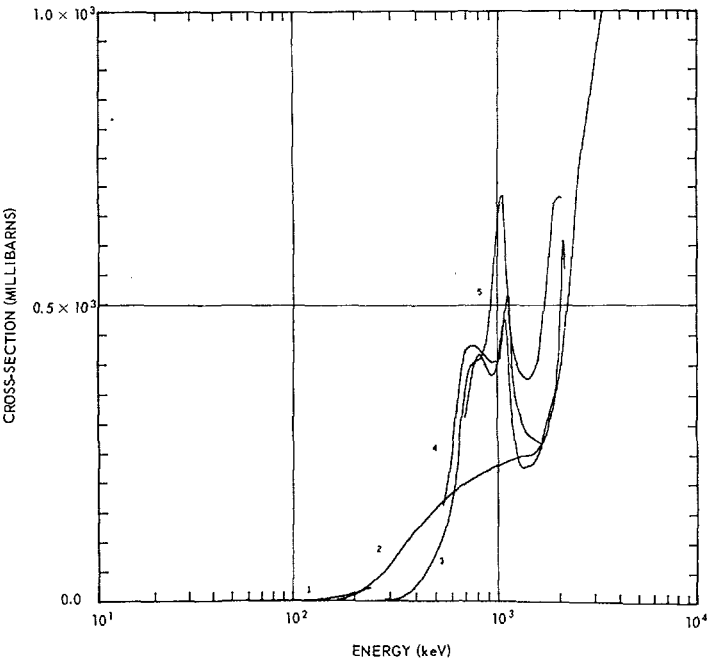

FIG. 12. $^{7}Li(d,n)\,^{8}Be$. Baggett[2], Bennett[4], Sawyer[1], Slattery[5] and Whaling[3].

material. There is then a thickness of graphite to slow down and reflect the neutrons. This is followed by a further lithium coolant channel. Surrounding this structure are the magnetic field windings and shield.

The list of materials above is not exhaustive but is considered at the present stage to represent a reasonable balance between strength, cost, and desireable neutronic properties. The first wall operates at 600°C, considered too high for stainless steel but suitable for the refractories niobium and molybdenum. Lithium in many respects is preferred to Flibe, but losses are incurred in pumping it across magnetic lines of force, and its hold up of tritium is high. Flibe is probably better from the safety view point but is poorer for tritium breeding.

This blanket model, Fig.14, Test Case 7, has been analysed neutronically (Blow et al 1969) and some of the reaction rates, based on one incident 14 MeV neutron are given in tabular form in the same Figure.

An accurate knowledge of the cross-sections of the materials composing the blanket is vital for estimating breeding (tritium production, neutron multiplication, parasitic capture); heat generation (particle reactions, recoil nuclei, Y-ray production); radiation damage (displacement damage, helium production, transmutation); and radioactivity (for maintenance, etc.).

The importance of the calculated neutron spectra for the blanket must not be overlooked. All the above features are influenced by the accuracy of these calculated spectra. The spectra are particularly important in areas where the physical limit is being approached. Such regions are those close to the first wall where heat fluxes are extremely high and radioactive damage severe. Similar limitations, but of a much smaller magnitude, could apply to the superconducting coils in which heat deposition and radiation damage must be limited. It is thus important that the neutron cross-sections, particularly of the bulk material, must be know accurately enough to enable the reactor spectra to be adequately calculated.

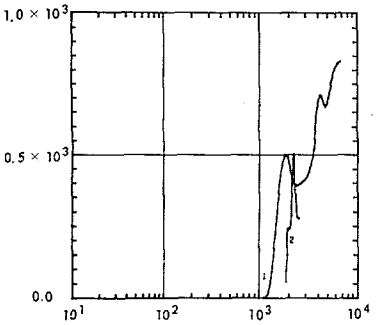

$^{7}Li(p,n)^{7}Be$ Blaser[1] Taschek[2]

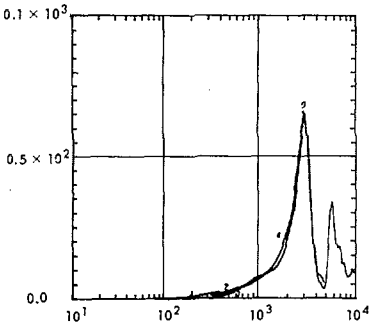

$^{7}Li(p,\alpha)^{4}He$ Herb[1] Heydenburg[2] Jeronymo[4] Mani[5] Sweeney[3]

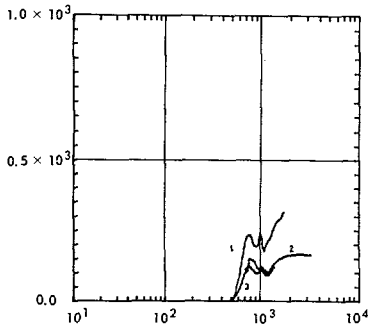

$^{7}Li(d,p)^{8}Li$ Baggett[1] Bashkin[2] Bennett[3]

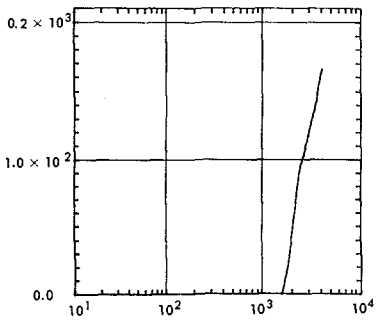

$^{7}Li(d,t)^{6}Li$ Macklin

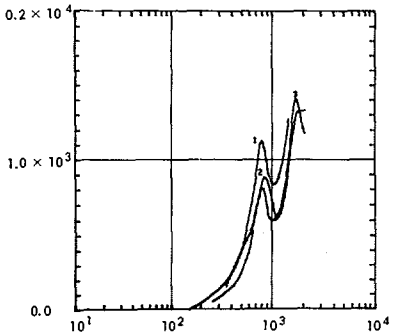

$^{7}Li(t,2n)^{4}He+^{4}He$ Crews[3] Serov[1] Valter[2]

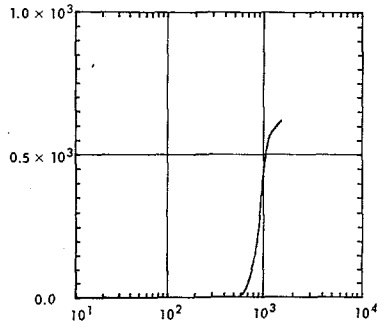

$^{7}Li(^{3}He,p)^{9}Be$ etc. Serov.

FIG. 13. ^{7}Li reactions.

TEST CASE	REGIONS 5,7,9,12	REGIONS 6,8,10	(n,2n)	T_6	T_7	T	ABS	LOST
6	98% Li 2% Nb	98% Li 2% Nb	0·131 ± 0·001	0·894 ± 0·015	0·398 ± 0·006	1·292 ± 0·021	0·207 ± 0·006	0·027 no reflection
7	98% Li 2% Nb	FLIBE	0·169 ± 0·003	0·908 ± 0·019	0·257 ± 0·006	1·165 ± 0·025	0·256 ± 0·005	0·005
8	FLIBE	FLIBE	0·187 ± 0·003	0·896 ± 0·013	0·131 ± 0·002	1·027 ± 0·015	0·290 ± 0·005	0·001

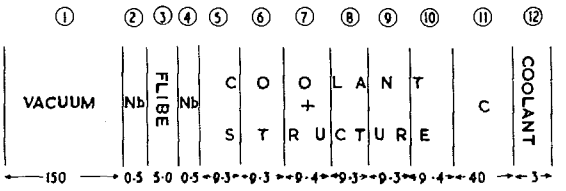

FIG. 14. Typical blanket design and reaction rates

Key: FLIBE = Li_2BeF_4.
T_6 = reaction rate from Li^6 (n, t)
T_7 = reaction rate from Li^7 (n, tn')
$T = T_6 + T_7$.

(iii) Tritium Breeding Reactions

Looking at the table in Fig. 14, Test Case 7, the value for total tritium production, T, is 1·17. The criterion of accuracy chosen is that we would like to know T to ± 1%. On this basis the required accuracy for any reaction rate is judged by its magnitude relative to 1·17.

a. $^6Li(n,t)^4He$: $T_6 \approx 0.91$. Obviously this important reaction should be known as accurately as possible – to about 1%. Recent measurements at Harwell (Silk, 1969) show that $\sigma_{thermal} = 953 \pm 5$ barns. The accuracy is ½%. Silk intends also to measure around the resonance peak at 250 keV ($\sigma \sim 2$ barns). He hopes to get 5% accuracy in this range which is as good as can be done at present.

b. $^7Li(n,n't)^4He$: $T_7 = 0{\cdot}26$. We would like to know this other important cross-section to at least 10% (preferably 5%) instead of the present ~ 25%. From Pendlebury (1964) the cross-section accuracy is ~ 15% at 14 MeV, and ~ 25% at 8 MeV (see Fig. 15). However, several of the published values lie well away from the preferred curve. Experimental results up to 1962 are included by Pendelbury. There appear to be no further measurements since ~ 1963. The American ENDF/B file (Honeck, 1967) values are based on the U.K. compilation (Pendlebury, 1964b). For a description of the format of the U.K. data file see Parker, 1963.

Fig. 15 shows the tritium production cross-sections in natural lithium (composed of 7.42% ^6Li and 92·58% ^7Li) in the high energy region. At lower energies the cross-section gradually assumes a V^{-1} dependence and reaches a value of 71 barns at thermal energy. This low energy contribution arises from the ^6Li isotope; pure ^6Li has a cross-section of 953 barns at 0·025 eV. We assume natural lithium will be used since no great advantage accrues from isotopic enrichment in ^6Li (typically, a 5% increase in breeding for a 50% ^6Li content, see Impink, 1965).

c. $^9Be(n,t)^7Li$: The contribution from this reaction is negligible.

(iv) Neutron Multiplication Reactions

From the table in Fig. 14 the total (n,2n) reaction rate is 0·17, so we would like to know the (n,2n) contribution to ~ 7% accuracy.

On the three most important reactions we make the following comments:

a. Nb(n,2n): The activation value (which is the one in the ENDF/B American file and the U.K. nuclear data file) for σ at 14 MeV is ~ 450 mb. Allen and Drake (1967) state that the current value may be up to 3 times as great. This is based on theoretical work done by H.C. Carter (1966). The activation value (Bramlitt and Fink, 1962; Basu et al, 1966) is derived from intensity measurements on the 10·1 day half-life of what is now established as the first excited state of ^{92}Nb with a spin of 2. The ground state of ^{92}Nb has a spin of 7. If this state has a long half-life then virtually no activity will be measured as a result of its decay. The question to ask is: how many decays from the ^{93}Nb(n,2n) ^{92}Nb reaction proceed to the first excited state, how many go to the ground state?

An estimate has been made using the Troubetzkoy formalism (Troubetzkoy, 1961) which gives a ratio of 1 to 1·5 for decays going to the first excited state and ground. This indicates that we should multiply the activation value (450 mb) by 2.5, giving ~ 1100mb, which closely agrees with Carter's estimate of 1136 mb.

Carter also points to the possibility of a significant (n,np) cross-section at 14 MeV (with a value ~ 350 mb).

b. Mo(n,2n): This cross-section has simply never been measured (up to 1966). Values in the ENDF/B and U.K. files are based on theoretical calculations by S. Pearlstein (1964). The value deduced at 14 MeV is 1·28 barns.

c. Be(n,2n): The accuracy at 14 MeV is about 10%. The preferred measurement of McTaggart and Goodfellow (1963) is 450 $\pm$ 40 mb. Data over the rest of the range (threshold is at ~ 2·5 MeV) are not very good (see BNL 325, Suppl.2, Vol.1, Goldberg et al., 1966). The preferred curve is probably accurate to within 25% away from the 14 MeV point.

(v) Parasitic Neutron Capture

From Fig.14, Test Case 7, the total contribution to absorption is 0·26, so we would like to attain 5% accuracy here.

Besides the four reactions given in Table III, reaction rates were calculated for ^{6}Li(np), ^{7}Li(nd), Nb(np), Nb(nα), ^{6}Li(nγ), ^{7}Li(nγ), Be(nγ), and C(nα). None of these contributed significantly in the present sense.

TABLE II. MULTIPLICATION REACTIONS IN BLANKET MODEL

REACTION	CONTRIBUTION	REQUIRED ACCURACY
Nb(n,2n)	0·03	~ 30%
Mo(n,2n)	~ 0·07	~ 20%
Be(n,2n)	0·09	~ 15%
F(n,2n)	0·02	~ 50%
^{6}Li(n,2n)D	0·003	ignore
^{7}Li(n,2n)^{4}He	0·01	~ 100%
^{7}Li(n,2n)^{6}Li	0·01	~ 100%

TABLE III. SIGNIFICANT ABSORPTION REACTIONS

REACTION	CONTRIBUTION	REQUIRED ACCURACY
Nb(nγ)	0·112	15%
Mo(nγ)	~ 0·11	15%
F(n,abs)	0·124	10%
Be(nα)	0·010	100%

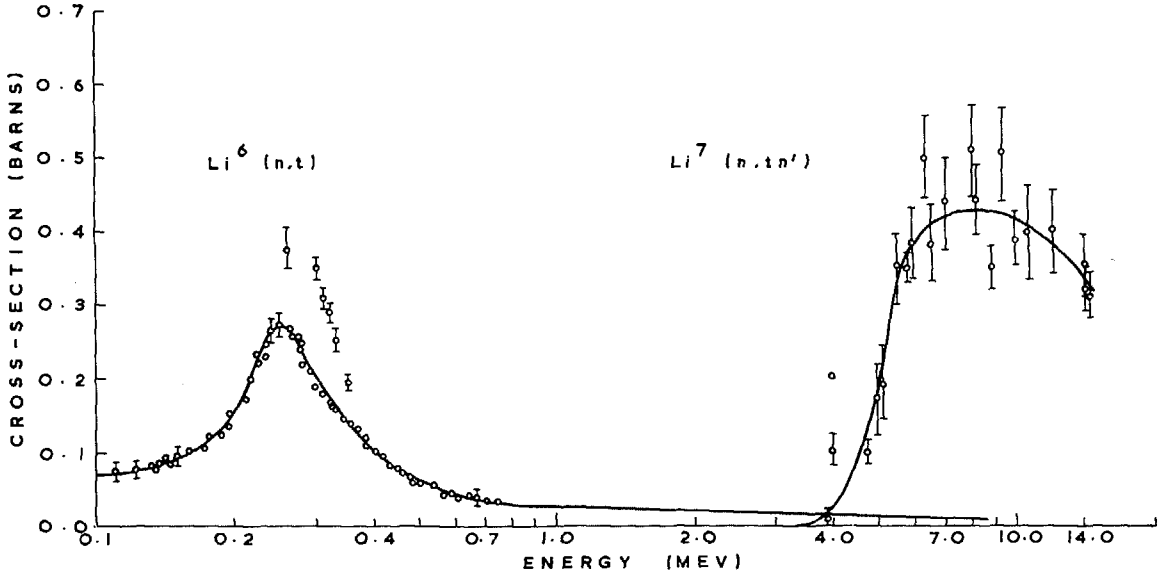

FIG. 15. Tritium breeding cross-sections for lithium isotopes in the high-energy region. The circles represent experimental points from several sources.

On the three important reactions we make the following comments:

a. Nb(nγ): Data in the region thermal to 10 keV should be accurate to within a few per cent. From 100 keV to 1 MeV the accuracy is ~ 25%. Above 1 MeV there are no measurements available but in any case the cross-section is dropping to a negligibly small value. These observations are made from graphs given in BNL 325, Suppl.2, Vol.IIB, 1966.

b. Mo(nγ): The state of the data is very similar to that of niobium.

c. F(n,abs): Contributions from (nt), (nd), (nα), (np) and (nγ) processes have all been lumped together in a total absorption cross-section by R.S. Buckingham et al (1960).

The data for (nα), the largest contributor, are very poor over the range 3.0 MeV to 9.0 MeV, with variations of up to 100%. (BNL 325, Suppl.2, Vol.1, 1964). The (nα) and (np) reactions have been re-measured recently (Prasad and Sarkar, 1966; Pasquarelli 1967; Mitra and Ghose, 1966). The measurements were taken only at around 14 MeV, and there is still a failure of overlap between the different experimental values.

The F^{19} (nγ) reaction has a value of only 10 mb at thermal energies (Glickstein and Winter, 1963).

(vi) Heating

Gamma-ray absorption cross-sections are derived from the well-known processes of Compton scattering, photoelectric effect, and pair production. There appears to be no problem with accuracy here. Details of heating effects thus revolve around having adequate knowledge of gamma-ray source intensity and spectral description, recoil effects, and charged particle emission. For the medium-heavy nuclides, niobium and molybdenum, these three effects are now considered in inverse order of importance.

a. Charged Particle Emission: The cross-sections for the only two reactions producing charged particles in Nb, (np and nα), are 30 mb and 10 mb respectively at 14 MeV. The accuracy is ~ 20%. Contributions to heating from these two processes are therefore insignificant. The (nα) cross-section is, however, very important in radiation damage work (see 3.(vii).b).

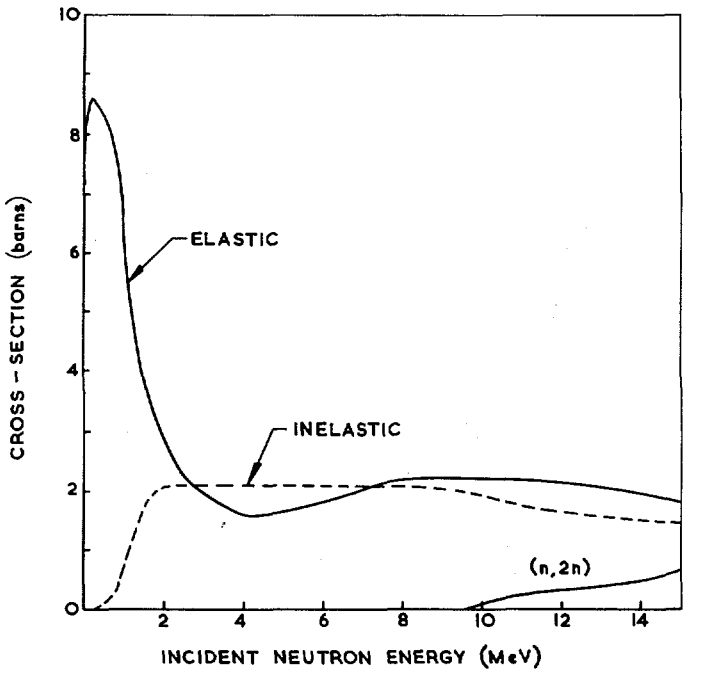

FIG. 16. Cross-sections for elastic, inelastic, and (n, 2n) scattering in niobium.

b. Recoil Effects: Steiner (1969) has calculated that ~ 8% of heating in the first wall of a reactor is caused by primary recoil processes. The important reactions are elastic scattering and inelastic scattering (quite well-known) and (n,2n) events (poorly known). The cross-sections from 0 to 14 MeV are shown in Fig.16.

The calculation of recoil is made using simple hard-sphere dynamics. The accuracy of the calculation depends on the adequacy of the secondary angular distribution. For elastic scattering only one measurement of anisotropy has been made (Western et al., 1966) at 14 MeV. For inelastic scattering isotropy in the centre of mass (c.m.) system is assumed. We would like to see a measurement of any anisotropy in inelastic scattering at 14 MeV.

The form of energy distribution of the two emitted neutrons in (n,2n) is a total unknown. The (n,2n) reaction contributes significantly to recoil, and therefore damage processes (see 3.(vii)), in a fusion spectrum.

c. Gamma-Ray Source Intensity and Spectral Description: Steiner (1969) calculates that ~ 92% of the heating in the first wall is caused by gamma absorption. Around 30% of the total energy released in the blanket is emitted as gamma-radiation. An adequate intensity and spectral description is therefore necessary.

The only two important processes are inelastic scattering and (nγ). For the first wall region neutron spectrum, the reaction rate for inelastic scattering is some eight times that for (nγ).

Following Groshev's early work (1959) a literature survey has not revealed a useful measurement of the gamma-ray spectrum from radiative capture, over the entire energy range. There is likewise a dearth of data for gamma-rays from inelastic scattering at, say, 14 MeV. Any γ-ray spectra produced from inelastic scattering have been mainly used for establishing excitation functions and energy values for excited states (see e.g., Degtyarev, 1970; Beghian et al., 1967). Such measurements have therefore been made in the energy region 1 to 2·5 MeV, whereas we would like to see γ-ray spectra from inelastic scattering in the 5 to 14 MeV regime.

(vii) Radiation Damage

(a) Displacement: Displacement damage is closely related to the magnitude of the recoil energy of struck nuclei. Recoil effects have been discussed in 3.(vi).b.

A comparison of the spectrum in the first wall of a fusion reactor (Blow et al, 1969) with that in the core centre of the Dounreay Fast Reactor (Birss and Bishop, 1966) is made in Fig.3. The flux values are nearly the same at $2{\cdot}8 \times 10^{15}$ n cm^{-2} sec^{-1}, and $2{\cdot}5 \times 10^{15}$ n cm^{-2} sec^{-1}, respectively. Despite the much greater energy available in the fusion spectrum the displacement rate is only twice that in the D.F.R. spectrum. The main reasons for this are: (a) forward peaking in elastic scattering at high energies; and (b) greater proportional loss of energy by excitation, rather than displacement of other atoms, by struck nuclei of high initial energy.

Displacement rates of niobium atoms in the first wall are high. A figure of .165 displacements per atom per year is calculated (Blow, 1970a). Fig.17 shows damage energy spectra from elastic, inelastic, and (n,2n) scattering in a fusion reactor first wall.

(b) Void and Bubble Formation: Helium tends to be trapped in a metal like niobium, even at 600°C, whereas hydrogen will diffuse out (Martin, 1969). It is essential to have an accurate value of the rate of helium formation for two reasons:

(a) helium nuclei may agglomerate to form mobile bubbles; and

(b) they may act as nuclei for void formation.

The creation and growth of bubbles and voids will cause swelling in the structural material and ultimate mechanical failure (Martin, 1969).

There have been several experimental measurements of the (nα) cross-section in niobium (BNL 325, Suppl.2, Vol.IIB). There is a discrepancy of some 20% at 14 MeV. The accepted value is 10 mb.

(viii) Radioactivity and Transmutation

A recent calculation (Blow 1970b) has shown that the activity of a segment of first wall, 300 cm in diameter, 0·5 cm thick and 100 cm in length, will be ~ 17 megacurles at the end of a 20 year irradiation period.

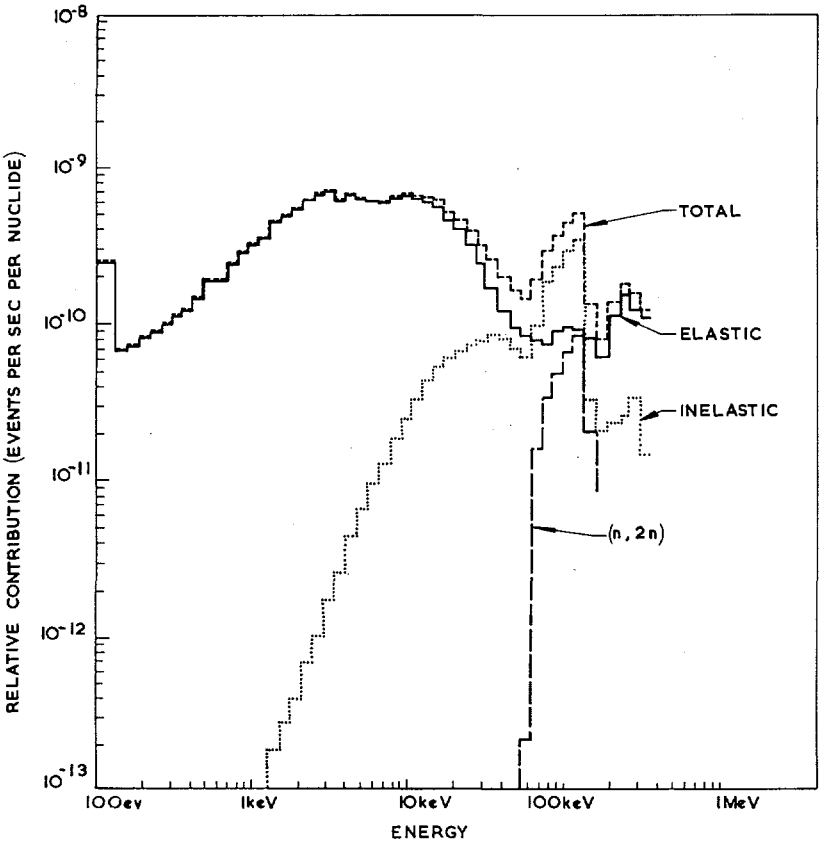

FIG.17. A histogram of the three contributing damage energy spectra and their sum in the neutron flux in the first wall of a model fusion reactor.

Nearly 80% of this activity is caused by excitation of the first excited state of ^{93}Nb in inelastic scattering. This state, of energy 30 keV, has a half-life of 13·7 years. It decays by internal transfer to the ground state. It is estimated, using a simple theoretical model of Troubetzkoy's (1961), that 23% of the decays following inelastic scattering at 14 MeV will land in the first excited state. It is highly desireable to have an experimental determination confirming or modifying this value.

Transmutation in the wall from niobium to zirconium depends critically on the magnitude of the (n,2n) cross-section. Using the recommended value of 450 mb, 7·5% of the niobium is converted to zirconium after 20 years. Using a higher value of 1,000 mb (see sec.(iv)a) the answer is 15%. This is a formidable transmutation rate which may have significant effect on structural integrity.

CONCLUSIONS

(i) Charged particle cross-sections

A rather large number of thermonuclear reactions are potentially of interest to the fusion reactor designer, although for good reasons attention has hitherto been focussed on the T(d,n)^{4}He reaction. The basic requirement for a reaction to be of interest is that it should have a cross-section in excess of about 10 millibarns at an energy not exceeding a few MeV, that the nuclei involved

should have a low charge (with Z certainly less than 10 and probably less than 4) and that the reaction Q value should be positive and reasonably large (several MeV). The reactions involving species with $Z < 4$ which satisfy these requirements are listed in Table 1, together with their peak cross-section and Q value, and compilations of the existing cross-section data in Figs.4–13. The data for the $D(d,n)^3He$, $D(d,p)T$ and $T(d,n)^4He$ reactions are seen to be in very reasonable (better than 90%) agreement. For all the other reactions, particularly those involving the isotopes of lithium, substantial discrepancies are observed. In many cases absolute normalizations of yield curves are absent, angular distributions unknown, branching ratios uncertain or known only at one energy, and in several cases the cross-section is still increasing at the highest energy at which a measurement is available. There is considerable scope for further work in this area.

(ii) Neutron cross-sections

Table IV summarises the conclusions from the sections of this report on neutron reactions for which the present state of data accuracy is insufficient. Reaction 5 in this table refers specifically to niobium, the currently preferred structural material, but a similar lack of data exists for both molybdenum and iron (stainless steel) which are other possible structural materials.

TABLE IV. NUCLEAR REACTIONS HAVING INADEQUATE DATA FOR NEUTRONICS, HEATING, DAMAGE AND ACTIVITY CALCULATIONS

REACTION	SPHERE OF INTEREST	PRESENT STATE OF DATA ACCURACY
1. $Li^7(n,n't)$	Tritium Breeding	~ 25% Accurate
2. Nb(n,2n) 3. Mo(n,2n)	(i) Recoil Heating (ii) Damage (iii) Transmutation	Nb Very uncertain Mo not measured
4. F(n,abs)	(i) Neutron Absorption (ii) Gamma-Ray Heating	Several Reactions contributing. Poor experimental agreement
5. Gamma-Ray spectra from (nγ) and inelastic scattering in Nb	(i) Gamma-Ray Heating	No complete spectral measurement
6. Nb(nα)	(i) Damage	~ 20% Accurate
7. Excitation of first state in Nb^{93}	(i) Radioactivity	Not measured

Three general comments can be made:-

(a) It is in the region 1–14 MeV that neutron cross-section data are relatively poor. This region is more important for fusion systems based on the D-T cycle, than for fission systems.

(b) the materials selected for the neutron blanket should not be regarded as unique, so that for any new structural material, say iron, the comments under (a) would apply.

(c) secondary γ-ray production appears to be very important in fusion systems and has been inadequately investigated.

(iii) Data library services

It appears that none of the existing nuclear data libraries compile or evaluate data on charged particle cross-sections or on γ-ray production in neutron interactions. It would be valuable if the data centres at Obninsk, Vienna, Saclay and Brookhaven were to consider extending their services in these directions. As regards charged particle interactions, the data required include total cross-sections, differential cross-sections, angular distributions, reaction product energy distributions, branching ratios and excited state energy levels for fusion, stripping, elastic and inelastic scattering processes. On the neutron side, the requirement is for neutron cross-sections for γ-ray production which could be integrated with neutron spectra in order to describe γ-ray source spectra emitted in non-elastic neutron interactions.

ACKNOWLEDGEMENTS

We acknowledge the efforts of the Culham Information Service, and particularly of Mr. D.J. Dancy, in performing the literature search upon which Part 2 of this paper is based, and the cooperation of the Culham Computing Service, especially Mr. T.J. Martin, in producing the software used to process the data. We are also grateful to Mr. P. Oliver for his assistance, and to Drs. R.S. Pease, M. Petravic and D. R. Sweetman, for valuable discussions.

GENERAL REFERENCES

ALLEN, M.S., and DRAKE, M.K., 1967, "Neutron Cross-Sections for Niobium", GA-8133.

BASU, D., SETHI, B., and BAKHRU, H., 1966, Proc. of Nucl. Phys. & Sol. State Phys. Symposium, Bombay, p.209.

BEGHIAN, L., et al., 1967, Proc. of Int. Conf. on Nucl. Structure, Tokyo, p.190.

BELL G.J. et al. BNES Nuclear Fusion Reactor Conf., Culham 1969, Proceedings p.242.

BIRSS, I.R., and BISHOP, T.P., 1966, TRG 1039(D).

BLOW, S., CROCKER, V.J., and WADE, B.O., 1969, BNES Nuclear Fusion Reactor Conf., Culham, Paper 5.5.

BLOW, S., 1970 (a) A.E.R.E. R-6320.

BLOW, S., 1970 (b) A.E.R.E. Report, to be published.

BRAMLITT, E.T., and FINK, R.W., 1962, J. of Inorg. Nucl. Chem., 24, 1321.

BUCKINGHAM, B.R.S., PARKER, N., and PENDLEBURY, E.D., 1960, A.W.R.E., O-28/60.

CARRUTHERS, R., DAVENPORT, P.A., and MITCHELL J.T.D., CLM-R85 (1967)

CARTER, H.G., 1966, Proc. of Conf. on Neutron Cross-Section Technology, Washington, D.C., Vol.2, p.682.

DEGTYAREV, Y.G., 1970, Russian J. of Nucl. Phys., No.11, Vol.2, 241.

FOWLER, T.K. and RANKIN, M. Plasma Physics 8, 121 (1966).

GLICKSTEIN, S.S., and WINTER, R.G., 1963, Phys. Rev. 129, 1281.

GOLDBERG, M.D., MUGHABGHAB, S.F., PUROHIT, S.N., MAGURNO, B.A., and MAY, V.M., 1966, BNL 325, 2nd edition.

GROSHEV, L.V. et al., 1959, Atlas of γ-Ray Spectra from Radiative Capture of Thermal Neutrons, Pergamon Press.

HOMEYER, W.G., 1965, M.I.T. Technical Report 435.

HONECK, H.C., 1967, BNL-50066.

IMPINK, A.J., 1965, M.I.T. Technical Report 434.

McNALLY, J.R. Oak Ridge Semiannual Progress Reports ORNL-3760, ORNL-3836.

McTAGGART, M.H., and GOODFELLOW, H., 1963, J. Nuclear Energy, A/B, 17, 437.

MARTIN, D.G., 1969, J. of Nucl. Materials, 33, 23.

MILLS, R.G., Princeton Report MATT-658 (1969).

MITRA, B., and GHOSE, A.M., 1966, Nucl. Phys. 83, 157.

PARKER, K., 1963, AWRE O-70/63.

PASQUARELLI, A., 1967, Nucl. Phys. A93, 218.

PEARLSTEIN, S., 1965, Nucl. Sci. Eng. 23, 238.

PENDLEBURY, E.D., 1964 (a), AWRE O-60/64.

PENDLEBURY, E.D., 1964 (b), AWRE O-61/64.

KUO-PETRAVIC, L.G., PETRAVIC, M., WATSON, C.J.H., BNES Nucl. Fusion Reactor Conf. Proc. p.144.

POST, R.F., BNES Nuclear Fusion Reactor Conference, Culham, 1969, p.88.

PRASAD, R., and SARKAR, D.C., 1966, Nucl. Phys. 85, 476.

ROSE, D.J., Nucl. Fusion 9, No.3 (1969).

SILK, M.G., 1970, Private Communication.

STEINER, D., 1969, BNES Nuclear Fusion Reactor Conference, Culham, 1969, p.483.

TROUBETZKOY, E.S., 1961, Phys. Rev. 122, No.1, 212.

WESTERN, G.T., et al., 1966, Proc. of Conf. on Neutron Cross-Section Technology, Washington, D.C., P.B. Hemming (ed.), Vol.2, p.675.

FUSION CROSS-SECTION BIBLIOGRAPHY

AGNEW, H.M., et al. Phys. Rev. Vol.84, p.862, 1951.
ALLEN, R.C. et al., Phys. Rev. Vol.111, No.4, p.1129, Aug.15, 1958.
ALLRED, J.C., Phys. Rev. Vol.84, No.4, p.695, Nov.15, 1951.
ALMQVIST, E., ALLEN, K.W., DEWAN, J.T. and PEPPER, T.P., Phys. Rev. Vol.83, p.202, 1951.
ARGO, H.V., TASCHEK, R.F., AGNEW, H.M., HEMMENDINGER, A.H. and LELAND, W.T., Phys. Rev. Vol.87 No.4, 1952
ARNOLD, W.R., et al. Phys. Rev. Vol.93, No.3, p.483, Feb.1, 1954.
BAGGETT, L.M. and BAME, S.J., Phys. Rev. Vol.85, No.3, Feb.1, 1952.
BALABANOV, E.M. et al. Sov. J. Atomic Energy. Supp.5, pp.43-52 (1958).
BALABANOV, E.M. et al. Sov. J. Atomic Energy. Supp.5, pp.37-42 (1958).
BAME, S.L. and PERRY, J.E., Phys. Rev. Vol.107, No.6, p.1616, Sept.15, 1957.
BARRY et al. Ruth. Conf.p.543, (1961)
BASHKIN, S., Phys. Rev. Vol.95, No.4, Aug.15, 1954.
BASHKIN, S., and RICHARDS, H.D. Phys. Rev. Vol.84, No.6, p.1124, Dec.15, 1951.
BEAUMEVIEILLE, CEA-R-2624.
BERTRAND, F., et al. Saclay Report CEA-R-3428, (1968),
BENNETT, W.E. et al. Phys. Rev. 71, 11 (1947)
BLAIR, J.M. et al. Phys. Rev. Vol.74. No.11, p.1599, Dec.1, 1948.
BLASER et al. Helv. Phys. Acta. 24 465 (1951).
BONNER, T.W., NSA: 4/6744, (1960)
BONNER, T.W. et al. Phys. Rev. Vol.88, No.3, p.473, Nov.1, 1952.
BOOTH, D.L., PRESTON, G. and SHAW, P.F.D. Proc. Phys. Soc. Vol.A69, p.265, 1955.
BOWERSOX, R.B. Phys. Rev. Vol.55, No.4, p.323, Feb.15, 1939.
BRETSCHER, E. and FRENCH, A.P. Phys. Rev. Vol.75, No.8, p.1154, Apr.15, 1949.
BROLLEY, J.E. et al. Phys. Rev. Vol.82, No.4, p.502, May 15, 1951.
BROLLEY, J.E. et al. Phys. Rev. Vol.107, No.3, p.820, Aug.1, 1957.
BRUNO et al. Journal de Physique 27 (1966) 517
BURCHAM, W.E. and FREEMAN, J.M. Phil.Mag. Ser.7, Vol.41, No.320, p.921, Sept.1950.
CONRAD et al. Naturwiss 45 (1958) 204
CONNER, J.P., BONNER, T.W. and SMITH, J.R. Phys. Rev. Vol.88, No.3, p.468, Nov.1, 1952.
COOK, C.J., JONES, E. and JORGENSEN, T., AECU 1834 (1951).
CREWS, Phys. Rev. 82 100 (1951).
DAVENPORT, P.A., et al. Proc. Roy. Soc. Vol.A216, p.66, (1953).
DAVIDENKO, V.A. et al. Sov. J. Atomic Energy, Suppl. No.5, p.7, (1958).
ELIOT, E.A., ROAF, D., and SHAW, P.F.D., Proc. Roy Soc. Vol.A216, p.57, (1953).
Von ENGEL, A. and GOODYEAR, C.C., Proc. Roy. Soc. Vol.A264, p.445 (1961).
ERICKSON, K.W., et al. Phys. Rev. Vol.76, No.8, p.1141, Oct.15, 1949.
FREIER, G., and HOLMGREN, H., Phys. Rev. Vol.93, No.4, p.825, Feb.15, 1954.
GALONSKY, A., and JOHNSON, C.H., Phys. Rev. Vol.104, No.2, Oct.15, 1956.
GANEEV, A.S., et al. Sov. J. Atomic Energy. Suppl.5, p.21-36, 1958.
GEMEINHARDT, W. et al. Zeitschrift fur Physik, Vol.197, p.53, (1966).
GOOD, W.M., KUNZ, W.E. and MOAK, C.D., Phys. Rev. Vol.94, No.1, p.87, Apr.1 1954.
GOVOROV, A.M., et al. Sov. Phys. JETP. Vol.15, No.2, p.266, Aug.1962.
HEMMENDINGER, A. and ARGO, H.V., Phys. Rev. Vol.98, No.1, p.70, April 1, 1955.
HENKEL, R.L., PERRY, J.E. and SMITH, R.K., Phys. Rev. Vol.99, p.1050 (1955).
HERB, R.G. et al, Phys. Rev. 48, 118 (1943).
HEYDENBURG, N.P., et al. Phys. Rev. Vol.74, No.4, p.405, Aug.15, 1948.
HIRST, F., JOHNSTONE, I. and POOLE, M.J. Phil. Mag. Vol.45, p.762, (1954).
HUNTER, G.T., and RICHARDS, H.T., Phys. Rev. Vol.76, No.10, p.1445, Nov.15, 1949.
JARMIE, N. and SEAGRAVE, J.D. (Editors). LA-2014.
JARVIS, G.A. et al. Phys. Rev.79 (1950), 929.
JARVIS, R.G. and ROAF, D. Proc. Roy. Soc. Vol.A218, p.432 (1953).
JERONYMO, J.M.F. et al. Nuclear Physics, Vol.38, p.11, (1962).
JERONYMO, J.M.F. et al. Nuclear Physics 43 (1963) 424
KUHN, B. and SCHLENK, B., Nuclear Phys. Vol.48, p.353-360. (1963)
KUNZ, W.E., Phys. Rev. Vol.97, No.2, p.456, Jan.15 1955.
LEBLANC, GOLDBERG, WASH1021, p.54.
LELAND, W.T. and AGNEW, H.M., Phys. Rev. 82 559 (1951).
MACKLIN, R.L. and BANTA, H.E., Phys. Rev. Vol.97, No.3, p.753, Feb.1, 1955.

MANI, G.S., et al. Proc. Phys. Soc. Vol.85, p.281 (1965).
MARION et al. Phys. Rev. 104 (1956) 1402.
MEYER, V., PFEIFER, W. and STAUB, H.H., Helv. Phys. Acta. Vol.36, p.465 (1963).
MOAK, C.D. Phys. Rev. Vol.92, No.2, p.383, Oct.15, 1953.
NICKELL, W. E. Phys. Rev. 95 426 (1954).
PEPPER, T.P. et al. Phys. Rev. Vol.85, p.155 (1952).
POPPE, C.H. et al. Phys. Rev. 129 733, (1963).
PRESTON, G., SHAW, P.F.D. and YOUNG, S.A. Proc. Phys. Soc. Vol.A226, p.206 (1954)
SAWYER, G.A. and PHILLIPS, J.A. LA1578, Aug. 1953.
SCHIFFER, J.P. et al. Phys. Rev. Vol.104, No.4, p.1064, Nov.15, 1956
SEROV et al. Soviet J. At. En. 12 (1962) 1.
SLATTERY et al. Phys. Rev. 108 (1957) 809.
SMITH, D.B., et al. Phys. Rev. Vol.129, No.2, p.785, Jan.15, 1963.
SMITH, R.C. and LEVIN, J. WASH1021, p.26 (1959)
STEWART, L., et al. Phys. Rev. Vol.119, No.5, p.1649, Sept.1 (1960)
SWEENEY, W.E. and MARION, J.B., Phys. Rev. Vol.182, No.4, p.1007, 20th June 1969.
TASCHEK, R. and HEMMENDINGER, A. Phys. Rev. Vol.74, No.4, p.373, 1948.
TASCHEK, R., Phys. Rev. 76 325 (1949).
THORNTON, S.T., Nucl. Phys. Vol.A136, p.25-34, (1969).
VALTER, et al. S.J. At.En. 10(1961) 574.
VOLKOV, V.V., et al., Sov. J. Atomic Energy - Suppl.5, p.13-20, 1958.
WENZEL, W.A. and WHALING, W. Phys. Rev. Vol.88, No.5, p.1149, Dec.1, 1952.
WHALING, W. and BONNER, T.W., Phys. Rev. Vol.79, No.2, July 15, 1950.
WHALING, et al. Phys. Rev. 75 (1949) 688.
WILLARD, H.R. et al. Phys. Rev. Vol.90, No.5, p.865 June 1 1953.
YARNELL, J.L. et al. Phys. Rev. Vol.90, No.2, p.292, Apr.15, 1953.
YOUN, L.G. et al. Sov. Phys. JETP. Vol.12 No.2, p.163 Feb.1961.

DISCUSSION

S. W. CIERJACKS: Have you made any recent calculations of the power deposited in the wall of a vacuum tank incorporating a lithium-cooled blanket system? I am referring to the power which is deposited by the gamma rays coming from interactions of fast neutrons with the blanket material. I ask this question mainly because the earlier calculations of Hameyer indicated that the heat produced by the gamma backshine is just at the upper limit of what can be cooled. This was shown, for example, in the case of a reactor of 5 GW thermal power in which a Li_2BeF_4 cooling system was used.

Also, do you have any plans for measuring the neutron flux distributions in some suitable blanket models instead of making measurements of a large number of detailed neutron cross-sections?

V. S. CROCKER: We are at present in the process of doing gamma-ray heating calculations and, thus, I cannot answer your question directly. However, I know that nuclear-heating calculations by other people indicate that the use of FLIBE as compared with natural lithium, increases the heat loading in the vacuum wall by ~ 40%. More than 90% of the nuclear heating in this wall is due to gamma rays.

Although we would like to do some experimental work on the neutron spectra, etc. in various blanket configurations, we feel that in the immediate future we should continue with the present type of calculations.

Invited Paper

PROGRESS IN UNDERSTANDING NEUTRON INTERACTIONS WITH NUCLEI

J.E. LYNN
UKAEA, AERE,
Harwell, Didcot, Berks,
United Kingdom

Abstract

PROGRESS IN UNDERSTANDING NEUTRON INTERACTIONS WITH NUCLEI.

The general development of neutron reactions is reviewed, with emphasis on the growing awareness of the importance of special, relatively simple, states of the nuclear motion in influencing the underlying microscopic structure of neutron cross-sections. The main illustrative case chosen is that of the coupling of single-particle motion and collective rotation of a heavy deformed nucleus. The description of this case is given in R-matrix theory, and it is shown how the coupling can give rise to correlation between elastic and inelastic scattering widths in the fine-structure resonances, thus influencing the average inelastic-scattering cross-section, provided that spreading of the special, coupled states into the fine structure is not too large. It is also shown how direct inelastic scattering cross-sections appear in the theory. The measured capture and inelastic scattering cross-sections of ^{238}U are discussed from the theoretical point of view, and it is pointed out how the capture data require a model of the radiative-capture process that favours high-energy transitions. This again may be evidence of the role of special modes that are not too strongly damped into the fine-structure levels. Finally, we mention the recent developments in fission that strikingly demonstrate the role played by the special states corresponding to excitation of a highly-elongated quasi-stable shape of the nucleus.

1. INTRODUCTORY SURVEY

It is fascinating to recall that the two extreme models of neutron reaction theory were both propounded within a very few years of the discovery of the neutron, and since that time we have gradually groped our way towards a highly refined synthesis of the two opposed points of view. The very first theory of neutron reactions, the Bethe-Fermi theory [1,2], described the interaction between neutron and nucleus as simply a refraction of the neutron by the average force field of the nucleus without any excitation of the internal degrees of freedom of the nucleus itself. The theory successfully described the statistical scatter of thermal neutron capture cross-section values among the elements, but very shortly after its inception the discovery was made of sharp, slow-neutron capture resonances [3,4], and this led to the original version of Bohr's compound nucleus theory [5] in which the degrees of freedom of the nucleus are so strongly excited that the original mode corresponding to the incident neutron is virtually lost.

For more than a decade afterwards, theories of neutron absorption and scattering, particularly of average cross-sections, were based on this extreme picture; these are the statistical theories [6,7]. A significant feature of such average cross-sections in the statistical theory was their monotonic decrease with energy. The discovery nearly twenty years ago of "giant resonances" in fast neutron cross-sections, together with the intellectual climate in nuclear structure physics at that time following the successes of the shell model, led to the optical or complex potential

model [8], in which it was recognised that the initial mode of the reaction, an incident neutron in the average field of the unexcited target nucleus, was only moderately damped by the excitation of the other degrees of freedom of the system. After some time it was realised that certain special degrees of freedom could be excited particularly strongly by the incident mode of motion. At high energies such selection is usually called direct reaction, and was basically understood quite early, but it took a little longer to appreciate that such processes could also occur at moderate and low energies. Particular examples are the real (or virtual) excitation of rotational or vibrational modes of the target nucleus, with the odd neutron losing some of its incident energy. The mathematical expression of these ideas is the coupled channel version of the complex potential model; with the availability of large, fast computers it now produces results of great sophistication (see for example [24]).

Above a few MeV these phenomenologically-based theories can hardly be improved upon at the present time, yet we know that at lower energies there is an underlying fine structure in the cross-sections, and often also, observed in some cases and suspected in others, an intermediate structure, sometimes of quite dramatic character. The intermediate structure can often be dealt with in the coupled channel theories, but the resonance fine-structure, from which the original compound nucleus theory directly stemmed, requires a deeper modification of the phenomenological theories at these low energies. Resonance fine structure was dealt with in the original optical model [8] on a statistical basis. The model is used to compute an average collision function $\bar{U}$ from which the total cross-section $2\pi\lambda^2(1-\Re\bar{U})$ and the shape elastic scattering, $\pi\lambda^2|1-\bar{U}|^2$, corresponding essentially to the smooth potential scattering between resonances are determined. The difference between the average of the true elastic scattering cross-section, $\pi\lambda^2|1-U|^2$, and the shape elastic scattering cross-section has the form of a variance; it is thus the average of a fluctuating term and is therefore interpreted as compound, or resonance, elastic scattering. If this is added to the average total reaction cross-section, $\pi\lambda^2(1-|U|^2)$, the quantity $\pi\lambda^2(1-|\bar{U}|^2)$ is obtained, and this is interpreted as the compound nucleus formation cross-section, the average of the sum of all reaction processes including elastic scattering proceeding through resonances.

The quantity $(1-|\bar{U}|^2)$ is proportional to the so-called transmission factor T of Hauser-Feshbach theory [9], or to the strength function of more formal reaction theories. In Hauser-Feshbach theory the average cross-section for a particular reaction process is obtained from the product of the transmission factors for the entrance and exit channels divided by the sum of the transmission factors for all open channels i.e. $\sigma_{ab}=\pi\lambda^2 T_a T_b/\Sigma_c T_c$. A similar expression is obtained for the cross-section averaged over a single narrow resonance, but now a highly statistical aspect of resonance properties prevents the result from being immediately extended to the average over many resonances to obtain the Hauser-Feshbach expression. This is, of course, the fluctuaction property of partial widths from resonance to resonance. It follows from the assumption of statistical randomness in the wave-functions of resonance levels that the reduced widths should have the well-known Porter-Thomas distribution [10]. If this statistical distribution is properly included in the computation of the average cross-section σ_{ab} over many resonances, an expression similar to the Hauser-Feshbach form is obtained, but an extra factor, δ, the averaging or fluctuation factor, which may differ from unity by a factor of up to two, or more, appears [11].

The prescription, therefore, of computation of strength functions from optical or coupled-channel models, followed by substitution of these in the Hauser-Feshbach theory to obtain particular reaction cross-sections is not

accurate to better than a factor of two or so, and average cross-sections should therefore be based on a better understanding of the microscopic structure, and, in particular, the way that special modes of the nucleus are mixed into this structure. Such an understanding is pursued in the remainder of this paper. Emphasis is placed mainly on the neutron channels, both elastic and inelastic, but some comments are made in later sections on two of the main reaction processes induced by neutrons, namely radiative capture and fission.

2. MIXING OF A SPECIAL STATE WITH NEIGHBOURING STATES

In this section we recall the simple mathematical treatment [12,13] for the line-broadening problem, i.e. the mixing of a single special discrete state with neighbouring discrete states through interactions not fully taken into account in defining the original basis states. The Hamiltonian of the system is split into a main part H_c and a residual part H'. The basis states are eigenfunctions of H_c. If all the basis states, except one special state, N, are diagonalised, there results the set of equations

$$\left.\begin{aligned} C_1^\lambda (E_1 - E_\lambda) &\qquad\qquad + C_N^\lambda H'_{1N} = 0 \\ C_2^\lambda (E_2 - E_\lambda) &\qquad\qquad + C_N^\lambda H'_{2N} = 0 \\ &\cdots \\ C_{N-1}^\lambda (E_{N-1} - E_\lambda) &+ C_N^\lambda H'_{N-1\,N} = 0 \end{aligned}\right\} \qquad (1a)$$

$$C_1^\lambda H'_{N1} + C_2^\lambda H'_{N2} + \cdots + C_{N-1}^\lambda H'_{NN-1} + C_N^\lambda (E_N - E_\lambda) = 0 \qquad (1b)$$

where E_i to E_{N-1} are the eigenvalues of the diagonalised sub-set, the E_λ are the final eigenvalues of the whole set and the C_i^λ are the coefficients of admixture of the state E_i into the final states E_λ.

Together with the normalisation condition $\sum_i C_i^{\lambda 2} = 1$ these equations can be solved. For the coefficients we find

$$C_i^\lambda = - C_N^\lambda H'_{iN} / (E_i - E_\lambda), \qquad i \neq N \qquad (2a)$$

$$C_N^{\lambda 2} = 1 \Big/ \left\{ \sum_{i \neq N} H'^2_{iN} / (E_i - E_\lambda)^2 + 1 \right\} \qquad (2b)$$

while the eigenvalues E_λ satisfy the equation

$$\sum_{i \neq N} \frac{H'^2_{iN}}{E_i - E_\lambda} = E_N - E_\lambda \qquad (3)$$

In the uniform model (equal spacing D_i of the states $E_i, i \neq N$, and equal values of H'^2_{iN}) equation (2b) becomes

$$C_N^{\lambda 2} = \frac{H'^2_{iN}}{(E_N - E_\lambda)^2 + \left(\frac{\pi H'^2_{iN}}{D_i}\right)^2 + H'^2_{iN}} \qquad (4)$$

This is just a Lorentz form for the intensity admixtures of the special state N into the eigenstates λ. The half-width, W, of the resonance-type

spreading is, for $H'^2_{iN} \gg D_i$, approximately $\pi H'^2_{iN}/D_i$; this is the so-called golden rule for spreading widths.

The same procedure can be used where there is more than one special state; the basis states defined by H_0 are now split into two sub-sets, and each set is diagonalised separately. One diagonalised sub-set comprises the widely-spaced special states. In the final diagonalisation of the entire system, we shall be faced with a number of sets of equations (for each special level) like equation (1), but with additional terms relating to the other special levels. If these can be neglected, the solutions expressed by equations (2) to (4) result. Clearly the condition for neglect of the additional terms is that the W_N are much less than the D_N

To be applied to nuclear reaction phenomena, these formal manipulations have to be extended to a continuum of eigenstates. This can be done very simply (in principle) by working within the framework of R-matrix theory. In R-matrix theory real, energy-independent boundary conditions are imposed on the wave-functions at the channel radii (of open particle channels) selected outside the range of nuclear forces. In this way the internal states of R-matrix theory are defined as discrete states, and the above relaionship on mixing of special states with their much denser neighbours can be applied to them.

It has to be remembered that the parameters of the R-matrix levels do not always correspond in a simple manner to the parameters of resonances in the cross-section. It has been shown in the work of Humblet and Rosenfeld [14] and their collaborators that the resonances correspond to poles of the collision matrix (or S-matrix) in the complex energy plane. When the widths associated with the R-matrix levels are greater than their spacings it has been shown [15] that the imaginary components (the half-widths) of the S-matrix poles can be very different from the R-matrix widths. This occurs when coupling of the internal region, in which the R-matrix levels are defined, to the continuum is strong. In the case in which the special level is strongly coupled to the continuum, and the others are not, it can be shown that the spreading of the special level into the S-matrix poles (rather than the R-matrix levels) is related to the width of the special level. When this width Γ_N is much greater than the spreading width $2W_N$ of the special level into the other R-matrix levels, the widths of the S-matrix poles corresponding to the narrow resonances will have a Lorentz envelope of width Γ_N, while the special level will appear in the cross-section as an underlying broad background term. Intermediate situations where $\Gamma_N \sim 2W_N$ have been discussed in papers by Weidenmüller and Mahaux and others [16,17]. In the subsequent discussion of this paper we generally assume that mixing of the special level with others, rather than coupling to the continuum, is predominant. This will almost certainly be the case for neutron reactions below about one MeV; in these, attenuation through centrifugal barriers and the reflectance factor at the edge of the nuclear well keep the coupling with the continuum tolerably small.

3. COUPLED CHANNELS IN R-MATRIX THEORY: ILLUSTRATIVE EXAMPLE

3.1 Single-particle and rotation coupling

The use of R-matrix theory to handle coupled channel phenomena in nuclear reactions is not new; it was first applied in the case of neutron reactions with ^{12}C by Buttle [18]. In this paper, however, we are considering its use for the reactions of heavier nuclei in which there is a dense fine structure of resonance states.

The illustrative example chosen here is that of neutron elastic and inelastic scattering coupled through rotational motion; the original work on the coupled-channel optical model in this case was that of Chase, Wilets and Edmonds [19]. The Hamiltonian of the system is split into the following terms:

$$H = T_n + V_n(r, \theta', \phi') + H_{coll} + H'' \qquad (5)$$

where T_n is the kinetic energy of the incident neutron (as usual, anti-symmetrisation is ignored), $V_n(r, \theta', \phi')$ is the average potential field, due to the target nucleus, acting on this neutron, the angular variables θ' and ϕ' being in the body-fixed frame of reference, H_{coll} is the Hamiltonian describing collective motion of the target nucleus, and H'' comprises the residual interactions that cannot be described by the simple scheme of single-particle motion and collective degrees of freedom.

The potential field is conveniently expanded in spherical harmonics:

$$V_n(r, \theta', \phi') = v_0(r) + \sum_{\lambda \geq 2} \sum_{\mu=-\lambda}^{\lambda} v_{\lambda\mu}(r) Y_\mu^\lambda(\theta', \phi') \qquad (6)$$

In general, the radial terms, $v_{\lambda\mu}$, in this expansion depend on the parameters of the collective motion of the target. If, as in the present example, the target nucleus is assumed to have a fixed, spheroidal shape, and the only collective motion considered is rotation, the terms $v_{\lambda\mu}$ depend only on the deformation parameter, β, entering the quadrupole moment of the target. Typical behaviour of the $v_{\lambda\mu}$ is shown in Fig. 1. Here, the radial dependence of the potential energy is assumed to have the Eckart form:

$$V_n(r, \theta', \phi') = \frac{V_0}{1 + \exp\{[r - a(\theta', \phi')]/d\}} \qquad (7a)$$

$$a(\theta', \phi') = a_0\left(1 + \beta Y_0^2(\theta', \phi')\right) \qquad (7b)$$

The numerical parameters for Fig. 1 are V_0 = -42.8 MeV, a_0 = 7.97 fm, d = 0.67 fm, β = 0.3; these are probably appropriate to an actinide nucleus. From Fig. 1 it is apparent that appreciable interaction extends out to nearly 15 fm, so the channel radii for elastic and inelastic scattering are set about here (actually at 15.07 fm). Spin-orbit interaction has a rather complex form in a non-spherical potential, so here it is simplified by just including the term

$$-\lambda \cdot \frac{1}{r} \frac{\partial v_0}{\partial r} (\vec{\sigma} \cdot \vec{l}) \qquad (8)$$

in the spherical component of equation (6). The eigenvalues ε_{nlj} of the odd orbital angular momentum radial wave-functions associated with v_0 (including spin-orbit coupling) are given in Table I for particular values of the boundary condition $B_c = (r/u)(\partial u/\partial r)$. The significance of these particular numerical choices is given in Section 3.4. The bound eigenstates in this Table have eigen values very close to the natural eigenvalues determined with the condition of vanishing wave-function at infinity. The lowest positive eigenvalues correspond to the 4p state which becomes just unbound among the actinide nuclei. The nearness of the next highest

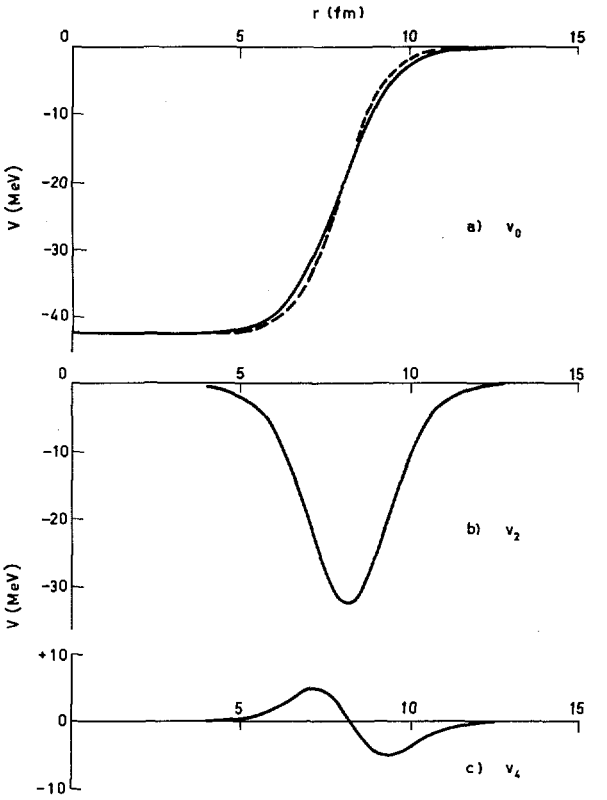

FIG. 1. Components of a non-sperical potential. The original Eckart potential is shown by the broken curve. Its components, for a deformed nucleus with $\beta = 0.3$, in a spherical harmonic analysis are shown by the full curves (a, b, c).

eigenvalue is a consequence of the channel radius being so much greater than the effective potential radius a_0. As explained in ref. [20] (see also ref. [21]) this results in compression of the R-matrix states, and even in the introduction of extra states.

We now proceed to discuss the nature of the R-matrix states in the Hamiltonian $H_0 = T_R + V_R + H_{coll}$. The collective Hamiltonian here corresponds only to the rotational degree of freedom. The eigenfunctions of H_{coll} are denoted by χ_I where I denotes the rotational angular momentum, and the eigenvalues are ϵ_I. The χ_I are the wave-functions of a symmetric top (see [22]):

$$\chi_{IM_I}\left(\equiv |I M_I\rangle\right) = \left((2I+1)/8\pi^2\right)^{1/2} \mathcal{D}^{I\,*}_{M_I 0} \tag{9}$$

$$\epsilon_I = \frac{\hbar^2}{2\mathcal{I}} I(I+1) \tag{10}$$

TABLE I. EIGENVALUES IN POTENTIAL v_0 OF FIG. 1, WITH BOUNDARY CONDITION B_c IMPOSED AT CHANNEL RADIUS $a_c = 15.07$ fm, ℓ DENOTES ORBITAL ANGULAR MOMENTUM, j IS TOTAL SPIN, n IS PRINCIPAL QUANTUM NUMBER, $u_n(a_c)$ IS VALUE OF WAVE-FUNCTION AT CHANNEL RADIUS a_c, AND γ_n^2 IS REDUCED WIDTH OF SINGLE PARTICLE STATE.

ℓ	B_c	j	n	E_n	$u_n(a_c)$	γ_n^2
1	-0.1545	3/2	3	-9.86	0.035	0.00017
			4	0.308	-1.19	0.194
			5	4.105	1.57	0.337
			6	12.71	-1.39	0.267
		1/2	3	-8.96	0.041	0.00023
			4	0.556	-1.29	0.230
			5	4.54	1.51	0.313
			6	13.11	-1.39	0.265
3	-1.652	7/2	3	0.779	0.65	0.058
			4	4.61	-1.56	0.335
		5/2	3	1.84	0.97	0.128
			4	5.47	-1.45	0.290
5	-4.138	11/2	2	0.0	-0.17	0.0038
			3	7.0	1.28	0.225
		9/2	2	3.39	-0.43	0.025

The eigenfunctions of H_c are written as an expansion in the product wave-functions $u_{n\ell j}(r)|s\ell; j\rangle$ and χ_I coupled to total angular momentum J:

$$\chi_\lambda^\circ = \sum_{n\ell j, I} C^\lambda_{n\ell j, I}\, u_{n\ell j}(r)\, |j\, I; J\rangle \tag{11}$$

Substitution of such expansions in the Schrödinger equation,

$$H_c \chi_\lambda^\circ = E_\lambda^\circ \chi_\lambda^\circ \tag{12}$$

gives

$$\sum_{n\ell j, I} C^\lambda_{n\ell j, I} \left(\mathcal{E}_I + \varepsilon_{n\ell j} - E_\lambda^\circ\right) u_{n\ell j}(r)\, |j\, I; J\rangle + \sum_{n\ell j, I} \sum_{\lambda \geq 2} v_{\lambda 0}(r)\, Y_0^\lambda(\theta, \phi) C^\lambda_{n\ell j, I}\, u_{n\ell j}(r)\, |j\, I; J\rangle = 0 \tag{13}$$

If this is projected out against $u_{n'\ell'j'}\langle j'I';J|$ we obtain the set of coupled equations for the internal R-matrix states:

$$C^{\lambda}_{n'\ell'j',I'}\left(\epsilon_{I'}+\varepsilon_{n'\ell'j'}-E^{o}_{\lambda}\right)+\sum_{n\ell j,I}\sum_{\lambda\geq 2}C^{\lambda}_{n\ell j,I}\left[\int_0^{a_c}dr\,u_{n\ell j}\,v_{\lambda}\,u_{n'\ell'j'}\right]\left\langle j'I',J\left|Y^{\lambda}_{0}(\theta',\phi')\right|jI,J\right\rangle=0 \qquad (14)$$

The radial integrals over v_λ have been numerically computed, while angular momentum matrix elements of $Y^{\lambda}_{0}(\theta',\phi')$ can be calculated by the usual methods of angular momentum algebra. Diagonalisation of the equations typified by (14) for coupled p and f states and I = 0,2 rotation gives the properties of the X^{o}_{λ} shown in Table II. It is interesting to note that among the terms with $\lambda \geq 2$ in equation (14) are some that are diagonal when $I \neq 0$ These correspond to a lowering of the eigenvalues of the $I \neq 0$ terms; the physical reason for this is that the rotational motion of the nucleus is correlated with the orbital angular momentum of the neutron in such a way that the neutron feels a net attraction from the quadrupole term in the potential expansion of equation (6).

TABLE IIa. PROPERTIES OF $J^{\pi} = 1/2^{-}$ R-MATRIX STATES IN THE ROTATIONAL COUPLING MODEL

E_λ	-1.711	0.318	1.64	3.02	4.49	6.00
$\gamma(I=0, \ell=1, j=1/2)$	-0.141	-0.168	-0.451	0.368	-0.121	0.356
$\gamma(I=2, \ell=1, j=3/2)$	-0.133	0.315	-0.009	0.537	0.273	-0.200
$\gamma(I=2, \ell=3, j=5/2)$	-0.044	0.276	0.182	0.198	0.522	-0.238

TABLE IIb. PROPERTIES OF $J^{\pi} = 3/2^{-}$ R-MATRIX STATES IN THE ROTATIONAL COUPLING MODEL

E_λ	-1.70	-0.283	0.350	1.50	1.78
$\gamma(I = 0, \ell=1, j=3/2)$	0.17	-0.069	0.0	-0.461	0.070
$\gamma(I = 2, \ell=1, j=3/2)$	0.0006	-0.295	0.119	0.155	-0.267
$\gamma(I = 2, \ell=1, j=1/2)$	-0.049	-0.149	-0.326	-0.087	0.261
$\gamma(I = 2, \ell=3, j=7/2)$	0.032	0.021	-0.106	-0.017	-0.070
$\gamma(I = 2, \ell=3, j=5/2)$	0.018	-0.020	0.058	0.132	0.237
E_λ	2.67	3.51	4.15	5.55	7.00
$\gamma(I = 0, \ell=1, j=3/2)$	-0.360	0.141	0.150	0.243	0.222
$\gamma(I = 2, \ell=1, j=3/2)$	-0.099	0.521	0.081	-0.021	-0.218
$\gamma(I = 2, \ell=1, j=1/2)$	0.247	0.339	-0.293	-0.120	0.243
$\gamma(I = 2, \ell=3, j=7/2)$	-0.377	-0.071	-0.430	-0.137	-0.156
$\gamma(I = 2, \ell=3, j=5/2)$	-0.231	0.015	0.239	-0.459	0.137

Examination of the p-wave admixture in the state X_λ° reveals that the p neutron orbitals are now spread over a considerable energy range. It is interesting to compare this spreading with that deduced from analysis of elastic scattering data using the traditional spherical optical model. Analyses of s-wave neutron strength function data indicate a spreading of the s-wave single particle state with a half-width of 1 to 2 MeV. Analysis of higher energy elastic scattering data (including angular distributions) result in a volume imaginary term (equivalent to a spreading half-width) of 1.5 to 3 MeV.

These figures are of the same order as the spreading of either the $p_{1/2}$ or $p_{3/2}$ states in Table II, and we conclude that further spreading into more complex states (see Section 3.2) may be comparatively small.

The role of the higher states (above one MeV) in Table II, should be pointed out. At energies corresponding to the eigenvalues of these states, their coupling to the continuum is very strong (their widths are well over one MeV). They do not correspond in any way to giant resonance phenomena in the cross-section, but rather contribute to the direct cross-sections (see Section 3.4).

3.2 Introduction of fine structure

We conclude from the last paragraph that coupling of neutron single particle motion with the rotational degrees of freedom already accounts for a great deal of the spreading of the mode corresponding to single particle motion in an unexcited nucleus. We now look at the possible impact of this on the resonance fine-structure of cross-sections.

The formal R-matrix states corresponding to fine structure may be introduced by returning to equation (5) and generalising the term to include other single particle excitations of the nucleus i.e. the single particle model becomes an independent particle model. The basis states now correspond to one or more excited single particles coupled to rotational motion of the target nucleus as a whole. The totality of states are now divided into two sub-sets: the single neutron + rotation states and the much denser 2 particle - 1 hole, 3 particle - 2 hole, etc. states. Both sub-sets are now separately diagonalised for the full Hamiltonian. If it is assumed that the residual component H'' of equation (5) consists only of particle-particle forces, this term will not enter the diagonalisation of the single-particle sub-set, which has therefore been fully considered in Section 3.1.

In the diagonalisation of the denser sub-set the states of 2p - 1h type will be spread to a greater or lesser degree over the resulting eigenvalues. These are, of course, the components of these states that will contribute to the matrix elements connecting them with the states of the 1p sub-set through the particle-particle residual forces of H''. In the final diagonalisation of the whole set the magnitude of these matrix elements is the key-point. If they are small, as they may well be following our considerations of the magnitude of optical model spreading in comparison with spreading due to rotational coupling, each individual line of the single-particle sub-set will be spread over an energy interval that is small compared to their spacing. The actual shape of the spreading profiles will depend on the 2p - 1h mixing among the other lines. If this is fairly uniform the spreading profiles will be essentially of Lorentz form as in equation (4). For non-uniform 2p - 1h admixture the profiles can be computed numerically from equations (26) and (3) or by the contour integral technique described by Bohr and Mattelson [13]. Large values of the matrix elements of H'' will obliterate any traces of the pattern of the coupled single particle-rotation states of the special set.

The two possibilities have distinct implications for the statistical behaviour of partial widths in the resonance fine structure as well as for the energy behaviour of strength functions for elastic and inelastic scattering. In the former case (small values of $\langle 1p\text{-}rot \mid H'' \mid 2p\text{-}1h\text{-}rot \rangle$) each individual 1p - rot state is mixed almost uniquely into its neighbouring complex states. Each complex (or fine structure) state therefore contains the same relative pattern of reduced widths for elastic and inelastic scattering to rotational states of the residual nucleus, i.e. elastic and inelastic widths of this type are correlated. Mid-way between 1p - rot states the complex states will receive on average equal admixtures from neighbouring 1p - rot states, but with random sign and magnitude about this average. In consequence, partial widths will generally be uncorrelated in this situation. This will also be true in the second case (large values of $\langle 1p\text{-}rot \mid H'' \mid 2p\text{-}1h\text{-}rot \rangle$) in which the structure of the single-particle-rotational states is lost.

3.3 Average cross-sections

Correlation properties in the reduced widths of the fine-structure resonances affect the values of average cross-sections deduced from resonance properties. For uncorrelated widths the average cross-section for a reaction (a,b) over many resonances has the form [23]

$$\sigma_{ab} = 2\pi^2\lambda^2 g_J \frac{\bar{\Gamma}_{(a)}\,\bar{\Gamma}_{(b)}}{\bar{\Gamma}}\,\delta_{ab} \tag{15}$$

with

$$\delta_{ab} = \frac{1}{2}\left(\frac{\Gamma_{(\gamma)}}{2}\right)^{\frac{m+2}{2}} \frac{\bar{\Gamma}}{\bar{\Gamma}_{(a)}\bar{\Gamma}_{(b)}\left(\bar{\Gamma}_{(a)}\bar{\Gamma}_{(b)}\cdots\bar{\Gamma}_{(m)}\right)^{1/2}} \int_0^\infty dt \frac{e^{-t}}{\left(t+\frac{\Gamma_{(\gamma)}}{2\bar{\Gamma}_{(a)}}\right)^{3/2}\left(t+\frac{\Gamma_{(\gamma)}}{2\bar{\Gamma}_{(b)}}\right)^{3/2}\left(t+\frac{\Gamma_{(\gamma)}}{2\bar{\Gamma}_{(c)}}\right)^{1/2}\cdots\left(t+\frac{\Gamma_{(\gamma)}}{2\bar{\Gamma}_{(m)}}\right)^{1/2}} \tag{16}$$

For full correlation between $\Gamma_{(a)}$ and $\Gamma_{(b)}$, but with no other widths correlated to $\Gamma_{(a)}$, the fluctuation factor δ_{ab} has the form

$$\delta_{ab} = \frac{k}{(1+k)^2}\cdot\frac{3}{2}\left(\frac{\Gamma_{(\gamma)}}{2}\right)^{\frac{m+1}{2}} \frac{\bar{\Gamma}}{\bar{\Gamma}_{(a)}\bar{\Gamma}_{(b)}\left[(1+k)\bar{\Gamma}_{(a)}\bar{\Gamma}_{(c)}\cdots\bar{\Gamma}_{(m)}\right]^{1/2}} \int_0^\infty dt \frac{e^{-t}}{\left(t+\frac{\Gamma_{(\gamma)}}{2(1+k)\bar{\Gamma}_{(a)}}\right)^{5/2}\left(t+\frac{(\Gamma_{(\gamma)}}{2\bar{\Gamma}_{(c)}}\right)^{1/2}\cdots\left(t+\frac{\Gamma_{(\gamma)}}{2\bar{\Gamma}_{(m)}}\right)^{1/2}} \tag{17}$$

where $k = \bar{\Gamma}_{(b)}/\bar{\Gamma}_{(a)}$.

As an example of the difference between (15) and (17) the inelastic scattering cross-sections of the 44 keV 2^+ state of ^{238}U through the $1/2^-$ and $3/2^-$ states of ^{239}U are calculated in the 0 to 1 MeV range with the following data. Neutron strength functions for even-parity neutron waves (s, d, etc.) are taken equivalent to $\bar{\Gamma}_n^{(e)}/\bar{D} = 1.0 \times 10^{-4}$. The odd-parity neutron strength functions are equivalent to $\bar{\Gamma}_n^{(o)}/\bar{D} = 1.85 \times 10^{-4}$. These strength function values are assumed for the inelastic as well as the elastic channels. Radiative capture widths are more fully discussed in Section 4. In the present calculation the radiative capture width is assumed to have the value of 24 meV at zero neutron energy and to fall as

in Fig. 6 to 14 meV at 1 MeV. The level density formula employed for the decrease in level spacing with energy is that of Newton [25] with the adjustments of Lang [26]:

$$\rho(J,E) = \frac{C(2J+1)e^{-J(J+1)/2\sigma_M^2}}{2\sigma_M^3\sqrt{2\pi}} \quad e^{\sqrt{aU}} \qquad (18)$$

where the parameter a turns out to have the value 125, the spin dispersion constant $\sigma_M \sim 6$, and the effective excitation energy U is the total excitation energy $E = E_n + E_{th,n}$ (neutron energy plus neutron separation energy) minus a pairing energy, here taken to be 0.7 MeV.

Most of the contribution to inelastic scattering to the 44 keV state comes from compound nucleus states of total angular momentum and parity $J^\pi = 1/2^-$ and $3/2^-$. These contributions are shown in Fig. 2 for the assumptions that the elastic and inelastic scattering widths are either uncorrelated or fully correlated. The assumption of full correlation increases the inelastic scattering cross-section by a factor of about two. This emphasises how important it is to know more about the mixing conditions of simple states into the fine-structure states; in other words, to understand properly the underlying microscopic behaviour of neutron cross-sections.

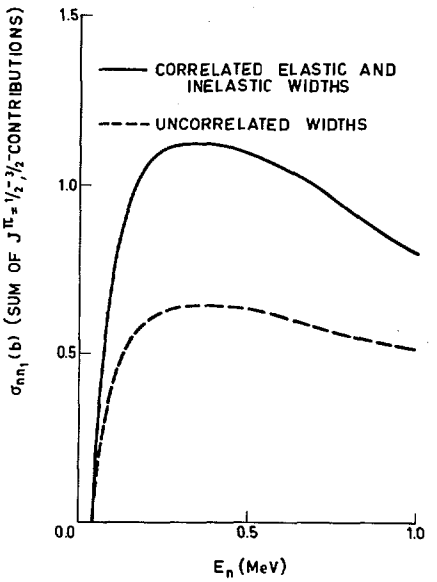

FIG. 2. Contributions to inelastic scattering to the 44 keV (2^+) state of ^{238}U from the compound states of $J^\pi = 1/2^-$ and $3/2^-$ under the assumption a) that the elastic and inelastic widths are uncorrelated and b) that they are fully correlated.

3.4 Direct inelastic scattering

The increased inelastic scattering to rotational states that may arise from correlated partial widths in resonances is not the source of increase that was postulated by earlier calculations using the coupled-channel version of the optical model [19]. In the latter model the extra cross-section is a

form of direct scattering. In the microscopic reaction theories, direct reaction arises from coherent contributions to the reaction amplitude from distant levels; the R-matrix element R_{ab} is written as the sum of contributions from local levels and distant levels:

$$R_{ab} = R_{ab}^{local} + R_{ab}^{\infty}$$

$$= \sum_{\lambda(local)} \frac{\gamma_{\lambda(a)}\gamma_{\lambda(b)}}{E_\lambda - E} + \sum_{\lambda'(distant)} \frac{\gamma_{\lambda'(a)}\gamma_{\lambda'(b)}}{E_{\lambda'} - E} \qquad (19)$$

The distant term alone gives rise to a direct cross-section of the form

$$\sigma_{ab}(dir) = \pi\lambda^2 \left| 2 P_a^{1/2} P_b^{1/2} R_{ab}^{\infty} d^{-1} \right|^2 \qquad (20)$$

where $d = (1 - iP_a R_{aa}^{\infty})(1 - iP_b R_{bb}^{\infty}) + P_a P_b R_{ab}^{\infty}$.

Direct inelastic scattering to the 2^+ rotational level, calculated from the level parameters of Table II is shown in Fig. 3 for extreme assumptions about the spreading width of the particle-rotation states into the fine-structure states. In these computations level shifts have had to be included. The original single-particle eigenvalues (see Section 3.1) were computed for numerical boundary conditions at the channel radii equivalent to the level

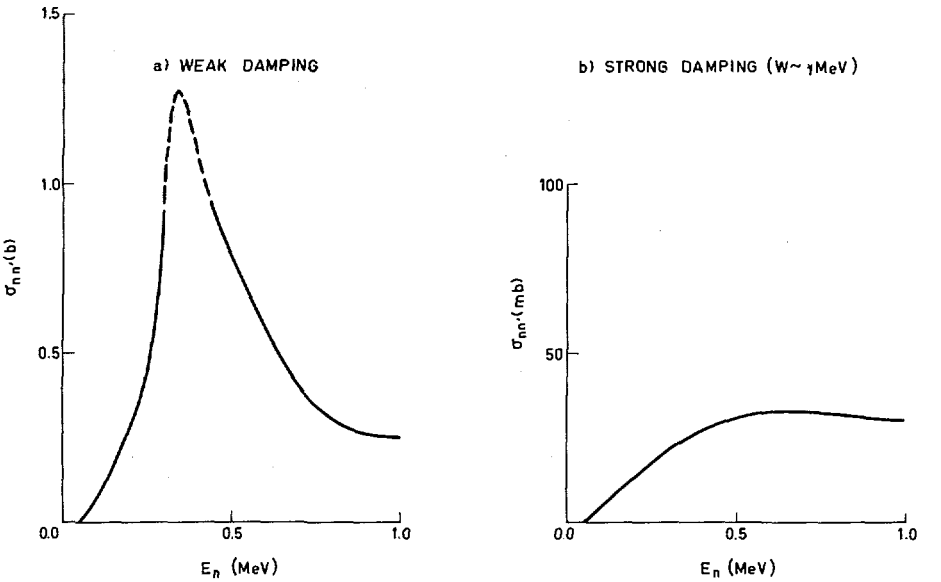

FIG. 3. Direct inelastic scattering to the 44 keV (2^+) state of ^{238}U through the $1/2^-$ total angular momentum and parity component. The left-hand diagram assumes that the 0.318 MeV state of Table IIa is only very weakly damped into the compound-nucleus states, while the right-hand diagram is based on the assumption that this state is so thoroughly damped as to have no influence on the direct cross-section.

shift factor of a free neutron of 0.5 MeV neutron energy. This means that in calculations of cross-sections at 0.5 MeV neutron energy no level shifts need be considered. At other neutron energies, E, the level energy E_λ has to be replaced by $E_\lambda - \Delta_\lambda$ where $\Delta_\lambda = \sum_c (S_c - B_c)\gamma_{\lambda c}^2(\omega)$, the shift factors S_c (the real part of the logarithmic derivative of an outgoing wave in channel c) being computed at E.

It is seen from Fig. 3 that there may be a direct inelastic scattering contribution of the order of 0.1 b or more at $E_n \approx 0.5$ MeV.

3.5 Comparison with data

The average capture and inelastic scattering cross-sections of ^{238}U have been calculated in standard compound nucleus theory using the numerical assumptions described in Section 3.3. The capture cross-section is shown in Fig. 4 and the inelastic scattering cross-sections are given in Fig. 5. Agreement with available data is reasonably good, particularly for the capture cross-section. The latter depends to a large extent on the behaviour of the radiative capture width and this is discussed further in Section 4. Careful consideration of the inelastic scattering cross-sections gives us little guide at present to the actual spreading of single-particle-rotation states into the fine structure states. For example, in the scattering to the 44 keV state, a direct inelastic scattering contribution of the order of 100 mb at 500 keV would bring closer agreement between calculation and data; at the same time it would imply that the inelastic and elastic widths are largely uncorrelated, and that the spreading of the 1p - rot states into the fine structure is at least as great as the spacing between these special states. On the other hand the assumption of very small spreading cannot be entirely ruled out; Fig. 3a shows that the direct contribution from the $J^\pi = 1/2^-$ term alone will give nearly the correct peak cross-section near 300 to 500 keV, although we would expect rather sharper peaking than given by the data. In the intermediate case (spreading into the fine structure over a width of one to two MeV) we would expect, for $1/2^-$ states, a p-wave elastic strength function $\bar{\Gamma}_{(n)}^{(1)}/\bar{D} \sim 1$ to 2×10^{-4} and an inelastic strength function

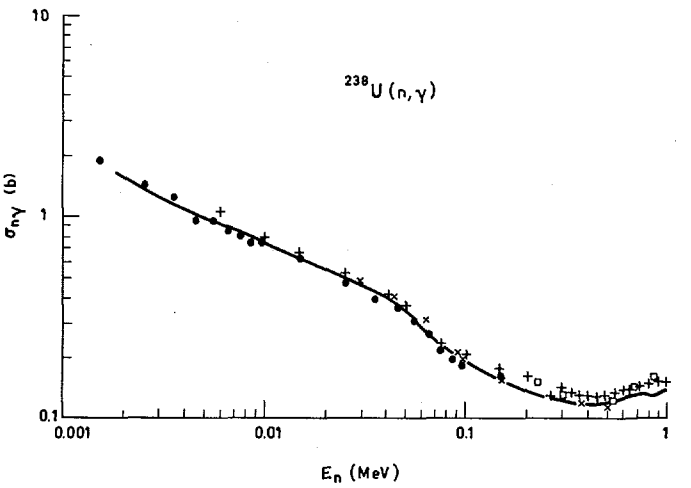

FIG. 4. Calculated capture cross-section of ^{238}U. Some data are also shown. These are: ● Moxon [32], x Menlove and Poenitz [33], + "selected best values" of evaluation by Davey [34].

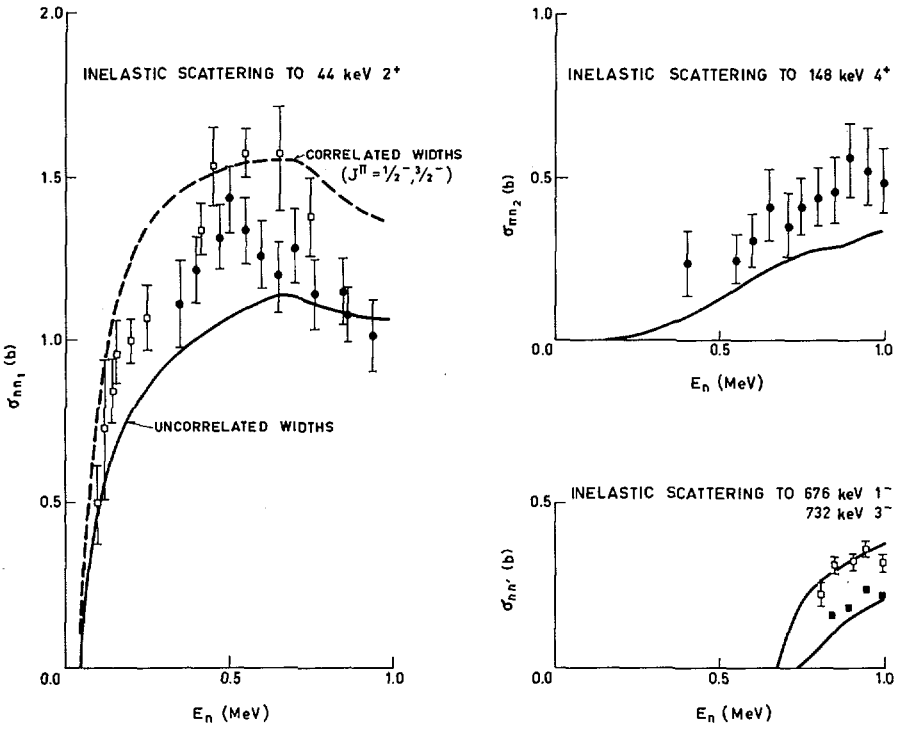

FIG. 5. Calculated inelastic scattering cross-sections to some low-lying states of ^{238}U. Data are due to: □ *Barnard et al. [35]*, ● *Smith [36]*.

$\bar{\Gamma}^{(0)}_{(n')}/\bar{D}$ ~ 3 to 6 x 10^{-4} (from the data of Table IIa), and, for $3/2^-$ states, an elastic strength function of ~6 x 10^{-4} and an inelastic strength function of ~.8 x 10^{-4}. Again, such values are feasible for explaining the data of Fig. 5.

4. PROBLEMS IN RADIATIVE CAPTURE

One of the difficulties yet remaining in using our understanding of neutron interactions as a precise tool in evaluating nuclear data is that we still lack a thorough comprehension of the radiative capture mechanism. The capture cross-section curve of Fig. 6 was calculated using a total radiative capture width based on a shell model level density law with the following form and parameters for the final states. The independent particle form of equation (18) with the parameters of Newton and Lang was used for excitation energies above 2.8 MeV. The constant C was adjusted to 2.46 x 10^{-5} to give a spacing of 20 eV for $1/2^+$ levels at 4.7 MeV. Below 2.8 MeV, and above 1.4 MeV, the level density was assumed to be constant,

$$\rho(J) = 53\,(2J+1)\,e^{-J(J+1)/2\sigma_M^2}, \qquad (18a)$$

and below 1.4 MeV it was assumed to be just (2J + 1); in other words a crude attempt is made to reproduce a pairing gap structure at low energies, this running smoothly into the independent particle form at E = 2Δ.

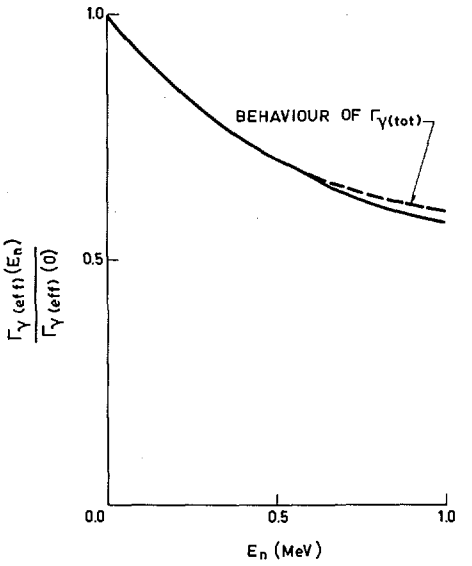

FIG. 6. Calculated radiative-capture width behaviour of ^{238}U + n. For model see text.

The strength of individual transitions was assumed to be governed by a photonuclear type of behaviour [25]:

$$\Gamma_{\gamma(\lambda\to\mu)} \propto \frac{\Gamma_G \varepsilon_\gamma^4}{(\varepsilon_\gamma^2 - E_G^2)^2 + (\Gamma_G \varepsilon_\gamma)^2} \qquad (21)$$

where E_G, Γ_G are the peak energy and width of the photonuclear giant resonance. When $\varepsilon_\gamma \ll E_G$ equation (22) can be simplified to $\Gamma_{\gamma(\lambda\to\mu)} \propto \varepsilon_\gamma^5$. The alternative model that is often used for the radiative transition is the statistical model; all factors governing the electric dipole matrix elements between initial and final states are thoroughly mixed, or damped out, over large energy intervals and the only energy dependence remaining in the partial width is the phase space factor proportional to ε_γ^3. The use of this model gives the curve in Fig. 7 for the behaviour with energy of the total radiation width in the ^{238}U + n reaction. The use of this model would increase the capture cross-section by almost 25% at 1 MeV. Discussion of this point is also stressed by Fricke et al. [26] in a contribution to this Conference. The importance of the choice of model certainly needs to be emphasised. For example, a simple change of the level density law can have a remarkable effect on the radiation width behaviour. A change in the constant of equation (18) from 53 to 10 gives the radiation width behaviour shown in Figs. 8 and 9 for the alternative choices of radiative transition behaviour. In both cases again a large rise in the calculated capture cross-section of ^{238}U towards 1 MeV would result.

Of the two models the first (Fig. 6) seems the preferable although it is by no means certain that it is a valid picture. It does, however, place extra emphasis on high energy transitions and this seems to be essential to explain most of the existing data on low energy neutron capture. An alternative

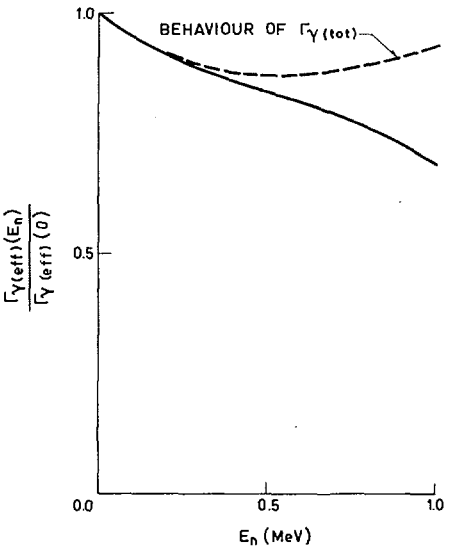

FIG. 7. Calculated radiative-capture width behaviour of $^{238}U + n$. For model see text.

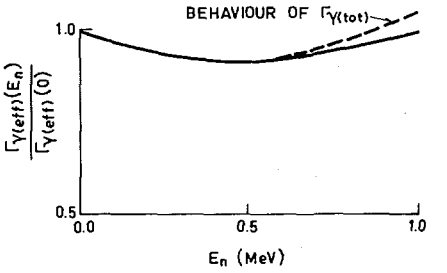

FIG. 8. Calculated radiative-capture width behaviour of $^{238}U + n$. For model see text.

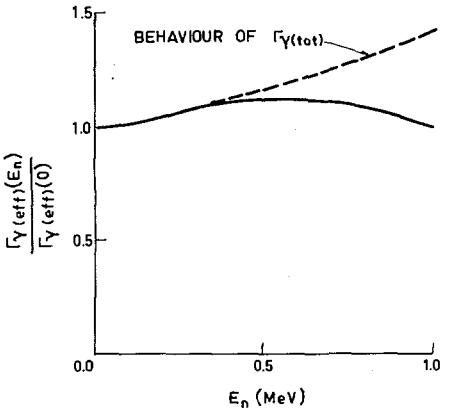

FIG. 9. Calculated radiative-capture width behaviour of $^{238}U + n$. For model see text.

model, for which however a thorough quantitative description still has to be completed, is the valency nucleon model in which it is assumed that most of the strength of a transition comes from a single particle (neutron or proton) state, coupled to a low-lying excited state of the residual nucleus, falling to a lower single particle state, the state of the residual nucleus remaining unchanged. For slow neutron capture by the actinide nuclei for instance, the important single-particle states coupled into the initial states would be 4p and 3f neutron states, while the final states, some 3 MeV below, would contain appreciable admixtures of $4s_{1/2}$, $3d_{3/2}$ and $2g_{7/2}$ states.

Some model such as this, i.e. one containing structural effects as opposed to a statistical type of picture, seems to be necessary to explain the various phenomena that have recently been found in the experimental study of radiative spectra. One such phenomenon is the pygmy resonance [27] at gamma-ray energies of about 5.5 MeV. An explanation that has been advanced for this is that special 2 particle - 1 hole states play an important part in the radiative mechanism, one of the particles falling into the vacant hole [28]. Such a mechanism could also explain phenomena like the correlation of neutron widths with partial radiation widths found, for example, in ^{169}Tm + n; Lane [29] has been studying this possibility. Very simply, one can visualise the neutron single-particle state corresponding to the entrance channel as coupled with a 2p - 1h state; if this special state is isolated in the sense that this is the only state introducing single-particle admixtures into the compound states then it follows immediately that there is correlation between the neutron widths and radiative transitions governed by the 2p - 1h admixtures. The fact that this particular correlation phenomena is not found in most other nuclei studied may emphasise that the isolation of such a special state is an uncommon occurrence.

5. THE FISSION PROCESS

Above 1 MeV in the neutron bombardment of ^{238}U, and at lower energies in the neutron interactions with most other actinide nuclei, the fission reaction becomes an important phenomenon. Until perhaps four years ago, fission was regarded as the reaction process perhaps the most amenable to statistical understanding and analysis. Now, however, it is known to be the reaction following neutron absorption in which special modes or states of the nucleus exert their most dramatic influence.

A quantitative understanding of many of the newly discovered features of fission is now being reached through the medium of Strutinsky's doubled-humped fission barrier; this was extensively discussed at the Vienna Symposium of 1969 [30] so there is no need to pursue the topic in detail here. The essential feature that emerges from the Strutinsky barrier is that the nucleus can have a heirarchy of excited levels associated with a highly elongated shape of the nucleus in addition to the (much denser) states associated with the normal ground state shape. The former states (class II states) have a much greater probability of fissioning than the normal (class I) states at a similar excitation energy. On weakly coupling the two sets through the potential barrier separating the normal and elongated shapes intermediate structure can appear in the fission decay of the neutron-excited compound nucleus.

One of the simplest examples of such intermediate structure is shown by James [31] in his paper to this conference; this is the neutron-induced fission cross-section of ^{230}Th showing a sharp peak (some 25 keV wide) at a neutron energy of 720 keV, and then an apparently normal rise to about 1100 keV. Detailed analysis of the shape of this cross-section curve, and of angular distributions of the fission products at various energies, reveals that the whole fission cross-section is dominated by the spectroscopy of the states of

the secondary minimum (the highly elongated nuclear shape). We deduce that the potential barrier for one set of states ($J^{\pi} = 1/2^{-}$) has the quantitative form shown in Fig. 10.

In this case (the compound nucleus ^{231}Th) it is seen from Fig. 10 that the secondary minimum in the Strutinsky potential is very shallow. In heavier nuclei it is known to be much deeper, and this introduces much greater complexity into the intermediate structure. At neutron reaction energies the effective excitation of the elongated nucleus is still much lower than the true excitation energy, but nevertheless is now sufficient that the simple multi-phonon vibration modes can be considerably mixed (or "damped") into more complex states of the class-II type. These more complex states are in turn weakly coupled to

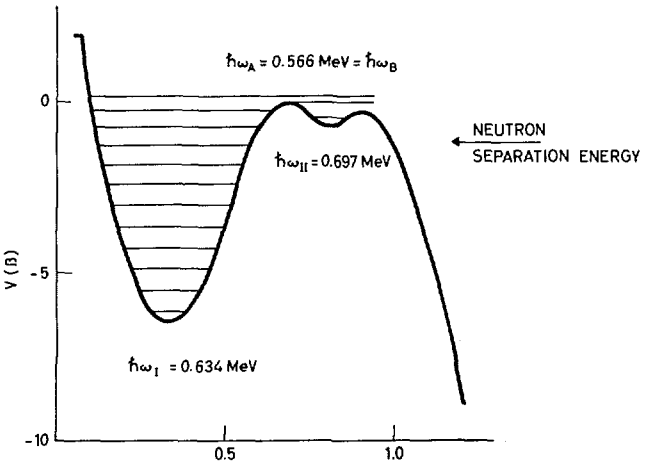

FIG. 10. Hypothesized fission barrier for quantitative explanation of fission cross-section of ^{230}Th. β-type vibrational states are indicated by horizontal lines.

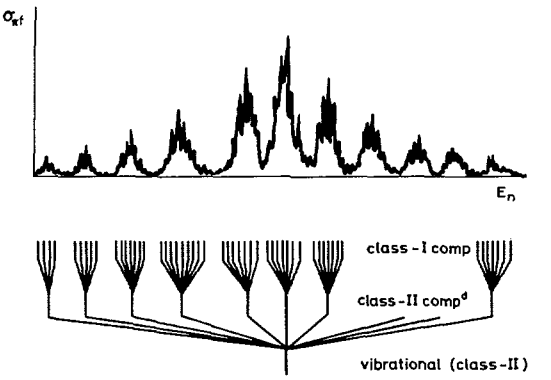

FIG. 11. Schematic diagram of neutron-induced fission cross-section across a weakly-damped class-II vibrational state.

the class I states and the resulting neutron-induced fission cross-section may have the form schematically shown in Fig. 11. It is believed that the fission cross-section of ^{234}U is an example of this behaviour but the full quantitative interpretation of the fission of this and other nuclei of practical importance is still being pursued.

6. CONCLUSION

The main theme of this paper has been the important role of special states, often corresponding to quite simple dynamic modes of the nucleus, in the interaction of neutrons with nuclei. The influence of some of these special states was recognised quite early, but it is only recently that it has been realised how they can affect aspects of the microscopic structure of neutron cross-sections that have always been believed to be purely statistical in nature. We are still groping towards a quantitative understanding of the mixing of special states into the fine-structure states, and it is clear that it is not possible to achieve this understanding without a great deal more of the excellent experimental data that have emerged in the field of neutron reactions in the last few years. It seems equally certain that it will be increasingly difficult to reconcile future sophisticated measurements with each other without a detailed understanding of the theory; the two aspects of the field covered by this Conference, namely the acquisition of accurate nuclear data for practical purposes, and the basic understanding of nuclear phenomena, are indivisible for satisfactory progress in each.

REFERENCES

[1] BETHE, H. A. Phys. Rev. 47, 747 (1935).
[2] AMALDI, E., D'Agostini, O., Fermi, E., Pontecorvo, B., Rasetti, F. and Segre, E. Proc. Roy. Soc. A149, 522 (1935).
[3] MOON, P. B. and Tillman, R. Proc. Roy. Soc. 153, 421 (1936).
[4] RASETTI, F., Segre, E., Fink, G., Dunning, J. R. and Pegram, G. B. Phys. Rev. 49, 104, (1936).
[5] BOHR, N. Nature, 137, 344 (1936).
[6] WEISSKOPF, V. F. and Ewing, D. F. Phys. Rev. 57, 472 (1940).
[7] FESHBACH, H., Peaslee, D. C. and Weisskopf, V. F. Phys. Rev. 71, 145 (1947).
[8] FESHBACH, H., Porter, C. E. and Weisskopf, V. F. Phys. Rev. 96, 448 (1954).
[9] HAUSER, W. and Feshbach, H. Phys. Rev. 87, 366 (1952).
[10] PORTER, C. E. and Thomas, R. G. Phys. Rev. 104, 483 (1956).
[11] LANE, A. M. and Lynn, J. E. Proc. Phys. Soc. A70, 557 (1957).
[12] LYNN, J. E. Harwell report AERE - R 5891 (1968).
[13] BOHR, A. and Mattelson, B. "Nuclear Structure", Vol. 1, 302 (1969).
[14] HUMBLET, J. and Rosenfeld, L. Nucl. Phys. 26, 529 (1961).
[15] LYNN, J. E. Proc. Int. Conf. on study of nuclear structure with neutrons, Antwerp, 1965 (Eds. M. Neve de Mevergnies et al.) p.125 (North-Holland, Amsterdam) (1966).
[16] MAHAUX, C. and Weidenmuller, H. A. "Shell Model Approach to Nuclear Reactions" (North-Holland, Amsterdam) (1969).
[17] LEJEUNE, A. and Mahaux, C. Nuc. Phys. A113, 272 (1968).
[18] BUTTLE, P. I. A. Phys. Rev. 160, 719 (1967).
[19] CHASE, D. M., Wilets, L. and Edmonds, A. R. Phys. Rev. 110, 1080 (1958).
[20] LYNN, J. E. "Theory of Neutron Resonance Reactions" (Clarendon Press, Oxford, 1968) p.65.
[21] LEJEUNE, A. and Mahaux C. Nuc. Phys. A145, 613 (1970).

[22] DAVIDSON, J. P. "Collective Models of the Nucleus" (Academic Press, New York, 1968) p.178.
[23] DRESNER, L. Proc. Int. Conf. on Neutron Interactions with Nuclei, New York, USAEC Report TID-7547, p.71 (1957).
[24] TAMURA, T. Ann. Rev. Nucl. Sc. 19, 99 (1969).
[25] BRINK, D. M. D. Phil. Thesis, Oxford (unpublished) (1955).
[26] FRICKE, M. P., Lopez, W. M., Friesenhahn, S. J., Carlson, A. D. and Costello, D. G. Paper CN-26/44, these proceedings.
[27] STARFELT, N. Nuc. Phys. 53, 397 (1964).
[28] BARTHOLOMEW, G. A. Proceedings of Studsvik Int. Symp. (IAEA Vienna) (1969).
[29] LANE, A. M. Phys. Lett. 31B, 344 (1970).
[30] "Physics and Chemistry of Fission", Proc. of 2nd Int. Symp., Vienna (IAEA, Vienna) (1969).
[31] JAMES, D. G. These proceedings.
[32] MOXON, M. C. Private communication (1970).
[33] MENLOVE, H. O. and Poenitz, W. P. Nucl. Sci. and Eng. 33, 24 (1968).
[34] DAVEY, W. G. Nucl. Sci. and Eng. 39, 337 (1970).
[35] BARNARD, E., Ferguson, A. T. G., McMurray, W. R., Van Heerden, I. J. Int. Conf. on Study of Nuclear Structure with Neutrons, Antwerp P/26 (1965).
[36] SMITH, A. B. Nucl. Phys. 47, 633 (1963).

DISCUSSION

J. J. SCHMIDT: In Fig. 4 of your paper you show a theoretical curve which fits nicely with some capture data for ^{238}U in the keV-range. Could you give some indication of the general confidence level which can be achieved by those capture cross-section calculations?

J. E. LYNN: From a theoretical point of view this is a curve that favours a model emphasizing high-energy transitions in the capture γ-ray mechanism. For reasons concerned with capture γ-ray spectra, which are outlined in the text of the paper, there is other support for such a model. I would feel therefore that a confidence limit of perhaps a $\pm$ 20% variation either way might be appropriate to this curve. I would be very surprised if it were out by as much as, say 50%.

A. PRINCE: In connection with Fig. 2 of your paper, I would like to comment on the scattering to the 44-keV state in ^{238}U. We carried out analyses in which we assumed uncorrelated widths and added the direct-interaction component. We found that the sum of these falls somewhere between your uncorrelated and correlated elastic and inelastic widths.

J. E. LYNN: I think this is probably quite reasonable. As you will have noted, the curve from the $J^{\pi}=1/2^-$ state would, if extrapolated to the $3/2^-$ state and added, give an extra 100 millibarns or so to add to my uncorrelated curve and this, in turn, would certainly bring it up towards the Smith data. However, it would still be a bit lower, I think, than the data of Barnard et al. Of course, a lot depends on the particular p-wave strength function that you take.

A. PRINCE: This was even more true in the scattering to the 4^+-level at 148 keV where, to describe the experimental data adequately, it was necessary to add the direct component also.

J. E. LYNN: Yes, the uncorrelated curve on my picture is definitely quite a long way under the data of Smith.

A. PRINCE: There is one more thing. We carried out analyses of the gamma-ray strength function and, using Musgrove's analysis, we showed the radiation width to vary by about 50% over 3 MeV, which would probably pull down your curve a little bit, as I think you showed in your curve, where you are down to 50% at about 1 MeV.

J. E. LYNN: What kind of model did you use for the gamma-ray strength function?

A. PRINCE: The dipole-transition model.

J. E. LYNN: What about the level density of the final states?

A. PRINCE: For this we used the Fermi model.

J. E. LYNN: Actually, the single-particle level density that goes into the Fermi model is rather crucial in these calculations. There is certainly some dependence on that parameter. In the calculation which I showed here, I was using the original Newton shell model, but with the adjustment that Lang gave in a paper a few years later. This comes out to a coefficient equal to about 125.

Section II

CROSS-SECTIONS AND TECHNIQUES FOR HIGH-PRECISION NEUTRON NUCLEAR DATA MEASUREMENTS

Chairman
E.R. RAE (UK)

PRECISE 2200 m/s FISSION CROSS-SECTIONS OF ^{239}Pu AND ^{235}U.

A.J. DERUYTTER, W. BECKER*
Central Bureau for Nuclear Measurements,
EURATOM, Geel, Belgium

Abstract

PRECISE 2200 m/s FISSION CROSS-SECTIONS OF ^{239}Pu AND ^{235}U.

A new precise measurement of the 2200 m/s fission cross-section of ^{239}Pu was performed with a slow chopper at the Belgian BR2-reactor (energy range from 0.005 to 0.1 eV). Simultaneous recordings of pulse-height and time-of-flight spectra of successively compared ^{239}Pu layers and standard natural boron layers were made. The detection of the ^{10}B (n, α) ^{7}Li and ^{239}Pu (n, f) reaction fragments is made with excellent pulse-height resolution in low geometry with a surface barrier detector. The separation between the pile-up tail produced by the α-particles of ^{239}Pu and the fission-fragment pulse-height distribution was very good. The relative ^{10}B contents of several standard boron foils were checked by their neutron-induced reaction rates. The absolute ^{10}B contents were determined from direct weighing in vacuum combined with careful chemical and isotopic analysis of witness foils. The fission foils were checked by α- and fission counting. Their absolute weights were obtained from absolute low-geometry α-counting.

A final value for the 2200 m/s fission cross-section of ^{235}U was also obtained, making use of a carefully redetermined value of the ^{234}U α-half-life.

A comparison of the obtained 2200 m/s values with the up-dated IAEA review for these quantities is included.

The fission cross-section of both isotopes was carefully studied down to 2 meV neutron energy and up to 0.1 eV and serves for the calculation of g-factors.

INTRODUCTION

Recently the 2200 m/s neutron constants for these fissile isotopes have been thoroughly reviewed by G. C. Hanna et al. [1]. The spread in the input data for σ_f^o (fission cross-section at a neutron velocity of 2200 m/s) is considerable, especially for ^{239}Pu. A measurement of the fission cross-section of ^{235}U in the energy range 0.005 eV to 0.1 eV was reported earlier [2]. In the meantime, these results were improved especially $T_{1/2}$ (^{234}U) for α-decay was studied in great detail at CBNM. Also a new group of data was obtained with another chopper rotor speed (resolution) for the comparison between σ_f (^{235}U) and $\sigma(n,\alpha)$ of ^{10}B as a standard cross-section.

New measurements were performed of σ_f (^{239}Pu) in the same neutron-energy range with the slow chopper installed at the tangential beam-tube T-7 of the belgian BR2-reactor, also by a direct comparison of known evaporated elemental boron layers and well-defined electrosprayed ^{239}Pu-layers, in order to deduce σ_f^o (^{239}Pu) by comparison to $\sigma^o(n,\alpha)$ of ^{10}B.

---

* EURATOM Research Fellow.

TABLE I. ISOTOPIC COMPOSITIONS OF TARGETS (IN ATOM %)

Elemental Boron				$^{235}UF_4$-Targets		Pu-acetate-Targets	
B64		B74		U4, U5(NBS-930)		Tp 442-1 and Tp 442-3	
^{10}B	20.127 ± 0.046	20.330 ± 0.065	^{234}U	1.0812 ± 0.0020	^{239}Pu	99.979	
^{11}B	79.873 ± 0.046	79.670 ± 0.065	^{235}U	93.336 ± 0.010	^{240}Pu	0.02	
			^{236}U	0.2027 ± 0.0006	^{241}Pu	0.001	
			^{238}U	5.380 ± 0.005			

TABLE II. WEIGHTS OF TARGETS

Boron (weights in μg ^{10}B)		U-targets (weights in μg ^{235}U)		Pu-targets (weights in μg ^{239}Pu)	
B64*	146.28 ± 0.38	U1	1505.0 ± 5.4	Tp 442-1*	267.55 ± 0.62
B69	91.89 ± 0.24	U3	798.1 ± 2.9	Tp 442-2-1	570.91 ± 1.31
B74*	99.11 ± 0.26	U4*	1590.5 ± 5.7	Tp 442-2-2	575.22 ± 1.32
B73	77.49 ± 0.20	U5*	3219.9 ± 11.1	Tp 442-3*	1011.54 ± 2.33

*Targets used in the experiments.

The main criticism about direct determinations of thermal fission cross-sections with choppers or crystal spectrometers has been the insufficient knowledge of the efficiency of the 2π - or 4π - ionisation chambers used to detect the fission events, caused by the appreciable low-energy tailing of the fission fragment spectra. Also the insufficient resolution of ionization chambers hampered the separation of the ^{7}Li-recoils and α-particles from the $^{10}B(n,\alpha)^{7}Li$, $^{7}Li^{*}$ reactions, and hence the knowledge of the efficiency of detection and use of the standard cross-section. In our experiments the detection of fission fragments and α-particles from ^{10}B was performed in identical low geometry with a large surface barrier detector, enabling the fission spectra and α-particles to be almost completely resolved. In this way no appreciable errors result from the extrapolation of the pulse-height spectra in order to obtain detection efficiencies.

EXPERIMENTAL PROCEDURE

1. The neutron beam extraction system and neutron energy selection was described previously in ref. [2]. The detection chamber allowed for reproducible positioning of targets in the beam and in counting position with respect to the surface barrier detector.

2. Targets: 4 targets are simultaneously in use: two evaporated elemental boron layers and two fissile layers, all deposited on gold-coated quartz disks. ^{235}U was evaporated as UF_4 and ^{239}Pu was deposited as Pu-acetate by electrospraying. During the boron-evaporation witness-layers were prepared for chemical and isotopic analysis. The amount of ^{10}B was determined from direct weighing in vacuum and correction for chemical and isotopic analysis. Several layers were intercompared by neutron-induced counting. Weights and counting rates are in good agreement [2]. In Table I the isotopic compositions of the evaporated natural boron, NBS-930 ^{235}U-material and ^{239}Pu-targets are given. The amounts of ^{235}U and ^{239}Pu on the foils were determined from precise low-geometry α-counting. The neutron induced fission rates were also checked as a relative control. The deduction of the amounts of ^{239}Pu from this method was not a severe problem as the different α-half-life measurements for ^{239}Pu agree so closely (certainly within 0.2%). The determination of the specific activity of NBS-930 material on the contrary is heavily dependent on the α-half-life of ^{234}U. An extensive study of this half-life has been performed at CBNM, yielding at present a value of $(2.445 \pm 0.010)\times10^{5}$ yrs [3] that confirms the previously quoted value (Ref. 2). Also at Argonne NL recent measurements were performed of this quantity, yielding values considerably lower than previous data [4]. The value of this quantity used in Ref. [1] e.g. was $(2.488 \pm 0.016)\times10^{5}$ yrs which is about 2% higher than the latest CBNM-results. The standard error quoted at present on the CBNM-value is only 0.4%, because the different methods used for the determination of the amount of uranium (controlled potential coulometry, isotope dilution, weighing in vacuum) only agree within these error limits, although each method is capable of better precision.

In Table II the weights of the different targets are listed. The boron weights are taken from a straight line fit through the neutron counting rate versus absolute ^{10}B weight plot as described in ref. [2]. The values from this fit are used with 0.26% standard errors.

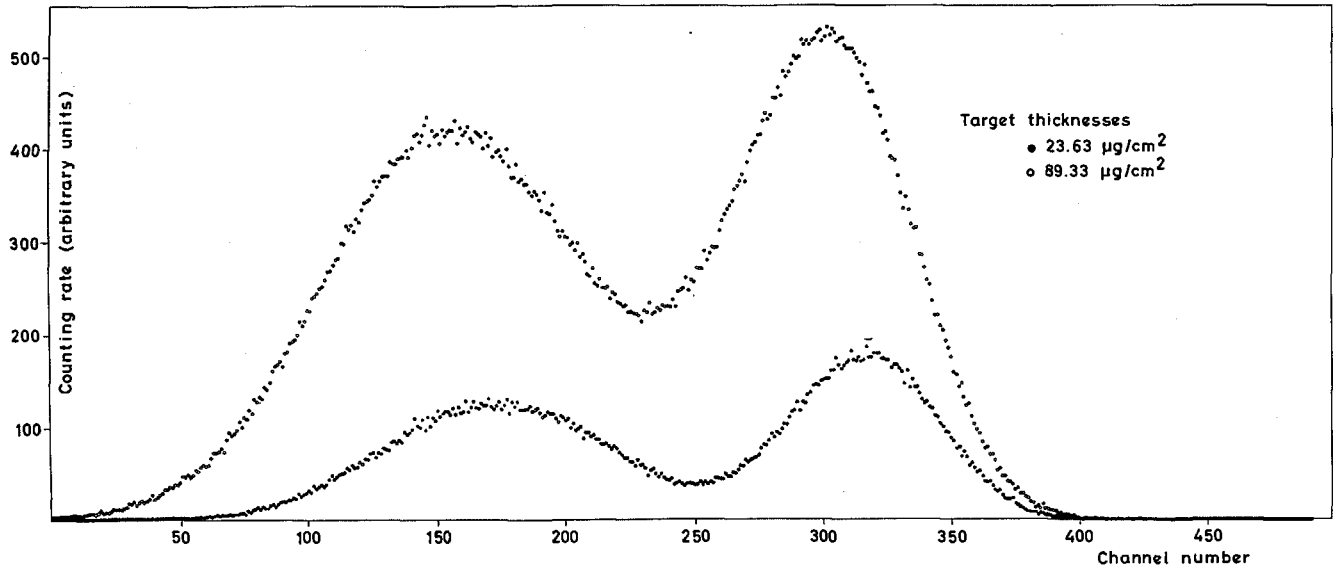

FIG. 1. The pulse-height spectra of two ^{239}Pu-targets: Tp 442-1, Tp 442-3.

For the determination of the amounts of the fissile elements an error of 0.20% was accepted for the low geometry counting of the UF_4-targets and 0.12% for the Pu-targets. For the specific activity the error resulting from ^{234}U for NBS-930 targets is 0.4%, for the ^{239}Pu-targets 0.2% resulting from a $T_{1/2}$ -value for ^{239}Pu of $(2.4380 \pm 0.0049) \times 10^4$ yrs. As standard errors we accept 0.45% on the amounts of ^{235}U and 0.23% on the amounts of ^{239}Pu.

RESULTS AND DISCUSSION

The method of analysis was briefly discussed in ref. [2] and figures of the ^{235}U fission fragment spectra are shown there. In the case of ^{239}Pu, due to the α-pile-up pulses the separation of α- and fission fragment pulses is more difficult. However as can be seen from Fig. 1 the fission fragment pulses from ^{239}Pu are well resolved and completely separated from the α- pile-up for both targets (cut-out by discrimination). Also the α-particles from the $^{10}B(n,\alpha)$ reaction are well separated from the ^{7}Li-recoils (cut-out by discrimination) (Fig. 2). Such spectra, together with the accurate positioning of the targets with respect to neutron beam and detector permit an accurate deduction of the relative efficiencies of (n, f) and $^{10}B(n,\alpha)$ detection [2].

In Fig. 3 the fission cross-section obtained for ^{239}Pu is shown in the neighbourhood of the 2200 m/s reference point. A straight line fit was used to interpolate between values to obtain the value at 2200 m/s. The result obtained in this way is σ_f^o (^{239}Pu) = 742.5 $\pm$ 3.7 barns, where the error should be considered as one standard deviation.

In Table III the estimated errors for ^{235}U and ^{239}Pu 2200 m/s fission cross-section values are tabulated.

The shape of the ^{239}Pu σ_f-curve obtained with the slow chopper, together with the shape from 0.1 to 0.5 eV obtained in a recent Linac experiment [5] were used to deduce the g_f-factor for a Maxwellian distribution with a temperature of 20.44°C to compare with the value of Westcott [1]. This g_f-factor was also calculated based on our low energy run at the Geel Linac [5] that comes down till 10 meV. Both values are in good agreement. (See Table IV). The results for ^{239}Pu: σ_f^o and the g_f-factor, very closely agree with the values recommended by the IAEA-evaluation as is evident from Table IV.

The values for ^{235}U are also shown in Table IV. The g_f-factor agrees with the recommended IAEA-value. However our σ_f^o-value of 587.9 $\pm$ 3.4 b, although obtained by the same method as for ^{239}Pu, and referred to the same standard is higher than the IAEA-value. An examination of ^{235}U 2200 m/s fission cross-sections used for the input to the IAEA-evaluation, based on the most recent $T_{1/2}$ -values for α-decay of ^{233}U and ^{234}U would yield a slightly higher input value for σ_f^o than the now accepted one. Also the fission cross-section ratio $\sigma_f^o(^{239}Pu)/\sigma_f^o(^{235}U)$ used as input datum in [1] is somewhat too high 1.28176 $\pm$ 0.00832, whereas our experiments yield 1.2629 $\pm$ 0.0099 in better agreement with previous data (cf. e.g. ref. [6]) except for the heavily weighted value of Lounsbury et al. [7] of 1.2947 + 0.0104.

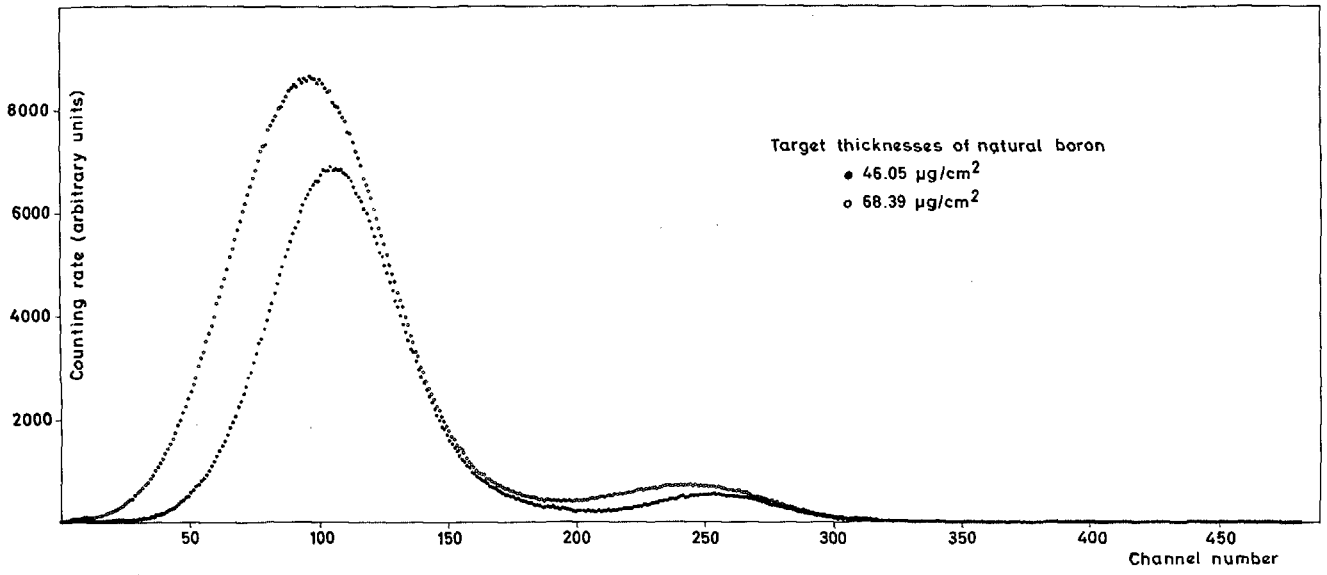

FIG. 2. The α-particle spectra of two natural boron targets B64 and B74.

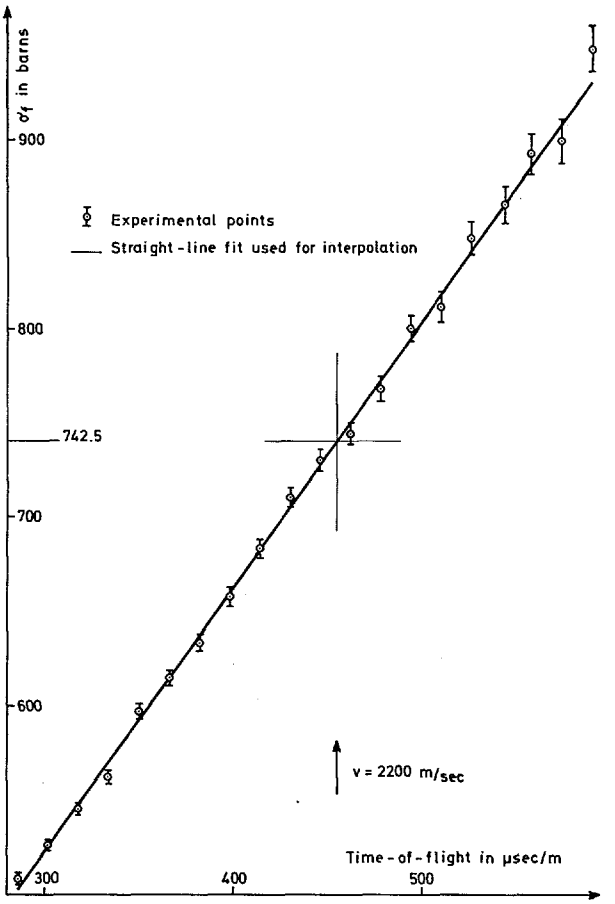

FIG. 3. The $^{239}Pu(n, f)$ cross-section in the neighbourhood of the reference velocity 2200 m/s. The dots are the experimental values. The full line is a straight-line fit used for interpolation.

Also the input datum for the capture-to-fission ratio for $^{235}\overline{U}$ may be on the high side if one considers all the available thermal α-data. The absorption cross-section, as recommended in [1] is deduced from $\sigma^{o}_{tot} - \sigma^{o}_{sc} = \sigma^{o}_{a}$. Very little information is available on the scattering cross-section of ^{235}U at 2200 m/s. At this conference Ceulemans and Poortmans [8] report a value at 2200 m/s of 14 ± 1 barns, which is lower than the values used to deduce the thermal absorption cross-sections in ref. [1]. The IAEA-review recommends $\sigma_s^{bound} = 17.6 \pm 1.5$ barns.

Based on this evidence we suggest that the thermal fission cross-section of ^{235}U as recommended by the IAEA-Review may be too low by a few barns. For ^{239}Pu however our results seem to confirm completely the recommended values.

TABLE III. ERRORS IN σ_f^o

Cause of error	Relative error on σ_f^o in %	
	^{239}Pu	^{235}U
Number of ^{10}B-atoms	0.26	0.26
Number of ^{239}Pu-atoms	0.23	
^{235}U-atoms		0.45
Ratio of efficiencies for detection (ϵ_B/ϵ_f)	0.13	0.14
σ_B^o (= 3835 barn)	0.13	0.13
Neutron velocity	0.20	0.05
Counting rate ratios (C_f/C_B)	0.23	0.15
Total standard error $= \sqrt{\Sigma \delta_i^2}$	0.50%	0.57%

TABLE IV. COMPARISON OF OUR RESULTS AND IAEA BEST VALUES

	IAEA Review[1]		These experiments	
	^{239}Pu	^{235}U	^{239}Pu	^{235}U
σ_f^o	741.6 ± 3.1b	580.2 ± 1.8b	742.5 ± 3.7b	587.9 ± 3.4b
g_f (20.44°C Maxwell-distribution)	1.0548±0.0030	0.9766±0.0016	1.0566±0.018 (Linac)	0.9780±0.0010
			1.0540±0.018 (BR2)	

ACKNOWLEDGEMENTS

The authors wish to thank Dr. J. Spaepen for active support and stimulating discussions throughout the experiments, Drs. G. C. Hanna, W. W. Havens Jr., A. Spernol for valuable discussions and comments.

We are very grateful to the CBNM sample preparation group who really made this work possible, and especially to Drs. P. De Bièvre, H. Eschbach, K. F. Lauer, Y. Le Duigou, H. Moret, A. Spernol and V. Verdingh.

We thank SCK-CEN (Belgium) and especially Dr. M. Nève de Mévergnies for the hospitality at BR2 and in the Neutron Physics Department during these experiments, for the electronic assistance

(E. Mies) and for the mechanical maintenance of the chopper (L. Van Steenlandt.

We further thank Dr. L. Schotsmans (SCK-CEN, Belgium) for the programming of the g-factor calculations, Dr. H. Depuydt and Mrs. De Corte L. (SCK-CEN Belgium) for programming, Mr. J. Brulmans (CBNM) for the accurate measurements on the sample changer and Mr. G. Le Dez for technical assistance in the experiment.

REFERENCES

[1] HANNA, G.C., WESTCOTT, C.H., LEMMEL, H.D., LEONARD JR., B.R., STORY, J.S., ATTREE, P.M., Atomic Energy Review Vol. VII 4 (1969) 3.

[2] DERUYTTER, A.J., SPAEPEN, J., PELFER, P., "Neutron Cross Sections and Technology" NBS Special Publication 299 Vol. I (1968) 494.

[3] SPERNOL, A., private communication, work performed by a CBNM-group.

[4] MEADOWS, J.W., private communication (1970).

[5] DERUYTTER, A.J., WAGEMANS, C., PENNING, G., EANDC(E) 131"AL" (1970).

[6] WHITE, P.H., REICHELT, J.M.A., WARNER, G.P., "Nuclear Data for Reactors" (Paris 1966) IAEA, Vienna (1967) 29.

[7] LOUNSBURY, M., DURHAM, R.W., BIGHAM, C.B., HANNA, G.C., KUSHNERIUK, S.A., INDC(CAN)-4 (1969) and EANDC(CAN)-40 (Sept. 1969) 7.

[8] CEULEMANS H., POORTMANS, F., this conference (1970).

Invited Paper

CROSS-SECTIONS AND TECHNIQUES FOR HIGH-PRECISION NEUTRON NUCLEAR DATA MEASUREMENTS

A.J. DERUYTTER
Central Bureau for Nuclear Measurements,
EURATOM, Geel, Belgium

Abstract

CROSS-SECTIONS AND TECHNIQUES FOR HIGH-PRECISION NEUTRON NUCLEAR DATA MEASUREMENTS.

The accuracy requirements for cross-sections of structural and fuel materials needed for the design of nuclear reactors (and for precision neutron dosimetry) have stimulated the investigation and selection of standard cross-sections and the improvement of the precision in neutron flux measuring techniques. In this paper, the present status in these fields is reviewed. Considerable attention is given to standard cross-sections, i.e. cross-sections that are used to obtain other cross-sections by comparison and especially to the so-called "primary" standards as, e.g. the cross-sections of the $^{10}B(n,\alpha)^{7}Li$-, H(n,n)H-reactions. Further, improvements in the knowledge of other "working standard" cross-sections such as $^{6}Li(n,\alpha)$ and $^{3}He(n,p)$ are discussed. Some special attention is given to the normalization of $^{235}U(n,f)$ and $^{239}Pu(n,f)$-reactions in the resonance region, as these cross-sections are both important reactor requests and, at the same time, may play the role of secondary standards.

Also the situation of absolute neutron-flux determination is briefly reviewed.

Finally, stringent requirements for improvements are set forth for the preparation and handling of samples for precise measurements with respect to chemical definition, isotopical analysis and enrichment and absolute counting (half-lives of α-active fissile isotopes).

INTRODUCTION

Highly precise measurements of neutron cross-sections in view of the establishment of the so-called set of standard cross-sections have been discussed by Spaepen [1] (1966), the IAEA Panel on nuclear standards for neutron measurements [2] (1967) and Gibbons [3] (1968). In the first two reports also methods of absolute flux determination were dealt with which are independent of or nearly independent of cross-sections (such as associated particle and activity methods, flat response detectors and photoneutron sources) as well as other standard nuclear data, especially $\bar{\nu}$ (^{252}Cf), and standard materials and foils for neutron measurements.

The primary set of standard cross-sections has to be the small set of well-defined cross-sections which are used to obtain other cross-sections by simpler relative measurements. The accuracy of the comparison will in general be better when the standard and relative cross-sections are of the same type. So standard cross-sections should preferably be found for each reaction type. However, it is not necessary that the standard cross-section be a reaction cross-section needed in reactor design, but because of the high accuracy demanded for these standard cross-sections they will automatically fulfill the reactor requirements for this cross-section. This request is sometimes the origin of their choice as a standard.

TABLE I. Typical high-precision data accuracies (in %) requested for reactor design and dosimetry (standards excluded)

Energy range	$\sigma_{n,f}(E)$	$\sigma_{n,\gamma}(E)$	$\sigma_{n,n}(E,\theta)$ different. $\sigma_{n,n'}(E;E'\theta)$	Threshold reactions	$\bar{\nu}$
Thermal	0.5 (e.g. ^{239}Pu)	0.2 - 1 (e.g. ^{233}U, ^{239}Pu, ^{238}U			0.5 to 1
E_n up to a few MeV	0.5 - 1 (e.g. ^{239}Pu, ^{235}U)	1 - 3 (e.g. ^{239}Pu, ^{233}U, ^{238}U) (^{151}, ^{153}Eu; ^{177}, ^{178}Hf)	2.5 - 5 (e.g. Fe, Ni, ^{238}U)		0.5 - 1 (e.g. ^{235}U, ^{239}Pu) 2 (e.g. ^{238}U, ^{240}Pu)
From threshold up to about 15-20 MeV				(n, p) 2 - 5 (e.g. ^{46}Ti, ^{58}Ni, ^{54}Fe) (n, α) 4 - 10 (e.g. ^{63}Cu, Be) (n, 2n) 5 (e.g. ^{55}Mn, ^{65}Cu) (n, n') 3 (^{115}In) tot. in. 5 (^{238}U, ^{103}Rh)	

In the last few years we have noticed on one side a demand for low energy cross-sections with ever increasing precision, and on the other hand a shift of the reactor requests towards higher neutron energies (fast reactor requests), entailing demands for higher accuracy on standards and (or) neutron measuring techniques in this region, especially in the keV-region where precision was seriously lacking.

How accurate should the standard cross-section be known? That, of course, depends on the precision requested for the other cross-sections. But if we note e. g. that in the RENDA request list [4] the thermal neutron fission cross-section for ^{239}Pu is demanded with 0. 5% accuracy, then the standard cross-section serving this purpose (e. g. $^{10}B(n,\alpha)$) should be known a few times better, which brings us for $\sigma^{o}_{n,\alpha}$ (^{10}B) at thermal energy to about 0. 1% accuracy, a formidable task. If we apply the same rule for other cross-sections and in other energy regions we arrive at very stringent requirements for the standard cross-sections and/or neutron flux determination.

In Table I we have summarized some of the high precision cross-section requests selected from the RENDA list [4] . It is obvious from this table that the requested accuracy of flux standards in the whole energy-range below about a couple of MeV is 0. 1 to 0. 3% to meet these cross-section accuracies, and in the higher energy region 1 to 2% is wanted.

Another condition for a standard cross-section is that the isotope to which it pertains can be conveniently used in cross-section experiments, target preparation, detection possibilities, and it is certainly very helpful if the cross-section can be measured via two or more independent ways.

In this text we are concerned especially with the cross-sections for the reactions $^{10}B(n,\alpha)^{7}Li$; $^{6}Li(n,\alpha)^{3}He$, $^{3}He(n,p)^{3}H$, H(n, n), by now nearly conventional standard cross-sections, but also some special attention is given to the normalization of $^{235}U(n,f)$- and $^{239}Pu(n,f)$-reactions as they are both important reactor requests and at the same time they are of interest as secondary standards (especially ^{235}U).

Very briefly some improvements obtained in the last years in the field of direct absolute neutron flux measurements will be mentioned. In fact, the problem of neutron flux measurements and standard cross-sections are very closely related. Only in a few cases each can be measured independently of the other. The typical examples are: a total cross-section can be measured by transmission without a knowledge of the neutron flux and a flux can be determined by the associated particle method without knowing the reaction cross-section.

1. STATUS OF NEUTRON STANDARD CROSS-SECTIONS (AND $\bar{\nu}$)

1. 1. The $^{3}He(n,p)$, $^{6}Li(n,\alpha)$ and $^{10}B(n,\alpha)$ processes

are charged particle producing reactions with cross-sections which nearly follow a 1/v-behaviour in the low energy region. They have rather large thermal cross-sections and are well-suited as standards in the thermal energy region and below $\approx$ 100 keV.

TABLE II. Binding energies (MeV) in ^{7}Li, ^{11}B, ^{4}He [5],[6].

Binding energies	^{7}Li	^{11}B	^{4}He
B(n)	7.2525	11.4559	20.5780
B(p)	9.9799	11.2283	19.8142
B(t)	2.4674	11.2264	19.8142
B(α)	2.4674	8.6644	
B(^{3}He)	28.250	27.2099	20.5780
B(d)	9.6831	15.8188	23.8471

TABLE III. Q-values in MeV of possible neutron induced reactions in ^{6}Li, ^{10}B and ^{3}He [5],[6] for $E_n < 100$ keV.

	^{6}Li	^{10}B	^{3}He
(n, α)	+ 4.7851	+ 2.7915	---
(n, γ)	+ 7.2525	+ 11.4559	+ 20.5780
(n, p)	- 2.7274	+ 0.2276	+ 0.7638
(n, d)	- 2.4306	- 4.3629	- 3.2691
(n, t)	+ 4.7851	+ 0.2295 ($^{8}Be \rightarrow 2\,^{4}He$ Q = + 0.095; yields Q = + 0.3245)	+ 0.7638
(n, ^{3}He)	- 20.9975	- 15.7540	---

1.1.1. Fundamental View-Points:

In Table II we have summarized the binding energies of several particles in the nuclei formed by these three reactions. We note that besides of the (n, γ)-reaction and elastic scattering no other reactions are energetically possible but $^{3}He(n, p)$ and $^{6}Li(n, \alpha)$ at the considered neutron energies (below 100 keV), but for boron $^{10}B(n, p)$ and $^{10}B(n, t)$ are energetically not excluded. These binding energy values result in the Q-values for possible neutron induced reactions in ^{6}Li, ^{10}B and ^{3}He tabulated in Table III. Here it is also evident that the Q-value for $^{6}Li(n, \alpha)$ of 4.7851 MeV is considerably larger than that of $^{10}B(n, \alpha)$ (=2.7915 MeV) and for $^{3}He(n, p)$ only 0.7638 MeV. Recently [7] we have measured the Q-values of the $^{10}B(n, \alpha)$ and $^{6}Li(n, \alpha)$ reactions with high resolution solid-state detectors with the following results: Q for $^{10}B(n, \alpha)$ = (2800.8 ± 7.6)keV and for $^{6}Li(n, \alpha)$: Q = (4794 ± 12)keV which are slightly higher than the values deduced from mass-excesses, although the deviation is probably not statistically significant. We note further that the Q-value for the $^{10}B(n, p)$-reaction is only 0.2276 MeV and for $^{10}B(n, t)2^{4}He$ it is 0.3245 MeV. Thus from the point of view of Q-values and competing reactions $^{6}Li(n, \alpha)$ has to be preferred over ^{10}B. Also the level density of ^{7}Li is less than that of ^{11}B in the neighbourhood of the neutron binding

energy and there is less chance of weak levels contributing to the ^{6}Li cross-section than to that of ^{10}B. In ^{7}Li the first known level is at 247 keV above the neutron binding energy, whereas ^{11}B has two known levels within the first 150 keV.

1.1.2. Practical View-Points:

The disadvantage for ^{10}B of competing reactions can be judged from Table IV. (Here neutron scattering is not considered). We note that they are all very small. Furthermore these reactions are not so cumbersome for direct measurements of the (n,α) cross-section when the produced α-particles or the 478 keV γ-rays accompanying the deexcitation of $^{7}Li^{*}$ are detected. Also for $\sigma(n,\alpha)$ determination via $\sigma_{tot}-\sigma_{sc}$ only small corrections have to be applied in the energy region considered here.

TABLE IV. Cross-sections for neutron-induced reactions in ^{10}B (scattering excluded).

Possible reactions	Thermal energy	At higher energies
$^{10}B(n,\gamma)^{11}B$	$\lesssim$ 1 b [8] [9]	0(< 10 mb) at 230 keV [10]
$^{10}B(n,\alpha)^{7}Li$	3835 ± 14 b [11]	1 keV:(19.03±0.15)b; 10 keV [11] (5.99±0.06)b; 100 keV (2.01±0.06)b
$^{10}B(n,t)2\,^{4}He$	---	0 (< 60 mb) at 230 keV [12]
$^{10}B(n,p)^{10}Be$	< 7 mb [13]	E_n(10 keV-500 keV) < 30 mb [14] [15]

The $^{6}Li(n,\gamma)$ cross-section as taken from BNL 325, Suppl. 2, Vol. 1 [16] is (45 ± 10)mb at thermal energies whereas $\sigma(n,\gamma)$ for ^{3}He at thermal is inferior to 1 mb [16]. For all three reactions the competing cross-sections are small or can be corrected for.

a. Thermal energy-values:

An important advantage of ^{10}B and ^{3}He are the much larger and better known thermal values. The recommended value for $^{10}B(n,\alpha)$ at 2200 m/s is 3835 ± 14 b [11]. Also the thermal branching-ratio for this reaction is now known to a high precision (0.1%) [7], [17]. A new value of σ_a^o (^{10}B) was obtained by the life-time method at Argonne NL [18] of 3855 ± 26 b in agreement with the recommended value, although somewhat higher (but with rather large spread on the individual runs). For $^{3}He(n,p)$ [16] a value of 5327 ± 10 b is recommended. For $^{6}Li(n,\alpha)$ the situation is not so clear, because a large number of experiments has been made on isotopically not well-defined natural Li-samples. It has been established that isotopic variations dependent on geological source and chemical history of the sample exist. Cameron in a survey of commercial chemicals [19] found ^{6}Li contents different by more than 4%. Wagner et al. [20] were able to reduce the ^{6}Li-content of a natural sample from 7.4% to 6.65% (10%) by repetitive partial precipitation. An illustration of these possible variations is the 3% difference between the results of Meadows and Whalen [21] of 70.4 ± 0.4 barns for natural Li leading to a $^{6}Li(n,\alpha)$ cross-section of 953 b for the pure isotope

(7.42% ^{6}Li) and the value of a recent [18] measurement of 68.3 ± 0.4 b yielding a value for the ^{6}Li-isotope of 924 ± 6 b. This shows with how much precaution recommended values have to be handled e.g. 70.7±0.7 b recommended for natural Li in BNL 325 [16]. Work is in progress at Argonne NL [18] by the neutron life-time method, at Saclay [22] by a pile oscillation technique and at CBNM, Geel, by a precise transmission experiment on solutions of natural and enriched Li_2SO_4 in D_2O.

Preliminary results are available from Argonne and yield a value of 938 ± 6 barns for the enriched samples, but a value of only 924 ± 6 barns is obtained with the "natural" Li-sample. The difference of about 1.5% may be due to an error in the ^{7}Li/^{6}Li-mass ratio (due to mass-discrimination) that has its largest effect on σ_a in the case of the natural sample. However, this important cross-section needs further examination, eventually also by looking directly at the ^{6}Li(n,α)-reaction in well-defined LiF-layers (weighed in vacuum) with a solid state detector in a known geometry in a comparison with "absolute" boron layers. Furthermore for the accurate determination of σ_a at 2200 m/s via transmission experiments the problem of the scattering cross-section remains unsolved. There is the disagreement between the coherent scattering length for the isotope ^{6}Li as measured by Peterson and Smith [23] with resonant neutrons $a_{coh} = +1.8f$($\sigma_{coh} = 0.4$b) and $a_{coh} = +7f$($\sigma_{coh} \cong 6$b) as calculated from the data of natural Li and ^{7}Li at thermal energy by Shull and Wollan [24]. From a fit to the total cross-section in an energy-region below 5 keV (1/v term + constant) Uttley and Diment [25] found a value for the constant term of 0.696 barns which is in very good agreement with the preliminary value for the low energy scattering cross-section obtained by Asami and Moxon [26] of 0.7 barn. However, a careful measurement of σ_s at exact thermal energy remains necessary for standardization of $\sigma(n,\alpha)$ via σ_{tot}.

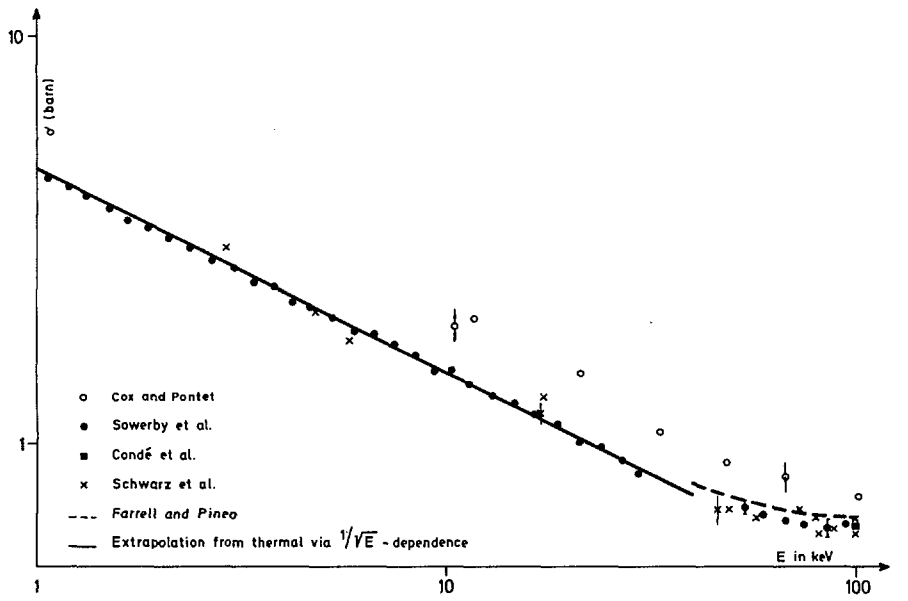

FIG.1. The ^{6}Li(n,α)-cross-section from 1 to 100 keV.

b. Higher energy-region (especially up to 100 keV)

(1) ^{6}Li: In fig. 1 we summarized some of the available data for $^6Li(n,\alpha)$ between 1 and 100 keV and in fig. 2 the recently available data from 100 keV to 1 MeV. A few remarks have to be made. The total cross-section of ^{6}Li has recently been measured by Farrell and Pineo [27] in the energy range 50 to 650 keV, by Hibdon and Mooring [28] in the energy range 10 to 1236 keV and by Uttley and Diment from 70 eV to 7 MeV [25]. These data agree reasonably well among each other in the energy-region below 100 keV, but not as well at the resonance peak of the 247 keV resonance (especially the data of Farrell and Pineo are lower). The total cross-section is considered as an s-wave contribution on which the 247 keV p-wave resonance is superimposed.

Resonance parameters were deduced by Uttley and Diment and by Farrell and Pineo based on the total cross-section results. The region below 5 keV is considered as the s-wave contribution by Sowerby et al. [29] represented by $\sigma_{nT}(Li) = 149.5/\sqrt{E(eV)} + 0.696$ barns with the $1/\sqrt{E}$-term being the (n,α) and the constant term the elastic scattering cross-section

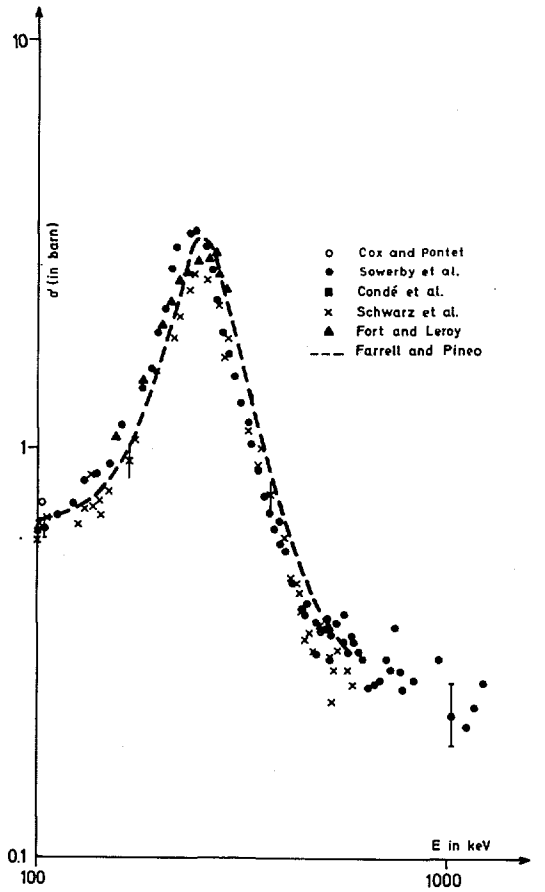

FIG. 2. The $^6Li(n,\alpha)$-cross-section above 100 keV.

in this region. The absorption cross-section was obtained in two ways by the Harwell-group: (1) by subtracting a calculated scattering cross-section [30] and (2) the absorption cross-section was calculated from the resonance parameters + s-wave absorption. Also Farrell and Pineo [27] calculated $\sigma(n,\alpha)$ from an analysis of their total cross-sections, and they disagree with the Harwell-results in the region of the 247 keV-resonance, but their measurements only come down in energy till about 50 keV. In the region below 100 keV, which is of very great importance for Li as a standard cross-section, there is agreement between the data of Sowerby et al. [29], Farrell and Pineo [27], Schwarz, Strömberg and Bergström [31], as well as with the absolute spot-point at 100 keV obtained by Condé et al. [32]. The data of Schwarz et al. [31], are, however, relative data normalized to a $1/\sqrt{E}$-extrapolation from a 945 b 2200 m/s $\sigma(n,\alpha)$ cross-section up to 10 keV. The data of Barry [33] and of Bame and Cubitt [34] are not present in the plot because they are normalized with respect to the ^{235}U fission cross-section. In fact, recent high resolution measurements of the ^{235}U fission cross-section reveal considerable structure in this cross-section up to at least 166 keV [35] [36] [37] and σ_f is certainly not suited there to deduce a secondary standard cross-section, as errors of up to 10% can be introduced, depending on the resolution of the experiment. This remark also applies to spot point measurements, e.g. with a Sb-Be-source (22 keV) because of the neutron source energy spread.

There is definitely a difference between the data of Sowerby et al., Schwarz et al., and Condé et al. on one side and the data of Cox and Pontet [38] on the other side, these latter data being considerably higher. The data of Cox and Pontet are obtained from the spherical shell transmission method. Also their data on ^{10}B obtained with the same technique would yield by extrapolation to thermal energy via a $1/\sqrt{E}$-law a higher value than the recommended thermal value ($\approx$ 6% higher). However, the technique is an absolute one and the difference remains unexplained. Certainly either the Cox-data or the Harwell data are wrong because at 10.7 and 12 keV the values of Cox coincide with the total cross-section Harwell data.

In the region above 100 keV the most recent data are shown in fig. 2. (Older data were deleted, because the accuracies are low or the multiple scattering corrections were not applied or the chosen standard was not suitable). New data also here are the data of Sowerby et al. [29] and new data of Leroy et al. between 100 and 500 keV energy not shown here will be presented at this conference [39]. The general agreement in this energy region is not better than 10%.

There is another region of interest for the $^{6}Li(n,\alpha)$ cross-section from 0.5 to 3.2 MeV for ^{6}Li semiconductor spectrometers in the measurement of fast reactor neutron spectra, where the $\sigma(n,\alpha)$-cross-section is only known to about 20%, and certainly needs further attention.

(2) ^{10}B: The $^{10}B(n,\alpha)$ cross-section and the branching ratio of this reaction have been recently reviewed by Gubernator and Moret [11]. They use essentially 4 data sets obtained from 4 different techniques, i.e. Mooring, Monahan and Huddleston [14], who measured the total cross-section and simultaneously the ratio of the scattering to total cross-section, Cox [40], [38], who used the spherical shell transmission method which gives a direct measure of the absorption cross-section; Diment [41] who measured the total cross-section from 100 eV to 10 MeV and determined the absorption cross-section up to 500 keV by subtracting

the scattering cross-section of Mooring et al. [14] from the total cross-section, and Macklin and Gibbons [42] who measured the inverse reaction and multiplied by the appropriate branching-ratio to obtain the $^{10}B(n,\alpha)$ cross-section by reciprocity. It was also dealt with in detail by Gibbons [3]. These authors, Gubernator, Moret and Gibbons conclude that the cross-section follows a 1/v law to within 2% below 100 keV. In the low keV and eV region the shape is the most critical as normalization is often established in this range by extrapolation from 2200 m/s. From their recent $^{6}Li(n,\alpha)/^{10}B(n,\alpha)$ cross-section ratio measurements however Sowerby et al. conclude making use of the shape of the $^{6}Li(n,\alpha)$ cross-section of Uttley and Diment [25] to deduce the $^{10}B(n,\alpha)$-shape, that $^{10}B(n,\alpha)$ does not vary as $1/\sqrt{E}$ and that the cross-section falls below that level reaching a minimum in the region of 25 keV where the cross-section is about 4% below the 1/v extrapolation, and then it rises and shows a resonance and peaks at about 150 keV ($\approx$8% above 1/v).

This resonance should correspond to a level at (140 $\pm$ 35) keV in ^{11}B as listed in the level compilation of Lauritsen and Ajzenberg-Selove [6]. Following Gubernator and Moret there is a similar but weaker deviation from 1/v in this energy range. We should note, however, that the Harwell data are obtained from a ratio-measurement and that in the energy region 150 - 200 keV the shape of the $^{6}Li(n,\alpha)$ cross-section is not so well established as was shown in fig. 2. Both Gubernator and Moret and Sowerby et al., derived formulas for $\sigma(n,\alpha)$, based on a formula proposed by Bergman and Shapiro [44]:

$$\sigma_r = A\,E_n^{-1/2} + \Delta\sigma + \beta\sqrt{E_n} + C\,E_n \qquad (1)$$

(constants for E in keV and σ in barns)

where Sowerby et al. added an s-wave resonance in the region of 150 keV to the first three terms of the expansion (1). Below 100 keV the recommended values agree within the assigned error. The values obtained for $\Delta\sigma$ are $\Delta\sigma$ = -0.32 b (Gubernator and Moret) and $\Delta\sigma$ = -0.31 b (Sowerby et al.), in reasonably good agreement with the value of Bergman and Shapiro of $\Delta\sigma$ = -0.40 $\pm$ 0.03 b from a $^{6}Li(n,\alpha)/^{10}B(n,\alpha)$ ratio measurement [43]. The sign of the β-correction term is different in the analysis of Harwell compared with the other authors. They attribute this change in sign to the fact that Bergman and Shapiro did not include the 247 keV-level in ^{6}Li that contributes about 5% of the cross-section at 25 keV, the upper limit of their analysis of the $^{6}Li/^{10}B$-ratio.

In fig. 3 we show both recommended $\sigma(n,\alpha)$ cross-sections for ^{10}B (from .1 to 200 keV).

In many experiments, especially at higher energies, one uses only the $^{10}B(n,\alpha\gamma)^{7}Li$-reaction as a standard via the detection of the 478 keV-γ-ray. So the branching-ratio of the reaction $\sigma(n,\alpha_0)/\sigma(n,\alpha\gamma)$ should be known. The requirements for this ratio are not so high below 100 keV as the uncertainty enters only in a correction of about 6%. Gubernator and Moret give an uncertainty of 5% (95% confidence limits) resulting in a cross-section error for $\sigma(n,\alpha\gamma)$ of 0.3%. From 100 keV to 1 MeV the uncertainties in the cross-section are of the order of 10% and of the order of 20% in the branching ratio.

(3) ^{3}He: The ^{3}He cross-sections from 0-10 MeV were reviewed recently by Als-Nielsen [44]. Below 11 eV, Als-Nielsen and Dietrich [45] have shown that the cross-section is 1/v to within 1%. Inverse reaction measurements $^{3}H(p,n)^{3}He$, of which the most recent and accurate have

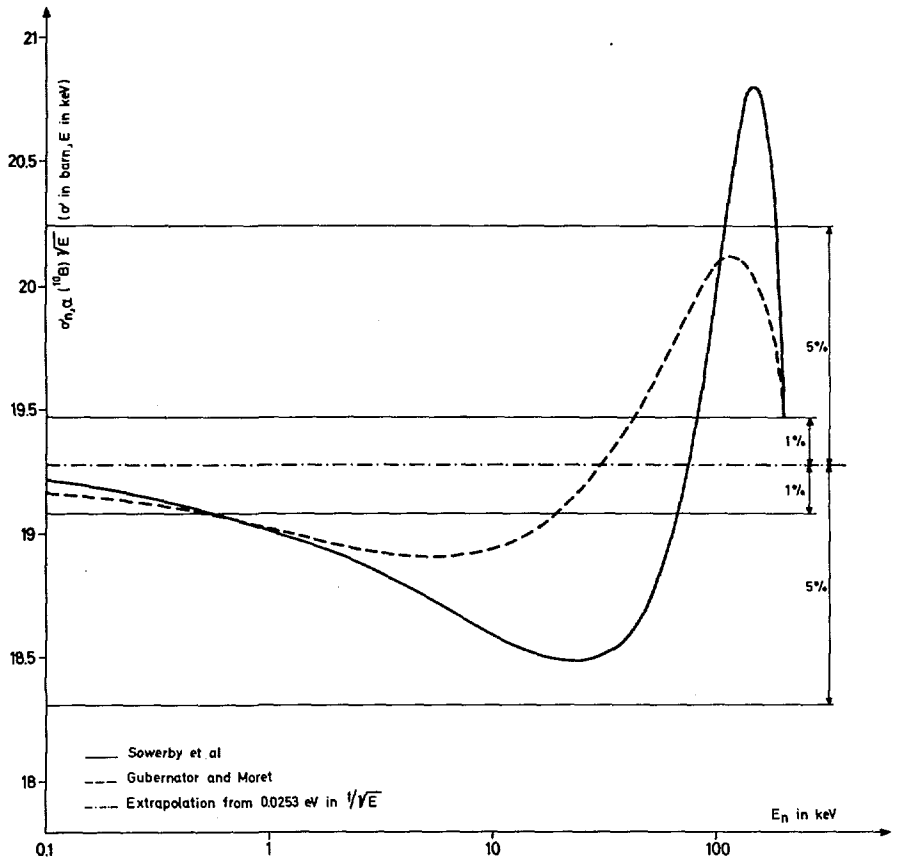

FIG.3. Comparison of recommended values for $^{10}B(n,\alpha)$ between 1 and 100 keV by Sowerby et al. and by Gubernator-Moret.

been reported by Macklin and Gibbons [46] extend the knowledge of the $^{3}He(n, p)$ cross-section down to 4 keV and cover the energy range up to 290 keV. The range from 11 eV to 4 keV is not covered. The inverse reaction measurements give very accurate relative cross-sections with about 2% relative precision following Macklin and Gibbons [17]. However, the absolute accuracy in the region above 4 keV seems not to be better than 10%, due to normalization of the inverse reaction. (Macklin and Gibbons normalize to a value of 1.98 b at 100 keV from a previous direct measurement [47]). The values of the cross-section in the keV-region (5 - 100 keV) are considerably lower than that what one would expect from a $1/v$-extrapolation of the thermal cross-section (i.e. 7% at 5 keV, 25% at 100 keV). This disagreement can be explained by the theory of Shapiro [48], that also can serve for an extrapolation in the region where the cross-section is not measured [44] up to the measurement of Macklin and Gibbons where the extrapolation is only 3%

lower than the measured values. So these data are in agreement with this extrapolation in view of the normalization errors. It is more difficult to use the $^{3}He(n, p)$ reaction as a standard above 4.4 MeV neutron energy, the threshold of the $^{3}He(n, d)^{2}H$ reaction, due to confusion of the desired protons with deuterons from the (n, d)-reaction.

1.1.3. Discussion

In Table V the estimated accuracy of the three cross-sections are given at typical energies.

So although the $^{10}B(n,\alpha)$-cross-section has some disadvantages: possible presence of resonances, competing reactions, smaller Q-value than $^{6}Li(n,\alpha)$, it is certainly known at present to a higher degree of accuracy. Furthermore it can be used in gaseous, solid or liquid form, has a considerably larger cross-section than $^{6}Li(n,\alpha)$ and emits a very useful γ-ray with the α-particles in a large fraction of the reactions, allowing for fast detection. ^{6}Li is most commonly used in a Li-glass detector. However, there is the gamma-ray sensitivity, the limitation of Li content in the glass to about 10%, as well as the relatively large scattering to capture probability in the scintillator which causes a deterioration of the fast time response as well as significant corrections for multiple scattering. $^{3}He(n, p)$ is well suited at low energies, but at higher energies (keV-region), its very low Q-value and the lack of a stable fast detector makes it unuseful as a primary standard.

The practical primary standard below 100 keV remains $^{10}B(n,\alpha)$, but $^{6}Li(n,\alpha)$, once the thermal value is known to a higher precision could become a serious competitor.

TABLE V. Estimated accuracies for $^{10}B(n,\alpha)$, $^{6}Li(n,\alpha)$, $^{3}He(n, p)$.

Reaction	$^{10}B(n,\alpha)$	$^{6}Li(n,\alpha)$	$^{3}He(n, p)$
Thermal (2200 m/s)	0.3%	2%	0.2%
1 keV	1%	3%	2%
10 keV	2%	5%	10%
100 keV	3%	5%	10%

1.2. $^{1}H(n, n)^{1}H$

has been reviewed in detail by Hopkins [2]. This reaction is the basis of the proton recoil detector, which is commonly used experimentally in one of the following forms: (1) hydrogen or methane filled proportional counter, (2) polyethylene radiator + semi-conductor detector, (3) telescope counter, (4) plastic or scintillation counters.

To obtain differential (with respect to angle) cross-sections one needs the total cross-section and relative angular distribution. For the total elastic cross-sections only a very small capture cross-section ($\lesssim$ 1 mb) has to be subtracted from the total cross-section ($\sim$ 1 b).

Very recently it had been suggested that a careful examination of the available experimental data indicates fluctuations of about 5% in the values of the n-p cross-section [49] , and that these fluctuations were most apparent in the energy region 3 to 20 MeV. Several authors [50], [51], [52] have since shown, however, that if such oscillations were present, their value should be extremely small, so it may be accepted that the cross-section has no structure. New measurements were also performed by Langsford and Clements [53]in the energy range between 0.8 and 5.8 MeV with an accuracy between about 0.3 to 0.5%. The results agree with the results of Engelke et al. [54] and lie about 0.7% higher than the earlier data. These authors hope to extend their measurements down to 100 keV. It is in the lower energy region (< 500 keV) from an experimental point of view, that the situation is especially unsatisfactory.

From a more theoretical point of view there is the work of Gammel [55] who uses an analytical form (based on effective range theory) for the total cross-section to interpolate between values, quoted with a precision of 0.5% up to 4.7 MeV and to about 1% at 14 MeV. Gammel states that the region below 1 MeV is more in doubt. He also gives an expression for the $\sigma(180°)/\sigma(90°)$-ratio. Very recently Hopkins and Breit [57] have calculated the best possible values of the free n-p scattering total cross-sections and differential cross-sections from phase-shift analysis between 100 keV and 30 MeV. The anisotropies (cross-section ratios (180°)/(90°)) obtained are approximately 1.023 at 7 MeV, 1.011 at 3 MeV, and 1.004 at 1 MeV whereas Gammel's phenomenological formula yields 1.012 at 7 MeV, 1.002 at 3 MeV, and 1.0002 at 1 MeV. The anisotropy following Hopkins and Breit is considerably larger. However, the 180° cross-sections (corresponding to the forward-going proton at 0°) which are of interest for proton recoil measurements have been estimated with reasonable accuracy by the Gammel expression. In Table VI the last experimental data on σ_{tot} of Langsford and Clements together with their calculated values and the calculated values of Gammel and Hopkins and Breit are represented.
The agreement between the data and the calculations is excellent.

Above 500 keV up to 10 MeV the total cross-section is known to about 0.5%. Below 500 keV down to 100 keV the cross-section may be known to 1%. Below 100 keV the problem of the detection of the proton-recoils becomes a major problem, although the cross-section is still well-known.

Hopkins in his recent report gives a representation of the C.-M. $^1H(n,n)^1H$ differential cross-section in terms of Legendre polynomials using phase shifts and quotes standard deviations for the differential cross-section differences $\sigma(90°) - \sigma(180°)$ of approximately $\pm$ 35% for incident neutron energies between 100 keV and 10 MeV, $\pm$ 20% for incident energies between 10 and 15 MeV, and $\pm$ 10% for energies between 15 and 30 MeV.

The accuracy of neutron flux determination above a few MeV with a proton recoil telescope counter is limited by insufficiently known differential cross-sections. Therefore new relative differential measurements between 5 and 20 MeV with $\pm$ 1% relative error are required, also in view of the new results of the anisotropy calculations by Hopkins and Breit. But generally speaking in the whole energy range considered the largest uncertainties in flux determination are due to the detectors used and not to the uncertainties in the cross-sections.

TABLE VI. $^{1}H(n,n)^{1}H$ cross-section values.

Energy MeV	Langsford and Clements (experimental) Cross-section in barn	Statistic. error in barn	System. uncertainties in barn	Langsford and Clements (theoret.)	Gammel (1963) in barn	Hopkins and Breit (1970) in barn (approx.)
0.8408	4.690	0.005	0.008	4.677	4.681	4.688
1.1615	3.947	0.004	0.007	3.936	3.930	3.934
1.4535	3.493	0.004	0.008	3.486	3.475	3.482
1.7503	3.156	0.003	0.007	3.146	3.132	3.142
2.0435	2.893	0.004	0.008	2.881	2.868	2.880
2.3463	2.674	0.004	0.007	2.661	2.672	2.685
2.7188	2.439	0.003	0.007	2.437	2.421	2.434
3.3239	2.164	0.003	0.007	2.152	2.142	2.156
4.3746	1.796	0.003	0.005	1.795	1.782	1.795
5.8581	1.455	0.003	0.004	1.456	1.447	1.456

1.3. C(n, n)Pb(n, n)

C(n, n) has been suggested as a secondary standard for use in the measurement of fast neutron scattering cross-sections below about 1.5 MeV by Batchelor [2] due to the absence of competing reactions apart from the small $^{12}C(n,\gamma)$-cross-section. It competes in this region with H(n, n) that has a smooth variation with energy and an angular distribution that is nearly isotropic. C(n, n), however, has also advantages. Pure carbon samples can be obtained whereas hydrogen is often used in a mixture such as polyethylene; scattered neutron energy varies more slowly with angle and is under most angles larger than for H(n, n), making detection easier and the "time-of-flight" peak narrower. This reaction is discussed in more detail by Knitter [57] at this conference.

Lead can be used in the low keV-range as a scattering standard and has the advantage of smaller energy-loss in collisions which is interesting when neutron detection is made with a detector that has an energy-dependent efficiency (e.g. Li-glass).

1.4. Capture cross-sections

Standard capture cross-sections have been discussed recently by Pönitz [2] and Gibbons [3]. The $^{197}Au(n,\gamma)$ cross-section is certainly the most commonly used standard. At thermal energy its value is known to a high precision (0.3%) 98.7 ± 0.3 b [2] [3]. (Also the thermal Co-activation cross-section is often used). In the keV-range several compilations have been made, but this capture cross-section will be discussed in more detail in connection with $^{235}U(n,f)$ by Pönitz [58] at this conference. We also want to remember the suggestion of Gibbons [3] to use $I(n,\gamma)$ as standard especially for non time-of-flight experiments because of the good ratio of keV- to thermal capture cross-sections for this isotope.

TABLE VII. ^{235}U fission integrals normalized at IAEA best value $\sigma_F^o = 580.2 \pm 1.8$ barn via our integral $\int_{7.8\ eV}^{11\ eV} \sigma_F(E)dE = 237.1 \pm 2.1$ barn · eV.

Energy interval	Our results	de Saussure	Cao et al.	Michaudon		Mostovaya	$\sqrt{\frac{\Sigma(I_n - \bar{I}_n)^2}{N(N-1)}}$	$\sqrt{\frac{\Sigma(I - \bar{I})^2}{N(N-1)}}$	Bowman	Brooks	Ryabov	Shore - Sailor
0.50 - 0.70	13.26	13.47		13.86			0.176	0.197	12.73	14.43		13.21
0.70 - 1.00	16.66	17.05		17.28			0.181	0.199	16.30	17.92		16.87
1.0 - 1.8	29.11	29.19		29.88		29.09	0.189	0.522	27.81	31.64		30.06
1.8 - 5.0	49.96	50.70		50.09		49.07	0.336	0.665	45.32	50.93	58.55	52.23
5.0 - 7.4	62.11	62.30		61.14		61.60	0.262	1.141	280.73	62.83	67.19	58.81
7.4 -10.0	220.00	219.6	219.9	215.5	216.5	216.14	0.858	3.148		221.56	211.84	210.41
10.0 -15.0	214.4	216.8	212.3	217.8	217.1	210.5	1.202	3.171	211.4	217.7	224.1	
15.0 -20.5	316.0	316.3	304.9	309.6	292.3	302.9	3.786	6.326	319.7	307.4	303.4	
Fission integral from 7.8 to 11 eV calculated from the original data	237.1	236.7	226.6	238.1	232.6	255.6	Standard deviations of the mean value of the fission integrals after and before renormalization		246.7	215.1	217.8	Renormalized at $\sigma_F^o = 580.2 \pm 1.8$ barn
20.5 - 33.0		447.8	430.2	457.9	435.3	451.9	5.17	13.01	439.9	459.6	456.6	
33.0 - 41.0		497.1	493.5	482.0	453.6	508.3	9.32	17.02	497.4	458.6	499.7	
41.0 - 60.0		918.4	882.1		855.2	941.5	19.12	41.25	930.9	914.9	888.3	
60.0 - 100.0		975.5	944.2 951.6		950.0	1018.5	13.72	35.98		914.9	1053.8	
100.0 - 200.0		2097.4	2040.6 2033.2		2067.1		14.34	35.24		1954.8	2183.5	
200.0 - 300.0		2085.3	1850		2098.7		75.5	97.6			2238	
300.0 -1000.0		8138.5	7297		8262.4		303.4	380.5			8830	

1.5. Fission cross-sections

$^{235}U(n,f)$ and $^{239}Pu(n,f)$ reactions from thermal to several MeV neutron energy are important reactor requests and have been studied in detail by many authors. At thermal energies and in the keV-region they have been used as secondary standards. Reasons for their use as standard cross-sections are the large Q-values of the reactions and the stability of the detectors. Another argument, the smooth variation of σ_f with E_n in the range above 10 keV, seems to be invalidated by recent measurements where structure was observed in $\sigma_f(^{235}U)$ up to 166 keV [35] [36] [37] (fluctuations of 30% in the region of 20 keV, and at least 5 to 10% in the region of 100 keV). The use of ^{235}U as a standard below 200 keV in the present situation is not to be recommended and older measurements relative to this isotope (e.g. $^{6}Li(n,\alpha)$, $^{197}Au(n,\gamma)$...) should be carefully reconsidered.

Structure in the ^{235}U-fission cross-section has been previously reported by Albert [59] in the energy range between 0.1 to 2 MeV. However, this structure was never confirmed by other authors [60] [61] [62] who found a smooth variation with energy.

In the paper CN 26/100 of this conference we deal with the 2200 m/s fission cross-sections of both isotopes. We would like to draw the attention here also to an often underestimated problem of normalization of fission cross-sections. Precise measurements of σ_f of ^{235}U were made at CBNM relative to a $1/v$-$^{10}B(n,\alpha)$ cross-section below 22 eV [63] for a direct normalization at 0.0253 eV of the relative cross-sections. Our data are normalized to the IAEA best 2200 m/s value of σ_f (580.2 $\pm$ 1.8) barn [64] and then fission integrals are calculated. For further normalization of σ_f (^{235}U) we propose our fission integral:

$$\int_{7.8\ eV}^{11\ eV} \sigma_f(E)dE = 237.1 \pm 2.1\ \text{barn}\cdot\text{eV},$$

a very suitable integral, because it contains a large resonance (high counting-rate) and timing errors will affect this integral only very little because of the small cross-sections at its limits.

In order to compare our results with previous results obtained by other ways of normalization and/or with other detection techniques we summarized the results of several authors [65] [66] [67] in Table VII. The integrals from 7.8 to 11 eV were obtained from the integration by CCDN of differential data retrieved from their files. These values show differences up to 20%. When examining the normalization procedures for these measurements we find that they are nearly all different. Only the measurement of Bowman et al. [68] and ours are directly normalized at σ_f^o. All the other normalization methods are indirect, thus less precise, and sometimes very peculiar, e.g. Mostovaya [69] normalized her cross-section curves to the mean σ_f-curve from 0.8 to 0.9 eV from BNL 325, Suppl. II. However, when normalizing the different measurements in the same way i.e. at our fission integral from 7.8 eV to 11 eV we obtain a considerable reduction of the discrepancies proving in this way that the existing differences between the results are for a large part due to the normalization method and not caused in most cases a different quality of the relative measurements.

From Table VII, we arrive at the following conclusions:
In the energy-region from 0.7 eV to 15 eV we obtain a very good agreement (within 3%) after renormalization between our results and those of

TABLE VIII. ^{239}Pu fission integrals.

Energy interval (eV)	Our results (preliminary)	GWIN [79]		BLONS [75]	BOLLINGER [76]	RYABOV [77]	IGNATIEV [78]
6.0 - 9.0	179.1	181.0		181.6	173.0	107.0	159.0
9.0 - 12.6	498.1	496	498	509.6	516.9	348.3	412.9
12.6 - 20.0	537.1	547	546	554.8	538.4	479.5	443.2
20.0 - 24.7	221.0	225	221	222.0	221.4	191.8	177.4

de Saussure [65], Cao et al. [66], Michaudon et al. [70]and Mostovaya [69]. The deviations from the mean are considerably reduced (compare columns 7 and 8). There is also a good agreement with the results of Bowman et al. [68] (except for the integral from 1.8 eV to 5.0 eV) and with those of Shore and Sailor [71]. The values of Brooks [72] (no direct measurement; σ_f obtained via σ_t and η) are systematically higher than all the other data after renormalization. The data of Ryabov [73] are doubtful as there exist differences of 20% between his two data sets.

In the energy region from 15 eV to 1 keV we now obtain a much better agreement between the results of Cao, Michaudon, Mostovaya and de Saussure (within 10%, before within 20%). The deviations from the mean are considerably smaller after renormalization (compare columns 7 and 8 of Table VII). Also the data of Bowman and Brooks are in much better agreement with the other data in this energy range. The data of Ryabov are generally higher than all the other data-sets.

Similar measurements of σ_f (^{239}Pu) were made below 40 eV [74] and normalization at the 2200 m/s σ_f-value recommended by IAEA of σ_f^o = 741.6 ± 3.1 barn was performed. Again fission integrals were calculated as shown in Table VIII. In this table are also shown integrals calculated by CCDN from their data files for Blons et al. [75], Bollinger et al. [76], Ryabov et al. [77] and Ignatiev et al. [78]. Gwin et al. [79] supplied us with the quoted fission integrals.

We note again the very large differences of the fission integrals, especially with the data of Ryabov and Ignatiev. Our data and the data of Gwin et al. were normalized independently in the same way and the agreement is excellent. The agreement with Blons et al. and Bollinger et al. is reasonably good (within 2 to 3%).

Certainly again a normalization to our integral from 9.0 - 12.5 eV would bring the data (especially Ryabov and Ignatiev) in much better agreement. We hope to obtain more information on results from Harwell and from Shunk et al. [80] to be able to make a more detailed comparison.

We will not discuss in detail the higher energy region for σ_f(^{239}Pu) as this will be treated in this conference by several authors, but from the available data on the fission cross-section it seems to be less energy-dependent than for ^{235}U.

1.6. Neutron multiplicity

$\bar{\nu}$ from spontaneous fission of ^{252}Cf is widely accepted as a standard and is requested to 0.25% accuracy. At this conference a report on $\bar{\nu}$ of fissionable nuclei will be presented by Colvin. The most recent discussion of $\bar{\nu}$ (Cf^{252}) has been made in detail by Hanna et al. [64], but discrepancies of 2% persist between different methods. Recently Axton et al. [81] have published a technique for absolute counting of nuclear fission events that they intend to use for a new measurement of this quantity with a better Cf sample.

1.7. Threshold-reactions

Cross-section curves of (n, p), (n, α), (n, 2n), (n, n') are often measured against working standards such as ^{32}S(n, p) or ^{27}Al(n, α). The differential cross-section results for these standards were critically reviewed by Liskien and Spaepen [2] and resulted in evaluated best curves which are presented in tabular and graphical form in reference 2. Recently

a precision measurement (± 1%) of the $^{27}Al(n,\alpha)$ cross-section at 14.4 MeV was reported [82]. For other working standards as $^{56}Fe(n,p)$ and $^{65}Cu(n,2n)$ more measurements and evaluation work have to be done.

2. NEUTRON FLUX MEASUREMENTS VIA STANDARD METHODS

Here we want to discuss briefly methods for flux measurements independent or nearly independent of absolute cross-sections. We will restrict the discussion to the latest new results and improvements that were communicated to us.

2.1. Associated particle method

The charged particle produced at the same time as the neutron in reactions such as $T(d,n)^4He$ ($E_n \approx 14$ MeV), $D(d,n)^3He$ (E_n: 1.9 to 2.1 MeV) and $T(p,n)^3He$ (E_n: 200 keV to 1.5 MeV) is identified (with or without coincidence between particle and neutron detector) and counted in a defined solid angle, thus determining the neutron flux in a defined solid angle according to the reaction kinematics. Leroy et al. [83] report a precision of about 2% in neutron flux determination between 10 keV and 1 MeV by intercomparison of three different absolute methods: associated particle counting with the reaction $T(p,n)^3He$, manganese sulfate bath method calibrated with a calibrated Ra Be-source, proton recoil proportional counter [83]. At present, however, his best results come from the manganese sulfate-bath in a collimated geometry (accuracy 1.6%).

Also Liskien and Paulsen [84] have made a comparison of the associated particle method based on $T(p,n)^3He$ recoil proton telescope and methane-filled proportional counter. The agreement at 1 MeV was within 2%. A comparison at 0.5 MeV was also made and is planned at 250 keV.

2.2. Associated activity method

The number of neutrons emitted in a nuclear reaction has been deduced in some cases from the activity of the reaction products. $^{51}V(p,n)^{51}Cr$, e.g. is being used in the 500 - 600 keV region by Pönitz with a spherical fission detector to determine $\sigma_f(^{235}U)$ [85]. Improvements in the deduction of the activity via the $^7Li(p,n)^7Be$ reaction can now been obtained, thanks to more precise measurements of the ^7Be branching-ratio of Taylor and Merritt [86] of 0.1035 ± 0.0008 and a preliminary result of Mutterer and Spernol [87] of 0.1044 (± 2%). Also a new preliminary value for the branching-ratio in the electron-capture decay of ^{51}Cr to the 320.1 keV level in ^{51}V has been obtained by Taylor and Merritt [86] of (0.0972 ± 0.0015).

2.3. Flat response counters

This method is generally based on the slowing-down of the neutron in a hydrogeneous medium (or graphite) and counting at thermal energy. Such detectors have a rather constant efficiency as a function of neutron energy and have to be carefully shielded for scattered neutrons. Several such detectors have been described in the literature, starting with the long counter of Hanson and McKibben [88] which is less flat in response over the graphite sphere detector of Macklin [89], the boron pile, etc. Recently Pönitz [90] has developed his "grey detector" which is a paraffine sphere with a neutron beam entrance channel and a lead shielded NaI(Tl)-crystal to detect the 2.2 MeV capture γ-rays. The sphere is large

enough for moderated neutrons to be captured in hydrogen but causes in this way the time response to be slow ~ 1 ms. The energy range of application depends on the sphere dimensions; Pönitz used it to measure in the range 25 - 500 keV with a precision of about 3%. At this conference a neutron detector with a flat energy response for use in time-of-flight experiments will be presented by E.R.Rae et al. [91] where the detector is a spherical homogeneous mixture of vaseline ($CH_{2.05}$) and ^{10}B with a radial re-entrant hole. Neutrons are moderated and then captured in ^{10}B to produce 478 keV γ-rays which are detected in the same way as with the Pönitz detector. The neutron energy limit (on the high side) and the neutron life-time increase with sphere size. It is of course desirable to have E_{max} as large as possible so that the sphere-size will be limited by the maximum acceptable neutron life-time. For a practical neutron time-of-flight detector the criterion will be set by the timing resolution needed. For the 300 m flight-path at the Harwell Linac-booster the life-time should not be longer than ~ 0.7 /usec, leading to a choice of a detector with 12 cm radius [91]. Of course this detector will have to be calibrated at low and higher energies.

2.4. Bath methods

Manganese sulfate baths and more recently vanadium sulfate baths have been used to calibrate the neutron output of (α, n) and (γ, n)-source and also in the determination of $\bar{\nu}$. The results of an international comparison analysed by BIPM of a Ra-Be (α, n) source show a spread of $\pm$ 1% about the mean value and are compatible within the errors quoted by each laboratory [2].

A $MnSO_4$-bath detector with a re-entrant hole calibrated with a Ra-Be source from BIPM has been developed and used by Leroy et al. for further calibration of neutron detectors.

3. CONCLUSIONS

(1) To avoid confusion in results on standard data it is absolutely necessary that measurements are only carried out on samples that have been analysed with all possible means (isotopic and chemical analysis on witness-samples of evaporated or electrosprayed materials; counting for radioactive samples with different counters and in different geometries; mass determination by weighing in vacuum and isotope dilution techniques or controlled potential coulometry afterwards, cross-comparison of methods, relative measurements in a neutron flux etc. . .). Typical examples from our laboratory are differences in the $^{10}B/^{11}B$-ratios in evaporated materials compared to the starting material of a few percent; considerable differences in $^6Li/^7Li$-ratios in "so-called" natural lithium etc.

(2) The $^{10}B(n,\alpha)^7Li$ cross-section below 100 keV is still the most useful standard cross-section. The recent results of Harwell indicate deviations from a 1/v-behaviour. However, these data are based on a measurement of $(\sigma_t - \sigma_{sc})$ of ^6Li and a ratio measurement $\sigma_a(^{10}B)/\sigma_a(^6Li)$. As the scattering cross-sections in the higher zone of this energy range are considerable it is recommended to make a direct comparison $^6Li(n,\alpha)/^{10}B(n,\alpha)$ to avoid the indirect methods. Such a measurement was started by CBNM Geel [92] at the Harwell Linac. Nevertheless from the preceding discussion of the standard cross-sections it follows that ^6Li, as it is often

used in ^{6}Li-glasses and as its energy dependence may be easier described than that of ^{10}B, might be a useful standard, but it is necessary to improve the accuracy of this standard cross-section considerably at thermal and at higher neutron energies. For the use of $^{10}B(n,\alpha\gamma)$ as a standard above 100 keV improvement of the knowledge of the cross-section and the branching-ratio are still requested.

For H(n, n) the new calculations of Hopkins and Breit yielded values for σ_{tot} in agreement with the phenomenological formula of Gammel, however considerably different anisotropies, which have to be verified by experiment. Efforts to improve the techniques of using the well-known H(n, n) cross-section, especially below 500 keV should be continued. H(n, n) remains the most suitable primary standard cross-section above 100 keV.

^{3}He(n, p) has been used in the low energy-region, an extension as standard cross-section to higher energies may be possible if ^{3}He gas-scintillation detectors with fast response time can be operated in a stable way.

H(n, n) above 100 keV and $^{10}B(n,\alpha)^{7}$Li seem still to be the most indicated as primary standard cross-sections. However, intercomparison with other cross-sections should yield secondary standards preferably for each type of reaction: $^{6}Li(n,\alpha)$, $^{3}He(n,p)$, $^{197}Au(n,\gamma)$, $^{235}U(n,f)$, C(n, n), Pb(n, n), etc.

(3) At present data obtained relative to ^{235}U especially in the lower keV-region seems to be seriously in doubt, and authors having used this standard cross-section should re-assess their values, in view of the later data. For fission cross-sections attention should be given to the way the data are normalized in the resonance region as this can introduce serious discrepancies. It may be worthwile to look for another standard fission cross-section, e.g. ^{233}U in view of the difficulties with ^{235}U.

(4) To fulfill reactor requests as tabulated in Table I still a long way of improvement of standard materials and detection techniques is required.

ACKNOWLEDGEMENTS

The author wishes to thank for private communications and release of data prior to publication Drs. E. J. Axton, R. S. Caswell, H. Condé, G. C. Hanna, J. C. Hopkins, J. L. Leroy, R. L. Macklin, J. W. Meadows, A. Paulsen, W. P. Pönitz, M. Sowerby.

He is very grateful to Dr. J. Spaepen for valuable discussions and guidance in the preparation of the text.

He is indebted to many colleagues of the CBNM for critical reading and comments, especially to Drs. A. Spernol, Prof. A. H. W. Aten and A. Paulsen and to Dr. M. Nève de Mévergnies of SCK-CEN (Mol) Belgium.

He also wants to thank Mrs. M. L. Mallants and Mr. Van Saene for the help in the preparation of this text.

REFERENCES

[1] SPAEPEN, J., Nuclear Data for Reactors, Vol.I, IAEA Vienna (1967) 241.
[2] Nuclear Standards for Neutron Measurements, Report of a Panel IAEA-107 (1968).
[3] GIBBONS, J.H., Neutron Cross Sections and Technology, Proceedings of a Conference, NBS special publication 299, Vol. I (1968) 111.
[4] RENDA, Compilation of EANDC Requests for Neutron Data Measurements EANDC 85"U" (April 1970).
[5] MATTAUCH, J.H.E., THIELE, W., WAPSTRA, A.H., Nucl.Phys. 67 (1965) 32.
[6] LAURITSEN, T. and AJZENBERG-SELOVE, F., Nucl.Phys. 78 (1966) 1.
[7] DERUYTTER, A.J. and PELFER, P., Journal of Nuclear Energy 21 (1967) 833.
[8] BARTHOLOMEW, G.A., CAMPION, P.J., Can.J.Phys. 35 (1957) 1347.
[9] THOMAS, G.E., BLATCHEY, D.E., BOLLINGER, L.M., Nucl.Instr. & Meth. 56 (1967) 325.
[10] BIGGERSTAFF, J.A., Oak Ridge Report ORNL TM 1271 (1965) 8.
[11] GUBERNATOR, K., and MORET, H., EUR.3950.e (1968).
[12] KLEIN, P.D., MOORING, F.P., cited in ref. 11.
[13] CRESPI, M.B., CAIRO, A.E., Journ.Inorg.Nucl.Chem. 3 (1956) 248.
[14] MOORING, F.P., MONAHAN, J.E., HUDDLESTON, C.M., Nucl.Phys. 82, (1966) 16.
[15] EGGLER, C., HUGHES, D.J., HUDDLESTON, C., Phys.Rev. 74 (1948) 1239.
[16] JOHN R.STEHN, et al., BNL 325, Vol. 1, Supplement 2 (1964).
[17] MACKLIN, R.L., GIBBONS, J.H., Phys.Rev. 165 (1968) 1147.
[18] MEADOWS, J.W., WHALEN, J.F., private communication (1970).
[19] CAMERON, A.E., J.Ann.Chem.Soc. 77 (1955) 2731.
[20] WAGNER, G., PILZ, A., HIGATSBERGER, M.J., Monatsh. 85 (1954) 464.
[21] MEADOWS, J.W., WHALEN, J.F., Nucl.Sci. & Engng. 9 (1961) 132.
[22] VIDAL, J., CARRE, Y., private communication (1970).
[23] PETERSON, S.W., SMITH, H.G., J.Phys.Soc. Japan 17 (Suppl. BII) (1962) 335.
[24] SHULL, C.G., WOLLAN, E.O., Phys.Rev. 81 (1951) 527.
[25] UTTLEY, C.A., DIMENT, K.M. (1970 to be published) (cited in AERE R 6316).
[26] ASAMI, A., MOXON, M.C. (1970 to be published).
[27] FARRELL, J.A., PINEO, W.F.E., Proceedings of the Conference on Neutron Cross Sections and Technology, Washington 1 (1968) 153.
[28] HIBDON, C.T., MOORING, F.P., Proceedings of the Conference on Neutron Cross Sections and Technology, Washington 1 (1968) 159.
[29] SOWERBY, M.G., PATRICK, B.H., UTTLEY, C.A., DIMENT, K.M., AERE R-6316 (1970).
[30] DIMENT, K.M., UTTLEY, C.A., AERE PR/NP 15, 12 and AERE PR/NP 16 (1969) 3.
[31] SCHWARZ, S., STROMBERG, L.G., BERGSTROM, A., Nucl.Phys. 63 (1965) 593.
[32] CONDE, H., SCHWARZ, S., STARFELT, N., Arkiv Fysik 29 (1965) 45.

[33] BARRY, J.F., Proceedings of the Conference on Neutron Cross Sections and Technology, Washington (1966) 763.
[34] BAME, S.J., CUBITT, R.L., Phys.Rev. 114 (1959) 1580.
[35] PATRICK, B.H., SOWERBY, M.G., SCHOMBERG, M.G., EANDC(UK), 119"AL" (1970).
[36] VAN HEMERT, R.L., UCRL 50501 (TID-4500) (1968).
[37] HAVENS, W.W., Jr., private communication (1970).
[38] COX, S.A., PONTET, F.R., J.Nucl.En. 21, (1967) 271.
[39] LEROY, J.L., et al., This conference papers CN 26/71 and CN 26/72 (1970).
[40] COX, S.A., Proceedings of the Conference on Neutron Cross Sections and Technology, Washington, Book 2 (1966) 701.
[41] DIMENT, K.M., UKAEA HL 67/762, EANDC(UK) 85 "S" (1967).
[42] MACKLIN, R.L., GIBBONS, J.H., Phys.Rev. 165 (1968) 1147.
[43] BERGMAN, A.A., SHAPIRO, F.L., Soviet Physics JETP 13 (1961) 895.
[44] ALS-NIELSEN, CCDN-NW/6 (1967).
[45] ALS-NIELSEN, J., DIETRICH, O., Phys.Rev. 133 (1964) B 925.
[46] MACKLIN, R.L., GIBBONS, J.H., Int. Conf. on the Study of Nucl.Structure with Neutrons, Antwerp, EANDC-50-S, Vol. I Comm. 13 (1966).
[47] GIBBONS, J.H., MACKLIN, R.L., Phys.Rev. 114 (1959) 571.
[48] SHAPIRO, F.L., Soviet Phys. JETP 7 (1958) 1132.
[49] HREHUSS, G., CZIBOK, T., Phys.Letters 28B (1969) 585.
[50] PAULSEN, A., LISKIEN, H., Phys.Letters 29B (1969) 562.
[51] CZIERJACKS, S., et al., Physical Review Letters 23 (1969) 866.
[52] SCHWARZ, R.B., SCHRACK, R.A., HEATON, H.T., Phys. Letters 30B (1969) 36.
[53] LANGSFORD, A., CLEMENTS, P.J. EANDC(UK) 120"AL" (1970).
[54] ENGELKE, C.E., BENONSEN, R.E., MELKONIAN, E., LEBOWITZ, J.M., Phys. Rev. 129 (1963) 324.
[55] GAMMEL, J.L. in Fast Neutron Physics, Intersci. Pub. N.Y. Chap. V Part II (1960) 2185.
[56] HOPKINS, J.C., BREIT, G., private communication (1970 to be published).
[57] UTTLEY, C.A., DIMENT, K.M., CN 26/24 and AHMED, N., et al. CN 26/23, this conference (1970).
[58] PONITZ, W.P., private communication, paper CN 26/111, this conference (1970).
[59] ALBERT, R.D., Phys.Rev. Letters 15 (1965) 637.
[60] MACKLIN, R.L., GIBBONS, J.H., Phys.Rev.Letters 16 (1966) 248.
[61] SMITH, A.B., WHALEN, J.F., Phys.Rev.Letters 16 (1966) 525.
[62] GILBOY, W.B., KNOLL, G.F., Phys. Letters 21 (1966) 432.
[63] DERUYTTER, A.J., WAGEMANS, C., to be published (EANDC(E) 129"AL").
[64] HANNA, G.C., WESTCOTT, C.H., LEMMEL, H.D., LEONARD, Jr., B.R., STORY, J.S., ATTREE, P.M., Atomic Energy Review Vol. VII, N° 4 (1969).
[65] DE SAUSSURE, G., et al., Nuclear Data for Reactors, Paris (1966) (IAEA) II, 233.
[66] CAO, M.G., et al. Journ. of Nucl. Eng. 22 (1968) 211.
[67] ENEA Neutron Data Compilation Centre, CCDN, Gif-sur-Yvette, Saclay, France.
[68] BOWMAN, C., et al. UCRL-1406 (1966) and Conf. on Neutron Cross-Sections and Technology, March 1966, Washington, Vol. II, 1004.

[69] MOSTOVAYA, O. BESPALOV, INDC-152 E (1967).
[70] MICHAUDON, A., et al, Nucl. Phys. 69 (1965) 545 and CEA R-2552 (1964).
[71] SHORE, F., SAILOR, V., Phys.Rev. 112 1 (1958) 191.
[72] BROOKS, F., et al., Report AERE-N 1670 (1966).
[73] RYABOV, Y., et al., Proceedings of the Symposium on Physics and Chemistry of Fission, Salzburg 1965, 287 and INDC-232 (1968).
[74] DERUYTTER, A.J., WAGEMANS, C., PENNING, G., EANDC(E) 131"AL" (1970).
[75] BLONS, J., et al., C.R. Acad. Sc. Paris 262 (1966) 79 and 267 (1968) 901.
[76] BOLLINGER, L.M., et al., Proc. of Sec. Int. Conf. on the Peaceful Uses of Atomic Energy, Geneva 1958 15 127.
[77] RYABOV, Y., et al., INDC-232 (1968).
[78] IGNATIEV, K., et al., Sov. At. En. 16 (1964) 121.
[79] GWIN, R., et al., ORNL-TM-2598 and private communication (1970).
[80] SHUNK, E.R., et al., Proceedings of the Conference on Neutron Cross Sections and Technology, Washington 1966 Book 2 (979).
[81] AXTON, E.J., BARDELL, A.G., AUDRIC, B.N., Journal of Nuclear Energy 23 (1969) 457 and private communication.
[82] VONACH, H., Dutch-German Spring Meeting of NNV and DPG, Contribution K-106, Eindhoven (1970).
[83] LEROY, J.L., et al., DRP/SMPNF 70/01 and DRP/SMPNF/70/08 (1970) and private communication.
[84] LISKIEN, H., PAULSEN, A., Nucl.Instr. Methods 69 (1969) 70 and private communication (1970).
[85] PONITZ, W.P., private communication (1970).
[86] TAYLOR, J.G.V., MERRITT, J.S., EANDC(CAN)-40"L" (1970).
[87] MUTTERER, M., SPERNOL, A., private communication (1970).
[88] HANSON, A.O., MCKIBBEN, J.L., Phys.Rev. 72 (1947) 673.
[89] MACKLIN, R.L., Nucl.Instr. & Methods 1 (1957) 335.
[90] PONITZ, W.P., Nucl.Instr. & Methods 58 (1968) 39.
[91] RAE, E.R., COATES, M.S., HART, W., CN 26/35 (1970)
[92] WARTENA, J., THEOBALD, J., private communication (1970).

NORMALIZATION OF RELATIVE ^{235}U AND ^{239}Pu FISSION CROSS-SECTIONS IN THE RESONANCE REGION *

A.J. DERUYTTER
Central Bureau for Nuclear Measurements,
EURATOM, Geel, Belgium
and
C. WAGEMANS**, G. PENNING***
SCK-CEN, Mol, Belgium

Abstract

NORMALIZATION OF RELATIVE ^{235}U AND ^{239}Pu FISSION CROSS-SECTIONS IN THE RESONANCE REGION.

Measurements were performed with the Linac of the CBNM in view of extending relative fission cross-sections down to below thermal energy for a direct normalization to the previously determined absolute thermal reference cross-section. Two series of measurements for both isotopes were performed at a well collimated short-flight path (about 8m). The first run goes down to below thermal energy and has been made with low repetition rate and long burst-width of the Linac to avoid overlapping of successive bursts in the low-energy region. The second run (0.1 eV - 30 eV) has a better resolution and has been made with higher repetition rate and smaller burst width such that there was a large overlap between both measurements.

The comparison of induced reaction rates in a back-to-back ^{239}Pu- (or ^{235}U) and ^{10}B-foil is made simultaneously with two sets of solid-state detectors (outside the beam) and registered in two halves of a 4096 channels time-of-flight analyser.

Background laws were determined by using "black-resonance" absorbing filters.

The neutron spectra (^{10}B-foil) were compared at different pulse repetition frequencies (from 10 to 100 Hz) to detect possible overlap of successive bursts.

From these data we calculate normalized fission cross-sections in the region 0.01 eV - 30 eV, based on the absolute reference 2200 m/s values recommended by the IAEA from which fission- and resonance integrals are calculated. For the ^{235}U fission cross-section, we show that normalization differences between different authors are, for a large part, responsible for the differences in quoted fission integrals.

We propose absolute reference fission integrals for further normalization of σ_f for both isotopes.

---

* This subject is treated in detail in chapter 5 of the invited paper IAEA-CN-26/106 by A.J. Deruytter.

** NFWO, Research Fellow.

*** IWONL, Research Fellow.

LOW-ENERGY NEUTRON-SCATTERING CROSS-SECTION OF ^{6}Li

A. ASAMI*
Japan Atomic Energy Research Institute, Tokai-mura, Naka-gun, Ibaraki-ken, Japan
M.C. MOXON
Atomic Energy Research Establishment, Harwell, Didcot, Berks, United Kingdom

Presented by M.G. Sowerby

Abstract

LOW-ENERGY NEUTRON-SCATTERING CROSS-SECTION OF ^{6}Li.

The neutron scattering cross-section of ^{6}Li has been measured in the energy region between 1 keV and 110 keV with a scattering detector on a 50-m flight path of the Harwell Electron Linac neutron time-of-flight spectrometer. The detector consists of eight ^{6}Li-glass scintillators, and the measurements were made at four angles to the incident beam: 39°, 65°, 120° and 144°. The ^{6}Li sample has a thickness of 5.88×10^{-2} atoms/b (93.7% ^{6}Li, 5.2% ^{7}Li, and 1.1% others). The sample is canned with a thin aluminium plate of thickness of 1.47×10^{-3} atoms/b, which is sealed with Araldite. The measurements were made relative to a carbon sample with a thickness of 2.06×10^{-2} atoms/b. The data were analysed mainly with the IBM 7044 at JAERI. In the analysis corrections for the effects of the following were made: (1) self-absorption in the sample before and after primary scattering (assuming neutrons are lost by any further interaction after primary scattering, and this may be called the first-order multiple scattering; (2) multiple scattering (only for the twice-scattered neutrons in the sample, e.g. the second-order multiple scattering); (3) the sample impurities; (4) the sample can; (5) difference in attenuation caused by an aluminium neutron-beam tube between the neutrons scattered by the ^{6}Li and the carbon samples (above 40 keV); and (6) the energy dependence of the detector efficiency. Thus the differential scattering cross-section was obtained, which showed no significant angular dependence in the low-energy region below 10 keV. The angular distributions of the scattered neutrons were analysed in terms of the scattering lengths a_+ and a_- for the channel spin 3/2 and 1/2, respectively, and the resonance parameters of th 250-keV level in ^{6}Li (n, α) cross-section from the 1/v law was obtained.

1. INTRODUCTION

In the energy region up to 100 keV, the ^{6}Li scattering cross-section of ^{6}Li is of importance, primarily because the $^{6}Li(n,\alpha)$ cross-section, one of the best standards in this region, can be obtained from the difference between the total and scattering cross-sections, as other reaction cross-sections are negligible. Up to the present, however, the scattering cross-section has been measured [1] only above 50 keV. Furthermore, Shapiro [2] showed that the 1/v law, a widely used assumption, for the $^{6}Li(n,\alpha)$ cross-section is an approximation and that the cross-section has the form

$$\sigma_{n,\alpha} = \frac{C}{\sqrt{E}} + \Delta\sigma + \beta\sqrt{E} \qquad (1)$$

where C, $\Delta\sigma$ and β are constants. At low energies the second term $\beta\sqrt{E}$ may be negligible and the constant term $\Delta\sigma$ is the dominant correction to the 1/v

* The measurements were carried out at the Atomic Energy Research Establishment, Harwell, when A. Asami was there.

law. This constant term could be directly obtained by comparing the scattering cross-section, which is expected to be constant at low energies, with the constant term determined from fits to the total cross-section with the formula $a/\sqrt{E} + b$.

In these measurements the scattering cross-section of ^{6}Li has been determined relative to that of carbon in the energy region between 1 and 110 keV with a ^{6}Li-glass scintillator detector system on a 53.6-m flight path of the Harwell Electron Linac neutron time-of-flight spectrometer. Measurements were made at angles of 39°, 65°, 120° and 144° to the direction of the incident neutron beam. The data were analysed mainly with the IBM 7044 and FACOM 230/65 computers at JAERI.

The experimental method is described in Section 2, and the analysis and results are presented in Sections 3 and 4 respectively. The present work is an extension of a similar study on ^{10}B, which is reported in ref. [3].

2. EXPERIMENTAL METHOD

The neutron detector and the experimental procedure were almost the same as in ref. [3], and are only briefly described below. The detector consisted of eight Li-glass scintillators (NE 905, 1-3/4 in. diameter and 1/2 in. thick), which were separated into two groups, placed at angles to the incident beam. In the first set of measurements the angles were 39° and 144°, and in the second set they were 65° and 120°. The distance between detector and sample was 11 cm in the first case, and 7 cm in the second. A signal from the detector was recorded on a magnetic tape using a 64 K channel recorder with a channel width of 1/16 μsec. The only modification made to the previous detector system [3] was that the neutron beam passing through the sample was defined by a collimator, 20-in. long with an inner diameter of 0.9 in.

The sample was 1.97 in. in diameter and had a total thickness of 5.899×10^{-2} atoms/b. The end plates of the aluminium can had a thickness of 1.47×10^{-3} atoms/b, and the can was sealed with Araldite. The isotopic ratio for the sample of ^{6}Li was 95.46% by atoms and the sample contained about 0.9 % by atoms of impurities, the major component being sodium. The measurements were made relative to a carbon sample, which was 1.37 in. in diameter with a thickness of 2.055×10^{-2} atoms/b. Both samples were mounted on a sample changer, which alternated the sample in and out of the neutron beam about every 10 minutes, half of the time being used to measure background. The background measurements were made using a second sample changer with a set of "black-resonance" filters of aluminium, manganese and cobalt, the aluminium filter being thicker than the one used in ref. [3] in order to make the 150-keV resonance black. A sodium sample was left permanently in the beam to obtain a normalization factor of the background. The signal-to-background ratio depends on the type of the sample, the neutron energy and the detector position. This ratio is poorer for the lithium than for the carbon particularly at low energies due to the large absorption cross-section of the lithium. Some of the ratio for the sample are shown in Table I.

In order to measure the effect of the Araldite used for sealing the sample can, additional short runs were made on two nearly identical carbon samples. One sample was the standard sample described above, the other one of the same diameter with a thickness of 2.013×10^{-2} atoms/b was placed in an Araldite-sealed dummy can.

TABLE I. SIGNAL-TO-BACKGROUND RATIO FOR ^{6}Li

Energy (keV) \ Θ (degree)	39	65	120	144
70	1.2	1.9	1.7	1.3
10	0.9	1.7	1.4	0.8
1	0.8	1.2	1.6	1.0

3. ANALYSIS OF THE DATA

3.1. Background

The background formula used is of the form $a + b/t^{c}$, where t is the time-of-flight and a, b and c are constants to be determined. As it was found difficult to fit the background over the whole energy region by this simple formula, the energy region was divided into two, the division being made at 35 keV for the data at 39° and 144°, and at 2.8 keV for the data at 65° and 120°. The background fitting method used was similar to that described in ref. [3].

3.2. Approximate formula for the cross-section

An approximate value of the cross-section σ_s was obtained with the formula

$$\sigma_{s(1)} = \frac{P(2)}{P(1)} \cdot \frac{C(1)}{C(2)} \cdot \sigma_{s(2)} \qquad (2)$$

where C is the count rate, and the numbers 1 and 2 in the parenthesis refer to the quantities for the lithium sample and for the carbon sample, respectively. $P\,d\Omega$ is the probability divided by σ_s for an incident neutron to escape from the sample into a solid angle $d\Omega$ between Θ and Θ + dΘ, where Θ is the scattering angle. P(Θ) is given by

$$P(\Theta) = \frac{F(\Theta)}{(\sigma_t'/\cos\Theta) - \sigma_t}\left[\exp(-n\sigma_t) - \exp(-n\sigma_t'/\cos\Theta)\right] \quad (\Theta < \pi/2) \qquad (3a)$$

$$= \frac{F(\Theta)}{\sigma_t - (\sigma_t'/\cos\Theta)}\left[1 - \exp\left\{-n(\sigma_t - \sigma_t'/\cos\Theta)\right\}\right] \quad (\Theta > \pi/2) \qquad (3b)$$

where σ_t and σ_t' are the total cross-sections at the incident and scattered energies respectively and n is the thickness of the sample in atoms/barn. F(Θ) is

$$F(\Theta) = f(\Theta)\left[1 + \frac{2m}{M}\cos\Theta + \left(\frac{m}{M}\right)^2\left(1 - \frac{3}{2}\cos^2\Theta\right)\right] \qquad (3c)$$

where f(Θ) is the angular dependence of the scattering cross-section ($\int f(\Theta)\, d\Omega = 1$), and m and M are the neutron and target nucleus masses, respectively.

In deriving equations (3a) to (3c) the assumptions were made that the neutrons are incident normally at the centre of an infinite plane sample

and that neutrons are lost by any further interaction after primary scattering, so that P(Θ) implies a correction for self absorption of the neutron in the sample.

The total cross-section of ^{6}Li is assumed to be [4] $151/\sqrt{E(eV)} + 0.7$ b and for the carbon the data of Uttley and Diment[5] were used. Due to the tail of the 250-keV resonance in ^{6}Li, the total cross-section decreases more slowly than the above formula with increase in energy, and the difference becomes appreciable towards 100 keV. The difference in P(1), however, with these two values for the cross-section is very small even at 100 keV, one per cent at most, and neglected. The self absorption is quite large at low energies, and some of the relative magnitudes of P(1) are shown in Table II.

TABLE II. RELATIVE MAGNITUDE OF SELF-ABSORPTION CORRECTION P (2) / P (1).
The values are normalized to unity at 70 keV.

Θ \ E (keV)	1	10	70
39	1.31	1.06	1.00
65	1.51	1.09	1.00
120	1.45	1.09	1.00
144	1.34	1.07	1.00

TABLE III. MAGNITUDES OF CORRECTIONS IN %.
The values are averages over detector position, and the cross-section increases if the correction is positive. The beam-tube correction is large at some other points, e. g. at 47 keV it is -11% at 144°.

E (keV)	1	10	70
multiple scattering	10	10	8
detector efficiency	- 8	- 8	- 6
impurity	- 7	- 4	- 1
can	- 10	- 7	- 8
Araldite	- 4	- 5	- 6
beam tube	0	0	1

3.3. Corrections

To obtain an accurate cross-section value, corrections are required for the effect of the following:- (1) multiple scattering, (2) the energy dependence of the detector efficiency, (3) finite size of the detector, (4) the sample impurities, (5) the sample can and the Araldite and (6) an aluminium beam-drift tube. These corrections are briefly described in the following paragraphs and their magnitudes averaged over the detector positions are listed at a few energy points in Table III.

A multiple-scattering correction was made for neutrons that are scattered more than once in the sample. Simplifying assumptions were made that (1) neutrons are primarily scattered at the centre of the sample

isotropically; (2) that the energy loss on the second collision corresponds to an angle of scatter of 90°; (3) that the probability that the neutrons escape from the sample towards the detector after a second collision is the same as for a primary scattering event. The efficiency of the detector was simply assumed to be $1 - \exp(-n\sigma_{n,\alpha})$, where $\sigma_{n,\alpha}$ is the Li(n,α) cross-section and n is the number of ^{6}Li atoms/cm^2 in the detector. The whole energy region was divided into four at 10, 65 and 90 keV, and the cross-section was approximated by $a + bE^c$, where a, b and c were determined from an evaluation of this cross-section [6]. The correction for the finite size of the detector is small, the largest value being 2.4 % at 1 keV at 65°.

The corrections for the ^{7}Li and other impurities present in the sample are small, but for the aluminium can the corrections are fairly large as is seen in Table III, and the energy variation of the total cross-section [7] had to be taken into account with reasonable accuracy. The correction for the Araldite was deduced from the measurements on the two carbon samples, one sample without any can, the other in the dummy one, in which only the total counts in two wide energy regions, 60 to 200 eV and 200 eV to 600 keV were measured. Although the ratio of the total counts for the two samples showed an energy dependence, being lower in the lower energy region by 30%, the ratio obtained in the higher region was used assuming it is constant. As is seen in Table III, this correction depends on the energy of the neutrons which result from the variation of the ^{6}Li (n,α) cross-section.

The last (small) correction is for the effect of the neutron-beam drift tube. Due to the large mass difference between lithium and carbon, the energies of neutrons scattered from the two samples are different, which causes an appreciable difference in the attenuation of the neutrons by the aluminium tube before reaching the detector in the energy region above 40 keV. In calculating the correction, simplifying assumptions were again made. Firstly an upper limit of the probability for a neutron scattered by the tube, after primary scattering towards the detector, to reach the detector is one half, in other words, all the neutrons scattered forwards by the tube reach the detector. Secondly a lower limit is given by the ratio of the solid angle of detector at the crossing point of the detector axis and the tube to the total solid angle 4π. Lastly the probability is assumed to be the mean of these two limits with the error being the difference between the mean and either of the limits.

3.4. Analysis of the cross-section

The differential scattering cross-sections at four detector positions were thus obtained, and analysed in terms of the scattering lengths a_+ and a_- for 3/2 and 1/2 s-wave spin sequences respectively and the resonance parameters of the 250-keV level. For the present case the angular distributions of the scattered neutrons [8] in the centre of mass system are given in terms of Legendre Polynomials by

$$\sigma(\Theta) = B_0 P_0 (\cos \Theta) + B_1 P_1 (\cos \Theta) + B_2 P_2 (\cos \Theta) \qquad (4a)$$

where the coefficients B are given by

$$B_0 = \lambda\!\!\!^{-2}\left\{\frac{1}{3}\sin^2 ka_- + \frac{2}{3}\sin^2 ka_+ + \frac{\Gamma_n^2/4}{(E_\lambda + \Delta_\lambda - E)^2 + \Gamma^2/4}\right\}$$

$$B_1 = -\lambda\!\!\!^{-2}\frac{(E_\lambda + \Delta_\lambda - E)\,\Gamma_n}{(E_\lambda + \Delta_\lambda - E)^2 + \Gamma^2/4}\sin ka_+ \qquad (4b)$$

$$B_2 = \lambda\!\!\!^{-2}\frac{1}{6}Z^2(1, 5/2, 1, 5/2, 3/2, 2)\frac{\Gamma^2 n/4}{(E_\lambda + \Delta_\lambda - E)^2 + \Gamma^2/4}$$

where Γ_n and Γ are the neutron and total widths respectively, E_λ is the characteristic energy associated with the level shift Δ_λ, E, $\lambda\!\!\!^{-}$ and k are the energy, wave length and wave number of the neutrons respectively and Z is the Z coefficient. For a p-wave resonance Γ_n is related to the reduced neutron width γ_n^2 by $\Gamma_n = 2\left[x^3/(1+x^2)\right]\gamma_n^2$, where $x = kR_n$ and R_n is the entrance-channel radius. The resonance energy E_R is given by $E_\lambda + \Delta_\lambda(E_R) - E_R = 0$, and $\Delta_\lambda = \gamma_n^2/(1+x^2)$.

Since even the highest energy point covered in the measurements is still far off the resonance, all the resonance parameters were fixed and only a_+ and a_- were determined by fitting equation (4a) to the cross-section. The resonance parameters from the data of Uttley and Diment [4] were used in these calculations. These are: E_R = 250 keV (laboratory system), R_n = 2.5 fm, Γ_n = 0.115 MeV, the alpha width Γ_α = 0.053 MeV ($\Gamma = \Gamma_n + \Gamma_\alpha$), and the total spin and parity 5/2-.

4. RESULTS AND DISCUSSIONS

The differential scattering cross-section is shown in Fig. 1. The cross-sections near 2.8, 35 and 89 keV were not measured because of the presence of the resonances in materials left permanently in the flight path, i.e. sodium (2.8 keV) and aluminium (35 and 89 keV).

Except in the higher-energy region above 40 keV there seems to be no significant difference between the cross-sections measured at the four angles. Below 20 keV down to 4 keV the cross-sections appear to be constant, but become a little lower below 2 keV. This decrease is likely to be due to inaccuracy in the applied corrections. The indicated errors are a combination of uncertainties arising from the following: (1) counting statistics, (2) background, (3) multiple scattering, for which $\pm$ 30% of the correction is assumed, (4) Araldite correction, $\pm$ 50% of the correction being assumed, and (5) the beam drift-tube correction. Among these the second is the most significant at all the detector positions, the first is next in significance at 39° and 144°, and the others contribute equally. According to the data of Lane et al. [1], which extended from 50 keV to 2250 keV, the total scattering cross-section of ^{6}Li is 0.530$\pm$0.026 b at 50 keV, and slowly increases up to 0.632$\pm$0.032 b at 100 keV. These values are significantly lower than the present results.

The solid lines in Fig. 1 are the cross-sections calculated by fitting equations (4) to the data. In the energy region below 2 keV the measured cross-sections are slightly too low, as already mentioned, and show deviation from the calculated cross-sections. In the other region agreement is fairly good. The values of the scattering lengths a_+ and a_- obtained by the above fit are 0.70 $\pm$ 0.15 fm and 4.12 $\pm$ 0.06 fm, respectively.

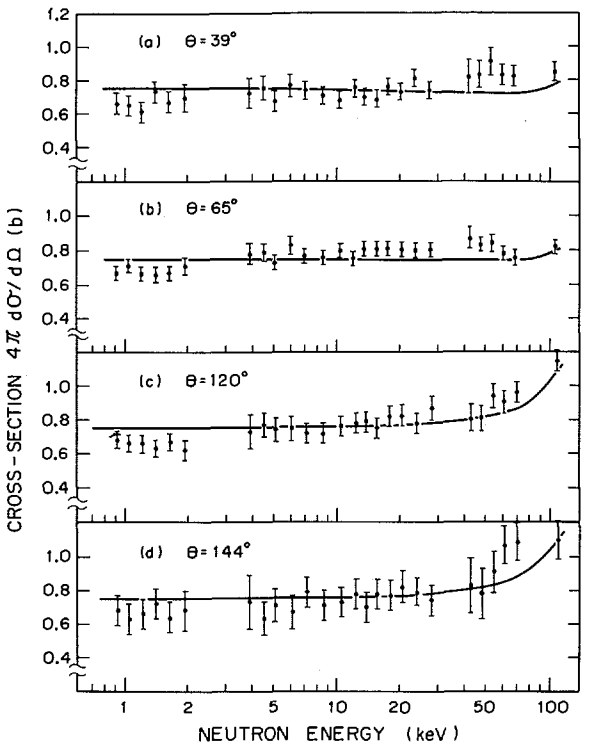

FIG. 1. Differential elastic scattering cross-sections (centre of mass system) of ^{6}Li are shown as a function of incident neutron energy (laboratory system) at the following angle θ (laboratory system): (a) $\theta = 39°$, (b) $\theta = 65°$, (c) $\theta = 120°$, and (d) $\theta = 144°$.

With these values the constant scattering cross-section at low energies is obtained to be 0.752 ± 0.043 b. Here the error is deduced from the errors of the measured cross-sections in the energy region between 1 and 10 keV. The least square fit to the total cross-section data of Uttley and Diment [4] gives $\sigma_t = (149.5 \pm 0.3)E^{-1/2} + (0.696 \pm 0.010)$ b. Using this expression and the value of the constant cross-section obtained in the present measurements, the constant term $\Delta\sigma$ of the (n,α) cross-section is - 0.056 ± 0.044 b. Bergman and Shapiro [9] measured the ratio of the $^{6}Li(n,\alpha)$ to $^{10}B(n,\alpha)$ cross-section and deduced that for ^{6}Li $\Delta\sigma$ = -0.03 ± 0.01 b. Since a fairly large error is associated with the present result, the agreement between this value and the present one seems reasonable.

ACKNOWLEDGEMENTS

The authors wish to thank Dr. E. R. Rae for useful discussions and encouragement and Dr. C. A. Uttley and Dr. M. G. Sowerby for useful discussions. One of the authors (A. Asami) is very grateful to Dr. E. Bretscher, Dr. B. Rose and Dr. E. R. Rae of Harwell and to Dr. T. Momota, and Dr. H. Takekoshi of JAERI for the opportunity to work at Harwell. He also wishes to thank Dr. H. Takekoshi for his encouragement.

REFERENCES

[1] LANE R. O., LANGSDORF A. S. Jr., MONAHAN J. E., ELWYN A. J., Annls Phys. 12 (1961) 135; and Argonne National Laboratory Report (unpublished).
[2] SHAPIRO F. L., Sov. Phys. JETP 7 (1958) 1132.
[3] ASAMI A., MOXON M. C., UKAEA Report AERE-R 5980 (1969).
[4] DIMENT K. M., UTTLEY G. A., UKAEA Report AERE-PR/NP, 14, 20 (1968).
[5] UTTLEY C. A., DIMENT K. M., UKAEA Report AERE-PR/NP, 13, 4 (1968).
[6] SOWERBY M. G., private communication (1967).
[7] Brookhaven National Laboratory Report BNL 325, Second Edn, Supplement No. 2 (1966).
[8] BLATT J. M., BIEDENHARN L. C., Rev. mod. Phys. 24 (1952) 258.
[9] BERGMAN A. A., SHAPIRO F. L., Sov. Phys. JETP 13 (1961) 895.

A MEASUREMENT OF THE RATIO OF THE $^{6}Li(n,\alpha)$ AND $^{10}B(n,\alpha)$ CROSS-SECTIONS FROM 10 eV TO 80 keV AND RECOMMENDED VALUES OF THE CROSS-SECTIONS UP TO 200 keV

M.G. SOWERBY, B.H. PATRICK, C.A. UTTLEY, K.M. DIMENT
UKAEA, AERE, Harwell, Didcot, Berks,
United Kingdom

Abstract

A MEASUREMENT OF THE RATIO OF THE $^{6}Li(n,\alpha)$ AND $^{10}B(n,\alpha)$ CROSS-SECTIONS FROM 10 eV TO 80 keV AND RECOMMENDED VALUES OF THE CROSS-SECTIONS UP TO 200 keV.

Measurements of the neutron spectrum produced by the Harwell 45 MeV Linear Accelerator have been made, using time-of-flight techniques, with detectors based upon the $^{6}Li(n,\alpha)$ and $^{10}B(n,\alpha)$ reactions. A 2-inch-diameter $^{10}BF_3$ counter, a "boron-plug" detector with 0.003547 ^{10}B atoms/barn and a 1/8-inch-thick ^{6}Li glass scintillator were used in the experiments, and their relative efficiencies as a function of neutron energy were calculated by Monte-Carlo methods. Since these detectors were "thin" ($n\sigma < 0.3$) the multiple-scattering corrections are small and almost energy-independent, and hence the experimental data can be used to obtain the ratio of the $^{6}Li(n,\alpha)$ to $^{10}B(n,\alpha)$ cross-sections in the energy range 10 eV to 80 keV. The ratio is normalized at 10 eV to a value of 0.245. The absorption cross-section of ^{6}Li has been obtained from total and scattering cross-section data. By combining these values with the data from the ratio measurement, the $^{10}B(n,\alpha)$ cross-section has been deduced with estimated errors ranging from 2 - 3%. The results are compared with other measurements, and there is very good agreement over the entire energy range. The data are all consistent with the $^{10}B(n,\alpha)$ cross-section falling below the $1/\sqrt{E}$ level, reaching a minimum at ~ 25 keV, where the deviation is about 4%. Above this energy the cross-section relative to the $1/\sqrt{E}$ level, rises and passes through a resonance at ~170 keV. The complete set of data has been fitted by an analytic expression which includes the first three terms of the Shapiro expansion describing the low-energy dependence of such cross-sections together with an s-wave resonance at 170 keV. A least-squares fitting procedure was used with five free parameters, two of which are the energy and total width of the resonance. It is concluded that the $^{10}B(n,\alpha)$ cross-section up to 200 keV is given by

$$\sigma_{n\alpha} = \frac{13.837}{\sqrt{E}} - 0.312 - 1.014\times 10^{-2}\sqrt{E} + \frac{2.809\times 10^{5}}{\sqrt{E}\,[(170.3-E)^2 + 2.243\times 10^{4}]} \text{ barns}$$

where E is in keV. This expression has an estimated accuracy ranging from ~1.5% at low energies to ~ 3% at the high-energy end, this being a considerable improvement in accuracy over previous determinations.

1. INTRODUCTION

In the course of some experiments by Patrick et al. [1] to measure eta, alpha and the neutron cross-sections of ^{239}Pu in the energy range 10 eV to 30 keV using the Harwell linear accelerator time-of-flight spectrometer, the relative incident neutron flux was measured using detectors based on the $^{6}Li(n,\alpha)$ and $^{10}B(n,\alpha)$ reactions. It was assumed that, over the energy range of interest, the energy dependence of these reaction cross-sections was adequately represented by a $1/\sqrt{E}$ law but the neutron spectra obtained from the two detectors were inconsistent at the higher energies. It is important to establish the energy dependence of these cross-sections accurately since they are the most useful reactions with which to measure neutron flux below 100 keV. The data from the two

TABLE I. EXPERIMENTAL RESULTS

Experiment	Low Energy	Low Energy	High Energy	High Energy
Spectrum detector	0.3 cm thick Li glass scintillator	5 cm diameter $^{10}BF_3$ counter	0.3 cm Li glass scintillator	"Boron Plug" Detector
Reaction detected	$^6Li(n,\alpha)$	$^{10}B(n,\alpha_0)+^{10}B(n,\alpha_1\gamma)$	$^6Li(n,\alpha)$	$^{10}B(n,\alpha_1\gamma)$
Neutron Pulse Width (unmoderated) (nS)	220	220	220	220
Timing Channel Width (nS)	125	125	125	125
Flight path length (m)	34.9	35.97	97.55	97.55
Nominal resolution (nS/m)	7.2	7.0	2.5	2.5
Permanent "black" filters	Na + Boron	Na + Boron	Al + Boron	Al + Boron
Resonance filters for background measurement	Mn, Mo, Ta	Mn, Mo, Ta	Mn, Au	Mn, Au

detectors can be used to obtain accurate values of the ratio of the $^{6}Li(n,\alpha)$ to $^{10}B(n,\alpha)$ cross-sections as a function of neutron energy and have been used as a basis to investigate the energy dependence of the $^{10}B(n,\alpha)$ cross-section. This has been done by combining the ratio measurement with the absorption cross-section of ^{6}Li deduced from an accurate measurement of the total cross-section over a wide energy range (70 eV to 7 MeV) and calculations of the scattering cross-section of ^{6}Li.

In this paper the measurements of the neutron flux are described and the ratio of the cross-sections obtained. A brief outline of the determination of the absorption cross-section of ^{6}Li is given and a comparison is made between the $^{10}B(n,\alpha)$ cross-section obtained by this method and that determined from recent measurements of the total and scattering cross-sections of ^{10}B.

2. EXPERIMENTAL METHOD

Two measurements covering the energy regions 10 eV to 2 keV and 50 eV to 80 keV have been made on the 45 MeV Harwell Linear Accelerator time-of-flight spectrometer. These experiments will be referred to as the low energy and high energy experiments respectively. In both experiments the relative incident neutron spectrum was measured with a 0.3 cm thick Li glass scintillator (NE 905). The glass was 6.35 cm diameter and was mounted 5.25 cm away from the photomultiplier to reduce the effect of neutrons scattered in the photomultiplier on the efficiency of the detector. In the low energy experiment the spectrum was also measured with a 5 cm diameter, copper-walled, $^{10}BF_3$ counter (20th Century Electronics Type 40 EB 70/50). In the high energy experiment the second spectrum measurement was made with a "Boron plug" detector [2] which consists of an array of NaI crystals which detect the 478 keV γ-rays from the $^{10}B(n,\alpha_1\gamma)$ reaction produced in a sample of ^{10}B in the neutron beam. The ^{10}B sample had a total mass of 3.38 gms and was 7.6 cms in diameter. The details of the experiments are given in Table I.

The time-of-flight of each event was recorded on a 1 inch magnetic tape recorder fitted with a six word input buffer so that several events could be recorded per machine cycle. The number of time channels was 8192. A PDP-4 computer was used to analyse the events into time spectra. The backgrounds were measured by the use of resonance filters.

If, for a given detector, $N(E)$ is the number of counts at energy E in the interval ΔE, then this is related to the efficiency of the detector $\epsilon(E)$ and the incident neutron flux $\phi(E)$ by the expression

$$N(E) = \epsilon(E)\phi(E) \qquad (1)$$

For a detector of uniform thickness

$$\epsilon(E) = k[1 - T(E)] \frac{n\sigma_\alpha(E)}{\log_e\{1/T(E)\}} S(E) \qquad (2)$$

where n is the number of ^{6}Li or ^{10}B atoms per cm^2; $\sigma_\alpha(E)$ is the appropriate (n,α) cross-section; $S(E)$ is a factor which allows for the effect of multiple scattering in the detector and surrounding material; k is a constant which allows for the fact that not all the (n,α) events are accepted because of solid angle, pulse height analysis, etc. - in the case of the "Boron plug" detector, k also includes the ^{10}B branching ratio because only ~93% of the (n,α) events are of the $(n,\alpha_1\gamma)$ type and in the

analysis of the results k has a small energy dependence because of the slight change in the branching ratio with energy at the upper end of the energy region covered by the measurements; T(E) is the neutron transmission of the detector and is given by

$$T(E) = A \exp[-n\sigma_\alpha(E)] \qquad (3)$$

where $A = \exp[-\{\sum_i n_i\sigma_i(E) + n\sigma_s(E)\}]$, n_i being the number of atoms per cm^2 of the ith constituent of the detector other than ^6Li or ^{10}B, $\sigma_i(E)$ its total neutron cross-section and $\sigma_s(E)$ the neutron scattering cross-section of the ^6Li or ^{10}B. Both detectors are sufficiently "thin" (small n-value) such that the energy dependence of σ_i and σ_s have a negligible effect on the value of A which can be taken to be a constant.

If for one of the experiments $N_L(E)$ and $N_B(E)$ are the number of counts in ΔE for the lithium and boron detectors, then from equations (1), (2) and (3) the ratio between these counts can be expressed as

$$\frac{N_L(E)}{N_B(E)} = \frac{k_L}{k_B}\,\frac{n_L\sigma_{\alpha L}(E)}{n_B\sigma_{\alpha B}(E)}\,\frac{S_L(E)}{S_B(E)}\,\frac{F_L(E)}{F_B(E)} \qquad (4)$$

where $F(E) = \dfrac{1 - A\exp[-n\sigma_\alpha(E)]}{\log_e(1/A)+n\sigma_\alpha(E)}$, the suffixes L and B referring to the lithium and boron detectors respectively.

For "thin" detectors both S(E) and F(E) approach unity and the measured ratio $N_L(E)/N_B(E)$ gives a direct determination of the ratio of the (n,α) cross-sections provided k_Ln_L and k_Bn_B are known. Now in the case of the detectors used in these measurements, both F(E) and S(E) do not differ greatly from unity and it can be shown that their values are insensitive to small changes in the cross-sections. Hence only an approximate value of σ_α at any energy is needed to obtain accurate values of F(E) and S(E). Thus by calculating F(E) and S(E) using approximate values for σ_α the ratio $N_L(E)/N_B(E)$ enables the ratio of the cross-sections to be determined. The ratio $N_L(E)/N_B(E)$ is normalised at low energies (~10 eV) where both the (n,α) cross-sections are well known, so that it is not necessary to know the values of k and the values of n are only required to obtain F(E) and S(E), these again being insensitive to the exact n values.

3. EFFICIENCY OF DETECTORS

The probability of a neutron producing an alpha particle in the Li glass detector has been calculated using two Monte Carlo codes assuming that σ_α for ^6Li varies as $1/\sqrt{E}$. In the first calculation, which used a code of Lynn and Moxon [3], it was assumed that the neutrons all interacted on the axis of the disc while in the second, which was performed by Hart [4] using the GEM code [5], the neutron beam was assumed to be 5 cm diameter. In order to obtain accurate values of A and n the neutron transmission of the glass was measured as a function of neutron energy (equation (3)). The results of the two Monte Carlo calculations agreed to better than 2%.

The calculations of the multiple scattering correction for the "Boron plug" were made using the code of Lynn and Moxon. It was assumed in the calculation that the boron was uniformly spread over the surface of the disc.

The efficiency of the BF_3 counter, which was mounted with its axis perpendicular to the neutron beam, was calculated by Hart using the GEM code assuming there are no neutron resonances in copper. The results of this calculation agreed to within $\pm 0.1\%$ with an analytical calculation made assuming that the counter had no walls.

4. RESULTS

The results of the experiments are plotted in Fig. 1. The low energy experiment has been normalised to a value of 0.2450 in the energy range 10 to 20 eV. This value was chosen because Diment [6] and Uttley and Diment [7] have deduced from their total cross-section measurements on ^{10}B and ^{6}Li that the low energy absorption cross-sections are given by $610.3/\sqrt{E(eV)}$ barns and $149.5/\sqrt{E(eV)}$ barns respectively. Extrapolating to 0.0253 eV these expressions give values of 3839 ± 20 and 940 ± 4 barns respectively which agree with the values of 3836 ± 7 and 945 barns given in the review by Spaepen [8]. The high energy experiment was normalised to the low energy one in the region of 1 keV. Corrections have been applied to the data to allow for the variation of the ^{10}B branching ratio above 10 keV.

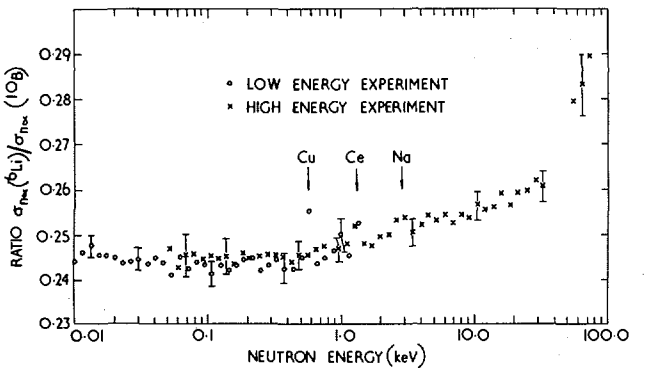

FIG. 1. The measured ratio of the $^{6}Li(n,\alpha)$ and $^{10}B(n,\alpha)$ cross-sections. The arrows labelled Cu and Ce indicate the positions of resonances in the cross-sections of the copper walls of the BF_3 counter and of the cerium present as a constituent of the lithium glass scintillator. The arrow marked Na indicates the position of the 2.85 keV resonance in sodium, where the effect of neutrons scattered from the glass of the photomultiplier is observed.

The errors in the measured ratios, which are shown on a few points in Fig. 1, are mainly systematic. The error in the normalising value of 0.245 is considered to be $\pm 0.5\%$ and statistics increase the low energy experiment normalisation error to 0.6%. The error in normalisation of the high energy experiment is $\pm 1.0\%$. By normalising the experiments the magnitudes of the systematic errors are reduced in the vicinity of the normalising regions.

There are three groups of data at approximately 570 eV, 1.3 keV and 2.8 keV which are high because of inadequate corrections. The first two are due to the fact that allowance has not been made in the Monte Carlo calculations for the effects of the 577 eV resonance in the cross-section of the copper of the BF_3 counter and the 1.3 keV resonance in the cross-section of cerium present in the Li glass scintillator. The high points

at 2.8 keV are due to the scattering of neutrons from the sodium in the glass face of the photomultiplier even although it is mounted 5.25 cms behind the Li glass scintillator in the neutron beam. The observed increase in counts agrees with a calculation which also shows that the scattering is negligible at all other energies.

There is only one other direct measurement of the ratio of the $^{6}Li(n,\alpha)$ and $^{10}B(n,\alpha)$ cross-sections which can be compared with the present experiment. Bergman and Shapiro [9] using the lead slowing-down spectrometer measured the ratio in the energy range 8 eV to 25 keV. The results agree well with the present experiment below 3 keV but are lower at higher energies by up to 3%. The discrepancy is probably not significant.

5. DISCUSSION

Having obtained values for the ratio of the (n,α) cross-sections of ^{6}Li and ^{10}B, we can calculate the cross-section for one if we know the values of the other. We choose to take $^{6}Li(n,\alpha)$ as the known cross-section and deduce the $^{10}B(n,\alpha)$ cross-section for the following reasons. In the neighbourhood of the neutron binding energy the level density of ^{7}Li is much less than that of ^{11}B and consequently there is less chance of weak levels contributing to the ^{6}Li cross-section than to that of ^{10}B. The first known level in ^{7}Li above the neutron binding energy lies at 247 keV whereas in ^{11}B there are two known levels within the first 150 keV. Over the range of neutron energies considered here, (n,α) and (n,γ) are the only possible reactions in ^{6}Li whereas in ^{10}B, (n,α), (n,γ), (n,p) and (n,t) are all possible. It is not surprising that the cross-sections for (n,p) and (n,t) are small since the Q-values are low and the charged particles have to be emitted with angular momentum $l \geq 2$ for s-wave neutron absorption. It has been assumed in this paper that all absorption cross-sections other than (n,α) are zero. As a result of these comments, we feel that there is a greater possibility of being able to obtain accurate values of the ^{6}Li cross-section, rather than that of ^{10}B, in particular by using total cross-section measurements; we shall now proceed along these lines.

Uttley and Diment [7] have recently measured the ^{6}Li total cross-section over the energy range 70 eV to 7 MeV, the details of which will be published later. However, some of the results will be used here. The data have been analysed to give the resonance parameters of the 247 keV resonance. Since this resonance is produced by p-wave neutrons, it is superimposed on an s-wave contribution which is conveniently found by analysing the data below 5 keV where the contribution from the resonance is negligible. In this region the total cross-section is found to be described by the expression

$$\sigma_{nT}\,(Li) = 149.5/\sqrt{E(eV)} + 0.696 \text{ barns} \qquad (5)$$

There have been two other recent measurements of the ^{6}Li total cross-section. The first, by Hibdon and Mooring [10] in the energy range 10 to 1236 keV, gives results which are in very good agreement with those of Uttley and Diment. The second, by Farrell and Pineo [11] who measured over the energy range 50 to 650 keV, is, in general, in good agreement with Uttley and Diment except on the peak of the resonance where Farrell and Pineo obtain values ~0.4 barn lower. However, we are interested here in the (n,α) cross-section below 100 keV only where the three experiments agree.

Asami and Moxon [12] have recently measured the scattering cross-section of ^{6}Li relative to that of carbon and their value of the potential scattering cross-section is 0.752 ± 0.043 barns. Diment and Uttley [13] have made an exact calculation of the scattering cross-section giving a value of 0.72±0.01 barns at low energies which is in reasonable agreement. However, since the values of Diment and Uttley are more accurate and they agree with the scattering cross-section data of Lane et al. [14] over the 247 keV resonance, we have chosen to use their data.

The absorption cross-section has been obtained from the total cross-section data by two methods. In the first, the exact calculation of the scattering cross-section was subtracted from the measured total cross-section and the results are plotted in Fig. 2. In the second method, the absorption cross-section was calculated and the resulting smooth curve is also shown in Fig. 2 where it can be seen that the agreement between the two sets of results is extremely good in the region of interest.

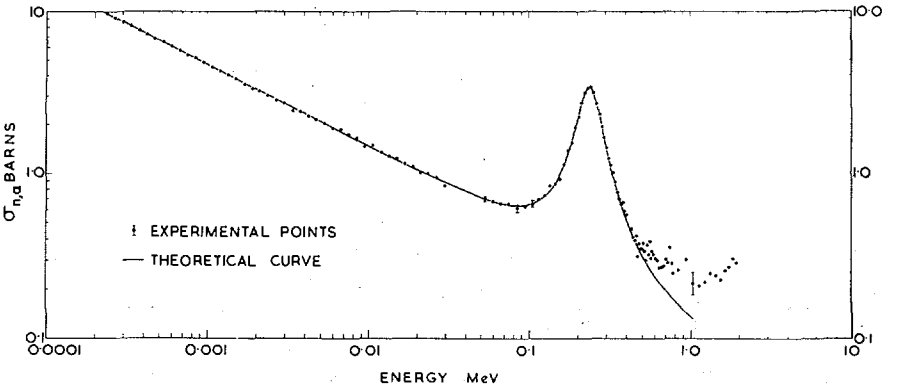

FIG.2. The absorption cross-section of ^{6}Li from 200 eV to 2 MeV. The points are the values obtained by subtracting the calculated scattering cross-section from the measured total cross-section. The curve represents the calculated absorption cross-section.

Fig. 3 shows the values of the ^{6}Li(n,α) cross-section as measured by various experiments in the energy range 10 to 150 keV. Also shown is the smooth calculated curve of Uttley and Diment along with their fit to the total cross-section which is included for comparison purposes. It is immediately clear that the (n,α) cross-section values at 10.7 and 12 keV, measured by Cox and Pontet [15] are much too high since they are essentially equal to the total cross-section and we have seen that the scattering cross-section is ~0.7 barn. The value at 22 keV is also clearly too large as the difference between it and the total cross-section is less than half of the scattering cross-section. It thus appears that the data of Cox and Pontet are probably in error and can be neglected.

Of the other sets of data between 10 and 150 keV, those of Barry [16] and Bame and Cubitt [17] have been measured relative to the ^{235}U fission cross-section. The lowest energy point of Barry at 25 keV was normalised to the Sb-Be source measurement of the ^{235}U fission cross-section made by Perkin et al. [18]. High resolution time-of-flight measurements of this cross-section by Patrick et al. [19] show that there is considerable structure in this energy region and the cross-section averaged over the

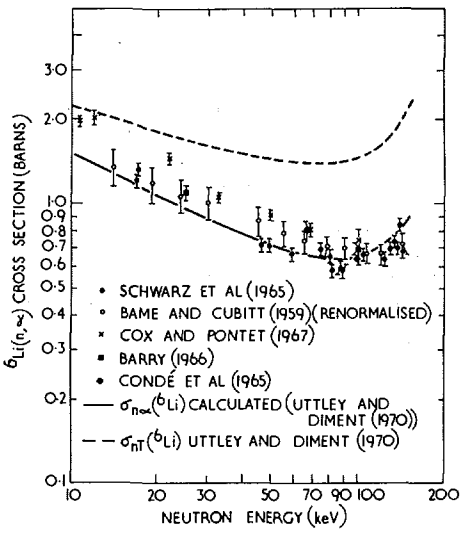

FIG. 3. The $^6Li(n,\alpha)$ cross-section from 10 to 150 keV.

source energy spectrum may be as much as 10% higher than that in the region of 25 keV. The results of Bame and Cubitt used here have been renormalised (see Bergstrom et al. [20]) to take account of later measurements of the ^{235}U fission cross-section. However, because of the presence of structure, it is felt that measurements based on the ^{235}U fission cross-section are subject to uncertainties of at least 5%. In the experiment of Bame and Cubitt, a $^6LiI(Eu)$ crystal was used as a combined ^6Li sample and detector. No corrections were made for the effects of multiple scattering in the crystal, although some were made for the presence of the crystal container and photomultiplier, and so it might be expected that their results will be too high.

In Fig. 3, the absorption cross-section values of Schwarz et al. [21] appear to be in reasonable agreement with the calculated values. However, this is not surprising since, in the region below 40 keV, the data were normalised to a $1/\sqrt{E}$ extrapolation from the thermal cross-section. Thus these results cannot be used to indicate deviations from a $(1/\sqrt{E}$ + resonance) dependence. The single energy measurement of Conde et al. [22] at 100 keV obtained 0.64 ± 0.02 barn in very good agreement with the calculated value of 0.65 barn.

In view of the above comments, we feel that, at present, the values of the (n,α) cross-section obtained from the fit to the total cross-section are the best available set. Since the total cross-section shows no sign of structure below the 247 keV resonance, there seems to be no reason for believing that the absorption cross-section is as high as the measured values indicate. Farrell and Pineo also obtained parameters for the 247 keV resonance and deduced the absorption cross-section over the resonance and down to 40 keV. The difference between the two calculations is never more than 5% but since Uttley and Diment had the advantage of data for their analysis extending well into the $1/\sqrt{E}$ region, it is likely that it will be the more accurate.

We can now find the $^{10}B(n,\alpha)$ cross-section using the results of the ratio measurement together with the $^{6}Li(n,\alpha)$ cross-section values obtained by Uttley and Diment. We have chosen to use the absorption cross-section found by subtracting the calculated smooth scattering cross-section from the measured total cross-section rather than use the calculated absorption cross-section for the following reasons. We shall want to compare the $^{10}B(n,\alpha)$ cross-section deduced from these data with that obtained from measurements of the total and scattering cross-sections. All the data are then as close as possible to being the actual experimentally measured averages containing similar statistical fluctuations rather than the results of a smooth fit. Clearly, since the $^{6}Li(n,\alpha)$ cross-section data obtained by the two different methods are in very good agreement, there will be no difference in the results and conclusions whichever set is used.

In obtaining the $^{10}B(n,\alpha)$ cross-section from the ratio and $^{6}Li(n,\alpha)$ data, the data were averaged over suitable energy intervals, weighting each point in the time-of-flight measurements by its energy width, and in order to show deviations from a $1/\sqrt{E}$ behaviour more clearly, the resulting data have been divided by $19.30/\sqrt{E(\text{keV})}$ averaged over the same energy intervals. The relative cross-section thus found is plotted in Fig. 4 with estimated errors being shown on a few representative points. Also shown are the absorption cross-section values of Mooring et al. [23] and the results obtained by subtracting the scattering cross-section data of Asami and Moxon [24] from the total cross-section data of Diment. Above 100 keV, the scattering cross-section data of Mooring et al. were used since the data of Asami and Moxon did not extend into this region. The data of Bogart and Nichols [25] and Nellis et al. [26] have been neglected because of their relatively large errors.

It can be seen from Fig. 4 that the agreement between the various sets of data is very good. It is clear that the $^{10}B(n,\alpha)$ cross-section does not vary as $1/\sqrt{E}$ as the relative cross-section falls below this level reaching a minimum in the region of 25 keV where the cross-section is ~4% below the $1/\sqrt{E}$ level. Because of this deviation and the large energy spread of their normalisation point at 30 keV, we have not included the data of Macklin and Gibbons [27] in Fig. 4. Above this energy the relative cross-section passes through a resonance and peaks at ~150 keV. That there appears to be a resonance in this region is quite reasonable since the energy level compilations of Ajzenberg-Selove and Lauritsen [28] show a level in ^{11}B, which decays by α-emission, at 140±35 keV above the neutron separation energy.

Although it is usually assumed that the $^{10}B(n,\alpha)$ and $^{6}Li(n,\alpha)$ cross-sections follow a $1/\sqrt{E}$ law until the vicinity of the first resonance above thermal energy, Shapiro [29] has shown that the cross-section σ cannot be strictly proportional to $1/\sqrt{E}$ but must have the form

$$\sigma = \frac{A}{\sqrt{E}} + \Delta\sigma + \beta\sqrt{E} + \gamma E^{3/2} + \ldots \qquad (6)$$

where A, $\Delta\sigma$, β and γ are constants. $\Delta\sigma$ depends on the square of the thermal cross-section and upon the fraction of that cross-section due to resonances of spin $J = I + 1/2$ and $J = I - 1/2$, where I is the spin of the target nucleus. The values of $\Delta\sigma$ are small and always negative, and only cause significant deviations from the $1/\sqrt{E}$ law above neutron energies of a few keV. β and the higher terms are usually considered to be small except in the vicinity of resonances. In regions where equation (6) is valid, β is positive if the levels responsible for most of the low energy cross-section lie above the neutron binding energy and negative if they lie below. Using the Shapiro expression for $\Delta\sigma$, it can be shown that for

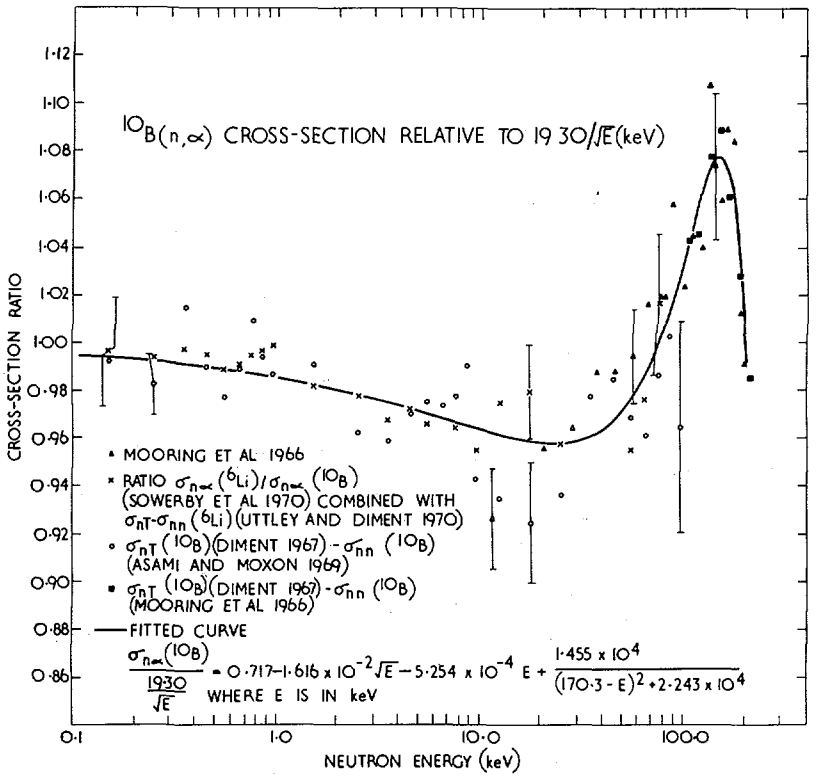

FIG.4. The $^{10}B(n,\alpha)$ cross-section relative to $19.30/\sqrt{E}$ (keV) from 100 eV to 200 keV.

^6Li, $\Delta\sigma \sim -0.02$ barn. However, the value for ^{10}B is expected to be much larger since the thermal cross-section is about four times that of ^6Li and Bergman and Shapiro deduced a value of -0.40 ± 0.03 barn from a measurement of the ratio of the (n,α) cross-sections of ^6Li and ^{10}B. Thus the deviation of the data from a $1/\sqrt{E}$ behaviour as shown in Fig. 4 is indicative of the presence of the $\Delta\sigma$ term and possibly also of a significant value of β.

The measured energy dependence of the cross-section suggests that it may be possible to fit the data with an expression which contains the first three terms of the Shapiro expansion (equation (6)) and an s-wave resonance in the region of 150 keV. We write the $^{10}B(n,\alpha)$ cross-section $\sigma_{n\alpha}(^{10}B)$ as

$$\sigma_{n\alpha}(^{10}B) = 19.30/\sqrt{E} + \Delta\sigma + \beta\sqrt{E} + \frac{K}{\sqrt{E}}\left[\frac{1}{(E-E_o)^2 + \frac{\Gamma^2}{4}} - \frac{1}{E_o^2 + \frac{\Gamma^2}{4}}\right] \text{ barns} \qquad (7)$$

where $\Delta\sigma$, β and K are constants, E is the neutron energy in keV, E_o is the resonance energy in keV and Γ is the total width of the resonance in keV.

It has been assumed that $\Gamma_\alpha >> \Gamma_n$ and hence $\Gamma_\alpha \sim \Gamma$. The second term in the square brackets is included to remove the $1/\sqrt{E}$ tail of the resonance term since it is already included in the term $19.30/\sqrt{E}$. It should be noted that if resonance interference effects are present then the energy dependence of the interference terms will be similar to equation (6) but with the addition of a term proportional to E.

Dividing equation (7) by $19.30/\sqrt{E}$ we obtain the following expression for the relative cross-section

$$\frac{\sigma_{n\alpha}(^{10}B)}{19.30/\sqrt{E}} = 1 + A\sqrt{E} + BE + C\left[\frac{1}{(E-E_o)^2 + \frac{\Gamma^2}{4}} - \frac{1}{E_o^2 + \frac{\Gamma^2}{4}}\right] \qquad (8)$$

where A, B and C are constants.

A programme was written to fit this expression to all the data plotted in Fig. 4 by adjusting the quantities A, B, C, E_o and Γ to minimise the sum of the squares of the differences, equal weight being given to all the data points. It can be seen from the curve drawn through the data in Fig. 4, which is the result of this fit, that it is not necessary to consider more than the first three terms in the Shapiro expansion. The resonance energy is found to be 170.3 keV and the width Γ = 299.5 keV. The value of $\Delta\sigma$ obtained is -0.31 barn and the best fit is obtained with $\beta = -1.01 \times 10^{-2}$ barns.$(keV)^{-1/2}$. If common terms in equation (7) are collected together and the expression simplified, then the cross-section $\sigma_{n\alpha}$ of ^{10}B is given by

$$\sigma_{n\alpha}(^{10}B) = \frac{13.837}{\sqrt{E}} - 0.312 - 1.014 \times 10^{-2}\sqrt{E} + \frac{2.809 \times 10^5}{\sqrt{E}[(170.3-E)^2 + 2.243 \times 10^4]} \text{ barns} \qquad (9)$$

where E is in keV.

While the above expression is a good description of the energy dependence of the cross-section, great care must be taken in interpreting the meaning of the various parameters. It is quite likely that other expressions can be found which give equally good fits. The s-wave resonance included in the present analysis accounts for 28% of the low energy cross-section, but, if the resonance is attributed to p-waves, an equally good fit is obtained. The presence of other small resonances would certainly destroy the validity of this analysis and it is to be noted that there is a level in ^{11}B at 6 ± 10 keV above the neutron separation energy. The data tend to suggest the existence of a resonance in the region of 40 keV but the inclusion of another resonance is not justified by the accuracy of the data. If we take equation (9) seriously, the negative sign of β would suggest that, in the absence of resonance interference effects, the levels responsible for the low energy $^{10}B(n,\alpha)$ cross-section lie below the neutron binding energy, which is opposite to the conclusion reached by Bergman and Shapiro. However, these authors did not allow for the contribution of the 247 keV resonance in the $^6Li(n,\alpha)$ cross-section. Since this contributes about 5% of the cross-section at 25 keV, the upper limit of their experiment, this omission makes their analysis invalid.

6. CONCLUSIONS

Summarising, the ratio of the (n,α) cross-sections of ^{6}Li and ^{10}B has been measured from 10 eV to 80 keV with an accuracy ranging from 0.9 to 2.5%. It has been shown that if these results are combined with the $^{6}Li(n,\alpha)$ cross-section values deduced by Uttley and Diment from fits to their measured total cross-section, the resulting values of the $^{10}B(n,\alpha)$ cross-section are in very good agreement with those derived or measured in other ways. The cross-section has been written in terms of an analytic expression, the form of which has been derived from theoretical arguments. This expression has been fitted to all the cross-section data and the result is given by equation (9). We conclude that equation (9) describes the $^{10}B(n,\alpha)$ cross-section up to 200 keV within an accuracy ranging from 1% up to 1 keV, 2% at 10 keV, 3% at 100 keV and 5% at 200 keV and it is recommended that this equation be used where neutron fluxes are determined with detectors based on the $^{10}B(n,\alpha)$ reaction.

It has been shown that the $^{10}B(n,\alpha)$ cross-section is now known to a considerably higher accuracy than previously since the results of three independent measurements agree so well. However, in the case of $^{6}Li(n,\alpha)$ although we believe that the Uttley and Diment calculated cross-section is probably equally accurate, the agreement between the various measurements is much poorer, as indicated in Fig. 3. Thus, at present, the $^{10}B(n,\alpha)$ cross-section is the better known one but in deciding whether ^{6}Li or ^{10}B should be considered as the primary standard, the following points should be noted. Several reactions besides (n,α) are energetically possible in ^{10}B whereas capture is the only other one possible in ^{6}Li. Although these cross-sections are known to be small, it is clearly desirable for a primary standard to have as few competing reactions as possible so that use can be made of accurate total cross-section data and scattering cross-section measurements to obtain the appropriate cross-section used in the flux determinations. The possible presence of resonances in the ^{10}B cross-sections below 150 keV means that the $^{10}B(n,\alpha)$ cross-section is by no means an ideal case for use as a standard.

Clearly, as a result of the greater accuracy with which the $^{10}B(n,\alpha)$ cross-section is known, it will continue to be used very widely in the determination of neutron fluxes. Nevertheless, in view of the statements above, we suggest that the $^{6}Li(n,\alpha)$ cross-section be considered as the primary standard in the region below 100 keV.

ACKNOWLEDGEMENTS

The authors are grateful to Dr. E. R. Rae for his continued interest in this work. The assistance of Mr. M. G. Schomberg during the measurements and in the analysis is greatly appreciated. We are also indebted to Drs. D. B. Gayther, M. S. Coates and Mr. J. S. Story for helpful discussions and to Dr. W. Hart for the Monte Carlo calculations of efficiencies.

REFERENCES

[1] PATRICK, B. H., Schomberg, M. G., Sowerby, M. G. and Jolly, J. E., Proc. Conf. on Nuclear Data for Reactors, IAEA Vienna, Vol. II (1967), p.117.
[2] RAE, E. R. and Bowey, E. M., Proc. Phys. Soc. A66 (1953) 1073.
[3] LYNN, J. E. and Moxon, M. C., private communication.
[4] HART, W., private communication.
[5] HEMMINGS, P. J., UKAEA Report AHSB(S)R105.

[6] DIMENT, K. M., UKAEA Report AERE - R 5224.
[7] UTTLEY, C. A. and Diment, K. M., to be published.
[8] SPAEPEN, J., Proc. Conf. on Nuclear Data for Reactors, IAEA Vienna, Vol. I (1967) p.241.
[9] BERGMAN, A. A. and Shapiro, F. L., Soviet Physics JETP 13 (1961) 895.
[10] HIBDON, C. T. and Mooring, F. P., Proc. Conf. on Neutron Cross Sections and Technology, Washington (1966) p.159.
[11] FARRELL, J. A. and Pineo, W. F. E., Proc. Conf. on Neutron Cross Sections and Technology, Washington (1966) p.153.
[12] ASAMI, A. and Moxon, M. C., (these Proceedings).
[13] DIMENT, K. M. and Uttley, C. A., Nuclear Physics Division Progress Reports AERE - PR/NP 15, p.12 and AERE - PR/NP 16, p.3.
[14] LANE, R. O., Elwyn, A., Mooring, F. P. and Langsdorf, A., Bull. Am. Phys. Soc. 12 (1967) 87.
[15] COX, S. A. and Pontet, F. R., J. Nuc. Energy 21 (1967) 271.
[16] BARRY, J. F., Proc. Conf. on Neutron Cross Sections and Technology, Washington (1966) p.763.
[17] BAME, S. J. and Cubbitt, R. L., Phys. Rev. 114 (1959) 1580.
[18] PERKIN, J. L., White, P. H., Fieldhouse, P., Axton, E. J., Cross, P. and Robertson, J. C., J. Nuc. Energy 19 (1965) 423.
[19] PATRICK, B. H., Sowerby, M. G. and Schomberg, M. G., UKAEA Report AERE - R 6350.
[20] BERGSTROM, A., Schwarz, S., Stromberg, L. G. and Wallin, L., Neutron Data Compilation Centre, Paris, Report CCDN-NW 3.
[21] SCHWARZ, S., Stromberg, L. G. and Bergstrom, A., Nuc. Phys. 63 (1965) 593.
[22] CONDE, H., Schwarz, S. and Starfelt, N., Arkiv. Fysik 29 (1965) 45.
[23] MOORING, F. P., Monohan, J. E. and Huddleston, C. M., Nuc. Phys. 82 (1966) 16.
[24] ASAMI, A. and Moxon, M. C., UKAEA Report AERE - R 5980.
[25] BOGART, D. and Nichols, L. L., Nuc. Phys. A125 (1969) 463.
[26] NELLIS, D. O., Tucker, W. E. and Morgan, I. L., to be published.
[27] MACKLIN, R. L. and Gibbons, J. H., Phys. Rev. 165 (1968) 1147.
[28] AJZENBERG-SELOVE, F. and Lauritsen, T., Nuc. Phys. A114 (1968) 1.
[29] SHAPIRO, F. L., Soviet Physics JETP 7 (1958) 1132.

DISCUSSION

TO PAPERS IAEA-CN-26/100, 106, 25, 26

J. R. ASKEW: In the introduction to his paper (CN-26/106) Dr. Deruytter refers to the requests for high-accuracy data on ^{239}Pu fission cross-sections and infers that measurements on standards are needed to an even higher accuracy than that requested (i. e. to better than $\frac{1}{2}$%). This appears to me to raise two questions: Is this practicable? Is it necessary? As a reactor physicist I cannot comment upon the first question. On the second, however, it seems to me that even ignoring integral data, the performance calculations in which we are interested are more sensitive to cross-section ratios than to absolute values. Where integral evidence is available it is the energy dependence of the cross-section which is most required from the differential measurement. Should this consideration affect the studies on standards?

A. J. DERUYTTER: As regards the first part of your question, it is shown in the paper that, thanks to the steady improvement in fission foils and in the knowledge of standard materials and cross-sections (such as ^{10}B (n, α), we may well be able at present to reach 0. 5% accuracy on the fission cross-section of ^{239}Pu (and ^{235}U) at a typical energy, e. g. the 2200 m/s-values. However, to reach a precision of 0. 5 to 1% over the entire energy range, from thermal up to MeV, as requested in the RENDA-list, it will still be necessary to make extensive improvements as far as standard cross-section materials and detection techniques are concerned.

In reply to the second part of your question, asking whether this degree of accuracy is necessary for these cross-sections, I would like to emphasize that Table I of the paper is based on Priority I requests from the recently edited RENDA-list. The latter is a compilation of data requests for reactor design and neutron dosimetry and the accuracy requirements for standards follow directly from these requests. For us, this RENDA-list is a working document. What you are questioning is, in fact, the necessity of the demands that are put forward as Priority I by reactor physicists and designers in that particular request compilation.

W. G. DAVEY: Mr. Askew's question regarding the need for precise standards seems to imply that only ratios of data are needed. As a reactor physicist, I believe that it is essential to have two sets of data in an absolute sense: the first is a single fission cross-section, and here the ^{235}U-cross-section is still the best despite recent evidence of structure; the second is an absolute $\bar{\nu}$-value. Without these absolute data, the often-used derivation of differential data to fit critical experiments is an exceedingly dangerous procedure.

M. ASGHAR: I should like to make a comment. We know that "standards" are very important and we are entitled to demand that they should be measured with an accuracy of, say, 1% or even 0. 1% or 0. 01%. However, this does not make much sense if the different laboratories carrying out these standard cross-section measurements do not co-ordinate and "standarize" the methods used to analyse these data.

J. P. THEOBALD: In the case of neutron-scattering experiments, in particular, the $^{6}Li, (n, \alpha)$ cross-section does not seem to be suitable owing to the absence of gamma-discriminating detectors. The most recent experiments have been performed with boron-loaded liquid scintillators

with pulse-shape discriminators or else with ^{3}He proportional or gas scintillator counters. The corrections for multiple scattering in glasses will always be a subject for discussion because of the complex structure of the glasses.

M. G. SOWERBY: I agree. We, too, consider that for practical use the boron reactions are of more use than the $^{6}Li(n,\alpha)$ reaction. However, if one requires the greatest accuracy in the long term the $^{6}Li(n,\alpha)$ is better for the reasons stated in our paper and the boron cross-sections can always be obtained from ratio measurements. It is a question of what you mean by a primary standard.

A. J. DERUYTTER: I think Mr. Sowerby's comment bears out the remarks made in our paper (CN-26/106) concerning lithium glasses and shows once again that the use of the ^{10}B (n,α) reaction as a practical primary standard is preferable to the ^{6}Li (n,α) reaction because one has to be able to use the standard cross-section accurately, otherwise it does not serve its purpose.

R. VIDAL: Mr. Deruytter points out in section 1 of paper CN-26/106 that the isotopic content of the lithium can be affected by the chemical preparation. Is there not the likelihood in mass-spectrometer measurements of isotopic content that, as a result of variations in isotopic composition, the measurement of content in the sample will be imprecise?

A. J. DERUYTTER: In our measurements with the layers of natural boron, we observed enrichments in ^{10}B in the evaporation process as compared with the natural boron at the start. This effect is due to the preparative evaporation of the boron layers under vacuum and not to the mass spectrometer with which the isotopic ratio is subsequently measured (the latter being calibrated with standards whose isotopic ratio is very well known).

As far as the lithium programme is concerned, we are still at the stage of using Li_2SO_4 solutions in heavy water for determining the 2200 m/s absorption cross-section by transmission. In the case of the lithium layers our procedure will probably be to use lithium fluoride layers. In this case, too, the mass spectrometer can be calibrated with standards whose $^{6}Li/^{7}Li$ ratio is known. The possibility of a residual chemical effect - which is not very probable - consists in an instability in isotopic composition during the dissolution of the evaporated L. F.

MEASUREMENTS OF NEUTRON ELASTIC SCATTERING FROM CARBON IN THE ENERGY REGION OF 0.50 TO 2.00 MeV

N. AHMED*, M. COPPOLA, H.-H. KNITTER
Central Bureau for Nuclear Measurements,
EURATOM, Geel, Belgium

Abstract

MEASUREMENTS OF NEUTRON ELASTIC SCATTERING FROM CARBON IN THE ENERGY REGION OF 0.50 TO 2.00 MeV.

Thirty-one differential cross-section angular distributions for the elastic scattering of neutrons from carbon were measured at primary neutron energies between 0.50 and 2.00 MeV, using fast neutron time-of-flight techniques. The fully corrected points of each angular distribution were fitted with a five-term Legendre-polynomial expansion. The obtained B_L-coefficients were then fitted with suited functions of the energy in order to obtain a smooth dependence of the differential neutron-scattering cross-sections on the primary neutron energy using a limited number of parameters. A phase-shift analysis based on the present experimental B_L-coefficients was performed. The obtained phase shifts are compared with the ones predicted by a coupled-channel calculation of ^{12}C-neutron scattering and with phase shifts resulting from neutron-polarization measurements.

INTRODUCTION

The accurate knowledge of the neutron cross section of carbon is of actual importance and usefulness in the field of neutron scattering measurements. The ^{12}C nucleus has its first excited state at 4.4 MeV and the nuclear reactions that can be induced by neutrons with lower energies are elastic scattering and neutron capture. The (n,γ) cross section is 1.86 mb in the neighbourhood of 0.1 eV [1] and becomes negligible as the incoming neutron energy increases. The total neutron cross section of carbon shows no resonance structure below 2 MeV and can be represented by simple parametric expansions. For these reasons the neutron cross section of carbon below 2.00 MeV is well suited to be used as a standard for the determination of the neutron scattering cross sections of other elements.

In addition, carbon samples are very easy to be prepared and analysed. Their use as standard samples is especially indicated in neutron scattering experiments, when the $^7Li(p,n)^7Be$ neutron producing reaction is used above 0.5 MeV. In fact, the other most commonly used standard material, that is polyethylene, can hardly be utilised when more than one primary neutron group is present.

In the past, neutron elastic scattering cross sections of carbon up to 4.1 MeV have been measured by several authors [2-7] using methods other than time-of-flight. A verification of the existing results was then thought to be necessary by means of the last mentioned technique which is most extensively used in our laboratory for the determination of cross sections of other elements or isotopes.

---

* Guest from Pakistan Atomic Energy Commission.

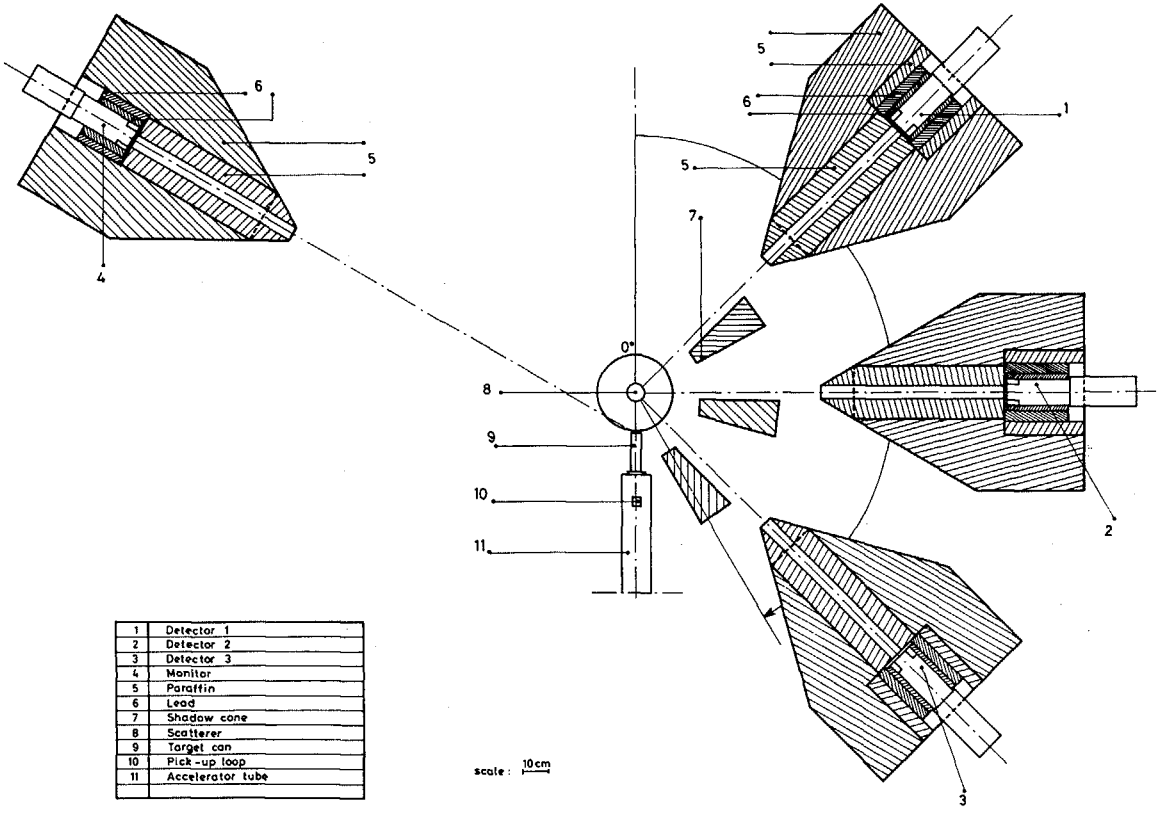

FIG. 1. Lay-out of the detecting system.

EXPERIMENTAL EQUIPMENT AND PROCEDURE

The measurements were done at the 3 MV Van de Graaff accelerator of CBNM using fast neutron time-of-flight techniques. The layout of the experiment is shown in Fig. 1. A pulsed proton beam of 1 ns pulse width and 1 MHz repetition rate was focussed on the neutron producing target.

For neutron production two different reactions were used. Between 0.50 and 0.70 MeV neutrons were produced through the $^{7}Li(p, n)^{7}Be$ reaction using a solid LiF target. Above 0.75 MeV neutrons were obtained by the $T(p, n)^{3}He$ reaction with occluded TiT targets. The target thicknesses and the scattering geometry were chosen in such a way that the total neutron energy spreads were between 30 and 45 keV for all the measurements.

The neutrons emitted around zero degree with respect to the direction of the incoming proton beam were scattered by the cylindrical carbon sample and collimated towards three detectors placed inside appropriate shieldings at an equal distance of 141.0 cm from the scatterer. The sample was positioned at 15.0 cm from the target. Each detector consisted of a cylindrical NE 102A plastic scintillator 5.0 cm x 2.5 cm, viewed by an AVP 56/03 photomultiplier. The fast outputs of the detectors gave the start signals for three time-to-pulse height converters. The stop signals were extracted from a pick-up loop placed before the target. The output signals of the converters were registered simultaneously in three different memory sections of a 4096 channel pulse height analyser. The overall time resolution of such a neutron time-of-flight spectrometer, including the ion pulse width of the accelerator, was about 2.3 ns. The relative neutron fluence was measured making use of an additional time-of-flight spectrometer with the detector inserted in a shielding collimating the neutrons coming from the neutron producing target. The part of the time spectrum corresponding to the direct target neutrons was selected by means of a window discriminator to monitor the measurements.

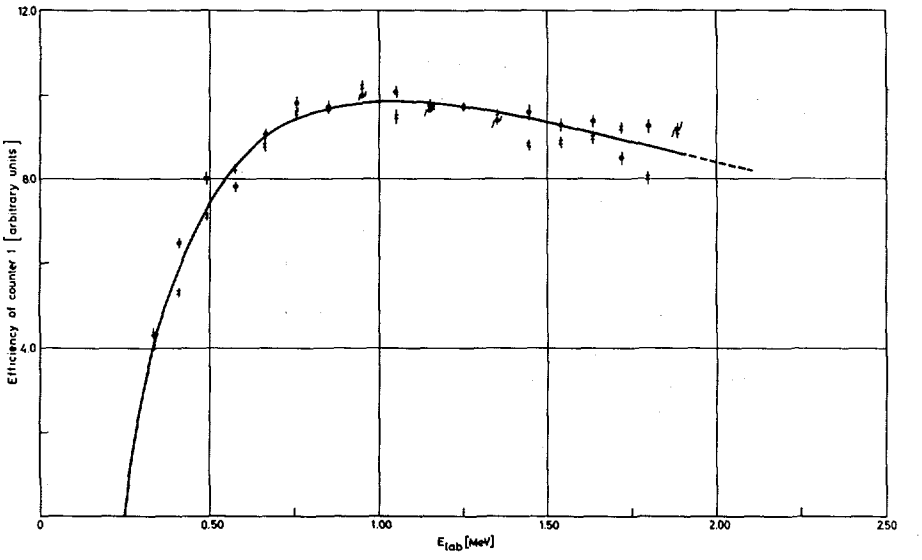

FIG. 2. Relative efficiency of detector 1 measured at the beginning and at the end of the present measurements.

The relative efficiency of the three detectors was measured by comparing the yield of neutrons scattered on a hydrogenous sample at several angles between 20° and 67.5° and the known n-p cross-section. The hydrogeneous sample was a polyethylene cylinder of 1.00 cm outside diameter, 0.60 cm inside diameter and 4.00 cm height. Its weight was 1.840 g and the content of hydrogen was 14.31%.

The relative efficiencies of the detectors were measured twice, at the beginning and at the end of the scattering measurements on carbon. Within the experimental errors, no variation of the efficiencies was found. The experimentally observed efficiency of the three detectors were fitted with a semiempirical expression. The result of the fit for detector 1 is shown in Fig. 2, along with the observed values.
The dimensions of the carbon samples used in the present experiment are shown in Table I. They were chosen in such a way, that the corrections due to beam attenuation and multiple scattering in the sample do not change appreciably with the incident neutron energy. The multiple scattering corrections at 20° turned out to be between 3.0 and 6.5%.

TABLE I. DIMENSIONS OF CARBON SAMPLES

Carbon Sample Dimensions				Neutron energy region (MeV)
Outside diameter (cm)	Inside diameter (cm)	Height (cm)	Weight (g)	
2.00	0.86	3.505	15.462	0.50 - 1.25
1.41	0.00	3.500	9.375	1.30 - 1.70
1.72	0.00	3.500	13.897	1.75 - 2.00

TABLE II. SOURCES OF ERRORS FOR THE DIFFERENTIAL ELASTIC CROSS-SECTIONS AND THEIR REPRESENTATIVE RELATIVE ERRORS

Sources of errors	Errors (%)
Detector efficiency	2.00
Total n-p scattering cross-section	0.50
Counting statistics on H	1.00
Flux factor in C-sample	
1) due to fluctuations in flux calculations	0.45
2) due to uncertainties of σ_T	0.70
Multiple scattering correction in carbon	0.70
α-factor in CH_2	1.00
H-content in CH_2	0.5
Total error	2.8

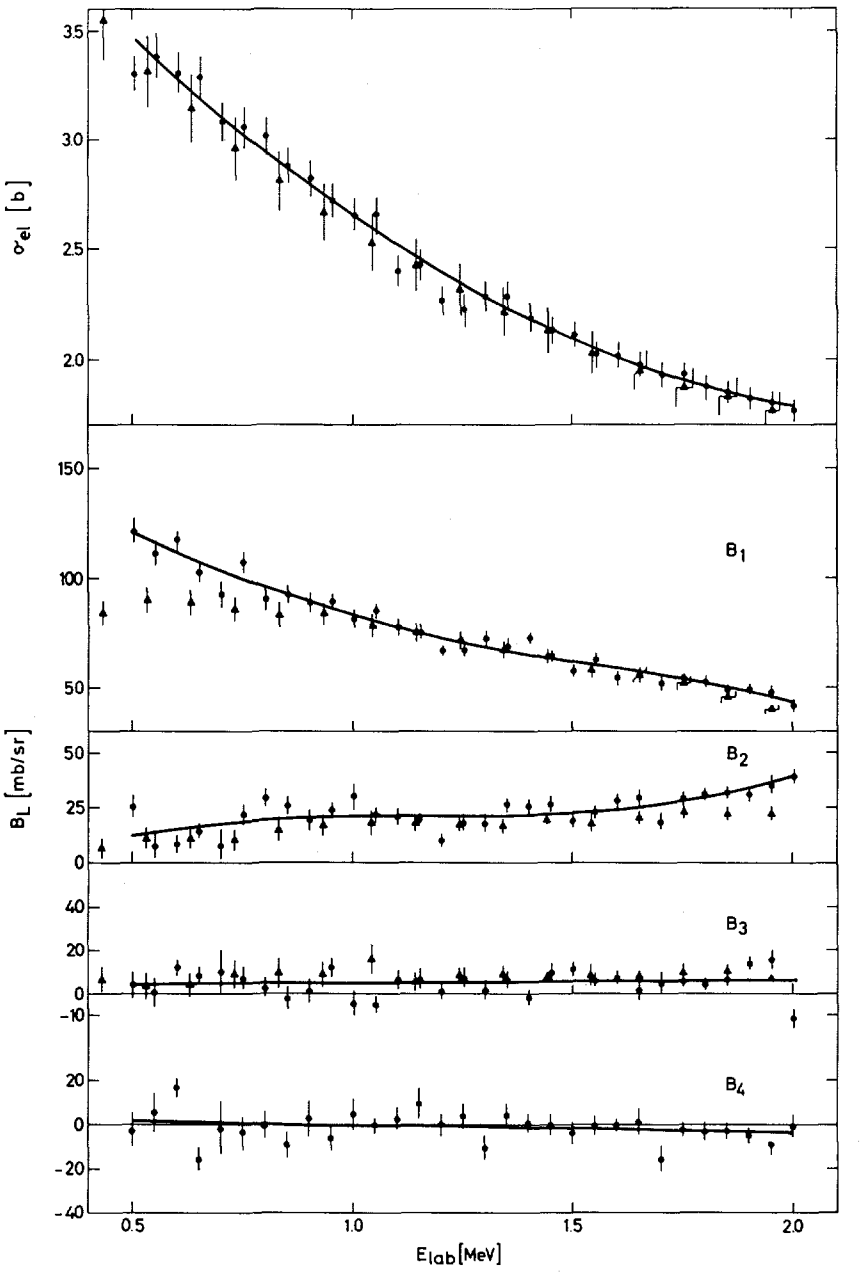

FIG. 3, Total elastic cross-section of carbon and B_1 to B_4 coefficients. Full circles are the results of the present measurements, and solid lines are the fits with Eq.(2). Triangles are the experimental points of Lane et al.[23].

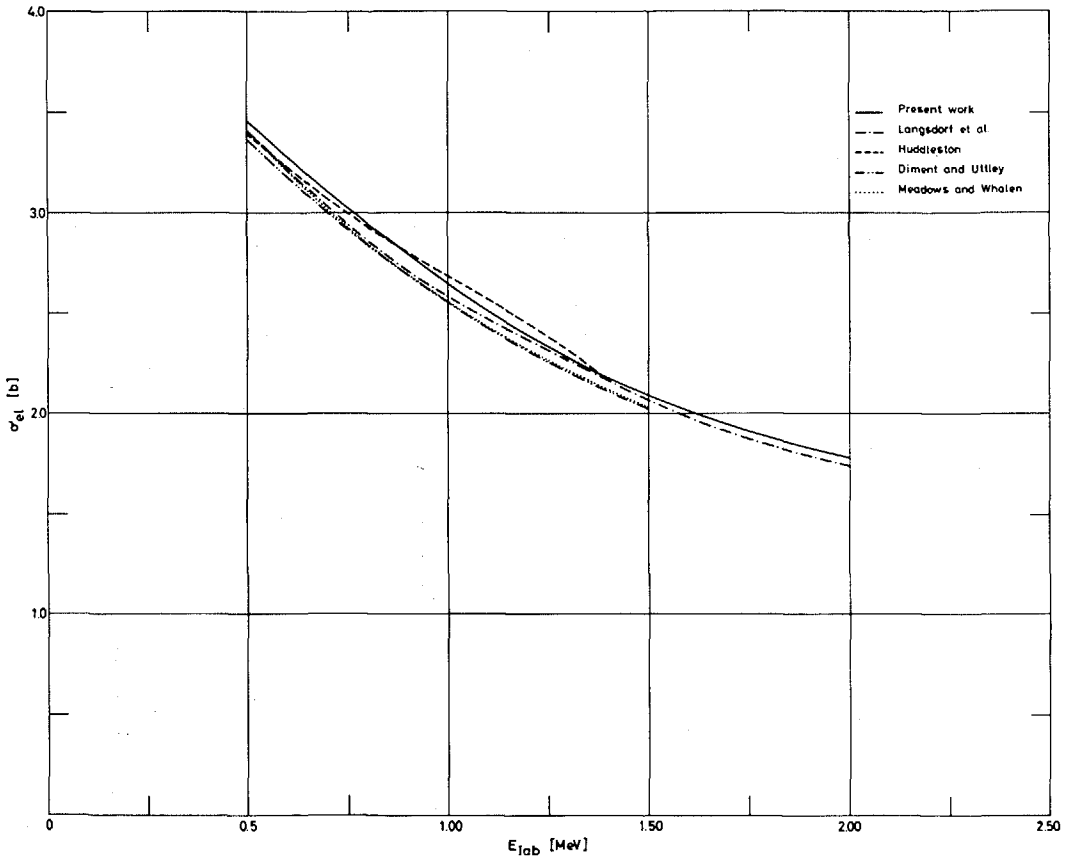

FIG. 4. Comparison between σ_{el} results from the present analysis and curves of other workers.

EXPERIMENTAL RESULTS

Angular distributions of neutrons scattered from carbon were measured at incident neutron energies between 0.50 and 2.00 MeV in energy steps of 50 keV. The scattered neutrons were detected between 20° and 150°, with an angular spacing of 10°. The neutron scattering from the polyethylene sample was measured at +30° and -30° for the energies between 0.50 and 0.85 MeV and at +40° and -40° for the energies between 0.90 and 2.00 MeV. In this way the presence of eventual experimental asymmetries of the neutron yield around zero degree was checked. No such asymmetry was observed within the experimental accuracy.

The absolute values of the differential cross section of carbon were determined comparatively to the H(n, n)H differential cross section. A number of corrections were applied to the observed data. The variation in the intensity of the $^{7}Li(p, n)^{7}Be$ and $T(p, n)^{3}He$ neutron yields as a function of angle and energy due to the finite target-to-sample geometry were taken into account. The attenuation of the incoming neutron flux in the scattering samples and the multiple scattering of neutrons within the polyethylene and carbon samples were also considered. The evaluation of these corrections were performed by the Monte Carlo program MAGGIE in the version modified at the CBNM [10]. The applicability of this program is illustrated elsewhere [11-15] in several cases.

In evaluating the errors to the individual experimental points, the ones introduced by the counting statistics and those originating from the statistical nature of the Monte Carlo method were considered. A complete list of the other sources of errors is presented in Table II.

A fit through the corrected differential scattering cross sections were made with a Legendre polynomial expansion of the form

$$\frac{d\sigma}{d\Omega}(\theta) = \sum_{L=0}^{4} B_L P_L(\cos\theta) \qquad (1)$$

The B_L coefficients obtained from (1) were then fitted using an expression of the type

$$B_L(E) = \sum_{i=0}^{3} A_{Li} E^{i} \qquad (2)$$

where the expansion on the right hand side of (2) was truncated after the second term for B_3 and B_4. The values of $\sigma_{el} = 4\pi B_0$ and of B_1 to B_4 from (1) are presented in Fig. 3, together with their errors, along with the fitted curves from (2).
For practical purposes, the explicit expression valid for σ_{el} in the energy region from 0.50 to 2.00 MeV is

$$\sigma_{el}(E) = (4.513\pm0.243) - (2.343\pm0.637)E + (0.465\pm0.520)E^{2} + (0.012\pm0.133)E^{3} \text{ barn} \qquad (3)$$

where E is the incoming neutron energy in MeV.
The overall error per point, including the computed error from the fitting procedure and errors from other sources, is evaluated to about 3%.

Attention must be paid to the large sensitivity of the coefficients of (3) to the shape of the total cross section curve due to the correlation between the coefficients themselves. It has been observed that a variation of the cross section values of about 1.5% at the low energy side produces a change of the first coefficient of (3) comparable to the quoted error.

In Fig. 4 the integrated elastic scattering cross sections from the present measurements are compared with the cross section results of other workers [4, 15-17]. The agreement between all these measurements, although made with different experimental methods, is good within the quoted errors.

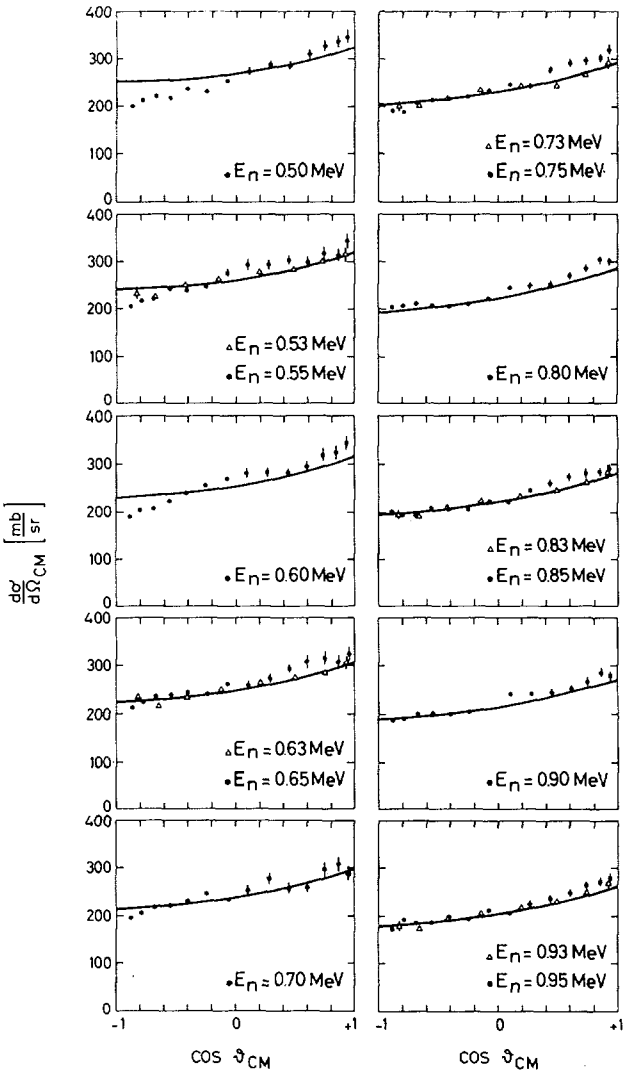

FIG. 5. Elastic scattering cross-section between 0.50 and 0.95 MeV. Full circles are from the present work, triangles are from Ref. [23]. Solid lines are the calculations using Reynolds' phase shifts.

DISCUSSION

Reynolds et al. [18] have recently done coupled-channel calculations on the $^{12}C+n$ system. They were able to generate a set of phase shifts in the incident neutron energy range from 0 to 5 MeV, which reproduced fairly well the total cross section and the available elastic scattering angular distributions in the above range, and the polarization above 2.4 MeV. In Figs. 5 to 7 the elastic scattering angular distributions calculated from the phase shifts of Reynolds et al. are shown along with the experimental results of the present work and of Lane et al. [23]. The agreement between the two measurements is good within the experimental errors, but

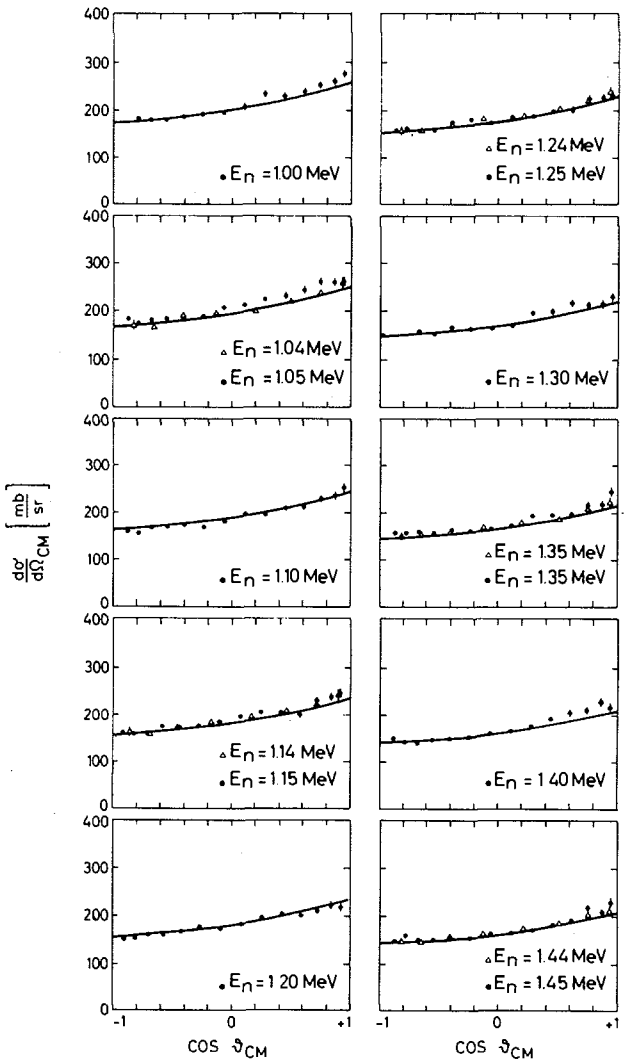

FIG. 6. Elastic scattering cross-section between 1.00 and 1.45 MeV. Full circles are from the present work, triangles are from Ref. [23]. Solid lines are the calculations using Reynolds' phase shifts.

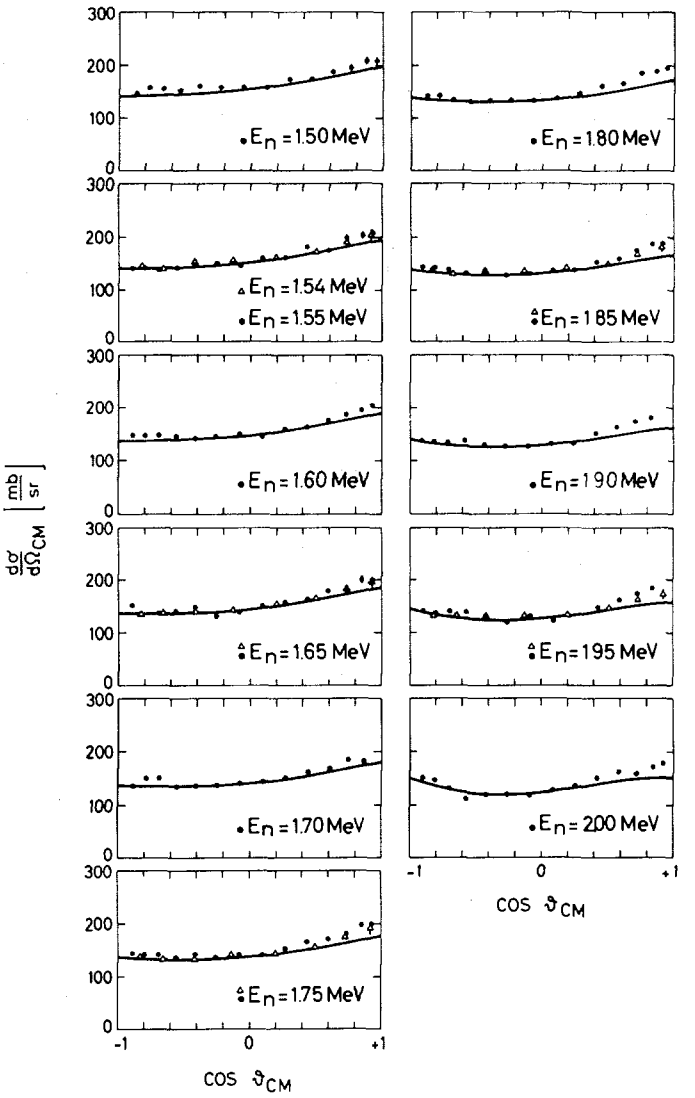

FIG. 7. Elastic scattering cross-section between 1.50 and 2.00 MeV. Full circles are from the present work, triangles are from Ref. [23]. Solid lines are the calculations using Reynolds' phase shifts.

the data of Lane et al. appear to agree slightly better with the calculations of Reynolds et al.. Therefore, a phase shift analysis for s, p and d waves using the present angular distribution results was performed. For this purpose the formalism of Blatt and Biedenharn [19] specified for pure elastic scattering of neutral spin-1/2 particles on spin-0 nuclei was used.

Phase shifts were calculated corresponding to the highest and to the lowest values of the experimental B_L-coefficients. The results are shown

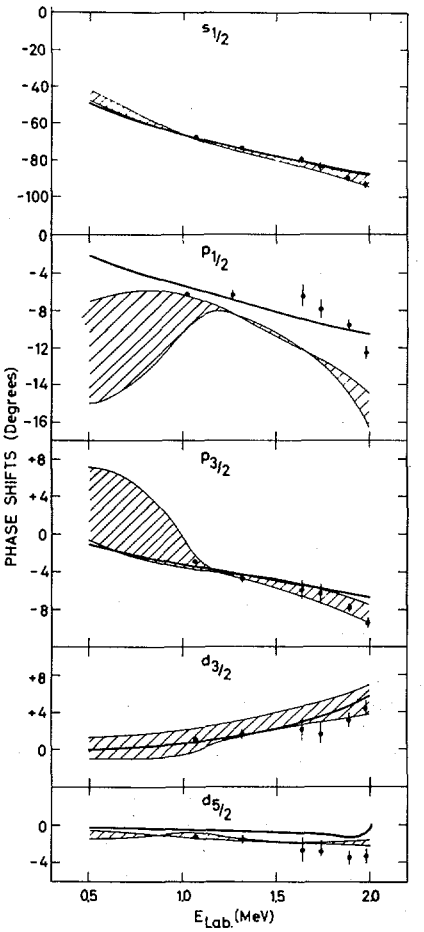

FIG. 8. Results of phase shift analysis. Hatched areas are obtained from the measured B_L- coefficients of the present work. Solid lines are Reynolds' phases. Full circles are measured points of Aspelund [20].

as the limits of the hatched areas in Fig. 8, along with the phase shifts of Reynolds et al. and the values determines by Aspelund [20] . The agreement between the measured and the calculated phase shifts is good for the s 1/2, p 3/2 and d 3/2 phases, while some discrepancies exist for the d 5/2, and more evident for the p 1/2 phase shifts.

The phase shifts obtained in the present investigation were used to calculate the polarization power of carbon. Use was made of formula (3.2) of Simon and Welton [21] specified to the case of neutron scattering on spin-zero nuclei. The results at $\theta_{lab} = 45°$ are shown in Fig. 9 along with the experimental values of Elwyn et al. [22] and of Aspelund [20], and with the calculations using Reynolds phase shifts. The hatched area has the same significance as before.

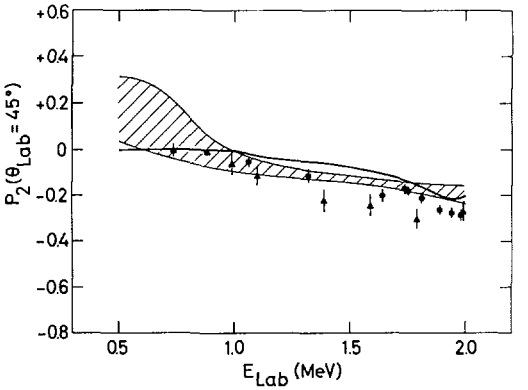

FIG. 9. Polarization power of carbon at $\Theta_{lab}=45°$. Hatched area represents calculations starting from the B_L-coefficients of the present measurement. The solid line is calculated from Reynolds' phases. Triangles are experimental values of Elwyn et al. [22]. Full circles are from Aspelund [20].

CONCLUSIONS

The present measurements on carbon give integrated neutron cross sections in agreement within 1.5% with the values obtained by other workers using different experimental techniques. The phase shifts calculated starting from the presently measured angular distributions are in reasonably good agreement with the phase shifts of Reynolds calculated on the basis of a coupled-channel model of the $^{12}C+n$ system. A certain discrepancy, however, has been noticed for the p 1/2 phase shift.

The comparison between measured and calculated polarization power of carbon suggests that additional valuable information could be drawn from a better knowledge of this quantity. It is, therefore, felt that more polarization angular distribution measurements should be carried out.

REFERENCES

[1] PARKER, K., AWRE Report n° 0-71/60, 1961.

[2] LANE, R.O., LANGSDORF, Jr., A.S., MONAHAN, J.E., ELWYN, A.J., Annals of Physics 12 (1961) 135.

[3] WILLS, Jr., J.E., BAIR, J.K., COHN, H.O., WILLARD, H.B., Phys. Rev. 109 (1958) 891.

[4] LANGSDORF, Jr., A., LANE, R.O., MONAHAN, J.A., ANL-5567 Rev. 1961.

[5] WILLARD, H.B., BAIR, J.K., KINGTON, J.D., Phys. Rev. 98 (1955) 669.

[6] MUEHLHAUSE, C.O., BLOOM, S.D., WEGNER, H.E., GLASOE, G.N., Phys.Rev. 103 (1956) 720.

[7] ROGERS, W.L., GARBER, D.I., SHRADER, E.F., Bull.Am.Phys. Soc. 6 (1961) 61.

[8] GAMMEL, J.L., "Fast Neutron Physics", Part II (MARION, J., FOWLER, J., Eds.) Interscience Publishers, Inc., New York (1963).

[9] Nuclear Data Sheets, Nuclear Data Group of the National Research Council, National Academy of Sciences.

[10] SCHMIDT, H., HORSTMANN, H., private communication.

[11] KNITTER, H.-H., COPPOLA, M., EUR 3903.e 1968.

[12] KNITTER, H.-H., COPPOLA, M., Z. Physik 228 (1969) 286.

[13] COPPOLA, M., KNITTER, H.-H., EUR 2798.e 1966.

[14] COPPOLA, M., KNITTER, H.-H., Z. Physik 232 (1970) 286.

[15] HUDDLESTON, C.M., LANE, R.O., LEE, Jr., L.L., MOORING, F.P., Phys. Rev. 117 (1960) 1055, ANL-6111, 1960.

[16] DIMENT, K.M., UTTLEY, C.A., EANDC(UK) 94 AL.

[17] MEADOWS, J.W., WHALEN, J.F., private communication (1969).

[18] REYNOLDS, J.T., SLAVIK, C.J., LUBITZ, C.R., FRANCIS, N.C., Phys. Rev. 176 (1968) 1213.

[19] BLATT, J.M., BIEDENHARN, L.C., Rev. Mod. Phys. 24 (1952) 258.

[20] ASPELUND, O., A.B. Atomenergi Report n° AE-282 (1967).

[21] SIMON, A., WELTON, T.A., Phys. Rev. 90 (1953) 1036.

[22] ELWYN, A.J., LANE, R.O., Nucl. Phys. 31 (1962) 78.

[23] LANE, R.O., LANGSDORF, Jr., A.S., MONAHAN, J.E., ELWYN, A.J., ANL 6172 (1960).

ANALYSIS OF THE TOTAL CROSS-SECTION OF CARBON FROM 70 eV TO 1.5 MeV

C.A. UTTLEY, K.M. DIMENT
UKAEA, AERE, Harwell, Didcot,
United Kingdom

Presented by M.G. Sowerby

Abstract

ANALYSIS OF THE TOTAL CROSS-SECTION OF CARBON FROM 70 eV TO 1.5 MeV.

The total cross-section of reactor grade graphite was measured from 0.07 keV to several MeV using the 120 m and 300 m flight paths on the Harwell 45 MeV Electron Linac. The data up to 1500 keV are well fitted with the following polynomial in energy (E in MeV):

$$\sigma_{nT} = 4.744 - 3.707E + 2.389E^2 - 1.11E^3 + 0.242E^4 \quad (1)$$

The effective range expansion can be applied to the carbon cross-section by expressing σ_{nT} (E) in terms of k cot δ_0, where k (= $k_0\sqrt{E}$) is the (c.m.) wave number and δ_0 is the s-wave phase shift. From effective range theory

$$k \cot \delta_0 = -1/a + r_0 k^2/2 - P_0 r_0^3 k^4 \quad (2)$$

where a is the scattering length, r_0 is the effective range of the nuclear potential and P_0 is a potential shape factor. Application of Eq.(2) enables the s-wave scattering cross-section to be expressed as a polynomial in energy and by equating the coefficients of E^0 and E^1 with those in Equation (1) the scattering length and the effective range are found to be 6.14 fm and 3.06 fm, respectively.

The coefficient of E^2 is determined by the value and sign of the shape factor P in addition to a and r_0 and furthermore p-wave scattering contributes a term αE^2. Assuming p-wave scattering to be negligible a value of P = -0.071 is obtained which is rather larger than the value (-0.033) expected for a sharply cut-off square well. If, however, P = 0 and p-wave scattering is interpreted as hard sphere scattering with radius R viz. $12\pi k^{-2} \sin^2 \delta_1$ with $\delta_2 = -k^3R^3/3$ a value of R = 3.76 fm is obtained corresponding to a p-wave cross-section of 0.2 barns at 1 MeV. Since P can be slightly positive for a well with a tail it is concluded that a significant p-wave interaction is present in the cross-section.

A least-squares fit to the total cross-section has been obtained after subtracting the above p-wave contribution, in terms of an s-wave potential scattering and the parameters of the $1/2^+$ state at -1.86 MeV (c.m.) in ^{13}C which yields a radius of 4.84 fm and a reduced neutron width of 0.51 MeV (c.m.).

1. INTRODUCTION

The measurement of the total cross-section of reactor grade graphite analysed in this paper was made by the transmission method using the 300 metre flight path of the Harwell 45 MeV electron linear accelerator which also includes a detector station at 120 metres. The purpose of the measurement was to determine the carbon cross-section, which is essentially all elastic scattering, with sufficient accuracy to enable it to be used as a standard particularly below about 0.2 MeV. In view of the relatively large amount of existing data below about 1 keV and the increasing volume of data above about 0.8 MeV, this measurement from 70 eV to ~7 MeV enables a comparison to be made with existing data at the extreme ends of the energy region of interest. The present data on the carbon cross-section below about 0.1 MeV have been used by Asami and Moxon as a standard relative to which they measured the elastic scattering cross-sections of ^{10}B [1] and ^{6}Li [2].

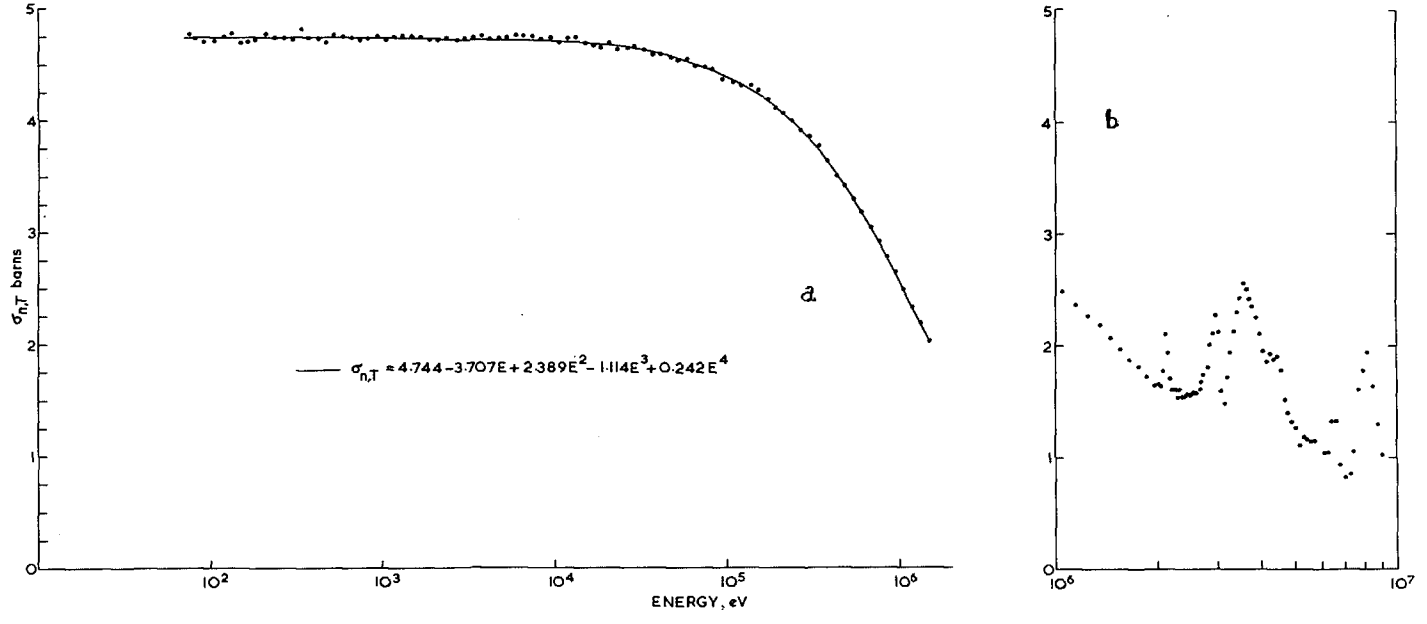

FIG. 1. The total cross-section of carbon. The solid line is a fit to the data below 1.5 MeV of a polynomial in energy. Fig 1b is the data above 1 MeV.

In these measurements no correction has been made for the 1.1% ^{13}C content. Existing data on this isotope [3] show that the cross-section is very close to that of natural carbon below 1.5 MeV apart from the resonance near .15 MeV.

2. EXPERIMENTAL DETAILS

The neutron detector at 300 metres is a 12 cm diameter cylinder of ^{10}B metal powder mixed with vaseline clad in a thin aluminium can and viewed with four NaI(Tl) crystals. The mixture of ^{10}B with a hydrogenous compound improves the efficiency of the detector for MeV neutrons. In principle a time jitter is introduced by the detector moderation, but this is negligible compared with the duration of the neutron burst from the Booster or with the 125 ns wide time channels.

A thin plug of ^{10}B metal powder is placed in the beam at 120 metres; it is of sufficient thickness to prevent overlap neutrons from reaching the 300 metre detector. This plug is also viewed by four NaI(Tl) crystals and acts as a further detector enabling the measurements to be extended to lower neutron energies with a better ratio of spectrum to background counts. The carbon sample is mounted on a sample changer and placed in the neutron beam in front of the 120 metre detector. Pulses from both detectors are fed into the same 8 MHz, 1" magnetic tape recorder which uses 13 bits to record time-of-flight and 2 bits to code the detector station and the position of the sample relative to the neutron beam.

Background filters of sulphur, aluminium, manganese and cobalt are used for the measurements; sets of runs were made using different combinations of background filters permanently in the neutron beam. In these measurements two samples of carbon were used with thicknesses of 0.0842 and 0.2997 atoms/barn. With the arrangement described above there is an overlap in energy between the two detectors from about 10 keV to 100 keV in which data averaged over the same energy intervals are of comparable statistical accuracy.

3. ANALYSIS OF DATA

Below 2 MeV there is no observable resonance structure in carbon apart from the small contribution from the 0.15 MeV resonance in ^{13}C. Below 1.5 MeV the smooth variation in the cross-section with neutron energy can conveniently be expressed by a polynomial in energy which is fitted to the experimental data by minimising X^2. A fit to the present data is shown in Fig. 1 and is given by

$$\sigma_{nT} = 4.744 - 3.707E + 2.389E^2 - 1.114E^3 + 0.242E^4 \qquad (1)$$

where E is neutron energy in MeV.

An expression of the form of equation (1) is expected adequately to represent the carbon cross-section up to about 1.5 MeV. Differential elastic scattering data [4] show that the p- and d-wave phase shifts are small below 1.5 MeV and that consequently almost all the cross-section is due to s-wave scattering. Hence one expects s-wave effective range theory, developed by Bethe [5] and others, to describe the cross-section in terms of at most three parameters. The shape-dependent effective range approximation expresses the energy dependence of the s-wave phase shift δ_o as follows

$$k \cot \delta_o = -\frac{1}{a} + \frac{1}{2} r_o k^2 - P r_o^3 k^4 \qquad (2)$$

where k is the neutron wave number, a is the scattering length, r_o is the effective range and P is a factor which represents the effect on the scattering of the radial dependence of the potential surface and is expected to be small. If expression (2) is substituted into the s-wave scattering cross-section $\sigma = 4\pi/k^2 \sin^2\delta_o$ then σ can be expressed as a polynomial in energy similar to equation (1) in which, in particular, the coefficients of E^o and E are $+ 4\pi a^2$ and $- 4\pi a^2 k_o^2(a^2 - ar_o)$ respectively where k_o is the neutron wave number at 1 MeV. If the p- and d-wave phase shifts are small and the p-wave resonances relatively distant from the energy region of interest, their respective scattering cross-sections will vary with energy as E^2 and E^4 and thus not contribute to the coefficients of E^o and E and we can equate the effective range coefficients with those in equation (1). Thus a = 6.14 fm and r_o = 3.05 fm.

The large value of the scattering length a relative to the expected hard sphere scattering radius for carbon can only be obtained if the s-wave scattering cross-section is determined by a bound $^1/_{2^+}$ state. Such a state is known at -1.86 MeV (C. of M.) and thus the formal R-matrix expression for the s-wave phase shift can be written

$$\delta_o = \tan^{-1}\left(\frac{\gamma_n^2\, kR}{E_\lambda - E}\right) - kR \qquad (3)$$

where γ_n^2 is the reduced neutron width of the $^1/_{2^+}$ state at energy E_λ relative to neutron binding and R is the hard sphere scattering radius. $k\cot\delta_o$ can be expanded from Equation (3) as a series in even powers of k to yield an expression equivalent to Equation (2). Equating coefficients of k^o and k^2 we obtain

$$a = R(1 - \gamma_n^2/E_\lambda)$$

$$r_o = 2[R^3/3a^2 - R^2/a + R(1 - \hbar^2/2\,\mu a^2 E_\lambda) + \hbar^2/2\,\mu E_\lambda a]$$

where μ is the reduced mass of the neutron-^{12}C system and these equations can be solved to give R = 4.625 fm and γ_n^2 = 0.611 MeV (θ^2= 0.192) using the effective range values of a and r_o determined above and E_λ = -1.86 MeV (C. of M.).

The s-wave cross-section resulting from these parameters gives a very good fit to the total cross-section up to near 1 MeV, as is seen in Fig. 2, but the experimental cross-section diverges increasingly towards 1.5 MeV. A small p-wave scattering cross-section can readily account for the remaining cross-section. If we assume this to be p-wave potential scattering

$$\sigma_{l=1} = \frac{12\pi}{k^2} \sin^2\delta_1$$

$$\text{with} \quad \delta_1 = (\rho - \pi/2) + \cot^{-1}\rho$$

where $\rho(= kr = \rho_o\sqrt{E})$ is the product of the neutron wave number and a scattering radius, the p-wave scattering depends only on one parameter r. Subtracting the p-wave scattering from the experimental data for various trial values of r and fitting the remainder in terms of an s-wave scattering radius and a reduced neutron width for the bound state shows that X^2 rapidly diverges from a minimum value as the p-wave scattering radius increases. Thus the data can be fitted in terms of three parameters, the s- and p-wave scattering radii and the reduced neutron width of the bound state. The values found for these quantities are 4.56 fm, 3.07 fm and 0.645 MeV respectively and result in the fit shown in Fig. 3.

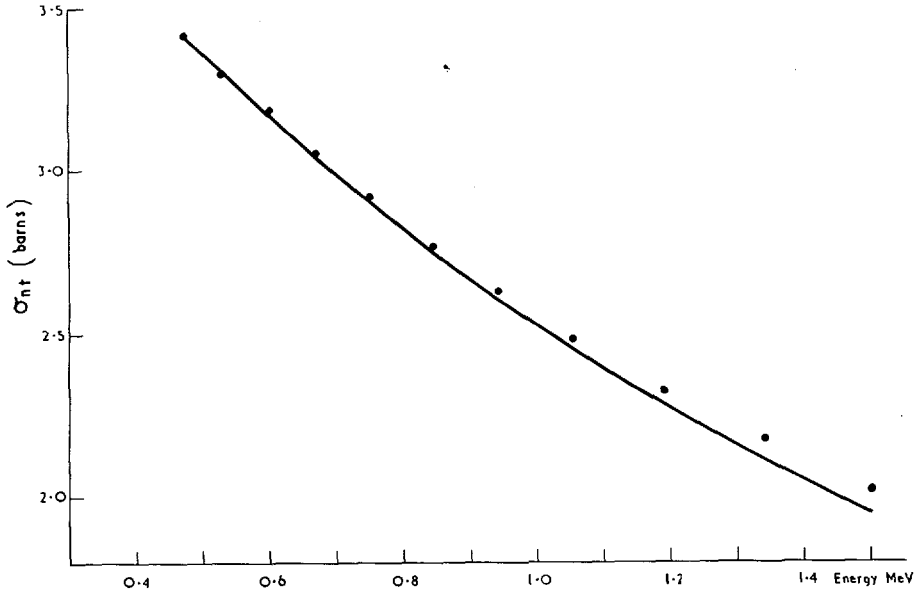

FIG. 2. Calculation of the s-wave interaction, using the s-wave parameters determined from effective-range theory, and comparison with the experimental data from ~ 0.5 to 1.5 MeV.

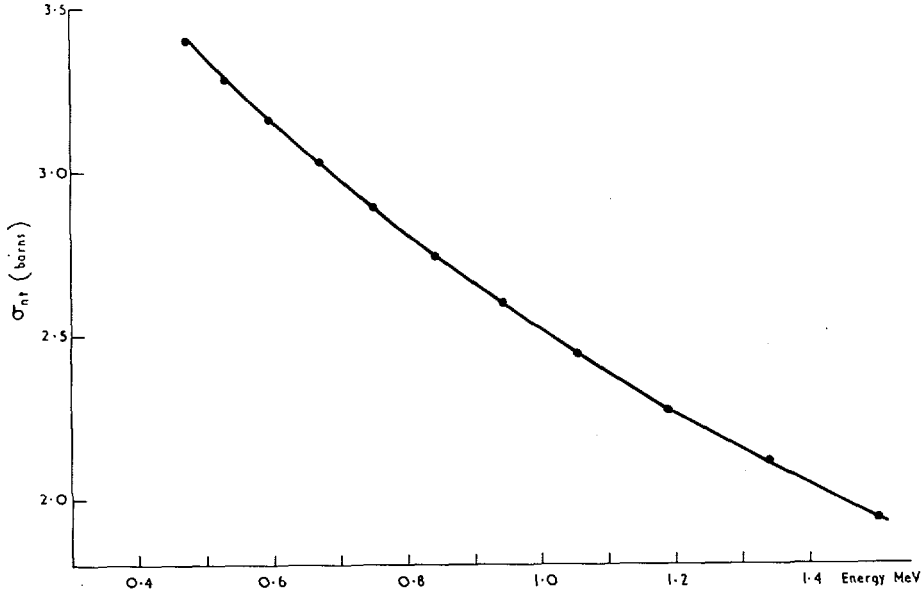

FIG. 3. s-wave fit to the carbon total cross-section after subtracting p-wave hard-sphere scattering with a radius of 3.07 fm.

The value of the p-wave scattering radius of 3.07 fm corresponds to a phase shift of 3.8° at 1 MeV which is consistent with the differential scattering data of Wells et al. [6]. These authors also deduce a $\delta_2(3/2)$ phase shift of +3° at 1.45 MeV and if this is taken into account in the present data the s- and p-wave parameters are changed slightly to 4.58 fm, 2.97 fm and 0.638 MeV. The value of the p-wave phase shift at 1.45 MeV will thus be 5.61° giving a p-wave scattering cross-section rather larger than the phase shifts of Wells but smaller than those of Ahmed et al. [7].

It is seen that the s-wave parameters of 4.58 fm and 0.638 MeV for the scattering radius and reduced neutron width of the bound $^1/2^+$ state are close to those determined from the effective range parameters even though the former are more concerned with the fit to the data at high energies in contrast to the values obtained from effective range parameters.

An extension of the effective range analysis taking into account the cross-section due to the higher partial waves shows that the value of the shape factor P is slightly negative indicating that scattering from carbon behaves like scattering from a sharply cut-off potential well.

REFERENCES

[1] ASAMI, A. and Moxon, M. C., UKAEA Report AERE - R 5980 (1969).
[2] ASAMI, A. and Moxon, M. C., contribution to this Conference.
[3] BNL 325, 2nd Edition, Supplement No. 2.
[4] LANE, R. O., Langsdorf, A. S. Jnr., Monahan, J. E. and Elwyn, A. J., ANL-6172 (1960).
[5] BETHE, H. A., Phys. Rev. 76, 38 (1949).
[6] WELLS, J. E., Jnr., Bair, J. K., Cohn, H. D. and Willard, H. B., Phys. Rev. 109, 891 (1958).
[7] AHMED, N., Coppola, M. and Knitter, H. H., contribution to this Conference.

RE-EVALUATION OF GOLD SHELL TRANSMISSION DATA AT 24-keV NEUTRON ENERGY

F.H. FRÖHNER
Institut für Angewandte Kernphysik,
Kernforschungszentrum Karlsruhe,
Federal Republic of Germany

Abstract

RE-EVALUATION OF GOLD SHELL TRANSMISSION DATA AT 24-keV NEUTRON ENERGY.

Quite different values of the 24-keV neutron-capture cross-section have been extracted by various authors from the shell transmission data reported by Schmitt and Cook. The differences are due to the different treatment of the rather important self-shielding and multiple-scattering corrections. A new attempt to calculate them was based on the best available total cross-section data and level statistics. Monte-Carlo methods were used to generate resonance cross-sections. The result is σ_γ (24 keV) = (650 ± 35) keV. Implications for the present gold-standard situation are discussed.

1. INTRODUCTION

Gold is a convenient reference nuclide in fast-neutron capture work. Consequently, the shape of the capture cross-section of gold in the keV region was repeatedly measured (see, e.g. Refs [1-4]). One of the possible methods to obtain an absolute value is the shell transmission method [5] used by Schmitt and Cook [6, 7] and Belanova [8] to find the absolute capture cross-section of gold at 24 keV with neutrons from an Sb-Be source. The published shell transmissions are quite accurate. However, the extraction of absolute cross-sections is seriously complicated by multiple scattering and by the (non-observed) resonance structure of the cross-section (self-shielding). The only practical way to account for these effects is the use of Monte-Carlo methods in conjunction with level statistics to generate representative resonance cross-sections [9].

The first Monte-Carlo interpretation of the data of Schmitt and Cook [6, 7] was based on relatively sparse resonance information. The two relevant s-wave strength functions S_{01} and S_{02} (for compound spins 1 and 2, respectively) were taken as equal. However, subsequent extensive resonance parameter determinations from transmission data between 0 and 1 keV yielded vastly differing values: $S_{01} = (1.17 \pm 0.3) \times 10^{-4}$, $S_{02} = (2.46 \pm 0.53) \times 10^{-4}$ [11]. Re-evaluation of the data seemed to be necessary. Two significantly differing average capture cross-sections for 24-keV neutrons were reported: $\langle\sigma_\gamma\rangle$ = (645 ± 35) mb [12] and $\langle\sigma_\gamma\rangle$ = (725 ± 25) mb [13]. A somewhat crude histogram representation of the Wigner and Porter-Thomas distributions in Ref. [13] may have introduced some error here. In the meantime, the resonance analysis has been extended to 2 keV, and the s-wave strength functions calculated for the whole range 0 - 2 keV are not significantly different [14]. Hence, it seems that the difference between S_{01} and S_{02} in the range 0 - 1 keV [11] is fortuitous, resulting from too small resonance samples. In the

present paper, we present a re-evaluation of the data of Schmitt and Cook [6, 7] with level-statistical parameters derived from the improved resonance data of Ref. [14].

2. CALCULATION

The theoretical background of the calculations was reported previously [12]. In the present work, we assumed spin-independent strength functions. The calculations were performed in three steps.

First, the resonance data of Ref. [14] were used in a least-squares analysis similar to that described in Ref. [15]. The following level-statistical parameters were obtained:

$S_0 = \left(2.05 \pm \begin{matrix} 0.24 \\ 0.21 \end{matrix}\right) \times 10^{-4}$ (s-wave strength function),

$D_0 = (18 \pm 1)$ eV (average s-wave level spacing),

$\Gamma_{\gamma 0} = (128 \pm 6)$ meV (average s-wave radiation width).

Then values of the p-wave strength function S_1 were calculated from the expressions (see Ref. [12]):

$$\langle\sigma\rangle = 2\pi^2\lambda^2 \sum_{\ell=0}^{1} (2\ell + 1)\, S_\ell\, (E/1\text{ eV})^{\frac{1}{2}}\, V_\ell \cos 2\xi_\ell + \sigma_p$$

with

$$\sigma_p = 4\pi\lambda^2 \sum_{\ell=0}^{1} (2\ell + 1) \sin^2 \xi_\ell$$

$$\xi_0 = -kR', \quad \xi_1 \approx \xi_0 - \arctan \xi_0$$

$$V_0 = 1 \quad , \quad V_1 = \xi_0^2\, (1 + \xi_0^2)^{-1}$$

S_0 values between 1.8 and 2.3×10^{-4} were chosen. The effective radius R' was chosen so as to reproduce the σ_p-values 9.5 b and 10 b given in Refs [11, 14], and $\langle\sigma\rangle$ values between 13.5 and 13.9 were used in accordance with the values published in the literature [6, 7, 13] and with our own measurements reported in these Proceedings [16]. In this way, self-consistent sets of the quantities $\langle\sigma\rangle$, S_0, S_1, R' were found. Eventually, these sets together with $\Gamma_{\gamma 0} = 128$ meV were used in Monte-Carlo calculations with the code SESH. The only remaining free parameter, the p-wave radiation width $\Gamma_{\gamma 1}$, was adjusted in such a way as to reproduce the measured shell transmission as well as possible. The best fit resulted from the following values:

$$\langle\sigma\rangle = 13.7 \text{ b}, \quad S_0 = 1.8 \times 10^{-4}, \quad D_0 = 18 \text{ eV}, \quad \Gamma_{\gamma 0} = 128 \text{ meV},$$

$$\sigma_p = 9.5 \text{ b}, \quad S_1 = 0.7 \times 10^{-4}, \quad D_1 = 9 \text{ eV}, \quad \Gamma_{\gamma 1} = 100 \text{ meV}.$$

The resulting sphere transmissions were

$T_s = 0.80 \pm 0.01$ for a shell thickness corresponding to 0.149 nuclei/b,

$T_s = 0.88 \pm 0.01$ for a shell thickness corresponding to 0.099 nuclei/b,

in agreement with the measured values 0.800 ± 0.004 and 0.876 ± 0.005 given in Refs [6, 7]. The average capture cross-section found with these input numbers is $\langle\sigma_\gamma\rangle = (660 \pm 20)$ mb. The uncertainties given here for $\langle\sigma_\gamma\rangle$ and T_s are due to the limited number of Monte-Carlo histories. Similar calculations with slightly different input numbers yield as final result

$$\langle\sigma_\gamma\rangle = (650 \pm 35) \text{ mb}$$

where the uncertainty reflects also the uncertainty of the input numbers, $\langle\sigma\rangle$, σ_p, S_0, D_0, $\Gamma_{\gamma 0}$. This result is not much different from that found for $S_{01} \neq S_{02}$ [12], (645 ± 25) mb.

3. CONCLUSION

Level statistics with spin-independent strength functions derived from the new Saclay resonance parameters [14] were used to reanalyse the shell transmission data of Schmitt and Cook [6, 7]. The result, $\langle\sigma_\gamma\rangle = (650 \pm 35)$ mb at 24 keV, is not much different from the numbers of Refs [12] which were obtained with spin-dependent strength functions derived from older Saclay data [11]. It also agrees with Semler's result for spin-independent strength functions [13]. Discrepancies exist with Semler's value (725 ± 25) mb for spin-dependent strength functions, which, however, can no longer be considered correct in view of the new Saclay results. Furthermore, our result does not agree with the high gold capture cross-section reported in Ref.[4]. These cross-sections, however, were revised recently and are now in agreement with our result [18]. Thus, the standard capture cross-section of gold used in our capture work, with a normalization value of 596 mb at 30 keV [2, 3], which was somewhat in doubt after publication of the high values of Refs [13] and [4], is reasonably confirmed by this re-evaluation.

REFERENCES

[1] HARRIS, K.K. et al., Nucl. Phys. 69 (1965) 37.
[2] PÖNITZ, W.P., MENLOVE, H.O., KOMPE, D., J. nucl. Energy 22 (1968) 505.
[3] KOMPE, D., Nucl. Phys. A133 (1969) 513.
[4] FRICKE, M.P., LOPEZ, W.M., Physics Lett. 29B (1969) 393.
[5] BETHE, H., BEYSTER, J.R., CARTER, R.E., J. nucl. Energy 3 (1956) 207.
[6] SCHMITT, H.W., COOK, C.W., Nucl. Phys. 20 (1960) 202.
[7] SCHMITT, H.W., UK Report EANDC-33U (1963) 41.
[8] BELANOVA, T.S. et al., J. nucl. Energy 20 (1966) 411.

[9] BOGART, D., USAEC Report Conf-660303, in Neutron Cross Section Technology (Proc. Conf. Washington, 1966) 1 486.
[10] BOGART, D., SEMLER, T.T., USAEC Report Conf-660303, in Neutron Cross Section Technology (Proc. Conf. Washington, 1966) 1 502.
[11] JULIEN, J. et al., Nucl. Phys. 76 (1966) 391.
[12] FRÖHNER, R.H., Report GA-8072 (1967).
[13] SEMLER, T.T., Trans. Am. nucl. Soc. 11 (1968) 162.
[14] ALVES, R.N. et al., Nucl. Phys. A131 (1969) 450.
[15] SLAVINSKAS, D.D., KENNETT, T.J., Nucl. Phys. 85 (1966) 641.
[16] SCHNEIDER, E., FRÖHNER, F.H., contribution CN-26/10 to these Proceedings.
[17] FRÖHNER, F.H., report GA-8380 (1968).
[18] PÖNITZ, W.P., private communication.

THE TEMPERATURE DEPENDENCE OF THE AVERAGE TRANSMISSION OF GOLD

E. SCHNEIDER, F.H. FRÖHNER
Institut für Angewandte Kernphysik,
Kernforschungszentrum Karlsruhe,
Federal Republic of Germany

Abstract

THE TEMPERATURE DEPENDENCE OF THE AVERAGE TRANSMISSION OF GOLD.

The average neutron transmission of gold was measured with fairly thick samples between 10 and 60 keV at 11°C and at 800°C. The observed temperature effect is caused by thermal expansion of the sample (which enhances the transmission) and by Doppler broadening of resonances (which tends to lower it on the average). The experimental data were used to check the adequacy of various methods for the calculation of resonance cross-sections from level statistics. In particular, one- and multi-level R-matrix representations were tested. The results are discussed.

1. INTRODUCTION

The temperature dependence of the average transmission of materials with unresolved resonance cross-sections is important for calculations of the Doppler coefficient of fast reactors. Measurements on fairly thick samples of natural tungsten at room temperature and at 755°K revealed an appreciable temperature effect on the average transmission between 5 and 100 keV [1]. An attempt was made to explain this effect as caused by (a) thermal expansion of the sample, and (b) Doppler broadening of unresolved resonances. Monte-Carlo methods based on level statistics were used to generate the resonance structure of the cross-sections by sampling from the appropriate width (Porter-Thomas) and level-spacing (Wigner) distributions. It was found that in order to reproduce the experimental data rather large strength functions and very small effective nuclear radii were required. A more detailed interpretation [1], however, suffered from the fact that tungsten is a mixture of essentially four isotopes. Furthermore, level-level interference effects could not be taken into account. It seemed desirable to make a similar study on a monotope.

In the present work, gold was used. There is only one isotope and its level statistics (strength functions, average level spacings, average level widths) are well known from analyses of resonances in the low-energy region up to 2100 eV [2, 3]. Level-level interference effects were studied by calculating the cross-sections with a multi-level formula. As the resonance structure of gold is similar to that of tungsten the results should be comparable.

2. MEASUREMENTS

The average transmission of a thick gold sample was measured between 10 and 60 keV with time-of-flight techniques. A pulsed 3-MV Van-de-Graaff accelerator was used to produce 10-ns bursts of neutrons via the ^{7}Li(p, n)

reaction. The energy resolution was ~3 keV at 30 keV, hence all data represent statistically meaningful averages over compound resonances (mean s-wave level spacing: 16.8 eV). The sample thickness, n_0 = 0.0808 nuclei/barn, corresponded to roughly one mean free path at 30 keV. Data were taken with the sample at room temperature (284°K) and at 1073°K. The measured transmission values, each an average of three experimental runs, are shown in Fig. 1 together with the corresponding values calculated with the multi-level formula (smooth curves). The temperature effect (relative change of average transmission by heating the sample from 284°K to 1073°K) is shown in Table I, the calculated one is given in Table II both for single-level and multi-level formulae. The measurement shows large fluctuations in contrast to the calculated values. There is evidence for intermediate structure (resulting from statistical fluctuations in level density and width) in the cross-section of gold, as was already pointed out by Seth in an earlier publication [4]. A comparison with high-resolution capture data [5,6] reveals that the peaks in the average total cross-section at 18, 24, 29 and 42 keV correspond to peaks in the capture cross-section (Fig. 2). This structure is important for the interpretation of shell transmission data at 24 keV which provide absolute capture cross-section values (see contribution CN-26/26 to these Proceedings).

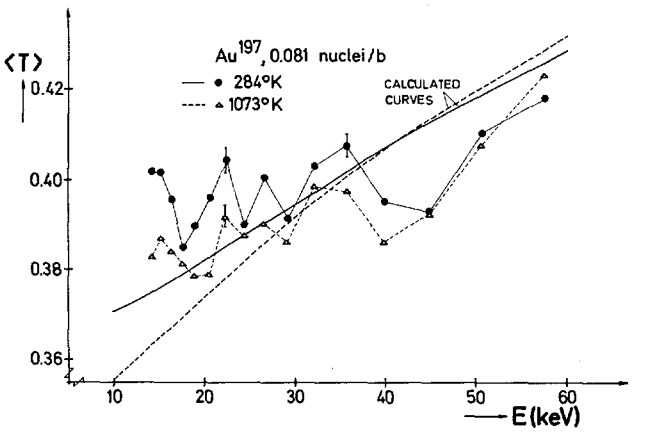

FIG. 1. Average transmission of gold versus energy at room temperature and at 1073°K.

3. CALCULATIONS

Two effects influence the transmission of a heated sample:

3.1. Thermal expansion

The thermal expansion of the sample was treated with the expression

$$n_t = \frac{n_0}{(1 + \alpha t)^2}$$

TABLE I. EXPERIMENTAL TRANSMISSION AND RELATIVE CHANGE

Energy (keV)	<T> 11°C	<T> 800°C	$\frac{\Delta<T>}{<T>}$ (%)	σ_{tot} (b)
14.24	0.4019	0.3828	4.75	14.26 ± 0.23
15.24	0.4016	0.3871	3.61	14.09 ± 0.19
16.36	0.3957	0.3843	2.88	14.10 ± 0.17
17.60	0.3848	0.3814	0.88	14.27 ± 0.15
18.99	0.3898	0.3785	2.89	13.94 ± 0.14
20.55	0.3962	0.3790	4.34	13.57 ± 0.12
22.31	0.4044	0.3919	3.09	13.16 ± 0.11
24.31	0.3901	0.3878	0.58	13.45 ± 0.10
26.59	0.4007	0.3904	2.57	12.96 ± 0.08
29.20	0.3914	0.3861	1.35	13.11 ± 0.08
32.22	0.4032	0.3986	1.14	12.60 ± 0.08
35.73	0.4074	0.3974	2.45	12.33 ± 0.08
39.85	0.3953	0.3863	2.27	12.58 ± 0.07
44.73	0.3929	0.3928	0.02	12.53 ± 0.07
50.56	0.4105	0.4074	0.75	11.87 ± 0.06
57.61	0.4182	0.4232	-1.19	11.53 ± 0.12

where n_t and n_0 are the sample "thicknesses" (nuclei/barn) at centigrade temperatures t and 0, respectively; the expansion coefficient in the temperature range about 800°C was taken as $\alpha = 18.56 \times 10^{-6}/°C$ [8]. The sample expansion tends to increase the transmission.

3.2. Doppler broadening of resonances

The measured transmission data are energy averages over many resonances,

$$\langle T \rangle = \langle e^{-n_t \sigma_t} \rangle$$

where σ_t is the Doppler-broadened total cross-section for centigrade temperature t; the brackets denote energy averages or, more precisely,

TABLE II. CALCULATED TRANSMISSION AND TEMPERATURE EFFECT

Energy (keV)	One level			Multi-level		
	$\langle T \rangle$ 11°C	$\langle T \rangle$ 800°C	$\frac{\Delta \langle T \rangle}{\langle T \rangle}$ (%)	$\langle T \rangle$ 11°C	$\langle T \rangle$ 800°C	$\frac{\Delta \langle T \rangle}{\langle T \rangle}$ (%)
10	0.3649	0.3497	4.16	0.3708	0.3557	4.07
15	0.3703	0.3599	2.80	0.3760	0.3649	2.95
20	0.3768	0.3701	1.77	0.3817	0.3736	2.12
24	0.3822	0.3778	1.15	0.3873	0.3815	1.49
30	0.3902	0.3886	0.41	0.3945	0.3920	0.63
40	0.4028	0.4044	-0.39	0.4075	0.4071	0.09
50	0.4144	0.4182	-0.91	0.4180	0.4205	-0.59
60	0.4250	0.4302	-1.22	0.4285	0.4322	-0.86

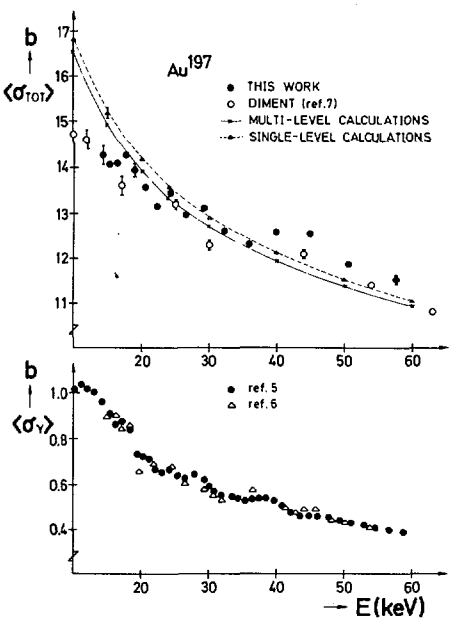

FIG. 2. Average total cross-section and average capture cross-section of gold versus energy.

TABLE III. INPUT VALUES FOR CALCULATIONS

A	$S_0 \times 10^4$	$S_1 \times 10^4$	D_0 (eV)	D_1 (eV)	Γ_γ (eV)	R' (Fm)
197	1.98	0.3	16.8	8.4	0.13	8.69

convolutions with the resolution function. For the calculation of $\langle T \rangle$ a modification of the SESH code [9] was used. This code yields energy averages of $\exp(-n_t\sigma_t)$ over many Doppler-broadened resonances from level statistics. The input parameters S_0, D_0 and Γ_γ (S-wave strength-function, mean level spacing and radiation width) were obtained from the Saclay data [2,3] and are summarized in Table III. The usual Fermi gas expression was used for the spin and energy dependence of the level spacings. To study level-level interference effects, the computations were performed with single-level and multi-level expressions for the total cross-section. In the first case, the cross-section was calculated as a sum of single-level Breit-Wigner terms. Doppler broadening can then be described analytically by the shape functions ψ and φ (also known as Voigt profiles). For the multi-level treatment it was calculated as convolution of the cross-section with the usual Gaussian [10]. An effective temperature as defined by Lamb [11] was used to account for the binding of the nuclei in the crystal lattice.

Doppler broadening lowers the average transmission, whereas the sample expansion increases it. Hence, one has two counteracting effects with heated samples.

Results of the multi-level calculations are shown in Figs 1 (smooth curves) and 2.

4. CONCLUSION

The average transmission of gold was measured in the keV-region at room temperature and at 800°C with a sample thickness of roughly one mean free path. The objective was to study the temperature effect caused by the unresolved resonance structure of the gold cross-section. The main conclusions from the present work are:

(1) The total cross-section of gold in the keV region (Fig. 1) shows intermediate structure closely corresponding to that observed in the neutron-capture cross-section [5, 6, 14].

(2) Two counteracting effects determine the temperature dependence of the average transmission $\langle T \rangle$: Doppler broadening of unobserved resonances tends to lower $\langle T \rangle$, thermal expansion of the sample tends to increase it with increasing temperature. Below ~ 50 keV Doppler broadening dominates for gold, at higher energies thermal expansion becomes dominant (Fig. 1).

(3) For a sufficiently high energy, i.e. when the resonance structure is practically completely smeared out by Doppler broadening, sample expansion dominates even below 50 keV. For example, around 24 keV Doppler broadening dominates below 400°C, sample expansion above 700°, Between 400 and 700°C the two effects balance each other (Fig. 3). Table IV shows the variation of transmission with temperature at 24 keV.

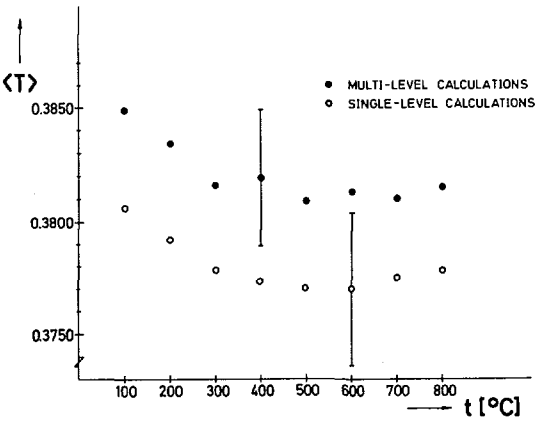

FIG. 3. Calculated average transmission at 24 keV versus temperature.

(4) Computer calculations using level statistics and Monte-Carlo methods appear to describe the temperature dependence of $\langle T \rangle$ adequately. The influence of level-level interference (multi-level effects) on the temperature effect is negligible, as verified by calculations with summed-single-level and multi-level cross-section expressions.

(5) The fluctuations of the average cross-section is correlated to fluctuations of the temperature effect. The temperature effect is found to be

TABLE IV. VARIATION OF TRANSMISSION WITH TEMPERATURE AT 24 keV

t (°C)	$n_t \times 10^2$ (nucl/barn)	$\langle T \rangle \pm \Delta\langle T \rangle$ Multi-level	$\langle T \rangle \pm \Delta\langle T \rangle$ Single-level
100	8.06	0.3849 ± 0.0029	0.3806 ± 0.0039
200	8.03	0.3834 ± 0.0029	0.3792 ± 0.0038
300	8.01	0.3816 ± 0.0030	0.3778 ± 0.0037
400	7.98	0.3819 ± 0.0030	0.3773 ± 0.0036
500	7.95	0.3809 ± 0.0031	0.3770 ± 0.0035
600	7.92	0.3813 ± 0.0032	0.3770 ± 0.0034
700	7.88	0.3810 ± 0.0032	0.3775 ± 0.0033
800	7.85	0.3815 ± 0.0033	0.3778 ± 0.0032

large whenever the average transmission is large and vice versa (Fig. 1). This behaviour indicates that the resonance structure is more pronounced (resonances are stronger and/or more widely spaced) in the intermediate-structure minima of the average cross-section. More detailed insights require additional information. Recently, attempts have been made to simulate such intermediate structures for fissile isotopes in the unresolved-resonance region [12-13]. Large numbers of resonance "ladders" were generated by sampling from the appropriate width and spacing distributions. Then the ladders which best describe measured average quantities were selected for further predictions. It would be interesting to know whether these ladders would also lead to the observed correlation between temperature effect and average transmission fluctuations.

REFERENCES

[1] FRÖHNER, F.H., RUSSEL, J.L., Jr., YOUNG, J.C., in Neutron Cross Sections and Technology (Proc. Conf. Washington, D.C., 1968) 1, NBS, Washington (1968) 61.
[2] JULIEN, J., et al., Nucl. Phys. 76 (1966) 391.
[3] JULIEN, J., et al., Nucl. Phys. A131 (1969) 450.
[4] SETH, K.K., Phys. Lett. 16 (1965) 306.
[5] KOMPE, D., Nucl. Phys. A133 (1969) 513.
[6] FRICKE, M.P., LOPEZ, W.M., Phys. Lett. 29B (1969) 393.
[7] DIMENT, K.M., UTTLEY, C.A., Report AERE-PR/NP 12 (1968).
[8] GMELINS Handbuch, Gold GL (1954) 479.
[9] FRÖHNER, F.H., Report GA-8380 (1968).
[10] FRÖHNER, F.H., Nucl. Instrum. Meth. 49 (1967) 89.
[11] LAMB, W.E., Phys. Rev. 55 (1939) 190.
[12] OHNSIHI, T., NEDA, Y., Nucl. Sci. Technol. 6 (1969) 715.
[13] ISHIGURO, Y. et al., Nucl. Sci. Engng 40 (1970) 25.
[14] PÖNITZ, W.P., KOMPE, D., MENLOVE, H.O., J. nucl. Energy 22 (1968) 505.

DISCUSSION

TO PAPERS IAEA-CN-26/8, 10

W. P. POENITZ: The result you obtained in the spherical shell transmission experiment strongly supports the results of the activation experiment conducted by Ryves et al. and also of our measurements at 30 keV. However, the question still arises whether the quoted accuracy is not too optimistic. This is suggested by the very existence of several different values resulting from different interpretations of the same experimental value by Schmitt and Cook (see Fig. A). A much more serious matter is the presence of the fluctuations in the capture cross-section for gold in this energy region, as shown in your paper CN-26/10. These fluctuations indicate that in local regions sets of parameters (Γ_n, $\langle D \rangle$, etc.) fairly different from those used for the low-keV-energy range may be valid.

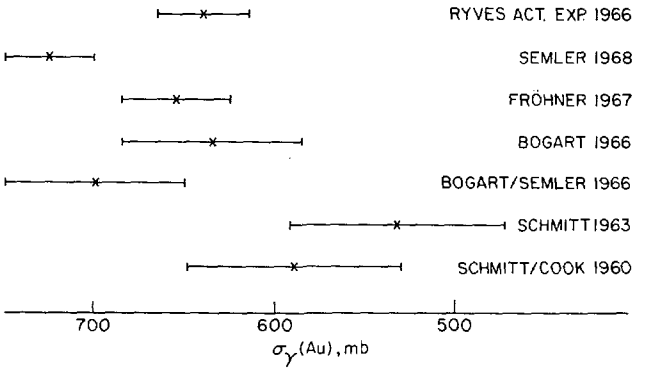

Fig. A. Results from different interpretations of spherical-shell transmission experiments (Experimental results from Schmitt and Cook).

F. H. FRÖHNER: We did not treat the structure seen in the cross-sections explicity. However, we varied the statistical input parameters within the rather wide confidence limits shown in the paper, using for example strength functions between 1.8 and 2.3×10^{-4} for the s-wave. We obtained a large number of input sets compatible with the measured total cross-sections, and from the quality of the fits achieved with these individual sets we estimated the error bars quoted. Fortunately, the spread in neutron energies from the Sb-Be source tends to reduce fluctuation effects. To ensure that such effects are not too extensive, one could utilize a procedure similar to that of Ohnishi et al. and Ishiguro et al. (Refs [12, 13], paper CN-26/10). These authors constructed resonance ladders by sampling from the Porter-Thomas and Wigner distributions and rejected all ladders that did not reproduce the investigated structures. With the remaining ladders we were able, in our case, to evaluate the effect of fluctuations. I agree that your point is a valid one.

A. ATEN: Mr. H. Pauw, one of my collaborators at Amsterdam, in a study of neutron spectra for his doctor's thesis, has measured the capture cross-section of gold at 22 keV by an absolute method. His result (655 ± 40 mb) is almost exactly the same as the value given in the paper under discussion.

A NEUTRON DETECTOR WITH A FLAT ENERGY RESPONSE FOR USE IN TIME-OF-FLIGHT EXPERIMENTS

M. S. COATES, G.J. HUNT, E.R. RAE
UKAEA, AERE, Harwell, Didcot, Berks,
United Kingdom

Abstract

A NEUTRON DETECTOR WITH A FLAT ENERGY RESPONSE FOR USE IN TIME-OF-FLIGHT EXPERIMENTS.

Monte-Carlo calculations have been carried out to assess the feasibility of making a neutron detector suitable for time-of-flight work whose efficiency can be accurately predicted (~±2%) ideally over the energy region 100 eV → several MeV. Accurate flux measurements are needed in this region to determine partial neutron cross-sections for use in fast-reactor design. The detector was taken to be a spherical homogeneous mixture of ^{10}B and vaseline with a radial re-entrant hole to allow a parallel neutron beam to fall near the sphere centre. Neutrons are moderated and captured in the ^{10}B to produce 478-keV γ-rays in the reaction $^{10}B(n,\alpha)^{7}Li^{*}$, $\gamma^{7}Li$ which are detected at the surface of the sphere in NaI scintillation counters. On the basis of the calculations a 12 cm radius counter has been built containing ~1 kg ^{10}B with a re-entrant hole 8 cm deep and 2.5 cm diameter. The counter is predicted to have an efficiency which is flat within 4% between 100 eV and 700 keV. The time response is such that an incident fast neutron has a probability of 0.99 of being captured within 0.67 μs. Measurements are being carried out on a 300 m flight path of the Harwell 45 MeV electron linac to test the theoretical predictions. If these are successful the flat response detector will be used as a standard for calibrating the counters actually used for flux determination in fast neutron partial cross-section measurements.

The measured characteristics of the detector will be presented and compared with the theoretical predictions.

1. INTRODUCTION

The theoretical design of a neutron detector suitable for use in time-of-flight systems and with a flat efficiency in the energy range 10 eV –> ~700 keV has already been reported[1][1]. In principle the detector should allow the measurement of neutron flux to an accuracy of $\lesssim \pm 2\%$ over this region. Although it is already possible to approach this accuracy using chiefly detectors based on standard cross-sections, such measurements only give precise determinations over a relatively limited energy region which gives rise to normalisation problems in the regions of overlap. The present detector will prove particularly useful in giving accurate flux measurements over such a wide energy range provided it can be demonstrated that the calculated efficiency is correct. A model of the detector has been constructed and set up on the 300 m flight path of the neutron booster-electron linac system [2] at AERE Harwell and a preliminary experimental test of the calculated response is described. Time-of-flight distributions of neutrons from the booster were measured with the detector operating under two different conditions and the ratio of the two distributions compared with the calculated ratio. Theory and experiment agree within the respective errors. While this result gives confidence that the theoretical treatment is correct, a rigorous test of the calculated efficiency requires cross check measurements against other detectors. Such experiments are

[1] Since this report has not received a wide distribution, the design study will be described again in some detail here.

planned for the immediate future. Should these prove that the predicted efficiency is correct, it will be possible to establish the flux spectrum from the neutron booster as a standard on which partial cross-sections can be measured to the accuracy ($\pm$2-3%) required for the fast reactor programme or alternatively other detectors can be cross calibrated to allow such measurements to be carried out elsewhere.

2. THE FLAT EFFICIENCY DETECTOR

The detector is a spherical homogeneous mixture of Vaseline (effectively $CH_{2.05}$) and ^{10}B with a radial re-entrant hole to allow a parallel neutron beam to fall on the inner end near the sphere centre. Neutrons are moderated and captured in the ^{10}B to produce 478 keV γ-rays, in the reaction $^{10}B(n,\alpha)^{7}Li^{*},\gamma Li^{7}$, which are detected at the surface of the sphere in NaI scintillation counters. This technique is well proved and was first used by Rae and Bowey [3] who used an unmoderated ^{10}B plug. More recently Coates et al. [4] used a Vaseline-^{10}B mixture to enhance the response to fast neutrons. This detector had a relatively large neutron leakage and the leakage neutrons produced γ-rays in the NaI crystals by inelastic scatter, which were indistinguishable from γ-rays produced in the ^{10}B reaction. Such events in the present detector would preclude an accurate prediction of the detector efficiency and in consequence the neutron leakage must be small. This requirement must also be met if the calculated efficiency is to be suitably insensitive to the input nuclear data. The parameters of the experimental detector chosen on the basis of the calculations to be described, are given in Table I.

A detector which has several features in common with the present one has been designed and built by Poenitz [5]. The major difference is that the detector material is paraffin wax with the sphere large enough for the moderated neutrons to be captured in the hydrogen, producing 2.2 MeV γ-rays which are detected at the sphere surface. The weak capture causes the time response to be slow (~1 msec) and so the detector is useful with monoenergetic neutron sources only.

3. METHOD OF CALCULATION

The calculations were carried out on the IBM 7090 computer at Risley using the Monte Carlo code GEM 4 [6]. The UKAEA Nuclear Data Library [7] provides the required nuclear data. The programme tracks monoenergetic neutrons incident on the inner end of the re-entrant hole and when a neutron is captured its energy, spatial co-ordinates and time to capture are recorded. [All significant captures are in ^{10}B]. A second part of the programme tracks the 478 keV γ-rays produced in the $^{10}B(n,\alpha)^{7}Li^{*},\gamma Li^{7}$ reaction and gives the γ-ray energy and emergent position on the sphere surface. The distribution of γ-rays in a chosen energy band, corresponding to a given instrumental acceptance, emerging from a chosen area on the sphere surface gives the efficiency for a practical detector at a given incident neutron energy.

4. RESULTS FROM THE DESIGN CALCULATIONS

The most detailed calculations carried out in the design stage were on the properties of a detector containing 1 kg of ^{10}B since this was approximately the amount readily available in the laboratory. The diameter of the re-entrant hole was arbitrarily fixed at 2.5 cm and the hole depth was taken to be one third of the sphere diameter. This depth was found to minimise the leakage of high energy neutrons for the given ^{10}B content. The neutron absorption as a function of incident neutron energy was calculated

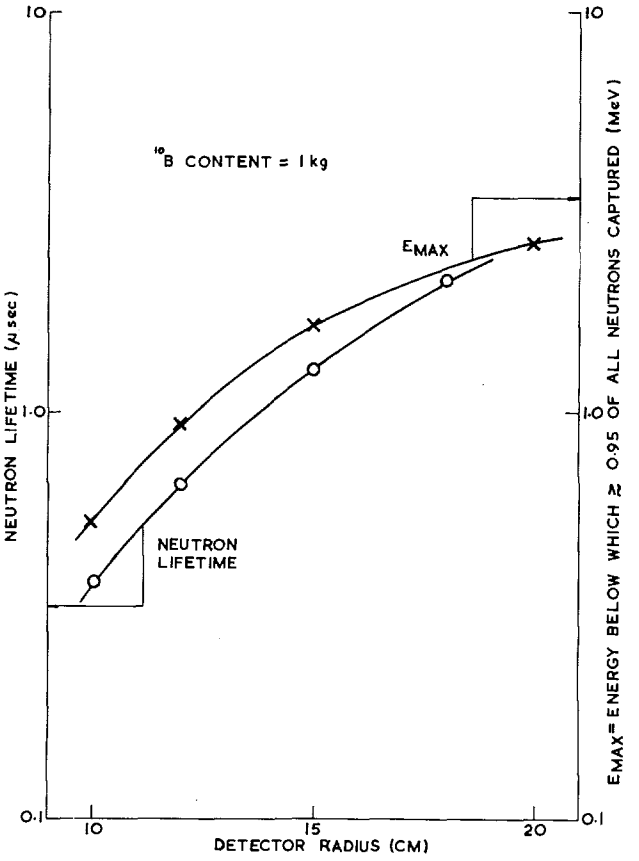

FIG. 1. Neutron capture and neutron lifetime as a function of detector radius.

for different sizes of sphere and the neutron lifetimes in the detector were obtained. Fig. 1 shows the variation with sphere radius of the incident neutron energy, E_{max}, below which the probability for capture is at least 0.95. Also shown is the variation of neutron lifetime with sphere radius. Neutron lifetime is defined here as the time taken to capture 99% of high energy incident neutrons. It will be seen that E_{max} and neutron lifetime both increase with sphere size. It is desirable to have E_{max} as high as possible and so the detector size is limited by the maximum acceptable neutron lifetime. For a practical neutron time-of-flight detector the criterion is set by the timing resolution needed to determine time dependent background events adequately using filters and the black resonance technique. For measurements to be made on the 300 m flight path of the neutron booster the neutron lifetime should not be longer than ~0.7 μsec which leads to the choice of a detector with radius ~12 cm (see Table I).

With the detector size chosen a detailed study of the γ-ray distribution at the surface of a 12 cm radius sphere was carried out. Although this distribution is symmetrical about the direction of the incident neutron beam it is not uniform over the sphere surface because high energy incident

TABLE I. EXPERIMENTAL DETECTOR PARAMETERS

Sphere radius	:	12 cm nominal
Re-entrant hole depth	:	8 cm nominal
Re-entrant hole diameter	:	2.5 cm nominal
Containment shell	:	Aluminium 0.175 cm thick
*Boron content	:	1059 gms powder (nominally 90% pure B with 90% ^{10}B content. Impurities C(2%), Fe(0.7%), Ni(0.3%), Si(2.4%), O_2(1%), (Cr + Al + Co + Cu) (1.9%)
Vaseline content	:	5389 gms
NaI crystals	:	Four crystals symmetrically placed and essentially in contact with the sphere surface. Each crystal 10.8 cm diameter and 5 cm thick.

Comments - The re-entrant hole is formed by having a thin walled (0.0125 cm) stainless steel tube crossing the sphere on a diameter and inserting into this a cylinder of ^{10}B-Vaseline contained in aluminium 0.025 cm thick. The NaI crystals have lead collars 2.5 cm thick, to ensure that they detect only Y-rays from the required area on the sphere surface.

* The isotopic content and the presence of impurities were included in the calculations.

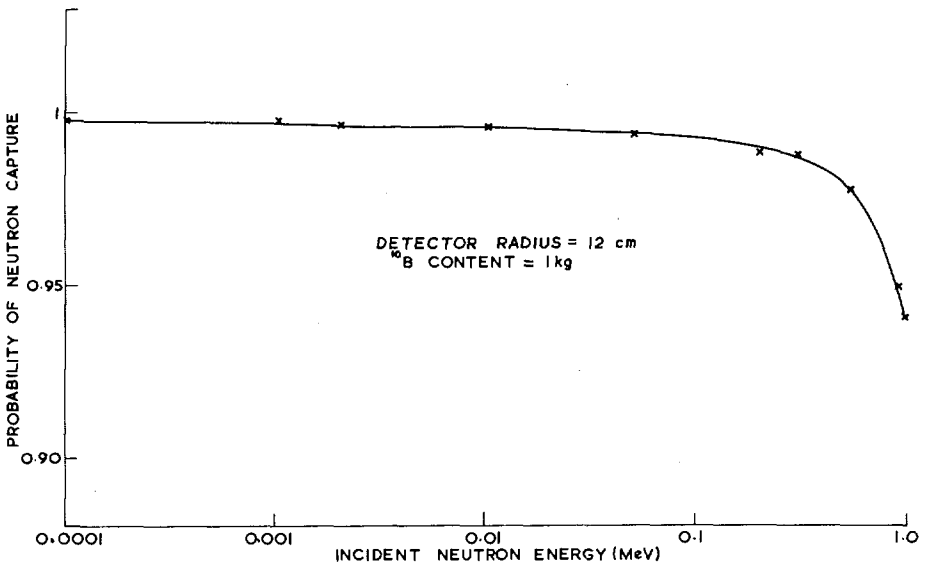

FIG. 2. Capture probability as a function of incident neutron energy.

neutrons tend to be absorbed beyond the sphere centre while low energy neutrons tend to be absorbed in front of the sphere centre. Fig. 2 shows the neutron capture probability as a function of neutron energy. Fig. 3 shows the distribution in the number of Y-rays in the energy range 400 -> 480 keV arriving at the surface of the sphere as a function of neutron energy for the five equal areas indicated in the inset. The angular distribution of the Y-rays from the $^{10}B(n,\alpha)^{7}Li^{*},Y_{Li}^{7}$ reaction is taken to be isotropic and allowance is made for the branching ratio of this reaction and the $^{10}B(n,\alpha)^{7}Li$ reaction using the data of Macklin and Gibbons [8]. (Although the branching ratio changes considerably above ~100 keV the calculated Y-ray distributions at the sphere surface are very insensitive to the change because most neutron captures occur below 100 keV). The distributions shown in Fig. 3 are relatively flat for the three central areas but the variation is large for the two outer areas. For a detector accepting Y-rays from areas 2 and 3 the efficiency varies by less than 4% over the energy range 10 eV -> 700 keV. Fig. 4 shows this distribution for the experimental detector. (The distribution differs slightly from that which would be derived from Fig. 3 since the results were calculated after the detector had been built in order to use more exact values of dimensions and ^{10}B concentration).

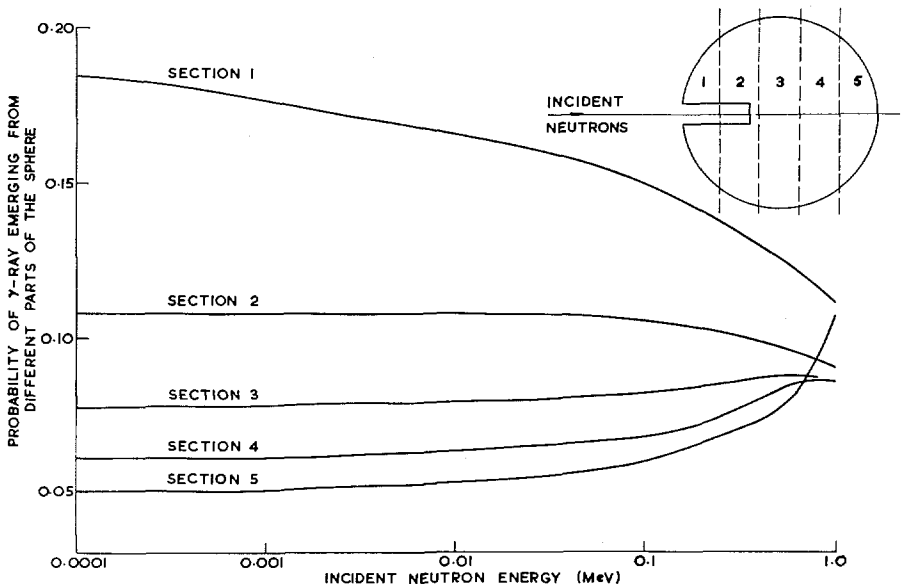

FIG. 3. Probability of γ-rays in energy range 400-480 keV emerging from different equal areas on sphere surface as a function of neutron energy.

To test the sensitivity of the results to the input nuclear data, the $^{10}B(n,\alpha)$ cross section and the hydrogen scattering cross-section were systematically altered from the best quoted values. Changes were made in the $^{10}B(n,\alpha)$ cross-section of 1% at 20 keV, 5% at 100 keV and 57% at 1 MeV, and a change of 3% was made in the hydrogen scattering cross-section. The distribution of Fig. 4 did not change within the statistical error of the calculation (1-2%). It is worth noting that calculations made for a 12 cm radius detector containing 2 kg ^{10}B gave a less acceptable efficiency variation at high incident neutron energies

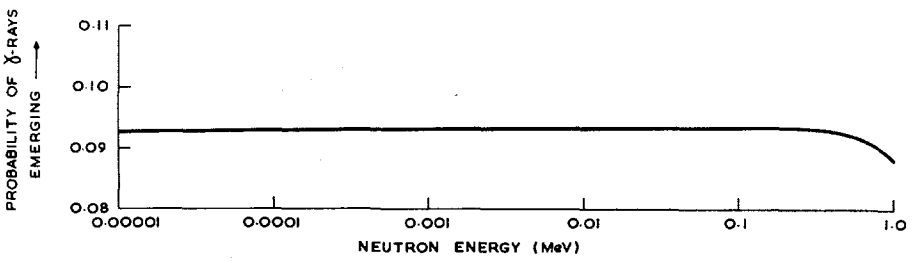

FIG. 4. Probability of γ-rays in range 400 → 480 keV emerging from areas 2 and 3 for experimental detector.

than obtained for the 1 kg ^{10}B content. The range over which the efficiency is flat to within 4% is 10 eV –> 300 keV for the 2 kg detector compared with a 700 keV upper limit for the 1 kg detector. The main interest in a detector with greater ^{10}B content lies in its faster time response, resulting from the increased neutron absorption, thus allowing the detector to be used on a shorter flight path with a consequent improvement in count rate.

Another conclusion from the design calculations was that the value of the maximum energy below which at least 95% of incident neutrons are captured is insensitive to the ^{10}B concentration. This means that the extension of the region of flat efficiency to higher energies can only be achieved by increasing the size of the sphere. To maintain the ^{10}B concentration (for timing purposes) would lead to a considerable expenditure on ^{10}B (commercial cost ~£2-10-0 per gm).

5. MEASUREMENTS WITH THE FLAT EFFICIENCY DETECTOR

The detector described in Table I was set up on the 300 m evacuated flight path of the neutron booster. A detailed description of the relevant booster construction has been given [9]. The only significant alteration is that the 2 cm thick water moderator and Al containers described in the reference have been replaced by 2.5 cm thick polyethylene slabs. The neutron beam was collimated at the booster end of the flight path so that the detector viewed a 12.5 cm diameter circle at the centre of the moderator face. A collimator of 90 cm borated resin and 20 cm Pb set ~3 metres from the detector limited the beam to fall within the diameter of the re-entrant hole. Alignment was checked by removing the insert from the centre hole (see Table I) and ensuring that the beam passed completely through without striking the remaining part of the detector. The detector was surrounded by shielding walls of 5 cm thick Pb inside 15 cm thick borated wax. The flight path had two breaks at the 60 m and 120 m positions to allow measurements to be made on shorter flight paths. The six vacuum windows through which the neutron beam passed were each of 0.0125 cm thick Melinex. Air gaps in the flight path totalled ~10 metres.

Time-of-flight distributions of neutrons from the booster were measured on an 8 MHz magnetic tape recorder with the linac operating at 192 c/s with an electron pulse width of 0.23 μsec. For the first set of measurements the NaI crystals viewed areas 2 and 3 (Figs. 3 and 4) which is the designed operating condition to give a flat efficiency. In the second set of measurements the NaI crystals viewed regions 3 and 4 where the predicted efficiency varies more with energy. Fig. 5 gives the

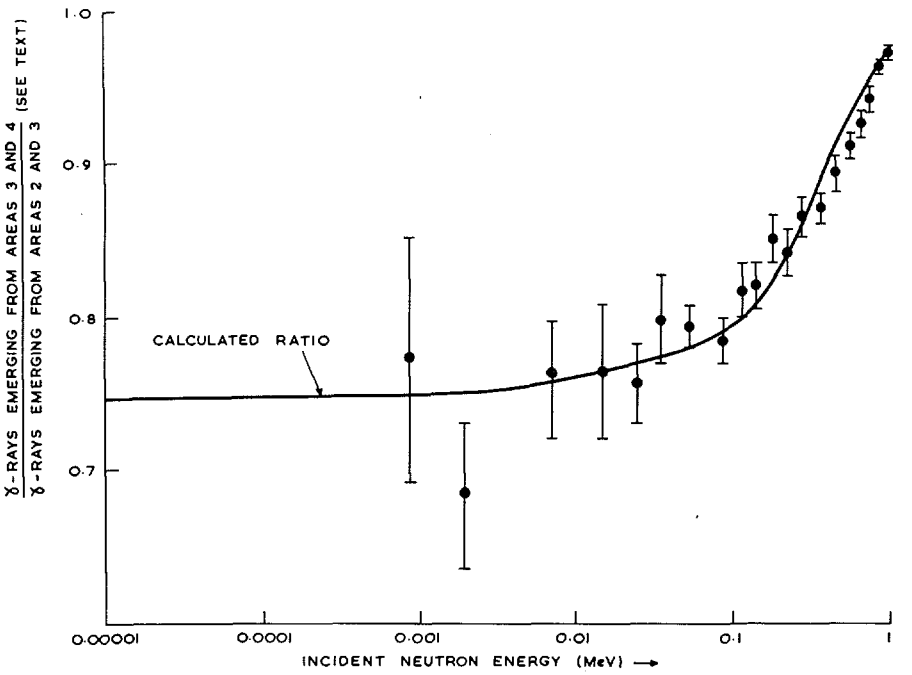

FIG. 5. Calculated and experimental ratio of detector response under different operating conditions.

calculated and experimentally determined ratio of the normalised, background corrected count rates in the two experiments. The experimental points, obtained by summing individual timing channels appropriately are normalised to the theoretical ratio at 1 MeV where the statistical accuracy of the data is greatest. Background was measured using the black resonance technique with Al and SiO_2 filters. The time dependent part of the background proved to be insignificant and the major (time constant) part of the background arose from cosmic ray events. This limited the accuracy of the experimental data towards low energies.

The agreement between theory and experiment in Fig. 5 is encouraging. In the region above ~100 keV where the accuracy of the experimental points is $\lesssim \pm 2\%$ there is some indication of a small systematic discrepancy ($< 2\%$ overall) with theory. However, since the points determining the theoretical curve have errors of 1-2% it is probably fair to conclude that theory and experiment agree within their respective errors. Further measurements are needed to improve the accuracy of the data below 100 keV and it should be possible to reduce cosmic ray background significantly by using anticoincidence techniques.

The cross check measurements against other detectors referred to in Section 1 will be carried out in several stages. Measurements on the booster linac system in the low energy range below ~100 keV will be made using detectors based on the $^{10}B(n,\alpha)$ and $^{6}Li(n,\alpha)$ cross-sections as standards. These measurements will be made with the flat efficiency detector at the 120 m position on the 300 m flight path in order to increase the count rate over that at 300 m. For measurements at high energies the

detector will be moved on to the pulsed Van de Graaff IBIS and cross check measurements made against the Harwell long counter [4]. Until recently the long counter efficiency had been established from proton recoil measurements (viz against the hydrogen total scattering cross-section as a standard) but recently the efficiency has been checked using a technique of associated radioactivity [10] which promises to give results of high accuracy in the energy region ~20 keV -> 1.4 MeV. Nuclei (V, Fe) are used as targets to produce neutrons in (p,n) reactions which leave the residual nucleus γ-radioactive. Analysis of the residual radioactivity and calibration in terms of standard sources allows the neutron flux to be determined with an ultimate accuracy hopefully of ~±1%.

REFERENCES

[1] COATES M. S. and Hart, W. EANDC(UK)109AL (1969).
[2] POOLE, M. J. and Wiblin, E. R. Proc. 2nd Int. Conf. on Peaceful Uses of Atomic Energy (Geneva) 14, 266 (1958).
[3] RAE, E. R. and Bowey, E. M. Proc. Phys. Soc. 66A, 1073 (1953).
[4] COATES, M. S., Gayther, D. B. and Goode, P. D. UKAEA Report AERE - R 5364 (1968).
[5] POENITZ, W. P. Nucl. Inst. and Methods 58, 39 (1968).
[6] HEMMINGS, P. J. UKAEA Report AHSB(S)R105 (1967).
[7] NORTON, D. S. UKAEA Report AEEW - M824 (1968).
[8] MACKLIN, R. L. and Gibbons, J. H. Phys. Rev. 165, 1147 (1968).
[9] COATES, M. S. and Tripp, D. J. UKAEA Report AERE PR/NP 7 (1964).
[10] ADAMS, J. M., Ferguson, A. T.G. and McKenzie, C. D. UKAEA Report AERE PR/NP 14 (1968).

DISCUSSION

N. ADIB: When measuring neutron fluxes in the reactor by the time-of-flight method, the neutrons are always accompanied by a large gamma background. What is the range of application of the detector in question for gamma background?

E. R. RAE: The detector, of course, operates by detecting the 478 keV gamma rays from the $^{10}B(n,\alpha\gamma)$ reaction and so is, in principle, sensitive to gamma rays. Nevertheless, the measurements described were made using the Harwell booster neutron source, and the gamma rays from the fission products in the booster core had only a small effect on the background. The main component of the background was due to cosmic rays.

R. F. TASCHEK: What would you expect to be the limitation to the flatness of the detector if it could be completely optimized?

E. R. RAE: This is a difficult question. Certainly, increasing the ^{10}B content of the experimental detector reduces the energy range over which the efficiency curve is flat, and for 2 kg of ^{10}B in the detector, the energy range over which the efficiency is flat to 4% extends only to 300 keV, as compared with 700 keV for 1 kg. Increasing the size of the detector would extend the flat region to higher energies, but the efficiency would be reduced. Perhaps the best hope for extending the energy range of the flat region and perhaps even improving the flatness, would be to study the properties of ^{10}B-vaseline assemblies of different shapes and also non-uniform

^{10}B loadings. The reason for studying homogeneous spheres in the first place was computational simplicity.

W. P. POENITZ: Some modification of Dr. Rae's answer may be required: The efficiency of the detector can be made very flat, but only for applications in a limited energy region. Extensions of the energy region makes necessary the use of larger spheres and this in turn causes a rise in the efficiency curve due to the absorption of γ-rays until the ultimate drop-off due to leakage occurs.

E. R. RAE: Yes. What I really meant was that to avoid the rather catastrophic drop-off just below 1 MeV, one should make it larger. I did not intend to suggest that one could maintain as good a flatness to very high energy.

Yu. POPOV: What is the geometrical arrangement of the gamma detectors?

E. R. RAE: The gamma-ray detectors consist of four sodium iodide detectors 10.8 cm in diameter by 5 cm thick arranged symmetrically around the sphere, and essentially in contact with it.

Yu. POPOV: What is the absolute efficiency of the neutron recording?

E. R. RAE: I do not have a figure for the overall efficiency of the experimental detector. However, the probability of the emission of gamma rays of energy 400-480 keV into the solid angle subtended by the sodium iodide detectors is 9-10%. The overall efficiency will then be this figure multiplied by the intrinsic efficiency of the sodium iodide detectors.

ABSOLUTE NEUTRON FLUX DETERMINATION

F. KÄPPELER, F.H. FRÖHNER
Institut für Angewandte Kernphysik,
Kernforschungszentrum Karlsruhe,
Federal Republic of Germany

Abstract

ABSOLUTE NEUTRON FLUX DETERMINATION.

A proton recoil counter with a solid-state detector and a solid radiator was developed for absolute neutron flux measurements in the energy region between 200 keV and 1 MeV. The radiator-detector geometry was chosen such that only the forward-peaked recoil protons within a maximum angle were detected. Thus, it was possible to measure the complete recoil proton spectrum even at energies of about 200 keV. A Monte-Carlo program serves to fit the experimental spectra and to normalize to the absolute neutron flux. The accuracy for the determination of the neutron flux is about 5%.

1. INTRODUCTION

For neutron energies higher than about 100 keV any partial neutron cross section measurement of good accuracy has to refer to the hydrogen (n,p) scattering cross section. This is the only standard cross section with an accuracy better than 3 % in this energy region, well established by experimental as well as by theoretical work [1] .

Therefore many efforts were made to design proton recoil counters for neutron flux measurements. In general one can distinguish between counters with solid radiator and counters filled with gas containing hydrogen [2,3] . The use of a solid radiator (for example a thin layer of stearic acid) has the advantages that the detector geometry is well defined even in a divergent neutron flux and that it is possible to determine the background by covering the radiator. The disadvantage of such a system is its small efficiency. Since the solid radiator has to be so thin that practically all protons can escape from it the efficiency is about three orders of magnitude lower than for a gas-filled counter.

The recoil protons from a solid radiator can be detected in a proportional counter or with a solid-state detector. The proportional counter has a good efficiency - the protons are detected in 2π - geometry - but it is sensitive to γ-rays. The γ-flash of an accelerator causes a background which masks the lower part of the step-like recoil proton spectrum. Because the proportional counter is too slow for time-of-flight-discrimination of the γ-ray background, one always has to extrapolate the spectrum to zero pulse height in order to find the full count rate. This extrapolated portion of the pulse-height distribution and thus the uncertainty of the number of recoil protons gets larger with decreasing energy. Additional uncertainties arise from the amount of protons absorbed in the radiator. These difficulties remain when the proportional counter is replaced by a solid state detector located close to the surface of the radiator as in Ref. [4] .

The uncertainty due to extrapolation of the recoil proton spectrum can be avoided with a solid state detector positioned at a certain distance from the radiator. Then only forward-peaked protons are detected. The minimum proton energy $E_{p\ min} = E_n \cos^2 \Theta_{max}$ is defined by the maximum scattering angle Θ_{max} between the radiator and the detector. Thus, it is not at all necessary to extrapolate the spectra to zero pulse height. Furthermore, all recoil protons impinging on the solid state detector have enough energy to be detected. No recoil protons are lost by absorption in the radiator or in the detector window. The penalty for the improvement in background discrimination is a further reduction of the efficiency. Nevertheless, this solution is valuable for neutron energies below about 1 MeV, where other recoil detector systems fail because of background problems.

2. EXPERIMENTAL ARRANGEMENT

2.1 The Proton Recoil Counter

In its first form, this detector was suggested by E. Pfletschinger. The principle was to measure the entire spectrum of recoil protons. When the spectrum is integrated for the calculation of the detector efficiency, it is not necessary to make corrections for an extrapolated part of the spectrum. Fig. 1a shows the counter. The materials used were bronze for the walls and brass for the lid and the flanges. During operation, the counter is evacuated to about 0.1 Torr. It was designed as light-weight as possible to keep the amount of scattered neutrons small. A coolant baffle filled with liquid nitrogen prevents oil vapors from contaminating the counter. Storage and handling of the counter is always done in Argon atmosphere.

The solid state detector and the radiator are mounted on the lid. Therefore deformations due to the air pressure outside the counter cannot change the solid angle between them.

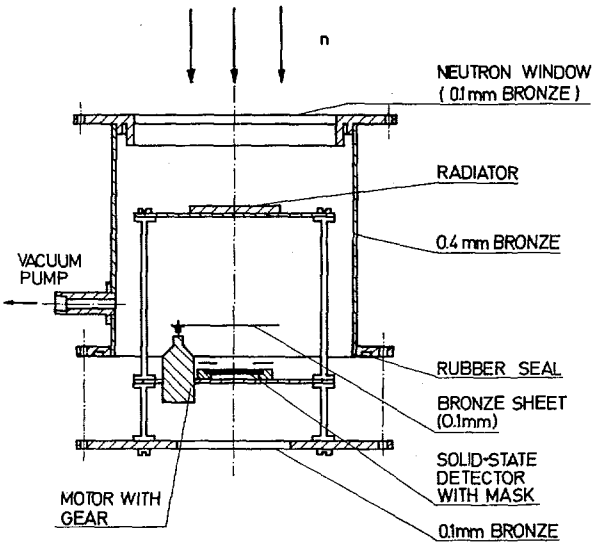

FIG. 1a. Schematic view of the proton recoil counter.

2.2 The Solid State Detector

An ion-implanted silicon detector was used as the proton detector [5] . Its surface was metallized with 20 $\mu g/cm^2$ gold and the thickness of the insensitive region, measured by a collimated beam of alpha particles impinging under different angles, was about 20 $\mu g/cm^2$ silicon under experimental conditions. The detector had an energy resolution of about 2 % and a sensitive area, defined by a mask with an aperture, of 1.76 cm^2. During measurements the detector can be covered with a 0.1 mm thick bronze sheet during every second cycle of an automatic sample changer. The distance between the aperture of the detector and the bronze sheet was 1.0 cm. The background spectrum measured with the detector covered can be stored in the memory of an on-line computer under exactly the same conditions as the recoil proton spectrum.

2.3 Radiator

The radiators were made by the CBNM/Euratom in Geel [6] . Stearic acid ($C_{18}H_{36}O_2$) was evaporated at a constant temperature of 240° C onto a 1 mm thick sheet of stainless steel. The polish of the backing is better than 1 µm, which was measured with an optical method. Evaporation times from one to several hours were used, depending on the layer thickness. Stearic acid was chosen because of the large hydrogen content of about 12 %, the high purity of this material and its resistance against air moisture.

The diameter of the layer was 4 cm and the thickness varied between 60 $\mu g/cm^2$ and 180 $\mu g/cm^2$, corresponding to 0.6 and 2.2 mg of stearic acid. The total mass was determined by weighing the samples with a vacuum balance before and after evaporation. The uncertainty is estimated to be $\pm$ 10 µg and is caused by the error of the balance. After storage in air as well as in Argon over long time periods (several months) no change in the weight of the samples greater than $\pm$ 10 µg was found.

A second method to determine the hydrogen content of the radiators is a quantitative chemical analysis which is supposed to be accurate to about 1 %. Such an analysis is being prepared.

2.4 Neutron Source

Neutrons were produced with the Karlsruhe 3 MV pulsed Van de Graaff accelerator via the $^7Li(p,n)^7Be$ reaction. The pulse width was 1 nsec and the repetition rate $10^6 \frac{1}{sec}$. The neutron energy was determined with a Li-glass detector at a distance of 1.80 m and with a time resolution $< 2 \frac{nsec}{m}$. Normally the ^7Li-targets were 30 to 70 keV thick. Ta-backings for the ^7Li-targets and a shielding of 2 cm Pb reduced the γ-flash of the accelerator.

2.5 Electronics

Fig. 1b shows a block diagram of the electronics. The pulses from a charge-sensitive preamplifier located close to the silicon detector are shaped and amplified by a spectroscopy amplifier. The width of the output pulses was 250 nsec. Time determination is achieved with a zero-crossing trigger, the time resolution depending on the pulse height, e.g. 18 nsec at 500 keV. The time-of-flight-spectrum produced

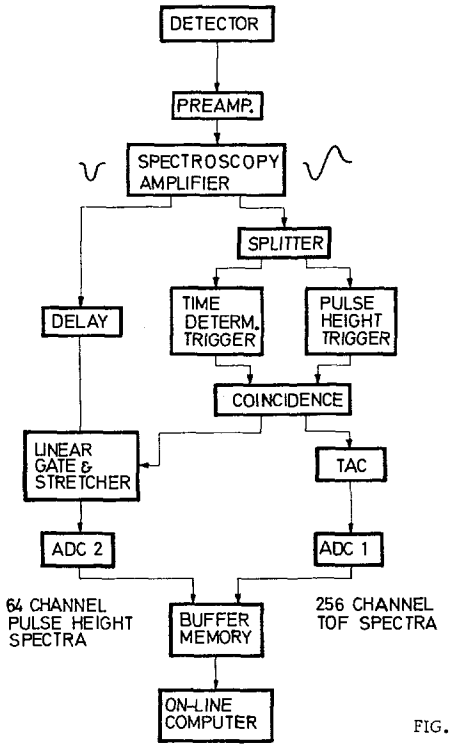

FIG. 1b. Block diagram of the electronics.

in a first analog-to-digital converter (ADC1 in Fig. 1b) contained 256 channels. By the computer program they were compressed to 64 channels in such a way, that the important part of the spectrum with the recoil protons is preserved with the original resolution. The two resulting 64 x 64 channel matrixes (for covered and uncovered silicon detector) contain pulse height spectra versus time of flight.

For data transmission from the buffer memory to the computer it is necessary that there are two coincident signals, one from every ADC.

3. MONTE CARLO PROGRAM

For the calculation of the efficiency and for the simulation of pulse-height spectra of the proton recoil counter a Monte Carlo program was written. Similar to that of Bame et al. [7] , the neutrons from a point source hit the (circular) radiator sheet, producing recoil protons. The laboratory scattering angles are sampled from the appropriate distributions, then the energy and the direction of the knock-on proton can be determined for a given neutron energy and direction. This is done for different places and depths in the radiator. To save computer time, angle sampling for each interaction is restricted to a cone containing the solid state detector. The geometry factors of the efficiency M, determined with about 10^5 hits of the

solid state detector agreed within the statistical uncertainties with the values of Bame et al. [7] . Energy losses in the radiator and in the entrance window of the solid state detector are calculated from known energy-range and dE/dx relationships [8,9,10,11] .

4. RESULTS AND DISCUSSION

First experiments without any radiator material confirmed that there was no difference in the spectra measured with the detector uncovered or covered by the 0.1 mm thick bronze sheet. Fig. 2a shows a spectrum taken with the radiator in place. Also shown is the background. The spectrum is due to neutrons with energies of (550 ± 20) keV from a pulsed 3 MV Van de Graaff accelerator. It demonstrates that measurements can be done with good discrimination against background. In Fig. 2b the experimental results at three neutron energies are plotted together with the theoretical curves. The agreement is satisfactory. Absolute fission cross section measurements with this detector are in progress.

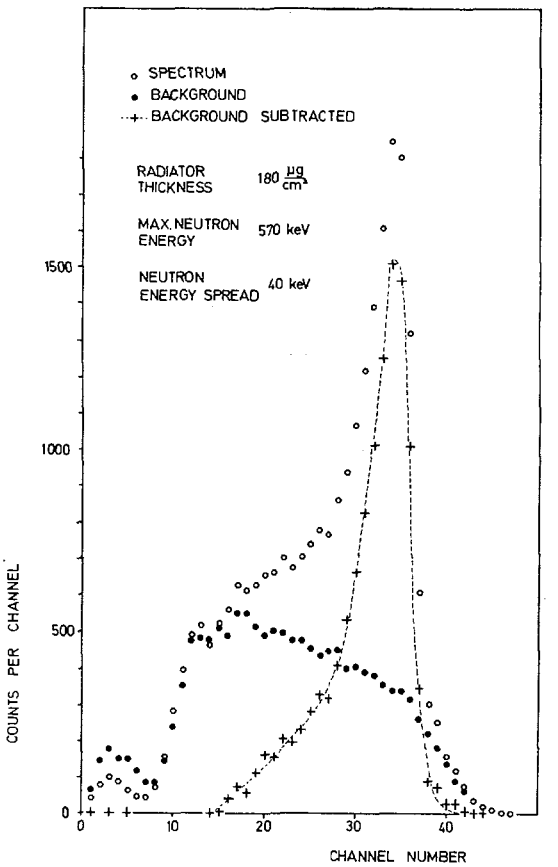

FIG. 2a. Spectrum with covered and uncovered solid-state detector.

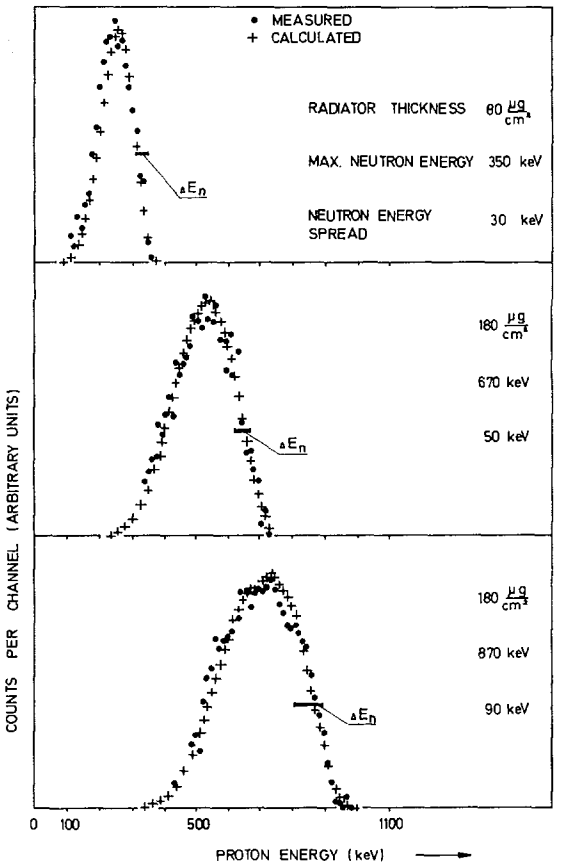

FIG. 2b. Experimental and calculated spectra at three energies.

ACKNOWLEDGEMENT

The authors wish to thank E. Pfletschinger for the initiation of, and Prof. Beckurts for his support and permanent interest in this work. We appreciate the careful preparation of the radiator foils by H.L. Eschbach and E.W. Kruidhof as well as the good work of the van de Graaff operators.

REFERENCES

[1] GAMMEL, J.L., Fast Neutron Physics - II (J.B. Marion and J.L. Fowler, Eds.) Intersci., N.Y. (1963) 2185.

[2] FERGUSON, A.T.G., Fast Neutron Physics - I (J.B. Marion and J.L. Fowler, Eds.) Intersci., N.Y. (1963) 179.

[3] JOHNSON, C.H., Fast Neutron Physics - I (J.B. Marion and J.L. Fowler, Eds.) Intersci., N.Y. (1963) 247.

[4] WHITE, P.H., J. Nucl. Energy 19 (1965) 325.

[5] MEYER, O., IEEE Trans. Nuc. Sci. NS-15 3(1968) 232.

[6] ESCHBACH, H.L., priv. comm.

[7] BAME, S.J., Jr., EUGENE HADDAD, PERRY, J.E., Jr., SMITH, R.K., and BLAIR SWARTZ, Rev. Sci. Instr. 31 (1960) 911.

[8] WHALING, WARD, Handbuch der Physik 34 (1958) 193.

[9] BICHSEL, HANS, Phys. Rev. 112 (1958) 1089.

[10] HIRSCHFELDER, J.O., and MAGEE, J.L., Phys. Rev. 73 (1948) 207.

[11] WILLIAMSON, C., and BOUJOT, J.P., CEA-2189 (1962 Saclay).

DISCUSSION

M. ASGHAR: I see that in your measurements with this solid-state detector, there is an important contribution from background. Could you not have decreased this background contribution by using a ΔE detector in coincidence with your detector?

F. KÄPPELER: No ΔE detector was used because of the low (below 1 MeV) proton energies. In a measurement of the neutron flux an additional uncertainty would arise from the correction for protons lost by absorption or scattering in the ΔE detector.

MESURE ABSOLUE DE LA SECTION EFFICACE DE FISSION DE L'URANIUM-235 ET DU PLUTONIUM-239 ENTRE 0,025 ET 1 MeV

I. SZABO, J.P. MARQUETTE,
E. FORT, J.L. LEROY
CEA, Centre d'études nucléaires de Cadarache,
France

Abstract — Résumé

ABSOLUTE MEASUREMENT OF THE FISSION CROSS-SECTION FOR ^{235}U AND ^{239}Pu BETWEEN 0.025 AND 1 MeV.

This measurement was made using monokinetic neutrons from the Van-de-Graaff accelerator at Cadarache. The neutron flux was measured with standard counters, the calibration of which is the subject of another paper at this Conference. The fission chamber used for ^{235}U was built by P.H. White (Aldermaston). The ^{239}Pu-foil was prepared and calibrated by BCMN. A special electronic assembly makes it possible to reduce the fluctuations of the response time of the fission chamber to less than 7 ns, by detecting the current of electron migration due to ionization. In this way, use can be made of the time-of-flight method to detect the fissions due to neutron background. The total error of the measurement points is ± 3%.

MESURE ABSOLUE DE LA SECTION EFFICACE DE FISSION DE L'URANIUM-235 ET DU PLUTONIUM-239 ENTRE 0,025 ET 1 MeV.

Cette mesure a été faite en utilisant des neutrons monocinétiques provenant du Van de Graaff de Cadarache. Le flux de neutrons a été mesuré au moyen de compteurs étalons dont la calibration a fait l'objet d'une autre communication à la même conférence. La chambre à fission utilisée pour ^{235}U a été construite par P.H. White (Aldermaston). Le dépôt de ^{239}Pu a été préparé et calibré par le BCMN. Un montage électronique spécial permet de réduire à moins de 7 ns les fluctuations du temps de réponse de la chambre à fission, en détectant le courant de déplacement des électrons dus à l'ionisation. Ceci permet d'utiliser la méthode du temps de vol pour déterminer les fissions dues au bruit de fond neutronique. L'erreur totale sur les points de mesures est de ± 3%.

1. INTRODUCTION

Depuis plusieurs années, la section efficace de l'uranium-235 fait l'objet de nombreuses mesures [1-7], mais l'accord entre les valeurs obtenues n'est pas excellent. En dessous de 100 keV notamment, les écarts atteignent parfois 16%, alors que les erreurs attribuées aux différentes mesures sont de l'ordre de 2 à 3%.

Dans le domaine des énergies plus élevées, un meilleur accord existait, mais une mesure faite récemment par Poenitz [7] donne, entre 260 et 1500 keV, des valeurs inférieures de 15% environ à celles obtenues précédemment par la plupart des autres auteurs.

Les écarts sont encore plus grands en ce qui concerne le plutonium-239, dont la section efficace de fission joue un rôle essentiel dans le calcul des réacteurs.

Etant donné l'importance de ces données microscopiques, une telle situation est loin d'être satisfaisante et de nouvelles mesures sont nécessaires.

La dispersion des résultats peut être expliquée en partie par la grande difficulté de la mesure absolue du flux de neutrons. Afin de diminuer les risques d'erreurs systématiques dans cette mesure, nous avons mis au point plusieurs méthodes indépendantes, destinées à la calibration absolue d'un dispositif simple dans son principe et d'un emploi commode, appelé «détecteur directionnel» [8].

L'expérience décrite ici consiste essentiellement en une comparaison des taux de comptage de détecteurs de ce type, et de chambres à fission contenant un nombre déterminé d'atomes de ^{235}U ou de ^{239}Pu. La section efficace de fission est ensuite déduite des rapports des taux de comptage et de l'efficacité absolue du détecteur directionnel utilisé.

Lors des premières mesures faites en 1967 sur l'uranium-235, l'étalonnage des détecteurs directionnels en était à son début, et la précision obtenue était insuffisante. Des progrès ont été accomplis depuis, et les résultats préliminaires publiés dans la référence [9] sont maintenant renormalisés par rapport aux valeurs définitives de l'efficacité absolue du détecteur directionnel, récemment obtenue avec une précision de 1,8%. Les dernières mesures faites simultanément sur le ^{235}U et le ^{239}Pu concernent un domaine d'énergies plus large, et quelques modifications ont été apportées à l'appareillage dans le but d'améliorer la précision et de diminuer le temps de mesure.

L'ensemble des mesures a permis d'obtenir la section efficace de fission du ^{235}U à 31 énergies de neutrons comprises entre 0,027 et 1 MeV et, dans la même gamme d'énergie, celle du ^{239}Pu à 13 énergies.

2. DISPOSITIF EXPERIMENTAL

2.1. Caractéristiques des détecteurs

2.1.1. Chambres à fission

Uranium-235. Nous avons utilisé une des chambres à fission construites par White, dont la description détaillée est donnée dans [6]. Le nombre d'atomes de ^{235}U contenu dans le dépôt d'oxyde est connu à ± 1%. Les méthodes de détermination de ce nombre ainsi que diverses corrections: absorption des fragments dans la couche d'oxyde, extrapolation du spectre d'amplitude vers l'origine, etc., sont également données dans cette référence.

Une détermination supplémentaire de la masse d'uranium a pu être effectuée dans notre laboratoire. En améliorant la résolution de la chaîne d'amplificateurs associés aux chambres à fission, nous avons pu séparer le spectre des α de désintégration du bruit de fond électronique.

Diverses corrections: extrapolation du spectre vers zéro (0,6%), perte dans la couche d'oxyde (4,7%), rétrodiffusion des α (2,4%), sont appliquées aux taux de désintégration bruts. Les masses d'uranium sont calculées en utilisant comme période des isotopes de l'uranium les valeurs mesurées par Flemming et al. [10] et Keinberger [11].

La méthode de comptage des α en géométrie 2π, utilisée ici, est légèrement différente de celle de White, en ce sens que la mesure a été

faite avec le dépôt fixé à l'intérieur de la chambre elle-même et non pas en l'incorporant dans une chambre à grille.

L'écart entre nos résultats et les valeurs que White a obtenues par quatre méthodes différentes est inférieur à 1%.

Plutonium-239. Afin de rendre nos mesures sur le ^{239}Pu entièrement indépendantes de celles de White, nous avons demandé au BCMN de Geel (Belgique) de fabriquer des dépôts de plutonium par la méthode de l'«electrospraying» [12] et de les étalonner par comptage α en géométrie définie [13].

L'échantillon utilisé se compose d'une couche d'oxyde de plutonium de 150 $\mu g/cm^2$ d'épaisseur et de 30 mm de diamètre, déposée sur un disque en platine de 0,3 mm d'épaisseur. L'ensemble est incorporé dans une chambre à ionisation en titane de 1 mm d'épaisseur et remplie d'un mélange d'argon + 10% CH_4, à une pression de 0,5 atm (fig. 1).

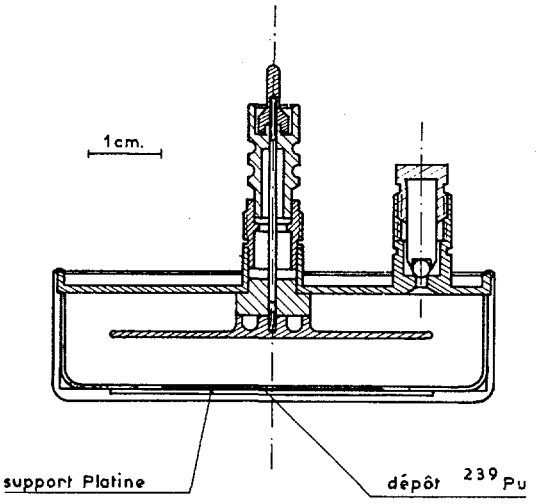

FIG. 1. Chambre à fission au plutonium.

La composition isotopique du plutonium utilisé: < 0,01% ^{238}Pu, 99,27% ^{239}Pu, 0,071% ^{240}Pu, 0,02% ^{241}Pu, < 0,01% ^{242}Pu, est donnée avec une incertitude relative de 0,1%, et l'activité avec une erreur quadratique moyenne de 0,2%. La précision sur le nombre d'atomes de ^{239}Pu, calculé en utilisant comme période des isotopes les valeurs de Wallmann [14], est de 0,6%.

Un échantillon similaire, fabriqué en même temps que celui utilisé pour la mesure, est conservé au BCMN en vue d'une analyse destructive ultérieure.

2.1.2. Détecteurs directionnels

Ces appareils, destinés à des mesures absolues de flux neutroniques, se composent essentiellement d'un bloc de polyéthylène et de deux compteurs à BF_3. L'ensemble est entouré d'une protection d'eau et les neutrons

sont amenés au cœur du dispositif par un collimateur. Le diamètre du trou de collimation est choisi suffisamment petit pour que les neutrons produits par la cible, en le traversant, aillent jusqu'au fond d'un puits aménagé dans le bloc de polyéthylène. La détection se fait au moyen des compteurs à BF_3, après ralentissement et thermalisation des neutrons.

Ce dispositif se rapproche de celui utilisé par Langsdorf et al. [15]. Une idée similaire est mise en œuvre dans le «grey detector» de Poenitz [16].

La structure détaillée du détecteur ainsi que les différentes méthodes mises en œuvre pour l'étalonner sont décrites de façon détaillée par Leroy et al. [8]. Les courbes d'efficacité des deux détecteurs directionnels utilisés dans la mesure simultanée des sections efficaces de fission du ^{235}U et du ^{239}Pu sont données dans la même référence.

2.2. Sources de neutrons

Les neutrons d'énergies comprises entre 25 et 550 keV sont produits par la réaction $^{7}Li(p,n)^{7}Be$, et, pour des énergies plus élevées, par la réaction $p(T,n)^{3}He$. Les cibles de lithium utilisées se composent d'un support de tantale de 0,5 mm d'épaisseur sur lequel on a déposé par évaporation sous vide du lithium naturel. La cible est placée au bout d'un tube très mince de 0,3 mm d'épaisseur. D'une façon générale les montages mécaniques situés au voisinage immédiat de la cible sont allégés au maximum afin de réduire le bruit de fond neutronique.

La dispersion en énergie due à l'épaisseur du dépôt de lithium est de 3 à 16 keV quand l'énergie passe de 25 à 540 keV. Pour les cibles de tritium sous forme de dépôt solide la résolution en énergie est de $\pm$ 30 keV. Le refroidissement de la cible se fait par jet d'air comprimé et le courant maximal admissible est de 15 μA.

2.3. Géométrie de l'expérience

La disposition des détecteurs est représentée à la figure 2. Dans un premier temps, la chambre à ^{235}U est placée à un angle de 20° et la chambre à ^{239}Pu à 135°. Les deux détecteurs directionnels sont placés aux angles symétriques de ceux des chambres. Le premier, situé vers l'avant, mesure le flux de neutrons d'énergie supérieure à 120 keV, tandis que le deuxième, placé vers l'arrière, permet de couvrir la région des basses énergies. On obtient ainsi, en une seule mesure, la section efficace de fission du ^{235}U et celle du ^{239}Pu, chacune à une énergie différente donnée par la cinématique de la réaction productrice de neutrons. En permutant ensuite les deux chambres à fission, on peut couvrir toute la gamme d'énergies.

Les détecteurs directionnels sont placés à des distances comprises entre 2,50 m et 3,50 m. La précision sur cette distance, mesurée entre le centre de la cible et la face arrière du collimateur, est de $\pm$ 1 mm. L'alignement angulaire est fait au moyen d'un théodolite dont la précision atteint 10^{-4} radian; l'erreur angulaire commise est de l'ordre de 0,05°.

Des gabarits, dont le rôle est de définir mécaniquement un angle et une distance, permettent de positionner la chambre à 0,3 mm près avec une erreur angulaire inférieure à 0,1°.

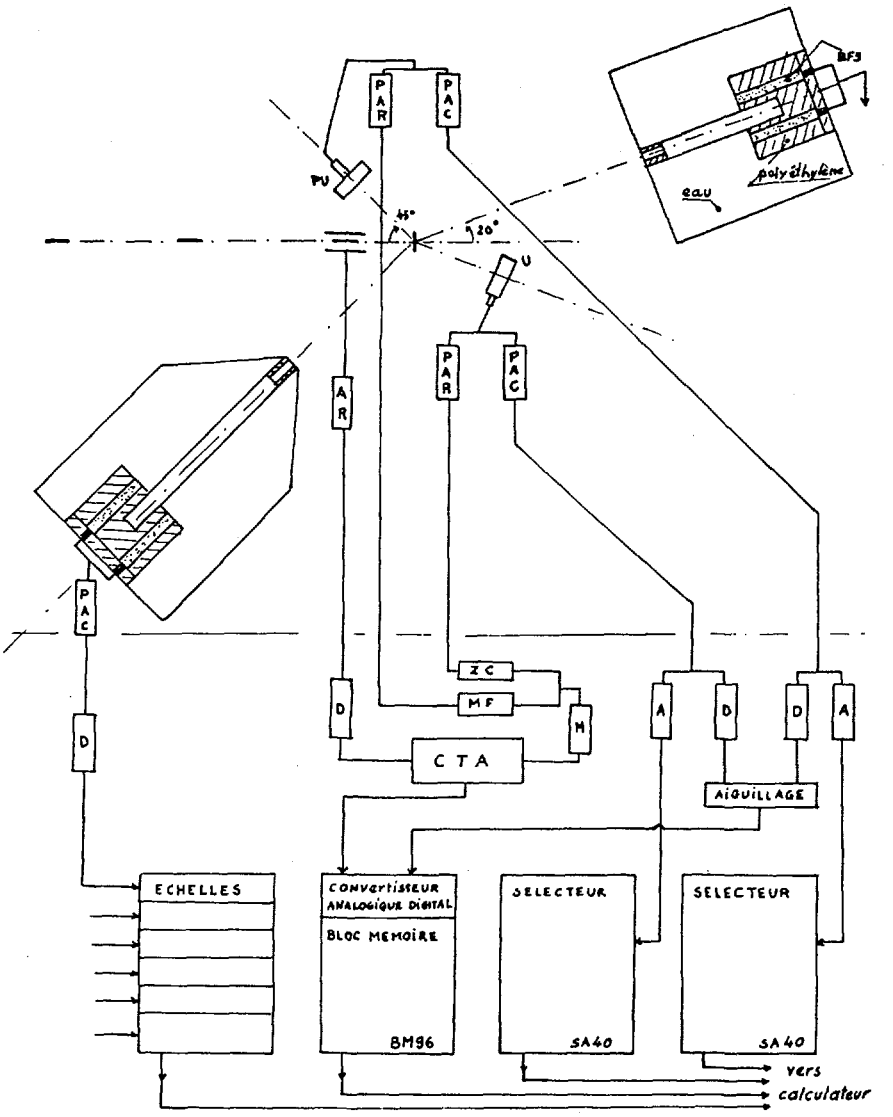

FIG. 2. Arrangement expérimental.
A amplificateur – D discriminateur – PAR préamplificateur rapide – PAC préamplificateur de charge – ZC «zero crossing» – MF mise en forme – M mélangeur – CTA convertisseur temps-amplitude.

L'alignement et le positionnement des détecteurs se font par rapport au centre de la cible qui, parfois, ne coïncide pas exactement avec l'impact du faisceau. En raison des dimensions des détecteurs directionnels, il ne nous est pas possible de les permuter avec les chambres correspondantes afin d'éliminer les erreurs de distance et d'angle solide dues à l'asymétrie; une correction dont la valeur ne dépasse pas 1% et qui tient compte à la fois de la position de l'impact et de son diamètre est appliquée aux distances et angles. La contribution de l'ensemble des erreurs associées au positionnement des détecteurs représente 0,3 à 0,6% de la valeur du flux neutronique.

2.4. Electronique associée

Le schéma synoptique de l'expérience est représenté à la figure 2.

Le signal délivré par l'un ou l'autre des deux compteurs à BF_3 incorporés dans chaque détecteur directionnel est envoyé après amplification dans un circuit de comptage comprenant un discriminateur suivi d'une échelle, le seuil de détection étant fixé juste au-dessus du bruit de fond électronique.

L'électronique associée à chacune des deux chambres à fission se sépare en deux voies distinctes. Dans la voie lente, les impulsions recueillies à la sortie d'un amplificateur de charge à faible bruit sont analysées dans un sélecteur à 400 canaux. Le nombre total de fissions est obtenu en extrapolant le plateau du spectre d'amplitude vers l'origine de la manière indiquée par White.

La voie rapide a été introduite dans le but d'utiliser la méthode du temps de vol pour déterminer la part du bruit de fond neutronique dans le taux de comptage de la chambre à fission. La section 3.2 traitera ce problème plus en détail.

3. DESCRIPTION DES MESURES

3.1. Principe de la mesure

Dans son principe la mesure consiste à comparer le taux de comptage d'une chambre U ou Pu à celui d'un détecteur directionnel:

$$N_{ch} = \frac{\phi}{D^2_{ch}} N\sigma_f + b_{ch}$$

$$N_{dir} = \frac{\phi}{D^2_{dir}} S_{dir}\epsilon_{dir} + b_{dir}$$

où ϕ est le flux de neutrons par unité d'angle solide dans la direction des détecteurs, S, D, ϵ désignant respectivement la distance, la surface et l'efficacité, N le nombre total de noyaux fissiles contenus dans le dépôt, σ_f la section efficace de fission, et b les bruits de fonds neutroniques.

3.2. Détermination du bruit de fond neutronique

De par leur conception, les détecteurs directionnels sont peu sensibles aux neutrons diffusés. Le collimateur utilisé est suffisamment long et efficace pour délimiter un cône de détection de telle sorte que tout neutron dont la trajectoire est extérieure à ce cône n'est pas détecté. En dehors de ce cône d'angle solide très faible (10^{-3} stéradian), les compteurs à BF_3 sont en effet protégés de toutes parts par une cuve cylindrique remplie d'eau. Le bruit de fond neutronique qu'on peut mesurer en intercalant une barre d'ombre en polyéthylène entre la cible et le détecteur croît avec l'énergie mais reste inférieur à 1% jusqu'à 2 MeV.

Les chambres à fission sont trop près de la cible pour qu'on puisse mettre une barre d'ombre suffisamment efficace. En supposant le bruit neutronique indépendant de la position de la chambre, la variation du taux de comptage en fonction de la distance suit une loi en $a/r^2 + b$. Des mesures faites à plusieurs distances s'échelonnant entre 10 et 50 cm on peut déduire, par une méthode de moindres carrés, la valeur du paramètre b qui représente le bruit de fond neutronique à l'énergie considérée.

Une bonne précision sur les paramètres a et b nécessite, pour chaque énergie, quatre ou cinq mesures à des distances différentes. Il est cependant difficile d'obtenir, dans des limites de temps raisonnables, une bonne statistique pour les mesures aux grandes distances. Dans les mesures où cette méthode a été appliquée, la détermination du bruit de fond a, en pratique, nécessité autant de temps que la mesure du rapport des taux de comptage. Dans certains cas, l'accord n'est pas très bon entre les points expérimentaux et la loi en $a/r^2 + b$ et les erreurs commises sont de l'ordre de 0,5 à 2%.

Afin d'améliorer la précision tout en diminuant le temps de mesure, nous avons adapté la méthode du temps de vol aux chambres à fission. A cet effet, une impulsion de courant de 10 ns de temps de montée et de largeur inférieure à 300 ns est extraite de chaque chambre au moyen d'un circuit «temps» dont la description détaillée est donnée dans [17]. Ce signal est ensuite envoyé sur l'une des deux voies d'un convertisseur temps-amplitude, l'autre voie étant déclenchée par des impulsions induites dans une électrode cylindrique par le faisceau de protons. Celui-ci est formé de paquets de 8 ns de large produits à une fréquence de 3,5 MHz par un dispositif de pulsation placé dans l'électrode haute tension du Van de Graaff (fig. 2). Dans ce dispositif, une pulsation supplémentaire, placée après accélération du faisceau et synchrone de celle effectuée au voisinage de la source, permet d'éliminer le courant résiduel subsistant entre deux paquets de protons. L'extinction complète du courant entre deux impulsions de protons est en effet indispensable pour s'assurer que la partie plate du spectre de temps de vol ne comporte que des événements aléatoires dus aux neutrons diffusés.

Un circuit mélangeur et d'aiguillage permet d'enregistrer les spectres de temps de vol des deux chambres dans deux sous-groupes de 252 canaux d'un bloc-mémoire. Un exemple de spectre est montré à la figure 3. Dans la résolution globale du pic, qui est de 11 ns à mi-hauteur, la contribution de l'électronique rapide associée aux chambres est de 7 ns. Avec de tels spectres, l'évaluation de la surface du pic qui représente la proportion de fissions «vraies» est faite avec une précision meilleure que 1%. Un

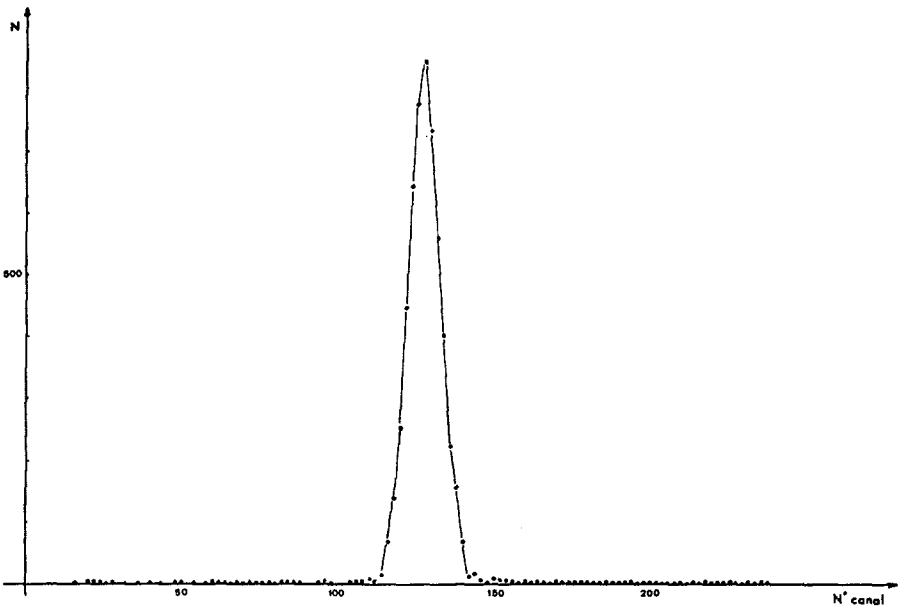

FIG. 3. Spectre de temps de vol, chambre à fission à ^{235}U (N = noyaux fissiles).

autre avantage de la méthode est de réduire le temps de comptage d'un facteur 3 environ.

La proportion de bruit de fond varie en fonction de l'énergie des neutrons et de la position de la chambre. Dans la gamme d'énergie considérée, et pour une distance comprise entre 15 et 20 cm, elle est de 3 à 10% lorsque la chambre à fission est positionnée à 20°, et de 7 à 20% quand l'angle est de 135°.

3.3. Déroulement des mesures

Pour une énergie déterminée, la mesure des taux de comptage bruts des détecteurs est suivie de la détermination du bruit de fond neutronique. Dans les mesures les plus récentes, bien que la méthode du temps de vol donne directement le taux de comptage réel des chambres à fission, le processus de mesure reste inchangé. Le courant moyen du faisceau pulsé est en effet limité à 4 μA et une mesure faite de bout en bout avec une pulsation serait trop longue. Aussi, dès que la statistique des spectres de temps de vol est suffisante pour obtenir une bonne précision sur le bruit de fond de chaque chambre, on enlève la pulsation pour effectuer une mesure avec un faisceau continu dont l'intensité est trois à quatre fois plus grande. La proportion de bruit neutronique, déterminée auparavant par la mesure en pulsé, est ensuite enlevée du taux de comptage brut enregistré en faisceau continu.

Les taux de comptage étant extrêmement faibles, de l'ordre d'une fission toutes les 2 ou 3 secondes, la durée totale d'une mesure est de 1 à 2 jours. Des résultats partiels sont prélevés et traités à intervalle régulier afin de détecter rapidement toute instabilité de l'électronique ou présence

d'impulsions parasites, qui se traduit soit par des résultats non reproductibles, soit par une déformation des spectres. Ces contrôles sont faits systématiquement, bien qu'en pratique la proportion des résultats partiels inexploitables soit très faible. L'électronique utilisée possède une grande stabilité et les impulsions parasites sont éliminées par l'emploi de filtres efficaces et de câbles de connexion à double blindage.

Le seuil et la stabilité des détecteurs directionnels sont contrôlés entre deux mesures, au moyen d'une source Ra-Be étalon placée à une position mécaniquement bien définie, à l'intérieur du trou de collimation. Les fluctuations de leurs taux de comptage ne dépassent pas 0,3% durant toute l'expérience.

Dans la dernière phase des mesures, l'enregistrement et le traitement des résultats ont été rendus automatiques au moyen d'un calculateur CAE 90-10.

4. RESULTATS

Les valeurs obtenues pour les sections efficaces de fission du ^{235}U et du ^{239}Pu sont groupées dans le tableau I, et représentées à titre de comparaison avec celles des autres auteurs sur les figures 4 et 5. Le détail des erreurs et des corrections dont nous avons tenu compte est donné dans le tableau II, pour deux énergies de neutrons. En ce qui concerne la correction de diffusion des neutrons sur les parois des chambres à fission, le calcul est fait au moyen de la méthode de Monte-Carlo.

Uranium-235. Un bon accord existe entre nos mesures et celles de White, sauf dans la région des énergies inférieures à 50 keV où les valeurs obtenues ici sont plus basses de quelques pour cent. Bien que dans cette région nos résultats tendent à confirmer ceux obtenus par Knoll et Poenitz [18] d'une part, et par Poenitz [7] d'autre part, la variation de la section efficace de fission en fonction de l'énergie a une forme différente de celle obtenue récemment par ce dernier auteur.

Plutonium-239. Les mesures effectuées sur le ^{239}Pu, à la différence de celles relatives au ^{235}U, sont entièrement indépendantes des mesures de White. De plus, la méthode utilisée est une méthode absolue qui donne directement la section efficace de fission du ^{239}Pu sans recourir au standard primaire ^{235}U.

Au-dessus de 150 keV, les valeurs obtenues sont en bon accord avec la plupart des mesures antérieures, notamment avec celles de White [19,20], Allen et Ferguson [1], Dorofeev et Dobrinin [3], et aussi avec les valeurs recommandées par Davey [21].

Vers les basses énergies, nos résultats s'écartent à la fois de ceux de White et de Allen et Ferguson, tout en restant en bon accord avec les points obtenus à 24 keV par Perkin et à 30 keV par Dorofeev et Dobrinin.

Une hypothèse avancée récemment par différents auteurs semble devoir fournir une explication plausible à la grande dispersion des résultats obtenus dans la région des keV. Les écarts seraient dus aux grandes fluctuations observées dans les sections efficaces de fission. Melkonian, en analysant ses résultats pour le ^{235}U entre 20 et 30 keV, a trouvé des

TABLEAU I. VALEURS OBTENUES POUR LES SECTIONS EFFICACES DU ^{235}U ET DU ^{239}Pu

^{235}U					^{239}Pu				
ΔE proton (keV)	$\theta_{lab} \pm \Delta\theta$		$E_n \pm \Delta E_n$ (keV)		$\sigma_f \pm \Delta\sigma_f$ (b)		ΔE proton (keV)	$\theta_{lab} \pm \Delta\theta$		$E_n \pm \Delta E_n$ (keV)		$\sigma_f \pm \Delta\sigma_f$ (b)	
9	135°	6°	17,5	3,5	2,16	0,08	7	135°	5,8°	35	4	1,71	0,07
6	135°	6°	27	3,5	2,22	0,07	8	135°	5,8°	49	5	1,61	0,06
7	135°	5,5°	42	5	1,84	0,05	9	135°	5,8°	102	8	1,63	0,06
6	135°	6°	68	5	1,78	0,04	12	135°	5,8°	152	10	1,49	0,05
15	135°	6°	72,5	6,5	1,78	0,04	22	135°	5,8°	165	13	1,47	0,04
8	135°	5,5°	95	5	1,59	0,05	9	20°	5,8°	197	16	1,52	0,03
20	135°	6°	110	10	1,59	0,05							
7	20°	4,5°	120	8	1,61	0,05	7	20°	5,8°	226	12	1,45	0,05
6	135°	6°	125	7	1,52	0,04	8	20°	5,8°	331	12	1,57	0,03
7	20°	5,5°	145	9	1,56	0,05	8	20°	5,8°	453	13	1,61	0,04
5	20°	5,5°	150	6	1,51	0,04	10	20°	5,8°	506	16	1,63	0,04
10	135°	6°	152	10	1,48	0,04	15	20°	5,8°	665	22	1,64	0,04
9	20°	5,5°	154	14	1,46	0,03	20	20°	5,8°	810	35	1,75	0,04
22	135°	6°	156	12	1,49	0,04	22	20°	5,8°	972	40	1,78	0,04
8	20°	4,5°	195	11	1,42	0,05							
7	20°	4,5°	215	10	1,34	0,04							
15	20°	4,5°	227	16	1,34	0,03							
8	20°	6,8°	251	11	1,32	0,03							
11	20°	4,5°	257	15	1,31	0,05							
11	20°	4,5°	272	15	1,32	0,04							
9	20°	5,5°	286	15	1,30	0,03							
10	20°	4,5°	313	15	1,32	0,04							
6	20°	5,5°	320	8	1,26	0,04							
11	20°	4,5°	331	15	1,24	0,04							
11	20°	4,5°	369	15	1,25	0,04							
9	20°	5,5°	407	15	1,25	0,03							
12	20°	5,5°	506	17	1,19	0,02							
8	20°	5,5°	540	10	1,19	0,04							
15	20°	5,5°	665	22	1,16	0,03							
20	20°	5,5°	810	35	1,16	0,03							
22	20°	5,5°	1,01	40	1,23	0,03							

fluctuations pouvant atteindre 20%, et plus récemment les résultats encore préliminaires de Diven, Kayworth, Moore, obtenus avec une explosion nucléaire, et de Bowman avec un Linac, montrent des fluctuations du même ordre [22]. Or les mesures faites au moyen d'un Van de Graaff [1, 6, 7, etc.] ou avec une source Sb-Be [5] supposaient implicitement que, dans le domaine défini par la résolution en énergie, qui est de quelques keV, les fluctuations de la section efficace ne dépassaient pas les erreurs de mesures.

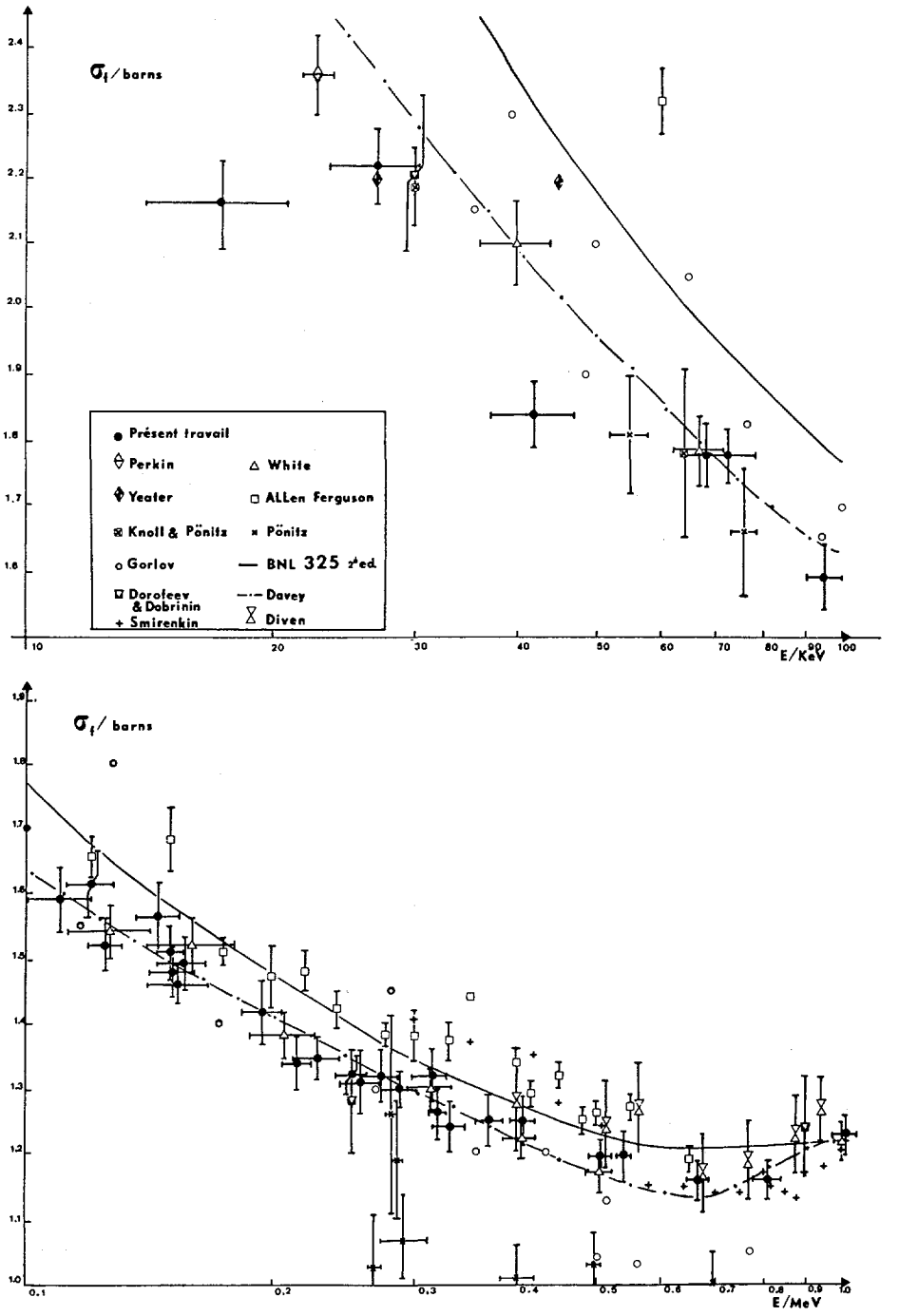

FIG.4. Section efficace de fission du ^{235}U.

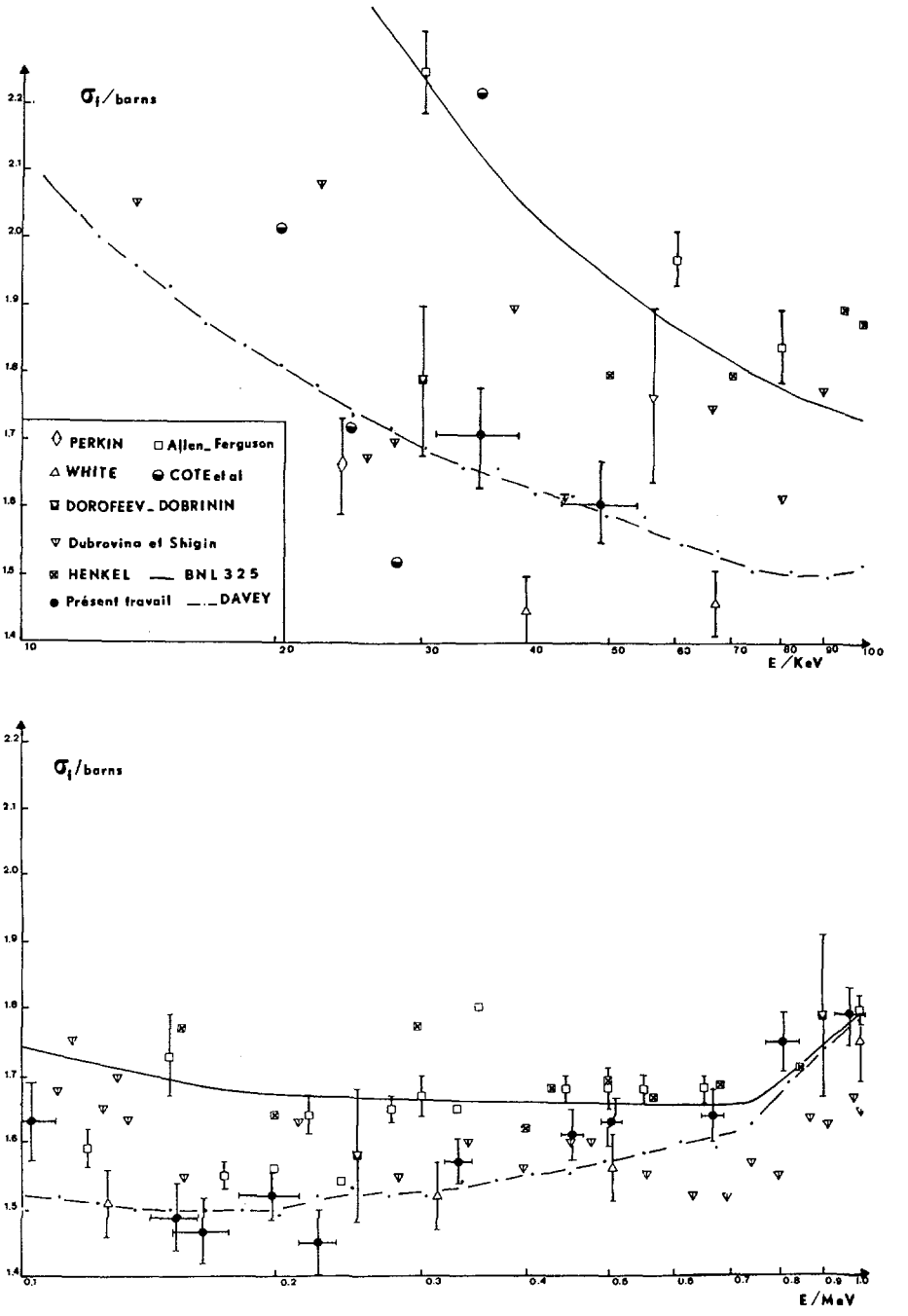

FIG. 5. Section efficace de fission du ^{239}Pu.

TABLEAU II. ERREURS ET CORRECTIONS

	^{235}U, E_n = 68 keV		^{239}Pu, E_n = 506 keV	
	Correction %	Erreur %	Correction %	Erreur %
Nombre d'atomes		1		0,6
Extrapolation du spectre vers l'origine	3	0,5	2	0,4
Pertes de fragments	5,9	0,5	1,7	0,3
Diffusion de neutrons sur les parois de la chambre	0,1	0,1	0,5	0,5
Distance	0,9	0,3	0,9	0,3
Bruit de fond de la chambre	9	0,7	3	0,3
Statistique		1,13		0,5
Efficacité du BF_3		1,8		2
Atténuation due à l'air	7	0,5	6	0,5
Total		2,7		2,4

Le problème soulevé par l'existence de grandes fluctuations mérite une attention particulière. Dans le tableau I sont indiqués, en même temps que les énergies moyennes, les épaisseurs des cibles utilisées, les angles et les résolutions angulaires. Ces grandeurs serviront à calculer la fonction de résolution qui sera utilisée ultérieurement dans une analyse plus détaillée des mesures dans ce domaine d'énergie.

REMERCIEMENTS

Les auteurs remercient tout particulièrement M. P.H. White pour avoir mis à leur disposition les chambres à ^{235}U et leur avoir donné de précieux renseignements, ainsi que MM. K.F. Lauer et V. Verdingh, du BCMN (Geel), pour la préparation et l'étalonnage des dépôts de plutonium.

Les auteurs remercient également MM. R. Sher (Stanford University) et Ph. Quentin pour la collaboration efficace qu'ils leur ont apportée durant ces mesures, M. Riou pour la fabrication des chambres à ^{239}Pu, M. M. Culot pour les études mécaniques, M. E. Pomelas pour le travail de documentation et l'équipe «Machine» pour la conduite du Van de Graaff, et M. J.Y. Tocquer pour les essais faits avec l'accélérateur Sames de 300 keV.

REFERENCES

[1] ALLEN, W.D., FERGUSON, A.T.G., Proc. phys.Soc.Lond. A70 (1957) 575.
[2] DIVEN, B.C., Phys. Rev. 105 (1957) 1350.
[3] DOROFEEV, G.A., DOBRININ, Y.P., J.nucl.Energy II 5 (1957) 217.
[4] GORLOV, G.V., et al., J.nucl.Energy A 12 (1960) 79.
[5] PERKIN, J.L., et al., J.nucl.Energy A/B 19 (1965) 423.
[6] WHITE, P.H., J.nucl.Energy A/B 19 (1965) 325.
[7] POENITZ, W.P., Neutron Cross Sections and Technology (Proc. Conf. Washington, 1968) I, NBS Special Publication 299 (1968) 503.
[8] LEROY, J.L., et al., «Développement des méthodes de mesure absolue des flux de neutrons rapides dans la gamme de 10 keV à 1 MeV», ces comptes rendus, IAEA-CN-26/70.
[9] Rapport EANDC(E) 115 "U" (mars 1968) 161.
[10] FLEMMING, E.H., GHIORSO, A., CUNNINGHAM, B.B., Phys.Rev. 88 (1952) 642.
[11] KEINBERGER, C.H., Phys.Rev. 87 (1952) 520.
[12] LAUER, K.F., VERDINGH, V., Nucl. Instrum. Meth. 21 (1963) 161.
[13] SPERNOL, A., LERCH, O., Nucl.Instrum.Meth. 32 (1965) 283-99.
[14] WALLMANN, J.C., UCRL (avril 1951).
[15] LANGSDORF, A.S., LANE, R.O., MONAHAN, J.E., Phys. Rev. 72 (1947) 673.
[16] POENITZ, W.P., Nucl. Instrum. Meth. 58 (1968) 39.
[17] MARQUETTE, J.P., SZABO, I., Rapport DRP/SMNF n° 17 (1970).
[18] KNOLL, G.F., PÖNITZ, W.P., J.nucl.Energy A/B 21 (1967) 643.
[19] WHITE, P.H., HODGKINSON, J.G., WALL, G.J., «Measurement of fission cross-sections for neutrons of energies in the range 40-500 keV», Physics and Chemistry of Fission (C.r. Coll. Salzbourg 1965) I, AIEA, Vienne (1965) 219.
[20] WHITE, P.H., WARNER, J.P., J.nucl.Energy A/B 21 (1967) 671.
[21] DAVEY, W.G., Nucl.Sci.Engng 26 (1966) 149; id. 32 (1967) 35.
[22] HAVENS, W.W. Jr., Communication privée.
[23] HENKEL, R.L., LA-2114 (1957).
[24] DUBROVINA, S.M., SHIGIN, V.A., Dokl. Akad.Nauk SSSR 157 (1964).
[25] COTÉ, R.E., et al., Bull. Am. phys.Soc. 2 1 (1956) 187.
[26] SMIRENKIN, G.N., et al., Atomn.Energ. 13 (1962) 974.
[27] YEATER, M.L., et al., KAPL-1109 (1954).

DEVELOPPEMENT DES METHODES DE MESURE ABSOLUE DES FLUX DE NEUTRONS RAPIDES DANS LA GAMME DE 10 keV A 1 MeV

J.L. LEROY, J.L. HUET, I. SZABO, E. FORT
CEA, Centre d'études
nucléaires de Cadarache,
France

Abstract — Résumé

DEVELOPMENT OF METHODS FOR THE ABSOLUTE MEASUREMENTS OF FAST NEUTRON FLUXES IN THE RANGE OF 10 keV TO 1 MeV.

The absolute measurement of a neutron flux is a necessary stage in the determination of all the reaction cross-sections. In the energy range of 10 keV to 1 MeV precise flux measurements are difficult. To provide a sound basis for cross-section measurements in their laboratory, the authors made a systematic comparison between the following monokinetic flux measurement techniques: the associated-particle method with neutrons produced by the $T(p, n)^3He$ reaction, using both the coincidence variant and the absolute counting variant for ^3He-particles; the manganese sulphate bath method in combination with a collimator for neutron selection; the method based on the use of recoil proton proportional counter. Since this comparative study was carried out over a fairly extended period, these different methods have been applied successively for the calibration of the same measurement instrument, the stability of which with time was carefully verified. This instrument consists of a BF_3-counter assembly in a paraffin block; it is fitted with a collimator for selecting the neutrons for measurement and a shield to eliminate the background due to scattered neutrons. The efficiency of this apparatus is virtually independent of energy. Calculations were made by the Monte-Carlo method. Overall the theoretical and measurement results are in good agreement. The authors consider this instrument capable at the present time of measuring neutron fluxes to an accuracy of ±2% within the energy range 10 keV to 1 MeV.

DEVELOPPEMENT DES METHODES DE MESURE ABSOLUE DES FLUX DE NEUTRONS RAPIDES DANS LA GAMME DE 10 keV A 1 MeV.

La mesure absolue d'un flux de neutrons est une étape nécessaire à l'obtention de toutes les sections efficaces de réaction. Dans le domaine d'énergie de 10 keV à 1 MeV, les mesures de flux précises sont difficiles. Pour donner une base solide aux mesures de sections efficaces faites dans leur laboratoire, les auteurs ont fait une comparaison systématique des méthodes de mesure de flux monocinétiques suivantes: la particule associée avec la réaction $T(p, n)^3He$, utilisée en version coïncidence et en version comptage absolu des particules ^3He; la cuve de sulfate de manganèse, couplée avec un collimateur de prélèvement des neutrons; le compteur proportionnel à protons de recul. Comme ce travail de comparaison a été échelonné sur un temps assez long, ces différentes méthodes ont été appliquées successivement à la calibration d'un même instrument de mesure dont la stabilité dans le temps a été soigneusement vérifiée. Cet instrument est un assemblage de compteurs à BF_3 dans un bloc de paraffine; il est équipé d'un collimateur pour prélever les neutrons à mesurer, et d'une protection destinée à éliminer le bruit de fond dû aux neutrons diffusés. L'efficacité de ce dispositif est pratiquement indépendante de l'énergie. Elle a été calculée par la méthode de Monte-Carlo. L'ensemble des résultats de calcul et de mesure est en bon accord. Les auteurs estiment que ce dispositif permet actuellement de mesurer les flux de neutrons avec une erreur inférieure à ±2% dans le domaine d'énergie compris entre 10 keV et 1 MeV.

1. INTRODUCTION

Pour obtenir la plupart des sections efficaces des réactions induites par les neutrons, il est nécessaire de procéder à une mesure absolue du flux des neutrons incidents. La difficulté de faire cette mesure avec précision a été soulignée à plusieurs reprises [1, 2].

Pour pouvoir garantir une précision meilleure que ±2% dans cette gamme d'énergie, il est indispensable de mesurer le même flux par différentes méthodes absolues indépendantes, et de vérifier qu'elles sont en accord dans la limite des erreurs prévues pour chacune. De cette façon, on réduit fortement la probabilité d'une erreur systématique importante.

Nous avons employé les méthodes suivantes:
- la particule associée avec la réaction $T(p, n)^3He$,
- la cuve de sulfate de manganèse, calibrée au moyen d'une source de Ra-Be étalonnée par le BIPM,
- le compteur proportionnel à protons de recul.

Comme ce travail de comparaison a été échelonné sur un temps assez long, les différentes méthodes absolues ont été appliquées successivement à la calibration d'un même instrument de mesure dont la stabilité dans le temps a été soigneusement vérifiée. Cet instrument, qui a déjà été décrit [3, 4], était un assemblage de compteurs à BF_3 dans la paraffine. Cet appareil, que nous appellerons par la suite «compteur directionnel», a été construit en plusieurs versions qui diffèrent principalement par la distance entre les compteurs.

2. METHODE DE LA PARTICULE ASSOCIEE

Quand on utilise la réaction $T(p, n)^3He$ pour produire les neutrons, on peut obtenir ceux-ci dans une gamme d'énergie allant de 100 keV à 1, 5 MeV tout en détectant des particules ^3He d'une énergie supérieure à 0, 8 MeV. Ces particules doivent être détectées dans une direction faisant avec le faisceau incident un angle compris entre 10° et 45°. Dans ces conditions, il est nécessaire que le support de la cible tritiée soit assez mince pour être traversé par le faisceau de protons incident. De plus, il est indispensable de pouvoir trier correctement les particules ^3He parmi les protons et tritons diffusés qui sont également émis par la cible, et qui sont beaucoup plus nombreux que les ^3He aux petits angles. Nous utilisons pour cela un analyseur qui combine un champ électrique et un champ magnétique [5]. On peut alors procéder de deux façons différentes:

2. 1. Mesure de l'efficacité d'un détecteur par coïncidence entre neutrons et ^3He

On enregistre d'une part ces coïncidences et d'autre part le nombre total de particules ^3He. Le rapport de ces deux nombres donne l'efficacité du détecteur de neutrons, à condition que celui-ci soit placé de façon à être traversé par les neutrons associés aux particules ^3He détectées. Il faut de plus que l'efficacité du détecteur de neutrons soit indépendante de la position du point d'entrée du neutron dans le détecteur. Avec un scintillateur de verre au ^6Li en forme de disque, la première condition

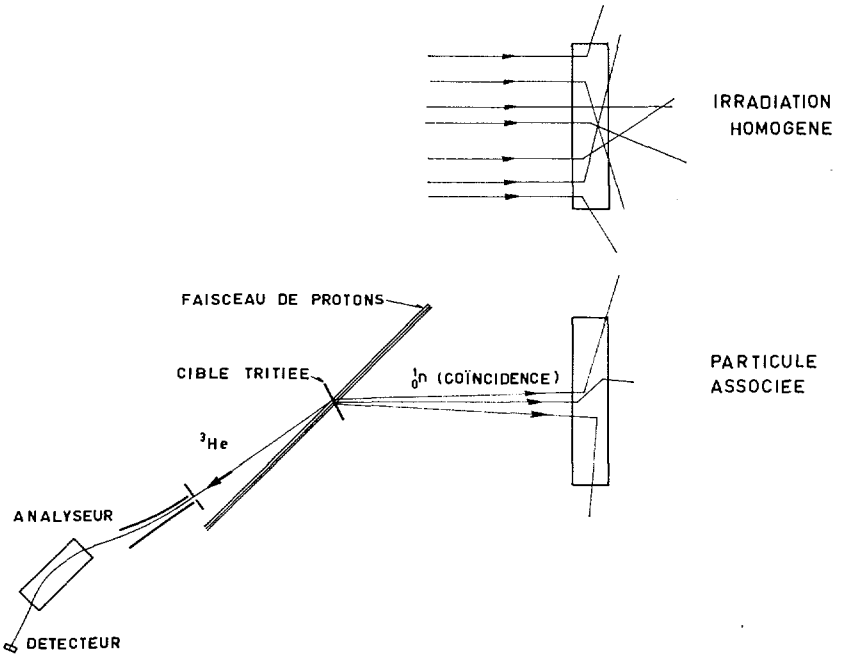

FIG. 1. Principe de la mesure d'efficacité par la méthode de la particule associée, et effet de la diffusion des neutrons dans le scintillateur.

est facile à réaliser, bien que la diffusion coulombienne multiple des ^{3}He dans la cible tritiée provoque un léger élargissement du cône des neutrons associés. La seconde condition n'est pas rigoureusement vérifiée à cause de la diffusion multiple des neutrons dans le verre; la figure 1 illustre cet effet. Si on veut utiliser les mesures d'efficacité faites par coïncidence pour mesurer un flux de neutrons qui est distribué de façon uniforme sur la face plane du disque, il faut appliquer une correction, qui peut être calculée par la méthode de Monte-Carlo [6]. La mesure de coïncidence a été faite sur un scintillateur NE 905 de 9,5 mm d'épaisseur et 44 mm de diamètre, puis ce scintillateur a été comparé dans un flux quasi parallèle avec le compteur directionnel. La figure 2 donne l'efficacité de la version n° 1 de ce compteur, déduite de ces deux mesures et affectée de la correction de diffusion multiple qui varie entre 3 et 10%.

2.2. Mesure du flux par comptage absolu des particules ^{3}He dans un angle solide défini

Cette façon de procéder, qui a également été utilisée par d'autres auteurs avec la réaction $T(p,n)^{3}He$ [7], permet de mesurer directement le flux de neutrons et de tourner la difficulté signalée au paragraphe précédent, au sujet de la définiton de l'efficacité du détecteur. De plus, elle met en œuvre un appareillage électronique plus simple et la suppression des coïncidences conduit à des taux de comptage beaucoup plus importants. En

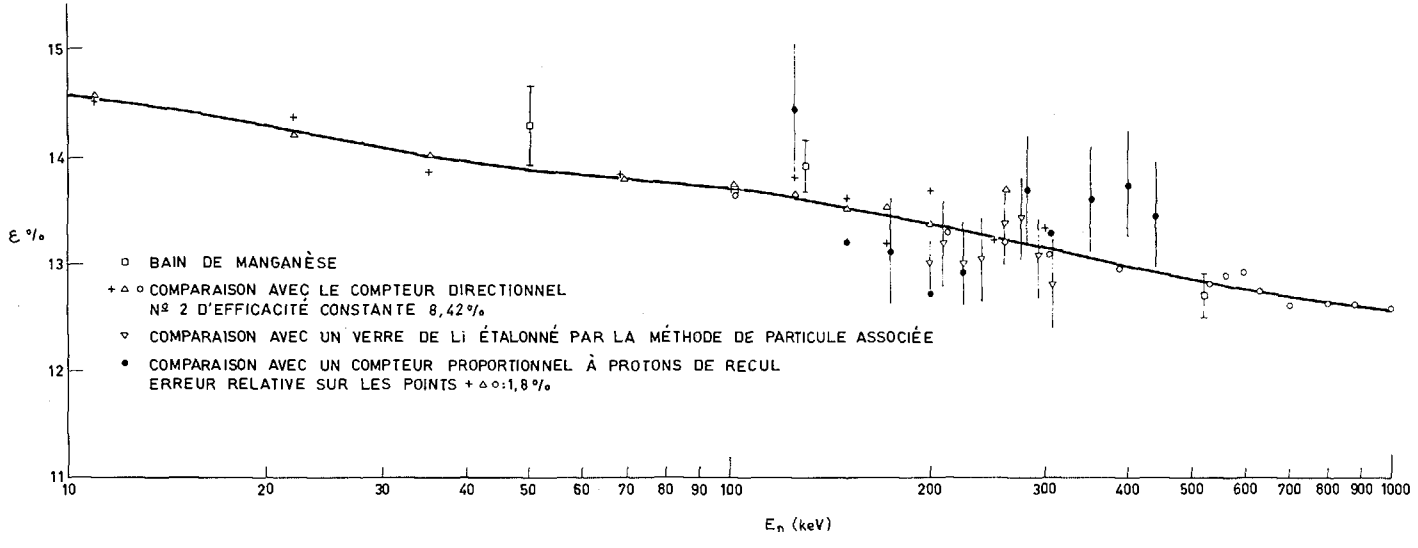

FIG. 2. Efficacité du compteur directionnel (version n° 1).

revanche, l'analyseur de particules chargées est soumis à des exigences plus sévères puisqu'il doit non seulement éliminer les particules qui ne sont pas des ^{3}He, mais il doit aussi ne perdre aucune de celles-ci. Les causes principales de pertes de particules dans l'analyseur sont:

- la dispersion angulaire des particules,
- leur dispersion en énergie,
- le phénomène d'échange de charge dans la cible qui fait que certaines particules ^{3}He émergent avec un ou deux électrons, et par conséquent ne suivent pas les mêmes trajectoires dans l'analyseur,
- les défauts d'alignement éventuels de l'analyseur.

Pour éviter ces pertes, l'analyseur électromagnétique [5] utilisé dans l'expérience de coïncidence a été transformé de la manière suivante:

– La résolution angulaire du collimateur précédant l'analyseur a été augmentée. De plus le bruit de fond de protons, qui provenait principalement de la diffusion sur les bords du diaphragme de définition, a été éliminé grâce à un second diaphragme, un peu plus large que le premier, placé juste avant l'analyseur électrostatique.

– La déflexion due au champ magnétique est double et de signe opposé à celle due au champ électrique; de la sorte, le système peut accepter sans perte de comptage une dispersion en énergie d'un facteur 2 environ. Le spectre d'énergie des impulsions fournies par le détecteur est donné par la figure 3. On peut voir que la contamination par d'autres particules est négligeable. Dans les conditions les plus sévères, c'est-à-dire lorsqu'on

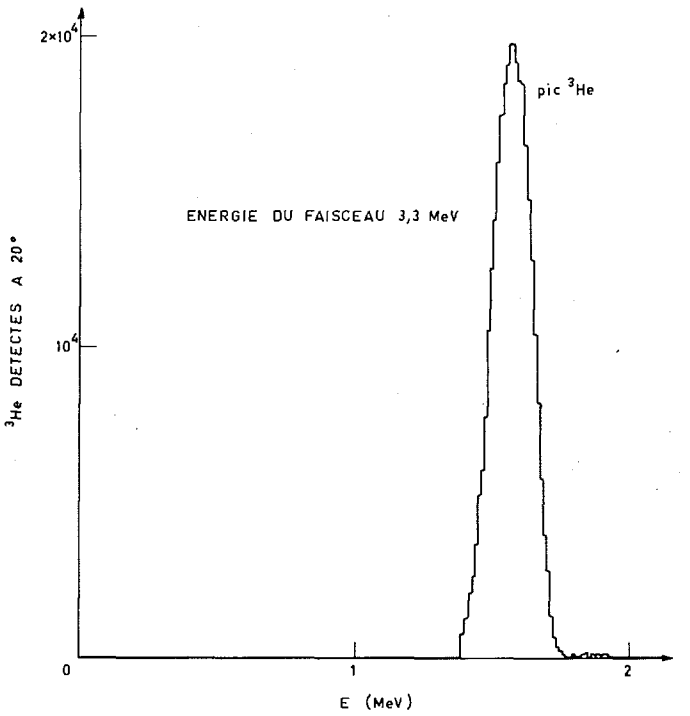

FIG. 3. Spectre d'énergie des particules ^{3}He.

détecte les particules ^3He à un angle de 10° par rapport au faisceau incident, le bruit de fond, mesuré avec une cible non tritiée, est inférieur à 1% du comptage ^3He.

– On peut tenir compte des $^3He^+$ en faisant une mesure séparée dans laquelle on multiplie par 2 les champs électrique et magnétique de l'analyseur. On trouve ainsi que la contribution des $^3He^+$ est de 12% des $^3He^{2+}$ pour une énergie moyenne de 1,3 MeV. Il n'est pas possible de mesurer les ^3He neutres avec ce dispositif, mais leur contribution est très faible.

– L'alignement des différents diaphragmes du collimateur et des analyseurs a été soigneusement vérifié, et les pertes de comptage dues à des défauts résiduels sont en principe négligeables.

Des mesures d'efficacité du compteur directionnel n°1 ont été faites pour des énergies comprises entre 450 et 800 keV. Les valeurs ainsi obtenues sont supérieures de 4 à 5% à celles qui proviennent de la cuve de manganèse, bien que la marge d'erreur calculée soit de ±2%. L'origine de ce désaccord n'est pas encore très claire.

3. UTILISATION DE LA CUVE DE SULFATE DE MANGANESE

La technique de la cuve de sulfate de manganèse est utilisée dans de nombreux laboratoires pour la mesure absolue des sources radioactives. La calibration de la même source par 14 laboratoires différents utilisant cette technique avait donné des résultats cohérents à 1% près [8], ce qui donne une idée de la précision qu'on peut en attendre. Nous avons adapté cette méthode à la mesure des flux neutroniques produits par une source quasi ponctuelle. Le dispositif est représenté à la figure 4. L'expérience consiste en fait à mesurer l'efficacité absolue du compteur directionnel.

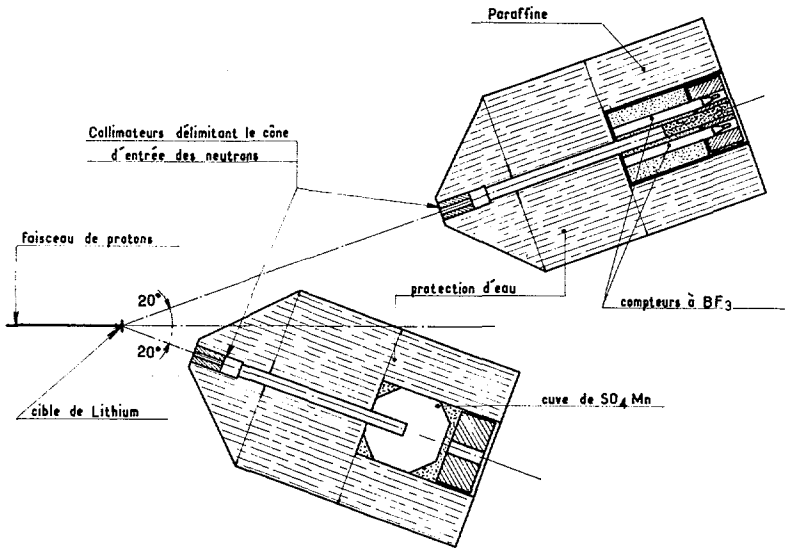

FIG. 4. Mesure de l'efficacité du compteur directionnel par la méthode du bain de sulfate de manganèse.

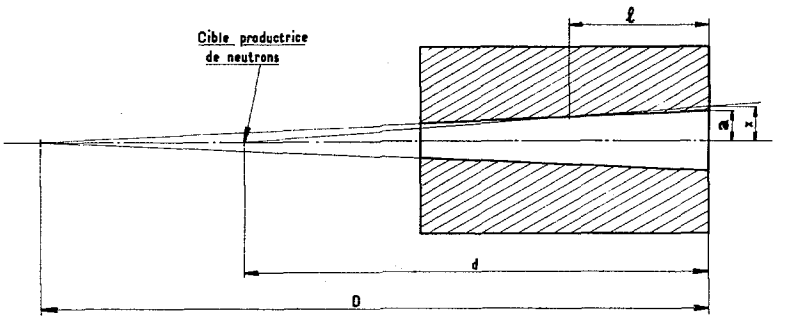

FIG. 5. Collimateur de définition du flux de neutrons, utilisé avec le compteur directionnel.

Dans les deux appareils, l'angle solide utile est limité par un collimateur de polyéthylène ou de plexiglas, représenté à la figure 5. Les dimensions du système sont choisies de manière telle que tout neutron qui part de la source et traverse le trou du collimateur va jusqu'au fond du puits. Toutefois, certains neutrons peuvent traverser une partie de la paroi du collimateur sans subir de choc, et continuer leur route jusqu'au fond du puits. On peut, avec une bonne approximation, tenir compte de cet effet en multipliant la surface du trou du collimateur par le facteur

$$f = 1 + 2\lambda\left|\frac{1}{D} - \frac{1}{d}\right|$$

λ est le libre parcours moyen des neutrons dans le matériau constituant le collimateur, d et D sont des paramètres géométriques définis par la figure 5. Le flux cherché est égal au nombre de neutrons détectés divisé par la surface corrigée du trou du collimateur. Les neutrons qui sont parvenus au fond du puits sont ralentis et capturés dans la solution. Une légère correction est nécessaire pour tenir compte de ceux qui sont capturés dans la paroi métallique du puits, et de ceux qui sortent de la sphère. Cette correction a été déterminée par un calcul de Monte-Carlo; dans tous les cas utiles, elle est inférieure à 4%. Le calcul de ces corrections est exposé avec plus de détails dans une publication récente [4]. La solution active est soutirée et brassée énergiquement en fin d'irradiation dans une cuve qui comporte un puits contenant un scintillateur NaI servant à mesurer l'activité de la solution. L'étalonnage du détecteur a été fait en mesurant l'activité de la solution après une irradiation faite dans une sphère de 90 cm de diamètre au moyen d'une source de Ra-Be de 100 mCi; calibrée par le BIPM. Cette façon de procéder élimine la nécessité de connaître la teneur exacte en manganèse de la solution, et de faire la mesure absolue de l'activité de la solution. Les mesures d'activité de la solution activée au moyen de la source sont reproductibles à 0,2% près. Si on admet l'erreur de 1,1% donnée pour la calibration de la source par le BIPM, on arrive, en tenant compte de toutes les causes d'erreur vraisemblables, à une erreur de ± 1,80% pour la mesure du flux neutronique.

La méthode a été appliquée successivement à plusieurs versions du compteur directionnel. Avec la version n°2, qui est caractérisée par un écartement des compteurs de 17 cm au lieu de 13 cm pour les versions

n° 1 et n° 3, on a fait 14 mesures entre 20 keV et 1 MeV. Aucune variation systématique en fonction de l'énergie n'a pu être mise en évidence, et il est possible de prendre pour l'efficacité la valeur 0,0842 ± 0,0014 dans tout ce domaine d'énergie. Quelques mesures ont été faites avec la version n° 1: elles sont représentées sur la figure 2 avec les résultats d'une comparaison entre ces deux versions du compteur directionnel.

4. COMPTEUR PROPORTIONNEL A PROTONS DE RECUL

Grâce à la collaboration de MM. Liskien et Paulsen, du BCMN, nous avons pu utiliser un compteur construit par eux d'après les travaux de Skyrme et al. [9] et White [10]. Une première comparaison a été faite dans le domaine d'énergie allant de 100 keV à 450 keV auprès du Van de Graaff de Geel, entre le compteur proportionnel et le scintillateur de verre au ^{6}Li déjà étalonné par la méthode de la particule associée. Compte tenu des marges d'erreur, les deux méthodes sont en bon accord, principalement entre 180 et 300 keV. En dessous de 180 keV et au-dessus de 350 keV, le compteur proportionnel donne des valeurs légèrement supérieures, ce qui est peut-être dû à une estimation imparfaite du bruit de fond du scintillateur dans l'expérience de comparaison. Une deuxième comparaison a été faite à Cadarache entre le compteur proportionnel et le compteur directionnel dans le domaine d'énergie allant de 800 keV à 2 MeV. Dans toutes ces mesures, le spectre expérimental des protons de recul n'avait pas exactement la même forme que le spectre théorique qui sert au calcul du flux. Ceci introduisait une erreur de ± 3%. L'incertitude totale était de ± 4%.

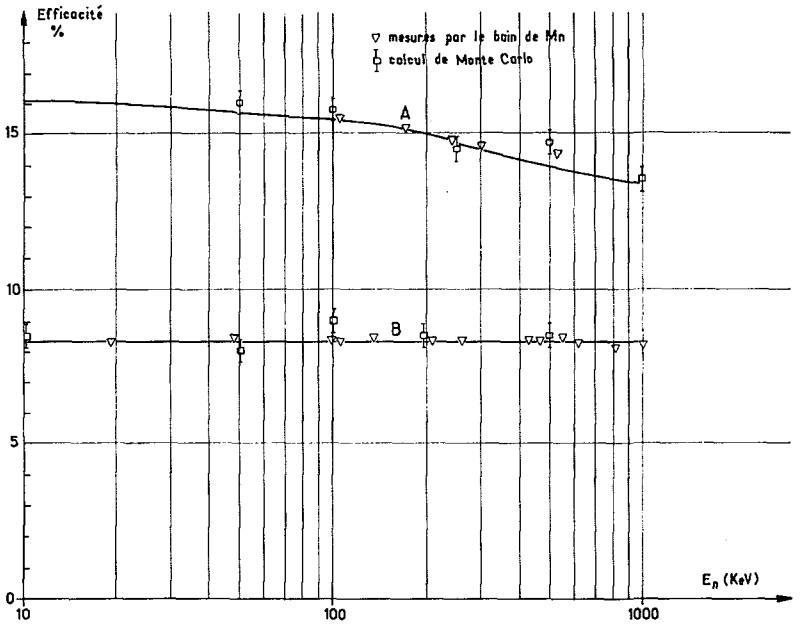

FIG. 6. Efficacité des compteurs directionnels n° 2 (A) et n° 3 (B) calculée par la méthode de Monte-Carlo.

5. CALCUL DIRECT DE L'EFFICACITE DU DETECTEUR DIRECTIONNEL PAR LA METHODE DE MONTE-CARLO [4]

Cette méthode de calcul est particulièrement commode dans ce cas à cause des cavités importantes constituées par le puits d'arrivée des neutrons et les trous des compteurs. Le résultat de ce calcul est donné à la figure 6 pour deux versions de l'appareil. Dans la version n° 2, l'écartement des compteurs est de 17 cm, dans la version n° 3, l'écartement est de 13 cm. Les autres dimensions sont inchangées. On voit qu'il existe un accord excellent avec les valeurs mesurées de l'efficacité. Ceci nous permet d'affirmer que les corrections de pertes de neutrons calculées pour la cuve de SO_4Mn au moyen d'un code tout à fait similaire n'introduisent pas d'erreur appréciable.

6. COMPARAISON DE CES DIFFERENTES METHODES

Dans l'état actuel des choses, la méthode du bain de sulfate de manganèse est la plus précise, et elle donne des résultats utilisables à partir de 10 keV et jusqu'à 2 MeV, avec une marge d'erreur estimée à ± 1, 8%. Pour appliquer la méthode à des énergies plus élevées, il faudrait dans doute augmenter le diamètre de la sphère.

La méthode de la particule associée en version coïncidence a permis l'étalonnage d'un scintillateur de verre au ^6Li, dans un domaine d'énergie plus réduit, mais la variation très rapide de la section efficace de la réaction $^6Li(n, \alpha)T$ en fonction de l'énergie introduit une erreur supplémentaire qui limite la précision de la mesure de flux ainsi faite à ± 3%. L'utilisation du compteur proportionnel à protons de recul a fourni des résultats moins reproductibles que ce qu'on pouvait espérer d'après les travaux faits ailleurs [10]. Néanmoins, ces deux dernières méthodes sont en accord avec la méthode du bain de manganèse dans la limite des erreurs inventoriées, ce qui laisse espérer qu'aucune erreur systématique importante n'est passée inaperçue.

La méthode de la particule associée en version comptage absolu n'est pas encore parfaitement au point, mais elle semble particulièrement séduisante par la rapidité des mesures qu'elle permet et la simplicité de sa mise en œuvre. Il ne paraît pas déraisonnable d'espérer atteindre prochainement par cette méthode une précision meilleure que ± 2%.

REMERCIEMENTS

Les auteurs remercient le BIPM, et en particulier M. Naggiar, d'avoir bien voulu se charger de l'étalonnage de la source de Ra-Be qui a servi de référence dans ce travail. Ils remercient également MM. Paulsen et Liskien, du BCMN (Geel), pour le prêt du compteur proportionnel à protons de recul, et pour leur aide dans l'interprétation des résultats obtenus au moyen de cet appareil.

REFERENCES

[1] Symposium on the absolute determination of the neutron flux in the energy range of 1 to 100 keV, EANDC-"33 V" (1963).
[2] INTERNATIONAL ATOMIC ENERGY AGENCY, Nuclear Standards for Neutron Measurements, IAEA-107, IAEA, Vienna (1968).
[3] LEROY, J.L., HUET, J.L., SZABO, I., LE RIGOLEUR, C., ABRAMSON, D., Revue Phys. appl. 4 (1969) 251.
[4] LEROY, J.L., HUET, J.L., GENTIL, J., à paraître.
[5] FORT, E., LEROY, J.L., à paraître dans Nucl. Instrum. Meth.
[6] FORT, E., á paraître.
[7] LISKIEN, H., PAULSEN, A., Nucl. Instrum. Meth. 69 (1969) 70.
[8] NAGGIAR, V., Rapport interne BIPM (27 février 1967).
[9] SKYRME, H.R., TONNICLIFFE, P.R., WARD, W.G., Rev. scient. Instrum. 23 (1952) 209.
[10] WHITE, P.H., J. nucl. Energy 19 (1965) 325.

SECTION EFFICACE DE LA REACTION $^{6}Li(n, \alpha)T$ DANS LA GAMME D'ENERGIE COMPRISE ENTRE 100 keV ET 500 keV

E. FORT
CEA, Centre d'études
nucléaires de Cadarache,
France

Présenté par J.L. Leroy

Abstract — Résumé

CROSS-SECTION OF THE $^{6}Li(n, \alpha)T$ REACTION IN THE 100-500 keV ENERGY RANGE.

The cross-section for the $^{6}Li(n, \alpha)T$ reaction is determined from the efficiency of a ^{6}Li glass scintillator measured by a coincidence-version associated particle method, for which a description is also given. The number of ^{6}Li atoms contained in the scintillator was determined by two methods of nuclear analysis: (a) By comparison with a glass whose ^{6}Li-content was calculated on the basis of a measurement of total absorption of thermal neutrons made in the ZOE reactor by the phase oscillation method; (b) a transmission method. In both cases it is assumed that the cross-section for the reaction at 2200 m/s is known. The multiple diffusion of the neutrons in the special case of the experiment was determined by a Monte-Carlo calculation.

SECTION EFFICACE DE LA REACTION $^{6}Li(n, \alpha)T$ DANS LA GAMME D'ENERGIE COMPRISE ENTRE 100 keV ET 500 keV.

La section efficace de la réaction $^{6}Li(n, \alpha)T$ est déduite de l'efficacité d'un scintillateur au verre de ^{6}Li mesurée par une méthode de particule associée, version coïncidence, qui est exposée ailleurs. Le nombre d'atomes de ^{6}Li contenus dans le scintillateur a été déterminé par deux méthodes d'analyse nucléaire: a) une méthode de comparaison avec un verre dont la teneur en ^{6}Li a été calculée à partir d'une mesure d'absorption totale des neutrons thermiques faite dans la pile Zoé par la méthode d'oscillation de phase; b) une méthode de transmission. Dans les deux cas, on suppose connue la section efficace de la réaction à 2200 m/s. La diffusion multiple des neutrons dans le cas particulier de l'expérience est obtenue par un calcul de Monte-Carlo.

1. INTRODUCTION

Considérons un matériau dont la composition est à base de ^{6}Li.

Si N désigne la concentration en ^{6}Li évaluée en nombre d'atomes par cm^3 et $\sigma(E)$ la section efficace de la réaction $^{6}Li(n, \alpha)T$ à l'énergie E, la probabilité de réaction (n, α) pour un neutron de cette énergie sur un parcours élémentaire $d\ell$ s'exprime par:

$$p = 1 - e^{-N \sigma(E)\, d\ell} \qquad (1)$$

Une relation semblable exprime l'efficacité $\epsilon(E)$ d'un scintillateur NE 905 d'épaisseur δ pour des neutrons incidents, parallèles, monocinétiques d'énergie E

$$\epsilon(E) = 1 - e^{-N \sigma(E)\, \delta} \qquad (2)$$

Cette relation, qui exprime que tous les neutrons ont la même probabilité d'être détectés, reste valable tant que la probabilité de diffusion par choc élastique ou non reste tout à fait négligeable.

Cette condition n'est satisfaisante, par suite des valeurs des sections efficaces macroscopiques des éléments constituant le verre, que pour de très faibles valeurs de δ, donc de $\epsilon(E)$.

S'il était possible de réaliser une expérience où les conditions idéales énoncées plus haut seraient respectées, il serait possible d'obtenir directement la valeur de la section efficace $\sigma(E)$ de la valeur expérimentale de l'efficacité par la relation

$$\sigma(E) = \frac{1}{N\delta} \log \frac{1}{1 - \epsilon(E)} \tag{3}$$

Dans la réalité on est conduit à utiliser un scintillateur épais et des neutrons issus d'une cible et qui, de ce fait, ne sont ni tout à fait monocinétiques ni parallèles.

Il en résulte des corrections à apporter à la relation (3) qui doivent être calculées de façon aussi précise que possible.

Désignons par un terme unique $F(E)$ l'ensemble de ces corrections.

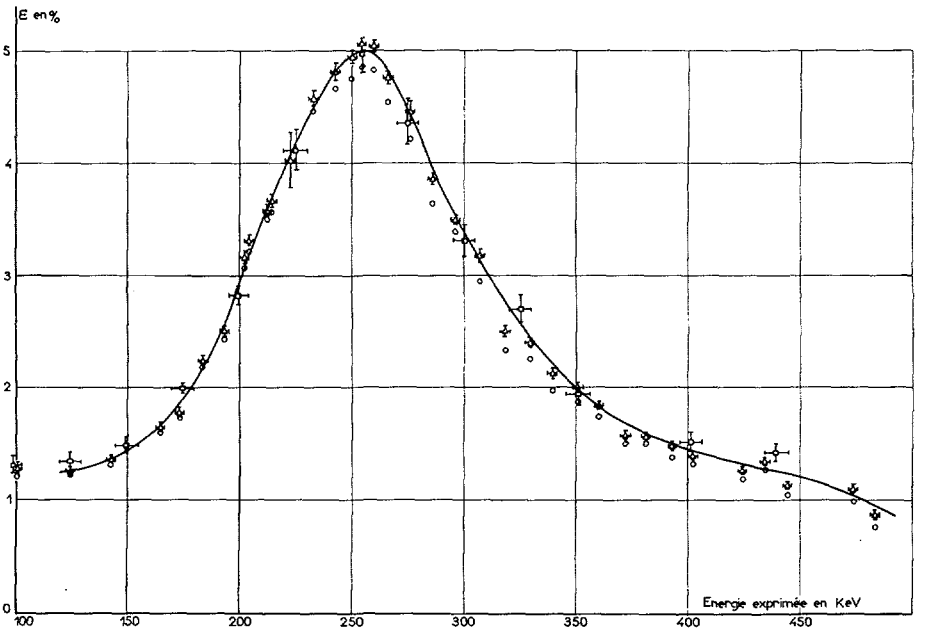

FIG. 1. Valeurs expérimentales de l'efficacité d'un scintillateur NE 905 (diamètre 4,44 cm, épaisseur 0,96 cm) mesurées par une expérience de particule associée en réaction $p(T, n)^3He$

△ particules associées, résultats corrigés.

□ compteur proportionnel à protons de recul.

○ particules associées, résultats bruts.

L'expérience choisie est une expérience de particule associée, version coïncidence, en réaction p(T, n)^{3}He, décrite en détail ailleurs [1].

Elle consiste à détecter à un angle «avant» les particules ^{3}He par un détecteur solide, et les neutrons associés, en coïncidence, par un détecteur de verre au ^{6}Li NE 905, relativement épais (9,5 mm).

L'efficacité $\epsilon(E)$, à caractère absolu, est égale au rapport du nombre de coïncidences sur le nombre des ^{3}He comptés dans le même temps (fig. 1).

Les corrections concernent:

- la diffusion coulombienne multiple des ^{3}He dans la cible avant leur émission; cette correction est spécifique de la nature de l'expérience;
- la diffusion multiple des neutrons dans le scintillateur; cette correction traduit le fait que le verre est épais, elle est fonction de l'énergie des neutrons et de la section efficace $\sigma(E)$ cherchée.

$F(E)$ est donc une fonction implicite de $\sigma(E)$; $F(E) \equiv F(\sigma(E))$. Pour les conditions expérimentales choisies l'expression (3) doit s'écrire:

$$\sigma(E) = \frac{1}{N\delta} \log \frac{1}{1 - \frac{\epsilon(E)}{F(\delta(E))}} \qquad (4)$$

On voit que la section efficace de réaction ^{6}Li(n, α)T ne pourra être tirée des valeurs expérimentales de l'efficacité du scintillateur que par itération à partir de valeurs des sections efficaces choisies au départ. En l'occurrence, celles-ci étaient celles publiées par Schwarz et al. [2].

2. CORRECTIONS - CALCUL DU FACTEUR CORRECTIF $F(\sigma(E))$

L'étude de ces corrections a fait l'objet d'une publication [3]. Le calcul par une méthode de Monte-Carlo se fait en simulant l'histoire du neutron depuis sa création jusqu'à son absorption éventuelle dans le scintillateur par réaction (n, α).

La diffusion coulombienne des particules ^{3}He à l'intérieur de la couche tritiée dévie légèrement les particules, si bien que celles qui sont comptées par le détecteur solide sont émises au moment de la réaction neutronigène dans une direction légèrement différente. Cette diffusion est affectée par les phénomènes d'échange de charges et par l'importance du trajet des particules à l'intérieur de la cible. Les proportions des trois états de charge $^3He^0$, $^3He^+$, $^3He^{2+}$ ont été mesurées expérimentalement [4] comme des fonctions de l'énergie. De même, la distribution spatiale des atomes de tritium dans la couche tritiée a été déterminée par l'expérience [5].

Le calcul de l'effet de la diffusion multiple coulombienne se fait en tirant successivement au hasard, selon les lois de probabilité propres à la méthode, la position de l'atome de tritium donnant lieu à la réaction, l'état de charge de la particule ^{3}He, son angle de diffusion au cours des chocs coulombiens successifs. On obtient ainsi l'angle d'émission de la particule à sa sortie de la cible. En supposant qu'elle parte dans la direction où elle sera détectée, on peut calculer l'angle que formait sa

direction avec celle du proton incident juste après la réaction qui la produit.

Par application des lois de la cinématique on obtient l'angle d'émission et l'énergie du neutron associé.

Il suffit que le scintillateur soit placé suffisamment près de la cible pour que tous les neutrons associés soient interceptés par lui. Dans le cas de l'expérience de particule associée le scintillateur se trouvait à une distance de 5 cm de la cible.

Il n'y avait donc pas lieu de corriger les valeurs expérimentales de l'efficacité. L'effet de la diffusion coulombienne multiple se réduit alors au fait que les neutrons incidents présentent un spectre angulaire d'incidence et un spectre énergétique autour de l'énergie moyenne E.

La diffusion multiple des neutrons dans le scintillateur a pour résultat d'allonger le parcours des neutrons et d'augmenter ainsi la probabilité de détection, qui n'est plus égale à

$$\bar{p} = 1 - e^{-N\sigma(E)\delta}$$

Soit $\bar{p}$ la moyenne des probabilités de détection des neutrons irradiant le scintillateur. La probabilité de détection d'un neutron est la somme des probabilités de réaction $^6Li(n, \alpha)T$ entre deux chocs successifs; chacune de ces probabilités, qui s'exprime par une relation du type (1), est conditionnée par l'histoire du neutron lors des chocs précédents. Le calcul suivant une méthode de Monte-Carlo se fait en tirant au hasard, selon leurs lois de probabilités propres, la nature du noyau sur lequel aura lieu le choc diffusant, l'angle de diffusion, la longueur de parcours entre deux chocs successifs. Le neutron est considéré comme perdu lorsque son parcours entre deux chocs est plus grand que la distance qui lui reste à parcourir dans le scintillateur ou la photocathode. On a supposé que les seuls processus nucléaires auxquels sont soumis les neutrons sont la réaction $^6Li(n, \alpha)T$ et la diffusion élastique avec perte d'énergie. Pour ce processus, les distributions angulaires retenues sont celles parues dans la littérature [6-8].

3. DETERMINATION DE LA TENEUR EN ^{6}Li DU VERRE NE 905

Le procédé de fabrication du verre NE 905 permet de présumer qu'il peut exister un écart entre la concentration réelle du ^{6}Li et la valeur annoncée par le constructeur, d'où la nécessité d'en faire une détermination aussi exacte et précise que possible.

Pour cela deux méthodes d'analyse nucléaire sont exposées: une méthode «comparative» et une méthode de transmission.

3.1. Méthode comparative

Cette méthode consiste à comparer le scintillateur étudié à un scintillateur de référence ou étalon «secondaire», lui-même étalonné à partir d'un scintillateur de base ou étalon «primaire». La teneur en Li naturel de ce dernier a été calculée par Carre et Vidal [9] à partir d'une mesure d'absorption totale des neutrons thermiques faite dans

la pile Zoé par la méthode d'oscillation de phase. Ceux-ci admettent pour la section efficace d'absorption thermique la valeur de 70,4 barn trouvée par Meadows et Walen [10]. La concentration en Li naturel qu'ils déterminent de cette façon est inférieure de 2% à la valeur donnée par le constructeur. Il en est de même pour la concentration en ^{6}Li.

La comparaison entre scintillateur étudié et scintillateur de référence se fait en les plaçant dans un flux de neutrons de 250 keV et en établissant le rapport de leurs efficacités, chacune corrigée de son facteur de diffusion multiple respectif. L'utilisation pour la comparaison d'une méthode de temps de vol permet par ailleurs de faire la correction de bruit de fond neutronique.

De cette manière la teneur en ^{6}Li a été trouvée par Szabo [11] inférieure de 3% à celle annoncée par le constructeur. Cette valeur paraît vraisemblable à priori. L'erreur est évaluée à 2,5%.

3.2. Méthode de transmission

Cette expérience a été réalisée à Saclay sur l'accélérateur linéaire de 45 MeV. Elle consiste à mesurer la transmission en temps de vol du scintillateur utilisé dans l'expérience de particule associée dans une gamme d'énergie comprise entre quelques eV et une centaine d'eV. La courbe de transmission T(E) en fonction de l'énergie incidente E permet d'obtenir la teneur en ^{6}Li. En effet, désignons par N le nombre d'atomes de ^{6}Li par cm^2, par σ_T la section efficace totale du ^{6}Li, par $\sum_\gamma n_\gamma \sigma_\gamma$ la somme des sections efficaces macroscopiques totales des autres éléments du verre.

$$T(E) = e^{-(N\sigma_T(E) + \sum_\gamma n_\gamma \sigma_\gamma(E))}$$

avec

$$\sigma_T(E) = \sigma_{nn}(E) + \sigma_{n\gamma}(E) + \sigma_{n\alpha}(E)$$

σ_{nn}, $\sigma_{n\gamma}$, $\sigma_{n\alpha}$ sont respectivement les sections efficaces de diffusion élastique, de capture radiative et de réaction (n, α).

Dans le domaine d'énergie qui est celui de l'expérience, σ_{nn} est une constante ainsi que les sections efficaces totales des matériaux autres que le ^{6}Li, tels ^{16}O, ^{27}Al, ^{28}Si.

Il est bien établi maintenant que la section efficace de réaction (n, α) à basse énergie est imputable à une onde s et que la contribution de l'interférence avec une résonance p (à 252 keV) est parfaitement négligeable. Les sections efficaces (n, α) et (n, γ) varient en $1/\sqrt{E}$, mais la seconde représente 0,005% de la première et peut être négligée.

On peut écrire

$$\log T(E) = -N\sigma_T(E) - \sum_\gamma n_\gamma \sigma_\gamma(E) = A + \frac{B}{\sqrt{E}}$$

avec

$$B = - N\sigma_{n\alpha}(E_{th})\sqrt{0,025}$$

et

$$A = - (N\sigma_{nn}(E) + \sum_{\gamma} n_\gamma \sigma_\gamma(E))$$

La constante B permet d'obtenir N à partir de la section efficace de réaction (n, α) à l'énergie thermique $\sigma_{n\alpha}(E_{th})$. Il ressort de la compilation des résultats de Diment et Uttley, de Havens et Rainwater, et de Devaney faite par Spaepen (Paris, 1966) que la valeur à attribuer à $\sigma_{n\alpha}(E_{th})$ est de 945 barn.

Le changement de variable $u = 1/\sqrt{E}$ transforme la courbe log T(E) en une droite log (T(u)) = A + Bu. Cette droite est obtenue à partir des points expérimentaux transformés par une méthode de lissage de moindres carrés.

L'analyse par cette méthode des résultats expérimentaux de Tellier [12] donne une concentration en ^{6}Li inférieure de 4% à celle donnée par le constructeur avec une précision évaluée à 2,6%. Bien que cette valeur concorde à 1% avec la valeur trouvée par Szabo, elle est peu sûre car un effet de diffusion parasite a été mis en évidence pour certaines énergies. Cette expérience sera reprise.

4. DISCUSSION DES CAUSES D'ERREURS

La valeur de la section efficace de la réaction ^{6}Li(n, α)T peut être affectée d'erreurs dont les causes apparaissent soit au niveau de la mesure de l'efficacité, soit au niveau du calcul à partir de cette efficacité.

4.1. Erreurs affectant la mesure de l'efficacité

a) L'erreur statistique est, selon les points, de 1 à 3%.

b) L'erreur provenant d'une contamination des ^{3}He par des protons est considérée comme nulle.

c) L'erreur liée à l'effet de diffusion coulombienne des ^{3}He dans la couche tritiée est également considérée comme nulle. En effet, la distance scintillateur-cible a été prise très inférieure à la distance minimale en dessous de laquelle l'effet a été calculé comme étant nul.

d) Il en est de même pour l'erreur due à une perte affectant les taux de comptage en neutrons.

4.2. Erreurs affectant le calcul de la section efficace de réaction ^{6}Li(n, α) T

Ce sont:

a) L'erreur provenant de l'incertitude sur la correction de diffusion multiple dans le scintillateur. Elle est liée à l'erreur statistique de la méthode de Monte-Carlo et à l'incertitude affectant les mesures expérimentales des distributions angulaires de diffusion des divers constituants. Cette erreur n'a pas été évaluée.

b) L'incertitude sur le nombre d'atomes de ^{6}Li. Elle est de 2,5%. Malheureusement la détermination de ce nombre d'atomes fait intervenir beaucoup de constantes parmi lesquelles la section efficace d'absorption thermique du Li naturel et la composition isotopique de celui-ci.

c) L'erreur affectant la mesure des dimensions géométriques du scintillateur qui, par suite des rugosités présentées par la surface latérale, ne peut être considérée comme inférieure à 0,5%.

d) L'erreur liée à la méthode d'itération. Elle est prise égale à 0,3%.

Au total, l'erreur sur la section efficace est évaluée comme étant comprise entre 2,8 et 4% selon les points de mesure.

5. RESULTATS

La courbe donnant l'évolution du facteur $F(\sigma(E))$ en fonction de l'énergie est représentée sur la figure 2. La figure 3 montre les valeurs de la section efficace pour la réaction $^{6}Li(n, \alpha)T$ qui s'en déduisent par la formule (4). La valeur retenue pour N est

$$16,8 \cdot 10^{21} \text{ atomes par cm}^3$$

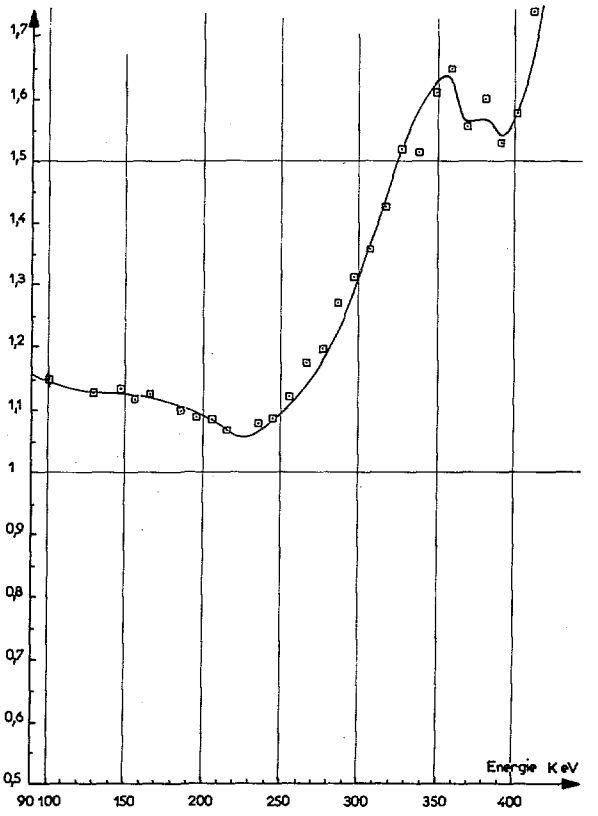

FIG.2. Variation du facteur de correction de diffusion multiple en fonction de l'énergie.

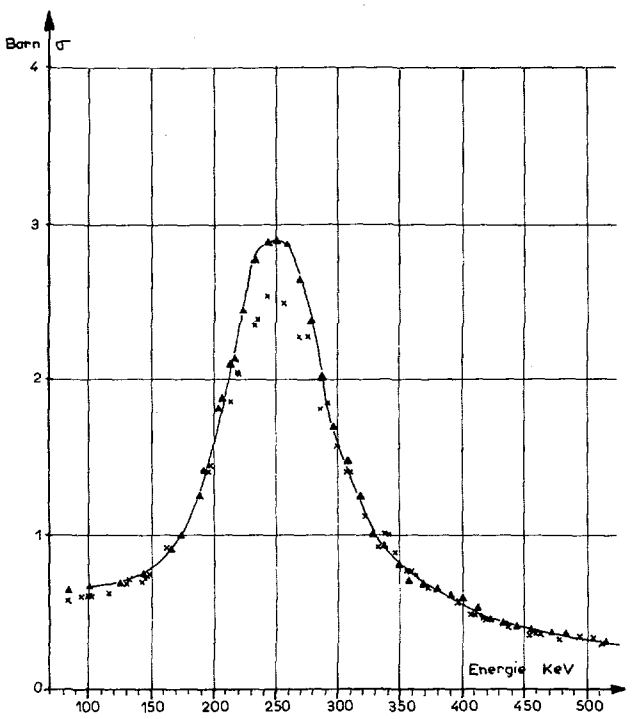

FIG. 3. Section efficace de la réaction $^{6}Li(n, \alpha)T$
X Schwarz et al., Δ présent travail.

Ces deux courbes sont obtenues par itération. Celle-ci a été arrêtée lorsque, d'un passage au suivant, les valeurs varient de moins de 0,3%. La figure 3 montre également les résultats obtenus par Schwarz et al. [2] et qui ont servi de point de départ pour l'itération. Par ailleurs, cette courbe représente les résultats les plus voisins des nôtres parmi ceux publiés dans la littérature. En effet, exception faite de la région de la résonance à 252 keV, l'écart entre les deux courbes résulte vraisemblablement de la différence des valeurs retenues pour les concentrations en ^{6}Li.

REMERCIEMENTS

L'auteur est reconnaissant à M. J.L. Leroy d'avoir suscité de fructueuses discussions. Il exprime ses remerciements à M. Szabo pour lui avoir communiqué ses résultats concernant la concentration en ^{6}Li, et à M. Tellier pour la réalisation de l'expérience de mesure de la transmission du verre NE 905 utilisé.

ANNEXE

TABLEAU DES VALEURS PROPOSEES POUR LA SECTION EFFICACE DE LA REACTION $^{6}Li(n, \alpha)T$
Ces valeurs sont sujettes à une renormalisation consécutive à une réévaluation de la concentration en ^{6}Li

Energie (keV)	Section efficace (barn)	Précision (%)
81,8	0,640	
99	0,680	3,9
125	0,707	3,2
143,7	0,754	3,2
164	0,920	3,2
174	1,002	3,1
183,6	1,281	3,1
193,4	1,438	3
203	1,832	3
205,5	1,918	10
213	2,114	3
215	2,156	3,1
223	2,416	7
233	2,724	3,1
243	2,805	3
250	2,884	2,9
255	2,860	3
266	2,643	2,8
276	2,353	3,1
286	1,965	3,1
296	1,663	3
307	1,434	3
317	1,230	3,1
327	0,995	3,1
338	0,915	3,1
348	0,785	3
358,4	0,694	3
369	0,679	3
379	0,623	3
390	0,610	3
401	0,560	3,1
411	0,494	3,1
422	0,443	3
432	0,415	3,1
444	0,385	3,2
454	0,361	3,2
472	0,366	4,6
482	0,337	3
493	0,310	
517	0,300	

REFERENCES

[1] FORT, E., LEROY, J.L., MARQUETTE, J.P., Nucl. Instrum. Meth., à paraître.
[2] SCHWARZ, S., STROMBERG, L.G., BERGSTROM, A., Nucl. Phys. 63 (1965) 593-609.
[3] FORT, E., Nucl. Instrum. Meth., à paraître.
[4] LEROY, J.L., CEA, CEN-CADARACHE, Communication privée.
[5] FORT, E., HUET, J.L., Proc. third Conf. on Accelerator Targets Designed for the Production of Neutrons, 1967, p.21.
[6] BEETS, C., DONNEAUX, E., ROBAYE, G., WINAND, L., J. nucl. Energy 16 (1962) 383.
[7] *Angular Distributions in* Neutron Induced Reactions 1, BNL-400 (1963).
[8] LANE, R.O., LANGSDORF, A.S., Jr., MONAMAN, J.E., ELWYN, A.J., Ann. Phys. 12 (1961) 135-71.
[9] CARRE, J.C., VIDAL, B., *Communication privée* et note technique CEA EN n°60.
[10] MEADOWS, J.W., WALEN, J.F., Nucl. Sci. Engng 9 (1961) 132-36.
[11] SZABO, I., CEA, CEN-CADARACHE, *Communication privée*.
[12] TELLIER, CEA, CEN-SACLAY, Communication privée.

DISCUSSION

TO PAPERS IAEA-CN-26/69, 70, 72

W. W. HAVENS: Recently; Bowman from the Lawrence Radiation Laboratory at Livermore informed me that he had analysed his ^{235}U fission cross-section data in the 10-15 keV region and had concluded that the fluctuations in the ^{235}U cross-section could not account for the discrepancies that occur in the 200-300 keV energy region.

Section III

NUCLEAR DATA IN THE THERMAL AND RESONANCE ENERGY REGION: A > 220

Chairmen

S.I. SUKHORUCHKIN (USSR)

R.L. JOLY (FRANCE)

Invited Paper

CROSS-SECTIONS OF THE HEAVY NUCLEI IN THE RESONANCE REGION

G.D. JAMES
UKAEA, AERE, Harwell,
Didcot, Berks,
United Kingdom

Abstract

CROSS-SECTIONS OF THE HEAVY NUCLEI IN THE RESONANCE REGION.

The first part of this paper reviews the available cross-section data of heavy nuclei of importance in reactor design with particular emphasis on the fission-cross-section results. In the second part, data which indicate inetrmediate structure in the cross-sections of the heavy elements are presented and discussed.

1. INTRODUCTION

This paper is intended to introduce the topic of nuclear cross-sections of the heavy nuclei in the resonance region by reviewing recent progress in experimental nuclear data research for this mass and energy region. In Section 2 we discuss some of the cross-sections required for reactor design and operation, as outlined in Section 2.1, and in Section 3 we discuss structure in the resonance cross-sections of the heavy elements. Experiments in this energy range are made predominantly on pulsed neutron sources arising from pulsed electron linear accelerators and on underground nuclear explosions and the merits of these methods are briefly illustrated in Section 4. The specification of nuclear data requirements is exemplified by the work of Greebler et al. [1] who highlighted the large changes in fast reactor doubling times due to data uncertainties in alpha and nu for ^{239}Pu and the capture cross-section of ^{238}U. The first two quantities are to be considered at meetings held before this conference and the results will be summarised in other papers. The available data on the capture widths of ^{238}U are presented in Section 2.3. As shown in the work of Greebler et al. in Section 2.1 errors in the fission cross-sections of ^{239}Pu and ^{241}Pu contribute to the uncertainty in fast reactor fuel costs. A number of recent measurements of these cross-sections as well as the fission cross-sections of ^{233}U, of interest for the thorium fuel cycle, and ^{235}U are now available on magnetic tape from the neutron data centres and these have been intercompared in Section 2.3. The observation of a short-lived decay component (0.34 ± 0.11y) in the time dependence of the reactivity of a sample of ^{241}Pu by Nisle and Stepan [2] may be explained by the existence of a long-lived spontaneously fissioning isomer or by a metastable state with a fairly large thermal fission cross-section. In Section 2.4 we give the results of an experiment to compare the low energy fission cross-sections of freshly prepared ^{241}Pu with that of ^{241}Pu which is many years old. No other reference will be made to thermal neutron cross-sections because the data for the main fissile nuclides has been reviewed in a recent publication [3].

Structure in neutron resonance cross-sections is known to arise from the existence of a second minimum in the fission potential barrier, predicted by Strutinski [4], and is expected to appear in the sub-threshold fission cross-sections of heavy nuclei in the mass range 230 to 240 atomic mass units [5]. The full significance of this structure for reactor design remains to be determined. There is clear evidence for structure in the fission cross-section of ^{239}Pu [6,7,8,9] and this may well have an effect on the details of plutonium fuel element construction. An ability to predict the structure below 10 keV in the energy dependence of alpha for ^{239}Pu would have enabled the consequences of this structure on the fuel doubling time of plutonium fuelled fast reactors to be anticipated. These considerations explain the emphasis given in this paper to an examination of structure in the resonance cross-sections of the heavy elements. Clear-cut examples of structure, such as narrow intermediate structure in the sub-threshold fission cross-sections, briefly reviewed in Section 3.1, present no problem of recognition. Structure arising in the presence of partially open fission channels presents a more difficult problem of recognition and proof. It is shown in Section 3.2 how a distribution free statistic, developed by Wald and Wolfowitz [10] to compare the unknown distributions of two sets of data, can be used to test for energy dependent structure superimposed on the chi-squared distribution of resonance parameters. The example chosen for analysis is the energy dependence of the reduced neutron widths of ^{232}Th which, as expected, show no structure. The same test is applied to show that the correlograms derived by James and Patrick [8] after removing a proposed structure in the fission cross-section, have no significant energy dependent structure, thus confirming the adequacy of the proposed structure. The concept of the resonance region is extended to include an analysis of a resonance at 715 keV in the fission cross-section of ^{230}Th which results in a direct estimate of the moment of inertia of a nucleus in a highly deformed shape isomeric state. Several cross-sections show structure similar to that in ^{230}Th near fission threshold and their study would improve our knowledge of the fission potential barrier as a function of atomic mass number.

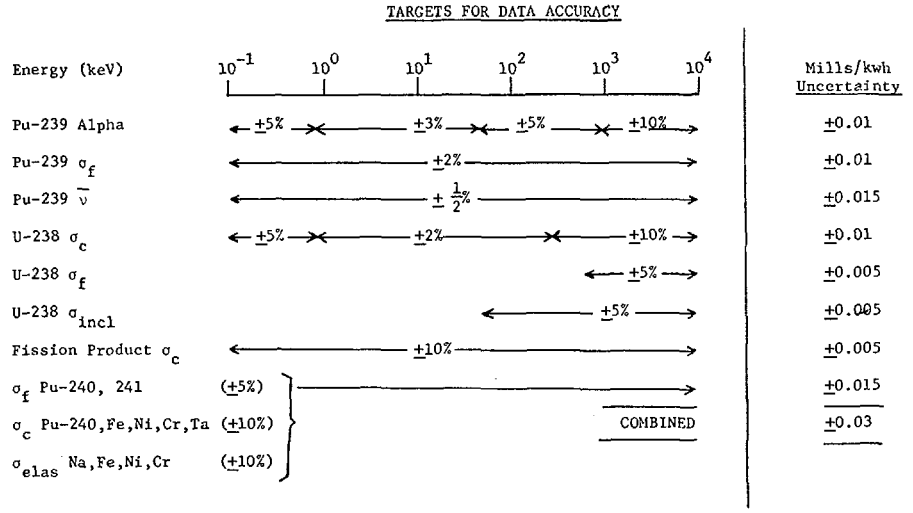

FIG.1. A diagram showing the accuracy requirements which will bring the fuel cost uncertainty of plutonium-fuelled fast reactors to 0.03 mill/kWh. This shows the relevance of heavy element cross-sections in the resonance region. Taken from Greebler et al. [1].

2. CROSS SECTIONS OF IMPORTANCE IN REACTOR DESIGN

2.1 Specification of nuclear data requirements

At the previous IAEA nuclear data conference, Kinchin [11] concluded that broadly speaking the nuclear data needs of thermal reactors had been met and that "the torch which had been carried in the quest for precise nuclear data could almost be handed over from the thermal to fast reactor field". At the same conference the nuclear data needs for fast reactor design and operation were reviewed by Smith [12] in a paper which illustrates the interplay between fast reactor safety and economic

TABLE I. ^{233}U FISSION RESONANCE INTEGRAL DATA FROM 0.4 eV TO 1222 eV[a]

Energy range eV		1	2	3	4	5	6	$\langle\sigma_f\rangle$	Error %
0.414	0.532	33.34	35.14		34.20	34.77		34.36	1.14
0.532	0.68	30.54	32.29		31.47	32.14		31.61	1.26
0.68	0.875	28.84	30.84		29.53	30.61		29.95	1.56
0.875	1.126	34.76	37.17		35.54	36.99		36.11	1.61
1.126	1.444	56.61	53.87		54.63	59.48		56.15	2.22
1.444	1.85	138.23	139.95		140.54	137.32		139.01	0.54
1.85	2.38	97.56	95.55	97.63	92.02	99.64	96.57	96.49	1.09
2.38	3.06	14.55	15.22	13.18	17.19	14.70	14.05	14.81	3.73
3.06	3.93	26.14	25.54	23.11	25.82	24.73	23.50	24.81	2.07
3.93	5.04	20.41	20.07	17.92	19.82	18.94	17.87	19.17	2.35
5.04	6.47	22.10	22.07	19.92	20.83	20.57	20.19	20.95	1.82
6.47	8.32	35.09	30.98	33.44	31.55	33.56	33.60	33.04	1.87
8.32	10.67	30.48	28.59	28.43	25.85	28.00	27.17	28.09	2.25
10.67	13.70	27.61		26.98	23.17	26.55	26.20	26.10	0.77
13.70	17.59	18.99		19.30	16.36	19.62	18.61	18.58	0.58
17.59	22.59	32.47		30.87	23.21	30.57	28.61	29.15	5.51
22.59	29.07	16.76		17.53	15.12	17.50	17.75	16.93	2.85
29.07	37.03	15.18		15.54	11.77	15.08	14.78	14.47	4.74
37.03	47.8	6.76		7.27	5.90	8.46	6.77	7.03	5.97
47.8	61.4	11.29		10.91	8.23	13.17	10.35	10.79	7.38
61.4	78.9	9.77			7.14	11.44	9.46	9.45	9.36
78.9	101.2	8.74			6.51	7.83	7.82	7.72	5.94
166.9	214.9	5.82			4.07	5.54	5.26	5.17	7.44
214.9	275	5.51			4.59	5.57	5.17	5.21	4.31
275	353	5.42			4.51	4.73	5.39	5.01	4.61
353	453	3.65			3.77	3.50	3.61	3.63	1.53
453	582	3.54			2.80	3.31	3.59	3.31	5.46
582	748	3.84			3.17	3.40	3.96	3.59	5.16
748	961	3.26				2.72	3.21	3.06	5.62
961	1222	2.44				2.00	2.45	2.30	6.46

(a) The data of columns 1 - 5 are taken from Cao et al. [18]

Column Number	SCISRS key or reference
1	Weston et al. (1968) ref. [51]
2	Brooks (1966) ref. [52]
3	Nifenecker (1964) ref. [53]
4	Moore et al. (1960) ref. [19]
5	Cao et al. (1970) ref. [18]
6	James (1970) to be published

TABLE II. ^{235}U FISSION CROSS-SECTION DATA FROM 10 eV TO 20 keV[a]

Energy range keV		1	2	3	4	5	6	7	8	9	$\langle\sigma_f\rangle$	Error %
10	20		2.801	2.768		3.271					2.947	
9	10		3.418	3.248		3.340		3.182		3.044	3.246	2.00
8	9		3.505	3.030		3.227		3.047		2.984	3.159	3.04
7	8		3.551	3.034		3.430		3.829		3.193	3.407	4.08
6	7		3.791	3.149		3.457		3.738		3.469	3.521	3.27
5	6		4.274	3.459		3.831		3.905		3.948	3.883	3.35
4	5		4.502	4.013		4.499		4.535		4.413	4.392	2.21
3	4		4.887	4.721		4.907		(b)		4.854	4.842	0.87
2	3		5.761	5.464		5.620		(b)		5.404	5.562	1.40
1	2		7.545	7.653		7.619		(b)	7.282	7.445	7.525	1.10
0.9	1	7.128	7.874	7.932		8.676		7.709	7.074	7.625	7.717	2.65
0.8	0.9	8.255	8.586	7.821		9.108		8.366	7.271	8.437	8.263	2.66
0.7	0.8	10.18	10.89	10.99		11.35		11.29	10.07	11.17	10.84	1.82
0.6	0.7	11.81	11.72	11.48		11.68		11.64	9.481	11.57	11.34	2.75
0.5	0.6	14.11	14.59	15.43		14.74		15.33	13.03	15.17	14.63	2.18
0.4	0.5	14.94	13.19	14.69		13.38		13.76	11.66	13.73	13.62	3.00
0.3	0.4	12.20	14.38	13.21		12.94		13.21	10.36	13.26	12.79	3.70
0.2	0.3	20.72	20.52	21.75		20.55		20.80	17.51	20.34	20.31	2.45
0.1	0.2	21.47	21.31	21.56		20.37		21.01	19.24	20.90	20.84	1.47
0.09	0.1	19.26	23.98	21.91		23.99	25.04	22.40	20.76	22.50	22.48	2.96
0.08	0.09	29.16	25.63	28.65		26.51	30.74	28.05	25.72	28.40	27.86	2.27
0.07	0.08	25.63	29.22	34.24		30.46	34.29	32.12	30.05	33.52	31.19	3.37
0.06	0.07	23.83	16.21	15.13	15.93	15.73	19.47	14.80	13.69	14.69	16.61	6.33
0.05	0.06	55.40	55.74	62.55	64.88	55.52	67.86	61.81	57.37	63.72	60.54	2.56
0.04	0.05	34.97	30.88	31.91	34.58	32.28	36.92	33.51	29.17	33.57	30.09	2.34
0.03	0.04	51.09	50.48	52.20	58.49	51.56	61.82	56.00	53.43	56.61	54.63	2.34
0.02	0.03	44.03	35.66		37.57	34.56	40.21	36.47	33.59	33.81	36.98	3.43
0.01	0.02	51.59	48.62		55.56	47.39	53.99		48.47		50.94	2.66

(a) This table gives energy weighted average fission cross-sections for the energy ranges shown.

(b) Data in this region were not available on the data tape.

Column number	SCISRS key or ref.
7	RPI PAR ND /48 66J
8	TF GEL JNE 22 211 68D
9	BLONS, J. (1970) private communication

Column number	SCISRS key or ref.
1	5TF KAPKPR 104 479 56J
2	5TF SACKJPR 21 429 60E
3	TF LASCNCS FF11 66C
4	TF LRL&UCRL-14606 66C
5	TF&DUBSSAL 86 65C
6	TF KURWT.MOSTOVAJA 66L

considerations and nuclear data requirements and which concludes that data that are sufficiently accurate for calculations of reactivity and breeding gain are also sufficiently good for most other reactor calculations with the exception of some of the temperature coefficients. In analysing the results of an intercomparison of calculations, made at several laboratories, for a dilute plutonium-fuelled fast critical assembly [13], Davey [14] concludes that the critical mass of such an assembly can be calculated to about 2% particularly if data sets adjusted for agreement with experimental critical assemblies are used. Such adjusted sets, however, are unlikely to be equally good for a different design of reactor and, taking this broader view there is no substitute for improved nuclear data. In order to focus our attention on the typical neutron data requirements of a fast reactor design we reproduce in fig. 1, taken from the work of Greebler et al. [1], a list of the accuracy requirements which will bring future designs of plutonium-fuelled fast reactors to an accuracy of 0.03 mill/kwh. In the resonance region, the heavy element cross-sections of importance, in addition to those already noted above as having a strong effect on fuel doubling times, are the fission cross-sections of ^{239}Pu, ^{241}Pu and ^{240}Pu and the capture cross-section of ^{240}Pu.

2.2 Fission cross-sections of ^{233}U, ^{235}U, ^{239}Pu and ^{241}Pu

In the last few years a large number of measurements of the resonance region fission cross-sections of the four main fissile nuclides have been carried out by time-of-flight experiment on pulsed electron linear accelerators or using underground nuclear explosions. Most of these data are available from the ENEA Neutron Data Compilation Centre at Saclay and have been read from magnetic tape and averaged into suitable groups (in collaboration with Schomberg [15]), and the results are shown in Tables I to IV. Some of the data are derived from published tabulations. The purpose of this analysis is to decide how well the various measurements agree with each other and to see whether any sets of data disagree with the mean value derived from all the data sets for a given isotope in an explicable way. This analysis should not be taken to be an evaluation. No steps have been taken to ensure that all the data are normalised in a consistent way to a chosen value of the thermal fission cross-section. The indications are that, because of the errors inherent in this process, there would be little reduction in the average errors derived in the present treatment if all the data were consistently renormalised. Furthermore, it is now known [16] that the $B^{10}(n,\alpha)$ cross-section does not have a strictly 1/v dependence up to 20 keV: data calculated assuming a 1/v dependence have not been corrected for the purpose of the present comparison. Apart from the inclusion of my own data [17], Table I is taken from the work of Cao et al. [18] and the quantities shown are energy weighted average values of the fission resonance integral. Results for the other three fissile nuclides show energy weighted average values of the fission cross-section for a standard set of energy intervals. These tables also show mean values for each energy range and the standard deviation in the mean value deduced from the spread of the data on the assumption that each datum has equal weight. Average percentage errors over broad energy bands are summarised in Table V, which shows that the data for ^{235}U show good agreement, the data for ^{241}Pu are within the specification in Fig. 1 whereas the data for ^{239}Pu are about twice as poor as the specification in Fig. 1. The data for ^{233}U in Table V are not strictly comparable with those for the other isotopes because of the different set of energy intervals used. An analysis was made to decide whether certain measurements show an improved agreement over all the data sets in Table II. The results are shown in Table VI which gives the average errors deduced for the data listed in the footnote.
This agreement between selected data sets, close to 2% for the energy

TABLE III. ^{239}Pu FISSION CROSS-SECTION DATA FROM 10 eV TO 20 keV[a]

Energy range keV		1	2	3	4	5	6	7	8	9	$\langle\sigma_f\rangle$	Error %
10	20	3.065			2.213		1.688	1.885	1.713	1.82	2.064	10.4
9	10	2.334			2.137		2.006	1.979	1.833	1.90	2.031	3.6
8	9	2.066			2.462		2.347	2.481	2.221	2.22	2.299	2.8
7	8	1.912			2.232		2.210	1.997	2.243	2.15	2.124	2.6
6	7	2.693			2.203		1.980	2.012	1.947	2.17	2.167	5.2
5	6	2.793	3.207		2.710		2.194	2.206	2.383	2.18	2.525	5.9
4	5	2.665	2.919		2.313		2.343	2.376	2.512	2.39	2.503	3.3
3	4	3.490	3.381		2.744		2.782	3.089	2.799	3.22	3.072	3.7
2	3	3.363	3.864		2.641		2.896	3.355	3.288	3.32	3.247	4.5
1	2	3.979	5.410		3.832		3.706	4.535	4.251	4.49	4.315	5.1
0.9	1	7.703	8.108		8.278		7.025	8.689	7.425	8.28	7.930	2.7
0.8	0.9	6.212	6.029		4.360		4.119	5.190	5.046	5.13	5.155	5.7
0.7	0.8	5.517	6.357		5.195		4.756	6.033	5.966	5.43	5.608	3.7
0.6	0.7	3.715	5.252		3.941		3.688	4.779		4.54	4.319	6.0
0.5	0.6	10.75	16.12		14.66		13.80	15.75	16.93	15.43	14.77	5.2
0.4	0.5	10.05	10.61		9.105		8.175	9.849	9.941	9.60	9.619	3.1
0.3	0.4	9.822	12.85		8.352		7.217	9.037	10.54	8.63	9.493	7.2
0.2	0.3	17.47	20.82		18.25		15.59	18.02	20.46	18.06	18.38	3.7
0.1	0.2	19.61	21.65	21.92	17.82	21.78	17.07	19.18	21.80	18.09	19.88	3.3
0.09	0.1	27.68	37.42	35.71	26.10	35.35		31.74	34.93		32.70	5.0
0.08	0.09	66.35	80.40	73.16	61.48	72.69		69.03	66.89		70.00	3.3
0.07	0.08	63.52	70.20	68.22	59.54	67.80		65.57	64.71		65.65	2.0
0.06	0.07	53.81	63.96	60.24	54.92	59.75		57.25			58.32	2.6
0.05	0.06	71.81	77.36		72.32	75.53		77.94	72.78		74.62	1.5
0.04	0.05	26.14	28.47	27.25	24.62	27.17			25.99		26.61	2.0
0.03	0.04	3.798	2.679	3.802	2.156	3.337			4.586		3.39	10.5
0.02	0.03	32.81	36.46	33.39	42.07	32.53			31.24		34.75	4.7
0.01	0.02	103.82		109.17		105.97					106.32	1.5

(a) This table gives energy weighted average fission cross-sections for the energy ranges shown.

Column number	SCISRS key or reference	Column number	SCISRS key or ref.
1	TF ANLCGEN2 15*127 58I	6	TF HAR EAN UK 96 68J
2	5GS SACCSAL SM60/13 65C	7	TF SAC CR 267 901 68J
3	GS SACYBLONS ET AL.66B	8	James - to be published
4	TF LASCNCS FF12 66C	9	Gwin. et al. ORNL TM 2598
5	5TF-SACCPAR ND 70 66J		

TABLE IV. ^{241}Pu FISSION CROSS-SECTION DATA FROM 10 eV TO 2 keV[a]

Energy range keV		1	2	3	4	5	$\langle\sigma_f\rangle$	Error %
1	2	9.327	8.431	8.587	7.64	8.786	8.554	3.2
0.9	1	10.73	9.976	10.87	9.71	10.95	10.45	2.4
0.8	0.9	9.317	9.363	9.64	8.37	9.844	9.307	2.7
0.7	0.8	11.02	9.787	10.63	9.55	11.13	10.42	3.1
0.6	0.7	11.56	10.93	11.41	9.98		11.56	5.6
0.5	0.6	16.58	17.47	16.76	14.36		16.29	4.1
0.4	0.5	20.60	21.05	19.39	14.78	19.86	19.14	5.9
0.3	0.4	22.14	23.43	22.41	18.20	21.46	21.53	4.1
0.2	0.3	28.98	31.85	27.61	26.08	29.37	28.78	3.3
0.1	0.2	27.48	28.91		24.98	32.11	28.37	5.2
0.09	0.1	33.03	28.58	25.98	27.70	31.29	29.32	4.3
0.08	0.09	(88.67) (b)	70.67	66.72	68.55	64.46	67.60	2.0
0.07	0.08	29.40	30.92	26.13	28.94	28.71	28.82	2.7
0.06	0.07	(88.79) (b)	51.64	55.67	56.45	58.98	55.68	2.7
0.05	0.06	19.26	16.09	16.60	16.80	20.25	17.80	4.6
0.04	0.05	41.80	35.31	40.25	36.54	41.01	38.98	3.3
0.03	0.04	46.44	38.73	46.91	46.50	44.95	44.71	3.4
0.02	0.03	85.96	72.77	81.37	82.86	74.94	79.58	3.1
0.01	0.02	152.74		148.37	146.82		149.31	1.2

(a) This table gives the energy weighted fission cross-sections for the energy ranges shown.

(b) These high values arise from platinum back scattering and have not been included in the averaging process.

Column number	SCISRS key or reference
1	5TF HARKNP 65+353 65C
2	TF LASCNCS F6 66C
3	Saclay data - private communication
4	Geel data - private communication
5	James - to be published

TABLE V. AVERAGE ERRORS IN FISSION CROSS-SECTION DATA DEDUCED FROM THE SPREAD OF SEVERAL MEASUREMENTS

Energy range keV	Average error - per cent			
	^{233}U (table I)[a]	^{235}U (table II)	^{239}Pu (table III)	^{241}Pu (table IV)
1 - 10		2.4	4.0	
0.1 - 1	5.1	2.5	4.5	4.0
0.01 - 0.1	4.7	3.1	2.8[b]	3.0

(a) The energy intervals used in Table I differ from those used in Tables II, III and IV.

(b) A 10% error on the low cross-section between 30 eV and 40 eV is omitted in calculating this error.

TABLE VI. AGREEMENT OF SELECTED DATA SETS[a]

Energy range (keV)	Average error – per cent		
	^{233}U	^{235}U	^{239}Pu
1 - 10		2.5	2.7
0.1 - 1	1.7	1.9	3.3
0.01 - 0.1	2.3	1.2	

[a] The errors quoted are standard deviations in the mean derived from the spread of data sets. The errors were evaluated for the energy intervals given in Tables I to III and averaged over the energy ranges given here. The data chosen are: for ^{233}U column 1 and 6 of Table I (RPI, HAR), for ^{235}U columns 7, 8 and 9 of Table II with column 8 renormalized (RPI, GEL, SAC) and for ^{239}Pu columns 7, 8 and 9 of Table II (SAC, HAR, RPI).

range below 10 keV, represents the limit achieved in our knowledge of the shape of the fission cross-section at the present time. It is hoped that an evaluation by people who have been involved in such measurements would reveal the reasons for the discrepancies between these selected data and others. Graphical plots of the data of Tables I to IV (not shown) enable the outstandingly discrepant data to be observed. The more obvious features of the data are the low values of the ^{233}U data of Moore et al. [19] above 10 eV, the higher values of the ^{241}Pu data of James [20] in the range 60-70 eV and 80-90 eV (these are due to back scattering from the platinum backing of the foil and have been corrected in the repeated measurement of James [17]) and the low values of the Geel data for ^{235}U and ^{241}Pu in the range 200 eV to 1 keV possibly due to the type of permanent filters used.

2.3 The radiation widths of ^{238}U

Three sets of measurements of the radiation widths of ^{238}U are available and, as shown in Fig. 2, they are not in good agreement with each other. The results of Glass et al. [22] are generally lower than the other two measurements but have some regions of high values which suggests the structure which these authors have indicated by the dashed line in Fig. 2. If this effect is genuine it indicates a low value of ν for the chi-squared distribution of these data, or as the authors have shown a component of the distribution with a low value of ν . An analysis of these data by the method given in Section 3.2 shows that the energy dependence of the data have a probability of only 1.5% arising from data that have no energy dependent structure. Because of the disparity between the measurements it is difficult to accept the structure as genuine at this stage.

2.4 An isomeric state of ^{241}Pu?

Significant differences between reported values of the half-life of ^{241}Pu ranging from 13.0 ± 0.2y [21] to 14.98 ± 0.33y [25] have led to a suggestion by Cabell [25] that a long lived ^{241}Pu isomer may exist. More recently in a measurement of the time-dependence of the reactivity of a sample of ^{241}Pu Nisle and Stepan [2] found evidence for a short-lived component (0.34 ± 0.11y) in the decay of this quantity which they attribute to a short lived isomeric state. Uncertainty about the history of the ^{241}Pu samples used in various experiments makes an interpretation of all

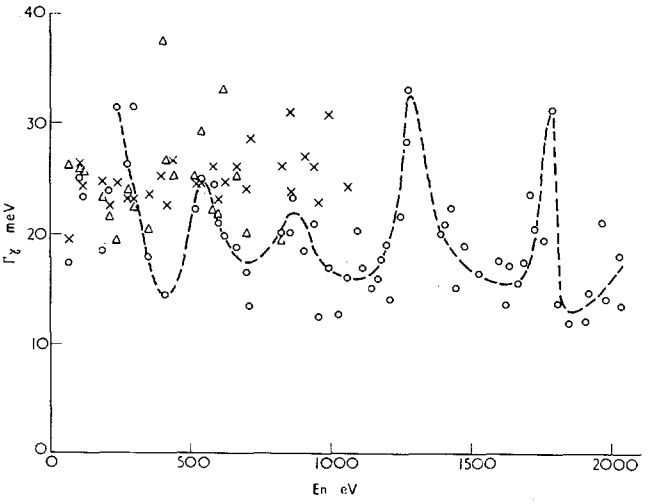

FIG.2. Measurements of the capture width for ^{238}U from three experiments. The data of Glass et al. [22] are indicated by circles, the data of Rohr et al. [23] by crosses and the data of Asghar et al. [24] by triangles. The dashed line indicates possible structure in the data of Glass et al. but these results are not confirmed by the other measurements.

the evidence very difficult. Lynn [27] has considered the possible explanations and concluded that a spontaneously fissioning isomer with a 0.34y half-life cannot explain the results but that a normal high spin isomer [28] with a high fission cross-section may provide an explanation. An experiment to compare the fission cross-section of freshly prepared ^{241}Pu with that of ^{241}Pu which is several years old has been carried out at Harwell. The data extend from 0.005 eV to 20 eV. In this energy range the resonant structure of the two sets of data are identical. By normalising the two sets of data to each other at the 0.24 eV resonance, it is found that the thermal fission cross-section of the two samples are equal to within about $1\frac{1}{2}\%$ at a time when the fresh sample, prepared by irradiating ^{240}Pu in a flux of 10^{14} neutrons/cm^2 sec for 3 weeks, was 2 months old.

3. STRUCTURE IN THE RESONANCE CROSS-SECTIONS OF THE HEAVY ELEMENTS

3.1 Structure phenomena in near barrier fission reactions

Perhaps the most spectacular development in neutron cross-section work in the last few years has been the discovery of narrow intermediate structure in the sub-threshold fission cross-section of ^{240}Pu [29]. It is now well known that these and similar results discovered in other nuclei (^{237}Np [30], ^{242}Pu [31], ^{234}U [32], ^{241}Am [33] and ^{238}Pu [34]) are explained by a second minimum in the fission potential barrier predicted by Strutinsky [4]. These results have been extensively interpreted and reviewed by Lynn [35]. Differences in the depth of the second minimum and in the heights of the intervening and outer potential barriers for different nuclei give rise to a range of structures in the sub-threshold fission cross-sections. An undamped vibrational level in a shallow second minimum gives rise to structure in the fission cross-section of the type exemplified [36] by the fission cross-section of ^{230}Th shown in Fig. 3. The curve of Fig. 3 and the fission fragment angular distributions shown in Fig. 4 have been

analysed in terms of the rotational band structure built on the vibrational level, to yield an estimate of the moment of inertia of the nucleus in the highly deformed shape isomeric state associated with the second minimum. This is found to be about five times that of the ground state. In this experiment the fission cross-section was determined on the Harwell IBIS Van de Graaff accelerator at a neutron energy resolution of 5 keV using surface barrier fission fragment detectors. The angular distribution was determined at a neutron energy resolution of about 15 keV using the Makrofol technique [37] to locate the fission fragment positions. Many threshold fission cross-sections (e.g. ^{231}Pa, ^{234}U and others) show resonances which are amenable to this kind of investigation and their study would greatly enhance our knowledge of the atomic mass dependence of the second fission potential minimum.

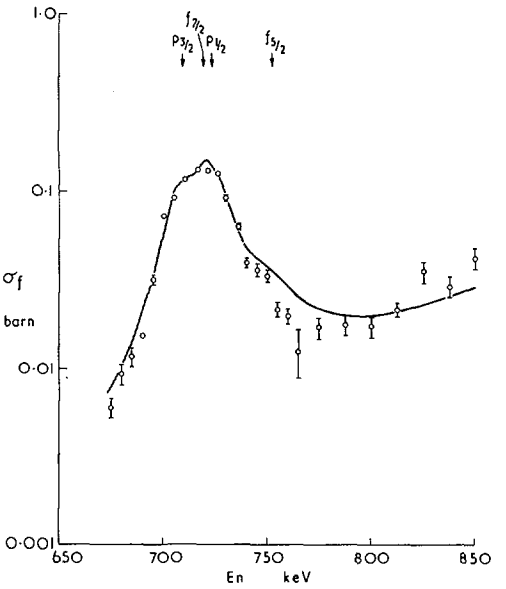

FIG.3. The fission cross-section of ^{230}Th [36] between 600 keV and 850 keV measured with an energy resolution of 5 keV. The resonance at 715 keV is attributed to a vibrational level in the second fission potential barrier minimum and the solid line is a theoretical fit based on the rotational band structure indicated.

At the other extreme the second minimum can be quite deep with the vibrational states rather strongly damped into much more complicated states (class II states) of a compound nucleus type. These states are coupled to the denser (class I) fine structure resonances of the first potential minimum. The strength of this coupling and the fission width of the class II level determine the nature of the observed fission cross-section. Very weak coupling to a narrow class II state gives rise to narrow intermediate structure, as found in the slow neutron-induced fission cross-sections of ^{240}Pu, ^{242}Pu and possibly ^{237}Np, which can be analysed by perturbation theory. Stronger coupling to a weak class II level or very weak coupling to a strong class II level gives rise to intermediate structure in which the fine structure fission widths have a Lorentzian energy dependence superimposed on a Porter-Thomas fluctuation. The first

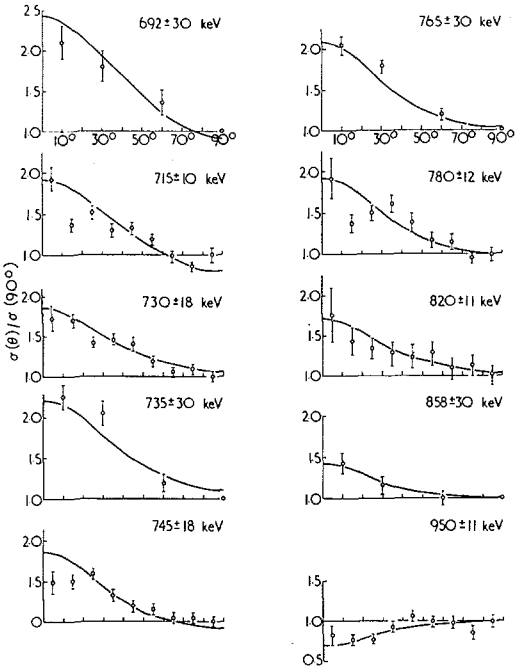

FIG.4. Fission fragment angular distributions for ^{230}Th(n, f) between 692 keV and 950 keV. Distributions with four data points are the measurements of Vorotnikov et al. [26]. The solid line is a theoretical fit for the rotational band structure indicated in Fig.3. These results are from James et al. [36] and provide an estimate of the moment of inertia of the ^{230}Th + n nucleus at a deformation corresponding to the second fission potential barrier minimum.

experimental demonstration of these predictions [38] is for the fission widths of fine structure resonances in the intermediate structure resonance centred at 638.4 eV in the fission cross-section of ^{234}U shown in Fig. 5. The solid line in this figure gives the Lorentzian energy dependence of the mean fission width and was derived from the individual fission widths shown. Because of worsening energy resolution only one fission width could be measured above the Lorentzian resonance energy chosen to be at the energy of the largest fission width which is interpreted as a predominantly class II resonance. Subsequently, mean fission widths over 100 eV intervals have been calculated from 700eV to 1100eV from average values of the fission cross-section and the neutron strength function. As shown in Fig. 5 these results lie close to the Lorentzian curve deduced from data below 700 eV thus confirming the choice of Lorentzian resonance energy.

3.2 A statistical test for structure

Probably the most direct influence of fission cross-section structure on the details of nuclear reactor design and safety considerations will come from structure in the fission cross-section of ^{239}Pu. The first evidence for this structure arose from a serial correlation analysis [6,7] of the cross-section below about 5 keV. The correlograms obtained showed highly significant values of the serial correlation coefficient at an energy

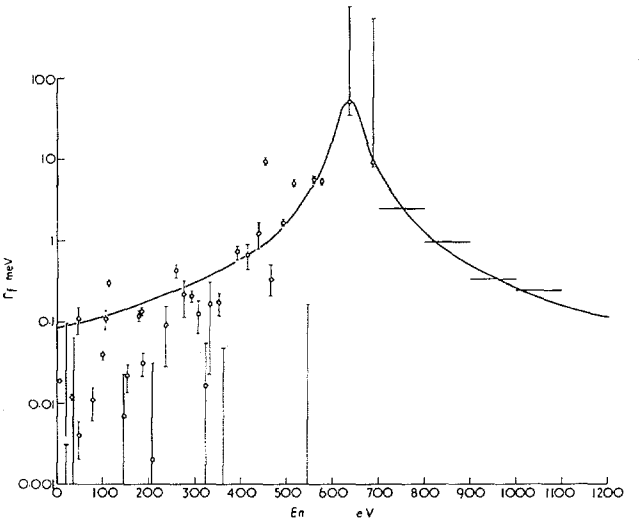

FIG.5. The energy dependence of the observed fission widths of ^{234}U resonances [38] within the narrow intermediate structure resonance centred at 638.4 eV. The solid line shows a Lorentzian energy dependence of the mean fission width deduced from the individual fission widths below 700 eV. It is seen that average fission widths over 100 eV intervals between 700 eV and 1100 eV are also fitted by this curve thus confirming the choice of resonance energy at 638.4 eV. The individual fission widths fluctuate about the energy-dependent mean value with a Porter-Thomas distribution.

TABLE VII[(a)]. MEASURED AVERAGE VALUES OF MEAN FISSION WIDTHS.

E (eV)	$\langle \Gamma_f \rangle_{10^+}$ (meV)	$\langle \Gamma_f \rangle_{1^+}$ (meV)
0 - 110	2065 ± 840	41 ± 10
110 - 220	970 ± 370	30 ± 8
220 - 330	3302 ± 1350	22 ± 5
330 - 440	3285 ± 1550	43 ± 11
440 - 550	2352 ± 925	38 ± 11
550 - 660	1800 ± 1040	7 ± 2

(a) From Paya et al. [41].

spacing between the data being tested of about 460 eV and were interpreted as implying a modulation of the fission cross-section with this energy spacing. This interpretation of the correlograms has been criticised by Perez et al. [39,40] who simulated a modulated cross-section and showed that for a Wigner distribution of the spacing of the modulations, peaks in the correlogram do not correspond to the average spacing introduced in the simulation. However, James and Patrick [9] have shown that by allowing for fairly obvious modulations of the fission cross-section with an average spacing of about 500 eV significant features of the correlogram, shown in

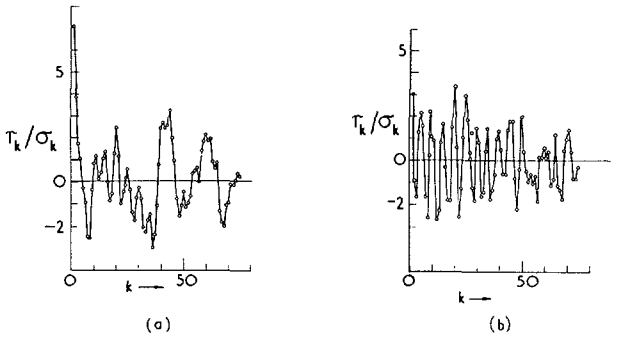

FIG.6. Correlograms for the fission cross-section of ^{239}Pu over the energy range 716 eV to 5683 eV [8]. Here, r_k is the serial correlation coefficient, σ_k the standard deviation in r_k and k is the spacing between regions being tested. In calculating (a) the mean fission cross-section is assumed to have a $1/\sqrt{E}$ energy dependence whereas in (b) an additional energy-dependent structure of the mean fission width is assumed. Correlogram (b) is more featureless than (a) as shown by the Wald and Wolfonitz test thus showing that the assumed structure is reasonably correct.

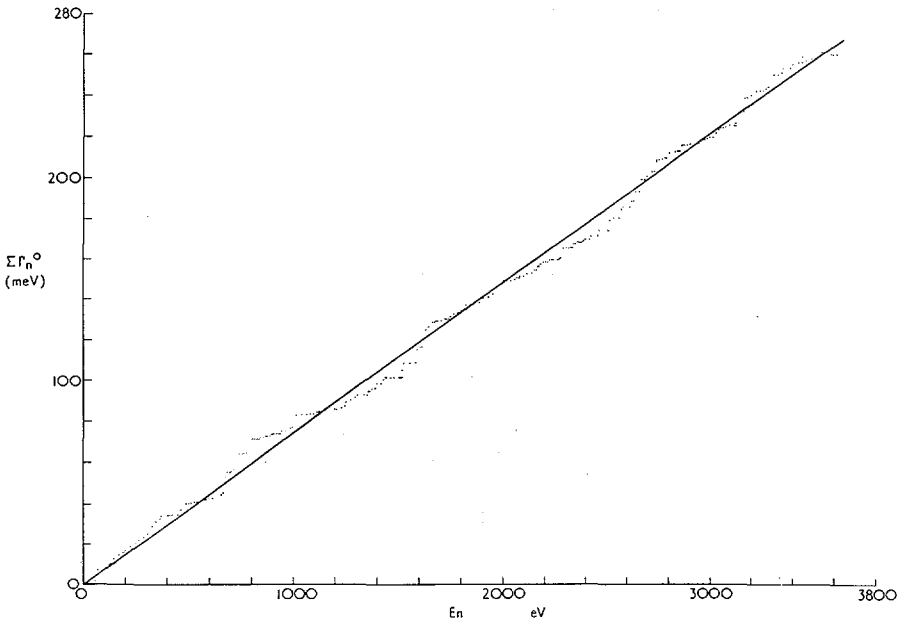

FIG.7. The cumulative sum of the reduced neutron widths of ^{232}Th as a function of neutron energy. An application of the Wald and Wolfonitz test to these data shows that, despite appearances, they have no energy-dependent structure.

Fig. 6(a) are removed and the correlogram is rendered featureless as shown in Fig. 6(b). Convincing direct evidence for variations of the mean fission widths of ^{239}Pu slow neutron resonances is provided by the work of Paya et al. [41] who have obtained resonance parameters for this nuclide by a combined analysis of fission and total cross-section data measured with samples cooled to liquid nitrogen temperature. Their measured average values of the mean fission widths over 110 eV intervals below 660 eV are shown for both spin states in Table VII which shows that between 110 eV and 550 eV the average fission width for the sub-threshold $J^\pi = 1^+$ state decreases by a factor of ten.

It was noted above that the correlogram of Fig. 6(b) is more featureless than that of Fig. 6(a) and it useful to obtain a numerical representation of this quantity. This can be done using the statistic U developed by Wald and Wolfowitz [10] to compare the unknown distributions of two sets of data. The statistic tests the probability of obtaining a sequence of zeros and ones when on a given occasion a zero and a one are equally likely. The method will be explained by showing how it can be used to test for structure in the energy dependence of the reduced neutron widths of ^{232}Th. In the energy range below 3.6 keV, 270 values of Γ_n^o are available for analysis (Stehn et al. [42]). They have a χ^2 distribution with a number of degrees of freedom $\nu = 0.94 \pm 0.07$ which is consistent with a Porter-Thomas distribution. Nevertheless, if all the large values of Γ_n^o occurred close together or at regular intervals, the data could have an energy dependent structure while still retaining a Porter-Thomas distribution and indeed such a structure is suggested to the eye by the cumulative plot of the Γ_n^o data for thorium (Fig. 7). The reality or otherwise of such apparent structure can be examined by the Wald and Wolfowitz test. For data with a Porter-Thomas distribution half the data have values greater than (approximately) half the mean value and the data can be divided into sets depending on whether they are greater or less than half the mean value. Let one set be marked as zeros and the other as ones. After writing down the sequence of zeros and ones for the reduced neutron widths taken in the order of the resonance energies, the Wald and Wolfowitz statistic U is found by counting the number of runs in the sequence. Here a run is an unbroken train of zeros or ones. If m is the total number of zeros and n is the total number of ones, Wald and Wolfowitz have shown that U is normally distributed about an expected value $\mathcal{E}(U)$ with a variance $\sigma^2(U)$ given by the formulae

$$\mathcal{E}(U) = 1 + 2mn/(m + n)$$
$$\sigma^2(U) = 2mn(2mn - m - n)/(m + n)^2 (m + n - 1) \qquad (1)$$

The significance level of a given value of U is found from normal probability tables using $X = (U - \mathcal{E}(U) + 0.5)/\sigma(U)$ which includes a half integer because the distribution is discrete. For the sequence obtained from the reduced neutron widths of ^{232}Th, it is found that U = 137, $\mathcal{E}(U) = 136$ and $\sigma = 8.2$ giving a significance level of 52% and showing that, despite appearances, the data have no energy dependent structure. A median dividing line giving m = n = 135 was used in the analysis. This analysis can be applied to any data that should be distributed about a median value with no energy dependence for the distribution, such as the data of Glass et al. noted in Section 2.3 and the distribution of Γ_f for ^{234}U about a median value which runs at approximately half the Lorentzian curve shown in Fig. 5.

The same basic method can be used to test for structure in the correlograms of Fig. 6 but, because a high value of r_k arising from structure in the data is likely to be accompanied by high values of r_{k-1} and r_{k+1}, the values of $\mathcal{E}(U)$ and $\sigma(U)$ should not be taken from equation (1) but can

be estimated by randomising the fission cross-section data a large number of times and evaluating U in each case. (A better estimate is obtained by simulating the cross-section from parameters with known distributions). In this way it is found that the probability of obtaining the observed values of U for Fig. 6(a) (U = 15) and Fig. 6(b) (U = 30) from data that have no energy dependent structure besides that allowed for is <0.003% and 7.35% respectively. This shows that the structure allowed for by James and Patrick [8] in deducing Fig. 6(b) is a good representation of the data although it could be improved to bring the probability nearer to 50%. In a similar way the method could be applied directly to testing the structure suggested by James and Patrick. The values of $\xi(U)$ and $\sigma(U)$ would best be established by simulation and this has not been done. However, using equation (1), it is found that for an energy independent mean of the ^{239}Pu fission cross-section examined by James and Patrick, U = 44, $\xi(U)$ = 76 and σ = 6.08 giving a significance level of <0.003% whereas for the modulated mean value suggested by these authors U = 62, $\xi(U)$ = 75.6, σ = 6.38 giving a significance level of 2.0%.

4. PULSED NEUTRON SOURCES

The measurement of neutron cross-sections of the heavy elements in the resonance region is carried out entirely by time-of-flight experiments and most modern experiments rely on pulsed particle accelerators, notably electron linear accelerators, or on underground nuclear explosions, to provide pulsed neutron sources. Improvements in the intensity and energy resolution of these sources reflect directly on improvements in the partial and total cross-sections measured and in Table VIII, taken from Rae and Good [44], we give the parameters which show the improvements in pulsed linear accelerator neutron sources over the two decades since this method was first suggested by Cockcroft [45]. If we arbitrarily take as a figure of merit, the neutron production rate during the pulse multiplied by the pulse repetition frequency and divided by the pulse duration we derive a figure for ORELA ($1.7.10^{21}$ neutrons $s^{-2}ns^{-1}$) which exceeds that for a 1.2 kilotonne underground nuclear explosion [46] ($4.7.10^{20}$ neutrons $s^{-2}ns^{-1}$) based on $1.8.10^{23}$ neutrons in 100ns at one explosion per annum. The Oak Ridge accelerator is being used to determine the total cross-section for separated isotopes of ^{241}Am and ^{243}Am [47] over the energy range from thermal to 10 keV. Measurements with both large diameter targets (to obtain precise results) and with very small samples, are being made to determine the precision of the latter measurements. These will then provide a criterion for judging measurements to be made on isotopes available only in small quantities, and transmission measurements on a sequence of curium isotopes and other heavy isotopes are planned [48].

The high neutron production rate during the pulse from an underground nuclear explosion ($1.8.10^{30}$ neutrons/sec for a 1.2 kilotonne explosion) enables fission cross-section measurements to be made for highly alpha active and spontaneously fissioning isotopes as exemplified by the recent measurements of Moore et al. [49] on curium isotopes. In this experiment fission yields from fourteen different isotopes were obtained, the sample for one of which (^{252}Cf) gave a spontaneous fission background rate of 10^6 fragments/sec. The experiment was undertaken to enable the production rate of ^{252}Cf in high flux reactors to be optimised. It was found that the sub-threshold fission widths of ^{244}Cm, ^{246}Cm and ^{248}Cm below 300 eV are reasonably constant and that there is qualitatively no evidence for intermediate structure in the fission yields of these isotopes and that of ^{252}Cf, between 300 eV and threshold. This confirms the calculations of Strutinsky and Pauli [5] and Nilsson [50] that intermediate structure should disappear for Cm and Cf sub-threshold fission.

TABLE VIII. SPECTROMETERS BASED ON ELECTRON LINEAR ACCELERATORS

Spectrometer installation	Frequency (MHz)	Number of klystrons	Total rf power (MW)	Beam current (mA)	Beam energy (MeV)	Pulse duration (nsec)	Max. prf (pps)	Target	Neutron production rate in pulse (neutrons/sec)	Flight path length (metres)	No. of flight paths	Best nominal resolution (nsec/metre)	No. of timing channels	Reference [a]
Harwell	3000	1 (mag)	2	125	3.5	2000	200	Pt/Be	2.5×10^{12}	10	1	200	32	Fry et al. (1948)
														Merrison and Wiblin (1952)
Yale (cavity accelerator)	600	8 (triodes)	0.5	100	10	1000	90	Au/Be	10^{14}	5-15	1	70	500	Schultz and Wadey (1951)
														Schultz et al. (1956)
Harwell	3000	1 (mag)	2	25	14	1000	400	U	2×10^{14}	3-60	4	2	500	Bareford and Kelliher (1953)
				100	15	100	400		10^{15}					Wiblin (1955)
														Firk et al. (1958)
Saclay	3000	3	15	0	55									
				650	40	100	1000	U	10^{17}	5-200	6	0.05	400 000	Leboutet et al. (1957)
				2000	50	10	1000	U	4.5×10^{17}				(4×10^{9})	Roland et al. (1967)
Kurchatov Institute (Moscow)	3000	1	20	0	32	50-600	120	U	3×10^{16}	2-110	7	0.5	10 000	Vladimirsky and Sokolovsky (1958)
				500	25									Voronkov et al. (1962)
														Malyshev (1966)
Harwell	2998	7	56	0	55									
				550	35	1700	500	U						
				650	40	100	500	^{235}U booster	10^{18}	5-300	12	0.5	650 000	Poole and Wiblin (1958)
				2000	50	10	750	U	4.5×10^{17}	100	1	0.1	(7×10^{10})	Poole and Robinson (1964)
Livermore	3000	3	15	0	50									Austin and Fultz (1959)
				250	30	20-2000	360	U	2×10^{16}	10-60	4	0.3	-	Fultz (1969)
San Diego	1300	3	30	0	46									
				750	23	4500			-	19-50	2	0.2	-	Sund et al. (1964)
				2000		10	720	-						
Yale	1300	5	50	0	60								2000	
				700	40	4500								
				1600		100	500	-	2×10^{17}	-	-	-		Harvey (1963)
RPI (Troy)	1300	9	90	0	100									
				800	60	4500			10^{17}					Gaerttner et al. (1962)
				2000		10	720	Ta	5×10^{17}	8-250	4	0.04	8000	Tatarczuk and Block (1967)
Tokai-Mura (Japan)	2857			(200)	2-20	4000		Pb	2×10^{15}	10-50	2			
						40	300					0.8	500	Takekoshi (1965)
Toronto	2856	2	40	0	43									
				500	27	2000		W	-	up to 60	3			McNeill (1967)
				500	35	< 10	960					< 0.16	-	
NBS (Washington)	1300	12	120	0	250									Harvey (1963)
				680	130	7000								Schwartz et al. (1968)
				(2000)		1.5	720	(Cd)	10^{18}	up to 40	-	0.04	16 000	

TABLE VIII. (cont.)

Spectrometer installation	Frequency (MHz)	Number of klystrons	Total rf power (MW)	Beam current (mA)	Beam energy (MeV)	Pulse duration (nsec)	Max. prf (pps)	Target	Neutron production rate in pulse (neutrons/sec)	Flight path length (metres)	No. of flight paths	Best nominal resolution (nsec/metre)	No. of timing channels	Reference [a]
Geel	2856	2	66	0	66									
				350	43	2000	250		6×10^{16}	30-400	9	0.025	(16 000)	Allard and Salome (1966)
				1200	59	100	880	U	3×10^{17}					
				3 600	64	10	1000		1.2×10^{18}					
San Diego	1300	4	70	0	80									
				700	50	7-4500	720	-	$(\sim 10^{17})$	19-220	3	0.03	-	Adcock et al. (1967)
				3 500	40	50	720		$(\sim 4 \times 10^{17})$					
Oak Ridge	1300	4	100	500	140	1000	1000	Ta	$(\sim 10^{17})$	10-80	11	0.03	$\sim 10^6$	Harvey (1969)
				15 000	140	2.3-24	1000		4×10^{18}					
Livermore	3000	6	120	0	200									
				700	80	3000	600	U	3×10^{17}	16-250	10	0.02	-	Fultz (1969)
				10 000	140	5	660		8×10^{18}					
							(1800)							

(a) These references will be found in the paper by Rae and Good [44] from which this table is taken.

5. CONCLUDING DISCUSSION

This introductory paper has concentrated attention on the fission cross-section data required for nuclear reactor design and operation and on data that have advanced our knowledge of the fission potential barrier. The presence of a second minimum in this potential for the mass range 230 to 240 atomic mass units can lead to structure in fission cross-sections which can have an effect on the details of nuclear reactor design and operation. A comparison of fission cross-sections below 10 keV indicates that the cross-section of ^{235}U is known to an accuracy of about 2% as determined from the spread of several measurements. Results for the other three important thermally fissile nuclei show a spread which is about twice as big as this. This does not, of course, preclude a particular data set from being more accurate but a smaller error can hardly be accepted until at least two measurements, preferably carried out by techniques which differ as much as possible, are found to agree. Evaluation of these data, which is now being actively pursued may result in recommended cross-sections with errors below those given in this paper. It is noted that the resonance region should now be extended to include structure near the fission threshold. Several nuclei are known to exhibit this structure [42] and its detailed study would clearly advance our knowledge of the second fission potential barrier minimum. The topic of resonance parameter determination and analysis has not been discussed but will be dealt with in the companion paper by Ribon [43]. However, a method of testing for structure in the presence of the well known fluctuations of resonance parameters [54] has been outlined which may prove useful in the investigation of energy dependent structure in resonance parameter and neutron cross-section data.

ACKNOWLEDGEMENTS

The author is grateful to Dr. E. R. Rae and Dr. J. E. Lynn for stimulating discussions during the preparation of this paper, to Dr. A. Schett of CCDN for promptly complying with our requests for data, to Mr. M. G. Schomberg who organised the processing of these data and Mr. D.A.J. Endacott for his assistance. He is also grateful to the many scientists who kindly communicated their results prior to publication and the Academic Press for permission to publish Table VIII.

REFERENCES

[1] GREEBLER, P., Hutchins, B. A. and Wolfe, B. Neutron cross-sections and technology, NBS Special Publication 299, 291 (1968).
[2] NISLE, R. G., Stepan, I. E. Idaho Nuclear Corporation, Progress report IN-1317, 149 (1969).
[3] HANNA, G. C., Westcott, C. H., Lemmel, H. D., Leonard, B. R., Story, J. S. and Attree, P. M. Atomic Energy Rev. VII, 3 (IAEA Vienna) (1969).
[4] STRUTINSKY, V. M. Nuc. Phys. A95, 420 (1967).
[5] STRUTINSKY, V. M. and Pauli, H. C. Physics and Chemistry of Fission (IAEA Vienna) 155 (1969).
[6] PATRICK, B. H. and James, G. D. Phys. Lett. 28B, 258 (1968).
[7] BLONS, J. et al. C.r. Seance. hebd. Acad. Sci. Paris 267, 901 (1968).
[8] JAMES, G. D., Patrick, B. H. Physics and Chemistry of Fission (IAEA Vienna) 391 (1969).
[9] PAYA, D., Blons, J., Derrien, H., Michaudon, A. Physics and Chemistry of Fission (IAEA Vienna) 307 (1969).

[10] WALD, A. and Wolfowitz, A. Annals Math. Stat. XI, No. 2 (1940).
[11] KINCHIN, G. H. Nuclear Data for Reactors I (IAEA Vienna) 13 (1967).
[12] SMITH, R. D. Nuclear Data for Reactors I (IAEA Vienna) 27 (1967).
[13] DAVEY, W. G. Proc. Int. Conf. on Fast Critical Experiments ANL-7320, 57 (1966).
[14] DAVEY, W. G. Neutron cross-sections and technology, NBS Special Publication 299 (1968).
[15] JAMES, G. D. and Schomberg, M. G. UKAEA Memorandum AERE - M 2157 (Revised).
[16] GUBERNATOR, K., Moret, H. Euratom Report EUR 3950 (1968).
[17] JAMES, G. D. to be published.
[18] CAO, M. G., Migneco, E., Theobald, J. P. and Merla, M. to be published.
[19] MOORE, M. S., Miller, L. G., Simpson, O. D. Phys. Rev. 118, 714 (1960).
[20] JAMES, G. D. Nuc. Phys. 65, 353 (1965).
[21] MACKENZIE, D. R., Lounsbury, M. and Boyd, A. W. Phys. Rev. 90, 327 (1953).
[22] GLASS, N. W., Schelberg, H. D., Tatro, L. D., Warren, J. M. Neutron cross-sections and technology, NBS Special Publication 299, Vol. I, 573 (1968).
[23] ROHR, G., Weigmann, H., Winter, J. to be published.
[24] ASGHAR, M., Chaffey, C. M., Moxon, M. C. Nuc. Phys. 85, 305 (1966).
[25] CABELL, M. J. J. Inorg. Nucl. Chem. 30, 2583 (1968).
[26] VOROTNIKOV, P. et al. Soviet Nucl. Phys. 5, 210 (1967).
[27] LYNN, J. E. private communication.
[28] NILSSON, S. G., Ohlen, G., Gustafson, C., Moller, P. Phys. Lett. 30B, 437 (1969).
[29] MIGNECO, E., Theobald, J. P. Nuc. Phys. A122, 603 (1968).
[30] PAYA, D., Derrien, H., Fubini, A., Michaudon, A. and Ribon, P. Nuclear Data for Reactors II (IAEA Vienna) 128 (1967).
[31] JAMES, G. D. Nucl. Phys. A123, 24 (1969).
[32] JAMES, G. D., Rae, E. R. Nucl. Phys. A118, 313 (1968).
[33] SEEGER, P. A., Hemmendinger, A., Diven, B. C. Nucl. Phys. A96, 605 (1967).
[34] SILBERT, M. G. LASL Report LA-4108-MS (1969).
[35] LYNN, J. E. Physics and Chemistry of Fission (IAEA Vienna) 249 (1969).
[36] JAMES, G. D., Lynn, J. E., Earwaker, L. to be published.
[37] LARK, N. Nuc. Inst. and Methods 67, 137 (1969).
[38] JAMES, G. D. and Slaughter, G. G. Nucl. Phys. A139, 471 (1969).
[39] PEREZ, P. B., de Saussure, G., Moore, M. N. Physics and Chemistry of Fission (IAEA Vienna) 283 (1969).
[40] DE SAUSSURE, G., Perez, P. B., Moore, M. N. Phys. Lett. 31B, 413 (1970).
[41] PAYA, D., Blons, J., Derrien, H., Michaudon, A. Physics and Chemistry of Fission (IAEA Vienna) 307 (1969)(also Blons et al. in these Proceedings).
[42] STEHN, J. R., Goldberg, R. D., Weiner-Chaseman, R., Mughabghab, S. F., Magurno, B. A., May, V. M. Report BNL 325, 2nd Ed. Suppl. No. 2 (1965).
[43] RIBON, P. Contribution to these proceedings.
[44] RAE, E. R. and Good, W. M. Experimental Neutron Resonance Spectroscopy (Ed. Harvey, J. A.) (Academic Press, New York) 28 (1970).
[45] COCKCROFT, J. D. Nature 163, 869 (1949).
[46] HEMMENDINGER, A. Nuclear data for reactors II (IAEA Vienna) 219 (1967).
[47] SIMPSON, F. B., Simpson, O. D., Harvey, J. A., Slaughter, G. G., Benjamin, R. W., Ahlfeld, C. E. Washington APS Meeting, April (1970).
[48] HARVEY, J. A. private communication.
[49] MOORE, M. S., Brown, W. K., Ennis, M. E., Fullwood, R. R., Keyworth, G. A., McNally, J. H., Simpson, F. B., Berreth, J. R., Baybarz, R. D., Thomson, M. C. Contribution to these proceedings.

[50] NILSSON, S. G. et al. Nucl. Phys. A131, 1 (1969); TSANG, C. F. and Nilsson, S. G. Nucl. Phys. A140, 275 (1970).
[51] WESTON, L. W., Gwin, R., de Saussure, G., Ingle, R. W., Fullwood, R. R., Hockenbury, R. W. Report ORNL-TM-1751 and Nucl. Sci. Eng. 34, 1 (1968).
[52] BROOKS, F. D. UKAEA Report AERE - M 1709 (1966).
[53] NIFENECKER, H. et al. J. de Physique 23, 254 (1963); J. de Physique 25, 877 (1964).
[54] PORTER, C. E. and Thomas, R. G. Phys. Rev. 104, 483 (1956).

DISCUSSION

M. ASGHAR: In Section 2.4 of your paper you mention a 0.34 year half-life isomer in ^{241}Pu and Lynn's conclusion that a spontaneously fissioning isomer of this half-life cannot explain the results but that a normal high-spin isomer with a high fission cross-section might provide an explanation. Could you say a few words about this? Where does this state have to be: in the first well or in the second well seen in the potential energy against deformation contour? What value of spin should it have?

G. D. JAMES: An explanation of how such a highly deformed high-spin nucleus can arise is given by Nilsson et al. (See Ref. [28] of the paper).

B. ROSE: Are you able to make any statement about the variation with time of the fission cross-section of the freshly prepared ^{241}Pu, which might be expected to contain the proposed ^{241}Pu-isomer?

G. D. JAMES: We have measured the fission cross-section of the freshly prepared sample at regular intervals for about three months. The thermal fission cross-section relative to the fission cross-section at 0.24 eV remains constant in time within the accuracy of the measurement, which is about 3%.

H. W. KÜSTERS: You state in Section 2.2 of the paper that the fission cross-sections for ^{235}U and ^{239}Pu below 10 keV are now known to an accuracy of 2%. Is this the statistical error of a sample measurement or is your statement to be understood as meaning that various measurements are now yielding consistent results and have an uncertainty margin of about 2%?

G. D JAMES: What I meant was that certain data sets for ^{233}U, ^{235}U and ^{239}Pu are consistent to about 2%, below 10 keV, as determined from the spread of the measurements. This means that the shapes of the cross-sections are in agreement to this accuracy and that they are well normalized to each other.

J. J. SCHMIDT: May I enlarge on the question of Dr. Küsters and ask whether it is meaningful to claim an accuracy of 2% for the resonance fission cross-sections of the main fissile nuclei below 10 keV when differences of the order of 10% are still found between different measurements?

G. D. JAMES: One cannot claim an accuracy of 2% but only an inter-consistency of 2%. This consistency of two data sets is a minimum prerequisite for assuming an accuracy of 2%. There may, of course, still be common reasons why the consistent data sets are wrong - i.e. in addition to those due to their normalization. An evaluation may reveal such reasons and lead to explanations of the 10% discrepancies which you mentioned. However, discrepancies of 10% between data sets do not vitiate an agreement of 2% between two of them.

MEASUREMENTS OF ALPHA AND OF FISSION CROSS-SECTION RATIOS FOR ^{233}U, ^{235}U AND ^{239}Pu AT THERMAL ENERGIES

M. LOUNSBURY, R.W. DURHAM, G.C. HANNA
Chalk River Nuclear Laboratories,
Atomic Energy of Canada Limited,
Chalk River, Ontario,
Canada

Abstract

MEASUREMENTS OF ALPHA AND OF FISSION CROSS-SECTION RATIOS FOR ^{233}U, ^{235}U AND ^{239}Pu AT THERMAL ENERGIES.

Measurements of alpha for ^{233}U, ^{235}U and ^{239}Pu, and of fission cross-section ratios for these nuclides, have been made in the NRU reactor at Chalk River in a special temperature-controlled thermal-flux irradiation facility designed by C.B. Bigham. Extensive thermalization calculations have been carried out by S.A. Kushneriuk and the uncertainty in the neutron spectrum is believed to be equivalent to a temperature uncertainty of only ± 4 °C.

The experiment consisted of irradiating mixtures of uranium and plutonium isotopes, to approximately 0.7 neutrons per kilobarn, and measuring the changes in isotopic composition. With a ^{233}U-^{238}U mixture the change in the (233/238) ratio gives the 233 destroyed and that in (234/238) the 234 produced, from which $\alpha(233)$ can be calculated. Similarly a ^{239}Pu-^{242}Pu mixture gives $\alpha(239)$. When they are mixed, so that they receive the same irradiation, a comparison of the fractions of ^{233}U and ^{239}Pu destroyed gives the ratio of the absorption cross-sections. Both ^{233}U-Pu and ^{235}U-Pu mixtures were irradiated. By combining the α and σ_a data fission cross-section ratios are obtained that do not depend on the assay (e.g. by alpha particle counting) of thin deposits.

The 2200 m/s α values obtained for ^{233}U, ^{235}U and ^{239}Pu were 0.0899 ± 0.0004, 0.1702 ± 0.0007, and 0.3597 ± 0.0021, respectively. The fission cross-section ratios were (239/233) = 1.4046 ± 0.0079, (239/235) = 1.2926 ± 0.0081 and (233/235) = 0.9203 ± 0.0057. Values of $g\sigma_\gamma$ = 95.6 ± 2.1 b for ^{234}U and σ_γ = 289.5 ± 1.4 b for ^{240}Pu were also obtained. The errors include the uncertainties in the neutron spectrum and in other cross-sections (e.g. of ^{241}Pu and ^{242}Pu), as well as the experimental errors, but not the uncertainties in the g-factors, which were taken from the latest reviews of C.H. Westcott.

INTRODUCTION

The 2200 m/s neutron data for ^{233}U, ^{235}U, ^{239}Pu and ^{241}Pu were reviewed by Westcott et al [1] in 1965 and again, in 1969, by Hanna et al [2]. It was emphasized in [1] that discrepant measurements of $\bar{\nu}$ and fission cross sections raised some difficulties, and the experiment described in the present paper was undertaken in order to improve the situation by providing more reliable values of α (the ratio of capture to fission, which would relate $\bar{\nu}$ to η and σ_f to σ_a), and of σ_f ratios, for ^{233}U, ^{235}U and ^{239}Pu. The latest measurements of $\bar{\nu}$ for ^{252}Cf have not satisfactorily disposed of the discrepancies noted in [1], and recent results on α-decay lifetimes have further complicated the interpretation of σ_f measurements [2]. In this situation the present experiment has been valuable in reducing the overall uncertainties, especially as it provides σ_f ratios that are independent of α-decay lifetime data.

The experiment was planned to improve on earlier Chalk River α measurements [3] by including ^{233}U as well as ^{235}U and ^{239}Pu, by using a more nearly Maxwellian neutron spectrum, and by using mixed uranium-plutonium

samples so as to obtain more precise information on uranium/plutonium fission cross section ratios. It consisted of irradiating small samples (∿ 8 mg) to a level of about 0.7 neutrons per kilobarn in a special temperature-controlled thermal-flux irradiation facility in the NRU reactor, and measuring the changes in isotopic composition by mass spectrometry.

When a ^{233}U-^{238}U mixture is irradiated, the change in the (233/238) ratio gives the fraction of ^{233}U destroyed (after a small correction for ^{238}U destruction) and the change in the (234/238) ratio the ^{234}U produced, from which $\alpha(233)$ can be calculated. Similarly a ^{239}Pu-^{242}Pu mixture gives $\alpha(239)$. When they are mixed, so that they receive exactly the same irradiation, comparison of the fractions of ^{233}U and ^{239}Pu destroyed gives the ratio of absorption cross sections ($\sigma_1/\sigma_2 = \log(1 - f_1)/\log(1 - f_2)$, where f denotes the fraction destroyed). By combining the α and σ_a data a value is obtained for the σ_f ratio ($^{239}Pu/^{233}U$) that does not depend on the assay (e.g. by alpha-particle counting) of thin deposits. A ^{235}U-^{238}U plus ^{239}Pu-^{242}Pu mixture gives similar information for ^{235}U and ^{239}Pu.

Sample Preparation and Analysis

Solutions of ^{233}U, ^{235}U, ^{238}U, ^{239}Pu and ^{242}Pu of high isotopic purity and of approximately known concentration were made up in nitric acid and mixed in appropriate proportions to give two solutions of paired fissile nuclides, $^{239}Pu/^{233}U$ and $^{239}Pu/^{235}U$, containing ^{242}Pu and ^{238}U as "spikes" for the isotopic analyses. These solutions were converted to oxide powders by heating. Samples containing some 7 mg of fissile material were prepared for irradiation from each powdered oxide by diluting with some 150 mg of aluminum (to reduce self shielding) and cold pressing into discs 8 mm in diameter 1 mm thick. These discs, protected from contamination by cold-welded aluminum covers, were loaded into a 1.4 cm I.D. sample tube, with aluminum spacers separating the samples, and the sample tube was inserted into the inner tube of the irradiation facility described briefly in the next section. (More complete details including the arrangement of samples are given in [4].) Duplicate samples were made in parallel with those to be irradiated and set aside for subsequent isotopic analyses.

The irradiation lasted about one year and was followed by a one year cooling period. The irradiated samples, and the unirradiated ones also, were then removed from their aluminum covers and dissolved in hydrobromic acid. The plutonium was separated by anion exchange, as described in [10], and purified by further anion exchange followed by electrolysis from an acetone solution. The separated uranium fraction was purified by solvent extraction with tributyl phosphate. Americium was removed from the plutonium fractions immediately before isotopic analysis. Quantitative chemistry was not required in any of these processes.

The isotopic compositions were measured with a Consolidated Electrodynamics mass spectrometer Model 21-703. This instrument, which is of the single-focusing 60°-sector type, has a radius of 30 cm and was operated with a resolving power of 400. It employs a triple-filament surface-ionization source. The mass spectra were scanned magnetically and the ion currents measured with a Faraday cage detector, vibrating-reed electrometer and pen recorder. Mass discrimination effects are believed to be negligible [5] and have been ignored in these experiments.

Each analysis presented in Table I represents the averaging of about thirty individual spectrograms, and the assigned errors are calculated from the dispersion of these individual results. The observed ^{241}Pu abundances have been corrected for decay, using a half life of 14.5 ± 0.5 years (see

TABLE I. MASS SPECTROMETER ANALYSES

Sample A (235/239)

Uranium Fraction			Plutonium Fraction		
Mass	Initial	Final	Mass	Initial	Final
234	0.062±0.002	0.091±0.002	238	0.057±0.002	0.112±0.002
235	100.	100.	239	100.	100.
236	0.065±0.003	8.728±0.009	240	1.214±0.002	32.861±0.030
238	9.529±0.009	15.099±0.012	241	0.290±0.002	3.235±0.004
			242	6.210±0.005	13.945±0.012

Sample B (233/239)

Uranium Fraction			Plutonium Fraction		
Mass	Initial	Final	Mass	Initial	Final
233	100.	100.	238	0.057±0.002	0.110±0.002
234	0.056±0.002	4.090±0.004	239	100.	100.
235	0.100±0.002	0.225±0.002	240	1.215±0.003	32.926±0.030
236	0.000±0.000	0.017±0.002	241	0.291±0.003	3.255±0.003
238	9.622±0.008	14.424±0.014	242	6.197±0.005	13.932±0.010

section 3.2 of ref [2]) to the dates of the beginning and end of the irradiation for the initial and final samples respectively. The uranium analyses given in Table I have not been corrected for the growth of uranium isotopes from the α decay of the accompanying plutonium so that they do not give exactly the initial and final compositions. These and other small corrections are discussed in the Interpretation section below.

The Irradiation Facility

The irradiation facility, which is described more fully in [4], was designed to provide a well thermalized neutron flux of accurately known temperature. It consisted essentially of two vertical tubes, a 5.1 cm O.D. outer tube and a 1.9 cm O.D. inner tube, with the space between them filled by light water at a controlled temperature. It was located in the 15 cm wide air-filled annulus separating the heavy water moderator and the graphite thermal column of the NRU reactor. The adjacent fuel sites were vacant during the irradiation to reduce the fraction of epithermal neutrons. The neutron flux was approximately 2×10^{13} $cm^{-2}sec^{-1}$ and the Westcott epithermal flux parameter r was 2.4×10^{-4}.

The value of r was determined before and after the irradiation from cadmium-difference measurements with gold detectors, and during the irradiation from a cadmium-difference measurement with silver; as expected (see ref [4] p 34) the presence of the samples did not appreciably increase the epithermal component. With such a small value of r the uncertainties in correcting the results for epithermal neutron effects are negligible.

On the other hand the "temperature" of the thermal neutrons is very important, especially for the interpretation of the ^{239}Pu results, and a detailed study was carried out by Kushneriuk [4] to establish the neutron spectrum with the necessary accuracy; only the results will be quoted here. The annulus of light water at 37.5 ± 0.5°C served to rethermalize neutrons from the heavy water moderator (average temperature 28°C with variations of ± 5°C during the irradiation) and from the graphite of the thermal column

(∿ 138°C with apparent fluctuations of ± 30°C depending on reactor power and other factors). It was estimated that the neutron temperature of the heavy-water component of the incurrent (into the light water annulus) was about 7°C higher than the physical temperature of the moderator, and that the intensities of the heavy-water and graphite components of the incurrent were in the ratio two to one. The spectrum of neutrons inside the light water annulus in the absence of samples was found to be well approximated by a Maxwellian distribution of temperature 47°C (i.e. 9.5°C higher than that of the light water, essentially because of absorption in hydrogen and aluminum) rather independent of the temperatures and relative intensities of the components of the incurrent. Absorption and self shadowing effects* increased the effective neutron temperature inside the samples by a further 5.5°C approximately (averaged over the irradiation -- as the samples are irradiated the effect drops from about 6°C to about 5°C).

Kushneriuk's results are expressed more precisely (i.e. without the oversimplified concept of temperature) in Table II which gives the values of σ_a and σ_f for ^{235}U and ^{239}Pu, averaged over the calculated spectra, relative to their values in a Maxwellian spectrum at 37.5°C. Multiplying these ratios, R, by 37.5°C g-factors gives the appropriate factors to convert measured cross sections to 2200 m/s values. From a study of the variation of these R values with incurrent temperatures and other model parameters Kushneriuk concludes that they are accurate to about ± 30% in R-1. For other nuclides where spectrum effects are much less serious (e.g. ^{233}U) or less important (e.g. ^{241}Pu) g factors at the appropriate neutron temperature have been used.

TABLE II. CROSS-SECTION CORRECTION FACTORS, R

(relative to 37.5°C Maxwellian values, averaged over the duration of the irradiation, see text)

	^{235}U	^{239}Pu
σ_a	0.99526	1.01269
σ_f	0.99521	1.00889

Interpretation

The interpretation of the mass spectrometer measurements involved first the assumption of certain input cross section data on which this experiment gave no useful information, and the adoption of trial values for those cross sections on which it did. The expected final isotopic compositions were then calculated, compared with what was observed and adjustments made to the trial values; repeated iterations resulted in final values for the cross sections that were to be determined. This iterative process was in fact unnecessary for the $^{235}U + ^{238}U$ system, which is simple enough to solve explicitly (using the equation given on p 21 of [3]), but for the $^{233}U + ^{238}U$ and $^{239}Pu + ^{242}Pu$ systems computer programs were written and

*The estimate of these effects given in [4] neglects the finite size of the mixed-oxide particles (∿60μm) and corresponds to a ∿ 4°C increase.

run on the Chalk River G-20 computer. The effects on the output cross sections of the errors in the input data (isotopic analyses and assumed cross sections) were determined by repeating the calculations with individually changed input data.

These calculations were carried out for idealized unmixed systems, i.e. with no ^{234}U or ^{238}Pu present initially, with no contribution to the plutonium fraction from neutron capture in the ^{238}U of the uranium fraction, and with no production of uranium isotopes by α decay from plutonium. The computer calculations on the ^{239}Pu + ^{242}Pu system also ignored the effects of neutron capture in ^{241}Am, which produces a small amount of ^{242}Pu (and also some ^{238}Pu from ^{242}Cm α decay). Preliminary hand calculations of these effects were carried out and the results applied as corrections to the observed isotopic compositions. The corrections were essentially trivial, i.e. much less than the error of the mass spectrometer measurements, for all but the ^{233}U + ^{238}U system where (correcting for α decay) the initial relative abundance of 235 was reduced from 0.100 to 0.095, and the final 235 and 236 abundances were reduced from 0.225 to 0.220 and from 0.017 to 0.013 respectively.

In fact no use was made of the measured ^{236}U abundance in the irradiated ^{233}U sample. In principle it would provide another value of $\alpha(235)$ but of much lower accuracy than the value obtained from the ^{235}U irradiation, which was used instead in the ^{233}U calculation (which gave a 236 abundance in satisfactory agreement with the observed value as corrected above for ^{240}Pu α decay).

Table III lists the values of the input cross sections and cross section ratios, and the sources of these data. The uncertainties are generally not important; exceptions are noted in the discussion of the individual results given in the next section. The uncertainties of the σ_a

TABLE III. INPUT DATA

(Cross Sections at 2200 m/s in barns, Resonance Integrals above 0.5 eV)

Nuclide	σ_o(abs)	Note	RI	Note
^{233}U	575.62±3.27	1	890	2
^{235}U	679.46±2.54	1	410	2
^{236}U	5.5 ±0.3	3	350	3
^{238}U	2.721±0.016	4	282	5
^{241}Pu	1375.5 ±9.6	6	740	2
^{242}Pu	19.4 ±1.0	7	1200	8
^{241}Pu	α = 0.3680±0.0096			6

Notes

1. From Table IV of [2]
2. From Table C II of [2]
3. Adopted from values given in Tables 5 and 6 of [6]
4. From [7]
5. From Table A III of [8]
6. From [2]. The values are appropriate for use with the g factors of [9] rather than the output g factors of [2]. The errors have been arbitrarily increased over the $\hat{\sigma}_a$ and $\hat{\alpha}$ errors of ± 7.6 b and ± 0.0066 (see text)
7. Compare values of 18.7±0.7 b [10] 22±2 b [11] and 19.8±1.1 b used in [3]
8. Compare values of 1220±200 b above 0.45 eV [12] and 1090±60 b [11]

and α values for ^{241}Pu have been arbitrarily increased, as noted in Table III, by more than the factor 1.125 recommended in section 5.2 of [2] because R factors were not calculated for this nuclide and an effective temperature was used instead.

Results

Table IV lists the results obtained, along with the individual contributions to the errors from the uncertainties in the isotopic analyses, the input cross sections and the neutron spectrum (using the estimate of ± 30% in R-1 for ^{235}U and ^{239}Pu and its equivalent, ∿ ± 4°C, for other nuclides). The sixth column gives the quadrature sum of these errors, and the last column the errors in the g factors, as given by Westcott [9], for ^{233}U, ^{235}U and ^{239}Pu.

TABLE IV. RESULTS

Quantity	Value at 2200 m/s	Errors				
		Isotopic Analysis	Other Cross Sections	Spectrum Uncertainty	Total	g factor
$\alpha(^{233}U)$	0.0899	±0.0004	±0.041	±0.042	±0.0004	±0.0017
$g\sigma_\gamma(^{234}U)$	95.6 b	±2.0 b	±0.4 b	±0.1 b	±2.1 b	-
$\alpha(^{235}U)$	0.1702	±0.0007	±0.042	±0.042	±0.0007	±0.0020
$\alpha(^{239}Pu)$	0.3597	±0.0009	±0.0011	±0.0015	±0.0021	±0.0045
$\frac{\sigma_f(^{239}Pu)}{\sigma_f(^{233}U)}$	1.4046	±0.0060	±0.0030	±0.0041	±0.0079	±0.0049
$\frac{\sigma_f(^{239}Pu)}{\sigma_f(^{235}U)}$	1.2926	±0.0054	±0.0027	±0.0053	±0.0081	±0.0042
$\frac{\sigma_f(^{233}U)}{\sigma_f(^{235}U)}$	0.9203	±0.0055	±0.0004	±0.0014	±0.0057	±0.0023
$\sigma_\gamma(^{240}Pu)$	289.5 b	±0.5 b	±1.2 b	±0.5 b	±1.4 b	small?

The results for α(239) and σ_γ(240) are in each case the weighted means of two semi-independent measurements from the A and B samples; the two values of α(239) differed by 0.0010 ± 0.0018 and the two values of σ_γ(240) by 1.1 ± 1.6 b, where these errors are the quadrature sum of the independent parts of the individual errors.

It will be seen that the values of α(233) and α(235) are very insensitive to the input cross section data and the neutron spectrum, and that the largest uncertainties arise in the conversion from Maxwellian to 2200 m/s values. For α(239) the g-factor error is also serious, but the mass-spectrometer error is smaller than the uncertainties due to the neutron spectrum and the input cross section data (mainly σ_γ for ^{241}Pu and ^{242}Pu).

The fission cross section ratios involving ^{239}Pu are also rather sensitive to neutron spectrum and cross section data (again mainly σ_γ for ^{241}Pu and ^{242}Pu). The value for the ratio of the ^{233}U and ^{235}U fission cross sections is obtained from the ^{239}Pu/^{233}U and ^{239}Pu/^{235}U results and is virtually independent of uncertainties in the cross sections for plutonium isotopes. The uncertainties in the input cross section data for uranium isotopes (mainly σ_a for ^{233}U and ^{235}U) have only a very small effect. The errors quoted for these σ_f ratio results are of course not independent, and using them as input data to a least squares fit raises problems that are discussed in [2].

The values of $g\sigma_\gamma$ for ^{234}U and σ_γ for ^{240}Pu are essentially a by-product of the present work, though their accuracy appears to be better than that of previously available data. The error in the ^{234}U cross section is due almost entirely to the uncertainties in the measurement of the small amounts of ^{235}U in the initial and final uranium fractions of the ^{233}U + ^{238}U mixture. The main contributions to the error in $\sigma_\gamma(240)$ are from uncertainties in the absorption cross sections of ^{233}U, ^{235}U and ^{241}Pu and in the ß-decay half life of ^{241}Pu.

Comparison with other Data

The values of α obtained in the present experiment are in agreement with previous less accurate data (see Table VIIIa of [2]). The fission cross section ratios are compared with other values in Table V and it will be seen that the present work tends to support the relatively high values for $^{239}Pu/^{233}U$ and $^{239}Pu/^{235}U$ of Bigham et al [13]. Table V only includes data taken in Maxwellian spectra so that uncertainties due to g factors are not involved. The errors quoted, which do not contain g-factor contributions, are the partially correlated errors of the "best values" from each measurement (and are therefore ~~larger~~ smaller (Peter Hemmo 72/11/16) than the "equivalent independent" errors given in Table Vb of [2]).

TABLE V. FISSION CROSS-SECTION RATIO MEASUREMENTS

	$^{233}U/^{235}U$	$^{239}Pu/^{233}U$	$^{239}Pu/^{235}U$
Bigham et al [13]	0.9141±0.0012	1.4189±0.0081	1.2970±0.0075
White et al [14]			1.253 ±0.030
Keith et al [15]	0.9227±0.0064	1.3773±0.0137	1.2709±0.0138
Present work	0.9203±0.0057	1.4046±0.0079	1.2926±0.0081

Values [13, 14, 15] recalculated as in [2]

The present results are compared in Table VI with the best values of α and σ_f ratios that can be obtained from all other available measurements. For this purpose the least squares fit program of [2] was rerun with the present results omitted from the input data set. The outputs of the fit are expressed as Maxwellian averages divided by g-factor values from [9] so that they are directly comparable with the present results as given in Table IV. Also tabulated, on the same basis, are the results from a similar least squares fit that does include the present results.* In all cases the errors exclude the g-factor errors. If they were included, as in Table XII of [2], the improvement in accuracy due to the present results would be much less striking, e.g. the error of the 2200 m/s value of $\alpha(239)$ only decreases from ± 0.0039 to ± 0.0035.

The results of the present experiment have been expressed as values of α and σ_f ratios because these quantities are relatively independent of other cross section data. However, the results that can be obtained for $\sigma_a(239)$ are of some interest. The values of σ_a for ^{233}U and ^{235}U given in Table III are, essentially, the weighted averages of all the monokinetic transmission data corrected for scattering. If the Table III value for

*The least squares fit [2] used preliminary, slightly different, values from the present experiment (cf Tables Vb and VIIIa of [2]) and gave (Maxwellian) output values that are higher than those in the last column of Table VI by 0.0003 for $\alpha(239)$, 0.0005 for $\sigma_f(239/233)$ and 0.0004 for $\sigma_f(239/235)$.

TABLE VI. COMPARISON WITH LEAST-SQUARES-FIT RESULTS

Quantity	Present Value	LSF Values Excluding present results	LSF Values Including present results
$\alpha(233)$	0.0899±0.0004	0.0902±0.0008	0.0900±0.0003
$\alpha(235)$	0.1702±0.0007	0.1699±0.0008	0.1701±0.0005
$\alpha(239)$	0.3597±0.0021	0.3650±0.0037	0.3609±0.0018
$\sigma_f(233/235)$	0.9203±0.0057	0.9138±0.0012	0.9140±0.0012
$\sigma_f(239/233)$	1.4046±0.0079	1.3986±0.0050	1.4021±0.0041
$\sigma_f(239/235)$	1.2926±0.0081	1.2780±0.0046	1.2816±0.0038

Values are (Maxwellian averages)/(g factors from [9])
Errors exclude g factor errors (see text)

$\sigma_a(233)$ is used to interpret the observed behaviour of the B sample a value of 1009.2 ± 8.6 b is obtained for $\sigma_a(239)$ at 2200 m/s, where the error includes the uncertainties in g factors; the corresponding value from the A sample and the Table III value of $\sigma_a(235)$ is 1020.1 ± 8.0 b. The expected error of the difference (10.9 b) is ± 8.4 b, and the weighted mean is 1015.1 ± 7.1 b, which may be compared with the weighted mean value from transmission measurements (Table IVc of [2]) of 1012.11 ± 6.17 b.

Acknowledgments

The authors wish to thank F.W. Molson for assistance with sample preparation and chemical processing, J.A. Schruder for mass spectrometric analyses, and Miss C.M. Sprague for programming and computation. The irradiation facility was designed by C.B. Bigham and the late N.H. Nielson, and the analysis of neutron spectra was the work of S.A. Kushneriuk.

REFERENCES

[1] WESTCOTT, C.H., EKBERG, K., HANNA, G.C., PATTENDEN, N.S., SANATANI, S., ATTREE, P.M., Atom. Energy Rev. 3 2 (1965) 3
[2] HANNA, G.C., WESTCOTT, C.H., LEMMEL, H.D., LEONARD, B.R., Jr., STORY, J.S., ATTREE, P.M., Atom. Energy Rev. 7 4 (1969) 3
[3] DURHAM, R.W., HANNA, G.C., LOUNSBURY, M., BIGHAM, C.B., HART, R.G., JONES, R.W., Nuclear Data for Reactors (Proc. Conf. Paris 1966) 2 IAEA, Vienna (1967) 17
[4] KUSHNERIUK, S.A., AECL-3364 (1969)
[5] LOUNSBURY, M., Can.J.Chem. 34 (1956) 259
[6] CARLSON, A.D., FRIESENHAHN, S.J., LOPEZ, W.M., FRICKE, M.P., Nuclear Physics A 141 (1970) 577
[7] BIGHAM, C.B., DURHAM, R.W., UNGRIN, J., Can. J. Phys. 47 (1969) 1317
[8] WESTCOTT, C.H., AECL-1101 (1960)
[9] WESTCOTT, C.H., AECL-3255 (1969)
[10] DURHAM, R.W., MOLSON, F., Can. J. Phys. 48 (1970) 716
[11] YOUNG, T.E., REEDER, S.D., IN-1132 (1968)
[12] CABELL, M.J., Nuclear Data for Reactors (Proc. Conf. Paris 1966) 2 IAEA Vienna (1967) 3
[13] BIGHAM, C.B., HANNA, G.C., TUNNICLIFFE, P.R., CAMPION, P.J., LOUNSBURY, M., MACKENZIE, D.R., Second Int. Conf. Peaceful Uses Atomic Energy (Proc. Conf. Geneva 1958) 16 UN, New York (1959) 125
[14] WHITE, P.H., REICHELT, J.M.A., WARNER, G.P., Nuclear Data for Reactors (Proc. Conf. Paris 1966) 2 IAEA, Vienna (1967) 29
[15] KEITH, R.L.G., MCNAIR, A., RODGERS, A.L., J. Nucl. Energy 22 (1968) 477

MESURE DES SECTIONS EFFICACES DE L'URANIUM-233 POUR LES NEUTRONS THERMIQUES

R. VIDAL, M. ROBIN, C. CARNEIRO DA SILVA*
CEA, Centre d'études nucléaires
de Fontenay-aux-Roses,
France

Présenté par G.C. Hanna

Abstract — Résumé

MEASUREMENTS OF ^{233}U CROSS-SECTIONS FOR THERMAL NEUTRONS.

The fission cross-section and the η of ^{233}U are determined for 2200 m/s by taking ^{235}U as a standard and using integral measurements made in a thermal neutron spectrum as a basis. This was done by using two complementary methods:

a) Measurement of fission cross-sections with fission chambers. The ratio of the fission cross-sections of ^{233}U and ^{235}U is determined by irradiating fission chambers containing ^{238}U in combination with either ^{233}U or ^{235}U in a Maxwellian spectrum. The originality of the method lies in the calibration of the chambers, which is carried out in a fast-neutron spectrum and takes advantage of the fissions produced in the ^{238}U. In this way, merely by knowing the isotopic contents of the foils, one can make a very accurate relative calibration. The results are $(\sigma_{f_3}/\sigma_{f_5})_{2200\ m/s} = 0.914 \pm 0.005$.

b) Measurement of η by the oscillation method. The ratio (η_3/η_5) is determined by measuring the variations in reactivity produced in a natural uranium-heavy water lattice by the oscillation of ^{238}U-samples containing between 0.1 and 0.7% of ^{233}U or ^{235}U. By weighting the differential cross-sections of ^{233}U and ^{235}U over the neutron spectrum in which the measurements were made, the authors derive the ratio of the η from the ratios of the effective $\hat{\eta}$. The results are $(\eta_{233}/\eta_{235})_{2200\ m/s} = 1.081 \pm 0.005$.

From all these results the following cross-sections of ^{233}U can be derived, considering the values of the ratio ν_3/ν_5, of σ_{f_5} and η_5 given: $\sigma_{f_3} = 530 \pm 4$ barns; $\eta_3 = 2.240 \pm 0.012$; $\sigma_{a_3} = 589 \pm 7$ barns.

MESURE DES SECTIONS EFFICACES DE L'URANIUM-233 POUR LES NEUTRONS THERMIQUES.

La section efficace de fission et le η du ^{233}U pour des neutrons de 2200 m/s, en prenant le ^{235}U comme étalon, ont été déterminés à partir de mesures intégrales faites dans un spectre de neutrons thermiques, en utilisant deux méthodes complémentaires.

a) Mesure de la section de fission à l'aide de chambres à fission. Le rapport des sections efficaces de fission du ^{233}U et du ^{235}U est déterminé en irradiant dans un spectre maxwellien des chambres à fission contenant du ^{238}U allié à du ^{233}U ou du ^{235}U. L'originalité de la méthode réside dans l'étalonnage des chambres, qui est effectué dans un spectre de neutrons rapides, en mettant à profit les fissions qui se produisent dans le ^{238}U. Ainsi, la seule connaissance des teneurs isotopiques des dépôts permet un étalonnage relatif très précis. On a obtenu $(\sigma_{f_3}/\sigma_{f_5})_{2200\ m/s} = 0,914 \pm 0,005$.

b) Mesure du η par la méthode d'oscillation. Le rapport (η_3/η_5) est déterminé en mesurant les variations de réactivité produites dans un réseau à uranium naturel et eau lourde par l'oscillation d'échantillons de ^{238}U contenant entre 0,1 et 0,7% de ^{233}U ou de ^{235}U. En pondérant les sections efficaces différentielles du ^{233}U et du ^{235}U sur le spectre neutronique où ont été faites les mesures, on déduit le rapport des η à 2200 m/s, à partir du rapport des $\hat{\eta}$ effectifs. On obtient: $(\eta_{233}/\eta_{235})_{2200\ m/s} = 1,081 \pm 0,005$.

De l'ensemble de ces résultats, on peut déduire, en se donnant les valeurs du rapport ν_3/ν_5 et de σ_{f_5} et η_5, les sections efficaces suivantes du ^{233}U: $\sigma_{f_3} = 530 \pm 4$ barns; $\eta_3 = 2,240 \pm 0,012$; $\sigma_{a_3} = 589 \pm 7$ barns.

---

* Stagiaire du « Centro de Energia Nuclear da Universidade Federal de Pernambuco».

INTRODUCTION

La mesure des sections efficaces thermiques du ^{233}U est faite par deux méthodes intégrales complémentaires et indépendantes [1, 2].

A l'aide de chambres à fission, on mesure dans un spectre maxwellien le rapport des sections de fission $\hat{\sigma}_{f3}/\hat{\sigma}_{f5}$. A partir de cette valeur expérimentale, on détermine $(\sigma_{f3}/\sigma_{f5})$, à 2200 m/s.

Par oscillation dans un réseau uranium naturel-eau lourde, on mesure le rapport $\hat{\eta}_3/\hat{\eta}_5$. Comme précédemment, à partir de cette valeur expérimentale, on détermine (η_3/η_5), à 2200 m/s.

En adoptant les valeurs de référence pour le ^{235}U, on en déduit les sections efficaces de capture et de fission pour le ^{233}U à 2200 m/s.

1. MESURE DU RAPPORT DES SECTIONS EFFICACES DE FISSION DU ^{233}U ET DU ^{235}U DANS UN SPECTRE MAXWELLIEN PAR CHAMBRES A FISSION

De nombreux auteurs se sont préoccupés d'effectuer cette mesure par la technique des chambres à fission; l'incertitude des résultats était liée à la connaissance de la quantité de matière fissile déposée et au rendement global de la chambre. Ces quantités étaient déterminées par comptage α et l'on supposait que le rendement de la chambre était le même pour les produits de fission et pour les α.

La méthode originale que nous avons mise au point permet de s'affranchir de ces hypothèses.

1.1. Principe de la méthode

L'étalonnage des chambres est effectué uniquement en fission. On utilise un spectre de référence riche en neutrons de fission et des chambres contenant une quantité importante de ^{238}U uniquement fissile aux hautes énergies et une faible quantité de ^{233}U ou de ^{235}U. Les chambres étant étalonnées en masse de ^{238}U, une simple mesure de la teneur isotopique du dépôt, qui est très précise, permet de connaître la masse de ^{233}U ou de ^{235}U contenu et de les utiliser dans un spectre thermique où le ^{238}U ne crée pas de fission.

Le taux de comptage C délivré par une chambre à fission contenant du ^{233}U et du ^{238}U placée dans un spectre quelconque s'exprime par la relation:

$$C = K \phi (N_8 \sigma_{f8} + N_3 \sigma_{f3}) \qquad (1)$$

K : rendement de la chambre
ϕ : flux au point de la mesure
σ_{f3}, σ_{f8} : sections efficaces de fission du ^{233}U et du ^{238}U dans le spectre considéré; $\sigma_{f8} = 0$ pour un spectre thermique
N_3, N_8 : quantités de ^{233}U et de ^{238}U déposées dans les chambres.

Lorsque l'on fait le quotient des rapports des taux de comptage d'un couple de chambres: 38 (^{233}U - ^{238}U) et 58 (^{235}U - ^{238}U), irradiées

simultanément dans le spectre de fission de référence F, puis dans le spectre thermique de mesure T, on obtient la relation suivante:

$$\left(\frac{\sigma_{f3}}{\sigma_{f5}}\right)_T = \frac{(C_{38}/C_{58})_T}{(C_{38}/C_{58})_F} \times \frac{(N_5/N_8)_{58}}{(N_3/N_8)_{38}} \times \frac{1 + (N_3/N_8)_{38} \times (\sigma_{f3}/\sigma_{f8})_F}{1 + (N_5/N_8)_{58} \times (\sigma_{f5}/\sigma_{f8})_F} \qquad (2)$$

On remarque dans cette expression que le dernier facteur est un terme correctif qui dépend de la teneur isotopique des dépôts et du rapport des sections de fission dans le spectre de référence.

Ce terme correctif est mesuré en associant à ces chambres 38 et 58 respectivement des chambres à ^{233}U pur et à ^{235}U pur. Lorsque l'on fait le quotient des rapports des taux de comptage des couples de chambres 38 et 3 ou 58 et 5 irradiées simultanément dans le spectre F, puis dans le spectre T, on obtient les relations suivantes:

$$Q_{38} = \frac{(C_{38}/C_3)_F}{(C_{38}/C_3)_T} = 1 + \left(\frac{N_8}{N_3}\right)_{38} \times \left(\frac{\sigma_{f8}}{\sigma_{f3}}\right)_F \qquad (3)$$

$$Q_{58} = \frac{(C_{58}/C_5)_F}{(C_{58}/C_5)_T} = 1 + \left(\frac{N_8}{N_5}\right)_{58} \times \left(\frac{\sigma_{f8}}{\sigma_{f5}}\right)_F \qquad (4)$$

On déduit ainsi de ces relations pour le spectre de référence:

$$(\sigma_{f3}/\sigma_{f8})_F \quad (\sigma_{f5}/\sigma_{f8})_F \quad \text{et} \quad (\sigma_{f3}/\sigma_{f5})_F$$

On peut aussi, à titre de vérification, n'utiliser que des couples de chambres sans ^{238}U et, en les mesurant successivement dans les spectres F et T, on obtient la relation:

$$\left(\frac{\sigma_{f3}}{\sigma_{f5}}\right)_T = \frac{(C_3/C_5)_F}{(C_3/C_5)_T} \times \left(\frac{\sigma_{f3}}{\sigma_{f5}}\right)_F \qquad (5)$$

Dans cette relation, la précision sur le rapport $(\sigma_{f3}/\sigma_{f5})_T$ dépend directement de celle sur le rapport des sections efficaces dans le spectre F. Cette méthode est donc en principe moins précise, mais elle constitue une excellente vérification d'erreurs systématiques éventuelles.

1.2. Technique de mesure

Les chambres à fission ont été construites par le laboratoire spécialisé du Commissariat à l'énergie atomique [3]. Elles sont d'un modèle de très petites dimensions. Le boîtier en titane a un diamètre extérieur de 4 mm et une longueur de 23,2 mm. L'électrode centrale, en titane également, a un diamètre de 2,5 mm et une longueur utile de 12 mm. Les différents dépôts ont été réalisés par électrolyse. Pour les chambres contenant le mélange ^{235}U-^{238}U, les dépôts sont en U naturel; pour celles contenant le mélange ^{233}U-^{238}U, l'uranium utilisé contient environ 350 ppm de ^{235}U et 1% de ^{233}U.

Le spectre de fission de référence est celui du convertisseur de la pile ZOE, constitué par un cylindre d'uranium naturel percé d'un trou dont les parois sont recouvertes de cadmium. Le spectre obtenu est riche en neutrons de fission et parfaitement reproductible, comme le montrent les nombreuses mesures faites avec des chambres utilisant différents matériaux fissiles: ^{238}U, ^{239}Pu, ^{235}U, ^{233}U. Les mesures dans un spectre thermique ont été faites dans la colonne thermique de la pile ULYSSE, réacteur du type ARGONAUT, constituée par un cube de graphite de 150 cm de côté. Des mesures faites avec différentes épaisseurs de parois de chambre montrent que le spectre thermique n'est pratiquement pas perturbé par la présence de la chambre.

Afin de s'assurer une excellente précision, la mesure des taux de comptage est effectuée par une technique originale. Pour chaque irradiation de chambre, on enregistre sur un sélecteur d'amplitude à 100 canaux le spectre des impulsions. Le taux de comptage est ensuite calculé à partir d'un seuil variable, dont la valeur est normalisée par rapport à une abscisse de référence qui est définie par rapport au maximum de spectre. Plusieurs seuils sont déterminés et constituent une caractéristique de la chambre. Les résultats sont ainsi indépendants des dérives du matériel électronique et même des fluctuations de mesure dues aux α ou aux parasites. La reproductibilité des mesures ne dépend, dans ces conditions, que de la précision statistique du comptage.

La précision atteinte sur le rapport du taux de comptage est grandement améliorée si on utilise les nombreux résultats obtenus dans un même spectre de référence, à des dates différentes et avec différents couples de chambres d'une même série de fabrication.

1.3. Résultats

Plusieurs couples de chambres (^{238}U, ^{233}U) et ^{233}U pur et (^{238}U, ^{235}U) et ^{235}U pur ont été utilisés pour mesurer les rapports des sections de fission dans le spectre de référence F. On a ainsi obtenu, pour le calcul des termes correctifs:

$$(\sigma_{f8}/\sigma_{f5})_F = 0,0478 \pm 0,0002$$

$$(\sigma_{f8}/\sigma_{f3})_F = 0,0234 \pm 0,0014$$

d'où:

$$(\sigma_{f3}/\sigma_{f5})_F = 2,043 \pm 0,015$$

On remarquera que la valeur de $(\sigma_{f8}/\sigma_{f5})_F$ est connue avec une meilleure précision, car, les chambres étant réalisées avec des dépôts d'uranium naturel, il n'y a aucune erreur sur la valeur de la teneur isotopique.

En utilisant la relation (2), on obtient, pour le rapport des sections de fission dans le spectre thermique:

$$(\sigma_{f3}/\sigma_{f5})_T = 0,932 \pm 0,007$$

La précision statistique sur le rapport des taux de comptage, soit dans le spectre de référence, soit dans le spectre thermique, est de ± 0, 5%. La précision sur les teneurs isotopiques est de ± 0, 1% et la précision sur le terme correctif de ± 0, 3%. Au total, on obtient une erreur expérimentale égale à ± 0, 8%.

En utilisant la relation (5), on obtient:

$$(\sigma_{f3}/\sigma_{f5})_T = 0,928 \pm 0,009$$

Dans ce cas, le rapport des taux de comptage est mesuré à ± 0, 5% dans chacun des spectres et, la valeur de l'indice dans le spectre de référence étant connue à ± 0, 7%, on obtient le résultat prévu avec une précision de 1%. En pondérant ces deux valeurs, on obtient:

$$(\sigma_{f3}/\sigma_{f5})_T = 0,931 \pm 0,005$$ Maxwellian result

Cette valeur représente le rapport des sections efficaces effectives dans un spectre maxwellien à 20° C, qu'il faut corriger pour en déduire les valeurs à 2200 m/s. Pour cette correction, on applique les coefficients calculés par Westcott [4]:

$$g_3 = \frac{\hat{\sigma}_{f3}}{(\sigma_{f3})_{2200}} = 0,9950 \pm 0,0021$$

$$g_5 = \frac{\hat{\sigma}_{f5}}{(\sigma_{f5})_{2200}} = 0,9766 \pm 0,0016$$

On en déduit:

$$(\sigma_{f3}/\sigma_{f5})_{2200} = 0,914 \pm 0,005$$

2. MESURE DU RAPPORT η_3/η_5 PAR LA METHODE D'OSCILLATION

2.1. Principe de la méthode

La méthode d'oscillation pour l'étude des matériaux fissiles a été développée au Commissariat à l'énergie atomique et a fait l'objet de nombreuses publications [5-7]. Nous n'en rappelons que le principe. On compare les signaux obtenus avec des échantillons d'uranium contenant de faibles quantités du matériau fissile à mesurer avec ceux fournis par des échantillons de référence, de géométrie identique et de caractéristiques neutroniques bien connues (uranium boré, enrichi ou appauvri en ^{235}U).

Considérons le réseau de référence critique, constitué par un ensemble de cellules identiques, formées de barreaux d'uranium naturel plongés dans de l'eau lourde. On remplace l'élément combustible central de ce réseau par un autre élément de propriétés neutroniques voisines. Une barre de pilotage automatique permet de rétablir l'état critique par variation de la réactivité. Celle-ci est fonction de la différence entre la production et l'absorption des neutrons de l'élément perturbateur et de l'élément du réseau. On

démontre que l'on peut définir autour de l'échantillon une zone ayant approximativement comme rayon le pas du réseau, au-delà de laquelle la perturbation de la densité neutronique est indépendante de la forme de la loi de capture du matériau fissile. Ceci permet de définir par le calcul un échantillon fictif E, composé d'uranium naturel, de ^{235}U et de bore, équivalent à l'échantillon à mesurer, P [7]. Pour ces échantillons E et P, qui produisent le même effet en réactivité, et la même perturbation de densité neutronique à l'extérieur de la zone perturbée, on a égalité des taux de capture et de production pour l'ensemble du réacteur. Le calcul détaillé de la cellule perturbée, effectué à l'aide du code THERMOS [8], permet de déterminer le rapport n_P/n_E des densités neutroniques moyennes dans les deux échantillons, ainsi que les rapports α et β des taux de capture et de production de neutrons pour l'échantillon à mesurer et pour l'échantillon équivalent.

L'équivalence des échantillons se traduit par les deux relations suivantes:

$$\alpha \times v_0 \times n_P \times \hat{\Sigma}_{aP} = v_0 \times n_E \times \hat{\Sigma}_{aE} \tag{6}$$

$$\beta \times v_0 \times n_P \times (\nu\hat{\Sigma}_{fP}) = v_0 \times n_E \times (\nu\hat{\Sigma}_{fE}) \tag{7}$$

Les deux échantillons sont caractérisés par le même signal de réactivité G, qui, pour l'échantillon équivalent, s'exprime sous la forme:

$$G = a\,N_5 + b\,N_B + C \tag{8}$$

N_5, N_B: quantités de ^{235}U et de bore qu'il faut ajouter à l'uranium naturel servant de référence pour obtenir la composition de l'échantillon équivalent.

Des trois équations avec quatre inconnues (N_5, N_B, Σ_{aP}, $\nu\Sigma_{fP}$), on déduit la relation linéaire suivante:

$$\hat{\eta}_P/\hat{\eta}_5 = A + B \times \frac{\hat{\sigma}_{a5}}{\hat{\Sigma}_{aP}} \tag{9}$$

A et B: constantes qui dépendent des sensibilités du signal de réactivité au ^{235}U et au bore, des sections efficaces du ^{235}U et du bore et des coefficients calculés α, β et n_P/n_E.

Avec la relation (9), on peut déduire le rapport $\hat{\eta}_P/\hat{\eta}_5$ des η si on se donne la section efficace de capture du matériau fissile à mesurer. La section efficace de fission étant mesurée par ailleurs, cette valeur de Σ_a est ensuite réajustée.

A partir du rapport des $\hat{\eta}$ effectifs, on peut déduire le rapport des η à 2200 m/s, en effectuant des corrections pour tenir compte de la loi de variation des sections efficaces avec l'énergie. L'intérêt de cette méthode est surtout de mesurer directement dans le réseau des valeurs des sections efficaces effectives, afin de les comparer directement à celles fournies par un formulaire de calcul de réseau.

2.2. Technique de mesure

Les mesures sont faites dans le réacteur MINERVE, au Centre d'études nucléaires de Fontenay-aux-Roses. Au centre de la pile, on place un réseau au pas carré de 130 mm, en uranium naturel de 29,2 mm de diamètre et eau lourde, contenu dans une cuve d'aluminium de 90 cm de côté et de 97 cm de hauteur. La criticité est assurée par des éléments d'uranium enrichi à 93%, placés autour de la cuve.

On fait osciller verticalement le combustible de la cellule centrale avec un mouvement carré, de période 20 secondes et d'amplitude 60 cm. L'échantillon à étudier séjourne alternativement au centre et à l'extérieur du réacteur. Il est inclus entre deux colonnes d'uranium naturel de hauteur telle qu'il y a toujours, au cours de l'oscillation, de l'uranium dans la cellule centrale. Pendant les mesures, le réacteur est maintenu à l'état critique à l'aide d'une barre de pilotage automatique [9]. La variation de position de cette barre au cours des oscillations est directement proportionnelle au signal de réactivité correspondant à la différence entre l'échantillon à mesurer et l'uranium naturel de référence.

Les mesures sont faites avec des échantillons de même géométrie (diamètre 2,92 cm; longueur 9,75 cm), dont on a mesuré avec précision les teneurs en uranium et en bore.

Les échantillons suivants ont été utilisés:

Echantillons pour l'étalonnage du signal en sensibilité au ^{235}U et au bore:
- uranium enrichi à 0,65, 0,71, 0,83, 0,86, 0,91, 0,95%
- uranium naturel avec 30 et 50 ppm de bore

Echantillons d'alliage uranium - ^{233}U
- uranium naturel avec 0,10 et 0,15% de ^{233}U
- uranium appauvri à 0,35% avec 0,25 et 0,35% de ^{233}U.

A titre de vérification, quelques échantillons contenant de faibles quantités de plutonium ont aussi été mesurés.

2.3. Résultats

Un résultat de mesure d'oscillation correspond à la valeur moyenne du signal de réactivité pendant 50 cycles de 20 s. Sur chaque échantillon, on effectue plusieurs mesures.

Afin de faciliter la comparaison des signaux obtenus, on effectue les corrections suivantes:
- correction de masse, pour que les signaux soient rapportés à des échantillons contenant la même masse de ^{238}U
- correction de linéarité de la barre de pilotage, qui rend le signal mesuré directement proportionnel à la variation de réactivité
- correction de courbure, qui permet de conserver, même pour les grandes perturbations, des signaux proportionnels à l'équivalence en ^{235}U et bore.

Suivant la méthode décrite dans le chapitre 2.1, on obtient le rapport $\hat{\eta}/\hat{\eta}_5$, qui correspond à chaque mesure, et, de là, le rapport (η/η_5) à 2200 m/s.

L'interprétation des résultats, et en particulier le passage des sections efficaces effectives mesurées aux valeurs à 2200 m/s qui s'en déduisent, est effectuée à l'aide du code CRUEL V [10], qui traite la thermalisation des neutrons dans les réacteurs à eau lourde et qui utilise la bibliothèque des sections efficaces différentielles de l'UKAEA (1967) [11].

Les résultats obtenus pour les quatre échantillons contenant du ^{233}U, affectés uniquement des erreurs de mesure, sont les suivants:

Echantillon	$(\eta_3/\eta_5)_{2200}$
U naturel + 0,10% de ^{233}U	1,082 ± 0,002
U naturel + 0,15% de ^{233}U	1,078 ± 0,002
U à 0,35% + 0,25% de ^{233}U	1,083 ± 0,002
U à 0,35% + 0,35% de ^{233}U	1,080 ± 0,002

Les échantillons à support d'uranium appauvri et plus chargés en ^{233}U donnent des résultats plus précis; on déduira donc la valeur moyenne de l'ensemble des échantillons en pondérant le résultat obtenu pour chaque échantillon par la quantité de ^{233}U qu'il contient.

En plus des erreurs aléatoires provenant de l'analyse des échantillons et des étalons et de la mesure des signaux, pour lesquelles la répétition des expériences et l'utilisation de plusieurs échantillons diminuent considérablement les erreurs statistiques, il faut tenir compte des erreurs systématiques introduites par les différentes corrections, par le calcul des coefficients de passage de l'échantillon à son équivalent et par le calcul du spectre.

Afin de confirmer les calculs de spectre, des mesures ont été effectuées avec des échantillons de plutonium, eux-mêmes beaucoup plus sensibles en raison de la forme de leur section efficace. Le résultat obtenu pour le ^{239}Pu avec des échantillons peu chargés en ^{240}Pu est de

$$(\eta_9/\eta_5)_{2200} = 1,017$$

Cette valeur est en parfait accord avec celle proposée par Hanna dans son évaluation de 1969 [4], égale à 1,018 ± 0,009, et la valeur expérimentale de 1,014 ± 0,003, obtenue aussi par la méthode d'oscillation sur les assemblages critiques MARIUS et CESAR.

Il faut aussi remarquer que, dans le calcul de η, les erreurs sur le spectre ne sont pas indépendantes sur $\hat{\sigma}_a$ et $\hat{\sigma}_f$ et elles se compensent partiellement lorsqu'on effectue le rapport. Ceci nous conduit à adopter, pour les erreurs dues à l'interprétation du résultat, une valeur de ± 0,003, à laquelle s'ajoute l'erreur statistique de mesure égale à ± 0,002. On obtient ainsi la valeur suivante:

$$(\eta_3/\eta_5)_{2200} = 1,081 \pm 0,005$$

CONCLUSION

Les mesures avec chambres à fission et par oscillation, ramenées à 2200 m/s, donnent les résultats suivants:

$$\frac{\sigma_{f3}}{\sigma_{f5}} = 0,914 \pm 0,005$$

$$\frac{\eta_3}{\eta_5} = 1,081 \pm 0,005$$

En remarquant que

$$\frac{\eta_3}{\eta_5} = \frac{\nu_3}{\nu_5} \frac{\sigma_{f3}/\sigma_{f5}}{\sigma_{a3}/\sigma_{a5}}$$

on peut, en admettant [4]

$$\frac{\nu_3}{\nu_5} = 1,0262$$

en déduire le rapport des sections d'absorption:

$$\frac{\sigma_{a3}}{\sigma_{a5}} = 0,868 \pm 0,008$$

Nos valeurs et celles déduites des mesures de Lounsbury [12] et tirées de l'évaluation de Westcott [4] sont les suivantes:

	Ce rapport	Lounsbury [12]	Westcott [4]
σ_{f3}/σ_{f5}	0,914 ± 0,005	0,921 ± 0,007	0,915 ± 0,004
σ_{a3}/σ_{a5}	0,868 ± 0,008	0,858 ± 0,001	0,851 ± 0,004

L'examen de ces résultats fait ressortir un bon accord avec les mesures de Lounsbury, dont la précision est excellente, pour le rapport des sections efficaces d'absorption.

Si on adopte les valeurs suivantes pour les sections efficaces du ^{235}U [5]:

[4] !!!

$$\sigma_{f5} = 580,2 \pm 1,8 \text{ barns}$$

$$\sigma_{a5} = 678,5 \pm 1,9 \text{ barns}$$

$$\eta_5 = 2,072 \pm 0,006$$

on en déduit le jeu de valeurs suivantes pour le ^{233}U, en incluant dans les marges d'erreur l'incertitude sur les sections efficaces du ^{235}U:

$$\sigma_{f3} = 530 \pm 4 \text{ barns}$$

$$\sigma_{a3} = 589 \pm 7 \text{ barns}$$

$$\eta_3 = 2,240 \pm 0,012$$

L'ensemble de ces résultats montre un bon accord avec les valeurs publiées par Lounsbury, qui sont obtenues par des méthodes totalement différentes, ce qui confirme que les erreurs systématiques éventuelles de l'une ou l'autre méthode sont relativement faibles.

REFERENCES

[1] CARNEIRO DA SILVA, C., ROBIN, M., VIDAL, R., Mesure des sections efficaces thermiques de l'uranium 233, Note CEA (à paraître).

[2] CARNEIRO DA SILVA, C., Mesure des sections efficaces de l'uranium 233 dans un assemblage critique, Thèse de Doctorat de 3ème cycle, Faculté d'Orsay (1969).

[3] GUERY, M., MENESSIER, P., Mesure d'indices de spectre par chambre à fission, Note CEA (à paraître).

[4] HANNA, G.C., WESTCOTT, C.H., LEMMEL, H.D., LEONARD, B.R., STORY, J.S., ATTREE, P.M., Revision of values for 2200 m/s neutron constants for four fissile nuclides, Atom. Energy Rev. 7 4 (1969) 3.

[5] TRETIAKOFF, O., VIDAL, R., CARRE, J.C., ROBIN, M., Mesure des sections efficaces effectives d'échantillons fissiles par une méthode d'oscillation dans les assemblages critiques, Rapport CEA-R-2487 (1964).

[6] VIDAL, R., TRETIAKOFF, O., ROBIN, M., « Mesure des sections efficaces effectives d'échantillons fissiles par une méthode d'oscillation dans les assemblages critiques», Exponential and Critical Experiments III (C.r. Coll. Amsterdam, 1963), AIEA, Vienne (1964) 141.

[7] LAPONCHE, B., LEFEBVRE, J.C., MENESSIER, D., MICHEL-VILLAZ, M., BASIUK, M.J., VANUXEEM, J., Expérience de remplacement d'un élément combustible, Méthode d'interprétation, Note CEA-N-1043 (1969).

[8] HONECK, H.C., THERMOS, BNL-5826 (1961).

[9] CARRE, J.C., Etude d'un pilote automatique pour les mesures précises de faibles variations de réactivité, Note CEA-N-1139 (1969).

[10] CHABRILLAC, M., Code CRUEL V, Communication personnelle.

[11] Bibliothèque UKAEA de sections efficaces.

[12] LOUNSBURY, M., DURHAM, R.W., BIGHAM, C.B., HANNA, G.C., KUSHNERIUK, S.A., Measurements of alpha and fission cross section ratios for U 233, U 235, and Pu 239 at thermal energies, INDC (CAN) 4 (1969) et EANDC (CAN) 40 (1969).

[13] Etude neutronique du plutonium dans les réacteurs à neutrons thermiques, Rapport final sur les études du contrat CEA-Euratom « Recyclage du Plutonium», Rapport EUR (à paraître).

DISCUSSION

TO PAPERS IAEA-CN-26/2, 97

A. J. DERUYTTER: Are there published data from irradiation experiments on the 2200 m/s fission cross-section ratio of ^{239}Pu to ^{235}U that support the Chalk River value?

G. C. HANNA: I am not aware of any such measurements.

J. Y. BARRÉ: Could you comment on the validity of applying the least-squares method to the case of the ratio σ_{f9}/σ_{f5}? It seems to me that there are two series of results: high values (1.29) and low values (1.26). The difference between these ratios is considerably higher than the precision of each of the measurements (0.7%).

G. C. HANNA: I admit that this is a real difficulty but it is not an isolated one. For example, there are also serious discrepancies in the measurements of $\bar{\nu}$ for Cf. In these circumstances some rather arbitrary decisions have to be taken. These decisions and their effects were discussed at length in the paper describing the IAEA least-squares fit (Atomic Energy Review, 7 (1969)3).

ВЕЛИЧИНА α ДЛЯ ^{239}Pu

С. И. СУХОРУЧКИН
Институт теоретической и экспериментальной физики Государственного комитета по использованию атомной энергии СССР, Москва, Союз Советских Социалистических Республик

Abstract — Аннотация

THE VALUE α FOR ^{239}Pu.

A short review of the results of the IAEA experts meeting on the α (^{239}Pu) problem held at Studsvik in Sweden on 12 June, 1970, is given. The findings and recommendations of the meeting are discussed, in particular the conclusion that the present accuracy in α can be assessed as ± 10% up to 10 keV-neutron energy.

ВЕЛИЧИНА α ДЛЯ ^{239}Pu.

В статье дается краткий обзор результатов работы совещания экспертов по проблеме величины α (^{239}Pu), проведенном МАГАТЭ в Студсвике (Швеция) 12 июня 1970 г. Приводятся и обсуждаются рекомендации, принятые этим совещанием, в частности вывод о том, что точность знания α в настоящее время может быть оценена величиной порядка 10% до энергии ~ 10 кэв.

Меня просили рассказать в обзорном докладе о результатах работы совещания экспертов, проведенном МАГАТЭ с целью рассмотрения современного состояния вопроса по величине α для ^{239}Pu. Это совещание проходило в Студсвике, Швеция, 12 июня, и на нем присутствовали Де Сасюр (из Ок-Риджа), Фаррелл (из Лос-Аламоса), Барре (из Кадараша), Роуландс (из Винфриза), Сухоручкин (из Москвы) и Шмидт и Коньшин из МАГАТЭ. В своем вводном докладе Д. Шмидт показал таблицу, где указаны требуемые в настоящее время точности измерений реакторных констант, а также уровень этой точности, достигнутый сейчас. Для величины α ^{239}Pu в области энергий от 100 эв до 100 кэв требуемая точность составляет 3-5% при достигнутом уровне 10-20%. Однако, чтобы оценить тот прогресс, который позволил совещанию экспертов констатировать, что в настоящее время в результате завершения первого поколения измерений реальная точность знания величины α может быть оценена величиной порядка 10%, нужно вспомнить ситуацию, существовавшую на Первой конференции по ядерным данным (Париж, 1966) и после нее, например во время Второй конференции (Вашингтон). Применявшиеся в то время системы ядерных констант в основном опирались на знание α в области больших энергий нейтронов и на экстраполяции к этим величинам значений, получавшихся усреднением резонансных параметров из области до 100 эв. Данные Канна 1955 года и предварительные данные Рябова (из Дубны) 1958 года не противоречили такой экстраполяции, показанной нижней кривой на рис. 2 работы [1]. Треугольниками внизу отмечены предварительные данные 1968 года из Дубны. Вслед за этим появились предварительные данные Шомберга и др. (из Харуэлла), а также данные Патрика (также из Харуэлла). Эти данные были существенно выше всех когда-либо рассматривавшихся и применявшихся в расчетах величин, что приводило при их использовании к исключительно плохим показателям для времени удвоения ядерного горючего в бридерных системах. На том же

ТАБЛИЦА 1. ЗНАЧЕНИЯ ВЕЛИЧИН α (^{239}Pu) ПО СОСТОЯНИЮ НА ИЮНЬ 1970 г. (взято из работы [2])

$\bar{E}$, кэв	Рябов [1]		Соверби [3]		Гвин [6]		Кзирр [7]		Сухоручкин [4]		Фаррелл [8]		Рябов [10]		Лоттин [9]		Оцененная величина [2]	
	α_1	$\Delta\alpha_1$	α_2	$\Delta\alpha_2$	α_3	$\Delta\alpha_3$	α_4	$\Delta\alpha_4$	α_5	$\Delta\alpha_5$	α_6	$\Delta\alpha_6$	α_7	$\Delta\alpha_7$	α_8	$\Delta\alpha_8$	$\bar{\alpha}$	
0.15	0.85	0.12	0.96	0.12	0.98	0.13	0.78	0.07	0.88	0.07	0.67	0.09	0.72	0.07			0.80	0.08
0.25	1.00	0.11	0.79	0.13	1.06	0.13	0.86	0.08	1.07	0.08	0.67	0.09	1.01	0.23			0.91	0.09
0.35	1.00	0.19	1.13	0.16	1.31	0.16	1.11	0.08	1.23	0.09	0.94	0.11	1.26	0.28			1.13	0.11
0.45	0.89	0.16	0.44	0.11	0.50	0.10	0.45	0.05	0.45	0.09	0.57	0.10	0.54	0.14			0.49	0.06
0.55	0.84	0.09	0.63	0.08	0.78	0.12	0.65	0.05	0.75	0.09	0.64	0.11	0.69	0.10			0.69	0.07
0.65	1.44	0.43	1.44	0.15	1.89	0.21	1.60	0.12	1.72	0.17	1.68	0.18					1.62	0.17
0.75	1.31	0.14	0.94	0.13	1.05	0.15	0.90	0.08	0.94	0.13	0.85	0.11	0.98	0.07			0.97	0.10
0.85	1.15	0.17	0.53	0.16	1.07	0.15	0.64	0.05	0.78	0.13	0.79	0.11	0.65	0.14			0.72	0.08
0.95	1.21	0.21	0.55	0.09	0.81	0.12	0.70	0.06	0.71	0.12	0.70	0.10	0.56	0.13			0.69	0.07
1.50	1.04	0.14	0.69	0.10	0.97	0.14	0.84	0.07	1.02	0.10	1.17	0.12	0.71	0.14			0.90	0.09
2.5	1.09	0.19	0.92	0.13	1.38	0.20	1.02	0.08	1.23	0.12	1.31	0.13	0.86	0.14			1.08	0.11
3.5	0.96	0.15	0.73	0.12	1.26	0.22	0.88	0.07	0.96	0.15	0.95	0.11	0.72	0.11			0.87	0.09
4.5	0.78	0.06	0.72	0.11	0.98	0.13	0.79	0.07	0.83	0.14	0.90	0.11	0.83	0.08			0.81	0.08
5.5	0.82	0.15	0.80	0.11	0.91	0.12	0.86	0.08			0.93	0.11	0.85	0.05			0.86	0.08
6.5	0.75	0.19	0.69	0.12	0.88	0.12	0.87	0.08			0.86	0.11	0.82	0.08			0.83	0.08
7.5	0.60	0.18	0.59	0.10	0.71	0.11	0.63	0.07	0.67	0.11	0.68	0.11					0.64	0.09
8.5	0.50	0.08	0.56	0.09	0.58	0.10	0.58	0.06			0.58	0.10					0.56	0.07
9.5	0.43	0.09	0.64	0.10	0.64	0.11	0.60	0.07			0.74	0.10					0.60	0.07
12.5			0.52	0.08	0.58	0.10	0.42	0.05			0.60	0.10					0.47	0.07
17.5			0.46	0.07	0.45	0.09	0.41	0.05							0.42	0.12	0.43	0.07
25.0			0.39	0.07	0.42	0.12	0.37	0.04			0.48	0.09			0.35	0.04	0.38	0.05
35.0															0.27	0.03	0.270	0.030
45.0															0.24	0.03	0.240	0.030
55.0															0.187	0.030	0.190	0.030
65.0															0.173	0.020	0.170	0.020
75.0															0.165	0.025	0.160	0.020
85.0															0.163	0.032	0.160	0.030
95.0															0.161	0.030	0.160	0.030
150.0																	0.150	0.024
250.0																	0.118	0.018
350.0																	0.095	0.011
450.0																	0.075	0.010
550.0																	0.060	0.011
650.0																	0.050	0.008
750.0																	0.042	0.008
850.0																	0.036	0.001
950.0																	0.029	0.001

рисунке вверху светлыми квадратами показаны данные из Харуэлла по состоянию на 1968 год. Теперь, на эту конференцию и на совещание в Студсвике, представлены окончательные результаты измерений, проведенных за последние годы в пяти лабораториях разных стран – в Дубне ([1] и [10]), в Москве [4], в Ливерморе [7], в Ок-Ридже ([5], [6]) и в Харуэлле [3] (см. табл. 1, взятую из работы [2]). Две работы, включая работу из Лос-Аламоса [8], содержат информацию предварительного характера, согласующуюся в основных чертах с остальными работами. Окончательные, пересмотренные данные Дубны приведены на вышеупомянутом рисунке.

Сотрудниками МАГАТЭ Коньшиным и Байэром был составлен и представлен совещанию в Студсвике обстоятельный обзор всей информации по величине α и методам измерений [2]. Этот обзор может быть получен из Секции по ядерным данным МАГАТЭ. В частности, там содержатся и рекомендации по усредненным величинам α (столбец 10, табл. 1) и обоснованное исключение из рассмотрения и окончательного усреднения некоторых точек, очень сильно расходящихся с остальными величинами[1]. По материалам работы Совещания экспертов в Студсвике будет составлен окончательный обзор, учитывающий всю имеющуюся численную информацию по этой величине.

Основное внимание совещание экспертов обратило на выявление возможных источников неопределенностей и систематических различий в имеющихся данных по α плутония-239 и наметило в ряде случаев возможные пути их устранения. Участники совещания экспертов пришли к выводу, что после уточнения нормировки и некоторых других уточнений, которые могут быть сделаны в Секции по ядерным данным МАГАТЭ, точность величины α для ^{239}Pu, усредненной по разным способам измерений, может быть оценена как $\pm 10\%$ (до энергии $\sim$ 10 кэв).

Я перечислю десять основных рекомендаций, которые приняло совещание экспертов.

1. В ряде работ производится нормировка результатов измерений на значения α для отдельных резонансов. Необходимо, чтобы принимаемые значения были унифицированы. Набор α-величин для различных резонансов, полученный Соверби и др. [3], достаточно оправдан для величин, меньших и близких к единице, но кажется, что большие величины α для некоторых резонансов несколько занижены. Следует, однако, иметь в виду, что не во всех методах нормировка осуществляется на резонансные параметры. В таких случаях авторы должны приводить, для сравнения, те величины, которые получаются у них для тех же самых хорошо разделенных резонансов, а также всю остальную численную информацию.

2. Необходимо стандартизовать интервалы усреднения. В области до 10 кэв в будущем следует стараться давать результаты для величин α, усредненных в интервалах как 1 кэв, так и 100 эв, учитывая наличие промежуточной структуры в α.

3. Величины α и другие данные, точка за точкой, должны быть присланы в МАГАТЭ для сбора и распределения по запросам.

4. До конца 1970 года Секция по ядерным данным МАГАТЭ в тесном сотрудничестве с авторами опубликует обзор данных по α.

---

[1] В группу измерений, результаты которых зависят от величины $\bar{\nu}$ – [3], [7], [4] и [1], – была введена 5%-поправка в величину α, определяемая возможной спиновой зависимостью величины $\bar{\nu}$.

5. Авторы должны более тщательно разбивать свои ошибки на флуктуирующие и систематические, указывая тенденции в последних. Поскольку во всех измерениях сечений захвата, включая измерения на взрывах, присутствует значительный фон, совещание рекомендовало унифицировать резонансные фильтры, помещаемые в пучки нейтронов при проведении фоновых измерений.

6. Из-за возможного влияния спиновой зависимости $\bar{\nu}$ для резонансов ^{239}Pu необходимо провести дополнительные измерения этой величины, так как величины Вайнштейна и Блока (из Ок-Риджа) и Ренселяйя и Рябова (из Дубны) антикоррелируют друг с другом. Поскольку в ряде методов регистрация сечения деления производится по быстрым нейтронам, все измерения могут быть рабиты на две группы. В работах, относящихся к первой из них, проводятся измерения величины α – отношения сечений, в работах другой группы измеряется произведение α на обратную величину $\bar{\nu}$.

7. При достижении точности в несколько процентов, влияние эффекта самоглокировки резонансов должно изучаться экспериментально и теоретически. Это особенно важно в связи с тем, что у экспериментатора обычно имеется желание применять более толстые образцы для получения лучшего отношения эффекта к фону.

8. Чтобы проверить верхнюю границу величин α, измеренных методом времени пролета, рекомендовано провести измерения этой величины другими способами и отличными от тех, которые применялись Де Сасюром и Лоттиным с сотрудниками.

9. Энергетические шкалы спектрометров по времени пролетов должны быть тщательно сопоставлены, применив согласованный список элементов.

10. Определенную помощь в дифференциальных измерениях может дать применение моноэнергетических нейтронов, полученных фильтрованием нейтронов через толстые образцы скандия, железа и т. д.

Как уже отмечалось выше, резюмируя результаты совещания, его участники пришли к выводу, что вся совокупность данных по величинам α характеризуется неопределенностью порядка 10%. На рис. 2 работы [2] показана часть результатов, полученная в Ренселайе и Харуэлле; данные, полученные в измерениях в ИТЭФ в Москве, лежат близко к этим результатам (см. табл. 1 и работу [4]). Недостаток времени в течение совещания в Студсвике помешал представить совместный рисунок, но большинство данных действительно группируется в пределах 10-20%, т. е. в пределах заявленной точности, хотя из более тщательного рассмотрения можно, например, обнаружить, что данные работы [2] в области нескольких кэв лежат систематически ниже данных Гвина и др. [5].

Следует подчеркнуть, что проникновение в область десятков и сотен килоэлектронвольт поднимает интересные вопросы о свойствах p-волновых резонансов, влиянии анизотропии угловых распределений, изменении числа быстрых нейтронов, числа и спектра гамма-лучей захвата и деления. Эти вопросы требуют тщательного изучения.

На совещании экспертов была высказана и та точка зрения, что многочисленные измерения не сразу дают требуемую для реакторостроения точность данных. Это привело даже к появлению таких "лозунгов", как "down with α". Однако мы считаем, что опыт, который должен быть извлечен из всей многолетней истории с α, говорит об обратном: необходимо в максимальной степени развивать измерения дифференциальных

сечений и других констант как источников важной дополнительной информации к результатам интегральных экспериментов.

В заключение я хотел бы отметить хорошую организацию совещания по величине α для ^{239}Pu и поблагодарить шведских ученых из Студсвика за их гостеприимство.

ЛИТЕРАТУРА

[1] КУРОВ, М.А., РЯБОВ, Ю.В., СО ДОН СИК, ЧИКОВ, Н., 2-я Междунар. конф. по ядерным данным, Хельсинки, 15-19 июня 1970, CN-26/124.

[2] KONSHIN, V.A., BYER, T.A., Review of Fission Cross Section in the Energy Region 5 keV to 15 MeV and α-values in the range 0.1 keV to 1 MeV for ^{239}Pu, INDC(NDS)-17/N, DRAFT, June 1970.

[3] SCHOMBERG, M.G., SOWERBY, M.G., BOYCE, D.A., MURRAY, K.J., SUTTON, D.L., IAEA Conf. no Nuclear Data for Reactors, Helsinki, 15-19 June 1970, CN-26/33.

[4] BELJAEV, F.N., IGNATIEV, K.G., SUKHORUCHKIN, S.I., BOROVLEV, S.P., PAVLOV, V.V., POLOZOV, M.V., SOLDATOV, A.N., IAEA Conf. on Nuclear Data for Reactors, Helsinki, 15-19 June 1970, CN-26/89.

[5] GWIN, R., WESTON, L.W., SAUSSURE, G. de et al., Nucl.Sci.Engng.40 (1970) 306.

[6] GWIN, R., WESTON, L.W., SAUSSURE, G.de et al., Private communication, June 1970.

[7] CZIRR, J.B., LINDSEY, J.S., Report UCRL-72080, November 1969, and IAEA Conf. on Nuclear Data for Reactors, Helsinki, June 1970, CN-26/47.

[8] FARRELL, J.A., AUCHAMPAUGH, G.F., MOORE, M.S., SEEGER, P.A., IAEA Conf. on Nuclear Data for Reactors, Helsinki, June 1970, CN-26/46.

[9] LOTTIN, A., WESTON, L.W., SAUSSURE, G. de, TODD, J.H., ANL-7320, October 1966, p.22; IAEA Conf. no Nuclear Data for Reactors, Paris 2 (1967) 233.

[10] РЯБОВ, Ю.В., СО ДОН СИК, ЧИКОВ, Н., КУРОВ, М.А., КОНОНОВ, В.Н., ПОЛЕТАЕВ, Е.Д., ПРОКОПЕЦ, Ю.С., СТАВИССКИЙ, Ю.Я., 2-я Междунар. конф. по ядерным данным, Хельсинки, июнь 1970 г., CN-26/57.

DISCUSSION

H.W. KÜSTERS: If I interpret your statement correctly, what you were discussing at Studsvik were the reasons for the discrepancies in the various measurements of alpha. This would seem to mean that the reasons for these differences are known. If that is true, could you make any recommendations regarding the measurements that should be preferred for reactor calculations: those from Dubna, from Harwell or from Oak Ridge?

S.I. SUKHORUCHKIN: The participants in the Panel reached agreement on a procedure for averaging the values of alpha as proposed in the report of the IAEA Nuclear Data Section. (Report INDC (NDS)-17/N by V.A. Konshin and T.A. Byer). It was suggested in this report that no account should be taken of series of measurements which did not satisfy certain obvious requirements. If the remaining results are averaged, with simple corrections being introduced for variations in ν and with re-calculation to uniform energy intervals, one can obtain very meaningful values. For these reasons the Panel recommended that the IAEA Nuclear Data Section should continue its work.

E.R. RAE: Were you talking about a total spread of approximately 10% in the experimental points, or about a standard deviation of 10% around the mean values?

S.I. SUKHORUCHKIN: The participants in the Panel came to the conclusion that in the neutron energy range up to 10 keV, the agreement of the

results in most of the energy intervals is such that the total uncertainty corresponds to a spread of ± 10% in the values and this figure can serve as a measure of the reliability of the averaged values of alpha.

J.Y. BARRE: As regards the stated precision of ± 10%, I should like to ask your opinion on the very considerable disagreements (50%) which exist between the Gwin (1970) measurements and those of Sowerby or Sukhoruchkin, for example.

S.I. SUKHORUCHKIN: You are apparently referring to the narrow neutron-energy range of 0.9-1.0 keV, where the data of Gwin and Sowerby do in fact differ by nearly a factor of two. Nevertheless, great significance should not be attached to irregular fluctuations in values, since you will in any case have to average them over a broad spectrum. It should be pointed out that the statistics allow very considerable random fluctuations. However, systematic differences really are present (see Fig. 2, CN-26/33) although they do not amount to the 50% mentioned by Mr. Barré.

J.L. ROWLANDS: I understand that, in the energy range Dr. Barré refers to, the background in the Harwell measurements was high, amounting to about 30% of the alpha value, and this may explain the difference between the Gwin and Harwell values of alpha. The Studsvik meeting assessed the accuracy which would be obtained in an evaluation of the measurements to be about ± 10% overall. However, as Dr. Barré points out, there are two energy ranges in which there are large differences between different sets of measurements. Although these may be within the larger uncertainties applying in these ranges, it is desirable to try to obtain accurate data in these ranges so that the structure of the ^{239}Pu cross-sections can be correctly analysed. Perhaps Dr. Sowerby would like to amplify my remarks.

M.G. SOWERBY: One of the energy regions mentioned by Dr. Barré is 0.8 to 0.9 keV and here the absorption cross-section is relatively low and the signal to background ratio for the gamma ray detector is poor in our experiment. This may also be the case for other experiments.

E.R. RAE: If the energy region in which the large discrepancy mentioned by Dr. Barré occurs is a region of low absorption cross-section, then it would be unimportant in determining an effective value of α, and so does not contradict Dr. Sukhoruchkin's general remarks about accuracy.

J.Y. BARRE: I agree with Dr. Rae that it is not a matter of great importance if the capture is low, but it is very difficult for someone using the cross-sections to accept the fact that the curve is good in one energy band and then suddenly to get such extensive differences in two particular energy regions. What I mean is that, even in trying to determine the shape of the variation of alpha as a function of energy, I am bothered by these two disagreements.

J.J. SCHMIDT: I would like to emphasize the fact that the overall confidence level figure of ± 10% for $\alpha(^{239}\text{Pu})$ which Dr. Sukhoruchkin quoted was certainly not meant to exclude the fact that systematic errors still exist. The aim of the recommendations of the Studsvik meeting is to encourage work directed towards finding an explanation of those systematic errors in the near future.

S.I. SUKHORUCHKIN: When we speak of an accuracy in alpha of 10%, we are referring essentially to measurements carried out up to neutron energies of approximately 10 keV. We assume that this is the boundary region between the Van-de-Graaff measurements and those made with time-of-flight spectrometers. This region, as well as the energy region

above 10 keV, needs to be investigated and, in accordance with one of our recommendations, it will be studied in the near future.

As regards the fluctuations of individual values of alpha in the detailed energy dependence, our recommendations are concerned with seeking out and with reducing errors in the data spread. The reason is that in the region which lies below 10 keV, or more accurately, below 5 keV, we experimentalists have generally measured very many points, and these values depend on the structure and thicknesses of the samples used, as well as on many other factors.

Obviously, it is not worth while for persons dealing with integral measurements to concern themselves with the above-mentioned spread of individual measuring points. As you know, the confidence level itself allows some fluctuation of individual experimental values.

RATIO OF THE CAPTURE AND FISSION CROSS-SECTIONS OF ^{239}Pu IN THE ENERGY RANGE 100 eV TO 30 keV

M.G. SCHOMBERG, M.G. SOWERBY, D.A. BOYCE,
K.J. MURRAY, (Miss) D.L. SUTTON
UKAEA, AERE,
Harwell, Didcot, Berks,
United Kingdom

Abstract

RATIO OF THE CAPTURE AND FISSION CROSS-SECTIONS OF ^{239}Pu IN THE ENERGY RANGE 100 eV TO 30 keV.

The ratio of the capture to fission cross-sections (alpha) of ^{239}Pu in the energy range 100 eV to 30 keV has been measured using the Harwell 45-MeV Linear Accelerator time-of-flight spectrometer. The method used has been described by Schomberg et al. in Fast Reactor Physics 1 (1968) 289 together with provisional results. In this paper, the final results are presented and compared with the other available data. Most experiments to measure alpha in this energy range are normalized to the values of alpha at the peaks of the low-energy resonances. It was recognized at the meeting of specialists organized by the International Working Group on Fast Reactors in July 1969 that some of the discrepancies between the various experiments were due to differences in the values used for normalization. It was, therefore, recommended that a best set of normalization values should be obtained and that, for comparison purposes, all experiments should be normalized to these. An evaluation to produce a best set has been performed, and the results are discussed in this paper.

1. INTRODUCTION

One of the important parameters required to calculate the breeding gain of a large sodium-cooled oxide-fuelled fast power reactor is the quantity alpha (the ratio of the capture and fission cross-sections) for ^{239}Pu and its dependence on neutron energy. For such a reactor system the neutron flux typically peaks in the range 100-300 keV but the peak neutron-capture-rate is a decade lower in energy and a significant number of capture events take place at energies as low as 0.1 keV. Because of experimental difficulties measurements of alpha for ^{239}Pu in the energy range 0.1 to 30 keV are extremely difficult and there were essentially no differential measurements in this energy range up to 1966. The present experiment was aimed at remedying this deficiency and the first provisional results [1], which were presented at the Karlsruhe Conference on Fast Reactor Physics, showed that α could be a factor 2 higher in the energy range 1 to 10 keV than the typical evaluated values favoured at that time (e.g. Schmidt [2] and Greebler et al. [3]). Such high α-values were not unexpected because similar values had been calculated [4] from total and fission cross-section measurements and the integral measurements of Fox et al. [5] indicated that α was underestimated in the current nuclear data sets (other confirmatory evidence was of course presented at the Karlsruhe Conference). The high α-values were initially difficult to understand theoretically because the values recommended for instance by

Greebler et al. were consistent with the values calculated from the distributions of resonance parameters and their mean values measured below 100 eV. This problem was solved by the discovery Weigman et al. [7]. There are now many experiments which show that α for ^{239}Pu is "high" below 10 keV but not as "high" as the first results of our experiment. This paper gives the final results of the experiment which supersede all previous data.

The remainder of the paper is essentially divided into six sections. In the first two sections, the experimental method is briefly discussed and the normalization of the experiment is considered. It was recognized at the meeting of specialists on ^{239}Pu-α organized by the International Working Group on Fast Reactors in July 1969 that some of the differences between experiments were due to differences in the resonance α-values used for normalization. It was recommended that a best set of values should be obtained and an evaluation is discussed in section 3. In sections 4 and 5 the results of the present experiment are given and their errors considered. These results are compared with other data in section 6, and final conclusions are drawn in section 7.

2. EXPERIMENTAL METHOD

The experimental method has previously been described [1] and will be discussed in more detail in a further report; therefore, only essential details will be given here. The measurements were made using the Harwell 45 MeV Electron Linear Accelerator time-of-flight spectrometer and the main experimental parameters are given in Table I. Data have been obtained with two detector systems which basically consist of fast-neutron detectors and gamma-ray detectors with Moxon-Rae characteristics. It was found with the first system which was described by Schomberg et al. [1], that the ratio of the efficiencies of the gamma-ray detector for fission and capture events was ~ 2.5 rather than $1.0 - 1.3$ as expected from the Moxon-Rae characteristic and the known total energy of prompt fission and capture gamma-rays. This was thought to be mainly due to coincidences produced by two gamma-rays and/or neutrons being detected in the two halves of the detector. The second system was built to overcome this effect and is shown in Fig. 1. Two new detectors similar to those described by Schomberg et al. were mounted above and below the sample and coincidences were taken between the following pairs of sections: AB, CD, AC and BD. The coincidences AC and BC (called cross-coincidences) give a measure of the contribution due to multiple events included in coincidences AB and CD (called gamma-coincidences). With these new detectors it was found to be impossible to use the individual sections A, B, C and D as fast neutron detectors because impurities in the liquid scintillators meant that the pulse shape discrimination technique would not work satisfactorily. Therefore, two sealed glass vessels ~ 12 cm in diameter and 7 cm thick filled with NE-213 liquid scintillator were mounted on either side of the sample and used with pulse-shape-discrimination techniques as fast-neutron detectors.

The results obtained with this modified detector system show that the ratio of the efficiencies of the gamma-ray detector for fission and capture events is 1.5 ± 0.2 and so is close to the expected value. It is also found

TABLE I. EXPERIMENTAL PARAMETERS

Energy range:	10 eV to 30 keV
Flight path length:	34.86 m
Neutron burst width: (unmoderated)	220 ns
Timing channel width:	125 ns
Nominal resolution:	7.2 ns/m
Resonance fitters for background measurement: (with resonance energies used)	Mn [a] (337 eV, 1.10, 2.38, 7.17 and 8.87 keV) Mo (45, 131 eV) Ta (10.34 eV) Na [b] (2.85 keV) Al (35 keV)
Permanent "Black" filters:	^{10}B, Al and Na [b]
Incident spectrum measurement:	3.2 mm thick ^{6}Li glass scintillator 6.35 cm in diameter and mounted 5.25 cm from the photomultiplier
Samples used:	3 samples 5.08 cm diameter, containing 1.07% Al, 0.7% ^{240}Pu, canned in 0.0127 cm Al and with sample thicknesses of 0.0012, 0.000579 and 0.00029 atoms per barn. 1 sample 7.4 cm diameter, containing 1.8% ^{240}Pu, thickness 0.0044 atoms per barn, canned in 30-cm-long Al cylinder with 0.092 cm end windows.

[a] 337 eV and 2.38 keV for one set of runs.
[b] For limited number of runs.

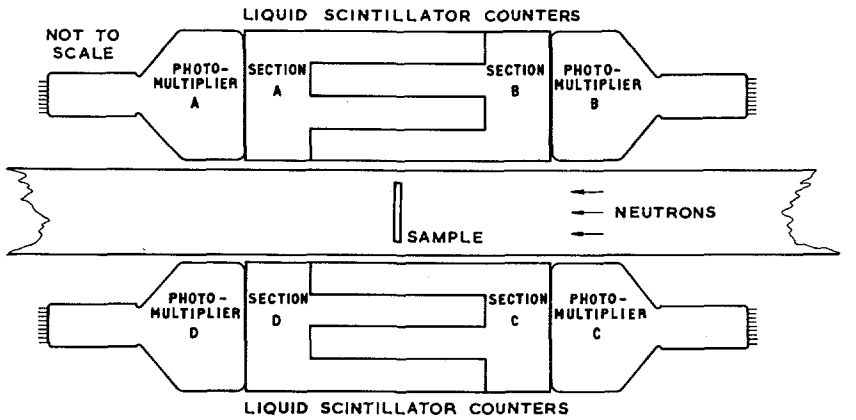

FIG.1. Sketch showing layout of detector sections.

that the cross-coincidences are mainly produced by fission events, the ratio of efficiencies for fission and capture being 4.4. These efficiencies are independent of neutron energy, and this means that the data obtained with the original detector system are not in error due to the detection of multiple events.

It was shown by Schomberg et al. that

$$\frac{n_c}{n_f} = \frac{\sigma_{n\gamma}}{\sigma_{nf}} S = \frac{A\frac{N_\gamma}{N_n} - 1}{B - C\frac{N_\gamma}{N_n}} \tag{1}$$

where $\sigma_{n\gamma}$ and σ_{nf} are the capture and fission cross-sections, N_γ and N_n are the counts of the gamma-ray and neutron detectors in a given time-of-flight channel, n_c and n_f are the number of capture and fission events, S is the multiple-scattering correction and A, B and C are constants involving the efficiencies of the detectors. (For the modified detector N_γ is the difference between the gamma and cross-coincidences.) This equation requires modification because recent measurements by Weinstein et al. [8] suggest that the number of neutrons per fission ($\bar{\nu}$) is not a constant in the resonance region but depends upon the spin of the resonance. In addition, it will be seen later that multiple-scattering effects can be neglected, and Eq. (1) is therefore modified to the form

$$\frac{n_c}{n_f} = \alpha = \frac{a\bar{\nu}\frac{N_\gamma}{N_n} - 1}{b - c\bar{\nu}\frac{N_\gamma}{N_n}} \tag{2}$$

c should be small and is effectively $c/\bar{\nu}$. The reactor physicist requires the ratio of the average values of the capture and fission cross-sections (i.e. $\langle\sigma_{n\gamma}\rangle/\langle\sigma_{nf}\rangle$) rather than the average value of α. Therefore, the values of N_γ and N_n should be replaced in Eq. (2) by

$$\sum_{i_1}^{i_2} \frac{N_\gamma(i)}{\phi(i)} \frac{\sigma_{nT}(i)}{(1 - T(i))} \Delta E(i) \quad \text{and} \quad \sum_{i_1}^{i_2} \frac{N_n(i)}{\phi(i)} \frac{\sigma_{nT}(i)}{(1 - T(i))} \Delta E(i)$$

where i_1 and i_2 are the channels corresponding to the energies over which the cross-section average is to be taken, ϕ is the incident neutron flux, σ_{nT} is the total cross-section, T is the transmission of the sample and ΔE is the energy interval per timing channel. The factor $\sigma_{nT}/(1-T)$ is essentially a correction for self-screening effects. The values of σ_{nT} required for these corrections were obtained from a transmission measurement of almost identical energy resolution performed on the same flight path. Measurements were made on the four samples listed in Table I and on an additional sample of thickness 0.0243 atoms per barn. The total cross-section was calculated as described by Patrick et al. [9].

A total of nine sets of experimental data have been obtained with the two detector systems. The first of these was the basis of the data presented by Schomberg et al. [1] at the Karlsruhe Conference. However,

TABLE II. COUNT-TO-BACKGROUND RATIOS FOR SAMPLE OF THICKNESS 0.0012 atoms/barn

Experiment	Energy interval (keV)			
	0.1 - 0.2	1 - 2	9 - 10	25 - 30
Original detector				
Neutrons	1.38	2.02	2.58	7.35
Gamma coincidences	0.50	0.65	1.16	3.15
Gamma coincidences (Ratio to time-dependent background)	1.51	1.22	2.0	5.34
Modified detector				
Neutrons	2.34	3.16	5.50	10.85
Cross-coincidences	2.68	3.42	5.71	12.35
Gamma coincidences	0.71	0.70	1.02	2.31
Gamma coincidences (Ratio to time-dependent background)	6.40	2.11	2.55	5.45

being the first runs with the detector the data were not taken under such controlled conditions as in subsequent runs and it has therefore been decided that they should be neglected. Table II gives the count to background ratios for various energy intervals for runs taken with both detector systems. It can be seen that the background is highest for the gamma-coincidence events. However, the time-constant background, which is well determined, is large for this detector and a more significant number to consider is the counts to time-dependent background ratios which are also given.

3. NORMALIZATION

The experiment is normalized and the values of a, b and c determined by obtaining the values of N_γ/N_n on the peaks of well resolved low-energy resonances where the values of α are known from other experiments measuring η and alpha. For our provisional results these resonance alpha values were obtained from the resonance parameters given by Derrien et al. [10]. Subsequently, they have been obtained from measurements of η and at the International Working Group on Fast Reactor Specialists Meeting on Plutonium Alpha in July 1969 the results given for the present experiment were normalized in this manner. At that meeting it was decided that some of the discrepancies between experiments were due to differences in the resonance alpha values used for normalization. It was therefore agreed that the experimenters involved should attempt to obtain a best set of resonance alpha values based on eta and alpha measurements

normalized in the thermal region so that the results of the various experiments could be compared when normalized consistently. An evaluation has, therefore, been performed and this is discussed below.

There are four experiments which need to be considered:

a) η-experiment Bollinger et al. [11] (normalized $\eta/\nu = 0.75$ at 2200 m/sec)
b) η-experiment Patrick et al. [9] (normalized to Brooks et al. [12] which is normalized to $\eta = 2.0$ at 0.08 eV)
c) α-experiment Gwin et al. [13] (normalized $\alpha = 0.359$ and 0.66 at 0.025 and 0.3 eV)
d) α-experiment Czirr and Lindsey [14] (normalized $\alpha = 0.460$ and 0.092 at 0.08 and 15.5 - 16.0 eV).

The data of Bollinger et al. are sensitive to $\overline{\nu}$ variations observed by Weinstein et al. [8] and they do not appear to agree in shape with other data in the thermal region. They have, therefore, been neglected. The normalization of the Czirr and Lindsey experiment is only partially made in the thermal region and, therefore, their data have also been largely ignored.

The primary normalization of the Brooks et al. experiment is essentially based on σ_{nF} and σ_{nT} data. An improvement can be made by normalizing to the value of 2.034 ± 0.007 obtained by Smith et al. [15] at 0.057 eV and this makes the values of η at 0.08 and 0.3 eV equal to 1.968 and 1.728 respectively. (The equivalent α values are 0.455 (for $\overline{\nu} = 2.864$) and 0.645 (for $\overline{\nu} = 2.842$). However, if the Weinstein et al. [8] $\overline{\nu}$-variations were ignored α would be 0.66 at 0.3 eV.) Changing the primary normalization of the Brooks et al. experiment does not remove the discrepancies between the α-values obtained by Patrick et al. and Gwin et al. and so a thorough re-appraisal of the cross-normalizations within the Brooks et al. experiment and between it and the Patrick et al. experiment has been made. This slightly modified the results and showed that the normalization of Patrick et al. is accurate to $\pm 3.8\%$.

Table III gives the resonance α values for the various experiments and also the $\overline{\nu}$ values used to obtain α from η. The values of Patrick et al. tend to be higher for low alphas and lower for high alphas than those of Gwin et al. However, in the measurement of alpha we are only interested in values in the range 0.2 - 1.6 and in this interval the Patrick et al. values are all high. The values of Czirr and Lindsey support the data of Gwin et al. and this suggests that the normalization of Patrick et al. is incorrect. We have, therefore, decided to re-normalize the latter experiment by combining the normalization through η (accurate to $\pm 3.8\%$) with a normalization based on Gwin et al. (accurate to $\pm 2.9\%$ and based on the 10.9, 14.3, 15.5, 22.3 and 32.3 eV resonances where $\alpha < 0.8$). The two normalizations differ by $6.3 \pm 4.8\%$ and their combination leads to the values given in column 6 of Table III.

The evaluated values given in Table III are obtained by taking the weighted average of the Gwin et al. and Patrick et al. (b) results. This procedure gives most weight to the Gwin et al. data but this is not unreasonable because in their experiment only one cross-normalization is required, and accurate flux measurements are not needed. In addition, they are supported by the data of Czirr and Lindsey in the low-energy

TABLE III. RESONANCE α-VALUES FROM VARIOUS EXPERIMENTS

Resonance energy (eV)	Gwin et al.	Czirr and Lindsey [a]	Patrick et al. [b]	$\bar{\nu}$	Patrick et al. [c]	Evaluated value
7.83	0.85 ± 0.05	0.83	0.97 ± 0.07	2.841	0.90 ± 0.08	0.86 ± 0.04
10.93	0.27 ± 0.06	0.26	0.41 ± 0.06	2.841	0.36 ± 0.04	0.33 ± 0.03
11.93	1.56 ± 0.10	1.54	1.58 ± 0.12	2.802	1.48 ± 0.09	1.52 ± 0.07
14.3	0.55 ± 0.04		0.66 ± 0.10	2.810	0.60 ± 0.08	0.56 ± 0.04
14.7	1.13 ± 0.06	1.11	1.48 ± 0.14	2.839	1.38 ± 0.12	1.18 ± 0.05
15.5	0.14 ± 0.06		0.11 ± 0.07	2.922	0.07 ± 0.07	0.11 ± 0.05
17.6	1.14 ± 0.06	1.05	1.20 ± 0.11	2.853	1.12 ± 0.08	1.13 ± 0.05
22.3	0.64 ± 0.04	0.64	0.78 ± 0.09	2.864	0.71 ± 0.07	0.66 ± 0.04
26.3	0.91 ± 0.05	0.88	0.96 ± 0.13	2.835	0.88 ± 0.11	0.90 ± 0.05
44.6	9.38 ± 0.70	10.1	8.21 ± 1.09	2.818	7.86 ± 1.06	8.94 ± 0.60
50.2	2.45 ± 0.28	1.90	2.23 ± 0.30	2.840	2.11 ± 0.29	2.27 ± 0.20
52.7	5.22 ± 0.45	5.1	4.94 ± 0.41	2.923	4.71 ± 0.37	4.92 ± 0.29
65.9	0.88 ± 0.06	0.84	1.07 ± 0.12	2.840	0.99 ± 0.10	0.91 ± 0.05
91.0	4.15 ± 0.36	3.6	4.18 ± 0.45	2.945	3.98 ± 0.42	4.08 ± 0.27

[a] No errors given
[b] Normalized through η to $\eta = 2.034$ at 0.057 eV
[c] Normalized to Gwin et al. and η

region where resolution differences are unimportant. It might be considered that the Patrick et al. data should be ignored but we feel that the eta-normalization does warrant some consideration and one should not neglect the fact that their relative values of alpha are found by an independent method.

The neutron yield data obtained in the experiment can be used to obtain fission cross-section data. The results obtained have been normalized in the 10-20 eV region to an average fission cross-section of 104.7 barns derived from the data of Bollinger et al. [11] and Gwin et al. [13].

4. RESULTS

The values of $\langle \sigma_{n\gamma} \rangle / \langle \sigma_{nf} \rangle$ obtained from the present experiment are given in Table IV and shown in Fig. 2. Also given are the values of $\langle \sigma_{nf} \rangle$, $\langle \sigma_{n\gamma} \rangle$ and $\langle \sigma_{nA} \rangle$ (σ_{nA} is the absorption cross-section). The fission cross-section values were deduced using the following formula and data taken with the samples of thickness 0.0012, 0.00579 and 0.00029 atoms per barn:

$$\langle \sigma_{nF} \rangle = \frac{\sum_{i_1}^{i_2} \frac{N_n(i)}{\phi(i)} \frac{\sigma_{nT}(i)}{1-T(i)} \Delta E(i)}{K(E_2 - E_1)} \qquad (3)$$

where K is the normalization constant and E_2 and E_1 are the energy limits over which the average is taken. The evaluated resonance α-values given in Table III have been used to normalize the experiment, and it has been assumed that multiple-scattering effects are negligible. No corrections have been made for the effect of ^{240}Pu in the sample, and it has been found that c in Eq. (2) is zero. This means that the neutron detector has zero efficiency for capture events. It has also been assumed that the efficiencies of the detectors for fission and capture events are independent of neutron energy. This assumption was discussed by Schomberg et al. [1] but since then Weinstein et al. have shown that $\overline{\nu}$ varies from resonance to resonance by up to ~3%. These $\overline{\nu}$ variations have been allowed for in the normalization procedure but otherwise it has been assumed that $\overline{\nu}$ is constant. If these assumptions were incorrect then the values of $\langle\sigma_{n\gamma}\rangle/\langle\sigma_{nf}\rangle$ above 20 keV might be expected to disagree with the data [16, 17] obtained using Van-de-Graaff accelerators. It can be seen from Fig. 2 that this is not the case.

TABLE IV. VALUES OF $\langle\sigma_{n\gamma}\rangle/\langle\sigma_{nf}\rangle$, $\langle\sigma_{nf}\rangle$, $\langle\sigma_{n\gamma}\rangle$ and $\langle\sigma_{nA}\rangle$

Energy interval (eV)		$\langle\sigma_{n\gamma}\rangle/\langle\sigma_{nf}\rangle$ (barn)		$\langle\sigma_{nf}\rangle$ (barn)		$\langle\sigma_{n\gamma}\rangle$ (barn)		$\langle\sigma_{nA}\rangle$ (barn)	
E_1	E_2	Value	Error	Value	Error	Value	Error	Value	Error
100	200	0.96	0.12	18.55	0.59	17.81	2.21	36.36	2.40
200	300	0.79	0.13	18.43	0.58	14.56	2.40	32.99	2.61
300	400	1.13	0.16	8.76	0.30	9.90	1.46	18.66	1.55
400	500	0.44	0.11	9.75	0.31	4.29	1.09	14.04	1.17
500	600	0.63	0.08	15.68	0.50	9.88	1.21	25.56	1.43
600	700	1.44	0.15	4.80	0.19	6.91	0.77	11.71	0.85
700	800	0.94	0.13	5.49	0.28	5.16	0.72	10.65	0.79
800	900	0.53	0.16	5.38	0.19	2.85	0.86	8.23	0.95
900	1 000	0.55	0.09	8.04	0.27	4.42	0.73	12.46	0.83
1 000	2 000	0.69	0.10	4.71	0.16	3.25	0.50	7.96	0.57
2 000	3 000	0.92	0.13	3.43	0.13	3.16	0.46	6.59	0.51
3 000	4 000	0.73	0.12	3.11	0.11	2.27	0.38	5.38	0.41
4 000	5 000	0.72	0.11	2.43	0.08	1.75	0.27	4.18	0.30
5 000	6 000	0.80	0.11						
6 000	7 000	0.69	0.12	2.03	0.07	1.40	0.24	3.43	0.27
7 000	8 000	0.59	0.10	2.16	0.07	1.27	0.21	3.43	0.24
8 000	9 000	0.56	0.09	2.20	0.08	1.23	0.20	3.43	0.23
9 000	10 000	0.64	0.10	1.90	0.06	1.22	0.19	3.12	0.21
10 000	15 000	0.52	0.08	1.72	0.06	0.89	0.13	2.61	0.16
15 000	20 000	0.46	0.07	1.60	0.05	0.74	0.11	2.34	0.13
20 000	25 000	0.45	0.07	1.56	0.05	0.70	0.10	2.26	0.13
25 000	30 000	0.34	0.06	1.62	0.06	0.55	0.10	2.17	0.13

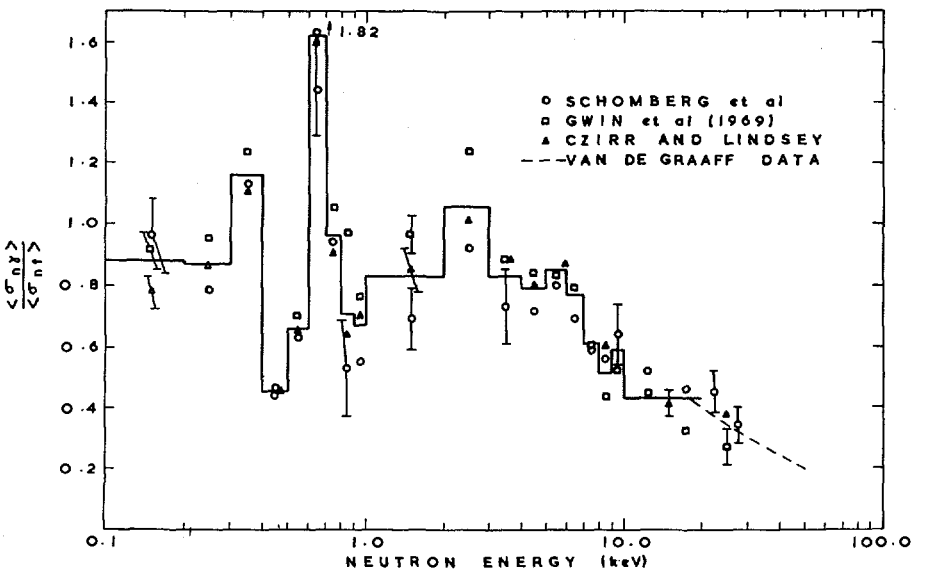

FIG.2. $\langle\sigma_{n\gamma}\rangle/\langle\sigma_{nf}\rangle$ for ^{239}Pu.

The assumption of negligible multiple-scattering effects is essentially only correct if (a) the sample is "thin" ($n\sigma_{nT} \ll 1$) or (b) the ratio of the scattering to total cross-sections is small or (c) in the case of $\langle\sigma_{n\gamma}\rangle/\langle\sigma_{nf}\rangle$ α is independent of neutron energy. At least one of these conditions is normally true for all regions where the experiments are normalized or the results accepted. However, there is additional evidence which suggests that multiple-scattering effects can be neglected. Patrick et al. [9] in their experiment to measure eta and fission cross-sections showed that the maximum error in the fission cross-section for essentially a sample of 0.00115 atoms per barn is 7% due to the neglect of the correction for the compound-elastic-scattering cross-section. This error occurs near the peak of the strong 52.6-eV resonance which has a large neutron and a small fission width. The error in the average cross-section over several resonances is likely to be much smaller, and this conclusion is supported by considering our average fission cross-section data obtained from neutron yields. In the energy range 10 eV to 100 eV the values of $\langle\sigma_{nf}\rangle$ obtained with the samples of thickness 0.0012, 0.00379 and 0.00029 atoms per barn are essentially the same and have a root-mean-square deviation of only $\pm\frac{1}{3}\%$.

5. ERRORS

The standard deviations in $\langle\sigma_{n\gamma}\rangle/\langle\sigma_{nf}\rangle$ given in Table IV are listed in more detail in Table V. The error due to statistics and background errors was evaluated for each set of experimental data (Table VI gives details for one of the sets of runs with the 0.0012 atoms/barn sample). The error in the mean value of $\langle\sigma_{n\gamma}\rangle/\langle\sigma_{nf}\rangle$ at a given energy due to

TABLE V. ERRORS IN $\langle\sigma_{n\gamma}\rangle/\langle\sigma_{nf}\rangle$

Energy range (keV)		$\langle\sigma_{n\gamma}\rangle/\langle\sigma_{nf}\rangle$	Error due to statistics and background errors	Error due to normalization	Error due to 2% uncertainty in $\bar{\nu}$	Total error
0.1	0.2	0.96	0.090	0.049	0.052	0.115
0.2	0.3	0.79	0.109	0.045	0.049	0.128
0.3	0.4	1.13	0.141	0.053	0.056	0.161
0.4	0.5	0.44	0.095	0.036	0.042	0.110
0.5	0.6	0.63	0.045	0.041	0.045	0.075
0.6	0.7	1.44	0.120	0.061	0.062	0.148
0.7	0.8	0.94	0.103	0.048	0.052	0.125
0.8	0.9	0.53	0.150	0.038	0.044	0.161
0.9	1.0	0.55	0.069	0.039	0.044	0.090
1.0	2.0	0.69	0.082	0.042	0.047	0.104
2.0	3.0	0.92	0.107	0.048	0.051	0.128
3.0	4.0	0.73	0.100	0.043	0.047	0.118
4.0	5.0	0.72	0.086	0.043	0.047	0.107
5.0	6.0	0.80	0.081	0.045	0.049	0.105
6.0	7.0	0.69	0.098	0.042	0.047	0.117
7.0	8.0	0.59	0.076	0.040	0.045	0.097
8.0	9.0	0.56	0.068	0.039	0.044	0.089
9.0	10.0	0.64	0.075	0.041	0.046	0.097
10.0	15.0	0.52	0.051	0.038	0.043	0.076
15.0	20.0	0.46	0.039	0.036	0.042	0.068
20.0	25.0	0.45	0.033	0.036	0.042	0.065
25.0	30.0	0.34	0.035	0.034	0.040	0.063

this cause can then be obtained from the errors of the individual sets of runs (internal error) or from the spread in the observations (external error) and the value given in column 4 of Table V is the larger of these. The error due to normalization uncertainties is difficult to assess. There is an error in fitting the normalizing curve to each set of runs due to errors in N_n/N_γ but these errors are random and essentially included in the spread of observations considered above. The systematic errors due to errors in determining the resonance α-values have been assumed to be 2.5% of $1+\alpha$ for α-values in the range 0 to 1.5.

In deducing $\langle\sigma_{n\gamma}\rangle/\langle\sigma_{nf}\rangle$ it is assumed that $\bar{\nu}$ is constant above 100 eV. There are only limited data available and there is no evidence that this assumption is not correct when wide energy intervals containing many resonances are considered. However, we feel it is advisable to assign a $\pm 2\%$ error to $\bar{\nu}$, and Table V lists the resulting errors.

Other possible errors have been neglected in determining the total error. It is, for instance, assumed that the efficiency of the gamma-coincidence detector for fission events is independent of neutron energy. Another possible error that has been considered and found negligible is the effect of delayed gamma rays from fission. With the present normalization the $\langle\sigma_{n\gamma}\rangle/\langle\sigma_{nf}\rangle$ values obtained above 20 keV agree within their experimental errors with the data obtained with Van-de-Graaff accelerators. The fact that the experiment agrees at both low energies (by normalization) and high energies with other experiments suggests that the assumptions made in analysing the results are probably correct and gives us confidence in the validity of the data in the intervening energy range.

The errors in the average fission cross-section data were determined in a similar manner. The error due to statistics and background is typically ±1 to 2% for the fission yield measurements and ~±1% for the spectrum determination. The error in the efficiency of the Li-glass detector varies between 0.5 and 1% and there are uncertainties of ±2% due to normalization errors and ±2% for possible errors in $\bar{\nu}$.

6. DISCUSSION

The results of our measurements of $\langle\sigma_{n\gamma}\rangle/\langle\sigma_{nf}\rangle$ are compared with other reliable data in Fig. 2 where the solid line is the mean value of the available data. The values of Gwin et al. and Czirr and Lindsey are not normalized to the evaluated resonance alpha values given in Table III but their normalizations lead to α values sufficiently close to these that we can consider all the normalizations to be consistent. It can be seen that below 0.8 keV and between 3 and 10 keV the three experiments agree reasonably well while between 0.8 and 3 keV our results tend to be systematically lower than the others. Above 20 keV the Van-de-Graaff data of Hopkins and Diven [16] and De Saussure et al. [17] (the basis of the curve labelled Van-de-Graaff data) are quite consistent with our data. The errors in the non-Van-de-Graaff-type measurements are mainly systematic but these errors are probably random between experiments. It is, therefore, interesting to consider the root-mean-square deviations of the data, and it is convenient to express these as percentages of $1+\alpha$. The mean root-mean-square deviations in the energy ranges 0.1 to 0.8, 0.8 to 3.0 and 3.0 to 10.0 keV are ±3.1, ±7.1 and ±2.7%, respectively. As far as the present experiment is concerned it is not surprising that the range 0.8 to 3 keV shows the greatest errors since it is demonstrated in Table VI that background errors have their maximum effect here. Making allowance for the common systematic normalization errors it is concluded that from these experiments $\langle\sigma_{nf}\rangle/\langle\sigma_{nA}\rangle$ is known to ~±4% over most of the energy range 0.1 to 20 keV. (The equivalent errors in α are ±0.05, ±0.065 and ±0.08 for $\alpha = 0.3$, 0.6 and 1.0). Above 20 keV the Van-de-Graaff data which are accurate to ~±10% in α are more accurate and should be preferred.

Table VII shows the average fission cross-sections obtained from the present experiment compared with other available data. The values have been corrected, where necessary, for the deviation from 1/v-dependence of the $^{10}B(n,\alpha)$ cross-section using the formula recommended by Sowerby et al. [18].

TABLE VI. ERRORS IN $\langle\sigma_{n\gamma}\rangle/\langle\sigma_{nf}\rangle$ FOR A TYPICAL SET OF RUNS WITH THE 0.0012 atoms/barn SAMPLE

Energy interval (keV)		Statistical errors			Background errors			Total statistical and background error
		Neutron detector	Gamma coincidences	Cross-coincidences	Neutron detector	Gamma coincidences	Cross-coincidences	
0.1	0.2	0.010	0.021	0.012	0.067	0.096	0.038	0.126
1.0	2.0	0.012	0.031	0.018	0.040	0.121	0.029	0.136
9.0	10.0	0.029	0.081	0.051	0.018	0.084	0.014	0.132
25.0	30.0	0.016	0.041	0.030	0.008	0.035	0.010	0.065

TABLE VII. COMPARISON OF THE AVERAGE FISSION CROSS-SECTIONS OF ^{239}Pu

Energy interval (keV)		Present experiment (barn)	Gwin et al.[13] (barn)	Bollinger[a] et al.[11] (barn)	James [19] (barn)	Shunk et al.[20] (barn)	Blons et al.[21] (barn)
0.1	0.2	18.55 ± 0.59	18.09	19.82		17.82	
0.2	0.3	18.43 ± 0.58	18.06	17.62		18.25	
0.3	0.4	8.76 ± 0.30	8.63	9.90		8.35	
0.4	0.5	9.75 ± 0.31	9.60	10.11		9.11	
0.5	0.6	15.68 ± 0.50	15.43	10.81		14.66	
0.6	0.7	4.80 ± 0.19	4.54	3.73		3.94	
0.7	0.8	5.49 ± 0.28	5.43	5.54		5.20	
0.8	0.9	5.38 ± 0.19	5.13	6.23		4.36	
0.9	1.0	8.04 ± 0.27	8.28	7.72		8.28	
1.0	2.0	4.71 ± 0.16	4.49	3.91	4.40	3.83	3.53
2.0	3.0	3.43 ± 0.13	3.32	3.35	3.46	2.64	3.35
3.0	4.0	3.11 ± 0.11	3.22	3.46	2.86	2.74	3.11
4.0	5.0	2.43 ± 0.08	2.39	2.63	2.55	2.31	2.38
5.0	6.0	-	2.18	2.75	2.42	2.71	2.23
6.0	7.0	2.03 ± 0.07	2.17	2.65	1.98	2.20	2.01
7.0	8.0	2.16 ± 0.07	2.15	1.87	2.29	2.23	2.01
8.0	9.0	2.20 ± 0.08	2.22	2.03	2.27	2.46	2.47
9.0	10.0	1.90 ± 0.06	1.90	2.30	1.87	2.14	1.98
10.0	20.0	1.66 ± 0.06	1.82		1.79		1.90
20.0	30.0	1.59 ± 0.06	1.71		1.67		
0.1	1.0	10.54	10.35	10.16		10.00	
1.0	5.0	3.42	3.36	3.33	3.32	2.98	3.34
6.0	10.0	2.07	2.11	2.21	2.10	2.26	2.12

[a] Renormalized to 742 barn at thermal energies.

$$\sigma_{n\alpha}(^{10}B) = \frac{13.837}{\sqrt{E}} - 0.312 - 1.014\times10^{-2}\sqrt{E} + \frac{2.809\times10^{5}}{\sqrt{E}[(170.3-E)^2 + 2.243\times10^{4}]} \text{ barns} \quad (4)$$

where E is the energy in keV. It can be seen that below 10 keV our values agree well with those of Gwin et al. [13], Blons et al. [21] and James [19]. The agreement is not so satisfactory with Bollinger et al. [11] and Shunk et al. [20] but these sets of data are less accurate. However, it is worth noting that the agreement is better when averaged over

larger intervals (e.g. 0.1 to 1.0, 1 to 4 and 6 to 10 keV). The root-mean-square deviations for these intervals are ±2.0, ±4.3 and ±2.8% respectively. Above 10 keV our results are the lowest values being 7.3% and 3.8% lower than the mean of all the values in the energy ranges 10 to 20 and 20 to 30 keV. The agreement with Gwin et al. in fission cross-section data implies that differences in $\langle\sigma_{n\gamma}\rangle/\langle\sigma_{nf}\rangle$ are due to errors in measuring the capture cross-section.

It has been shown by Patrick and James [22] and Blons et al. [21] using correlation analyses that there are modulations in the fission cross-section with a spacing of ~460 eV. James and Patrick [23] have also shown by analysing both the total and fission cross-section data that below 700 eV these modulations must be partially attributed to variations of neutron width. Above 700 eV, however, the variation of the cross-section is probably due to variations in the mean fission width of the spin 1^+-resonances due to the presence of levels in the second fission potential-barrier minimum and the average fission cross-section can be represented by a series of Lorentzian terms on a smooth background. It is, therefore, expected that where there are regions of high fission cross-section above 700 eV there should be regions of low $\langle\sigma_{n\gamma}\rangle/\langle\sigma_{nf}\rangle$ and vice-versa. Figure 3 shows a plot of $\langle\sigma_{nF}\rangle\sqrt{E}$ and $\langle\sigma_{n\gamma}\rangle/\langle\sigma_{nf}\rangle$ in 100 eV intervals below 4 keV. It can be seen that regions of high fission cross-section on the whole have corresponding minima in $\langle\sigma_{n\gamma}\rangle/\langle\sigma_{nf}\rangle$. The arrows on the figure show the positions where James and Patrick put the Lorentzian peaks in their analysis of the fission cross-section data. The strong fluctuations of the

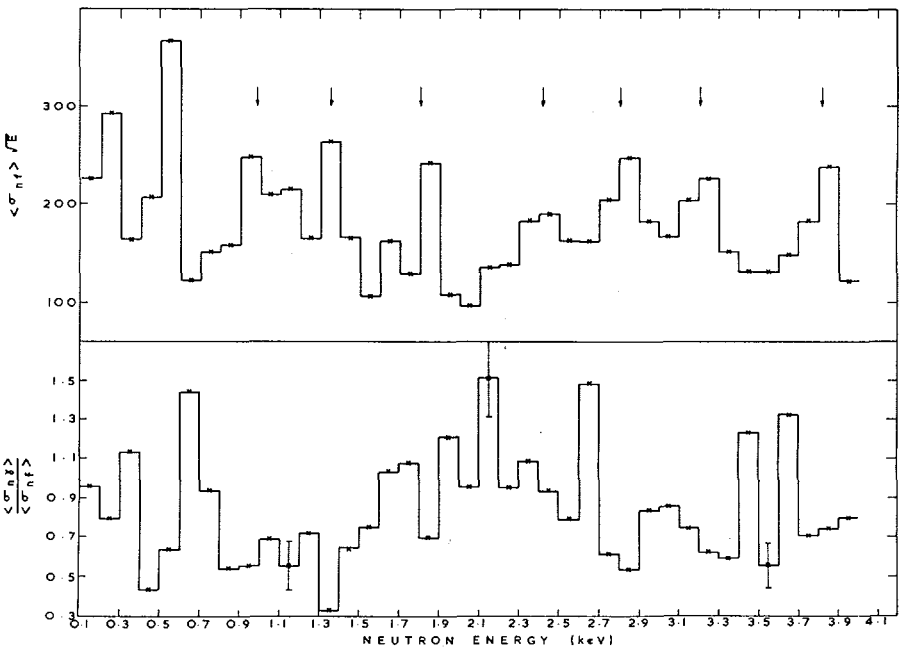

FIG.3. $\langle\sigma_{n\gamma}\rangle/\langle\sigma_{nf}\rangle$ and $\langle\sigma_{nf}\rangle\sqrt{E}$ between 0.1 and 4.0 keV.

cross-sections due the fine compound-nuclear resonances make it extremely difficult to evolve objective criteria for determining the parameters of the intermediate-structure modulations present in these data. However, Fig. 3 does show that similar fluctuations in $\langle\sigma_{n\gamma}\rangle/\langle\sigma_{nf}\rangle$ to those observed below 1 keV occur at higher energies.

7. CONCLUSIONS

The present experiment has measured $\langle\sigma_{n\gamma}\rangle/\langle\sigma_{nf}\rangle$ for ^{239}Pu in the energy range 0.1 to 30 keV to an accuracy of between ±5 and 8% in $\langle\sigma_{nf}\rangle/\langle\sigma_{nA}\rangle$. The experiment has been normalized to an evaluation of resonance α-values discussed in section 3 of the paper and which gives greatest weight to the data of Gwin et al. Our values of $\langle\sigma_{n\gamma}\rangle/\langle\sigma_{nf}\rangle$ agree reasonably well with those of Gwin et al. and Czirr and Lindsey below 10 keV while above 20 keV they are consistent with the data of Hopkins and Diven and De Saussure et al. The experiments considered together enable $\langle\sigma_{nf}\rangle/\langle\sigma_{nA}\rangle$ to be obtained to ~±4% over most of the energy range between 0.1 and 20 keV. The measured values of $\langle\sigma_{n\gamma}\rangle/\langle\sigma_{nf}\rangle$ in the energy range 1 to 10 keV are significantly higher than the evaluated values favoured two or three years ago but are not as high as the provisional results of the present experiment [1].

Values of $\langle\sigma_{nf}\rangle$ have also been determined and these agree well with the other available data except in the energy range above 10 keV where our results tend to be low. It has been shown that where there are broad peaks in $\langle\sigma_{nf}\rangle$ there are usually corresponding minima in $\langle\sigma_{n\gamma}\rangle/\langle\sigma_{nf}\rangle$. The structure in the latter quantity, which is probably due to intermediate structure in sub-threshold fission and is well known below 1 keV, is seen to continue to at least 4 keV.

ACKNOWLEDGEMENTS

We gratefully acknowledge the help, support and encouragement given by Dr. E.R. Rae throughout this experiment. We would also like to thank Dr. G.D. James, Dr. J.E. Lynn, Mr. M.C. Moxon, Dr. B.H. Patrick and Dr. C.A. Uttley for their advice and for many helpful discussions and Mr. F.W. Evans and Mr. V. Sherriffs for the assistance they have given us. Mr. G. White developed the pulse-shape-discrimination equipment, and we are indebted to him for all his help.

REFERENCES

[1] SCHOMBERG, M.G., SOWERBY, M.G., EVANS, F.W., in Fast Reactor Physics (Proc. Symp. Karlsruhe, 1967) 1, IAEA Vienna (1968) 289.
[2] SCHMIDT, J.J., KFK 120 Part 1 (1966).
[3] GREEBLER, P., ALINE, P., HUTCHINS, B., GEAP-5272 (1966).
[4] UTTLEY, C.A., JAMES, G.D., (1965) unpublished.
[5] FOX, W.N., RICHMOND, R., SKILLINGS, D.J., WHEELER, R.C., J. Br. nucl. Energy Soc. 6 (1967) 63.
[6] PAYA, D., DERRIEN, H., FUBINI, A., MICHAUDON, A., RIBON, P., Nuclear Data for Reactors (Proc. Conf. Paris, 1966) 2, IAEA, Vienna, (1967) 129.

[7] WEIGMANN, H., SCHMID, H., J. nucl. Energy 22 (1968) 317.
[8] WEINSTEIN, S., REED, R., BLOCK, R.C., Physics and Chemistry of Fission (Proc. Symp. Vienna, 1969), IAEA, Vienna (1969) 477.
[9] PATRICK, B.H., SCHOMBERG, M.G., SOWERBY, M.G., JOLLY, J.E., in Nuclear Data for Reactors (Proc. Conf. Paris, 1966) 2, IAEA, Vienna (1967) 117.
[10] DERRIEN, H., BLONS, J., EGGERMAN, C., MICHAUDON, A., PAYA, D., RIBON, P., in Nuclear Data for Reactors (Proc. Conf. Paris, 1966) 2, IAEA, Vienna (1967) 195.
[11] BOLLINGER, L.M., COTE, R.E., THOMAS, G.E., Int. Conf. peaceful Uses atom. Energy (Proc. Conf. Geneva) 15 (1958) 127.
[12] BROOKS, F.D., JOLLY, J.E., SCHOMBERG, M.G., SOWERBY, M.G., UKAEA Report AERE-M 1709 (1966).
[13] GWIN, R., WESTON, L.W., DE SAUSSURE, G., INGLE, R.W., TODD, J.H., GILLESPIE, F.E., HOCKENBURY, R.W., BLOCK, R.C., ORNL-TM-2598 (1969).
[14] CZIRR, J.B., LINDSEY, J.S. (1969) private communication.
[15] SMITH, J.R., READER, S.D., FLUHARTY, R.G., IDO-17083 (1966).
[16] HOPKINS, J.C., DIVEN, B.C., Nucl. Sci. Engng 12 (1962) 169.
[17] DE SAUSSURE, G., WESTON, L.W., GWIN, R., INGLE, R.W., TODD, J.H., HOCKENBURY, R.W., FULLWOOD, R.R., LOTTIN, A., in Nuclear Data for Reactors (Proc. Conf. Paris, 1966) 2, IAEA, Vienna (1967) 233.
[18] SOWERBY, M.G., PATRICK, B.H., UTTLEY, C.A., DIMENT, K.M., UKAEA Report AERE-R 6316 (1970).
[19] JAMES, G.D., Data given in UKAEA Report AERE-M 2065.
[20] SHUNK, E.R., BROWN, W.K., LA BAUVE, R., CONF 660303 (1966) 979.
[21] BLONS, J., EGGERMANN, C., MICHAUDON, A., C.r. Acad. Sci. Paris 267 (1968) 901.
[22] PATRICK, B.H., JAMES, G.D., Physics Letts 28B (1968) 258.
[23] JAMES, G.D., PATRICK, B.H., in Physics and Chemistry of Fission (Proc. Conf. Vienna, 1969) IAEA, Vienna (1969) 391.

^{235}U AND ^{239}Pu CAPTURE-TO-FISSION RATIO*

J.B. CZIRR, J.S. LINDSEY
Lawrence Radiation Laboratory,
University of California,
Livermore, Calif.,
United States of America

Abstract

^{235}U AND ^{239}Pu CAPTURE-TO-FISSION RATIO.

A new experimental technique has been used to measure the neutron capture-to-fission cross-section ratio, α, for ^{235}U and ^{239}Pu. Data were obtained in the 0.1 eV to 30 keV energy range using neutron time-of-flight methods, with the Livermore 33-MeV linac providing a pulsed neutron source. The detector for both capture gammas and fission neutrons was a one-liter liquid scintillator viewed by a single 5-in photomultiplier tube.

Fission neutrons were identified by pulse-shape-discrimination techniques applied to the signals from the deuterated-benzene scintillator. Capture-and-fission gamma events were pulse-height weighted on-line in order to obtain a signal which is independent of variations in the gamma spectra. The use of deuterated benzene as the scintillator solvent reduced the background arising from the capture of scattered neutrons. The fission-gamma contamination of the capture data was removed by a subtraction technique based on normalization at a resolved resonance with small capture-to-fission ratio. The resulting capture cross-section was averaged over energy bins and divided by the averaged fission data after normalization to accepted α values near thermal neutron energy. The quantity $\langle \sigma_C \rangle / \langle \sigma_F \rangle$ is presented for both isotopes from 100 eV to 30 keV to provide the data necessary for detailed reactor calculations.

For ^{239}Pu, $\frac{\langle \sigma_C \rangle}{\langle \sigma_F \rangle} = 0.80 \pm 0.05$ when averaged from 0.10 to 10 keV. (The quoted error includes estimated systematic uncertainties.) The present results indicate a considerably larger loss to ^{240}Pu production than previously assumed, for some fast-breeder reactor designs.

I. INTRODUCTION

The ratio of the capture and fission cross sections in the keV neutron energy range is an important quantity in the design of fast breeder reactors. The breeding ratio is a sensitive function of the neutron fraction wasted in capture in the low-flux but high-capture region below 20 keV.

Because of large variations in the flux as a function of neutron energy, it is necessary to know the detailed energy dependence of the capture-to-fission cross-section ratio (α). Early measurements of α were of the integral type and yielded only average values for the cross-section ratio over broad energy regions[1]. Current time-of-flight techniques, on the other hand, easily provide measurements with an energy resolution of 5% in the 10-keV region.

The present experiment was undertaken to provide accurate ($\pm$5%) values for α up to the energy range covered by measurements with Van de Graaff generated neutrons (~20 keV).

---

* Work performed under the auspices of the US Atomic Energy Commission.

II. EXPERIMENTAL TECHNIQUE

The Livermore 33-MeV electron linear accelerator was used as a pulsed source of neutrons at a repetition rate of 360 pps. The neutrons were generated by bremsstrahlung photons striking a 2-in.-thick Pb target, and then were moderated into a 1/E spectrum by a 2-in.-thick polyethelene block next to the source. Neutron velocities were measured by time-of-flight with a resolution of 50 nsec/m.

The metallic foils of 4×10^{-4} atoms/barn thickness were placed 11 meters from the neutron source and viewed by a 1-liter liquid scintillator detector. Capture and fission gamma rays and fission neutrons were observed in the single detector, using pulse shape discrimination (PSD) to identify the particle type. A complete description of the detector system is given in Ref. [2].

The gamma events were pulse-height weighted on-line to provide data which are essentially independent of variations in the capture-gamma de-excitation spectrum. The number of counts (proportional to pulse height) from a single event were added to the appropriate time-of-flight channel of a 4096-channel analyzer. This linear weighting assures spectral independence for capture events if the fraction of the capture-gamma energy spectrum below the threshold level is not a function of the incident neutron energy[2]. The gamma threshold was set at approximately 0.56-MeV (electron energy) to avoid the background arising from the radioactive decay of the sample foils. Fission gamma events were treated in the same way and then separated from capture events by a method described in Section III.

Events which were labeled "neutron" by the PSD system were routed to the other half of the 4096-channel analyzer and stored in the appropriate time-of-flight channel. The effectiveness of the PSD system for eliminating gamma rays from the neutron signal was checked by inserting a thin Ho foil in place of the fission foils. Under these conditions, the observed rate of neutron counts implies that the fraction of the neutron signal which resulted from PSD leakage was less than 0.3%

The incident neutron flux was measured with a single BF_3 tube inserted into the beam pipe during separate data runs. The measured spectrum is described by the relation $d\Phi/dE \propto E^{-0.97}$ for $E > 100$ eV.

The background for the fission data was assumed to consist of three main components: Ambient background, fissions induced by out-of-time neutrons (measured at 4, 10, 120 and 2800 eV by inserting totally black resonance absorbers of Na, Co and Ta during a separate background run), and prompt detection of scattered neutrons (without fission). This last component was measured by replacing the fission foils with a graphite foil which scattered the same fraction of the beam.

The gamma background was measured in a similar manner, with an exception arising from the fact that the last two components cannot be added. If this were done, the background resulting from delayed neutron capture in materials other than the sample foil would be added twice. To avoid this problem, the following approximation was used: $\alpha(E)$ was assumed to be a constant throughout the energy range of interest. It then follows that the fractional background due to the absorption of out-of-time neutrons in the foil would be the same for the fission and gamma signals. (Due to a systematic trend in $\langle \alpha \rangle$ above 7 keV, the above approximation introduces a 5% uncertainty in $\alpha(E)$ in the 7- to 30-keV region for ^{239}Pu.)

III. DATA ANALYSIS

The time-of-flight data for gamma and neutron events were stored in separate halves of a 4096-channel memory. Deadtime corrections were made, background were subtracted, and the resulting signal was divided by the measured incident neutron spectrum using an available computer program.

The gamma signal for each time-of-flight channel represents the total gamma energy deposited in the detector by fission and capture events at the corresponding beam neutron energy, and as such is proportional to the weighted capture and fission cross sections at that energy. The neutron signal is directly proportional to the fission cross section if the number of detected neutrons per fission is independent of incident neutron energy. Variations in the fission neutron spectrum and $\bar{\nu}$ are expected to be small in the energy region below 30 keV.

In order to extract the capture cross section from the total gamma signal, the fission-gamma contamination must be subtracted. The normalization required for this subtraction is best done where the capture-to-fission ratio is small. For ^{239}Pu we used the low-α region from 15.5- to 16.0-eV and for ^{235}U, the region from 13.5- to 14.4-eV was chosen.

The unnormalized capture cross section is obtained from the relation

$$k\ \sigma_C(E) = N_\gamma(E) - A\ N_n(E)$$

where $N_\gamma(E)$ is the total gamma signal (capture plus fission) at energy E, $N_n(E)$ is the fission neutron signal and $A = \frac{\text{weighted fission gammas}}{\text{detected fission neutron}}$, as determined in the above low-α region.

For ^{239}Pu, the ratio of the capture and fission cross sections was normalized in the 0.070- to 0.090-eV energy band. Using a thermal value for $\alpha = 0.3653 \pm 0.0036$,[3] and the ENDF/B file data on $\eta(E)$ from thermal energy to 0.09 eV,[4] we obtain $\bar{\alpha}$ (.07 - .09 eV) = 0.460 ± 0.009. The 2% error is an estimate which includes the uncertainties in the absolute thermal value and in the shape of the $\eta(E)$ curve[5].

For ^{235}U, the resonance at 11.7-eV was used for normalization of σ_C/σ_F. From Ref. [6], we obtain a value of $\langle \sigma_C \rangle / \langle \sigma_F \rangle = 4.57$ from 11.45- to 12.0-eV. The error on this normalization is taken to be ± 3% [6].

IV. RESULTS

A. Group-Averaged Alpha

Tables I and II show the values of $\langle \sigma_C \rangle / \langle \sigma_F \rangle$ when averaged over energy groups which were chosen to yield acceptable statistical errors at all energies.

A measure of the random errors was obtained directly from the data in order to include effects of unknown variations in the experimental conditions during data collection. For each energy group the random deviation in α was calculated by comparing one-half of the data to the average of both halves. The results are listed in the tables under $\Delta\alpha$ (random).

B. ^{239}Pu Resonance Alphas (0.10 eV < E_n < 100 eV)

Measurements of capture and fission reaction rates with the same detector system (and therefore essentially the same energy resolution)

TABLE I. $^{239}Pu < \sigma_C >/< \sigma_F >$ for $E_n \geq 100$ eV

E_{max} (keV)	E_{min} (keV)	$< \sigma_C >/< \sigma_F >$	$\pm \Delta \alpha$ (random)	$\pm \Delta \alpha$ (systematic)
30.1	19.0	0.37	0.02	0.03
19.0	11.4	0.41	0.02	0.03
11.4	7.23	0.56	0.03	0.05
7.23	5.44	0.86	0.04	0.06
5.44	4.24	0.77	0.03	0.05
4.24	3.40	0.93	0.03	0.06
3.40	2.62	0.85	0.03	0.06
2.62	2.02	1.13	0.04	0.07
2.02	1.57	1.21	0.04	0.08
1.57	1.23	0.68	0.02	0.04
1.23	0.968	0.62	0.02	0.04
0.968	0.745	0.66	0.02	0.04
0.745	0.583	1.47	0.03	0.10
0.583	0.456	0.54	0.01	0.04
0.456	0.355	0.52	0.01	0.03
0.355	0.275	1.11	0.02	0.07
0.275	0.214	1.07	0.01	0.07
0.214	0.167	0.54	0.005	0.04
0.167	0.130	0.80	0.006	0.05
0.130	0.101	0.97	0.006	0.06
10.0	0.10	0.799	0.002	0.05

TABLE II. $^{235}U < \sigma_C >/< \sigma_F >$ for $E_n \geq 50$ eV

E_{max} (keV)	E_{min} (keV)	$< \sigma_C >/< \sigma_F >$	$\pm \Delta \alpha$ (random)	$\pm \Delta \alpha$ (systematic)
28.0	23.1	0.43	0.04	0.03
10.9	7.34	0.37	0.04	0.03
7.34	4.29	0.30	0.03	0.02
4.29	2.64	0.28	0.02	0.02
2.64	1.58	0.33	0.02	0.02
1.58	0.955	0.37	0.02	0.03
0.955	0.585	0.39	0.01	0.03
0.585	0.355	0.30	0.008	0.02
0.355	0.214	0.37	0.007	0.03
0.214	0.130	0.54	0.008	0.05
0.130	0.079	0.56	0.006	0.05
0.079	0.048	0.42	0.002	0.04
10.2	0.10	0.340	0.001	0.025

TABLE III. $\langle\alpha\rangle$ FOR RESOLVED RESONANCES

E_0	$\langle\alpha\rangle$	ΔE (eV)	Resolution Width (eV)
0.29	0.675	(0.25-0.35)[a]	0.015
7.85	0.819	0.199	0.027
10.95	0.260	0.373	0.044
11.90	1.57	0.224	0.049
14.68	1.09	0.307	0.068
17.7	1.04	0.315	0.090
22.2	0.625	0.382	0.13
26.2	0.879	0.491	0.16
41.7	4.51	0.812	0.32
44.6	9.79	0.721	0.36
47.8	0.188	0.800	0.40
50.1	1.94	0.863	0.43
52.7	4.99	0.926	0.46
66.0	0.827	0.972	0.65
74.9	0.533	1.18	0.79
91.0	3.57	1.58	1.05

[a] Region of constant α.

yield potentially accurate resonance α information in the resolved-resonance region. Statistical errors are easily reduced to $\pm$ 1% and self-shielding effects due to thick samples are essentially eliminated when the ratio of σ_C/σ_F is calculated.

Table III lists the value of this ratio for 16 prominent resonances from 0.29- to 91-eV. The quantity shown is

$$\langle\alpha\rangle = \int_{E_\ell}^{E_h} \frac{\sigma_C(E)}{\sigma_F(E)}\, dE/\Delta E$$

where the limits correspond to the energies at which the measured capture rate is one-half of the peak value (except for the resonance at 0.29 eV). The interval ΔE, when chosen in this way, is a function of the sample thickness (4.3×10^{-4} atoms/b) and resolution (50 nsec/m). As seen from Table III, ΔE is considerably larger than the resolution width for most of the resonances listed.

V. SYSTEMATIC ERRORS AND CORRECTIONS

The sources of systematic errors which have been considered are given in this section.

A. Errors in Assumed Background

The major source of uncertainty arises from the assumption of equal out-of-time background for the neutron and gamma data. Since this background is defined by the use of resonance absorbers placed well upstream of the fission foils, it is important to consider variations in $\alpha(E)$ at energies below the energy of interest. The effect of the factor-of-two increase in α from 30 to 7 keV (for ^{239}Pu) was investigated by doubling the assumed out-of-time gamma background between these energies.

The results indicate that $|\Delta \alpha/\alpha| \leq 0.05$ in those regions where $\alpha(E)$ shows a systematic trend of the above magnitude. Below 7 keV $\alpha(E)$ shows rapid fluctuations, but no large trends away from $<\alpha> \approx 0.8$. The same fractional error is assigned to ^{235}U.

The statistical uncertainties in the other background components lead to approximately $\pm 2\%$ uncertainties in $<\alpha>$.

B. Variations in $\nu(E)$

A recent measurement on ^{239}Pu has shown that $\bar{\nu}$ for J = 0 resonances is 1.03 ± 0.02 times that for J = 1 resonances [7]. The fission-gamma subtraction procedure for the present measurement is normalized at a J = 0 resonance ($E_0 = 15.5$ eV) and this could result in a 3% reduction in the calculated $<\alpha>$ values at those energies dominated by J = 1 resonances. Because of the large relative error in this correction, it has not been applied to the present data. The effect should be smaller for ^{235}U and was again neglected.

C. ^{240}Pu Contamination (^{239}Pu data only)

The data have been corrected for the effect of the 0.875% ^{240}Pu (99.11% ^{239}Pu) concentration upon the normalization at 0.080 eV. The effect of this correction is to increase the calculated values of α by approximately 0.7%. It should be noted that the values of α listed in Table I apply to the above isotopic mixture and not to pure ^{239}Pu.

D. Multiple Collisions

Because of the small energy loss combined with the small probability for elastic scattering (4% scattering probability for $\sigma_S = 100$ b), the effects of multiple collisions were neglected in the analysis of the data.

E. Fission-Gamma Subtraction Errors

The ^{239}Pu normalization point at 15.5-16.0 eV is potentially subject to a large absolute error. The early η data of Bollinger yield $\alpha \approx 0.3$ at 15.5 eV [8], even when renormalized to recent thermal η values. Most analyses of σ_T and σ_F data yield a fission width for the 15.5 eV resonance in the range 600-800 meV [9]. An $\alpha = 0.3$ implies that either $\Gamma_\gamma \approx 200$ meV or that nearby resonances contribute a large portion of the capture cross section at 15 eV. The few determinations of Γ_γ for J = 0 resonances yield values in the 30-50 meV range and are consistent with the J = 1 value of 40 meV [9].

The $<\alpha>$ for the present normalization was obtained by combining calculated $\sigma_C(E)$ values with measured $\sigma_F(E)$ data. The calculated contributions from the 14.68-, 15.5- and 17.7-eV resonances [9] were added together for 15.5 eV $< E_n <$ 16.0 eV and divided by measured σ_F values [9]. This procedure is chosen in order to take advantage of the reliability of calculations based on the non-interfering capture levels and the more-

easily-measured fission cross section. The result is $\langle \alpha \rangle = 0.092$. It is considered likely that the errors on this value are less then $^{+}_{-}\,^{0.02}_{0.03}$, where the lower limit is obtained by neglecting the contributions from nearby resonances and the upper limit includes the effect of a possible non-resonant component in σ_C. These latter errors introduce an uncertainty of $\pm 3\%$ in the data in Table II.

For ^{235}U, an alpha of 0.107 was obtained from Ref. [6] in the region of the 14.0-eV resonance. Statistical uncertainties in the present data predominate in this case and introduce an uncertainty of $\pm 4\%$ in the tabulated data.

F. Variations in Capture Spectra

The remaining uncertainty arises from imperfect compensation for variations in the capture-gamma spectra with changes in neutron energy. This problem can conveniently be divided into two portions: variations in the prompt capture spectra for $E_\gamma > 1.5$-MeV and for $E_\gamma < 1.5$-MeV. For the former case, the calculated deviations from the ideal linear detector response are approximately $\pm 10\%$, as seen in Fig. 1. This characteristic, when combined with expected small variations in high-gamma-energy average transition probabilities [10], yields a negligible uncertainty in $\alpha(E)$.

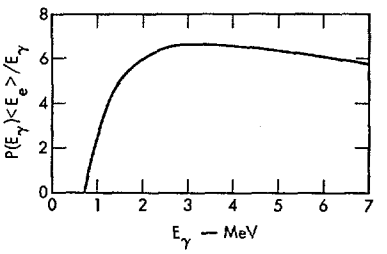

FIG.1. Calculated fractional response function versus incident gamma energy. The ordinate is proportional to the quantity $P(E_\gamma)\langle E_e\rangle/E_\gamma$ where $P(E_\gamma)$ is the interaction probability (including bias effect) for a gamma of energy E_γ incident upon a 7.6 cm-thick deuterated benzene scintillator shielded by 11 g/cm^2 of Pb. $\langle E_e\rangle$ is the first moment of the electron pulse height distribution. The electronics bias is set at 0.56 MeV electron energy.

For $E_\gamma < 1.5$-MeV, the situation is somewhat less certain. As seen from Fig. 1, a 1.0-MeV gamma ray receives only one-half of the required weight, so this energy may be considered as the effective threshold level. A systematic error can therefore arise from changes with neutron energy in the fraction of the total capture-gamma energy carried by gamma rays of $E_\gamma < 1.0$-MeV.

A measure of the size of this effect may be obtained from calculated gamma spectra, using numerical simulation of the complex decay process[11]. These calculations indicate changes in gamma-ray multiplicity of $\leq 10\%$ from one capture spin state J to another of spin J + 1 (ℓ=0 neutrons only). The effect of changes in multiplicity upon the low-energy spectrum fraction (< 1.0-MeV) is therefore considered to be less than $\pm 5\%$ from resonance to resonance. This is the assigned systematic uncertainty arising from variations in the capture spectra, for both isotopes.

The root mean squares of the systematic errors from A to F are listed in Tables I and II.

VI. SUMMARY

The average ^{239}Pu σ_C/σ_F ratio over the 0.10 to 10-keV energy range is 0.80 ± 0.05. The present values of $\alpha(E)$ are consistent with published Van de Graaff data in the 20-keV energy range. The results of the present experiment are in disagreement with the early integral measurements and indicate a considerably larger loss to ^{240}Pu production for some fast breeder reactor designs.(a)

The average ^{235}U σ_C/σ_F ratio over the 0.10- to 10-keV energy range is 0.34 ± 0.0.

ACKNOWLEDGMENTS

We would like to thank Dr. C. D. Bowman for suggesting the experimental technique and for his continued support throughout the measurement.

We also appreciate the discussions held with Dr. M. Sowerby and Dr. R. Gwin concerning the various experimental techniques in use.

REFERENCES

[1] W. R. KANNE, H. B. STEWART and F. A. WHITE, Intern. Conf. Peaceful Uses Atomic Energy (Geneva, 1955) 4, UN, New York (1955) 315.
[2] J. B. CZIRR, Nucl. Instr. Methods, 72 (1969) 23.
[3] G. C. HANNA (private communication, April 1969).
[4] P. GREEBLER, P. G. ALINE and B. A. HUTCHINS, Evaluation and Compilation of Pu-239 Cross Section Data for the ENDF/B Files, General Electric, Sunnyvale, Calif. Rep. GEAP-5272 (1966).
[5] B. R. LEONARD (private communication, May 1969).
[6] G. deSAUSSURE, R. GWIN, L. W. WESTON, R. W. INGLE, R. R. FULLWOOD and R. W. HOCKENBURY, Simultaneous Measurements of the Neutron Fission and Capture Cross Sections for U-235 for Incident Neutron Energies from 0.4-eV to 3-keV, Oak Ridge National Laboratory, Rep. ORNL-TM-1804 (1967).
[7] S. WEINSTEIN and R. C. BLOCK, Phys. Rev. Letters, 22 (1969) 195.
[8] L. M. BOLLINGER, R. E. COTÉ and G. E. THOMAS, 2nd Intern. Conf. Peaceful Uses Atomic Energy (Geneva, 1958) 15, UN, New York (1958) 127.
[9] H. DERRIEN, J. BLONS, C. EGGERMAN, A. MICHAUDON, D. PAYA and P. RIBON, "Sections efficaces totale et de fission du ^{239}Pu," Conf. Nuclear Data, Microscopic Cross Sections, and Other Data Basic for Reactors,(Paris, October, 1966) CN-23-48, IAEA (1966).
[10] H. WEIGMANN, J. WINTER and M. HESKE, Nucl. Phys., A134 (1969) 535.
[11] C. COCEVA, F. CORVI and P. GIACOBBE, Nucl. Phys., A117 (1968) 586.
[12] R. GWIN, L. W. WESTON, G. deSAUSSURE, R. W. INGLE, J. H. TODD, F. E. GILLESPIE, R. W. HOCKENBURY, and R. C. BLOCK, Measurements of the Neutron Fission and Absorption Cross Sections of ^{239}Pu over the Energy Region 0.02-eV to 30-keV, Oak Ridge National Laboratory Rep. ORNL-TM-2598 (1969).

(a) A paper recently published by Gwin et al.[12] indicates an average alpha over the 0.10- to 10-keV energy range of 0.80, in agreement with the average of the present results. This agreement is particularly significant in view of the very different experimental techniques employed.

ИЗМЕРЕНИЕ ВЕЛИЧИНЫ АЛЬФА ДЛЯ ^{235}U и ^{239}Pu

Ф. Н. БЕЛЯЕВ, К. Г. ИГНАТЬЕВ,
С. И. СУХОРУЧКИН, С. П. БОРОВЛЕВ,
В. В. ПАВЛОВ, М. В. ПОЛОЗОВ,
А. Н. СОЛДАТОВ
Институт теоретической и экспериментальной физики Государственного комитета по использованию атомной энергии СССР, Москва,
Союз Советских Социалистических Республик

Abstract — Аннотация

MEASUREMENT OF ALPHA VALUES FOR ^{235}U AND ^{239}Pu.

Because of inconsistences in alpha values for ^{239}Pu in the neutron energy range of several kev, measurements of this parameter for ^{235}U and ^{239}Pu were performed by means of the neutron spectrometer of the ITEF cyclotron. Fission and capture effects from metal foil were measured independently by two methods using different kinds of detectors, located on 14,6 - meter path - flight. Alpha values for ^{235}U and ^{239}Pu were obtained in the energy range of neutrons from thermal to 10 kev.

ИЗМЕРЕНИЕ ВЕЛИЧИНЫ АЛЬФА ДЛЯ ^{235}U И ^{239}Pu.

В связи с наличием расхождений в величине $\alpha = \sigma_c/\sigma_f$ для ^{239}Pu в области энергий нейтронов в несколько кэв, были проведены измерения этой величины для ^{235}U и ^{239}Pu на нейтронном спектрометре циклотрона ИТЭФ. Делительный и захватный эффекты из металлических образцов измерялись независимо двумя способами с применением разных типов детекторов на 14,6-метровой базе нейтронного спектрометра. В результате измерений были получены величины альфа ^{235}U и ^{239}Pu в области энергий нейтронов от тепловой до 10 кэв.

В работах [1,2] по измерению величины альфа ^{239}Pu имеются значительные расхождения в результатах в области энергий нейтронов в несколько килоэлектронвольт. В связи с этим нами были проведены измерения этой величины на циклотроне ИТЭФ, в результате которых были получены величины $\alpha(E)^{235}U$ и ^{239}Pu в области энергий нейтронов от тепловой до 10 кэв.

МЕТОДИКА ИЗМЕРЕНИЙ

Измерения проводились на нейтронном спектрометре по времени пролета циклотрона ИТЭФ. В таблице 1 приведены основные экспериментальные параметры установки.

Измерения проводились независимо двумя способами с применением разных типов детекторов. В обоих случаях величина $\alpha = \sigma_c/\sigma_f$ определялась из отношения экспериментальных счетов радиационного эффекта к делительному. В первом способе делительный эффект измерялся по выходу вторичных быстрых нейтронов из металлического образца счетчиками, состоящими из покрытия парафина с сернистым цинком, нанесенного на два ФЭУ-49. Импульсы с выходов ФЭУ суммировались. Эти детекторы практически нечувствительны к гамма-лучам, что позволяет надежно проводить измерения делительного эффекта. Гамма-лучи захвата и деления из этого же образца регистрировались одним кристаллом

ТАБЛИЦА 1. ОСНОВНЫЕ ПАРАМЕТРЫ УСТАНОВКИ

Параметры	1	2
Измеряемый энергетический интервал (эв)	*0,3 – 10000*	*0,025 – 10*
Пролетное расстояние (м)	14,56	14,56
Ширина нейтронного импульса (мксек)	3	8
Ширина временного канала анализатора (мксек)	1	8
Период следования нейтронных импульсов (мксек)	2300	17000
Фильтры для измерения фона	Mn,Na,Ag	
Фильтр в пучке от рециклических нейтронов	Cd	–

йодистого натрия размером 80 × 80 мм. При этом вводилось дискриминационное "окно", которое позволяло регистрировать гамма-лучи только в интервале энергий 1,0-2,0 мэв. Экспериментально было найдено, что в данном интервале энергий наблюдается наилучшее соотношение между выходами γ-лучей захвата и деления ($\sim$ 1 : 1). Кроме того, в этом энергетическом интервале в спектре γ-лучей нейтронного захвата у йода нет переходов с большой интенсивностью, т.е. выбор такой дискриминации приводит к снижению фона от рассеянных нейтронов.

Во втором способе оба эффекта (захват и деление) измерялись с помощью детектора с кристаллом стильбена (размерами 70 × 50 мм), с выхода которого нейтронные импульсы и импульсы от гамма-лучей разделялись по форме электронной схемой.

В измерениях применялся металлический образец ^{239}Pu толщиной $2{,}2 \cdot 10^{-3}$ атом/барн, содержащий 1,8% примеси ^{240}Pu. Фон определялся с помощью резонансных фильтров, приведенных в табл. 1, и свинцового рассеивателя, который ставился на место образца. От рассеянных нейтронов из образца кристаллы защищались фильтром из ^{10}B, толщиной 4 см. Радиационные и делительные эффекты с обоих типов детекторов регистрировались одновременно на четырех анализаторах типа АИ-4096.

РЕЗУЛЬТАТЫ ИЗМЕРЕНИЙ

С помощью описанной методики были получены величины альфа ^{235}U и ^{239}Pu от тепловой энергии нейтронов до 10 кэв. На рис. 1 приведены некоторые экспериментальные кривые делительного и радиационного эффектов ^{239}Pu после вычитания фона, измеренные первым типом детекторов. В радиационной кривой фон состоял из постоянной составляющей, возникающей из-за естественной радиоактивности образца (достигавшей $\sim$ 30% в резонансной области), и переменной составляющей, определявшейся при помощи резонансных фильтров, указанных в табл. 1 (ее максималь-

ная величина достигала ~ 50% на NaI детекторе и ~ 40% на стильбеновом детекторе при энергии нейтронов 5-10 кэв). В резонансной области переменная составляющая фона отсутствовала. В делительной кривой фон состоял только из постоянной составляющей от спонтанного деления примеси ^{240}Pu, достигавшей ~ 20% в резонансной области. Нечувствительность обоих делительных детекторов к гамма-лучам проверялась по полному отсутствию на экспериментальных делительных кривых захватного резонанса ^{240}Pu с энергией 1 эв.

Величина эффектов, регистрируемых радиационными (N_γ) и делительными (N_f) детекторами, в отдельном временном канале анализатора после вычитания фона может быть записана в следующем виде:

$$N_\gamma = n_c \cdot \epsilon_{\gamma c} + n_f \cdot \epsilon_{\gamma f}$$

$$N_f = n_f \cdot \epsilon_{nf}$$

где: n_c – число событий радиационного захвата нейтронов в образце,

n_f – число событий деления,

$\epsilon_{nf}, \epsilon_{\gamma f}, \epsilon_{\gamma c}$ – эффективности регистрации событий деления и радиационного захвата.

Отсюда, величина

$$\alpha = A \frac{N_\gamma}{N_f} - B \qquad (1)$$

где A и B – константы, не зависящие от энергии нейтронов и определяющиеся из нормировки.

При этом предполагается, что $\epsilon_{\gamma c}$ мало чувствительна к возможным изменениям спектра γ-лучей радиационного захвата. Это предположение проверялось специально проведенными измерениями спектров гамма-лучей радиационного захвата нейтронов с резонансов ^{235}U и ^{239}Pu. Обычно константы A и B определяются при нормировке результатов на отдельные разрешенные резонансы. Однако, если сравнивать данные по величинам этих резонансов, полученные в разных работах, то такое сопоставление показывает, что величины отличаются в некоторых случаях друг от друга на 20-30%, что приводит к значительным неопределенностям в α в киловольтной области энергий.

В данной работе был использован другой метод нормировки. Для этого были проведены специальные измерения отношений

$$\alpha = \frac{\sigma_c}{\sigma_f} \quad \text{и} \quad \frac{\sigma_f}{\sigma_t} = \frac{\sigma_f}{\sigma_c + \sigma_f} = \eta/\nu$$

от тепловой энергии до 10 эв, что позволило нормировать величины основных измерений на тепловую точку, где величины α и η/ν известны с высокой точностью [3]. Эти измерения проводились на том же пролетном расстоянии с увеличенным периодом следования нейтронных импульсов (см. табл. 1, столбец 2). При этом делительный и захватный эффекты измерялись теми же, что и в основных измерениях, детекторами, а эффект пропускания образца (σ_t) измерялся в условиях "хорошей" геометрии детектором медленных нейтронов, состоящим из сплава B_2O_3 и ZnS(Ag), нанесенного на фотокатод ФЭУ-2б.

В табл. 2 приведены величины η для ^{239}Pu, полученные в этих измерениях, отнормированные на величину η/ν в тепловой точке (ν = 2,88 для ^{239}Pu [3]).

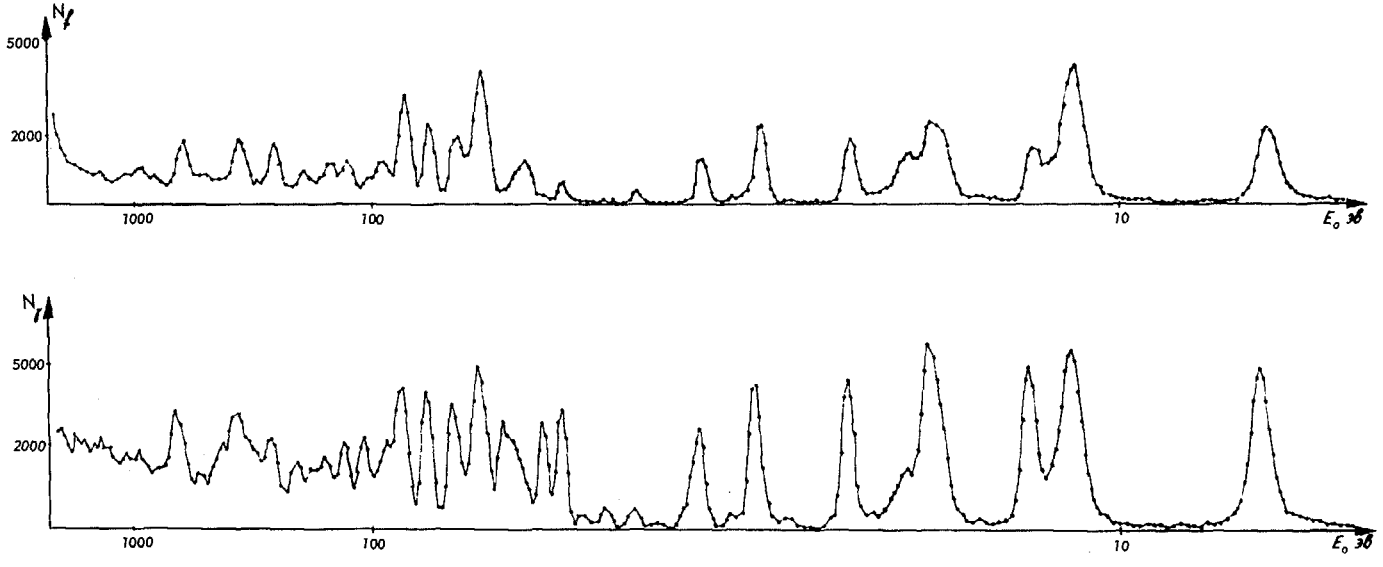

Рис. 1. Аппаратурные спектры делительного (N_f) и захватного (N_γ) эффектов в зависимости от энергии нейтронов (E_0).

ТАБЛИЦА 2. ВЕЛИЧИНЫ η ДЛЯ ^{239}Pu

E_0 (эв)	η	α	Примечание
0,025	2,11	0,36	[3]
0,30	1,728 ± 0,026	$0,66\ ^{+0,03}_{-0,02}$	Данная работа

ТАБЛИЦА 3. ВЕЛИЧИНЫ АЛЬФА ДЛЯ ПОЛНОСТЬЮ РАЗРЕШЕННЫХ РЕЗОНАНСОВ ^{239}Pu

E_0 (эв)	7,85	17,7	22,3	26,3	44,5
α	0,86 ± 0,03	1,14 ± 0,05	0,60 ± 0,04	0,99 ± 0,06	9,60 ± 0,60

ТАБЛИЦА 4. ВЕЛИЧИНЫ АЛЬФА ^{239}Pu, ПОЛУЧЕННЫЕ РАЗНЫМИ СИСТЕМАМИ ДЕТЕКТОРОВ, И ИХ СРЕДНИЕ ЗНАЧЕНИЯ

Энергия (кэв)	$\alpha\ ^{239}Pu$ (NaI и ZnS)	$\alpha\ ^{239}Pu$ стильбен	$<\alpha>\ ^{239}Pu$
0,1 – 0,2	0,87 ± 0,03	0,92 ± 0,07	0,88 ± 0,03
0,2 – 0,3	1,09 ± 0,04	1,03 ± 0,07	1,07 ± 0,04
0,3 – 0,4	1,24 ± 0,06	1,20 ± 0,10	1,23 ± 0,05
0,4 – 0,5	0,47 ± 0,05	0,42 ± 0,10	0,45 ± 0,05
0,5 – 0,6	0,76 ± 0,06	0,73 ± 0,10	0,75 ± 0,05
0,6 – 0,7	1,71 ± 0,15	1,74 ± 0,24	1,72 ± 0,13
0,7 – 0,8	0,92 ± 0,10	0,99 ± 0,20	0,94 ± 0,09
0,8 – 0,9	0,87 ± 0,11	0,63 ± 0,17	0,78 ± 0,09
0,9 – 1,0	0,75 ± 0,09	0,63 ± 0,17	0,71 ± 0,08
1,0 – 2,0	1,06 ± 0,07	0,96 ± 0,10	1,02 ± 0,06
2,0 – 3,0	1,23 ± 0,09	1,23 ± 0,17	1,23 ± 0,08
3,0 – 4,0	0,98 ± 0,13	0,92 ± 0,20	0,96 ± 0,11
4,0 – 5,0	0,87 ± 0,11	0,76 ± 0,20	0,83 ± 0,10
5,0 – 10,0	0,67 ± 0,08	0,66 ± 0,14	0,67 ± 0,07
1,0 – 10,0	0,83 ± 0,04	0,80 ± 0,06	0,82 ± 0,03

Величины α рассчитывались из η. Эти величины для тепловой области и резонанса с E_0 = 0,3 эв использовались для нахождения нормировочной зависимости между отношениями экспериментальных счетов N_γ/N_f и α, т. е. для определения констант A и B в соотношении (1). Такой метод нормировки делает полученные результаты независимыми от данных

других лабораторий. Нормировочная прямая, проведенная через точки, соответствующие величинам α тепловой области и резонанса 0,3 эв у ^{239}Pu, приводит к неопределенностям $\sim$ 5% для величин α = 0,6 - 1,1.

При помощи проведенной таким методом нормировочной прямой были получены величины α для полностью разрешенных в нашем эксперименте резонансов ^{239}Pu, которые приводятся в табл. 3. Эти данные могут быть использованы для сравнения нашего метода нормировки с нормировкой, проводимой в других работах.

В табл. 4 приведены величины альфа ^{239}Pu, полученные в данной работе разными системами детекторов, и их средние значения (в предпоследнем столбце таблицы) вместе с их статистическими ошибками.

На основании результатов, приведенных в табл. 4, были определены средние величины Z для ^{239}Pu в интервале энергий 1-10 кэв (в нижней строке таблицы) и α = 0,82 ± 0,07 для этого интервала с учетом статистической ошибки и ошибки из нормировки. В полученных величинах α хорошо прослеживается структура в области энергий 0,1-1 кэв.

Для проверки и отработки указанной выше методики были проведены также измерения величины α ^{235}U в том же энергетическом интервале. Результаты этих измерений показали, в отличие от ^{239}Pu, отсутствие у ^{235}U каких-либо особенностей в поведении величин α в энергетическом интервале 0,1-10 кэв.

В заключение авторы выражают благодарность сотрудникам А. Д. Харитонову, В. В. Ротману и В. А. Красноштанову, принимавшим участие в измерениях, а также коллективу циклотронной установки.

ЛИТЕРАТУРА

[1] РЯБОВ, Ю. В. и др., Атомная энергия 24 (1968) 351.
[2] SCHOMBERG, M.G. et al., AERE-PR/NP 14, Nucl. Phys. Div. Progress Report, 1968.
[3] HANNA, G.C. et al., Atomic Energy Review, IAEA, Vienna 7 4 (1969) 3.

ИЗМЕРЕНИЯ ОТНОШЕНИЯ СЕЧЕНИЙ РАДИАЦИОННОГО ЗАХВАТА И ДЕЛЕНИЯ (α) ДЛЯ ^{235}U И ^{239}Pu В ОБЛАСТИ ЭНЕРГИЙ НЕЙТРОНОВ НИЖЕ 30 кэв

M.A. KUROV Yu.V. RYABOV

М. А. КУРОВ, Ю. В. РЯБОВ, СО ДОН СИК, Н. ЧИКОВ,
Объединенный институт ядерных исследований,
Дубна,
В. Н. КОНОНОВ, Е. Д. ПОЛЕТАЕВ, Ю. С. ПРОКОПЕЦ,
Ю. Я. СТАВИССКИЙ
Физико-энергетический институт Государственного комитета по использованию атомной энергии СССР,
Обнинск,
Союз Советских Социалистических Республик

Abstract — Аннотация

MEASUREMENTS OF THE RADIATIVE - CAPTURE - TO - FISSION CROSS SECTIONS (α) FOR ^{235}U AND ^{239}Pu IN THE NEUTRON ENERGY RANGE BELOW 30 keV.

In this paper the results of measurements of the radiative - capture - to - fission cross sections $\alpha(E)$ for ^{239}Pu and ^{235}U in the neutron energy range below 30 keV are presented. The measurements were carried out with two different methods which are described in detail in this paper.

ИЗМЕРЕНИЯ ОТНОШЕНИЯ СЕЧЕНИЙ РАДИАЦИОННОГО ЗАХВАТА И ДЕЛЕНИЯ (α) ДЛЯ ^{235}U И ^{239}Pu В ОБЛАСТИ ЭНЕРГИЙ НЕЙТРОНОВ НИЖЕ 30 кэв.

В данной работе приводятся результаты измерений отношения сечений радиационного захвата и деления $\alpha(E)$ для ^{235}U и ^{239}Pu в области энергий нейтронов ниже 30 кэв. Измерения проводились двумя различными методами, которые описываются подробно в данной статье.

ВВЕДЕНИЕ

Подробная информация об энергетической зависимости $\alpha(E)=\sigma_c(E)/\sigma_f(E)$ для ^{239}Pu и ^{235}U в последние годы представляет особый интерес с точки зрения выбора оптимальных направлений развития ядерной энергетики. В связи с неудовлетворительным состоянием экспериментальных данных о величине $\alpha(E)$, особенно в области энергий нейтронов 0,1 ÷ 30 кэв, в данной работе были предприняты измерения $\alpha(E)$ ^{239}Pu и ^{235}U в указанной энергетической области двумя различными методами.

ЧАСТЬ I

На пролетном расстоянии 1000 м от импульсного реактора с разрешением 60 нсек/м были проведены измерения временных спектров деления и радиационного захвата образцов ^{235}U и ^{239}Pu с помощью жидкостного сцинтилляционного детектора объемом 500 л с введенным в раствор кадмием. Принцип регистрации актов деления и радиационного захвата подробно описан в работах [1,2]. При проведении данных измерений основное внимание обращалось на уменьшение влияния систематических ошибок на экспериментальные результаты.

Измерения временной зависимости скорости счета деления и радиационного захвата при небольших запаздываниях относительно нейтронного импульса реактора предъявляют жесткие требования к точности учета фонов.

Переменная составляющая фона при работающем реакторе по сравнению с первыми измерениями [1] была уменьшена с помощью:

а) формирования нейтронного пучка коллиматорами и фильтрами за пределами экспериментального помещения, что существенно понизило рассеяние быстрых нейтронов в помещение на коллиматорах, конструкционных материалах детектора и т. д.;

б) оборудования вакуумного тракта внутри детектора, что исключило вклад рассеяния нейтронов на воздухе;

в) фильтров из ^{10}B и ^{6}Li с парафином, окружающих образец, что приблизительно в 10 раз уменьшило эффективность регистрации детектором рассеянных образцом нейтронов;

г) дополнительного свинцового фильтра толщиной 0,6 см, помещенного между чувствительным объемом детектора и образцом, что понизило постоянный фон в 2-3 раза за счет уменьшения эффективности регистрации "мягких" γ-квантов, возникающих в результате интенсивного α-распада ядер образца.

Кроме того, по всей длине 1000-метрового нейтроновода в пучке оставалось минимальное количество материалов (алюминиевые вакуумные заглушки), которые в первых измерениях [1] не только уменьшили нейтронный поток, но и искажали его вблизи нейтронных резонансов марганца (E_i = 0,337 и 2,35 кэв) и алюминия (E_i = 35 кэв), что также приводило к увеличению ошибки в этих энергетических областях.

В итоге все это позволило понизить суммарный фон в канале регистрации актов радиационного захвата в области энергий 10-30 кэв с $\sim$ 50% [1] до $\sim$ 30% для ^{235}U и с $\sim$ 70% [1] до $\sim$ 40% для ^{239}Pu. Суммарный фон в канале рагистрации актов деления в той же области энергий для ^{235}U и ^{239}Pu уменьшился приблизительно на 30%. Для экспериментального определения уровня фона при работающем реакторе, кроме "черных" фильтров серебра, кобальта и марганца [1], использовались также фильтры натрия (E_i = 2,85 кэв) и титана (E_i = 17,5 кэв).

Для вычисления значений $\alpha(E)$ использовалось выражение, полученное в [1]:

$$\alpha(E_i) = A\,\frac{N_\gamma(E_i) - \text{фон}}{N_f(E_i) - \text{фон}} - B \qquad (1)$$

где: $N_\gamma(E_i)$ – число отсчетов при энергии E_i в i-том канале временного анализатора при регистрации актов радиационного захвата; $N_f(E_i)$ – число отсчетов при энергии E_i в i-том канале временного анализатора при регистрации актов деления; $A = \mathscr{E}_f/\mathscr{E}_c$ и $B = \omega/\mathscr{E}_c$ – константы, характеризующие детектор; $\mathscr{E}_f$, $\mathscr{E}_c$ – эффективности регистрации детектором акта деления и радиационного захвата, ω – эффективность регистрации актов деления в канале радиационного захвата.

Для различных серий измерений значения A и B лежали в пределах 1,2 ÷ 1,4 и 0,2 ÷ 0,8, соответственно. Величины A и B в данной работе были получены не нормировкой $(N_\gamma - \varphi)/(N_f - \varphi)$ на тепловую точку и прямым определением $\mathscr{E}_f$ и $\mathscr{E}_c$ [1,2], а нормировкой на α_i для 12 хорошо разрешенных резонансов ^{239}Pu и 14 резонансов ^{235}U. Такой способ нормировки имеет то преимущество, что позволяет использовать не одно зна-

чение α_0^{th}, причем низкое, а целый набор значений α_i от 0,2 до 9,5 (табл. 1). Погрешности в величинах α_i для отдельных резонансов составляют от 10 до 40%, поэтому для расчета на ЭВМ величин A и B методом наименьших квадратов использовались все известные в литературе данные по α_i. Ошибки величин A и B определялись с учетом ошибок нормировочных величин α_i [3-7] и отношения $\Sigma N_\gamma(E_i)/\Sigma N_f(E)$ для каждого резонанса. Ошибки при определении значений A и B составляли не более 5 и 15 ÷ 20%, соответственно. Чтобы не вводить расчетным путем поправки на многократные взаимодействия нейтронов в образце, что само по себе является сложной и трудоемкой задачей, требующей большого машинного времени, измерения были проведены с набором образцов, отличающихся по толщине. Для использования набора толщин образцов ($8{,}31\cdot10^{-5}$, $4{,}27\cdot10^{-4}$ и $4{,}21\cdot10^{-3}$ ядер/барн для ^{235}U и $2{,}85\cdot10^{-4}$, $5{,}8\cdot10^{-4}$, $8{,}7\cdot10^{-4}$, $1{,}42\cdot10^{-3}$ и $2{,}7\cdot10^{-3}$ ядер/барн для ^{239}Pu не было обнаружено зависимости величины $\alpha(E)$ от толщины образца. Это позволило сделать заключение, что многократные взаимодействия при достигнутой точности измерений, по-видимому, не играют существенной роли. Окончательные результаты по $\alpha(E)$ для ^{235}U и ^{239}Pu, представленные в таблицах 2 и 3, получены путем усреднения по всем сериям измерений, а приведенные ошибки характеризуют среднеквадратичный разброс значений $\alpha(E)$ отдельных измерений. Величины $\langle \alpha(E) \rangle$ также усреднены по энергетическим интервалам 0,1; 1,0 и 10 кэв.

ЧАСТЬ II

а) Аппаратура

Измерения $\alpha(E) = \sigma_c(E)/\sigma_f(E)$ проводились методом времени пролета на пролетном расстоянии Li = 250 м с разрешением ~ 220 и ~ 15 нсек/м. В качестве источника резонансных нейтронов в первом случае использовался импульсный быстрый реактор Объединенного института ядерных исследований (ОИЯИ), во втором – импульсный быстрый реактор с электронным инжектором – микротроном [8]. Методика эксперимента заключалась в сравнении счетов ионизационной делительной камеры, содержащей слои ^{239}Pu, и большого жидкостного сцинтилляционного детектора, регистрирующего в зависимости от времени пролета нейтронов γ-лучи радиационного захвата и деления из образца ^{239}Pu.

В опыте использовалась высокоэффективная ионизационная камера деления [9], содержащая 120 мг ^{239}Pu. Эффективность регистрации событий деления в камере составляла ~ 70%. Увеличение эффективности регистрации осколков деления в присутствии большого фона α-частиц ($3{,}2\cdot10^8$ α-частиц/сек) было достигнуто благодаря значительному увеличению быстродействия ионизационной камеры. Длительность импульсов от камеры на выходе усилителя, определяющая уровень фона многократных наложений α-частиц, составляла ~ 20 нсек.

Детектор, использовавшийся для регистрации γ-лучей захвата и деления, представляет собой большой сцинтилляционный бак объемом 500 л. Детектор имеет центральный канал, в котором располагался образец в геометрии, близкой к 4π, и через который проходит пучок нейтронов. Для уменьшения фона от радиоактивности образца и космических лучей, детектор разделен на две половины, включенные на совпадения. Для уменьшения фона, связанного с регистрацией рассеянных образцом нейтронов,

ТАБЛИЦА 1. ЗНАЧЕНИЯ α_i РАЗРЕШЕННЫХ РЕЗОНАНСОВ, ИСПОЛЬЗОВАННЫЕ ДЛЯ КАЛИБРОВКИ

Лаборатория / E_0, эв	Saclay [11]	ANL [15]	BNL [12]	Harwell [3]	ORNL-RPI [3]		ЛНФ-ОИЯИ [5]	
7,83	0,85 ± 0,09	0,98 ± 0,10	1,04 ± 0,09	1,0 ± 0,1	0,85 ± 0,02	0,84 ± 0,04	0,87 ± 0,07	0,85 ± 0,02
10,97	0,38 ± 0,08	0,22 ± 0,10	0,32 ± 0,08	0,36 ± 0,08	0,27 ± 0,05	0,24 ± 0,03	0,27 ± 0,04	0,35 ± 0,08
11,91	1,75 ± 0,25	1,86 ± 0,35	1,86 ± 0,20	1,59 ± 0,20	1,56 ± 0,10	1,52 ± 0,10	1,38 ± 0,21	1,54 ± 0,16
14,36	0,51 ± 0,14	0,66 ± 0,16	0,82 ± 0,20	0,67 ± 0,13	0,55 ± 0,02	0,58 ± 0,04	0,67 ± 0,10	–
14,75	1,25 ± 0,07	1,21 ± 0,18	1,32 ± 0,25	1,31 ± 0,13	1,13 ± 0,05	1,11 ± 0,08	1,25 ± 0,14	–
17,69	1,15 ± 0,04	0,84 ± 0,21	1,0 ± 0,2	1,15 ± 0,10	1,14 ± 0,05	–	0,92 ± 0,13	1,04 ± 0,08
22,33	0,71 ± 0,07	0,46 ± 0,24	0,59 ± 0,14	0,76 ± 0,07	0,64 ± 0,01	–	0,71 ± 0,06	0,80 ± 0,08
26,31	0,84 ± 0,17	1,07 ± 0,21	1,22 ± 0,26	1,21 ± 0,15	0,91 ± 0,03	0,91 ± 0,05	0,68 ± 0,21	0,82 ± 0,09
44,6	9,28 ± 0,40	9,61 ± 0,91	7,3 ± 1,7	8,5 ± 0,5	9,52 ± 1,00	9,38 ± 0,30	4,6 ± 2,5	–
47,92	0,31 ± 0,10	0,13 ± 0,05	0,16 ± 0,07	0,36 ± 0,08	0,32 ± 0,06	–	0,11 ± 0,06	–
50,18	3,5 ± 0,4	1,20 ± 0,33	1,27 ± 0,23	2,08 ± 0,30	–	2,45 ± 0,10	1,51 ± 0,43	–
52,8	5,25 ± 0,20	4,40 ± 0,66	4,6 ± 1,2	4,99 ± 0,49	–	5,22 ± 0,20	4,1 ± 0,9	–

ТАБЛИЦА 2. УСРЕДНЕННЫЕ ВЕЛИЧИНЫ $\langle \alpha(E) \rangle$ ДЛЯ ^{235}U

ΔE,эв	$\langle \alpha(E) \rangle$	ΔE,эв	$\langle \alpha(E) \rangle$
100 – 200	0,776 ± 0,073	3000 – 4000	0,480 ± 0,050
200 – 300	0,538 ± 0,050	4000 – 5000	0,421 ± 0,043
300 – 400	0,500 ± 0,049	5000 – 6000	0,267 ± 0,029
400 – 500	0,374 ± 0,036	6000 – 7000	0,340 ± 0,033
500 – 600	0,253 ± 0,026	7000 – 8000	0,287 ± 0,032
600 – 700	0,426 ± 0,043	8000 – 9000	0,332 ± 0,037
700 – 800	0,351 ± 0,034	9000 – 10000	0,203 ± 0,021
800 – 900	0,301 ± 0,037	10000 – 15000	0,334 ± 0,040
900 – 1000	0,458 ± 0,043	15000 – 20000	0,370 ± 0,045
1000 – 2000	0,352 ± 0,037	20000 – 25000	0,373 ± 0,047
2000 – 3000	0,400 ± 0,041	25000 – 30000	0,347 ± 0,048

ТАБЛИЦА 3. УСРЕДНЕННЫЕ ВЕЛИЧИНЫ $\langle \alpha(E) \rangle$ ДЛЯ ^{239}Pu

ΔE, эв	Толщина образца n, ядер/барн					$\langle \alpha(E) \rangle$
	$8{,}7 \cdot 10^{-4}$	$5{,}8 \cdot 10^{-4}$	$2{,}85 \cdot 10^{-4}$	$1{,}42 \cdot 10^{-3}$	$2{,}7 \cdot 10^{-3}$	
100 – 200	0,82 ± 0,21	1,01 ± 0,24	0,86 ± 0,14	0,85 ± 0,17	0,69 ± 0,13	0,85 ± 0,11
200 – 300	0,96 ± 0,24	1,09 ± 0,26	1,02 ± 0,16	1,09 ± 0,21	0,86 ± 0,14	1,00 ± 0,10
300 – 400	0,95 ± 0,26	1,11 ± 0,31	1,09 ± 0,17	1,14 ± 0,22	0,70 ± 0,15	1,00 ± 0,18
400 – 500	0,98 ± 0,29	0,92 ± 0,23	0,89 ± 0,15	0,91 ± 0,18	0,75 ± 0,13	0,89 ± 0,09
500 – 600	0,92 ± 0,23	0,89 ± 0,27	0,82 ± 0,13	0,85 ± 0,17	0,71 ± 0,12	0,84 ± 0,08
600 – 700	1,02 ± 0,20	1,21 ± 0,36	1,73 ± 0,24	2,05 ± 0,40	1,18 ± 0,13	1,44 ± 0,43
700 – 800	1,46 ± 0,39	1,19 ± 0,33	1,17 ± 0,19	1,42 ± 0,27	1,29 ± 0,12	1,31 ± 0,13
800 – 900	1,36 ± 0,36	0,97 ± 0,29	1,17 ± 0,19	1,21 ± 0,23	1,02 ± 0,14	1,15 ± 0,16
900 – 1000	1,35 ± 0,37	1,06 ± 0,32	1,16 ± 0,18	1,43 ± 0,28	1,03 ± 0,13	1,21 ± 0,18
1000 – 2000	1,15 ± 0,22	0,96 ± 0,29	1,06 ± 0,17	1,19 ± 0,23	0,85 ± 0,14	1,04 ± 0,13
2000 – 3000	1,34 ± 0,25	1,01 ± 0,26	1,17 ± 0,19	1,08 ± 0,26	0,87 ± 0,17	1,09 ± 0,18
3000 – 4000	0,95 ± 0,21	0,79 ± 0,20	1,09 ± 0,18	1,11 ± 0,22	0,86 ± 0,15	0,96 ± 0,14
4000 – 5000	0,80 ± 0,19	0,70 ± 0,21	0,77 ± 0,14	0,85 ± 0,18	0,78 ± 0,13	0,78 ± 0,05
5000 – 6000	1,02 ± 0,24	0,76 ± 0,18	0,88 ± 0,17	0,83 ± 0,18	0,63 ± 0,14	0,82 ± 0,14
6000 – 7000	1,07 ± 0,21	0,61 ± 0,17	0,68 ± 0,14	0,72 ± 0,16	0,69 ± 0,12	0,75 ± 0,18
7000 – 8000	0,88 ± 0,22	0,58 ± 0,15	0,45 ± 0,11	0,46 ± 0,13	0,65 ± 0,11	0,60 ± 0,17
8000 – 9000	0,62 ± 0,20	0,43 ± 0,12	0,46 ± 0,11	0,51 ± 0,16	0,48 ± 0,10	0,50 ± 0,07
9000 – 10000	0,44 ± 0,18	0,51 ± 0,14	0,50 ± 0,13	0,39 ± 0,15	0,32 ± 0,11	0,43 ± 0,08
10000 – 20000	0,34 ± 0,15	0,40 ± 0,13	0,41 ± 0,14	0,33 ± 0,11	0,39 ± 0,10	0,37 ± 0,05

в сцинтиллятор введен бор. Специальный опыт показал, что эффективность регистрации нейтронов, рассеянных образцом, не превышает 0,3%. Эффективный порог регистрации γ-лучей для обеих половин детектора составлял ~ 0,8 Мэв. При этом эффективность регистрации захвата составляла ~ 20%. Использование совпадений между двумя половинами детектора, которое позволило значительно уменьшить фон, приводит к заметному уменьшению эффективности регистрации событий, сопровождающихся испусканием только одного γ-кванта. Однако использование совпадений не влияет существенно на энергетическую зависимость эффективности при незначительных изменениях спектра γ-лучей радиационного захвата [10]. Уровень фона определялся экспериментально с помощью поглощающих резонансных фильтров (Al – 35 кэв, Na – 2,85 кэв, Mn – 0,337 кэв, Co – 0,132 кэв, Ag – 5,2 эв), которые исключали из пучка нейтроны с данной энергией.

б) Обработка экспериментальных данных

Число отсчетов камеры деления и детектора γ-лучей в отдельном временном канале анализатора после исключения фона можно представить в виде:

$$N_f = n_f^0 \mathscr{E}_f$$

$$N_\gamma = n_c \mathscr{E}_c + n_f \mathscr{E}_{\gamma f}$$

где n_f^0, n_f – число делений в камере и образце; n_c – число событий радиационного захвата нейтронов в образце; $\mathscr{E}_f$, $\mathscr{E}_{\gamma f}$, $\mathscr{E}_c$ – эффективности регистрации событий деления в камере и событий деления и радиационного захвата в образце. Из этих соотношений можно получить величину α:

$$\alpha = A \frac{N_\gamma}{N_f} - B$$

где $A = (m_0/m)(\mathscr{E}_f / \mathscr{E}_c)$; $B = \mathscr{E}_{\gamma f} / \mathscr{E}_c$ (m и m_0 – количество ^{239}Pu в образце и камере) – константы, которые, очевидно, не зависят от энергии нейтронов, если предполагать, что $\mathscr{E}_c$ слабо чувствительна к возможным изменениям спектра γ-лучей радиационного захвата.

В данной работе были проведены 3 серии измерений с образцом, 1 серия – с камерой деления в микротронном режиме и по одной серии – с камерой и образцом в реакторном режиме. Вся обработка экспериментальных данных производилась на ЭВМ "СДС 1604 А". Кроме величины α, в данном эксперименте были получены сечения деления ^{239}Pu до энергий нейтронов 30 кэв. Абсолютная нормировка сечений деления производилась согласно выражению:

$$\sigma_f(E) = \frac{k N_f(E) E^q}{\Delta E}$$

где ΔE – энергетическая ширина временного канала. E^{-q} – относительный ход нейтронного потока, измеренный с помощью пропорционального счетчика с BF_3, k – константа нормировки сечения, определяемая по известным значениям $\pi/q(\sigma_0\Gamma_f)$ нескольких изолированных резонансов [5, 11,12]. Точность, с которой известен этот параметр для низколежащих резонансов, составляет 2%, но неопределенность в полученных (в данном

ТАБЛИЦА 4. СРЕДНИЕ СЕЧЕНИЯ $\langle \sigma_f(E) \rangle$* ^{239}Pu, ПОЛУЧЕННЫЕ В СЕРИЯХ ИЗМЕРЕНИЙ С РАЗРЕШЕНИЕМ 15 нсек/м (I) И 220 нсек/м (II)

ΔE,кэв	$\langle \sigma_f(E) \rangle \pm 15\%$ барн (I)	Данная работа (II)	$\langle \sigma_f(E) \rangle$ [13] барн
20 – 29,6	2,05	1,72	1,57
10,1 – 20	2,09	1,78	1,71
9,1 – 10,1	2,22	2,17	2,06
8 – 9,1	2,32	2,26	2,25
7 – 8	2,55	2,39	2,14
6 – 7	2,13	2,18	2,19
5 – 6	2,36	2,20	2,50
4 – 5	2,65	2,36	2,45
3 – 4	3,65	2,95	2,95
2 – 3	3,61	2,91	3,07
1 – 2	5,56	5,01	3,85
0,9 – 1	10,93	7,16	
0,8 – 0,9	7,03	5,68	
0,7 – 0,8	6,57	5,34	
0,6 – 0,7	7,34	7,32	
0,5 – 0,6	18,33	15,61	
0,4 – 0,5	12,30	9,38	
0,3 – 0,4	7,30	8,77	
0,2 – 0,3	17,88	18,39	
0,1 – 0,2	21,63	18,94	

* Примечание: Полученные абсолютные $\sigma_f(E)$ имеют иллюстративный характер, не влияют на величину $\alpha(E)$, и отличия серии (I) от рекомендованных $\sigma_f(E)$ [13], по-видимому, связаны с неточностями определения энергетической зависимости нейтронного потока.

ТАБЛИЦА 5. ВЕЛИЧИНА ПОГРЕШНОСТИ В $\alpha(E)$

Значение α	Ошибка, связанная с калибровкой
0,2	35%
0,5	14,8%
1	7,4%
1,5	4,9%

ТАБЛИЦА 6. УСРЕДНЕННАЯ ВЕЛИЧИНА $\langle\alpha\rangle$ ДЛЯ ^{239}Pu, ПОЛУЧЕННАЯ В СЕРИЯХ ИЗМЕРЕНИЙ С РАЗРЕШЕНИЕМ 15 нсек/м (I) И 220 нсек/м (II)

Интервал уреднения, ΔE, кэв	$\langle\alpha\rangle$ (I)	$\langle\alpha\rangle$ (II)
10,1 – 29,5	0,48 ± 0,10	0,36 ± 0,08
9,1 – 10,1	0,43 ± 0,06	0,46 ± 0,09
8 – 9,1	0,49 ± 0,06	0,43 ± 0,08
7 – 8	0,46 ± 0,07	0,44 ± 0,08
6 – 7	0,97 ± 0,08	0,59 ± 0,10
5 – 6	0,90 ± 0,05	0,65 ± 0,09
4 – 5	0,95 ± 0,08	0,71 ± 0,08
3 – 4	0,67 ± 0,08	0,77 ± 0,11
2 – 3	0,89 ± 0,14	0,83 ± 0,14
1 – 2	0,65 ± 0,14	0,78 ± 0,13
0,9 – 1	0,48 ± 0,11	0,65 ± 0,15
0,8 – 0,9	0,68 ± 0,14	0,63 ± 0,14
0,7 – 0,9	1,03 ± 0,07	0,70 ± 0,16
0,6 – 0,7	0,75 ± 0,13	0,92 ± 0,21
0,5 – 0,6	0,68 ± 0,10	0,70 ± 0,10
0,4 – 0,5	0,48 ± 0,16	0,60 ± 0,12
0,3 – 0,4	1,71 ± 0,28	0,82 ± 0,23
0,2 – 0,3	1,31 ± 0,23	0,72 ± 0,16
0,1 – 0,2	0,71 ± 0,07	0,73 ± 0,05

эксперименте) сечениях деления обусловлена главным образом статистической ошибкой, которая составляла от 5 до 15% в пределах интервала усреднения. Полученные сечения деления приводятся в табл. 2. Наблюдается согласие в пределах ошибок со средними сечениями деления, рекомендованными Джеймсом и Патриком [13], но во всем энергетическом интервале сечения, полученные в данной работе, систематически на 5 ÷ 20% выше.

Для нормировки величины α были использованы также значения α_i для 12 хорошо разрешенных резонансов, приведенные в табл. 1. Величина погрешности в $\alpha(E)$, обусловленная калибровкой и использованием данных табл. 1 и метода наименьших квадратов для вычисления коэффициентов A и B, указана в табл. 5.

Значения α, полученные в данной работе, приведены в табл. 4. В экспериментах использовался образец ^{239}Pu толщиной $0{,}7\cdot10^{21}$ ядер/см^2. Результаты для микротронного режима получены путем усреднения по трем сериям измерений, а указанные ошибки характеризуют среднеквадратич-

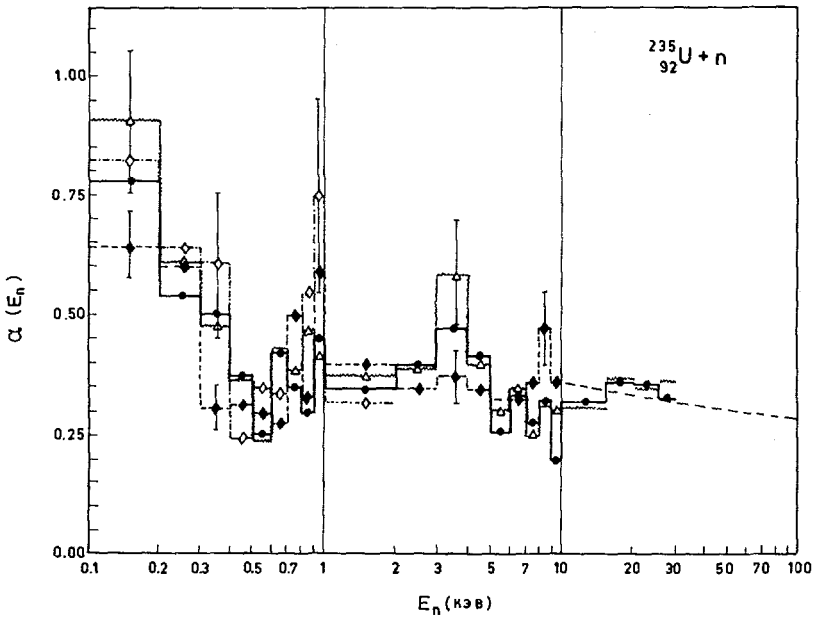

Рис. 1. Результаты измерений величины $\langle \alpha \rangle$ для ^{235}U в интервале 0,1 – 100 кэв:
——●—— – данные настоящей работы,
∿∿∿▲∿∿∿ – данные работы [1],
—·—◇—·— – данные работы [12],
— — ◆ — — – данные, полученные вычитанием $\langle \sigma_f(E) \rangle$ [6] из полных сечений $\langle \sigma_T(E) \rangle$ [13],
— — — — — — – данные, полученные в измерениях на электростатических генераторах [12].

ный разброс данных этих серий. Неопределенность в α, связанная со статистической ошибкой измерений отношения N_γ/N_f и учетом фона для каждой серии, составляет 20-50% и зависит от величины α. Окончательные данные для микротронного режима получены путем усреднения сечений деления и радиационного захвата по интервалам 0,1 кэв, 1 кэв и 20 кэв. Для реакторного режима оценка точности результатов измерений, основанная на учете статистических ошибок в отношении N_γ/N_f, статистических ошибок определения уровня фона, ошибок, связанных с калибровкой, приводит к величине неопределенности в $\alpha \pm 15$-20%.

ОБСУЖДЕНИЯ

Сравнение полученных результатов с имеющимися в настоящее время экспериментальными данными (рис. 1 и 2) показывает, что все данные об $\alpha(E)$ для ^{235}U согласуются в пределах $(10 \div 20)$% между собой, а для ^{239}Pu в некоторых энергетических областях еще наблюдаются расхождения, выходящие за 3-4 экспериментальные ошибки. Так, результаты данных измерений $\alpha(E)$ для ^{239}Pu удовлетворительно согласуются с результатами работы Гвина и др. [3] и отличаются от результатов работ [1,14] в области энергий $2 \div 5$ и $2 \div 30$ кэв, соответственно. Вместе с тем мож-

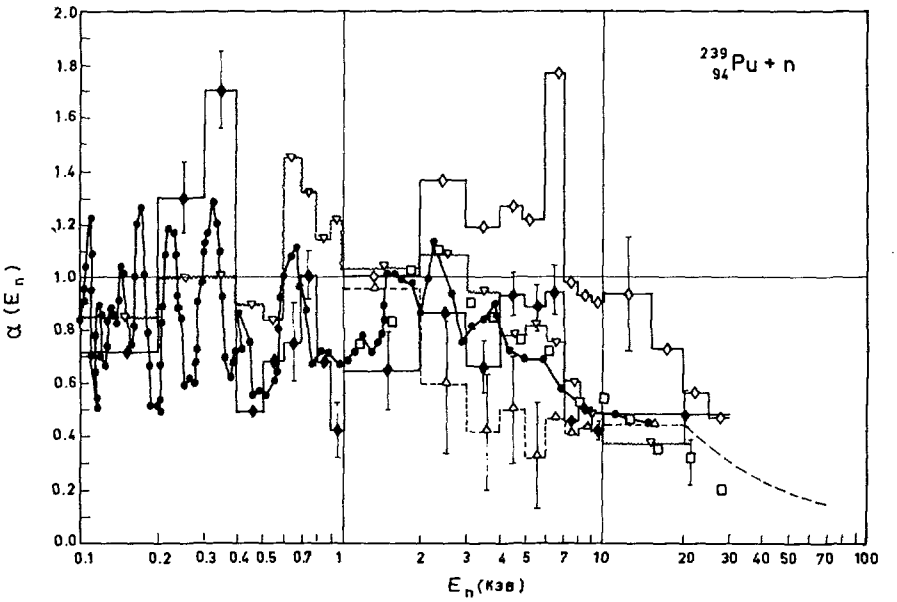

Рис. 2. Результаты измерений величины $\langle\alpha\rangle$ в интервале 0,1 – 100 кэв для ^{239}Pu:
- настоящая работа, разрешение 60 нсек/м,
- настоящая работа, разрешение 220 нсек/м,
- настоящая работа, разрешение 15 нсек/м (образец $0{,}7\cdot10^{21}$ ядер/см^2),
- работа [3],
- работа [1],
- работа [14] (приводится средний результат по нескольким сериям измерений),
- работа [12].

но отметить, что в тех случаях, когда энергетическое разрешение спектрометров по времени пролета оказывается достаточно высоким (область энергий ниже 1 кэв), структура в величине $\alpha(E)$, вызванная большими флуктуациями делительных ширин, хорошо согласуется, исключая область $0{,}2 \div 0{,}4$ кэв в данных измерениях с разрешением 15 нсек/м.

Значительное расхождение результатов измерений величины $\alpha(E)$, полученных в разных лабораториях, в диапазоне энергий нейтронов $1 \div 30$ кэв, видимо, нельзя объяснить только недостаточной точностью значений резонансных параметров, которые используются для калибровки. Вероятной причиной этих расхождений, скорее всего, является неадекватность процедуры измерения уровня фона методом резонансных фильтров. Это особенно относится к экспериментам на линейных ускорителях, где используются небольшие пролетные базы (25-35 м), так как переменная составляющая фона, связанная с нейтронами, рассеянными в измерительное помещение, при временах пролета, меньших 200 мксек, может оказаться значительной. Поэтому для получения более надежных данных по величине α в диапазоне энергий нейтронов 1-30 кэв кажется более целесообразным использование спектрометров с большими пролетными базами. Перспективным также может оказаться распространение в область более низких энергий нейтронов экспериментов на импульсных ускорителях

Ван-де-Граафа путем использования в качестве источника нейтронов реакции $^{7}Li(p,n)^{7}Be$ под большими углами или (p, n) реакций на тяжелых ядрах (V, Se).

В заключение авторы выражают глубокую признательность А. И. Лейпунскому, Ф. Л. Шапиро, Л. Н. Усачеву за постоянный интерес к работе, Л. Б. Пикельнеру – за предоставленную возможность проведения измерений на сцинтилляционном (n, γ) – детекторе, Л. Н. Седлаковой, Ц. Пантелееву, Ю. Колгину – за помощь при обработке результатов на ЭВМ и при измерениях.

ЛИТЕРАТУРА

[1] РЯБОВ, Ю. В. и др., Атомная энергия 24 4 (1968) 351.
[2] ВАН ШИ-ДИ, РЯБОВ, Ю. В., ПТЭ 14 (1965) 87.
[3] Материалы Совещания экспертов МАГАТЭ по α (^{239}Pu) 30 июня 1969 г., Винфрит (Англия).
[4] ВАН ШИ-ДИ, ВАН ЮН-ЧАН, ДЕРМЕНДЖИЕВ, Е, РЯБОВ, Ю. В., Препринт ОИЯИ, Дубна, Р-2024, 1965.
[5] РЯБОВ, Ю. В., ВАН ЮН-ЧАН и др., Препринт ОИЯИ, Дубна, Р-2713, 1966.
[6] MICHOUDON, A. et al., Nucl. Phys. 69 (1965) 545.
[7] CAO, M.G. et al., Nucl. Energy 22 (1968) 211.
[8] АНАНЬЕВ, В. Д., АНЦУПОВ, П. С., КАПИЦА, С. П. и др. Атомная энергия 20 (1966) 106.
[9] КОНОНОВ, В. Н., МЕТЛЕВ, А. А., ПОЛЕТАЕВ, Е. Д., ПРОКОПЕЦ, Ю. С., ПТЭ 6 (1969), 51.
[10] АЛЕКСАНДРОВ, Ю. А., РЯБОВ, Ю. В., САМОСВАТ, Г. С., Препринт ОИЯИ, Дубна, Р-2014, 1965.
[11] DARRIEN, H. et al., Nucl. Data for Reactors, IAEA, Vienna 2 (1967) 195.
[12] BNL-325, Suppl. 2 (1965).
[13] JAMES, G.D., PATRICK, B.H., AERE-M2068 (1968).
[14] SOWERBY, M.G. et al., Fast reactor phys. IAEA, Vienna 1 (1968) 289.
[15] БОЛЛИНГЕР, Л. и др., Труды II Международ. конф. по мирному использованию атомной энергии, Атомиздат, 2 стр. 123.

МЕТОДИКА ПРЯМОГО ИЗМЕРЕНИЯ ОТНОШЕНИЯ СЕЧЕНИЯ ЗАХВАТА К СЕЧЕНИЮ ДЕЛЕНИЯ

Г. В. МУРАДЯН, Т. А. МОСТОВАЯ,
В. И. МОСТОВОЙ, Ю. Г. ЩЕПКИН
Институт атомной энергии им. И. В. Курчатова,
Москва,
Союз Советских Социалистических Республик

Abstract — Аннотация

A METHOD OF DIRECT MEASUREMENT OF THE CAPTURE-TO-FISSION CROSS-SECTION.

A method of direct measurement of the capture-to-fission (α) cross-section is described. The fission events are recorded by an ionization chamber. A layer of the substance to be studied is located along the neutron beam and, at the same line, serves as a sample for the capture measurements. Neutron capture is recorded by NaI(Tl) crystals. The α-values for ^{235}U obtained by the method are given in a neutron energy region of 0.3-5000 eV.

МЕТОДИКА ПРЯМОГО ИЗМЕРЕНИЯ ОТНОШЕНИЯ СЕЧЕНИЯ ЗАХВАТА К СЕЧЕНИЮ ДЕЛЕНИЯ.

Описывается методика прямого измерения отношения сечения захвата к сечению деления (α). Случаи деления регистрируются с помощью ионизационной камеры. Слой исследуемого вещества располагается вдоль нейтронного пучка и служит одновременно образцом для измерения захвата. Захват нейтрона регистрируется кристаллами NaJ(Tl). Приводятся значения α для ^{235}U, полученные этим методом, в области энергии нейтронов 0,3 – 5000 эв.

1. ОСНОВНЫЕ ТРУДНОСТИ ИЗМЕРЕНИЯ

Экспериментальное определение отношения сечения захвата к сечению деления (α) в зависимости от энергии нейтрона имеет большое значение для реакторостроения и представляет интерес для понимания механизма взаимодействия нейтронов с делящимися ядрами. Измерение α в широкой энергетической области, от долей эв до нескольких десятков кэв, связано с многочисленными трудностями. Основные причины этих трудностей следующие:

1. Как при акте захвата, так и при акте деления испускаются γ-кванты. Исключение фона γ-квантов деления в измерениях захвата является нетривиальной задачей. Этот фон зависит от величины α и во многих случаях может быть значительно больше эффекта от γ-лучей захвата.

2. В киловольтовой области энергий нейтронов сечение захвата значительно меньше сечения рассеяния. Поэтому к детектору, регистрирующему захват, предъявляется жесткое требование в отношении его эффективности регистрации нейтронов. Эффективность регистрации нейтронов должна быть много меньше величины $\epsilon_\gamma (\sigma_\gamma/\sigma_s)$, где ϵ_γ – эффективность регистрации гамма-лучей захвата, σ_γ и σ_s – сечение захвата и рассеяния, соответственно. Кроме того, γ-детектор должен иметь достаточно низкую эффективность к нейтронам деления, в противном случае деление может регистрироваться как захват.

3. Для получения абсолютной величины α необходимо значение эффективности регистрации деления и захвата. Обычно эти эффективности не известны и поэтому для калибровки используется значение α в области разрешенных резонансов. Такая калибровка приводит к ошибке в α, величина которой зависит от способа измерения и точности знания величин, привлекаемых для калибровки.

Рассмотрим этот вопрос более подробно. В области $E \geqslant 1$ кэв для всех прямых измерений α деление регистрируется либо по γ-квантам деления [1], либо по нейтронам деления [2], либо по тем и другим одновременно [3,4]. Во всех этих случаях имеется заметная вероятность регистрации захвата в "канале деления". В измерениях захвата, как уже указывалось, всегда присутствует фон, связанный с γ-лучами деления. Поэтому непосредственно в эксперименте с одновременным измерением захвата и деления получаются следующие величины:

$$\left.\begin{aligned} N_\gamma &= A\cdot k\cdot\sigma_\gamma + B\cdot k\cdot\sigma_f \\ N_f &= C\cdot k\cdot\sigma_\gamma + D\cdot k\cdot\sigma_f \end{aligned}\right\} \qquad (1)$$

(предполагается, что исследуемый образец достаточно тонкий).

Здесь:

N_γ – число отсчетов в "канале захвата",
N_f – число отсчетов в "канале деления",
A – эффективность регистрации захвата в "канале захвата",
B – эффективность регистрации деления в "канале захвата",
C – эффективность регистрации захвата в "канале деления",
D – эффективность регистрации деления в "канале деления",
к – постоянный коэффициент.

Из (1) имеем:

$$\alpha \equiv \frac{\sigma_\gamma}{\sigma_f} = \frac{\frac{N_\gamma}{N_f}\frac{D}{A} - \frac{B}{A}}{1 - \frac{N_\gamma}{N_f}\frac{C}{A}} \qquad (2)$$

т. е. для определения α необходимо знание трех постоянных – B/A, C/A и D/A. Ошибка в α, связанная с ошибкой $[\Delta(N_\gamma/N_f)]$, в сильной степени зависит от соотношения абсолютных величин этих постоянных и сводится к минимуму при $B = C = 0$. Уменьшение числа калибровочных постоянных от трех до двух (это может быть, например, в том случае, когда в "канале деления" отсутствует фон, связанный с захватом) уже существенно уменьшает ошибку в α. Отметим, что с ростом B/A и C/A быстро растут требования к точности знания как самых величин, так и отношения N_γ/N_f.

4. Сечения захвата и деления, особенно в области разрешенных резонансов, где производится калибровка, имеют довольно резкую зависимость от энергии. Поэтому для получения приемлемой скорости набора информации при условии тонкости образца ($n\sigma_T < 1$, где n – число ядер на 1 $см^2$ образца, σ_T – полное сечение) приходится пользоваться образцами различной толщины, в зависимости от σ_T. Привязка серий измерений, соответствующих разным толщинам образцов, приводит к дополнительной ошибке.

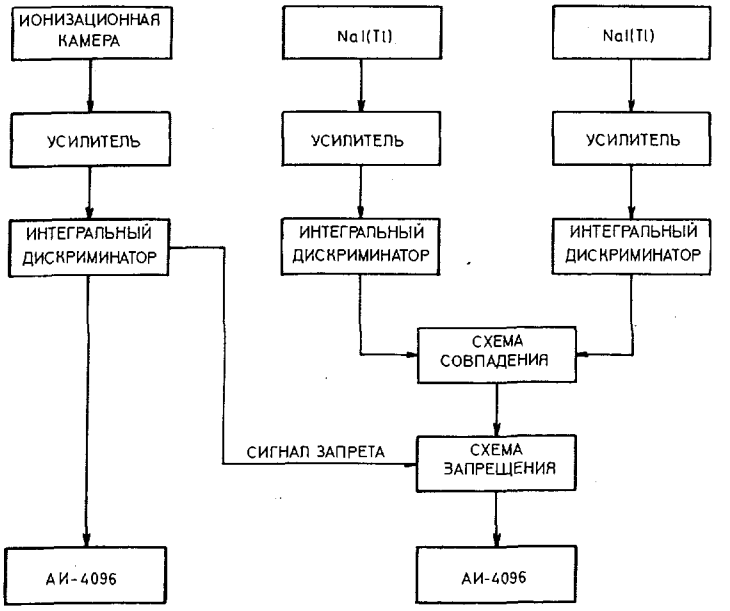

Рис. 1. Блок-схема измерений.

2. МЕТОДИКА ПРЯМОГО ИЗМЕРЕНИЯ α

При выборе методики измерения мы исходили из следующих предпосылок:

1. Поскольку в результатах измерений α, произведенных разными авторами (особенно в случае ^{239}Pu), существуют расхождения, превышающие экспериментальные ошибки, желательно выбрать независимую методику.

2. В целях уменьшения ошибок желательно сократить число калибровочных постоянных.

3. Большая величина фона сильно влияет на точность определения α, поэтому фон (особенно нейтронный) необходимо свести до минимума, так чтобы результаты не были критичны к точности определения фона.

Была выбрана следующая схема эксперимента. Измерение деления производится ионизационной камерой по осколкам деления. Одновременно с помощью двух кристаллов NaJ(Tl) регистрируется захват нейтронов. В качестве образца для измерения захвата служит слой делящегося вещества, находящийся в камере. Чтобы уменьшить вероятность регистрации γ-квантов деления кристаллами NaJ(Tl), сигналы от ионизационной камеры поступают в электронную схему "запрещения", которая при наличии сигнала деления в течение времени 5 мксек блокирует попадание сигналов из кристаллов NaJ(Tl) во временной анализатор импульсов (рис. 1), регистрирующий захват.

Измерения α с помощью аналогичной методики (вместо кристаллов NaJ(Tl) использовался жидкостный сцинтиллятор с объемом 750 л) предпринимались и ранее [5]. Однако наличие большого фона в "канале зах-

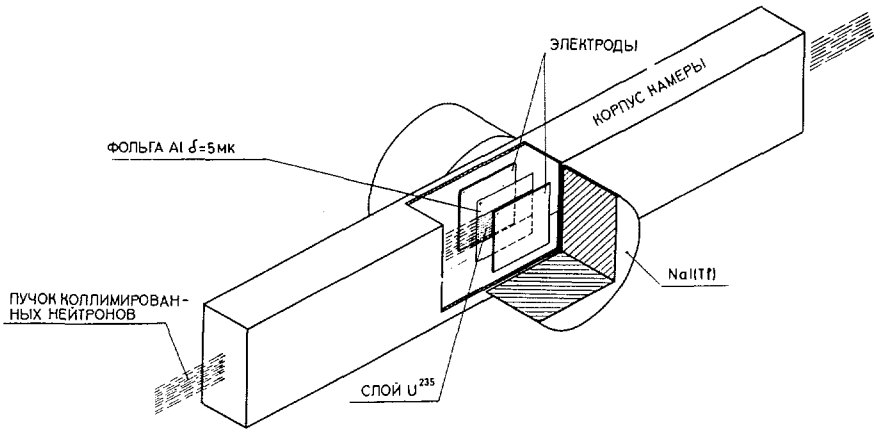

Рис. 2. Расположение камеры и детекторов NaJ(Tl) на пучке нейтронов.

вата" не позволяло получить приемлемые результаты в области энергий $E \gtrsim 1$ кэв. Прохождение большого фона при $E \gtrsim 1$ кэв связано с тем, что на пути нейтронного пучка, помимо исследуемого слоя, неизбежно присутствуют конструкционные материалы – входная и выходная диафрагмы, электроды, подложка слоя и рабочий газ камеры, вероятность рассеяния на которых намного превышает вероятности захвата в исследуемом слое. Например, для слоя ^{235}U 0,5 мгр/см^2, нанесенного на алюминиевую подложку толщиной 100 мк, рассеяние нейтронов от подложки при энергии 5 кэв в ~ 500 раз больше, чем захват в ^{235}U. Рабочий газ и диафрагмы дают еще больший вклад в рассеяние. Для быстродействующей камеры, описанной в [6], вероятность рассеяния на газе в ~ 4000 раз превышает вероятности захвата в исследуемом слое. Заметим, что при $E \leqslant 1$ кэв относительная доля рассеянных нейтронов существенно меньше, а защита от них проще, и поэтому измерение захвата в этой области энергии не встречает больших трудностей.

Таким образом, для проведения измерения захвата в киловольтовой области энергий прежде всего необходимо в десятки раз уменьшить нейтронный фон, обусловленный рассеянием нейтронов на конструкционных материалах. Это является основной проблемой в данной методике.

Уменьшение рассеяния от подложки слоя не связано с принципиальными трудностями. Для этого достаточно взять более тонкую подложку. Мы использовали алюминиевую подложку толщиной 5 мк. Столь тонкая подложка одновременно дала возможность за счет использования суммарного импульса от обоих осколков увеличить эффективность регистрации деления, что крайне необходимо для снижения фона γ-лучей деления в "канале захвата".

Более важной задачей является уменьшение рассеяния нейтронов от электродов и рабочего газа камеры. Рассеяние от этих элементов можно сильно уменьшить, расположив слой делящегося вещества не поперек нейтронного пучка, как это обычно делается, а вдоль (рис. 2). Действительно, как видно из рис. 2, если при таком расположении слоя сформировать узкий нейтронный пучок, то электроды и большая часть рабочего газа окажется вне пучка.

В качестве рабочего газа ионизационной камеры можно использовать аргон при относительно небольшом давлении (130 мм Hg). Выбор аргона связан с тем, что он является одноатомным газом и обладает малым сечением рассеяния ($\sigma_s < 1$ барн в области $E \leqslant 10$ кэв). В результате рассеяние нейтронов от газа становится не существенным. Это дало нам возможность, удлинением корпуса камеры, отодвинуть ее торцы от γ-детектора.

Приведем геометрические данные камеры, которая была использована в работе:

длина камеры	1000 мм
толщина торцов	1 мм
расстояние между электродами	25 мм
толщина подложки слоя (положительный электрод)	5 мк
размеры исследуемого слоя по пучку (длина слоя)	100 мм
высота слоя	30 мм.

Отсюда, при ширине пучка 4 мм и слое ^{235}U толщиной 0,8 мг/см^2, получаем:

вероятность рассеяния на подложке	$1{,}3 \cdot 10^{-3}$
вероятность рассеяния на ^{235}U	$0{,}8 \cdot 10^{-3}$
вероятность рассеяния на газе (с учетом CO_2)	$0{,}9 \cdot 10^{-3}$

Таким образом, вероятность рассеяния нейтронов в камере составляет $3 \cdot 10^{-3}$.

Вероятность же захвата в слое ^{235}U составляет $\sim 8 \cdot 10^{-3} E^{-1/2}$. Поэтому отношение вероятности рассеяния нейтронов и вероятности их захвата равно $\sim 0{,}38\sqrt{E}$. При E=5000 эв это дает величину ~ 27, т. е. относительная доля рассеянных нейтронов для такой камеры намного (~ 100 раз) меньше, чем для обычно применяемой камеры. Если внутри корпуса описанной камеры слой с электродами (допустим, что толщина электродов 5 мк) повернуть поперек пучка, то доля рассеянных нейтронов значительно увеличится. Кроме того, если эксперимент ставится на электронном ускорителе (используемом как источник нейтронов), то γ-детектор и камера при малых временах пролета нейтрона и при большом рассеянии на рабочем газе и электродах могут потерять линейность из-за первоначального γ-импульса ускорителя.

По-видимому, продольное расположение слоя предпочтительно еще и потому, что вследствие сильной коллимации нейтронное поле в районе γ-детектора сильно уменьшено, что, в свою очередь, приводит к уменьшению внешнего нейтронного фона.

Следует отметить, что расположение слоя вдоль пучка приводит к увеличению неопределенности в пролетном расстоянии нейтронов, из-за чего в области малых энергий, в данном случае в области $E \leqslant 20$ эв, ухудшается энергетическое разрешение. Однако для поставленной задачи высокое разрешение не является существенным и, кроме того, в области $E \leqslant 20$ эв достаточно хорошие результаты уже получены с обычным расположением слоя [5,7].

Наконец, заметим, что расположение слоя вдоль пучка не приводит к эффектам самоэкранирования. Даже для сильных резонансов $n\sigma_T \ll 1$ (n – число атомов ^{235}U на см^2 по направлению пучка, σ_T – полное сечение

^{235}U), что объясняется естественной расходимостью нейтронного пучка и тем, что подложка слоя не представляла собой идеальной плоскости.

3. РЕГИСТРАЦИЯ ДЕЛЕНИЯ

Как уже указывалось, случаи деления регистрировались ионизационной камерой. Камера работала при наполнении смесью химически чистого аргона (95%) и CO_2 (5%) до давления 130 мм Hg. При этом время собирания электронов составляло 0,2 мксек. Для увеличения стабильности работы и во избежание различного рода помех от линейного ускорителя высокое напряжение на электроды камеры, а также напряжение для питания транзисторного предварительного усилителя подавалось от сухих анодных батарей.

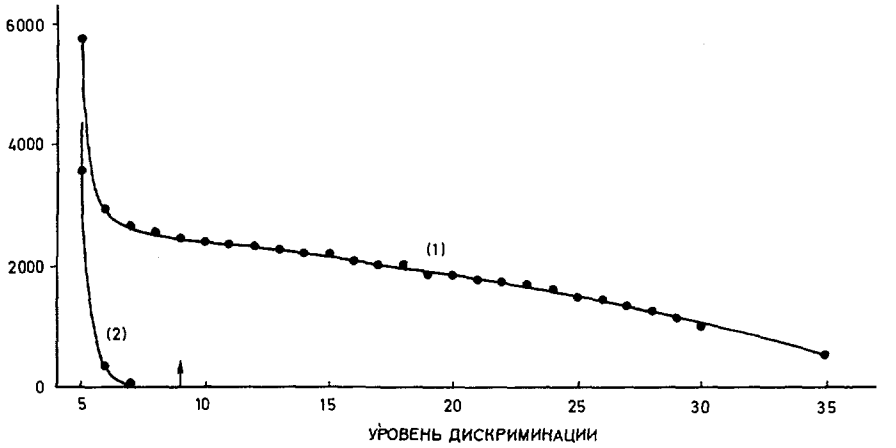

Рис. 3. Счетная характеристика камеры.

На рис. 3 приведено распределение амплитуд выходных импульсов камеры. Кривая 1 соответствует скорости счета осколков (число отсчетов за 1 мин.) с нейтронным источником, кривая 2 – без нейтронного источника. Там же стрелкой указан уровень дискриминации, который был выбран при измерениях α. Видно, что эффективность регистрации случаев деления для выбранного уровня дискриминации составляет ~95%. Последнее означает, что в "канале захвата" могут регистрироваться не более чем 5% случаев деления.

После дискриминации сигналы деления поступали на 4096-канальный временной анализатор и схему запрещения, которая блокировала регистрацию γ-квантов деления в "канале захвата".

4. РЕГИСТРАЦИЯ ЗАХВАТА

Поскольку в данной работе количество исследуемого вещества составляет очень малую величину – 24 мг, к детектору, регистрирующему захват, предъявляются жесткие требования в отношении его естествен-

ного фона и величины внешнего фона. Если бы мы использовали такой же жидкостный детектор, как и в [5], то отношение эффекта к естественному фону, не связанному с ускорителем, уменьшилось бы в ~200 раз, так как в [5] использовался образец в количестве 4,5 г. При этом величина фона была бы намного больше эффекта, из-за чего результаты обработки в сильной степени зависили бы от точности определения фона, от стабильности работы всей аппаратуры и т. д. То же самое относится к внешнему фону, обусловленному рассеянными нейтронами в помещении.

Для уменьшения указанных фонов необходимо сильно (в ~200 раз) уменьшить объем детектора. При этом эффективность детектора должна оставаться в приемлемых пределах.

Для регистрации захвата были использованы два кристалла NaJ(Tl) (рис. 2), размерами $\varnothing$ 200 × 100 мм^2. Сигналы от ФЭУ дискриминировались (уровень дискриминации 600 кэв) и поступали на схему совпадения, после чего через схему запрещения поступали на 4096-канальный временной анализатор (рис. 1).

Эффективность кристаллов NaJ(Tl) на единицу объема очень высокая. Поэтому при обычных небольших значениях эффективности (< 20%) они обеспечивают низкий уровень естественного и внешнего фона и не требуют громоздкой защиты[1].

Основным недостатком кристаллов NaJ(Tl) является их большая чувствительность к нейтронам. Регистрация нейтрона происходит в основном из-за их захвата в йоде. Однако число γ-лучей, испускаемых при захвате йодом нейтрона, по сравнению с ^{235}U (или другим делящимся ядром) довольно мала (приблизительно 1,2 γ-квантов/акт захв. при $E \geqslant 0{,}6$ Мэв), так что введение режима совпадения может существенно уменьшить нейтронный фон.

Оценим отношение эффективности регистрации рассеянного нейтрона и акта захвата в ^{235}U. Введем обозначения:

$\epsilon_{геом.}$ – телесный угол, под которым каждый кристалл видит исследуемый слой,

ϵ_γ – средняя вероятность регистрации кристаллом γ-кванта, когда последний попадает в кристалл,

$\epsilon_n(E)$ – средняя вероятность захвата кристаллом нейтрона, когда последний попадает в кристалл,

ν – количество γ-квантов, возникающих при захвате нейтрона в ^{235}U.

Допустим, что внутри камеры произошло рассеяние нейтрона. Оценим вероятность регистрации такого нейтрона. Вероятность захвата нейтрона в любом из двух кристаллов есть $2\,\epsilon_{геом.}\cdot\epsilon_n(E)$. При захвате в ~20% случаев возникают два γ-кванта с энергией выше порога регистрации. Если один из γ-квантов зарегистрируется в одном кристалле, а другой – в другом, возникает импульс совпадения. Вероятность такого совпадения будет:

$$0{,}2\,(1-\epsilon_\gamma)\,[2\epsilon_{геом.}\cdot\epsilon_n(E)]\cdot\epsilon_\gamma\frac{\epsilon_\gamma\cdot\epsilon_{геом.}}{4}\cdot 2 = 0{,}2\,\epsilon^2_{геом.}\cdot\epsilon_n(E)\cdot\epsilon^2_\gamma$$

[1] В настоящее время полученная эффективность регистрации акта захвата составляет 13% при естественном фоне 50 отсч./мин.

Зависимость $\epsilon_n(E)$ можно оценить, зная среднее сечение захвата $\sigma_\gamma(E)$ в йоде. Имеем:

$$\epsilon_n(E) \approx (1-e^{n\sigma_\gamma(E)}) \approx (1-e^{-\frac{15}{\sqrt{E}}}) \quad (3)$$

и поэтому эффективность регистрации рассеянного нейтрона будет:

$$W_n = 0{,}2\cdot\epsilon^2_{\text{геом.}}\cdot\epsilon^2_\gamma\,(1-e^{-\frac{15}{\sqrt{E}}})(1-e_\gamma) \quad (4)$$

Эффективность регистрации захвата в ^{235}U детектором NaJ(Tl) дается следующей приближенной формулой:

$$W_\gamma \approx (\epsilon_{\text{геом.}}\cdot\epsilon_\gamma)^2\cdot\nu(\nu-1) \quad (5)$$

Из (4) и (5) находим отношение эффективностей регистрации захвата и рассеяния:

$$\frac{W_\gamma}{W_n} = \frac{5\cdot\nu\,(\nu-1)}{(1-e^{-\frac{15}{\sqrt{E}}})(1-\epsilon_\gamma)} \quad (6)$$

Имея в виду, что между камерой и кристаллами введена защита из ^{10}B толщиной 3 г/см^2, окончательно получаем:

$$\frac{W_\gamma}{W_n} = \frac{5\cdot\nu\,(\nu-1)e^{\frac{100}{\sqrt{E}}}}{(1-e^{-\frac{15}{\sqrt{E}}})(1-\epsilon_\gamma)} \quad (7)$$

Заметим, что формула (7) приближенная. В ней не учтено, в частности, что захват нейтрона происходит на разных глубинах кристалла, что эффективная толщина защиты ^{10}B для рассеянных нейтронов больше 3 г/см^2 из-за их углового разброса, что совпадения могут происходить при испускании йодом (захватившим нейтрон) и одного γ-кванта и т. д.

По-видимому, в (7) переоценена вероятность регистрации нейтронов. Но даже при этом отношение W_γ/W_n достаточно высокое. Полагая $\nu = 4$, из (7) находим, что при E = 100 эв, 1000 эв, 10 000 эв величина W_γ/W_n составляет $\sim 4\cdot10^6$, $8\cdot10^3$, $2\cdot10^3$.

Чтобы оценить отношение эффекта к фону, необходимо найти отношение вероятности рассеяния и захвата. Как уже отмечалось, это отношение равно $\sim 0{,}38\sqrt{E}$.

Поделив (7) на $0{,}38\sqrt{E}$, получим искомую величину:

$$\chi \equiv \frac{\text{эффект}}{\text{фон}} \approx \frac{13\cdot\nu(\nu-1)\,e^{\frac{100}{\sqrt{E}}}}{(1-e^{-\frac{15}{\sqrt{E}}})(1-\epsilon_\gamma)\sqrt{E}} \quad (8)$$

При E = 100 эв, 1000 эв, 10 000 эв отношение χ равно 10^6, 600 и 60, соответственно.

Таким образом, внутренний нейтронный фон составляет небольшую величину и поэтому точность его определения слабо скажется на результаты измерения α.

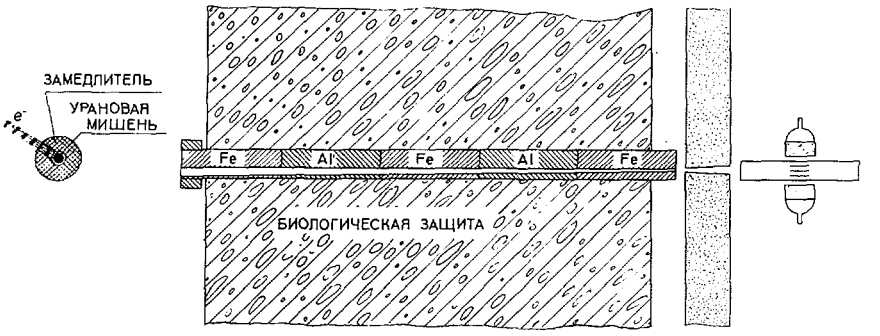

Рис. 4. Схема коллимации пучка.

5. ФОРМИРОВАНИЕ НЕЙТРОННОГО ПУЧКА И ЗАЩИТА

Измерения проводились на линейном электронном ускорителе Института атомной энергии [8] методом времени пролета. Камера и γ-детектор находились на расстоянии 5 м от урановой мишени ускорителя. Для формирования нейтронного пучка сечением 3×30 мм^2 использовался секционный коллиматор общей длиной 3,5 м, состоящий из железа и алюминия (рис. 4). Коллиматор расположен в нейтронном канале биологической защиты ускорителя и имеет конусную щель с квадратным сечением (входные размеры щели – 20×80 мм^2, выходные – $2{,}5 \times 28$ мм^2). Отверстие коллиматора расположено таким образом, чтобы исследуемый образец не видел урановую мишень, являющуюся источником первоначального импульса γ-лучей, и быстрых нейтронов. Между камерой и концом коллиматора расположен еще один коллиматор со встречным конусом. Это уменьшает вероятность попадания нейтронов в детектирующую систему после их рассеяния на конце предыдущего коллиматора.

Для защиты от фона нейтронов, рассеянных внутри камеры, между камерой и кристаллами введены диски из ^{10}B ($\varnothing$ 230 мм) толщиной 3 г/см^2. От внешнего фона детектор защищался последовательно слоем карбида бора (20 см), слоем свинца (10 см) и слоем смеси карбида бора с парафином (20 см). Кроме того, для поглощения мягкой компоненты γ-излучения ^{235}U кристаллы окружались свинцовым слоем толщиной 3 мм (кроме одного торца, который предусмотрен для укрепления ФЭУ).

На пути пучка постоянно находились Cd (0,5 мм) и Al (20 мм). Cd введен для поглощения рециклических нейтронов, а Al – для уменьшения фона, связанного с резонансным рассеянием на алюминиевой подложке слоя в камере. Введение кадмия одновременно позволяет получить величину постоянного во времени фона по интенсивности счета в последних каналах анализатора, где Cd поглощает практически все нейтроны.

6. ИЗМЕРЕНИЕ ФОНА

Для измерения фона, присутствующего в "канале захвата", была создана имитирующая камера, во всем идентичная с основной камерой, за исключением только того, что вместо урана на Al подложку был нанесен

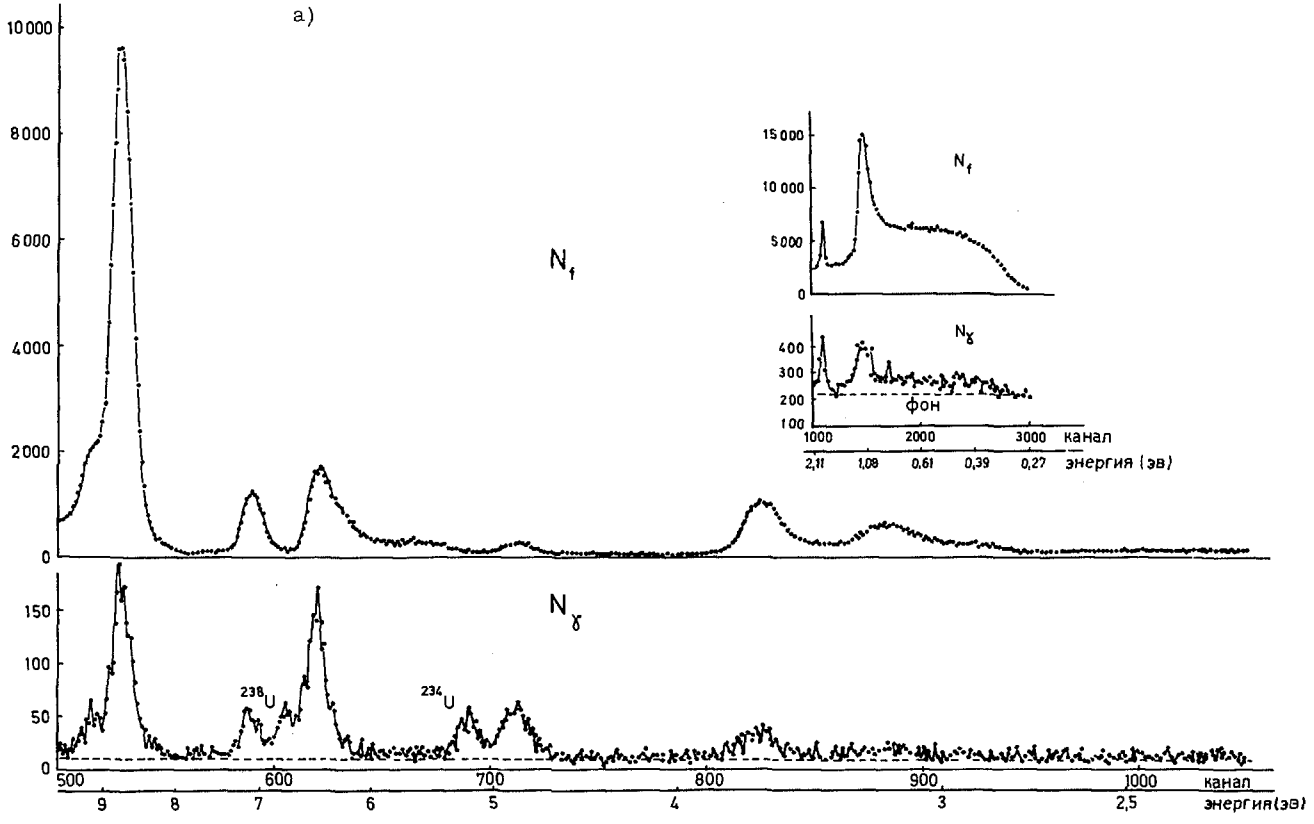
а)
N_f
N_γ
^{238}U
^{234}U
фон
канал
энергия (эв)
энергия(эв)

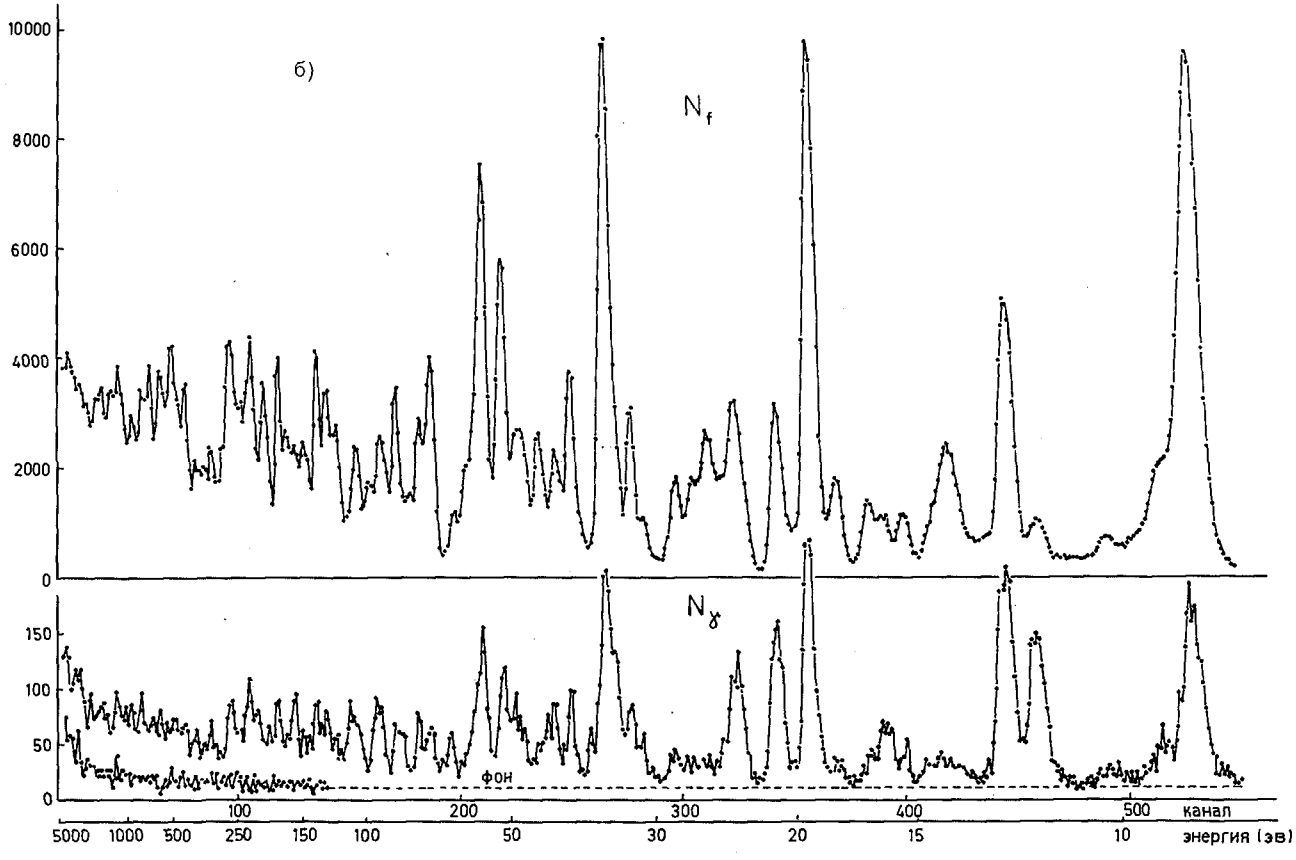

Рис. 5(а,б). Зависимость числа отсчетов N_γ,N_f и N_ϕ в каналах анализатора от номера канала и энергии нейтронов.

свинец. Толщина свинца подобрана таким образом, чтобы имитировать рассеяние нейтронов на уране. Измерения этой камерой со слоем свинца и без него показали, что фон практически не зависит от наличия в камере свинца. Это указывает на то, что основной фон связан не с рассеянием внутри камеры.

Для произведения серий измерений с имитирующей и рабочей камерами к одному нейтронному потоку использовались три монитора – два пропорциональных BF_3 – счетчика и один сцинтилляционный счетчик NaJ(Tl) в сочетании с образцом из серебра.

Обычно в измерениях α для определения фона применяют метод резонансных фильтров. В данном эксперименте (в той или иной степени и в других экспериментах) метод резонансных фильтров ничего не дает для определения "мгновенного фона", т.е. фона, связанного с рассеянием исследуемым образцом и конструкционными материалами. Этот метод позволяет получить величину внешнего и естественного фонов, а также фона, непосредственно связанного с нейтронным пучком, проходящим через камеру (нетаймированный фон).

В принципе можно было бы применять метод резонансных фильтров для определения фона в "канале деления", где "мгновенный фон" отсутствует. Однако в области больших энергий из-за низкого энергетического разрешения затруднено получение приемлемой точности.

Помимо описанных источников фона, в "канале захвата" существует фон случайных наложений. Действительно, если два рассеянных нейтрона или γ-кванта (или то и другое) зарегистрируются в разных кристаллах NaJ(Tl) в пределах времени разрешения схемы совпадения, то на выходе схемы появится сигнал, не связанный с эффектом. Чтобы оценить величину этого ложного эффекта, были проведены измерения в режиме сложения импульсов от кристаллов NaJ(Tl). Исходя из времени разрешения схемы совпадения, мы оценили фон случайных наложений. В области $E \leqslant 10$ кэв он оказался меньше 2%. Его величина сильно растет с ростом энергии и импульсной мощности ускорителя.

7. ИЗМЕРЕНИЕ И РЕЗУЛЬТАТЫ

Измерение захвата и деления проводились одновременно на двух 4096-канальных анализаторах с шириной канала 0,25 мксек. При этом ускоритель работал в следующем режиме: частота посылок 244 имп/сек, длительность импульса электронов – 0,2 мксек, ток в импульсе – 0,5 а, энергия электронов – 25 Мэв.

Были получены результаты 5 серий измерений с рабочей и 5 серий измерений с имитирующей камерами. Суммарное время измерений – 250 часов.

На рис. 5а и 5б приведена зависимость захвата N_γ, деления N_f и фона N_Φ от номера канала и энергии нейтронов, полученная в измерениях. При энергии выше 5 кэв в измерениях захвата обнаруживается зависимость получаемых результатов от мощности ускорителя. Происхождение этой зависимости, по-видимому, связано с регистрацией первоначального γ-импульса ускорителя. В случае регистрации деления такая зависимость не обнаруживается.

Одна из серий измерения N_f для области $E \geqslant 5$ кэв приведена на рис. 6, где четко видны уровни Al при 35 кэв и 89 кэв. Экспериментальная пло-

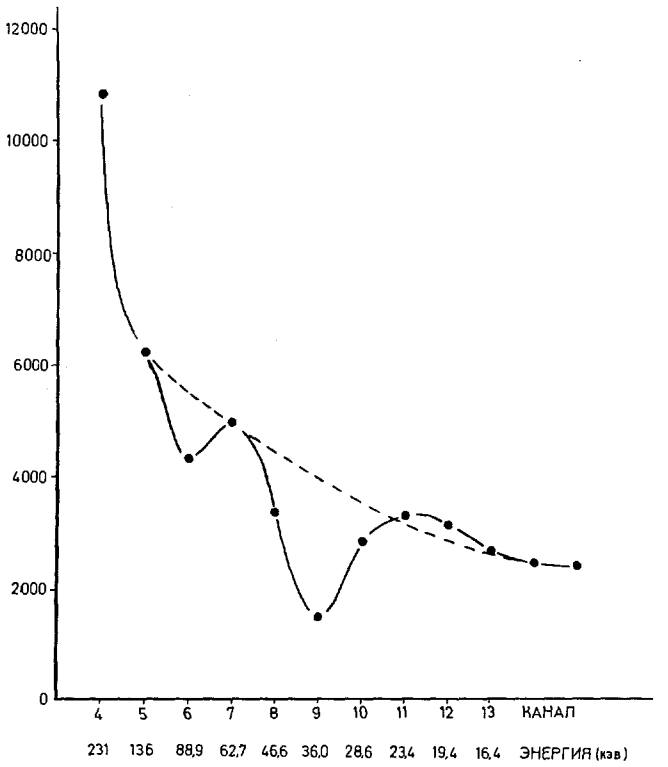

Рис. 6. Измеряемый эффект деления N_f на каналах анализатора для E > 5 кэв.

щадь уровня 35 кэв хорошо согласуется с расчетной, в предположении отсутствия фона. В измерениях захвата этот резонанс проявлен слабее. В измерениях с имитирующей камерой 35-кэв – резонанс не проявляется, откуда следует, что основным источником фона является внешний и естественный фон. Так как сам по себе внешний фон, зарегистрированный кристаллами NaJ(Tl) составляет небольшую величину, а количество вещества в кристаллах намного больше, чем количество ^{235}U, то фон в измерениях деления должен практически отсутствовать.

Из-за низкого разрешения энергетическая ширина канала довольно большая (~400 эв при E = 5000 эв). Поэтому очень важно установить соответствие между номерами каналов в измерениях деления и захвата. В наших измерениях это делалось одновременно по 35-кэв – резонансу Al и по первоначальному γ-импульсу ускорителя. Точность такой привязки получается не хуже чем половина канала временного анализатора.

Для определения абсолютного значения α была проведена калибровка. Поскольку в измерениях деления примесь захвата отсутствует, калибровка сводится к определению двух постоянных (см. формулу 2).

$$\alpha = a\frac{N_\gamma}{N_f} - b \qquad (9)$$

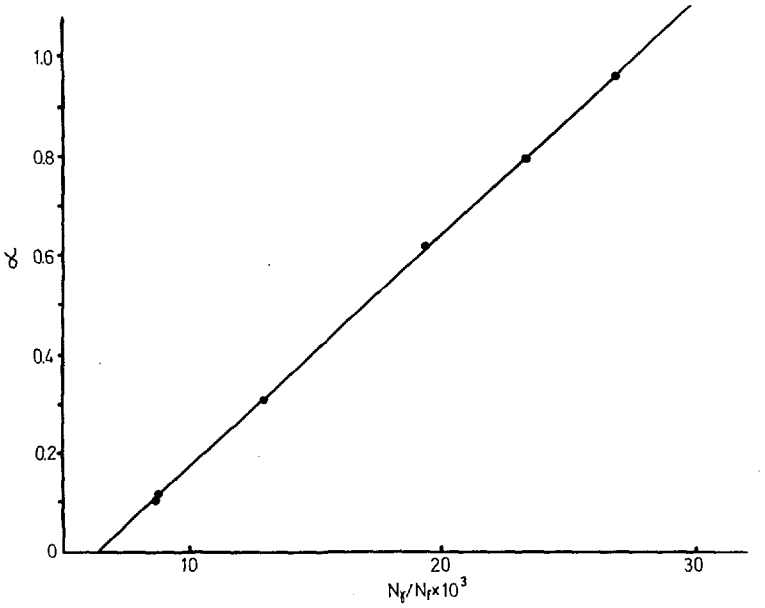

Рис. 7. Зависимость α от N_γ/N_f (калибровочная прямая).

ТАБЛИЦА 1. ЗНАЧЕНИЯ α

Интервал усреднения эв		$\langle\alpha\rangle$	$\pm\Delta\langle\alpha\rangle$
E_1	E_2		
10	20	0,96	0,02
20	30	0,92	0,03
30	40	0,81	0,03
40	50	0,73	0,04
50	60	0,53	0,03
60	80	0,55	0,05
80	100	0,60	0,04
100	200	0,65	0,03
200	300	0,55	0,03
300	400	0,63	0,06
400	600	0,38	0,03
600	800	0,51	0,05
800	1000	0,64	0,08
1000	2000	0,46	0,05
2000	3000	0,64	0,07
3000	5000	0,50	0,08

где N_γ – число отсчетов в "канале захвата" за вычетом фона, N_f – число отсчетов в "канале деления", a и b – искомые постоянные. Для определения a и b были использованы данные по α в области 0,55 – 20 эв из работы [9].

На рис. 7 приведены значения α из указанной работы и отношения N_γ/N_f, взятые из наших измерений. Тот факт, что калибровочные точки хорошо ложатся на прямую, указывает на правильность методики измерения α в целом.

Прямая рис. 7 описывается уравнением:

$$\alpha = 47{,}4\frac{N_\gamma}{N_f} - 0{,}3 \qquad (10)$$

которое одновременно служит формулой для определения α по известным величинам N_γ/N_f. Из формулы (10) следует, что эффективность регистрации деления кристаллами NaJ(Tl) примерно в 6 раз больше, чем эффективность регистрации захвата.

Действительно, выразив коэффициент b через эффективности регистрации деления камерой (ϵ_f) и кристаллами ($\epsilon_{\gamma f}$) и эффективность регистрации захвата ($\epsilon_{\gamma\gamma}$), имеем:

$$b = (1 - \epsilon_f)\frac{\epsilon_{\gamma f}}{\epsilon_{\gamma\gamma}} = 0{,}3$$

Положив $\epsilon_f = 0{,}95$, получим $\epsilon_{\gamma f} = b\epsilon_{\gamma\gamma}$. Такой же результат получается и без привлечения эффективности камеры, при использовании результатов измерений полного счета γ-лучей. Большая эффективность регистрации деления кристаллами связана с большим числом γ-квантов (частично регистрируются и нейтроны деления), вылетающих при делении.

Несмотря на столь большую относительную эффективность регистрации деления кристаллами, сам по себе фон деления в "канале захвата" составляет небольшую величину (30% для $\alpha = 1$). В известных к настоящему времени измерениях α этот фон намного больше, что, как уже отмечалось, приводит к сильной зависимости ошибки $\Delta\alpha$ от точности привлекаемых калибровочных величин и экспериментально получаемой величины N_γ/N_f.

В таблице 1 приведены значения $\langle\alpha\rangle\equiv$, вычисленные усреднением экспериментальных величин N_γ и N_f с учетом спектра нейтронов. Эти данные приведены также на рис. 8, где для сравнения нанесены известные результаты других авторов [7,10 – 13].

В области энергий от 10 до 300 эв, полученные значения $\langle\alpha\rangle$ находятся практически посередине других данных. Исключение составляет интервал 60-70 эв и 90-100 эв, где измерения различных авторов сильно расходятся.

В области $E_n > 900$ эв, полученные значения α систематически выше других данных. Это обстоятельство требует дополнительного анализа и контрольных экспериментов. Возможно, что это является следствием того, что имитирующая камера по фону неполностью адекватна рабочей. Так, эта камера не имитирует γ-излучение слоя за счет распада изотопов урана и осколков. Это может приводить к занижению фона. Имитирующая камера также не дает фона, связанного со случайными совпадениями γ-излучения захвата и γ-излучения фона. Вклад этих совпадений растет с увеличением фона.

Однако это систематическое превышение $\langle\alpha\rangle$ в области $E_n > 300$ эв над другими данными не выходит за пределы ошибок измерений. Поэто-

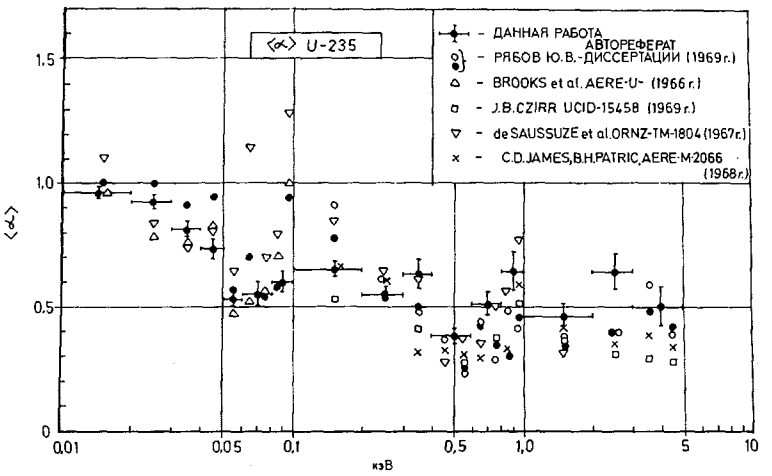

Рис. 8. Экспериментальные данные по α и сравнение с результатами других авторов.

му результаты данной работы несомненно свидетельствуют о том, что разработанная методика пригодна для измерений α.

В заключение перечислим вкратце особенности этой методики.

1. Деление измеряется с помощью ионизационной камеры, рабочий слой которой одновременно является образцом для измерения захвата. Благодаря высокой эффективности камеры (95%) в сильной степени подавлен фон деления в "канале захвата".

2. Слой камеры располагается под очень малым углом ($\sim 0°$) к нейтронному пучку, что существенно уменьшает фон рассеянных нейтронов в измерениях захвата.

3. Разработанная методика рассчитана для изучения малых количеств делящихся веществ (10-30 мг), что позволит проводить измерение α для ^{239}Pu и некоторых других изотопов.

ЛИТЕРАТУРА

[1] GWIN, R. et al., ORNL – 3499, 1 (1963) 15.
[2] SCHOMBERG, M.G., SOWERBY, M.G., EWANS, F.W., A new method of measuring alpha (E) for ^{239}Pu. AERE, Harwell U.K. HL 67/5474 (1967).
[3] ВАН ШИ-ДИ, ВАН ЮК-ЧАН, ДЕРМЕДЖИЕВ, Е., РЯБОВ, Ю.В.. Proc. Symp. Physics and Chemistry of Fission I 1965, p. 285.
[4] HOPKINS, J.C., DIVEN, B.C., Nucl.Sci. Eng. 12 (1962) 169.
[5] SAUSSURE, G. de, WESTON, L.W., GWIN, R., RUSSELL, J.E., HOCKENBURY, R.W., Nucl. Sci. Eng. 23 (1965) 45.
[6] КОНОНОВ, В.Н., МЕТЛЕВ, А.А., ПОЛЕТАЕВ, Е.Д., ПРОКОПЕЦ, Ю.С., ПТЭ 6 (1969) 51.
[7] РЯБОВ, Ю.В., Автореферат диссертации ОИЯИ, Дубна (1969).
[8] ВОРОНКОВ, Р.М., ПЕВЗНЕР, М.И., ФЛЕРОВ, Н.Н. и др., Атомная энергия 13 (1962) 327.
[9] BROOKS, F.D., JOLLY, J.E., SCHOMBERG, M.G., SOWERBY, M.G., AERE – M 1670 (1966).
[10] BROOKS, F.D. et al., AERE – U (1969).
[11] CZIRR, J.B., UCID – 15458 (1969).
[12] SAUSSURE, G.de et al., ORNL-TM-1804 (1967).
[13] JAMES, C.D., PATRIC, B.N., AERE – M 2065 (1969).

OBSERVATION OF AN ISOMERIC LEVEL IN ^{239}U BY MEANS OF THE ^{238}U(n, γ)^{239}U REACTION

B.W. THOMAS, J. MURRAY, E.R. RAE
UKAEA, AERE Harwell, Didcot, Berks,
United Kingdom

Abstract

OBSERVATION OF AN ISOMERIC LEVEL IN ^{239}U BY MEANS OF THE ^{238}U(n,γ)^{239}U REACTION

Low-energy-capture gamma-ray spectra (< 1 MeV) have been measured for several resonances in ^{238}U up to a neutron energy of 350 eV. The data were obtained using a 25-cm^3 Ge(Li) detector at the Harwell 45 MeV Electron Linac. Capture events were recorded as functions of gamma-ray energy and neutron time-of-flight, and by suitable analysis of the data time-of-flight spectra have been obtained for individual gamma-rays.

The strongest low-energy gamma-ray, at 134 keV, depopulates a level in ^{239}U at the same energy by an E2-transition to the ground state. The time-of-flight spectrum for this transition indicates that the 134-keV level is isomeric with a half-life of approximately 1 microsecond. This is evident from the long tails on the low-energy side of each resonance, which are not present for other regions of the gamma-ray spectrum.

The possibility of using low-energy gamma-rays as a measure of the total capture cross-section is investigated by comparing the time-of-flight spectrum for the 134-keV transition with that for a Moxon-Rae detector under the same experimental conditions.

In recent years the advent of Ge(Li) detectors has opened up the study of the radiative decay of the compound states formed in neutron resonance capture, by making possible the detailed study of the intensities of large numbers of discrete lines in the corresponding gamma-ray spectra. Because of the nature of the capture gamma-ray spectra (and of the Ge(Li) response function) these discrete lines are most easily seen and interpreted at the high and low energy ends of the spectra, the middle energy range being confused by a high density of lines and ambiguity in the detector response. Much of the earlier interest in this work has been concentrated on the relatively high energy primary transitions from the capturing states, in the fluctuations in the intensities of these transitions from resonance to resonance, and in the correlations between the strengths of different transitions, and between single transitions and the neutron widths of the resonances. These correlations, if they exist, indicate the presence of (weak) nuclear structure effects even above the neutron separation energy, while the study of the variation in mean primary transition strength with photon energy allows a comparison to be made with different models for predicting the photon strength function. More recently attention has been given to the discrete low energy transitions which occur between low lying levels in the compound nucleus. One interest in this work has been that the strengths of transitions from various low lying levels to the ground state, which reflect the strength with which these states are fed from the capture cascade, can in some cases be strongly correlated with the spin of the capturing state, thereby permitting the spins of many neutron resonances to be determined. Here we are concerned with another nuclear quantity which can, in certain special circumstances, be determined from a study of the low energy lines in neutron resonance capture, namely the lifetime of the excited state involved. This is obtained as a by-product of a neutron time of flight study of the yield of a particular gamma-ray excited in

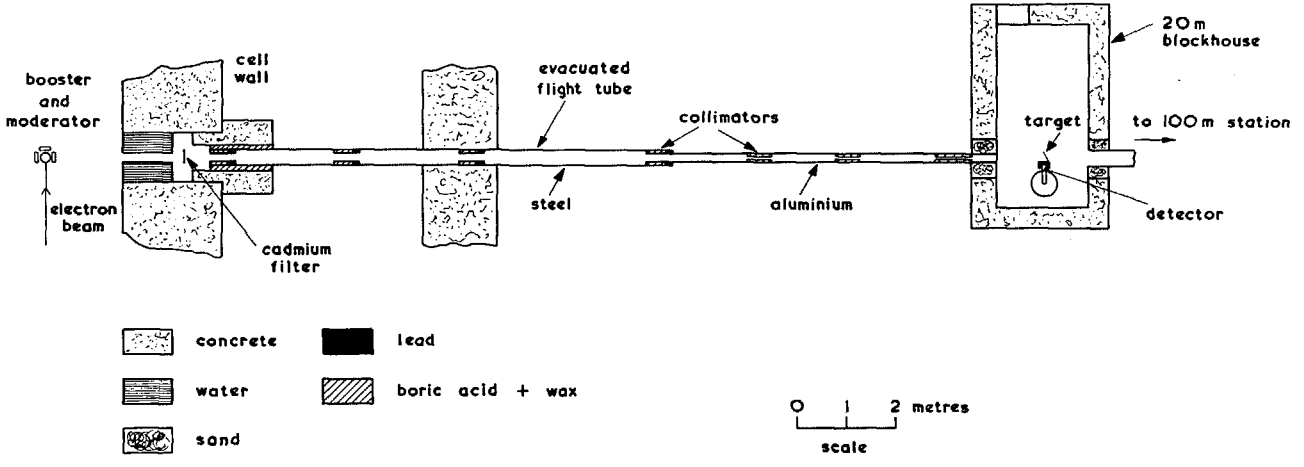

FIG. 1. 20-metre flight path.

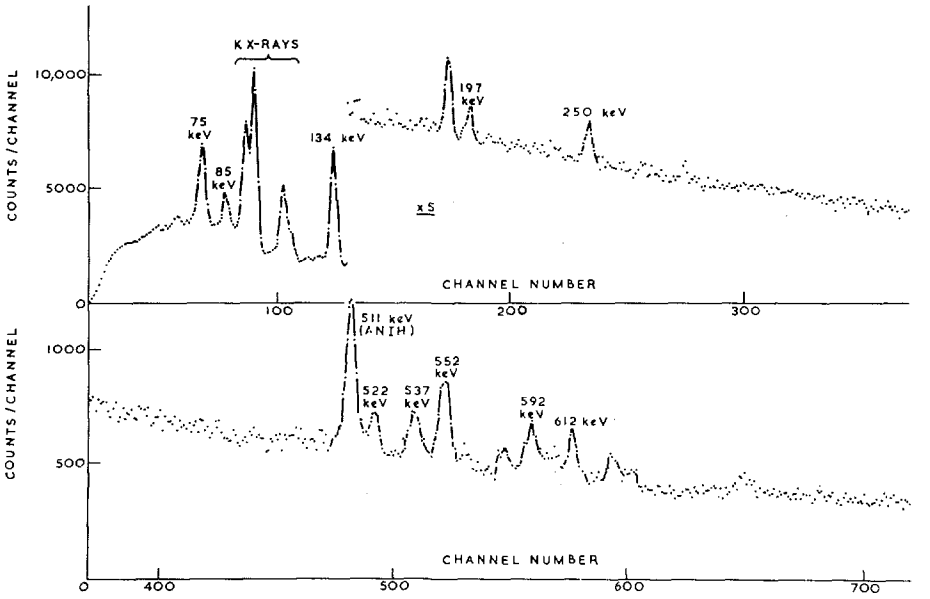

FIG.2. Low-energy-capture gamma-ray spectrum — 6.67 eV resonance $^{238}U(n,\gamma)^{239}U$.

resonance capture. If the lifetime of the initial state involved in the transition is of the order of a few microseconds, then the slow decay of the excited state shows itself as a tail on the neutron resonance shape observed in the plot of gamma-ray yield as a function of time of flight.

An example of such a relatively long lived state not previously reported has been found in the course of a study of neutron resonance capture in ^{238}U. The observations were made with a 25 cm^3 Ge(Li) detector on a 20 metre flight path of the Harwell 45 MeV Electron Linear Accelerator with its Neutron Booster target. The experimental layout is shown in Fig. 1 and the data were collected on-line using a two parameter programme on a PDP-4 computer. The gamma-ray energy range in the experiment was 70 to 900 keV and neutron energies up to 350 eV were recorded. Suitable analysis of the raw data yields complete gamma-ray spectra for individual resonances, or time of flight spectra for single transitions. The low energy gamma-ray spectra vary little in this case from resonance to resonance and are in general agreement with the data for thermal neutron capture. A typical spectrum (for the 6.67 eV resonance) is shown in Fig. 2. The time of flight yield curves for most transitions show the normal clean resonance shapes, but for one strong transition, of 134 keV, the resonance shapes show a long tail indicating that the initial state involved is isomeric with an experimental lifetime of approximately 1 microsecond. This effect is clearly seen in Fig. 3, where the shapes for the 134 keV transition of the resonances at 66 and 103 eV are compared with the corresponding resonance shapes for a section of the continuum of the gamma-ray spectrum which represents a complicated summation of the compton distributions of all higher energy gamma-rays. A detailed measurement of the low energy gamma-ray spectrum (< 1 MeV) produced in thermal neutron capture by ^{238}U has been published by Maier [1]. The strong gamma-ray at 134 keV was thought to depopulate a level in ^{239}U at the same excitation. Data from (d,p) measurements [2] and high energy capture spectra [3] confirm this assumption

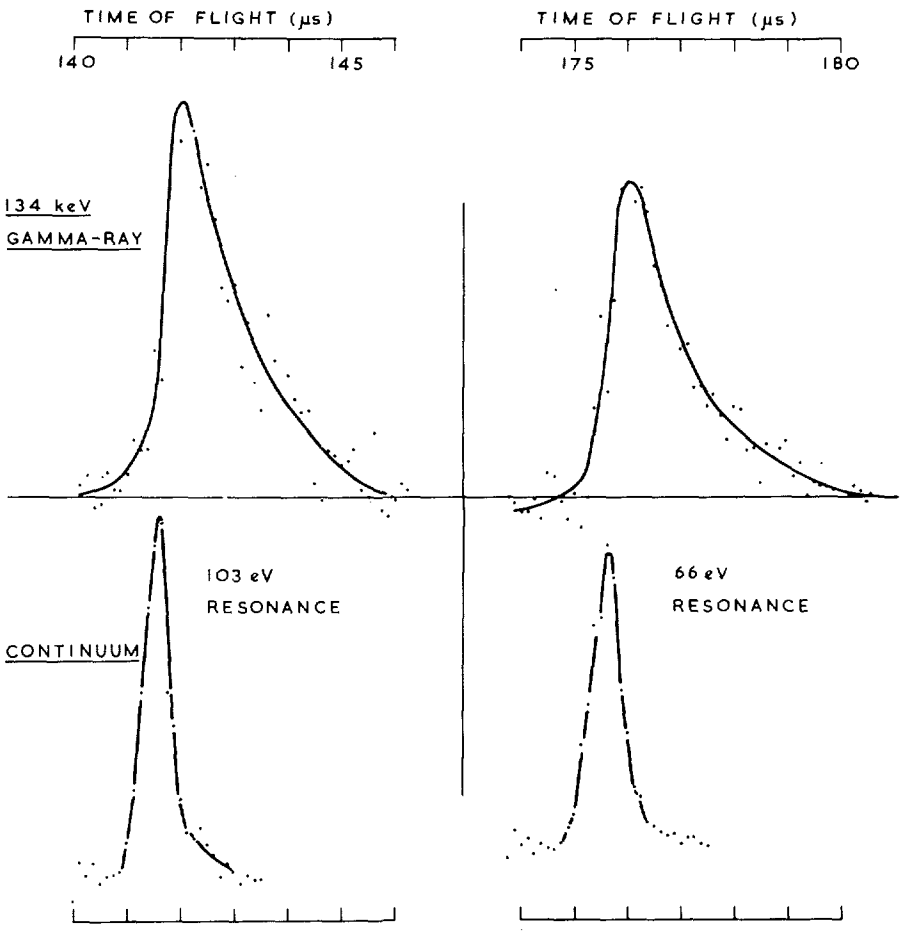

FIG.3. Neutron resonance shapes for the 134-keV capture gamma-ray produced in the reaction $^{238}U(n,\gamma)^{239}U$.

and suggest that the transition is of E2 character. If this assignment is correct, an estimate of the internal conversion coefficient for this transition yields a value of 3.5. This coefficient leads to a value for the intrinsic gamma-emission lifetime of the isomeric transition to the ground state of approximately 4.5 microseconds. This can be compared with the single particle estimate for an E2 transition of 60 nanoseconds.

REFERENCES

[1] MAIER, B. P. K., Zeit. Phys. 184 (1965) 143.
[2] SHELINE, R. K., Shelton, W. N., Udagawa, T., Jurney, E. T. and Motz, H. T., Phys. Rev. 151 (1966) 1011.
[3] PRICE, D. L., Chrien, R. E., Wasson, O. A., Bhat, M. R., Beer, M., Lone, M. A. and Graves, R., Nuc. Phys. A121, No. 3 (1968) 630.

HIGH-ENERGY γ-RAYS FOLLOWING NEUTRON CAPTURE IN ^{239}Pu AND ^{235}U*

R.E. CHRIEN, O.A. WASSON
Brookhaven National Laboratory

S. DRITSA
Brookhaven National Laboratory
and
NRC Demokritos, Athens, Greece

S. BOKHAREE, J.B. GARG
Brookhaven National Laboratory
and
State University of New York at Albany, New York,
United States of America

Abstract

HIGH-ENERGY γ-RAYS FOLLOWING NEUTRON CAPTURE IN ^{239}Pu AND ^{235}U.

The study of thermal-neutron-capture γ-ray spectra, which has proved useful in investigating the nuclear properties of many nuclei, is difficult for fissionable nuclides because of the large fission γ-ray background. The authors have attempted to observe primary high-energy γ-rays, representing direct transitions to low-lying states of the residual nucleus, in resonant neutron capture, using the BNL fast-chopper time-of-flight facility.

Capture γ-rays may be distinguished from fission γ-rays on the basis of four criteria: a) lack of Doppler broadening, b) wide fluctuations in transition strength, c) correspondence to known states in the residual nucleus, and d) correlation with values for Γ_γ/Γ_F for different resonances.

In ^{235}U such transitions are too weak to be easily observed; however, strong capture γ-rays are observed in ^{239}Pu resonances. Two of these transitions populate known states in ^{240}Pu at 597.4 keV (1^-) and at 42.8 keV (2^+), giving a neutron binding energy of 6533.7 ± 1.5 keV.

Other γ-rays are seen which correspond to the population of levels heretofore unobserved in ^{240}Pu. These levels probably have spin 0^-, 1^-, or 2^- and are located at 858.1, 936.4, 958.5, 1241.4, and 1438.3 keV. There is weaker evidence for several additional levels.

The observation of the M-1 transition permits the assignment of the spins of two resonances in ^{239}Pu. The 0.3-eV resonance and the 41.7 eV resonance are both assigned spin 1. These are in agreement with recent spin assignments derived from neutron-multiplicity measurements and scattering measurements; the former is in disagreement, however, with multilevel cross-section fitting. A comparison is made between the delayed fission γ-ray spectra of ^{235}U and ^{239}Pu, which appear as backgrounds in the time-of-flight studies.

1. INTRODUCTION

The methods of neutron-capture γ-ray spectroscopy have been successfully applied to a large variety of nuclei throughout the periodic table and have been useful in determining the characteristics of the low-lying levels of the residual nucleus, and of the highly excited states formed by neutron capture – the neutron resonances.

* This work was supported by the US Atomic Energy Commission.

These methods are, however, affected by certain difficulties when they are applied to the fissile nuclides, due to the background of fission γ-rays and neutrons. These difficulties are especially severe when studying thermal-neutron capture. In fact, no radiative transitions connecting capturing states and low-lying levels of ^{240}Pu and ^{236}U have ever been observed in thermal-capture work. In resonance capture, however, the situation is somewhat ameliorated by the advantage of being able to examine a variety of resonances, with various values of the ratio of capture width to fission width. It was with this advantage in mind that the authors initiated an attempt to search for high-energy radiative transitions after neutron capture in ^{239}Pu and ^{235}U.

2. DESCRIPTION OF EXPERIMENT

Large samples (84 grams of 96% ^{239}Pu and 150 grams of 93% ^{235}U) were examined at the 22- and 48-metre flight stations of the BNL fast chopper at the High Flux Beam Reactor [1]. With rotor speeds of 10 000 RPM and 2500 RPM (and a resolution of 300 ns/m) the resonance structure from thermal to ~50 eV could be observed, and most of the resonances adequately separated.

To establish absolute radiative partial widths for the plutonium resonances, it was necessary to prepare and run in a separate experiment a composite sample of plutonium and platinum. The 7921-keV transition found in the 11.9-eV Pt-resonance was used as a standard for line intensities.

3. RESULTS

The time-of-flight spectra, over selected portions of the incident-neutron-energy range, are shown in Figs 1 and 2, for ^{235}U and ^{239}Pu, respectively. The former was recorded at the 48-*m* station, for γ-rays above 2.5 MeV in energy deposited in a 35-cm^3 Ge(Li) detector with a resolution of 8.0 keV at 6 MeV. The plutonium spectra were recorded in a similar, but not identical detector.

From these spectra it can easily be inferred that: a) the γ-ray spectra from Pu-resonances are harder, or richer in high-energy components than for ^{235}U resonances, and b) there is a considerable background of delayed fission γ-rays appearing under the resonances. Within the time scale of this time-of-flight experiment, the delayed fission γ-rays constitute an essentially time-independent background.

In addition, there is some background due to fission neutrons which subsequently capture in materials near the detector, which was shielded from the target by approximately 1 in. of polythene, and 1/4 in. of lead. The presence of this background is inferred from the appearance of strong γ-rays from capture in ^{56}Fe.

The high background in these experiments was sufficient to obscure the relatively weak capture γ-rays in ^{235}U. No attempt was made to observe secondary low-energy γ-rays from ^{236}U, as reported by other groups, such as Weigman et al. [2], at Geel. Considerable structure is noticeable in the spectrum of delayed γ-rays, as observed between

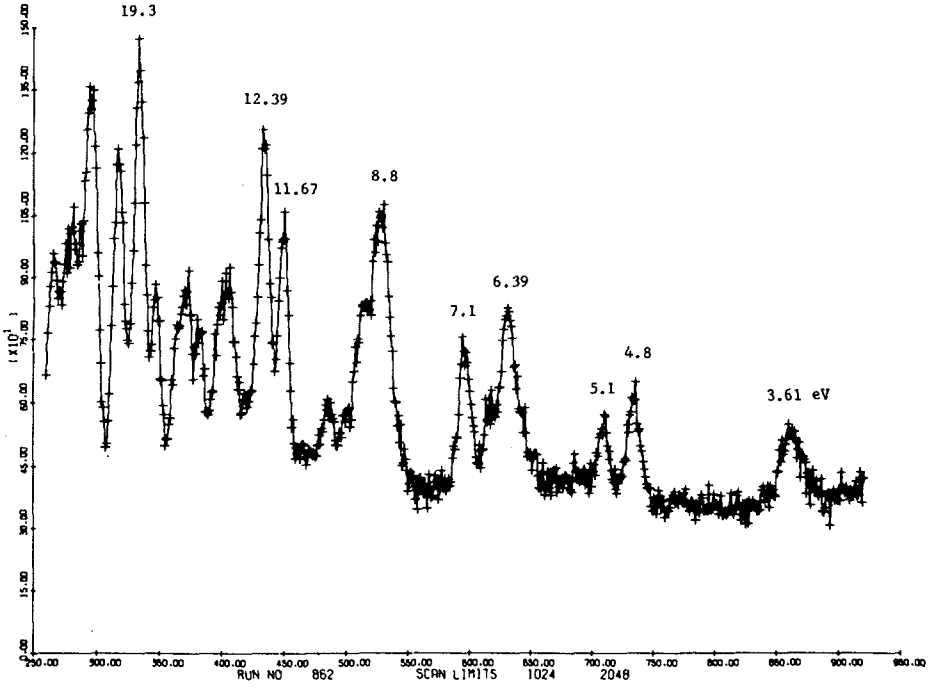

FIG. 1. A portion of the time-of-flight spectrum for ^{235}U. Events depositing more than ~2.5 MeV in the detector are recorded.

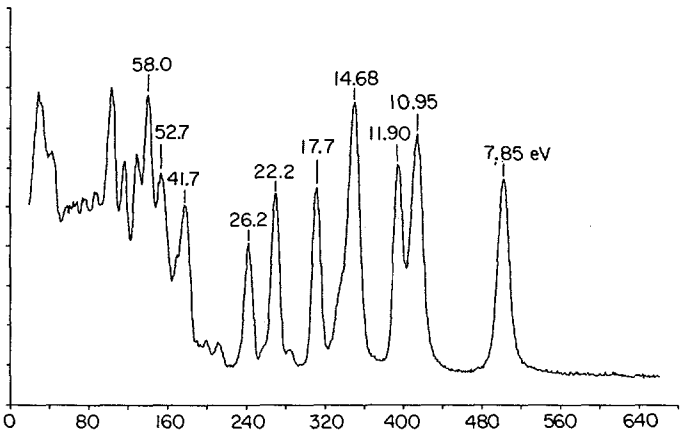

FIG. 2. A portion of the time-of-flight spectrum for ^{239}Pu.

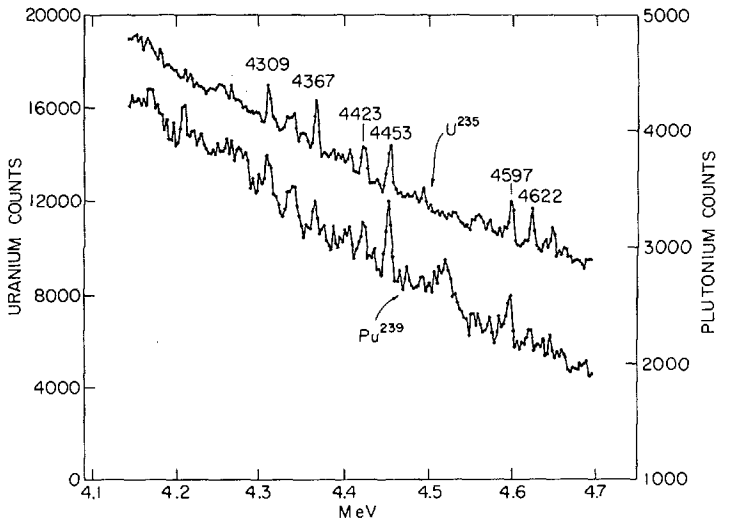

FIG. 3. Portions of the spectra of delayed γ-rays from ^{235}U and ^{239}Pu: 4.1 - 4.7 MeV. The energies shown are for assumed two-escape peaks.

resonances, in both ^{235}U and ^{239}Pu. Spectra were recorded, for the off-resonance time regions, from 2.6 to 7.0 MeV for both samples. Examples of the comparison between these spectra are shown in Figs 3, 4, and 5 for the energy regions from 4.1 to 5.8 MeV.

Some of these lines may be due to gammas following the moderation and capture of fission neutrons, but most are undoubtedly delayed γ-rays following beta-decay of the fission fragments.

The energies of the principal lines which are common to both spectra are indicated in the figures, and are believed known to a precision of ± 1.5 keV, having been calibrated against the Th C'' and ^{56}Fe lines in the spectrum.

While many of the stronger lines appear in both spectra, some differences between the spectra are evident. These differences suggest that it may be useful to carry out non-destructive assaying methods using delayed fission γ-rays for uranium and plutonium.

The relatively high delayed fission γ-ray background coupled with the relatively poor time-of-flight resolution available with the chopper made the observation of high-energy γ-rays impossible for ^{235}U. In ^{239}Pu, the situation is strikingly different. Here, strong rays in the neutron resonances are observed above the fission background. The identification of these γ-rays as capture γ-rays proceeds from several arguments:

1) Several of the γ-rays have energies corresponding to transitions to known states of ^{240}Pu.
2) These lines are narrow and exhibit no Doppler broadening, which would be expected to smear the energies of prompt fission γ-rays.
3) The transitions do not appear between resonances, hence they are not delayed γ-rays.
4) The transitions fluctuate widely in strength among the resonances, and the strengths are not correlated with the fission widths. Hence, they cannot be fission-induced events.

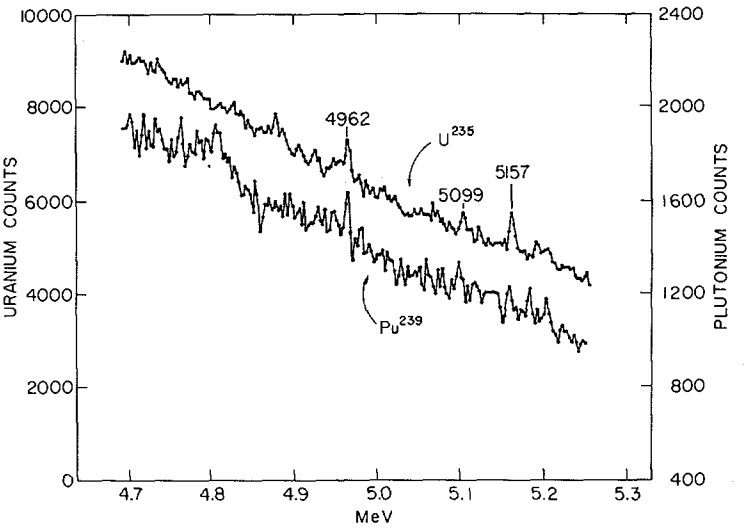

FIG. 4. The delayed γ-ray spectra from 4.7 to 5.2 MeV.

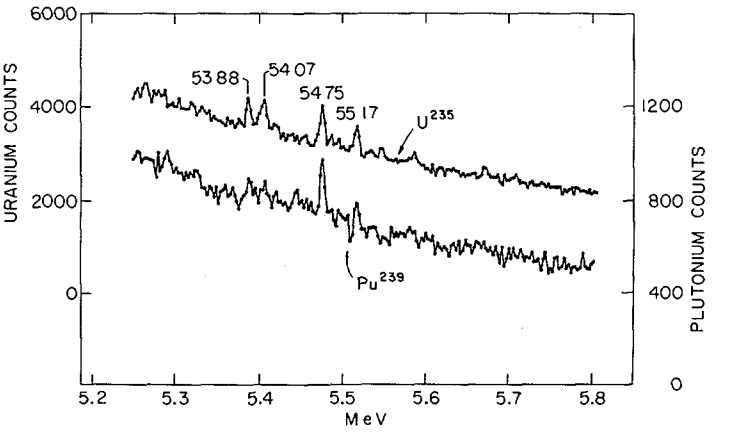

FIG. 5. The delayed γ-ray spectra from 5.2 to 5.8 MeV.

Some of the low-lying levels in ^{240}Pu are known from the decay of the 7.3 min and 63 min isomers of ^{240}Np, and from the alpha decays of ^{244}Cm [3]. Of particular interest are the ground-state band, with the 2^+ level at 42.80 keV, and the 1^- level at 597.4. The energies are those determined from recent work of Zender, Bemis, and Schmorak at Oak Ridge [4].

The spectrum of the 7.8-eV resonance is dominated by a strong line, as shown in Fig. 6, which populates the lowest 1^--level at 597.4, with an energy of 5936.3 ± 1.5 keV. This leads to a neutron binding energy of 6533.7 ± 1.5 keV. The energy calibration is based on background lines from ^{56}Fe capture in the spectrum, whose energies were supplied by R. C. Greenwood [5]. These energies were also indirectly compared, via the Fe-lines, with nitrogen capture lines [6].

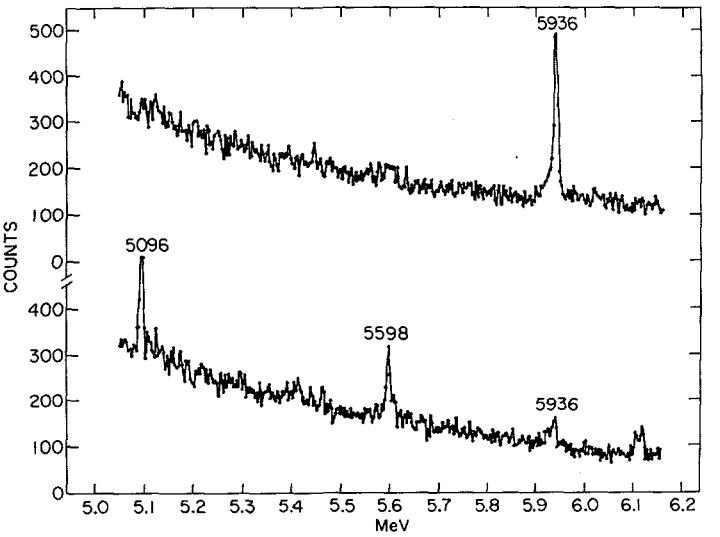

FIG. 6. Capture γ-ray spectra from the 7.8-eV (above) and 11.9-eV (below) resonances of ^{239}Pu.

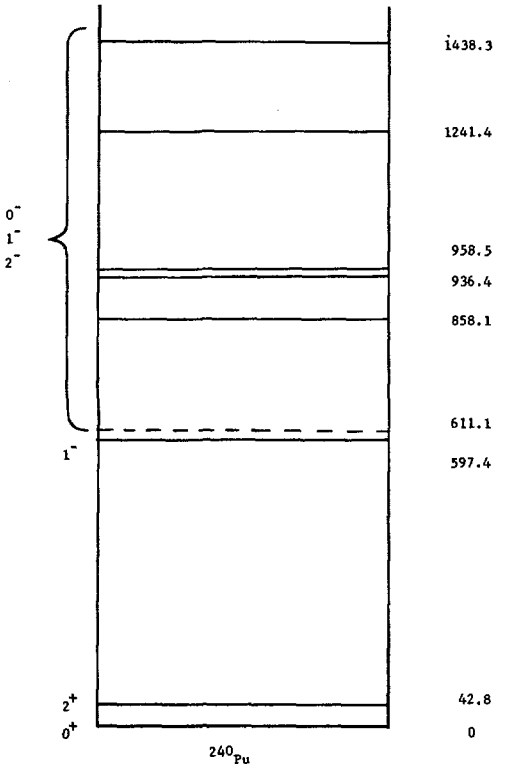

FIG. 7. A level diagram of ^{240}Pu, showing states populated by capture γ-rays in this experiment. Electric-dipole transitions would imply population of states with spin and parity 0^-, 1^-, 2^-.

Gamma rays leading to previously unreported states at higher excitations in ^{240}Pu are seen in other resonances. For example, Fig. 6 also shows lines observed in the 11.9-eV resonance, at 5598 and 5096, in addition to the 5936-keV line cited above.

Figure 7 shows the level diagram of ^{240}Pu obtained from transitions observed in this experiment.

In the 0.3 eV and in the 41.8-eV resonance, weak lines are observed leading to the 42.8-keV 2^+ state. These lines must be M-1 in character and the energy, 6490.9 keV, is consistent with the quoted binding energy.

Several interesting consequences arise from the observation of the transitions to the 42.8-keV 2^+-state. If we assume that these are magnetic dipole γ-rays, then spin assignments of 1^+ can be made for the 41.8- and 0.3-eV resonances in ^{239}Pu. The former is in agreement with the scattering experiments of Sauter and Bowman [7], and Asghar [8], and with the assignment of Weinstein and Block [9] based on neutron multiplicity measurements. The 0.3-eV resonance has been assigned 0^+ in BNL-325, based on multilevel fitting by Vogt [10]. This evidence is contradicted by the multiplicity measurement of Weinstein and Block, and by the results of the present experiment, which definitely require a 1^+-assignment for this level.

4. THE DETERMINATION OF PARTIAL RADIATIVE WIDTHS

In non-fissile targets, radiative intensities are conventionally determined by forming the ratio of the events recorded for a specific transition to the total of all events recorded by the detector above an arbitrary discriminator limit. The total number of recorded events in a resonance, N_γ, can be written as follows:

$$N_\gamma = (A_T T)\, \phi(E_n) \int_{\Delta E_n} (1 - e^{-n\sigma_T T})\, (\sigma_\gamma / \sigma_T)\, dE_n \int_{E_d}^{E_B} \nu_T (E_\gamma)\, \epsilon(\Omega, E_\gamma)\, dE_\gamma$$

where $(A_T T)$ is the product of target area and elapsed time, $\phi(E_n)$ is the incident neutron flux, $\int_{\Delta E_n} (1 - e^{-n\sigma_T T})\, (\sigma_\gamma / \sigma_T)\, dE_n = A_\gamma$ is the radiative capture area, and $\int_{E_d}^{E_B} \nu_T \epsilon(\Omega, E_\gamma)\, dE_\gamma$ represents the integrated detector response for an efficiency $\epsilon(\Omega, E_\gamma)$ from the discrimination level E_d, to the binding energy E_B, for the total spectrum ν_T ($\int \nu_T dE = \nu$, the photon multiplicity).

An effective efficiency may be defined for the γ-ray detector:

$$\epsilon_{eff}(\gamma) = \int_{E_d}^{E_B} \nu_T (E_\gamma)\, \epsilon(\Omega, E_\gamma)\, dE_\gamma$$

and we can write

$$N_\gamma = (A_T T)\,\phi\,(E_n)\,A_\gamma\,\epsilon_{eff}\,(\gamma)$$

The events for a single transition, n_γ, are related to the absolute photon intensity I_γ, as follows:

$$n_\gamma = (A_T T)\,A_\gamma\,\epsilon\,(\Omega,\,E_\gamma)\,I_\gamma$$

The peak-to-total area is thus proportional to the absolute intensity,

$$n_\gamma/N_\gamma = \frac{\epsilon\,(\Omega,\,E_\gamma)}{\epsilon_{eff}\,(\gamma)}\,I$$

and it is usually assumed that the effective efficiency ϵ_{eff} does not vary appreciably among the resonances.

For fissile nuclei this expression must be modified by including a contribution due to fission γ-rays:

$$N_\gamma = (A_T T)\,\phi\left\{\epsilon_{eff}\,(\gamma)\,A_\gamma + \epsilon_{eff}\,(F)\,A_F\right\}$$

where A_F and $\epsilon_{eff}\,(F)$ are defined in analogous fashion. In the present experiment, we evaluate $\epsilon_{eff}\,(F)/\epsilon_{eff}\,(\gamma)$ by calculating values of N_γ, using parameters obtained from Ref. [11], and comparing these to the experimentally determined N_γ. A least-squares adjustment yields the best value for $\epsilon_{eff}\,(F)/\epsilon_{eff}\,(\gamma)$, 0.16. This ratio is then used to correct the observed values of n_γ/N_γ for the fission component.

To obtain an absolute intensity, the method outlined by Carpenter [12] is used. The 5936-keV transition in the 7.8-eV ^{239}Pu-resonance is compared with the 7921-keV ground-state transition in the 11.9-eV resonance of ^{195}Pt. A composite of thin samples (n = 0.000705 and 0.000851 atoms/barn of plutonium and platinium, respectively) was fabricated and placed in the beam. From the known intensity, I = 0.048 photons/capture, for the platinum line, an intensity of 0.018 photons/capture for the 5936-keV transition was obtained. A correction for the energy variation of the detector efficiency $\epsilon\,(\Omega,\,E_\gamma)$ was obtained by recording the intensities of nitrogen-capture γ-rays from a melamine target and comparing these to previously

TABLE I. PARTIAL RADIATIVE WIDTHS FOR ^{239}Pu (n, γ) ^{240}Pu (10^{-6} eV)

E_γ (keV)	0.3	7.85	10.95	11.9	14.68	17.7	22.2	41.7	52.7	58
6491.2 ± 1.5	65							66		
5936.3	80	726		120	28			48	126	93
5674.6	96							76		
5597.3		227		286	25	169	72	76		
5575.2	295	64	156		38		136		103	99
5292.3					78			110		
5095.4				344	44			160	96	

measured intensities [6]. In this way, the quantity $\epsilon(\Omega, E_\gamma)/\epsilon_{eff}(\gamma)$ was evaluated, and the absolute intensities for the plutonium lines were obtained.

The widths of Table I are obtained from the γ-ray intensities under the assumption of a constant total radiation width of 0.04 eV for ^{239}Pu, the recommended value from BNL 325.

5. THE ^{240}Pu RESONANCE

The γ-ray spectrum following neutron capture in the 1.056-eV resonance of ^{240}Pu was also observed in this experiment. This resonance appears as a sizable impurity in the plutonium run. Relative intensities for transitions definitely ascribable to this resonance are given in Table II. The binding energy of the last neutron in ^{241}Pu is expected to be 5.412 MeV, from the tables of Mattauch [13]. Since electric dipole transitions proceed only to 1^--final states in this case, none of the low-lying, positive-parity states of ^{241}Pu is populated.

TABLE II. RELATIVE INTENSITIES FOR THE PRINCIPAL γ-RAYS FROM THE 1.056-eV RESONANCE OF ^{240}Pu

E_γ (keV)	Intensity
5170.4	110 ± 22
5076.5	140
4298.7	259
4279.8	208
4273.8	230
3942.6	601
3882.3	641
3874.2	368 ± 56

6. SUMMARY OF RESULTS

Gamma rays following neutron capture in ^{235}U and ^{239}Pu have been examined. In ^{235}U, the radiative transitions are weak and not readily observable above the fission γ-ray background. There is, however, considerable structure in the spectrum of delayed γ-rays following fission. This structure is seen to be similar to the structure observed for a target of ^{239}Pu. In the latter case, however, the radiative transitions are stronger and are seen to dominate the spectra of several resonances. Several transitions to known states of ^{240}Pu allow a precise determination of the binding energy of the last neutron of ^{240}Pu and the assignment of spins in two ^{239}Pu resonances. The partial widths of the stronger transitions were measured by correcting the detector for the fission γ-ray component and standardizing against a known transition in ^{195}Pt. Several γ-ray lines in ^{241}Pu, resulting from capture in the 1.056-eV ^{240}Pu impurity resonance, were also observed.

REFERENCES

[1] CHRIEN, R.E., REICH, M., Nucl. Instrum. Methods 53 (1967) 93.
[2] WEIGMANN, H., WINTER, J., in Neutron Capture Gamma-Ray Spectroscopy (Proc. Symp. Vienna, 1969), IAEA, Vienna (1969) 687.
[3] LEDERER, C.M., HOLLANDER, J.M., PERLMAN, I., Table of Isotopes (1967) 434.
[4] ZENDER, M.J., BEMIS, C.E., Jr., SCHMORAK, M.R., in Radioactivity in Nuclear Spectroscopy (Int. Conf. Nashville, Tennessee, August 1969).
[5] GREENWOOD, R.C., private communication.
[6] JONSSON, L., HARDELL, R., Neutron Capture Gamma-Ray Spectroscopy (Proc. Symp. Vienna, 1969), IAEA, Vienna (1969) 199.
[7] SAUTER, G.D., BOWMAN, C.D., Phys. Rev. Lett. 15 (1965) 761.
[8] ASGHAR, M., Nucl. Physics, A98 (1967) 33.
[9] WEINSTEIN, S., BLOCK, R.C., Phys. Rev. Lett. 22 (1969) 195.
[10] VOGT, E., Phys. Rev. 118 (1960) 724.
[11] Neutron Cross Sections, BNL 325, 2nd Ed., Suppl. No.2 (Feb.1965).
[12] CARPENTER, R.T., ANL-6589, Aug.1962.
[13] MATTAUCH, J.H.E., THIELE, W., WAPSTRA, A.H., Nucl.Phys. 67 (1965) 32.

DISCUSSION

M. S. MOORE: Mass distributions also provide a very reliable method of assigning spins in ^{239}Pu resonances. If one compares the results obtained by Regier at the MTR for the 0.3 eV resonance with the work of Cowan et al. at Los Alamos for the higher energy resonances, one can infer that the spin of the 0.3 eV resonance is 1^+.

G. J. KIROUAC: Your assignment of spin and parity depend on the assumed nature of the transition. I wonder how certain you are of the nature of the transition.

O. A. WASSON: The final-state spin and parity assignment of 2^+ for the 42.8 keV state was based on previous decay experiments. This eliminates the possibility that the X-ray transition is E1. Since it is unlikely that the transition is of E2 multipolarity, we assign it to be M1 and, thus, require the 1^+ assignment for the resonance spins.

TOTAL NEUTRON CROSS-SECTION OF ^{233}U FROM 0.7 eV TO 320 eV

W. KOLAR, G. CARRARO, G. NASTRI
Central Bureau for Nuclear Measurements,
EURATOM, Geel, Belgium

Presented by J.P. Theobald

Abstract

TOTAL NEUTRON CROSS-SECTION OF ^{233}U FROM 0.7 eV TO 320 eV.

The total neutron cross-section of ^{233}U has been measured in the energy range of 0.7-320 eV. The experiments were carried out at the 60-MeV electron linear accelerator of the CBNM. Two metal samples of ^{233}U with a thickness of 1.78 gr/cm^2 were available. The nominal resolution of the different measurements varied between about 50 ns/m at 0.7 eV and about 1 ns/m at 320 eV.

Up to 93 eV, the results have been analysed using the multilevel fit program CODILLI of D.B. Adler and F.T. Adler. In addition, from 2.5 eV to 53 eV a single-level analysis with the shape program of S.E. Atta and J.A. Harvey has been performed.

From the single-level resonance parameters up to 30 eV a mean level spacing $< D > = 0.61 = 0.07$ eV was obtained. Assuming that all resonances in that energy range are due to s-wave neutrons the strength function is $S_0 = (2.25 \pm 0.55) \times 10^{-4}$.

1. INTRODUCTION

Up to now three measurements [1], [2], [3] of the total neutron cross section of ^{233}U in the resonance region have been published. The first one was done with a crystal spectrometer, while the two others were performed at a reactor using a fast chopper to pulse the neutron beam and BF_3 counters as neutron detectors. The observed cross sections agree for energies below 10 eV but show discrepancies for higher neutron energies (see BNL 325 second edition). In the course of the measurement program at the CBNM on fissile isotopes the low energy fission cross section [4] and the total neutron cross section of ^{233}U have been remeasured.

The evaluation of the resonance parameters has been done using the multilevel fit program CODILLI as developed by D.B. Adler and F.T. Adler [5] and the single level shape fit program of S.E. Atta and J.A. Harvey [6]. In the latter case only an "adjustment fit" (see chapter 4) to the observed cross section data was possible.

The energy range analysed with the multilevel fit program extends from 0.9 eV to 93 eV, while for the single level evaluation the energy range is limited from 2.5 eV to 53 eV.

2. SAMPLES

Two metal foils (dimensions 76 mm x 38 mm) of ^{233}U with a total weight of 51.7 g have been available. The foils were canned in a manganese free aluminium can. The total thickness of the aluminium was 0.6 mm.

TABLE I. EXPERIMENTAL CONDITIONS

Neutron energy range	1st Experiment	2nd Experiment	3rd Experiment
	0.7 eV - 62 eV	15 eV - 97 eV	64 eV - 320 eV
neutron burst width	1 μsec	0.050 μsec	0.070 μsec
repetition rate	40 pps	400 pps	300 pps
analyser channel width	ch. Nr. 1-2560: .640 μsec 2561-3072: 2.56 " 3073-4096: 5.12 "	ch. Nr. 1-4096: .320 μsec	ch. Nr. 1-2048: 0.080 μsec 2049-4096: 0.160 "
nominal resolution	1.2 nsec/m - 50 nsec/m	~3 nsec/m	1 nsec/m - 1.7 nsec/m
statistical error "sample-IN"	0.6% - 1.2%	0.8% - 1.5%	0.6% - 0.75%
permanent background filter	Co	Co	Bi
background filter in background run	Co, Mo, W, Au, In	Mo, W	Mn, Co
flight path length	99.89 m	99.89 m	98.99 m

The isotopic composition of the samples as determined by L. Collins (KAPL) is:

^{232}U: < 0.6 ppm

^{233}U: $99.76\% \pm 0.01\%$

^{234}U: $0.022\% \pm 0.001\%$

^{236}U: ≤ 0.1 ppm

^{238}U: $0.21\% \pm 0.01\%$.

A spectrochemical analysis of the metal foils is published in reference [3].

3. EXPERIMENTAL TECHNIQUE

The experiments were performed at the 60 MeV linear accelerator of the CBNM. The fast neutrons, which are produced in the mercury cooled uranium target are slowed down in a 2.4 cm thick polyethylene slab (dimensions 20 cm x 20 cm) which is mounted close to the target.

The neutron detector was placed at a distance of about 100 m. For the measurements between 0.7 and 97 eV (see Table I) a 1 cm thick ^{10}B-loaded liquid scintillator (NE 321A) was chosen. The liquid was filled into a cylindric container (diameter 11 cm), the front and back side of which consisted of 4 mm thick glass. The detector assembly was mounted on a XP 1040 photomultiplier, equipped with a pulse shape discriminator against the detection of gamma radiation. The measurement run 65 - 320 eV was performed with the conventional B^{10}-NaI neutron detector. The ^{10}B slab consisted of 1 cm thick sintered pieces of $^{10}B_4C$ (overall dimensions 10.5 cm x 10.5 cm x 1 cm) and was viewed laterally by 4 NaI crystals (4 inch diameter, 3 inch height) mounted on XP 1040 photomultipliers. Only those pulses, which passed a fast threshold and fell into an amplitude window around the 480 keV peak of the $^{10}B(n,\alpha\gamma)Li^7$ reaction were accepted for analysis.

The evacuated neutron flight path tube (inclination 9° with respect to the normal to the moderator surface) which connected the target bunker with the detector station was interrupted at about 50 m where the 2-row 4-position sample changer and two collimators were placed. The time sequence of the different sample changer positions was controlled by preset monitor counts from a BF_3 counter, also installed in the 50 m station. The monitor was shielded against neutrons scattered by the samples.

Neutron flight times were sorted in a 4096 channel time analyser. After a monitor scaler had reached the preset numbers of counts for the different sample positions, the acquisition of data stopped. The analyser data were transferred via an analyser-computer interface system [7], [8] to an IBM 1800 computer where they, provided several conditions are fulfilled, are added to the already collected data and stored on disk. In some measurements a conditioner [9] has been used. With this conditioner system it is possible to subdivide the analyser channels into groups with different channel widths. This technique allows, that a much greater energy range can be measured at the same time.

The background was determined by the "black resonance" method. A suited background sample was placed permanently in the neutron beam. Additional background samples to determine the shape of the background

are inserted in the neutron beam in a third run which followed each "sample-in", "sample-out" sequence.

The influence of the aluminium can was corrected by using and equivalent amount of aluminium in the "sample-out" run. The reaction rate due to overlap was always kept below 1 per cent of the useful neutrons.

4. MEASUREMENTS AND ANALYSIS OF THE RESULTS

In total three measurements have been performed. Table I shows the main characteristics of the different runs. The raw data reduction and the calculation of the observed total neutron cross section is described elsewhere [10].

Two different computer programs, the multilevel fit program CODILLI [5] and the single level shape fit program of Atta and Harvey [6] have been used to analyse the resonance parameters.
In the program CODILLI the total neutron cross section is given by the expression

$$E^{1/2}\sigma(T) = \sum_i \frac{G_i^{(T)}\cdot\nu_i + H_i^{(T)}(\mu_i - E)}{(\mu_i - E)^2 + \nu_i^2} + \sigma_{pot}\cdot E^{1/2} \qquad (1)$$

where μ_i, ν_i, $G_i^{(T)}$ and $H_i^{(T)}$ are the resonance parameters of the i-th resonance. The results of the evaluation for neutron energies between 0.9 eV and 93 eV are shown in Table II, the corresponding plots of the fits obtained with these parameters are given in Fig. 1a-1g. For the resonances at 1.78 eV and 2.29 eV the observed peak cross sections are not meaningful, because the ^{233}U samples were too thick.

The calculations have been performed under the assumption that the Doppler broadening kernel and the resolution kernel are gaussians. The listed set of resonance parameters is not unique in that sense that also other sets might yield fits of the same quality as the presented one. Because of this ambiguity it is not meaningful to assign standard deviations to the resonance parameters.

The agreement of the parameters μ and ν of this work with those of de Saussure [12] and Cao et al. [4] is in general good. Discrepancies appear, when due to overlapping resonances the shapes of the single resonances are lost. In these cases it was tried to fit the experimental data with the smallest number of resonances.

The expression for the total neutron cross section in the single level program is

$$\sigma(T) = 4\pi r^2 + \frac{A}{E}\cdot\sum_i \frac{\Gamma_i (fg\Gamma_n^o)_i}{(E_i-E)^2+(\Gamma_{i/2})^2} - B\sum_i \frac{(fg\Gamma_n^o)_i (E_i - E)}{(E_i-E)^2+(\Gamma_{i/2})^2} \qquad (2)$$

The first term of the sum represents the potential scattering. For the calculations a potential scattering radius r = 9.6 fm was assumed. This value results from an extrapolation of compiled data [13]. The second term describes the resonance reactions and the third the interference between

resonance and potential scattering. Due to the mathematical structure of the program, which demands at the same time the iteration of the resonance energy E_i, the total width Γ_i and the reduced neutron width $(fg\Gamma_n^o)_i$ and due to the small resonance spacing of the ^{233}U cross section, it was not possible to apply the least square fit iteration technique. The resonance parameters have been determined so that the visual inspection of the plots gave the best agreement between the theoretical fit and the observed cross section data.

TABLE II. MULTILEVEL RESONANCE PARAMETERS OF ^{233}U

μ (eV)	ν (eV)	$G^{(T)}$(barn·eV$^{3/2}$)	$H^{(T)}$(barn·eV$^{3/2}$)
1.56	0.324	101.40	41.19
1.78	0.110	172.13	-24.03
2.30	0.042	92.01	12.19
3.62	0.425	62.90	36.03
3.65	0.065	24.58	5.93
4.65	0.654	168.00	-55.86
5.80	0.194	28.46	-30.36
6.83	0.099	239.73	37.76
7.51	0.250	29.01	2.36
8.72	0.595	91.55	-8.73
9.15	0.141	10.76	-25.01
10.39	0.159	336.20	-7.16
11.39	0.226	42.14	19.75
12.00	0.360	33.56	2.96
12.83	0.168	291.37	37.90
13.53	0.159	52.35	29.96
13.69	0.132	53.27	-53.10
15.36	0.111	160.67	-42.70
16.29	0.220	143.00	50.06
16.57	0.103	112.82	-18.33
18.02	0.106	50.38	2.54
18.59	0.190	66.28	34.31
18.96	0.148	279.84	-67.45
20.65	0.207	144.41	4.02
21.94	0.123	193.27	70.25
22.35	0.189	512.63	-63.09
22.96	0.459	152.63	30.53
23.71	0.336	106.25	-76.46
25.29	0.193	117.03	-30.58
26.18	0.224	10.41	16.50
26.69	0.220	77.74	13.87
28.46	0.145	15.50	33.09
29.23	0.308	283.15	158.64
29.55	0.153	33.42	-52.27
30.90	0.160	68.85	93.89
31.20	0.385	154.88	-114.47
32.11	0.135	133.79	26.58
33.20	0.450	125.58	23.53
34.00	0.500	171.15	39.77
34.55	0.320	165.45	-16.94
35.40	0.800	220.64	-91.28
36.65	0.076	97.62	1.07
37.55	0.225	89.19	-1.89
39.20	0.482	67.25	-73.54
40.36	0.897	201.77	26.67
41.16	0.064	28.17	4.97
42.76	0.117	89.25	16.02

TABLE II. (cont.)

μ (eV)	ν (eV)	$G^{(T)}_{(barn \cdot eV^{3/2})}$	$H^{(T)}_{(barn \cdot eV^{3/2})}$
43.61	0.175	54.31	3.46
44.46	0.467	54.50	-26.89
46.19	0.098	47.47	-8.82
47.43	0.258	96.72	26.24
48.83	0.100	225.59	4.39
49.49	0.269	40.51	43.85
50.40	0.835	197.63	-82.75
52.12	0.155	10.41	-5.71
53.08	0.399	183.14	-127.99
53.95	0.180	69.83	-91.54
54.81	0.068	78.03	-17.38
56.06	0.260	164.26	47.80
56.42	0.218	152.09	-87.41
57.60	0.390	243.34	5.57
58.63	0.181	97.12	27.61
61.47	0.275	200.82	32.45
62.66	0.061	138.11	-14.05
64.10	0.200	91.02	7.81
65.50	0.100	110.84	-26.28
65.27	0.150	49.49	12.12
66.44	1.27	205.35	-153.19
68.06	0.141	22.80	-11.95
69.21	0.362	114.00	-52.16
70.39	0.287	155.13	47.34
71.95	0.343	53.45	-28.63
73.53	0.107	200.92	-49.11
74.15	0.186	271.65	-24.13
75.64	0.197	303.13	65.25
78.35	0.271	163.97	7.86
79.97	0.280	184.39	70.10
82.69	1.30	333.11	22.29
82.98	0.073	233.22	87.58
85.38	0.485	136.92	-13.57
87.35	0.084	28.01	1.08
88.99	0.164	148.99	-23.05
90.71	0.125	639.87	12.52
93.04	0.415	159.53	73.27
93.96	0.121	166.87	9.02

Table III lists the results for neutron energies from 2.5 eV to 53 eV. The corresponding plots are shown in Fig. 2a-2d . Also in this case it was assumed that the Doppler broadening and the resolution function can be represented by gaussian distributions. Because of the ambiguity of the resonance parameter, it is as in the multilevel analysis not meaningful to calculate standard deviations.

5. STATISTICAL PROPERTIES

The resonance parameter of the single level analysis can be used to determine the statistical properties of the nucleus. Fig. 3 shows the cumulative number of levels. Up to 30 eV the observed level density is nearly constant. For this energy range comprising 46 levels , a mean level spacing of

$$\langle D \rangle = (0.61 \pm 0.07)\ eV$$

was calculated [14] . The error has been determined using the formula $\sigma^2 = 0.54 \cdot \frac{\langle D \rangle^2}{n}$, where n is the number of resonances.

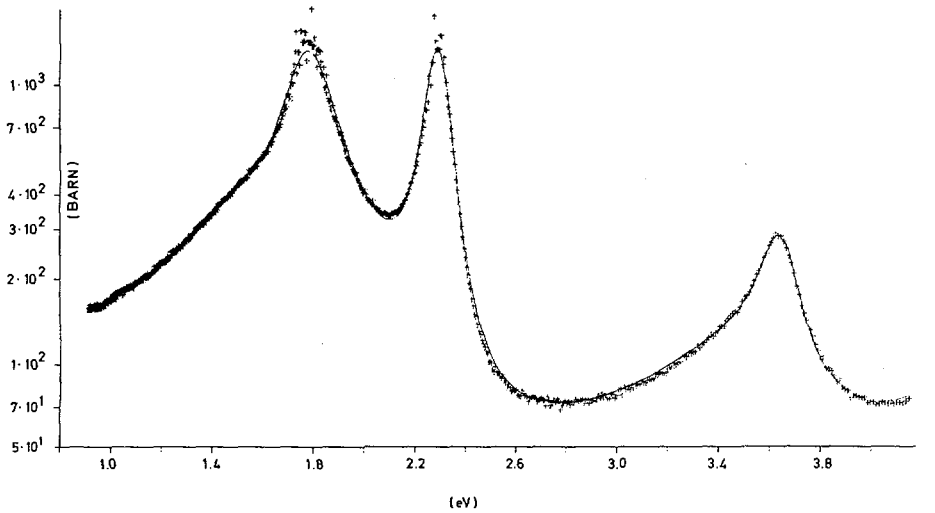

FIG. 1a. Multilevel fit to the total cross-section data. The crosses and the dots are the measured points. The solid lines are the computed total cross-section with the parameters of Table II.

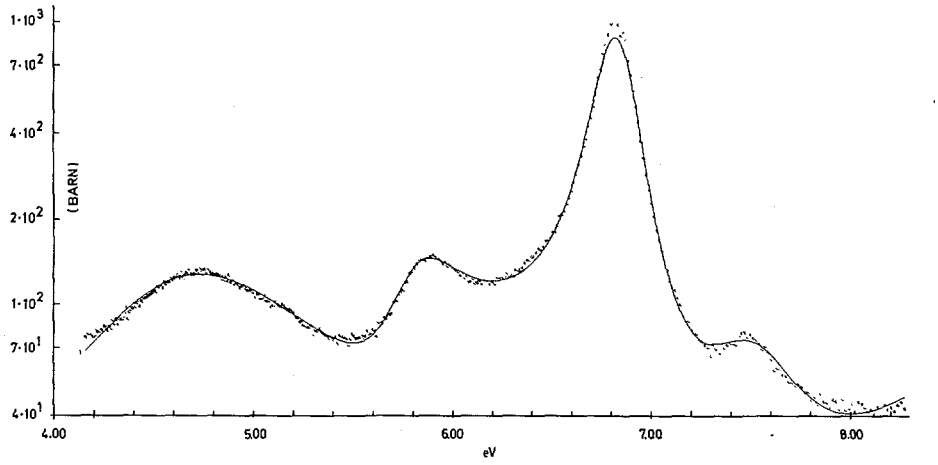

FIG. 1b. Continued.

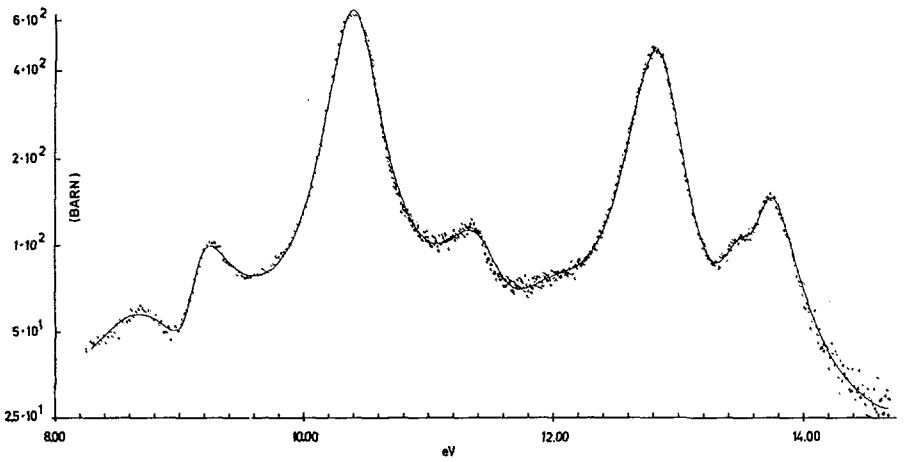

FIG. 1c. Continued.

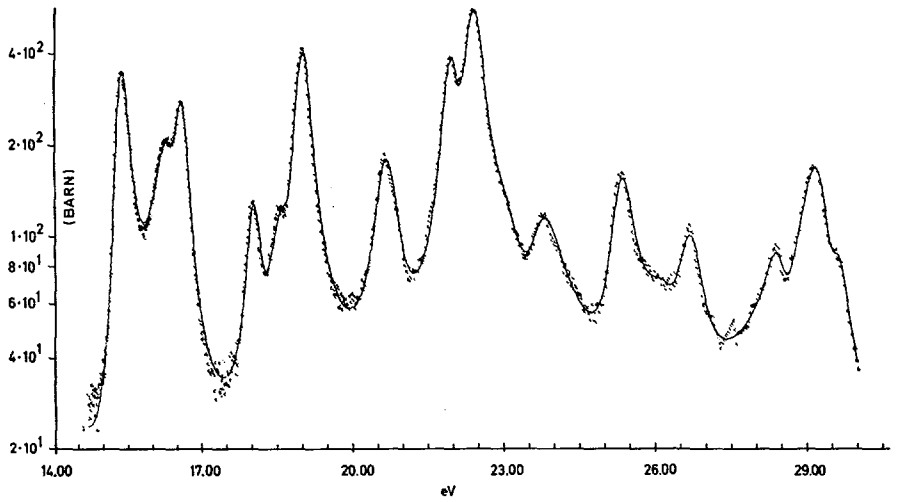

FIG. 1d. Continued.

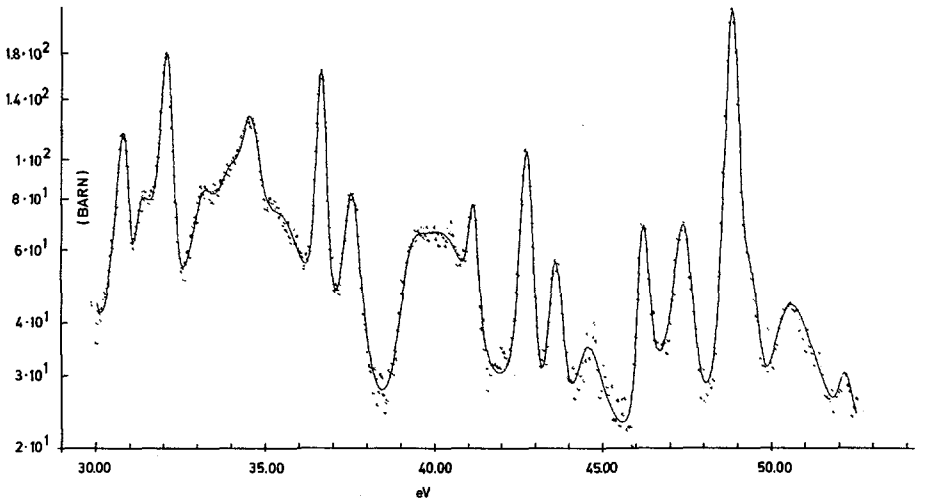

FIG. 1e. Continued.

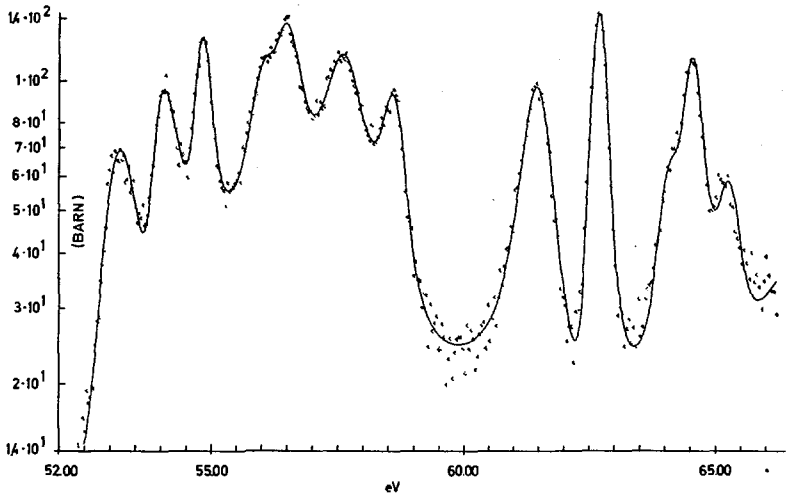

FIG. 1f. Continued.

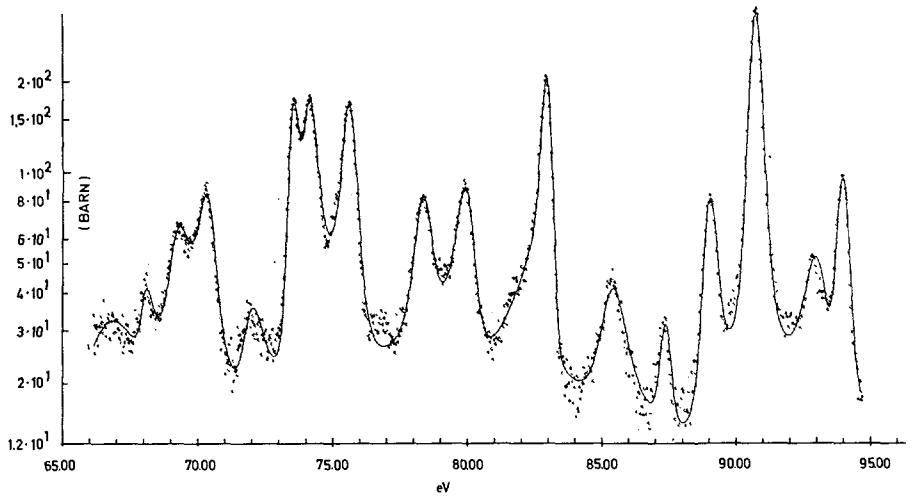

FIG. 1g. Continued.

TABLE III. SINGLE-LEVEL RESONANCE PARAMETERS OF ^{233}U

E (eV)	Γ (eV)	$2g\Gamma_n^o \cdot 10^{-3}$ (eV)	E (eV)	Γ (eV)	$2g\Gamma_n^o \cdot 10^{-3}$ (eV)
2.80	0.500	0.012	25.30	0.320	0.174
3.49	0.700	0.089	25.89	0.900	0.152
3.66	0.130	0.040	26.33	0.150	0.007
4.77	1.00	0.186	26.66	0.300	0.098
5.89	0.350	0.060	27.15	0.600	0.032
6.40	0.650	0.086	28.05	0.800	0.102
6.81	0.170	0.380	28.38	0.170	0.038
7.50	0.200	0.014	29.11	0.530	0.352
7.80	0.500	0.012	29.65	0.250	0.036
8.33	0.500	0.010	30.43	0.400	0.028
8.68	0.390	0.024	30.79	0.250	0.114
9.25	0.250	0.039	31.44	0.550	0.126
9.66	0.650	0.041	32.09	0.350	0.278
10.38	0.320	0.520	33.18	1.000	0.218
11.00	0.350	0.022	34.02	1.000	0.228
11.32	0.350	0.060	34.58	0.600	0.206
12.05	0.900	0.090	35.20	0.500	0.034
12.81	0.300	0.408	35.75	1.500	0.264
13.45	0.150	0.015	36.65	0.170	0.156
13.74	0.300	0.106	37.55	0.430	0.128
15.36	0.090	0.120	39.42	0.850	0.170
15.51	0.225	0.108	40.00	0.600	0.074
16.26	0.600	0.334	40.50	0.600	0.112
16.59	0.150	0.118	41.15	0.300	0.094
18.01	0.250	0.099	42.05	0.800	0.040
18.50	0.250	0.061	42.72	0.230	0.138
18.98	0.270	0.406	43.62	0.330	0.072
19.40	0.500	0.060	44.75	1.100	0.114
19.94	0.400	0.018	46.23	0.250	0.090
20.64	0.450	0.258	46.73	0.200	0.012
21.47	0.400	0.038	47.38	0.470	0.152
21.90	0.250	0.314	48.83	0.200	0.362
22.37	0.350	0.714	49.35	0.300	0.048
22.93	0.700	0.178	50.60	1.100	0.172
23.77	0.450	0.124	51.45	0.400	0.019
24.28	0.700	0.088	52.15	0.300	0.023

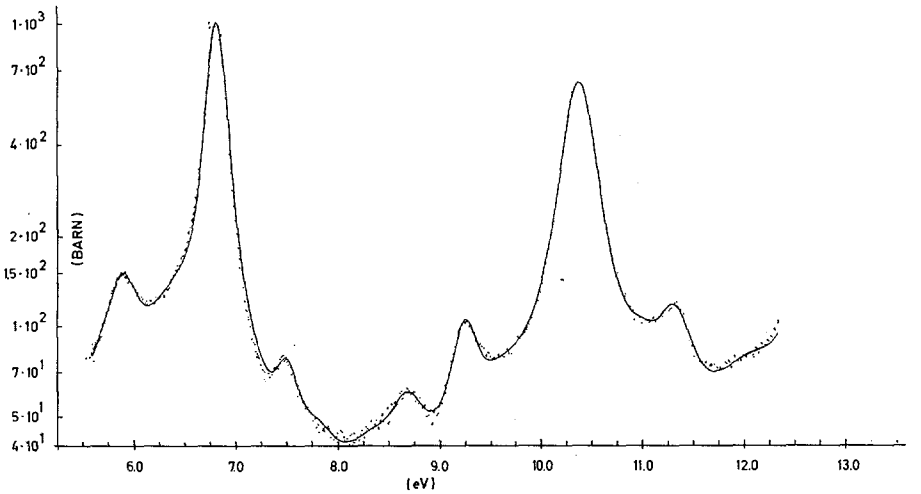

FIG. 2a. Single-level fit to the total cross-section data. The dots are the measured points. The solid lines are the computed total cross-section with the parameters of Table III.

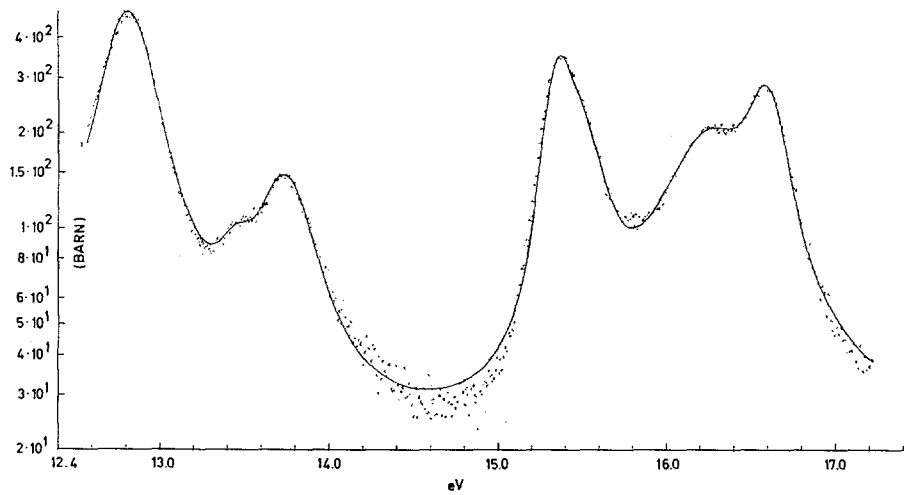

FIG. 2b. Continued.

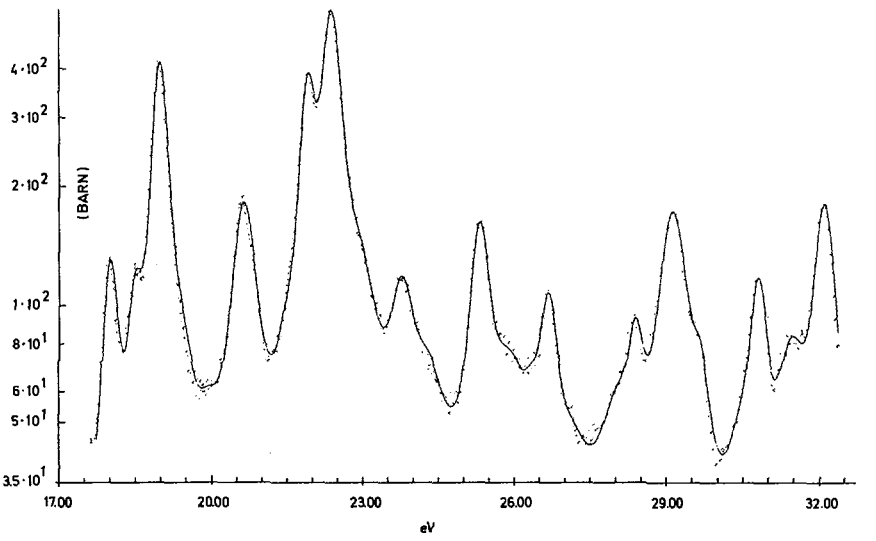

FIG. 2c. Continued.

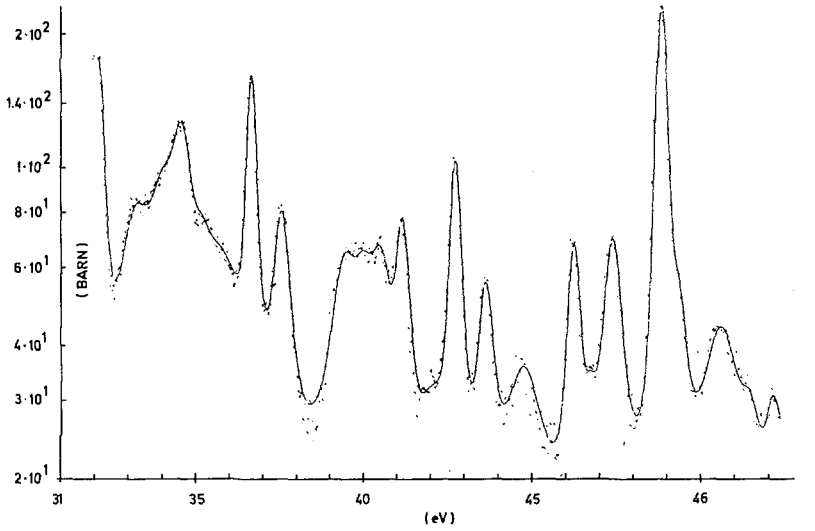

FIG. 2d. Continued.

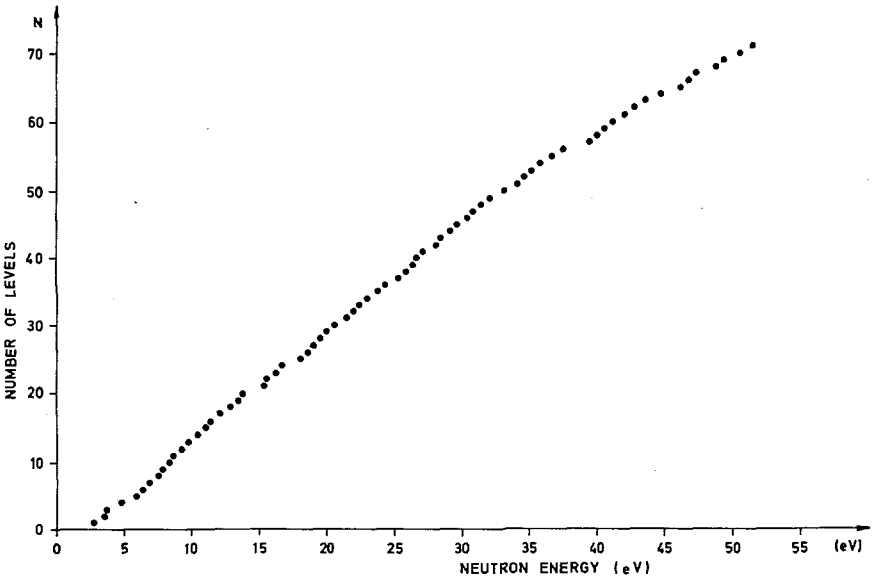

FIG. 3. Cumulative number of levels versus neutron energy.

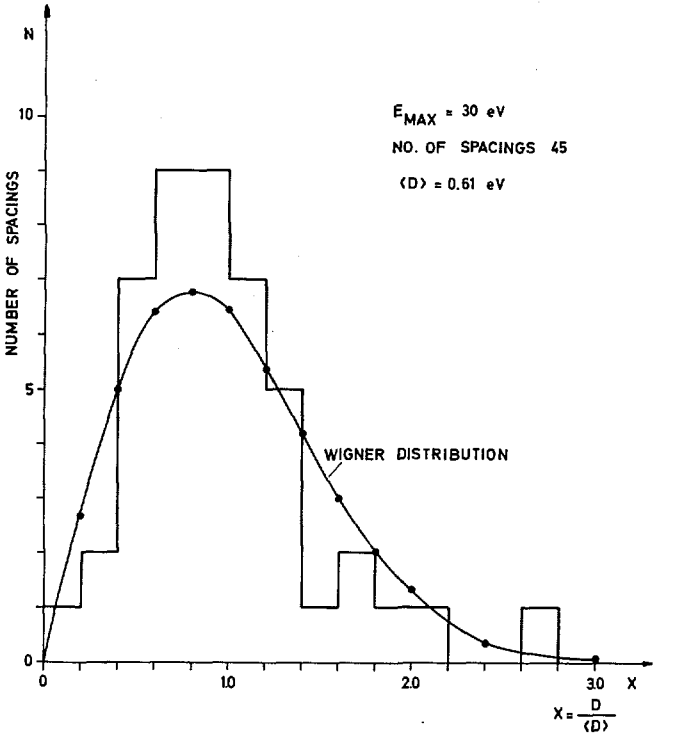

FIG. 4. Histogram of the observed distribution of the nearest-neighbour spacing together with the Wigner distribution.

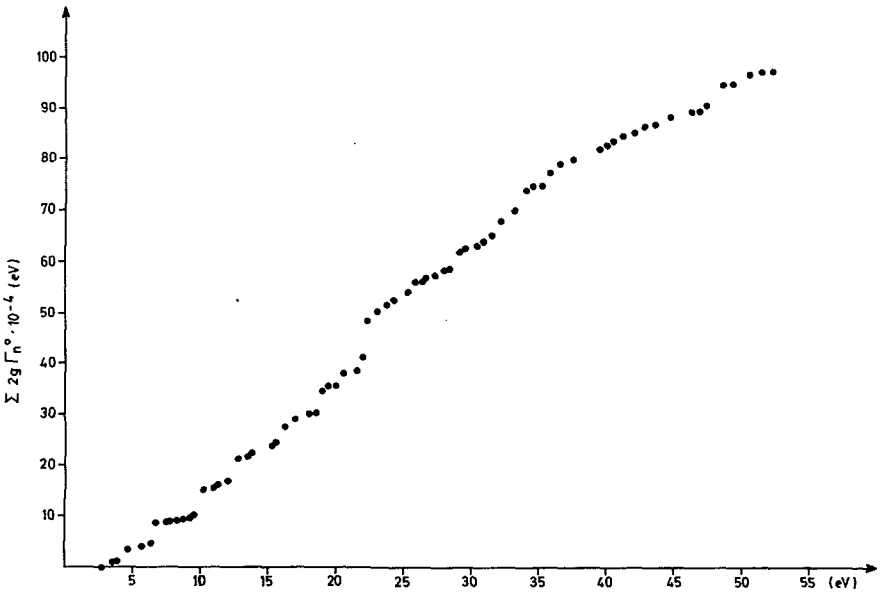

FIG. 5. $\Sigma 2g\Gamma_n^0$ versus neutron energy.

The level spacing distribution of the same number of resonances together with the theoretical predicted Wigner distribution is given in Fig. 4.

Other statistical quantities are the s-wave strength function

$$S_o = \frac{\sum_j (2g\Gamma_n^o)_j}{E_1 - E_2}$$

and the mean neutron width

$$\langle 2g\Gamma_n^o \rangle = \frac{\sum_j (2g\Gamma_n^o)_j}{n}$$

E_2 and E_1 are the energy values of the first resp. the last resonance where $2g\Gamma_n^o$ are taken for the sum of reduced neutron widths and n the number of levels. Assuming that all resonances are due to s-wave neutrons one determines for the same above-mentioned set of parameters up to 30 eV

$$S_o = (2.25 \pm 0.55) \cdot 10^{-4}$$

and as mean neutron width

$$\langle 2g\Gamma_n^o \rangle = (0.136 \pm 0.03) \cdot 10^{-3} \text{ (eV)}$$

The values of $\Sigma 2g\Gamma_n^o$ versus neutron energy E for the resonances up to 53 eV are given in Fig. 5.

The distribution of the amplitudes of the reduced neutron widths up to 30 eV is shown in Fig. 6 together with the theoretical distributions for $\nu = 1$ and $\nu = 2$ degrees of freedom.

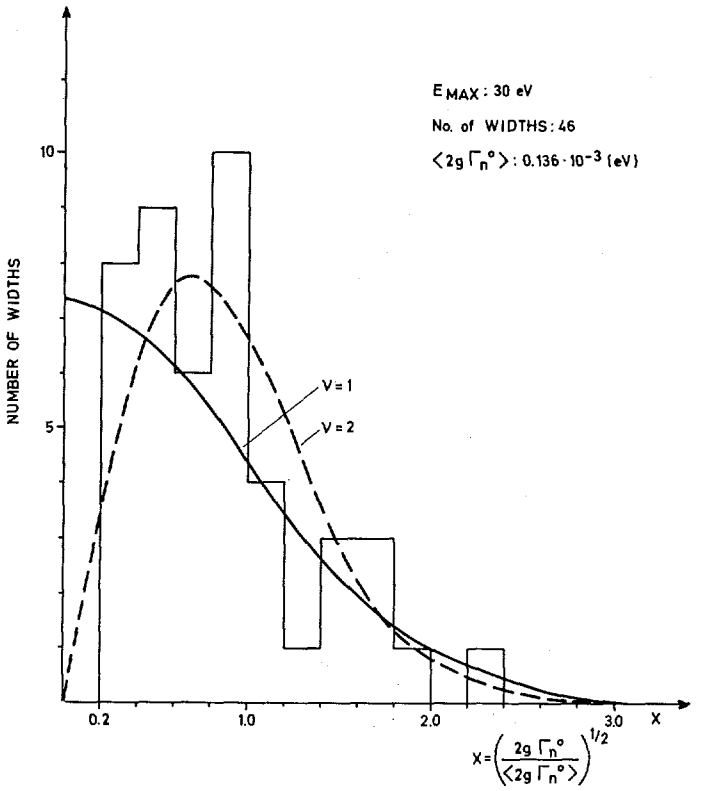

FIG. 6. Histogram of the observed distribution of $(2g\Gamma_n^0 / < 2g\Gamma_n^0 >)^{\frac{1}{2}}$. The theoretical curves are the distributions for $\nu = 1$ and $\nu = 2$.

ACKNOWLEDGEMENTS

The authors thank Dr. J. Spaepen and Mr. K. H. Böckhoff for their interest and support in this work. They are very indebted to Mr. A. De Keyser and Mr. S. De Jonge from the electronic group of the CBNM. They thank Dr. M. G. Cao who adapted the multilevel fit program CODILLI to the IBM 7090. They thank the USAEC for the loan of the samples. They wish to express their gratitude to Mr. A. Dufrasne for his help during the execution of the measurements and to Mr. U. Meloni for his very active support during the evaluation of the measurements.

REFERENCES

[1] SAILOR, V. L., BNL 325 second edition.

[2] MOORE, M. S., MILLER, L. G., SIMPSON, O. D., Phys. Review 118 (1960) 714.

[3] PATTENDEN, N. J., HARVEY, J. A., Nucl. Science and Engng. 17 (1963) 404.

[4] CAO, M. G., MIGNECO, E., THEOBALD, J. P., MERLA, M., Journal of Nuclear Energy (to be published).

[5] ADLER, D. B., ADLER, F. T., Report COO 1546-3, University of Illinois, Urbana (1966).

[6] ATTA, S. E., and HARVEY, J. A., Report ORNL-3205 (1961)

[7] DE KEYSER, A., DE JONGE, S., VAN DER VEEN, T., TER MEER, P., International Symposium on Nuclear Electronics, Versailles 1968, Vol. II (1968) 135.

[8] HORSTMANN, H., DE KEYSER, A., SCHMID, H., Proceedings on the Effective Use of Computers in the Nuclear Industry, Knoxville 1969, Conf-690401 (1969) 143.

[9] COLLING, F., and STÜBER, W., Nucl. Instr. and Meth. 64 (1968) 52.

[10] CARRARO, G., and KOLAR, W., Neutron widths of ^{238}U from 60 eV to 5.7 keV, this conference.

[11] ADLER, F. T., and ADLER, D. B., Proc. Conf. on Neutron Cross Section and Technology Vol. II (1968) 967.

[12] DE SAUSSURE, G., Rep. ORNL-TM-2745 (1969).

[13] LYNN, J. E., "The Theory of Neutron Resonance Reactions", Chapter VI, Clarendon Press, Oxford (1968) 272.

[14] LYNN, J. E., "The Theory of Neutron Resonance Reactions", Chapter IV, Clarendon Press, Oxford (1968) 108.

NEUTRON WIDTHS OF ^{238}U FROM 60 eV TO 5.7 keV

G. CARRARO, W. KOLAR
Central Bureau for Nuclear Measurements,
EURATOM, Geel, Belgium

Presented by G. Rohr

Abstract

NEUTRON WIDTHS OF ^{238}U FROM 60 eV TO 5.7 keV

The neutron total cross-section of ^{238}U has been measured from about 60 eV to about 14 keV and the resonance parameters have been evaluated up to 5.7 keV. The experiments were carried out at the 60 MeV linear accelerator of the CBNM. The thickness of the ^{238}U sample (99.6% of ^{238}U) was 91 barn/at. The nominal resolution of the different measurements varied between 3.2 ns/m at 60 eV and 0.5 ns/m at about 5.7 keV. About 260 resonances were observed and the resonance parameters E_0 and Γ_n^0 have been determined using the area program of S.E. Atta and J.A. Harvey [1]. Up to 0.5 keV, the resonance parameters are in good agreement with those of Garg et al. [2], while for higher neutron energies there appear discrepancies. The statistical properties for the resonances observed between 60 - 2000 eV are determined. One calculates a mean level spacing $\langle D \rangle = 17.8 \pm 0.9$ eV and a mean reduced neutron width $\langle \Gamma_n^0 \rangle = (1.95 \pm 0.27) \times 10^{-3}$ eV assuming that all resonances in that energy range are s-wave resonances. The s-wave strength function is determined to $S_0 = (1.09 \pm 0.15) \times 10^{-4}$.

INTRODUCTION

The total neutron cross section of U^{238} in the resonance region has been measured several times [2, 3, 4, 5]. In view of the importance of U^{238} and of the discrepancies in the Γ_n^o values reported by different authors, the total neutron cross section was remeasured between 60 eV and 14 keV neutron energy.

For the resonance parameter analysis only resonances up to 5.7 keV have been taken into account due to resolution limits.

EXPERIMENTAL TECHNIQUE

The measurements were performed at the 60 MeV linear accelerator of the CBNM. The technique applied is conventional and was described elsewhere [6].
Experimental parameters used are the following:

Sample
It was a slab of metallic U^{238} (dimensions: 200 x 200 x 2.27 mm). Its total weight was (1745 ± 0.1)gr which corresponds to 4.345 gr/cm^2 or 90.94 barn/at. The U^{238} concentration was 99.6%.

Moderator
It was a polyethylene slab (dimensions 20 x 20 x 2.4 cm).

Detector
It consisted of 4 NaI crystals (4 inch diam. and 3 inch thickness) mounted on XP 1040 photomultipliers which viewed laterally a slab of an assembly of sintered $^{10}B_4C$ pieces (overall dimensions: 10.5 x 10.5 x 1 cm).

Flightpath length: 100 m (the sample was placed at 50 m).

Angle of the flightpath with the normal to the moderator: 9°.

TABLE I. MAIN CHARACTERISTICS OF DIFFERENT RUNS

	1st Run	2nd Run	3rd Run
Total energy range	65 eV - 800 eV	750 eV - 3600 eV	2.5 keV - 14 keV
Burst width	50 nsec	50 nsec	50 nsec
Repetition rate	400 Hz	600 Hz	600 Hz
Electron energy	55 MeV	60 MeV	60 MeV
Number of bursts "IN"	$2.059 \cdot 10^8$	$1.937 \cdot 10^8$	$2.057 \cdot 10^8$
Number of bursts "OUT"	$0.512 \cdot 10^8$	$0.483 \cdot 10^8$	$0.517 \cdot 10^8$
Black resonances	Bi, Mn, Co	Bi, Co, Na	Bi, Al, Na
Energy range (eV): (a)	799.62 - 297.01	3627.5 - 2029.8	2.5 keV - 14 keV
(b)	297.01 - 153.60	2029.8 - 1294.7	
(c)	153.60 - 62.98	1294.7 - 763.8	
Channel widths: (a)	0.08 μsec	0.02 μsec	0.02 μsec
(b)	0.16 μsec	0.04 μsec	
(c)	0.32 μsec	0.08 μsec	
Overlap filter	0.29 gr of $^{10}B/cm^2$	0.60 gr of $^{10}B/cm^2$	0.60 gr of $^{10}B/cm^2$

TABLE II: ^{238}U Resonance Parameters: Neutron Widths

Energy (eV)	Γ_n (meV)	Γ_n^o (meV)
66.00 ± 0.10	25.3 ± 1.0	3.11 ± 0.12
80.74 ± 0.06	2.00 ± 0.15	0.22 ± 0.02
89.29 ± 0.08	0.096 ± 0.02	0.010 ± 0.002
102.55 ± 0.10	69.5 ± 7	6.86 ± 0.69
116.88 ± 0.11	27.2 ± 2.0	2.53 ± 0.18
145.58 ± 0.15	0.89 ± 0.10	0.074 ± 0.008
165.27 ± 0.09	3.4 ± 0.2	0.264 ± 0.016
189.63 ± 0.18	169 ± 7	12.27 ± 0.51
208.45 ± 0.13	53 ± 6	3.67 ± 0.42
237.32 ± 0.16	28.2 ± 2	1.83 ± 0.13
242.69 ± 0.17	0.16 ± 0.03	0.010 ± 0.002
263.99 ± 0.19	0.23 ± 0.03	0.014 ± 0.002
273.62 ± 0.20	25.9 ± 1.2	1.57 ± 0.07
290.81 ± 0.22	15.0 ± 1.2	0.88 ± 0.07
311.23 ± 0.12	1.1 ± 0.1	0.062 ± 0.006
347.76 ± 0.14	83.6 ± 4	4.48 ± 0.21
376.82 ± 0.16	1.26 ± 0.005	0.065 ± 0.003
397.63 ± 0.17	6.33 ± 0.5	0.32 ± 0.03
410.22 ± 0.18	20.6 ± 1.0	1.02 ± 0.05
434.10 ± 0.20	9.6 ± 0.4	0.46 ± 0.02
439.49 ± 0.40	0.46 ± 0.10	0.022 ± 0.005
453.72 ± 0.42	0.46 ± 0.1	0.022 ± 0.005
463.16 ± 0.21	5.55 ± 0.4	0.258 ± 0.019
478.33 ± 0.23	3.97 ± 0.3	0.182 ± 0.014
488.79 ± 0.24	0.57 ± 0.1	0.026 ± 0.005
518.29 ± 0.25	55.5 ± 4	2.44 ± 0.02
535.20 ± 0.27	45.2 ± 2.0	1.95 ± 0.09
556.08 ± 0.28	0.7 ± 0.2	0.030 ± 0.008
580.04 ± 0.30	44.1 ± 2.7	1.83 ± 0.11
594.98 ± 0.34	84.4 ± 5.0	3.46 ± 0.20
619.84 ± 0.34	32.5 ± 1.5	1.31 ± 0.06
624.08 ± 0.34	0.72 ± 0.1	0.029 ± 0.004
628.53 ± 0.35	6.7 ± 0.2	0.267 ± 0.008
661.08 ± 0.37	132.0 ± 7.0	5.13 ± 0.27
677.35 ± 0.38	0.96 ± 0.2	0.037 ± 0.008
693.03 ± 0.40	43.8 ± 2.0	1.66 ± 0.08
708.02 ± 0.41	22.2 ± 2.0	0.83 ± 0.08
721.38 ± 0.43	1.46 ± 0.2	0.054 ± 0.007
729.93 ± 0.43	0.44 ± 0.20	0.016 ± 0.007
732.09 ± 0.44	1.59 ± 0.30	0.059 ± 0.011
756.04 ± 0.46	0.84 ± 0.20	0.031 ± 0.007
765.18 ± 0.54	3.8 ± 1.0	0.14 ± 0.04
779.49 ± 0.53	2.2 ± 0.2	0.079 ± 0.007
791.03 ± 0.52	6.9 ± 0.2	0.245 ± 0.070
821.81 ± 0.52 *	65.3 ± 3.0	2.28 ± 0.10
847.09 ± 0.54 *		
851.42 ± 0.55	63 ± 3	2.16 ± 0.10

* Levels which are uncertain

TABLE II: continued

Energy (eV)	Γ_n (meV)	Γ_n^o (meV)
856.32 ± 0.55	86.3 ± 4	2.95 ± 0.14
866.83 ± 0.55	5.7 ± 0.5	0.194 ± 0.017
891.90 ± 0.58	0.7 ± 0.2	0.023 ± 0.007
905.44 ± 0.59	56.2 ± 2	1.87 ± 0.07
910.22 ± 0.6	0.8 ± 0.2	0.027 ± 0.007
925.42 ± 0.62	13.9 ± 1.5	0.46 ± 0.05
937.22 ± 0.63	137.3 ± 8	4.48 ± 0.26
958.91 ± 0.65	196.3 ± 9	6.34 ± 0.29
991.86 ± 0.69	377 ± 15	11.97 ± 0.48
1011.6 ± 0.7	1.9 ± 0.3	0.060 ± 0.009
1023.2 ± 0.7	10 ± 1	0.31 ± 0.03
1029.4 ± 0.7	2.6 ± 0.2	0.081 ± 0.006
1033.7 ± 0.70*		
1054.8 ± 0.7	92.5 ± 5	2.85 ± 0.15
1067.6 ± 0.4	0.4 ± 0.3	0.012 ± 0.009
1081.8 ± 0.4	1.04 ± 0.20	0.032 ± 0.006
1095.2 ± 0.4	2.7 ± 0.20	0.082 ± 0.006
1099.1 ± 0.4	22.9 ± 0.20	0.691 ± 0.006
1103.1 ± 0.4	1.3 ± 0.30	0.039 ± 0.009
1109.6 ± 0.4	32.5 ± 1.0	0.98 ± 0.03
1131.7 ± 0.4	1.8 ± 0.7	0.054 ± 0.021
1140.9 ± 0.4	218 ± 7	6.45 ± 0.21
1168.0 ± 0.4	84 ± 4	2.46 ± 0.12
1177.5 ± 0.5	67.4 ± 2	1.96 ± 0.06
1195.0 ± 0.5	95.7 ± 2	2.77 ± 0.06
1211.4 ± 0.5	9.3 ± 0.5	0.27 ± 0.27
1245.3 ± 0.5	237 ± 10	6.72 ± 0.28
1267.7 ± 0.5	28.6 ± 0.5	0.803 ± 0.014
1273.6 ± 0.5	30.4 ± 0.5	0.810 ± 0.014
1299.8 ± 0.5	2.6 ± 0.3	0.072 ± 0.008
1317.4 ± 0.5	3.4 ± 0.4	0.094 ± 0.011
1331.6 ± 0.5	1.2 ± 0.2	0.033 ± 0.005
1394.3 ± 0.6	211 ± 8	5.65 ± 0.21
1406.3 ± 0.5	71.4 ± 3	1.90 ± 0.08
1417.4 ± 0.6 }	91 ± 0.2	0.241 ± 0.005
1420.9 ± 0.6 }		
1428.8 ± 0.6	29.6 ± 1.0	0.78 ± 0.03
1444.9 ± 0.6	15.4 ± 1.1	0.41 ± 0.03
1474.4 ± 0.6	129 ± 3	3.36 ± 0.08
1523.5 ± 0.7	260 ± 7	6.66 ± 0.18
1548.2 ± 0.6 }	7.5 ± 1	0.19 ± 0.03
1550.9 ± 0.4 }		
1566.0 ± 0.4	5.7 ± 0.5	0.144 ± 0.013
1598.7 ± 0.4	334 ± 30	8.35 ± 0.75
1623.4 ± 0.4	108 ± 10	2.68 ± 0.25
1639.3 ± 0.4	56.3 ± 2	1.39 ± 0.05
1663.5 ± 0.4	228 ± 8	5.59 ± 0.20

* Levels which are uncertain

TABLE II: continued

Energy (eV)	Γ_n (meV)	Γ_n^o (meV)
1689.7 ± 0.4	98 ± 5	2.38 ± 0.12
1710.8 ± 0.6	93 ± 4	2.25 ± 0.10
1723.6 ± 0.4	15.8 ± 1	0.38 ± 0.02
1756.9 ± 0.4	133 ± 6	3.17 ± 0.14
1783.8 ± 0.4	632 ± 40	14.96 ± 0.95
1798.7 ± 0.4	1.8 ± 0.7	0.042 ± 0.017
1809.6 ± 0.4	17.8 ± 2	0.418 ± 0.005
1847.2 ± 0.5	11 ± 1	0.256 ± 0.023
1904.0 ± 0.5	43.1 ± 2	0.988 ± 0.046
1914.9 ± 0.5*		
1918.1 ± 0.5	43 ± 6	0.982 ± 0.137
1954.9 ± 0.5	4.7 ± 0.4	0.106 ± 0.009
1970.1 ± 0.6	690 ± 50	15.54 ± 1.13
1975.9 ± 0.5	510 ± 40	11.47 ± 0.90
2024.8 ± 0.5	185 ± 15	4.11 ± 0.33
2031.8 ± 0.5	63.5 ± 5	1.41 ± 0.11
2090.0 ± 0.5	26 ± 3	0.569 ± 0.066
2097.9 ± 0.5	24.2 ± 1	0.528 ± 0.022
2147.0 ± 0.5	78.5 ± 4	1.69 ± 0.09
2154.4 ± 0.6	288 ± 15	6.2 ± 0.3
2173.4 ± 0.6*		
2188.4 ± 0.6	600 ± 25	12.83 ± 0.53
2203.0 ± 0.6	113 ± 6	2.41 ± 0.13
2261.2 ± 0.6	115 ± 5	2.42 ± 0.11
2268.3 ± 0.6	248 ± 12	5.21 ± 0.25
2283.7 ± 0.6	189 ± 4	3.95 ± 0.08
2298.7 ± 1.2	5.8 ± 0.5	0.121 ± 0.010
2317.4 ± 0.6	19.6 ± 1.0	0.407 ± 0.021
2328.5 ± 0.7	2.1 ± 0.5	0.044 ± 0.010
2334.0 ± 0.6	1.6 ± 0.2	0.033 ± 0.004
2340.2 ± 0.6	11.2 ± 0.5	0.23 ± 0.01
2348.2 ± 0.6	3.5 ± 1.0	0.07 ± 0.02
2355.7 ± 0.6)		
2357.6 ± 0.6)	204 ± 10	4.20 ± 0.21
2370.1 ± 0.6	2.8 ± 2.8	0.058 ± 0.058
2386.6 ± 0.6	2 ± 0.7	0.041 ± 0.014
2393.6 ± 0.6	31.7 ± 1	0.648 ± 0.020
2399.4 ± 1.2	3.7 ± 0.5	0.076 ± 0.010
2403.9 ± 1.2	3.1 ± 0.5	0.063 ± 0.010
2413.0 ± 0.7	4.7 ± 0.6	0.096 ± 0.012
2428.6 ± 0.7	161 ± 6	3.27 ± 0.12
2448.3 ± 0.6	222 ± 8	4.49 ± 0.16
2457.6 ± 0.7	17.2 ± 1	0.347 ± 0.020
2491.2 ± 0.6	107 ± 5	2.14 ± 0.10
2523.5 ± 0.7	20.1 ± 0.5	0.40 ± 0.01
2550.0 ± 0.7	706 ± 36	13.98 ± 0.71
2561.3 ± 0.7	234 ± 10	4.62 ± 0.20
2583.0 ± 0.7	394 ± 20	7.75 ± 0.39

* Levels which are uncertain

TABLE II: continued

Energy (eV)	Γ_n (meV)	Γ_n^o (meV)
2599.7 ± 0.7	790 ± 50	15.49 ± 0.98
2621.8 ± 0.8	51.6 ± 3	1.01 ± 0.06
2661.2 ± 0.7*		
2674.0 ± 0.8	280 ± 10	5.41 ± 0.19
2698.4 ± 0.7	31.6 ± 2	0.61 ± 0.04
2719.2 ± 0.8	170 ± 10	3.26 ± 0.19
2752.8 ± 0.8	39.4 ± 3	0.751 ± 0.057
2764.7 ± 0.8	16.5 ± 2.5	0.314 ± 0.048
2790.3 ± 0.8	10.1 ± 2.5	0.191 ± 0.047
2801.6 ± 0.8*		
2831.8 ± 0.8	22.8 ± 6	0.428 ± 0.113
2867.5 ± 0.8	280 ± 50	5.23 ± 0.93
2885.2 ± 0.8	557 ± 20	10.37 ± 0.37
2899.7 ± 0.5	17 ± 4	0.316 ± 0.074
2926.3 ± 0.8	7.3 ± 1.2	0.135 ± 0.022
2935.9 ± 0.8	37 ± 4	0.683 ± 0.074
2959.5 ± 0.9	19 ± 5	0.349 ± 0.092
2970.1 ± 0.9	3.9 ± 2.5	0.072 ± 0.046
2990.5 ± 0.9	5 ± 2.5	0.091 ± 0.046
3006.2 ± 0.9	124 ± 10	2.26 ± 0.18
3031.1 ± 0.9	151 ± 8	2.74 ± 0.15
3062.4 ± 0.5	28.3 ± 2	0.511 ± 0.036
3113.0 ± 1.0	228 ± 10	4.09 ± 0.18
3136.8 ± 0.9	8.4 ± 1	0.15 ± 0.02
3151.3 ± 1.0	113 ± 5	2.01 ± 0.09
3172.7 ± 1.0	6.8 ± 1	0.121 ± 0.018
3181.5 ± 1.0	93 ± 5	1.65 ± 0.09
3191.3 ± 1.0	108 ± 5	1.91 ± 0.09
3208.1 ± 1.0	100 ± 5	1.76 ± 0.09
3229.1 ± 1.0	23 ± 7	0.405 ± 0.123
3252.3 ± 1.0	28 ± 3	0.491 ± 0.053
3281.8 ± 1.0	270 ± 50	4.71 ± 0.87
3300.4 ± 2.0	3.6 ± 2.6	0.063 ± 0.045
3315.0 ± 1.0	159 ± 10	2.76 ± 0.17
3324.4 ± 1.0	125 ± 5	2.17 ± 0.087
3336.5 ± 1.1	102 ± 4	1.77 ± 0.07
3358.1 ± 1.1	128 ± 10	2.21 ± 0.17
3393.5 ± 1.1	22.4 ± 2.6	0.38 ± 0.045
3402.2 ± 1.2*		
3411.9 ± 1.2	219 ± 10	3.75 ± 0.17
3439.3 ± 1.2	370 ± 15	6.31 ± 0.26
3461.0 ± 1.2	719 ± 30	12.22 ± 0.51
3488.5 ± 1.2	104 ± 5	1.76 ± 0.08
3497.8 ± 1.2	9.8 ± 2	0.166 ± 0.034
3564.4 ± 1.2	261 ± 15	4.37 ± 0.25
3576.6 ± 1.2	417 ± 20	6.97 ± 0.33
3597.8 ± 1.2	57 ± 3	0.95 ± 0.05
3612.0 ± 1.2*		
3626.3 ± 1.2*		

* Levels which are uncertain

TABLE II: continued

Energy (eV)	Γ_n (meV)	Γ_n^o (meV)
3632.7 ± 1.2	559 ± 55	9.27 ± 0.91
3696.3 ± 1.2	415 ± 20	6.83 ± 0.33
3719.8 ± 1.3	102 ± 10	1.67 ± 0.16
3737.2 ± 1.2	225 ± 10	3.68 ± 0.16
3767.9 ± 1.3	94 ± 5	1.53 ± 0.08
3785.1 ± 1.3	466 ± 25	7.57 ± 0.41
3835.2 ± 1.3	12.6 ± 2.5	0.20 ± 0.04
3861.3 ± 1.3	560 ± 30	9.01 ± 0.48
3876.5 ± 1.3	201 ± 10	3.23 ± 0.16
3904.9 ± 1.3	327 ± 30	5.23 ± 0.48
3918.3 ± 1.3	110 ± 8	1.76 ± 0.13
3943.2 ± 1.4	212 ± 12	3.38 ± 0.19
3958.2 ± 1.3	136 ± 7	2.16 ± 0.11
4044.6 ± 1.4	60.7 ± 5	0.95 ± 0.08
4067.1 ± 1.4	17.5 ± 4	0.27 ± 0.06
4094.2 ± 1.4	97.3 ± 5	1.52 ± 0.08
4128.8 ± 1.5	35.7 ± 12	0.56 ± 0.19
4172.6 ± 1.5	160 ± 20	2.48 ± 0.31
4182.9 ± 1.4	28.0 ± 12	0.43 ± 0.19
4214.2 ± 1.4	55.5 ± 10	0.85 ± 0.15
4229.1 ± 1.5*		
4262.4 ± 1.5	33.1 ± 4	0.51 ± 0.06
4303.7 ± 1.5	140 ± 15	2.13 ± 0.23
4311.5 ± 1.6	122 ± 10	1.86 ± 0.15
4329.3 ± 1.6	96.3 ± 8	1.46 ± 0.12
4375.6 ± 1.6	160.0 ± 12	2.42 ± 0.18
4380.3 ± 1.6		
4439.6 ± 1.7	104.5 ± 7	1.57 ± 0.10
4493.4 ± 1.7	5.2 ± 4.5	0.08 ± 0.07
4516.5 ± 1.7	606 ± 30	9.02 ± 0.45
4548.2 ± 1.7	100 ± 5	1.48 ± 0.07
4571.7 ± 1.7	44.9 ± 4	0.66 ± 0.06
4599.8 ± 1.7	31.30 ± 7	0.46 ± 0.10
4622.8 ± 1.7	15.9 ± 12	0.23 ± 0.18
4636.6 ± 1.7	27.9 ± 5.0	0.41 ± 0.07
4667.8 ± 1.7	142.5 ± 30	2.09 ± 0.44
4699.3 ± 1.7	15 ± 9	0.22 ± 0.13
4709.9 ± 1.8	390 ± 120	5.68 ± 1.75
4733.0 ± 1.7	20 ± 9	0.29 ± 0.13
4770.5 ± 1.8	22.4 ± 15	0.32 ± 0.22
4804.9 ± 1.8	179.4 ± 33	2.59 ± 0.48
4841.5 ± 1.8	16 ± 16	0.23 ± 0.23
4864.6 ± 1.8	250 ± 50	3.58 ± 0.72
4903.8 ± 1.8	105.3 ± 30	1.50 ± 0.43
4913.1 ± 1.9	139 ± 30	1.98 ± 0.43
4925.4 ± 1.9	178 ± 20	2.54 ± 0.28
4959.6 ± 1.9	178 ± 20	2.53 ± 0.28

* levels which are uncertain

TABLE II: continued

Energy (eV)	Γ_n (meV)	Γ_n^o (meV)
4978.8 ± 1.9	70 ± 18	0.99 ± 0.25
5011.5 ± 1.9	50 ± 24	0.71 ± 0.34
5040.8 ± 1.9	299 ± 40	4.21 ± 0.56
5092.0 ± 2.0	51 ± 15	0.71 ± 0.21
5123.9 ± 2.0	156 ± 16	2.18 ± 0.22
5225.6 ± 2.0*		
5248.4 ± 2.0*		
5265.0 ± 2.1	185 ± 55	2.55 ± 0.76
5315.5 ± 2.1	9.3 ± 8	0.13 ± 0.11
5351.7 ± 2.2	160 ± 30	2.19 ± 0.41
5358.1 ± 2.2		
5425.1 ± 2.2	55.5 ± 10	0.75 ± 0.14
5491.2 ± 2.2	550 ± 90	7.42 ± 1.21
5536.0 ± 2.3	30 ± 6	0.40 ± 0.08
5557.4 ± 2.3	133 ± 30	1.78 ± 0.40
5585.8 ± 2.3	38.2 ± 16	0.51 ± 0.21
5643.3 ± 2.3	465 ± 55	6.19 ± 0.73
5656.0 ± 2.3	484.5 ± 50	6.44 ± 0.66
5680.5 ± 2.3	222 ± 60	2.94 ± 0.80
5687.6 ± 2.3		
5701.7 ± 2.4*		
5762.1 ± 2.4	128.7 ± 15	1.70 ± 0.20

* Levels which are uncertain

MEASUREMENTS AND ANALYSIS OF THE RESULTS

In total three measurements have been performed. Table I shows the main characteristics of the different runs. The calculation of the total cross section is done with a computer program [7] . The area analysis program of S. E. Atta and J. A. Harvey [1] has been used to analyse the resonance parameters. This program calculates Γ_n for an assumed value of Γ (where $\Gamma = \Gamma_n + \Gamma_\gamma$).
For most of the resonances up to 1000 eV Γ_n was evaluated making use of the Γ_γ values obtained by Rohr and Weigmann [8] ; for the other resonances in this range the value $\langle \Gamma_\gamma \rangle = (24.64 \pm 0.85)$ meV was used as communicated by the same authors.
For nearly all resonances above 1000 eV practically no dependence of Γ_n from the Γ_γ parameter was observed in the Γ_n, Γ_γ -plane.
The results are shown in Table II.

The errors of Γ_n^o result from: a) the statistical error of the transmission values b) the error due to the choice of the boundaries for area analysis c) the uncertainty of base line (see program of S. E. Atta and J. A. Harvey [1] d) the uncertainty of the sample thickness. If one calculates all these different error contributions using the method described in [6] and combines them, one gets the resulting error as quoted in Table II.

Up to 0. 5 keV the present resonance parameters agree quite well with those of [2, 3, 4, 5] .
For higher energies discrepancies occur which cannot be explained at the moment. Therefore it is planned to repeat some of the measurements with different sample thicknesses.

STATISTICAL PROPERTIES

The large number of observed resonances allows the evaluation of the statistical properties of the nucleus. Fig. 1 shows the cumulative number of levels vs. neutron energy. Up to 2 keV the level density is nearly constant. For this energy range a mean level spacing of $\langle D \rangle = 17.8 \pm 0.9$ eV was calculated which agrees with that of Garg and al. [2] (17.7 ± 0.7)eV and of Firk and al. [3] (18.0 ± 1.3)eV.

The error has been determined using the formula $\sigma^2 = 0.54 \cdot \frac{\langle D \rangle^2}{n}$, where n is the number of levels [9] .

The theoretical Wigner distribution [2]:

$$P(x) = \frac{\pi}{2} x \exp\left(-\frac{\pi}{4} x^2\right) \quad \text{where} \quad x = \frac{D}{\langle D \rangle}$$

fits better the experimental histogram than the random distribution (Fig. 3)

$$P(x) = e^{-x}$$

The other statistical quantity is the mean value of the reduced neutron width. For the energy range 60 eV - 2 keV a value of $\langle \Gamma_n^o \rangle = (1.95 \pm 0.27)\ 10^{-3}$ eV was determined, which agrees quite well with Firk and al. [3] $(1.8 \cdot 10^{-3}$ eV) but is somewhat higher than that of Garg and al. $(1.60 \cdot 10^{-3}$ eV) [2] .

In Fig. 2 is reported the $\Sigma \Gamma_n^o$ vs. neutron energy. Assuming that all resonances are due to s-wave neutrons, the strength function $S_o = \frac{\langle \Gamma_n^o \rangle}{\langle D \rangle}$ results to be $S_o = (1.09 \pm 0.15) \cdot 10^{-4}$.

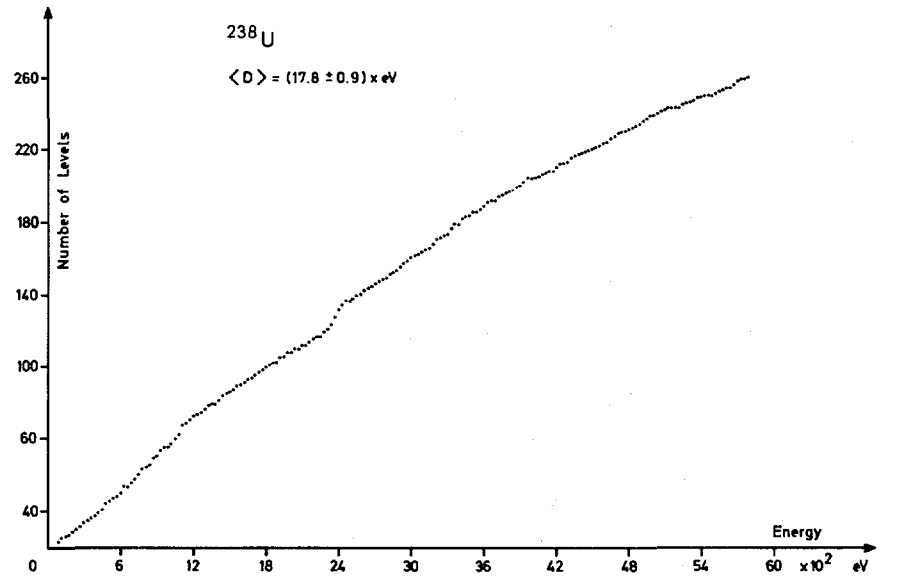

FIG.1. Plot of the cumulative number of levels observed in ^{238}U.

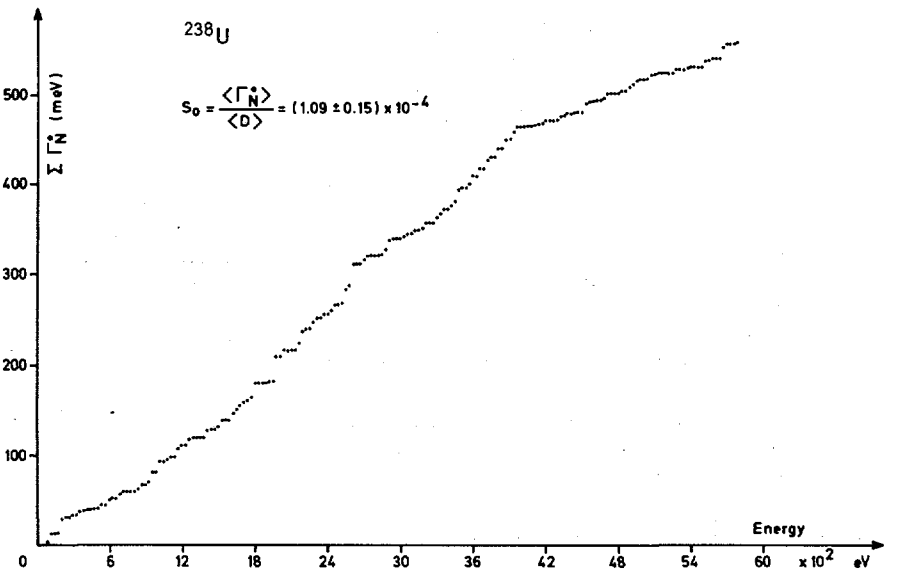

FIG.2. $\Sigma\Gamma_n^0$ versus neutron energy E. The slope of the curve determines the strength function.

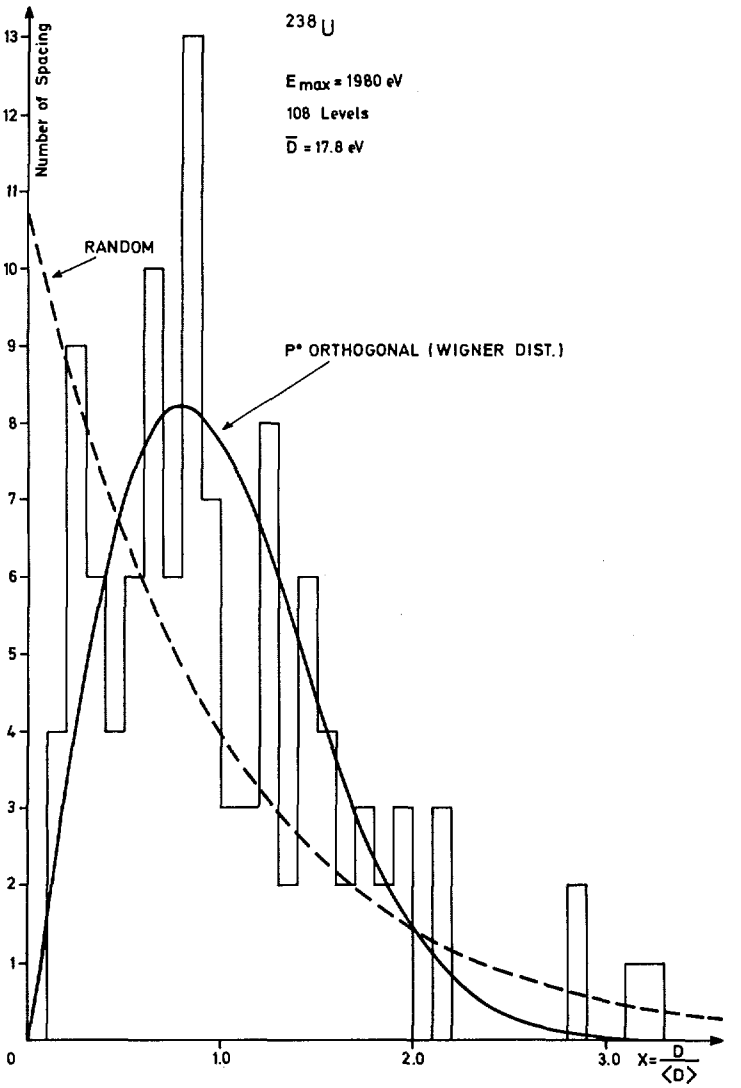

FIG. 3. Histogram plot of the observed distribution of nearest-neighbour level spacings $x = D/\langle D \rangle$ for ^{238}U. The two theoretical curves correspond to random and Wigner distribution, respectively.

The result is in good agreement with Firk and al. $(1.00 \pm 0.15) \cdot 10^{-4}$ but is again somewhat higher than that of Garg and al. $(0.90 \pm 0.10) \cdot 10^{-4}$. The theoretical distribution [10]

$$P(x, \frac{\nu}{2})dx = \frac{(\frac{\nu x}{2})^{(\frac{\nu}{2} - 1)}}{\Gamma} \exp\left[- \frac{\nu}{2} x \right] dx$$

agrees better with the histogram for $\nu = 1$ (where ν = number of degree of freedom). See Fig. 4.

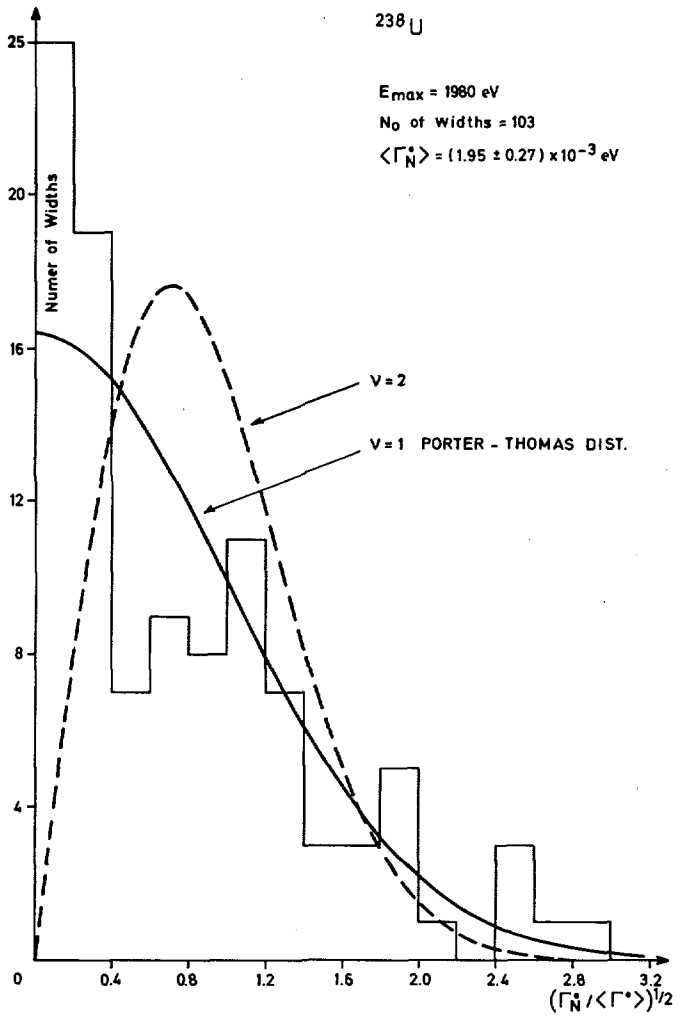

FIG. 4. Histogram of the observed distribution of $(\Gamma_n^0/\langle\Gamma_n^0\rangle)^{1/2}$. The Porter-Thomas ($\nu = 1$) and the $\nu = 2$ theoretical distributions are shown for comparison.

CONCLUSIONS

Up to 500 eV the present results agree well with those published earlier. At higher energies some discrepancies appear. Measurements will be repeated with other sample thicknesses.

ACKNOWLEDGEMENTS

The authors thank Dr. J. Spaepen and Mr. K. H. Böckhoff for their interest and support in this work. They are very grateful to Mr. A. De Keyser and Mr. S. de Jonge from the electronics group of CBNM. They thank Dr. G. Nastri who prepared the

data reduction programs for the IBM 1800. They wish to express their gratitude to Mr. A. Dufrasne for his help during the execution of the measurements and to Mr. U. Meloni and Mr. C. Cervini for their very active support during the evaluation of the measurements.

REFERENCES

[1] ATTA, S.E., HARVEY, J.A., Numerical Analysis of Neutron Resonances, ORNL-3205 (1961).

[2] GARG, J.B., RAINWATER, J., PETERSEN, J.S., HAVENS, W.W., Jr., Physical Rev. 134 (1964) 985.

[3] FIRK, F.W.K., LYNN, J.E., MOXON, M.C., Nucl. Phys. (1963) 614.

[4] ASGHAR, M., CHAFFEY, C.M., MOXON, M.C., Nucl. Phys. 85 (1966) 305.

[5] ROSEN, J.L., DESJARDINS, J.S., RAINWATER, J., HAVENS, W.W., Jr., Physical Rev. 118 (1960) 687.

[6] KOLAR, W., BÖCKHOFF, K.H., Journ. of Nucl. Energy 22 (1968) 299.

[7] NASTRI, G., SCHMID, H., Data Reduction Programs for Total Cross Section Experiments, EUR 4456.e (1970).

[8] ROHR, G., WEIGMANN, H., WINTER, J., Resonance parameters from neutron radiative capture in ^{238}U (this conference).

[9] LYNN, J.E., International Course of Nuclear Physics, (1966) Trieste.

[10] PORTER, C.E., THOMAS, R.G., Phys.Rev. 104 (1956) 483.

RESONANCE PARAMETERS FROM NEUTRON RADIATIVE CAPTURE IN ^{238}U

G. ROHR, H. WEIGMANN, J. WINTER
Central Bureau for Nuclear Measurements
EURATOM, Geel, Belgium

Abstract

RESONANCE PARAMETERS FROM NEUTRON RADIATIVE CAPTURE IN ^{238}U.

Neutron radiative capture in ^{238}U has been studied in the neutron energy range from 50 eV to 1 keV. Combined area analysis of these data together with data from total cross-section measurements performed at the CBNM yields the resonance parameters of 28 resonances. A mean value of $\bar{\Gamma}_\gamma = (24.64 \pm 0.85)$ meV has been obtained. The results are compared with earlier measurements. No evidence for a non-statistical variation of the radiative widths with neutron energy has been found.

INTRODUCTION

The knowledge of the radiative widths of (^{238}U + n) resonances is of importance for calculations of the breeding ratio of fast reactors. A redetermination of these quantities seemed to be desirable in view of the rather large discrepancies in existing data [1-3]. Moreover, recent measurements [3] seemed to indicate an intermediate structure type variation of the radiative widths as a function of neutron energy; such a structure would be of special interest in view of the intermediate structure observed in subthreshold fission cross sections of several heavy elements.

MEASUREMENTS

The measurements have been performed at a 60 m flight path of the CBNM 60 MeV electron linac. The nominal resolution varied between 20 nsec/m and 1 nsec/m for different energy ranges.

After suitable collimation the neutrons fall onto the sample which is placed in the centre of a modified Moxon Rae detector. Samples of depleted U (0.2% ^{235}U) with thicknesses of $3.06\ 10^{-3}$ atoms/b and $1.01\ 10^{-2}$ atoms/b have been used. The detectors have been described in detail elsewhere [4]. The detector signals, after passing the electronics associated with the detector, were sorted in an Intertechnique 4096-channel analyser.

The energy spectrum of the neutrons at the detector station was measured with BF_3 counters as well as with a ^{10}B slab viewed by a NaI crystal; the $^{10}B(n,\alpha)^7Li$, $^7Li^+$ cross section is assumed to vary as 1/v in the energy range of interest. Absolute calibration of the product detector efficiency times neutron flux was done with the black resonance technique by observing neutron capture events in the peak region of the 6.67 eV resonance in ^{238}U.

ANALYSIS OF THE DATA AND RESULTS

For determination of the resonance parameters the CBNM transmission data [5] could be used together with the capture data. Therefore it was possible to apply a combined area analysis method for transmission and

capture data by means of the TACASI-program [6] . In this program the area below the resonances is computed by taking into account the finite resolution and Doppler-broadening. The influence of the multiscattering effect on the capture area is determined by a Monte-Carlo calculation. In general the area analysis of each measurement determines a curve in the Γ_n - Γ_γ -plane. The TACASI-program calculates for two independent measurements the intersection point of these curves, or if there are more than two, this program chooses the resonance parameters by means of a least square method. The uncertainties of the resonance parameter caused by the input data (statistical and systematical errors of the area) are determined by using the normal methods of error propagation.

In the energy range of 50 eV - 1 keV the parameters of 28 resonances have been obtained. Normally for each resonance two capture and one transmission areas were used. Only the parameter of resonances marked by an asterisk were obtained with only one capture and one transmission area.

TABLE I. ^{238}U RESONANCE PARAMETERS IN THE ENERGY RANGE FROM 50 eV UP TO 1 keV IN COMPARISON WITH EARLIER DATA

E_o[eV]	this paper		Asghar et al. [1]		Garg et al. [2]	Glass et al. [3]
	Γ_n[meV]	Γ_γ[meV]	[a] Γ_n[meV]	[a] Γ_γ[meV]	Γ_n[meV]	[a] Γ_γ[meV]
66.0*	24.8 ± 1.5	19.6 ± 3.0	22.74 ± 0.73	26.07 ± 1.48	25.2 ± 1.0	17.35 ± 3.0
102.6*	72.6 ± 0.5	26.1 ± 2.3	58.64 ± 1.74	25.95 ± 1.40	65.9 ± 2.0	24.9 ± 4.1
116.9*	28.3 ± 0.4	24.3 ± 1.4	23.10 ± 0.66	25.72 ± 1.52	36.0 ± 1.5	23.3 ± 3.6
189.6*	168.8 ± 3.4	24.7 ± 2.0	133.2 ± 5.05	23.21 ± 1.59	150.4 ± 2.8	18.5 ± 5.6
208.5	49.0 ± 1.2	22.4 ± 0.6	50.1 ± 1.79	21.49 ± 1.26	56.3 ± 6.0	23.8 ± 3.6
237.3	26.1 ± 0.7	24.5 ± 1.0	25.0 ± 1.25	19.53 ± 1.48	27.7 ± 1.6	31.4 ± 3.5
273.6	25.6 ± 0.8	23.1 ± 1.0	20.76 ± 1.45	23.91 ± 2.33	25.2 ± 1.7	26.1 ± 2.3
290.8	16.1 ± 1.7	23.1 ± 1.8	13.97 ± 0.73	22.40 ± 2.22	15.4 ± 1.7	31.4 ± 8.0
347.8*	81.7 ± 1.6	23.5 ± 1.4	57.4 ± 3.26	20.40 ± 0.58	82.1 ± 7.5	17.9 ± 1.5
397.6	6.4 ± 0.3	25.2 ± 5.2	4.95 ± 0.82	37.5 ± 33.6	6.0 ± 1.0	
410.2	19.9 ± 0.5	22.6 ± 1.4	14.23 ± 1.10	26.61 ± 3.96	19.1 ± 1.0	14.4 ± 1.4
434.1	10.1 ± 0.5	26.5 ± 3.7	7.87 ± 1.0	25.1 ± 8.70	8.3 ± 1.5	
518.3	48.9 ± 1.5	24.4 ± 1.2	39.1 ± 2.22	25.12 ± 2.58	43.3 ± 2.3	22.4 ± 1.5
535.2	43.0 ± 1.4	24.7 ± 1.2	38.8 ± 2.52	29.30 ± 3.63	37.0 ± 2.3	24.9 ± 1.5
580.0	42.5 ± 1.6	26.1 ± 1.5	37.54 ± 2.62	22.00 ± 3.31	27.0 ± 0.7	24.4 ± 3.8
595.0	85.2 ± 2.4	23.1 ± 1.0	71.4 ± 3.60	21.79 ± 2.77	81.7 ± 2.9	20.8 ± 1.6
619.8	30.0 ± 1.2	24.6 ± 1.6	25.5 ± 2.7	33.10 ± 7.1	28.3 ± 1.0	19.8 ± 2.1
661.1	123.2 ± 2.9	26.0 ± 1.2	104.7 ± 5.51	25.12 ± 5.0	115.7 ± 6.5	18.8 ± 1.5
693.0	42.3 ± 2.0	24.1 ± 1.5	31.7 ± 3.30	20.2 ± 4.6	34.2 ± 1.3	16.5 ± 1.1
708.0	22.3 ± 1.3	28.5 ± 2.6			18.6 ± 2.7	13.4 ± 2.9
821.8	57.0 ± 3.2	26.0 ± 1.7	45.9 ± 4.2	19.5 ± 3.6	58.8 ± 2.9	20.0 ± 2.5
851.4	55.6 ± 3.6	30.9 ± 1.6			55.4 ± 3.0	20.1 ± 1.6
856.3	78.4 ± 3.9	23.6 ± 1.4			80.5 ± 4.4	23.1 ± 1.5
905.4	49.3 ± 3.8	26.8 ± 1.9			45.1 ± 1.5	18.4 ± 1.8
937.2	129.5 ± 9.8	23.6 ± 1.3			147.0 ± 15.0	20.9 ± 1.6
958.9	180.5 ± 11.5	22.7 ± 1.3			158.0 ± 16.0	12.3 ± 1.6
991.9	341.2 ± 10.5	30.7 ± 1.6			346.4 ± 16.0	16.9 ± 1.3
1054.8	99.7 ± 11.2	24.2 ± 1.7			74.7 ± 16.0	16.1 ± 1.3

[a] The uncertainties of Γ_n and Γ_γ in columns 4, 5 and 7 include only the statistical error.

In Table I the results are listed for comparison with earlier measurements. The resonance energies in column 1 were taken from ref. [5]. The values obtained for Γ_n are systematically somewhat higher than those determined by Asghar et al. [1], using a combined area method for neutron capture and scattering. A much better agreement is observed with the data of Garg et al. [2], measured in a transmission experiment. Only in a few cases the resonance parameters do not coincide within the given errors. Concerning the largest deviation between the two sets, i.e. for the resonance at 580 eV our result seems to be in favour, since the Γ_n of ref. [2] in this case is even smaller than that of ref. [1].
The values obtained for Γ_γ are in accord with those determined by Asghar et al. [1]. This is especially true for the mean radiative widths. The value determined in this paper is $\bar{\Gamma}_\gamma = (24.64 \pm 0.85)$ meV and is in accord with $\bar{\Gamma}_\gamma = (23.74 \pm 1.09)$ meV of ref. [1]. Both values are calculated in the same manner as reported in ref. [7] and the uncertainties given include a systematic error common to all resonances which in our case is ± 0.74 meV. The standard deviation for the frequency distribution in our case is given by $\sigma = (1.54 \pm 0.78)$ meV. We cannot reproduce the small $\bar{\Gamma}_\gamma = (19.1 \pm 1.6)$ meV which was obtained [3] from measurements with an underground nuclear explosion with the aid of the Γ_n -values of Garg et al. [2]. An indication that this mean $\bar{\Gamma}_\gamma$ -value may be too small lies in the fact, that the resonance integral computed with this mean width is by more than 10 barns too small as compared to the well-known experimental value [8].
As mentioned above, the data of Glass et al. [3] show a quasi-periodic variation of the radiative widths with neutron energy. Such a structure could be an indication for the influence of a second minimum of the potential energy surface as a function of deformation, which in other actinide elements has been shown to produce an intermediate structure in subthreshold fission cross sections. Although no subthreshold fission has been observed for ^{238}U, a second energy minimum could still produce an effect on the radiative widths, provided certain conditions concerning the magnitudes of the two humps of the fission barrier are fulfilled. Therefore, some interest is due to the question whether or not the structure observed by Glass et al. is real.
No evidence for such an intermediate structure in the total radiative widths was observed in the present experiment. Although in the data of table I there seems to be a slight increase of the radiative widths with neutron energy, the quasi-periodic structure of ref. [3] is clearly not reproduced up to 1 keV.

REFERENCES

[1] ASGHAR, M., CHAFFEY, C.M., MOXON, M.C., Nuclear Physics 85 (1966) 305.

[2] GARG, J.B., RAINWATER, J., PETERSEN, J.S., HAVENS, W.W., Jr., Phys. Rev. 134 (1964) B 985.

[3] GLASS, N.W., SCHELBERG, A.D., TATRO, L.D., WARREN, J.H., Neutron Cross Sections and Technology, Washington, Vol. 1 (1968) 573.

[4] WEIGMANN, H., CARRARO, G., BOCKHOFF, K.H., Nucl. Instr. 50 (1967) 265.

[5] CARRARO, G., KOLAR, W., Paper of this conference.

[6] FRÖHNER, F.H., General Atomic Report: GA-6906 (1966).

[7] ASGHAR, M., CHAFFEY, C.M., MOXON, M.C., PATTENDEN, N.J., RAE, E.R., UTTLEY, C.A., Nuclear Physics 76 (1966) 196.

[8] KÜSTERS, H., SCHMIDT, J.J., BROEDERS, C.H.M., EISEMANN, E., METZENROTH, M., SCHROETER, K.E., THIEM, D., KFK 793 (1968).

DISCUSSION

TO PAPERS IAEA-CN-26/17, 18

P. H. RIBON: I think it is better to compare the values of the capture resonance area (proportional to $\Gamma_n \Gamma_\gamma/\Gamma$) than the values of Γ_γ in the case of ^{238}U. This comparison shows an agreement between the Harwell and Los Alamos findings, whereas your values are higher by about 9%.

FISSION-CROSS-SECTION MEASUREMENT OF ^{233}U

M. G. CAO, E. MIGNECO, J. P. THEOBALD, M. MERLA
Central Bureau for Nuclear Measurements
EURATOM, Geel, Belgium

Abstract

FISSION-CROSS-SECTION MEASUREMENT OF ^{233}U.

The neutron-induced fission cross-section of ^{233}U has been measured in the energy range between 0.018 eV and 2 keV. Up to 80 eV, a spark-chamber fission-fragment detector has been used, the properties of which are described to some extent. From 10 eV up to 2 keV the data are taken with a fission neutron scintillator detector.

A multilevel fit has been performed for resonances below 65 eV. Resonance integrals are compared with results of other laboratories.

INTRODUCTION

The fission cross section of ^{233}U is of interest for the reactor design based on the thorium cycle [1]. As there are systematic discrepancies in the existing data [2], which seem to result from the normalization procedure, this measurement has been extended down to thermal neutron energies, where the cross section has been adapted to the value of 524.5±1.9 b recommended by the Sigma Centre of Brookhaven [3].

EXPERIMENTAL TECHNIQUE

The CBNM linear electron accelerator with its mercury cooled natural uranium target and polyethylene moderators served as the pulsed neutron source in the time-of-flight experiments. Two detector systems have been used. For the energy range between 0.018 eV and 80 eV a wire-to-plane spark chamber and from 10 eV to 2 keV a liquid scintillation neutron detector. The experimental lay-out is shown in figure 1.
The measurement with the spark chamber has been performed with uran-uranyl-acetate layers of 2 mg/cm^2 thickness and the following isotopic composition

^{232}U	0.01%
^{233}U	87.82%
^{234}U	0.84%
^{235}U	0.189%
^{236}U	0.001%
^{238}U	11.14%

The sample for the neutron detector is a metalic sheet of 3.18 x 7.65 cm^2 and a thickness of 222.5 mg/cm^2 and is canned in aluminium foils of 0.1

mm thickness. It has to be strongly depleted in ^{232}U because of the high γ-sensitivity of the scintillator liquid and is composed of

^{232}U < 0.6 ppm
^{233}U = 99.76%
^{234}U = 0.022%
^{235}U = 0.007%
^{236}U ≤ 1 ppm
^{238}U = 0.21%

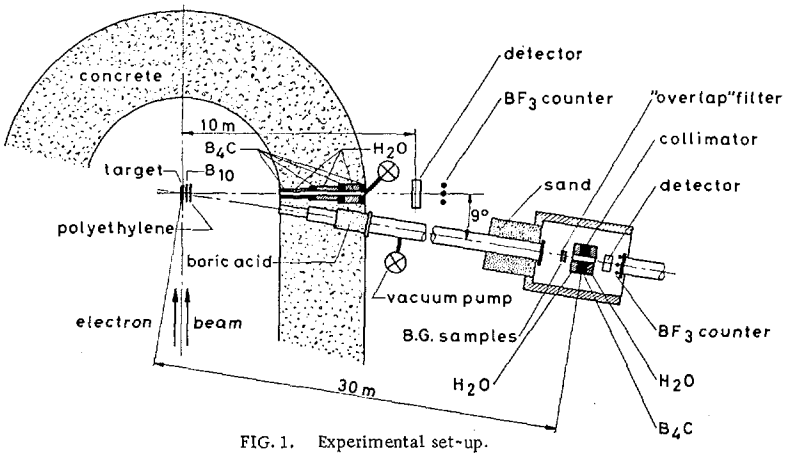

FIG. 1. Experimental set-up.

The data have been recorded either into a 4096 channel time-of-flight analyser equipped with an 'accordeon' allowing the subdivision of the 4096 channels into up to eight groups of different channel widths and different initial delay times, or into a 65536 channel analyser consisting of: fast logic units, a 10 ns time coder, a derandomizer and a magnetic tape address recorder. The measurement is composed of four runs, the parameters of which are shown in table I. The first row of the table indicates the neutron energy interval being finally taken out for the data evaluation. For the background measurement the black resonance technique has been applied. Banks of BF_3 counters with a diameter of one inch have measured and controlled the neutron spectra. The counting gas in the low energy range was natural boron-trifluoride at 40 Torr, in the higher energy range boron-10-trifluoride at 70 Torr.
In the special case of the first run supplementary experiments were necessary to study the influence of overlapping neutrons in the background correction due to the absence of the cut-off filter.

DETECTORS

The fission fragment detector

In order to extend the measurement down to thermal neutron energies low burst repetition rates and a short flight path of about 10 m are necessary to avoid overlap from preceding neutron bursts. Consequently

TABLE I. PARAMETERS OF THE TIME-OF-FLIGHT SPECTROMETER

	1st run	2nd run	3rd run	4th run
Neutron-energy range	0.018 - 0.68 eV	0.68 - 30 eV	30 - 52 eV	52 - 1200 eV
Detector type	spark chamber	spark chamber	liquid scintillator	liquid scintillator
Linac energy	55 MeV	62 MeV	60 MeV	55 MeV
Beam-peak current	400 mA	1800 mA	1500 mA	1200 mA
Neutron-burst width	1000 ns	100 ns	100 ns	70 ns
Burst frequency	40 Hz	220 Hz	280 Hz	300 Hz
Analyser-channel width	1280 ns	640 ns	160 ns	80 ns
Permanent background filters	W	Cd, Mo	Au, Mn	Co
Filter set for the background law	Cd, In, Au, W	Cd, Au, Mo	Au, W, Mo, Mn	Mo, Co, Mn, Na
Cut-off filter	none	Cd	B	B
Flight-path length	10.10 m	30.67 m	30.61 m	30.61 m
Moderator	polyethylene $20 \times 20 \times 2.4$ cm^3			

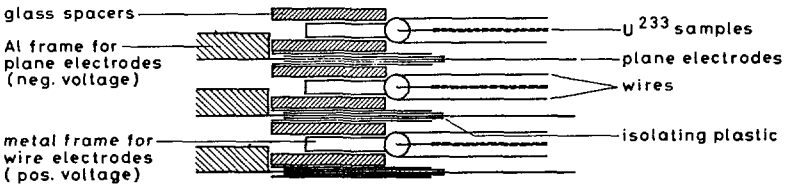

FIG. 2. Spark-chamber detector.

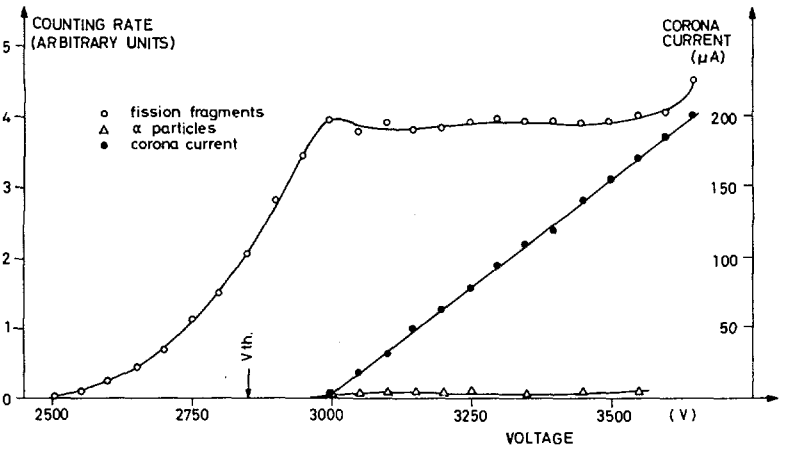

FIG. 3. Detector characteristics of the spark chamber.

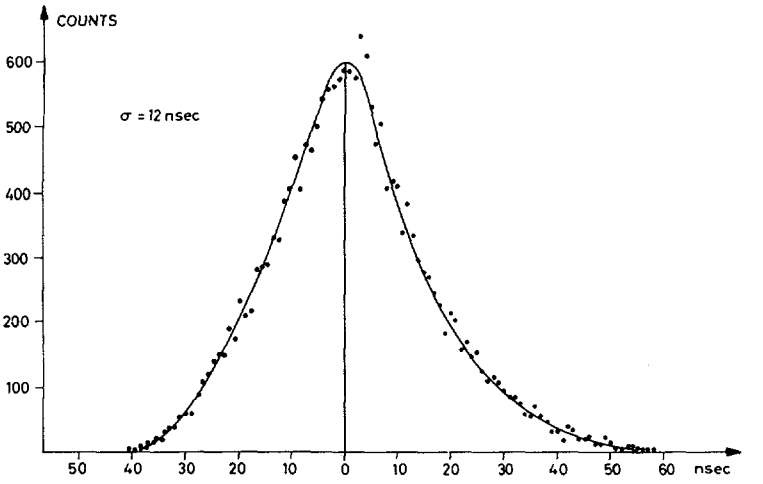

FIG. 4. Time-resolution function of the spark chamber.

the detector is exposed to a very strong gamma flash, which can seriously disturb its function. Therefore in the low energy run a spark chamber detector has been chosen, which is very insensitive to high gamma intensity and moreover to the high natural activity of the sample.

The detector used for this experiment consists of six wire-to-plane chambers each with a sensitive area of 20 x 20 cm^2 with electrosprayed ^{233}U samples (fig. 2). The gap between the wire and plane electrodes is 2 mm, the wire-to-wire distance is 3 mm and the wire diameter 0.15 mm. The plane cathodes are spanned 50 μ thick nickel plated aluminium foils. The electrodes are isolated with glass spacers.
In this construction the clamped assemblage of the six chambers has a thickness of 2.6 cm.
The detector is mounted in a vacuum tight aluminium box filled with pure nitrogene with a pressure of 250 Torr. The interelectrode voltage is 2750 V, which guarantees a negligible efficiency for the α particle background. The ^{233}U samples have a distance from the wire electrodes of 2 mm. The backings are spanned aluminium foils.

The general properties of this detector for time-of-flight experiments have been published [4]. Figure 3 shows the characteristic curve of the spark chamber obtained with a fission fragment source of ^{252}Cf with an activity of 32 fragments per second and a ^{241}Am α source with $1.2 \cdot 10^6$ α per second. The efficiency for fission fragments at the working voltage is 17%. The time jitter of the spark chamber has been measured using the γ-signal of a prompt ^{252}Cf fission event as zero time pulse. The result is shown in figure 4.

The fission neutron detector has been described elsewhere [5].

RESULTS

The fission cross section is determined from the raw data by a data reduction procedure published by M. G. Cao [6]. For the normalization of the fission cross section the expression for the relative fission/neutron ratio

$$\frac{1}{\Delta E}\int_{E_{th}-\frac{\Delta E}{2}}^{E_{th}+\frac{\Delta E}{2}} R(E)dE = \langle R(E)\rangle$$

has been calculated for different ΔE in the energy range between 0.019 eV and 0.031 eV. E_{th} is the thermal energy of 0.025 eV. It has been verified that the values vary within 5‰. With $\sigma_f(E_{th}) = 524.5 \pm 1.9$ barn [3] the relation

$$K\langle R(E)\rangle = \sigma_f(E_{th}) \cdot \sqrt{E_{th}}$$

yields the normalization constant K.

At thermal energies the subtracted background contribution measured with a Cd-filter in the neutron beam was 0.8%. The modification by overlapping neutrons during the first run after removing the Cd-filter has been measured in a seperate run. It turned out that the background law is not significantly affected by the addition or removal of the Cd-filter.

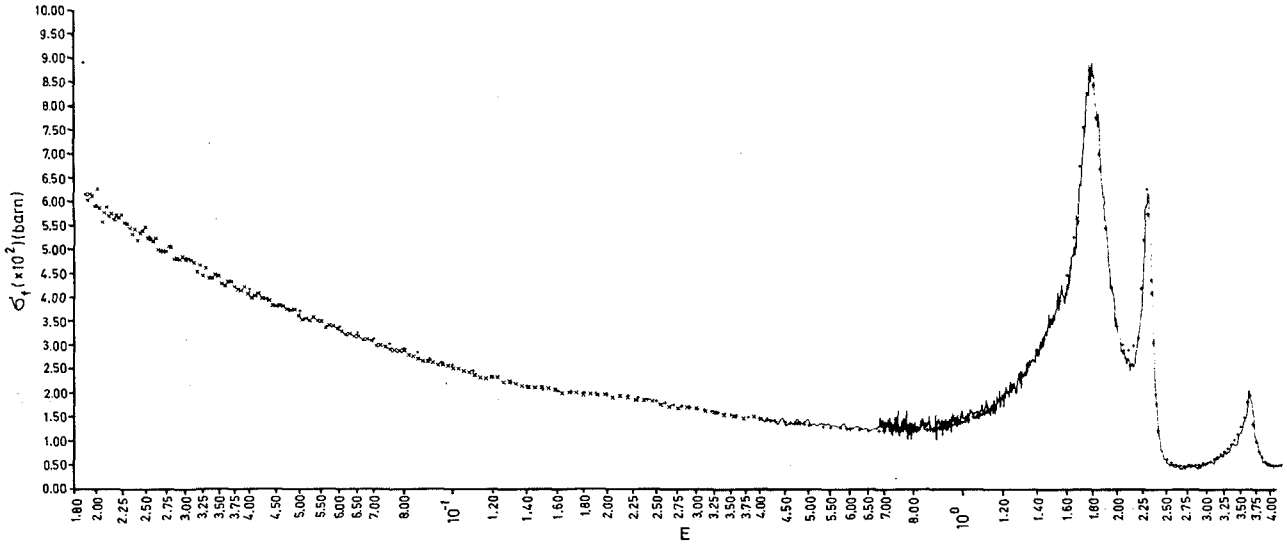

FIG. 5. Fission cross-section of ^{233}U between 0.018 and 4 eV together with recommended data [7].

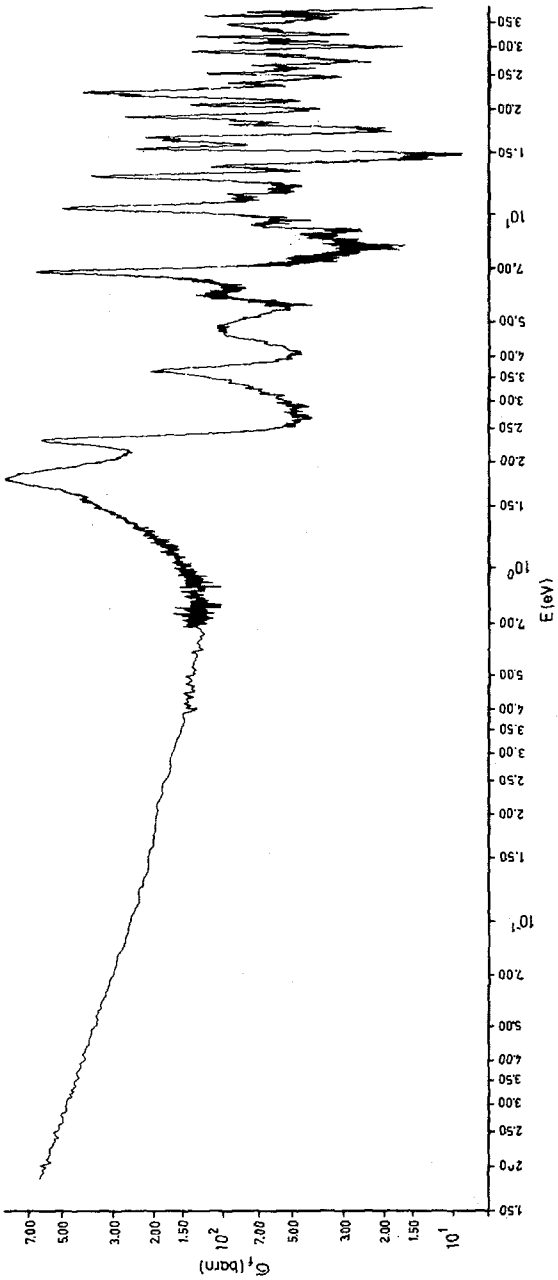

FIG. 6. Experimental fission cross-section of ^{233}U.

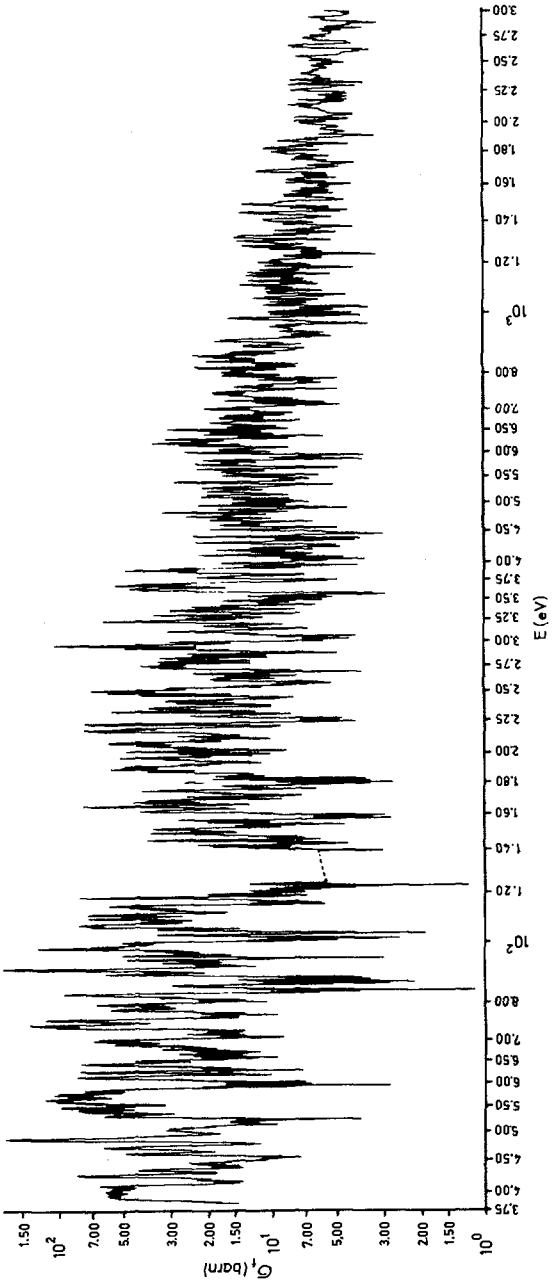

FIG. 7. Experimental fission cross-section of ^{233}U.

TABLE II. COMPARISON OF RESONANCE INTEGRALS FOR ^{233}U

$E_1 - E_2$ (eV)	$\int_{E_1}^{E_2} \sigma_f(E) \frac{dE}{E}$ (b)				
	Weston et al. (1968)	Brooks et al. (1966)	Nifenecker (1964)	Moore et al. (1960)	present data
0.414- 0.532	33.34	35.14		34.20	34.77
0.532- 0.68	30.54	32.29		31.47	32.14
0.68 - 0.875	28.84	30.84		29.53	30.61
0.875- 1.126	34.76	37.17		35.54	36.99
1.126- 1.444	56.61	53.87		54.63	59.48
1.444- 1.85	138.23	139.95		140.54	137.32
1.85 - 2.38	97.56	95.55	97.63	92.02	99.64
2.38 - 3.06	14.55	15.22	13.18	17.19	14.70
3.06 - 3.93	26.14	25.54	23.11	25.82	24.73
3.93 - 5.04	20.41	20.07	17.92	19.82	18.94
5.04 - 6.47	22.10	22.07	19.92	20.83	20.57
6.47 - 8.32	35.09	30.98	33.44	31.55	33.56
8.32 - 10.67	30.48	28.59	28.43	25.85	28.00
10.67 - 13.70	27.61		26.98	23.17	26.55
13.70 - 17.59	18.99		19.30	16.36	19.62
17.59 - 22.59	32.47		30.87	23.21	30.57
22.59 - 29.07	16.76		17.53	15.12	17.50
29.07 - 37.03	15.18		15.54	11.77	15.08
37.03 - 47.8	6.76		7.27	5.9	8.46
47.8 - 61.4	11.29		10.91	8.23	13.17
61.4 - 78.9	9.77			7.14	11.44
78.9 -101.2	8.74			6.51	7.83
166.9 -214.9	5.82			4.07	5.54
214.9 -275	5.51			4.59	5.57
275 -353	5.42			4.51	4.73
353 -453	3.65			3.77	3.50
453 -582	3.54			2.80	3.31
582 -748	3.84			3.17	3.40
748 -961	3.26				2.72
961 -1222	2.44				2.00

TABLE III. SURVEY OF RESONANCE INTEGRALS FOR ^{233}U

$E_1 - E_2$ (eV)	$\int_{E_1}^{E_2} \sigma_f(E) \frac{dE}{E}$ (b)				
	Weston et al.	Brooks et al.	Nifenecker	Moore et al.	present data
0.414 – 10.67	568.65	567.28		559.00	571.45
1.85 – 61.42			362.03		371.9
0.414-101.2	716.24			676.4	721.17
166.9 – 748	27.78			22.91	25.87
166.9 – 1222	33.48				30.59

The neutron spectrum has been corrected for self screening in the BF_3 counter filled with natural gas. These corrections are in the order of 1% at thermal energy.

A comparison with data points between 0.018 and 4 eV recommended by Drake [7] based on the results of Moore et al [8] are shown in figure 5.

The cross section spectrum obtained is shown in figures 6 and 7. The resonance integrals $\int \sigma_f(E) \frac{dE}{E}$ are shown in tables II and III together with results of other laboratories. The statistical error in the peaks is about $\pm$ 3% between the resonances about 20%.

Self screening and multiple scattering corrections are neglected. This is justified for the spark chamber data. For the neutron detector data above 30 eV the self absorption effect is of importance at the peaks of the highest resonances. This effect will lower the resonances at 32.0, 36.5 and 48.7 eV about 4%.

Moreover the self screening and multiple scattering can be the reason for cross normalization uncertainties. To keep these errors as small as possible, the large overlap of the spark chamber and neutron detector spectra has been utilized to perform the cross normalizations in energy ranges, where self absorption and multiple scattering corrections are less than about 2%. The error due to background contributions is negligible besides the statistical error, if the assumption is right that between the black resonances the background law can be interpolated with smooth analytical functions of the polynomial type.

For the high energy run used from 52 eV - 1.2 keV the fission neutron detector has been applied because of the higher counting rate. This run is normalized with the spark chamber data between 47 and 78 eV.

The third run from 20 to 60 eV was used to fill the gap due to the permanent Mo black resonance in the spark chamber run and it was normalized with the low energy spectrum from 20 to 37 eV.

What concerns the comparison with the results of other laboratories, one can say the following:

The agreement of the integral taken over the range from 0.4 to 100 keV between present result and that of the Oak Ridge group is within 1% [9]. Between 0.4 and 10.5 eV Brooks' result [10] agrees within 1% with these data, while Nifenecker's integral is about 2% lower [11].

TABLE IV. RESONANCE PARAMETERS OF ^{233}U

μ (eV)		ν (eV)		$G_f(beV^{3/2})$		$H_f(beV^{3/2})$	
ORNL*	CBNM	ORNL	CBNM	ORNL	CBNM	ORNL	CBNM
-2.79	-2.790	0.37	0.370	-1511.99	-1514.986	-513.24	-521.078
0.180	0.180	0.07	0.070	-0.190	-0.190	-0.830	-0.830
1.43	1.598	0.35	0.495	66.91	147.741	-31.81	-26.875
1.78	1.800	0.12	0.092	111.08	79.521	-1.78	-1.024
2.29	2.307	0.05	0.041	42.47	34.867	17.64	12.311
3.29	3.040	0.51	0.420	36.93	-14.624	-42.08	-34.259
3.63	3.657	0.08	0.103	20.91	23.992	7.23	8.730
4.53	4.750	0.39	0.390	44.29	56.798	-51.91	-23.455
5.74	5.810	0.18	0.210	11.04	16.120	-24.25	-26.671
6.80	6.856	0.09	0.091	168.68	1.283	35.89	0.240
7.5	7.450	0.11	0.251	5.93	13.155	2.23	1.221
8.67	8.860	0.26	0.412	15.01	45.952	4.05	20.862
9.15	9.180	0.15	0.200	17.63	13.691	-15.41	-36.038
10.35	10.420	0.16	0.162	276.95	263.003	7.65	-8.185
11.2	11.210	0.27	0.300	41.21	42.445	-4.76	-19.462
12.76	12.860	0.16	0.166	226.13	221.875	44.65	37.340
13.51		0.14		-12.21		4.42	
13.63	13.760	0.24	0.200	101.85	70.416	3.03	4.577
15.28	15.400	0.12	0.094	118.4	99.618	-33.36	-29.328
16.15	16.460	0.22	0.220	106.78	210.856	7.14	142.435
16.51	16.540	0.13	0.080	97.21	13.088	17.74	-83.245
17.92	18.110	0.10	0.100	37.37	35.860	4.27	13.040
18.46	18.580	0.25	0.260	78.36	138.367	20.69	17.923
18.86	19.000	0.15	0.150	213.21	173.698	-61.33	-94.971
20.53	20.620	0.21	0.205	116.58	125.0	6.91	-20.31
21.85	21.950	0.13	0.114	131.87	123.2	95.43	49.97
22.23	22.380	0.24	0.220	545.37	492.40	-90.62	-33.67
22.94	23.040	0.38	0.380	96.53	170.95	-6.68	1.234
23.54	23.640	0.33	0.315	61.03	48.730	-95.86	-125.0
25.13	25.270	0.19	0.190	85.0	84.040	-44.81	-48.650
26.57	26.700	0.28	0.230	58.7	60.270	19.73	22.44
28.42	28.480	0.28	0.260	29.85	43.420	86.46	54.37
28.91	29.080	0.31	0.310	233.67	225.30	-62.48	-32.29
29.68	29.750	0.11	0.110	-0.16	0.679	13.34	16.606
30.15	30.200	0.10	0.105	2.27	-0.068	-0.61	1.632
30.76	30.810	0.15	0.140	52.79	57.09	51.39	41.620
31.20	31.270	0.47	0.470	149.57	123.0	-72.18	-85.67
31.97	32.030	0.15	0.150	113.99	102.30	6.79	6.781
32.74	32.800	0.43	0.430	42.61	17.95	-96.58	-98.84
34.03	34.100	0.66	0.660	112.79	40.85	26.7	73.87
34.53	34.590	0.42	0.420	168.73	209.1	21.71	65.79
35.19	35.200	0.12	0.155	27.07	42.17	-8.85	-12.068
35.49	35.550	0.16	0.190	10.72	25.095	-24.48	-33.81
36.52	36.500	0.09	0.085	59.13	75.57	11.5	-10.46
37.46	37.470	0.19	0.218	64.0	88.93	14.4	19.42
39.48	39.480	0.22	0.300	67.55	90.164	76.24	116.940
39.71	39.710	0.11	0.160	34.07	47.736	-27.73	-26.458
40.15	40.150	0.45	0.460	97.39	156.800	-80.0	-101.442
41.08	41.080	0.10	0.100	19.88	33.903	13.37	15.608
	41.900		0.400		16.117		7.380
42.62	42.600	0.11	0.160	62.23	99.103	15.86	0.629
43.47	43.450	0.13	0.146	32.49	45.692	6.16	-10.375
44.70	44.480	0.56	0.339	93.00	38.679	36.62	-13.902

TABLE IV (cont.)

μ (eV)		ν (eV)		G_f(beV$^{3/2}$)		H_f(beV$^{3/2}$)	
ORNL*	CBNM	ORNL	CBNM	ORNL	CBNM	ORNL	CBNM
45.21	45.300	0.25	0.050	1.91	-0.806	-23.98	0.875
45.99	46.070	0.12	0.070	33.33	32.437	-26.17	-8.864
47.17	47.270	0.23	0.230	75.74	90.760	-9.08	30.471
48.64	48.670	0.13	0.130	167.38	200.033	-21.20	-12.940
49.12	49.000	0.09	0.300	9.68	19.330	-6.64	-0.949
50.21	50.300	0.45	0.400	55.75	51.313	-31.14	4.922
50.99	51.150	0.38	0.200	16.84	4.937	-4.13	18.371
51.95	51.905	0.62	0.620	12.00	53.557	-41.84	34.837
52.93	53.000	0.22	0.230	53.45	91.480	-62.43	-36.482
53.97	54.000	0.14	0.150	61.95	90.750	-25.09	-14.953
54.77	54.770	0.09	0.090	61.08	80.866	6.13	7.288
56.09	56.090	0.27	0.270	69.62	106.698	128.22	146.752
56.35	56.440	0.30	0.270	211.98	225.687	-60.39	-31.019
57.48	57.500	0.49	0.460	282.72	345.336	20.92	8.529
58.51	58.510	0.23	0.250	91.51	117.092	26.41	2.895
61.30	61.350	0.40	0.375	185.51	233.236	47.48	53.202
62.50	62.520	0.20	0.098	107.86	96.786	-14.96	-14.487
	64.080		0.500		282.465		57.830
64.30	64.300	0.40	0.257	228.02	58.479	-22.05	-126.008
	64.770		0.106		-20.249		-33.864

* ORNL-TM-1751 Report

At energies higher than 100 eV the present data tend to be lower than those of the Oak Ridge group.
The cross section integrals $\int \sigma_f(E)dE$ of Bergen et al [2] are 40% higher than the present results.

EVALUATION

For reactor calculations it is of importance to have the resonance parameters in a form to reproduce the fission cross section at different temperatures by the application of conventional Doppler broadening corrections. For this reason it is convenient to analyse the data with the multilevel formalism of D. B. Adler and F. T. Adler [12], where the fission cross section is given by the expression

$$\sigma_f = g \cdot \frac{\pi}{k^2} \cdot \sum_i \frac{G_i + (\mu_i - E)H_i}{(\mu_i - E)^2 + \nu_i^2}$$

which has a structure like a sum of Wigner's single level terms, but μ_i and ν_i are modified level energies and widths. In fact μ_i and ν_i are the resp. real and imaginary parts of complex quantities c_i representing in a generalized Kapur-Peierls-formalism the complex poles of the collision matrix. *The coefficients* G_i *and* H_i *describing* the symmetric and asymmetric components in the resonances are functions of the resonance parameters only [13].
The results of this analysis are given in table IV. The fit obtained is shown in figures 8 - 11.

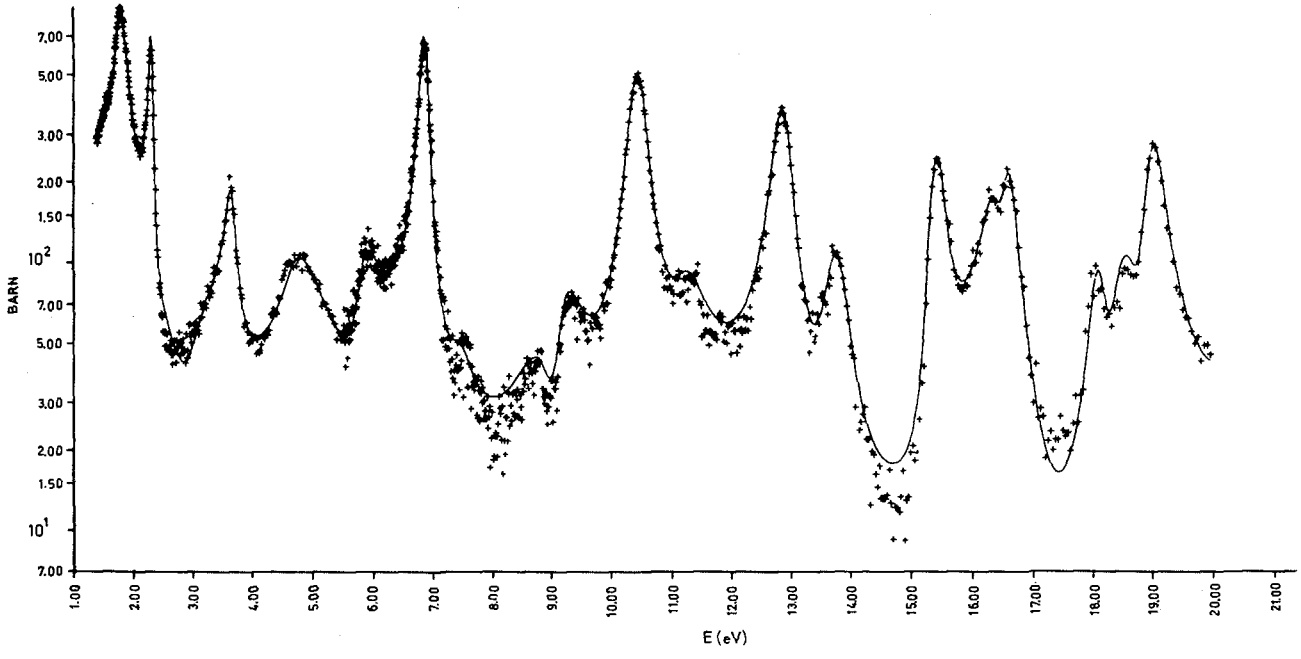

FIG. 8. Analytical fit between 1.39 and 20 eV.

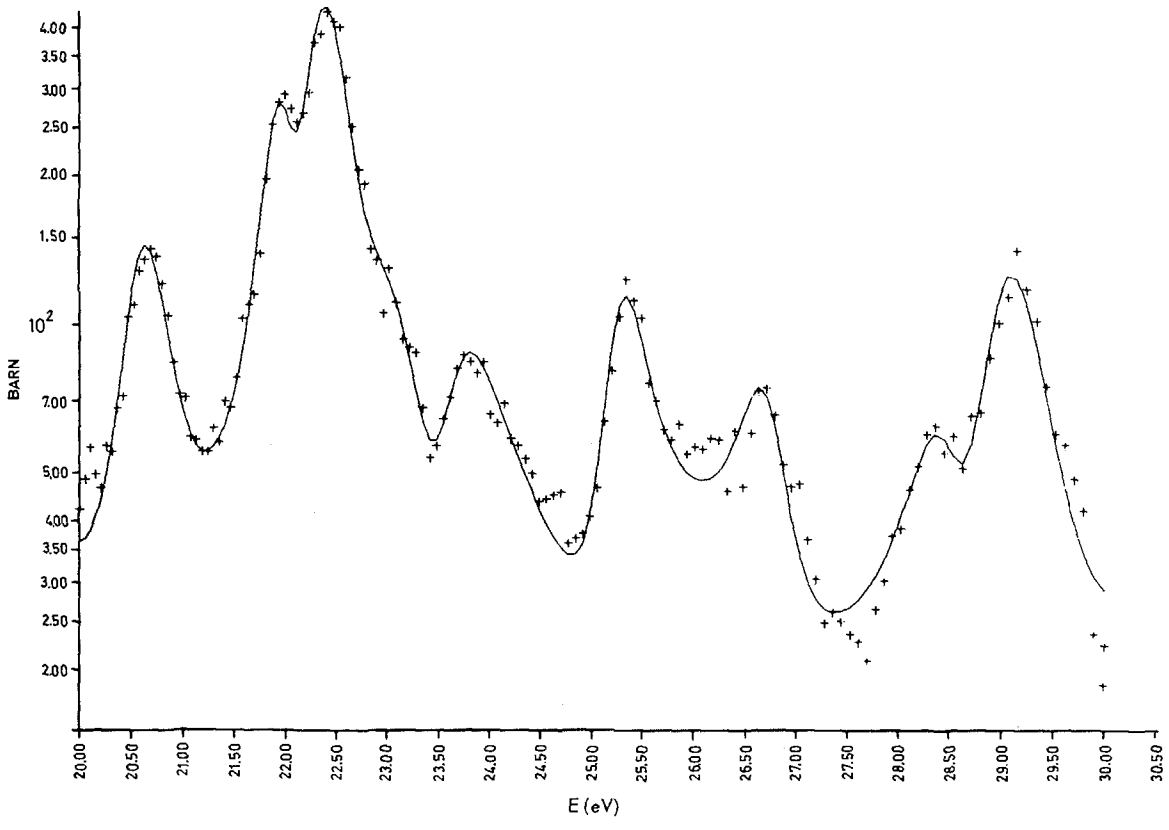

FIG. 9. Analytical fit between 20 and 30 eV.

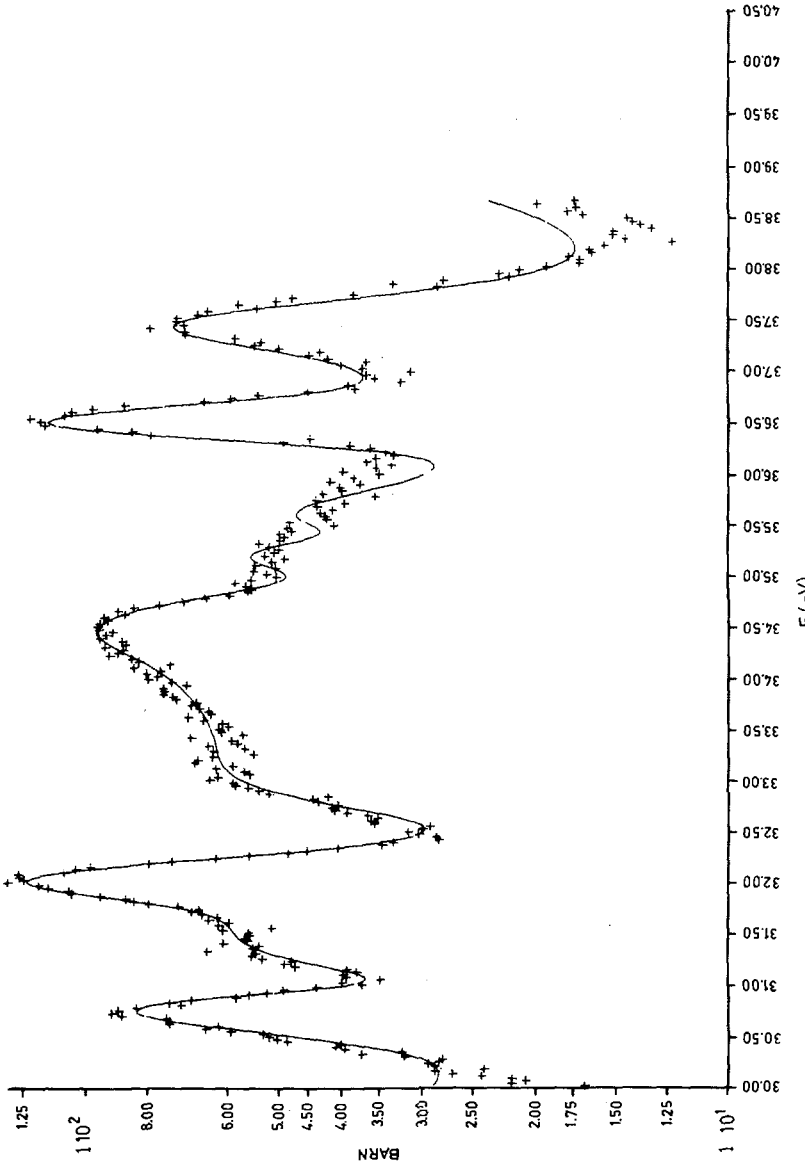

FIG. 10. Analytical fit between 30 and 38.7 eV.

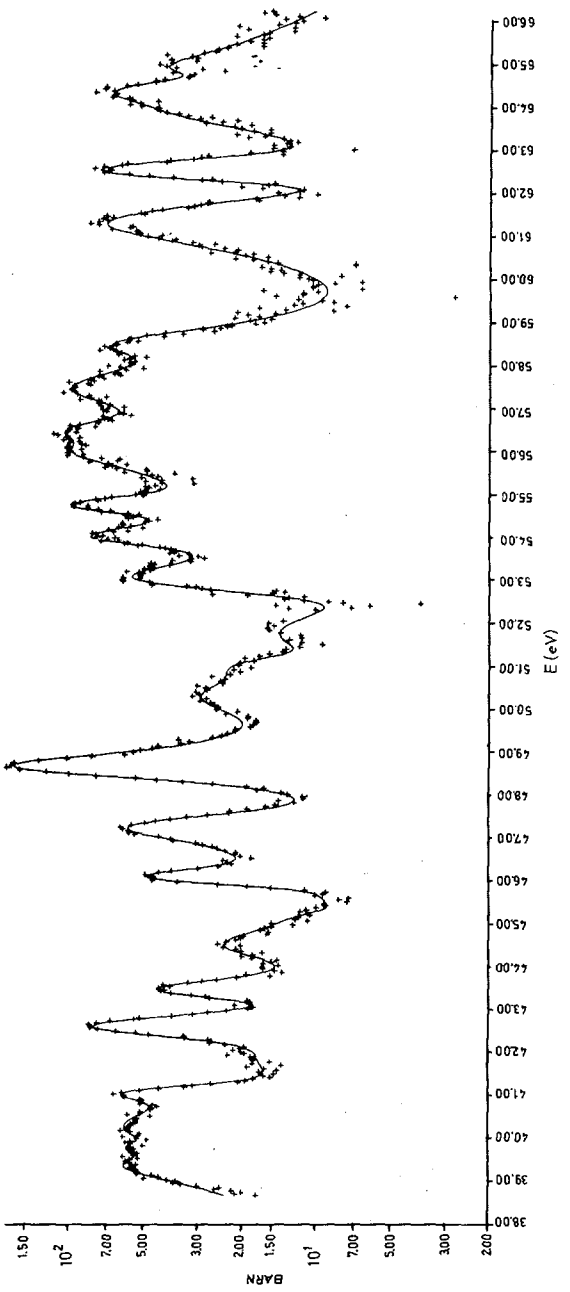

FIG. 11. Analytical fit between 38.7 and 66.2 eV.

The type of resonance analysis used for this evaluation does not give one unique set of resonance parameters, if like in the present case only one partial cross section measurement is analysed. In table IV is listed this set of parameters, which is the nearest to that of de Saussure [15], who has evaluated fission and capture cross section data with the same method simultaneously.
For comparison the Oak Ridge results are given in table IV too.
An autocorrelation analysis, which yielded a periodical correlogram in the case of the ^{235}U neutron induced fission cross section [14], gives in the case of $^{233}U(n, f)$ insignificant serial autocorrelation coefficients and the correlogram has no periodicity. From this result, one can deduce that either the ^{233}U fission cross section has no intermediate structure in subthreshold fission channels or that the actual spacings of possible intermediate levels are too randomly distributed inside the finite statistical sample given by the present ^{233}U fission cross section.

ACKNOWLEDGEMENT

The authors are indebted to the CBNM target preparation group for the preparation of the spark chamber samples. Special thank is due to the U.S.A.E.C., which put the very pure neutron detector sample at their disposal. The support of the experiments by Dr. J. Spaepen and Mr. K.H. Böckhoff is acknowledged.

REFERENCES

[1] SCHWARZ, S., HÄUSSERMANN, H., RENDA Compilation of EANDC Requests, EANDC Rep. 78 AL (1968).
[2] BERGEN, D.W., SILBERT, M.G., Phys.Rev. 116 (1968) 1178 and Report LA-3586, Los Alamos.
[3] STEHN, J., GOLDBERG, M.D., WIENERCHASMAN R., MUGHABGHAB, S.F., MAGURNO, B.A., MAY, V.M., Neutron Cross Sections, Report BNL 325 III (1965) page 92 - 233 - 2, Brookhaven.
[4] MIGNECO, E., THEOBALD, J.P., MERLA, M., Report EUR.4077.e (1968).
[5] CAO, M.G., MIGNECO, E., THEOBALD, J.P., WARTENA J.A., WINTER, J., Journal of Nucl. Energy 22 (1968) 211.
[6] CAO, M.G., Report EUR.3652.f (1967).
[7] DRAKE, M.G., Report G.A.-2076, General Atomic San Diego (1966).
[8] MOORE, M.S., MILLER, L.G., SIMPSON, O.D., Phys.Rev. 118 (1960) 714.
[9] WESTON, L.W., GWIN, R., de SAUSSURE, G., INGLE, R.W., FULLWOOD, R.R., HOCKENBURY, R.W., Report ORNL-TM-1751, Oak Ridge, see also Nucl.Sci.and Engng. 34 (1968) 1.
[10] BROOKS, F.D., Report AERE-M-1709, Harwell (1966).
[11] NIFENECKER, H., et al., J. de Physique 23 (1963) 254 and NIFENECKER,H., J. de Physique 25 (1964) 877.
[12] ADLER, D.B., ADLER, F.T. Report COO 1546-3, University of Illinois, Urbana (1966).
[13] ADLER, D.B., ADLER, F.T., A simple approach to the multilevel-multichannel formalism, University of Illinois, Urbana (1962).
[14] CAO, M.G., MIGNECO,E., THEOBALD, J.P., Physics Letters 27B (1968) 409.
[15] de SAUSSURE, G., Report ORNL-4280, Oak Ridge (1968).

NEUTRON-INDUCED FISSION CROSS-SECTION OF ^{241}Pu

E. MIGNECO, J.P. THEOBALD, J.A. WARTENA
Central Bureau for Nuclear Measurements,
EURATOM, Geel, Belgium

Abstract

NEUTRON-INDUCED FISSION CROSS-SECTION OF ^{241}Pu

A time-of-flight experiment has been performed to measure the neutron-induced fission cross-section for neutrons of energies in the range 2 - 2000 eV. The CBNM linear accelerator with a mercury-cooled uranium target served as pulsed neutron source. The nominal resolution of the time-of-flight spectrometer was 20 ns/m between 2 and 46.5 eV and 2ns/m at higher energies. The fission events were detected by a liquid scintillation neutron detector.

The reduced data are presented together with a set of resonance integrals, which are compared with results from other laboratories.

INTRODUCTION

The compilations of partial fission resonance integrals, which were published in the last years by G. D. James and M. G. Schomberg [1] and H. H. Hennies [2], show that there exist still considerable discrepancies in the cross section data of the $^{241}Pu(n, f)$ reaction in the resonance region. Therefore reactor physicists ask still for this cross section in the compilation of EANDC requests for neutron data measurements with a high priority [3]. This is one reason why the fission cross section of ^{241}Pu has been remeasured with the CBNM time-of-flight spectrometer. Another reason is that the interesting structure of this cross section (Fig. 2) and the typical distribution of the fission width of the resonances had invited already since some years the physicists to study the multichannel character of the fission process on just this isotope [4].

EXPERIMENTAL TECHNIQUE

The experimental set up is shown in figure 1. The fission neutron scintillator detector as well as details of the collimation system have been described elsewhere [5]. For the experiment on ^{241}Pu the electronic circuits of the detector have been refined by a pile-up rejection system against γ-induced pulses passing through the pulse shape discriminators.
The characteristic parameters of this time-of-flight experiment are given in table I.
The samples were in the low energy range 25 mg/cm^2 in the high energy range 100 mg/cm^2 Pu oxide layers immediately prepared after ^{241}Am seperation. The isotopic composition, as determined by ORNL, was the following:

^{238}Pu	0.008%	($\leq$ 0.009%)	^{241}Pu	94.474%	(94.658%)
^{239}Pu	0.0832%	(0.868%)	^{242}Pu	1.49%	(1.497%)
^{240}Pu	2.93%	(2.968%)	^{244}Pu	< 0.0001%	

chemical impurities $\leq$ 0.318%

in brackets are given the values as determined by the CBNM.

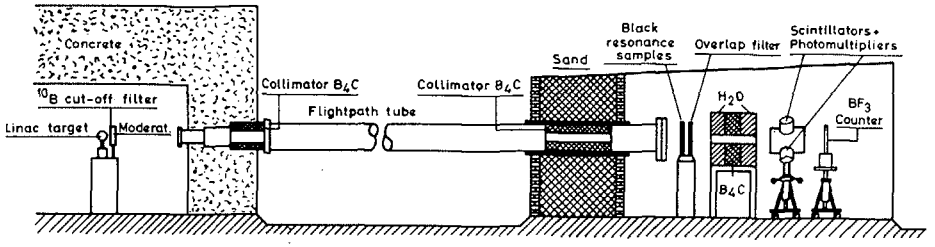

FIG. 1. Experimental set-up.

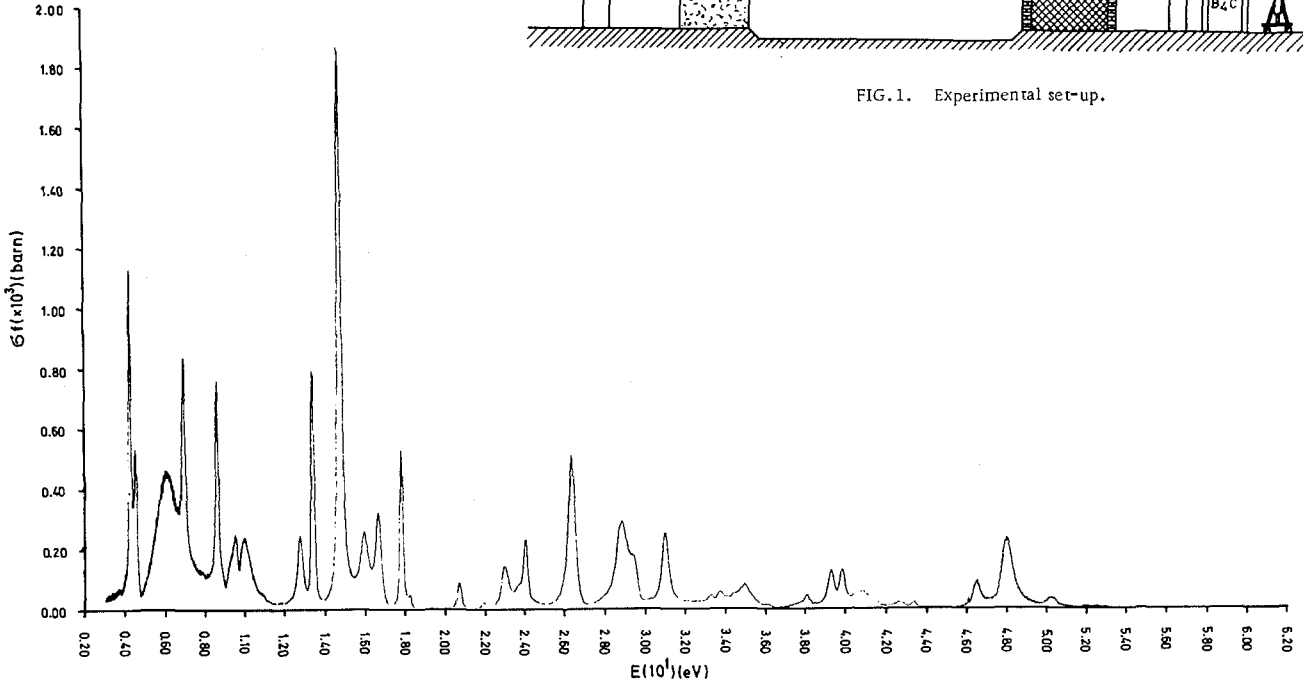

FIG. 2. Experimental fission cross-section.

TABLE I. CHARACTERISTIC PARAMETERS OF TIME-OF-FLIGHT EXPERIMENT

	Low energy	High energy
Energy range (effective)	2 - 46.5 eV	46.5 - 2000 eV
Linac energy	50 MeV	50 MeV
Burst width	600 ns	50 ns
Burst frequency	100 Hz	400 Hz
Analyser channel width	320 ns	40 ns
Permanent filter	In	In
Filter for background law	In, Ta, W, Mo, Co	Mo, Co, Mn, Na
Cut-off filter	B_4C	^{10}B
Flight path length	30.617 m	30.617 m
Moderator	polyethylene 20 x 20 x 2.4 cm^3	

MEASUREMENT

The measurement is performed in two runs, one for low energy neutrons from 2 to 46.5 eV and one for higher neutron energies up to 2000 eV. Each run consists of two parts, in the first one the fission yield and the neutron spectrum are recorded with a permanent resonance filter in the neutron beam for the normalization of the following background measurements. In the second part the background law is determined with the same set-up but with several resonance filters.

The time-of-flight analysers are described in another paper of this conference [6].

RESULTS

The fission cross section has been calculated from the raw data with the following expression

$$\sigma_f \sqrt{E} = \text{Normalization constant} \cdot \frac{\text{fission yield - background}}{\text{neutron rate - background}}$$

where the neutron spectrum is the result of a least square fit to the experimental data with polynomials. The background rates on the fission yield and the neutron spectrum have been determined with the "black resonance method" and expressed by smooth analytical curves.

The resulting cross section of this experiment is shown in figures 2 to 4 on a linear scale and in order to present more clearly the residual fission cross section between the resonances in figures 5 and 6 on a logarithmic scale.

The cross section has been normalized by equating the partial fission resonance integral $\int_{4.65\,eV}^{10\,eV} \sigma_f(E)\frac{dE}{E}$ to the value of 193.6 barn recommended by H. Hennies [2]. This normalization procedure does not exclude the possibility of a systematic error, because there exists a lack of up-to-date measurements of the fission cross section between thermal neutron energies and some eV.

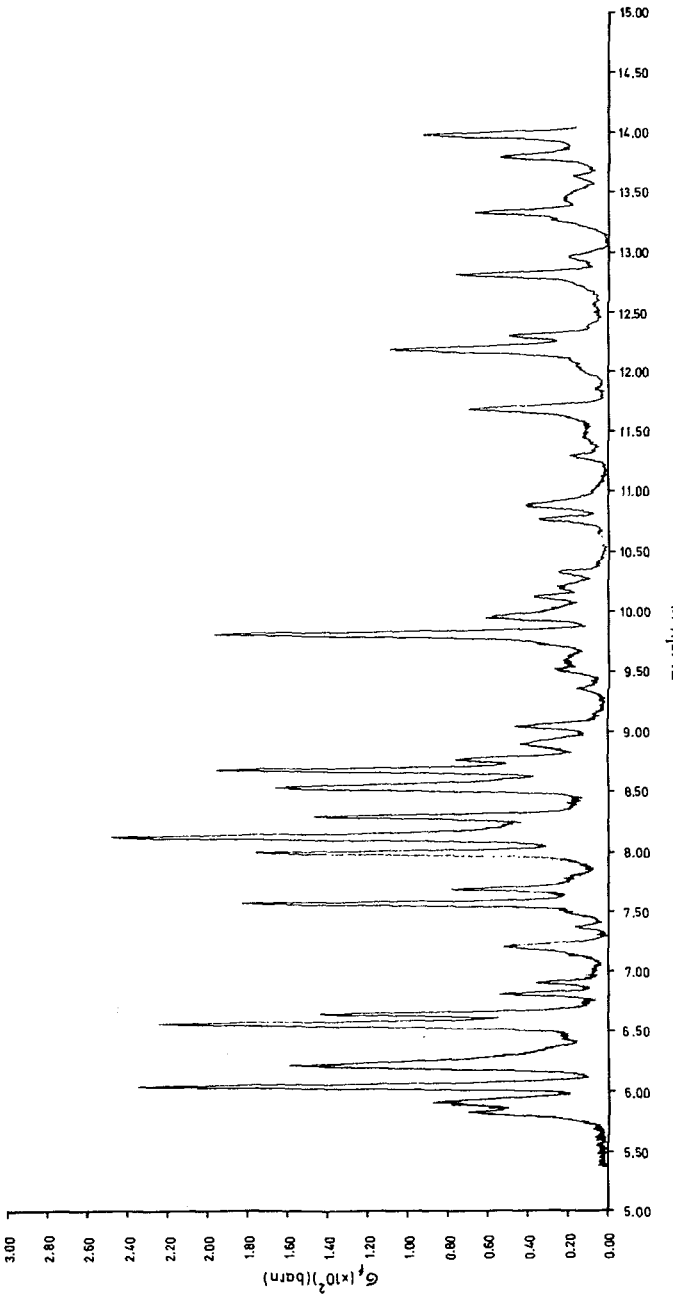

FIG. 3. Experimental fission cross-section.

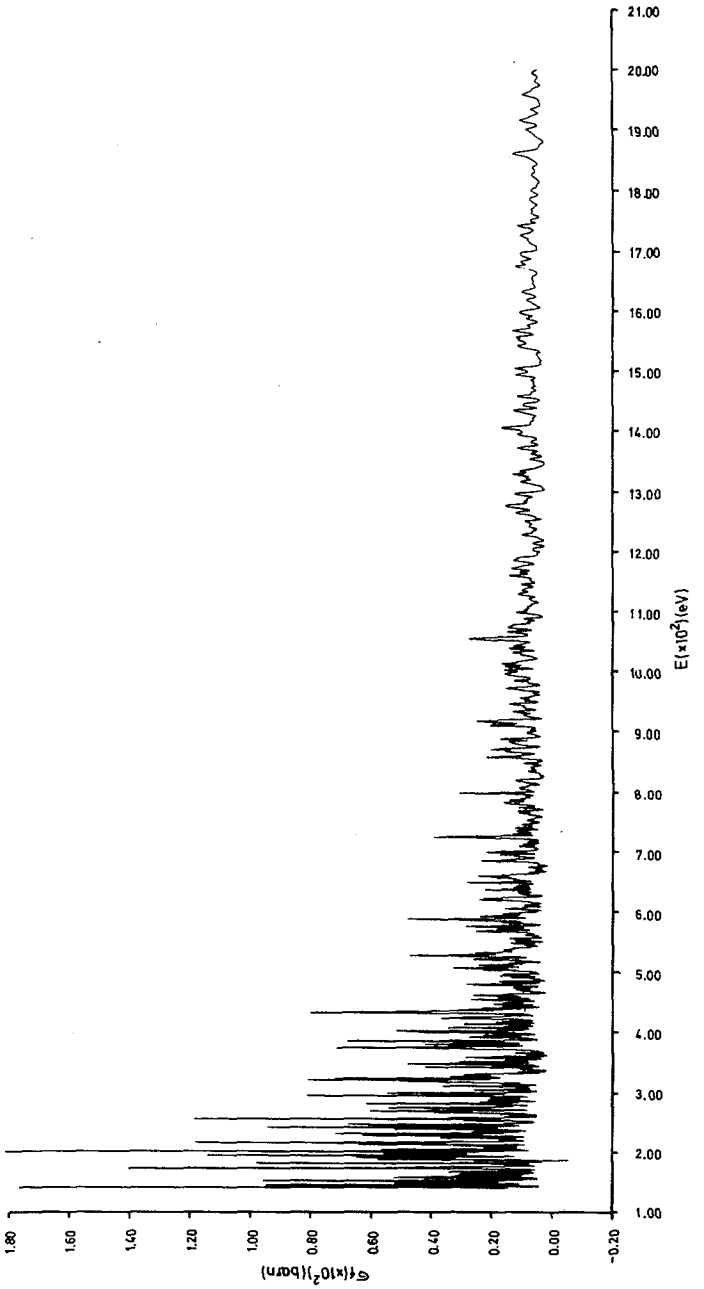

FIG. 4. Experimental fission cross-section.

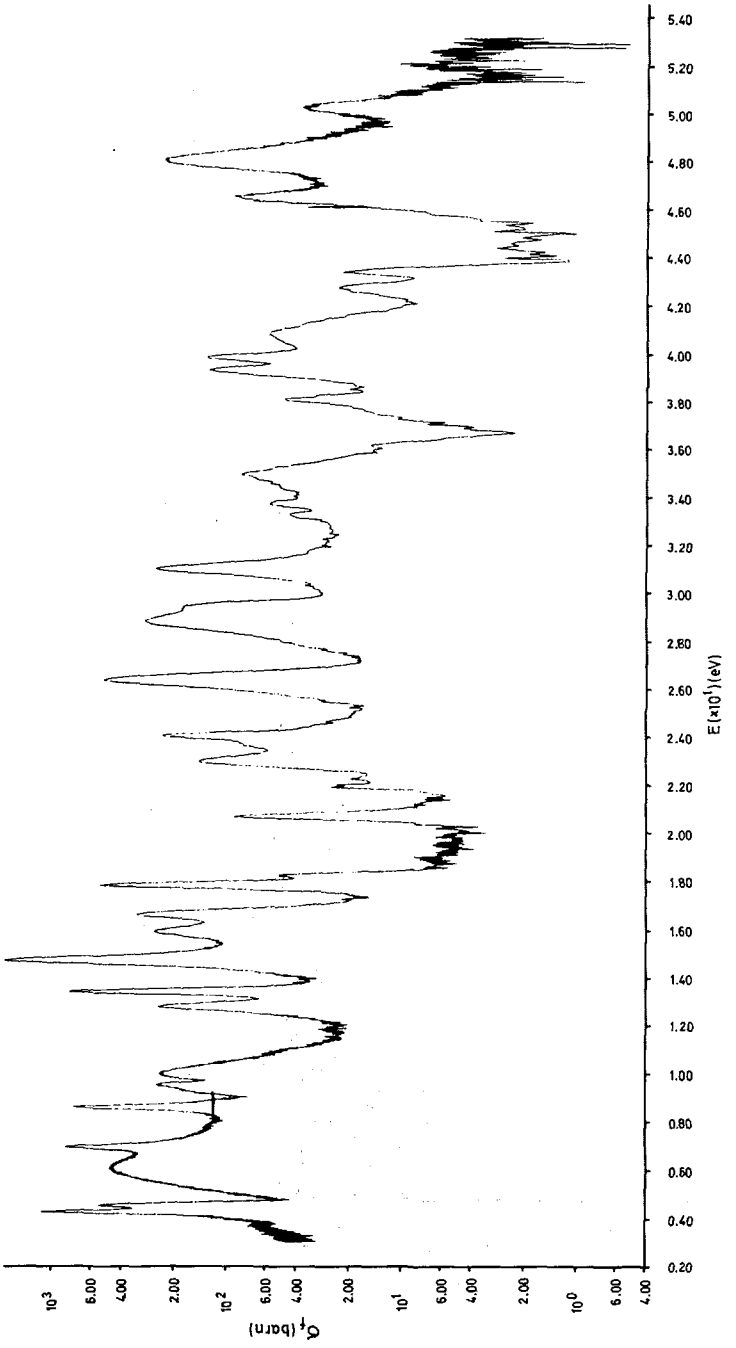

FIG. 5. Experimental fission cross-section.

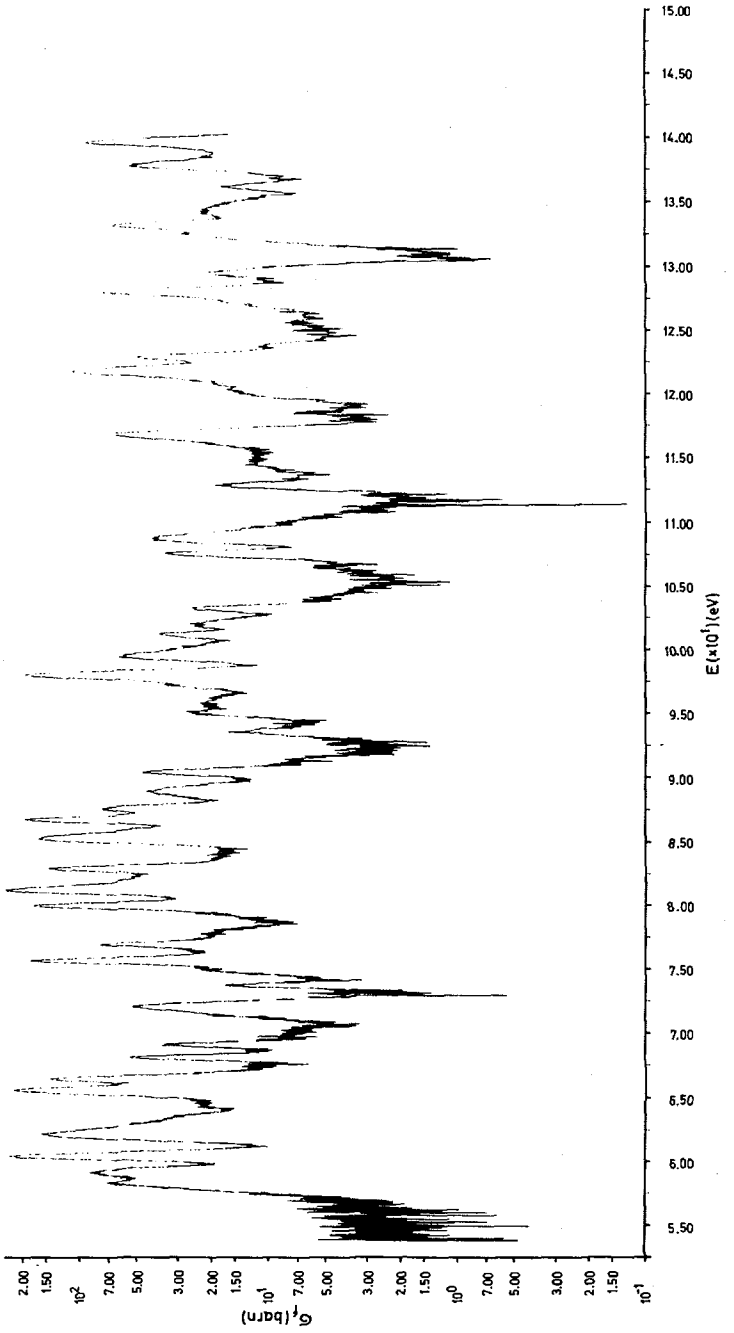

FIG. 6. Experimental fission cross-section.

TABLE II. FISSION RESONANCE INTEGRAL FOR ^{241}Pu IN BARNS

Energy limits (eV) High	Low	CCCP [9]	RPI [4]	RPI [4]	HAR [7]	HAR [7]	LASL [8]	MTR [8]	CBNM
20 000	10 000						2.351		
10 000	9 000						0.3364		
9 000	8 000						0.4408		
8 000	7 000						0.4975		
7 000	6 000						0.6963		
6 000	5 000						0.7846		
5 000	4 000						1.133		
4 000	3 000						1.834		
3 000	2 000						2.626		
2 000	1 000				6.612		6.014		5.43
1 000	900				1.125		1.053		1.024
900	800				1.102		1.101		0.98
800	700				1.468		1.306		1.27
700	600				1.788		1.687		1.54
600	500				3.044		3.195		2.63
500	400				4.621		4.754		3.36
400	300				6.382		6.776		5.26
300	200				12.06		13.11		10.76
200	100				18.44		18.95		16.44
100	90				3.439		2.951	3.568	2.87
90	80		8.607	9.680	10.44		8.394	10.50	8.15
80	70		5.015	5.831	3.871		4.070	5.316	3.81
70	60		10.42	10.51	13.69		8.096	10.62	8.85
60	50		4.836	5.057	3.389		2.817	3.734	2.96
50	40	10.88	10.81	10.62	9.168		7.674	9.902	7.98
40	30	21.54	13.86	14.73	13.67		11.30	15.10	13.58
30	20	19.21	33.00	33.98	32.58	30.35	27.78	35.27	31.69
20	10	113.2	108.40	102.5	105.8	102.1			102.2

The cross normalization between the low and high energy run has been done in the energy range between 21.7 and 30.2 eV by equalizing the integrals $\int \sigma_f(E)dE$. The possible error introduced by this can be about 2%. In table II are listed the resonance integrals of different laboratories and of this experiment. The data of column 1 to 7 are taken from the compilation of G. D. James and M. G. Schomberg.

The integrals of the present data agree up to 40 eV with the Harwell data and between 30 and 100 eV with the LAS data relatively well. In the range from 100 eV to 600 eV the present resonance integrals are considerably

TABLE III. AVERAGE FISSION CROSS-SECTION FOR ^{241}Pu IN BARNS

Energy limits (eV)		CEN [10]	CBNM
High	Low		
300	200	27.41	26.08
200	100		24.98
100	90	25.98	27.7
90	80	66.72	68.55
80	70	26.13	28.94
70	60	55.67	56.45
60	50	16.60	16.80
50	40	40.24	36.54
40	30	46.91	46.50
30	20	81.37	82.86
20	10	148.37	146.82

lower than the two comparative results from Harwell and LAS. From 600 to 2000 eV the agreement tends to be better. The strong discrepancies of certain resonance integrals can hardly be explained by isotopic or chemical impurities in the samples of the different experiments.

A comparison of the average cross section with preliminary results of Saclay [10] shows up to 200 eV a good agreement, as is seen from table III.

ACKNOWLEDGEMENT

We wish to thank our sample preparation group for the preparation and purification of the sample, and the USAEC for the loan of the ^{241}Pu material.

REFERENCES

[1] JAMES, G. D., SCHOMBERG, M. G., Report AERE-M 2157 (1969)
[2] HENNIES, H. H., IAEA Conference on Nuclear Data for Reactors, Paris 1966, Proceedings, 333 (1967).
[3] SCHWARZ, S., HÄUSSERMANN, W., Report EANDC 78 "AL" (1968).
[4] MOORE, M. S., SIMPSON, O. D., WATANABE, T., RUSSEL, J. E., HOCKENBURY, R. W., Phys. Rev. 135 (1964) 945.
[5] CAO, M. G., MIGNECO, E., THEOBALD, J. P., WARTENA, J. A., WINTER, J., J. of Nucl. Energy 22 (1968) 211.
[6] CAO, M. G., MIGNECO, E., THEOBALD, J. P., MERLA, M., this conference.
[7] JAMES, G. D., Nucl. Phys. 65 (1965) 353.

[8] MOORE, M.S., Report IN 1222 (1969)
and SIMPSON, O.D., FLUHARTY, R.G., MOORE, M.S., MARSHALL, N.H., DIVEN, B.C., HEMMENDINGER, A., Proceedings of the Conference on Neutron Cross Section and Technology, Washington, Vol. II, 910 (1966).
[9] ADAMCHUK, Y.B., GERASIMOV, V.F., YEFIMOV, B.V., ZENKEVICH, V.S., MOSTOVOI, V.J., PEVZNER, M.J., CHERNYSHOV, A.A., TSITOVICH, A.P., Proceedings of the Intern. Conf. on Peaceful Uses of Atomic Energy, Geneva, 216 (1956).
[10] BLONS, J., private communication (1970).

DISCUSSION

TO PAPERS IAEA-CN-26/16, 19, 95

P. H. RIBON: Do you have any idea of the number or percentage of levels of ^{233}U which you have not identified?

J. P. THEOBALD: No, I do not, because the analysis of the CODILLI programme is not unequivocal.

P. H. RIBON: This being so, what differences are there in the analyes: identification of resonances or only values of parameters?

J. P. THEOBALD: The identification of resonances is not unequivocal with just one partial experiment.

A. M. MICHAUDON: The question of missed levels is a serious one for the multilevel fits of cross-sections of certain fissile nuclei, e. g. ^{233}U. When the proportion of missed levels becomes large, multi-level analyses are not very significant, even if they adequately fit the cross-sections. This seems to be the case for ^{233}U where the analysis of simulated cross-sections demonstrates that the proportion of missed levels is about 30-40%.

C. M. NEWSTEAD: The strength function you have obtained for ^{233}U, $S_0 = (2.25 \pm 0.55) \times 10^{-4}$, is about a factor of two greater than the s-wave neutron strength function of other odd mass fissile nuclei, such as ^{235}U and ^{239}Pu, which have values near unity.

W. KOLAR: The value of the strength function in paper CN-26/16 which you are referring to is given by the expression $S_0 = \Sigma_j(2_g \Gamma_n^0) / (E_1 - E_2) = (2.25 \pm 0.55) \times 10^{-4}$ and so corresponds to twice the value of the actual s-wave strength function.

C. M. NEWSTEAD: So in fact, your result is actually only about 10% greater, that is, 1.13×10^{-4}. Since your analysis was confined to levels below 53 eV, do you think this is evidence for an energy variation (intermediate structure) in the strength function? I have in mind the fact that in ^{239}Pu there is such a difference over 100 eV intervals.

J. P. THEOBALD: No, there is no evidence for intermediate structure. For instance, there was no significant value of the serial auto-correlation coefficient found in a statistical analysis of the fission data.

J. J. SCHMIDT: I have two questions relating to your ^{233}U resonance results. First, did you try, from plots of the experimental distributions of D and $g\Gamma_n^0$ and comparison with the theoretical distributions, to obtain some idea of the missed levels? Secondly, if, according to the remark of Dr. Michaudon, there is a chance of missing 40% of the levels not necessarily with small neutron widths, would this not account, at least, to some extent for the rather high strength-function value which you obtained?

J. P. THEOBALD: The answer to the first part of your question is, yes, we did make such comparisons. However, when there is an influence on the strength function, it will not be very significant (in particular for the small Γ_n).

E. R. RAE: I would like to comment on Dr. Schmidt's remark. I think it is true that the addition or loss of extra resonances of zero neutron width does not affect the strength function as determined from $<\Gamma_n^0>/D$. Hence, even the loss of 40% of the resonances, if of very low Γ_n, will probably have a very small effect on the strength function obtained.

SCATTERING CROSS-SECTION OF ^{235}U BELOW 100 eV DETERMINATION OF Γ_n AND J OF RESONANCES

F. POORTMANS, H. CEULEMANS
SCK/CEN, Mol, Belgium
E. MIGNECO, J. P. THEOBALD
CBNM, EURATOM, Geel, Belgium

Abstract

SCATTERING CROSS-SECTION OF ^{235}U BELOW 100 eV. DETERMINATION OF Γ_n and J OF RESONANCES.

The scattering cross-section of ^{235}U has been measured for two reasons. First of all, it is one of the most reliable methods for determining the resonance spins which are important for a better understanding of the fission process in the resonance region and for multilevel fits to the fission cross-section. Secondly, the scattering cross-section can improve the accuracy on the resonance parameters Γ_n and Γ. Of course, this is only possible for resonances which have a resonant scattering cross-section not much smaller than the potential scattering.

In this experiment, the detector array is composed of nine 10-atmosphere ^3He proportional counters with low jitter time. The measurements were performed below 100 eV at a 30 meter flight path of the liner electron accelerator of CBNM, Euratom, Geel. The main advantages of the detectors are their good discrimination properties against gamma rays and fission neutrons. The very low background allowed the measurements to be made with thin samples (7.81×10^{20} and 2.58×10^{20} nuclei/cm^2) so that the corrections for self-screening and absorption were small. The total error on the scattering cross-section data is of the order of 5%. In the whole energy range, the scattering cross-section is consistent with a potential scattering of 11.7 barn. The total cross-section was measured with the same samples and the same time-of-flight resolution.

Taking the published values (A. Michaudon et al., Nucl. Phys. 69 (1965) 545) of resonance parameters $g\Gamma_n$ and Γ the total cross-section and the scattering cross-sections corresponding to the two possible spin states were calculated, taking into account resolution and Doppler broadening. In general, the agreement with our experimental data is very good and the spin of 14 resonances below 60 eV could be determined. For some resonances, the accuracy of the resonance parameters Γ_n and Γ could be improved by the simultaneous fit of the scattering and total cross-section.

The experimental results obtained by the authors and the correlation between their spin values and previously obtained data from different fission experiments (fission width, mass and kinetic energy of fission fragments, ternary-fission anisotropy of fission fragments from aligned nuclei and average number of neutrons per fission) will be discussed.

1. INTRODUCTION

Many experiments have been performed in recent years, in order to determine the spins of low energy neutron resonances in ^{235}U. Knowledge of the resonance spins is interesting for different reasons. First of all, it allows to check if there is any correlation between the spin and some other properties of slow neutron induced fission such as the mean fission width, the fragment mass and kinetic energy distribution, the probability of ternary fission and the number of neutrons per fission. Secondly, the knowledge of the resonance spins is necessary for the analysis of the fission neutron cross section with a multi-level formalism. Moreover, the angular anisotropy of fission fragments from slow

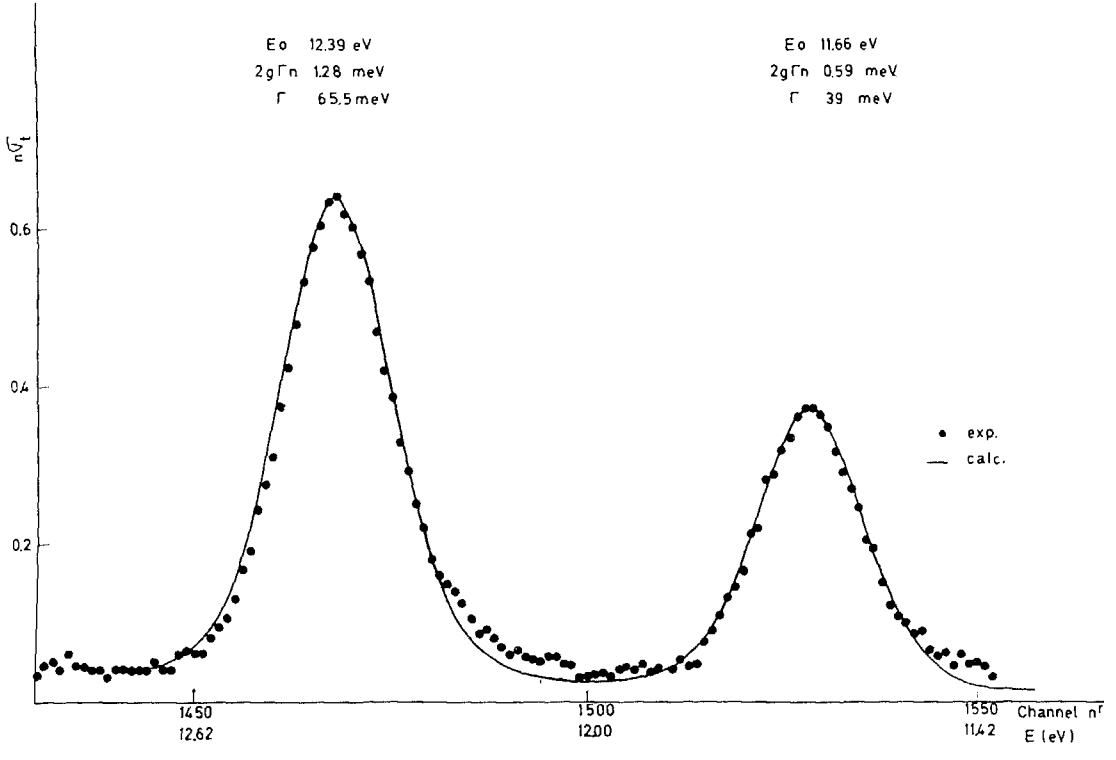

FIG. 1. Total cross-section σ_t times sample thickness ($n = 7.806 \times 10^{-4}$ atoms of ^{235}U per barn) around 12 eV. Points are experimental results. The solid line is a single-level Breit-Wigner curve calculated with resonance parameters of Table I.

neutron induced fission of aligned ^{235}U nuclei has been measured recently [1,2]. These results, together with the resonance spins, give some information about the nature (J and K quantum numbers) and the number of open channels for fission.

The spins of three resonances below 2 eV have been measured with the method of polarized neutrons and polarized nuclei [3]. Some scattering experiments have also been performed previously [4,5,6] but only a very limited number of spins could be assigned. Because of difficulties associated with the experiments mentioned above, a number of other less direct methods have been applied, all based on some property of the γ decay from the resonant states [7,8,9].

Up to now, the number of resonances for which the spin has been measured is still very small and there are many discrepancies between the existing data. For this reason we have measured the scattering and total cross sections, from which the spin of the resonances can be deduced. Moreover, in this way, it is possible to increase the accuracy of the resonance parameters, especially the ratio Γ_n/Γ. The measurements covered the energy range between 7 eV and 60 eV.

2. EXPERIMENTAL METHOD

2.1. Principle of the Method.

The measurements were performed at a 30 meter flight path of the pulsed neutron source of the linear accelerator of CBNM, Euratom Geel. We have measured the scattering and the total cross section with the same time of flight resolution. For both experiments, the same neutron detector was used in the same geometrical arrangement, but for the total cross section measurements, a 14 mm thick sample of lead was placed in the scattering chamber and the ^{235}U sample in transmission geometry. The width of the resolution function was mainly determined by the spread in flight path length (about 9 cm). For the transmission measurements, this spread was increased by 0.7 cm due to multiple scattering in the lead sample.

Starting with the known resonance parameters $g\Gamma_n$ and Γ, the total cross section was calculated, taking into account resolution and Doppler broadening. This calculated single level cross section curve was compared with our experimental data. An example is shown in fig. 1. In general, the agreement is very good if we take the parameters $g\Gamma_n$ and Γ, published by A. Michaudon [10]. In some cases the agreement could be improved by slightly changing the resonance parameters. However, in all cases, the new parameters we obtain in this way agree with the results of ref. [10] within the experimental error.

We then calculated the scattering cross section corresponding to the two possible spin states, and compared them with the experimental scattering cross section data. Examples are shown in figures 2, 3 and 4.

For both the σ_t and σ_n calculations, we took into account the contribution of the 20 most nearby resonances of ^{235}U and of all the resonances below 100 eV of the other uranium isotopes present in the sample.

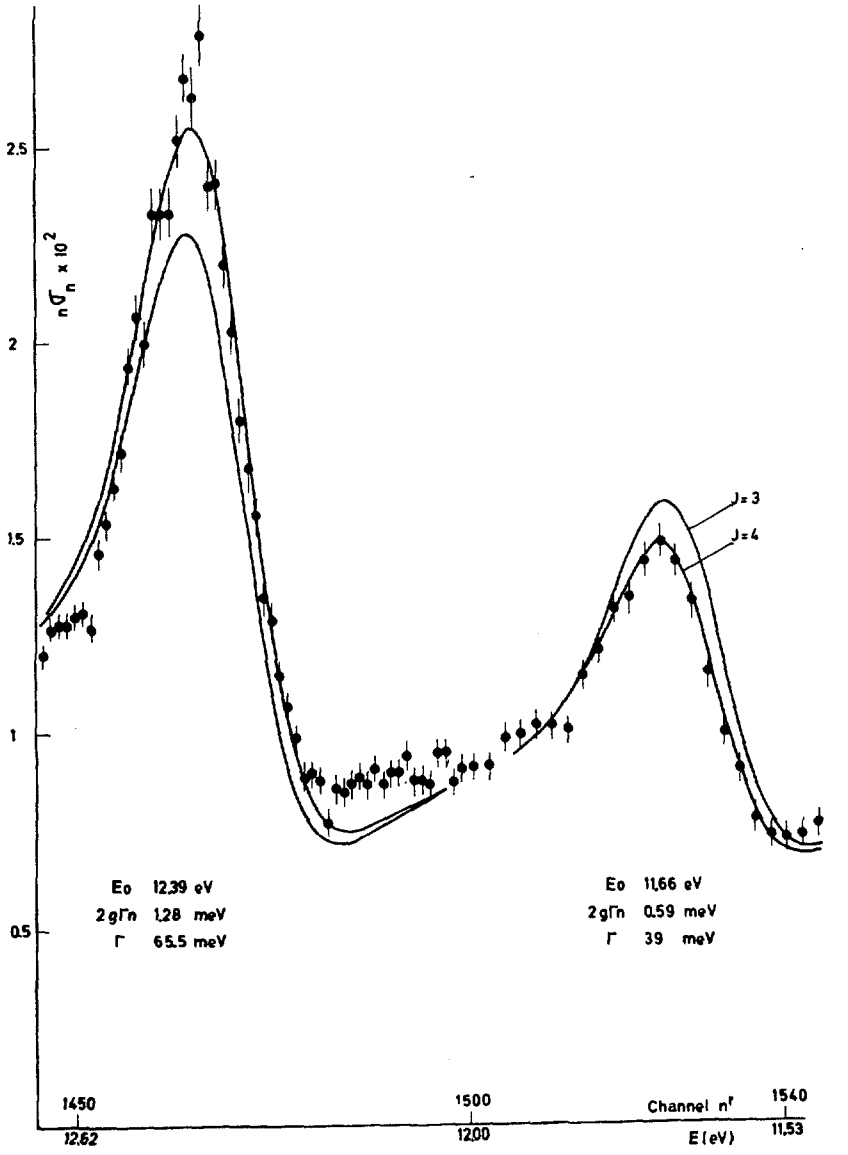

FIG. 2. Scattering cross-section σ_n times sample thickness (n = 7.806 x 10^{-4} atoms of ^{235}U per barn) around 12 eV. Points are experimental results. The solid lines are single-level Breit-Wigner curves for the two possible J values.

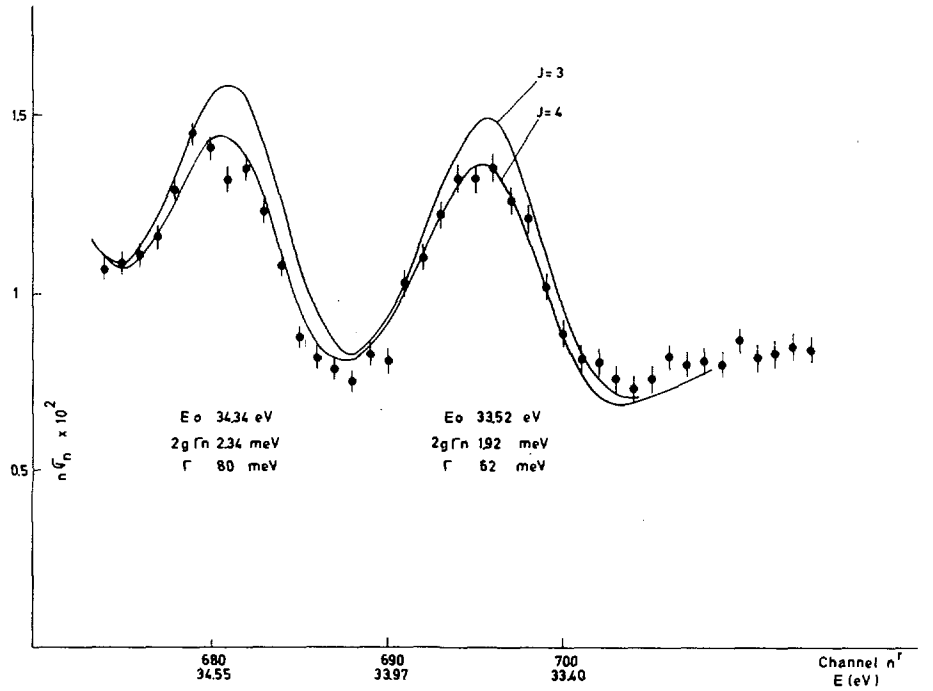

FIG. 3. Scattering cross-section σ_n times sample thickness (n = 7.806 × 10^{-4} atoms of ^{235}U per barn) around 34 eV. Points are experimental results. The solid lines are single-level Breit-Wigner curves for the two possible J values.

2.2. Experimental Details.

The specifications of the main items were as follows :

- Linac :	burst frequency	400 Hz
	burst width	50 nsec.
	channel width	320 nsec.
	detector distance	30.62 m
- Samples :	for background spectrum	Au, W, Mo, Co
	cut-off filter	Cd
^{235}U samples :	(a) $7.806\ 10^{-4}$ nuclei of ^{235}U per barn	
	(b) $2.366\ 10^{-4}$ nuclei of ^{235}U per barn	
	for both: diameter 12 cm	
	isotopic composition (by weight) :	
	^{234}U (0.72 %) ^{236}U (0.17 %) ^{235}U (93.1 %)	
	^{238}U (5.9 %)	
Pb sample :	Pb sample thickness : $6.60\ 10^{-3}$ atoms per barn	
	Pb scattering cross section [11] : 11.28 ± 0.06 barn	
detectors :	9 ^3He detectors, diameter 2.5 cm	
	active length 15 cm	
	total jitter time : approximately 0.8 μsec	
	pressure : 10 atmospheres	
	overall efficiency : approximately $4\ 10^{-3} \sqrt{E(eV)}$	

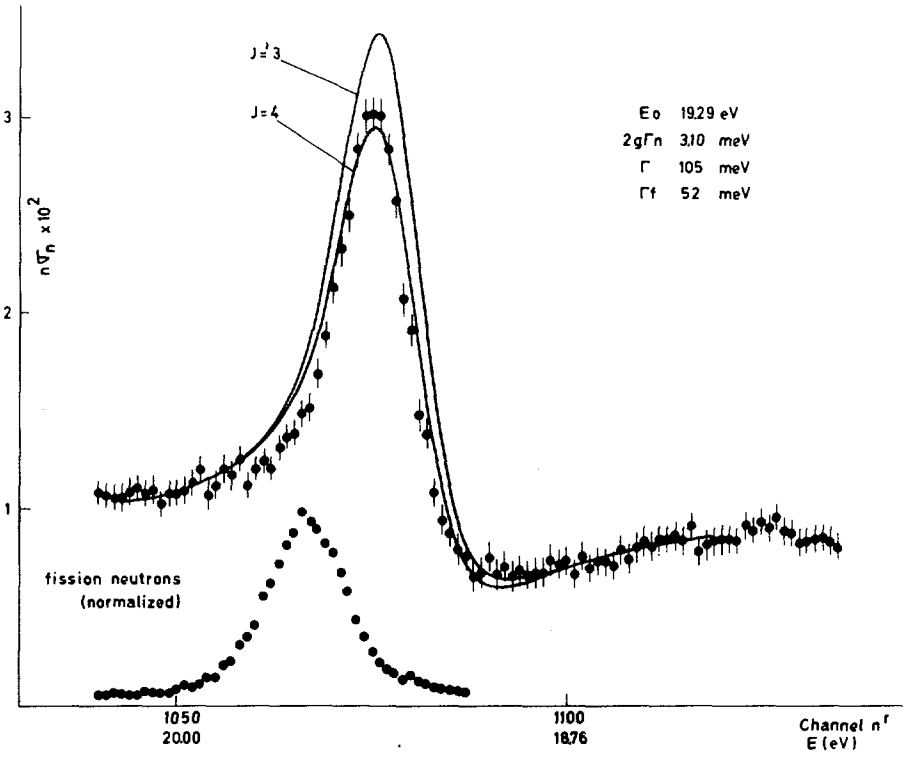

FIG. 4. Scattering cross-section σ_n times sample thickness (n = 7.806 × 10^{-4} atoms of ^{235}U per barn) in the 19.29 eV resonance. Points are experimental results. The solid lines are single-level Breit-Wigner curves for the two possible J values. The fission neutron correction is shown on the bottom of the figure.

The scattering experiments with the thickest ^{235}U sample were made in 7 runs (total time of 200 hours). Background measurements and normalization measurements with the Pb sample were made between each of these runs. The total count rate in the time of flight analyzer, normalized to the monitor value and the measuring time remained always constant to better then 1 %. Moreover, no change in the neutron spectrum could be detected in the energy range up to 100 eV. A ^{3}He proportional counter was used as neutron monitor; it was located besides the neutron beam, just before the entrance window of the scattering chamber.

2.3. Background conditions.

The sample-out background was only 2 x 10^{-3} times the count rate one would obtain if all the incident neutrons were scattered by the sample. This corresponds to 20 per cent of the count rate due to the potential scattering of the thickest ^{235}U sample.

A marked advantage of the ^{3}He detectors is their insensitivity to gamma rays and their good discrimination properties for fission neutrons. Indeed, an important part, Nf, of the fission neutron pulses are eliminated by pulse-height discrimination. The remaining ones, N'f, have the same pulse height as the low energy scattered neutrons, Ns.

This remaining part is mainly due to ^{3}He recoil pulses. The ratio $K = N'f/Nf$ was determined at low neutron energy ($En < 0.3$ eV) with a cadmium shield for the slow neutrons between detector and ^{235}U sample. During the scattering experiment, time-of-flight spectra were taken simultaneously of both the scattered neutrons and remaining fission neutron background ($Ns + KNf$) and of the high fission neutron pulses Nf. Later the count rate in the second time-of-flight spectrum was multiplied by the known factor K and subtracted from the first. The magnitude of this correction is shown in fig. 4 for the 19.3 eV resonance. The mean distance between detector and sample was 20 cm, so that the fast fission neutrons arrived earlier at the detector than the slow scattered neutrons. Due to this effect, the correction for fission neutrons was important only in the high energy wing of the strongest fission resonances as can be seen on the example given in fig. 4.

2.4. Corrections for self screening and absorption of the scattered neutrons.

A more detailed description of the experimental conditions and of the method of analysis will be published elsewhere, so we will not derive here the mathematical formula for the different corrections. With the chosen target thicknesses, these corrections were small and could be calculated very accurately from the experimental total cross sections which were measured with the same time-of-flight resolution.

3. RESULTS AND DISCUSSION

The precision on the scattering cross section data from the thickest sample is of the order of 5 %. In the whole energy range, from 7 eV up to 60 eV, the results agree very well with a potential scattering cross section $\sigma_p = 11.7$ barns. An example is given in fig. 5 for the region around 16 eV. This value for σ_p is in good agreement with other results [4,10].

The statistical accuracy of the measurements with the thinnest sample was only sufficient in the strong resonances. In fact, these measurements were only performed to test the results at 8.8 eV, 12.4 eV and 19.3 eV, where the thickest sample transmission was of the order of 0.5. The agreement between the two experiments is very good in these strong resonances.

In Table I, we give the results for the ratio $g\Gamma_n/\Gamma$ and for the spin J. We also give the resonance parameters $g\Gamma_n$ and Γ which were used to calculate the total cross section and the two possible (for $g = 7/16$ and $g = 9/16$) scattering cross section Breit Wigner curves. In case we do not give a value for $g\Gamma_n$ and Γ, the results from ref. [8] were used.

For all resonances, different sets of parameters were tried. The resonance parameters given in Table 1 form a consistent set such that good agreement was obtained simultaneously with our total cross section results and with our scattering results fitted to one of the two possible scattering cross section curves. A change of the resonance parameters $g\Gamma_n$ and Γ such that our scattering data fits the calculated Breit-Wigner curve corresponding to the other spin state, always resulted in a worse agreement with our total cross section data. In general, the precision on the ratio $g\Gamma_n/\Gamma$ so obtained is of the order of 10 %.

In Table II, we have compared our spin assignments with those of other authors. We have previously obtained another result for the spin of the 12.4 eV resonance at Mol, from scattering cross section measurements with a crystal spectrometer [4].

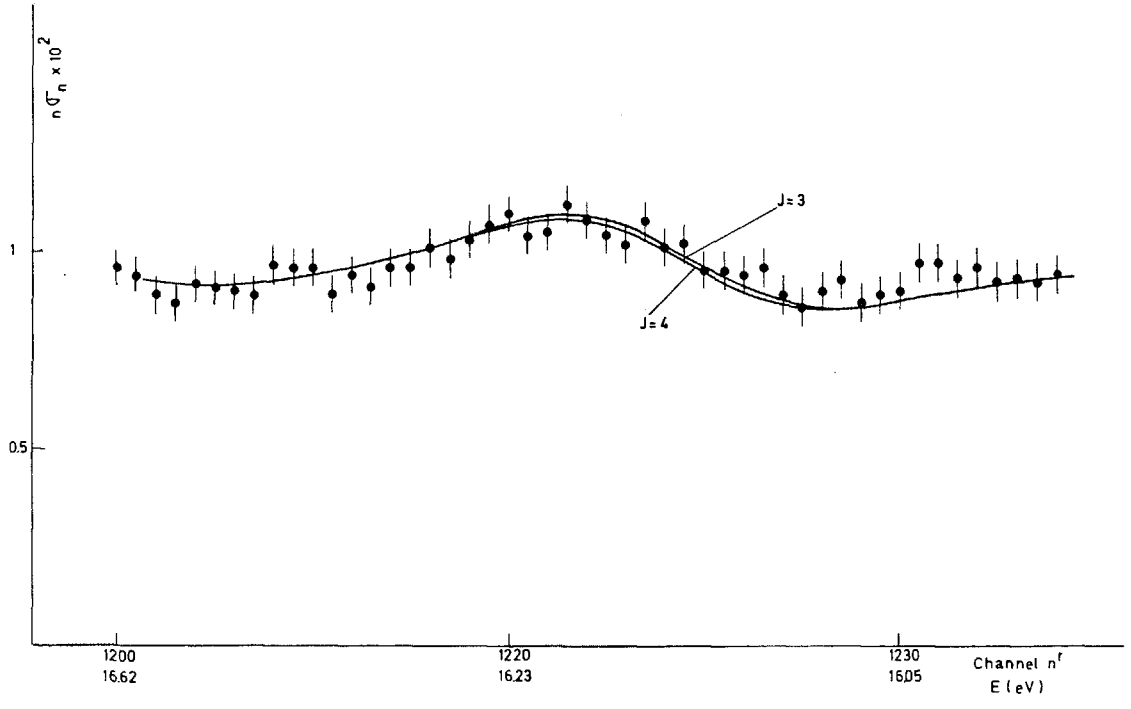

FIG. 5. A typical example of the good agreement between the experimental scattering cross-section and the calculated (solid line) taking as potential scattering cross-section the value of 11.7 barn. The small hump around 16 eV is due to the weak resonance of 16.08 eV.

TABLE I. RESONANCE PARAMETERS WHICH GIVE BEST FIT TO OUR TOTAL AND SCATTERING CROSS-SECTION MEASUREMENTS. IF NO RESULTS FOR $2g\Gamma_n$ AND Γ ARE QUOTED, THE RESULTS OF REF. [10] GIVE VERY GOOD AGREEMENT. FOR ALL RESONANCES WHERE J HAS BEEN DETERMINED, THE ERROR ON $2g\Gamma_n/\Gamma$ IS LESS THAN 10%

E_o (eV)	$2g\Gamma_n$ (meV) ref. [10]	present	Γ (meV) ref. [10]	present	$2g\Gamma_n/\Gamma \times 10^2$	J
8.78	1.18 ± 0.05	1.13	133 ± 13	133	0.85 ± 0.06	3
11.66	0.59 ± 0.04		40 ± 5		1.48 ± 0.1	4
12.39	1.29 ± 0.06	1.28	69 ± 6	65	1.95 ± 0.14	3
19.29	3.10 ± 0.15		105 ± 10		2.95 ± 0.2	4
22.93	0.45 ± 0.03	0.60	92 ± 10		0.65 ± 0.1	
23.40	0.69 ± 0.06		37 ± 4		1.86 ± 0.2	(4)
23.61	0.95 ± 0.10	0.70		133	0.53 ± 0.1	
32.07	1.95 ± 0.15	1.90	100 ± 10	100	1.90 ± 0.19	4
33.52	1.92 ± 0.12		62 ± 8		3.10 ± 0.3	4
34.34	2.20 ± 0.20	2.34	85 ± 10	80	2.93 ± 0.3	4
35.17	4.5 ± 0.3	4.5	175 ± 25	165	2.73 ± 0.27	4
39.41	2.5 ± 0.20		95 ± 10		2.63 ± 0.26	3
41.86	1.45 ± 0.10		90 ± 10		1.61 ± 0.16	(3)
51.26	3.76 ± 0.20	3.60		111	3.24 ± 0.3	4
55.06	3.28 ± 0.08	3.55		110	3.23 ± 0.3	(4)
55.84	2.3 ± 0.4	1.95		129	1.51 ± 0.25	
56.49	4.89 ± 0.35	5.0		149	3.36 ± 0.3	3

However, the experimental conditions of this earlier experiment were much worse: the neutron energy resolution was very bad, reducing the experimental ratio of resonant scattering to potential scattering strongly. Moreover, we did not have, of course, the time-of-flight discrimination between the fission neutrons and the scattered neutrons.

The mean fission width for the two possible spin states deduced from Table I does not seem to be significantly different:

$J = 3 \quad \langle \Gamma_f \rangle = 57$ meV

$J = 4 \quad \langle \Gamma_f \rangle = 43$ meV

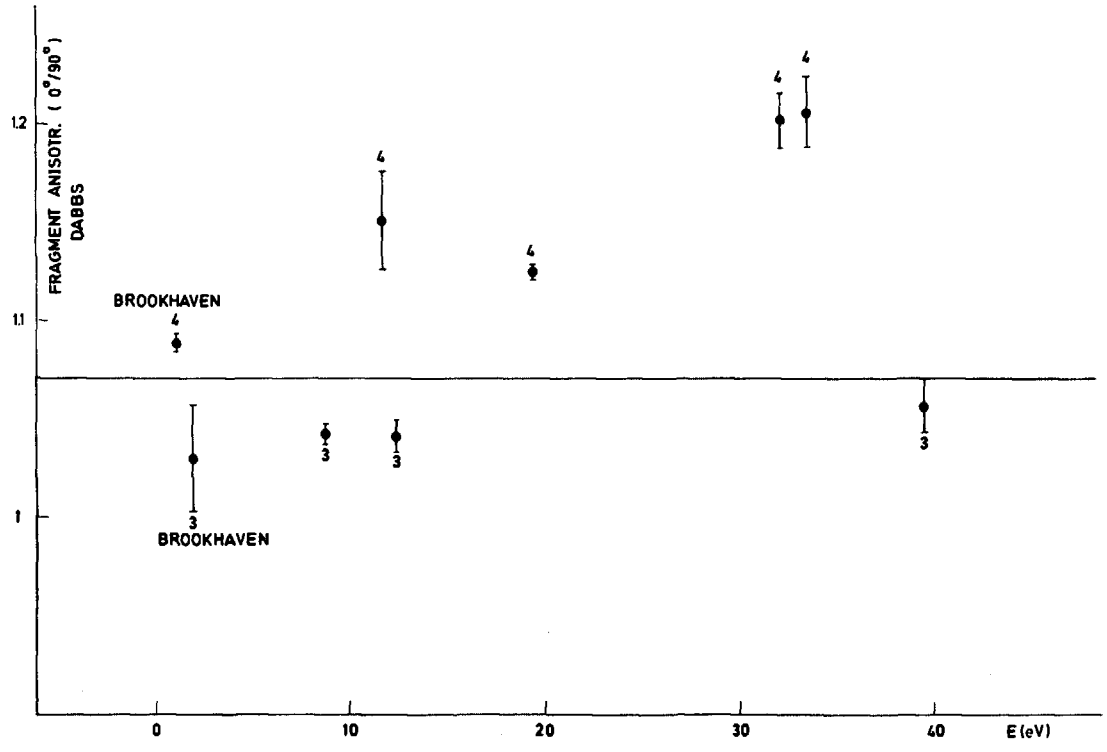

FIG. 6. Results of the anisotropy of fission fragments from aligned nuclei [1] together with the present spin values and those determined at Brookhaven [3]. For this comparison, we left out the resonances for which important contributions of neighbouring resonances with unknown spin were present as reported in Ref. [1].

TABLE II. RESONANCE SPINS FOR ^{235}U

Energy (eV)	Present results	Asghar a	Weigman b
8.78	3	3	
11.66	4	4	
12.39	3	4	4
19.29	4	4	4
23.40	(4)		4
32.07	4	(4)	4
33.52	4	4	4
34.34	4	4	(3)
35.17	4	4	4
39.41	3	4	4
41.86	(3)		
51.26	4		
55.06	(4)		
56.49	3		

a. ref. [7] : gamma-ray multiplicity method

b. ref. [8] : relative population of 2^- level at 687 keV of ^{236}U

However, the number of resonances, for which we determined the spin is still too small to draw any firm conclusion.

There is a lot of experimental information about different properties of slow neutron induced fission in the resonance region such as mass and kinetic energy distribution of fission fragments, probability for ternary fission and number of neutrons per fission, but, we do not find conclusive evidence for a correlation between these data and our spin assignments.

There seems to be a correlation between our spin values and those of Brookhaven [3] and the published results for the anisotropy of fission fragments from aligned nuclei [1] . As shown in fig. 6, the ratio 0°/90° seems to be systematically higher for the J = 4 resonances than for the J = 3 resonances. We took only into account the resonances which were well isolated in the experiments of Dabbs [1] and the group of two resonances around 39.5 eV which is largely dominated by the J = 3 resonance of 39.4 eV, and left out the resonances for which an important contribution from neighbouring resonances with unknown spin was present as reported in [1] .

On the other hand, preliminary results from anisotropy measurements performed at Harwell [2] seem to be significantly different from the results of ref. [1] for the individual resonances, and no correlation with our spin assignments is found.

REFERENCES

[1] DABBS J.W., EGGERMAN C., CAUVIN B., MICHAUDON A., SANCHE M., Physics and Chemistry of Fission (Proc. 2nd IAEA Symp. Vienna) (1969) 321

[2] POSTMA, private communication

[3] SCHERMER R.I., PASSEL L., BRUNHART G., REYNOLDS C.A., SAILOR L.V., SHORE F.J., Phys. Rev. 167 (1968) 1121

[4] POORTMANS F., CEULEMANS H., M. NEVE de MEVERGNIES, Nuclear Data for Reactors (Proc. IAEA Conf. Paris) IAEA, Vol. II (1967) 211

[5] SAUTER G.D., BOWMAN C.D., Phys. Rev. 174 (1968) 1413

[6] ASGHAR M., MICHAUDON A., PAYA D., Phys. Let. 26B (1968) 664

[7] WEIGMANN H., WINTER J., HESKE M., Nucl. Phys. A134 (1969) 535

[8] MICHAUDON A., DERRIEN H., RIBON P., SANCHE M., Nuol. Phys. 69 (1965) 545

[9] RAYBURN L.A., WOLLAN E.O., Nucl. Phys. 61 (1965) 381

[10] UTTLEY C.A., Congres Int. de Phys. Nucl. (Edit. CNRS Paris) II (1964) 700

THE SCATTERING CROSS-SECTION OF ^{235}U BETWEEN 0.025 eV AND 1 eV*

H. CEULEMANS, F. POORTMANS
SCK/CEN Mol, Belgium

Abstract

THE SCATTERING CROSS-SECTION OF ^{235}U BETWEEN 0.025 eV AND 1 eV.

In view of the importance of the ^{235}U scattering cross-section for cross checks between, for example, total and fission cross-sections, this quantity was measured at the BR2 reactor of SCK/CEN, Mol, in the energy region of 0.025 eV to 1 eV. The results of the experiments are presented together with a short description of the method and a discussion of the overall accuracy of the experiments.

1. INTRODUCTION

It is generally recognized that our information on the scattering cross section of ^{235}U in the thermal energy region is much less accurate than our knowledge of other parameters such as the total and the fission cross sections, and the capture to fission ratio. An accurate measurement of this quantity would allow us to make meaningful cross checks between the other parameters. As was pointed out in the recent review paper by Hanna et al. [1] , there has been no activity on this subject in recent years and according to the same paper, the best value of the ^{235}U scattering cross section for a rolled metal sample is (15.3 ± 4.6) barn.

2. MEASUREMENTS

The measurements were performed at the BR2 reactor of our institute. A crystal spectrometer was used to diffract monochromatic neutrons into the direction of the scattering chamber and the transmission counter. The diffraction occurred on the (111) planes of a silicon crystal, in order to avoid higher-order contamination of the diffracted beam. The second order diffraction is forbidden and third plus higher order contamination amounted to less than 1%. Both transmission, scattering and where applicable, fission counting rates were recorded for a number of samples. The scattering and fission signals were detected in a scattering chamber of a design similar to the one described in [2] but equipped with ^{3}He proportional counters. The axis of these counters is parallel with the incident beam and scattering between 15° and 165° angles can be detected. Low-energy neutrons are absorbed in the ^{3}He gas of the detectors and give a narrow peak due to the proton generated in the reaction. Fission neutrons are either absorbed or elastically scattered giving a distribution of pulses starting well above the peak of the low-energy neutrons but extending also below this peak. If we use a high channel and a low channel, then the high channel will contain only fission neutrons and the low channel will contain scattered neutrons plus a number of fission events. This number is a certain,

* This research was supported in part by the IAEA under contract number 726/RB.

constant fraction of the number detected in the high channel. In so doing a simple yet reliable correction for fission neutrons can be made. The ratio of fission counts in the high channel to those in the low channel was measured at approximately 0.036 eV neutron energy. A thin Cd-shield around the sample absorbed all scattered neutrons and produced a pure fission neutron source. It was found that the low channel contained 82% of the fission neutrons counted in the high channel.

The scattering signal from ^{235}U was compared with the scattering signal from a thin vanadium sample. Vanadium was chosen because unlike lead it does not show coherent scattering effects. The vanadium cross section however is not too well known and it proved necessary to measure this cross section again with higher accuracy. The total cross section was measured between 1 eV and 0.025 eV and the scattering and capture cross sections were extracted from a fit of these data to an expression of the form $(a + b\ E^{-1/2})$. The scattering cross section was further checked by a direct comparison with lead at about 0.76 eV where no coherent scattering effects occur in lead and where the absorption cross-section of vanadium has decreased to about 1 barn.

3. ANALYSIS OF THE DATA

The ^{235}U sample has been prepared at the Central Bureau for Nuclear Measurements of Euratom. Its characteristics are listed in Table I. The neutron beam had a diameter of about 0.20 cm and

TABLE I. CHARACTERISTICS OF SAMPLES

1. ^{235}U sample

   chemical composition : rolled metal sample
   diameter : 3.09 cm
   average thickness : 0.3318 ± 0.0002 g/cm^2
   total mass : 2.4884 ± 0.0002 g
   isotopic composition : ^{235}U 93.154 %
   ^{234}U 0.781 %
   ^{236}U 0.227 %
   ^{238}U 5.838 %

2. Vanadium sample

   - transmission sample:
     diameter : 3.002 cm
     total mass : 12.394 g
     average thickness : 1.751 g/cm^2
     2.07 x 10^{22} atoms/cm^2

   - scattering sample:
     diameter : 3.002 cm
     total mass : 4.153 g
     average thickness : 0.5867 g/cm^2
     6.936 x 10^{21} atoms/cm^2

3. Lead sample

   diameter : 2.998 ± 0.001 cm
   total mass : 15.998 g
   average thickness : 2.266 g/cm^2
   6.691 x 10^{21} atoms/cm^2.

covered only part of the sample surface. As a check on local thickness fluctuations the total cross section was measured with high statistical accuracy. At 0.0253 eV the apparent cross-section after corrections for higher order and isotopic composition was (686 ± 2.5) barn. If this is compared with the value (694 ± 4.0) barn given in ref. [1] , it may be concluded that the local thickness is lower than the average thickness by (1 ± 0.5)% . In this case and in all other similar cases, a large number of individual measurements was taken and a statistical analysis applied, such that an internal , rather than an external (i.e. based on the number of counts) standard deviation was obtained. Whenever measurements were repeated even with time intervals of several weeks, the results agreed within the limits derived from the experimental standard deviations. In this way we obtained from transmission measurements in the region between 1 eV and 0.025 eV, the following values for respectively, the scattering and capture cross sections of vanadium

$$\sigma_n = (4.87 \pm 0.05) \text{ barn}$$
$$\sigma_\gamma = (0.81 \pm 0.01) \times E^{-1/2} \text{ barn}$$

It is noteworthy that the same result was obtained for σ_n by direct comparison of the scattering signal with a lead sample of nominal thickness 6.69×10^{21} atoms/cm^2 and with an assumed cross-section [3]:

$$\sigma_n \text{ (Pb)} = 11.28 \pm 0.06 \text{ barn}$$

The result obtained for σ_γ of vanadium agrees closely with the recommended value of BNL-325 [4] : 5.06 ± 0.06 barn, versus our value 5.12 ± 0.06 barn. The value for σ_n on the contrary is only in reasonable agreement with the values of 4.74 ± 0.07 barn quoted in ref. [3] and of 5.07 ± 0.15 barn of ref. [5] . The vanadium sample used in the transmission experiments had 2.07×10^{22} atoms/cm^2 and the one used in the scattering experiments had 6.94×10^{21} atoms/cm^2.

During the first series of scattering experiments on uranium data were taken at discrete energy points between 0.02 eV and 0.2 eV. Samples of U, V and an empty holder were sequentially rotated into the beam and for each sample the number of counts in the transmission detector and in the low-energy and fission neutron channel were recorded. After suitable corrections the ratio of uranium scattering to vanadium scattering was calculated. At each point the data taking was repeated a large number of times, such that the variance of the mean was less than 0.5 % at each point. The relation between the ratio of the scattering yields and the scattering and total cross-sections is as follows

$$R = \frac{(\sigma_n/\sigma_t)_U \, (I_1 + I_2)_U}{(\sigma_n/\sigma_t)_V \, (I_1 + I_2)_V} \qquad (1)$$

The integral I_1 is

$$I_1 = \iint \exp(-\alpha) \cdot \exp\left[-(\alpha_o - \alpha)\sec\vartheta\right] \cdot \left[1 - \exp(-\xi_o \operatorname{cosec}\vartheta)\right] \cdot \sin\vartheta \, d\vartheta \, d\alpha \qquad (2)$$

The ϑ-integration is in the interval ϑ_o, $\pi/2$ with $\vartheta_o = \pi/12$, and the α-integral in the interval 0, α_o with $\alpha_o = n\sigma_t t$, the product of the number of nuclei/cm^3, the total cross section and

the sample thickness. The parameter ε_0 is the detector efficiency at $\vartheta = \pi/2$.

The integral I_2 is the same as the first except for the term $\exp\left[-(\alpha_0-\alpha)\sec\vartheta\right]$ which now becomes $\exp\left[-\alpha\sec\vartheta\right]$

For all practical purposes the term $\left[1-\exp\left(-\varepsilon_0\ \mathrm{cosec}\,\vartheta\right)\right]$ can be considered as a constant because ε_0 is large. ($\varepsilon_0 \approx 0.9$ at $E_n = 1$ eV and proportional to $(E_n)^{-1/2}$. This simplifies somewhat the expressions for I_1 and I_2 which prove to be simple combinations of the exponential integrals $E_1(x)$ and $E_2(x)$ and of the transmission T.

The value used for the transmission is not the experimentally determined value in each point, but the value calculated from the evaluated total cross section as given in ENDF/B-II, material number 1102. Although the experimental value agrees within statistical errors with the evaluated value, the latter is to be preferred. For the contribution of the other isotopes the values used are:

^{234}U : $\sigma_n = 17$b $\quad \sigma_\gamma = 95$ b

^{236}U : $\sigma_n = 10$b $\quad \sigma_\gamma = 6$ b

^{238}U : $\sigma_n = 8.95$ b $\quad \sigma_\gamma = 2.7$ b

The figures quoted are for 0.0253 eV energy. A $E_n^{-1/2}$ dependence is assumed for σ_γ and in an approximative way, σ_n is assumed to be constant.

The second series of measurements consisted of a scan between 0.8 eV and 0.025 eV neutron energy. The experimental standard deviation in this case was about 1%. The scattering cross-section σ_n calculated from the two series of data are presented together in fig. 1, with different labels. The error bars represent two standard deviations on each side. There exists evidence for some coherent scattering structure in the data below 0.040 eV. The value found at 0.0253 eV is

$$\sigma_n\ (0.0253\ \mathrm{eV}) = (14.3 \pm 0.5)\ \mathrm{barn}$$

This value is obtained by excluding geometry-dependent coherent effects.

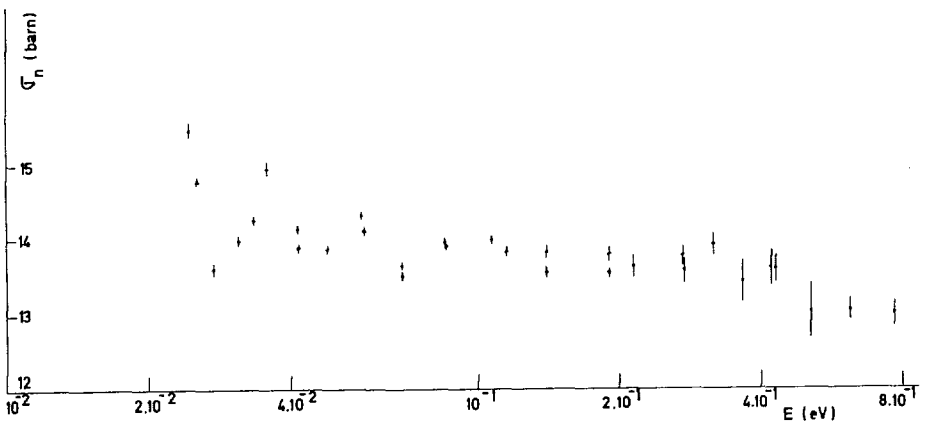

FIG. 1. Scattering cross-section of ^{235}U below 1 eV.

4. CONCLUSION

The values of σ_t for rolled metal samples given in Table IV of ref. [1] give an average of 696.0 ± 3.5 barn. Subtracting our value for σ_n, this would give σ_a = 681.7 ± 3.5 barn. Combining this with the capture to fission ratio value α = 0.1694 ± 0.0019 of Table VIIIa, ref. [1] , the value found for the fission cross section is σ_f = 583 ± 4.5 barn, and for the capture cross section σ_γ = 98.7 ± 4.5 barn. The errors on these values are probably overestimated and largely due to the 3.5 barn error on σ_t. The values proper, especially σ_f, show however a trend towards higher values as indicated also in paper CN-26/100 to be presented at this conference.

The data contained in this paper will be made available in numerical form to the C.C.D.N. Saclay, France.

REFERENCES

[1] Hanna, G.C., et al., Atomic Energy Review, Vol. VII (1969) N° 4

[2] Ceulemans, H., Poortmans, F., Nucl. Instr. Meth., 17 (1962) 342

[3] Rayburn, L.A., Wollan, E.O., Nucl. Phys. 61 (1965) 381

[4] Goldberg, M.D., Mughabghab, S.F., Magurno, B.A., May, V.M., BNL-325 Second Edition, Suppl. 2, Vol. IIA (1966)

[5] Brockhouse, B.N., Can. J. Phys. 31 (1953) 432

DISCUSSION

TO PAPERS IAEA-CN-26/20, 21

A. J. DERUYTTER: On the subject of paper CN-26/21, I would like to ask Dr. Poortmans whether he could make an accurate determination of the total cross-section of ^{235}U at 2200 m/s so as to be able to obtain a precise value for the absorption cross-section at 2200 m/s by subtracting his precise scattering value.

F. POORTMANS: We intend to perform total and scattering cross-section measurements on the same sample and in this way to get an accurate measurement of the absorption cross-section.

M. ASGHAR: I would like to congratulate Dr. Poortmans on his high-quality neutron-scattering data (paper CN-26/20). I am sure that they have been collected with great care, patience and control. However, the disagreement between your spin assignment of the 12.39 eV resonance and other data listed in Table II, worries me, because this resonance (along with that at 19 eV) is very "clear" and well isolated. Morever, in your previous assignment, you had assigned a spin J = 4 to this resonance. Do you think that this difference in assignment might be due to the change in resolution of these two measurements? Or could this simply be a double resonance.

F. POORTMANS: If the 12.4 eV resonance is not a single resonance, it could explain the disagreement between the different results. We previously obtained another result for the spin of the 12.4 eV resonance. The earlier experiments were performed with the BR2 crystal spectrometer and the experimental conditions were much less satisfactory than in the present experiments. The neutron energy resolution was very bad, strongly reducing the experimental ratio of resonant scattering to potential scattering. Moreover, the fission neutron correction was more important in the resonance peak because we did not have the time-of-flight discrimination between the fission neutrons and the scattered neutrons.

A. M. MICHAUDON: In reply to Dr. Asghar about the 12.39 eV resonance in ^{235}U, I can say that it is very unlikely that this resonance is a doublet since it is well separated and rather narrow, especially when measured with cooled samples.

I would then like to comment on the correlation which Dr. Poortmans showed between the spin state of ^{235}U resonances and the anisotropy of the fission fragments in the same resonances. There are two reasons for believing that such a correlation is rather fortuitous. first, the correlation disappears if the Harwell data on the anisotropy are used instead of the Saclay data; and second, such a correlation is not to be expected on the basis of the channel theory of fission because since the K = 0 band is found to be inhibited, the 3^- and 4^- states are found with equal probability in the other bands ($K = 1^-$ and $K = 2^-$) with comparable anisotropies.

F. POORTMANS: As regards the comparisons between our spin assignments and the results of the fission-fragment angular-distribution measurements with aligned ^{235}U nuclei by Dabbs et al., I was merely drawing attention to a striking experimental correlation between these two results. Furthermore, for $K = 2^-$, the calculated difference in the ratio $0°/90°$ between J = 3 and J = 4 states is about 6%, which is larger than the errors given for the anisotropy data.

MESURE ET ANALYSE DES SECTIONS EFFICACES DE FISSION DE L'URANIUM-235 ET DU PLUTONIUM-241

J. BLONS, G. DEBRIL,
J. FERMANDJIAN, A. MICHAUDON
CEA, Centre d' études
nucléaires de Saclay,
France

Abstract — Résumé

MEASUREMENT AND ANALYSIS OF ^{235}U AND ^{241}Pu FISSION CROSS-SECTIONS

The fission cross-sections of ^{235}U between 17 eV and 30 keV and of ^{241}Pu between 1 eV and 3 keV have been measured by a time-of-flight method making use of a gas scintillator operated at a temperature of 77°K. The Saclay 45-MeV linear accelerator has been used as pulsed neutron source. For either of these two measurements, the experimental conditions are presented and the average fission cross-section is compared with those of other laboratories. Moreover, the fission cross-section of ^{241}Pu has been analysed from 1 to 6 eV and from 14 to 63 eV by means of a least-squares program based on a single-level formalism, and from 6 to 14 eV by a least-squares program based on a multi-level formalism. Finally, the preliminary results of a higher-resolution measurement (2 ns/m) of ^{241}Pu are also presented.

MESURE ET ANALYSE DES SECTIONS EFFICACES DE FISSION DE L' URANIUM-235 ET DU PLUTONIUM-241.

Les sections efficaces de fission de ^{235}U entre 17 eV et 30 keV et de ^{241}Pu entre 1 eV et 3 keV ont été mesurées par la méthode du temps de vol avec un scintillateur gazeux fonctionnant à la température de 77°K. L' accélérateur linéaire de 45 MeV de Saclay a été utilisé comme source pulsée de neutrons. Pour chacune de ces deux mesures, les conditions expérimentales sont présentées et la section efficace moyenne de fission est comparée avec celles d' autres laboratoires. De plus, la section efficace de fission de ^{241}Pu a été analysée de 1 à 6 eV et de 14 à 63 eV par un programme de moindres carrés basé sur un formalisme à un niveau, et de 6 à 14 eV par un programme de moindres carrés basé sur un formalisme multiniveaux. Enfin, les résultats préliminaires d' une mesure à meilleure résolution (2 ns/m) de ^{241}Pu sont également présentés.

1. INTRODUCTION

Les améliorations apportées à la technique du temps de vol et à la détection de la fission nous ont conduits à mesurer les sections efficaces de fission de ^{235}U et ^{241}Pu.

Les mesures ont été faites en utilisant l'accélérateur linéaire de 45 MeV de Saclay comme source pulsée de neutrons et une base de vol inclinée de 10° par rapport à la normale à la face de sortie du ralentisseur.

Le détecteur était un scintillateur gazeux fonctionnant à la température de l'azote liquide afin de réduire l'effet Doppler particulièrement important dans ce type de mesures [1, 2].

La technique utilisée consistait à mesurer simultanément le taux de comptage dû aux événements de fission et le spectre de neutrons incidents grâce à un compeur à BF_3 situé juste derrière le détecteur de fission. Le bruit de fond était déterminé par des écrans à résonances noires placés dans le faisceau de neutrons. Les impulsions émises par les détecteurs étaient enregistrées sur bandes magnétiques à 16 pistes dont 13 étaient affectées à l'enregistrement des informations de temps de vol codées,

2 autres au codage des voies (3 voies pour la fission correspondant aux 3 plans du détecteur et une voie pour la mesure simultanée du spectre de neutrons); la dernière piste servait au contrôle de parité.

Dans le calcul de la section efficace de fission, on a supposé que la section efficace de la réaction ^{10}B (n, α) était donnée par la relation suivante:

$$\sigma_{(n,\alpha)(barn)} = \frac{610,3}{\sqrt{E_{(eV)}}} - 0,28 \qquad (1)$$

Les conditions expérimentales et les résultats obtenus sont décrits ci-dessous séparément pour ^{235}U et ^{241}Pu.

2. SECTION EFFICACE DE FISSION DE ^{235}U

La section efficace de fission de ^{235}U a été mesurée entre 17 eV et 30 keV avec une résolution nominale de 1 ns/m et une quantité de 1,5 g de ^{235}U sous la forme de dépôts minces répartis dans les 3 plans du détecteur.

La composition isotopique en masse des échantillons était la suivante:

^{234}U : 0,02% ^{235}U : 99,87%

^{236}U : 0,04% ^{238}U : 0,07%

Les conditions expérimentales sont résumées dans le tableau I.

TABLEAU I. CONDITIONS EXPERIMENTALES

	$\sigma_{f\ ^{235}U}$	$\sigma_{f\ ^{241}Pu}$
Accélérateur	Fréquence de répétition: 500 Hz	
	Largeur d' impulsion: 50 ns	100 ns
Sélecteur de temps de vol	Gamme d' énergie — Largeur de canal 17 eV - 31 eV — 400 ns 31 eV - 68 eV — 200 ns 68 eV - 205 eV — 100 ns 205 eV - 50 keV — 50 ns	Gamme d' énergie — Largeur de canal 1 eV à 14 eV — 200 ns 14 eV à 3,5 keV — 100 ns
Longueur de vol	50,05 m	10,89 m
Filtre	Bore naturel, épaisseur 860 mg/cm^2	Bore naturel, épaisseur 420 mg/cm^2
Mesure de bruit de fond		
Ecran permanent	Aluminium	Cobalt
Ecrans temporaires	Manganèse-cobalt	

La section efficace de fission a été normalisée en égalant la valeur de σ_f intégrée de 60 eV à 200 eV à celle d'une mesure antérieure faite à Saclay [3].

La figure 1A montre la section efficace de fission de 17 eV à 100 eV, Cette figure met en évidence l'amélioration apportée à la mesure par les nouvelles conditions expérimentales, notamment aux environs de 19 eV, 31 eV et 42 eV, ainsi que la valeur très basse de la section efficace résiduelle entre les résonances. D'autre part, on observe sur la figure 1C des fluctuations relativement importantes de la section efficace de fission dans la région des résonances non résolues, par exemple entre 200 eV et 5 keV. De semblables fluctuations se retrouvent dans la section efficace totale sur la figure 1B. Elles proviennent donc principalement de la voie d'entrée et, a priori, ne seraient pas dues à un phénomène de structure intermédiaire dans la section efficace de fission correspondant aux voies partiellement ouvertes 3^- ou 4^-.

Dans le tableau II nous comparons nos valeurs de σ_f moyennées dans plusieurs gammes d'énergie à celles d'autres laboratoires [4-7]. On remarquera qu'elles sont légèrement plus basses entre 900 eV et 3 keV et entre 8 keV et 20 keV et sont en excellent accord avec celles de ORNL-RPI entre 30 eV et 900 eV [6].

3. SECTION EFFICACE DE FISSION DE ^{241}Pu

La mesure décrite ci-dessous est préliminaire; nous n'avions en effet à notre disposition qu'une quantité limitée de ^{241}Pu (129 mg). C'est la raison pour laquelle nous l'avons effectuée avec une base de vol assez courte ($L \simeq 11$ m). Une autre mesure est actuellement en cours avec une quantité plus importante de ^{241}Pu (448 mg), ce qui permet d'utiliser une base de vol plus longue (50 m).

La première mesure a été effectuée entre 1 eV et 3 keV. Les conditions expérimentales sont résumées dans le tableau I.

Les dépôts de ^{241}Pu, sous la forme de PuO_2, d'épaisseur variant de 0,2 à 0,76 mg/cm^2, étaient répartis dans 8 cellules situées dans 2 plans différents.

Les échantillons ont été purifiés 3 semaines avant le début de la mesure pour réduire la contamination en ^{241}Am. La composition isotopique environ 6 mois avant le début de la mesure était la suivante [8]:

^{239}Pu : 1,38%	^{240}Pu : 3,041%
^{241}Pu : 94,399%	^{242}Pu : 1,177%

La faible contamination en ^{239}Pu est visible dans nos résultats expérimentaux par l'apparition des résonances à 7,83 eV, 10,53 eV et 10,86 eV.

La section efficace de fission de ^{241}Pu a été normalisée sur les valeurs de $\sigma_0\Gamma_f$ déduites des paramètres des résonances à 15,95 eV et 16,66 eV [9].

La courbe de σ_f en fonction de l'énergie est tracée de 3 eV à 3 keV sur la figure 2A.

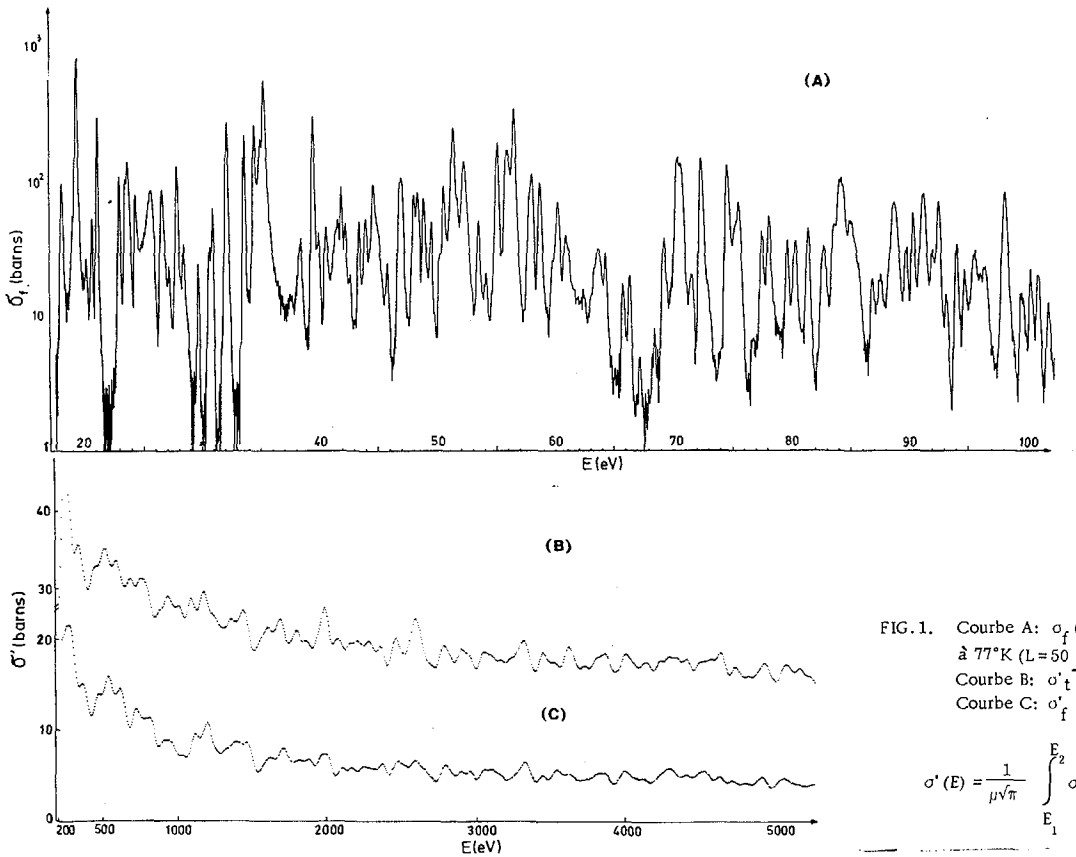

FIG. 1. Courbe A: $\sigma_f(E)$, section efficace de fission de ^{235}U à 77°K (L = 50 m).
Courbe B: $\sigma'_t(E)$, section efficace totale moyennée.
Courbe C: $\sigma'_f(E)$, section efficace de fission moyennée.

$$\sigma'(E) = \frac{1}{\mu\sqrt{\pi}} \int_{E_1}^{E_2} \sigma_f(E') \exp\left[-\frac{(E-E')^2}{2\mu^2}\right] dE'$$

E_1 et E_2 sont les bornes de l'intervalle d'intégration centré sur E et grand par rapport à μ (ici pris égal à 21,2 eV).

TABLEAU II. SECTION EFFICACE MOYENNE DE FISSION DE ^{235}U

Intervalles d'énergies (eV)	$<\sigma_f>$ (barns)					Intervalles d'énergies (eV)	$<\sigma_f>$
	Saclay 1958 [4]	Dubna 1965 [5]	ORNL-RPI 1966 [6]	Los-Alamos 1966 [7]	Saclay (ce travail)		Saclay (ce travail)
						30 - 29	2,242
30 000 - 20 000					2,106	29 - 28	2,242
20 000 - 10 000	2,801	3,271		2,768	2,467	28 - 27	2,176
10 000 - 9 000	3,418	3,340	3,101	3,248	3,074	27 - 26	2,065
9 000 - 8 000	3,505	3,227	3,122	3,030	2,984	26 - 25	2,006
8 000 - 7 000	3,551	3,430	3,931	3,034	3,193	25 - 24	2,101
7 000 - 6 000	3,791	3,457	3,612	3,149	3,469	24 - 23	1,960
6 000 - 5 000	4,274	3,831	3,910	3,459	3,948	23 - 22	2,186
5 000 - 4 000	4,502	4,499	4,728	4,013	4,413	22 - 21	2,080
4 000 - 3 000	4,887	4,907	5,117	4,721	4,854	21 - 20	1,994
3 000 - 2 000	5,761	5,620	5,680	5,464	5,404	20 - 19	2,200
2 000 - 1 000	7,545	7,619	7,601	7,653	7,445	19 - 18	2,409
1 000 - 900	7,874	8,676	7,939	7,932	7,625	18 - 17	2,261
900 - 800	8,586	9,108	8,233	7,821	8,437	17 - 16	2,304
800 - 700	10,89	11,35	11,29	10,99	11,17	16 - 15	2,345
700 - 600	11,72	11,68	11,63	11,48	11,58	15 - 14	2,568
600 - 500	14,59	14,74	15,41	15,43	15,17	14 - 13	2,659
500 - 400	13,19	13,38	13,65	14,69	13,73	13 - 12	2,496
400 - 300	14,38	12,94	13,24	13,21	13,26	12 - 11	2,683
300 - 200	20,52	20,55	20,84	21,75	20,34	11 - 10	2,741
200 - 100	21,31	20,37	21,00	21,56	20,90	10 - 9	3,074
100 - 90	23,98	23,99	22,34	21,91	22,50	9 - 8	2,984
90 - 80	25,63	26,51	28,10	28,65	28,40	8 - 7	3,193
80 - 70	29,22	30,46	32,02	34,24	33,52	7 - 6	3,469
70 - 60	16,21	15,73	14,78	15,13	14,69	6 - 5	3,948
60 - 50	55,74	55,52	61,22	62,55	63,72	5 - 4	4,413
50 - 40	30,88	32,28	33,06	31,91	33,57	4 - 3	4,854
40 - 30	50,48	51,56	56,21	52,20	56,61	3 - 2	5,404
30 - 20	35,66	34,56	36,60		33,82	2 - 1	7,445
20 - 10	48,62	47,39	51,71				

Dans le tableau III, les valeurs de σ_f moyennées dans plusieurs gammes d'énergie sont comparées à celles d'autres laboratoires [10-12]. Les écarts entre nos valeurs et celles de la moyenne des quatre mesures sont inférieurs à 5%, sauf de 70 eV à 80 eV et de 90 eV à 100 eV où ils sont de l'ordre de 10%.

Cette analyse conjuguée avec les valeurs de 2 g Γ_n déduites de la section efficace totale [9] permet, dans la majorité des cas, d'obtenir les largeurs de fission jusqu'à une énergie de 50 eV. Le tableau IV montre cependant qu'il y a parfois incompatibilité entre les valeurs de 2 g Γ_n et celles de σ_0 Γ_f déduites de notre mesure.

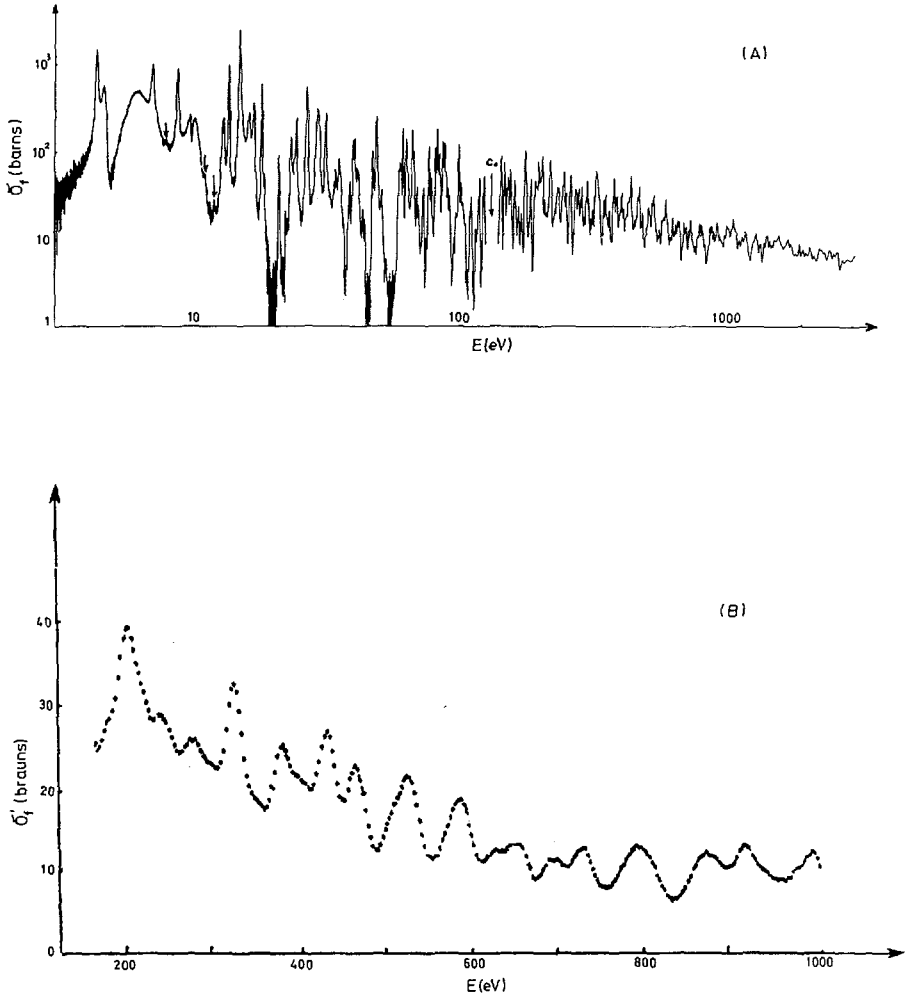

FIG. 2. Section efficace de fission de ^{241}Pu à 77°K (L = 10, 89 m). Les résonances dues à ^{239}Pu sont représentées par des flèches sur la courbe A.

Courbe A: σ_f (E) non moyennée.
Courbe B : σ'_f (E) moyennée (voir texte).

Dans quelques cas où les effets d'interférences sont très marqués, par exemple entre 6 eV et 14 eV, nous avons utilisé un programme de moindres carrés basé sur le formalisme de Reich et Moore et mis au point par Derrien [13].

La figure 3 montre un bon accord de 8 eV à 14 eV entre les points expérimentaux et la courbe calculée en choisissant les spins proposés par Moore [14] sauf pour les résonances à 9, 55 eV et 10, 00 eV auxquelles nous attribuons le même spin.

TABLEAU III. SECTION EFFICACE MOYENNE DE FISSION DE ^{241}Pu

Intervalles d'énergies (eV)	$<\sigma_f>$ (barns)					
	(1)	(2)	(3)	(4)	(5)	
	Harwell [10]	Los Alamos [11]	Geel [12]	Saclay (ce travail)	Moyenne de (1), (2), (3), (4)	(4)/(5)
3000 - 2000		6,515		6,193		
2000 - 1000	9,327	8,431	7,64	8,587	8,496	1,011
1000 - 900	10,73	9,976	9,71	10,87	10,32	1,053
900 - 800	9,317	9,363	8,37	9,64	9,17	1,051
800 - 700	11,02	9,787	9,55	10,63	10,25	1,037
700 - 600	11,56	10,93	9,98	11,41	10,97	1,040
600 - 500	16,58	17,47	14,36	16,76	16,29	1,029
500 - 400	20,60	21,05	14,78	19,39	18,96	1,023
400 - 300	22,14	23,43	18,20	22,41	21,55	1,040
300 - 200	28,98	31,85	26,08	27,61	28,63	0,964
200 - 100	27,48	28,91	24,98			
100 - 90	33,03	28,58	27,7	25,98	28,82	0,901
90 - 80		70,67	68,55	66,72		
80 - 70	29,40	30,92	28,94	26,13	28,85	0,905
70 - 60		51,64	56,45	55,67		
60 - 50	19,26	16,09	16,80	16,60	17,19	0,966
50 - 40	41,80	35,31	36,54	40,24	38,47	1,046
40 - 30	46,44	38,73	46,50	46,91	44,65	1,051
30 - 20	85,96	72,77	82,86	81,37	80,74	1,008
20 - 10	152,74		146,82	148,37		

Pour certaines résonances dont la valeur Γ est supérieure à 300 meV on suppose $g = 1/2$ et on calcule Γ_f par la formule suivante:

$$\Gamma_{f\,(meV)} = \Gamma_{(meV)} - (40 + \Gamma_{n\,(meV)}) \qquad (2)$$

La distribution intégrale des largeurs de fission des résonances est tracée sur la figure 4. On ne constate pas l'apparition de deux familles de résonances ayant des largeurs moyennes $<\Gamma_f>$ très différentes [15]. L'histogramme expérimental peut être bien décrit par une seule distribution en χ^2 dont les paramètres déterminés par la méthode des moindres carrés sont les suivants:

$$<\Gamma_f> = 236 \text{ meV}, \quad \nu = 0,9$$

TABLEAU IV. PARAMETRES DE RESONANCES DE ^{241}Pu

E (eV)	$2g\Gamma_n$ (meV) [9]	$\sigma_0\Gamma$ (b·eV)	Γ (meV)	$\sigma_0\Gamma_f$ (b·eV)	Γ_f (meV)
4,28	0,66	200	72	113	41,2
4,56	0,43	122,6	180	90	132
6,05	2,43	522,1	1300	470	1268 [a]
6,93	0,71	133,2			118 [b]
8,62	1,0	150,8	103	107	54 [b]
9,55	0,18	24,5			221 [b]
10,00	1,5	195			968 [b]
12,81	0,79	80,2	261	61,9	201
13,43	2,2	213,0	60	106,1	30
14,77	6,2	545,7	145	411,2	109
15,95	1,52	123,9	519	114	477,5
16,66	1,23	96,0	225	79	185
17,85	3,2	233,1	55	71	16,8
18,26	0,16	11,4	100	7	61,4
20,71	0,34	21,3	55	12,4	32
21,90	0,15	8,9	50	1,8	10
23,04	1,2	67,7	300	50	214
23,70			190	16,6	
24,08	1,6	86,4	180	45	68
24,61				10	
26,42	4,4	216,5	280	181	234
28,91	4,8	215,8	650	202	608,4
29,48	0,7	30,9	90	19	55
31,03	2,9	121,5	240	84,7	167,3
32,20			1800	50	1760 [a]
33,36	0,40	15,6	180	8,4	97
33,81	0,114	4,4	150	9,9	
34,52			400	14,4	360 [a]
35,05	2,1	77,9	600	50	558 [a]
36,10			300	5	
37,50			400	7	
38,15	1,12	38,2	230	15,7	95
38,8				6	
39,39	1,34	44,2	201	45	
39,95	2,12	69	80	33	38
40,7	0,83	26,5	400	20	302
41,16	1,64	51,8	106	47,4	97
42,72	0,12	3,7	240	8,8	
43,45	0,2	6	114	4,4	83,6
46,62	1,5	41,8	300	44	258 [a]
48,17	6,26	168,9	500	177,3	454 [a]
50,32			700	31,4	660 [a]
52,28				1,4	
52,8				0,8	
58,45				44,8	
59,31				53,9	
60,59				86	
62,40				126,8	

[a] Valeur de Γ_f obtenue par la formule (2) (voir texte).

[b] Valeur obtenue par une analyse multiniveaux.

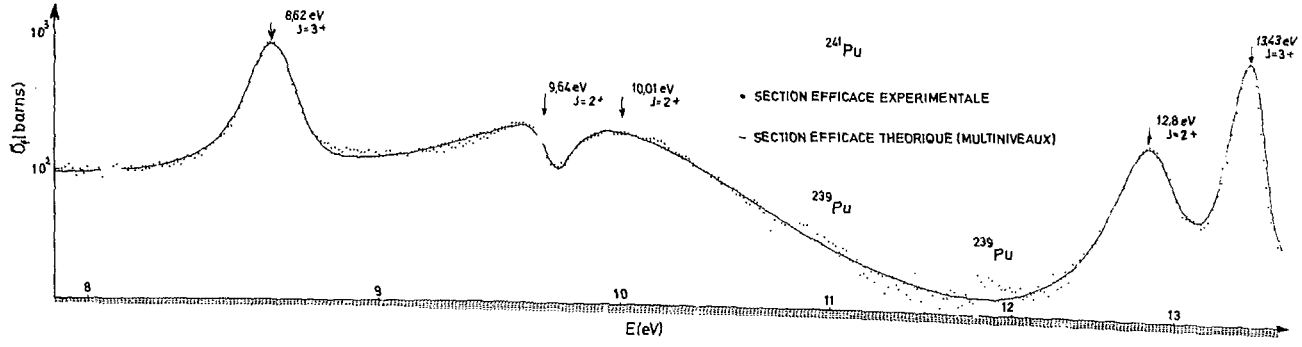

FIG. 3. Résultat de l' analyse par un programme de moindres carrés basé sur un formalisme multiniveaux de σ_f de ^{241}Pu entre 8 eV et 14 eV.

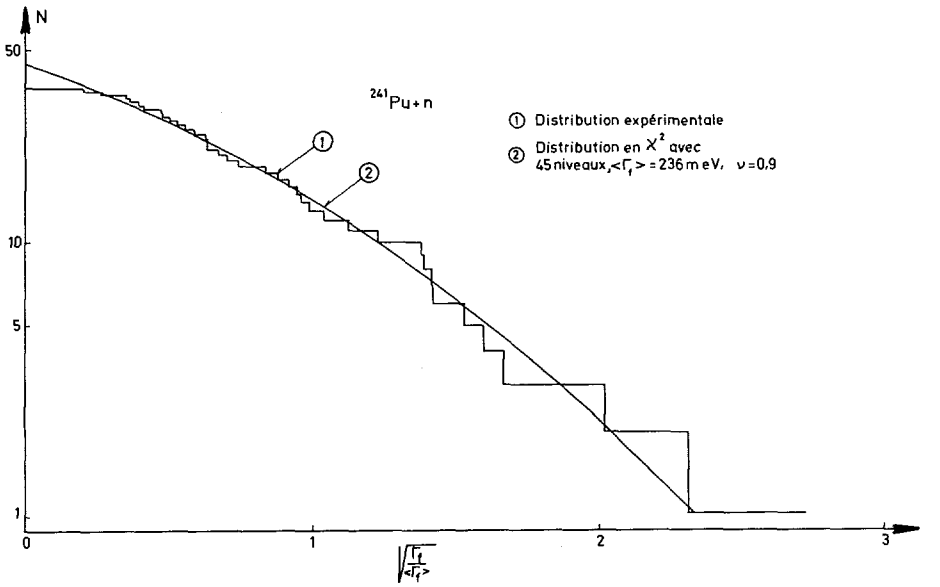

FIG. 4. Distribution intégrale des largeurs de fission des résonances de ^{241}Pu de 0 à 50 eV.

Dans la région des résonances non résolues de 150 eV à 1 keV, la section efficace de fission présente d'assez grandes fluctuations qui sont illustrées par la figure 2B où l'on a tracé, en fonction de l'énergie, la quantité suivante:

$$\sigma_f^1 (E) = \frac{1}{\mu\sqrt{\pi}} \int_{E_1}^{E_2} \sigma_f (E') \exp\left[-\frac{(E - E')^2}{2\mu^2}\right] dE'$$

μ est pris égal à 8,5 eV.

De semblables fluctuations se retrouvent aussi dans la section efficace totale.

Les résultats de la deuxième mesure (avec L = 50 m) sont encore préliminaires. Cependant, la qualité de la mesure apparaît sur la figure 5 où le nombre de coups par canal des événements de fission est tracé en fonction du numéro du canal dans la gamme d'énergie comprise entre 20 eV et 300 eV. Une fois la mesure terminée, la précision statistique sera encore meilleure et permettra une analyse des résonances jusqu'à 200 eV environ.

4. CONCLUSION

Nous avons montré dans les sections efficaces moyennes totale et de fission de ^{235}U de grandes fluctuations.

Nous avons également mis en évidence dans la section efficace moyenne de fission de ^{241}Pu des fluctuations importantes, de l'ordre de 60% vers 500 eV.

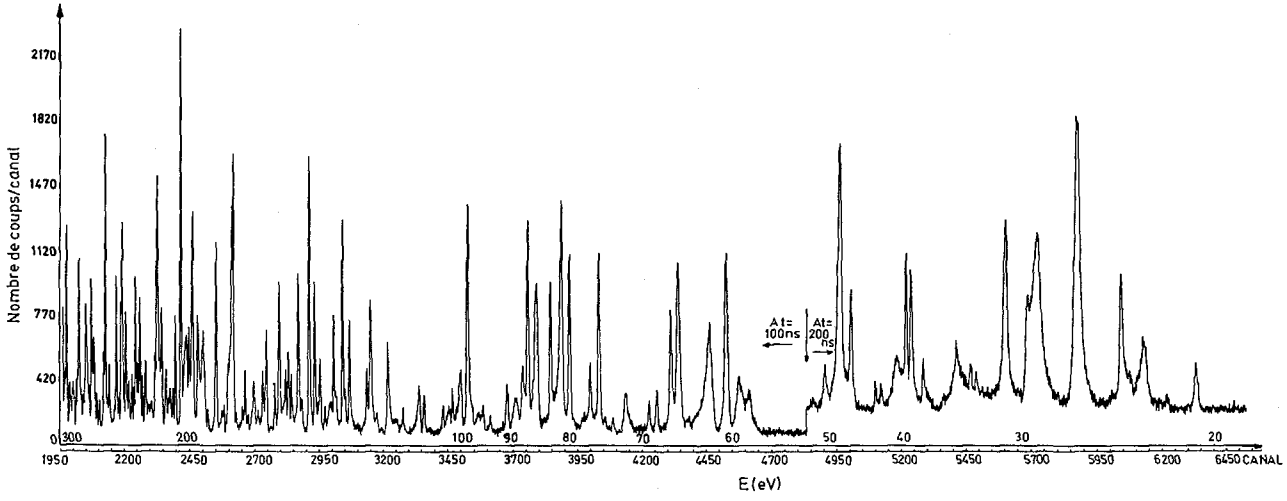

FIG. 5. Taux de comptage de fission de ^{241}Pu à 77°K (L = 50 m).

Ces fluctuactions semblent dues à la voie d'entrée et vont être étudiées plus en détail.

Enfin nous avons présenté les résultats d'une première mesure de σ_f de ^{241}Pu. Cette mesure nous a permis d'analyser les résonances jusqu'à une énergie de 50 eV. L'analyse sera poursuivie jusqu'aux environs de 200 eV à l'aide de la deuxième mesure à meilleure résolution.

REMERCIEMENTS

Nous remercions l'UKAEA, qui nous a fourni le ^{241}Pu pour la mesure préliminaire.

Nous remercions également Mlle Valentin pour la préparation et la purification des échantillons.

REFERENCES

[1] EGGERMANN, C., et al., Détecteur de fission à basse température (77°K), Nucl. Instrum. Meth. (à paraître).
[2] BLONS, J., et al., Rev. Phys. appl. 4 (juin 1969) 287.
[3] MICHAUDON, A., Rapport CEA n° 2252 (1964).
[4] MICHAUDON, A., Rapport CEA n° 1093 (1958).
[5] VAN SHI-DI, et al., «Interaction entre neutrons et noyaux de ^{235}U dans la région des énergies de 2 eV à 30 keV» (en russe), Physics and Chemistry of Fission (C.r. Coll. Salzbourg, 1965) I, AIEA, Vienne (1965) 287.
[6] DE SAUSSURE, G., et al., «Measurement of the neutron capture and fission cross-sections and of their ratio alpha for ^{233}U, ^{235}U and ^{239}Pu», Nuclear Data for Reactors (C.r. Conf. Paris, 1966) II, AIEA, Vienne (1967) 233.
[7] WILBURK, et al., Neutron Cross Section Technology (Proc. Conf. Washington, 1966) II (1966) 97.
[8] GLOVER, K.M., Communication privée (déc. 1968).
[9] Neutron Cross Sections, BNL-325, Suppl. No. 2 (1965).
[10] JAMES, G.D., Nucl. Phys. 65 (1965) 353.
[11] SIMPSON, O.D., et al., Neutron Cross Section Technology (Proc. Conf. Washington, 1966) II, (1966) 910.
[12] MIGNECO, E., et al., Communication privée (1970).
[13] DERRIEN, H., BLONS, J., MICHAUDON, A., «Analyse simultanée de 5,7 à 160 eV des sections efficaces totale et de fission du plutonium-239 par un formalisme multiniveaux», ces comptes rendus, IAEA-CN-26/61.
[14] MOORE, M.S., et al., Phys. Rev. 135 (1964) B945.
[15] MICHAUDON, A., «Détermination du spin des résonances des noyaux fissiles», Nuclear Data for Reactors (C.r. Conf. Paris, 1966) II, AIEA, Vienne (1967) 161.

ANALYSE SIMULTANEE DE 5, 7 A 160 eV DES SECTIONS EFFICACES TOTALE ET DE FISSION DU PLUTONIUM-239 PAR UN FORMALISME MULTINIVEAUX

H. DERRIEN, J. BLONS, A. MICHAUDON
CEA, Centre d'études
nucléaires de Saclay,
France

Abstract — Résumé

SIMULTANEOUS ANALYSIS OF TOTAL AND FISSION CROSS-SECTIONS OF ^{239}Pu FROM 5.7 TO 160 eV USING A MULTI-LEVEL FORMALISM

Total and fission cross-sections have been measured at Saclay using the 45-MeV linear accelerator as a pulsed source of neutrons. The two measurements were carried out with a nominal resolution of 0.5 and 1 ns/m, respectively, the samples being held at the temperature of liquid nitrogen. In most cases analysis of the shape of the resonances by the Breit-Wigner single-level formula gave a satisfactory value for the parameters. However, this formula cannot always reproduce a cross-section shape in agreement with the measurements. More particularly, certain differences between the theoretical and experimental curves can be definitely reduced by adding resonances, the existence of which has not been definitely established. To reproduce as faithfully as possible the cross-section shape and thus define accurately certain parameters, the analysis has been carried out using a multi-level formalism allowing for interference between resonances of the same spin; the formalism used is that of Reich and Moore. The programme makes use of a least squares method of adjustment applied simultaneously to the total and fission cross-sections. Analytical results are presented, covering in particular: a comparison of the theoretical curves with the experimental results; a statistical study of the parameters and a comparison with an equivalent study made on the results of a single-level analysis; a determination of the spin of certain levels by systematic study of the shape of the interferences; the number of exit channels of the 0^+ and 1^+ states of the compound nucleus.

ANALYSE SIMULTANEE DE 5,7 A 160 eV DES SECTIONS EFFICACES TOTALE ET DE FISSION DU PLUTONIUM-239 PAR UN FORMALISME MULTINIVEAUX.

Les sections efficaces totale et de fission ont été mesurées à Saclay en utilisant l'accélérateur linéaire de 45 MeV comme source pulsée de neutrons. Les deux mesures ont été faites avec une résolution nominale de 0, 5 et 1 ns/m respectivement, et avec des échantillons portés à la température de l'azote liquide. L'analyse de forme des résonances, à l'aide du formalisme de Breit-Wigner à 1 niveau, permet d'obtenir, dans la plupart des cas, une bonne valeur des paramètres. Cependant, ce formalisme ne peut pas toujours reproduire la forme des sections efficaces telles qu'elles sont mesurées. En particulier, certains écarts entre les courbes théoriques et les courbes expérimentales peuvent être nettement diminués en ajoutant des résonances dont l'existence n'est pas établie d'une façon certaine. C'est pour pouvoir reproduire le plus fidèlement possible la forme des sections efficaces, et par là même préciser certains paramètres, que l'analyse a été poursuivie avec un formalisme multiniveaux qui tient compte de l'interférence entre résonances de même spin; le formalisme utilisé est celui de Reich-Moore. Le programme utilise une méthode d'ajustement par moindres carrés, simultanément sur les sections efficaces totale et de fission. Les résultats de l'analyse sont présentés, notamment: la comparaison des courbes théoriques aux résultats expérimentaux; l'étude statistique des paramètres et la comparaison avec la même étude faite sur les résultats de l'analyse à 1 niveau; la détermination des spins de certains niveaux par l'étude systématique de la forme des interférences; le nombre de voies de sortie des états 0^+ et 1^+ du noyau composé.

1. INTRODUCTION

Les sections efficaces totale et de fission de ^{239}Pu ont été mesurées auprès de l'accélérateur linéaire de 45 MeV de Saclay utilisé comme source pulsée de neutrons, avec une résolution nominale de 0,5 ns/m et 1 ns/m respectivement. Dans les deux cas, les échantillons étaient portés à la température de 77°K pour diminuer l'effet Doppler et obtenir ainsi une meilleure séparation des résonances. Les sections efficaces ont été analysées par la méthode des formes jusqu'à 660 eV, en utilisant le formalisme de Breit-Wigner à 1 niveau [1-3]. Cette analyse a permis d'aboutir aux conclusions suivantes:

1°) La distribution des espacements et des largeurs neutroniques réduites a montré qu'environ 95% des niveaux sont identifiés dans l'intervalle d'énergie de 0 à 300 eV; les espacements moyens des résonances des deux états de spin 0^+ et 1^+ sont respectivement $<D_0> = 9,6$ eV et $<D_1> = 3,2$ eV.

2°) La distribution des largeurs de fission est composée de deux familles de résonances dont les largeurs moyennes sont très différentes. Ces deux familles correspondent très vraisemblablement aux deux états de spin 0^+ et 1^+. La largeur moyenne de fission de l'état 0^+ est $<\Gamma_f>_{0^+} \simeq 2200$ meV et le nombre de voies de sortie est voisin de 1,4; pour l'état 1^+, la largeur moyenne est $<\Gamma_f>_{1^+} = 36$ meV et le nombre de voies de sortie est égal à 1.

3°) Le spin a pu être attribué pour un très grand nombre de résonances, soit par des méthodes indirectes (valeurs de Γ_f ou de Γ_γ [1, 2], distribution en masse de produits de fission [4]), soit par des mesures de diffusion élastique [5].

4°) L'étude de la variation, en fonction de l'énergie, de la largeur moyenne $<\Gamma_f>_{1^+}$ calculée sur des intervalles de 110 eV a mis en évidence un phénomène de structure intermédiaire dans la section efficace de fission due à la voie de sortie 1^+ [6].

Toutefois quelques réserves sont à apporter à cette analyse; le formalisme de Breit-Wigner à un niveau n'est une bonne approximation, dans l'analyse des sections efficaces des noyaux fissiles, que si l'effet d'interférence entre résonances, dû aux voies de sortie de fission, est faible. Cette condition est probablement réalisée pour les résonances 1^+ pour lesquelles $<\Gamma_f>/<D> \simeq 0,01$; mais elle l'est beaucoup moins pour les résonances 0^+ pour lesquelles $<\Gamma_f>/<D> \simeq 0,16$.

Les sections efficaces dues aux voies 0^+ risquent donc d'être sensiblement perturbées par l'effet d'interférence; pour reproduire fidèlement ces perturbations, il est nécessaire, en se limitant au formalisme à un niveau, d'ajouter d'une façon artificielle des résonances supplémentaires, par exemple à 11,5 eV, 57,8 eV et 83,5 eV.

Il est donc souhaitable, pour préciser le phénomène de fission dans les voies 0^+, de reprendre l'analyse par un formalisme multiniveaux. Les sections efficaces de ^{239}Pu semblent bien se prêter à une telle analyse, pour les raisons suivantes:

a) le nombre de voies de sortie de fission est très limité;
b) presque tous les niveaux sont identifiés dans la zone d'analyse; les dissymétries sont donc dues principalement à des interférences;
c) le spin a pu être attribué à un nombre important de résonances, ce qui facilite leur classification.

2. CHOIX DU FORMALISME

Une théorie complète des réactions nucléaires, aboutissant à un formalisme capable d'expliquer la forme des sections efficaces neutroniques dans le domaine des résonances, est extrêmement complexe. Certaines approximations sont nécessaires pour que les calculs soient possibles. Les formalismes utilisés jusqu'à présent sont basés sur la théorie dite de la matrice R de Wigner-Eisenbud [7] qui établit la relation suivante entre la matrice R et la matrice de collision U:

$$U = \omega \frac{1 + i\,(BRB + C)}{1 - i\,(BRB + C)}\,\omega \qquad (1)$$

Cette relation matricielle est définie dans l'espace des voies d'entrée et de sortie. Les éléments de la matrice R sont égaux à:

$$R_{\alpha\beta} = \sum_{\lambda} \frac{\gamma_{\lambda\alpha}\,\gamma_{\lambda\beta}}{E_\lambda - E}$$

$\gamma_{\lambda\alpha}$ et $\gamma_{\lambda\beta}$ sont les amplitudes de désexcitation du niveau λ dans les voies α and β; E_λ est l'énergie du niveau λ.

Le calcul des éléments de la matrice U à partir de la relation (1) présente certaines difficultés si le nombre de voies de sortie est trop élevé. Mais, pour l'étude des noyaux fissiles, le problème peut être simplifié; en effet, les voies de désexcitation par émission de rayons γ sont très nombreuses et ainsi les interférences correspondantes s'annulent en moyenne; les largeurs de diffusion neutronique sont, en général, faibles devant les largeurs de fission; les interférences dues à la voie d'entrée sont donc négligeables; il suffira de tenir compte des voies de fission qui, étant peu nombreuses, peuvent conduire à de très forts effets d'interférence.

Trois méthodes ont été proposées pour l'analyse des sections efficaces des noyaux fissiles. La méthode de Vogt [8] utilise la matrice des niveaux A dont on connaît l'inverse [9]; le temps de calcul devient très important si on veut tenir compte d'un grand nombre de résonances. La méthode de Adler et Adler (diagonalisation de la matrice A^{-1}) [10] aboutit à une formulation simple des sections efficaces en une somme de termes de Breit-Wigner à un niveau; mais l'interprétation des paramètres est très difficile, car leur relation avec les paramètres de la matrice R est très complexe.

La troisième méthode, celle de Reich-Moore [11], utilise une relation formellement identique à la relation (1); mais l'espace des voies dans lequel les matrices sont définies est limité à quelques-unes d'entre elles: la voie d'entrée (neutrons s) et les voies de fission considérées. Dans les calculs, la matrice R est remplacée par la matrice R' définie par la relation:

$$R'_{\alpha\beta} = \sum_{\lambda} \frac{\gamma_{\lambda\alpha}\,\gamma_{\lambda\beta}}{E_\lambda - E - \frac{i}{2}\Gamma_{\lambda\gamma}} \qquad (2)$$

dans laquelle $\Gamma_{\lambda\gamma}$ est la largeur totale de capture radiative du niveau λ.

La matrice U est donc liée à R' par la relation:

$$U = \omega \frac{1 + i\,(BR'B + C)}{1 - i\,(BR'B + C)}\,\omega \tag{3}$$

Cette méthode semble la mieux adaptée à l'analyse des sections efficaces de ^{239}Pu, car le nombre de voies de sortie de fission est au maximum égal à 2 alors que le nombre des résonances est beaucoup plus important; les calculs peuvent donc s'effectuer avec des matrices d'ordre 3 au maximum (une voie de diffusion, deux voies de fission).

3. DESCRIPTION DES CALCULS

La matrice U est calculée à partir de la relation (3) dans laquelle les matrices B et C sont diagonales.

Les éléments de B apparaissent dans la définition des largeurs partielles $\Gamma_{\lambda\alpha}$ de désexcitation du niveau λ dans les voies α par la relation:

$$\tfrac{1}{2}\Gamma_{\lambda\alpha} = B_\alpha^2\,\gamma_{\lambda\alpha}^2 \tag{4}$$

La matrice C est choisie égale à 0 par les conditions aux limites dans les voies de fission.

Dans la matrice des phases ω, les seuls éléments à considérer sont ceux qui correspondent à la voie d'entrée ($\alpha = 1$):

$$\omega_1 = \exp(-i\,k\,R) \tag{5}$$

k est le nombre d'onde du neutron incident, R est le rayon du noyau.

Les sections efficaces σ_T^J et σ_f^J, pour chaque état de spin, sont égales à:

$$\sigma_T^J = 2\pi\,\lambda\!\!\!^{-2}\,g^J\,\mathrm{Re}\,(1 - U_{11}^J) \tag{6}$$

$$\sigma_f^J = \pi\,\lambda\!\!\!^{-2}\,g^J\left[\,|U_{12}^J|^2 + |U_{13}^J|^2\right] \tag{7}$$

Dans les calculs, les voies sont repérées par les indices suivants:
1: voie d'entrée (neutrons s); 2 et 3: voies de sortie de fission.

Le programme permet d'effectuer les opérations suivantes:

a) calcul des sections efficaces théoriques σ_T^J et σ_f^J;
b) calcul des sections efficaces élargies par un effet Doppler gaussien et par la résolution expérimentale (supposée également gaussienne);
c) ajustement des courbes théoriques aux points expérimentaux par une méthode de moindres carrés, simultanément sur les sections efficaces totale et de fission;
d) tracé superposé des points expérimentaux et des courbes théoriques.

Les calculs effectués avec le calculateur CDC-6600 du CEN de Saclay, peuvent porter au maximum sur 3000 points et 100 résonances; 20 paramètres peuvent varier simultanément. Le temps de calcul est de l'ordre d'une minute pour 1000 points, 60 résonances et un paramètre variable.

4. ANALYSE ET INTERPRETATION DES RESULTATS

4.1. Généralités

Les sections efficaces totale et de fission ont été analysées de 5,7 à 160 eV; cette gamme d'énergie a été découpée en quatre zones: de 5,7 à 40 eV; de 40 eV à 78 eV; de 70 eV à 112 eV; de 112 eV à 160 eV.

Un tel découpage est rendu nécessaire par le nombre de points maximal que le programme peut traiter et aussi par le temps de calcul; mais, dans chaque zone, on tient compte des résonances des autres zones. De 5,7 eV à 40 eV, seule la section efficace totale est analysée.

Au cours de l'ajustement par moindres carrés, tous les paramètres peuvent être variables sauf:

- la largeur totale de capture radiative Γ_γ qui est fixée à la valeur obtenue par l'analyse à 1 niveau [1, 2];
- le spin des résonances.

La valeur du spin J est choisie de la façon suivante:

a) Lorsque J est déterminé soit par une mesure directe [5], soit par une mesure indirecte [1, 4], nous avons adopté cette valeur.
b) Lorsque la largeur de la résonance est supérieure à 500 meV, nous avons adopté la valeur J = 0 [1].
c) Dans certains cas, le spin a pu être déterminé par l'analyse elle-même.
d) Les résonances restantes sont généralement de faible amplitude et ne donnent lieu qu'à de faibles effets d'interférences; leur largeur de fission est dans tous les cas inférieure à 200 meV et, pour cela, nous les avons classées dans la famille de spin J = 1, ce qui est justifié pour la plupart d'entre elles.

4.2. Résultats

Les résultats obtenus sont montrés sur les figures 1 à 4, où sont tracés et comparés les points expérimentaux et les courbes théoriques résultant de l'analyse. Il y a en général un bon accord entre les points expérimentaux et les courbes théoriques. Dans la zone de 5,7 eV à 40 eV, où seule la section efficace totale a été analysée, les résultats sont en accord avec la section efficace de fission de Bollinger [12].

Les paramètres des résonances sont rassemblés dans le tableau I. Ils peuvent être comparés à ceux qui résultent de l'analyse des mêmes sections efficaces par un formalisme à 1 niveau [1, 2]. On constate que:

a) Un nombre plus faible de résonances permet d'expliquer la forme des sections efficaces; trois résonances à 11,5 eV, 57,8 eV et 83,5 eV, introduites dans l'analyse à 1 niveau, ne sont pas nécessaires quand on utilise un formalisme multiniveaux; il en résulte, dans les zones d'énergie correspondante, quelques différences significatives pour les largeurs neutroniques et les largeurs de fission.
b) Les paramètres des résonances de spin 1^+ sont pratiquement inchangés; en particulier, une seule voie de sortie 1^+ permet d'expliquer la forme des sections efficaces.

L'attribution du spin a pu être faite dans les quatre cas suivants:

a) La forte dissymétrie de la résonance à 23,87 eV ne peut être expliquée que par une interférence avec la résonance à 22,23 eV qui est de spin 1^+; la résonance à 23,87 eV est donc aussi de spin 1^+.

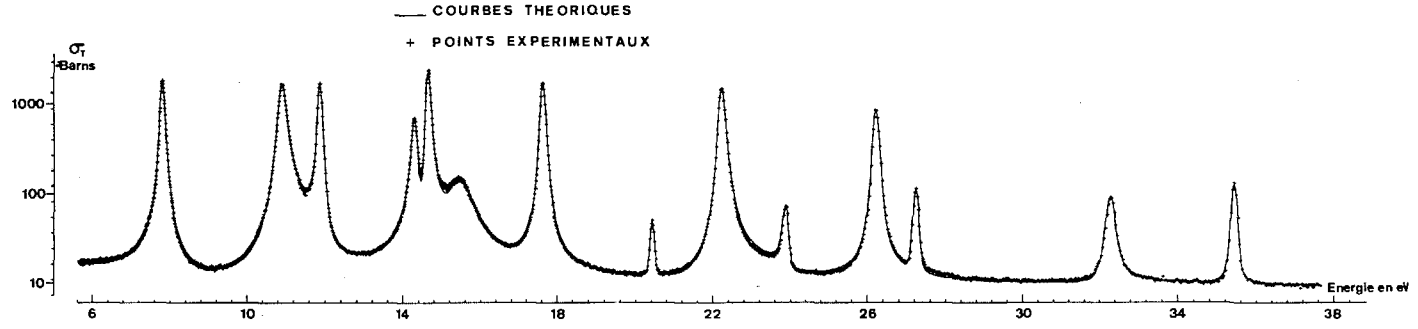

FIG. 1. Section efficace totale de ^{239}Pu entre 5, 7 et 36 eV.

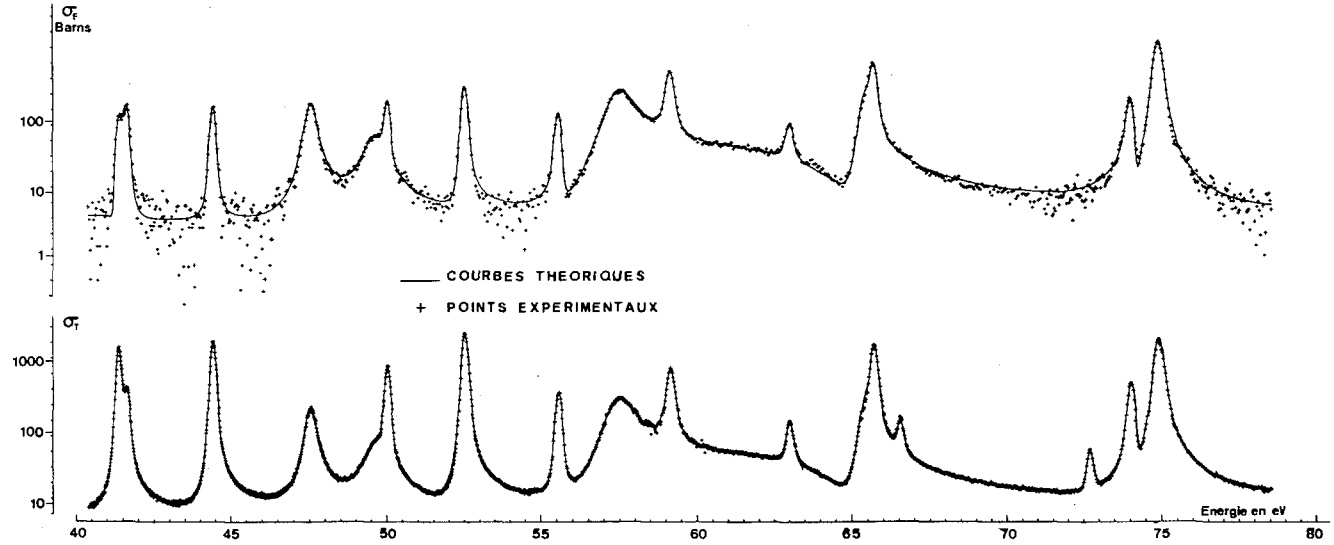

FIG. 2. Sections efficaces totale et de fission de ^{239}Pu entre 40 et 78 eV.

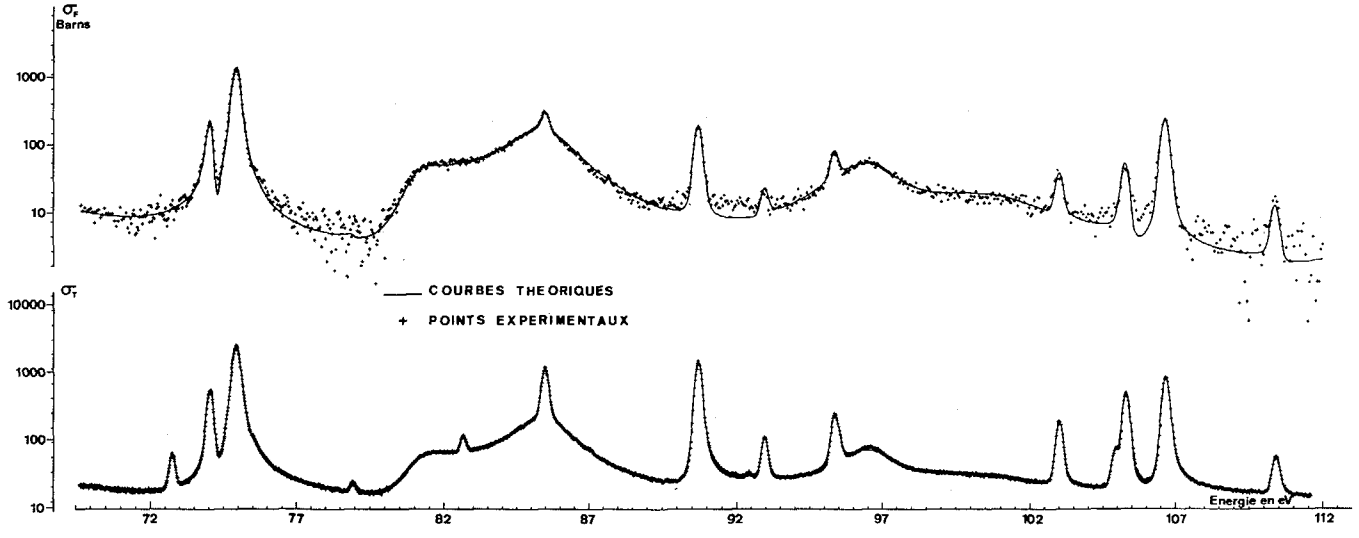

FIG. 3. Sections efficaces totale et de fission de ^{239}Pu entre 70 et 112 eV.

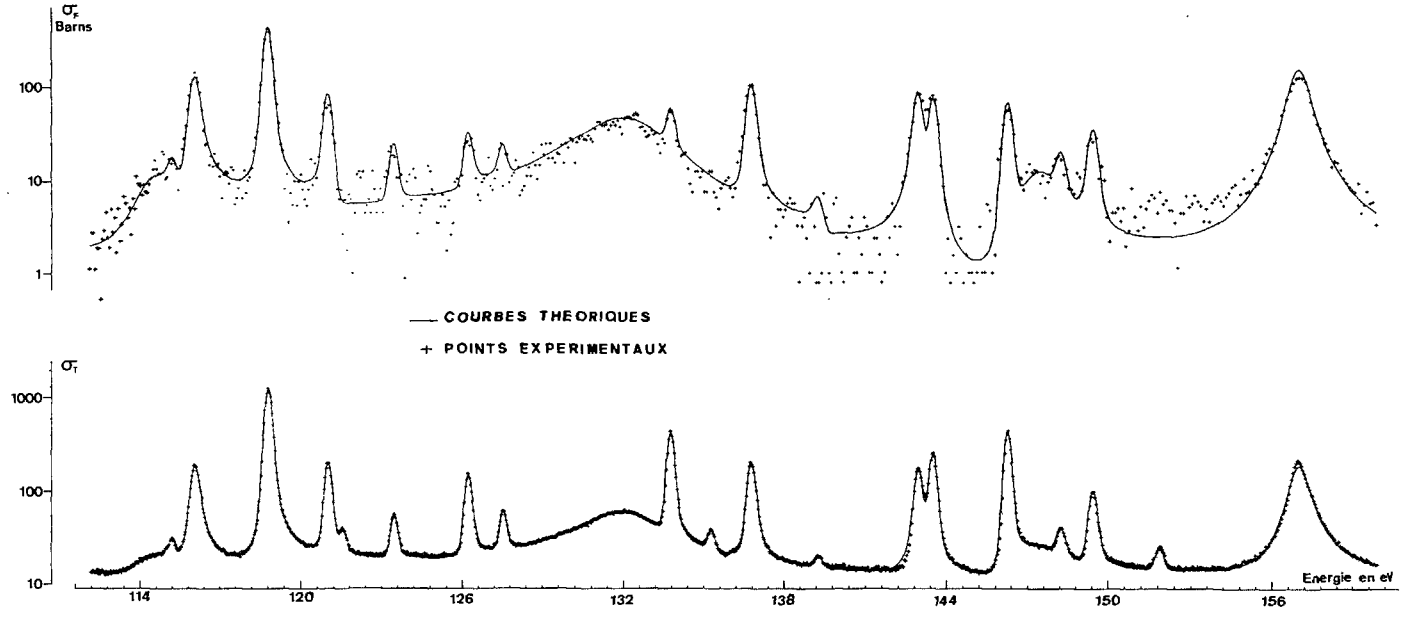

FIG. 4. Sections efficaces totale et de fission de ^{239}Pu entre 112 et 160 eV.

TABLEAU I. PARAMETRES DES RESONANCES

Energie (eV)	Γ_n (meV)	Voie 1^+	Voies 0^+		J		Energie (eV)	Γ_n (meV)	Voie 1^+	Voies 0^+		J	
		Γ_f (eV)	Γ_{f1} (eV)	Γ_{f2} (eV)	(a)	(b)			Γ_f (eV)	Γ_{f1} (eV)	Γ_{f2} (eV)	(a)	(b)
0,296	0,24			0,0600	0		82,666	0,39	0,0100				1
7,800	0,77	- 0,0470			1		85,490	7,45	0,0094			1	
10,910	1,85	- 0,1200			1		85,534	53,41		- 2,0100	0,0550	0	
11,878	0,98	0,0210			1		90,711	11,86	0,0090			1	
14,307	0,66	0,0610			1		92,953	0,70	0,0090				1
14,660	1,92	0,0370			1		95,374	1,90	- 0,0250			1	
15,405	1,73		- 0,4420	0,0994	0		96,332	20,66		0,8420	1,8160	0	
17,633	1,83	- 0,0405			1		101,751	9,05		- 4,8230	0,0250	0	
22,234	2,59	- 0,0640			1		103,010	1,61	0,0100			1	
23,876	0,09	0,0300				1	105,301	4,78	- 0,0060			1	
26,223	1,52	0,0440			1		106,670	8,93	- 0,0260			1	
27,233	0,15	- 0,0080				1	110,410	0,44	0,0130				1
32,265	0,84			- 0,1140	0		114,692	2,50		- 1,6540	- 0,0170	0	
35,422	0,25	0,0053			1		115,185	0,21	0,1600				1
41,373	3,79	- 0,0036			1		116,075	11,75		- 0,1170	- 0,1390	0	
41,623	1,38	0,0434				1	118,831	16,85	- 0,0340			1	
44,435	5,83	- 0,0050			1		121,006	2,38	0,0360				1
47,494	5,25		0,2810	- 0,0700	0		123,467	0,51	- 0,0390				1
49,446	3,44		- 0,7860	- 0,0610	0		126,226	1,93	- 0,0200				1
50,033	2,97	- 0,0125			1		127,557	0,51	0,0250				1
52,533	10,02	0,0090			1		132,321	35,06		3,9910	- 0,0350	0	
55,582	1,51	0,0220			1		133,784	5,59	- 0,0060			1	
57,003	14,47		- 1,5540	0,0280	0		136,770	10,24			- 0,0840	0	
59,153	4,80	0,1020			1		139,340	0,10	0,1200			1	
61,866	26,25		7,1020	0,0200	0		142,963	3,24	0,0820			1	
63,018	0,70	0,0800				1	143,470	4,08	0,0310			1	
65,497	13,66		0,2380	0,1510		0	146,250	7,05	0,0130			1	
65,711	9,17	0,0285			1		147,496	3,53		1,4990	0,0860	0	
74,053	3,37	- 0,0260			1		148,242	0,44	0,1020				1
74,937	22,78	- 0,0870			1		149,442	1,69	0,0500				1
78,968	0,04	0,0020				1	157,009	32,55		0,0290	0,4730	0	
80,915	4,95		0,9630	0,5820	0								

[a] Spins attribués antérieurement [4, 5].

[b] Spins donnés dans ce travail (voir texte).

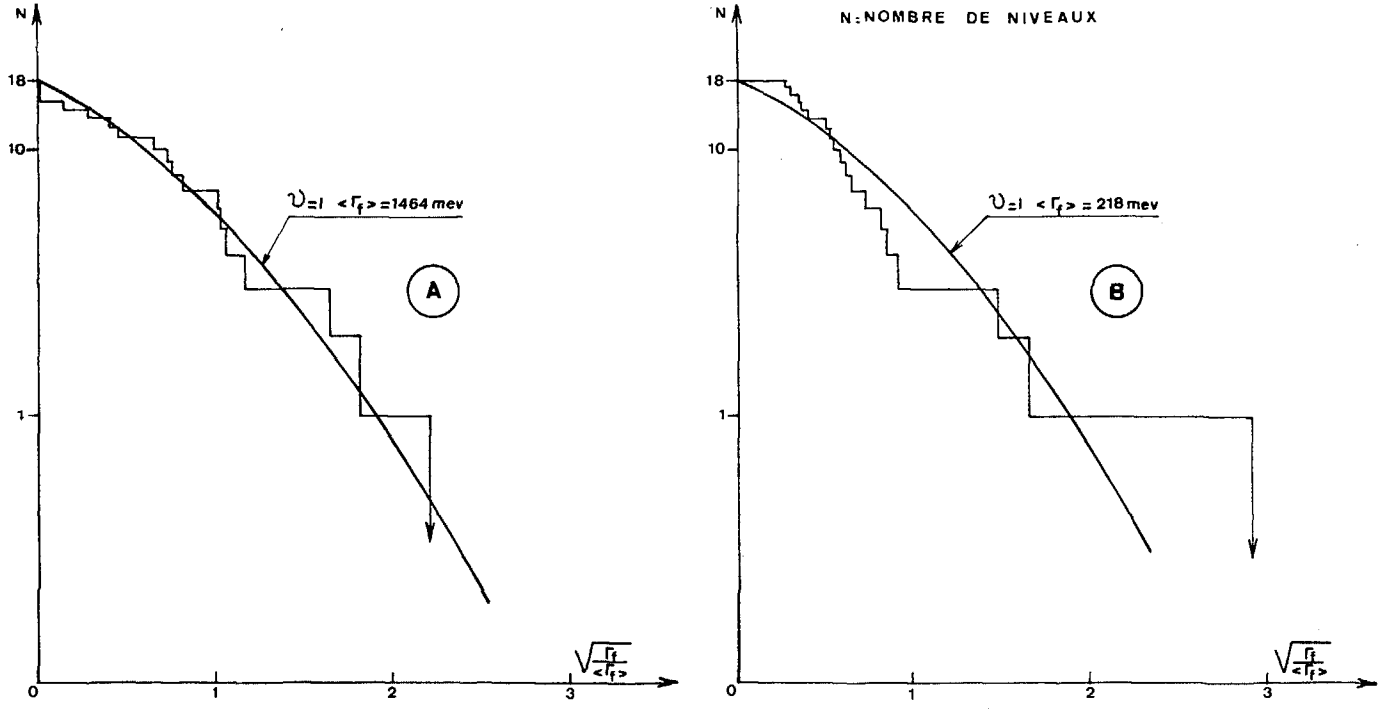

FIG. 5. Distribution intégrale des largeurs partielles de fission dans les deux voies 0^+.

A - première voie, $<\Gamma_f>$ = 1464 meV, ν = 1.

B- deuxième voie, $<\Gamma_f>$ = 218 meV, ν = 1.

b) On ne peut expliquer les résultats expérimentaux vers 41 eV qu'en donnant à la résonance à 41,62 eV le même spin 1^+ qu'à la résonance à 41,37 eV.
c) La résonance à 63,02 eV est très symétrique et on ne peut obtenir cette symétrie qu'en l'empêchant d'interférer avec les résonances voisines de spin 0^+; elle est donc de spin 1^+.
d) La forme très caractéristique des sections efficaces totale et de fission au voisinage de 65 eV ne peut être expliquée que par une interférence très forte entre la résonance à 65,50 eV et la résonance très large de spin 0^+ à 61,87 eV; la résonance à 65,50 eV est donc aussi de spin 0^+.

Certaines propriétés de la fission dans les voies 0^+ ont pu être précisées; en particulier l'existence de deux voies de sortie dans l'état 0^+ est mise en évidence par les constatations suivantes:

a) Les formes complexes des sections efficaces entre 66 eV et 70 eV d'une part et entre 80 eV et 90 eV d'autre part ne sont expliquées que si on admet l'existence de deux voies 0^+.
b) La résonance étroite à 136,77 eV, de spin 0^+ d'après des mesures de diffusion élastique [5], ne peut se trouver dans la même voie que la résonance large de spin 0^+ à 132,56 eV; sinon elles interféreraient trop fortement.
c) A un degré moindre, la forme légèrement dissymétrique de la résonance à 32,26 eV est assez bien expliquée si on la place totalement dans une deuxième voie 0^+.
d) D'une façon générale, il apparaît que l'existence de la deuxième voie 0^+ soit nécessaire pour atténuer les effets d'interférences, qui seraient trop forts si on ne considérait qu'une seule voie.

La figure 5 montre la distribution des largeurs partielles de fission correspondant aux deux voies 0^+. La distribution correspondant à la première voie est compatible avec une loi en χ^2 à 1 degré de liberté; cela est moins évident pour la distribution relative à la deuxième voie, probablement à cause de l'imprécision sur la détermination des largeurs de fission de cette voie, surtout dans les résonances larges. La valeur moyenne de la largeur de fission dans la première voie est voisine de 1400 meV (donc $N_{eff} \simeq 1$); cette voie de fission, complètement ouverte, correspondrait à l'état de transition 0^+ fondamental. La valeur moyenne pour la deuxième voie 0^+ est de l'ordre de 200 meV (donc $N_{eff} \simeq 0,13$), ce qui situerait l'état de transition correspondant à environ 150 keV au-dessus de l'énergie d'excitation du neutron. La fission dans cette deuxième voie 0^+ serait donc au-dessous du seuil et pourrait conduire à une structure intermédiaire dans la section efficace de fission correspondante. Un tel effet est pratiquement impossible à mettre en évidence actuellement.

4.3. Comparaison avec d'autres analyses multiniveaux

Une analyse par le même formalisme, mais sans moindres carrés, a été faite par James sur la section efficace de fission dans une zone restreinte allant de 78 eV à 88 eV [13]; ses conclusions sont qualitativement les mêmes que les nôtres, mais les paramètres qu'il obtient sont très différents, probablement parce qu'il n'a pas tenu compte des paramètres exacts des résonances très larges en dehors de la zone étudiée,

à 60,94 eV, 96,49 eV et 100,25 eV. Ceci montre l'importance des effets d'interférence et la nécessité de tenir compte des paramètres exacts des niveaux éloignés de la zone à étudier.

En utilisant également ce même formalisme, sans ajustement par moindres carrés, Farrell a analysé, entre 14 eV et 90 eV, la section efficace de fission mesurée à Los Alamos [14]. Cette analyse, qui détermine tous les paramètres des résonances (largeurs neutroniques comprises) à partir de la seule section efficace de fission, donne des résultats différents des nôtres. Il n'est pas possible, dans le cadre de cette communication, de faire une critique détaillée des deux ensembles de résultats. On peut noter cependant que les paramètres de Farrell, surtout pour les résonances 1^+, ne permettent pas de reproduire la section efficace totale, ce qui jette un doute sur la valeur des largeurs neutroniques et, par là même, des largeurs de fission ainsi obtenues.

5. CONCLUSION

Nous avons présenté ici une analyse multiniveaux simultanée, par la méthode des moindres carrés, de σ_f et de σ_T de ^{239}Pu. Les paramètres obtenus restent en assez bon accord avec ceux de l'analyse avec le formalisme à 1 niveau, sauf pour quelques résonances larges. Un bon accord entre les points expérimentaux et les courbes théoriques est obtenu avec un nombre de résonances plus faible qu'avec le formalisme à 1 niveau. Cet accord ne peut être obtenu qu'avec 2 voies de sortie pour la fission dans les résonances 0^+; les largeurs de fission des deux voies 0^+ sont très différentes, l'une d'entre elles est probablement située au-dessus de l'énergie de liaison du neutron.

L'analyse dans les mêmes conditions est en cours jusqu'à 210 eV.

REMERCIEMENTS

Les auteurs remercient Mlle M. Sanche pour l'aide précieuse qu'elle a apportée dans de nombreux calculs, et M. Alix, dont la collaboration a permis l'utilisation maximale des possibilités de l'ordinateur CDC 6600 du Centre d'études nucléaires de Saclay.

REFERENCES

[1] DERRIEN, H., et al., «Sections efficaces totale et de fission du ^{239}Pu», Nuclear Data for Reactors (C.r. Conf. Paris, 1966) II, AIEA, Vienne (1967) 195.

[2] BLONS, J., DERRIEN, H., MICHAUDON, A., «Mesure à haute résolution et analyse de la section efficace de fission du plutonium-239», ces comptes rendus, IAEA-CN-26/63.

[3] DERRIEN, H., et al., A paraître.

[4] COWAN, G.A., et al., Phys. Rev. 144 (1966) 979.

[5] TROCHON, J., DERRIEN, H., LUCAS, B., MICHAUDON, A., «Détermination du spin des résonances induites par des neutrons lents dans le plutonium-239», ces comptes rendus, IAEA-CN-26/62.
ASGHAR, M., «Spin assignments of low-energy resonances in ^{239}Pu», Nuclear Data for Reactors (C.r. Conf. Paris, 1966) II, AIEA, Vienne (1967) 185.
FRASER, J.S., SCHWARTZ, R., Nucl. Phys. 30 (1962) 269.
SAUTER, G.S., BOWMAN, C.A., Rapport UCRL-14200.

[6] PAYA, D., et al., «Structure intermédiaire dans les sections efficaces de fission du neptunium-237 et du plutonium-239», Physics and Chemistry of Fission (C. r. Coll. Vienne, 1969) AIEA, Vienne (1969) 307.
[7] WIGNER, E.P., EISENBUD, L., Phys. Rev. 72 (1947) 29.
[8] VOGT, E., Phys. Rev. 118 (1960) 724.
[9] WIGNER, E.P., Phys. Rev. 70 (1946) 15.
[10] ADLER, D.B., ADLER, F.T., Rapport C00-1546-4.
[11] REICH, C.W., MOORE, M.S., Phys. Rev. 111 3 (1958) 929.
[12] BOLLINGER, L.M., et al., «Slow neutron cross sections», Conf. int. util. énergie atom. fins pacif. (Actes 2e Conf. Genève, 1958) 15 (1958) 127.
[13] JAMES, G.D., J. nucl. Energy 22 (1968) 263.
[14] FARRELL, J.A., Phys. Rev. 165 (1968) 1371.

DETERMINATION DU SPIN DES RESONANCES INDUITES PAR DES NEUTRONS LENTS DANS LE PLUTONIUM-239

J. TROCHON, H. DERRIEN, B. LUCAS, A. MICHAUDON
CEA, Centre d'études
nucléaires de Saclay,
France

Abstract — Résumé

DETERMINATION OF THE SPIN OF SLOW-NEUTRON INDUCED RESONANCES IN ^{239}Pu.

A high-resolution measurement of slow-neutron elastic scattering from ^{239}Pu has been carried out by the time-of-flight method, using the Saclay 45-MeV linear accelerator as pulsed neutron source. An analysis of the experimental data, in conjunction with that of the total cross-section of Saclay, allowed the spin of 112 resonances in the energy range of 0-660 eV to be determined. With the help of certain assumptions, these results allow a classification of all resonances analysed into two groups corresponding to the two spins $J = 0^+$ and $J = 1^+$. A study of the mean widths $\langle \Gamma_f \rangle_{0^+}$ and $\langle \Gamma_f \rangle_{1^+}$ in energy intervals of 110 eV confirms the existence of an intermediate structure in the fission cross-section due to channel 1^+. This intermediate structure is responsible for the large fluctuations of α in the energy range of 0-660 eV.

DETERMINATION DU SPIN DES RESONANCES INDUITES PAR DES NEUTRONS LENTS DANS LE PLUTONIUM-239.

Une mesure à bonne résolution de la diffusion élastique de neutrons lents par ^{239}Pu a été effectuée par la technique du temps de vol, en utilisant l'accélérateur linéaire de 45 MeV de Saclay comme source pulsée de neutrons. L'analyse des données expérimentales conjuguée avec celle de la section efficace totale de Saclay a permis de déterminer le spin de 112 résonances dans la gamme d'énergie 0-660 eV. Ces résultats permettent, à partir de certaines hypothèses, de séparer toutes les résonances analysées en deux familles correspondant aux deux spins $J = 0^+$ et $J = 1^+$. L'étude des largeurs moyennes $\langle \Gamma_f \rangle_{0^+}$ et $\langle \Gamma_f \rangle_{1^+}$ dans des intervalles d'énergie de 110 eV confirme l'existence d'une structure intermédiaire dans la section efficace de fission due à la voie 1^+. Cette structure intermédiaire est responsable des grandes fluctuations de α dans la gamme d'énergie 0-660 eV.

1. INTRODUCTION

L'interprétation des expériences relatives à la fission induite par des neutrons de résonances [1] est souvent gênée par le peu d'informations concernant leurs spins [2]. En effet, dans la fission d'un noyau de nombre de masse A impair, de spin et de parité I^π, les niveaux excités par des neutrons s appartiennent à l'une des deux familles de spin et de parité $J^\pi = (I + \frac{1}{2})^\pi$ et $J^\pi = (I - \frac{1}{2})^\pi$. Généralement, le spin J ne peut être déterminé que par une mesure séparée. Dans le cas de ^{239}Pu, il semble qu'une mesure directe, comme celle de la diffusion élastique, puisse donner des résultats intéressants jusqu'à une énergie assez élevée [2], grâce à l'utilisation d'un détecteur de neutrons lents diffusés, récemment mis au point [3].

2. ETUDE EXPERIMENTALE

La diffusion élastique de neutrons de résonances par ^{239}Pu a été étudiée par la technique du temps de vol, en utilisant l'accélérateur linéaire d'électrons de 45 MeV de Saclay comme source pulsée de neutrons.

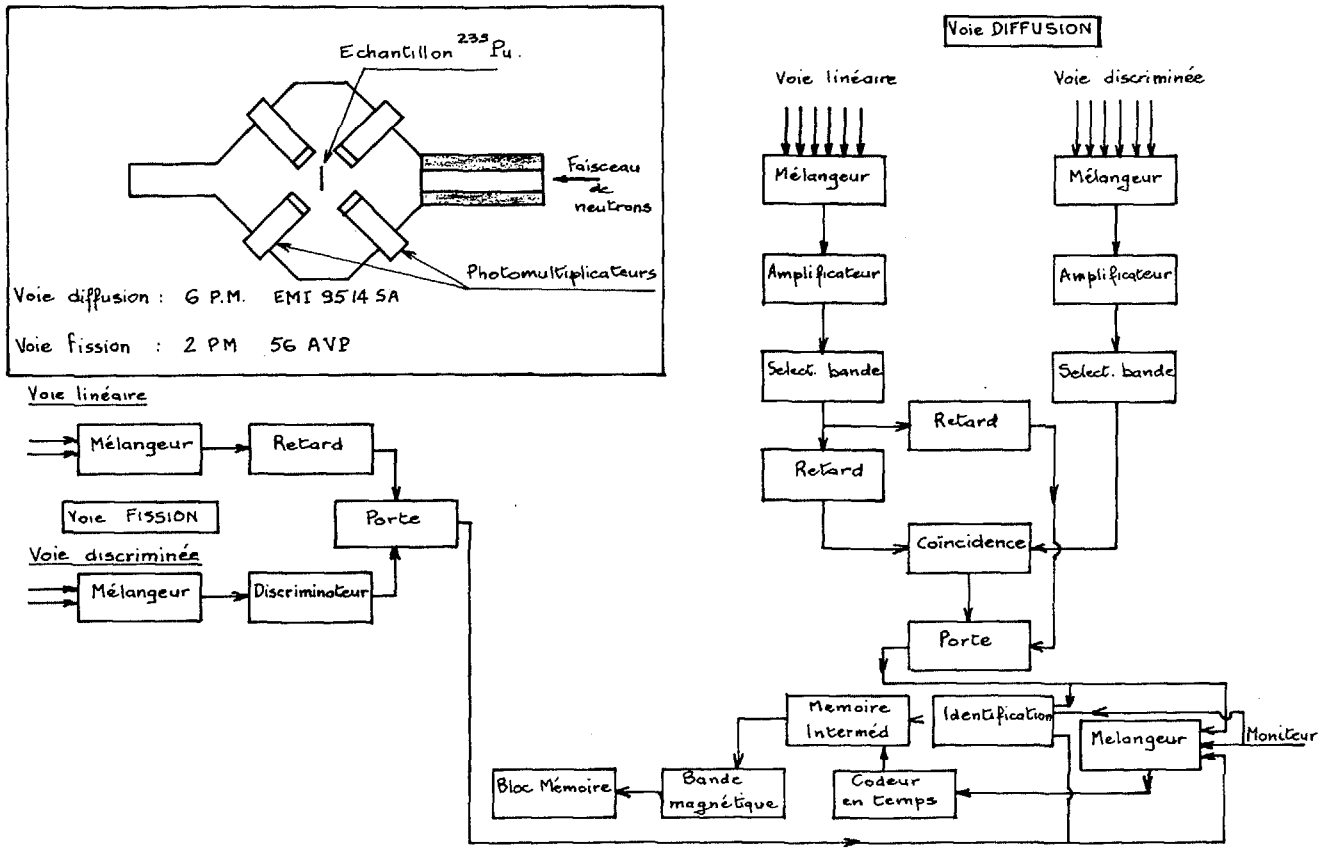

FIG. 1. Ensemble électronique de l'expérience de diffusion sur le ^{239}Pu.
Le dispositif expérimental (en haut, à gauche) est à une trentaine de mètres environ de la salle où l'électronique de cette figure est installée. La liaison est réalisée par câbles.

Le détecteur est constitué d'un ensemble de huit scintillateurs liquides disposés autour de l'échantillon [3]. Six sont chargés en ^{10}B (NE 321 A)[1] et sont sensibles aux neutrons lents et aux neutrons rapides. Ils fournissent des signaux qui, groupés, forment ce que l'on appellera la «voie diffusion». Cette voie est contaminée par des impulsions dues à des neutrons de fission qui ne peuvent être éliminées électroniquement. Les deux autres scintillateurs ne sont pas chargés en ^{10}B (NE 213)[1] afin de mesurer cette contamination. Les signaux qui en sont issus forment la «voie fission» (non contaminée par des impulsions dues aux neutrons diffusés). Les huit cellules, placées à environ 7 cm du centre de l'échantillon, ont un diamètre de 5 cm et une épaisseur de 1,5 cm (fig. 1).

Les impulsions dues aux rayons γ sont éliminées par un dispositif de discrimination de forme. Dans le cas de la voie diffusion, le taux de réjection est de 10^5 pour une perte d'efficacité de 38% dans la détection des neutrons diffusés.

Le rapport des efficacités ϵ_d et ϵ_f de détection des neutrons de fission, respectivement dans les voies diffusion et fission, a été déterminé à l'aide d'une source de ^{252}Cf. La mesure a donné le résultat suivant:

$$\frac{\epsilon_d}{\epsilon_f} = 0,36 \pm 0,04 \qquad (1)$$

Le même rapport a été calculé en utilisant une autre méthode qui consiste à comparer, parmi les résultats obtenus par temps de vol, les aires des résonances dans lesquelles la contribution de la fission est bien connue et très importante; en choisissant les résonances à 10,93 eV et 11,89 eV, nous avons trouvé:

$$\frac{\epsilon_d}{\epsilon_f} = 0,39 \pm 0,02 \qquad (2)$$

Cette valeur, en très bon accord avec (1) et plus précise, a été adoptée pour l'analyse des résultats.

La mesure a été faite avec deux échantillons de $6,5 \cdot 10^{-4}$ atome/barn (environ 0,13 mm) et $4,0 \cdot 10^{-4}$ atome/barn (environ 0,08 mm) d'épaisseur contenant très peu de ^{240}Pu et gainés par deux feuilles d'aluminium de 0,12 mm d'épaisseur chacune.

Par ailleurs, le spectre des neutrons incidents a été mesuré en remplaçant l'échantillon de ^{239}Pu par une plaque de plomb de 5 mm d'épaisseur. Le bruit de fond a été évalué à l'aide d'écrans à résonances noires (Co, Mn, Mo et W) placés dans le faisceau de neutrons incidents.

Au cours de ces mesures, l'accélérateur linéaire fonctionnait à raison de 1000 impulsions de 50 ns par seconde.

L'analyse en temps de vol a été effectuée avec un sélecteur dont la largeur de canal a été réglée, suivant la gamme étudiée, de la façon suivante:

de 10 eV à 35 eV	Δt = 400 ns
de 35 eV à 70 eV	Δt = 200 ns
>70 eV	Δt = 100 ns

[1] Appellation de la Société Nuclear Enterprise.

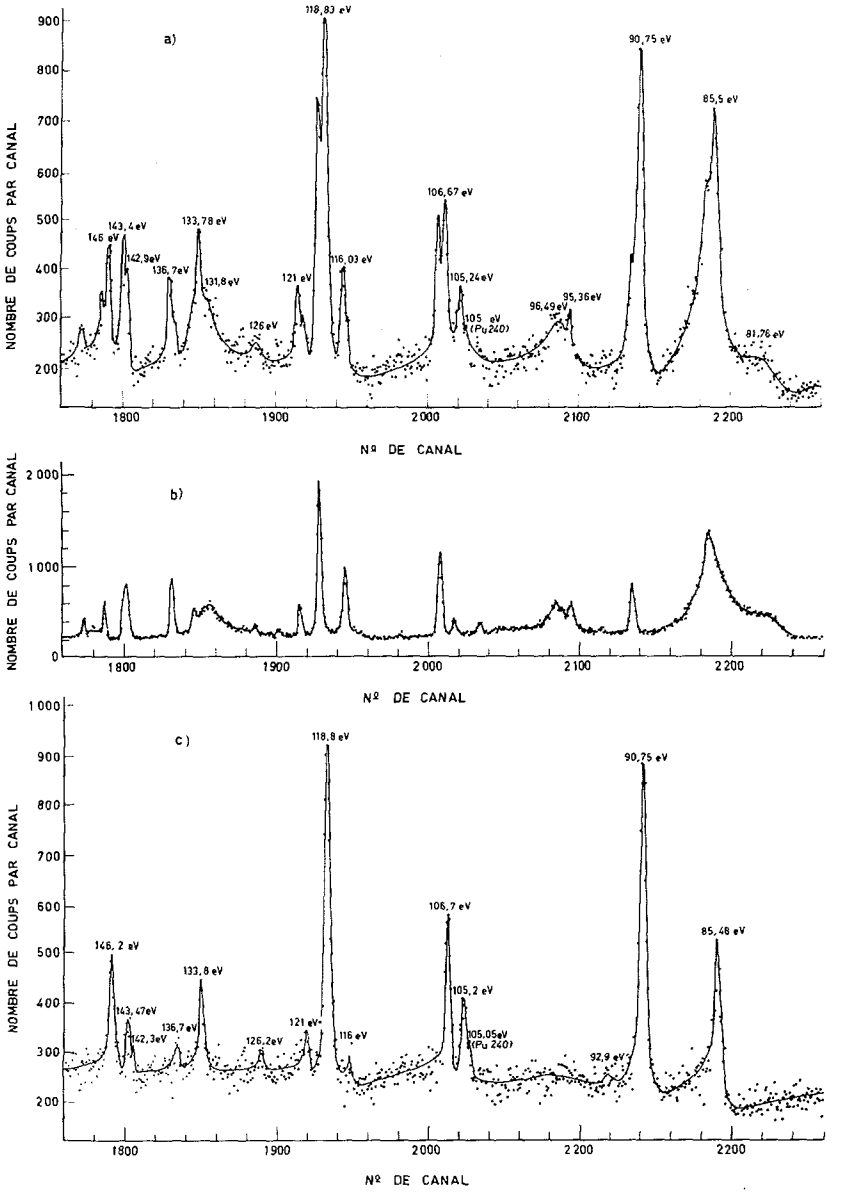

FIG.2. Exemple de l'obtention d'une courbe de diffusion pure (échantillon le plus épais).

a) Courbe de diffusion brute obtenue avec les six scintillateurs chargés en ^{10}B. Les neutrons de fission parcourent beaucoup plus vite que les neutrons diffusés la distance qui sépare l'échantillon des détecteurs (environ 7 cm). Il en résulte un dédoublement des pics obtenus par la mesure du temps de vol.

b) Courbe de fission obtenue avec les deux scintillateurs sans bore. Le sommet des résonances coïncide avec ceux de la fission de la figure 2a grâce à un décalage de l'origine.

c) Après soustraction de la courbe b (multipliée par le rapport ϵ_d/ϵ_f) de la courbe a, nous btenons la courbe c, exempte de fission. Les larges résonances de la figure 2a, principalement dues à la fission dans la voie 0^+, ont disparu car leur section efficace de diffusion est très petite. Il ne sera pas possible de déterminer leur spin par cette mesure.

3. ANALYSE DES RESULTATS

Les résultats relatifs aux voies diffusion et fission et à la mesure du spectre sont d'abord corrigés du bruit de fond. Ensuite, la voie diffusion doit être débarrassée de la contamination due aux neutrons de fission. Cette contamination est nettement visible sur la figure 2a où les résonances de la voie diffusion sont dédoublées. Pour chaque résonance, le premier pic, du côté des basses énergies, est dû aux neutrons diffusés alors que le deuxième, du côté des hautes énergies, correspond à la fission. Ce dédoublement provient simplement de la différence de temps de parcours entre l'échantillon et le détecteur pour les neutrons lents diffusés et les neutrons rapides de fission. La contribution parasite des neutrons de fission est éliminée en soustrayant des résultats de la voie diffusion ceux de la voie fission multipliée par la valeur (2) du rapport ϵ_d / ϵ_f (fig. 2). Ensuite, les résultats relatifs aux neutrons diffusés seuls sont normalisés, par rapport, d'une part, au spectre des neutrons incidents, et, d'autre part, à l'aire des résonances à 38,34 eV, 66,66 eV, 71,83 eV, 287,3 eV de l'impureté ^{240}Pu dont on connaît les paramètres [4]. Cette normalisation est confirmée par l'aire de certaines résonances bien connues de ^{239}Pu. Pour l'ensemble des résonances analysées et pour les deux épaisseurs d'échantillon, les aires expérimentales $(A_0)_{exp}$ sont rassemblées dans le tableau I. Elles sont corrigées des effets d'autoabsorption et de diffusion multiple par un programme analytique simple. Pour chacune d'elles, nous avons également porté la valeur de $(A_0)_{th}$ donnée par l'expression suivante:

$$(A_0)_{th} = \frac{1,02 \cdot 10^3 \, (2g\,\Gamma_n)^2}{E\,g\,\Gamma} \qquad (3)$$

où
E est l'énergie de la résonance,
Γ et Γ_n sont respectivement les largeurs totale et de diffusion élastique
$g = \frac{2J+1}{2(2I+1)}$ est le facteur statistique ($g = \frac{1}{4}$ ou $g = \frac{3}{4}$).

Pour calculer $(A_0)_{th}$ à l'aide de l'expression (3), nous avons choisi les valeurs de Γ et de $2g\Gamma_n$ déterminées par l'analyse de forme de la section efficace totale [5, 6]. Pour chaque résonance, on calcule ainsi deux valeurs de $(A_0)_{th}$ correspondant à $g = 1/4$ et $g = 3/4$.

A de très rares exceptions près, une seule valeur de $(A_0)_{th}$ correspond aux valeurs expérimentales, ce qui permet d'attribuer le spin sans ambiguïté à 112 résonances sur les 254 observées jusqu'à l'énergie de 660 eV.

4. DISCUSSION DES RESULTATS

Dans le tableau I, nous avons rassemblé les résultats d'autres laboratoires avec lesquels nous sommes généralement en très bon accord [7-11]. Par exemple, dans tous les cas nous avons les mêmes attributions que celles qui sont déduites de l'analyse des résonances dans σ_f et σ_T [5, 6]. En revanche les résultats de Asghar [12], obtenus par une méthode semblable à la nôtre, sont parfois en désaccord avec nos attributions (dans 7 cas sur 47) et toujours dans le même sens: une résonance $J = 0$ d'après Asghar devient $J = 1$ d'après nos mesures. Un tel effet avait déjà été noté [2].

TABLEAU I. RESULTATS

(Certains groupes de deux résonances n'ont pas été bien résolus dans l'expérience de diffusion. Cela n'a pas toujours empêché la détermination du spin. Dans ce tableau une accolade rassemble les résonances non résolues, et l'aire expérimentale est alors la somme des deux aires individuelles.)

E (eV)	$2g\Gamma_n$ (meV)	Γ (meV)	A_0 expérimental (b·eV)		A_0 théorique (b·eV)		Spin J				
			échantillon épais	échantillon mince	g = 1/4	g = 3/4	1	2	3	4	5
0,3									0		
7,8										1	
10,9										1	
11,9										1	
14,3										1	
14,7	2,9	70		9,5 ± 3	32,5 ± 3,4	10,8 ± 1,1	1	1		1	
15,5									0	0	
17,7	2,7	75		8,0 ± 2	23,1 ± 2,7	7,7 ± 0,9	1	1		1	1
22,3	4,0	109	4,5 ± 3	8,0 ± 2	26,9 ± 2,8	9,0 ± 0,9	1	1	1	1	1
23,9									1		
26,2								1			1
32,3									0	0	
35,5										1	
41,4	6,2	52	} 22,0 ± 2		72,8 ± 12,4	24,3 ± 4,1	1	1		1	1
41,7	2,0	105			3,8 ± 1,1	1,3 ± 0,4					
44,5	10,0	58	49,0 ± 5	51,0 ± 5	157,2 ± 19,9	52,4 ± 6,6	1	1		1	1
47,6	2,6	398	5,0 ± 3	4,0 ± 3	1,5 ± 0,2	0,5 ± 0,1	0	0	0	0	1
49,4									0		0
50,1	4,5	57	12,0 ± 2	9,3 ± 3	29,6 ± 7,6	9,9 ± 2,5	1	1			1
52,6	15,7	68	89,0 ± 7	93,0 ± 9	281,2 ± 66,4	93,7 ± 22,1	1	1		1	1
55,6	2,2	59	2,6 ± 1,3	1,8 ± 1,5	6,0 ± 3,1	2,0 ± 1,0	1	(0)			
57,0									0		0
59,2	8,4	191	8,6 ± 4		25,3 ± 3,4	8,4 ± 1,1	1	0			1
61,9									0		
63,1									1		
65,7	18,8	137	49,0 ± 4		160,5 ± 18,1	53,5 ± 6,0	1	1	(1)		1
65,5									0		
74,0	4,7	71	5,0 ± 1	4,0 ± 2	17,5 ± 2,4	5,8 ± 0,8	1	1			
74,9	33,2	147	91,0 ± 9		408,2 ± 54,9	136,1 ± 18,3	1	1	1	1	1
80,9									0		
85,5	11,8	85	26,0 ± 2		78,2 ± 10,6	26,1 ± 3,5	1	0			
85,5									0		
90,8	18,4	60	67,0 ± 7		255,1 ± 44,9	85,0 ± 15,0	1	1	1		
95,4	3,1	98	0,7 ± 0,6	1,0 ± 1	4,3 ± 0,6	1,4 ± 0,2	1	0			
96,5									0		
100,4									0		
103,0	2,4	48	1,2 ± 0,4	< 1,8	4,8 ± 0,6	1,6 ± 0,2	1	0			
105,3	7,0	48	12,8 ± 2	19,0 ± 8	39,1 ± 7,4	13,0 ± 2,5	1	1			
106,7	14,0	75	32,0 ± 3	33,0 ± 8	99,4 ± 9,7	33,1 ± 3,2	1	1	1		
114,7									0		
116,0	5,4	257		6,1 ± 2,4	4,0 ± 0,3	1,3 ± 0,1	0	0			
118,8	25,9	102	72,0 ± 5	85,0 ± 13	226,2 ± 17,1	75,4 ± 5,7	1	1	1		
121,0	3,7	78	6,8 ± 2	10,0 ± 3	5,9 ± 1,0	2,0 ± 0,3	0				
126,2	3,0	96	3,9 ± 1		3,0 ± 0,4	1,0 ± 0,1	(0)				
131,7								0	0		
133,8	8,4	81	16 ± 4		38,2 ± 4,7	12,7 ± 1,6	1	1			
136,7	5,1	126	5,0 ± 1,5	9,0 ± 5	6,2 ± 0,6	2,1 ± 0,2	0	0			
142,9	4,9	137	1,4 ± 0,7		4,9 ± 0,9	1,6 ± 0,3	1				
143,5	6,1	83	4,7 ± 1		12,8 ± 1,9	4,3 ± 0,6	1				
146,2	10,6	70	18,8 ± 3	14,0 ± 3	44,6 ± 5,2	14,9 ± 1,7	1	1			
147,4									0		
157,1	17,2	673	11,0 ± 2,0	12,0 ± 5	11,4 ± 1,1	3,8 ± 0,4	0	0	0		
164,5	42,0	79	189,0 ± 11	184,0 ± 15	553,7 ± 103,8	184,6 ± 34,6	1	1	1		
167,1	8,7	112	6,0 ± 2		16,7 ± 1,9	5,6 ± 0,6	1	1	1		
171,1									0		

TABLEAU I (suite)

E (eV)	$2g\Gamma_n$ (meV)	Γ (meV)	A_0 expérimental (b·eV)		A_0 théorique (b·eV)		Spin J		
			échantillon épais	échantillon mince	g = 1/4	g = 3/4	1	2	3
177,2	5,4	51	2,9 ± 1		13,0 ± 1,8	4,3 ± 0,6	1	1	
178,9	1,8	58	<1,1		1,3 ± 0,1	0,4 ± 0,0	(1)		
184,9									0
190,6	2,5	67	2,8 ± 1,4	2,5 ± 1,2	2,0 ± 0,3	0,7 ± 0,1	(0)		
195,4	30,0	447	23,0 ± 3	39,0 ± 10	42,0 ± 5,1	14,0 ± 1,7	0	0	0
196,7	7,0	112	4,6 ± 1,4		9,2 ± 1,8	3,1 ± 0,6	1	1	
199,4	14,5	133	12,8 ± 2		32,3 ± 4,7	10,8 ± 1,6	1	1	(1)
203,9	26,6	430	34,6 ± 3		32,9 ± 16,6	11,0 ± 5,5	0	0	
207,4	10,5	57	17,2 ± 3		38,1 ± 4,6	12,7 ± 1,5	1	1	1
211,1									0
212,0									0
216,5	9,4	67	9,0 ± 2		24,8 ± 3,2	8,3 ± 1,1	1	(1)	
219,5	5,4	70	1,0 ± 1		7,6 ± 1,3	2,5 ± 0,4	1		
220,2	11,1	52	15,0 ± 2		44,2 ± 8,9	14,7 ± 3,0	1		1
223,2	5,1	59	3,7 ± 2		8,1 ± 0,9	2,7 ± 0,3	1		
227,8									0
227,9	2,5	67	<1,1		1,7 ± 0,3	0,6 ± 0,1	(1)		
231,4	17,8	54	27,4 ± 4		103,5 ± 21,9	34,5 ± 7,3	1	1	1
234,3	15,3	74	18,7 ± 4	21 ± 4	55,4 ± 8,0	18,5 ± 2,7	1	0	
239,0	8,1	73	5,8 ± 1,7		15,5 ± 2,4	5,2 ± 0,8	1	1	
242,9	9,9	97	4,6 ± 1,4		17,0 ± 1,8	5,7 ± 0,6	1	0	1
248,9	22,1	62	48 ± 5		129,5 ± 16,6	43,2 ± 5,5	1	1	1
251,2	41,2	83	93,7 ± 10	104 ± 15	332,1 ± 28,2	110,7 ± 9,4	1	1	1
254,6	4,2	55	2,5 ± 1,2		5,1 ± 1,2	1,7 ± 0,4	(1)		
256,1	9,5	91	4,8 ± 2,4		15,8 ± 3,1	5,3 ± 1,0	1	1	
262,4									0
269,5	5,8	72	1,9 ± 0,8		7,1 ± 2,6	2,4 ± 0,9	1		
272,6	41,8	92	71 ± 10		284,2 ± 37,4	94,7 ± 12,5	1	1	1
274,8									0
275,6	35,1	150	41 ± 6		121,6 ± 26,5	40,5 ± 8,8	1	1	1
277,2									0
279,6	10,6	111	14,9 ± 3		14,8 ± 1,4	4,9 ± 0,5	0	0	
282,9	37,8	85	83 ± 8	114 ± 30	242,4 ± 39,3	80,8 ± 13,1	1	1	1
288,0									0
292,3	5,8	115	4,2 ± 1,8		4,1 ± 0,5	1,4 ± 0,2	0		
296,5	4,9	81	2,3 ± 1		4,1 ± 0,7	1,4 ± 0,2	(1)		
298,6	15,8	74	13 ± 5		46,1 ± 5,8	15,4 ± 1,9	1	1	1
301,8	27,3	108	27 ± 4	42 ± 9	93,3 ± 8,9	31,1 ± 3,0	1	(1)	1
309,0	21,1	85	24,0 ± 3	23,0 ± 5	69,2 ± 10,8	23,1 ± 3,6	1		1
313,6	20,4	62	30 ± 4	20 ± 6	87,3 ± 10,7	29,1 ± 3,6	1		1
316,7	7,7	73	3,9 ± 1,5		10,6 ± 8,6	3,5 ± 2,9	1		
323,4	30,2	160	49 ± 10	42 ± 15	71,9 ± 9,1	24,0 ± 3,0	(0)		0
325,3	12,8	105	10 ± 3		19,6 ± 2,5	6,5 ± 0,8	1		
329,6									0
333,9	8,2	67	7 ± 3		12,4 ± 1,5	4,1 ± 0,5	1		
335,9	26,6	83	27 ± 5	32 ± 8	103,5 ± 9,0	34,5 ± 3,0	1		1
337,9	12,1	74	6,3 ± 4		23,8 ± 2,9	7,9 ± 1,0	1		
339,2	4,9	81	5,2 ± 2		3,6 ± 0,6	1,2 ± 0,2	0		
343,2	23,7	75	33 ± 6	31 ± 8	89,0 ± 30,0	29,7 ± 10,0	1		1
346,6									0
350,3	32,2	97	44 ± 4	52 ± 10	124,9 ± 10,2	41,6 ± 3,4	1		1
352,8	5,8	69	3,2 ± 2		5,7 ± 1,2	1,9 ± 0,4	(1)		
357,9									0
366,0									0
371,7									0

TABLEAU I (suite)

E (eV)	2g Γ_n (meV)	Γ (meV)	A_0 expérimental (b·eV)		A_0 théorique (b·eV)		Spin J	
			échantillon épais	échantillon mince	g = 1/4	g = 3/4	1	3
375,0	4,0	43	3,7 ± 1,7		4,0 ± 1,3	1,3 ± 0,4	0	
384,3	8,5	109	2 ± 1		7,1 ± 2,3	2,4 ± 0,8	1	
385,9								0
394,4	9,8	106	3 ± 1,5		9,3 ± 1,3	3,1 ± 0,4	1	
401,6	29,1	220	10 ± 3		39,1 ± 5,0	13,0 ± 1,7	1	1
404,2	34,8	155	22 ± 6		78,9 ± 13,2	26,3 ± 4,4	1	1
412,3	13,4	145	3,4 ± 1,7		12,3 ± 1,7	4,1 ± 0,6	1	
419,8	9,1	139	2,8 ± 1,1		5,8 ± 1,2	1,9 ± 0,4	1	
426,4								0
429,6								0
437,8	4,0	62	<1,3		2,5 ± 0,7	0,8 ± 0,2	(1)	
431,3								0
438,7	4,4	61	<1,3		2,9 ± 0,8	1,0 ± 0,3	1	
442,4	10,5	422	2,8 ± 1		2,4 ± 0,4	0,8 ± 0,1	0	
451,3	21,1	81	14,8 ± 4	22 ± 8	49,7 ± 15,7	16,6 ± 5,2	1	
455,7	39,7	503	26 ± 7		28,1 ± 5,1	9,4 ± 1,7	0	
457,3	11,1	303	} 5,3 ± 2		3,6 ± 0,4	1,2 ± 0,1		
458,8	6,9	83			5,1 ± 1,7	1,7 ± 0,6	1	
468,2								0
470,0								0
473,1	6,2	60	1,6 ± 1,5		5,5 ± 2,3	1,8 ± 0,8	1	
475,3								0
476,9								0
490,6								0
494,1	6,9	96	<1,5		4,1 ± 1,3	1,4 ± 0,4	1	
500,5	5,1	84	<1,5		2,4 ± 1,1	0,8 ± 0,4	(1)	
502,9	17,8	207	3,6 ± 2,5		12,4 ± 3,2	4,1 ± 1,1	1	
509,7	78,2	292	69 ± 7	69 ± 15	166,8 ± 30	55,6 ± 10	1	
511,5								0
520,2	22,4	172	14 ± 4	13 ± 6	22,9 ± 7,5	7,6 ± 2,5	(1)	
524,2	46,0	101	65 ± 12	74 ± 15	163,1 ± 36	54,4 ± 12	1	
525,4								0
530,5	63,8	192	110 ± 12	123 ± 18	163,2 ± 30	54,4 ± 10	0	0
539,2	17,0	70	17 ± 7		31,2 ± 14,4	10,4 ± 4,8	1	
543,1	17,6	67	8,6 ± 4		34,7 ± 17,4	11,6 ± 5,8	1	
545,8								0
549,7	17,7	51	9 ± 6	8,5 ± 7	45,6 ± 19,3	15,2 ± 6,4	1	
554,1								0
559,2	41,0	127	41 ± 11	46 ± 18	96,6 ± 26,8	32,2 ± 8,9	1	1
571,1	12,9	71	6 ± 6		16,7 ± 3,6	5,6 ± 1,2	(1)	(1)
574,0	79,5	180	} 161 ± 24		121 ± 12	40 ± 4	(0)	(0)
575,8	59,7	115			219,6 ± 65,2	73,2 ± 21,7	1	1
579,1	10,3	77	5,7 ± 2,8		9,4 ± 1,6	3,1 ± 0,5	1	
588,1	16,9	78	13 ± 3		25,4 ± 2,3	8,5 ± 0,8	(1)	
597,3	13,0	65	8,7 ± 4		17,8 ± 8,9	5,9 ± 3,0	1	
598,0								0
604,0	37,5	75	33 ± 6	25 ± 7	126,7 ± 45,7	42,2 ± 15,2	1	1
607,6	14,6	83	6 ± 5		17,2 ± 5,6	5,7 ± 1,9	1	
609,3	23,6	85	15 ± 7		43,9 ± 14,7	14,6 ± 4,9	1	(1)
620,8	17,8	77	} 7 ± 4		27,0 ± 11,3	9,0 ± 3,8	1	
622,6	14,7	60			23,6 ± 9,9	7,9 ± 3,3	1	1
625,2	11,8	65	6,6 ± 4		14,0 ± 6,1	4,8 ± 2,0	(1)	
632,9								0
639,3	13,9	63	6,4 ± 4		19,6 ± 6,3	6,5 ± 2,1	1	
644,9	8,8	57	<3,5		8,6 ± 3,6	2,9 ± 1,2	(1)	
658,5	128,0	271	109 ± 15	83 ± 16	374,5 ± 85,0	124,2 ± 28,3	1	

1: ce travail; 2: Asghar; 3: Derrien; 4: Sauter; 5: Cowan.

Parmi les 112 résonances dont nous avons attribué le spin, 95 sont de spin 1^+ et 17 de spin 0^+, soit un rapport des populations pour les deux états de spin:

$$\frac{N_1}{N_0} = \frac{N(J = 1)}{N(J = 0)} = \frac{95}{17} = 5,6 \qquad (4)$$

Apparemment, un tel rapport est en désaccord avec la loi en $(2J + 1)$. Cependant, il faut tenir compte du fait que la mesure de diffusion élastique opère une discrimination dans le choix des résonances analysées. Un calcul simple, basé sur l'hypothèse que seules pouvaient être observées les résonances ayant une valeur de Γ_n/Γ supérieure à un seuil donné, donne [2]: $N_1/N_0 = 4,6$. Cette nouvelle valeur du rapport N_1/N_0 est très proche de la valeur expérimentale donnée en (4).

Nous allons maintenant aborder quelques aspects de la fission de ^{239}Pu par des neutrons lents, ce qui devient possible grâce à la connaissance des spins. Nous terminerons par une évaluation de la fonction densité.

4.1. Résonances de spin 0^+

Aux 17 niveaux 0^+ déterminés ici nous pouvons en ajouter 43 autres attribués, soit à partir de l'analyse des sections efficaces totale et de fission par un formalisme multiniveaux [13], soit parce que les largeurs de fission Γ_f sont plus grandes que 500 meV [5, 6]. Le nombre d'attributions $J = 0^+$ est ainsi porté à 60 alors que le nombre total de résonances 0^+ devrait être de 64 environ sur 254 résonances observées. Ceci indique que presque toutes les résonances 0^+ sont identifiées. La figure 3 représente la distribution des largeurs de fission de cette famille. Elle est compatible avec une loi en χ^2 dont les paramètres sont donnés dans le tableau II.

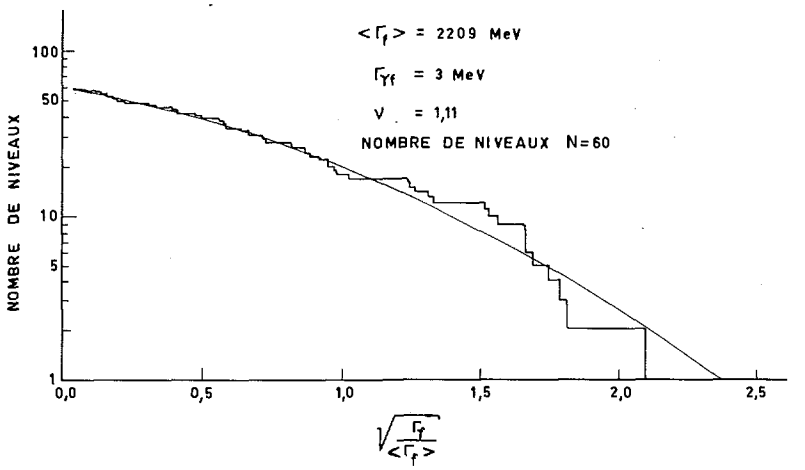

FIG. 3. Distribution intégrale des largeurs de fission Γ_f de la voie 0^+.

N est le nombre de niveaux dont le rapport $\sqrt{\Gamma_f/\langle\Gamma_f\rangle}$ est supérieur à l'abscisse. Le diagramme expérimental (en escalier) est très bien lissé par une loi de Porter et Thomas avec $\nu = 1,11$ et $\langle\Gamma_f\rangle = 2209$ meV.

TABLEAU II. ETUDE DES LARGEURS DE FISSION DE LA VOIE 0^+

	Nombre de résonances	$\langle\Gamma_f\rangle_{0^+}$ (meV)	Erreur statistique (meV)	Erreur d'échantillonnage (meV)	Nombre de voies de sortie ν
Distribution de tous les niveaux observés	59	2270			1,40
Distribution des niveaux attribués 0^+	60	2209			1,11
Valeur moyenne calculée des niveaux attribués 0^+	60	2160	270	390	

L'étude des distributions des largeurs de fission Γ_f a montré que les niveaux 0^+ ont probablement deux voies de sortie ($1<\nu<1,5$) [5, 6], dont l'une au moins est complètement ouverte. L'observation de certaines résonances étroites confirme que la fission n'est pas due à une voie 0^+ unique. En effet, quelques résonances 0^+ de faible largeur de fission n'interfèrent que très faiblement avec les résonances larges voisines. Ceci a été observé par l'analyse des sections efficaces par un formalisme multiniveaux [13] qui donne la largeur partielle de fission des deux voies pour chaque résonance 0^+. Un exemple caractéristique se trouve vers 134 eV, où il y a deux résonances, une à 136,70 eV classée 0^+ à partir des mesures de diffusion (réf. [2] et ce travail), et une autre à 132,36 eV dont la largeur est de 4 eV environ, donc 0^+ également. D'après [13], les composantes dans chacune des voies sont:

E = 132,56 eV	Γ_{f_1} = 3,96 eV	Γ_{f_2} = 0,008 eV
E = 136,70 eV	Γ_{f_1} = 0 eV	Γ_{f_2} = 0,084 eV

Nous avons donc deux niveaux de même spin qui interfèrent très peu car leurs vecteurs de fission sont dans deux voies 0^+ différentes.

4.2. Résonances de spin 1^+

Nous avons procédé à 95 attributions $J = 1^+$, auxquelles on peut en ajouter 9 autres, dont 7 relatives à des résonances à basse énergie que nous n'avons pas analysées, mais dont le spin $J = 1^+$ a été déterminé par d'autres laboratoires [7, 9], et 2 dont le spin a pu être connu par l'analyse multiniveaux de σ_T et de σ_f [13]. Ceci porte à 104 le nombre de résonances $J = 1^+$ dont la largeur moyenne est

$$\langle\Gamma_f\rangle_{1^+} = 29 \pm 6 \text{ meV} \qquad (5)$$

Cette valeur est plus faible que celle obtenue à partir de la distribution des largeurs de fission de tous les niveaux observés ($\langle\Gamma_f\rangle_{1^+} = 35,5$ meV) [6]. Cela provient en partie d'un effet systématique dans la mesure. L'aire A_0 d'une résonance de diffusion est proportionnelle à $g\,\Gamma n^2/\Gamma$ (3). Or la largeur de capture radiative est constante et la largeur neutronique Γ_n est en général assez petite. Si une résonance a une largeur de fission Γ_f

élevée, la largeur totale Γ l'est également et l'aire A_0 devient faible. Cette résonance peut alors ne pas être observée tandis qu'une autre, ayant la même largeur Γ_n mais une largeur Γ_f plus petite, l'aurait été. Les largeurs moyennes de fission ainsi déduites sont donc sous-estimées.

Par ailleurs nous avons vu (sous 4.1) que presque toutes les résonances 0^+ avaient été identifiées. Nous pourrons donc former une famille comprenant les 104 résonances $J = 1^+$ et les résonances restantes dont la largeur Γ_f est déterminée (au nombre de 45, presque toutes de spin 1^+). On obtient ainsi une famille de résonances faiblement contaminée en résonances 0^+ et dont la largeur moyenne de fission, appelée aussi $\langle\Gamma_f\rangle_{1^+}$, sera légèrement supérieure à la valeur vraie. Par cette méthode, on trouve:

$$\langle\Gamma_f\rangle_{1^+} = (33,7 \pm 5)\,\text{meV} \qquad (6)$$

valeur en très bon accord avec celle déduite de la distribution des largeurs de fission [6].

Toutes ces valeurs sont corrigées de la largeur $\Gamma_{\gamma_f} = 3,5$ meV correspondant à la réaction (n,γ_f).

4.3. Variation, en fonction de l'énergie, de la valeur moyenne locale de fission pour les deux états de spin

La faible valeur de $\langle\Gamma_f\rangle_{1^+}$ signifie que la fission dans la voie 1^+ est en dessous du seuil [14]. Il est donc possible que la section efficace de fission due à cette voie présente un phénomène de structure intermédiaire [15], par analogie avec la section efficace de la fission en dessous du seuil de certains noyaux non fissiles. Un tel effet a été mentionné en 1969 [16] lors d'une étude des fluctuations des largeurs moyennes $\langle\Gamma_f\rangle_{0^+}$ et $\langle\Gamma_f\rangle_{1^+}$, déduites de l'analyse de la distribution des largeurs de fission pour différentes gammes d'énergie. Cet effet est d'ailleurs confirmé par une étude similaire mais plus complète, présentée à cette Conférence [6].

La connaissance du spin d'un grand nombre de résonances permet maintenant une étude directe de ce phénomène en calculant $\langle\Gamma_f\rangle_{1^+}$ et $\langle\Gamma_f\rangle_{0^+}$ pour les six gammes de 110 eV considérées [16].

Les valeurs que nous obtenons sont consignées dans le tableau III. Pour $\langle\Gamma_f\rangle_{1^+}$ nous donnons deux valeurs, correspondant aux deux familles des résonances 1^+ considérées sous 4.2, qui constituent les limites inférieure et supérieure de la valeur vraie. Chacune des valeurs $\langle\Gamma_f\rangle_{1^+}$ et $\langle\Gamma_f\rangle_{0^+}$ est donnée avec deux barres d'erreur:

- une barre d'erreur d'origine expérimentale égale à:

$$\frac{1}{N}\sqrt{\sum_i (\Delta\Gamma_{f_i})^2} \qquad (7)$$

- une barre d'erreur correspondant à l'échantillonnage égale à:

$$\sqrt{\frac{2}{N}} \cdot \langle\Gamma_f\rangle \qquad (8)$$

Γ_{f_i} est la largeur de fission de la résonance i
N est le nombre de résonances de spin $J = 0$ ou $J = 1$ considérées.

TABLEAU III. VARIATION DES LARGEURS DE FISSION EN FONCTION DE L'ENERGIE

Zones d'énergie (eV)	Résonances 1^+						Résonances 0^+					
	$\langle\Gamma_f\rangle_{1^+}$ réf. [11] (meV)	$\langle\Gamma_f\rangle_{1^+}$ (meV)	Nombre de niveaux	Erreur statistique	Erreur d'échantillonnage	Erreur totale (meV)	$\langle\Gamma_f\rangle_{0^+}$ réf. [11] (meV)	$\langle\Gamma_f\rangle_{0^+}$ (meV)	Nombre de niveaux	Erreur statistique	Erreur d'échantillonnage	Erreur totale (meV)
0-110	41,2	38[a] 35[a]	27 29	2 2	10 9	12 11	2065	1820	12	620	730	1350
110-220	30,0	29 31	15 26	2 2	10 9	12 11	970	903	14	100	320	420
220-330	22,1	23 26	21 27	2 3	7 7	9 10	3302	3370	9	860	1580	2440
330-440	43,4	41 60	14 25	3 4	15 16	18 20	3285	2748	10	170	1240	1410
440-550	38,3	32 43	12 19	7 9	13 12	20 21	2352	2469	11	1060	1020	2080
550-660	7	7,1 7,7	15 23	1,3 1,3	2,6 2,2	3,9 3,5	1800	2560	4	800	1800	2600

[a] *La méthode choisie pour déterminer les valeurs extrêmes de* $\langle\Gamma_f\rangle$ est faussée dans cette zone car nous y avons un grand nombre d'attributions qui sont dues à différentes mesures.

Les valeurs de $\langle\Gamma_f\rangle$ sont données après déduction de $\Gamma_{\gamma f} = 3,5$ meV.

Pour la famille de spin 1^+ pour chaque intervalle d'énergie, les calculs faits avec les résonances identifiées sont sur la première ligne et les calculs faits avec toutes les résonances non identifiées 0^+ sont sur la deuxième.

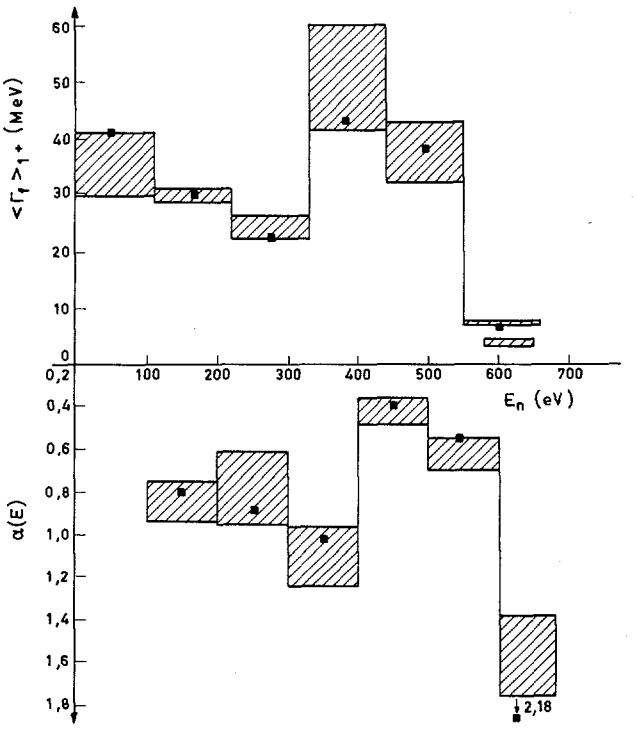

FIG.4. Comparaison des variations des largeurs de fission $\langle \Gamma_f \rangle_{1^+}$ et de $\alpha(E)$ de 0 à 660 eV pour ^{239}Pu.

a) $\langle \Gamma_f \rangle_{1^+} = f(E)$. Les deux lignes en traits pleins reliées par des hachures représentent les limites inférieure et supérieure de $\langle \Gamma_f \rangle_{1^+}$. Les petits carrés ■ sont les valeurs de $\langle \Gamma_f \rangle_{1^+}$ déterminées à partir des distributions des largeurs de fission de toutes les résonances observées (d'après [6]).

b) $\alpha(E) = f(E)$ d'après [17]. Les traits pleins reliés par des hachures sont les limites des valeurs de α les plus probables. Les petits ronds ● sont les valeurs calculées à partir de nos paramètres d'après la relation

$$\alpha = \frac{(\sigma_0 \Gamma_\gamma)_{0^+} + (\sigma_0 \Gamma_\gamma)_{1^+}}{(\sigma_0 \Gamma_f)_{0^+} + (\sigma_0 \Gamma_f)_{1^+}} \qquad \text{(voir tableau IV)}$$

C'est dans l'intervalle de 580 à 650 eV que l'effet de la structure intermédiaire est le plus important et la valeur de α trouvée est plus élevée que les évaluations faites de 600 à 700 eV: α (de 580 à 650 eV) = 2,33.

Compte tenu des barres d'erreur, les fluctuations de $\langle \Gamma_f \rangle_{0^+}$ ne sont pas significatives, même pour la valeur extrême correspondant à la zone 110 eV-220 eV où l'on observe pourtant un nombre inhabituel de résonances 0^+ ayant une faible largeur Γ_f.

En revanche, les fluctuations de $\langle \Gamma_1 \rangle_{1^+}$ sont plus importantes et incompatibles avec une valeur unique. En effet, les valeurs extrêmes sont les suivantes, avec une erreur totale égale à la somme des deux erreurs (7) et (8):

- Valeurs sous-estimées
  gamme 330-440 eV $\quad 23 \text{ meV} \leqslant \langle \Gamma_f \rangle_{1^+} \leqslant 59 \text{ meV}$
  gamme 550-660 eV $\quad 3,2 \text{ meV} \leqslant \langle \Gamma_f \rangle_{1^+} \leqslant 11 \text{ meV}$ (9)

- Valeurs surestimées
  gamme 330-440 eV $\quad 40 \text{ meV} \leqslant \langle \Gamma_f \rangle_{1^+} \leqslant 80 \text{ meV}$
  gamme 550-660 eV $\quad 4,2 \text{ meV} \leqslant \langle \Gamma_f \rangle_{1^+} \leqslant 11,2 \text{ meV}$ (10)

Remarquons que le découpage, en six zones de 110 eV de 0 à 660 eV, n'est pas celui qui donne le plus grand écart dans les valeurs de $\langle \Gamma_f \rangle_{1^+}$; il a été choisi pour pouvoir comparer nos résultats avec ceux de [6]. En prenant une zone un peu différente, de 580 à 650 eV, on obtient alors les valeurs suivantes:

- Valeur surestimée $\quad \langle \Gamma_f \rangle_{1^+} = 4,2 \pm 2,8$
- Valeur sous-estimée $\quad \langle \Gamma_f \rangle_{1^+} = 3,0 \pm 2,9$ (11)

Ces calculs accentuent encore les fluctuations de $\langle \Gamma_f \rangle_{1^+}$ déjà notées plus haut.

Les différentes valeurs de $\langle \Gamma_f \rangle_{1^+}$ sont tracées sur la figure 4a, où il peut être constaté que les variations de α (fig. 4b) dans la gamme d'énergie 0-660 eV sont bien corrélées avec celles de $\langle \Gamma_f \rangle_{1^+}$. Le tableau IV, où la valeur de α est déduite des paramètres individuels des résonances dans les gammes d'énergie considérées, montre bien que les variations importantes de α sont dues à celles de $\langle \Gamma_f \rangle_{1^+}$. Notons au passage l'excellent accord entre les valeurs de α calculées et celles qui sont déduites de mesures directes [17].

TABLEAU IV. DETERMINATION DE $\alpha(E)$ DE ^{239}Pu
(Voir également figure 4b)

Gamme d'énergie (eV)	$\sum \sigma_0 \Gamma_\gamma$ 0^+ (b·eV)	$\sum \sigma_0 \Gamma_\gamma$ 1^+ (b·eV)	$\sum \sigma_0 \Gamma_\gamma$ $0^+ + 1^+$ (b·eV)	$\sum \sigma_0 \Gamma_f$ 0^+ (b·eV)	$\sum \sigma_0 \Gamma_f$ 1^+ (b·eV)	$\sum \sigma_0 \Gamma_f$ $0^+ + 1^+$ (b·eV)	$\alpha(E)$
100-200	112	824	936	687	482	1169	0,801
200-300	33	936	969	540	565	1105	0,877
300-400	58	478	536	164	303	467	1,147
400-500	14	219	233	328	254	582	0,401
500-600	53	475	528	668	285	953	0,553
600-650	1	300	301	68	70	138	2,18

L'analyse des résonances n'a été faite que jusqu'à 660 eV et nous ne pouvons donner une valeur de α de 600 à 700 eV. Dans la zone de 600 à 650 eV, l'effet de la structure intermédiaire est maximal et la valeur calculée est bien supérieure à celles qui, par ailleurs [17], sont données de 600 à 700 eV.

Les différentes valeurs de $\sigma_0 \Gamma_\gamma$ ont été déduites des mesures de transmission [5,6]. Lorsque cela n'était pas possible, nous avons supposé $\Gamma_\gamma = 42$ meV.

5. FONCTION DENSITE S_0

Nous avons vu précédemment comment nous avons pu séparer les 254 résonances observées jusqu'à 660 eV en deux familles correspondant aux deux états de spin. On peut en déduire facilement la fonction densité S_0 pour les neutrons s relative à chacun de ces deux états de spin.

$$S_0^J = \frac{\langle \Gamma_n^0 \rangle_J}{\langle D \rangle_J} = \frac{\sum_0^{\Delta E} (\Gamma_n^0)_J}{\Delta E} \qquad (12)$$

Dans cette relation,
Γ_{nJ}^0 est la largeur neutronique réduite d'une résonance de spin J
$\langle D \rangle_J$ est l'espacement moyen des résonances de spin J
ΔE est l'intervalle d'énergie considéré pour la détermination de S_0^J
(ici ΔE = 660 eV).

La valeur S_0^J est dérivée de la pente de l'histogramme $\sum_0^E \Gamma_{nJ}^0 = f(E)$ tracé sur la figure 5. Nous obtenons:

$$S_0^1 = (1,13 \pm 0,12) \cdot 10^{-4} \qquad (13)$$

$$S_0^0 = (1,56 \pm 0,28) \cdot 10^{-4} \qquad (14)$$

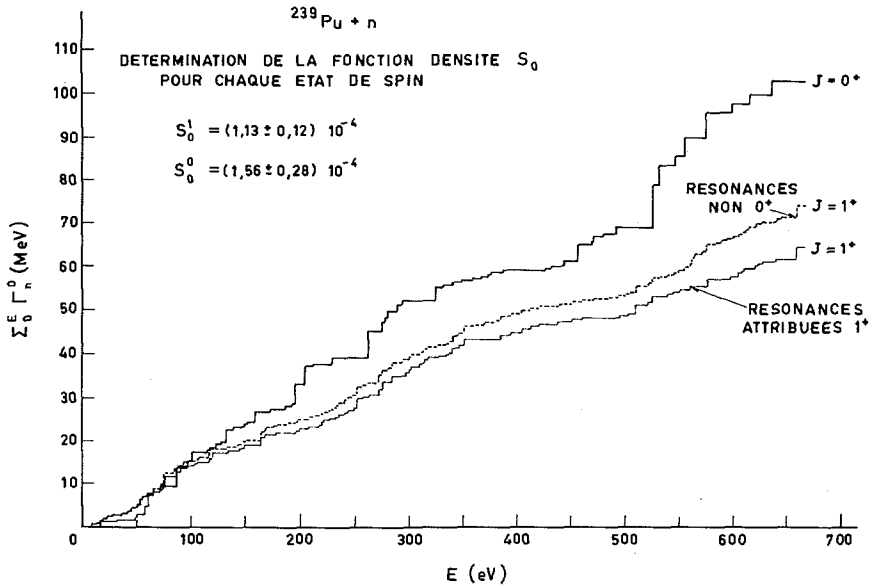

FIG.5. Détermination de la fonction densité S_0 pour chaque état de spin $\sum \Gamma_n^0 = f(E)$. Les diagrammes ont été réalisés avec les résonances dont le spin a été attribué et avec la famille de résonances 1^+ déterminée dans le paragraphe 4.2. Malgré le nombre important de niveaux pris en compte, il n'est pas possible de se prononcer sur une différence entre S_0^1 et S_0^0.

soit une valeur moyenne, pour les deux états de spin:

$$\langle S_0 \rangle = (1,24 \pm 0,11) \cdot 10^{-4} \qquad (15)$$

En se limitant uniquement aux résonances dont le spin a été attribué, on obtient:

$$S_0^1 = (1,01 \pm 0,14) \cdot 10^{-4} \qquad (16)$$

$$S_0^0 = (1,56 \pm 0,28) \cdot 10^{-4} \qquad (17)$$

Ces résultats donnent des valeurs de S_0 différentes pour les deux états de spin, mais juste à la limite des barres d'erreur. Malgré le nombre considérable de niveaux pris en compte, une précision de 10% a seulement pu être obtenue pour S_0^1 et si l'effet existe, il est inférieur à cette valeur. Une étude est en cours à ce sujet.

6. CONCLUSION

Les mesures de diffusion élastique décrites ici, venant en complément de celles de la section efficace totale, ont permis de déterminer le spin de 112 résonances dans la gamme d'énergie 0-660 eV. D'autre part, certaines hypothèses relatives au processus de fission et à la densité de niveaux ont permis de séparer les autres résonances situées dans la même gamme d'énergie en deux familles correspondant aux deux états de spin 0^+ et 1^+.

Dans ces conditions, il a été possible d'étudier certaines propriétés de la fission en fonction de l'énergie pour les deux états de spin. Il apparaît en particulier que la largeur moyenne $\langle \Gamma_f \rangle_{1^+}$ accuse de fortes variations en fonction de l'énergie, corrélées avec celles de α, confirmant ainsi la présence d'une structure intermédiaire dans la section efficace de fission due à la voie 1^+. Ce phénomène peut être interprété comme une des conséquences d'une barrière de fission à deux bosses pour le noyau composé ^{240}Pu [18] mise en évidence d'une façon tout à fait indépendante par l'existence d'un isomère de fission ^{240}Pu [19-23]. Dans le cas présent nous considérons la barrière de fission pour l'état 1^+, dont la partie la plus élevée est au-dessus de l'énergie de séparation S_n du neutron dans ^{240}Pu, ce qui conduit à une fission au-dessous du seuil pour cette voie de sortie.

Ce phénomène de structure intermédiaire dans la section efficace de fission d'une voie de sortie a pu être clairement mis en évidence dans le cas de ^{239}Pu grâce à l'analyse microscopique des sections efficaces totale et de fission et la détermination du spin d'un grand nombre de résonances. Ce phénomène existe probablement pour d'autres noyaux, notamment ^{235}U, mais n'a pas pu être décelé ni par la méthode précédente, ni par les techniques d'autocorrélations dont l'interprétation est particulièrement délicate.

REFERENCES

[1] BOHR, A., Conf. int. util. énergie atom. fins pacif. 2 (Actes Conf. Genève, 1955), ONU, New York (1956) 151.
[2] MICHAUDON, A., Nuclear Data for Reactors II (C.r. Conf. Paris, 1966), AIEA, Vienne (1967) 161.
[3] TROCHON, J., et al., Nucl. Instrum. and Meth. 72 (1969) 307.
[4] BÖCKHOFF, K.H., et al., Nuclear Data for Reactors II (C.r. Conf. Paris, 1966), AIEA, Vienne (1967) 135.
[5] DERRIEN, H., et al., Nuclear Data for Reactors II (C.r. Conf. Paris, 1966), AIEA, Vienne (1967) 195.
[6] BLONS, J., et al., ces comptes rendus, IAEA-CN-26/63.
[7] COWAN, G.A., et al., Phys. Rev. 144 (1966) 979.
[8] MELKONIAN, E., MEHTA, G.K., Physics and Chemistry of Fission II (C.r. Coll. Salzbourg, 1965), AIEA, Vienne (1965) 355.
[9] SAUTER, G.D., BOWMAN, C.D., Phys. Rev. Letters 15 (1965) 761.
[10] SHAPIRO, F.L., Nuclear Structure (C.r. Coll. Doubna, 1968), AIEA, Vienne (1968) 283.
[11] WEINSTEIN, S., et al., Physics and Chemistry of Fission (C.r. Coll. Vienne, 1969), AIEA, Vienne (1969) 477.
[12] ASGHAR, M., Nuclear Data for Reactors II (C.r. Conf. Paris, 1966), AIEA, Vienne (1967) 185.
[13] DERRIEN, H., et al., ces comptes rendus, IAEA-CN-26/61.
[14] MICHAUDON, A., J. Phys. 29 Suppl. n°1 (1968) 51.
[15] MICHAUDON, A., Neutron Cross Sections and Technology (Proc. Conf. Washington, 1968) 1, NBS Special Publication 299 (1968) 427.
[16] PAYA, D., et al., Physics and Chemistry of Fission (C.r. Coll. Vienne, 1969), AIEA, Vienne (1969) 307.
[17] SOWERBY, M.G., Meeting on the value of α for ^{239}Pu, Winfrith, U.K., June 1969.
[18] STRUTINSKY, V.M., Nucl. Phys. A95 (1967) 420.
[19] VANDENBOSCH, R., WOLF, K.L., Physics and Chemistry of fission (C.r. Coll. Vienne, 1969), AIEA, Vienne (1969) 439.
[20] WOLF, K.L., Spontaneous Fission Isomers, Rapport RLO-1388-107, Washington University, Seattle (1969).
[21] BURNETT, S.C., et al., Submitted to Phys. Letters, 1970.
[22] ELWYN, A.J., Physics and Chemistry of Fission (C.r. Coll. Vienne, 1969), AIEA, Vienne (1969) 457.
[23] METAG, V., et al., Z. Phys. 226 (1969) 1.

MESURE A HAUTE RESOLUTION ET ANALYSE DE LA SECTION EFFICACE DE FISSION DU PLUTONIUM-239

J. BLONS, H. DERRIEN, A. MICHAUDON
CEA, Centre d'études
nucléaires de Saclay,
France

Abstract — Résumé

HIGH-RESOLUTION MEASUREMENT AND ANALYSIS OF THE ^{239}Pu FISSION CROSS-SECTION.

The fission cross-section of ^{239}Pu has been measured up to an energy of 30 keV with a gas scintillator containing 960 mg of ^{239}Pu and operated at a temperature of 77°K. The measurement has been made with a resolution of 1 ns/m using the Saclay 45-MeV linear accelerator as pulsed neutron source. The resonances have been analysed up to 660 eV by the shape method, by using a least-squares program based on a single-level formalism. A detailed study of the fission-width distribution for different energy intervals of 110 eV shows the existence of an intermediate structure in the fission cross-section due to the exit channel 1^+. This phenomenon is confirmed by measuring the spin of the resonances up to 660 eV. Finally, the fission cross-section averaged over different energy intervals is compared with those obtained in other laboratories.

MESURE A HAUTE RESOLUTION ET ANALYSE DE LA SECTION EFFICACE DE FISSION DU PLUTONIUM-239.

La section efficace de fission de ^{239}Pu a été mesurée jusqu'à une énergie de 30 keV avec un scintillateur gazeux contenant 960 mg de ^{239}Pu et fonctionnant à la température de 77°K. La mesure a été faite avec une résolution de 1 ns/m en utilisant l'accélérateur linéaire de 45 MeV de Saclay comme source pulsée de neutrons. Les résonances ont été analysées jusqu'à 660 eV, par la méthode des formes, en utilisant un programme de moindres carrés basé sur un formalisme à un niveau. L'étude détaillée de la distribution des largeurs de fission pour différents intervalles d'énergie de 110 eV montre l'existence d'une structure intermédiaire dans la section efficace de fission due à la voie de sortie 1^+. Ce phénomène est confirmé par une mesure de spin des résonances jusqu'à 660 eV. Enfin, la section efficace de fission, moyennée dans différents intervalles d'énergie, est comparée à celles obtenues dans d'autres laboratoires.

1. INTRODUCTION

Jusqu'à présent les paramètres des résonances de ^{239}Pu n'étaient connus que jusqu'à 250 eV [1, 2]. Cette limite en énergie était imposée par la section efficace de fission qui était mesurée avec une moins bonne résolution que celle de la section efficace totale. Pour étendre cette analyse à de plus hautes énergies, il a semblé possible d'utiliser les récents progrès dans la détection de la fission et dans la technique du temps de vol pour la mesure à haute résolution de la section efficace de fission de ^{239}Pu.

2. CONDITIONS EXPERIMENTALES

La mesure a été faite par la méthode du temps de vol en utilisant l'accélérateur linéaire de 45 MeV de Saclay comme source pulsée de neutrons. Le principe du détecteur est basé sur la détection des fragments de fission dans un scintillateur gazeux fonctionnant à la température de l'azote liquide [3, 4]. Ce détecteur comprend 12 cellules identiques

TABLEAU I. CONDITIONS EXPERIMENTALES

Accélérateur	Fréquence de répétition: 500 Hz	
	Largeur d'impulsion: 50 ns	
Sélecteur de temps de vol	Gamme d'énergie	Largeur de canal
	40 eV - 70 eV	200 ns
	70 eV - 192 eV	100 ns
	192 eV - 50 keV	50 ns
Longueur de vol	50,05 m (l'inclinaison de la base par rapport à l'axe du ralentisseur est de 10°)	
Filtre	Bore naturel, épaisseur 960 mg/cm²	
Mesure de bruit de fond		
Ecran permanent	Aluminium	
Ecrans temporaires	Manganèse-cobalt	

réparties dans 3 plans différents. Pendant la mesure, il contenait 960 mg/cm² de ^{239}Pu sous la forme de dépôts minces de PuO_2 de 1,4 mg/cm² d'épaisseur.

La composition isotopique en masse des échantillons était la suivante: ^{239}Pu, 98,6%; ^{240}Pu, 1,37%; ^{241}Pu, 0,025%.

Le spectre des neutrons incidents était mesuré par un compteur proportionnel à BF_3 placé immédiatement derrière le détecteur de fission. Les conditions expérimentales sont résumées dans le tableau I.

Les résultats ont été enregistrés sur bandes magnétiques à 16 pistes dont 13 étaient affectées aux informations de temps de vol codées, 2 autres au codage des voies (3 voies pour la fission correspondant aux 3 plans du détecteur et une voie pour la mesure simultanée du spectre de neutrons); la dernière piste servait au contrôle de parité.

3. ANALYSE DES RESULTATS

La section efficace de fission σ_f a été obtenue de 40 eV à 30 keV, après soustraction du bruit de fond, en divisant pour chaque canal le nombre de coups de fission par celui du compteur à BF_3.

Dans le calcul de σ_f, on suppose que la section efficace de la réaction $^{10}B\,(n, \alpha)$ est donnée par la relation suivante:

$$\sigma_{(n,\alpha)\,(barn)} = \frac{610,3}{\sqrt{E_{(eV)}}} - 0,28 \qquad (1)$$

Pour chaque canal la correction a été faite pour la différence de temps de vol entre les 4 voies (3 voies fission et 1 voie spectre).

La section efficace de fission a ensuite été normalisée sur les valeurs de $\sigma_0\Gamma_f$ des résonances à 44,48 eV; 47,6 eV; 52,6 eV et 74,95 eV obtenues par une mesure antérieure faite à Saclay [2].

La figure 1 montre la section efficace de fission ainsi obtenue de 192 eV à 1300 eV [5]. On remarquera, à de nombreux endroits, l'amélioration apportée par la qualité de la résolution et la réduction de l'effet Doppler. La brusque décroissance de σ_f vers 570 eV est très apparente sur cette figure [6].

Dans le tableau II nous comparons la section efficace de fission moyennée dans plusieurs gammes d'énergie avec celles obtenues dans d'autres laboratoires [7-9]. Nos valeurs sont en général plus faibles pour des énergies supérieures à 5 keV et plus élevées pour des énergies inférieures à 100 eV.

Les résonances qui apparaissent dans cette section efficace ont été analysées par la méthode des formes jusqu'à 660 eV en utilisant un programme de moindres carrés basé sur le formalisme à un niveau. Cette analyse, conjugée avec celle de la section efficace totale [2, 10], a permis de déterminer la plupart des paramètres des résonances situées dans cette gamme d'énergie (tableaux III et IV). La détermination de la largeur Γ_f est faite de la façon suivante:

a) De 0 eV à 450 eV, où la fonction de résolution est bien connue, les largeurs Γ_f sont calculées à partir des paramètres E_0, $2\,g\Gamma_n$, et $\sigma_0\Gamma_f$.

b) De 450 eV à 660 eV, les largeurs totales sont connues avec moins de précision; dans ce cas, et lorsque la largeur totale Γ est inférieure à 500 meV, Γ_f est calculée par la formule suivante:

$$\Gamma_f = \left[\Gamma_\gamma + \frac{2\,g\Gamma_n}{2\,g}\right] \times \frac{\sigma_0\Gamma_f}{\sigma_0\Gamma - \sigma_0\Gamma_f} \qquad (2)$$

Dans cette formule, Γ_γ est pris constant et égal à 42 meV [10]. La valeur de g est déterminée par celle du spin, lorsque celui-ci a pu être mesuré [11]. Lorsque le spin n'est pas connu, on prend $g = 1/2$.

c) Dans toute la gamme d'énergie, lorsque la largeur Γ est supérieure à 500 meV, la résonance correspondante est certainement de spin 0 [2, 12]; il est alors préférable de calculer Γ_f par la formule suivante:

$$\Gamma_f = \Gamma - \left(\Gamma_\gamma + \frac{2\,g\Gamma_n}{1/2}\right) \qquad (3)$$

La figure 2A montre la distribution des largeurs de fission dans la gamme d'énergie de 0 à 660 eV. Cet histogramme est bien décrit par une somme de deux distributions en χ^2 dont les paramètres, obtenus par une méthode de moindres carrés, sont les suivants:

Famille des résonances étroites (de spin 1^+):

$$171 \text{ résonances}, \quad \langle\Gamma_f\rangle_{1^+} = 35,5 \text{ meV}, \quad \nu = 1, \quad N_{eff} = 0,07$$

Famille des résonances larges (de spin 0^+):

$$58 \text{ résonances}, \quad \langle\Gamma_f\rangle_{0^+} = 2270 \text{ meV}, \quad \nu = 1,4, \quad N_{eff} = 1,48$$

(On a soustrait une valeur de $\Gamma_{\gamma f}$ égale à 3,5 meV pour tenir compte du processus (n, γf) [13, 14]).

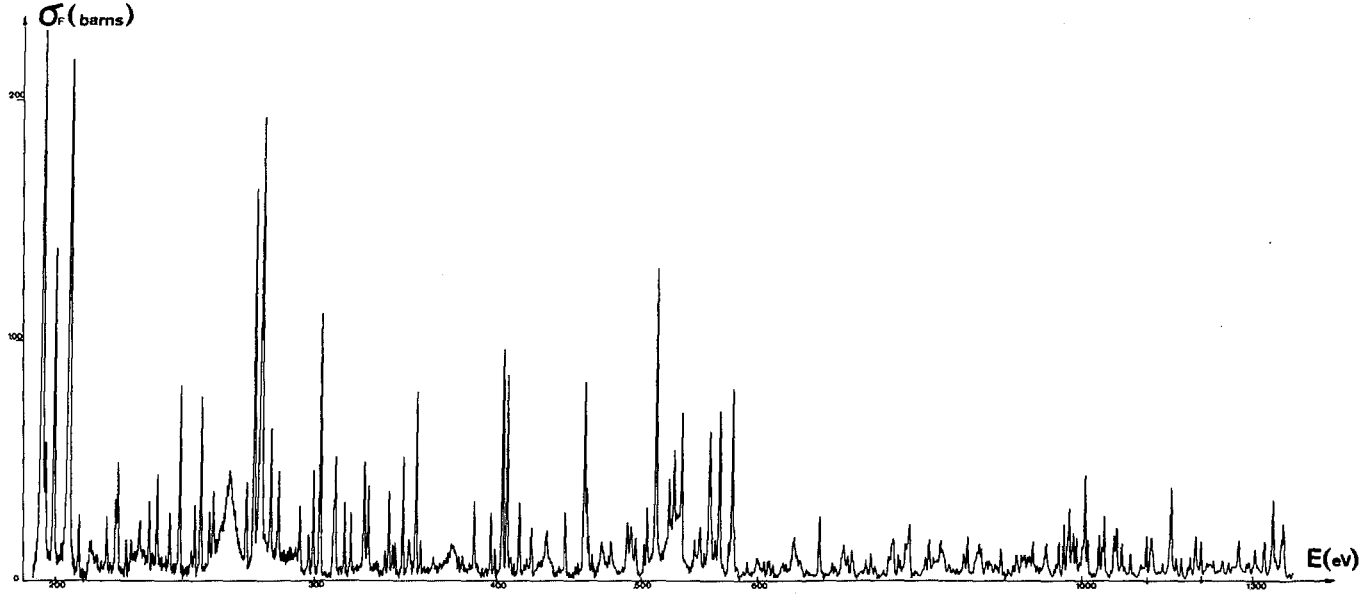

FIG. 1. Section efficace de fission de ^{239}Pu.

TABLEAU II. SECTION EFFICACE MOYENNE DE FISSION DE ^{239}Pu

Intervalles d'énergies (eV)	$\langle\sigma_f\rangle$ (barns)			
	Argonne [7]	Los Alamos [8]	Dubna [9]	Saclay (ce travail)
30 000 - 20 000				1,859
20 000 - 10 000	3,065	2,213	1,980	1,885
10 000 - 9 000	2,334	2,137	2,381	1,960
9 000 - 8 000	2,066	2,462	2,492	2,482
8 000 - 7 000	1,912	2,232	2,435	2,004
7 000 - 6 000	2,693	2,203	2,431	2,002
6 000 - 5 000	2,793	2,710	2,485	2,219
5 000 - 4 000	2,665	2,313	3,156	2,374
4 000 - 3 000	3,490	2,744	3,825	3,087
3 000 - 2 000	3,363	2,641	3,911	3,353
2 000 - 1 000	3,979	3,832	5,966	4,528
1 000 - 900	7,703	8,278	9,080	8,708
900 - 800	6,212	4,360	7,795	5,175
800 - 700	5,517	5,195	6,607	6,051
700 - 600	3,715	3,941	5,471	4,773
600 - 500	10,75	14,66	12,38	15,742
500 - 400	10,05	9,105	2,891	9,853
400 - 300	9,822	8,352	4,219	9,037
300 - 200	17,47	18,25	13,67	18,025
200 - 100	19,61	17,82	12,21	19,179
100 - 90	27,68	26,10	23,62	31,74
90 - 80	66,35	61,48	46,21	69,02
80 - 70	65,32	59,54	29,94	65,57
70 - 60	53,81	54,92	34,40	57,10
60 - 50	71,81	72,32	39,15	77,71
50 - 40	26,14	24,62	13,80	29,35
40 - 30	3,798	2,156	2,674	
30 - 20	32,81	42,07	23,94	
20 - 10	103,82		82,21	

Le nombre de résonances analysées permet d'étudier la distribution des largeurs de fission dans plusieurs gammes d'énergie et d'observer comment les paramètres moyens $\langle\Gamma_f\rangle_{0^+}$ et $\langle\Gamma_f\rangle_{1^+}$ varient en fonction de l'énergie. Nous donnons dans le tableau V les valeurs de ces deux paramètres, obtenues par moindres carrés, pour 6 intervalles de 110 eV entre 0 et 660 eV, à partir des distributions des largeurs de fission.

TABLEAU III. PARAMETRES DES RESONANCES DE ^{239}Pu

E(eV)	2 g Γ_n (meV) [10]	$\sigma_0\Gamma$ (b·eV) [10]	Γ (meV) [10]	$\sigma_0\Gamma_f$ (b·eV)	Γ_f (meV)
0,30			99 ± 4		60 ± 4
7,82	1,21 ± 0,04	201,0 ± 6,6	87 ± 5	108,2 ± 2,1	47 ± 3
10,93	2,84 ± 0,15	338,2 ± 17,9	200 ± 20	242,1 ± 5,0	143 ± 16
11,5	0,15				
11,89	1,54 ± 0,10	168,6 ± 11,0	67 ± 7	60,9 ± 2,4	24 ± 3
14,31	0,91 ± 0,05	82,8 ± 4,5	102 ± 8	54,7 ± 3,3	67 ± 7
14,68	2,86 ± 0,05	253,6 ± 4,3	70 ± 7	107,5 ± 2,1	30 ± 3
15,46	0,98 ± 0,08	82,6 ± 6,3	700 ± 50	80 ± 8	656
17,66	2,74 ± 0,05	201,9 ± 3,6	75 ± 7	92,7 ± 1,9	34 ± 4
22,29	4,00 ± 0,10	233,6 ± 5,8	109 ± 9	132,3 ± 2,6	62 ± 6
23,94	0,13 ± 0,01	7,1 ± 0,5	70 ± 12	3,8 ± 0,9	38 ± 10
26,24	2,20 ± 0,15	109,1 ± 7,4	83 ± 10	58,0 ± 2,9	44 ± 7
27,24	0,21 ± 0,01	10,0 ± 0,3	42 ± 8	1,1	5
32,31	0,42 ± 0,02	16,9 ± 0,7	153 ± 20	12,2 ± 0,5	110 ± 15
34,60	0,02				
35,50	0,43 ± 0,02	15,8 ± 0,6	47 ± 9	1,5	4 ± 2
41,42	6,20 ± 0,20	194,9 ± 6,2	52 ± 8	15,7 ± 3,5	4 ± 1
41,66	2,02 ± 0,25	63,1 ± 7,9	105 ± 16	28,1 ± 4,2	46 ± 12
44,48	9,97 ± 0,20	291,7 ± 5,9	58 ± 7	24,0 ± 1,2	5 ± 1
47,60	2,90 ± 0,15	79,3 ± 4,0	322 ± 25	61,0 ± 2,5	248 ± 30
49,71	2,2 ± 0,2	58 ± 6	810 ± 200	53,2 ± 2,7	746 ± 200
50,08	4,55 ± 0,20	118,2 ± 5,2	57 ± 10	26,2 ± 2,1	13 ± 3
52,60	15,70 ± 0,30	388,5 ± 7,4	68 ± 10	51 ± 1	9 ± 2
55,13	2,20 ± 0,12	51,5 ± 2,9	59	18,7 ± 1,9	21
57,44	6,5	147	500	130	445
58,84	5,5	122	1100	118	1047
59,22	8,37 ± 0,46	184,0 ± 10,1	191 ± 16	119 ± 8	123 ± 15
60,94	11	235	6800	200	6736
63,08	1,20 ± 0,25	24,3 ± 5,2	155 ± 17	18 ± 4	111 ± 37
65,36	0,54				
65,71	18,22 ± 0,50	372,8 ± 9,7	137 ± 14	203 ± 6	74 ± 8
74,05	4,75 ± 0,20	86,1 ± 6,5	71 ± 8	37,9 ± 1,9	32 ± 4
74,95	33,20 ± 1,50	576,5 ± 10,4	147 ± 14	330 ± 6	84 ± 9
78,95	0,16	2,6			
81,76	6	95 ± 30	2050	61	1996
82,68	0,75 ± 0,15	11,8 ± 2,4	70		
83,52	1,2	18,7	1750	18	1706
85,32	28 ± 4	427 ± 60	2300	360	2002
85,48	11,80 ± 0,36	179,7 ± 5,5	75 ± 20	39	16
90,75	18,45 ± 0,42	264,6 ± 6	60 ± 10	38 ± 3	9 ± 2
92,97	1,05 ± 0,04	14,7 ± 0,6	57 ± 5	2,3	9
95,36	3,15 ± 0,15	43 ± 2	98 ± 10	13 ± 2	30 ± 6
96,49	6,68 ± 0,26	90,1 ± 3,5	1700 ± 350	86 ± 9	1645
100,25	5,60	72	6000	72	5947
102,99	2,42 ± 0,08	30,6 ± 0,3	48 ± 5	6,6 ± 1,7	10 ± 3
105,30	6,96 ± 0,40	86,0 ± 5,0	48 ± 7	9,8 ± 1,0	5 ± 2
106,67	13,96 ± 0,60	170,3 ± 7,3	75 ± 4	59,7 ± 1,8	26 ± 2
110,38	0,66 ± 0,07	7,8 ± 0,8	43 ± 16	2,4	13
114,44	0,8	9	1500	7	1456
115,10	0,32 ± 0,10	3,6 ± 0,1	200	3	
116,03	5,41 ± 0,13	60,7 ± 1,5	257 ± 15	51 ± 3	215 ± 20
118,83	25,92 ± 0,60	283,9 ± 6,9	102 ± 6	118 ± 6	42 ± 4
120,99	3,70 ± 0,15	39,8 ± 1,6	78 ± 12	20 ± 2	39 ± 7
123,44	0,70 ± 0,08	7,4 ± 0,9	63 ± 13	4,6	39
126,20	2,96 ± 0,12	30,5 ± 1,2	96 ± 10	6,2	20
127,51	0,77 ± 0,12	7,8 ± 1,2	64 ± 10	3,1	25
131,75	18,26 ± 1,20	180,3 ± 12,0	3800 ± 250	158 ± 20	3722

TABLEAU III. (suite)

E(eV)	$2g\Gamma_n$ (meV) [10]	$\sigma_0\Gamma$ (b·eV) [10]	Γ (meV) [10]	$\sigma_0\Gamma_f$ (b·eV)	Γ_f (meV)
133,78	8,38 ± 0,30	81,5 ± 2,9	56 ± 6	8,7 ± 2,2	6 ± 2
136,75	5,12 ± 0,16	48,7 ± 1,5	126 ± 10	32,6 ± 3,3	84 ± 10
139,28	0,18	1,7		1,5	
142,92	4,86 ± 0,21	44,3 ± 1,9	137 ± 20	26,6 ± 3,2	82 ± 15
143,47	6,12 ± 0,15	55,5 ± 1,4	83 ± 12	21 ± 3	31 ± 5
146,25	10,58 ± 0,30	94,2 ± 2,7	70 ± 7	16,8 ± 1,0	12 ± 2
147,44	1,20 ± 0,60	10,6 ± 5,3	1000	9,3	956
148,21	0,70 ± 0,10	6,1 ± 0,9	150	4,2	102
149,42	2,62 ± 0,12	22,8 ± 1,1	120 ± 20	9,5 ± 1,8	50 ± 13
157,08	17,2 ± 0,4	142,5 ± 3,3	670 ± 50	114 ± 5	537 ± 50
160,8	0,2	1,7			
161,96	0,21 ± 0,07	1,7 ± 0,6	150		
164,54	42 ± 3	332 ± 22	79 ± 10	34 ± 2	8 ± 2
167,10	8,75 ± 0,40	68,2 ± 3,1	112 ± 8	42,2 ± 2,5	69 ± 7
170,49	0,86 ± 0,02	6,6 ± 0,2	158 ± 60	5	120
171,08	0,89 ± 0,30	6,8 ± 2,3	1000	6	956
174,56	0,06				
175,98	3,14 ± 0,10	23,2 ± 0,8	73 ± 5	10 ± 2	31 ± 6
177,22	5,36 ± 0,18	39,4 ± 1,3	51 ± 6	5 ± 1	6 ± 2
178,90	1,83 ± 0,06	13,3 ± 0,5	58 ± 9	3,3 ± 0,8	14 ± 4
183,64	2,29 ± 0,12	16,2 ± 0,8	72	6,4	28
184,87	10 ± 2	70,4 ± 14	2200 ± 200	58 ± 12	1800 ± 500
188,27	0,92 ± 0,07	6,4 ± 0,5	53 ± 10	1,1	9
190,64	2,51 ± 0,09	17,1 ± 0,6	67 ± 9	3,4	13
195,36	30,0 ± 1,2	200 ± 8	447 ± 40	150 ± 9	335 ± 40
196,69	7,04 ± 0,42	46,6 ± 2,8	112 ± 18	22,5 ± 2,3	54 ± 12
199,39	14,49 ± 0,75	94,6 ± 4,8	133 ± 13	57 ± 3	80 ± 10
203,46	6	38,4		14	
203,93	26,6 ± 1,0	169,7 ± 6,4	430	145 ± 22	366
207,37	10,5 ± 0,4	65,9 ± 2,5	57 ± 5	6,8 ± 1,1	6 ± 2
211,09	1,4	8,6	800	8	745
212,02	1,2	7,4	1500	7,2	1456
213,28	0,7	4,3	200 ± 60	3,5	163
216,53	9,40 ± 0,40	56,5 ± 2,3	67 ± 7	9,3 ± 2,8	11 ± 4
219,49	5,36 ± 0,27	31,8 ± 1,6	70 ± 10	11,9 ± 3,6	26 ± 6
220,22	11,14 ± 0,50	65,8 ± 1,5	52 ± 8	13,9 ± 4,2	11 ± 3
223,16	5,12 ± 0,15	29,8 ± 0,9	59 ± 6	4,3	9
224,89	2,56 ± 0,15	14,8 ± 0,9	85 ± 17	4,4	25
227,77	17 ± 3	97 ± 15	9000	75 ± 18	8024
227,89	2,54 ± 0,15	14,5 ± 0,9	67 ± 10	7 ± 2	32 ± 10
231,40	17,8 ± 1,0	100 ± 6	54 ± 8	9,2 ± 1,8	5 ± 2
232,63	0,66 ± 0,15	3,7 ± 0,2	130	2	
234,32	15,35 ± 0,60	85,2 ± 3,3	74 ± 9	16,8 ± 2,0	15 ± 3
239,04	8,15 ± 0,40	44,4 ± 2,2	73 ± 8	9,9 ± 1,4	16 ± 4
240,60	0,05	0,27			
242,88	9,92 ± 0,45	53,2 ± 2,6	97 ± 6	31 ± 2	56 ± 6
247,50	1,39 ± 0,20	7,3 ± 1,2	312 ± 60	5,3 ± 1,3	227
248,86	22,13 ± 0,72	115,7 ± 3,7	62 ± 6	9,7 ± 1,2	5 ± 1
251,23	41,2 ± 1,2	213,4 ± 6,3	83 ± 5	31,1 ± 2,5	12 ± 2
254,58	4,2 ± 0,3	21,5 ± 1,5	55 ± 5	9,6 ± 1,5	25 ± 4
256,11	9,5 ± 0,5	48,2 ± 2,5	91 ± 16	16,8 ± 2,2	32 ± 7
259,00	0,4 ± 0,1	2,0 ± 0,5			
262,37	50 ± 4	248 ± 20	6300	233 ± 24	6148
262,74	3,64 ± 0,45	18,0 ± 2,3	60 ± 10	3,1	10
264,23	0,25	1,2			
269,11	2,1 ± 0,5	10,1 ± 2,5	140	6 ± 2	83
269,54	5,8 ± 0,6	28,0 ± 2,7	72 ± 20	11 ± 2	28 ± 10
272,62	41,8 ± 1,5	199,3 ± 7,2	92 ± 10	68,4 ± 3,5	31 ± 12
274,80	14,0 ± 2,0	66,2 ± 9,4	800	60 ± 20	730
275,57	35,1 ± 1,5	165,8 ± 7,2	150 ± 30	80 ± 13	72 ± 20
277,23	9	42	5300	42	5260

TABLEAU III. (suite)

E(eV)	2 g Γ_n (meV) [10]	$\sigma_0\Gamma$ (b·eV) [10]	Γ (meV) [10]	$\sigma_0\Gamma_f$ (b·eV)	Γ_f (meV)
279,59	10,64 ± 0,33	49,3 ± 1,5	111 ± 8	25 ± 3	56 ± 8
282,92	37,8 ± 2,7	174 ± 12	85 ± 6	22,2 ± 2,2	11 ± 2
285,73	0,10	0,45			
288,00	15	68	7000	60	6028
288,30	0,08	0,36			
292,33	5,82 ± 0,24	25,9 ± 1,1	115 ± 13	16,3 ± 2,1	72 ± 12
296,46	4,89 ± 0,21	21,4 ± 0,9	81 ± 12	8	30
298,59	15,80 ± 0,60	68,8 ± 2,6	74 ± 7	19 ± 4	20 ± 5
301,81	27,3 ± 1,0	117,6 ± 4,4	108 ± 6	52 ± 7	48 ± 10
308,20	4,40 ± 0,27	18,9 ± 1,2	150 ± 30	12,2 ± 3,6	98 ± 45
309,01	21,10 ± 0,72	88,8 ± 3,1	85 ± 12	25,4 ± 2,6	24 ± 5
311,12	0,73 ± 0,18	3,1 ± 0,8		1,6	
313,62	20,40 ± 0,72	85 ± 3	62 ± 6	13,0 ± 1,3	10 ± 3
316,66	7,75 ± 0,30	31,8 ± 0,9	73 ± 10	10,8 ± 1,6	25 ± 5
321,75	0,20	0,9			
323,36	30,2 ± 0,9	121,4 ± 3,6	160 ± 20	35,5 ± 5,3	47 ± 9
325,30	12,8 ± 0,5	51,2 ± 2,1	105 ± 9	22,6 ± 3,2	46 ± 12
329,65	5,6	22	2000	20	1947
333,91	8,24 ± 0,30	32,1 ± 1,2	67 ± 7	4,7	10
335,93	26,60 ± 0,72	102,9 ± 2,7	83 ± 6	22,1 ± 3,3	18 ± 4
337,95	12,09 ± 0,42	46,5 ± 1,6	74 ± 7	7,2 ± 2,2	11 ± 4
339,24	4,92 ± 0,21	18,9 ± 0,8	81 ± 12	7,8 ± 2,3	33 ± 12
343,18	23,69 ± 0,78	89,7 ± 3,0	75 ± 6	22,2 ± 2,2	18 ± 3
346,56	5,2 ± 0,6	19,5 ± 2,3	1200	18,0 ± 3,6	1148
350,30	32,25 ± 0,90	119,7 ± 3,4	97 ± 6	44 ± 3	35 ± 4
352,82	5,84 ± 0,24	21,5 ± 0,9	69 ± 13	5,2 ± 1,0	17 ± 5
354,89	0,60 ± 0,10	2,2 ± 0,4		1	
357,87	4,5	16	6000		5949
359,99	1,66 ± 0,18	6,0 ± 0,7	114 ± 20	4,2	80
361,28	0,33 ± 0,10	1,2 ± 0,4			
366,00	5,4	20	5000	20	4947
368,33	0,6 ± 0,2	2,1 ± 0,7		1,6	
370,31	3,90 ± 0,24	13,7 ± 0,8	105 ± 20	3	23
371,72	11,5 ± 1,4	41 ± 5	3400	41 ± 5	3335
375,02	4,0 ± 0,3	13,9 ± 1,1	43 ± 12	2	6
377,10	2,98 ± 0,30	10,3 ± 1,1	100 ± 20	4 ± 1	39 ± 16
378,04	1,88 ± 0,30	6,5 ± 1	223 ± 60		
382,43	0,63 ± 0,15	2,1 ± 0,5	130	1,4	85
384,26	8,55 ± 0,50	28,9 ± 1,7	109 ± 30	20 ± 3	75 ± 25
385,90	1,4	4,3	1000	4,3	955
389,51	2,09 ± 0,18	7,0 ± 0,6	74 ± 14	2	21
391,52	1,89 ± 0,18	6,3 ± 0,6	142 ± 28	3	68
394,43	9,78 ± 0,33	32,2 ± 1,0	106 ± 13	16,0 ± 2,4	52 ± 10
396,91	3,17 ± 0,21	10,4 ± 0,7	108 ± 20	5,9 ± 1,2	61 ± 20
401,56	29,1 ± 1,2	94,2 ± 3,8	220 ± 20	66 ± 7	154 ± 25
404,24	34,8 ± 1,3	111,9 ± 4,1	155 ± 25	55 ± 6	76 ± 15
406,03	2,73 ± 0,60	8,7 ± 1,9	320	1,5	
406,95	1,46 ± 0,60	4,7 ± 1,9	330	4,3	302
408,71	1,94 ± 0,30	6,2 ± 0,9	150	2,4	58
412,31	13,41 ± 0,63	42,3 ± 2,0	145 ± 15	20,4 ± 3,1	70 ± 13
415,66	4,89 ± 0,36	15,3 ± 1,2	152 ± 30	1,8	18
417,60	2,40 ± 0,36	7,5 ± 1,1	267 ± 64	5	178
419,85	9,11 ± 0,45	28,2 ± 1,4	139 ± 25	15 ± 3	74 ± 20
425,67	0,40	1,2			
426,37	14,8	45	7000	45	6913
429,64	5,66 ± 0,81	17,1 ± 2,4	780	15	727
431,29	7,3	22	3500	20	3443
432,73	1,54 ± 0,30	4,6 ± 0,9			
437,76	4,04 ± 0,30	12,0 ± 0,9	62 ± 15	2	10
438,72	4,36 ± 0,30	12,9 ± 0,9	61 ± 15	0,6	8
440,07	0,42 ± 0,15	1,2 ± 0,4			
442,41	10,5 ± 0,5	30,9 ± 1,5	422 ± 50	24,7 ± 4	337 ± 70

TABLEAU IV. PARAMETRES DES RESONANCES DE ^{239}Pu

E (eV)	$2 g \Gamma_n$ (meV) [10]	$\sigma_0 \Gamma$ (b·eV) [10]	$\sigma_0 \Gamma_f$ (b·eV)	g	Γ_f (meV)
449,75	2,0 ± 0,3	5,8 ± 0,9	3,9	1/2	90
451,35	21,1 ± 1,4	60,8 ± 4,2	3,8	3/4	3,7
454,45	0,7	2,0			
455,73	39,7 ± 2,5	113,3 ± 7,5	91,0	1/4	495
457,33	11,1 ± 1,1	31,6 ± 3,2	21,8	1/2	118
458,80	6,9 ± 0,6	19,6 ± 1,7	8,1	3/4	33
461,26	3,5 ± 0,4	9,9 ± 1,2	5,3	1/2	52,4
462,64	0,8 ± 0,2	2,2 ± 0,6	1,4	1/2	86
468,20	6,5	18,0		1/4	2045
470	15	41,5		1/4	5030
473,10	6,2 ± 0,4	17,0 ± 1,1	3	3/4	10
475,31	5,7	15,7	12,5	1/4	535
476,90	2,7	7,4	7	1/4	1950
479,24	0,2	0,5			
484,15	3,9 ± 0,4	10,4 ± 1,1	2,5	1/2	14,5
487,29	3,3	8,8	} 19,8		
487,81	5,2	15,4			
490,65	20 ± 3	53 ± 8		1/4	2220
494,10	6,9 ± 0,4	18,2 ± 1,1	10,5	3/4	70
495,63	1,2	3,1			
500,50	5,1 ± 1,3	13,2 ± 3,4	5,6	3/4	32
502,86	17,8 ± 1,4	46,0 ± 3,6	17,3	3/4	32
505,78	0,9	2,3			
508,22	0,7	1,8			
509,74	78,2 ± 4,0	199,4 ± 10,4	127,4	3/4	167
511,52	12,9	32,8		1/4	3300
515,16	1	2,5			
516,57	0,3	0,8			
517,98	0,7	1,8			
520,22	22,4 ± 1,8	56,0 ± 4,5	24	3/4	43
524,21	45,9 ± 4,8	113,6 ± 11,9	25	3/4	20
525,40	121	299		1/4	10500
526,00	1,5	3,7	2	1/2	51
527,38	1,5	3,7	~1	1/2	~16
530,52	63,8 ± 5,1	156,3 ± 12,8	48	1/4	75
539,17	17,1 ± 3,0	41,2 ± 7,2	1,8	3/4	2,4
540,71	4	9,6	} 14		
541,55	8	19			
543,08	17,6 ± 3,0	41,0 ± 7,2	3,5	3/4	5
545,85	17,5 ± 2,5	41,7 ± 6,0	34	1/4	1120
547,14	1,8	4,3			
549,67	17,7 ± 1,5	41,9 ± 3,5	5	3/4	7
553,50	17	39,9	~2		~3
554,13	52,2	122,5		1/4	1140
555,72	4,9	11,5	10,5		
559,16	40,8 ± 2,4	94,9 ± 6,7	22	3/4	21
562,84	53,6 ± 4,0	123,8 ± 9,3	81		
564,03	9,8 ± 1,6	22,6 ± 3,7	1		~2
565,81	14,2 ± 1,2	32,6 ± 2,7	2,9	1/2	5
571,11	12,9 ± 0,9	29,4 ± 2,1	11,5	3/4	33
574,00	79,5 ± 6,0	180,0 ± 13,6	94	1/4	220

TABLEAU IV. (suite)

E (eV)	$2 g \Gamma_n$ (meV) [10]	$\sigma_0 \Gamma$ (b·eV) [10]	$\sigma_0 \Gamma_f$ (b·eV)	g	Γ_f (meV)
575,77	59,7 ± 5,6	134,8 ± 12,6	12	3/4	8
578,00	2,5	5,6	2,5	1/2	36
579,04	10,3 ± 0,9	23,1 ± 2,1	2,8	3/4	7
584,81	0,7	1,6			
588,09	16,9 ± 1,2	37,4 ± 2,6	6	3/4	10
589,94	0,5	1,1			
593,52	3,2 ± 0,5	7,0 ± 1,2	0,6	1/2	4
597,35	12,9 ± 1,5	27,0 ± 1,7	2,6	3/4	5
598,04	21,6 ± 4,0	47,0 ± 8,2	44	1/4	5915
604,01	37,6 ± 3,3	80,9 ± 6,8	4	3/4	3,5
607,64	14,6 ± 1,2	31,2 ± 2,5	4,2	3/4	7,7
609,29	23,6 ± 2,4	50,4 ± 5,1	5,2	3/4	6,6
612,82	8,8 ± 0,8	18,7 ± 1,8	4	1/2	14
620,24	17,8 ± 1,5	37,3 ± 3,2	3,4	3/4	5,4
622,39	14,7 ± 1,2	30,7 ± 2,6	4,9	3/4	9,8
625,17	11,8 ± 1,2	24,5 ± 2,6	3,2	3/4	7,5
628,21	2,2 ± 0,7	4,6 ± 1,5	0,8	1/2	9
632,97	34 ± 4	69,8 ± 8,2	68	1/4	3800
636,47	8,0 ± 1,2	16,3 ± 2,5	4	1/2	16
639,28	13,9 ± 1,5	28,3 ± 3,1	2,8	3/4	6
641,42	0,7	1,4			
644,94	8,8 ± 1,2	17,7 ± 2,4	1	3/4	3
646,65	1,5	3			
658,29	122 ± 13	253 ± 25	33,2	3/4	19

TABLEAU V. VALEURS DES PARAMETRES $\langle \Gamma_f \rangle_{0^+}$ ET $\langle \Gamma_f \rangle_{1^+}$ POUR SIX INTERVALLES DE 110 eV

E(eV)	$\langle \Gamma_f \rangle_{0^+}$ (meV)	$\langle \Gamma_f \rangle_{1^+}$ (meV)
0 - 110	2065 ± 840	41 ± 10
110 - 220	970 ± 370	30 ± 8
220 - 330	3302 ± 1350	22 ± 5
330 - 440	3285 ± 1550	43 ± 11
440 - 550	2352 ± 925	38 ± 11
550 - 660	1800 ± 1040	7 ± 2

Ces paramètres sont assez voisins de ceux publiés précédemment [6]. On note cependant quelques différences car, d'une part, l'ensemble des largeurs Γ_f est plus complet et, d'autre part, l'analyse par moindres carrés des distributions donne des valeurs plus précises de $\langle \Gamma_f \rangle_{0^+}$ et $\langle \Gamma_f \rangle_{1^+}$. Ces dernières sont données avec une erreur qui correspond à l'échantillonnage. Les erreurs d'origine statistique, beaucoup plus faibles, ne sont pas considérées ici. Les valeurs de $\langle \Gamma_f \rangle_{0^+}$ et de $\langle \Gamma_f \rangle_{1^+}$ ainsi obtenues sont en accord avec celles de Trochon [11] déduites d'une mesure directe du spin des résonances. Ces deux résultats montrent que les fluctuations de

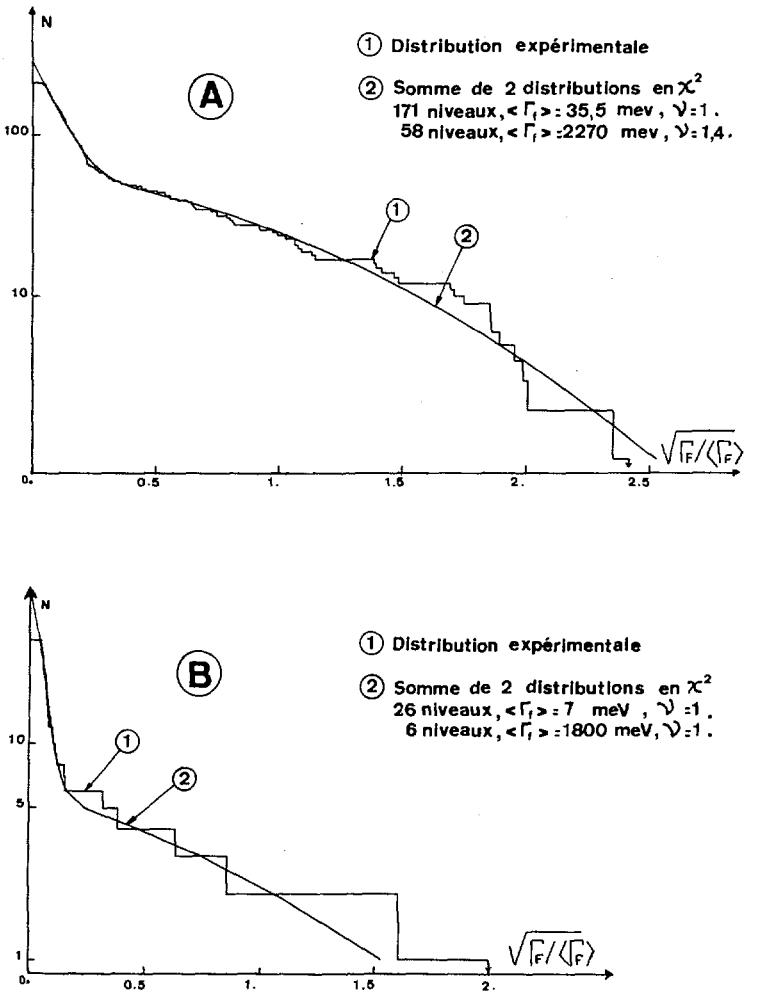

FIG. 2. Distribution des largeurs de fission: A, de 0 à 660 eV; B, de 550 à 660 eV.

$\langle\Gamma_f\rangle_{0^+}$ en fonction de l'énergie ne sont pas significatives. En revanche, celles de $\langle\Gamma_f\rangle_{1^+}$ sont beaucoup plus importantes et sont associées à des barres d'erreur plus faibles; les fluctuations de $\langle\Gamma_f\rangle_{1^+}$ sont incompatibles avec un modèle statistique et confirment l'existence d'une structure intermédiaire dans la section efficace de fission due à la voie de fission 1^+ [15], phénomène déjà présenté en 1969 [6]. L'interprétation de cet effet de structure intermédiaire est maintenant classique; elle consiste à considérer que les résonances 1^+ observées sont des états de classe I dont le couplage à la fission se fait par l'intermédiaire d'états de classe II situés dans le deuxième puits d'une barrière de fission à 2 bosses [13, 16]. Dans cette gamme d'énergie, le couplage semble maximal vers 400 eV.

4. CONCLUSION

La précision avec laquelle la section efficace de fission de ^{239}Pu a été mesurée, grâce à l'amélioration de la résolution expérimentale et à la réduction de l'effet Doppler, a permis d'étendre l'analyse microscopique des résonances jusqu'à 660 eV, énergie très élevée pour un noyau fissile. Cette analyse a mis en évidence une structure intermédiaire dans la section efficace de fission due à la voie de sortie 1^+. Actuellement, un tel effet est très difficile à mettre en évidence d'une autre façon, notamment par des techniques d'autocorrélation.

REMERCIEMENTS

Nous remercions Mlle Valentin pour la préparation des dépôts de ^{239}Pu, ainsi que Mlle Sanche pour sa collaboration efficace lors de l'analyse des paramètres de résonances.

REFERENCES

[1] BLONS, J., et al., C.r. hebd. Séanc. Acad. Sci., Paris 262 (1966) 79.
[2] DERRIEN, H., et al., «Sections efficaces totale et de fission du ^{239}Pu», Nuclear Data for Reactors (C.r. Conf. Paris, 1966) II, AIEA, Vienne (1967) 195.
[3] EGGERMANN, C., et al., Détecteur de fission à basse température (77°K), Nucl. Instrum. Meth. 81 2 (1970) 243.
[4] BLONS, J., et al., Rev. Phys. appl. 4 (1969) 287.
[5] BLONS, J., et al., C.r. hebd. Séanc. Acad. Sci., Paris 267 (1968) 901.
[6] PAYA, D., et al., « Structure intermédiaire dans les sections efficaces de fission du neptunium-237 et du plutonium-239 », Physics and Chemistry of Fission (C.r. Coll. Vienne, 1969), AIEA, Vienne (1969) 307.
[7] BOLLINGER, L.M., et al., « Slow neutron cross sections », Conf. int. util. énergie atom. fins pacif. (Actes 2e Conf. Genève, 1958) 15 ONU, New York (1958) 127.
[8] SHUNK, E.R., et al., Neutron Cross Section Technology (Proc. Conf. Washington, 1966) II (1966) 979.
[9] RYABOV, U.V., et al., Atomn. Energ. 24 4 (1968) 351.
[10] DERRIEN, H., et al., A paraître.
[11] TROCHON, J., DERRIEN, H., LUCAS, B., MICHAUDON, A., « Détermination du spin des résonances induites par des neutrons lents dans le plutonium-239 », ces comptes rendus, AIEA-CN-26/62.
[12] MICHAUDON, A., « Détermination du spin des résonances des noyaux fissiles », Nuclear Data for Reactors (C.r. Conf. Paris, 1966) II, AIEA, Vienne (1967) 161.
[13] LYNN, J.E., « Structure effects in nuclear fission », Nuclear Structure (C.r. Coll. Doubna, 1968), AIEA, Vienne (1968) 463.
[14] LE COQ, G., Thèse, Orsay, Octobre 1967.
[15] MICHAUDON, A., Neutron Cross Sections and Technology (Proc. Conf. Washington, 1968) 1, NBS Special Publication 299 (1968) 427.
[16] STRUTINSKY, V.M., BJØRNHOLM, S., « Intermediate states in fission », Nuclear Structure (C.r. Coll. Doubna, 1968), AIEA, Vienne (1968) 431.
[17] LYNN, J.E., Phys. Lett. 18 (1965) 31.
[18] DERRIEN, H., BLONS, J., MICHAUDON, A., « Analyse simultanée de 5,7 à 160 eV des sections efficaces totale et de fission du plutonium-239 par un formalisme multiniveaux », ces comptes rendus, IAEA-CN-26/61.

DISCUSSION

TO PAPERS IAEA-CN-26/60, 61, 62, 63

M. S. MOORE: I should like to question the uniqueness of the partial fission width distribution shown for 0^+ resonances in ^{239}Pu. As you know, in a two-fission-channel analysis, the vector orientations are invariant to a rotation of the reference axes. But such a rotation will completely change the partial fission width distribution.

A. M. MICHAUDON: In a few cases there are two neighbouring 0^+ resonances which have very different widths and which do not interfere. It was assumed that fission in two resonances of this kind proceeds in two different modes corresponding to two different channels, thus providing a unique reference axis.

M. S. MOORE: For ^{241}Pu, below 40 eV, the spin determinations of Sauter and Bowman seem to provide good evidence for a spin dependence of $< \Gamma_f >$. It would appear that an integral distribution of fission widths is not a sensitive test for a spin dependence of $< \Gamma_f >$, especially if the distributions overlap.

A. M. MICHAUDON: I quite agree and this is the reason for my showing that the fission width cannot be used as a means of separating the resonances into two groups corresponding to the two spin states in the case of ^{241}Pu, even though this has been done in the past.

E. R. RAE: I would like to refer to Dr. Michaudon's comment that the structure observed in the fission cross-section of ^{235}U below 5 keV was probably due to the entrance channel. Is there any evidence that the same argument applies to the rather broader structure observed at higher energies in the fission cross-section?

A. M. MICHAUDON: The comparison between averaged values of the fission and total cross-section of ^{235}U was limited to the energy of 5 keV because, at the time the paper was written, the quality of available total cross-section data had been checked up to this energy only. However, such a comparison can certainly be extended up to a higher energy limit.

J. Y. BARRÉ: In your oral presentation you gave some very interesting results of your high-resolution measurements relating to resonance parameters and spin determination. However, I should like to dwell on the importance of the average cross-section findings as far as reactor physicists are concerned. In the various papers which you presented you give average cross-section measurements up to 30 keV for ^{235}U and ^{239}Pu. I should like to request your comments on a number of points. First, what is the accuracy of these cross-sections, e. g. at 1 keV, 5 keV and 30 keV?

A. M. MICHAUDON: The error bars of statistical origin on the average cross-sections have not been given since they are certainly smaller than the systematic errors (normalization at low energy, subtraction of background etc.).

J. Y. BARRÉ: What can you say about the Van-de-Graaff measurements (Leroy) in the overlapping energy range of the two 25-30 keV measurements?

A. M. MICHAUDON: A comparison with the values obtained using the Van-de-Graaff electrostatic accelerator at Cadarache cannot be made immediately because it has to take into account fluctuations in cross-section and also different experimental conditions (e. g. resolution). However, it would appear that the fission cross-section of ^{235}U for the two laboratories

(Saclay and Cadarache) are systematically below the average in the energy range where they can be compared.

J. Y. BARRÉ: And lastly, could you comment on comparisons with average cross-sections obtained by other laboratories (e. g. for ^{239}Pu). In Table I of paper CN-26/63 your values are 20% higher than those of Los Alamos towards 1-2 keV and 20% lower towards 9-10 keV.

A. M. MICHAUDON: The comparison of our values with those of other laboratories is summarized in the tables which you have seen. The source of the differences between various measurements can be found only by making a detailed initial analysis of the various experimental conditions. This would be an important line of work and it deserves being carried out. However, we have not embarked upon it at our facilities.

J. L. LEROY: A comparison between the results of Saclay and Cadarache in the matter of the fission cross-sections for ^{235}U and ^{239}Pu could not be carried out directly because the fluctuations are rather considerable and the energy resolutions of the two series of measurements are very different.

We are working on such a comparison at present, by calculating

$$\sigma(E, E+\Delta E) = \int_{E}^{E+\Delta E} \sigma_{sa}(E')\, R(E')\, dE'$$

where $\sigma_{sa}(E')$ is the Saclay result and $R(E')$ represents the resolution function of the measurement made at Cadarache.

σ can be compared directly with the result of the Cadarache measurement.

FISSION AND CAPTURE CROSS-SECTIONS OF CURIUM*

M. S. MOORE, W. K. BROWN, M. E. ENNIS, R. R. FULLWOOD,
G. A. KEYWORTH, J. H. McNALLY,
Los Alamos Scientific Laboratory, Los Alamos, N. Mex.,
F. B. SIMPSON, J. R. BERRETH,
Idaho Nuclear Corporation, Idaho Falls, Idaho,
R. D. BAYBARZ,
Oak Ridge National Laboratory, Oak Ridge, Tenn.,
M. C. THOMPSON,
Savannah River Laboratory, Aiken, S. C.,
United States of America

Abstract

FISSION AND CAPTURE CROSS-SECTIONS OF CURIUM.

Optimization of the production of ^{252}Cf and heavier isotopes requires knowledge of the capture and fission cross-sections of various isotopes formed in the production chain. Most important are minimization of losses due to fission of ^{245}Cm, ^{247}Cm, and ^{251}Cf target material by neutrons. Also of interest are the capture cross-sections of the isotopes which undergo sub-barrier fission for resonance energy neutrons. In a recent experiment (Physics-8), utilizing a nuclear explosion as the neutron source, both fission and capture cross-sections were measured for ^{244}Cm and ^{246}Cm, and fission cross-sections were measured for the other Cm isotopes in the production chain: ^{245}Cm, ^{247}Cm, and ^{248}Cm, from 20 eV to several MeV. Fission cross-sections were also determined for a number of other heavy isotopes, including ^{252}Cf. This technique appears to be reasonably well suited for such studies, since only limited quantities (20 to 100 μg) of separated target isotopes are required, and the sample activity (up to 10^8 fissions/s) is no problem. Analysis of the data in the resolved resonance region above 20 eV yields all the partial cross-sections for the isotopes ^{244}Cm, ^{246}Cm, and ^{247}Cm, under the assumption that the capture width for the odd-A target is constant and given by nuclear systematics.

These measurements are also of interest because they offer experimental evidence concerning nuclear-structure-model predictions by Strutinsky and Nilsson on sub-barrier fission. The even curium and californium isotopes measured all show fission thresholds and appreciable sub-barrier resonance fission. However, the characteristic enhancement of sub-barrier resonance fission attributed to eigenstates in the second shape minimum does not seem to be present for the even Cm and Cf targets studied. More detailed statistical tests are required to establish the existence of such effects.

1. INTRODUCTION

The unique properties of the isotope ^{252}Cf make it highly desirable for industrial and medical use as a high-specific-activity neutron source. Potential applications which have been metnioned are radiotherapy, neutron activation analysis in medical diagnostics and in mineral exploration, short-lived radionuclide production for medical use, neutron well logging, and neutron radiography. Development of the market potential of ^{252}Cf is reported in a series of brochures [1, 2] issued by the Savannah River Operations Office of the US Atomic Energy Commission.

* Work performed under the auspices of the US Atomic Energy Commission.

At present, practical quantities of ^{252}Cf can only be produced by long term irradiation of isotopes of lower atomic weight in high-flux reactors. Less than 50 mg of material are presently available, but estimates of the demand in the early 1980's range as high as tens of grams per year. To meet such a demand, it is essential that production be optimized as far as is possible.

In considering this optimization, one can assume that the starting point in the production chain is ^{244}Cm, produced in substantial quantity in plutonium-fuelled power reactors. The production chain requires successive neutron capture by all the curium isotopes through ^{248}Cm, then by ^{249}Bk, ^{250}Cf, and ^{251}Cf. Loss of material occurs by fission, with most of the loss occurring by neutron capture in isotopes which are fissionable by thermal neutrons, ^{245}Cm, ^{247}Cm, and ^{251}Cf. These losses can be rather substantial. For example, ^{245}Cm has a 2200 m/s capture cross-section of 390 barns and a fission cross-section of 2250 barns [3], representing a loss of material by 570% at just this one stage.

The thermal cross-section primarily reflects the parameters of one or two resonances which occur close to the neutron binding energy. It has been conjectured that these resonances in fissile ^{245}Cm or ^{247}Cm might happen to have a lower than average value of α, the capture-to-fission ratio. If so, then loss of material in the production chain could be minimized by hardening the spectrum so that most of the neutron absorption occurs in the resonance region.

To help decide the question of whether a resonance reactor will optimize ^{252}Cf production, three different types of cross-section measurements are in progress. Using small quantities of electromagnetically separated sample material produced at Oak Ridge National Laboratory, groups at Oak Ridge and at the Savannah River Laboratory are measuring resonance capture and fission integrals and 2200 m/s cross-sections for the isotopes of interest. The fast chopper group at the Materials Testing Reactor in Idaho Falls, Idaho, is measuring microscopic total cross-sections of ^{244}Cm, ^{245}Cm, and ^{246}Cm below ~100 eV, using several more massive samples which have differing isotopic content by virtue of their irradiation history. The third effort is the measurement of the partial cross-sections of Cm above 20 eV, using the nuclear explosion as a neutron source. The present paper gives the preliminary results of this measurement.

2. EXPERIMENTAL METHOD

The technique of measuring cross-sections with a single burst of neutrons from a nuclear explosion has been discussed in detail [4], and will be reviewed here only briefly. In the most recent event, Physics-8, the foils of fissionable material were placed consecutively in twin stacks. In each stack, the foils were separated by about 21 cm, and each foil was viewed by two p-n junction Si solid-state detectors, at 55° and at 90° to the beam. The fissionable material, ranging from a few μg to several mg, was deposited on stainless steel backings, 2.5×10^{-3}mm thick. The beams were collimated several meters below the first sample, and trimmed to a circle of diameter 1.943 cm just below the stack. In the stack containing the Cm and ^{252}Cf samples, there were a number of other fissionable and

TABLE I. ISOTOPIC ANALYSIS OF SAMPLES

	% ^{243}Am	% ^{244}Cm	% ^{245}Cm	% ^{246}Cm	% ^{247}Cm	% ^{248}Cm
^{244}Cm fission (83.5 μg)	0.1	99.2	0.12	0.37	~0.1	~0.1
^{245}Cm fission (34.1 μg)	-	23.14	76.52	0.334	0.0025	0.0016
^{246}Cm fission (16.3 μg)	0.38	5.00	0.164	94.70	0.072	0.068
^{247}Cm fission (26.9 μg)	-	50.23	0.613	26.32	20.9	1.96
^{248}Cm fission (67.6 μg)	-	7.86	0.119	2.71	0.039	89.27
Mixed Cm capture (397 mg)	-	81.71	0.705	16.20	0.478	0.905
	% ^{249}Cf	% ^{250}Cf	% ^{251}Cf	% ^{252}Cf	% ^{253}Cf	% ^{254}Cf
^{252}Cf fission (60.8 μg)	0.03	0.56	0.158	99.23	0.027	0.044

monitor samples. The complete list of samples in this stack, in the order in which the beam passed through, is as follows: ^{243}Cm, ^{244}Cm, ^{246}Cm, ^{248}Cm, ^{238}U, Blank, ^{6}Li, ^{235}U, ^{245}Cm, ^{247}Cm, ^{242}Pu, ^{244}Pu, ^{237}Np, ^{243}Am, ^{10}B. After passing through this stack, located on the first floor of a 100-foot tower, the beam was passed undisturbed to the sixth and seventh floors. On the sixth floor, a collimator reduced the size of the beam to a circle 9.53 mm in diameter. The beam was then passed through a ribbon of ^{197}Au and ^{238}U, spinning on a drum, to serve as an absolute calibration for Moxon-Rae capture detectors [5]. Next, the beam passed through thin foils of ^{235}U, ^{252}Cf, Blank, ^{6}Li, and ^{236}U, and then through a Bi-^{243}Am blank, a ^{6}Li foil, the Cm capture sample, and another ^{6}Li foil. Higher on the seventh floor was located the polarization experiment, where the beam was polarized by transmission through a lanthanum magnesium nitrate crystal, analysed, and finally dumped.

Recording of the signals from the detectors was done in the standard way: The current from each detector was amplified logarithmically, and the voltage signal was displayed on an oscilloscope and recorded photographically on moving film, to be developed some hours later. The raw traces were then digitized over the next several months, which allowed cross-sections to be determined.

Sample preparation and assay was a crucial part of the experiment. The target material used in most of the fission measurements was electromagnetically separated in an isolated calutron facility at Oak Ridge National Laboratory. The ^{248}Cm sample consisted of material from ^{252}Cf decay, and the ^{252}Cf sample was recycled Cf from the High Flux Isotopes Reactor at ORNL. The Cm-capture sample resulted from a high-flux irradiation at the Savannah River Plant, and consisted of material with an extraordinarily high ^{246}Cm and ^{248}Cm content. The isotopic analysis of these samples is shown in Table I. The fission foils were prepared by electrodeposition from an organic solvent; the technique was described by Kappelmann and Baybarz [6]. Target foils of ^{244}Cm and ^{246}Cm, and a back-up foil of ^{248}Cm were prepared at the Savannah River Laboratory, and were assayed there by detection of the 44-keV ^{244}Cm gamma ray. Target

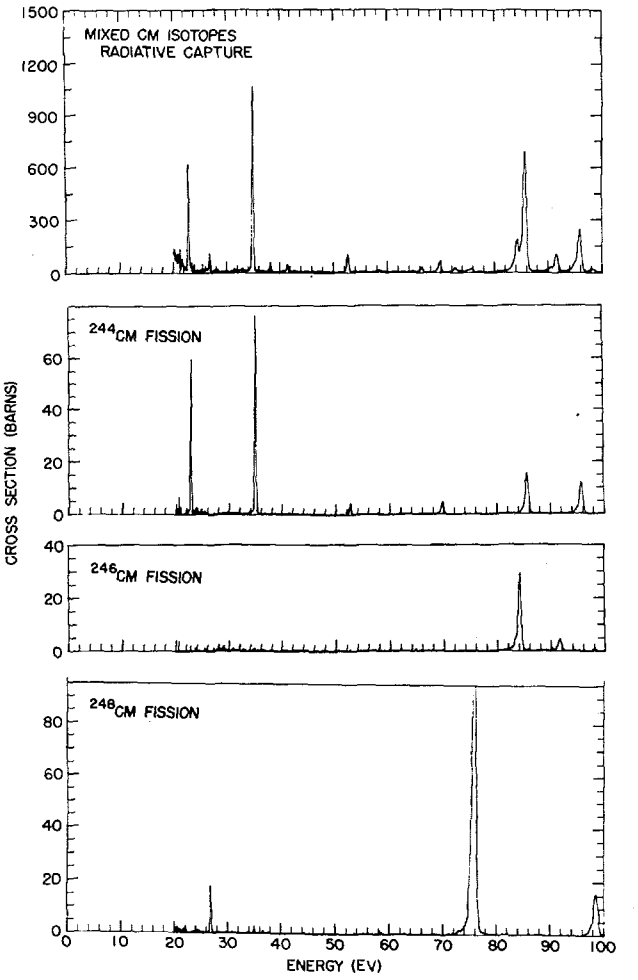

FIG. 1. Radiative-capture cross-section of a sample of mixed Cm isotopes, and fission cross-sections of ^{244}Cm, ^{246}Cm, and ^{248}Cm, between 20 and 100 eV. While the capture sample contained predominantly ^{244}Cm and the cross-section shown corresponds to the ^{344}Cm content, resonances also are seen which are due to ^{246}Cm and ^{248}Cm. Isotopic identification was made possible by the fission data shown.

foils of ^{245}Cm, ^{247}Cm, ^{248}Cm, and ^{252}Cf were prepared at the Oak Ridge National Laboratory. All target foils were assayed at ORNL by low geometry alpha counting. Certain of the foils also had a thin surface coating ($\sim 50 \times 10^{-6}$cm) of Ni, to hold the target material in place. In this experiment, the signal observed is proportional to the product of the number of events and the energy deposited in the detector per event. At the Los Alamos Scientific Laboratory, assay was made of the amount of target material by low geometry alpha counting. The energy deposited per fission was also determined by observing the pulse-height spectrum of fragments of spontaneous fission incident on a typical solid-state detector and in the

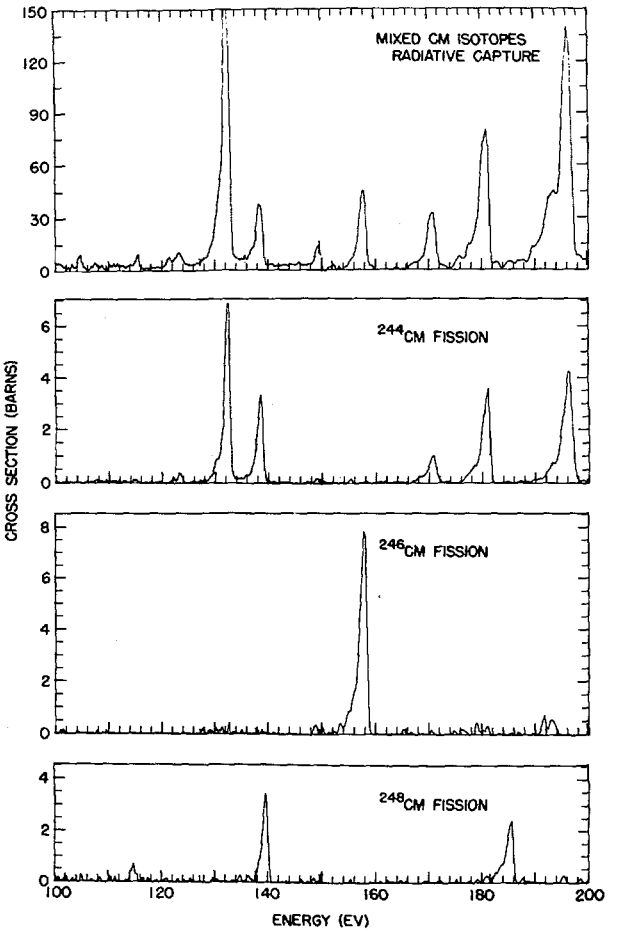

FIG. 2. Radiative-capture cross-section of a sample of mixed Cm isotopes, and fission cross-sections of ^{244}Cm, ^{246}Cm, and ^{248}Cm, between 100 and 200 eV. While the capture sample contained predominantly ^{244}Cm and the cross-section shown corresponds to the ^{244}Cm content, resonances also are seen which are due to ^{246}Cm. Isotopic identification was made possible by the fission data shown.

geometry of those used in the measurement. Slight corrections in the energy deposit were made both for the differences in detector-window thickness and for the expected differences in energy release for spontaneous and neutron-induced fission, as deduced from the systematics discussed by Viola and Seaborg [7].

The Cm-capture sample was prepared at Idaho Nuclear Corporation by mixing curium oxide and aluminum powder and pressing into a wafer. This technique is virtually that previously described by Berreth [8]. To maximize the thickness of the sample, the wafer had a diameter somewhat smaller than that of the sample can, and was held in place by a ring of aluminum. Unfortunately, the sample integrity was not preserved throughout the experiment. The sample was radiographed after the experiment, and

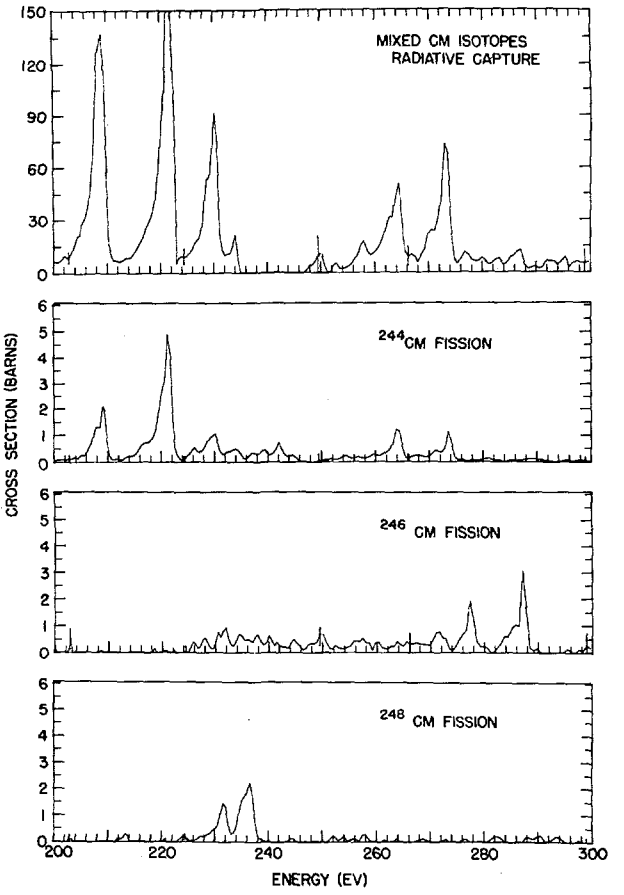

FIG. 3. Radiative-capture cross-section of a sample of mixed Cm isotopes, and fission cross-sections of ^{244}Cm, ^{246}Cm, and ^{248}Cm, between 200 and 300 eV. While the capture sample contained predominantly ^{244}Cm and the cross-section shown corresponds to the ^{244}Cm content, resonances also are seen which are due to ^{246}Cm. Isotopic identification was made possible by the fission data shown.

the radiograph showed that the Cm-wafer had shifted in the sample can, presumably in shipment. This, coupled with a discrepancy in the resonance parameters, was considered to be sufficient evidence to require that the capture data be renormalized to earlier work; that chosen was the total cross-section measurement of Cotė et al [9].

All fission cross-sections have been determined with reference to ^{235}U fission as a standard. The reference cross-section chosen in the energy region presented here is the measurement of de Saussure et al [10]. Backgrounds were determined by measuring the signal from the blank stainless steel backings, or, in the case of the Cm-capture signal, from a canned wafer of bismuth pressed with aluminum and calculated to have the same effective macroscopic scattering cross-section as the Cm-sample while yielding no gamma radiation.

The resolution in a measurement utilizing the nuclear explosion technique does not have a simple energy dependence. In the 1/E-neutron spectrum, the resolution is < 1 ns/m, determined by the amplifier and oscilloscope response. In the thermal neutron range, the resolution becomes much poorer, described by an exponential decay of 4.9 μs, or an effective resolution of ~20 ns/m. The thermal Maxwellian spectrum peaked at about 80 eV in the Physics-8 event, and extended to about 300 eV. In the low-resolution recording of the data, an R-C smoother of time constant 0.6 μs was used to ensure readability of the traces. Since the smoother operates on the output of a logarithmic amplifier, the low resolution recordings should be used only in the range below 300 eV, where the resolution is poorer than the time constant of the smoother. Only the low-resolution recordings from the Physics-8 event have been read completely, and the present paper is generally restricted to resonance-region cross-sections below 300 eV.

TABLE II. PRELIMINARY RESONANCE PARAMETERS FOR EVEN CURIUM TARGETS, FOR NEUTRON ENERGY BETWEEN 20 AND 300 eV.

The neutron widths were normalized to data of Coté between 20 and 100 eV, under the assumption that Γ_γ = 37 mV.

1) ^{244}Cm

E_0 (eV)	$\frac{\pi}{2}\sigma_0\Gamma_\gamma$ (b-eV)	$\frac{\pi}{2}\sigma_0\Gamma_f$ (b-eV)	Γ_n (mV)	Γ_γ (mV)	Γ_f (mV)	Γ_n (Coté) (mV)
22.8	160	13.5	0.98	(37)	2.9	0.97
34.9	354	23.8	3.5	(37)	2.4	4.30
52.7	45	1.9	0.61	(37)	1.5	0.70
69.8	35	2.7	0.65	(37)	2.6	0.48
85.7	621	12.5	20.4	(37)	0.8	20.0
95.9	228	10.5	6.5	(37)	1.6	6.2
132.0	297	9.8	13.2	(37)	1.1	15.1
139.0	49	4.5	1.9	(37)	3.1	
149.0[a]	$\lesssim$9	0.2	$\lesssim$0.3	(37)	$\lesssim$0.8	
171.0	46	1.6	2.1	(37)	1.2	
181.0	163	6.1	9.2	(37)	1.2	8.8
196.0	390	10.0	38.0	(37)	0.9	22.0
209.0	392	5.4	44.0	(37)	0.5	42.7
222.0	469	12.4	83.0	(37)	0.9	39.0
230.0	222	3.7	19.0	(37)	0.6	18.3
265.0	148	2.6	13.1	(37)	0.6	
273.0	181	2.7	18.0	(37)	0.5	43.0

[a] Partly ^{246}Cm.

TABLE II. cont.

2) ^{246}Cm

E_0 (eV)	$\frac{\pi}{2}\sigma_0\Gamma_\gamma$ (b-eV)	$\frac{\pi}{2}\sigma\Gamma_f$ (b-eV)	Γ_n (mV)	Γ_γ (mV)	Γ_f (mV)
84.3	666	22.2	22.3	(37)	1.1
91.6	608	4.1	22.8	(37)	2.4
158.0	246	10.3	13.2	(37)	1.5
277.0		3.6			
287.0		4.2			

3) ^{248}Cm

26.8	2325	4.4	25.8	(37)	0.06
75.8	1260	132.0	68.7	(37)	3.6
98.4	1290	15.1	187.0	(37)	0.4
140.0		4.6			
186.0		3.9			
232.0		2.9			
237.0		6.4			

TABLE III. PRELIMINARY FISSION RESONANCE PARAMETERS OF (^{252}Cf + n)

E_0 (eV)	$\frac{\pi}{2}\sigma_0\Gamma_f$ (b-eV)
24.72	5.4
36.32	138.0
51.41	0.23
68.2	450.0
79.0	20.1
88.0	1.2
138.0	4.5
188.0	3.9
216.0	81.0
243.0	11.5

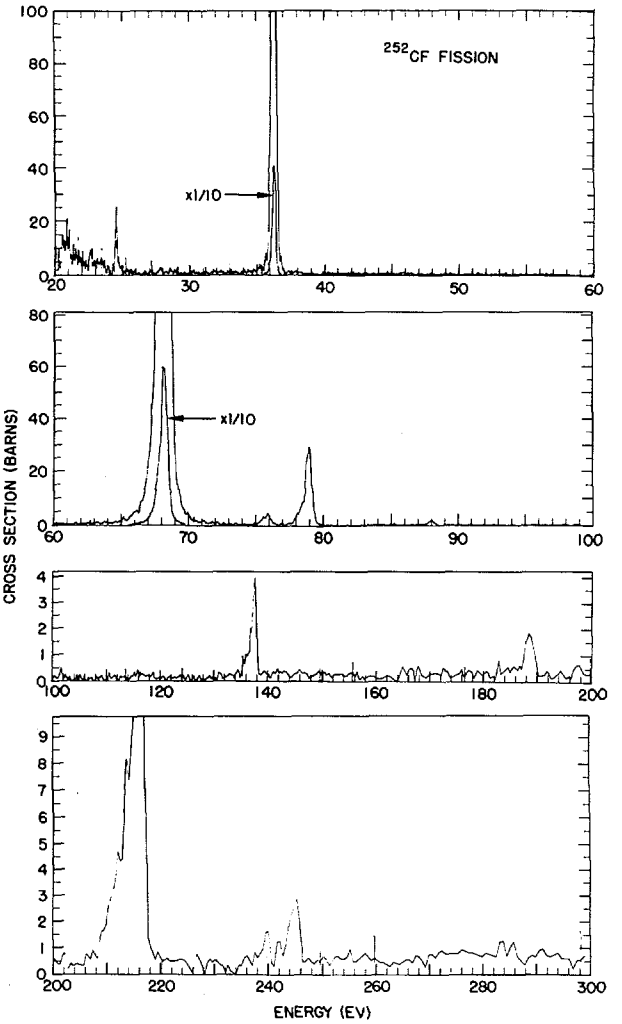

FIG. 4. The fission cross-section of ^{252}Cf, between 20 and 300 eV.

3. DATA AND ANALYSIS

The capture sample consisted primarily of ^{244}Cm and ^{246}Cm, and all the resonances observed could be identified as ^{244}Cm, ^{246}Cm, or ^{248}Cm. Figures 1 to 3 show radiative capture from the mixed sample, and fission in ^{244}Cm, ^{246}Cm, and ^{248}Cm, which permitted isotopic identification of the resonances. These data were analyzed by single-level area analysis; resonance parameters are listed in Table II. For comparison, parameters determined by Coté et al [9] are also listed. (As noted above, the present capture data were normalized through the parameters of Coté between 20 and 100 eV.) The fission data on ^{244}Cm agree well with previous data obtained on the Persimmon event by Fullwood [11].

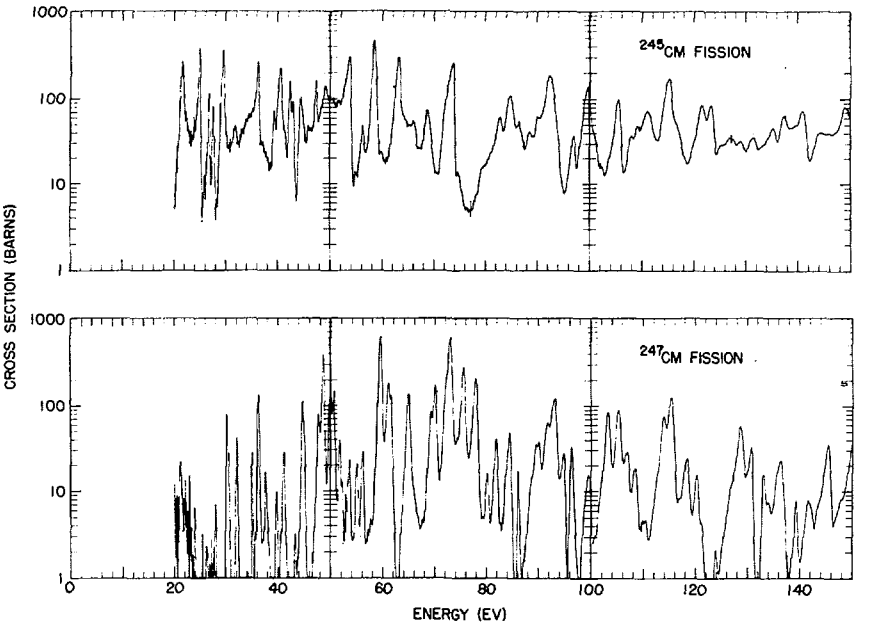

FIG. 5. The fission cross-sections of ^{245}Cm and ^{247}Cm between 20 and 150 eV. Differences in the interference and in the average fission width for the two isotopes are readily apparent.

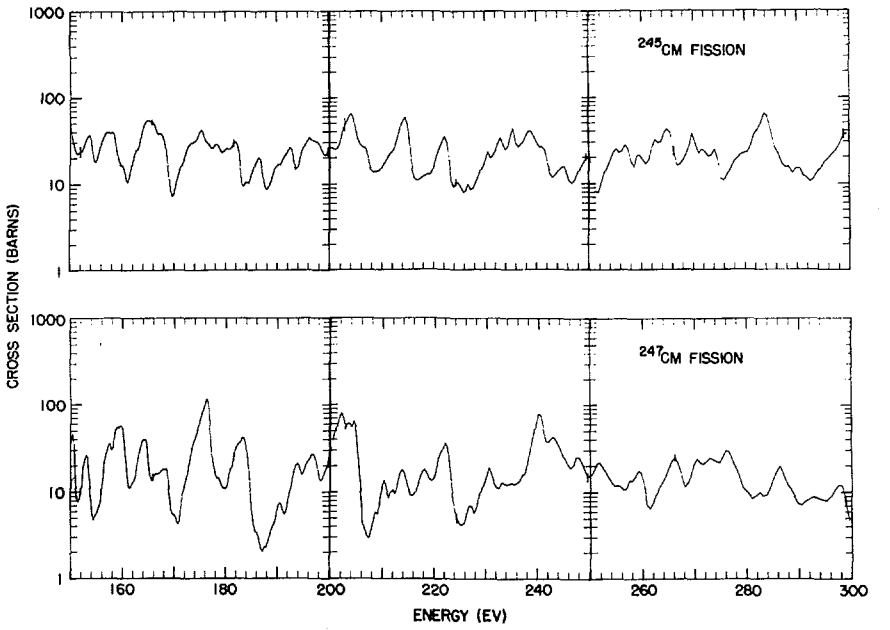

FIG. 6. The fission cross-sections of ^{245}Cm and ^{247}Cm between 150 and 300 eV.

TABLE IV. RESONANCE PARAMETERS FOR RESONANCES IN (^{245}Cm + n) BETWEEN 20 AND 60 eV. PHASE ANGLES REFER TO THE FISSION-WIDTH-VECTOR ORIENTATION IN A TWO-FISSION-CHANNEL, SINGLE-SPIN-STATE ANALYSIS.

E_0 (eV)	$2g\Gamma_n^0$ (mV)	Γ_γ (mV)	Γ_f (mV)	θ (degrees)
21.36	0.457	(40)	485	-16
24.90	0.521	(40)	226	99
25.84	0.007	(40)	549	89
26.83	0.147	(40)	131	160
27.63	0.114	(40)	165	90
29.42	0.638	(40)	328	-171
31.71	0.088	(40)	691	-69[a]
32.99	0.064	(40)	4	-61
34.59	0.039	(40)	61	113
35.31	1.276	(40)	4195	54
36.32	0.256	(40)	189	177
39.45	0.104	(40)	102	-126[a]
40.44	0.705	(40)	585	128
42.45	0.824	(40)	10	56
43.10	0.264	(40)	537	-55
44.57	0.391	(40)	694	-67
45.74	0.087	(40)	901	-9
47.51	0.516	(40)	28	28
49.20	0.718	(40)	1399	58
50.48	0.252	(40)	751	92
51.64	0.087	(40)	207	106
53.63	1.687	(40)	896	-173
54.63	0.045	(40)	1057	174
56.32	0.186	(40)	505	54
58.54	1.811	(40)	393	162
59.99	0.079	(40)	518	-39

[a] Best fits were obtained by placing those resonances marked with an a in a different spin group.

TABLE V. RESONANCE PARAMETERS FOR RESONANCES IN (^{247}Cm + n) BETWEEN 20 AND 60 eV. PHASE ANGLES REFER TO THE FISSION-WIDTH-VECTOR ORIENTATION IN A TWO-FISSION-CHANNEL, SINGLE-SPIN-STATE ANALYSIS.

E_0 (eV)	$2g\Gamma_n^0$ (mV)	Γ_γ (mV)	Γ_f (mV)	θ (degrees)
21.30	0.027	(40)	404	-61
24.03	0.009	(40)	134	-153
25.35	0.002	(40)	26	-103
26.19	0.003	(40)	220	-129
28.04	0.011	(40)	53	35
30.25	0.627	(40)	4	-94
30.62	0.034	(40)	52	-30
32.23	0.089	(40)	26	-92
36.36	0.270	(40)	61	-38
37.74	0.004	(40)	555	-153
37.76	0.217	(40)	13	-178
39.52	0.001	(40)	705	-163
39.95	0.015	(40)	167	19
40.61	0.005	(40)	48	-134
41.25	0.103	(40)	20	105
41.76	0.008	(40)	546	-11
43.39	0.029	(40)	4	117
44.87	0.313	(40)	32	11
45.21	0.086	(40)	60	-119
47.92	0.169	(40)	164	-75
48.85	0.973	(40)	82	25
50.08	0.334	(40)	55	-127
50.69	0.447	(40)	52	22
51.78	0.231	(40)	14	-154
52.19	0.175	(40)	4	-48
53.63	0.062	(40)	324	121
55.10	0.072	(40)	38	88
56.18	0.088	(40)	69	63
59.66	2.037	(40)	114	-68

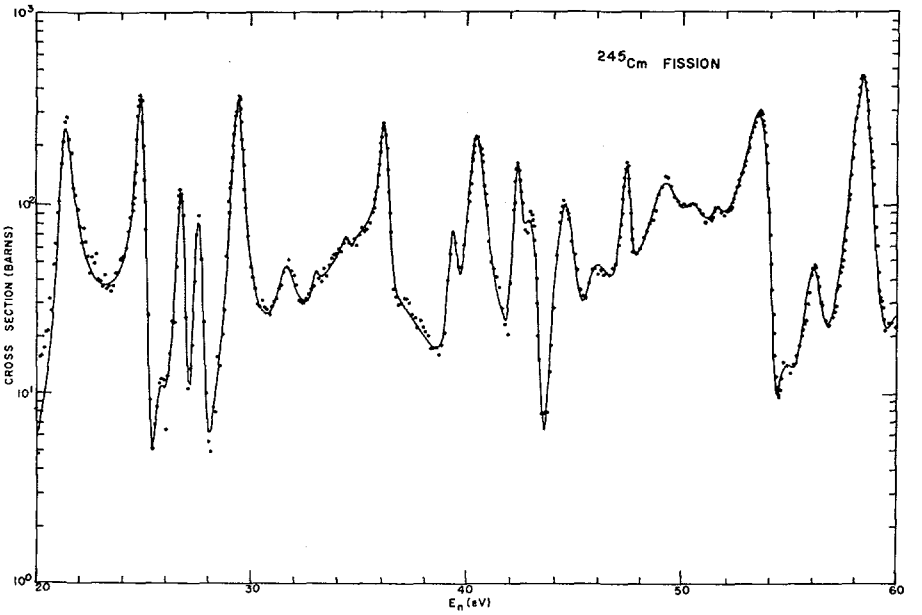

FIG. 7. Typical fit obtained by least-squares multilevel analysis of the fission cross-section of ^{245}Cm. The analysis was carried out between 20 and 70 eV.

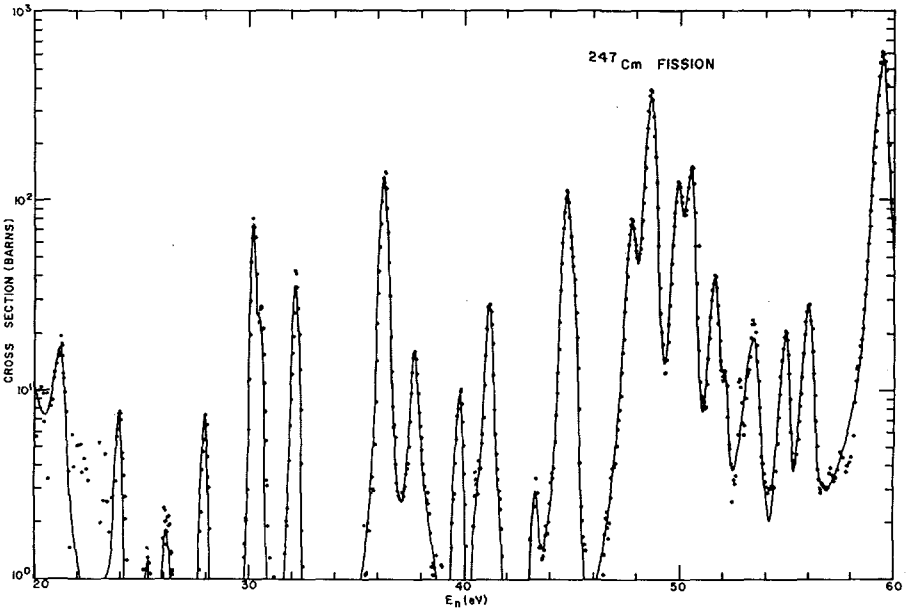

FIG. 8. Typical fit obtained by least-squares single-level analysis of the fission cross-section of ^{247}Cm. The analysis was carried out between 20 and 85 eV. While for the most part, a single-level treatment appears adequate, in some regions the need for a multi-level treatment is apparent.

Fission data on ^{252}Cf are shown in Fig. 4, and the single-level fission parameters are listed in Table III. This sample had a moderately high natural background rate, ~10^6 fragments/s, which appeared in the experiment as a fluctuating baseline, but gave no other problem.

These low-resolution readings can also be used to derive some preliminary values for the positions of the fission thresholds in the even-even targets. All the Cm-targets show smooth thresholds, at approximately 530 keV, 680 keV, and 660 keV for ^{244}Cm, ^{246}Cm, and ^{248}Cm respectively. Preliminary data on ^{252}Cf show a much gentler smooth rise below 1 MeV, but do not seem to show the characteristic plateau. All these results are very preliminary, based on one or two low-resolution records, and may be changed by the higher-resolution readings when they become available.

Fission cross-sections of ^{245}Cm and ^{247}Cm are shown in Figs 5 and 6. There is a qualitative difference in the appearance of the cross-sections: ^{245}Cm fission shows marked interference effects among rather wide resonances, while the structure in ^{247}Cm is narrower and shows few asymmetries in shape. This observation was confirmed in the analysis. The cross-section of ^{245}Cm required a full-scale multilevel treatment. This was carried out between 20 and 70 eV, with the least-squares search routine developed by Auchampaugh [12]. Fission in ^{247}Cm, on the other hand, could be surprisingly well described by a single-level treatment, which was carried out between 20 and 85 eV. Preliminary resonance parameters for ^{245}Cm are listed in Table IV, those for ^{247}Cm in Table V. Typical fitted data for these two isotopes are shown in Figs 7 and 8, respectively.

4. DISCUSSION

The even isotopes, ^{244}Cm, ^{246}Cm, and ^{248}Cm, show sub-threshold fission in every resonance seen in capture. The fission widths are moderately large and reasonably constant, at least below 300 eV. Qualitative examination of the fission data between 300 eV and threshold shows no apparent evidence of the type of intermediate structure observed in sub-threshold fission of even uranium and plutonium isotopes. It, thus, appears that the calculations of Strutinsky [13] and Nilsson [14], showing that this structure should disappear for Cm and Cf sub-threshold fission, have been experimentally verified.

The analysis of ^{245}Cm was carried out under the assumption that resonances could interfere in two channels in a single spin state. This, of course, is not correct in principle, but it is the simplest procedure in practice, because it allows the search routine to have maximum freedom.

The target ^{245}Cm appears to show strong interference in fission, and the sizes and variations of the fission widths are rather large. For ^{247}Cm, both the small variation in the fission widths and the adequacy of the single-level treatment show that here fission is a few- to many-channel process. The target ^{245}Cm, with a ground-state spin of $7/2^+$, resembles $5/2^+$ ^{233}U and ^{241}Pu. As might be expected, $9/2^-$ ^{247}Cm more nearly follows $7/2^-$ ^{235}U.

The present measurement has also yielded information which may be useful in the production of ^{252}Cf. If it is true that the resonance parameters determined here are representative of those in a resonance reactor, then these data can be used to predict the conversion efficiency of such a reactor. If the average assumed Γ_γ of 0.040 eV is correct, the ratio of the average

resonance capture to absorption integrals between 20 and 80 eV is 0.17 for ^{245}Cm and 0.33 for ^{247}Cm. The 2200 m/s values are 0.15 and 0.36, respectively [3]. Thus a resonance reactor, at least if the 20- to 80-eV region is representative, would not appear to enhance production of ^{252}Cf significantly above that which can be realized with a thermal reactor. These numbers also agree reasonably well with the measured resonance integral ratios of 0.12 and 0.39 for ^{245}Cm and ^{247}Cm, respectively [3].

ACKNOWLEDGEMENTS

The authors would like to take this opportunity to thank C. E. Bemis, Jr., of the Oak Ridge National Laboratory, who assayed the curium and californium fission foils by low-geometry alpha counting. The efforts of G. F. Auchampaugh of Los Alamos Scientific Laboratory, who provided the multilevel least-squares fitting code used in the analysis, are also gratefully acknowledged. Finally, it was through the interest and encouragement of B. C. Rusche of the Savannah River Laboratory that arrangement was made for the loan and fabrication of samples, making the entire measurement possible.

REFERENCES

[1] "Californium-252, Its Use and Market Potential", published by the Savannah River Operations Office, U.S. Atomic Energy Commission (may 1969).
[2] "Californium-252 Progress", Number 1, October 1969, published by the Savannah River Operations Office, U.S. Atomic Energy Commission.
[3] HENNELLY, E.J., private communication through B.C. Rusche (1970). Fission and capture cross-sections and resonance integrals quoted represent the results of an evaluation by Dr. Hennelly.
[4] DIVEN, B.C., in "Nuclear Structure Study with Neutrons" (NEVE DE MÉVERGNIES, M., VAN ASSCHE, P., VERVIER, J., Eds., North-Holland, Amsterdam (1966) 441.
[5] ELLIS, A.N., BROWN, W.K., FARRELL, J.A., FULLWOOD, R.R., IEEE Trans. NS-17 (to be presented at the 1970 Nuclear Science Symposium, New York).
[6] KAPPELMANN, F.A., BAYBARZ, R.D., Trans. Am. Nucl. Soc. 12 (1969) 515.
[7] VIOLA, V.E., Jr., SEABORG, G.T., J. inorg. nucl. Chem. 28 (1966) 697.
[8] BERRETH, J.R., Nucl. Applications 1 (1965) 230.
[9] COTÉ, R.E., BARNES, R.F., DIAMOND, H., Phys. Rev. 134 (1964) B1281.
[10] DE SAUSSURE, G., WESTON, L.W., GWIN, R., INGLE, R.W., TODD, J.H., HOCKENBURY, R.W., FULLWOOD, R.R., LOTTIN, A., in "Nuclear Data for Reactors," (Proc. Conf. Paris, 1966) 2 IAEA, Vienna (1967) 233.
[11] FULLWOOD, R.R., MCNALLY, J.H., SHUNK, E.R., in "Neutron Cross Sections and Technology" (GOLDMAN, D.T., Ed.), NBS Spec. Publ. 299 1 (1968) 567.
[12] AUCHAMPAUGH, G.F., paper submitted to this conference, but not published in these Proceedings.
[13] STRUTINSKY, V.M., PAULI, H.C., in "Physics and Chemistry of Fission", (Proc. Symp. Vienna, 1969) IAEA, Vienna (1969) 155.
[14] NILSSON, S.G. et al., Nucl. Phys. A131 (1969) 1; TSANG, C.F., NILSSON, S.G., Nucl. Phys. A140 (1979) 275.

A SIMULTANEOUS MEASUREMENT OF THE FISSION, CAPTURE, SCATTERING AND TOTAL CROSS-SECTIONS OF ^{239}Pu*

J. A. FARRELL, G.F. AUCHAMPAUGH, M.S. MOORE, P.A. SEEGER
University of California,
Los Alamos Scientific Laboratory,
Los Alamos, N.Mex.,
United States of America

Abstract

A SIMULTANEOUS MEASUREMENT OF THE FISSION, CAPTURE, SCATTERING, AND TOTAL CROSS-SECTIONS OF ^{239}Pu.

The fission, capture, scattering, and total cross-sections of ^{239}Pu have been measured from 14 eV to 1 MeV using an underground nuclear explosion as a pulsed neutron source. The flight path was 245 meters and the resolution was approximately 15 ns/metre in the resonance region. The cross-sections were measured simultaneously so that the source function is the same for each cross-section. All measurements were made with solid-state detectors. The current induced in the detectors by the detected particles was amplified with logarithmic amplifiers, displayed on oscilloscopes and photographed with moving film cameras.

The capture and scattering cross-sections were measured from a ^{239}Pu sample which was 8.8×10^{-4} atoms/barn thick. The neutron flux was measured on each side of the sample by ^{6}LiF foils and solid-state detectors to determine the transmission through the sample and therefore the total cross-section and the self-absorption correction to the capture and scattering signals.

The capture cross-section was measured with solid-state detectors equipped with Moxon-Rae converters. The fission gamma-ray sensitivity was determined from the broad 0^+ resonances which have very little capture. The ratio of capture to fission, alpha, has been computed. The result from 1 to 30 keV is in good agreement with the measurements of other laboratories.

The scattered-neutron detector was a stack of 10 thin solid-state detectors surrounded by 21 atmospheres of ^{3}He. The fission-neutron and gamma-ray background was measured by a similar detector filled with CH_4. The pressure of CH_4 was adjusted to match the responses of the two detectors to fission neutrons. The two signals were subtracted electronically in order to reduce recording errors. An additional transmission measurement was made on a thicker (6.1×10^{-3} atoms/barn) sample to provide a more accurate total cross-section in the valleys between resonances.

1. INTRODUCTION

The technique of measuring neutron cross sections using an underground nuclear explosion as a pulsed neutron source has been well developed [1,2]. The high intensity and low background of this source have made it possible to measure cross sections of highly radioactive samples, samples with very low fission cross sections, and samples for which only a few tens of micrograms of material is available; all of which would be difficult or impossible to measure with conventional sources. For example, the fission cross section of ^{237}U which has a half life of 6.9 days was recently measured with this technique [3].

Most of the measurements using the nuclear explosion source have been neutron induced fission cross sections because such measurements are relatively easy although measurements of the other partial cross sections of

* Work performed under the auspices of the US Atomic Energy Commission.

fissile isotopes are of equal or greater interest. In order to develop methods for measuring capture and scattering as well as total cross sections it was decided to attempt a "complete" cross section experiment on a fissile nucleus. Plutonium-239 was chosen as the subject of this experiment primarily because its low energy resonances are relatively well understood.

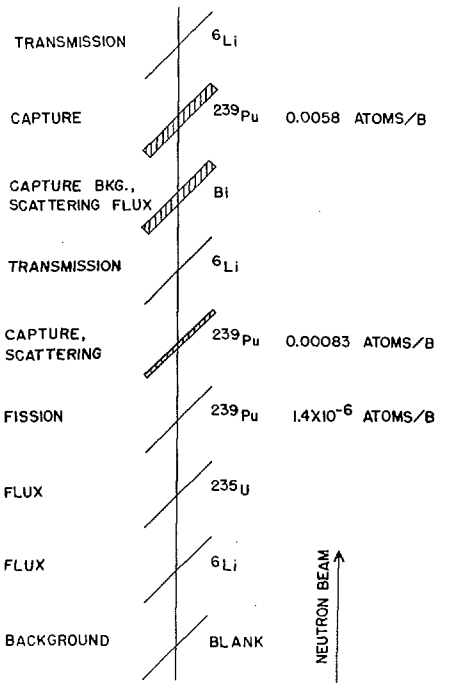

FIG. 1. Schematic diagram of the experiment. The neutron beam traversed the stack of foils from bottom to top. Two solid-state detectors were used with each foil except for the 0.00083 atoms/b ^{239}Pu sample which had two capture, one scattering, and one scattering background detector and the Bi which had one capture and one scattering detector.

2. EXPERIMENTAL METHOD

The general arrangement of the experiment is shown in Fig. 1. The neutron beam was brought to the surface of the ground in an evacuated pipe and collimated to a circle of 1.74 cm diameter before passing through the stack of samples. All of the samples except for the Bi and the two thick ^{239}Pu foils were evaporated on stainless steel backings 2.5 x 10^{-3}mm thick. Each of these foils was viewed by two Si solid state detectors at 55° and 90° to the beam. The neutron flux was determined from the ^{6}Li and ^{235}U foils. There was a 10-15% discrepancy at the higher energies between the two flux monitors which is probably due to errors in the cross sections used for ^{6}Li and ^{235}U. It was decided to use the ^{235}U evaluation of Davey [4] as the reference cross section. Background for the flux monitors and the fission cross section measurement was measured with the blank foil.

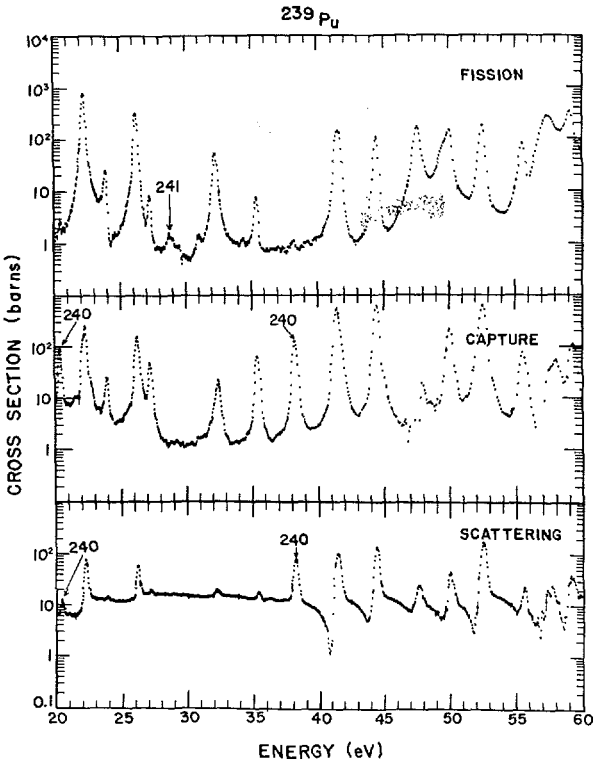

FIG.2. The fission, capture, and scattering cross-sections of ^{239}Pu from 20 to 60 eV. Resonances in ^{240}Pu and ^{241}Pu are identified. The apparent drop in the scattering cross-section below 22 eV is spurious and due to a rapidly decreasing neutron flux.

There were three ^{239}Pu samples, a thin foil, 1.4 x 10^{-6}atoms/barn, for the fission cross section measurement and two thicker foils, 0.00083 atoms/barn and 0.0058 atoms/barn, for the capture, scattering, and transmission measurements. The Pu samples used were 94.41% ^{239}Pu, 5.27% ^{240}Pu, and 0.30% ^{241}Pu. A bismuth sample provided a measurement of the scattered neutron background in the capture detectors and also provided the reference cross section for the scattering measurement. Transmission through the Pu samples was measured by ^{6}Li foils located above each sample.

Both sample thicknesses were used for the capture cross section measurements. Each was viewed by two solid state Moxon-Rae [5,6,7] type detectors. The efficiency of these detectors was determined by a separate experiment on the same event in which a ribbon of gold was mounted on the inside of a spinning drum and viewed by two of the capture gamma ray detectors [8]. The neutron beam was collimated to 9.5 mm diameter and passed through the drum. The drum speed was sufficient to resolve the individual low energy gold resonances which appear as spots of activation on the gold strip. The activated areas were located with an autoradiograph and were then cut out and beta counted. A comparison of the absolute activation in each of the gold resonances with the integrated signal in the detectors provided a

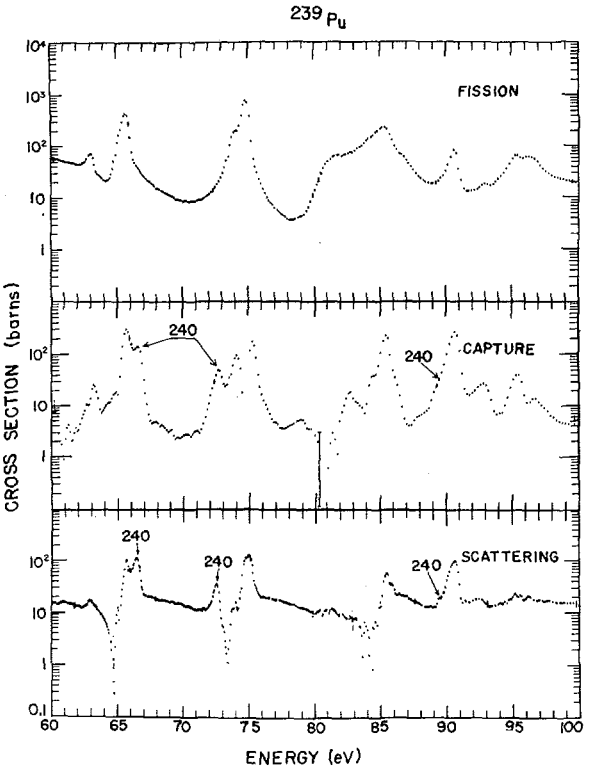

FIG.3. The fission, capture, and scattering cross-sections of ^{239}Pu from 60 to 100 eV.

determination of the detector efficiency that is independent of any knowledge of the neutron flux or gold cross section but dependent on the assumption that the efficiency is independent of the gamma ray spectrum. The estimated error in the efficiency measurement is 5%.

The scattered neutron detector was a stack of 10 thin Si solid state detectors surrounded by 21 atm of ^3He. The primary sources of background in the detector are fission neutrons and gamma rays from fission and capture. This background was determined by a similar detector filled with CH_4. The pressure of CH_4 was adjusted to match the response of the background detector to the ^3He detector for fission neutrons. In order to reduce the effect of recording errors, the scattering background signal was subtracted electronically from the ^3He signal before recording.

The currents from the solid state detectors were amplified with logarithmic amplifiers, displayed on oscilloscopes and photographed with two types of moving film cameras. The first type had a film speed of 30 m/sec and had an effective time resolution of about 1 μsec. An R-C smoother with a time constant of 0.6 μsec was used on these recordings to improve the readibility of the traces. Since the smoother was on the output of the logarithmic amplifiers, a small error is introduced above 300 eV where the burst width is less than the time constant of the smoother. The second

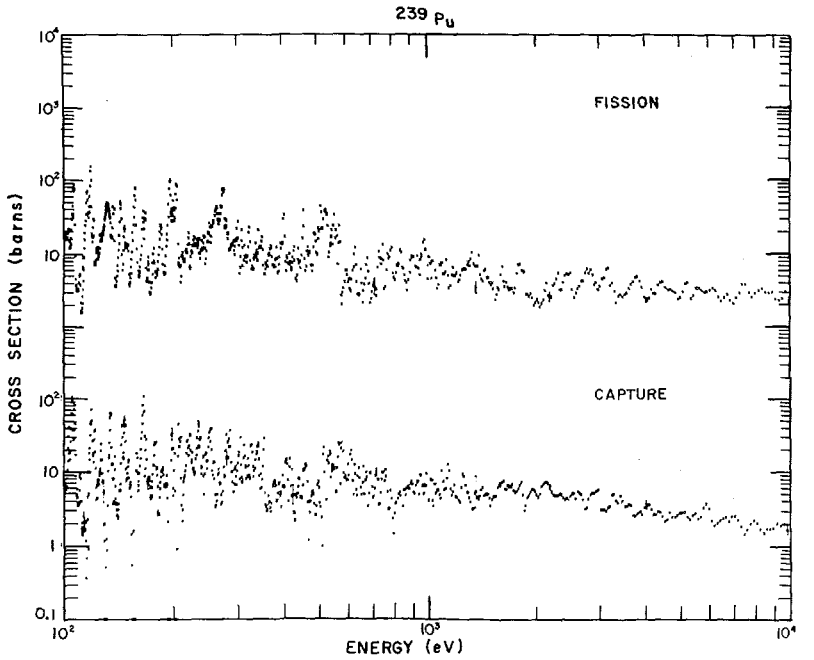

FIG.4. The fission and capture cross-sections of ^{239}Pu from 100 eV to 10 keV.

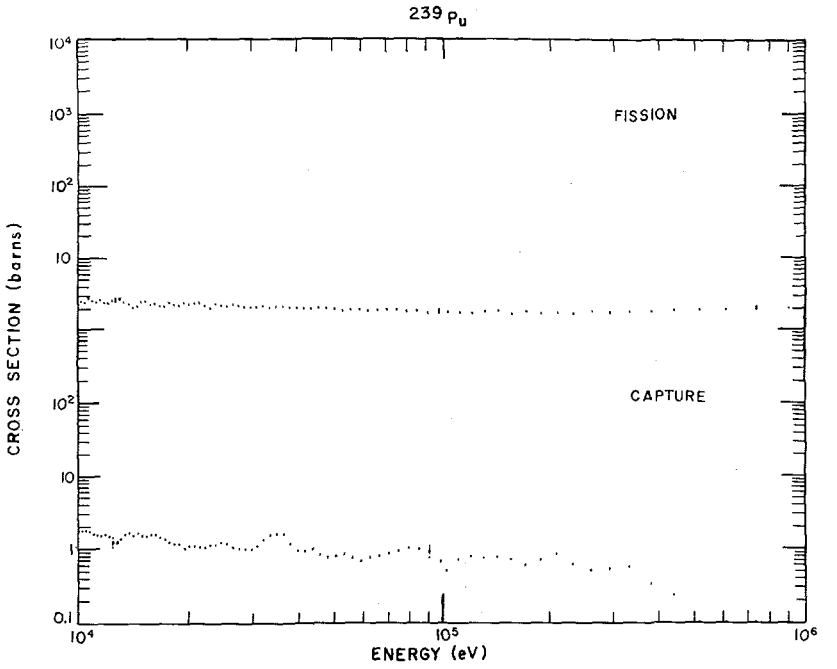

FIG.5. The fission and capture cross-sections of ^{239}Pu from 10 keV to 1 MeV. The structure in the capture cross-section at 30 keV and above is due to background from the aluminium sample can.

type of camera used a strip of film on the inside of a rotating drum. The film speed was 250 m/sec and the time resolution was approximately 0.2 μsec. After the event, the films were digitized using a projection microscope and reduced to cross sections. Only the low resolution recordings have been completely processed at this time.

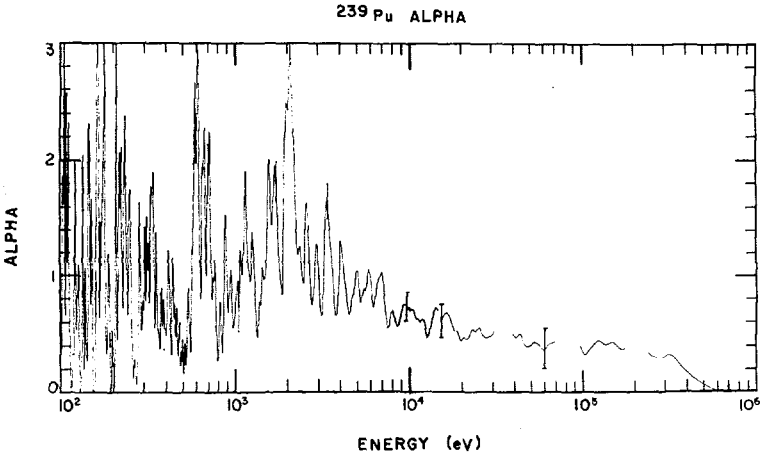

FIG.6. The ratio of capture to fission, alpha, for ^{239}Pu from 100 eV to 1 MeV. The data below 10 keV have been averaged over 5 μs intervals.

3. DATA REDUCTION AND RESULTS

The neutron flux for this experiment consisted of two parts, a thermal Maxwellian spectrum peaking at 80 eV and extending to 300 eV, and a 1/E spectrum at higher energies. The resolution in the thermal region was about 20 nsec/m which is somewhat poorer than in previous experiments of this type. Above 300 eV the resolution improved to better than 1 nsec/m but was limited to about 4 nsec/m by the recording system in the data presented here. Analysis of the high resolution recordings is underway and will give improved results above 300 eV.

The partial cross sections obtained are shown in Figs. 2, 3, 4, and 5. The fission cross section does not exhibit the low valley at 30 eV that was observed in the Petrel data [9,10]. This is due mostly to the presence of 0.3% of ^{241}Pu which has a resonance at this energy.

The signal recorded from the Moxon-Rae detectors consists of both capture and fission gamma rays. Since individual events cannot be recorded in this type of experiment, it was not possible to do coincidence or pulse height analysis to discriminate between capture and fission gammas. Thus, to obtain the capture cross section, it is necessary to subtract the fission contribution from the raw capture plus fission signal. The capture plus fission data were corrected for self absorption using the signals recorded from the Li foils positioned on each side of the capture samples. The fission gamma efficiency was determined from eight broad 0^+ resonances to be 1.27 ± 0.08 times the capture efficiency, thus the errors in the subtraction may be quite large at high energy where the capture cross section is small.

Above 30 keV there was an additional background due to the aluminum sample can which caused the capture signal to be too high in this region. The cross section shown in the figures is derived from the thin sample data when greater than 100 b, the thick sample below 30 b and is an average of the two in between. No multiple scattering correction has been made. The correction is estimated to be 5-10% on the highest peaks.

The scattering cross section was normalized to the known scattering cross section of Bi of 9 barns. The average error on the peaks is about 15% but the deep interference minima may be in error by a factor of two or more because of error in background subtraction.

The ratio of capture to fission, alpha, has been computed from the capture and fission cross sections and is shown in Fig. 6. Averaged values of α are given in Table I. The agreement with other measurements is quite good below 30 keV but above 30 keV our data appear to be too high. This is probably due to gamma rays from the aluminum can and the large errors in the subtraction of the fission background which represents 85% of the signal at 30 keV.

TABLE I. AVERAGED VALUES OF ALPHA FOR ^{239}Pu

Neutron energy (keV)	$\langle \alpha \rangle$	Percent error
0.1 - 0.2	0.67	0.14
0.2 - 0.3	0.67	0.14
0.3 - 0.4	0.94	0.12
0.4 - 0.5	0.57	0.18
0.5 - 0.6	0.64	0.18
0.6 - 0.7	1.68	0.11
0.7 - 0.8	0.85	0.13
0.8 - 0.9	0.79	0.14
0.9 - 1	0.70	0.15
1 - 2	1.17	0.10
2 - 3	1.31	0.10
3 - 4	0.95	0.12
4 - 5	0.90	0.12
5 - 6	0.93	0.12
6 - 7	0.86	0.13
7 - 8	0.68	0.16
8 - 9	0.58	0.17
9 -10	0.74	0.15
10 - 20	0.60	0.16
20 - 30	0.48	0.19

The total cross section obtained from the transmission has large errors except on the peaks of the resonances. The errors are due mostly to uncertainties in the geometry, ^{6}Li foil thicknesses, and detector characteristics. For this reason the data have been used only for making the self absorption correction in the capture and scattering data.

4. CONCLUSIONS

Capture and scattering cross sections of fissile nuclei can be measured with the nuclear explosion technique. The predominant errors in the capture cross section and consequently in alpha are due to the subtraction of the large fission background. In the present experiment, the energy dependence of alpha for ^{239}Pu is well determined below 10 keV. From 10 to 30 keV the error in alpha is about 30%, which is not as good as can be achieved in an accelerator measurement. Thus, this technique is best suited for highly radioactive materials which would be impossible to measure with an accelerator.

REFERENCES

[1] DIVEN, B. C., in "Nuclear Structure Study with Neutrons," (NEVE DE MÉVERGNIES, M., VAN ASSCHE, P., VERVIER, J., Eds.), North-Holland, Amsterdam (1966), 441.

[2] SEEGER, P. A., HEMMENDINGER, A., DIVEN, B. C., Nucl. Phys. A96 (1967) 605.

[3] McNALLY, J. H., WOLFSBERG, K., DROPESKY, B. J., BARNES, J. W., Bull. Am. Phys. Soc. 13 (1968) 1665.

[4] DAVEY, W. G., Nucl. Sci. Engng. 32 (1968) 35.

[5] MOXON, M. C., RAE, E. R., Nucl. Instr. Meth. 24 (1963) 445.

[6] MACKLIN, R. L., GIBBONS, J. H., INADA, T., Nucl. Phys. 43 (1963) 353.

[7] HEMMENDINGER, A., SILBERT, M. G., MOAT, A., IEEE Trans. NS-12, (1965) 304.

[8] ELLIS, A. N., BROWN, W. K., FARRELL, J. A., FULLWOOD, R. R., IEEE Trans. NS-17 (to be presented at the 1970 Nuclear Science Symposium, New York).

[9] SHUNK, E. R., BROWN, W. K., LaBAUVE, R., in "Proceedings of the Conference on Neutron Cross Section Technology," Washington, D. C. (1966) 979.

[10] FARRELL, J. A., Phys. Rev. 165 (1968) 1371.

DISCUSSION

TO PAPERS IAEA-CN-26/45, 46

J. P. THEOBALD: In one of the latest WASH reports you show sub-threshold fission-cross-section spectra of a curium isotope, where the fission fragments were recorded at different angles relative to the neutron beam. These spectra are significantly different from each other. Can you explain this fact?

M. S. MOORE: No, I cannot. The angular distribution observed is much too large to be physically meaningful and can only be explained by some unknown systematic error.

C. M. NEWSTEAD: Were you able to obtain transmission results from this measurement by taking the ratio of the outputs from the lithium detectors placed behind and in front of the ^{239}Pu samples? This would also provide an interesting check on the functioning of the lithium detectors.

J. A. FARRELL: We did indeed compute the transmission and the total cross-section. As you know, with an accelerator total cross-sections are done by sample-in and sample-out. We cannot do that. We have to measure the flux on either side of the sample. The results obtained are in reasonable agreement on the peaks of the resonances but the data are very inaccurate where the transmission is high.

M. S. MOORE: What Mr. Farrell is saying is that the data are not of very good technical quality.

C. W. NEWSTEAD: But do they agree on peaks?

M. S. MOORE: Yes, they do.

DETERMINATION OF RESONANCE PARAMETERS OF ^{240}Pu USING A CRYSTAL SPECTROMETER

D.V.S. RAMAKRISHNA, M.P. NAVALKAR
Nuclear Physics Division,
Bhabha Atomic Research Centre, Trombay, Bombay,
India

Abstract

DETERMINATION OF RESONANCE PARAMETERS OF ^{240}Pu USING A CRYSTAL SPECTROMETER.

In view of their considerable importance in reactor design, measurements of resonance parameters of ^{240}Pu have been undertaken by using a high-resolution crystal spectrometer.

Three different samples of plutonium in the form of Pu-Al alloy foils have been used to study the important 1-eV resonance energy level of ^{240}Pu. The experimental data have been analysed by the method of area analysis and also by shape analysis incorporating Doppler broadening and the resolution function of the crystal spectrometer. The parameters E_0 = 1.059 eV, σ_0 = 173 000 barn, Γ_n = 2.18 meV and Γ = 31.0 meV show a best fit to the experimental transmission curve. The results are compared with the other data published.

1. INTRODUCTION

The study of the total neutron cross-section of ^{240}Pu is important because it plays a significant role in reactor design. ^{240}Pu possesses a high resonance capture cross-section which affects the neutron economy of a reactor, and, in particular, the size and position of the resonance at 1 eV are such that most of the absorptions occur in this resonance. The measurement of the resonance parameters of this energy level is, therefore, justified by its considerable importance in reactor-physics calculations.

2. EXPERIMENTAL DETAILS

Transmission measurements were made with standard techniques whereby a monoenergetic beam of neutrons from a crystal spectrometer was used in conjunction with the heavy-water-moderated reactor CIRUS. The spectrometer gives a resolution of about 5% at 1.059 eV with the Be $(10\bar{1}1)$ plane. The resolution width has been determined by the relation given by Sailor et al. [1] from the knowledge of the angular divergence of the collimating beam and the half-width of the crystal rocking curve. The same fact has been verified by measuring the transmission through a thin foil of indium at 1.46 eV resonance and estimating the width. The higher-order contamination for this plane is of the order of one per cent.

Three samples of plutonium are used in the form of Pu - Al alloy foils with 13.58% plutonium. The isotopic concentrations of ^{239}Pu, ^{240}Pu and ^{241}Pu are 89.82%, 9.24% and 0.94%, respectively. The foils have the dimensions of 3.8 cm × 3.8 cm with mean thicknesses of 5.19×10^{19}, 1.035×10^{20} and 1.548×10^{20} Pu-atoms/cm^2. Typical transmission curves obtained with the samples are shown in Fig. 1.

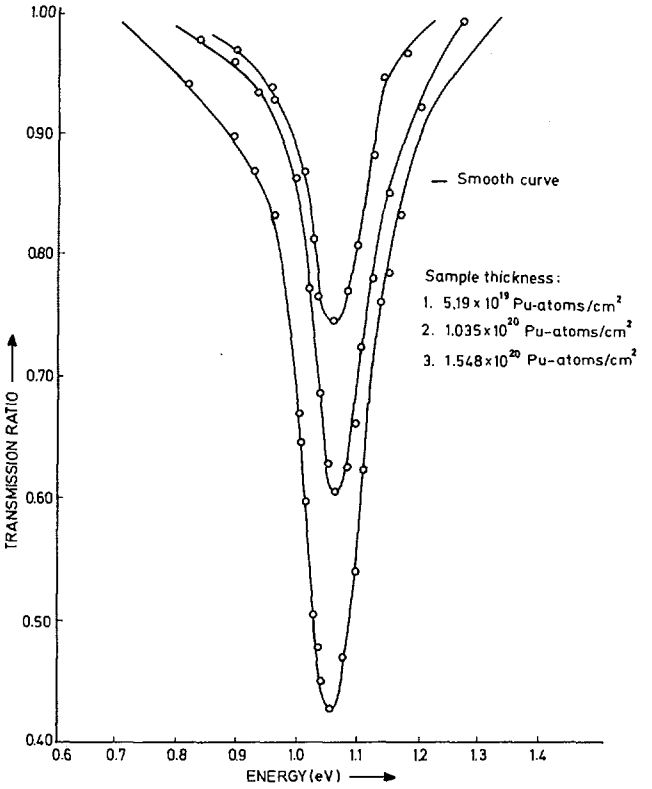

FIG. 1. Transmission curve for the 1-eV resonance of ^{240}Pu.

3. ANALYSIS AND RESULTS

The experimental data have been analysed by area and by shape analysis. The effect of the sample thickness which results in multiple scattering has been studied by doing a Monte-Carlo calculation and is seen to be negligible.

The uncertainty in the accurate determination of the area in the wings is avoided by treating the partial area of the transmission curve for the analysis as given by Marion and Bollinger [2]. The wings of the experimental curve are cut off symmetrically about the resonance energy at the points where the transmission is unaffected by Doppler broadening, and the area is measured. The same energy limits were set in obtaining the theoretical curves of the partial area as a function of $n\sigma_0$ for different values of Γ. Using these set of curves and the experimental areas, the analysis has been carried out as in the case of full area measurement.

The formalism of Atta and Harvey [3] has been used to determine the parameters by shape analysis. Taking into account all the three isotopes present in the sample, the total cross-sections are computed

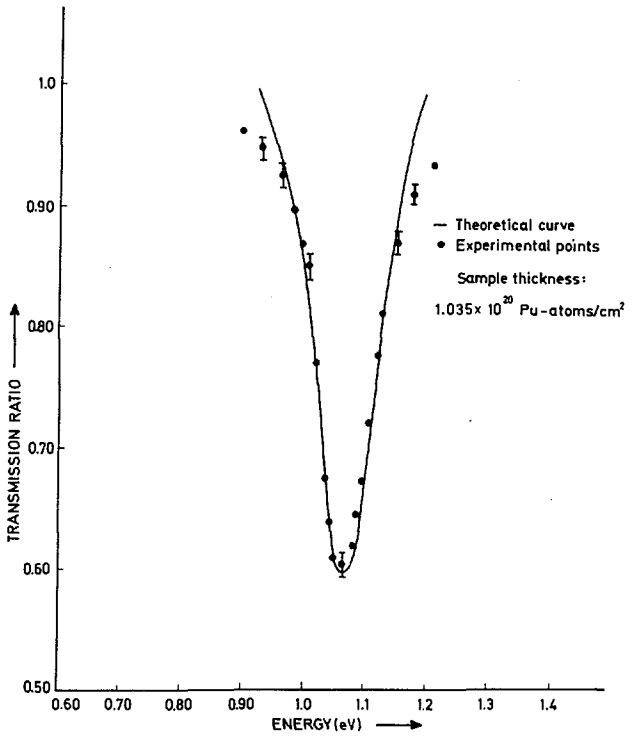

FIG. 2. Theoretical curve obtained with the resonance parameters to give the best fit of the experimental data.

TABLE I. COMPARISON OF RESONANCE PARAMETERS OF ^{240}Pu

Author	E_0 (eV)	Γ (meV)	Γ_n (meV)	σ_0 (barn)
Abov (1955)	1.075 ± 0.005	42 ± 5	3.1 ± 0.4	178 000 ± 16 000
Egelstaff (1958)	1.057 ± 0.002	40 ± 3	2.06 ± 0.10	-
Cote' (1959)	1.053	34.5 ± 3	2.4 ± 0.05	173 000 ± 15 000
Pattenden (1959)	1.0575 ± 0.001	30.6 ± 4.0	2.30 ± 0.2*	189 000 ± 20 000
Present measurement				
Area analysis	1.059 ± 0.007	30.8 ± 2.0	2.15 ± 0.10	172 000 ± 12 000
Shape analysis		31.0 ± 3.0	2.18 ± 0.10	173 000 ± 14 000

* Reduced width.

from the sum of the cross-sections of individual isotopes weighted over their fractional abundances. Incorporating the Doppler broadening and the resolution function of the spectrometer, theoretical transmissions have been computed by the process of convolution. A comparison has been made of the theoretical plot obtained with a set of parameters, with the experimental transmission curve and the process repeated until a best fit is obtained. The solid line in Fig. 2 represents the theoretical curve obtained with the adjusted parameters (listed in Table I) which are the best fit for the experimental observations.

As seen from the Fig. 2, fitting is good except at the wings where our computations for the theoretical transmissions are subject to large uncertainties. The sensitivity of the area-analysis method is improved by treating the partial area instead of the full area of the transmission curve. Furthermore, the parameters σ_0 and Γ could be determined separately (and not as a product) with better accuracy since Doppler and resolution effects are minimized. The parameters obtained by this method compare well with the values determined by shape analysis.

The 1-eV resonance level of ^{240}Pu has been studied by different authors and their values of the resonance parameters are listed in Table I along with our experimental results. The parameters obtained by the present measurement show, in general, agreement with the other values reported. The total width (Γ), though disagreeing with the values obtained by Abov [4] and by Egelstaff et al. [5], agrees well with those of Cote'[6] and of Pattenden [7]. The neutron width (Γ_n) obtained by our measurement has comparatively lower value than the value obtained by Cote' et al. However, it agrees well with the Egelstaff's value. Pattenden used the Be ($10\bar{1}1$) plane in his measurement with a crystal spectrometer, as in our case, and obtained a value of 172 000 barns for σ_0 which conforms with ours. Because of the limitations of the collimating system, higher-order-index planes could not be used in the present case, but the resolution is good enough to allow conclusions to be drawn from the area analysis.

ACKNOWLEDGEMENTS

Our thanks are due to Dr. P.K. Iyengar for suggesting the problem and for useful discussions. Our thanks are also due to Shri K. Subbukutty for his help in computer calculations and to Shri J.S. Coachman for his help in experimental work.

REFERENCES

[1] SAILOR, V.L., FOOTE, H.L., Jr. LANDON, H.H., WOOD, R.E. Rev. scient. Instrum. 27 (1956) 26.
[2] MARION, J.P., BOLLINGER, L.M., Bull. Amer. Phys. Soc. II 3 (1958) 103.
[3] ATTA, S.E., HARVEY, J.A., Rep. ORNL-3205.
[4] ABOV, Y.G. in Conf. of Academy of Science of the USSR on the Peaceful Uses of Atomic Energy, Moscow (1955) 294.
[5] EGELSTAFF, P.A., GAYTHER, D.B., NICHOLSON, K.P., J. nucl. Energy 6 (1958) 303.
[6] COTE', R.E., BOLLINGER, L.M., BARNES, R.F., DIAMOND, H., Phys. Rev. 114 (1959) 505.
[7] PATTENDEN, N.J., RAINEY, V.S., J. nucl. Energy 11 (1959) 14.

DISCUSSION

M. ASGHAR: Your data on the total width Γ and the neutron width Γ_n give a value of $\Gamma_\gamma \approx 28$ meV. However, the average value of $<\Gamma_\gamma>$ up to ~ 1 keV neutron energy range (but not including this resonance) is ~ 22 meV. The difference between these two values is very significant. Could you please comment on this?

D. V. S. RAMAKRISHNA: I might mention that there are independent measurements of the radiation width for this energy level and there is a good consistancy between our data and the reported value of ~ 30 meV for Γ_γ.

P. H. RIBON: Have you calculated the effective capture cross-section at 2200 m/s in accordance with your parameters?

D. V. S. RAMAKRISHNA: No, I have not.

P. H. RIBON: Your values of Γ_γ and Γ_n are lower than those previously assumed and therefore you would get a decrease in the contribution to the σ_c (2200 m/s) of this resonance. It would be necessary to introduce levels at negative energy to explain the experimental value. In any case, this value of Γ_γ (~ 29 meV) is abnormally high.

ТЕМПЕРАТУРНАЯ ЗАВИСИМОСТЬ СТРУКТУРЫ ПОЛНОГО СЕЧЕНИЯ УРАНА-238 В ОБЛАСТИ НЕРАЗРЕШЕННЫХ РЕЗОНАНСОВ

А. А. ВАНЬКОВ, Ю. В. ГРИГОРЬЕВ,
М. Н. НИКОЛАЕВ, В. В. ФИЛИППОВ,
Физико-энергетический институт, Обнинск,
Союз Советских Социалистических Республик
Б. БЁМЕР, З. КОЛЛАТЦ,
Центральный институт ядерных исследований,
Россендорф,
Германская Демократическая Республика
Л. Б. ПИКЕЛЬНЕР
Объединенный институт ядерных исследований, Дубна,
Союз Советских Социалистических Республик

Presented by Yu.P. Popov

Доклад представлен Ю.П. Поповым

Abstract — Аннотация

TEMPERATURE DEPENDENCE OF THE TOTAL CROSS-SECTION STRUCTURE OF URANIUM-238 IN THE UNRESOLVED RESONANCE REGION.

The authors measure the transmission of neutrons in the range 1-100 keV through uranium-238 samples varying in thickness between 1 mm and 128 mm at -196°C, 20°C and 770°C using the time-of-flight neutron spectrometer at the Joint Institute for Nuclear Research, Dubna. The IBR pulsed fast reactor was used as neutron source. By using programmes for calculating transmission and parameter optimization to process the experimental data, they obtained a set of average resonance parameters for uranium-238 describing the structure of the cross-section and its temperature dependence.

ТЕМПЕРАТУРНАЯ ЗАВИСИМОСТЬ СТРУКТУРЫ ПОЛНОГО СЕЧЕНИЯ УРАНА-238 В ОБЛАСТИ НЕРАЗРЕШЕННЫХ РЕЗОНАНСОВ

Измерялись пропускания нейтронов через образцы урана-238 с толщинами от 1 до 128 мм при температурах -196°C, 20°C и 770°C в диапазоне энергий нейтронов 1-100 кэв. Использовался нейтронный спектрометр по времени пролета Объединенного института ядерных исследований (г. Дубна). Источник нейтронов – импульсный быстрый реактор ИБР. Из обработки совокупности экспериментальных данных с помощью программ расчета пропусканий и оптимизации параметров был получен набор средних резонансных параметров для урана-238, описывающий структуру сечений и ее температурную зависимость.

1. ВВЕДЕНИЕ

В энергетических быстрых реакторах с керамическим топливом и натриевым теплоносителем допплеровский температурный коэффициент реактивности является основным фактором, компенсирующим рост реактивности, которая возникает при аварийном выбросе натрия из активной зоны. Поэтому для надежной оценки ядерной безопасности атомных электростанций с реакторами такого типа необходимо обе эти конкурирующие составляющие знать с достаточно высокой степенью точности. При этом наибольшую сложность представляет учет допплер-эффекта, так как надеж-

ность информации о средних резонансных параметрах, определяющих допплер-эффект в области неразрешенных резонансов (весьма важной в случае быстрых реакторов) невелика. Таким образом, возникла проблема достаточно прямого измерения параметров, определяющих допплер-эффект на основных делящихся изотопах во всей энергетической области, где он проявляется. На решение этой проблемы и направлена данная работа. В качестве первого объекта исследования был выбран уран-238, обуславливающий примерно 20% полного допплер-эффекта в энергетических быстрых реакторах.

2. МЕТОДИКА

Сечения захвата и рассеяния и коэффициент диффузии среды, усредненные по нейтронному спектру, в резонансной области энергий в приближении постоянства плотности столкновений и изотропного рассеяния (оправданных в рассматриваемом случае) могут быть представлены в виде [1,2]:

$$\bar{\Sigma}_c = \frac{\langle \Sigma_c/\Sigma_t \rangle}{\langle 1/\Sigma_t \rangle} \qquad (1\,а)$$

$$\bar{\Sigma}_s = \frac{\langle \Sigma_s/\Sigma_t \rangle}{\langle 1/\Sigma_t \rangle} \qquad (1\,б)$$

$$\bar{D} = \frac{\langle 1/\Sigma_t^2 \rangle}{\langle 3/\Sigma_t \rangle} \qquad (1\,в)$$

Здесь угловые скобки означают усреднение по энергетическому интервалу, содержащему много резонансов, но достаточно узкому, чтобы энергетическая зависимость средних резонансных параметров или плотности столкновений слабо сказывалась на результатах усреднения. Чертой сверху отмечены эффективные параметры среды, с помощью которых может быть рассчитан усредненный по резонансам нейтронный поток.

Допплеровское уширение резонансов приводит к изменению результатов усреднения, т. е. к изменению эффективных параметров, а поэтому и размножающих свойств среды.

Примем, что уран-238 является единственным резонансным поглотителем в среде при рассматриваемых энергиях. Тогда

$$\langle \Sigma_c/\Sigma_t \rangle = \left\langle \frac{\sigma_c^8}{\sigma_t^8 + \sigma_0} \right\rangle + \sum_{n \neq 8} \frac{\rho_n \langle \sigma_c^n \rangle}{\langle 1/\Sigma_t \rangle} \qquad (2)$$

где индекс 8 указывает, что величина относится к урану-238, ρ_n – плотность ядер сорта n.

$$\sigma_0 = \frac{1}{\rho_n} \sum_{n \neq 8} \rho_n \langle \sigma_c^n \rangle \qquad (3)$$

– "сечение разбавления" урана-238 другими компонентами среды. Температурная зависимость $\langle \Sigma_c/\Sigma_t \rangle$ определяется при рассматриваемых условиях первым членом в правой части равенства (2). Аналогично могут быть представлены и другие средние величины в правых частях равенств (1).

Таким образом, для определения температурной зависимости эффективных макроскопических параметров (1), обусловленных допплер-эффектом на уране-238, нам необходимо знать средние значения

$$\left\langle \frac{1}{\sigma_t^8 + \sigma_0} \right\rangle; \left\langle \frac{\sigma_c}{\sigma_t^8 + \sigma_0} \right\rangle; \left\langle \frac{\sigma_s^8}{\sigma_t^8 + \sigma_0} \right\rangle; \left\langle \frac{1}{(\sigma_t^8 + \sigma_0)^2} \right\rangle \qquad (4)$$

в зависимости от средней энергии интервала усреднения при любых, вообще говоря, σ_0 .

Величины (4) могут быть выражены через интегралы от функций пропускания $T(t)$ и $T_x(t)$ пучка нейтронов (распределенных в энергетическом интервале ΔE, по которому производится усреденение), пропущенного через фильтры из исследуемого вещества толщиной t, измеренной в условиях "хорошей" геометрии с помощью детектора с постоянной энергетической чувствительностью ($T(t)$) или детектора, который регистрирует реакции типа (x) в тонком образце из исследуемого материала, установленного за фильтром ($T_x(t)$):

$$\left\langle \frac{1}{(\sigma_t^8 + \sigma_0)^n} \right\rangle = \frac{1}{(n-1)!} \int_0^\infty t^{n-1} T(t) e^{-N\sigma_0 t}\, dt \qquad (5\ а)$$

$$\left\langle \frac{\sigma_x^8}{\sigma_t^8 + \sigma_0} \right\rangle = \langle \sigma_x^8 \rangle \cdot \int_0^\infty T_x(t) e^{-N\sigma_0 t}\, dt \qquad (5\ б)$$

где

$$T(t) = \frac{1}{\Delta E} \int_{\Delta E} e^{-N\sigma_t^8(E)t} dE \qquad (6\ а)$$

$$T_x(t) = \frac{\int_{\Delta E} \sigma_x^8(E)\, e^{-N\sigma_t^8(E)t} dE}{\int_{\Delta E} \sigma_x^8(E) dE} \qquad (6\ б)$$

Цель нашего исследования заключается в измерении функции $T(t)$ и $T_x(t)$ и их температурной зависимости, в первую очередь, для урана-238. В настоящее время завершены измерения температурных зависимостей функций $T(t)$ в энергетической области до 120 кэв (то есть во всей области энергий, в которой существенен допплер-эффект на уране-238) и проведен их предварительный анализ. Произведены также пробные измерения функций $T_c(t)$.

3. ЭКСПЕРИМЕНТАЛЬНАЯ УСТАНОВКА

Схема эксперимента изображена на рис. 1. Пучок нейтронов из активной зоны импульсного быстрого реактора ИБР через вакуумированный нейтроновод попадал на детектор, устанавливавшийся на пролетной базе 1000 м. На расстоянии 75 м от реактора в разрыве нейтроновода помещалась вакуумная печь с набором образцов из металлического урана толщиной от 1 до 128 мм и диаметром 195 мм. Перед печью пучок нейтронов с помощью коллиматора сужался до диаметра 50 ÷ 180 мм. Измеря-

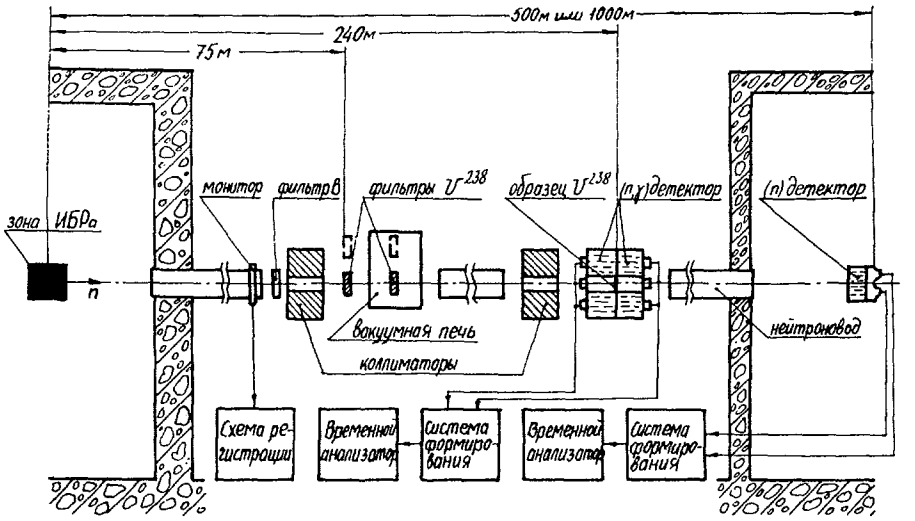

Рис. 1. Схема эксперимента для изучения Допплер-эффекта в ^{238}U.

лись функции пропускания при комнатной температуре и изменения этих функций при повышении температуры до 770°C ± 30°C. Последнее определялось в результате чередующихся измерений скоростей счета с горячим и с равным по толщине холодным образцом (устанавливавшимся вне печи, так как нагрев и, особенно, расхолаживание образцов в печи требовали значительных затрат времени).

Для толщин урановых образцов 16, 32 и 64 мм измерялись изменения пропусканий при охлаждении этих образцов до температуры жидкого азота – 77°K. Процедура измерения была такая же, как и в случае нагревания образцов: измерялось отношение скорости счета с охлажденным образцом к скорости счета с таким же образцом, находящимся при комнатной температуре. Для охлаждения образцов использовалась та же вакуумная печь, в которую после удаления нагревателя вводился охлаждающий "пояс", заполнявшийся жидким азотом.

Для измерения функций пропускания использовался жидкостной сцинтилляционный детектор [3] со сцинтиллятором площадью 800 $см^2$. Эффективность этого детектора слабо зависела от энергии и составляла при 10 кэв около 30%.

Проводились также предварительные, прикидочные измерения "захватных" функций пропускания $T_c(t)$. Для этой цели использовался жидкостной сцинтилляционный детектор [4] с отношением эффективностей к гамма-лучам и рассеянным нейтронам около 150. Детектор устанавливался на пролетной базе 240 м. Полученные с его помощью результаты являются, однако, недостаточно надежными из-за высокого уровня фона и трудностей его вычитания. В будущем предполагается провести измерения функций $T_c(t)$ с помощью более совершенных детекторов. Основные измерения были получены в одном из двух режимов работы ИБРа – реакторном и микротронном. В первом из них средняя мощность составляла w = 3 квт, частота нейтронных вспышек f = 5 гц, ширина вспышки на поло-

вине высоты $\tau = 60$ мксек. Во втором режиме реактор работал в качестве бустера, размножающего нейтроны, генерируемые в мишени электронного ускорителя-микротрона. В этом режиме $w = 0{,}6$ квт, $f = 50$ гц, $\tau = 3$ мксек. Разрешение с учетом ширины временного канала анализатора составляло либо 68 нсек/м (реакторный режим), либо 3,5 нсек/м (микротронный режим).

Временной анализ импульсов с детекторов осуществлялся с помощью 2048- или 4096-канальных анализаторов, иформация с которых для предварительной обработки передавалась на ЭВМ Минск-2 или БЭСМ-4.

4. УЧЕТ ФОНА И ДРУГИХ ПОПРАВОК

Собственный фон детектора был весьма стабилен и мог быть легко учтен. Обозначим через $N(t)$ скорость счета детектора в некотором временном канале при наличии на пучке фильтра толщиной t за вычетом собственного фона детектора. Пусть α – доля фоновых отсчетов в полной скорости счета детектора, связанных с работой реактора. Тогда для рассматриваемого канала

$$T(t) = \frac{N(t)[1 - \alpha(t)]}{N(0)[1 - \alpha(0)]} = \frac{N(t)}{N(0)}\left[1 - \frac{\alpha(t) - \alpha(0)}{1 - \alpha(0)}\right] \qquad (7)$$

Величины $\alpha(t)$ определялись методом резонансных фильтров (использовались фильтры из марганца, железа, натрия, алюминия, а также урана-238) до энергии 7 кэв в случае реакторного режима, до энергии 35 кэв в микротронном режиме для толщин $t \leqslant 64$ мм. Оказалось, что фон составляет от 5 до 15% от общей скорости счета и с точностью до ошибок ($\sim 2\%$) не зависит от толщины в указанном диапазоне толщин и области энергий. Было принято, что независимость фона от толщины для $t \leqslant 64$ мм сохраняется и для более высоких энергий, но точность этого утверждения падает с ростом энергии, достигая $\pm 4\%$ при $E = 100$ кэв. Очень слабая зависимость фона от толщины обусловлена слабой энергетической зависимостью пропускания от энергии при толщинах до 64 мм: среднее по энергии в интервале 1 – 100 кэв пропускание отличается от максимального всего на 15%. Поскольку сам фон составляет 15% от полного числа отсчетов, отличие его ослабления в фильтрах от ослабления полезных нейтронов, действительно, не должно превышать 2%.

При больших толщинах фильтров измеряемыми величинами являлись не сами функции пропускания, а их отношения:

$$\frac{T(t_1)}{T(t_2)} = \frac{N(t_1)}{N(t_2)}\left[1 - \frac{\alpha(t_1) - \alpha(t_2)}{1 - \alpha(t_1)}\right] \qquad (8)$$

Причем $t_1 - t_2$ не превышало 64 мм. Поэтому величина, стоящая в квадратных скобках в равенстве (8), также близка к единице и с той же точностью. Необходимо отметить, что γ-компонента реакторного фона, как показали измерения с полиэтиленовыми фильтрами, составляет весьма малую долю сравнительно с нейтронной компонентой фона, а кривая пропускания последней, соответствующая в основном жесткому спектру, сближается и пересекается с кривыми пропусканий (для выделенных энергетических групп) в области толщин 150-250 мм. Очевидно, в этой области толщин поправочный коэффициент наиболее близок к единице.

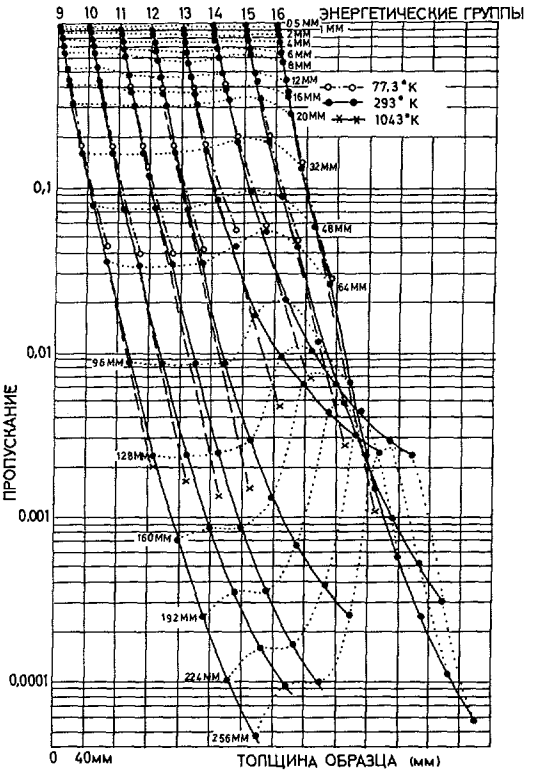

Рис. 2. Экспериментальные значения пропусканий на уране-238 при температуре образцов θ = 77,3°K; 293°K; 1043°K.

Кроме поправки на фон, влияющей, как отмечено, лишь на ошибку, но не на определяемую величину T(t), в скорости счета вводились поправки на просчеты. В случае измерения функции пропускания для относительно малых t (32, 64 мм) в реакторном режиме в области высоких энергий эти поправки могли быть весьма значительными и неопределенными из-за временной зависимости мертвого времени регулирующей системы, обусловленной перегрузкой детектора. Для устранения перегрузки детектора в этих случаях приходилось уменьшать интенсивность путем коллимации пучка и ослабления его свинцовым фильтром. При работе в микротронном режиме перегрузок детектора не происходило.

Изменение пропускания при нагреве фильтра производится не только за счет допплер-эффекта, но также и за счет уменьшения толщины фильтра в результате теплового расширения: $t \to t(1 - 2\alpha\Delta\theta)$, где α – линейный коэффициент теплового расширения, $\Delta\theta$ – приращение температуры. Таким образом, пропускание через горячий образец относится к несколько меньшей толщине фильтра, чем пропускание через холодный образец. При сравнении эксперимента с расчетом это обстоятельство учитывалось: пропускания рассчитывались для реальных толщин, соответствующих условиям эксперимента.

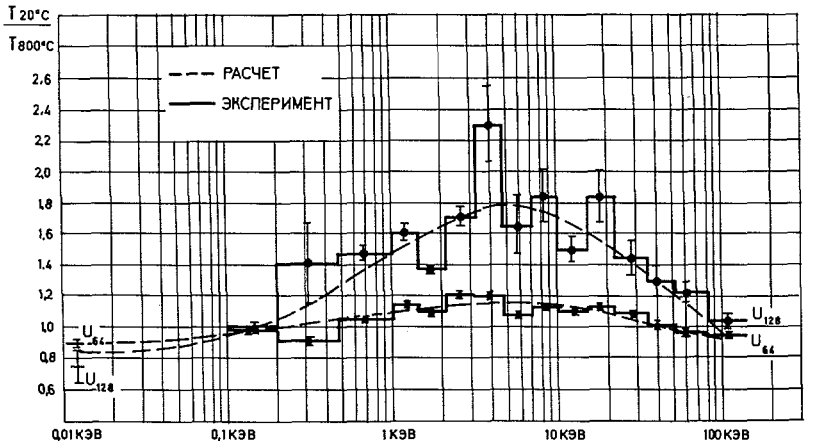

Рис. 3. Допплер-эффект в отношениях пропусканий $T_{20°C}/T_{800°C}$ на образцах урана-238 толщиной 64 мм и 128 мм.

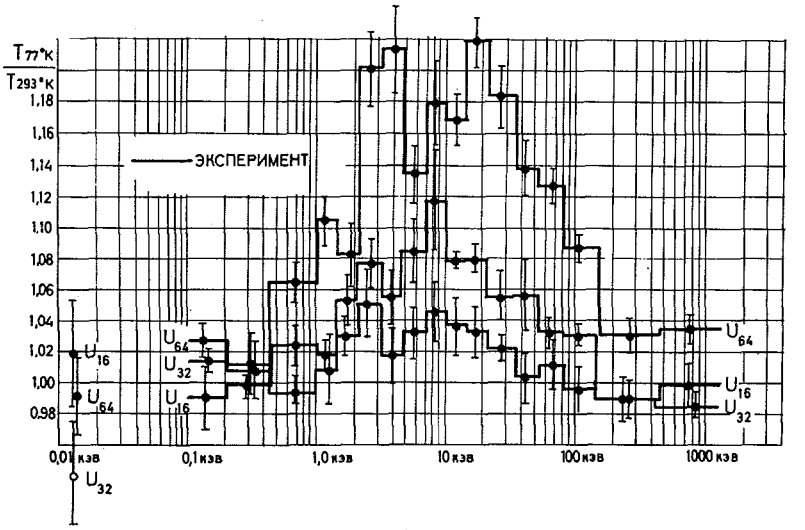

Рис. 4. Допплер-эффект в отношениях пропусканий $T_{77°K}/T_{293°K}$ на образцах урана-238 толщиной 16 мм; 32 мм; 64 мм.

5. РЕЗУЛЬТАТЫ

Исходным экспериментальным материалом для последующей обработки служили пропускания, измеренные для восьми энергетических интервалов (близко соответствующих энергетическим группам 26-групповой системы констант [1]) в диапазоне энергий от 0,2 до 140 кэв для толщин урановых образцов от 0,5 до 256 мм при комнатной температуре (по 19 точек на каждой кривой пропускания), температуре 1043°K (по 6 точек) и температуре жидкого азота (по 3 точки на каждой кривой). (Рис. 2,3,4).

ТАБЛИЦА 1. СРАВНЕНИЕ ЭКСПЕРИМЕНТАЛЬНЫХ СРЕДНЕГРУППОВЫХ СЕЧЕНИЙ (барн) УРАНА-238 С РЕЗУЛЬТАТАМИ ОЦЕНКИ Л. П. АБАГЯН

Номер группы		9	10	11	12	13	14	15	16
Интервал энергии (кэв)	Эксперимент	142 ÷ 42.0	42.0 ÷ 20.0	20.0 ÷ 10.5	10.5 ÷ 3.93	3.93 ÷ 1.97	1.97 ÷ 0.985	0.985 ÷ 0.400	0.400 ÷ 0.196
	Оценка	100 ÷ 46.5	46.5 ÷ 21.5	21.5 ÷ 10.0	10.0 ÷ 4.65	4.65 ÷ 2.15	2.15 ÷ 1.00	1.00 ÷ 0.465	0.465 ÷ 0.215
$\langle \sigma_t \rangle$	Эксперимент	$11.7^{+0.2}_{-0.2}$	$14.8^{+0.8}_{-1.0}$	$16.5^{+2.0}_{-1.0}$	$18.0^{+3.0}_{-2.0}$	$20.0^{+3.0}_{-1.0}$	$22.0^{+3.0}_{-0.5}$	$24.5^{+3.0}_{-0.5}$	$27.0^{+3.0}_{-1.0}$
	Оценка	12.9	13.7	14.7	16.1	18.2	21.6	22.4	22.0
$\langle 1/\sigma_t \rangle^{-1}$	Эксперимент	11.2 ± 0.2	11.5 ± 0.2	11.8 ± 0.2	12.0 ± 0.2	10.9 ± 0.2	10.2 ± 0.2	10.8 ± 0.2	13.0 ± 0.2
	Оценка	12.2	12.6	12.6	12.3	11.8	11.3	10.9	12.1
$\sigma^{*}_{tr}\|_{\sigma_0=0}$	Эксперимент	10.5 ± 0.3	10.6 ± 0.3	10.5 ± 0.3	9.8 ± 0.3	6.2 ± 0.2	6.0 ± 0.2	9.1 ± 0.3	11.3 ± 0.3
	Оценка	11.9	11.8	11.3	10.4	9.1	7.6	8.6	11.1
$\sigma^{*}_{tr}\|_{\sigma_0=10}$	Эксперимент	11.2 ± 0.3	11.5 ± 0.3	11.6 ± 0.3	12.4 ± 0.3	11.0 ± 0.3	10.0 ± 0.3	10.4 ± 0.3	12.0 ± 0.3
	Оценка	12.3	12.5	12.4	12.1	11.5	11.1	10.5	11.9

* $\sigma_{tr} = [\langle 1/\sigma_t + \sigma_0 \rangle / \langle 1/(\sigma_t + \sigma_0)^2 \rangle] - \sigma_0$; σ_0 – сечение разбавления.

ТАБЛИЦА 2. СРАВНЕНИЕ ТЕМПЕРАТУРНЫХ ПРИРАЩЕНИЙ (миллибарн/°К) ЭКСПЕРИМЕНТАЛЬНЫХ И ОЦЕНЕННЫХ СРЕДНЕГРУППОВЫХ СЕЧЕНИЙ УРАНА-238

Номер группы		9	10	11	12	13	14	15	16
Интервал энергии (кэв)	Эксперимент	142 ÷ 42.0	42.0 ÷ 20.0	20.0 ÷ 10.5	10.5 ÷ 3.93	3.93 ÷ 1.97	1.97 ÷ 0.985	0.985 ÷ 0.400	0.400 ÷ 0.196
	Оценка	100 ÷ 46.5	46.5 ÷ 21.5	21.5 ÷ 10.0	10.0 ÷ 4.65	4.65 ÷ 2.15	2.15 ÷ 1.00	1.00 ÷ 0.465	0.465 ÷ 0.215
$\frac{\Delta \langle 1/\sigma_t \rangle^{-1}}{\Delta \theta}$	Эксперимент	0.2 ± 0.2	0.5 ± 0.2	1.0 ± 0.3	0.8 ± 0.2	2.0 ± 0.3	1.3 ± 0.2	0.8 ± 0.2	0.3 ± 0.2
	Оценка	0.33	0.67	1.17	1.50	1.67	1.67	1.17	0.5
$\frac{\Delta \sigma_{tr}}{\Delta \theta}\|_{\sigma_0=0}$	Эксперимент	0.5 ± 0.3	0.9 ± 0.3	1.6 ± 0.4	1.5 ± 0.3	4.8 ± 0.4	3.6 ± 0.3	1.5 ± 0.3	0.7 ± 0.3
	Оценка	0.5	1.17	1.67	2.17	2.83	3.17	2.00	0.83
$\frac{\Delta \sigma_{tr}}{\Delta \theta}\|_{\sigma_0=10}$	Эксперимент	0.3 ± 0.3	0.5 ± 0.3	1.1 ± 0.4	0.8 ± 0.3	1.3 ± 0.4	1.2 ± 0.3	0.8 ± 0.3	0.4 ± 0.3
	Оценка	0.33	0.67	1.17	1.17	1.33	1.00	0.83	0.33

Применялось два подхода к анализу и дальнейшему использованию полученной информации. Первый состоял в том, чтобы подобрать такие значения средних резонансных параметров, которые обеспечили бы наилучшее согласие между наблюденными пропусканиями и пропусканиями, рассчитанными на основе средних резонансных параметров. Подбор параметров осуществлялся методом наименьших квадратов по программе MIRESPA, которая использовала для расчета пропусканий программу TAS [5]. Варьируемыми параметрами являлись средние приведенные нейтронные ширины для s- и p-резонансов, среднее расстояние между s-резонансами, сечение потенциального рассеяния в области низких энергий и радиационная ширина.

Для анализа использовался как полный набор полученных данных (объединенных в 8 энергетических групп), так и различные выборки из этого набора.

Оказалось, что параметры s-волны сравнительно слабо чувствительны к тому, какие данные включены в анализ: силовая функция для s-волны варьируется от 0,9 до 1,05; среднее расстояние между s-резонансами – от 21,0 до 23,4; сечение потенциального рассеяния – от 10,6 до 11,0 барна. Наиболее вероятные значения этих параметров:

$$\overline{\Gamma}_n^0/\overline{D}_{\frac{1}{2}} = (0,96 \pm 0,07)\cdot 10^{-4}$$

$$\overline{D}_{\frac{1}{2}} = (21,5 \pm 1,0) \text{ эв}$$

$$\sigma_{pot} = (10,7 \pm 0,2) \text{ бн}$$

Что касается радиационной ширины и силовой функции для p-волны, то значения этих параметров оказались чрезвычайно чувствительными к возможным небольшим систематическим ошибкам в данных и к естественным флуктуациям результатов, обусловленных конечным числом резонансов в группе. В разных вариантах расчета их значения варьировались от 18,5 мэв до 46 мэв ($\overline{\Gamma}_\gamma$) и от $0,46\cdot 10^{-4}$ до $2,2\cdot 10^{-4}$ ($\overline{\Gamma}_n^0/\overline{D}|_{l=1}$). Определить эти параметры таким образом не удалось; их значения, определенные путем усреднения параметров низколежащих резонансов ($\overline{\Gamma}_\gamma = 22,5 \pm 1,5$; $\overline{\Gamma}_n^0/\overline{D}|_{l=1} = (2,2 \pm 0,3)\cdot 10^{-4}$ не противоречат нашим результатам.

Другой подход к обработке полученных экспериментальных данных заключался в их непосредственном использовании для расчета величин типа (4). Для этой цели проводилась аппроксимация экспериментальных кривых пропускания суммами экспонент. Введем понятие функции распределения сечения в интервале усреднения – $P(\sigma)$, тогда:

$$T(t) = \int_0^\infty P(\sigma) e^{-\sigma t}\, d\sigma \approx \sum_n P_n \langle e^{-\sigma_n t} \rangle \Delta\sigma_n \qquad (9)$$

где $P_n \Delta\sigma_n$ – вероятность обнаружения в интервале усреднения полного сечения, равного $\Delta\sigma_n$.

Кривые пропускания аппроксимировались суммой экспонент с помощью программы OPAC, реализующей алгоритм, разработанный М. Тарско. Этот алгоритм обеспечивает положительность и необходимую гладкость решения при любом числе экспонент с заданными σ_n (практически использовались от 20 до 50 экспонент).

Другой использованный для обработки алгоритм – это аппроксимация кривой пропускания суммой минимального числа экспонент, обеспечиваю-

щего описание экспериментальных данных с точностью до ошибок. Поиск параметров P_n и σ_n осуществляется методом наименьших квадратов по программе МНК, составленной В. Ф. Хохловым [7].

После аппроксимации кривых пропускания аналитическими формами производилось вычисление среднегрупповых характеристик – $\langle \sigma_t \rangle$, $\langle 1/(\sigma_t + \sigma_0) \rangle$, $\langle 1/(\sigma_t + \sigma_0)^2 \rangle$. Различие в этих характеристиках, полученных при использовании двух указанных способов аппроксимации кривых пропускания, служило мерой их неточности, связанной с неопределенностью экстраполяции кривых пропускания на область очень больших и очень малых толщин.

Результатам расчетов, приведенным в табл. 1, приписаны ошибки, учитывающие как только что отмеченные обстоятельства, так и статистические неопределенности результатов. В табл. 1 приведены результаты расчета этих характеристик, выполненные Л. П. Абагян по параметрам разрешенных резонансов (до 2,15 кэв) и по средним резонансным параметрам (при более высоких энергиях).

Расхождения, имеющиеся в группах 15 и 16 (табл. 1), вполне объясняются различием интервалов усреднения расчетных и экспериментальных данных. В области неразрешенных резонансов, измеренное среднее сечение систематически выше расчетного на величину порядка ошибки (исключение составляет 9-я группа (табл. 1), в которой, однако, интервалы усреднения расчетных и экспериментальных сечений сильно разнятся). В то же время заблокированные сечения $\langle 1/\sigma_t \rangle^{-1}$ и особенно $\langle 1/\sigma_t \rangle / \langle 1/\sigma_t^2 \rangle$ в эксперименте получаются более низкими, чем это следует из расчета. Таким образом, резонансная самоэкранировка сечения оказывается более сильной, чем это следует из расчетов, хотя различия невелики даже в случае максимальной самоэкранировки ($\sigma_0 = 0$) и резко снижаются при разбавлении.

В табл. 2 сравниваются расчетные и экспериментальные приращения заблокированных сечений при нагреве среды (в предположении об их линейной зависимости от температуры в диапазоне 300°К ÷ 1000°К). Как видно из табл. 2, экспериментальные и оцененные данные согласуются между собой в пределах ошибок. Наибольшие расхождения имеют место в 12-ой и 13-ой группах (табл. 2): в первой из них экспериментальные температурные приращения оказались ниже, а в другой – выше, чем следует из оценки. Из характера кривой пропускания (см. рис. 2) видно, что основной причиной отличия является малая статистика уровней в этих группах, так что наблюдающиеся расхождения являются вполне естественными отклонениями средних выборочных от среднестатистических.

В целом характер расхождений указывает на небольшую переоценку температурных приращений (Л. П. Абагян); при разбавлении урана-238 нерезонансным разбавителем роль этой тенденции быстро уменьшается.

ЛИТЕРАТУРА

[1] АБАГЯН, Л. П., БАЗАЗЯНЦ, Н. О., БОНДАРЕНКО, И. И., НИКОЛАЕВ, М. Н., Групповые константы для расчета ядерных реакторов. М., Атомиздат, 1964.

[2] АБАГЯН, Л. П., МИХАЙЛУС, Ф. Ф., НИКОЛАЕВ, М. Н., ОРЛОВ, В. В., Распространение резонансных нейтронов в гомогенных средах. Теория и специальные функции. Бюллетень информационного центра по ядерным данным, вып. 5, приложение №1, М., Атомиздат, 1968.

[3] ВИЗИ, И. и др., Nuclear Electronics, IAEA, Vienna 1 1967, pp. 27-36.

[4] ПИКЕЛЬНЕР, Л.Б. и др., "Приборы и техника эксперимента" 2 (1963) 48-50.
[5] COLLATZ, S., Kernenergie 11 (1968) 1.
[6] ВАНЬКОВ, А.А. и др., Советско-бельгийско-голландский семинар по ядерным данным. Мелекесс, 1970.
[7] ХОХЛОВ, В.Ф., Бюллетень информационного центра по ядерным данным, вып. 4 (1967) 420.

DISCUSSION

C.M. NEWSTEAD: By extending the energy range of your measurement up to about 200 keV and increasing the accuracy of the measurement, do you think you would be able to extract the p-wave strength function?

Yu. POPOV: I do not think that extension of the energy range is involved here. It is obvious that the p-wave contribution plays an important part up to 100 keV and that beyond this the d-wave contribution begins to play a substantial role. To determine the contribution of the p-wave neutrons more exactly, it is better to improve the accuracy of the average cross-section measurements in the 10-100 keV range.

C.M. NEWSTEAD: I don't entirely agree with that because although it is true that the d-waves come in at this energy in capture cross-sections, they do not make their contribution to a higher energy in the case of total cross-sections. Therefore the p-wave contribution would be maximized in the region of 200 keV.

Yu. POPOV: This may be true. I cannot say right now in what region the p-wave neutrons cease to exert their effect. However, I think that for measuring the p-wave, it is better to achieve accuracy in the range up to 100 keV than to extend the range as a whole.

C.M. NEWSTEAD: Yes, I would agree with that. Accuracy in the measurement is probably what is most important.

Invited paper

EVALUATION DANS LE DOMAINE DES RESONANCES POUR LES NOYAUX DE NOMBRE DE MASSE SUPERIEUR A 220

P. RIBON
CEA, Centre d'études
nucléaires de Saclay,
France

Abstract — Résumé

EVALUATION IN THE RESONANCE RANGE OF NUCLEI WITH A MASS NUMBER ABOVE 220.

The author discusses the problems posed by the evaluation of neutron data for fissile or fertile nuclei in the range of resolved or unresolved resonances. It appears to take several years until the data of an experiment are used by the reactor physicists. If one wants to have recent data at one's disposal, one cannot have recourse to evaluated-data libraries. Moreover, the existing parameter sets are only fragmentary. A new evaluation is, therefore, necessary for nearly all of these nuclei, but it cannot be based upon different parameter sets; these are indeed contradictory, and the evaluator will have to go back to the original data.

The author shows for the set of σ_f of ^{235}U, that a careful comparison of the data shows up unsuspected local defects. Some examples illustrate the deviation between analyses carried out by different methods and between the results on the established divergences.

The parameters or cross-sections are far from being known with the precision one would desire. This fact gives rise to anomalies in the interpretation of data necessary for understanding and simulation in the range of unresolved resonances. But the introduction of concepts connected with sub-threshold fission noticeably furthers this understanding. Therefore a comparison of the methods of analysis must be made in more and more accurate measurements (evaluation and correction of systematic errors).

EVALUATION DANS LE DOMAINE DES RESONANCES POUR LES NOYAUX DE NOMBRE DE MASSE SUPERIEUR A 220.

L'auteur examine les problèmes posés par l'évaluation des données neutroniques pour les noyaux fissiles ou fertiles dans le domaine des résonances résolues ou non. Tout d'abord il apparaît un écart de plusieurs années entre l'exécution d'une expérience et l'utilisation des données de celle-ci par les physiciens des réacteurs. On ne peut, si l'on veut disposer de données récentes, se reporter aux bibliothèques de données évaluées. De plus les jeux de paramètres qui existent sont fragmentaires. Une nouvelle évaluation est donc nécessaire pour à peu près tous ces noyaux; mais elle ne pourra se faire à partir des différents jeux de paramètres; ceux-ci sont en effet contradictoires. Et l'évaluateur devra remonter aux données originales.

L'auteur montre, pour l'ensemble de σ_f du ^{235}U, qu'une comparaison soignée des données fait apparaître des défauts locaux insoupçonnés. Quelques exemples illustrent la dispersion des analyses effectuées par différentes méthodes et des résultats sur les divergences constatées. On est loin de connaître les paramètres ou les sections efficaces avec la précision désirée. Il en résulte des anomalies dans l'interprétation des données, nécessaire pour la compréhension et la simulation dans le domaine des résonances non résolues. Mais l'introduction des concepts liés à la fission sous le seuil fait nettement progresser cette compréhension. Ainsi il faut effectuer, en plus de mesures plus précises (évaluation et correction des défauts systématiques), une comparaison des méthodes d'analyse.

INTRODUCTION

Depuis 1965, plusieurs conférences ont traité, directement ou indirectement, de l'interaction de neutrons lents avec les noyaux fissiles ou fertiles [1-6]. Certaines de ces conférences concernaient plus particulièrement la fission; lors de la dernière en date [6] les phénomènes liés

à la fission sous le seuil (structures intermédiaires dans les sections efficaces de fission notamment) furent l'objet de nombreuses communications.

Plusieurs exposés généraux furent consacrés lors de ces conférences aux différents aspects des problèmes posés par la mesure des sections efficaces des noyaux fissiles et fertiles, leur analyse et leur interprétation. Il faut enfin signaler certains ouvrages récents consacrés en partie [Ly 68] ou en totalité [Mo 69] à ces sujets.

L'étude qui m'est demandée, à savoir: « Evaluation dans le domaine des résonances (résolues et non résolues) pour les noyaux de nombre de masse supérieur à 220», implique un certain recoupement avec ces publications récentes. Le lecteur est prié de s'y reporter car je ne pourrai que mentionner la plupart des sujets qui y sont traités.

Je devrais examiner les données dans le domaine thermique. Ce domaine est un cas particulier de celui des résonances résolues, compliqué par l'existence de niveaux inconnus à des énergies négatives, et avec une demande de précision très grande sur les valeurs absolues: 0,5% en priorité 1 sur les sections efficaces de fission et de capture du ^{239}Pu, par exemple. La détermination précise de ces valeurs absolues est l'objet d'une session spéciale de cette conférence, et l'évaluation de l'ensemble des données vient d'être refaite [Ha 69]. Aussi ne prêterai-je pas une attention particulière à ce domaine.

Pour situer le problème, je rappellerai d'abord quelles sont les demandes formulées par les physiciens des réacteurs, puis je suivrai la démarche de l'évaluateur à qui ces demandes sont adressées:

- Sous quelle forme dois-je fournir ces évaluations (sections efficaces ou paramètres des résonances)?
- Puis-je satisfaire la demande par les évaluations existantes?
- Si non, puis-je effectuer une évaluation à partir des valeurs de paramètres publiées?
- Si non, comment comparer les données expérimentales afin de retenir celles qui paraissent les plus sûres? Comment analyser ces données?

J'examinerai ensuite les principaux désaccords entre les différents laboratoires, puis l'interprétation de ces analyses.

1. GENERALITES

1.1. Demande des physiciens des réacteurs

Le tableau I donne la liste des demandes de données formulées par les physiciens des réacteurs en 1969 avec une priorité 1 pour $A > 220$; nous n'avons retenu que les demandes les plus exigeantes quant à la précision. Nous ferons plusieurs remarques.

a) Peu de demandes concernent les paramètres de résonances.

b) En 1968, ils étaient demandés, pour les noyaux fissiles, dans des gammes d'énergie où il est impossible de les obtenir [7]. Ces demandes ont disparu.

c) La précision demandée sur les paramètres de résonances ($\sim 10\%$) est inférieure à celle requise pour σ_f, σ_c etc. Par exemple, dans le cas du ^{237}Np, les trois demandes figurant dans Renda 68 émanent des mêmes laboratoires; il apparaît que leurs auteurs pensent que les mesures qui

TABLEAU I. LISTE DE DEMANDES DE DONNEES NEUTRONIQUES FIGURANT EN PRIORITE 1 DANS RENDA-68

Noyau	Donnée	Gamme énergie (eV)	Précision (%)
^{232}Th	Γ_γ	< 4000	10
	$l_{c\ eff}$	> 2000	5
	σ_c	> 4000	5
^{233}Pa	σ_a	< 500	5
	$l_{c\ eff}$	> 0,5	10
^{233}U	σ_f	< 1000	1
	σ_c	1 à 30	1
		30 à 1000	4
		1000 à 30 000	2
		1 à 100	3
^{235}U	par. rés.[a]	< 300	10
		300 à 5000	20
	σ_f	1 à 40 000	3
	σ_c	< 2000	5
	σ_a	1 à 15	5
		15 à 100	6
		< 2000	2
^{236}U	σ_t	< 1000	5
	σ_c	< 1000	10
^{238}U	σ_c	< 3	3
		100 à 40 000	3
^{237}Np	Γ_n	< 1000	5
	Γ_γ	< 1000	10
	σ_c	< 1000	3
^{238}Pu	σ_c	< 1000	10
^{239}Pu	par. rés.	< 5000	10
	σ_t	> 500	5
	σ_f	toutes énergies	3
	σ_c	< 500	5
		> 500	4
	$l_{c\ eff}$		1
	σ_a	1 à 15	3
		15 à 300	4
		300 à 2000	10
		11 à 300	4
		300 à 2000	5
		100 à 40 000	5
^{240}Pu	par. rés.	50 à 5000	< 10
	σ_c	< 100	3
		100 à 500	8
		> 500	5
^{241}Pu	par. rés.	< 2000	10
	σ_f	100 à 40 000	5
	σ_c	< 2000	10
	σ_a	150 à 300	8
		1000 à 2000	20
	n	400	5
	α	100 à 40 000	20
^{242}Pu	par. rés.	< 10 000	10-20
	σ_c	< 100	3
		100 à 1000	10
		> 1000	15-20
^{241}Am	σ_c	< 1000	10
^{243}Am	σ_t, σ_c	< 10 000	10

[a] Une demande précise: analyse multiniveau si possible.

permettront de déterminer Γ_n et Γ_γ à 5 - 10% donnent σ_c à 3%. Ceci conduit à s'interroger sur l'intérêt des paramètres des résonances.

1.2. Présentation des évaluations

Sections efficaces ou paramètres de résonances?

Est-il nécessaire de paramétriser les sections efficaces dans le domaine des résonances résolues puisque, d'une part, le résultat expérimental est généralement une courbe de sections efficaces en fonction de l'énergie, et que, d'autre part, c'est ce résultat qui intéresse le plus les physiciens des réacteurs?

Je retiendrai deux arguments en faveur de la non-paramétrisation des sections efficaces.

a) Le travail de dépouillement est plus aisé, puisqu'il n'y a pas d'analyse.

b) Il évite des erreurs d'analyse: les sections efficaces moyennes calculées d'après les jeux de paramètres sont souvent très différentes des sections efficaces expérimentales [Ri 69a].

Mais il existe de nombreux arguments en faveur de cette paramétrisation:

a) Elle permet mieux que tout autre moyen de comparer entre elles les expériences de même type effectuées par différents laboratoires (résolution ou effet Doppler différents) et de vérifier la cohérence des divers types d'expériences:
- identification des mêmes résonances, des impuretés;
- pour chaque résonance, vérification de $\Gamma = \Gamma_\gamma + \Gamma_n + \Gamma_f$.

b) Elle permet de calculer les effets de l'autoabsorption et des diffusions multiples lorsque l'épaisseur de l'échantillon n'est pas suffisamment faible, cas fréquent en pratique.

c) Elle est nécessaire lorsque le résultat n'est pas une section efficace (cas de la transmission).

d) Elle permet de définir les lois statistiques qui rendent possibles le calcul des sections efficaces simulées dans le domaine des résonances non résolues, permettant ainsi de répondre à la demande des physiciens des réacteurs.

e) On ne peut enfin négliger l'intérêt de cette analyse au point de vue de la physique nucléaire, les progrès de celle-ci se répercutant à son tour sur l'évaluation (voir 6).

1.3. Etat de l'évaluation

La première réaction du physicien auquel il est demandé de fournir un jeu de paramètres «recommandés» sera d'examiner ce qui existe.

a) Il constatera que les dernières évaluations datent de quelques années (1967 ou avant pour le ^{235}U, 1968 pour le ^{239}Pu et le ^{238}U) et que les données analysées dataient déjà de 3 ou 4 ans; par exemple les données les plus récentes utilisées par Ravier [Ra 68] ou par Wittkopf et al. [Wi 67] pour leurs évaluations du ^{238}U sont celles de Garg et al. [Ga 64] publiées en 1964, alors que Adler et Adler ont utilisé, pour leur analyse multiniveau du ^{239}Pu en dessous de 40 eV [Ad 68], les données obtenues à

Argonne en 1958 [Bo 58] et, en dessous de 20 eV, celles obtenues à Saclay en 1964-1965 [De 66].

Les nombreux résultats expérimentaux acquis depuis 5 ou 6 ans ne sont donc pas actuellement utilisables par les physiciens des réacteurs.

Plus généralement, il faut remarquer l'importance du laps de temps entre l'acquisition du résultat expérimental et son exploitation pour une évaluation: il y a certainement là un problème qu'il n'est pas dans mon propos d'examiner.

b) Le physicien constatera aussi que ces évaluations sont très souvent partielles et inutilisables, telles quelles, par les physiciens des réacteurs.

c) Enfin il verra qu'elles sont souvent en désaccord entre elles. Nous expliciterons ce point en 2.

Ceci conduira l'évaluateur à conclure qu'il doit effectuer lui-même une évaluation afin d'obtenir un jeu cohérent de paramètres utilisant toute l'information disponible.

La première idée sera évidemment d'effectuer cette évaluation en utilisant les valeurs des paramètres de résonances publiées par les expérimentateurs (ou d'autres évaluateurs). C'est le moyen classiquement utilisé jusqu'à présent (par exemple [Sc 66]). Nous allons examiner la possibilité d'opérer ainsi.

2. EVALUATION A PARTIR DES PARAMETRES DES RESONANCES

Chaque expérimentateur n'analyse que ses résultats, indiquant dans quelle mesure il utilise ceux obtenus par un autre laboratoire. On peut donc penser que l'évaluation pourra se limiter à une certaine moyenne pondérée des différents jeux de paramètres. Ceci n'est possible que s'il y a au moins deux jeux de paramètres indépendants: c'est-à-dire, au-delà d'une dizaine d'eV, pour un nombre très limité de noyaux: thorium-232, uranium-237, 235 et 238, plutonium-239, 240 et 241. Ce sont en fait les plus importants pour les réacteurs.

Nous allons prendre quelques exemples pour voir comment se présente la situation.

2.1. Cas du ^{235}U

C'est très probablement l'élément le plus étudié jusqu'à présent; mais il est loin d'être le mieux connu. Nous examinerons quelques données partielles.

a) Identification des résonances entre 21,5 et 27,5 eV

La figure 1 représente les énergies des résonances identifiées entre 21,5 et 27,5 eV:

Colonnes 1 à 4: Résultats obtenus par quatre expérimentateurs indépendamment les uns des autres.

Colonne 5: Résultats obtenus par un évaluateur, celui-ci ayant pratiquement supposé l'existence de toutes les résonances données une fois ou l'autre par un expérimentateur.

Colonne 6: Il s'agit d'une analyse simultanée de la section efficace totale mesurée à Saclay et des résultats de ORNL-RPI pour la capture et

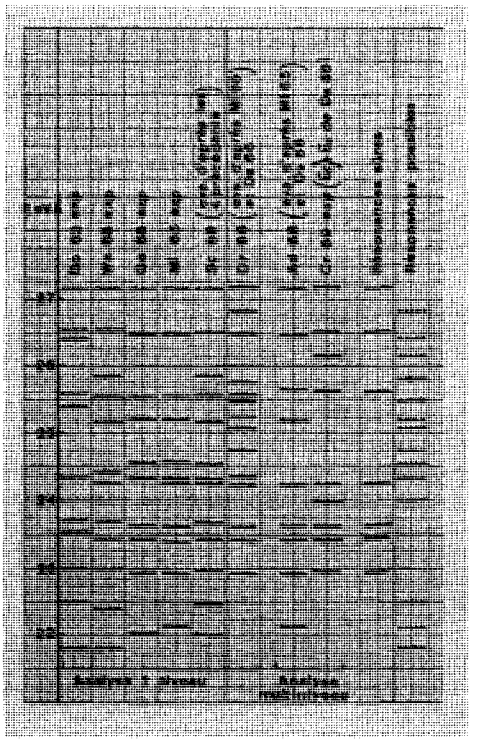

FIG. 1. Résonances du ^{235}U identifiées entre 21,7 et 27,5 eV.

la fission. Les auteurs de cette analyse concluent à l'absence de niveau entre 21,5 et 22,8 eV, mais en introduisent trois par ailleurs.

Colonne 7: Il s'agit d'une analyse multiniveau (méthode Adler-Adler) des mêmes résultats que ceux utilisés dans la colonne 6; les auteurs introduisent moins de niveaux, ce qui est normal, et sont en bon accord avec l'analyse à un niveau faite à Saclay (à deux résonances près).

Colonne 8: L'identification des résonances résulte de l'analyse multiniveau (méthode Reich-Moore) de la section efficace de fission mesurée à Los Alamos au cours du tir PETREL et en tenant compte de la capture de ORNL-RPI.

Toutes les expériences s'accordent sur l'existence de sept résonances, bien dessinées, mais diffèrent pour 14 autres. Les analyses multiniveaux devraient identifier les mêmes résonances, avec sans doute des énergies légèrement différentes: or les deux résonances que les analyses multiniveaux (colonnes 7 et 8) introduisent en plus des sept niveaux incontestés n'ont rien à voir entre elles.

Il faut remarquer que Drawbaugh et Gibson, qui introduisent le plus de niveaux, sont les seuls à donner une valeur correcte de $\overline{\sigma}_f$ d'après les paramètres de résonances à un niveau [Ri 69a].

L'évaluateur ne peut plus supposer que l'existence d'une résonance est probable parce qu'elle a été identifiée au moins une fois; les jeux de pa-

ramètres sont en fait incompatibles entre eux sans qu'on puisse faire la part des résultats expérimentaux et des méthodes d'analyses.

b) Paramètres des niveaux du ^{235}U entre 30, 7 et 41 eV

On peut penser que la gamme d'énergie de 21, 5 à 27, 5 eV est particulièrement délicate, et que l'identification des résonances posera moins de problèmes ailleurs; tel est effectivement le cas entre 30, 7 et 41 eV: il existe dix grandes résonances sur lesquelles tout le monde s'accorde, et peut être trois petites introduites par Cramer lors de son analyse multiniveau [Cr 69].

Le tableau II représente les valeurs des paramètres publiées par différents auteurs en utilisant parfois les mêmes expériences. Il apparaît de très grandes divergences entre les quatre jeux:

- le rapport $<\sigma_{f\,Sac}>/<\sigma_{f\,Las}>$ est de $\sim 0,75$, alors que le rapport $<\sigma_{c\,Sac}>/<\sigma_{c\,Las}>$ vaut 1, 30 (les valeurs de $<\sigma_\alpha>$ étant proportionnelles à $\sum \frac{2g\,\Gamma_n\,\Gamma_\alpha}{\Gamma}$)
- La valeur absolue de l'écart entre les valeurs de $2g\,\Gamma_n$ de Saclay et de Los Alamos est en moyenne de 25%.
- Les fluctuations de Γ_γ et Γ_f résultent de ces deux divergences et sont plus importantes.

Il existe une sous-estimation (ou une surestimation) de $\overline{\sigma_f}$ d'une analyse à l'autre, et un désaccord aléatoire sur $2g\,\Gamma_n$, et l'évaluateur devra se reporter aux résultats expérimentaux originaux.

2.2. Cas du ^{232}Th

L'étude des noyaux fertiles paraît plus aisée; on peut espérer, en particulier, avoir de bonnes données sur le ^{232}Th, élément monoisotopique à l'état naturel. Il n'y a pas, effectivement, d'ambiguïté sur l'identification des résonances, mais il n'en est pas de même pour la largeur neutronique réduite qui est pourtant le paramètre le plus facile à déterminer.

La figure 2 représente le rapport de Γ_n donné par différents expérimentateurs [As 66, Bo 64, Ga 64, Ha 65] à la valeur déterminée à Saclay [Ri 69]. J'ai normalisé par rapport à nos valeurs car nous sommes les seuls à les donner à toutes énergies (jusqu'à 3 keV).

On constate que la dispersion des valeurs est nettement supérieure aux 10% recherchés et qu'elle présente un caractère systématique:

- Les valeurs de General Atomics [Ha 65] sont toujours supérieures aux nôtres.
- Celles de Harwell [As 66] sont inférieures en dessous de 200 eV, supérieures au-dessus.
- Celles de Columbia [Ga 64] sont à peu près égales ou légèrement inférieures aux nôtres jusqu'à 1 keV, nettement inférieures au-delà.

La différence sur $\sum_{E_i}^{E_f} g\Gamma_n^0$ entre Columbia et Saclay montre clairement l'existence d'un désaccord au-delà de 1 keV (tableau III).

TABLEAU II. PARAMETRES DES RESONANCES DU ^{235}U ENTRE 30, 7 ET 41 eV

	Michaudon et al. [Mi 65] d' après σ_t et σ_f de Saclay					Cao et al. [Ca 68] d' après σ_f de Geel avec valeurs de Γ et $2g\,\Gamma_n$ de Saclay				Drawbaugh et Gibson [Dr 66] d' après σ_t de Saclay et σ_c, σ_f et ORNL-RPI					Cramer [CR 69] d' après σ_f de Los Alamos, en tenant compte de σ_c de ORNL-RPI						
E (eV)	$2g\,\Gamma_n$ (meV)	Γ_γ (meV)	Γ_f (meV)	$\frac{2g\,\Gamma_n\Gamma_f}{\Gamma}$ (meV)	$\frac{2g\,\Gamma_n\Gamma_\gamma}{\Gamma}$ (meV)	Γ_f (meV)	Γ_γ (meV)	$\frac{2g\,\Gamma_n\Gamma_f}{\Gamma}$ (meV)	$\frac{2g\,\Gamma_n\Gamma_\gamma}{\Gamma}$ (meV)	$2g\,\Gamma_n$ (meV)	Γ_γ (meV)	Γ_f (meV)	$\frac{2g\,\Gamma_n\Gamma_f}{\Gamma}$ (meV)	$\frac{2g\,\Gamma_n\Gamma_\gamma}{\Gamma}$ (meV)	$2g\,\Gamma_n$ (meV)	Γ_γ (meV)	Γ_{f_2} (meV)	Γ_{f_3} (meV)	Γ_{f_4} (meV)	$\frac{2g\,\Gamma_n\Gamma_f}{\Gamma}$ (meV)	$\frac{2g\,\Gamma_n\Gamma_\gamma}{\Gamma}$ (meV)
30,86	0,52	42	17	0,15	0,36	19	40	0,16	0,35	0,49	37	20	0,17	0,32	0,39	29	+ 20			0,16	0,23
31,55															0,01	29	- 40			0,01	0,00
32,07	1,95	52	46	0,90	1,01	53	45	1,03	0,88	1,87	46	66	1,08	0,75	1,49	29	+ 42			0,87	0,60
33,52	1,92	40	20	0,62	1,24	23	37	0,71	1,15	1,82	44	33	0,77	1,03	1,47	29	+ 22			0,62	0,82
34,34	2,20	47	34	0,88	1,22	38	44	0,98	1,14	2,18	48	48	1,07	1,07	2,18	45		- 42		1,03	1,10
34,83	0,90	60	49	0,40	0,49	84	25	0,69	0,20	1,25	41	116	0,92	0,32	0,60	45		+175		0,48	0,12
35,17	4,50	63	107	2,75	1,62	126	45	3,24	1,16	4,55	52	105	2,95	1,46	5,47	45		-225	-180	4,28	1,07
36,6															0,05	45		-425		0,04	0,01
37,4															0,04	45				0,04	0,00
38,31	0,55	-	-	-	-	-	-	-	-	0,56	84	471	0,48	0,08	0,40	45			+275	0,34	0,06
39,41	2,55	45	47	1,24	1,18	55	38	1,45	1,00	2,46	41	61	1,43	0,96	3,32	45		+450		1,69	1,52
39,90	0,46	-	-	-	-	-	-	-	-	0,31	22	153	0,27	0,04	0,38	45		-150		0,29	0,09
40,51	0,45	-	-	-	-	-	-	-	-	0,41	54	217	0,33	0,08	0,47	45		+200		0,38	0,09
Somme partielle				6,94	7,12			8,26	5,88				8,39	5,91						9,22	5,47
Somme totale	15,95									15,90			9,47	6,11	16,27					10,23	5,71

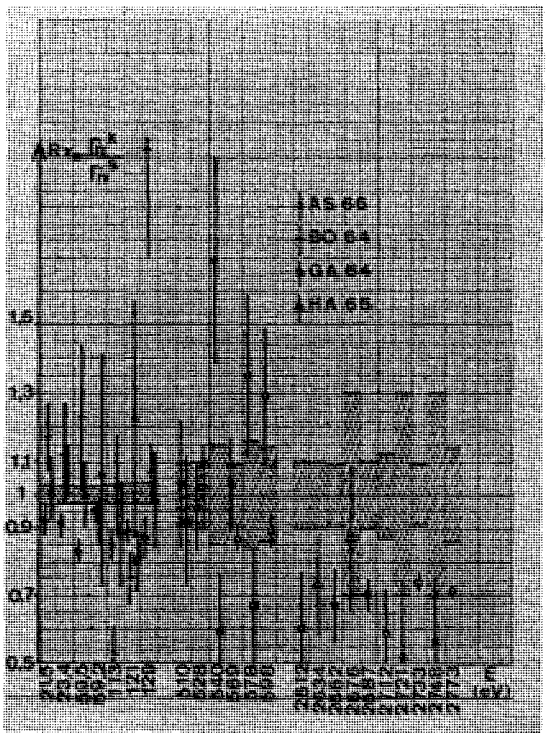

FIG. 2. ^{232}Th – rapport de Γ_n donné par différents laboratoires à Γ_n donné par Saclay [Ri 69] pour quelques résonances de ^{232}Th.

TABLEAU III. VALEUR DE $\sum_{E_i}^{E_f} g\,\Gamma_n^0$ POUR ^{232}Th

Gamme d'énergie	Saclay	Columbia
0 à 1 keV	83 meV	80 meV
1 à 2 keV	92 meV	63 meV
2 à 3 keV	89 meV	65 meV

2.3. Cas du ^{240}Pu

Le meilleur exemple de ces effets systématiques est certainement fourni par les résultats obtenus au BCMN à Geel sur le ^{240}Pu. Ce laboratoire a publié, à la même conférence [5], deux séries de valeurs de Γ_n^0 obtenues l'une d'après une expérience de transmission [Ko 68], l'autre d'après une expérience de diffusion [Ca 68a], différant de ~ 30%.

2.4. Conclusion

Devant une telle situation, l'évaluateur ne peut prétendre effectuer une moyenne des différents paramètres en se fiant uniquement aux valeurs publiées avec leurs barres d'erreurs, mais devra:
- soit choisir un jeu de paramètres publié par un laboratoire,
- soit se reporter aux données expérimentales originales, les étudier, essayer de détecter leurs défauts, et comprendre comment ceux-ci se répercuteront sur les valeurs des paramètres, éventuellement enfin les réanalyser.

3. EXAMEN DES DONNEES EXPERIMENTALES

Ce point a déjà été examiné par James au cours de cette Conférence, mais je vais le reprendre sous un éclairage différent, car un tel examen est essentiel pour une évaluation.

3.1. Distribution en énergie des valeurs expérimentales

Dans la gamme d'énergie qui nous intéresse tous les résultats expérimentaux sont obtenus par la méthode du temps de vol (à part quelques-uns acquis à l'aide de spectromètres à cristal en dessous de ~ 10 eV). Ils sont caractérisés par une largeur de canal constante en temps (à un facteur 2^n, n entier). Un examen des valeurs numériques peut déjà déceler certains défauts; mais pour aller plus loin, il faut comparer entre elles plusieurs expériences.

a) La comparaison des énergies des maximums de sections efficaces (résonances ou groupes de résonances) permet d'évaluer la correction à apporter à une expérience par rapport à une autre; cette correction est de la forme:

$$\delta E = fE + gE^{3/2}$$

Il faut signaler, à ce sujet, un petit défaut assez fréquent; lors d'un changement de la largeur du canal (par exemple doublement de τ à 2τ) il doit exister un intervalle de valeur intermédiaire (soit $1,5\,\tau$ dans l'exemple choisi). Ceci n'est souvent pas le cas.

Nous nous sommes aperçus de ce défaut lors de la comparaison des énergies obtenues par ORNL-RPI sur le ^{235}U [Ds 66] avec celles de BCMN [Ca 68b] (fig. 3).

De tels défauts paraissent avoir peu d'importance, mais ils empêchent de réaliser une analyse de forme simultanée correcte de plusieurs expériences.

b) Cette comparaison permet de mettre en évidence des pertes de canaux résultant d'erreurs lors de la manipulation des données – sans qu'il en résulte une discontinuité en énergie. Nous l'avons constaté dans un cas concernant σ_f de ^{235}U.

Mais un tel défaut est parfois voulu: c'est le cas pour les résultats de Los Alamos. Les physiciens de ce laboratoire appliquent en effet des

lois de transformation temps énergie différentes en dessous et au-dessus de 300 eV, et suppriment quatre ou cinq canaux [Br 66].

c) Cette comparaison peut mettre en évidence des défauts insoupçonnés, tels qu'un dédoublement des résonances dans le cas de Los Alamos (fig.4). Ce défaut apparaît entre 150 et 300 eV. Il est dû au même phénomène qui oblige les physiciens de Los Alamos à utiliser deux lois en temps différentes, à savoir l'existence de deux spectres de neutrons (thermique est de ralentissement) ayant des temps d'émission différents. Ils existent simultanément entre ~ 150 et 300 eV. Et, en comparant les résultats de σ_f de ^{235}U de LASL avec ceux du BCMN, nous avons constaté que le pic de gauche correspond au spectre thermique, celui de droite au spectre de ralentissement.

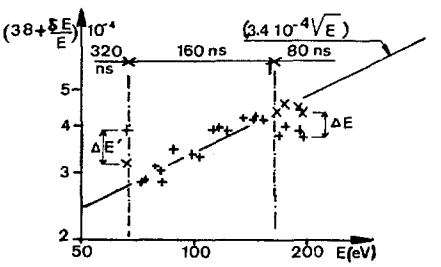

FIG.3. Ecart en énergie entre deux expériences de fission de ^{235}U [Ds 66 et Ca 68]. Les décalages ΔE, ΔE' se produisent lors du changement de largeur de canal de [Ds 66] et proviennent de l'absence d'un canal de largeur 1,5 τ.

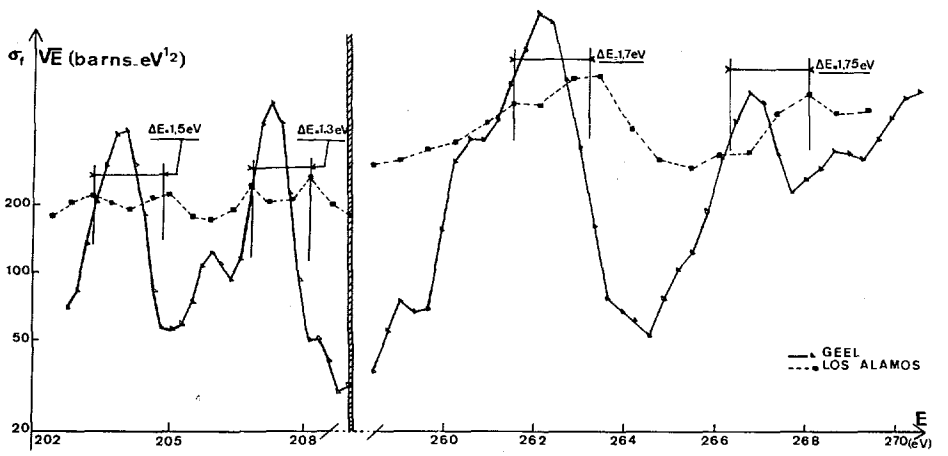

FIG.4. Comparaison de σ_f de ^{235}U mesuré par LASL [Br 66] et BCMN [Ca 68]. La structure très écrasée de LASL montre un dédoublement des pics.

3.2. Comparaison des sections efficaces moyennes

De telles comparaisons sont classiques; James en a présenté au cours de cette Conférence. Les tableaux montrent qu'il y a des différences, sans pouvoir expliquer d'où elles proviennent.

Pour cela nous proposons:

a) De choisir une expérience comme référence en énergie et de corriger les autres expériences pour les amener au même étalonnage en énergie.

b) D'élargir les sections efficaces par une fonction de résolution gaussienne dont la largeur est grande par rapport aux résolutions expérimentales. (Nous avons pris un écart type égal à $0,15\sqrt{E}$.) Les différences entre les sections efficaces ainsi élargies seront alors indépendantes des résolutions expérimentales.

c) De calculer une section efficace moyenne:

$$\sigma(E) = \frac{\sum_i p_i \, \sigma_i (E)}{\sum_i p_i}$$

σ_i étant la section efficace élargie de l'expérience i, p_i étant un poids.

d) De tracer pour chaque expérience:

$$\delta \sigma_i (E) = \sigma_i (E) - \bar{\sigma}(E)$$

Nous pensions que, les défauts étant différents d'une expérience à l'autre, $\bar{\sigma}(E)$ représenterait une moyenne où ces défauts seraient atténués, alors qu'ils apparaîtraient nettement, pour chaque expérience, dans $(\sigma_i (E) - \bar{\sigma}(E))$; plus précisément, nous nous attendions à voir des résultats à peu près confondus dans les zones où il n'y a pas de défauts.

Nous présentons quelques résultats concernant les sections efficaces de fission de ^{235}U.

La figure 5 représente $(\sigma_{f_i}(E) - \bar{\sigma}_f (E))$ entre 650 et 1000 eV. Cette différence présente de nombreuses structures. Nous avons pu en expliquer un certain nombre:

Les grands creux observés dans les données de Geel sont dus à un écran de Mo présent dans le faisceau.

L'interprétation est plus compliquée dans le cas de LASL. On sait que des marques de temps, espacées de 20 μs, sont ajoutées au signal utile; la valeur expérimentale est perturbée, et n'est souvent pas donnée, d'où l'absence de données (perte de un ou deux canaux) à 393, 582, 1045 eV, etc. Mais cette marque existe régulièrement, notamment à 542, 626, 676, 732, 795, 866, 948 eV, et provoque un creux dans σ_f élargi.

Nous n'avons pas pu expliquer les autres fluctuations. Elles existent aux énergies inférieures.

La figure 6 représente $\delta\sigma_i$ entre 40 et 260 eV. On constate un très bon accord entre les récents résultats de Saclay [Bl 70] et ceux de ORNL-RPI [Sa 66] entre 85 et 160 eV. On peut penser que ces deux expériences sont exemptes de défauts dans cette gamme d'énergie. Nous avons pu identifier certains défauts: W pour Geel, notamment.

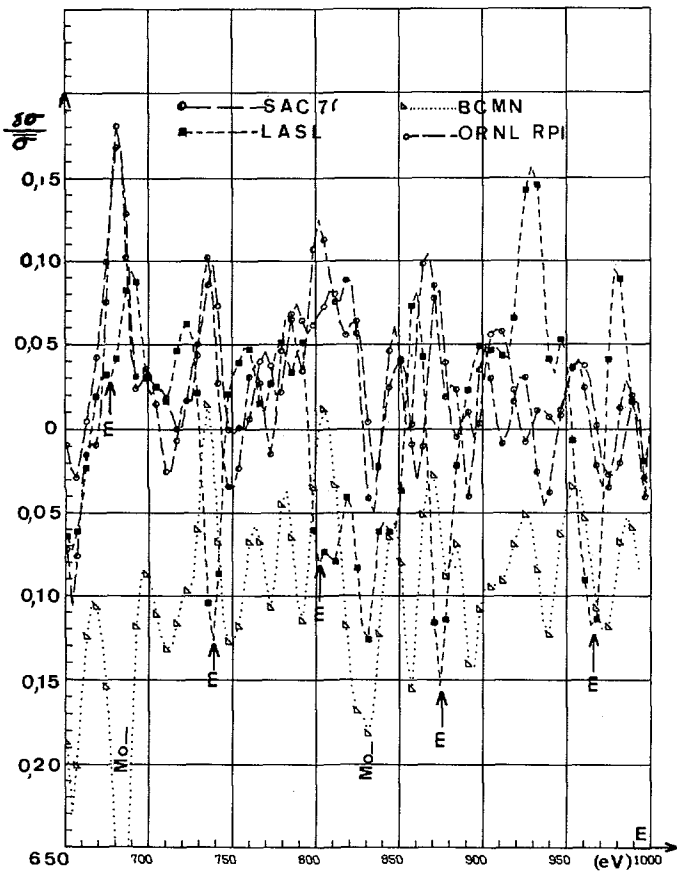

FIG. 5. Comparaison de $\delta\sigma_{f_i} = \sigma_{f_i} - \bar{\sigma}_f$ pour quatre mesures de σ_f de ^{235}U entre 650 et 1000 eV (voir texte).

L'interprétation des données de Doubna est plus difficile; il faut remarquer qu'elles sont les seules à fluctuer considérablement de part et d'autre de 0, et que ces fluctuations sont en opposition de phase avec σ_f (E). Nous voyons deux explications à cela:

a) La résolution réelle est nettement moins bonne que prévu. L'élargissement que nous avons effectué est de 2,6 eV à 55 eV (largeur à mi-hauteur de la gaussienne), alors que la résolution prévue est de 0,45 eV. Il faudrait donc que la résolution équivalente soit six fois plus mauvaise. Ceci serait encore plus net à 20 eV (il faudrait plus d'un facteur 10) [Kr 70].

Si une grande résolution peut expliquer le phénomène observé vers 500 eV, il nous paraît difficile qu'il en soit de même en dessous de 100 eV, bien que nous n'ayons pas analysé les effets de la queue de neutrons du réacteur pulsé de Doubna.

b) Admettre que, systématiquement, la section efficace de fission est sous-évaluée lorsqu'elle est grande et vice versa. Nous ne voyons pas

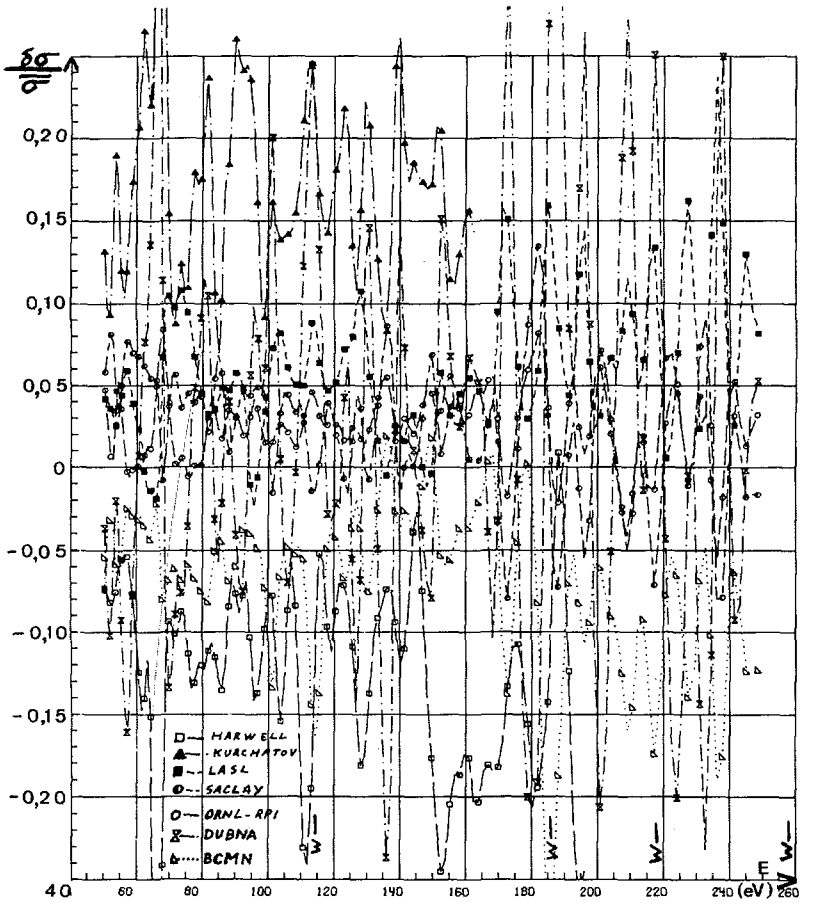

FIG.6. Comparaison de $\delta\sigma_{f_i} = \sigma_{f_i} - \bar{\sigma}_f$ pour quatre mesures de σ_f de ^{235}U (voir texte).

d'explication à cela (il faut néanmoins remarquer que l'effet des diffusions multiples est d'augmenter la probabilité de fission lorsque σ_f est petit).

L'examen de la zone à basse énergie (en dessous de 40 eV) montre des défauts similaires (voir [Kr 70]). De telles courbes montrent qu'en plus d'une différence sur la normalisation il existe des structures fines, en général dues à des défauts locaux, que l'on ne peut ignorer.

3.3. Résolution

C'est un problème bien connu, je ne l'examinerai pas; je rappellerai seulement qu'il peut être très intéressant de réduire l'effet Doppler afin de mieux séparer les résonances – ce qui est une spécialité de Saclay.

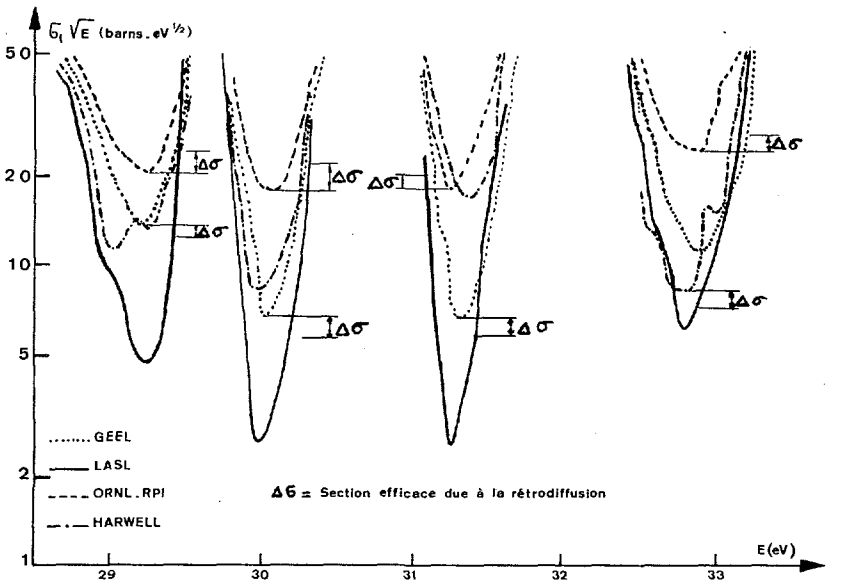

FIG.7. Sections efficaces de fission de ^{235}U entre les résonances d' après quatre expériences. La correction due aux diffusions multiples dans le détecteur est représentée par $\Delta\sigma$.

3.4. Section efficace résiduelle

Il s'agit de la section efficace dans les creux de résonances; sa connaissance est essentielle pour une analyse multiniveau. Elle est perturbée:

- par la résolution
- par des phénomènes expérimentaux divers (diffusions multiples dans les détecteurs, etc.).

Le premier facteur joue peu lorsque les résonances sont assez éloignées l'une de l'autre, et il est en principe toujours possible d'en tenir compte dans l'analyse.

Le second est par contre mal connu: la figure 7 représente les sections efficaces résiduelles pour ^{235}U vers 30 eV.

On constate des différences considérables; les valeurs données par LASL sont les plus faibles de toutes jusqu'à ~50 eV; à partir de cette énergie la résolution obtenue à LASL est insuffisante et elles ne sont plus inférieures aux autres. Ces faibles valeurs sont probablement dues à:

- une très bonne collimation du faisceau de neutrons
- peu de matières dans le faisceau
- peu de bruit de fond, et donc pas d'erreur résultant de son estimation.

La diffusion des neutrons par le détecteur est certainement une des causes de ce défaut; les expérimentateurs n'effectuent jamais la correction correspondante (à l'exception de ORNL-RPI). Cette correction peut être calculée rigoureusement; nous l'avons fait [Le 70] pour quelques expériences, et avons, en particulier, retrouvé les 3% annoncés par de Saussure et al. [Ds 67]. Mais cette correction est toujours insuffisante pour expliquer la différence avec LASL.

Il faut constater que l'amélioration des conditions expérimentales va toujours dans le sens d'une réduction de la section efficace résiduelle. Le cas le plus typique est celui de Bowmann qui, après une expérience donnant des valeurs de σ_f supérieures à celles des autres expérimentateurs [Bo 63], en refit une en soignant particulièrement le problème de la collimation et en diminuant la quantité de matière dans le faisceau: il obtint des valeurs plus faibles que tout autre expérimentateur (hormis Brooks [Br 66a]).

Mais le grave problème est l'impossibilité d'évaluer même approximativement les corrections autres que celles dues aux diffusions multiples dans le détecteur. On ne peut disposer de valeurs correctes de σ_f entre les résonances que de 20 à 40 eV grâce à LASL. Partout ailleurs les résultats des analyses multiniveaux seront sujets à caution.

4. ANALYSES

Ayant des données propres, ou dont les défauts sont connus, l'évaluateur va essayer de les paramétriser. Il dispose pour cela de deux méthodes:
- analyse de forme
- analyse des aires.

La première utilise toute l'information; elle inclut la méthode des aires; celles-ci sont correctes même si les largeurs sont fausses. Elle nécessite de gros moyens de calcul, permet de séparer les résonances superposées, mais ne permet pas, dans ses versions actuelles, d'effectuer des corrections d'autoabsorption ou de diffusions multiples.

Le résultat de la seconde méthode (aire totale) peut être évalué sans gros moyen de calcul; il est indépendant de la résolution et peut être corrigé des effets de l'autoabsorption et des diffusions multiples.

On constate qu'il se produit une spécialisation par laboratoire et par type de noyau: l'analyse de forme est presque seule utilisée pour les noyaux fissiles, alors que l'analyse d'aire l'est pour les éléments fertiles aux résonances bien séparées.

Il est très rare que les mêmes résultats expérimentaux soient analysés par les deux méthodes à la fois, si bien que l'on ne peut exclure la possibilité que certains désaccords soient dus aux méthodes d'analyse. Par exemple, j'ai signalé que les valeurs du Γ_n^0 obtenues à Columbia pour le ^{232}Th entre 1 et 3 keV étaient plus faibles de $\sim 30\%$ que celles que nous avons obtenues (voir § 2.2; [Ri 69]). Or les méthodes expérimentales étaient voisines (même type de détecteur, plusieurs échantillons à la température ambiante à Columbia, une seule épaisseur à basse température à Saclay) alors que les méthodes d'analyse étaient très différentes (méthodes des aires à Columbia, analyse de forme à Saclay).

Je signalerai que les méthodes d'aires partielles, très en vogue il y a quelques années, qui sont en fait des méthodes d'analyse de forme manuelles (avec abaques), ne sont pratiquement plus employées.

Analyses multiniveaux

Il s'agit de méthodes d'analyse de forme tenant compte des interférences dues aux voies de fission. Il en existe plusieurs versions qui supposent toutes que les interférences dues aux voies de capture s'annulent en moyenne (hypothèse statistique). Elles sont basées sur le formalisme de

la matrice R, sauf celle d'Adler et Adler [Ad 66] qui repose sur un formalisme voisin de celui de Kapur et Peierls. Les paramètres introduits peuvent être déduits de ceux de la matrice R, mais non l'inverse: c'est le principal inconvénient de cette méthode.

Les analyses à un niveau introduisent des résonances supplémentaires afin de décrire les interférences; il est donc normal que les niveaux identifiés soient différents de ceux donnés par les analyses multiniveaux; mais quel que soit le formalisme utilisé, ces dernières devraient identifier les mêmes résonances; or nous avons déjà vu qu'il n'en était pas ainsi.

Le tableau IV présente quelques paramètres du ^{239}Pu déterminés par analyse multiniveau.

Les trois auteurs sont bien d'accord pour supprimer la résonance large introduite par l'analyse un niveau à 83,5 eV [De 66]. Ils sont d'accord pour introduire une interférence dominante négative entre les niveaux à ~ 81 et à ~85,5 eV, mais diffèrent sur:

- l'importance de la contribution d'une interférence positive entre ces deux niveaux due à une seconde voie de fission (n'existant pas pour Farrell, valant à peu près 20% de l'interférence négative pour James)
- la nature des interférences avec les autres niveaux
- les valeurs de Γ_f.

La méthode d' Adler et Adler a le gros avantage de ne pas nécessiter l'explicitation des interférences: il ne devrait pas y avoir d'ambiguïté sur les paramètres ainsi déterminés. Les paramètres des niveaux du ^{233}U publiés à cette conférence par les physiciens du BCMN [Ca 70] montrent la comparaison des valeurs de G_f et de H_f obtenues à Geel et à Oak Ridge; ces valeurs ne sont égales (à ±10% près) que 1 fois sur 7, alors que 2 fois sur 7 elles diffèrent de plus d'un facteur 2 et qu'elles sont de signe opposé 1 fois sur 10.

Il faut s'interroger sur l'origine des différences constatées; celle-ci réside en grande partie dans l'imprécision des données expérimentales; l'explicitation des interférences est très délicate, et une faible différence sur les sections efficaces entre résonances peut changer considérablement l'interprétation. Par ailleurs les analyses montrent que l'inclusion des interférences avec des niveaux lointains peut changer sensiblement les valeurs de Γ_f [De 66]; ceci peut être la cause des divergences constatées entre Derrien et James qui analysent les mêmes données par le même formalisme.

5. COMPARAISON DES RESULTATS

Le problème a déjà été abordé en 2.

5.1. Valeurs de Γ_n

5.1.1. Noyaux fertiles

a) Différences entre diffusion et transmission. Le désaccord observé à Geel entre les valeurs de Γ_n du ^{240}Pu obtenues d'après la diffusion et d'après la transmission fut également observé à Harwell [As 69]; comme à Geel, il semble que l'utilisation de la diffusion tende à donner des valeurs de Γ_n plus faibles. (Dans tous les cas l'analyse fut effectuée par la méthode des

TABLEAU IV. PARAMETRES DES RESONANCES DU ^{239}Pu VERS 80 eV D'APRES TROIS ANALYSES MULTINIVEAUX

James [Ja 68], données de Saclay [De 66]. Seuls les niveaux à 81,36 et 85,22 eV sont ajustés					Farrell [Fa 68]					Derrien et al. [De 70]				
E (eV)	Γ_n (meV)	Γ_{f_1} (meV)	Γ_{f_2} (meV)	J	E (eV)	Γ_n (meV)	Γ_{f_1} (meV)	Γ_{f_2} (meV)	J	E (eV)	Γ_n (meV)	Γ_{f_1} (meV)	Γ_{f_2} (meV)	J
57,44					57,30	19,7	1040		0	57,00	14,47	-1554	28	0
60,94	30	5930		0	62,70	13,37	-4250		0	61,86	26,25	7102	20	0
					63,16	0,69	- 54		1	63,02	0,70	80		1
					65,40	0,80	- 39		1	65,50	13,66	2380	1510	0
65,71					65,75	7,57	- 127		1	65,71	9,17	28,5		1
66,57					66,75	4,21		1355	0					
					68,05	0,014	- 250		1					
74,05					74,19	3,32	92		1	74,05	3,37	- 26		1
74,95					74,97	16,4	148		1	74,94	22,78	- 87		1
					77,80	0,35		2000	0					
78,95	0,107	140		1	78,60	0,008	50		1	78,97	0,04	2		1
81,36	5,39	-456	416	0	81,1	8,54	1950		0	80,92	4,95	963	582	0
82,68	0,50	29.5		1						82,67	0,39	10		1
					83,62	0,22	- 74		1					
85,22	57,6	2686	571	0										
85,48	7,86	37		1	85,40	1,48	48		1	85,49	7,45	9,4		1
					85,60	43,5	-1916		0	85,53	53,4	-2010	55	0
96,49	(6,68)	1647		0						96,54	20,66	842	1816	0
100,25	(5,60)		5949	0						101,75	9,05	-4823	25	0

aires.) Les échantillons utilisés étaient les mêmes: aussi les physiciens concernés incriminent-ils un défaut de ceux-ci.

Mais le désaccord existe pour d'autres noyaux. Par exemple, pour le ^{238}U: le tableau publié à cette conférence par Rohr et al. [Ro 70] l'illustre. D'après ces valeurs, on constate que, en moyenne:

$$\Gamma_n \text{ (Harwell)} \sim 0,83\ \Gamma_n \text{ (Geel)}$$

$$\Gamma_n \text{ (Columbia)} \sim 0,94\ \Gamma_n \text{ (Geel)}$$

Nous avons vu que ce désaccord existait aussi pour le thorium (fig.1, [Ri 69]); les largeurs neutroniques des noyaux fertiles ne sont certainement pas déterminées à mieux que ~ 15% en dessous de 1 keV.

b) Différence en fonction de l'énergie. Nous avons en fait remarqué l'existence d'un désaccord croissant avec l'énergie entre Saclay et Columbia pour le ^{232}Th: entre 1 et 3 keV les valeurs données par Columbia sont en moyenne inférieures de 30% à celles de Saclay.

Le même effet existe pour le ^{238}U entre Columbia et Geel; en moyenne, les valeurs de Columbia sont inférieures à celles de Geel de 20% entre 1,5 et 2 keV, et de plus de 40% entre 3 et 3,5 keV. Les méthodes d'analyse étaient en principe les mêmes (méthodes des aires, mais programmes différents); les résolutions sont voisines. La principale différence semble être l'utilisation d'une seule épaisseur d'échantillon à Geel contre cinq à Columbia.

Je ne peux que constater ces désaccords; je ferai néanmoins remarquer que les largeurs neutroniques sont souvent sous-estimées lorsque la résolution est insuffisante; mais ceci ne semble pas devoir expliquer le désaccord entre Geel et Columbia.

Pour conclure, il faut bien se rendre compte que l'incertitude sur Γ_n est de l'ordre de 30% au-delà de 1 keV.

5.1.2. Noyaux fissiles

a) La section efficace totale de ces noyaux a été mesurée à plusieurs reprises depuis 7-8 ans; je citerai, pour ^{235}U, les résultats de Saclay à basse température [Mi 65], ceux de Doubna [Wa 65], de Columbia (non analysés) [Ga 65]; pour le ^{239}Pu, ceux de Saclay (toujours à basse température) [De 66], ceux des deux expériences de Harwell [Pa 66, Ut 67]. Les sections efficaces de diffusion ne sont pas utilisées pour obtenir les valeurs de $g\,\Gamma_n$. Celles-ci sont généralement déterminées par une analyse de forme.

Une comparaison des valeurs de $2g\,\Gamma_n$ données à partir d'expériences indépendantes par des méthodes d'analyse différentes pour le ^{235}U et le ^{239}Pu montre que les désaccords sont importants, mais compatibles avec les barres d'erreurs: surtout il n'apparaît pas d'effet systématique.

b) Utilisant le fait que $\Gamma_n \ll \Gamma$, et donc que la section efficace de diffusion composée est faible, de nombreux auteurs déterminent σ_t d'après des mesures de σ_f et σ_c, en ajoutant une diffusion potentielle constante. On peut montrer qu'il y a un bon accord avec des mesures directes de σ_t (pour le ^{233}U par exemple).

c) Mais il existe une autre possibilité de déterminer g Γ_n: d'après l'analyse multiniveau de la section efficace de fission. Cette méthode est très utilisée par les physiciens de Los Alamos [Cr 69, Fa 68, etc.]. Malheureusement, si les valeurs de Γ_n sont à peu près correctes lorsque les effets des interférences sont importants, c'est-à-dire lorsque Γ_f est grand, il n'en est pas de même dans le cas inverse, et les valeurs de Γ_n n'ont souvent aucun sens: ceci est apparent dans les tableaux II et IV. Les valeurs des aires sont exactes, ce qui prouve que l'erreur provient de l'analyse (partage de l'aire entre Γ_n et Γ_f).

5.2. Valeurs de Γ_γ

Les méthodes d'analyse sont spécialisées: méthode des aires pour noyaux fertiles (avec correction de l'autoabsorption et des diffusions multiples), analyse de forme pour les noyaux fissiles.

Le problème a été examiné par James au cours de cette Conférence, aussi n'en parlerai-je pas. Il faut seulement être bien conscient que la connaissance précise de Γ_γ implique d'abord celle de Γ_n et ne pourra pas lui être supérieure (sauf si $\Gamma_n > \Gamma_\gamma$). Par ailleurs, il apparaît des différences systématiques d'un laboratoire à l'autre: nous avons calculé $\Sigma(\Gamma_n \Gamma_\gamma / \Gamma)$ pour les 20 résonances du ^{238}U étudiées simultanément à Geel [Ro 70], Harwell [As 66a] et Los Alamos [Gl 68] entre 66 et 821 eV; nous obtenons respectivement 290, 266 et 262 meV: il apparaît donc que les aires déterminées à Geel sont systématiquement supérieures de 9 à 10% à celles données par Harwell et Los Alamos. Pour le ^{240}Pu nous avons observé un effet du même ordre, dans le même sens, entre Geel et Harwell [Lh 70].

5.3. Largeurs de fission

J'ai présenté quelques tableaux montrant les valeurs des largeurs de fission selon différents auteurs; les désaccords sont considérables pour le ^{235}U.

Il semble, au contraire, que les valeurs des paramètres (et de Γ_f en particulier) commencent à être bien connues pour le ^{239}Pu.

5.4. Spins

Il existe de nombreuses méthodes de détermination du spin. Il n'est pas dans nos propos de les examiner ici; je ferai seulement remarquer que si les méthodes directes sont assez sûres, l'interprétation des résultats des méthodes indirectes est souvent sujette à caution.

a) ^{239}Pu. La connaissance des spins des résonances de ce noyau a sensiblement progressé ces dernières années [De 66, Fa 68]; les derniers résultats de diffusion de Saclay, qui figurent dans ces comptes rendus, ont encore amélioré cette connaissance. Le ^{239}Pu est sans doute le noyau pour lequel le plus de spins ont été identifiés.

b) ^{241}Pu. Les spins de 22 résonances ont été déterminés à la fois par des mesures de diffusion et par des analyses multiniveaux des sections efficaces de fission; il y a accord complet entre ces déterminations pour

21 résonances, et un désaccord à 29,3 eV qui peut s'expliquer par un manque de résolution. Ceci constitue un bon exemple de la confiance que l'on peut avoir dans la détermination des spins d'après une analyse multiniveau (il faut noter que les spins attribués de 12,78 à 17,83 eV par Moore [Mo 64] doivent être inversés [Lh 70].

6. INTERPRETATION

Il est nécessaire de connaître les lois régissant les fluctuations des sections efficaces dans le domaine des résonances non résolues et les valeurs moyennes des paramètres. Je ferai d'abord une remarque générale sur les distributions des largeurs partielles: le mélange de population, les variations de la largeur moyenne (structures intermédiaires), les erreurs expérimentales aléatoires augmentent tous la dispersion des valeurs, donc réduisent le nombre de degrés de liberté de la loi en χ^2 décrivant la distribution.

6.1. Largeurs neutroniques réduites

Leur distribution est toujours en accord avec une loi en χ^2 à un degré de liberté, même lorsque les valeurs numériques sont très différentes, par exemple pour le ^{239}Pu [De 66, Fa 68] ou pour le ^{235}U [Mi 65].

6.2. Largeurs radiatives moyennes

Il est connu qu'elles fluctuent très peu pour les noyaux fertiles, davantage pour les noyaux fissiles. Les auteurs s'accordent en général à caractériser ces fluctuations par le nombre de degrés de liberté de la loi en χ^2 décrivant la distribution. Ce n'est qu'un moyen commode. Le nombre de voies de capture est toujours supérieur à ce ν équivalent. Mais il existe de grandes différences entre les résultats pour le même noyau, par exemple pour le ^{235}U (tableau V). On peut avancer deux explications à cela:

a) Les valeurs de ν sont déduites de la variance de la distribution expérimentale; or cette variance doit être corrigée des erreurs aléatoires d'origines expérimentales:

$$\frac{2}{\nu_{eq}} = \text{var. distribution} - \text{var. erreurs expérimentales}$$

Ceci n'est pratiquement jamais fait, et suffirait à donner un ν_{eq} très grand (dans le cas des paramètres de Doubna: variance de la distribution = 0,035 – alors que l'erreur sur Γ_γ est, en moyenne, de ~26% – correspondant à une variance due aux erreurs expérimentales de $N \sim 0,067$! Ceci signifie soit que l'erreur sur Γ_γ est en partie d'origine systématique, soit qu'elle vaut plus de 1,5 écart type).

b) Drawbaugh et Gibson ont introduit des résonances en surnombre pour décrire les données expérimentales, sans chercher une réalité physique.

TABLEAU V. INTERPRETATION DES DISTRIBUTIONS DE Γ_γ ET DE Γ_f

	Capture			Fission		Essais de séparation en deux groupes
	ν	Γ_γ (meV)	Remarques	ν	$\bar{\Gamma}_f$ (meV)	
Michaudon et al. [Mi 65]	32	46, 2		4	44, 8	3^- : $\bar{\Gamma}_f = 61$; 4^- : $\bar{\Gamma}_f = 30$
Wang Shi Di et al. [Wa 65]	58	40, 1	a	4		3^- : $\bar{\Gamma}_f = 81$; 4^- : $\bar{\Gamma}_f = 32$
Schmidt [Sc 66]	27	47, 9		4	65	
Drawbaugh et Gibson [Dr 66]	5, 9	46, 8	a	~ 1	144	
Cao et al. [Ca 68]	41	45, 2 ± 1, 2		4 ± 1, 5	53, 2 ± 1, 5	3^- : $\bar{\Gamma}_f = 114$; 4^- : $\bar{\Gamma}_f = 27$
Vorotnikov et Otroshchenko				4, 8 ± 1, 2		D'après 18 résonances
Cramer [Cr 69]		{ 29 pour 3^- 45 pour 4^-	supposé constant	~ 3	131	3^- : $\bar{\Gamma}_f = 114$; 4^- : $\bar{\Gamma}_f = 142$

[a] Nous avons calculé ν et Γ_γ d'après les données expérimentales.

6.3. Largeur de fission moyenne

Les résultats de l'analyse à un niveau du ^{239}Pu et du ^{241}Pu [Yi 67] sont cohérents avec $\nu = 1$ ou 2. La plupart des analyses donnent $\nu = 4$ pour le ^{235}U (tableau V) et pour le ^{233}U [Sc 68]. Ce résultat est anormal car il signifie que le nombre des voies de fission ayant une contribution significative est > 4 pour chaque état de spin, ce qui ne peut être expliqué théoriquement [Gr 65, Ly 66, Ly 68]. Il faut noter que l'analyse de Drawbaugh et Gibson donne $\nu \sim 1$, ce qui paraît plus réaliste. Mais, ainsi que nous l'avons déjà dit, ils introduisent des résonances en surnombre.

Il faut signaler une autre anomalie: les analyses multiniveaux faites en supposant l'existence de deux voies de fission pour chaque état de spin et en supposant qu'il n'y a qu'une voie pour chaque résonance (c'est-à-dire que pour chaque résonance une des deux voies est nettement prépondérante) donnent une distribution des Γ_f compatibles avec $\nu \sim 3$ pour ^{235}U, $\nu = 2$ pour ^{239}Pu ($J = 0^+$), etc., alors que l'on devrait trouver $\nu \sim 1$; l'analyse sommaire de la distribution de Γ_f pour chacune des quatre voies du ^{235}U donne:

1ère voie	$\overline{\Gamma_f} = 72$ meV	$\nu_{ap} = 5,4$
2e voie	$\overline{\Gamma_f} = 144$ meV	$\nu_{ap} = 2$
3e voie	$\overline{\Gamma_f} = 145$ meV	$\nu_{ap} = 3,1$
4e voie	$\overline{\Gamma_f} = 137$ meV	$\nu_{ap} = 5,3$

Le problème de l'interprétation en termes de voies de fission de la structure résonante des noyaux fissiles n'est pas résolu, sauf, peut-être, pour le ^{239}Pu.

6.4. Corrélation entre paramètres

Une corrélation positive entre largeurs partielles, pour le même niveau, a été prévue théoriquement [Kr 63, La 60] et observée entre Γ_n et Γ_γ (ou $\Gamma_{\gamma i}$) pour des noyaux de nombre de masse < 220.

Il n'existe pas de résultat probant quant à une corrélation entre Γ_γ et Γ_f ; celle-ci peut être difficile à mettre en évidence car une erreur systématique, même faible, sur Γ ou sur Γ_f se répercute sur Γ_γ et peut donner une corrélation apparente.

Il faut remarquer que la définition du coefficient de corrélation n'est pas suffisante en soi. Si, par exemple, on a:

$$\Gamma_\gamma = \text{constante} + \epsilon \Gamma_n \qquad \epsilon > 0$$

le coefficient de corrélation entre Γ_γ et Γ_n vaut 1 quel que soit ϵ. En pratique le problème n'est pas du tout le même selon que ϵ vaut 0, 1 ou 10^{-3}. Il faut caractériser une corrélation entre deux paramètres par une autre donnée, une amplitude de corrélation, par exemple le rapport des dispersions des deux paramètres.

TABLEAU VI. PLUTONIUM-240
Valeurs de $(\pi/2)\sigma_0 \Gamma_f$ pour les résonances de deux structures intermédiaires d'après LASL et BCMN

E (eV)	Γ_n^0 (meV)	Aire LASL (b · eV)	Aire BCMN (b · eV)	Remarque
1389	0,38	13,4	8,9	
1401	0,14	26,1	17	superposées
1408	0,29	16,1	25,2	superposées
		Zone morte pour LASL		
1450	1,67	11,4	6,1	
1462	0,55	12,2	2,9	
1841	2,93	27,1	20,1	
1852	0,80			
1873	1,79	5,3	5,4	
1901	4,80	21,2	8,3	superposées
1916	0,82	16,9	38,0	superposées
1943	0,18			
1949	1,89	39,6	46,0	
1956	5,90			
1973	1,53	3,9	8,1	
1991	2,57	1,3	0,02	
1998	0,12			
2016	1,17	10,0	3,4	
2022	1,23			superposées
2033	2,25	16,4	8,7	superposées

6.5. Structures intermédiaires de fission

L'évaluateur ne peut ignorer ce phénomène; James en a traité au cours de cette Conférence. Il a fait l'objet de plusieurs communications à Vienne [6]. Je ferai seulement deux remarques:

a) Le phénomène existe mais est quantitativement mal défini. Le tableau VI représente les valeurs des aires de fission pour les résonances situées dans deux pics de structures intermédiaires du ^{240}Pu, d'après les données de Geel [Mi 68] et de Los Alamos [By 66]. Il apparaît un effet systématique (Geel donne une aire plus grande que Los Alamos lorsque cette aire est grande). Les physiciens de Geel, sont, par ailleurs, en désaccord avec Los Alamos pour le ^{241}Pu [Th 69].

b) L'existence de corrélations entre σ (E) et σ (E + δE) est soupçonnée depuis 13 ans [Eg 58]. De telles corrélations ont été l'objet de nombreuses études. Mais l'interprétation des corrélogrammes est sujette à caution [Pe 69]. Plus récemment plusieurs auteurs ont annoncé l'existence de structures dans les sections efficaces de fission du ^{239}Pu et du ^{235}U [Pa 70] ou montré, d'après des études sur Γ_f, l'existence d'une structure intermédiaire pour la voie 1^+ du ^{239}Pu [Pa 69, Ki 70].

Cet aspect du problème (structure dans les noyaux fissiles) est actuellement en cours d'étude, et on peut penser que nous le connaîtrons beaucoup mieux d'ici un à trois ans.

CONCLUSION

Nous ne connaissons pas encore, à 10% près, les paramètres des niveaux des noyaux de nombre de masse > 220 dans le domaine des résonances résolues, et les interprétations en sont souvent divergentes et contradictoires. Ceci peut être dû:

- aux données expérimentales; il est souhaitable que des mesures plus précises soient effectuées; en particulier, il est nécessaire, pour les analyses multiniveaux, de corriger la section efficace résiduelle entre les résonances;
- aux différences entre les méthodes d'analyse.

Les mêmes données sont rarement analysées par différentes méthodes, si bien que l'on sait difficilement faire la part des deux facteurs.

Il y a quelques années, un exercice de calcul d'une expérience critique a été réalisé sur un plan international; l'expérience a été réalisée après et a permis à chaque participant de comparer les résultats théoriques aux valeurs expérimentales.

Je propose, pour essayer de vérifier les différentes méthodes d'analyse multiniveau, de faire de même: les différents laboratoires participants analyseraient des sections efficaces simulées dont, bien sûr, il ne connaîtraient pas les paramètres. Ceci permettrait de comparer les méthodes d'analyse sur un résultat exempt d'erreur expérimentale et dont on connaîtrait les vrais paramètres.

Je voudrais enfin demander aux physiciens des réacteurs de préciser l'importance que présente pour eux:

a) Les interférences entre résonances: au-delà de quelques dizaines d'eV, est-il nécessaire de recourir à une description multiniveau des sections efficaces ou une description à un niveau, donnant les mêmes sections efficaces moyennes, est-elle suffisante?

b) Les structures intermédiaires: dans quelle mesure est-il nécessaire de décrire en termes de structures intermédiaires la section efficace de fission des noyaux fertiles, tels que le ^{240}Pu?

REMERCIEMENTS

Je remercie M. G. Le Coq pour l'aide qu'il m'a apportée à la préparation de cette étude.

REFERENCES

1/ Nuclear Structure Study with neutron - Anvers 1965 - North Holland Publishing Company, Amsterdam, 1966.

2/ Physics and Chemistry of fission - Conference IAEA, Salzbourg, 1965

3/ Neutron cross section technology, Washington 1966 (CONF. 660 303).

4/ Nuclear data for reactors - Conference IAEA, Paris 1967

5/ Neutron cross section and technology, Washington 1968 (NBS special publication 299).

6/ Physics and chemistry of fission - Conference IAEA, Vienna 1969

7/ RENDA - Compilation of EANDC Requests for neutron data measurements - W. HÄUSSERMANN and S. SCHWARZ (1968)

Ad 66	F.T. ADLER and D.B. ADLER - ref 3 (1966) 873
Ad 68	F.T. ADLER and D.B. ADLER - ref 5 (1968) 967
As 66	M. ASGHAR and al. - Nucl. Phys. 76 (1966) 196
As 66 a	M. ASGHAR and al. - Nucl. Phys. 85 (1966) 305
As 69	M. ASGHAR and al. - rapport EANDC (UK) 103 AL (1969)
Bl 65	J. BLONS et al. - réf. 1 (1965) 564
Bl 70	J. BLONS et al. - ce congrès et communication privée (1970)
Bo 58	L.M. BOLLINGER et al. - Conf. Genève 15 (1958) 127
Bo 63	C.D. BOWMANN et al. - Phys. Rev. 130 (1963) 1482
Bo 64	L.M. BOLLINGER et al. - Phys. Lett. 8 (1964) 45 (voir aussi BNL 325)
Br 66	W.K. BROWN et al. - réf. 3 (1966) 971
Br 66 a	F.D. BROOKS et al. - rapport AERE - ND/GEN 35 (1966)
By 66	D.H. BYERS et al. - réf. 3 (1966) 903
Ca 68	M.G. CAO et al. - J.N.E. 22 (1968) 211
Ca 68 a	M.G. CAO et al. - réf. 5 (1968) 513
Ca 68 b	M.G. CAO et al. - réf. 5 (1968) 481
Ca 70	M.G. CAO et al. - ce congrès
Cr 69	J.D. CRAMER - Nucl. Phys. A 126 (1969) 471
De 66	H. DERRIEN et al. - réf. 4 vol. II (1966) 195
De 70	H. DERRIEN et al. - ce congrès et communication privée

Dr 66 D.W. DRAWBAUGH et G. GIBSON - réf. 4 - vol. II (1966) 251

Ds 66 G. de SAUSSURE et al. - réf. 4 - vol. II (1966) 233

Ds 67 G. de SAUSSURE et al. - rapport ORNL - TM 1804 (1967)

Eg 58 P.A. EGELSTAFF - J. Nucl. Energy 7 (1958) 35

Fa 68 J.A. FARRELL - Phys. Rev. 165 (1968) 1371

Ga 64 J.B. GARG et al. - Phys. Rev. 134B(1964) 985

Ga 65 J.B. GARG et al. - Non publié

Gl 68 N.W. GLASS et al. - réf. 5 (1968) 573

Gr 65 J.J. GRIFFIN - réf. 2, I (1965) 23

Ha 65 E. HADDAD et al. - rapport GA 6272 (1965)

Ha 69 G.C. HANNA et al. Atomic Energy Review VII (1969) 4

Ja 68 G.D. JAMES - Jour. Nucl. En. 22 (1968) 263

Ki 70 Y. KIKUCHI - communication privée à paraître dans N.S.E. (1970)

Ko 68 W. KOLAR et K.H. BÖCKOFF - réf. 5 (1968) 519

Kr 63 T.J. KRIEGER et C. PORTER - J. Math.Phys. 4 (1963) 1272

Kr 70 J. KREBS et al. - ce congrès

La 60 A. LANE et E. LYNN - Nucl.Phys. 17 (1960) 563

Le 70 G. LE COQ - note interne SMPNF

Lh 70 J.P. L'HERITEAU et P. RIBON - EANDC (E) 126 AL

Lh 70 a J.P. L'HERITEAU - note interne SMPNF

Ly 66 J.E. LYNN - réf. 1 (1966) 125

Ly 68 The Theory of Neutron Resonance Recations J.E. LYNN - Clarendon Press, Oxford (1968)

Mi 65 A. MICHAUDON - Thèse - rapport CEA N 2552 (1965)
A. MICHAUDON et al. - Nucl. Phys. 69 (1965) 545

Mi 68 E. MIGNECO et J.P.THEOBALD - réf. 5 (1968) 527

Mo 64 M.S. MOORE et al. - Phys. Rev. 135B(1964) 945

Mo 69 Low Energy Neutron Spectroscopy - Measurements on Fissile nuclides - M.S. MOORE - IN 1222 (1969)

Pa 66 B.H. PATRICK et al. - réf. 4, vol. II (1966) 117

Pa 69 D. PAYA et al. - réf. 6 (1969) 307

Pa 70 B.H. PATRICK et al. - rapport AERE R 6350 (1970)

Pe 69 P.B. PEREZ et al. - réf. 6 (1969) 283

Ra 68	J. RAVIER - rapport PNR/SETR - R 025 (rapport interne CEN/Cadarache) - 1968 -
Ri 69	P. RIBON - rapport CEA - N - 1149 (1969)
Ri 69 a	P. RIBON et J. P. L'HERITEAU - rapport EANDC-E- 115 U (1969) 151 et 156
Ro 70	G. ROHR et al - ce congrès.
Sc 66	J. J. SCHMIDT - rapport KFK 120 - EANDC-E- 35 - U (1966)
Sc 68	M.J. SCHNEIDER - réf. 5 (1968) 615
Th 69	J.P.THEOBALD et al. - communication privée (1969)
Ut 67	UTTLEY et al. - rapport AERE-PP/NP 11 (1967)
Wa 65	S.D. WANG et al. - réf. 2 - vol. I (1965) 287
Wi 67	W.A. WITTKOPF et al. - ENDF 103 (BAW 316) 1967
Yi 67	S. YIFTAH et al. - rapport IA - 1152 (1967)

DISCUSSION

G. ROHR: I would like to make a comment on the variation of the Γ_γ as a function of the neutron energy in ^{238}U, indicated by the measurement of Glass et al. We observed that the Γ_γ curve has a very similar shape to the capture cross-section curve determined with our resonance parameters. We have determined the correlation coefficient for these two curves and have obtained a value of 0. 75. This means that the probability of observing a larger value for non-correlation is less than 3. 5%.

M. ASGHAR: Dr. Ribon's paper is most stimulating but, more than that, it attempts to make an evaluation in depth for the purpose of bringing out the inconsistencies and differences found in the various data on total fission, total capture and scattering cross-sections for various nuclei. I should like to consider the case of our resonance parameters and the Saclay data on ^{232}Th. While the Saclay data consist only of total cross-sections analysed by means of a shape-analysis technique, our values of parameters were obtained from total cross-section measurements on different sample thicknesses which were processed by an area-analysis method in combination with total capture and scattering data. This combining of different types of data should tend to minimize the systematic effects but the fact remains that the disagreement between these two sets of data is still there!

This is also true for both Geel and Harwell, when we compare the resonance parameters of ^{240}Pu (using the same samples) obtained from total cross-sections alone with those determined from the total capture and scattering data. Why is this so? Is it because of the methods of analysis used? Should we not evaluate the methods of analysis too?

P. H. RIBON: My purpose was not to indicate which is the good set of parameters for ^{232}Th, for example, but to draw attention to a systematic effect found in the case of ^{232}Th, ^{238}U and ^{240}Pu, i. e. the values of Γ_n de-

duced by taking scattering experiments into account are lower than those obtained on the basis of transmission alone.

M. ASGHAR: I have one more question. You say in your paper that the number of degrees of freedom ν in fission of ^{235}U is about 4 for one spin state. I thought that this was for both spin states.

P. H. RIBON: The mixing of the populations (i. e. the 3^- and the 4^- levels in the case of ^{235}U) can only increase the variance and thus reduce the number of degrees of freedom ν of the χ^2 -law describing the distribution of Γ_f . If this latter is equal to 4, this means that for one-spin state ν is, at least, equal to 4.

Section IV

NUCLEAR DATA IN THE THERMAL AND RESONANCE ENERGY REGION: A < 220

Chairman
W. HAVENS (USA)

Invited paper

НЕЙТРОНОСПЕКТРОСКОПИЧЕСКОЕ ИССЛЕДОВАНИЕ ЯДЕР С A < 220 В РЕЗОНАНСНОЙ ОБЛАСТИ ЭНЕРГИЙ

Г. В. МУРАДЯН, Ю. Г. ЩЕПКИН,
Ю. В. АДАМЧУК
Институт атомной энергии им. И. В. Курчатова,
Москва,
Союз Советских Социалистических Республик

Abstract — Аннотация

NEUTRON-SPECTROSCOPY STUDY OF NUCLEI WITH A < 220 IN THE RESONANCE ENERGY REGION.

The review paper deals with the possibilities of present-day neutron-spectroscopy experiments from the point of view of obtaining nuclear constants in the resonance energy range required for reactor calculations. It is shown that a further increase of accuracy of the constants is connected with the development of pulsed neutron sources. An analysis of the existing methods for selection of one systems of levels is presented. Several reasons for the discrepancy between the experimental data and the theoretical prediction are considered.

НЕЙТРОНОСПЕКТРОСКОПИЧЕСКОЕ ИССЛЕДОВАНИЕ ЯДЕР С A < 220 В РЕЗОНАНСНОЙ ОБЛАСТИ ЭНЕРГИЙ.

В обзорном докладе рассмотрены возможности современного нейтроноспектроскопического эксперимента с точки зрения получения ядерных констант в резонансной области энергии, необходимых для расчета реакторов. Показано, что дальнейшее уточнение констант связано с развитием импульсных источников нейтронов. Приводится анализ существующих методов выделения одной системы уровней. Рассмотрены некоторые причины отклонения экспериментальных данных от предсказания теории.

I. ВВЕДЕНИЕ

Исследование нейтронных сечений в резонансной области имеет ряд особенностей как с точки зрения получаемой информации, так и с точки зрения требования к технике измерений.

При взаимодействии нейтрона с ядром в этой области проявляются четкие резонансы с шириной от нескольких десятков мэв и выше. Тот факт, что резонансы практически изолированы, дает возможность достаточно точно определить параметры отдельных уровней и проводить их анализ. Из данных по параметрам можно определить усредненные характеристики сечения, такие, как среднее расстояние между уровнями, средние ширины уровней, силовые функции и т. д. Систематизация экспериментальных данных позволяет экстраполировать полученную информацию в область трудноизучаемых энергетических интервалов и ядер, что очень важно для практики и, в первую очередь, для реакторостроения. Эти данные полезны также при анализе проблемы образования элементов во вселенной.

В соответствии с резонансной структурой сечения, техника измерений должна обеспечить такое энергетическое разрешение и статистическую точность, чтобы заметно не искажать ход сечения. Современный уровень техники нейтронного эксперимента вплотную приблизил нас к решению этой задачи. Мы уже давно перешли от единицы мксек/м, характери-

зующей энергетическое разрешение, к единице наносек/м. На лучших спектрометрах достигнуто разрешение, измеряемое долями этой единицы [1-5]. С ростом разрешения и интенсивности нейтронных источников расширяется круг исследуемых проблем и область энергии, которую мы называем резонансной. Одновременно растет точность измерений в "привычной" низкой области энергии.

Для того чтобы оценить уровень развития нейтроноскопических измерений, остановимся несколько подробнее на возможностях экспериментов.

II. НЕЙТРОННЫЙ ИСТОЧНИК

Исследование нейтронных резонансов имеет 30-летнюю историю. За это время создано много различных спектрометров. Наиболее эффективными из них являются спектрометры по времени пролета, которые используют импульсные источники нейтронов. В настоящее время способы регистрации нейтронов и продуктов реакции находятся на довольно высоком уровне, поэтому дальнейшее развитие техники нейтронного эксперимента во многом определяется развитием импульсных нейтронных источников.

Допустим, что мы имеем возможность выбрать нейтронный источник. Попытаемся оценить значения его оптимальных параметров с точки зрения "идеального" нейтроноспектроскопического эксперимента. Это позволит понять качество существующих источников и возможности нейтронных экспериментов на сегодняшний день.

Разумно требовать, чтобы энергетическое разрешение для ядер с $A \sim 100$ в области энергий $E \geqslant 100$ эв не превышало величины

$$\Delta E \simeq 0{,}005\sqrt{E} \qquad (1)$$

так как ширина уровня в этом случае определяется в основном допплеровским уширением:

$$\Delta = 2\sqrt{kT\frac{m}{M}E} \sim 0{,}03\sqrt{E} \qquad (2)$$

Это требование не является чрезмерным, если к тому же иметь в виду область $E < 100$ эв и возможность охлаждения образца.

Для нахождения величины пролетного расстояния зададимся неопределенностями во времени и в пролетном расстоянии. Пусть $\Delta L = 0{,}04$ м, а $\Delta t = 2/\sqrt{E}$ мксек. Последняя величина всего в $\sim 1{,}5$ раза больше времени замедления. Отсюда находим величину пролетного расстояния, которое обеспечивает разрешение (1):

$$L_M = 20\sqrt{E(\text{эв})} \qquad (3)$$

Как видно из этого выражения, при $E = 10$ кэв пролетная база составляет 2000 м! Пока что ни на одном источнике с такими Δt и ΔL не имеется столь длинная база. Имеющиеся базы не превышают 300 м (исключая ОИЯИ, где $\Delta t = 2$ мксек), что обеспечивает разрешение $\Delta E \leqslant 0{,}005\sqrt{E}$ только до энергии ~ 250 эв. Таким образом, по всей вероятности, в будущем нам понадобятся более длинные пролетные базы.

Зная величину необходимого пролетного расстояния, можно определить параметры источников. Найдем частоту посылок импульсов. Если потребовать, чтобы максимальная энергия рециклических нейтронов была в ~10 раз меньше исследуемой, то получим $\nu \simeq 220$ гц.

Для того чтобы оценить интенсивность источника, рассмотрим конкретно измерение сечения захвата. Предположим, что спектр нейтронов $\sim E^{-0,8}$. Такой спектр получается в результате замедления быстрых нейтронов ($E_{нач}$ 1-3 Мэв) с помощью полиэтиленового замедлителя толщиной 2,5 см [6]. Пусть количество изучаемого изотопа составляет 20 г, атомный вес – 100, эффективность детектора – 20%, статистическая точность измерений – 2%. Полагая далее, что разрешение задается формулой (1), найдем

$$\Phi \cdot t \cdot \sigma_\gamma \simeq 1,7 \cdot 10^{14} \cdot E^{1,3} \qquad (4)$$

где Φ – полное число нейтронов, вылетаемых из мишени за секунду, t – время измерения в часах, σ_γ – измеряемое сечение в барнах, E – энергия нейтронов, при которой проводится измерение σ_γ.

Для $E = 10^4$ эв, $t = 100$ час и $\sigma_\gamma = 2$ барна получаем $\Phi = 1,3 \cdot 10^{17}$ нейтр/сек. При этом длительность нейтронного импульса составляет ~10 наносек, а пролетная база ~2000 м.

Заметим, что мы здесь нашли параметры необходимого источника, не принимая во внимание многих "деталей". В частности, частота $\nu = 220$ гц и пролетная база $L = 20\sqrt{E}$ обеспечивают возможность измерения с разрешением $\Delta E = 0,005\sqrt{E}$ только при заданной энергии E. Чтобы одновременно получить и область низких энергий, где разрешение более чем достаточно, необходимо уменьшить частоту и, соответственно, увеличить интенсивность. Эта мера полезна также и с точки зрения уменьшения как естественного фона, так и фона, связанного с источником нейтронов.

Рассмотрение задачи для измерения полного сечения ($\sigma_T \simeq 15$ барн), аналогичной измерению сечения захвата, также приводит к интенсивности 10^{17} нейтр/сек. При расчете этой величины мы считаем, что площадь детектора составляет ~5000 см^2, площадь излучающей поверхности источника – 100 см^2, а $n\sigma_T \simeq 1$.

Ни один из существующих источников не имеет таких параметров. Наиболее сильный источник, недавно запущенный в Ок-Ридже [7], при частоте посылок $\nu = 1000$ гц имеет интенсивность $\Phi \simeq 10^{14}$ нейтр/сек. Таким образом, для проведения указанных экспериментов при ~10 кэв не хватает трех порядков по интенсивности. Поставленную задачу можно решить только в области $E \leqslant 0,5$ кэв. При $E > 0,5$ кэв необходимо увеличить количество исследуемого вещества, время измерения или ограничиться исследованием сечений в районе достаточно сильных резонансов. По оценкам [8] для получения интенсивности $\sim 10^{17}$ нейтр/сек линейный электронный ускоритель уже не пригоден. Если бы даже можно было получить нужное количество электронов в импульсе, то перед нами встала бы проблема теплосъема. Это дает основание думать, что перспектива получения $\Phi \sim 10^{17}$ нейтр/сек связана с применением протонных ускорителей.

Если же при проведении описанных выше экспериментов ограничиться разрешением $\Delta E \simeq 2\Delta$, то требуемая интенсивность источника составит величину $\Phi \simeq 10^{14}$ нейтр/сек, т. е. решение задачи уже возможно на существующих ускорителях.

В последние годы, наряду с изучением зависимости сечения от энергии падающего нейтрона, измеряются еще и другие характеристики, в том числе зависимость сечения от энергии продуктов реакции. К таким измерениям относятся, в частности, спектр γ-лучей захвата [9] и спектр α-частиц [10,11]. Заметим, что эти двухмерные измерения требуют несравненно более мощный нейтронный источник.

III. ВОЗМОЖНОСТИ ВЫДЕЛЕНИЯ ОДНОЙ СИСТЕМЫ УРОВНЕЙ

Для наиболее эффективного сопоставления нейтронных сечений с предсказаниями теории, а также для их использования в реакторостроении необходимо выделение уровней, принадлежащих определенному изотопу и имеющих одинаковые квантовые характеристики – спин и четность. Такое разложение сечений является непростой задачей. Однако большая актуальность этой задачи постоянно стимулирует экспериментаторов искать методические возможности ее решения.

В сущности для определения квантовых характеристик уровней требуется измерение определенного класса сечений. Измерение некоторых из них в общем случае вызывает большие трудности, поэтому наши возможности выделения одной системы уровней в известной мере характеризует развитие экспериментальных методов исследования сечений.

1. Возможности определения спинов уровней

Классический метод разделения уровней по спину сводится к измерению сечений поляризованных ядер с помощью поляризованных нейтронов. Проблема получения поляризованных нейтронов в широкой энергетической области от долей эв до нескольких десятков кэв успешно решается в Объединенном институте ядерных исследований (ОИЯИ) [12,13]. В настоящее время при уменьшении интенсивности всего в 5 раз степень поляризации нейтронов составляет ~60%. Слабым звеном осуществления программы измерения спина является трудность получения поляризованных ядер.

Универсальным методом поляризации ядер является метод Саймона (метод "грубой силы"). До сих пор он еще не использовался в нейтронных исследованиях, хотя в последнее время здесь достигнут существенный прогресс в связи с развитием сверхпроводимости и криогенной техники. С помощью растворения ^{3}He в ^{4}He (гелиевые холодильники) удается получить температуры $t° \sim 0{,}01°K$ при хладопроизводительности $\sim 10^3$ эрг/сек [14,15]. Имея ввиду, что поляризация $p = 10^{-7}$ H/t°, а достигнутые поля в достаточно большом объеме $\sim 10^5$ гаусс, можно получить заметную степень поляризации.

Другие методы, например метод с использованием внутреннего магнитного поля ядер, достаточно эффективны, но могут применяться только для ограниченного круга элементов [13,16].

Другая принципиальная возможность идентификации уровней по спину сводится к измерению полных и парциальных сечений. В качестве парциальных сечений можно использовать сечения захвата (σ_γ) или рассеяния (σ_s). Если для простоты предположить, что Γ и $g\Gamma_n$ известны без ошибок и для определения I использовать какое-либо из сечений σ_γ или σ_s, то точность определения последних должна быть не хуже следующих

$$\frac{\Delta\sigma_\gamma}{\sigma_\gamma} = \frac{1}{2I+1}\cdot\frac{\Gamma_n}{\Gamma_\gamma}\cdot 100\% \qquad (5)$$

$$\frac{\Delta\sigma_s}{\sigma_s} = \frac{1}{2I+1}\cdot 100\% \qquad (6)$$

где I – спин ядра мишени.

Зависимость этих величин от Γ_n/Γ_γ и I приведена на рис.1. Видно, что при $\Gamma_n/\Gamma_\gamma \leqslant 1$ (в случае $\Gamma_n/\Gamma_\gamma \geqslant 1$ определение спина не вызывает больших затруднений) к измерениям рассеяния предъявляются менее жесткие требования. К сожалению, это достоинство рассеяния практически не реализуется из-за экспериментальных трудностей, связанных с низкой эффективностью регистрирующих устройств и с резонансным фоном γ-лучей захвата [17]. Наоборот, в этом отношении измерение захвата имеет значительные преимущества. Для измерения захвата характерна высокая эффективность регистрации и хорошее соотношение эффекта к фону. Основная трудность измерения σ_γ сводится к обеспечению постоянной эффективности регистрации акта захвата для исследуемых резонансов. В настоящее время использование детекторов Моксона-Рая [18-20] и жидкостных сцинтиллирующих баков [21,22] позволяет получить постоянство эффективности ϵ_γ в пределах нескольких процентов.

Интересно оценить времена измерений, обеспечивающих точность (5) и (6). Оценка показывает, что для Γ_n = 10 мэв и Γ_γ = 100 мэв отношение времен измерений составляет: $t_s/t_\gamma \sim 10$ и ~ 300 при E = 100 и 1000 эв, соответственно. При оценке мы предположили, что пролетная база составляет 50 м, временная неопределенность $-2/\sqrt{E}$ мксек, неопределенность в пролетном расстоянии – 3 см, а эффективность регистрации захвата и рассеяния – 50% и $15\%/\sqrt{E}$, соответственно. Из приведенной оценки ясно видно преимущество измерения захвата. Это преимущество усиливается по мере увеличения энергии нейтрона.

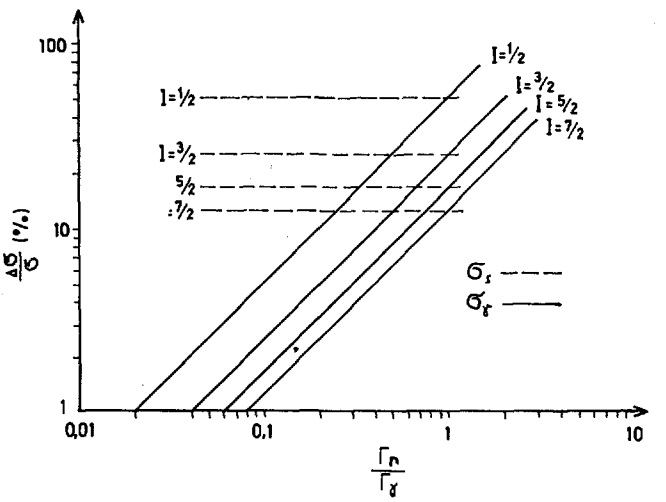

Рис. 1. Зависимость величины допустимой ошибки от Γ_n/Γ_γ в измерениях сечения захвата и рассеяния при определении спина уровня составного ядра I.

Для определения спинов уровней в последнее время интенсивно развиваются методы, использующие зависимость способа распада составного ядра от спина. По сравнению с предыдущими двумя методами, они пригодны для определенного круга ядер, но в большинстве случаев, когда их применение не вызывает сомнений, они позволяют идентифицировать гораздо большее число уровней. Один из таких методов, с помощью которого промерены ядра ^{177}Hf, ^{179}Hf, ^{95}Mo, ^{97}Mo, ^{99}Ru, ^{101}Ru, ^{105}Pd [23], основан на зависимости числа испущенных γ-квантов (множественность) от спина уровня. Измеряется отношение числа актов захвата в режиме регистрации одиночных γ-квантов к числу случаев в режиме совпадений. Оказывается, что это отношение (R_I) зависит от спина I. Для измеренных ядер ΔR_I^0 лежит в пределах $10 \div 20\%$. Наблюдаемая величина R_I^0 находится в качественном согласии с расчетным значением [23,24], а результаты по ^{105}Pd полностью согласуются с данными Боллингера [25], где спины идентифицированы по относительной интенсивности двухкаскадных переходов. На рис.2 приведено распределение величины R_I^0 для палладия. Четко видны две группы уровней.

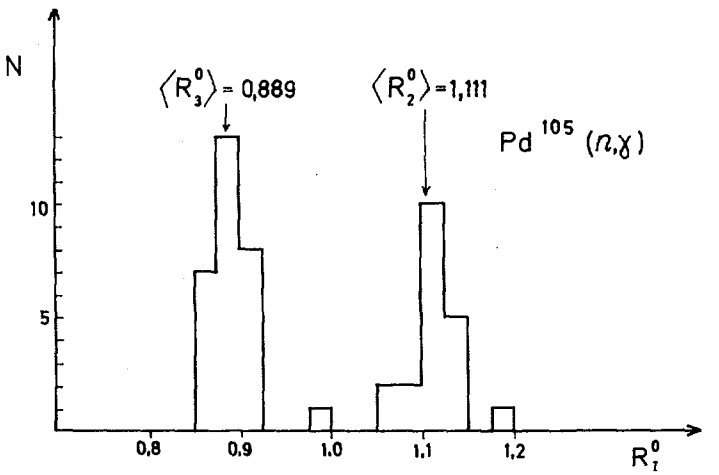

Рис. 2. Гистограмма величины R_I^0 для резонансов ^{105}Pd [23].

Благодаря применению кристаллов NaJ(Tl) метод идентификации по множественности является простым и светосильным.

При определении спинов уровней по γ-переходам можно использовать также и различную заселенность низлежащих уровней от спина [24]. Это приведет к различным интенсивностям переходов на основное или окололежащие состояния. В частности, таким образом определены спины ряда уровней ^{235}U [26]. Различие указанных интенсивностей переходов в этом случае составляет $20 \div 40\%$.

Для ядер, у которых при захвате нейтрона образуются состояния 0^- или 1^-, а основным состоянием является 0^+, заключение о спине уровней можно сделать на основе анализа спектров γ-лучей захвата [27]. В этом случае отсутствие перехода на основное состояние указывает, что $I^\pi = 0^-$.

2. Идентификация уровней по орбитальному моменту налетающего нейтрона

Отсутствие систематических экспериментальных данных по орбитальным моментам резонансного взаимодействия налетающего нейтрона (ℓ) с ядром связано, в основном, с недостаточной мощностью нейтронных источников. При существующих источниках проведение идентификации уровней по ℓ возможно только в ограниченной области E и Γ_n и при наличии достаточного количества разделенных изотопов высокого обогащения.

При $E \leqslant 100$ кэв во взаимодействии участвуют нейтроны с $\ell = 0$ и 1 (s и p – нейтроны), поэтому задача по определению ℓ сводится к идентификации s и p – уровней. В этой области энергии s и p – уровни значительно отличаются по силе интерференционного члена в сечении рассеяния и, естественно, в полном сечении. Практически это приводит к тому, что в отличие от p-уровней, s-уровни являются асимметричными по отношению к резонансной энергии E_0 .

Для выявления степени асимметрии уровня необходимо проводить измерения пропускания (или сечения рассеяния) с разрешением $\Delta E \leqslant \Delta/2$. При существующих нейтронных источниках такой метод позволяет идентифицировать s-уровни с $\Gamma \leqslant \Delta$ в области $E \leqslant 2$ кэв [5,28].

Намного более светосильным методом обнаружения асимметрии уровня является метод движущегося образца [29,30], где, в отличие от предыдущего, разрешение спектрометра должно обеспечить возможность лишь разделения уровней ($\Delta E \leqslant D/3$, где D – расстояние между уровнями). Этим способом на относительно слабом нейтронном источнике идентифицированы уровни ^{93}Nb [31] до энергии ~1,5 кэв, ^{120}Sn [32] до энергии ~10 кэв и уровень 1256 эв (ℓ=1) ^{56}Fe.

Для нахождения орбитального момента можно использовать и другой принцип – угловое распределение продуктов реакции. В измерениях упругого рассеяния нейтронов s и p идентификацию можно провести по интерференции потенциальной s-амплитуды с резонансной p-амплитудой. Для таких измерений также требуется наличие хорошего разрешения $\Delta E \sim \Delta$. Недавно опубликована первая удачная попытка такого измерения [33].

В ряде случаев p-уровни можно идентифицировать по преимущественному рассеянию p-нейтронов вперед и назад, когда $d\sigma_{l=1} \sim \cos^2\theta$. При этом разрешение спектрометра должно обеспечить возможность лишь разделения уровня ($\Delta E \leqslant D/3$).

Идентификация уровней по четности для некоторых возможных значений I проводится по анизотропии углового распределения прямых γ-переходов, проявляющейся при взаимодействии p-нейтронов [34]. Величина анизотропии составляет от нескольких процентов до нескольких десятков процентов в зависимости от спина начального и конечного состояния. Основное ограничение метода – низкая светосила, связанная с малой эффективностью используемых в этой задаче Ge-Li детекторов.

В ряде случаев заключение о четности уровня составного ядра можно сделать из характера спектра γ-лучей захвата нейтрона. Однако, из-за больших флуктуаций парциальных ширин $\Gamma_{\gamma i}$ и широкого диапазона в соотношении интенсивностей E1, M1, E2-переходов, идентификация по ℓ носит в значительной степени вероятностный характер.

На рис.3 приведено сравнение рассмотренных методов идентификации уровней по ℓ с точки зрения необходимого времени измерений. При этом время измерения в экспериментах по рассеянию рассчитывалось для

случая обнаружения преимущественного рассеяния p-нейтронов вперед и назад.

Рассматривался случай ядра с A = 100 и σ_p = 5 барн для резонансного уровня с Γ_n = 20 мэв, Γ_γ = 100 мэв, $\Gamma_{\gamma i}$ = 1 мэв и расстоянием между уровнями D = 30 эв.

При идентификации уровней величина разрешения в методе изучения формы принималась равной Δ/2, а в остальных экспериментах D/3. Остальные параметры, используемые в оценке времени измерений, приведены в табл. 1.

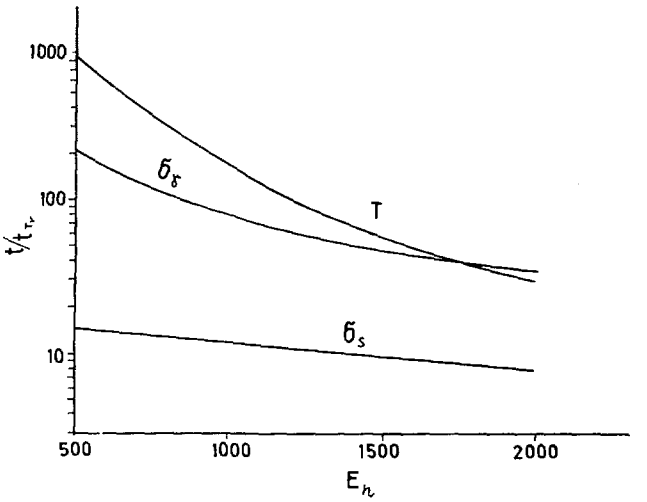

Рис. 3. Время измерения, необходимое для идентификации s и p-уровней в экспериментах по пропусканию (T), угловому распределению γ-лучей захвата ($\sigma_{\gamma i}$) и рассеянию нейтронов (σ_s) в единицах времени измерения, необходимого в эксперименте методом движущегося образца (T_v). E_n – энергия падающего нейтрона.

ТАБЛИЦА 1. ПАРАМЕТРЫ, ИСПОЛЬЗУЕМЫЕ В ОЦЕНКЕ ВРЕМЕНИ ИЗМЕРЕНИЙ

Параметры \ Энергия		(E эв)		
		500	1000	2000
n_T ат/барн	T, T_v	0,035	0,035	0,035
n_D ат/барн	T_v, $\sigma_{\gamma i}$	0,01	0,01	0,01
	σ_s	0,0025	0,0025	0,0025
ϵ (%)	T	20	20	20
	T_v	50	50	50
	σ_s	3	3	3
	$\sigma_{\gamma i}$	1	1	1
S	T	5	5	5
	T_v, σ_s, $\sigma_{\gamma i}$	1	1	1
δE	T	Δ	Δ	Δ
	σ_s	2ΔE	2ΔE	2ΔE
a	T	0,1	0,2	0,4
	T_v, σ_s, $\sigma_{\gamma i}$	0,5	1	2

В табл.1 $T, T_v, \sigma_s, \sigma_{\gamma i}$ обозначают методы определения ℓ в измерениях пропускания, движущегося образца, углового распределения рассеянных нейтронов и прямых γ-переходов. n_T, n_D – числа атомов на барн соответствующих образцов, ϵ – эффективности детекторов, δE – энергетический интервал, в котором заключен уровень, ΔE – ширина функции разрешения, "a" – отношение фона к эффекту, S – площадь образца в относительных единицах.

Время измерений определялось из условия получения статистической точности, равной разности ожидаемых эффектов между s – p -взаимодействием.

В расчете не учитывалось влияние рециклических нейтронов, фон от γ-лучей захвата и вторичные процессы в измерениях дифференциального сечения рассеяния.

Таким образом, хотя представленный расчет носит в значительной степени качественный характер, видно, что для идентификации резонансов по орбитальному моменту методом движущегося образца в рассматриваемой области энергий требуется значительно меньшая длительность циклов измерений, что особенно существенно при низкой интенсивности источника нейтронов или при малых количествах исследуемого вещества.

IV. О НЕКОТОРЫХ ТЕНДЕНЦИЯХ ТРАКТОВКИ ЭКСПЕРИМЕНТАЛЬНЫХ ДАННЫХ

При рассмотрении нейтронных сечений в области, где проявляются резонансные уровни, возникает естественный вопрос – каким закономерностям подчинены параметры резонансов?

В случае простых систем, например в случае гармонического осциллятора, по одному расположению уровней можно было бы получить много сведений о взаимодействии. Однако для подавляющего большинства ядер взаимодействие настолько запутано, что по резонансной картине невозможно сколько-нибудь однозначно определить детали внутриядерного взаимодействия.

При взаимодействии нейтрона с ядром энергия возбуждения составной системы имеет величину 5-10 Мэв. При столь высоких возбуждениях навряд ли можно надеяться, что для ядер с $A \geqslant 10$ современная теория сможет предсказать расположение уровней и их ширины. Эта ситуация в какой-то мере является общей для всей ядерной физики и связана со сложностью проблемы многих тел и недостаточно хорошо известной природой ядерных сил, имеющей весьма непростой характер [35].

Отказываясь от точного решения задачи, мы вынуждены пользоваться моделями, которые лишь приближенно передают различные стороны поведения ядра. В настоящее время в рамках различных моделей удается описывать поведение таких характеристик резонансных нейтронных сечений, как среднее расстояние между уровнями, распределение расстояний и ширин уровней, силовые функции и т.д. Хотя эти величины в совокупности и не определяют ход сечений с энергией, тем не менее, они несут большую информацию о сечении взаимодействия нейтрона с ядром.

В некоторых случаях, в частности, при расчете силовой функции по оптической модели и при описании распределения расстояний между уровнями, индивидуальные свойства отдельных ядер не входят в теорию. Совершенно не исключено, что такое пренебрежение является весьма гру-

бым с точки зрения отдельно взятого ядра. Но даже в этом случае теория является полезной, поскольку из сопоставления результатов измерений с такой теорией можно определить, насколько ядра сохраняют свою индивидуальность при возбуждениях $\sim 7 \div 10$ Мэв.

В последние годы многие экспериментаторы уделяют большое внимание именно такому подходу к результатам своих измерений. Следует отметить, что обнаружение отпечатков индивидуальности не является простой задачей. Здесь мы сталкиваемся с трудностями, связанными как с экспериментом, так и с флуктуациями самих измеряемых величин.

Рассмотрим, в частности, распределение расстояний (D) между уровнями – $P(D/\langle D\rangle) \equiv P(x)$. Теория этого распределения исходит из того, что все возможные типы внутриядерных взаимодействий равновероятны [36-38]. На выбор ансамбля взаимодействий налагаются лишь общие требования – инвариантность по отношению к инверсии времени и пространственных вращений. Получаемое распределение имеет плавную форму и стремится к нулю при $x \to 0$ ("отталкивание уровней"). В случае наложения двух независимых систем уровней это распределение также является плавным.

Для сопоставления экспериментального распределения с теоретическим необходимо, чтобы сведения о положении уровней были получены на спектрометрах с высоким разрешением. Такие измерения в последние несколько лет проведены в основном на колумбийском синхрофазотроне и на линейном электронном ускорителе в Сакле. Хорошее согласие эксперимента с теорией получены, в частности, для ^{238}U [39] и ^{197}Au [3], имеющих одну и две системы s-уровней, соответственно.

Вопрос отклонения экспериментального распределения P(x) от распределения Вигнера $P_w(x)$ обсуждался в связи с данными по ^{232}Th [40]. Сейчас появились и другие данные, в частности по ^{109}Ag [41] и ^{123}Sb [42] (рис.4), где также обнаружены отклонения от теоретического распределения.

В работе [43] обращается внимание на то, что отклонения в P(x) можно рассматривать с точки зрения существования выделенных интервалов (между уровнями), которые имеют тенденцию совпадать у ряда ядер. Эти интервалы отсчитываются от нулевого значения кинетической энергии нейтрона.

Для более определенных выводов необходимо проведение измерений большого количества ядер с достаточно хорошим разрешением.

Значительное количество информации о взаимодействии нейтрона с ядром получается из исследования нейтронных силовых функций $S_{\ell Ij} = \langle \Gamma^{(\ell)}_{nIj} \rangle / \langle D_{\ell Ij} \rangle$ (здесь $\langle \Gamma^{(\ell)}_{nIj} \rangle$ – средняя приведенная нейтронная ширина для системы уровней со спином I, j – полный момент нейтрона, ℓ – орбитальный момент). В отличие от распределения расстояний между уровнями в случае силовой функции мы имеем дело со средним параметром ядра $S_{\ell Ij}$, что упрощает экспериментальную задачу по его определению.

Величину силовой функции можно получить из измерений средних полных сечений [44], из измерений среднего сечения радиационного захвата [45,46] и путем определения параметров уровней в резонансной области [47].

Наибольшее количество данных по S_0 – силовой функции получено в резонансной области энергии, а по S_1 – из измерений средних сечений, позволяющих обойти вопрос идентификации уровней по четности. Для боль-

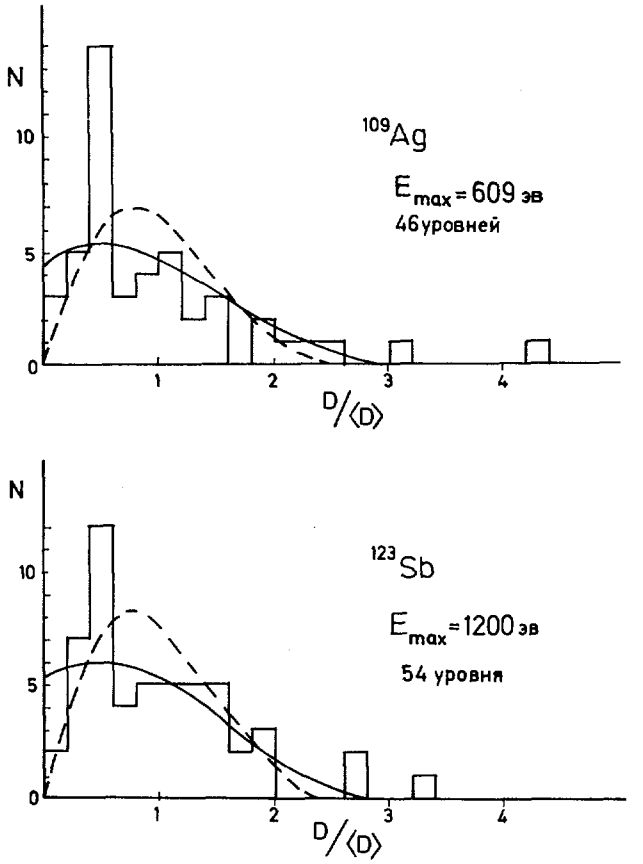

Рис. 4. Распределение расстояний между уровнями для изотопов ^{109}Ag [41] и ^{123}Sb [42]. Пунктирная и сплошная кривые – ожидаемые распределения для одного из двух систем уровней, соответственно.

шинства ядер точность определения S_0 выше чем S_1. Величины S_0, полученные из разных экспериментов, согласуются между собой, в то время как для S_1 силовых функций существуют значительные расхождения. Например, для ^{93}Nb наиболее последние данные, полученные из измерений $\langle \sigma_\gamma \rangle$, дают (в единицах 10^{-4}) значения $S_1 = 11{,}0 \pm 3{,}2$ [46] и $S_1 = 3{,}3 \pm 1{,}8$ [48]; для ^{238}U из измерений $\langle \sigma_T \rangle$ получены величины $S_1 = 2{,}47 \, ^{+0{,}16}_{-0{,}28}$ [49] и $S_1 = 0{,}50 \pm 0{,}25$ [44].

Исследование силовых функций оказывает большое влияние на понимание механизма взаимодействия нейтрона с ядром. Одни из первых результатов по S_0 [50] показали неприменимость модели ядра как сильно поглощающей среды и подтвердили предложенную Портером и др. [51] оптическую модель.

В дальнейшем, по мере накопления информации, оказалось, что оптическая модель в своем простейшем виде не в состоянии описать всю со-

вокупность экспериментальных данных по силовым функциям. Возникла необходимость к усовершенствованию модели, путем введения дополнительных параметров – диффузной границы, ядерной деформации, спин-орбитальной связи и различных видов поглощения (объемного, поверхностного, смешанного, вынесенного за пределы ядра). Введение деформации явилось шагом к учету некоторых индивидуальных свойств ядра [52]. Однако получить удовлетворительное согласие для всех ядер не удалось, в особенности, в районе минимума S_0 – силовой функции (A = 90 ÷ 130). В частности, значение S_0 для ^{120}Sn, полученное с учетом идентификации уровней по ℓ [32], составляет $(0{,}08\ ^{+0{,}1}_{-0{,}04})\cdot 10^{-4}$, что в ~10 раз меньше предсказываемого значения по оптической модели [52].

В то же время значение S_1 – силовой функции для ^{120}Sn, равное $(3{,}7\ ^{+1{,}8}_{-0{,}9})\cdot 10^{-4}$, согласуется с оптической моделью. Низкое значение S_0 в данной области A получено также для некоторых других изотопов олова [53,54], для изотопов сурьмы [42] и Te [1].

Другая особенность экспериментальных данных, не укладывающихся в рамки оптической модели, – скачкообразное изменение силовой функции для соседних ядер. Хотя в этом вопросе отсутствует статистический анализ, аналогичный проведенному в работе [55], тем не менее, для ряда ядер, например изотопов серебра [41], существует различие, лежащее вне пределов ошибок.

Блок и Фешбах [56] предложили механизм взаимодействия нейтрона с ядром, в котором учитывается оболочечная структура ядра. Они предположили, что образование составного ядра происходит через промежуточные трехквазечастичные состояния. По этой схеме падающий нуклон испытывает действие потенциала ядра и образует виртуальное одночастичное состояние. Затем, вследствие остаточного взаимодействия, нейтрон может возбудить один из нуклонов ядра, образуя состояние "две частицы – дырка" (2p - 1h). Это состояние является более сложным, чем одночастичное, но более простым, чем составное ядро. Остаточное взаимодействие может затем перевести 2p - 1h состояние в более сложные образования (3p - 2h, 4p - 3h и т. д.), пока не образуется составное ядро. Таким образом, вероятность образования составного ядра и степень сложности его конфигурации определяется вероятностью перехода из начального одноквазичастичного во все трехквазичастичные и более сложные состояния, допустимые принципом Паули и законами сохранения энергии, полного момента и четности.

Рассмотренный механизм образования составного ядра был подтвержден рядом экспериментальных данных. Например, в работе [57] были проведены измерения средних полных сечений для широкого круга ядер в области энергии 10 ÷ 650 кэв с разрешением ~ 10 кэв. Для большинства исследуемых ядер обнаружена структура в виде резонансов с шириной 75 ± 25 кэв.

В пользу существования промежуточной стадии реакции говорят и результаты измерений полных сечений Mo, Sn [58], ^{206}Pb и ^{208}Pb [59] в интервале энергий до нескольких Мэв.

В измерениях ^{59}Co, проведенных в Сакле [60], наблюдалась зависимость силовой функции от энергии в области разрешенных резонансов (0 ÷ 120 кэв) и периодическое изменение среднего сечения в области 120 ÷ 500 кэв.

Расчет S_0 силовой функции, проведенный Блоком и Фешбахом [56] и Шейкиным [61] для изотопов Sn и Pb с учетом оболочек, значительно улучшил согласие теории с экспериментом. В частности, для ^{120}Sn получено значение $S_0 \simeq 0{,}1$. Однако, пока что в расчетах существует значительная неопределенность в выборе потенциала парного взаимодействия. Расчеты ограничены четно-четными ядрами и наиболее простыми типами возбуждения.

В последнее время, в связи с развитием методов определения спина составного ядра (I), интенсивно изучается вопрос о зависимости S_0 от I.

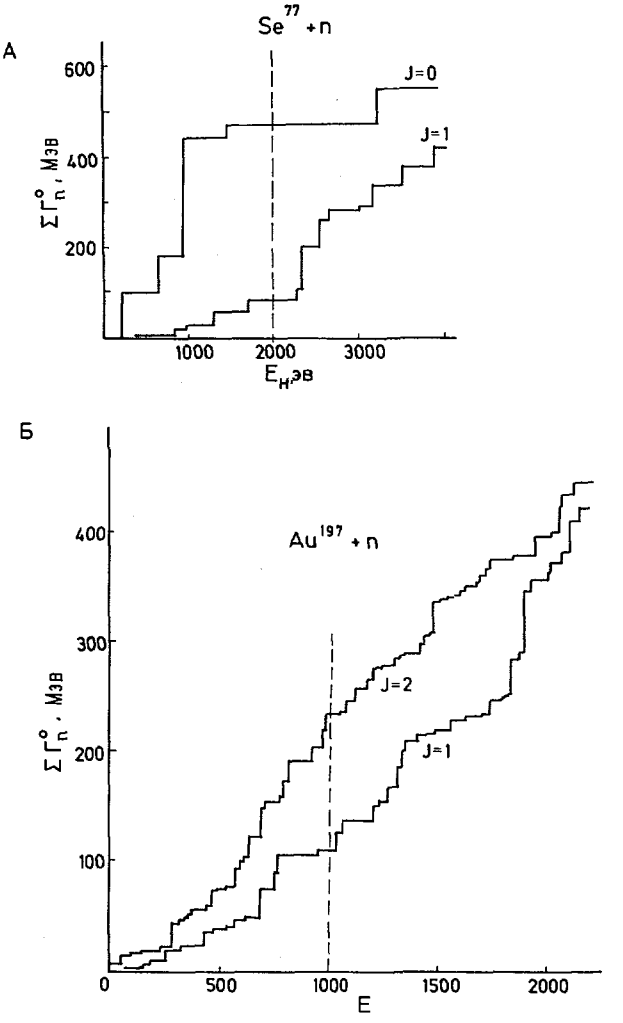

Рис. 5. Зависимость суммы приведенных нейтронных ширин $\Sigma\Gamma_{ni}^{(0)}$ от граничной энергии интервала усреднения для двух спиновых состояний ядра ^{77}Se [64] и ^{197}Au [3] ($I = I \pm \frac{1}{2}$). Пунктирная линия соответствует граничной энергии более ранних работ [62] и [21].

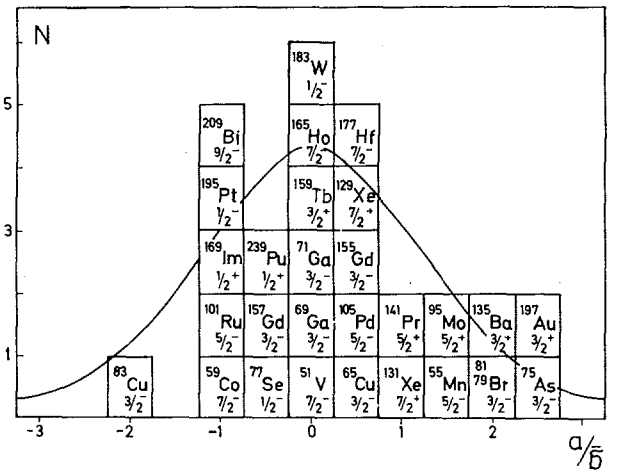

Рис. 6. Гистограмма разностей силовых функций для двух спиновых состояний, выраженных в единицах средней абсолютной ошибки. Плавная кривая – соответствующее теоретическое распределение [55].

В работах группы Сакле отмечается зависимость $S_0(I)$ для ^{69}Ga, ^{77}Se, ^{197}Au, ^{75}As, ^{79}Br и ^{81}Br [62,63,21]. Последующее измерение ^{197}Au [3] и ^{77}Se [64] показали, что при увеличении энергетического интервала $S_{I+\frac{1}{2}}$ и $S_{I-\frac{1}{2}}$ уравниваются (рис.5а, 5б). Измерения ^{69}Ga и ^{71}Ga, проведенные в ОИЯИ [65], не подтвердили результатов работы [62]. В настоящее время наблюдаемая зависимость $S_0(I)$ для всей совокупности ядер, для которых выделены две системы уровней, можно объяснить флуктуациями силовой функции [47,55]. На рис.6 приводятся результаты статистического анализа, приведенного в [55]. Следует отметить, что такой анализ не отвергает существование различия $S_{I+\frac{1}{2}}$ и $S_{I-\frac{1}{2}}$ для отдельно взятого ядра, так как очевидно, что, чем больше ядер мы включаем в анализ, тем больше вуалируется зависимость $S_0(I)$ для отдельно взятого ядра.

Сложность задачи многих тел и недостаточно известный закон ядерного взаимодействия не дают возможность детально описать сечения взаимодействия нейтрона с ядрами. Нейтронные сечения пока что можно получить только на эксперименте. Экспериментальные исследования сечений уточняют наши представления о ядре и служат базой для получения весьма ценных для реакторостроения констант.

ЛИТЕРАТУРА

[1] WYNCHANK, S., GARG, J.B., HAVENS, W.W., RAINWATER, J., Phys. Rev. 166 (1968) 1234.
[2] ROHR, G., FRIEDLAND, E., Nucl. Phys. A104 (1967) 1.
[3] ALVES, R.N., JULIEN, J., MORGENSTERN, J., SAMOUR, C., Nucl. Phys. A131 (1969) 450.
[4] ALVES, R.N., BARROS, S. De, CHEVILLON, P.L., JULIEN, J., MORGENSTERN, J., SAMOUR, C., Nucl. Phys. A134 (1969) 118.
[5] MORGENSTERN, J., ALVES, R.N., JULIEN, J., SAMOUR, C., Nucl. Phys. A123 (1969) 561.

[6] MICHAUDON, A., Special issue "Tailored" Neutron Beams. J. Nucl. Energy 17 N4/5 (1963)."Оптимизация нейтронных пучков" (русский перевод) Атомиздат, М., 1965, стр.38.
[7] PERING, N.C., LEWIS, T.A., Particle Accelerator Conference, D.C., Washington, March 5-7, 1969.
[8] LEISS, J.E., Electron Linear Accelerators as Sources of High Intensity Neutron Bursts, NBS-265, Washington, 1967.
[9] ALVES, R.N., KUCHLY, J.M., JULIEN, J., SAMOUR, C., MORGENSTERN, J., Nucl. Phys. A135 (1969) 241.
[10] КВИТЕК, И., ПОПОВ, Ю.П., РОДИОНОВ, К.Г., ПТЭ 2 (1967) 90.
[11] KOICHI OKAMOTO, Nucl. Phys. A141 (1970) 193.
[12] DRAGHICESCU, P., LUSHCHIKOV, V.I., NIKOLENKO, V.G., TARAN, Yu.V., SHAPIRO, F.L., Phys. Lett. 12 (1964) 334.
[13] АЛФИМЕНКОВ, В.П., ЛУЩИКОВ, В.И., НИКОЛЕНКО, В.Г., ТАРАН, Ю.В., ШАПИРО, Ф.Л., ЯФ 3 (1966) 55.
[14] НЕГАНОВ, Б., БОРИСОВ, Н., ЛИБУРГ, М., ЖЭТФ 50 (1966) 1445.
[15] ПЕШКОВ, В.П., Труды X Междунар. конф. по физике низких температур. Москва, т. 1 1966, стр. 162.
[16] MARSHAK, H., POSTMA, H., SHORE, F.J., SAILOR, V.L., REYNOLDS, C.A., Phys. Rev. 128 (1962) 1287.
[17] KING, T.J., BLOCK, R.C., Nucl. Phys. A138 (1969) 556.
[18] MACKLIN, R.L., GIBBONS, J.H., INADA, T., Nucl. Phys. 43 (1963) 353.
[19] WEIGMAN, H., CARRARO, G., BÖCKHOFF, K.H., Nucl. Instr. Meth. 50 (1967) 265.
[20] ПОПОВ, Ю.П., СТЕМПИНСКИЙ, М., ПТЭ №2 (1967) 94.
[21] JULIEN, J., BARROS, S.De., BIANCHI, G., CORGE, C., HUYNH, V.D., POITTEVIN, G. Le, MORGENSTERN, J., NETTER, F., SAMOUR, C., VASTEL, F., Nucl. Phys. 76 (1966) 391.
[22] BLOCK, R.C., RUSSELL, J.E., HOCKENBERRY, R.W., ORNL - 3425 (1963) 64.
[23] COCEVA, C., CORVI, F., GIACOBBE, P., Nucl. Phys. A117 (1968) 586.
[24] PÖNITZ, W.P., Zeit. Physik 197 (1966) 262.
[25] BOLLINGER, L.M., COTE, R.E., JACKSON, H.E., Compt. Rend. Cong. Int. de physique nucléaire, Paris 2 1964, p. 673.
[26] WEIGMANN, H., WINTER, J., HESKE, M., Nucl. Phys. A134 (1969) 535.
[27] SAMOUR, C., JULIEN, J., ALVES, R.N., BARROS, S. De, MORGENSTERN, J., Nucl. Phys. A123 (1969) 581.
[28] POITTEVIN, G. Le, BARROS, S. De, HUYNH, V.D., JULIEN, J., MORGENSTERN, J., NETTER, F., SAMOUR, C., Nucl. Phys. 70 (1965) 497.
[29] MURADYAN, H.V., Phys. Letters 14 (1965) 123.
[30] МУРАДЯН, Г.В., АДАМЧУК, Ю.В., МОСКАЛЕВ, С.С., ПТЭ 6 (1966) 43.
[31] MURADYAN, H.V., ADAMCHUK, Yu.V., Доклад на конф. по изучению структуры ядра нейтронами. Бельгия, июль 1965.
[32] MURADYAN, H.V., SHCHEPKIN, Yu.G., ADAMCHUK, Yu.V., ARUTIUNOV, M.G., Nucl. Phys. (1970) in press.
[33] ASAMI, A., MOXON, M.C., STEIN, W.E., UK/USSR Seminar. June 1968, N.UK/18.
[34] BHAT, M.R., CHRIEN, R.E., WASSON, O.A., BEER, M., LONE, M.A., Phys. Rev. 166 (1968) 1111.
[35] МИГДАЛ, А.Б., "Теория конечных Ферми-систем и свойства атомных ядер". Наука, М., 1965.
[36] WIGNER, E.P., Gatlinberg Conference on Neutron Physics ORNL-2309 (1957), 59.
[37] MEHTA, M.L., GAUDIN, M., Nucl. Phys. 18 (1960) 395, 420; Nucl. Phys. 25 (1961) 447.
[38] DYSON, F.J., J. Math. Phys. 3 1, Part I-III (1962) 140, 157, 166.
[39] GARG, J.B., HAVENS, W.W., RAINWATER, J., Phys. Rev. B136 (1964) 177.
[40] HAVENS, W., Progress in Fast Neutron Physics. Univ. Chicago Press, 1963, p. 215.
[41] МУРАДЯН, Г.В., АДАМЧУК, Ю.В., Доклад на Междунар. конф. по ядерным данным. Париж. 1966, № CN-23/107.
[42] МУРАДЯН, Г.В., АДАМЧУК, Ю.В., ЩЕПКИН, Ю.Г., ЯФ 8 (1968) 852.
[43] SUKHORUCHKIN, S.I., Proc. 2nd Conf. on Neutron Cross Section and Technology, Washington, 1968, p. 923.
[44] SETH, K.K., TABONY, R.H., BILPUCH, E.G., NEWSON, H.W., Phys. Letters 13 1 (1964) 70.
[45] ПОПОВ, Ю.П., ФЕНИН, Ю.И., ЖЭТФ 43 (1962) 2000.
[46] KOMPE, D., Nucl. Phys. A133 (1969) 513.
[47] MURADYAN, H.V., ADAMCHUK, Yu.V., Nucl. Phys. 68 (1965) 569.
[48] SPITZ, L.M., BARNARD, E., BROOKS, F.D., Nucl. Phys. A121 (1968) 655.

[49] UTTLEY, C.A., NEWSTEAD, C.M., DIMENT, K.M., Доклад на Междунар. конф. по ядерным данным. Париж, № CN-23/36, 1966.
[50] CARTER, R., HARVEY, J., HUGHES, D., PILCHER, V., Phys. Rev. 96 (1954) 113.
[51] FESHBACH, H., PORTER, C.E., WEISSKOPF, V.F., Phys. Rev. 96 (1954) 448.
[52] BUCK, B., PEREY, F., Phys. Rev. Letters 8 (1962) 444.
[53] FUKETA, T., KHAN, F.A., HARVEY, J.A., ORNL-3425 (1963).
[54] АДАМЧУК, Ю.В., ЗЕНКЕВИЧ, В.С., МОСКАЛЕВ, С.С., МУРАДЯН, Г.В., ЩЕПКИН, Ю.Г., ЯФ 10 (1969) 18.
[55] МАЛЭЦКИ, Х., ПИКЕЛЬНЕР, Л.Б., САЛАМАТИН, И.М., ШАРАПОВ, Э.И., ЯФ. 11 (1970) 111.
[56] BLOCK, B., FESHBACH, H., Ann. Phys. 23 (1963) 47.
[57] SETH, K.K., Phys. Letters 16 (1966) 306.
[58] MONAHAN, J.E., ELWYN, A.J., Nucl. Phys. A93 (1967) 683.
[59] FARRELL, J.A., KYKER, G.C., BILPUCH, E.G., NEWSON, H.W., Phys. Letters 17 (1965) 286.
[60] BARROS, S. De, CHEVILLON, P.L., HUYNH, V.D., JACKSON, H.E., JULIEN, J., MORGENSTERN, J., SAMOUR, C., Phys. Letters 23 (1966) 683.
[61] SHAKIN, C., Ann. Phys. 22 (1963) 373.
[62] JULIEN, J., BIANCHI, G., CORGE, C., HUYNH, V.D., POITTEVIN, G. Le, MORGENSTERN, J., NETTER, F., SAMOUR, C., Phys. Letters 10 (1964) 86.
[63] JULIEN, J., HUYNH, V.D., MORGENSTERN, J., NETTER, F., Comp. Rend 254 (1962) 4162.
[64] МАЛЭЦКИ, Х., ПИКЕЛЬНЕР, Л.Б., САЛАМАТИН, И.М., ШАРАПОВ, Э.И., Препринт ОИЯИ № Р3-3956, 1968.
[65] МАЛЭЦКИ, Х., ПИКЕЛЬНЕР, Л.Б., САЛАМАТИН, И.М., ШАРАПОВ, Э.И., Препринт ОИЯИ № Р3-4152, 1968.

TOTAL CROSS-SECTIONS OF ^{45}Sc, ^{47}Ti, ^{49}Ti, ^{53}Cr, AND ^{61}Ni IN THE keV-REGION

M. CHO, F.H. FRÖHNER, M. KAZEROUNI, K.-N. MÜLLER, G. ROHR
Kernforschungszentrum Karlsruhe
Karlsruhe, Federal Republic of Germany

Abstract

TOTAL CROSS-SECTIONS OF ^{45}Sc, ^{47}Ti, ^{49}Ti, ^{53}Cr, AND ^{61}Ni IN THE keV-REGION.

Neutron total cross-sections of separated isotopes were measured with the time-of-flight spectrometer at the 3-MeV Karlsruhe Van-de-Graaff accelerator. The neutron energy ranged from 10 to 250 keV. The energy resolution was between 0.2 and 0.5 ns/m.

The measured cross-sections were shape-analysed in terms of an R-matrix multi-level formula. Thus, neutron widths and spins for up to 50 resonances per isotope could be determined. Average neutron widths, level densities and strength functions were derived. The spin dependence of strength functions and the distribution of widths and spacings were investigated.

1. INTRODUCTION

High-resolution measurements of neutron total cross-sections in the keV-region are of interest, both for the construction of fast breeders and for the investigation of physical questions. The keV-spectrometer, installed at the pulsed 3-MeV Karlsruhe Van-de-Graaff generator, is characterized by high resolution and by the need for only gram amounts of sample material. This allows the measurement of separated isotopes. The nuclei studied in Karlsruhe are selected according to these facts from the mass region between A = 40 and A = 70. For this region and for neutron energies E_n = 10 to 250 keV, most of the cross-section is due to elastic scattering because the capture widths are small compared with the neutron widths and in most cases further reactions are not possible.

The analysis of the measured cross-section requires the use of a multi-level formula, which can describe the level-level interference effects due to overlapping resonances of the same spin state. The parametrization of the cross-section yields resonance parameters, which allow investigations of level densities, strength functions, and distributions of level widths and spacings.

2. EXPERIMENTAL METHOD AND ANALYSING TECHNIQUES

The total cross-section was measured in a transmission experiment by the time-of-flight method. Neutrons were generated in a thick lithium target by the (p, n)-reaction. The flight time was measured with a digital time coder. For energies up to about 60 keV a boron slab detector was used and a proton recoil detector at higher energies. The resolution was between 0.2 and 0.5 ns/m for flight paths of 6, 10, and 22 metres. To eliminate fluctuations of the neutron yield, an automatic sample changer,

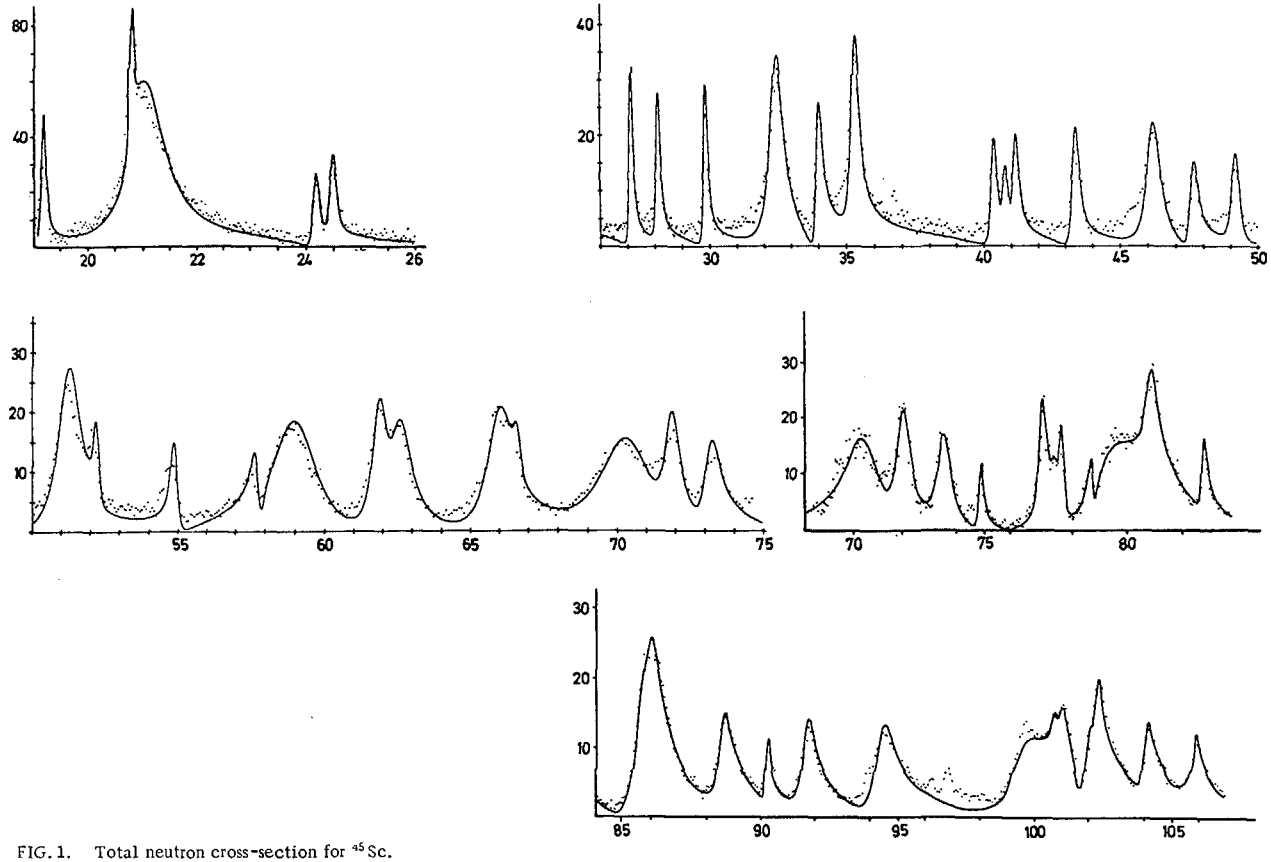

FIG. 1. Total neutron cross-section for ^{45}Sc.
X-axis: σ_{tot} (barn)
Y-axis: E_n (keV)

controlled by a beam current integrator, was used. More detailed descriptions of the experimental set-up are already published [1, 2].

With the exception of scandium all sample materials were provided by the EANDC-Pool. Scandium was used in the form of metal plates, the titanium isotopes as TiO_2 powder enriched to 79.5% (16.5% ^{48}Ti) in the case of ^{47}Ti and to 76.1% (18.5% ^{48}Ti) in the case of ^{49}Ti. ^{53}Cr was available in the form of 5.8 g Cr_2O_3 powder enriched to 95.2% (2.7% ^{52}Cr) and ^{61}Ni as metal powder enriched to 91.78% (5.2% ^{60}Ni). The material was filled into thin-walled aluminium containers. In the measurements without sample, equivalent empty containers were used. Different sample thicknesses, depending on the energy range and the cross-section structure, were chosen to obtain optimal statistical error and inscattering conditions. The influence of the oxygen content of the samples is easily corrected for because its cross-section, 3.5 barns, is constant up to 300 keV.

For analysis of the cross-section, an R-matrix multi-level formula [3] was used. Because of the minimum of the p-wave strength function in the mass region under consideration and because of the low penetration factors for higher partial waves in the keV region, all resonances of analysable width were assumed to be due to s-wave neutrons. The fits to the ^{49}Ti and ^{53}Cr data were achieved by trial and error. For the other isotopes, a least-squares fit program was written. The influence of the resonances outside the analysed region [4] was taken into account using a scattering phase of the form

$$\varphi_{0J} = ka\ (1 - R_{0J}^{\infty})$$

with

$$R_{0J}^{\infty} = A_J + B_J\ (E - E_M) + C_J\ (E - E_M)^2$$

Here k is the wave number, a the nuclear radius and E_M the middle of the energy interval analysed. The coefficients A_J, B_J, and C_J were chosen to give the best fit in the valleys between resonance peaks.

3. RESULTS

The cross-sections obtained are presented in Figs 1 to 5. The points give the experimental values and the curves give the fits achieved. The resonance parameters (resonance energy E_λ, width Γ_λ, and spin state J) yielding these fits are collected in Tables I to VI. Table VII contains the parameters describing the influence of the resonances outside of the analysed region.

The scandium data reveal a very high level density. Because of the many resonances analysed, an investigation of the distribution of widths and spacings was possible. Figure 6 shows the experimental distributions in the usual integrated form. The theoretical curves - Porter-Thomas distributions of the widths and Wigner distributions of the spacings - are plotted as smooth curves. The agreement between experimental and theoretical distributions is obvious.

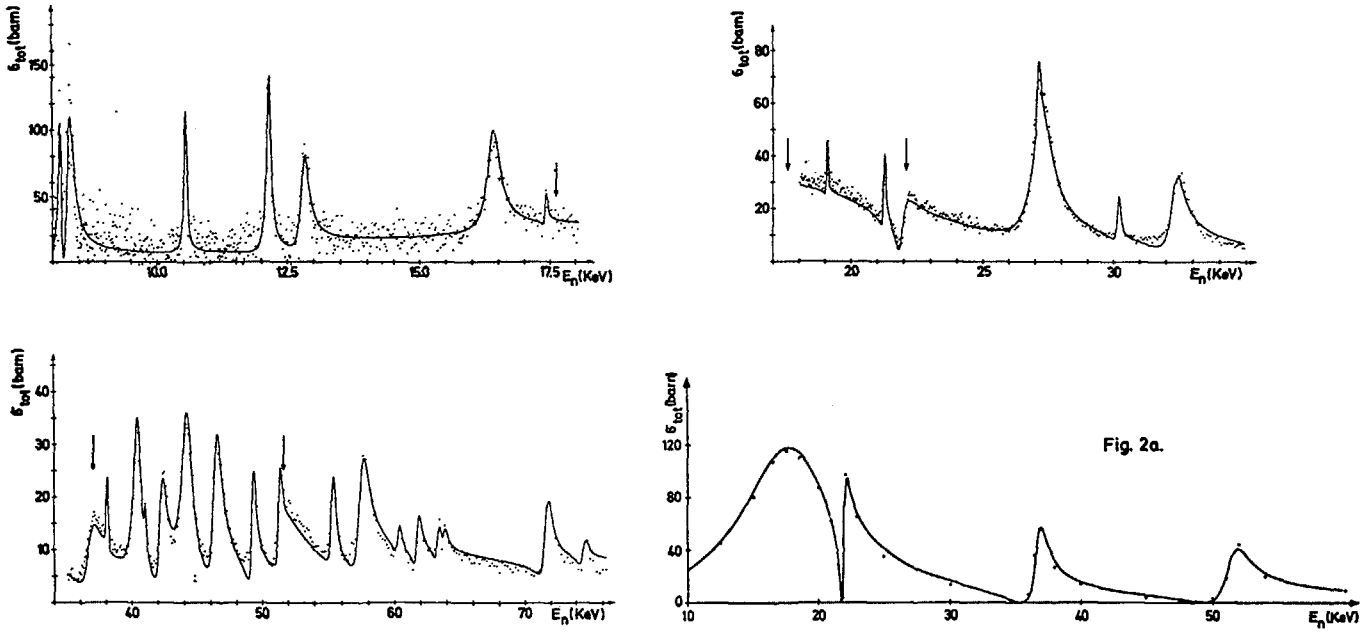

FIG. 2. Total neutron cross-section curve for ^{47}Ti. 0.795 σ (^{47}Ti) + 0.165 σ (^{48}Ti), arrows indicate ^{48}Ti resonances. Fig. 2a shows the total neutron cross-section curve for ^{48}Ti, 0.739 σ (^{48}Ti).

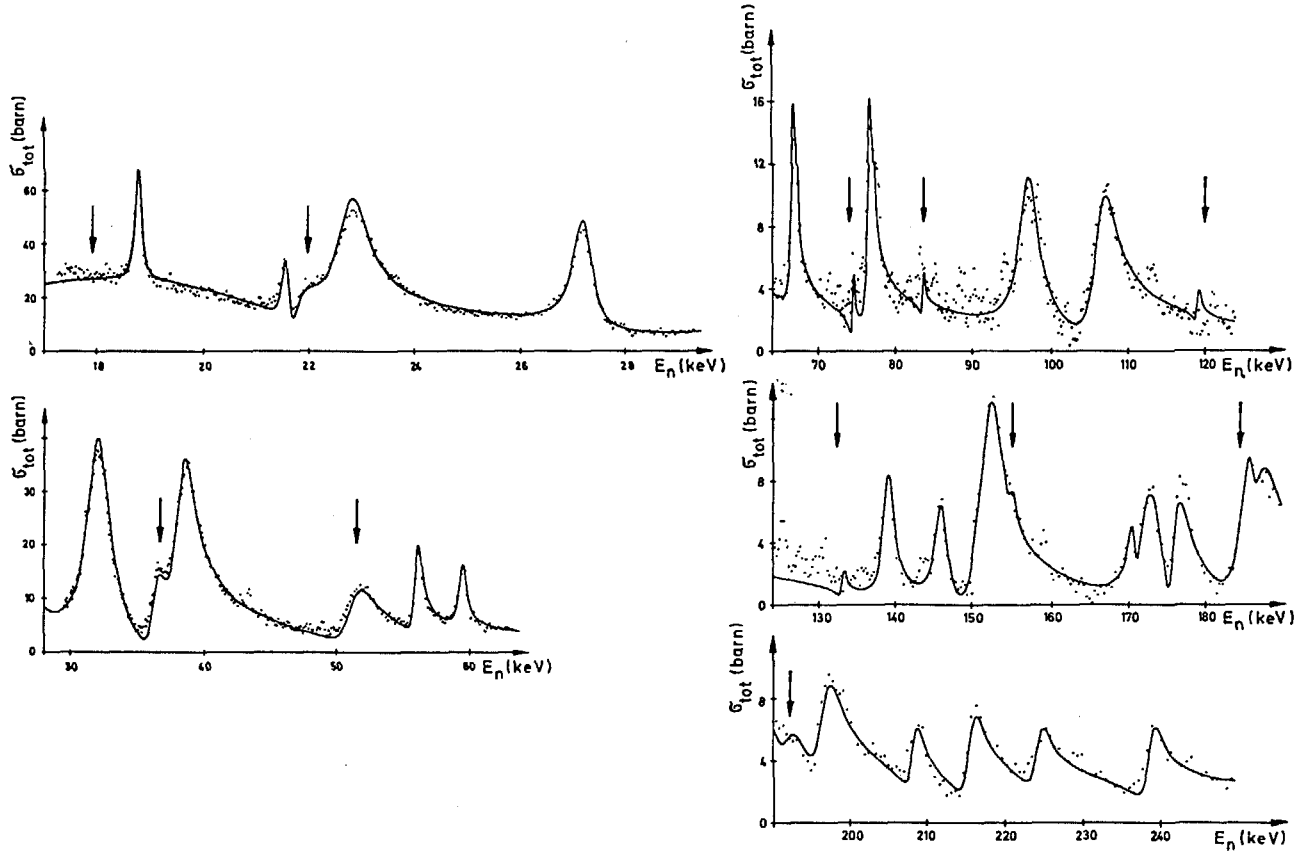

FIG. 3. Total neutron cross-section curve for ^{49}Ti. 0.761 σ (^{49}Ti) + 0.185 σ (^{48}Ti), arrows indicate ^{48}Ti resonances.

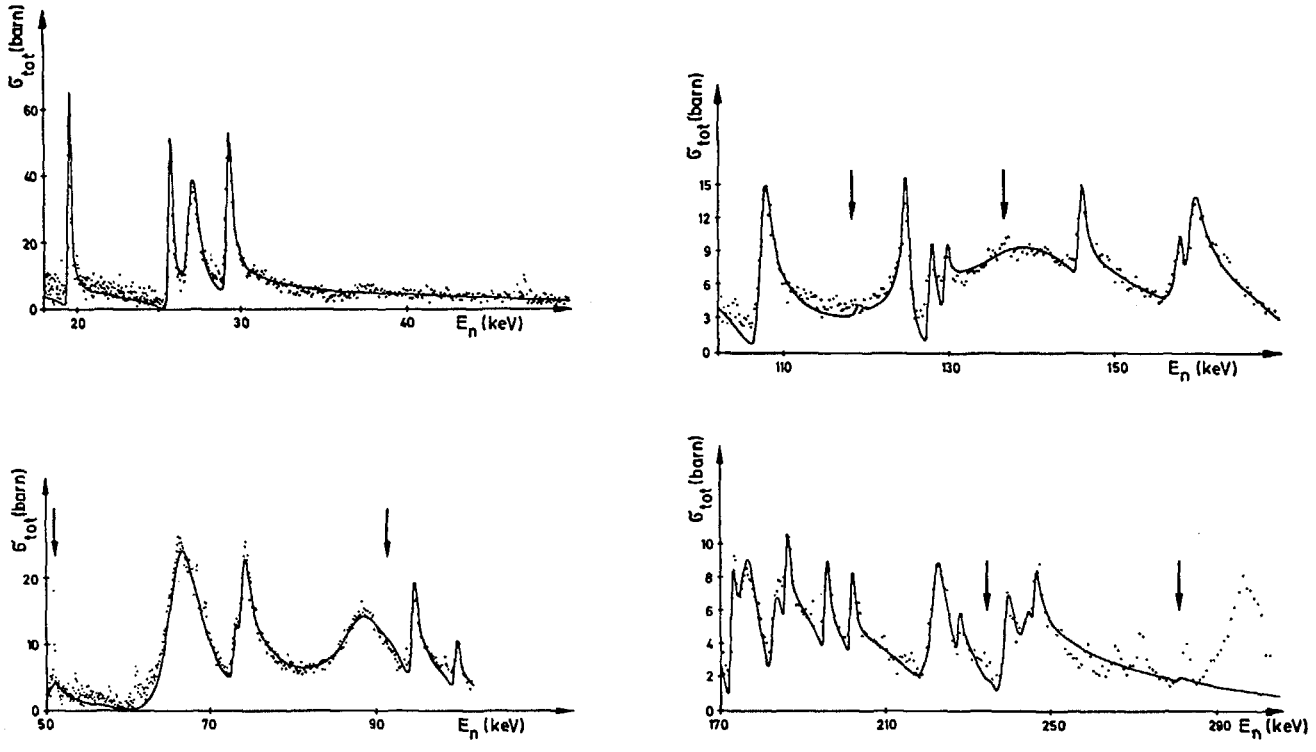

FIG. 4. Total neutron cross-section curve for ^{53}Cr. 0.952 σ (^{53}Cr) + 0.027 σ (^{52}Cr), arrows indicate ^{52}Cr resonances.

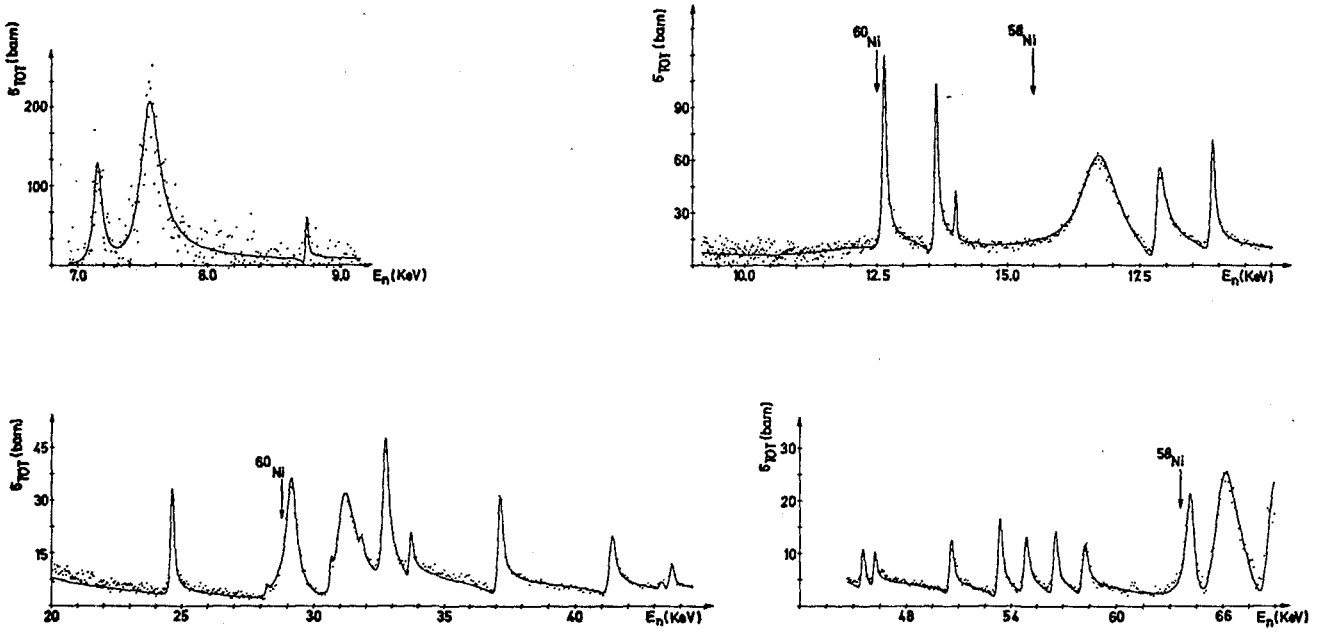

FIG. 5. Total neutron cross-section curve for ^{61}Ni. 0.9178 σ (^{61}Ni) + 0.052 σ (^{60}Ni) + 0.021 σ (^{58}Ni).

TABLE I. RESONANCE PARAMETERS OF ^{45}Sc

E_λ (keV)	Γ_λ (keV)	$(2g\,\Gamma)_\lambda$ (keV)	J	E_λ (keV)	Γ_λ (keV)	$(2g\,\Gamma)_\lambda$ (keV)	J
19.17	0.06	0.0675	4	65.94	1.04	1.17	4
20.80	0.06	0.0675	4	70.11	1.69	1.48	3
20.95	0.8	0.7	3	71.76	0.41	0.46	4
24.18	0.06	0.0525	3	73.18	0.35	0.307	3
24.48	0.06	0.0675	4	74.90	0.15	0.131	3
27.12	0.09	0.1012	4	77.15	0.25	0.28	4
28.12	0.11	0.09625	3	77.55	0.6	0.525	3
29.85	0.1	0.1125	4	77.85	0.15	0.168	4
32.40	0.57	0.4987	3	79.00	0.2	0.175	3
34.0	0.19	0.166	3	79.80	2.8	2.45	3
35.3	0.28	0.315	4	81.10	0.6	0.675	4
40.37	0.13	0.146	4	83.00	0.15	0.169	4
40.77	0.10	0.0875	3	85.60	0.85	0.956	4
41.15	0.11	0.124	4	86.00	0.65	0.569	3
43.35	0.17	0.19	4	88.60	0.55	0.481	3
46.15	0.48	0.42	3	90.20	0.12	0.135	4
47.60	0.18	0.1575	3	91.70	0.55	0.481	3
49.17	0.16	0.18	4	94.40	0.8	0.7	3
51.16	0.84	0.952	4	99.80	2.0	1.75	3
52.18	0.1	0.091	3	100.7	0.3	0.337	4
54.83	0.22	0.193	3	101.0	0.4	0.35	3
57.68	0.22	0.189	3	102.1	0.3	0.337	4
58.77	1.64	1.438	3	102.3	0.35	0.306	3
61.84	0.52	0.589	4	104.0	0.15	0.169	4
62.54	0.57	0.494	3	105.7	0.15	0.169	4

Errors of energies ~ 0.3%, errors of widths ~ 10%.

Because of the relatively high ^{48}Ti content of the two titanium samples a separate multi-level fit to the Columbia measurements [5] of natural titanium (73.9% ^{48}Ti) was carried out. The curve in Fig. 2a shows the fit obtained with the parameters of the first four resonances listed in Table III. The points are typical Columbia values. The cross-section contribution of these four resonances is easily visible in the data obtained for both titanium samples. The parameters of the other resonances listed in Table III were estimated from the Columbia data but they could not be uniquely identified with our measured resonance structures.

An important point in the parametrization of the ^{53}Cr cross-section is the existence of a big spin-one resonance at 135 keV and a super-

TABLE II. RESONANCE PARAMETERS OF ^{47}Ti

E_λ (keV)	Γ_λ (keV)	$(2g\,\Gamma)_\lambda$ (keV)	J	E_λ (keV)	Γ_λ (keV)	$(2g\,\Gamma)_\lambda$ (keV)	J
8.14	0.066	0.055	2	40.37	0.692	0.807	3
8.32	0.147	0.122	2	41.03	0.058	0.048	2
10.54	0.058	0.068	3	42.23	0.582	0.484	2
12.13	0.120	0.140	3	42.08	0.881	1.027	3
12.16	0.022	0.018	2	46.40	0.706	0.823	3
12.81	0.175	0.146	2	49.27	0.315	0.367	3
16.38	0.396	0.462	3	51.34	0.180	0.210	3
17.39	0.050	0.042	2	55.37	0.276	0.322	3
19.08	0.020	0.023	3	57.56	0.859	1.002	3
21.26	0.062	0.052	2	60.29	0.089	0.074	2
27.12	0.111	0.092	2	61.78	0.213	0.177	2
27.17	0.957	1.116	3	63.37	0.097	0.113	3
30.18	0.074	0.062	2	63.80	0.053	0.062	3
32.33	0.599	0.498	2	71.68	0.490	0.571	3
38.11	0.080	0.093	3	74.55	0.128	0.107	2

Errors of energies ~ 0.3%, errors of widths ~ 10%.

TABLE IIIa. RESONANCE PARAMETERS OF ^{48}Ti

E_λ (keV)	Γ_λ (keV)	$(2g\,\Gamma)_\lambda$ (keV)	J	E_λ (keV)	Γ_λ (keV)	$(2g\,\Gamma)_\lambda$ (keV)	J
17.76	8.43	16.86	0.5	119.0	0.2	0.4	0.5
22.11	0.78	1.56	0.5	133.2	0.2	0.4	0.5
36.9	1.3	2.6	0.5	154.9	0.25	0.5	0.5
51.7	2.4	4.8	0.5	185.6	0.65	1.3	0.5
74.4	0.15	0.3	0.5	192.4	3.0	6.0	0.5
83.6	0.12	0.24	0.5				

position of two resonances of different spin states at 124 keV. This interpretation is based, e. g. on the slow rise and steep decline of the 124-keV structure. Such a shape contrary to the normally steep rise and slow decline of an isolated resonance is typical for an interference with a large higher-energy resonance of the same spin. The influence of the large spin-one resonance on the spin dependence of the strength function is decisive. The strength function, evaluated for the energy range up to 120 keV, does not show spin dependence. Because of the 135-keV resonance the strength function for spin 1 calculated for the whole range up to 250 keV is twice that for spin two.

TABLE IV. RESONANCE PARAMETERS OF ^{49}Ti

E_λ (keV)	Γ_λ (keV)	$(2g\,\Gamma)_\lambda$ (keV)	J	E_λ (keV)	Γ_λ (keV)	$(2g\,\Gamma)_\lambda$ (keV)	J
18.76	0.09 ± 0.01	0.10	4	151.2	3.3 ± 1.0	2.9	3
21.54	0.15 ± 0.04	0.13	3	152.2	2.8 ± 1.0	3.1	4
22.77	0.70 ± 0.10	0.61	3	170.5	0.8 ± 0.2	0.9	4
27.14	0.42 ± 0.05	0.47	4	172.3	3.5 ± 0.7	3.9	4
31.9	2.0 ± 0.2	2.3	4	176.2	1.8 ± 0.5	2.0	4
38.4	1.7 ± 0.2	1.9	4	184.7	3.0 ± 0.6	2.6	3
56.1	0.45 ± 0.1	0.5	4	185.8	2.5 ± 0.5	2.8	4
59.4	0.45 ± 0.1	0.39	3	187.7	4.0 ± 1.0	3.5	3
66.75	0.8 ± 0.1	0.7	3	197.0	3.0 ± 0.6	3.4	4
76.6	0.9 ± 0.2	1.0	4	208.5	1.5 ± 0.3	1.3	3
96.6	3.0 ± 0.5	2.6	3	216.0	2.2 ± 0.4	2.5	4
106.4	3.3 ± 0.5	2.9	3	224.5	2.0 ± 0.4	1.8	3
138.8	1.6 ± 0.2	1.8	4	239.0	2.0 ± 0.5	2.3	4
145.7	1.9 ± 0.3	1.7	3				

TABLE V. RESONANCE PARAMETERS OF ^{53}Cr

E_λ (keV)	Γ_λ (keV)	$(2g\,\Gamma)_\lambda$ (keV)	J	E_λ (keV)	Γ_λ (keV)	$(2g\,\Gamma)_\lambda$ (keV)	J
19.53	0.13 ± 0.02	0.16	2	135.0	24.0 ± 5.0	18.0	1
25.64	0.22 ± 0.03	0.28	2	145.9	0.6 ± 0.1	0.8	2
26.95	0.70 ± 0.10	0.53	1	157.8	0.9 ± 0.1	1.1	2
29.23	0.33 ± 0.03	0.41	2	159.0	2.0 ± 0.3	2.5	2
65.7	4.5 ± 0.07	5.6	2	172.7	1.2 ± 0.2	1.5	2
73.1	1.05 ± 0.25	0.8	1	175.7	4.0 ± 0.8	3.0	1
74.06	1.2 ± 0.2	1.5	2	183.0	3.5 ± 0.7	2.6	1
87.2	7.8 ± 1.0	5.9	1	186.0	0.5 ± 0.2	0.6	2
94.5	0.6 ± 0.1	0.75	2	195.7	0.6 ± 0.1	0.8	2
99.7	0.4 ± 0.1	0.3	1	201.7	0.55 ± 0.1	0.7	2
107.4	1.5 ± 0.15	1.9	2	221.6	4.2 ± 0.8	5.2	2
123.6	4.0 ± 1.0	3.0	1	227.5	0.3 ± 0.1	0.4	2
124.5	0.5 ± 0.2	0.6	2	239.0	3.0 ± 0.6	3.8	2
127.6	0.4 ± 0.2	0.5	2	244.5	4.0 ± 1.0	3.0	1
129.5	0.2 ± 0.1	0.3	2	246.0	0.5 ± 0.3	0.6	2

TABLE VI. RESONANCE PARAMETERS OF ^{61}Ni

E_λ (keV)	Γ_λ (keV)	$(2g\,\Gamma)_\lambda$ (keV)	J	E_λ (keV)	Γ_λ (keV)	$(2g\,\Gamma)_\lambda$ (keV)	J
7.15	0.074	0.056	1	33.68	0.058	0.044	1
7.55	0.177	0.221	2	37.13	0.133	0.166	2
8.74	0.006	0.008	2	41.34	0.176	0.132	1
12.64	0.075	0.094	2	43.25	0.010	0.013	2
13.63	0.061	0.076	2	43.61	0.030	0.038	2
14.02	0.017	0.013	1	45.49	0.066	0.050	1
16.70	0.817	0.613	1	46.16	0.054	0.041	1
17.86	0.177	0.133	1	50.51	0.133	0.100	1
18.87	0.069	0.086	2	53.30	0.141	0.176	2
24.62	0.129	0.097	1	54.81	0.189	0.142	1
28.21	0.003	0.004	2	56.49	0.119	0.149	2
29.11	0.409	0.307	1	58.16	0.178	0.134	1
30.64	0.013	0.016	2	64.07	0.535	0.669	2
31.13	0.788	0.591	1	65.87	1.430	1.788	2
31.83	0.008	0.010	2	68.77	1.100	1.375	2
32.70	0.220	0.275	2				

Errors of energies ~ 0.3%, errors of widths ~ 10%.

TABLE VII. PARAMETERS FOR R_{0J}^{∞}

Target nucleus	E_H	A_J	B	$C(E < E_H)$	$C(E > E_H)$
^{45}Sc	60 kev	0.2	0.01	-1.0×10^{-6}	$+1.0 \times 10^{-6}$
^{47}Ti	-	J = 2 - 0.63 J = 3 + 0.14	0	0	0
^{48}Ti	-	0.33	0	0	0
^{49}Ti	130 keV	2.6×10^{-1}	1.9×10^{-3}	-5.5×10^{-6}	$+5.5 \times 10^{-6}$
^{53}Cr	160 keV	2.8×10^{-3}	2.33×10^{-3}	-2.22×10^{-5}	$+2.22 \times 10^{-5}$
^{61}Ni	-	J = 1 + 0.12 J = 2 - 0.23	0	0	0

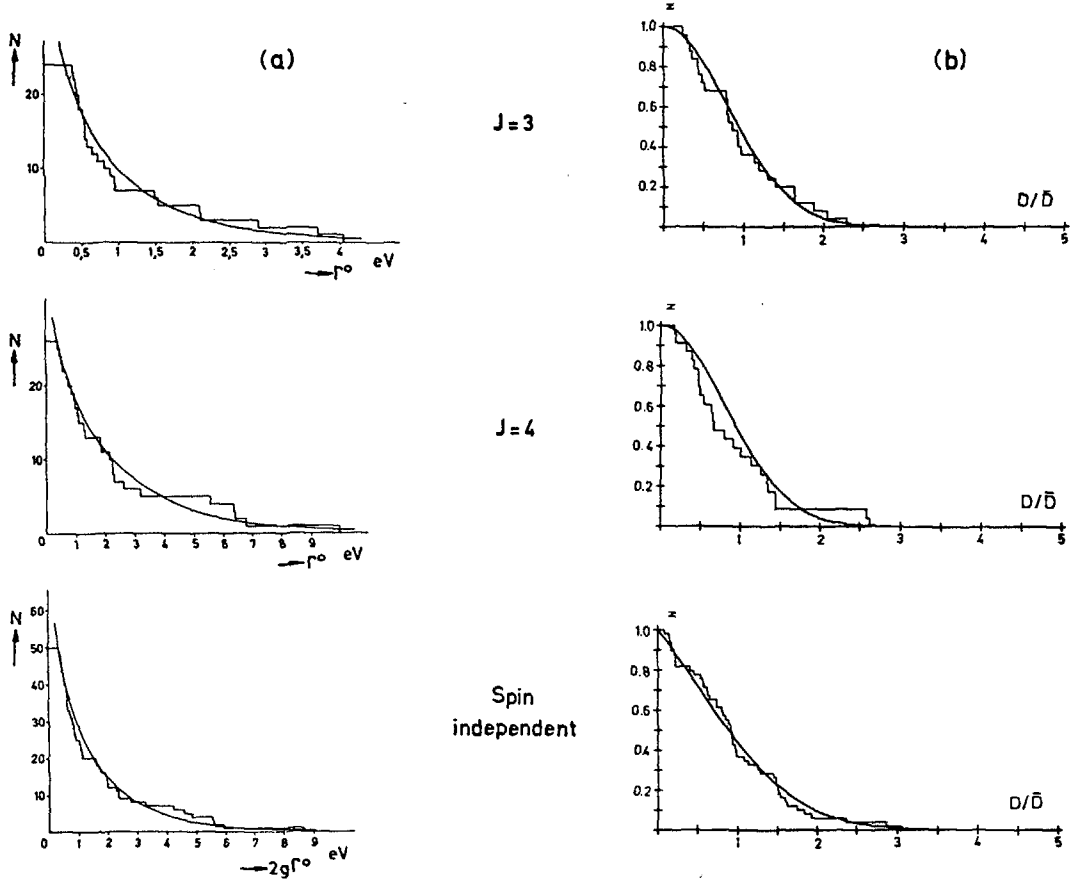

FIG. 6. Distribution of widths (a) and spacings (b) for ^{45}Sc + n.

TABLE VIII. AVERAGED VALUES

Target nucleus	Spin state	Energy range (keV)	$\bar{D}$ (keV)		$\bar{\Gamma}^0_n$ (eV)		$S \times 10^4$		Number of levels	
			a	b	a	b	a	b	a	b
^{45}Sc	J = 3	19 - 107	3.13	2.15	2.37	1.66	7.6	7.7	26	38
	J = 4		3.76	1.98	1.18	0.67	3.2	3.4	24	46
	independent		1.77	1.10	1.75	1.13	5.0	5.1	50	80
^{47}Ti	J = 2	8 - 76	5.11	3.04	1.0	0.6	2.0	2.1	14	24
	J = 3		4.08	2.95	2.0	1.4	4.8	4.9	16	22
	independent		2.29	1.59	1.6	1.1	3.5	3.6	30	43
^{49}Ti	J = 3	17 - 250	18.45	13.41	5.6	4.1	3.1	3.1	12	17
	J = 4		15.73	11.06	5.1	3.6	3.2	3.3	15	21
	independent		8.47	6.04	5.3	3.9	3.2	3.2	27	38
^{53}Cr	J = 1	18 - 250	27.19	22.70	15.4	12.9	5.7	5.7	9	11
	J = 2		11.32	6.91	3.2	2.1	2.9	3.0	21	38
	independent		7.81	5.73	6.3	4.7	4.0	4.1	30	41
^{61}Ni	J = 1	7 - 69	3.92	2.79	1.4	1.0	3.7	3.7	14	20
	J = 2		3.83	2.44	1.1	0.7	2.9	3.0	17	27
	independent		2.05	1.36	1.3	0.9	3.1	3.2	31	47

[a] Only number of analysed levels used.

[b] "Missed levels" included.

The influence of the ^{52}Cr content of the chromium samples was taken into account using the Duke [3] resonance parameters. For nickel the ^{60}Ni resonances at 12.5 keV (Γ_λ = 2.6 keV) and 28.7 keV (Γ_λ = 1.11 keV) [3,5] were considered. The influence of the 12.5-keV resonance was clearly evident as a background structure raising the interference valleys of the two spin-2 resonances at 12.7 and 13.6 keV. For ^{52}Cr A = B = C = 0 was chosen, and A = -0.15, B = C = 0 for ^{60}Ni [3].

The statistical parameters obtained from the analysed resonances are listed in Table VIII. The average level distance $\bar{D}$, the average reduced width $\bar{\Gamma}_n^0$, the s-wave neutron strength function S, and the number of levels are listed in an (a) and a (b) version. Version (a) gives the values obtained directly from the analysed resonances. Due to the energy-dependent detection and analysing limit for resonances, levels are missed. In the case (b) a correction for these "missed levels" [6] was carried out. It is based on the assumption of the validity of the Porter-Thomas distribution for the level widths. Though many levels are missed in some cases, their contribution to the strength function is small in general. A more pronounced difference between (a) and (b) strength function values (e.g. ^{45}Sc) is due to low average level widths relative to the detection threshold.

For some of the measured isotopes a spin dependence of the strength function was found, for others not. At the moment, no general description or explanation for the observed spin dependence is available. Recent calculations of strength functions in the 3s-resonance region [7], carried out for nuclei with and without spin, yielded a good description of the fluctuations of experimental strength functions around the optical model values. This agreement between calculations and experiment can be interpreted as an indication for a spin independence of the strength function [8]. A spin dependence would be caused by shell effects producing a deviation from the average spin dependence of the doorway-state density. The existing experimental data, in general, do not show a systematic tendency if one compares spin-up and spin-down strength functions [9].

With the exception of ^{45}Sc all nuclei had already been measured by the Oak Ridge Group [10] in the energy range of about 3 to 50 keV. The advantage of the present measurement is an improvement in resolution by a factor of ten and the extension of the energy range. Moreover, a thorough analysis of the data was carried out. The use of a multilevel formula allows a description of most of the complicated cross-section structures occurring. A fit of the typical interference shapes yields a determination of spins even in the case of not completely resolved resonances.

REFERENCES

[1] ROHR, G., thesis, Karlsruhe University, 1967.
[2] ROHR, G., MÜLLER, K.-N., Z. Physik 227 (1969) 1.
[3] BOWMAN, C.D., BILPUCH, E.G., NEWSON, H.W., Ann. Phys. 17 (1962) 319.
[4] FIRK, F.W.K., LYNN, J.E., MOXON, M.C., Proc. Phys. Soc. 82 (1963) 477.
[5] GARG, J.G., RAINWATER, J., HAVENS W.W., Jr., EANDC(US) - 54 "L", CR-1860.
[6] FUKETA, T., HARVEY, J.A., Nucl. Instrum. Meth. 33 (1965) 107.
[7] MÜLLER, K.-N., ROHR, G., KFK-Report 1114, Karlsruhe, 1969.
[8] MÜLLER, K.-N., ROHR, G., to be published.
[9] MALETSKI, Kh., PIKELNER, L.B., SALAMATIN, I.M., SHARAPOV, E.I., JINR-P_3-4484, Dubna, 1969.
[10] GOOD, W.M., PAYA, D., WAGNER, R., TAMURA, T., Phys. Rev. 151 (1966) 912.

HIGH-RESOLUTION MEASUREMENTS OF RADIATIVE NEUTRON-CAPTURE IN ^{47}Ti, ^{56}Fe, ^{58}Ni, ^{60}Ni AND ^{61}Ni BETWEEN 7 AND 200 keV*

A. ERNST
University of Vienna, Austria,
and
Kernforschungszentrum Karlsruhe,
F.H. FRÖHNER, D. KOMPE**
Kernforschungszentrum Karlsruhe,
Federal Republic of Germany

Abstract

HIGH-RESOLUTION MEASUREMENTS OF RADIATIVE NEUTRON CAPTURE IN ^{47}Ti, ^{56}Fe, ^{58}Ni, ^{60}Ni AND ^{61}Ni BETWEEN 7 AND 200 keV.

Neutron capture in enriched samples of ^{47}Ti, ^{56}Fe, ^{58}Ni, ^{60}Ni and ^{61}Ni has been measured in the energy range 7 - 200 keV using the time-of-flight method. The time resolution is better than 2 ns/m. Neutron pulses are produced by a 3 MV Van-de-Graaff accelerator via the ^{7}Li (p, n)^{7}Be reaction. Capture is detected with a large liquid scintillator tank. The $^{197}Au(n, \gamma)$ cross-section serves as standard.

Resonance parameters are given for many resolved resonances. For the determination of spins and radiation widths, transmission data were incorporated in the analysis.

1. INTRODUCTION

High-resolution measurements of radiative neutron capture in the keV region are of interest to the designers of fast reactors, to nuclear structure physicists and to astrophysicists. The measurements described here are part of a program to investigate structural materials for fast reactors.

2. EXPERIMENTAL APPARATUS

Capture yield versus neutron energy was measured using the time-of-flight method. 1 ns neutron pulses with a broad energy spectrum were produced with a repetition frequency of 500 kc/s by the ^{7}Li (p, n)^{7}Be reaction with protons from a pulsed 3 MV Van-de-Graaff accelerator. Samples were exposed to the well-collimated neutron beam in a cylindrical hole at the center of a 1.1 m liquid scintillator tank at a distance of 2 m from the target. The sample to be analysed was interchanged at short time intervals with a carbon sample, which served to determine the time-dependent background, and with a gold sample, which was used to determine

---

* Work performed within the association in the field of fast reactors between the European Atomic Energy Community and Gesellschaft für Kernforschung mbH, Karlsruhe.

** Present address: Philips Elektrologica, 5904 Eiserfeld, Federal Republic of Germany

the neutron flux [1]. All signals from the detector exceeding a bias equivalent to 3 MeV were sorted by an on-line computer into a three-dimensional spectrum according to the time-of-flight, the total gamma ray energy absorbed in the scintillator and the number of the sample. This enabled us to obtain crude gamma ray spectra for individual resonances. Gamma ray spectra averaged over many resonances were also recorded separately down to 0.5 MeV pulse height. The scintillator tank described in [2] was optically separated into four parts to allow majority coincidence operation in an attempt to get qualitative information on gamma ray multiplicities for individual resonances.

3. EXPERIMENTAL METHOD

Because the storage space of the on-line computer was insufficient to cover the whole energy region, there were two experimental runs for each isotope: a low-energy run and a high-energy run. In the-low energy run, capture yields in the energy range from 6 to 11 keV were measured with 4 ns per channel, from 11 to 43 keV with 2 ns per channel and from 43 keV upwards with 16 ns per channel with a maximum neutron energy of 70 keV. In the high-energy run, capture yields from 6 to 19 keV were measured with 8 ns per channel and from 19 keV upwards with 2 ns per channel with a maximum neutron energy between 160 and 230 keV, depending on the isotope. A typical experimental run took about 3 days. Every 12 hours, data were read out and time and energy calibrations were established to check the stability of the electronics. Each isotope was also measured down to 1 keV neutron energy in order to determine the possible overlap of neutrons from one pulse of the accelerator with low-energy neutrons from the preceeding pulse of the accelerator. Only in the case of ^{47}Ti a correction had to be applied to the data due to neutron capture in a resonance at 3 keV.

4. SAMPLES

All samples to be analyzed were powders pressed into flat cylindrical bronze containers with a diameter of 8 cm. Carbon samples were graphite discs with thicknesses chosen to match the scattering cross-section of the sample to be analyzed. They were placed into the same type of container. The gold sample was a disc 1 mm thick. The sample characteristics are listed in Table I.

5. ANALYSIS

From a three-dimensional spectrum obtained during one experimental run pulse height spectra for all samples were extracted covering the gamma energy range from 3 MeV to well above the neutron binding energy. These pulse height spectra were extrapolated to zero gamma ray energy with the aid of the average pulse height spectrum shapes obtained from the separately recorded pulse height data going down to 0.5 MeV gamma ray energy. The pulse height channels to be included in the capture-yield analysis were

TABLE I. SAMPLE CHARACTERISTICS

Sample	Chemical form	Total weight (g)	Enrichment (%)	Thickness (10-3 nuclei/barn)
^{47}Ti	TiO_2	41.7	79.5	4.664
^{56}Fe	Fe_2O_3	71.5	99.7	9.924
^{58}Ni	Ni	55.0	99.9	10.567
^{60}Ni	Ni	55.0	99.8	10.215
^{61}Ni	Ni	27.4	91.8	4.598
^{197}Au	Au	120.3	100.0	5.782

determined by a separate calculation in order to get a minimum for the combined statistical and systematic error in the capture yield. Then the time-of-flight spectra contained in these pulse height channels were added and the spectrum fraction contained in the resulting time-of-flight spectrum was calculated. In another calculation, the average neutron energy for each channel was computed from the flight path, from the position of the accelerator gamma flash (corrected for the photon flight time) and from the channel widths obtained from the time calibration data. Non-linearities in the time-to-digital conversion electronics were taken into account. From all these data the capture yield divided by the sample thickness was calculated for each time-of-flight channel by the formula

$$"\sigma_\gamma" = \frac{(C_X - C_{SX}) \cdot N_A \cdot \epsilon_A}{(C_A - C_{SA}) \cdot N_X \cdot \epsilon_X} \sigma_{\gamma A}$$

where C_X denotes the counting rate for the analyzed sample, C_{SX} the counting rate for the carbon sample, obtained by adding up the same pulse height channels as in the case of the analyzed sample, C_A is the counting rate for the gold sample, C_{SA} is the corresponding carbon sample counting rate, N_A and N_X are the sample thicknesses of the gold and of the analyzed sample and ϵ_A and ϵ_X are the average spectrum fractions. Although "σ_γ"

TABLE II. NUMBERS AND AVERAGE SPACING OF RESONANCES

Nuclide	Energy interval (keV)	Number of observed resonances	Average spacing (eV)
^{47}Ti	30	35	860
^{56}Fe	100	20	5000
^{58}Ni	100	33	3000
^{60}Ni	100	26	3800
^{61}Ni	30	38	790

TABLE III. RADIATION WIDTHS AND MULTIPLE-SCATTERING CONTRIBUTION

Nuclide	Resonance energy (keV)	Radiation width (eV)	Multiple-scattering contribution to primary capture yield (%)
^{47}Ti	8.11	1.4 ± 0.3	5
	8.33	2.0 ± 0.4	27
	10.5	1.6 ± 0.2	3
	12.2	2.1 ± 0.5	6
	12.8	2.5 ± 0.5	5
	16.4	2.0 ± 0.4	11
	17.4	2.0 ± 0.3	1
	19.0	2.5 ± 0.5	1
	21.2	1.7 ± 0.3	1
	average:	1.81 ± 0.11	
^{56}Fe	27.8	1.4 ± 0.2	59
^{60}Ni	12.5	3.4 ± 0.7	159
	28.5	1.2 ± 0.4	54
	65.5	2.2 ± 0.3	5
^{61}Ni	7.16	2.5 ± 0.4	11
	7.55	2.3 ± 0.6	70
	8.75	2.6 ± 0.8	2
	12.6	1.7 ± 0.3	7
	13.6	1.6 ± 0.4	7
	14.0	3.1 ± 0.5	7
	16.7	2.2 ± 0.4	
	17.9	1.6 ± 0.5	10
	18.9	0.9 ± 0.3	12
	24.6	1.4 ± 0.3	2
	28.2	3.0 ± 1.0	1
	29.1	2.4 ± 0.4	25
	33.7	2.8 ± 0.5	1
	37.1	3.0 ± 0.5	1
	average:	1.94 ± 0.12	

TABLE IV. DETAILS ON SPECTRA

Figure 8 spectrum No.	Resonance energy (keV)	Isotopic assignment	Relative coincidence efficiency
1	10.2	54	
2	13.9	57	
3	14.4	54	
4	22.8	56	0.84
5	27.7	56	0.66
6	30.5	54	
7	34.2	56	0.43
8	36.7	56	0.81
9	38.3	56	0.71
10	45.8	56	0.95
11	52	56	0.73
12	53	56	0.94
13	59	56	0.60
14	63	56	1.00
15	73	56	0.45
16	77	56 + 54	
17	81	56	0.80
18	83	56	
19	90	56	
20	93	56	
21	96	56	
22	102	56	0.70
23	105	56	0.44
24	112	56	
25	129	56	

has the dimensions of a cross-section, it should be noted that it is not identical to the true capture cross-section, since it still contains the effects of resonance self-shielding, multiple scattering and resolution broadening. Furthermore, possible deviations of resonance pulse height spectra from the average pulse height spectrum and differences between the detector efficiencies for the measured sample and for gold are neglected. All these effects were taken into account in the next step of the calculations, the determination of radiation widths. For resonances with known spin and total width the radiation width can be found by shape or area analysis. In the present work detailed multi-level fits of the transmission of ^{47}Ti and ^{61}Ni had yielded spins and total widths [3], and for ^{56}Fe, ^{58}Ni and ^{60}Ni

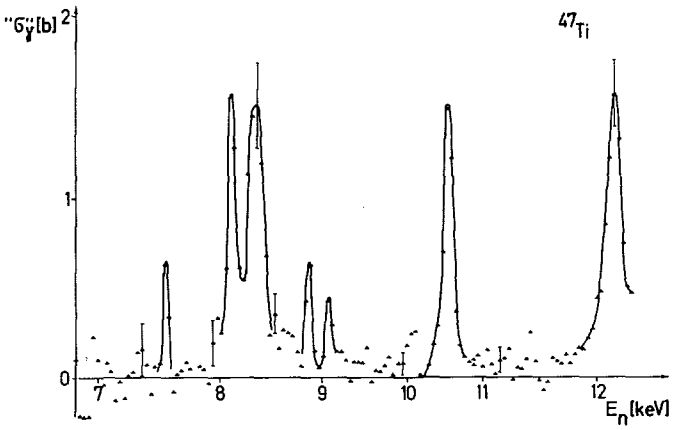

Figure 1

FIGS 1-5. ^{47}Ti capture yield divided by sample thickness versus energy; triangles: low-energy run, circles: high-energy run.

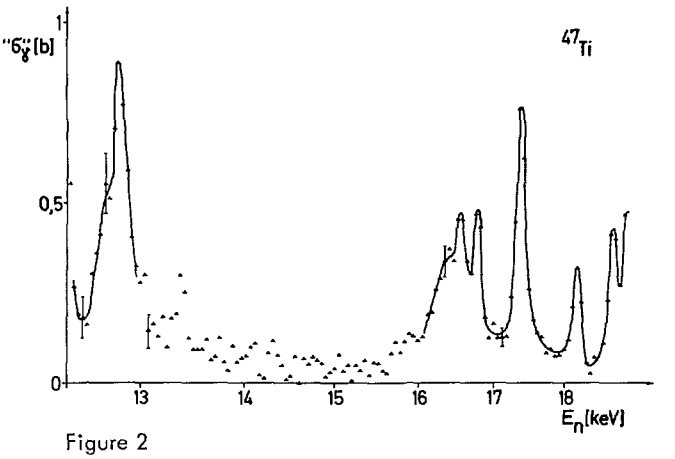

Figure 2

FIGS 1-5 (continued).

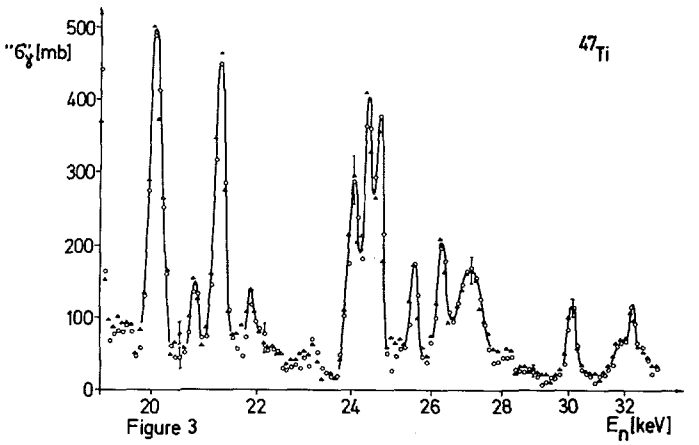

Figure 3

FIGS 1-5 (continued).

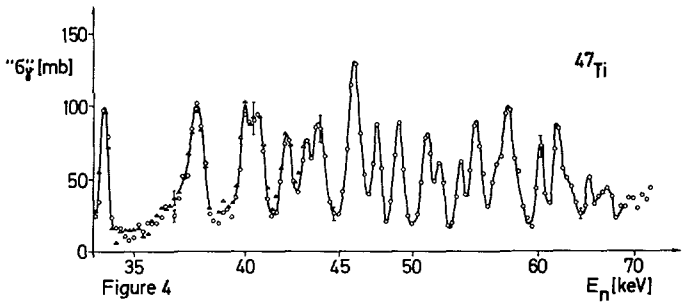

Figure 4

FIGS 1-5 (continued).

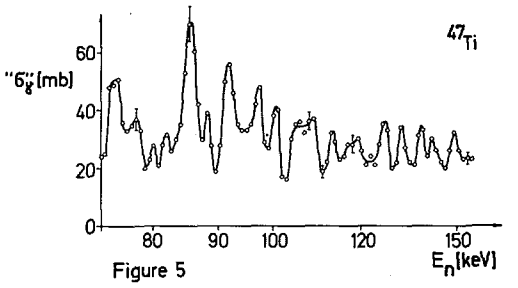

Figure 5

FIGS 1-5 (continued).

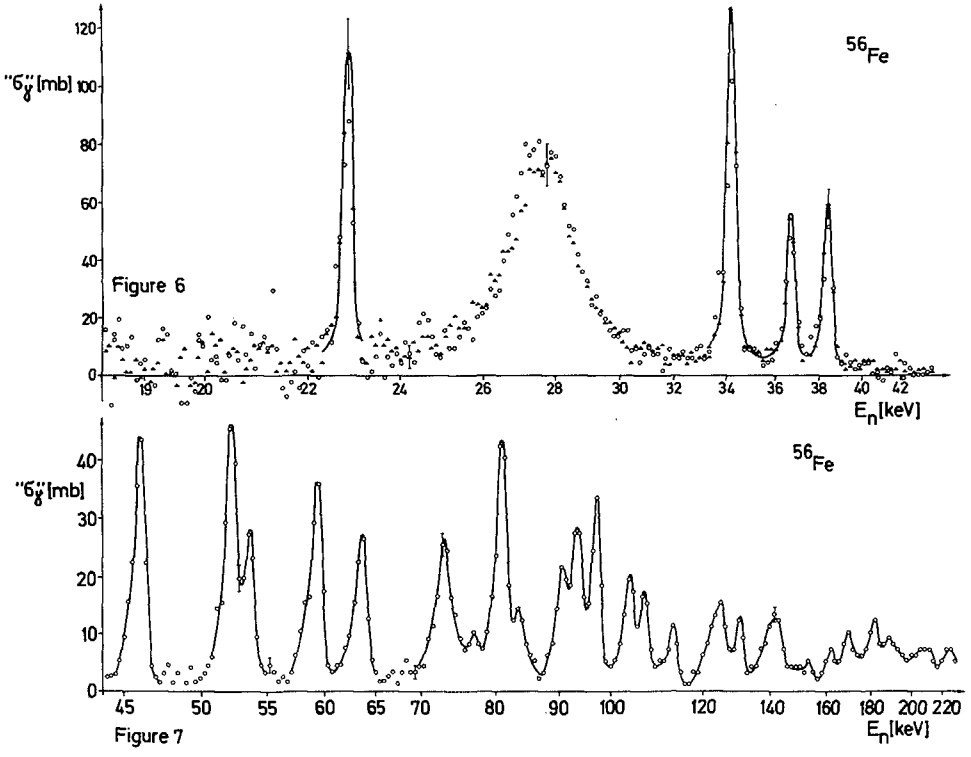

FIGS 6 and 7. ^{56}Fe capture yield divided by sample thickness versus energy; triangles: low-energy run, circles: high-energy run.

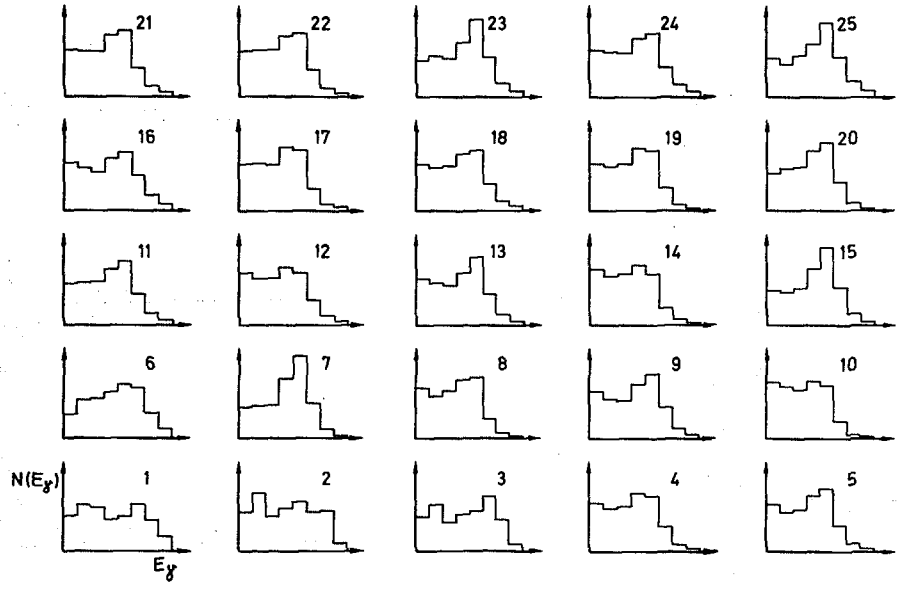

FIG. 8. Natural iron. Pulse-height spectra of individual resonances (see Table IV).

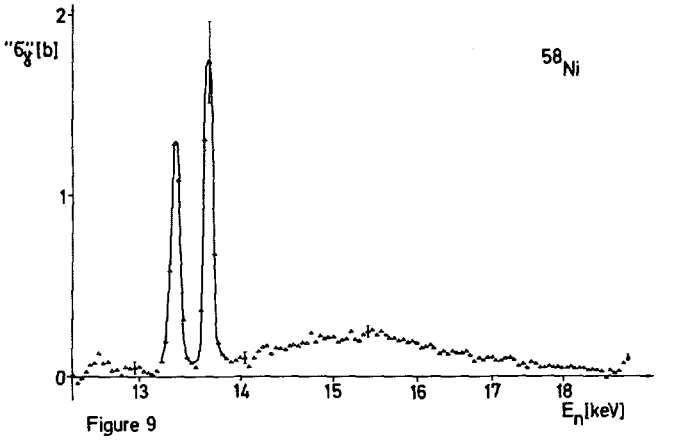

Figure 9

FIGS 9-12. ^{58}Ni capture yield divided by sample thickness versus energy; triangles: low-energy run, circles: high-energy run.

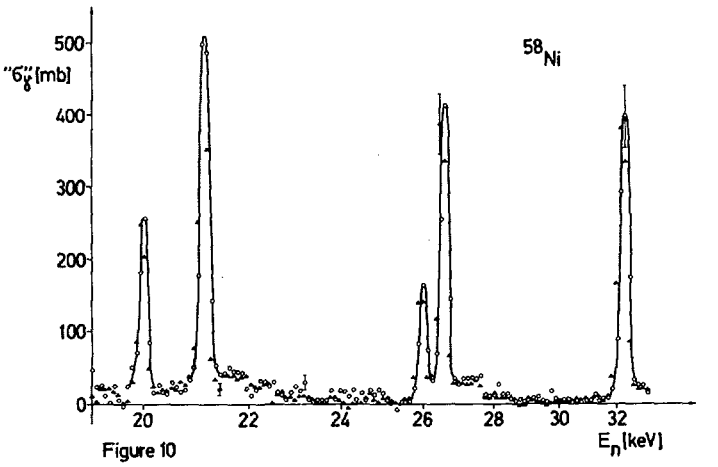

Figure 10

FIGS 9-12 (continued).

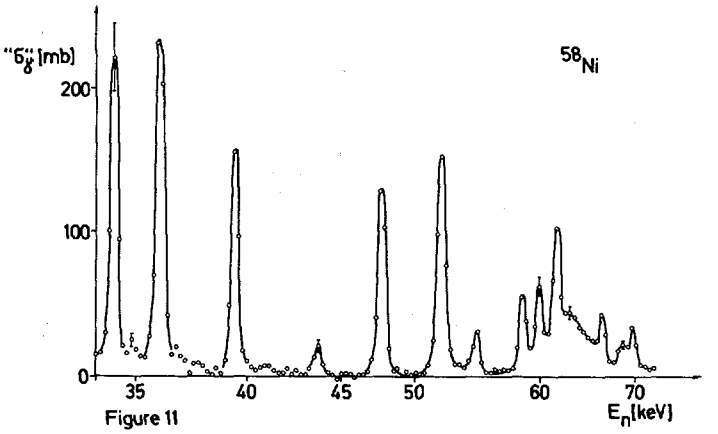

FIGS 9-12 (continued).

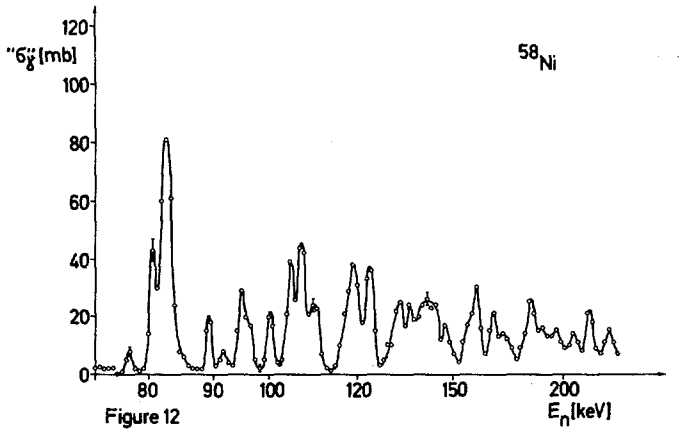

FIGS 9-12 (continued).

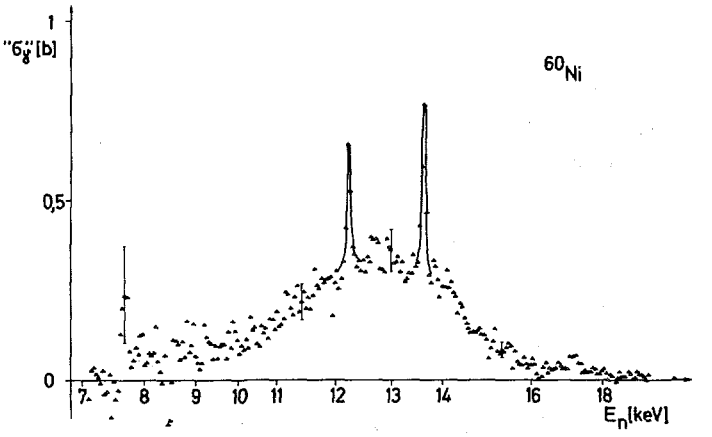

FIGS 13-16. ^{60}Ni capture yield divided by sample thickness versus energy; triangles: low-energy run, circles: high-energy run.

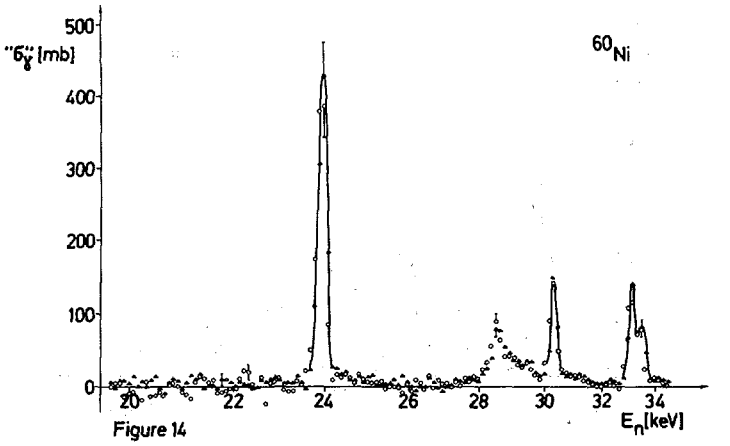

FIGS 13-16 (continued).

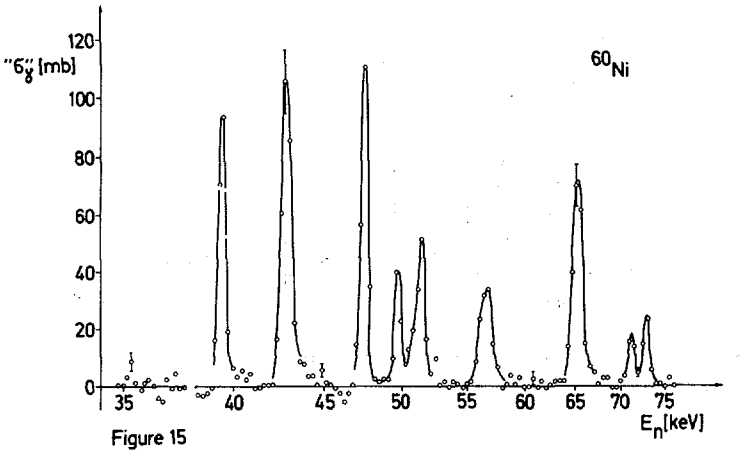

Figure 15

FIGS 13-16 (continued).

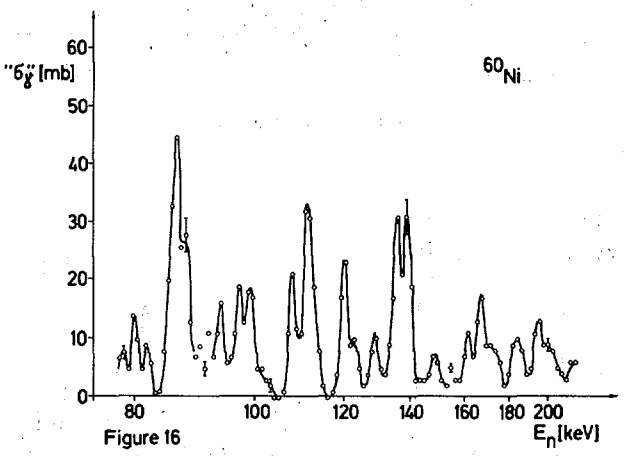

Figure 16

FIGS 13-16 (continued).

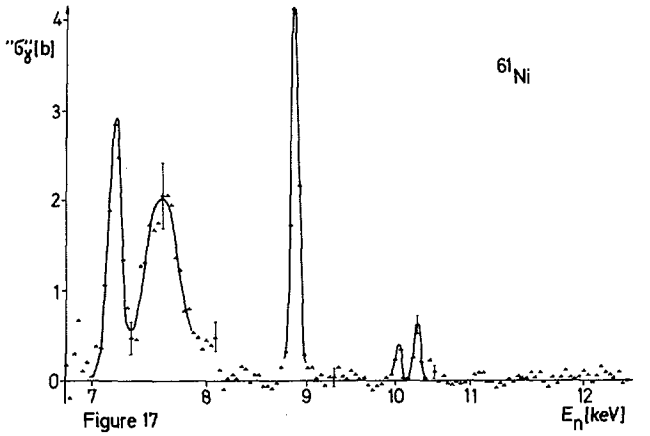

FIGS 17-21. ^{61}Ni capture yield divided by sample thickness versus energy; triangles: low-energy run, circles: high-energy run.

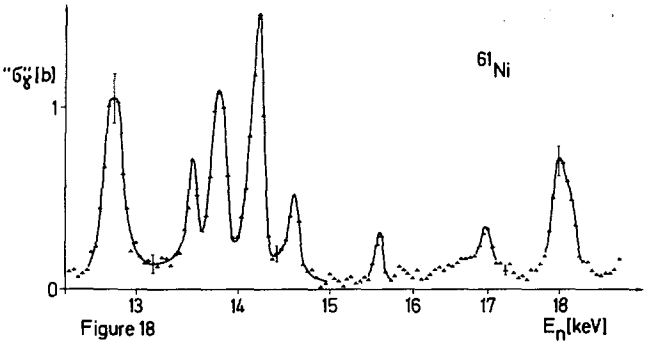

FIGS 17-21 (continued).

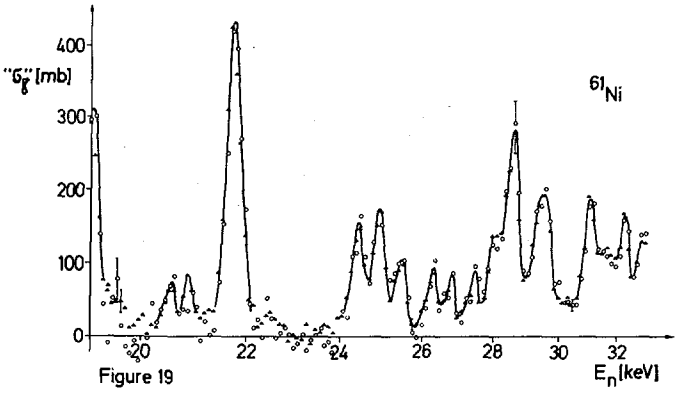

FIGS 17-21 (continued).

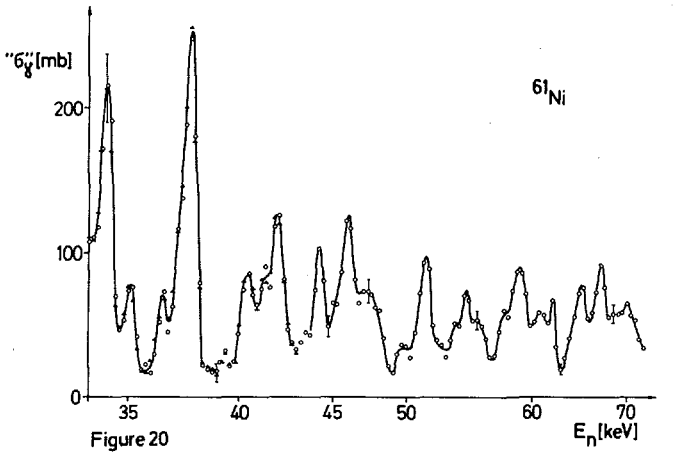

FIGS 17-21 (continued).

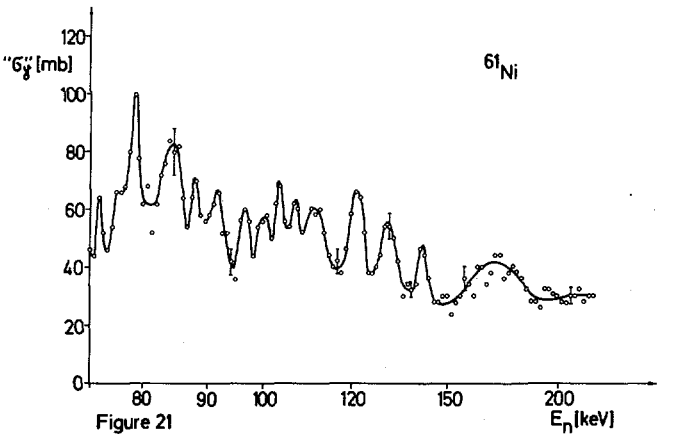

FIGS 17-21 (continued).

a few values were known from the literature [4]. Capture yield analysis was performed with a modified version of the program TACASI [5]. This program fits measured capture areas by adjusting the radiation widths. The TACASI code uses sums of single-level terms to represent the total cross-section and the capture cross-section. The effect of multiple scattering is calculated by Monte-Carlo methods. Since the resonances investigated have usually much larger neutron width than radiation width, multiple interactions were important. The contribution of multiple interactions are listed in Table III.

6. RESULTS

Capture yields divided by the sample thicknesses are shown in Figures 1 - 7 and 9 - 21. Many resolved resonances can be seen in the capture yield. The number of resonances observed over a fixed neutron energy interval is given in Table II.

The calculations of radiation widths are not yet finished. The results obtained until now are given in Table III.

Pulse height spectra obtained from a natural iron sample are given in figure 8. Table IV gives details on the spectra. The relative coincidence efficiency is the relative efficiency obtained with majority coincidence (at least two quarters of the scintillator tank must give a signal for a capture event to be recorded).

7. DISCUSSION

The main result of the present work are the capture cross sections presented in Figs. 1 - 7 and 9 - 21 and the radiation widths listed in Table III.

In several cases the isotopic assignments differ from those given in [6], where essentially the same samples were used. An important improvement of the analysis methods applied in the present work over those of [6] is the inclusion of well-analyzed total cross-section data, especially resonance spins and neutron widths, in the analysis. This enabled us to extract a large number of radiation widths, particularly for most of the broad s-wave resonances. The only level where previously reported values could be compared to our numbers is the 27.9 keV resonance of ^{56}Fe+n. Our result, (1.4 ± 0.2) eV, agrees well with the published values (1.5 ± 0.3) eV [8], 1.3 eV [7] and (1.44 ± 0.14) eV [6]. The radiation widths for ^{60}Ni and ^{61}Ni are much larger (roughly 2 eV) than those of other nuclei with similar masses (roughly 0.5 eV, see [9]). This seems to confirm conclusions reached by Moldauer [10] who had to assume radiation widths of the order of 1 eV for the nickel isotopes in order to fit unresolved capture data. Schmitt [11] estimated even higher radiation widths, using measured resonance integrals and thermal capture cross sections. Kuklin [12] gives a simple formula to estimate average radiation widths from the nuclear mass, the effective excitation energy and the single-particle level density at the Fermi energy. With this formula one finds values between 1 and 2 eV, depending a little on the way in which pairing corrections are applied to the excitation energy and on the single-particle level densities chosen. The main effect, according to Kuklin's formula, comes from the rather small single-particle level densities and high binding energies of the nickel isotopes, which in turn are related to the magic proton number of nickel.

ACKNOWLEDGEMENT

We wish to acknowledge the cooperation of the USAEC and Euratom agencies and committees who helped us to get the enriched isotopic samples. We thank Professor Beckurts for his interest in this work. The help of the Van de Graaff crew is also appreciated.

REFERENCES

[1] KOMPE, D., ERNST, A., FRÖHNER, F.H., Nucl. Phys. A141 (1970) 602.
[2] KOMPE, D., Nucl. Phys. A133 (1966) 513.
[3] CHO, M., et al., these Proceedings.
[4] BNL 325, Second Edition, Supplement No. 2 (1966).
[5] FRÖHNER, F.H., General Atomic Report GA-6906 (1965).
[6] HOCKENBURY, R.W., et al., Phys. Rev. 178 (1969) 17.
[7] MOXON, M.C., International Conference on the Study of Nuclear Structure with Neutrons, Antwerpen, 1965 (North Holland Publishing Co., Amsterdam, 1966).
[8] MACKLIN, R.L., PASMA, P.J., GIBBONS, J.H., Phys. Rev. 136 (1964) B695.
[9] JULIEN, J., et al., Nucl. Phys. A132 (1969) 129.
[10] MOLDAUER, P.A., in Physics of Fast and Intermediate Reactors, 1961) (Proc. Sem. Vienna) 1, IAEA (Vienne, 1962) 171.
[11] SCHMIDT, J.J., Report KFK 120 (1966).
[12] KUKLIN, R.N., Soviet Phys. Nucl. Phys. 7 (1968) 337.

DISCUSSION

M. C. MOXON: Can you say what effect the variation of γ-ray spectra from resonance to resonance has on the efficiency of detecting neutron-capture events in these isotopes? What effects do these variations in efficiency have on the capture cross-section, especially if interference effects are present due to initial high-energy γ-ray transitions?

A. ERNST: The effect of variations in γ-ray spectra is that the detector efficiency is not the same for all resonances. Therefore, the spectrum fraction and the probability that not all photons escape the detector without interaction have to be determined separately for each resonance from the corresponding pulse-height spectrum. Estimates for the non-escape probability lie between 0.8 ± 0.1 and 0.95 ± 0.05 for ^{56}Fe. I agree that in these cases of very low multiplicities interference might be possible, but so far we have not included interference effects in our neutron-capture calculations.

НЕЙТРОННЫЕ СЕЧЕНИЯ ИЗОТОПОВ-ПОГЛОТИТЕЛЕЙ, ИСПОЛЬЗУЕМЫХ В АТОМНЫХ РЕАКТОРАХ

В. П. ВЕРТЕБНЫЙ, М. Ф. ВЛАСОВ,
Н. Л. ГНИДАК, В. В. КОЛОТЫЙ,
А. Л. КИРИЛЮК, Е. А. ПАВЛЕНКО,
М. В. ПАСЕЧНИК, В. Ф. РАЗБУДЕЙ,
А. Ф. ФЕДОРОВА
Институт физики Академии наук УССР, Киев,
Украинская Советская Социалистическая Республика

Presented by G.V. Muradyan

Доклад представлен Г.В. Мурадяном

Abstract — Аннотация

NEUTRON CROSS-SECTIONS OF ISOTOPES USED AS ABSORBERS IN ATOMIC REACTORS.

The authors present the principal results of measurements of the energy dependence of the total neutron cross-sections, the neutron scattering cross-sections and the radiative capture cross-sections of a large number of non-fissionable isotopes. For their measurements they used the VVR-M (water-moderated, water-cooled) reactor of the Physics Institute of the Ukrainian SSR Academy of Sciences and the time-of-flight method in the energy range 0.007-10 eV. The paper contains a review of methods for increasing substantially the accuracy of total and partial cross-section measurements (reduction of multiple scattering, determination of the influence of impurities, irradiation of samples in the reactor core, etc.). Particular attention is paid to strong absorbers. In view of the fact that europium and dysprosium are used in reactor control, a careful analysis is made of all the neutron constants of these isotopes with a view to ascertaining the reasons for discrepancies between the results of different authors. Questions connected with the systematics of neutron cross-sections are discussed and experimental results are compared with theory.

НЕЙТРОННЫЕ СЕЧЕНИЯ ИЗОТОПОВ-ПОГЛОТИТЕЛЕЙ, ИСПОЛЬЗУЕМЫХ В АТОМНЫХ РЕАКТОРАХ.

Приводятся основные результаты измерений энергетической зависимости полных нейтронных сечений, нейтронных сечений рассеяния и сечений радиационного захвата большого количества неделящихся изотопов. Измерения выполнены на атомном реакторе ВВР-М Института физики АН УССР по методу времени пролета в диапазоне 0,007-10 эв. Дан обзор методов, позволивших существенно повысить точность измерений полных и парциальных сечений (снижение многократного рассеяния, определение влияния примесей, облучение образцов в активной зоне атомного реактора и т. п.). Особое внимание уделено сильным поглотителям. В связи с тем, что европий и диспрозий являются материалами, применяемыми для регулирования мощности атомных реакторов, проведен тщательный анализ всех нейтронных констант изотопов диспрозия и европия, позволивший выяснить в ряде случаев причины расхождений в результатах различных авторов. Рассмотрены вопросы, связанные с систематикой нейтронных сечений. Результаты экспериментов сравниваются с теорией.

ВВЕДЕНИЕ

На реакторе ВВР-М Института физики АН УССР ведутся систематические измерения полных и парциальных сечений изотопов для тепловых и эпитепловых нейтронов с целью получения более точных данных. Необходимость подобных измерений определяется различными соображениями,

в том числе и запросами реакторной техники. В прошлом в этой области энергий выполнено много измерений, тем не менее, точность нейтронных констант даже ряда распространенных изотопов не высока. Например, для сечения захвата ^{153}Eu при v = 2200 м/сек приводится 317 ± 5 барн [1] и 639 ± 7 барн [2]. Далеко не всегда имеются сведения об энергетической зависимости радиационного захвата и сечений рассеяния: для радиационного захвата чаще всего приводятся данные, усредненные по тепловому спектру: для рассеяния — только сечение когерентного рассеяния и, так называемое, $\bar{\sigma}_s$ — значение сечения рассеяния, полученное экстраполяцией σ_{tot} к $E_n \to \infty$. Ошибки при этом могут быть большими. В результате измерения как энергетической зависимости полных сечений, так и сечений рассеяния в прямом опыте (а в ряде случаев и сечений радиационного захвата) авторы надеются получить информацию, более полно и точно характеризующую взаимодействие медленных нейтронов с атомными ядрами. Особое внимание уделено изотопам редкоземельных элементов, у которых, благодаря высокой плотности уровней и сравнительно большой величине силовой функции $\bar{\Gamma}_n^0/D$, часто встречаются резонансы, близкие к нулевой энергии, а поэтому и большие сечения для тепловых и эпитепловых нейтронов.

1. МЕТОДИКА ЭКСПЕРИМЕНТА

Измерения полных сечений выполняются методом времени пролета с помощью механических прерывателей с разрешением 1-6 мксек/м (вблизи энергии нейтронов ~0,01 эв) [3,4]. Пролетные расстояния — от 20 до 70 м. Диаметр прерывателей — 200 и 300 мм. Наименьшая ширина щели — 0,2 и 0,5 мм, соответственно. Фон в этих измерениях в большей области энергий составляет несколько процентов. Измерения сечений рассеяния и энергетической зависимости сечения радиационного захвата также ведутся по методу времени пролета с разрешением 3-10 мксек/м [5] в энергетическом диапазоне 0,01-9 эв. Прерыватель диаметром 300 мм имеет прямые щели шириной 2 мм. Пролетное расстояние — примерно 6 м. В экспериментах по рассеянию фон обусловлен рассеянием нейтронов на контейнере. Обычно он составляет 20-30% от эффекта. На долю остальных источников фона приходится 2-3% от эффекта.

Отличительной чертой всех вышеперечисленных установок является то, что они приспособлены для измерений на малых количествах вещества. Именно эта особенность позволяет вести измерения на редких изотопах, а также образцах, подвергшихся облучению в активной зоне атомного реактора, а при определении сечений рассеяния использовать сравнительно тонкие образцы ($n\sigma_t \leq 0,1$) и тем самым уменьшить влияние эффектов ослабления и многократного рассеяния в образце.

Измерение полных сечений

Полные сечения определяются методом пропускания. Сравнительно нетрудно получить статистическую точность пропускания порядка 0,2-0,3%. Однако точное определение ядерных констант из пропускания образца сопряжено с целым рядом трудностей, которые, с одной стороны, связаны с нейтронно-оптическими эффектами (дифракцией нейтронов на упорядоченных структурах, рассеянием под малыми углами на зернах, магнитным и неупругим рассеяниями), с другой стороны, — с неидеальностью приготовления самого образца.

Трудности первого типа особенно существенны. Для исключения их желательно вести измерения по возможности в области более быстрых нейтронов и использовать образцы в виде растворов или достаточно мелкодисперсных порошков. Однако это не исключает полностью нейтронно-оптических эффектов, магнитного и неупругого рассеяний. Точность результатов окончательной обработки данных в известной мере зависит от точности теоретического описания тех или иных эффектов, которые всегда относятся к идеализированным объектам. Поэтому желательно проводить измерения на образцах различных составов.

Некоторые из нейтронно-оптических эффектов хорошо иллюстрируются рис. 1 и 2. На рис. 1 представлено полное сечение рассеяния природного германия при различных размерах зерен. В верхней части рис. 1 экспериментальные данные для зерен диаметром $\leq 5 \cdot 10^{-2}$ см изображены кривой 1; результаты расчета сечения рассеяния на решетке (сдвинута по вертикали) – кривой 2; в нижней части рис. 1 приведены экспериментальные данные для зерен диаметром $\leq 10^{-3}$ см. Эффект экстинкции на достаточно больших зернах ведет к уменьшению сечения. На рис. 2 приведено полное сечение для образца аэросила-300 (SiO_2). Средний радиус зерна – 40 Å. Эффект рассеяния на малые углы должен всегда приниматься во внимание при измерении методом времени пролета, т. к. углы, под которыми обычно виден детектор с образца, составляют всего лишь 10^{-2}–10^{-3} рад. В приведенном примере для $\lambda \sim 10$Å полное сечение, отнесенное к молекуле, в тридцать раз больше ядерного. Полное сечение при этом пропорционально λ^2. Отметим, что при измерениях на металлических фольгах надо учитывать эффект кристаллитов; на растворах – влияние структурных факторов и неупругого рассеяния нейтронов.

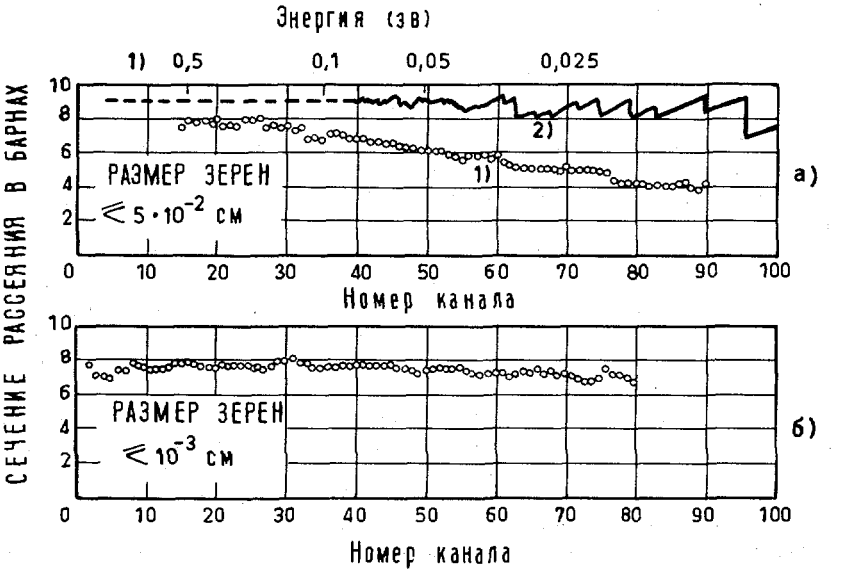

Рис. 1. Полное сечение рассеяния нейтронов на образцах германия в зависимости от энергии и времени пролета.

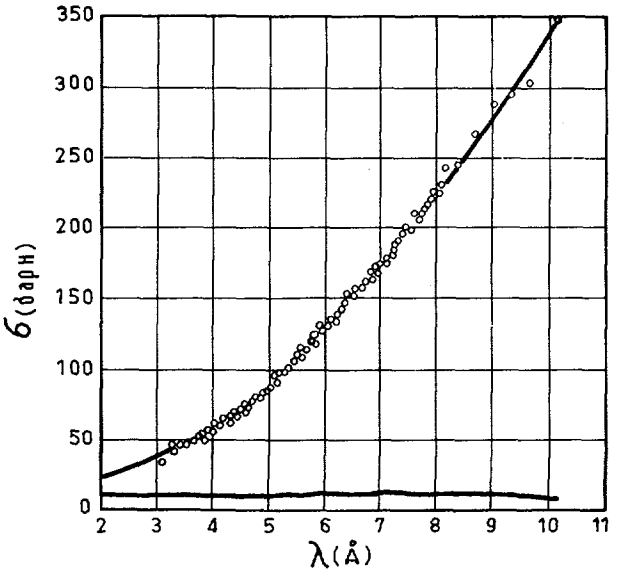

Рис. 2. Полное сечение образца аэросила-300 в зависимости от длины волны нейтронов.

Сечение магнитного рассеяния для ряда случаев, например для редкоземельных элементов, может быть сравнимо по величине с ядерным [5]. Сечение парамагнитного рассеяния нетрудно рассчитать, если известен магнитный форм-фактор:

$$\sigma_M = \text{const} \cdot \lambda^2 M^2 \int_0^{1/2} i(s)\,sds$$

где i – магнитный форм-фактор; λ – длина волны нейтрона; $s = \sin\theta/\lambda$; M – магнитный момент. Сечение парамагнитного рассеяния на ионе Dy^{+++}($M = 10{,}7\ M_B$) составляет при $v = 2200$ м/сек 20,3 барн, тогда как для Eu^{+++} – всего лишь 2 барна ($M = 3{,}6\ M_B$).

Подчеркнем, что в случае $\sigma_a \sim \sigma_s$ желательны тщательное изучение физических свойств исследуемого образца и измерения на образцах различного состава в возможно более широком диапазоне энергий, с тем чтобы при сопоставлении эксперимента с теорией оценить вклад различных искажающих эффектов и выбрать тот энергетический диапазон, где этот вклад достаточно мал.

Трудности, связанные с неидеальностью образцов, могут быть самыми разнообразными. Так, например, в случае порошков следует учитывать неоднородность набивки образцов. Для этого необходимо знать распределение концентрации по образцу. Это распределение может быть получено либо фотографированием образца в монохроматических гамма-лучах, либо зондированием его узким пучком монохроматических нейтронов. Для сравнительно толстого образца ^{164}Dy ($n\sigma_t \approx 1{,}6$) нами проведено такое исследование неоднородности последним из перечисленных методов, причем прозрачность измерялась в двух взаимно перпендикулярных

направлениях с помощью нейтронов со средней энергией 0,03 эв (рис. 3). Поправка на неоднородность вводилась по формуле, предложенной в работах [3,6]:

$$\sigma_{ист} = \sigma_{изм}(E) + \frac{\Delta n^2}{2n}\sigma''_{изм}(E)$$

Несмотря на сравнительно большую неоднородность образца, поправка в сечении, обусловленная ею, была $\leq 1\%$. Это свидетельствует о том, что поправки, связанные с неоднородностью приготовления образца, невелики и существенно не сказываются на определении σ_t.

На определение величины сечения иногда могут существенно влиять примеси других веществ в образце. В редкоземельных элементах – это примеси сильнопоглощающих, нечетных изотопов Gd и Sm. Содержание примесей определяется либо масс-спектрографическим, либо спектроскопическим методом по гамма-лучам захвата, если при этом учитывается разница в энергии связи нейтронов B_n и в особенности спектров жестких гамма-лучей. Последний метод и был использован авторами при определении примесей Gd в образцах четных изотопов Dy.

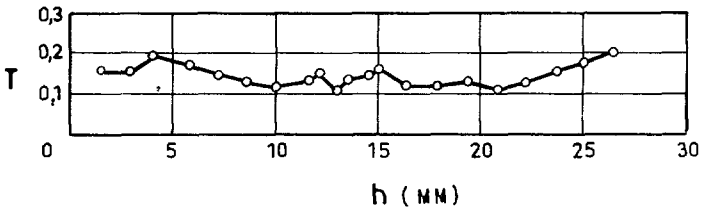

Рис. 3. Распределение пропускания по высоте образца. Измерения сделаны с шагом 1,41 мм. Поперечное сечение пучка нейтронов – 2 × 0,2 мм.

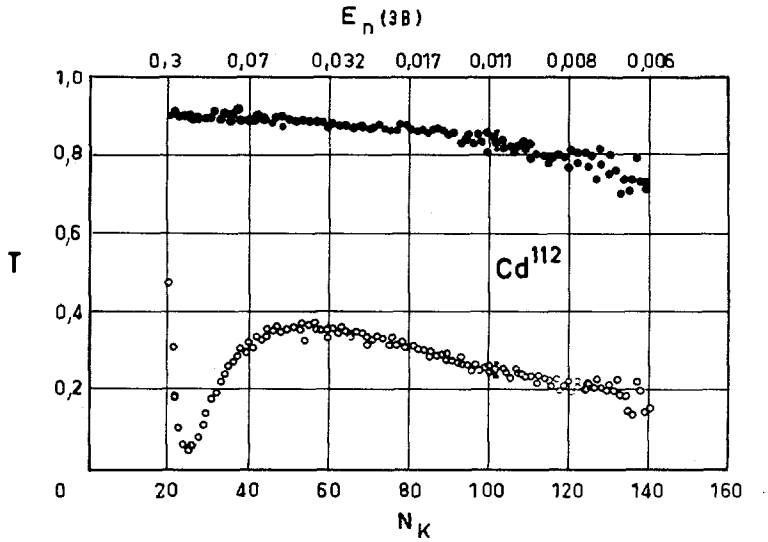

Рис. 4. Пропускание образцов ^{112}Cd до облучения (светлые точки, толщина образца – 0,6 мм) и после облучения (темные точки, толщина – 6 мм) в зависимости от энергии нейтронов и времени пролета. В пропускании облученного образца исчез провал, соответствующий резонансу $E_0 = 0{,}178$ эв ^{113}Cd.

Бывают случаи, когда в образце, обогащенном исследуемым изотопом, содержится некоторое количество сильнопоглощающего изотопа того же элемента; тогда малейшие ошибки в определении концентрации сильнопоглощающего изотопа приводят к существенным ошибкам в определении сечений исследуемого. Чтобы избавиться от этого, мы "выжигаем" сильнопоглощающую примесь, облучая образец в активной зоне атомного реактора [7]. На рис. 4 показано пропускание образца ^{112}Cd до и после облучения. Содержание сильнопоглощающего изотопа ^{113}Cd в первом случае – 4,8%, во втором $\leq 10^{-3}$ %. Отметим, что измерением пропускания образца-поглотителя до и после облучения в реакторе сравнительно нетрудно определить абсолютный поток нейтронов [8].

Измерение сечений рассеяния

Измерение сечений рассеяния производится в 4π-геометрии. Диаметр образцов равен примерно 10 мм. Поток нейтронов с помощью коллиматора "фокусируется" на образец [5]. Толщина образца выбирается, как правило, так, что $n\sigma_t \leq 0{,}1$. Диапазон энергии – 0,01-10 эв. Измерения ведутся относительно V, при этом сечение его принимается равным 5,1 барн. Определенные нами величины сечений C и Pb хорошо согласуются с общепринятыми. В большинстве случаев поправки на многократное рассеяние были несущественными. Для введения поправок на ослабление нейтронов в образце, разработаны расчетные методы, которые проверены измерением на стандартных образцах. Для детектирования нейтронов ранее использовался 4π-борный счетчик; сейчас используется детектор, собранный из счетчиков, наполненных ^3He до семи атмосфер (СНМ-37). Гелиевые счетчики позволили увеличить эффективность регистрации нейтронов под всеми углами (η = 92-99% при E_n = 0,04 эв и η = 72-99% при E_n = 0,16 эв) и тем самым уменьшить поправки на изменение эффективности регистрации за счет угловой анизотропии рассеянных нейтронов и изменения энергии нейтронов при рассеянии. Правда, сейчас гелиевые счетчики охватывают лишь одну шестую часть телесного угла, но в ближайшее время мы собираемся дополнить батарею до 4π и довести эффективность почти до 100% в большем диапазоне энергии нейтронов.

Определение энергетической зависимости сечения радиационного захвата

Энергетическая зависимость сечения радиационного захвата также определялась методом времени пролета. Использовался тот же нейтронный пучок и тот же механический прерыватель, что и в опытах по рассеянию. Гамма-лучи из реакции (n, γ) регистрировались с помощью сцинтилляционного спектрометра. Спектрометрический кристалл NaJ(Tl) диаметром и высотой 80 мм, защищенный от рассеянных нейтронов слоем карбида бора с парафином, помещался в конце пролетной базы под углом 90° к пучку. Использовались те же образцы, что и в опытах по рассеянию. Было показано с помощью измерений на "чистом" рассеивателе-фторопласте, что эффектом рассеянных нейтронов можно пренебречь. Чтобы исключить энергетическую зависимость падающего потока, измерения проводились относительно "черного" образца In.

Для тонкого исследуемого образца ($n\sigma_t \ll 1$) счет от гамма-лучей захвата N_x определяется следующей формулой:

$$N_x(E) = \Phi(E) n_x \sigma_{ax}(E) \eta_x \qquad (1)$$

где: $\Phi(E)$ – поток нейтронов, n_x – число ядер на квадратный сантиметр, η_x – эффективность регистрации гамма-лучей, σ_{ax} – сечение радиационного захвата нейтронов исследуемым образцом.

В случае "черного" образца (индия) счет гамма-лучей

$$N_{In} = \Phi(E) \frac{\sigma_a(In)}{\sigma_t(In)} (1 - T) \eta_{In} = \Phi(E) \eta_{In} \qquad (2)$$

если $\sigma_s \ll \sigma_a$.

Отсюда, разделив (1) на (2), получим

$$\sigma_{ax}(E) = \text{const} \frac{N_x(E)}{N_{In}(E)} \qquad (3)$$

Таким образом, этот опыт позволяет определить лишь энергетический ход сечения радиационного захвата; абсолютное значение сечений остается неизвестным. Тем не менее, соотношение (3) важно при определении параметров отрицательного уровня.

Гамма-спектрометр оказывается полезным также для экспериментального, независимого от масс-спектрографического, определения наличия в четных изотопах примесей сильнопоглощающих нечетных изотопов, таких, как ^{157}Gd. Например, энергия возбуждения ядра при захвате нейтрона ^{164}Dy составляет 5,8 Мэв, тогда как при захвате нечетными изотопами – 8,5-8 Мэв. Если выбрать порог дискриминации так, чтобы он превышал 5,8 Мэв, то отношение скоростей счета с образцом ^{164}Dy и "черным" образцом Gd равно

$$\frac{N_{Dy}}{N_{Gd}} = \frac{\Phi(E)}{\Phi(E)} \frac{n\sigma_a(^{155,157}Gd)}{\eta_{Gd}} \eta_{Gd} = n\sigma_a(^{155,157}Gd) \qquad (4)$$

В случае ^{164}Dy это отношение оказалось равным $0 \pm 0{,}015$, т. е. примеси нечетных изотопов не вносили существенного вклада в радиационный захват.

2. РЕЗУЛЬТАТЫ ИЗМЕРЕНИЙ

В этом разделе приведены некоторые результаты измерений, выполненных в последнее время на атомном реакторе ВВР-М Института физики АН УССР: полные сечения рассеяния и радиационного захвата для $^{161,162,163,164}Dy$ и сечения рассеяния для ряда других изотопов.

Нейтронные сечения изотопов диспрозия

Зависимости полных сечений σ_t $^{161,162,163,164}Dy$ от энергии и времени пролета изображены на рис. 5-8, а сечения рассеяния – на рис. 9 (^{161}Dy – верхняя, ^{163}Dy – нижняя кривая) и на рис. 10 (^{162}Dy). Нижняя кривая на рис. 11 изображает зависимость сечения рассеяния ^{164}Dy, а верхняя – энергетический ход радиационного захвата в относительных единицах.

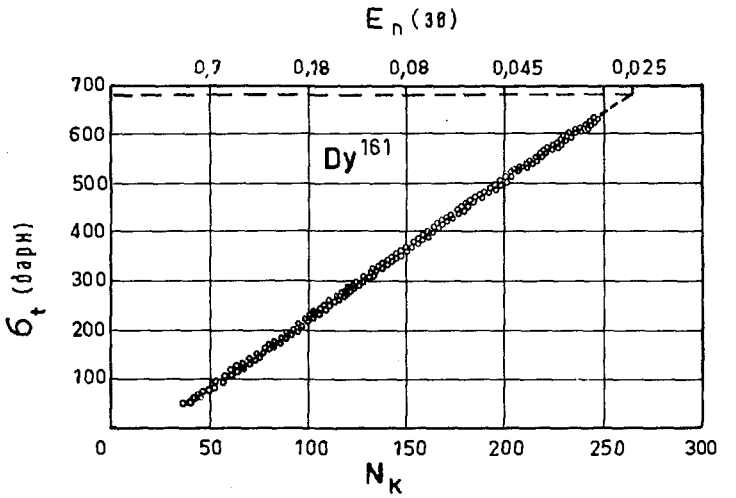

Рис. 5. Полное сечение ^{161}Dy в зависимости от энергии (времени пролета) нейтронов. Разрешение – 1,8 мксек/м.

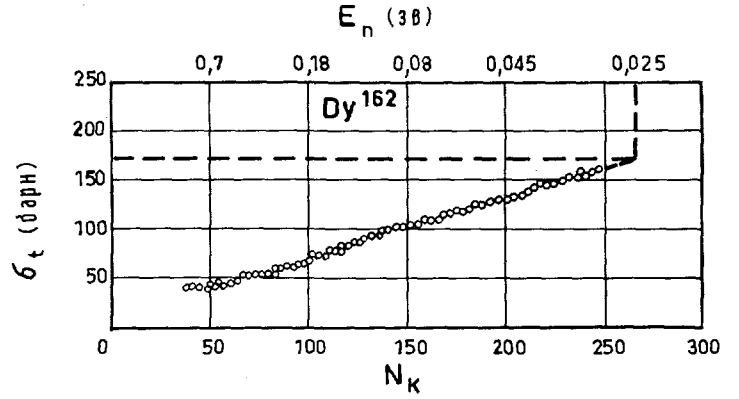

Рис. 6. Полное сечение ^{162}Dy в зависимости от энергии (времени пролета) нейтронов. Разрешение – 1,8 мксек/м.

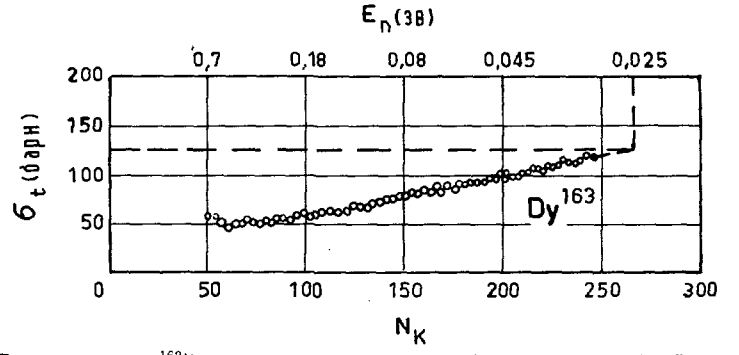

Рис. 7. Полное сечение ^{163}Dy в зависимости от энергии (времени пролета) нейтронов. Разрешение – 1,8 мксек/м.

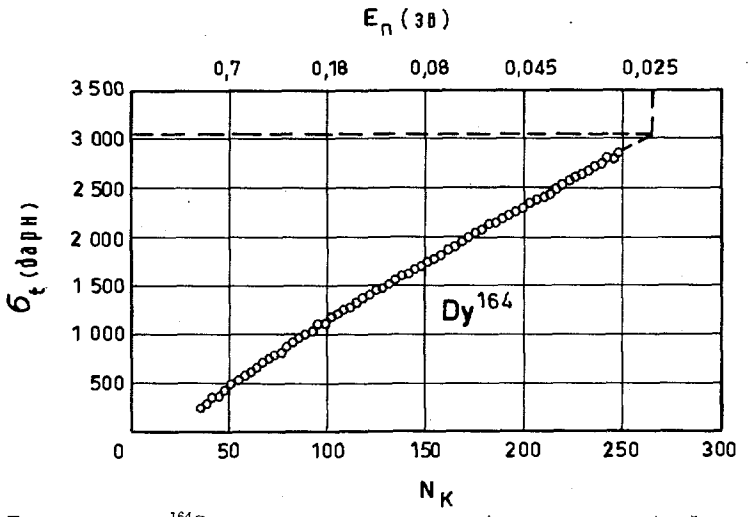

Рис. 8. Полное сечение ^{164}Dy в зависимости от энергии (времени пролета) нейтронов. Разрешение – 1,8 мксек/м.

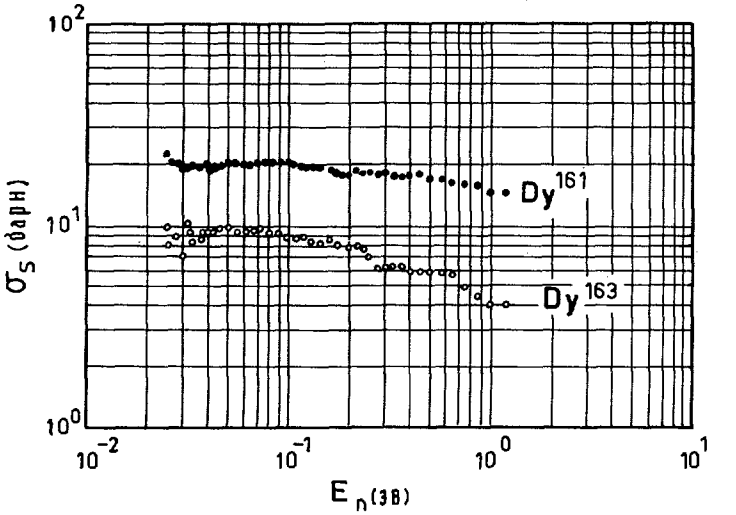

Рис. 9. Полные сечения рассеяния ^{161,163}Dy в зависимости от энергии нейтронов. Разрешение – 5,5 мксек/м.

Измерения выполнены на образцах окиси диспрозия, изотопный состав которых приведен в табл. 1. При обработке данных сделаны поправки на магнитное рассеяние (~20 барн при v = 2200 м/сек) и на неоднородность (меньше 1%). Экспериментально было показано, что примеси Gd не могут привести к завышению сечения более чем на 2% для ^{164}Dy и на 8% для ^{162}Dy. Для четных изотопов Dy в энергетическом интервале 0,01-0,5 эв в пределах 2-3% существует соответствие между абсолютной величиной сечения радиационного захвата $\sigma_t - \sigma_s$ и относительной величиной, опре-

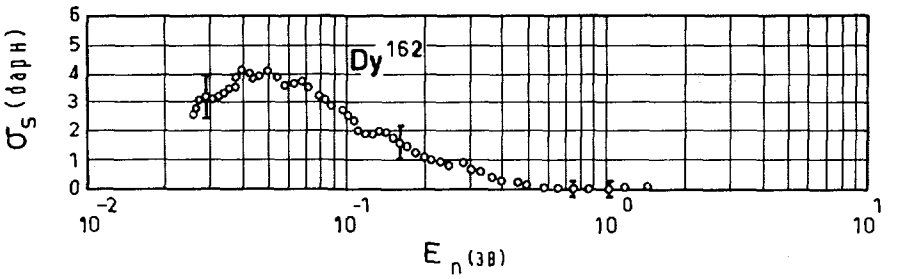

Рис. 10. Полное сечение рассеяния ^{162}Dy в зависимости от энергии нейтронов. В области 0,8-1,5 эв наблюдается интерференционный минимум резонанса 5,44 эв.

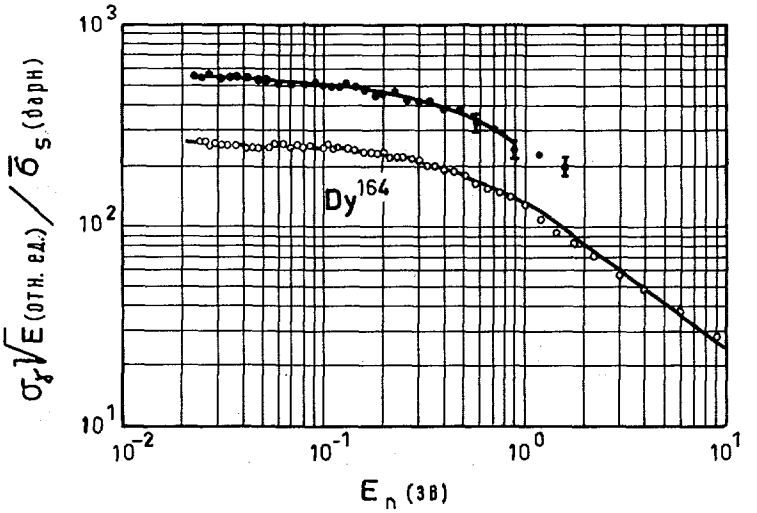

Рис. 11. Полное сечение рассеяния (в барнах) и сечение поглощения ^{164}Dy (в относительных единицах) в зависимости от энергии нейтронов. Разрешение – 3 и 5,5 мксек/м.

ТАБЛИЦА 1. ИЗОТОПНЫЙ СОСТАВ ОБРАЗЦОВ Dy

Образец	Концентрация изотопов				
	^{160}Dy	^{161}Dy	^{162}Dy	^{163}Dy	^{164}Dy
^{161}Dy	0,6	94,2	3,5	1,1	0,6
^{162}Dy	0,2	1,6	94,0	3,3	0,9
^{163}Dy	0,2	0,4	2,1	92,8	4,5
^{164}Dy	0,1	0,3	0,8	1,8	97

ТАБЛИЦА 2. НЕЙТРОННЫЕ КОНСТАНТЫ ИЗОТОПОВ Dy при v = 2200 м/сек

Изотоп	Полное сечение σ_t барн	Сечение поглощения σ_a барн	Сечение рассеяния σ_s барн	σ_a^* барн
^{161}Dy	677^{+12}_{-20}	655^{+12}_{-20}	22 ± 1	630 ± 17
^{162}Dy	172^{+6}_{-16}	170^{+6}_{-16}	2,5 ± 0,8	176^{+6}_{-9}
^{163}Dy	126^{+6}_{-12}	116^{+6}_{-12}	9,7 ± 0,4	126^{+6}_{-12}
^{164}Dy	3000^{+45}_{-70}	2740^{+45}_{-70}	262 ± 7	2740^{+45}_{-70}

* Сечения, усредненные по данным авторов и данным других работ.

ТАБЛИЦА 3. СЕЧЕНИЯ РАССЕЯНИЯ при v = 2200 м/сек

Изотоп	Сечения рассеяния барн	Изотоп	Сечения рассеяния барн
^{11}B	4,9 ± 0,2	^{140}Ce	4,0 ± 0,2
C	4,8 ± 0,1	^{142}Ce	3,7 ± 0,2
V*	5,10	^{153}Eu	8,0 ± 0,2
Cu	6,9 ± 0,3	Dy	82,6 ± 0,3
^{63}Cu	4,8 ± 0,4	^{161}Dy	22,0 ± 0,4
^{65}Cu	11,4 ± 0,4	^{162}Dy	2,5 ± 0,8
Ge	7,5 ± 0,2	^{163}Dy	9,7 ± 0,4
^{70}Ge	8,8 ± 0,8	^{164}Dy	262,0 ± 7
^{72}Ge	7,5 ± 0,7	Ho	9,5 ± 0,2
^{73}Ge	1,0 ± 0,9	Er	11,0 ± 0,8
^{74}Ge	6,1 ± 0,4	^{162}Er	3,8 ± 2,0
Cd**	5,6 ± 0,3	^{164}Er	12,1 ± 0,7
^{110}Cd**	4,3 ± 0,2	^{166}Er	19,1 ± 1,0
^{111}Cd**	5,2 ± 0,3	^{167}Er	7,9 ± 0,8
^{112}Cd**	6,9 ± 0,3	^{168}Er	13,1 ± 0,7
^{114}Cd**	5,2 ± 0,3	^{170}Er	15,9 ± 0,8
^{116}Cd**	6,4 ± 0,3	Yb	25,0 ± 0,8
Ce	4,7 ± 0,3	Lu	6,0 ± 0,2
		Pb	11,4 ± 0,2

* Эталонный образец.

** Измерено σ_s лишь при E_n = (0,4-9) эв.

деленной с помощью сцинтилляционного спектрометра. Выше 0,5 эв расхождения достигают 5-8%, но не превышают статистических ошибок. В табл. 2 приведены полные сечения, сечения захвата и рассеяния при v = 2200 м/сек. Полные сечения и сечения захвата получены экстраполяцией экспериментальных данных к этой же точке. Законность экстраполяции подтверждается тем, что $\sigma_a\sqrt{E}$ постоянно в интервале энергий, значительно большем, чем 0,005 эв в окрестности E_n = 0,03 эв. В значения сечений выше 1,5 эв не введены поправки на конечность разрешения, связанные с существованием резонанса 1,73 эв ^{163}Dy. В табл. 2 учтены не только статистические ошибки, но и ошибки, вызванные дрейфом всей аппаратуры в целом – 1,5-2%. При измерении полных сечений образцы в точке v = 2200 м/сек имели толщину $n\sigma_t$ = 1,6; 0,86; 0,68 и 2,9, соответственно, для ^{161,162,163,164}Dy. Образцы для измерений сечений рассеяния в диапазоне энергии 1-0,0253 эв имели толщину $n\sigma_t$ для ^{161}Dy от 0,02 до 0,23; для ^{162}Dy – от 0,04 до 0,17; для ^{163}Dy – от 0,03 до 0,23 и для ^{164}Dy – от 0,05 до 0,30, соответственно.

Сечения рассеяния изотопов

Результаты измерений даны в табл. 3. Измерения проведены в энергетическом диапазоне 0,02-3 эв на образцах разделенных изотопов. Данные усреднены по области, где сечение постоянно. Для изотопов Cd, чтобы исключить влияние резонанса ^{113}Cd, рассеяние измерялось выше 0,4 эв. Для ^{11}B, C, Cu, $^{63-65}$Cu, Ge, Cd, $^{110-116}$Cd образцы брались в виде простых веществ, для остальных изотопов – в виде окислов: GeO_2, CeO_2, $^{153}Eu_2O_3$, Dy_2O_3, Er_2O_3, Ho_2O_3, Sb_2O_3, Lu_2O_3. Где было необходимо, вводились поправки на магнитное рассеяние. Лишь в случае изотопов Dy после вычитания магнитного рассеяния остается энергетическая зависимость в сечении рассеяния.

3. ОБСУЖДЕНИЕ РЕЗУЛЬТАТОВ

Изотопы диспрозия

Обсуждение данных для изотопов диспрозия по измерениям, выполненным до 1967 года, проведено одним из авторов данной работы в обзоре [9]. После этого появились краткие сообщения об определении энергетической зависимости сечений рассеяния изотопов $^{161-164}$Dy [10] и амплитуд когерентного рассеяния и полных нейтронных сечений $^{160-164}$Dy при λ = 1,08 Å [11].

Прежде всего, хотелось бы отметить, что сечения радиационного захвата, определенные нами по разнице $\sigma_t-\sigma_s$, при v = 2200 м/сек хорошо согласуются со средними значениями, взвешенными по данным различных лабораторий [9]. Значения полных сечений при λ = 1,08 Å, определенные нами и авторами работы [11], находятся также в хорошем согласии (табл. 4). Результаты по зависимости сечений захвата от энергии можно сопоставить лишь с работами [12] и [13]. Для ^{161,162,163}Dy между нашими данными и данными Л. С. Данеляна и др. [12] нет существенных расхождений. Правда, в случае ^{162}Dy наши результаты примерно на 20% ниже, чем результаты Л. С. Данеляна и др. Расхождения между величинами полных сечений ^{164}Dy, определенными в этой работе и в работе [11], составляют не более 3% в диапазоне 0,0253-0,5 эв; выше 0,5 эв наши значе-

ТАБЛИЦА 4. ПОЛНЫЕ СЕЧЕНИЯ ИЗОТОПОВ Dy λ = 1,08 Å (E_n = 0,07 эв)

Изотоп	Полные сечения барн		Сечения рассеяния барн	
	Данные настоящей работы	Данные [11]	Данные настоящей работы	Данные [11]
^{161}Dy	389 ± 9	366 ± 13	20,0 ± 0,3	13,3* ± 1
^{162}Dy	109 ± 2	111 ± 6	3,0 ± 0,7	$0{,}25\ ^{+0{,}20}_{-0{,}10}$
^{163}Dy	83 ± 2	85,9 ± 8	9,3 ± 0,4	3,14 ± 0,75
^{164}Dy	1826 ± 30	1880 ± 30	250 ± 3	306 ± 15

* Ошибки оценены авторами данной работы.

ния σ_t на 5-10% меньше, тогда как значения сечений захвата, определенные нами, систематически больше, чем в [13]; причем для $E_n \leq 0{,}2$ эв эта разница примерно равна 7%, а в области $E_n \approx 1$ эв – 20%. Причина этих расхождений не ясна. Возможно, она связана с некоторым произволом при нормировке сечения активации в [13].

Расхождения между значениями сечений рассеяния, полученными в [11] и в данной работе, довольно большие (безусловно, нельзя придавать значения расхождению между данными для ^{162}Dy, так как здесь $\sigma_{магн} \gg \sigma_{яд}$). Найти объяснение этому трудно. Однако мы хотим высказать несколько доводов в пользу наших результатов. Во-первых, нами проделаны измерения как на природном диспрозии, так и на всех основных изотопах, составляющих природную смесь, тогда как в [11] непосредственных измерений на ^{164}Dy не было сделано. Кроме того, при v = 2200 м/сек значение сечения рассеяния для природного диспрозия, вычисленное по данным для отдельных изотопов, хорошо согласуется с результатом нашего эксперимента на природном диспрозии [14] (81 и 82,6 барн, соответственно). Полные сечения рассеяния природного диспрозия, определенные нами, хорошо согласуются и с результатами [15] во всем энергетическом диапазоне, если из последних вычесть магнитное рассеяние. По данным же [11] сечение когерентного рассеяния природного диспрозия на 10% больше полного сечения, определенного нами. Сам ход энергетической зависимости сечения рассеяния ^{164}Dy в какой-то мере также свидетельствует в пользу наших значений (корректность введения поправок).

Данные по полным сечениям, по сечениям рассеяния и радиационного захвата, полученные нами, согласуются с предположениями о существовании отрицательных резонансов у ^{161,163,164}Dy, высказанными в [12,13]. Мы сделали попытку определить параметры отрицательного уровня для ^{164}Dy. Это было желательно, во-первых, потому, что в настоящее время только из такого анализа можно определить радиационную ширину ^{164}Dy (для положительного уровня $\Gamma_n \gg \Gamma_\gamma$), во-вторых, из-за некоторой противоречивости между значениями параметров, приведенных в [13]. Возможно, последнее и является причиной отмеченного в этой же работе несоответствия вычисленного отношения σ_s/σ_a результатам [15].

При анализе данных предполагалось, что сечения описываются следующими формулами (обозначения общепринятые):

$$\sigma_s(E) = 0{,}1257\,R^2 + \frac{0{,}572\,R\,g\Gamma_n^0}{E + |E_0|} + 0{,}650\,\frac{g\Gamma_n^{0^2}}{(E + |E_0|)^2} \qquad (5)$$

$$\sigma_a = \frac{0{,}650}{\sqrt{E}}\,\frac{g\Gamma_n^0\Gamma_\gamma}{(E + |E_0|)^2} \qquad (6)$$

Из (6) получена энергия отрицательного резонанса E_0 и произведение $\Gamma_n^0\Gamma_\gamma = (2309 \pm 30)$(мэв)^2, тогда как формула (5) использована для получения параметров Γ_n^0, R, а следовательно, и Γ_γ. При анализе были учтены и значения σ_t ^{164}Dy для E_n – 1-10 эв, полученные в [16]. С помощью набора параметров $E_0 = -2{,}19$ эв, $\Gamma_n^0 = 37$ мэв, $\Gamma_\gamma = 89$ мэв, $R = 7{,}7$ ферми удается одновременно описать $\sigma_a(E)$ и $\sigma_s(E)$ с точностью 1-2% в диапазоне энергии 0,0253-0,5 эв, а в интервале от 0,5 до 3 эв – с точностью, не хуже 10%. Однако выбор параметров отрицательного резонанса не однозначен. Чтобы уменьшить пределы неоднозначности, необходимы данные по сечениям в диапазоне 0,5-10 эв, определенные с точностью, лучше 2%. Пределы варьирования параметров: $-2{,}3$ эв $\leq E_0 \leq -1{,}8$ эв; 31 мэв $\leq \Gamma_n^0 \leq 45$ мэв; 72 мэв $\leq \Gamma_\gamma \leq 98$ мэв и 4 ферми $\leq R \leq 10$ ферми. Следует отметить, что пределы различных параметров коррелируют друг с другом определенным образом, т. к. все параметры связаны между собой определенными соотношениями. Выбор крайних пределов ведет к систематическим отклонениям расчетных сечений от экспериментальных больше чем на 10%.

Общие закономерности в сечениях рассеяния

В настоящее время получены данные о сечениях рассеяния для довольно большого количества изотопов. Мы попытались использовать все эти данные, в том числе и полученные нами, для сравнения с предсказаниями оптической модели. На рис. 12 приведен график величины $(\sigma_s - 4\pi R'^2)/4\pi R'^2$ в зависимости от массового числа A, причем R' определено по расчетам [17]. Аналогичный график построен и для случая, когда $R' = 1{,}45\,A^{1/3}\cdot 10^{-13}$, однако отклонение от нулевого положения было гораздо больше. Сильные отклонения от нуля в районе $A \sim 50, 140, 190$, по-видимому, обусловлены большим влиянием резонансного и интерференционного членов от ближайших к нулевой энергии отрицательных уровней.

Для ряда четно-четных изотопов по сечениям рассеяния вблизи $E_n = 0$ нам удалось определить R' (оптическую длину рассеяния). Необходимое условие для этого – наличие информации о сечении захвата и параметрах положительных уровней. При анализе вклада отрицательных уровней в сечение рассеяния мы предполагали в соответствии с распределениями Вигнера и Портера-Томаса, что первый отрицательный уровень отстоит от первого положительного не более чем на $2\bar{D}$, и при этом его приведенная нейтронная ширина не больше чем $3\bar{\Gamma}_n^0$. Ошибки в определении R' связаны не столько с точностью эксперимента, сколько с природными флуктуациями величин. Вычисленные значения R' для ^{166,168,170}Er равны $9{,}6^{+2}_{-1}$; (10,5 ± 0,6); (10,3 ± 1) ферми, соответственно, а для ^{112,114,116}Cd – $7{,}4^{+0{,}3}_{-0{,}7}$; $\leq 6{,}5$, $7{,}15^{+0{,}4}_{-1{,}6}$ ферми, соответственно.

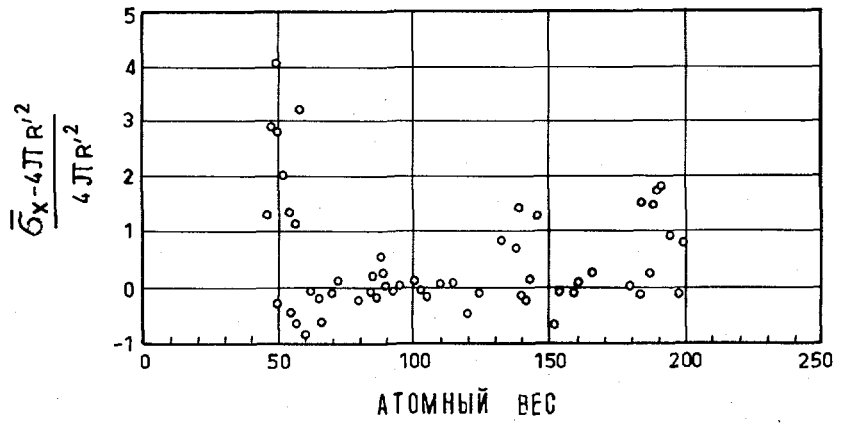

Рис. 12. Зависимость $\bar{\sigma}_x - 4\pi R'^2 / 4\pi R'^2$ от A.

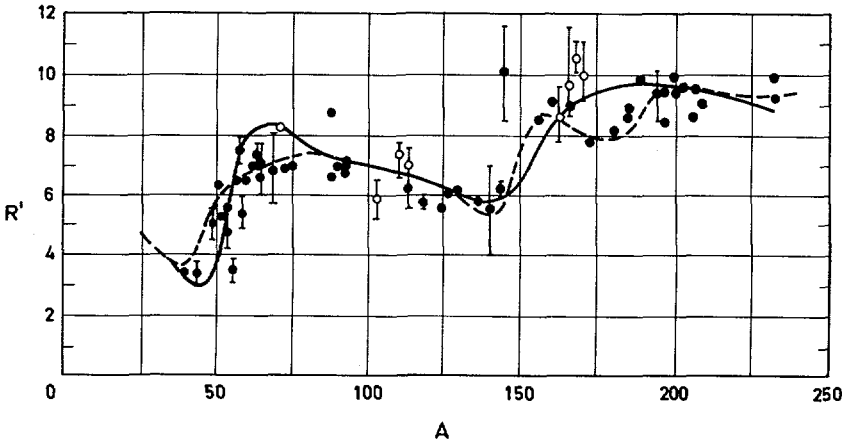

Рис. 13. Зависимость оптической длины рассеяния R' от A.

На рис. 13 приведен график, иллюстрирующий зависимость R' от массового числа A (по данным на декабрь 1969 г.). Сплошная кривая соответствует расчету по оптической модели без учета деформации ядра (потенциал Вудса-Саксона), штриховая – расчету с учетом деформации [17]. Данные авторов изображены открытыми кружками. Кривые заимствованы из работы [18]. В области A = 155-190 экспериментальные данные лучше согласуются с расчетом по Вилетсу. В области A ~150 чувствуется недостаток экспериментальных данных. Следует также отметить, что в общем точность многих существующих данных недостаточна для безапелляционного выбора модели.

В заключение авторы считают своим приятным долгом выразить благодарность за внимание к работе В. И. Мостовому и за помощь при измерениях и обработке данных Г. С. Падуну, И. П. Столяревскому, В. Б. Кисловскому, А. И. Игнатенко, В. К. Рудишину и Н. А. Трофимовой.

ЛИТЕРАТУРА

[1] TATTERSAL, R.B. et al., J.Nucl.Energy 12 (1960) 32.
[2] SIMS, G.H.K., JUHNKE, D.G., J.Inorg.Nucl.Chem. 29 (1967) 2671.
[3] ВЕРТЕБНЫЙ, В.П. и др., Атомная энергия 12 (1962) 324.
[4] ВЛАСОВ, М.Ф., КИРИЛЮК, А.Л., УФЖ 8 (1963) 947.
[5] КОЛОТЫЙ, В.В. и др., УФЖ 13 (1968) 599; ВЕРТЕБНЫЙ, В.П. и др., УФЖ 13 (1968) 605.
[6] SIMPSON, O.D. et al., Nucl.Instr. and Methods 16 (1962) 97.
[7] ВЕРТЕБНЫЙ, В.П. и др., Атомная энергия 27 (1969) 349,
[8] ВЕРТЕБНЫЙ, В.П. и др., Препринт Института физики АН УССР, ИФ-68-11, Киев, 1968.
[9] ВЕРТЕБНЫЙ, В.П., БИЦЯД 4 (1967) 7.
[10] ВЕРТЕБНЫЙ, В.П. и др., Ядерно-физические исследования в СССР, вып. 6 (1968) 108.
[11] CHILD, et al., Phys.Rev. 174 (1968) 1553.
[12] ДАНЕЛЯН, Л.С. и др., Атомная энергия 16 (1964) 56.
[13] SHER, R. et al., Nucl.Sci.Eng. 11 (1961) 369.
[14] ВЕРТЕБНЫЙ, В.П. и др., Ядерно-физические исследования в СССР, вып. 4 (1967) 38.
[15] BROCKHOUSE, B.N., Can.J.Phys. 31 (1953) 432.
[16] ВЕРТЕБНЫЙ, В.П. и др., Ядерно-физические исследования в СССР 7 (1969) 37.
[17] CHASE, D. et al., Phys.Rev. 110 (1958) 1080.
[18] MORGENSTERN, I. et al., International Conference on Nuclear Structure, Paper N87, Antwerpen, 1965.

DISCUSSION

TO PAPERS IAEA-CN-26/109, 87

C. M. NEWSTEAD: In your oral presentation you showed a slide dealing with the spin dependence of the s-wave strength function. The slide did not demonstrate that there was no such dependence: it merely indicated that existing data do not include enough resonances to specify accurately whether there is or is not a spin dependence.

G. V. MURADYAN: A study of Pikelner states that, on the basis of the data now available for the identification of levels by spin, no unequivocal conclusion can yet be drawn concerning the existence of a spin dependence of the strength function. This study does not deny the existence of a spin dependence but merely asserts that, within the limits of the existing errors, this can be dealt with in such a way that the spin dependence does not exist. This is all that is claimed. However, in my opinion this scheme does not exclude the possibility of a spin dependence in the case of individual nuclei.

C. M. NEWSTEAD: I have one further comment. It comes as a surprise to learn that there is such a disagreement in the p-wave strength function of niobium, because measurements made at Harwell by Uttley and myself over average total cross-sections determined a strength function of about 5 and measurements made at Saclay in the low-energy region for individual resonances also give a strength function of about this magnitude, i. e. 5. So I am surprised that you say that there is a factor-of-5 difference in the strength function.

G. V. MURADYAN: I said that there is a discrepancy by a factor of 3 in the strength function values for niobium. But what I was talking about had to do with the strength functions which were obtained from average radiative capture measurements. The source of the values is given in the paper: for the figure of 11, see Ref. [76]; for that of 3. 3, see Ref. [48].

G. J. KIROUAC: I would like to make a comment on the identification of resonance ℓ-values. Following the lead of Asami, Moxon and Stein, we have investigated theoretically and experimentally the possibility of assigning resonance ℓ-values by studying the differential scattering cross-section shape as a function of angle.

We tested the shape-analysis methods on ^{12}C and did a high-resolution differential-scattering measurement on ^{40}Ca at three angles. We believe we have been able to assign unique ℓ-values to about 50 resonances in ^{40}Ca between 500 keV and 1. 5 MeV.

АЛЬФА-ШИРИНЫ НЕЙТРОННЫХ РЕЗОНАНСОВ

Ю. П. ПОПОВ, М. ПШИТУЛА, Р. Ф. РУМИ,
М. СТЭМПИНСКИ, М. ФЛОРЕК, В. И. ФУРМАН
Объединенный институт ядерных исследований,
Дубна,
Союз Советских Социалистических Республик

Abstract — Аннотация

ALPHA WIDTHS OF NEUTRON RESONANCES.

Radiation damages of the crystal lattice of construction materials due to the α-particle escaping after capture of a slow neutron are considerably more serious than in the case of γ-ray emission. Fortunately, in the region of heavy nuclei $\sigma(n,\alpha)/\sigma(n,\gamma) \leq 10^{-6}$. For light nuclei, however, the cross-sections become closer to each other, for which reason allowance for a possible contribution of the (n,α)-reaction to radiation damages will, in a number of cases, undoubtedly be of vital importance in choosing the construction materials for nuclear reactors. On the basis of the statistical and optical models of the atomic nucleus the problem of the mean values of α-widths of neutron resonances for various nuclei and the problem of α-width fluctuations are discussed in this paper. The results of calculations are compared with the experimental data obtained by the authors. The possible reasons of the discrepancy between the calculated mean α-widths and the results of the measurements are discussed. A method of determining the spin of the nuclear resonance state from the values of total and partial α-widths measured in the (n,α)-reaction is proposed. The results of this spin identification are presented for a number of atomic nuclei.

АЛЬФА-ШИРИНЫ НЕЙТРОННЫХ РЕЗОНАНСОВ.

Радиационные повреждения кристаллической решетки конструкционных материалов, производимые α-частицей, вылетающей после захвата медленного нейтрона, значительно более серьезные, чем в случае испускания γ-кванта. К счастью, в области тяжелых ядер $\sigma(n,\alpha)/\sigma(n,\gamma) \leq 10^{-6}$. В то же время для легких ядер сечения становятся более близкими, поэтому учет возможного вклада в радиационные повреждения реакции (n,α) в ряде случаев будет несомненно актуален при выборе конструкционных материалов для ядерных реакторов. На основе статистической и оптической моделей атомного ядра рассматривается вопрос о средних значениях α-ширин нейтроиных резонансов для различных ядер и о флуктуациях α-ширин. Результаты расчетов сравниваются с экспериментальными данными, полученными авторами. Предлагается метод определения спина резонансного состояния ядра по значениям полиых и парциальных α-ширин, измеряемых в реакции (n,α). Приводятся результаты такой идентификации по спинам для ряда атомных ядер.

1. ВВЕДЕНИЕ

Исследование резонансных реакций (n,α), вызванных медленными нейтронами, дает ценные сведения для проверки теории ядерных реакций и дополнительную информацию о структуре высоковозбужденных состояний ядер.

Хотя сечение реакции (n,α) в этой области энергий нейтронов, как правило, значительно меньше сечений других реакций, однако радиационные повреждения, вызванные α-частицами, более значительны, чем в случае γ-лучей. Поэтому учет сечения реакции (n,α) при выборе конструкционных материалов в некоторых случаях может оказаться необходимым.

В докладе приводятся экспериментальные значения полных α-ширин для ядер-мишеней ^{95}Mo, ^{123}Te, $^{143,145}Nd$, $^{147,149}Sm$ и спектр α-частиц для резонанса ^{145}Nd. Проводится сравнение экспериментального распределения полных α-ширин с рассчитанным на основе предположений статисти-

ческой теории реакции. Даются спины некоторых резонансов, определенные из распределения ширин.

Сравниваются средние экспериментальные ширины с рассчитанными на основе оптической модели. Такое сравнение полезно для оценки точности и надежности предсказания сечений (n,α)-реакции на ядрах, для которых не имеется экспериментальных данных.

2. ЭКСПЕРИМЕНТ

В настоящее время в резонансной области энергий нейтронов исследование реакции (n,α) проведено лишь для шести ядер [1-3]. Приведенные в докладе данные включают полученные нами результаты дополнительных измерений и уточнения. Столь малое число изученных ядер связано с тем, что измерения полных α-ширин сильно затруднены малыми значениями сечений (n,α)-реакции и присутствием большого фона γ-лучей из конкурирующей реакции радиационного захвата нейтронов. Отношение $\sigma_\alpha/\sigma_\gamma$ для тяжелых ядер составляет $\leqslant 10^{-5} - 10^{-6}$. Еще более трудны измерения парциальных α-ширин, поскольку на детекторы налагаются дополнительные требования по спектрометрии вылетающих α-частиц.

Для этих измерений нами разработаны специальные детекторы с большой рабочей площадью, малой эффективностью регистрации γ-квантов и малым собственным фоном.

Измерения проводились на импульсном реакторе Объединенного института ядерных исследований. Энергия нейтронов определялась по времени пролета с разрешением 0,1 мксек/м для полных и 0,6 мксек/м для парциальных ширин.

а) Измерения *полных* α-ширин

Измерения полных α-ширин проводились ксеноновым сцинтилляционным детектором с использованием электрического поля для усиления светового выхода. Полная рабочая площадь мишени в детекторе – 0,7 м^2.

Конструкция детектора позволяла одновременно проводить независимые измерения счета с мишенью и без мишени, что давало возможность определять уровень фона детектора на пучке, т. е. в условиях измерения. Применялись мишени толщиной 4-10 мг/см^2 из окиси естественных смесей или обогащенных изотопов ^{95}Mo, ^{123}Te, ^{143,145}Nd и ^{147,149}Sm, нанесенных на алюминиевые подложки. Независимо от измерений (n,α)-реакции регистрировались γ-кванты из радиационного захвата нейтронов с помощью детектора, не чувствительного к форме γ-спектра в отдельных резонансах. Относительные α-ширины определялись из формулы

$$\frac{\Gamma_\alpha}{\Gamma_\gamma} = \frac{\sigma_\alpha}{\sigma_\gamma} = K\frac{N_\alpha}{N_\gamma}$$

где N_α и N_γ – числа счетов для соответствующих резонансов, зарегистрированные детекторами α-частиц и γ-квантов, а K – коэффициент, зависящий от характеристик детекторов и от отношения времен измерений.

Для вычисления абсолютного значения α-ширин значение K определялось из тепловой области, где σ_α и σ_γ были известны из других измерений или из одновременных измерений с другим калибровочным элементом [1].

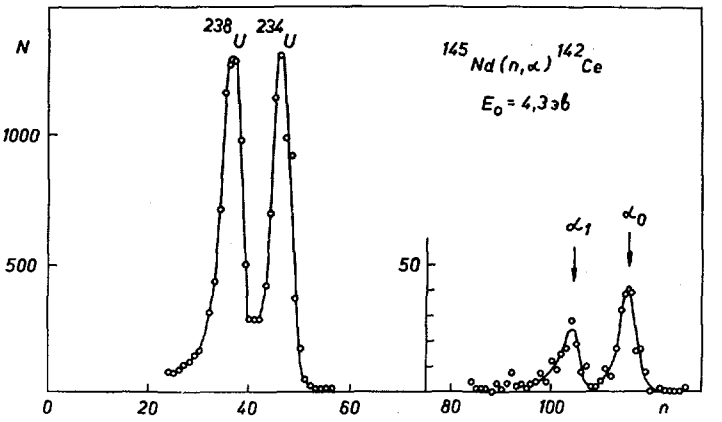

Рис. 1. Спектр α-частиц из реакции $^{145}Nd(n,\alpha)$ в резонансе 4,3 эв. Энергия α-частиц, соответствующих переходам в основное (α_0) и первое возбужденное (α_1) состояние: 8,58 и 7,96 Мэв. Показан калибровочный спектр α-частиц урана.

Таким образом были получены α-ширины почти пятидесяти резонансов для ^{95}Mo, ^{123}Te, $^{143,145}Nd$ и $^{147,149}Sm$.

б) Исследование парциальных α-ширин

Спектр α-частиц в отдельных резонансах измерялся ионизационной камерой с сеткой. Мишень из окиси обогащенного изотопа (например, ^{145}Nd), толщиной 0,2 мг/см^2, наносилась на алюминиевую фольгу. Площадь мишени – 0,14 м^2. Разрешение по энергии α-частиц $\Delta E_\alpha \approx 200$ кэв, для $E_\alpha = 4{,}2$ Мэв. Коды времени и амплитуды импульсов камеры записывались на магнитную ленту многомерного анализатора. Собственный фон импульсов с амплитудой > 5 Мэв составлял ~3 имп/час. Типичный спектр α-частиц резонанса 4,37 эв ^{145}Nd показан на рис. 1. Аналогичные измерения были проведены для резонансов ^{147}Sm.

3. ТЕОРИЯ

а) Статистические свойства α-ширин

Для ядер-мишеней со спином $I \neq 0$ захват s-нейтронов приводит к двум возможным значениям спинов составного ядра: $I_1 = I - 1/2$ и $I_2 = I + 1/2$. Парциальная ширина α-распада возбужденного состояния λ составного ядра в выходной канал "c" дается формулой

$$\Gamma_{\lambda c} = 2\gamma_{\lambda c}^2 P_c \qquad (1)$$

а полная ширина

$$\Gamma_\lambda = \sum_c \Gamma_{\lambda c} = 2\sum_c \gamma_{\lambda c}^2 P_c \qquad (2)$$

где: $\gamma_{\lambda c}$ – амплитуда приведенной ширины,

P_c – фактор проницаемости потенциального барьера, а индекс "c" фиксирует энергию и орбитальный момент вылетающей α-частицы. Суммирование проводится по всем выходным каналам, допускаемым правилами отбора по угловому моменту и четности.

По-видимому, для распада составного ядра можно принять предположения статистической теории о случайном характере распределения и взаимной независимости амплитуд приведенных ширин для отдельных резонансов [4]. Предполагается, что $\gamma_{\lambda c}$ распределены по нормальному закону со средним значением $\langle \gamma_{\lambda c} \rangle = 0$ и заданной для определенного спина I дисперсией $\langle \gamma^2_{\lambda c} \rangle$. В таком случае парциальные ширины $\Gamma_{\lambda c}$ подчиняются распределению χ-квадрат.

$$p(\chi) = \frac{\left(\frac{\nu}{2}\right)^{\frac{\nu}{2}}}{\Gamma\left(\frac{\nu}{2}\right)} \cdot \frac{1}{\langle \chi \rangle^{\frac{\nu}{2}}} \cdot \chi^{\frac{\nu}{2}-1} \cdot \exp\left[-\frac{\nu}{2}\frac{\chi}{\langle \chi \rangle}\right] \tag{3}$$

с числом степеней свободы $\nu = 1$. Дисперсия этого распределения дается формулой

$$D(\chi) = \frac{2\langle \chi \rangle^2}{\nu} \tag{4}$$

откуда для парциальных ширин получаем:

$$D(\Gamma_{\lambda c}) = 2\langle \Gamma_{\lambda c} \rangle^2 = 8\langle \gamma^2_{\lambda c} \rangle^2 P_c^2 \tag{5}$$

Распределение $p_i(\Gamma_\lambda)$ полных ширин (2), для распада состояний со спинами I_i, является сверткой парциальных распределений вида (3) с $\nu = 1$ и различающимися средними $\langle \Gamma_{\lambda c} \rangle = 2\langle \gamma^2_{\lambda c} \rangle P_c$. Попытки получить точный аналитический вид распределения полных ширин для общего случая (с различными средними парциальными ширинами) путем свертки приводит к серьезным математическим затруднениям [4,5]. Для облегчения расчетов, исходя из общих соображений, мы предположили, что распределение полных ширин можно апроксимировать также формулой (3) со средним

$$\langle \Gamma_\lambda \rangle = \sum_c \langle \Gamma_{\lambda c} \rangle = 2\langle \gamma^2_{\lambda c} \rangle \sum_c P_c \tag{6}$$

и дисперсией

$$D(\Gamma_\lambda) = \sum_c D(\Gamma_{\lambda c}) = 8\langle \gamma^2_{\lambda c} \rangle^2 \sum_c P_c^2 \tag{7}$$

Это предположение сразу приводит к выражению для числа степеней свободы

$$\nu = \frac{2\langle \Gamma_\lambda \rangle^2}{D(\Gamma_\lambda)} = \frac{\left(\sum_c P_c\right)^2}{\sum_c P_c^2} \tag{8}$$

Справедливость этого предположения проверялась нами методом Монте-Карло для пяти выходных каналов и для различных наборов P_c. Провер-

ка показала, что распределение полных ширин, в случае выполнения статистических предположений, хорошо описывается формулой (3) с параметрами (6) и (8).

На основе результатов этого рассмотрения проводился анализ распределений экспериментальных α-ширин. Для вычисления ν использовались значения факторов проницаемостей потенциального барьера, приведенные в работе [6]. По формуле (8) рассчитывались значения ν_1 и ν_2, соответственно для спинов I_1 и I_2. Для привязки теоретических распределений α-ширин к экспериментальным применялась следующая методика. Поскольку во многих случаях спины резонансов неизвестны, из эксперимента могут быть определены значения полных α-ширин, усредненные как по энергии, так и по двум возможным спиновым состояниям

$$\langle \Gamma_\lambda \rangle_э = \frac{\sum_{\lambda=1}^{n} \Gamma_{\lambda э}}{n} = \frac{\rho_1}{\rho} \langle \Gamma_\lambda \rangle_1 + \frac{\rho_2}{\rho} \langle \Gamma_\lambda \rangle_2 \qquad (9)$$

где:

$$\rho_i = \rho_0 (2I_i + 1) \exp\left[- \frac{\left(I_i + \frac{1}{2} \right)^2}{2\sigma^2} \right] \qquad (10)$$

Плотность уровней I_i, i = 1 или 2 нумерует два возможных спиновых состояния и $\rho = \rho_1 + \rho_2$. Величины $\Gamma_{\lambda э}$ – измеренные полные α-ширины, а n – число резонансов в исследуемом диапазоне энергий.

ТАБЛИЦА 1. ПАРАМЕТРЫ ДЛЯ РАСЧЕТА РАСПРЕДЕЛЕНИЙ α-ШИРИН

Ядро – мишень	$2\sigma^2$	$\frac{\rho(3)}{\rho(4)}$	$I_1^\pi = 3^-$		$I_2^\pi = 4^-$	
			ν_1	$\langle \Gamma \rangle_1 \cdot 10^7$ эв	ν_2	$\langle \Gamma \rangle_2 \cdot 10^7$ эв
^{143}Nd	47,8	0,92	1	146	1,8	1,21
^{147}Sm	54,9	0,90	1,8	9,25	2,2	0,88
^{149}Sm	58	0,89	2,6	3,48	2,5	0,58

Используя для оценки отношения средних полных α-ширин выражение

$$\frac{\langle \Gamma_\lambda \rangle_1}{\langle \Gamma_\lambda \rangle_2} = \frac{\rho_2}{\rho_1} \cdot \frac{(\sum_c P_c)_1}{(\sum_c P_c)_2} \qquad (11)$$

мы получаем из формулы (9) нормированные на эксперимент средние значения α-ширин для каждого спинового состояния. На основе полученных таким образом параметров $\langle \Gamma_\lambda \rangle_i$ и ν_i (см. табл. 1) рассчитывались распределения $p_1(\Gamma_\lambda)$ и $p_2(\Gamma_\lambda)$.

В случае небольшого количества резонансов (n = 10 ÷ 15) и при неизвестных спинах удобнее для сравнения пользоваться интегральным распределением, сложенным из интегральных распределений для обоих спинов:

$$nP(\Gamma_\alpha > \Gamma) = n_1 \int_\Gamma^\infty p_1(\Gamma_\lambda)\,d\Gamma_\lambda + n_2 \int_\Gamma^\infty p_2(\Gamma_\lambda)\,d\Gamma_\lambda \qquad (12)$$

где:

$$n_i = n\frac{\rho_i}{\rho}$$

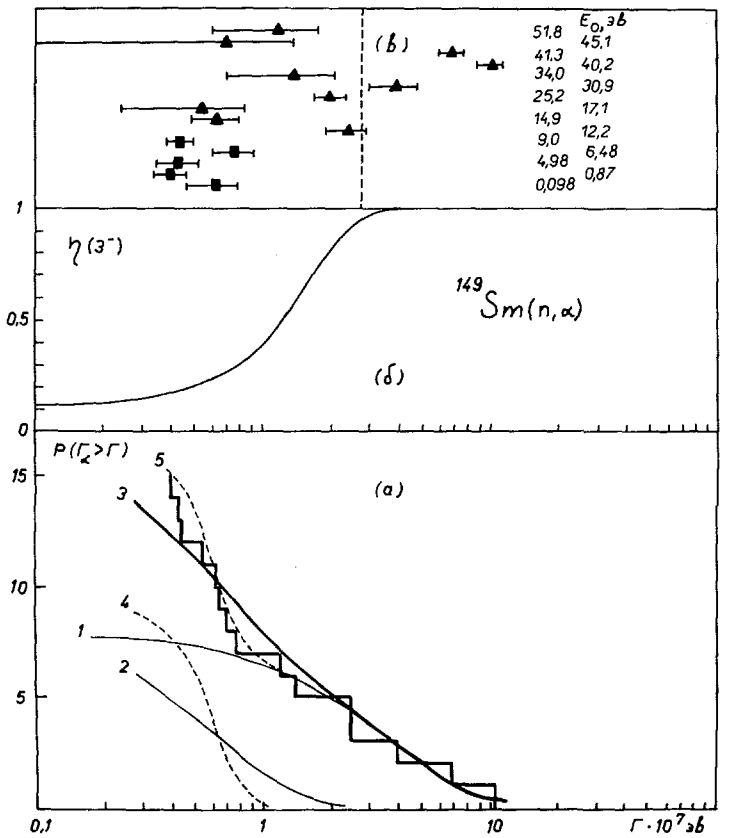

Рис. 2.

а – экспериментальное и рассчитанное интегральное распределение полных α-ширин из реакции $^{149}Sm(n,\alpha)$: 1 – рассчитанное распределение α-ширин резонансов со спином 3^-; 2 – то же для резонансов со спином 4^-; 3 – суммарное распределение для спинов 3^- и 4^-; 4 – рассчитанное распределение для спинов 4 – в предположении $\nu = 20$; 5 – сумма распределений 1 и 4.

б – вероятность приписать спин 3 резонансу с α-шириной, равной Γ.

в – экспериментальные α-ширины с указанием ошибок и энергии резонансов. Ширины, лежащие справа от вертикальной линии, по расчетам принадлежат с вероятностью $\eta > 0{,}95$ резонансам со спином 3^-.

▲ – спин резонанса не известен по другим работам,
■ – спин резонанса 4 по другим работам.

На рис. 2 а в качестве примера приводится интегральное распределение полных α-ширин, рассчитанное по формуле (12), и экспериментальное распределение для ^{149}Sm (гистограмма). Тонкими линиями показаны распределения для ширин со значениями спина I_1 и I_2. В пределах имеющейся статистической точности, согласие экспериментального распределения с теоретически ожидаемым надо считать хорошим.

Если средние значения α-ширин для разных спинов I_1 и I_2 заметно отличаются, то появляется возможность определить спины тех резонансов, значение ширин которых оказывается в областях, где отношение $n_1 p_1 / n_2 p_2$ или очень большое, или очень маленькое. Вероятность найти среди всех ширин ширину, принадлежащую резонансу со спином I_1, равна:

$$\eta(I_1) = \frac{n_1 p_1}{n_1 p_1 + n_2 p_2}$$

В области $\eta(I_1) > 0{,}95$ ширины принадлежат с большой вероятностью резонансам со спином I_1, а в области $\eta(I_1) < 0{,}05$ – резонансам со спином I_2.

На рис. 2б показана кривая $\eta(I_1)$ в зависимости от Γ. Несколько выше (рис. 2в) нанесены ширины с ошибками. Уровням, ширины которых лежат в области $\eta > 0{,}95$, приписываются значения $I^\pi = 3^-$. Аналогично определялись спины для других исследованных ядер. В результате получены спины 12-ти резонансов, из которых 7 не были известны ранее (см. табл. 2). Остальные совпадают со значениями спинов, измеренными другими авторами. Три спина, данные в скобках, приписаны с вероятностью $\simeq 0{,}9$.

Имеется еще одна интересная возможность определения спинов нейтронных s-резонансов из данных по спектрам α-частиц. Согласно законам сохранения момента и четности α-переход в конечное состояние 0^+ может происходить только для одного из двух возможных спиновых состояний. Тогда по наличию (отсутствию) соответствующей линии α-спектра можно провести идентификацию распадающегося состояния по спину. Таким образом, значение спина и четности 3– было приписано следующим резонансам: ^{147}Sm ; 3,4; 83,5; 161; 183 и 235 эв.

б) Расчет абсолютных значений α-ширин по оптической модели

Для того чтобы использовать оптическую модель для оценок абсолютных значений α-ширин, удобно рассматривать обратную реакцию. При этом усредненное сечение реакции взаимодействия α-частицы с конечным ядром представляется в виде разности сечения поглощения α-частиц, рассчитываемого в оптической модели, и среднего сечения упругого рассеяния через составное ядро. В нашем случае ($\Gamma_\alpha \ll \Gamma_n, \Gamma_\gamma$) вкладом упругого рассеяния через компаунд-ядро можно пренебречь и для ℓ-ой компоненты парциальной ширины (2) можно записать:

$$2\pi \rho_i \langle \Gamma_{\lambda \ell} \rangle_i = T_{\alpha \ell i} \equiv T_{ci} \qquad (13)$$

Или, переходя к полным α-ширинам (9), имеем:

$$\langle \Gamma_\alpha \rangle_{оп} = \frac{D_н}{2\pi} \left(\sum_c T_{c1} + \sum_c T_{c2} \right) \qquad (14)$$

ТАБЛИЦА 2. ПОЛНЫЕ α-ШИРИНЫ И СПИНЫ РЕЗОНАНСОВ

Ядро – мишень	E_0 эв	$\Gamma_\alpha \cdot 10^7$ эв	Спины резонансов	
			Данная работа	Другие авторы
^{143}Nd	-6	51 ± 13	3	3 [10]
	55,8	3,2 ± 1,6	–	–
	128	86 ± 12	3	3 [11]
	138	336 ± 30	3	3 [11]
	157	2	–	–
	184	17 ± 4	3	3 [11]
	190	4	–	3 [11]
	410	420 ± 120	3	–
	713	190 ± 100	3	–
^{147}Sm	3,4	20 ±3,0	3	3 [11]
	18,3	2,8 ± 0,3	–	4 [12], 3 [10]
	27	3,2 ± 0,65	–	3 [10]
	29,8	1,7 ± 0,45	–	3 [11]
	32,1	3,08 ± 1,10	–	–
	39,9	1,7 ± 0,25	–	–
	49,7	4,8 ± 1,0	(3)	–
	58	1,67 ± 0,56	–	–
	76	2,8 ± 1,3	–	–
	83,5	17,7 ± 3,0	3	–
	100	8,4 ± 4,2	(3)	–
	183	27 ± 4	3	–
^{149}Sm	0,098	0,63 ± 0,16	–	4 [11]
	0,87	0,40 ± 0,07	–	4 [11]
	4,98	0,43 ± 0,09	–	4 [11]
	6,48	0,76 ± 0,16	–	4 [11]
	9,0	0,44 ± 0,06	–	4 [11]
	12,2	2,4 ± 0,5	(3)	–
	14,9	0,64 ± 0,16	–	–
	17,1	0,54 ± 0,30	–	–
	25,2; 26,1	2,4 ± 0,31	–	–
	30,9	3,9 ± 0,9	3	–
	34,0	1,4 ± 0,7	–	–
	40,2	10,2 ± 1,4	3	–
	41,3	6,9 ± 0,9	3	–
	45,1	0,7 ± 0,7	–	–
	51,8	1,2 ± 0,6	–	–

ТАБЛИЦА 3. ТЕОРЕТИЧЕСКИЕ И ЭКСПЕРИМЕНТАЛЬНЫЕ ПОЛНЫЕ СРЕДНИЕ α-ШИРИНЫ

Ядро – мишень	Число ширин	n	$D_н$ эв	$\langle\Gamma_\alpha\rangle_э$ мкэв	$\langle\Gamma_\alpha\rangle_{оп}$ мкэв	$\langle\Gamma_\alpha\rangle_э/\langle\Gamma_\alpha\rangle_{оп}$
^{95}Mo	6	12	80 ± 20	5,6 ± 3,6	40 ± 10	0,14 ± 0,12
^{123}Te	6	10	30 ± 7	1,2 ± 0,8	1,3 ± 0,3	0,92 ± 0,77
^{143}Nd	8	13	38 ± 6	8,3 ± 2,8	6,6 ± 1,1	1,26 ± 0,63
^{145}Nd*	3	3	20 ± 3	2,6 ± 0,7	2,6 ± 0,4	1,0 ± 0,4
^{147}Sm	11	14	6,8 ± 1,6	0,49 ± 0,12	2,4 ± 0,6	0,2 ± 0,1
^{149}Sm	15	17	2,7 ± 0,5	0,19 ± 0,04	0,4 ± 0,08	0,47 ± 0,2

* Примечание: В случае ^{145}Nd все три изученных резонанса имеют спин 3$^-$.

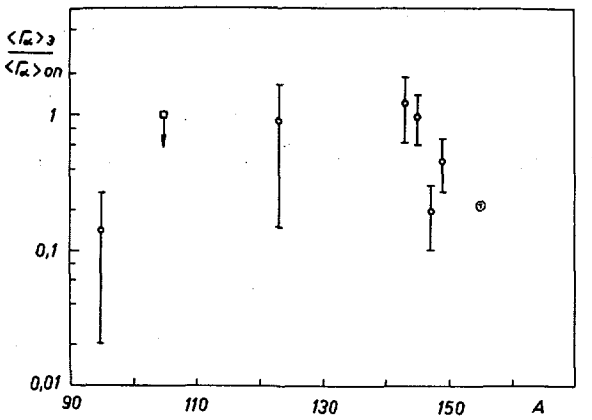

Рис. 3. Отношения абсолютных значений экспериментальных и теоретических полных α-ширин из табл. 3. В случае ^{105}Pd (□) использовалась верхняя оценка для $\langle\Gamma_\alpha\rangle_э$. Для ^{155}Gd (Ⓣ) оценка $\langle\Gamma_\alpha\rangle_э$ получена из сечения реакции (n,α) в тепловой точке [9].

Суммирование по "c" имеет тот же смысл, что и в формуле (2), а $D_н$ – экспериментальное среднее расстояние между резонансами без различия спина.

Коэффициенты прилипания T_c вычислялись с использованием оптического потенциала α-частиц из работы [7]. Единственным подгоночным параметром была глубина мнимой части потенциала W_0. Приведенные в табл. 3 величины $\langle\Gamma_\alpha\rangle_{оп}$ получены для $W_0 = -2$ Мэв (подробнее см [8]). Ошибки в значениях $\langle\Gamma_\alpha\rangle_{оп}$ связаны с неточностью определения $D_н$. Наглядное представление о соотношении экспериментальных и расчетных α-ширин дает рис. 3, из которого видно, что оптическая модель приводит к несколько завышенным абсолютным значениям α-ширин. (среднее по ядрам отношение $\langle\Gamma_\alpha\rangle_э/\langle\Gamma_\alpha\rangle_{оп} \approx 0,7$). В то же время для отдельных ядер указанное отношение отклоняется от среднего до трех раз в ту и другую стороны. Разброс точек на рис. 3 отражает степень

надежности экстраполяции расчетных величин $\langle \Gamma_\alpha \rangle$ в область экспериментально не изученных ядер.

Таким образом, проведенный выше анализ статистических свойств α-ширин и их абсолютных значений показывает, что полученные к настоящему времени экспериментальные данные более или менее укладываются в рамки современных теоретических представлений.

ЛИТЕРАТУРА

[1] ПОПОВ, Ю. П., ФЛОРЕК, М., Ядерная физика 9 (1969) 1163.
[2] КВИТЕК, И., ПОПОВ, Ю. П., Письма ЖЭТФ 5 (1967) 365.
[3] КВИТЕК, И., ПОПОВ, Ю. П., Известия АН СССР, сер. физ. XXX 8 (1966) 1371.
[4] PORTER, C.E., THOMAS, R.G., Phys. Rev. 104 (1956) 483.
[5] SHAKER, M.O., LUKYANOV, A.A., Phys. Lett. 19 (1965) 197.
[6] ДАДАКИНА, А. Ф., Бюллетень информационного центра по ядерным данным 3 Атомиздат, М., 1967, стр. 226.
[7] КАДМЕНСКИЙ, С. Г., КАЛЕЧИН, В. Е., ФУРМАН, В. И. и др., Ядерная физика 10 (1969) 730.
[8] МАРТЫНОВ, А. А., ПОПОВ, Ю. П., ФУРМАН, В. И., Программа и тезисы докладов на XX ежегодном совещании по ядерной спектроскопии и структуре атомного ядра. Ленинград, ч. II, 1970, стр. 251.
[9] BEG, K., MACFARLANE, R.D., Nucl. Phys., A129 (1969) 571.
[10] CHEIFETZ, E., GILAT, J., COHEN, S.G., Phys. Lett. 1 (1962) 289.
[11] GOLDBERG, M.D., MUGHABGHAB, S.F., PUROHIT, S.N. et al., BNL-325, Second edition, Supplement 2, vol II B and C (1966).
[12] POORTMANS, F., CEULEMANS, H., Conf. on Study of Nuclear Structure with Neutrons, Antwerp., 1965.

MEASUREMENTS OF NEUTRON-RESONANCE TOTAL CROSS-SECTIONS FOR FISSION PRODUCT ISOTOPES

H. H. JUNG, H. G. PRIESMAYER, H. SULITZE †
Institut für Reine und Angewandte Kernphysik der Universität Kiel
Reaktorstation, Geesthacht,
Federal Republic of Germany

Abstract

MEASUREMENTS OF NEUTRON RESONANCE TOTAL CROSS-SECTIONS FOR FISSION PRODUCT ISOTOPES.

The following measurements have been made by means of the fast-chopper time-of-flight spectrometer at the FRG 1-5-MW research reactor. The spectrometer resolution was between 160 ns/m and 30 ns/m, depending on the rotor speed.

A) Total neutron cross-sections of ^{133}Cs, ^{135}Cs and ^{137}Cs:

In the energy range from 1.7 eV to 1100 eV measurements have been made on stable ^{133}Cs and a mixture of fission product ^{133}Cs, ^{135}Cs and ^{137}Cs. The isotopic abundance 133 : 135 : 137 was 0.488 : 0.171 : 0.341. Two resonances were found in $^{135/137}$Cs. Resonance parameters have been determined.

B) Total neutron cross-sections of ^{100}Ru, ^{101}Ru, ^{102}Ru and ^{104}Ru:

In the energy range from 1 eV to 1.5 keV the total neutron cross-sections of the stable separated isotopes ^{100}Ru, ^{101}Ru, ^{102}Ru and ^{104}Ru have been measured. These measurements are needed for fast-reactor burn-up calculations since the yield for these isotopes of approximately 5% is relatively high. Several new resonances have been found and known resonances could be assigned isotopically. Measurements with different sample thicknesses were made using natural ruthenium in order to determine resonance parameters.

C) Total neutron cross-sections of gross fission products:

Samples of uranium enriched to 90% in ^{235}U have been burned up to 40% in the FRG 2-15-MW research reactor. A first time-of-flight spectrum, taken after 70 days of cooling, is presented. The covered energy range is from 1 eV to 30 eV. From the build-up and/or decay of resonances with time it will be tried to find isotopic assignments.

1. INTRODUCTION

At the research reactor FRG-1 at Geesthacht we operate a fast-chopper time-of-flight spectrometer. We concentrate on the investigation of total cross-sections of fission products. The knowledge of these cross-sections – especially of radioactive fission-product isotopes – is still comparatively incomplete. On the other hand, such measurements are interesting both from the technical and physical points of view.

After completion of total cross-section measurements on a mixture of radioactive fission-product caesium 135/137 and stable ^{133}Cs [1], we have investigated the four stable isotopes ^{100}Ru, ^{101}Ru, ^{102}Ru and ^{104}Ru. (The samples were given as a loan from the USAEC, Oak Ridge Isotopes Division).

---

† Present address: Institut für Reine und Angewandte Kernphysik der Universität Kiel, Aussenstelle Stohl, D 23 Kiel, Olshausenstrasse 40.

TABLE I. SPECTROMETER SETTINGS USED IN EXPERIMENTS

Rotor speed (rpm)	Covered energy range	Burst width (μs)	Channel width (μs)	Resolution (ns/m)
2250	2 eV - 20 eV	3.40	0.8	163
6000	13 eV - 140 eV	1.28	0.4	62
12000	70 eV - 1500 eV	0.64	0.15	30

2. EXPERIMENTAL FACILITY

Our fast chopper is run at a 5-MW reactor of the swimming-pool type. The rotor can be turned with 12 000 rpm maximum speed, which enables us to investigate the energy range between 1 eV and approximately 1.5 keV. The flight-path length is 21.5 m, but can be extended up to 90 m. As neutron detectors we use six lithium glass scintillators NE 912, each viewed by a photomultiplier [2]. Flight times are measured with a 4096-channel time-of-flight analyser with 0.1 μs or 0.15 μs minimum channel width. The 4096 channels can be divided into groups of 1024 channels each.

We have used three spectrometer settings as shown in Table I.

3. MEASUREMENTS ON $^{133/135/137}$Cs

We have measured the total neutron cross-section of stable ^{133}Cs in the energy region from 1.7 eV to 1100 eV, using five different samples of pure CsCl with thicknesses between 0.0000746 and 0.02023 Cs-atoms/barn. 24 resonances could be resolved. The resonance parameters are in fairly good agreement with previous measurements.

We found $\bar{\Gamma}_\gamma$ = 120 ± 10 meV, an average level spacing per spin state of D = 40 ± 2 eV and a strength function S = (1.15 ± 0.1) × 10^{-4}.

We then measured the total cross-section of a sample of fission product caesium containing stable ^{133}Cs and radioactive $^{135/137}$Cs. The isotopic contents 133 : 135 : 137 were 48.8% : 17.1% : 34.1%.

The sample thickness was 0.00703 Cs-atoms/barn. Two resonances have been discovered, which belong to either ^{135}Cs or ^{137}Cs: at 42.3 ± 0.1 eV and at 880 ± 20 eV. The neutron widths under the assumption of Γ_γ = 120 meV are 7 ± 2 meV and 700 ± 300 meV, respectively. Isotopic assignments could not be made since further samples with different isotopic enrichments were not available to us. Although above 300 eV resonances might be lost because of insufficient resolution, very large average level spacings can be concluded, which is consistent with the behaviour of near-magic nuclei.

4. MEASUREMENTS AND RESULTS FOR RUTHENIUM

All previous measurements were made using samples of natural ruthenium [3, 4] and in one case [5] of isotopically enriched ruthenium. Therefore, some resonances could not be assigned isotopically. Besides,

TABLE II. ISOTOPIC ENRICHMENTS AND SAMPLE THICKNESSES

Isotope No.	Enrichment (atom.%)	Sample thickness (atoms/barn)	Natural abundance (atom.%)
^{100}Ru	97.24	0.01102	12.62
^{101}Ru	97.73	0.00988	17.07
^{102}Ru	99.53	0.00784	31.61
^{104}Ru	99.70	0.00654	18.58

TABLE III. ISOTOPIC ASSIGNMENTS AND RESONANCE ENERGIES (in eV)

^{100}Ru	^{101}Ru	^{102}Ru	^{104}Ru	others
231.5	15.9	1306	227.5	10.1
	42.5		635	25.4
	52.5		1066	57
	62.4			82
	67.2			104
	100.1			
	113			
	142			
	159			
	200			
	247			
	316			
	385			
	437			
	463			
	543			
	679			

in previous measurements the resolution had been worse. In cases where the isotopic assignment was done by the 'total-width-determination' method this led to incorrect results, both for resonance parameters and assignment, as this experiment has shown.

The isotopic enrichments and the thicknesses of our samples are given in Table II.

To determine resonance parameters, measurements with different sample thicknesses were made with natural ruthenium since the amount of separated isotopes was limited to less than 3 g each. The abundance of

the isotopes in natural ruthenium considered is also given in Table II. Background determination was made by the method of black resonances, using the resonances of ^{197}Au at 4.9 eV, ^{186}W at 18.8 eV, ^{59}Co at 132 eV and ^{55}Mn at 334 eV.

Table III shows the results of this experiment. In this experiment many of the previous results have been confirmed, but some differences should be pointed out:

1. The resonance at 200 eV does not belong to ^{102}Ru, but to ^{101}Ru.
2. The two adjacent resonances at 227.5 and 231.5 eV had not been resolved, which led to the incorrect assumption of a big (Γ = 660 meV) resonance in ^{99}Ru at 227 eV.

In both cases, isotopic assignment was made by the 'total-width-determination' method.

3. The resonances at 142 eV and at 159 eV could be assigned to ^{101}Ru.
4. There is another resonance in ^{101}Ru at 247 eV.
5. Above 500 eV, we have discovered five more resonances because of better resolution.

The resonance parameters will be calculated by means of the AREA program of Atta and Harvey, which was altered for use on a CD-3400 computer.

5. GROSS-FISSION-PRODUCT MEASUREMENTS

Since fission produces a large number of different isotopes, a tremendous number of resonances is to be expected in the cross-section of a sample of gross fission products. It is to be feared that a time-of-flight measurement will not be able to resolve any of these resonances. We therefore made a theoretical investigation prior to this experiment [6]: total neutron cross-sections for the 195 mean fission product isotopes were calculated by Monte-Carlo methods, using the well-known statistical properties of the resonance parameters. About 17 000 resonances were calculated in the energy range between 1 eV and 1000 eV. It turned out that only 2 - 3% of them are large enough to contribute noticeably to the cross-section of the fission-product mixture. Below 100 eV, many of these resonances are expected to be resolved with our time-of-flight spectrometer.

The influence of the parameters neutron flux, burn-up and time after shut-down was also investigated.

We burned a sample of 8 g of uranium, enriched to 90% in ^{235}U, for half a year in the FRG-2, 15-MW research reactor at a thermal neutron flux of 10^{13} n/cm^2 s, thus achieving a burn-up of approximately 40%.

The first time-of-flight spectrum lay between 1 eV and 30 eV. The spectrum was taken 70 days after the burning ceased. At least six unassigned resonances were found. The total cross-section measurements on this sample will be repeated several times.

Further samples will be burnt at different neutron fluxes and to other amounts of burn-up. From the build-up and/or decay of resonances with time we hope to find isotopic assignments.

REFERENCES

[1] JUNG, H.H., Doctoral thesis. Kiel (1969).
[2] JUNG, H.H., PRIESMEYER, H.G., Nucl. Instrum. Meth. 68 (1969) 353.
[3] MELKONIAN, E., HAVENS, W.W., RAINWATER, L.J., Phys. Rev. 92 (1953) 702.
[4] KIM HI SAN, PIKELNER, SHARAPOV, SIRASHED, Nuclear Structure Study with Neutrons (Proc. Conf. Antwerp 1965) EANDC-50-S.
[5] BOLOTIN, H.H., CHRIEN, R.E., Nucl. Phys. 42 (1963) 676.
[6] SULITZE, H., JUNG, H.H., Atomkernenergie 15 (1970) 189.

THE EVALUATION OF FISSION PRODUCT YIELDS

W.H. WALKER
Atomic Energy of Canada Limited,
Chalk River Nuclear Laboratories,
Chalk River, Ontario
Canada

Abstract

THE EVALUATION OF FISSION PRODUCT YIELDS.

An evaluation of fission-product data is in progress at Chalk River. The report on cross-sections has been published earlier as AECL-3037. The present paper gives a detailed description of the evaluation of yields from the thermal-neutron fission of ^{235}U and these results, with yields from preliminary evaluations of ^{233}U and ^{239}Pu data, are used in the fission-product program, FISSPROD, to calculate fission-product absorption for comparison with reactivity measurements using irradiated fuel.

Earlier evaluations of fission-product yields have taken weighted averages using both spectrometric and radiometric data. In the present evaluation the relative mass-spectrometric yields from different experimenters are normalized to the isotopes of an element near the maxima of the light and heavy mass peaks and compared. Very divergent relative yield values are rejected and the isotopic yields of a particular element are re-normalized when the original normalization is suspect. This establishes the shape of the light and heavy mass peaks accurately. Final normalization requires an estimate of yields not included in mass-spectrometric data. The uncertainty in ^{235}U fission-product absorption calculations due to uncertainties in yields only is estimated to be about 1.4%. The major contributor is ^{135}Xe.

1. INTRODUCTION

Fission product yield measurements have played an important part in the study of fission since its discovery. The main interest initially was the general shape of the fission fragment distribution as a function of mass, and this evolved into detailed studies of deviations from the smooth curve (fine structure) and of the charge distribution for a given mass (direct yields). More recently work has been directed to precise yield measurements of specific fission products which can be used for accurate determination of fuel burnup. In the case of fission product absorption, however, most of the experimental effort has been directed to determining nuclide cross sections accurately and very little to reducing the uncertainty in yields, although neutron absorption by a high-cross-section fission product at equilibrium concentration is independent of its cross section, or nearly so, but is still proportional to its yield and absorption by a slowly-saturating fission product is proportional to both its yield and cross section.

The earliest yield measurements were of radioactive nuclides using counting techniques. These gave absolute yields with rather large errors or relative yields normalized to some

standard such as 67-h ^{99}Mo. Later, mass spectrometers were used to determine relative yields of the fission product isotopes of a particular element. The introduction of isotope dilution techniques enabled mass spectrometrists to determine absolute yields for the first time and radiochemists to improve the accuracy of their absolute yield measurements.

2. EVALUATION OF FISSION PRODUCT YIELDS

The fission product yield evaluation in this paper is intended to reduce the uncertainty in fission product absorption calculations in thermal reactors, in particular for use in the Chalk River computer program FISSPROD [1].

Both radiometric and mass spectrometric yield measurements are subject to the usual chemistry difficulties, but the latter have the advantage, from the evaluator's viewpoint, that they give the shape of a portion of the yield vs. mass curve (the relative yields) with high precision. In the case of thermal neutron fission of ^{235}U, which is the only fission process discussed in detail in this paper, several mass spectrometer measurements have been made for the majority of elements near the peak of the light and heavy mass distributions so that significant deviations from the average of a particular relative yield, such as might be caused by an unidentified contaminant or a β-decay correction based on out-of-date half-lives, can be detected by intercomparison.

There have been many earlier evaluations of fission product yields including the recent comprehensive work of Meek and Rider [2]. These have usually proceeded on a mass by mass basis taking weighted averages of all reasonable values at each mass and making final adjustments to give a total yield close to 100% each for the light and heavy mass peaks. In the present evaluation the shape of the yield vs. mass curve for each element is determined first by comparing all available relative mass spectrometric yields, then the shape of the main portion of the yield vs. mass distribution is obtained by linking the elemental shapes together. The linking together is done either using isotope dilution data, which give the number of atoms of each element per fission [3 - 7] or using measured abundances of two isotones, each relative to other isotopes of its own element, and then completing the link using known β-decay half-lives [8,9]. The first method is subject to errors arising in the chemistry, and the second to errors due to the use of incorrect decay data.

Once the yields giving the shape over the main portion of the light and heavy mass peaks are determined using mass spectrometric measurements they are normalized as a group to

fit radiometric data. This is done by using radiometric yields to estimate the contribution from masses not covered by the mass spectrometric data (mostly on the outer slopes of the peaks and in the valley between them) and normalizing the mass spectrometric values so that the sum over each peak is 100%. Finally the normalization of the mass spectrometric yields is checked by comparing them to available radiometric yields.

3. EVALUATION OF YIELDS FROM THE THERMAL FISSION OF ^{235}U

3.1 Selection of Mass Spectrometric Data

Some measurements, in which fissile material irradiated in a high flux ($\gtrsim 10^{13}$ n/cm^{2}s) for a considerable period was used, and require corrections for neutron capture as well as β-decay, have not been used. These include the work of Inghram et al. [10] Steinberg and Glendenin [3] and Gorshkov et al. [11] which were corrected at the time of publication but used cross section data that were incomplete and often wrong. Since no information is given on the magnitude of the original corrections re-evaluation is not possible and the heavy mass yields given in these papers (mostly for rare earths) have not been included in this evaluation. However, the capture corrections in the light mass region are small so that the light mass yields of [3] are used in this evaluation. The measurements of Rider et al. [6] and Lisman et al. [7] required similar corrections but the magnitude of the correction as well as the cross section and half-lives used are available for checking.

3.2 Corrections for β-Decay and Capture

Wherever possible FISSPROD which uses the half-lives and recommended cross sections of Walker [12] has been used to check the corrections made for β-decay and capture in the original papers. Where changes were made in the relative yields the percentage change and the old and new data used is indicated in footnotes to the tables displaying the yields.

3.3 The Shape of the Light Mass Peak

The evaluation of the mass spectrometric data proceeds in a series of steps beginning with an essentially arbitrary normalization of all sets of yields using the isotopes of an element near the maximum of the peak (about mass 95 for the light masses). The steps are indicated in Table I, which lists the normalized data, and the reasons for each normalization are discussed below. Except when noted below, the adopted yields are the averages of all measured values listed in the table at that mass.

TABLE I. ANALYSIS FOR THE SHAPE OF THE LIGHT MASS PEAK

Mass	Element	Steinberg Glendenin [3]	Lisman et al. [7,7a]	Farrar et al. [8]	A[a]	Farrar et al. [8]	A[a]	Petruska et al. [4]	Farrar et al. [8]	A[a]	Farrar et al. [8]	Petruska et al. [4]	A[a]
		Step 1				Step 2		Step 3			Step 4		
83	Kr		0.529									0.533[h]	0.53
84	Kr		1.005									0.981[h]	0.99
85	Rb(+Kr)		1.33					1.30[e]		1.32			
86	Kr		1.94									1.97[h]	1.95
87	Rb		2.55					2.49[e]		2.53			
88	Kr / Sr	3.60	3.63					3.53[e]	3.39[x]	3.60	(3.60)		
89	Sr/Y								4.5/4.5		4.75		4.75
90	Sr	5.79	5.93					5.74[e]	5.45[x]	5.84	(5.84)		
91	Zr / Sr/Y	5.83	5.93	5.89[b]	5.88				(5.88)[f] (5.71)[g]				
92	Zr	6.02	5.98	5.94	5.98								
93	Zr	6.44	6.37	6.41	6.40								
94	Zr	6.39	6.44	6.45	6.43								
95	Zr / Mo	6.26[x]	6.49	6.47[b]			6.48						
96	Zr	6.32	6.26	6.31	6.29								
97	Mo	6.08	5.89			6.06[d]	6.01						
98	Mo	5.77	5.80			5.68[d]	5.75						
100	Mo	6.29	6.27			6.31[d]	6.29						
101	Ru	4.99[c]	5.06				5.04						
102	Ru	4.09[c]	4.21				4.17						
104	Ru	1.80[c]	1.83				1.82						
106	Ru	0.38[c]	0.39				0.39						

a Adopted relative yield

b +0.3% corrections ^{91}Y - 58.8 d instead of 58.0 d
^{95}Zr - 65.5 d instead of 65.8 d

c Relative values normalized by absolute β-counting given only ½ weight in taking average.

d Normalized to average of [3] and [7] using sum of yields for masses 97, 98 and 100

e Given only ½ weight in taking average

f Y normalized to this value. Includes a +4% correction in the ratio of $^{91}Y/^{89}Y$
^{89}Sr - 50.8 d instead of 51.8 d
^{91}Y - 58.8 d instead of 58.0 d

g Sr normalized to this value (equals 5.88 less 3% for direct ^{91}Y yield). Includes a +1% correction in ^{91}Sr
^{91}Sr - 9.48 h instead of 9.67 h

h Normalized to [7] using sum of yields for masses 83, 84 and 86

x Value not used in obtaining average

( ) Normalizing value.

Step 1: All sets of data except [4] are normalized so that $\Sigma(y_i) = 31.000$ for the Zr isotopes of masses 91,92,93, 94 and 96. y_i is the normalized yield at mass i. The normalizing value should be considered as arbitrary. The normalization is applied to all yields linked to Zr by isotope dilution [3,7]. A comparison of the three sets show the relative Zr yields at each mass to be in excellent agreement, with a maximum deviation from the mean of less than 1%.

Step 2: Additional yields at masses 97,98 and 100 may be obtained using the relative yields of [8]. Since there is no link between this group and the yields already adopted the relative yields of [8] are normalized to give a value of $\Sigma(y_i)$ for masses 97,98 and 100 equal to the average of the normalized yields of [3] and [7] in columns 3 and 4. At mass 95 the Mo yield obtained by [3] is appreciably lower than the Mo yield of [7] and Zr yield of [8]. Since a half-life of 63 d used in [3] to correct for ^{95}Zr decay compared to a currently accepted value of 65.5 d the correction for hold-up of mass 95 atoms as Zr and Nb was too small, so this yield is omitted in taking the average.

Step 3: The Sr and Rb yields of [4] obtained by isotope dilution are in good relative agreement with the Rb and Sr yields of [7] and Sr yields of [3] but are about 2% lower in absolute value. In taking averages at masses 88,89 and 90 they are given only half weight because they could not be normalized to Zr.

Both the Y and Sr relative yields of [8] include mass 81 so that they can be normalized to the adopted value of 5.88. Both results are quite sensitive to β-decay half-lives used to correct measured ratios. The use of more recent half-lives [1] increases the relative yield at mass 91 by 1% for Sr and 4% for Y. Also Meek and Rider [2] estimate that ^{91}Y has a direct yield of 3% based on a semi-empirical charge distribution. Taking these factors into account (2nd column of step 3) the Sr and Y yields at mass 89 agree, but the ^{88}Sr and ^{90}Sr yields are about 6% lower than the yields of [3], [7] and [4]. There is no obvious explanation for this discrepancy but in view of the agreement between the other yield sets the Sr and Y yields of [7] are omitted in taking averages.

Step 4: The Sr yields of [8] are increased by 6% to agree with the recommended values at masses 88 and 90. This gives the adopted yield for mass 89. The same paper ([8]) also includes relative Kr yields for masses 86, 87 and 88 but, since the reference is to unpublished work with no data given for the half-lives or irradiation time, these results have been omitted.

TABLE II. LIGHT MASS YIELDS: MASS SPECTROMETRIC, RADIOMETRIC AND RECOMMENDED

Mass	Stable Fission Product[a]			Yields (%) of Radioactive F.P.[b]		Recommended	
	Elem	Z	Yield (%)	Z - 1	Z - 2	This Paper	Meek, Rider [2]
≤76						0.006[g]	0.0052
77	Se	34		.0083 [16]		0.008	0.0083
78	Se	34		.020 [16]	.018 [16]	0.020	0.020
79	Se	34		.056 [16]		0.056	0.056
80	Se	34				0.11[g]	0.094
81	Br	35		.22±.02 [16]		0.22	0.18
82	Se	34				0.35[g]	0.24
83	Kr	36	0.53	.56 [16]	.56±.04 [16]	0.53	0.52
84	Kr	36	1.00	.92±.06 [16]		1.00	0.97
85	Rb	37	1.33	.273±.004 [17][f]		0.273[f] 1.33	0.271[f] 1.30
86	Kr	36	1.96			1.96	1.89
87	Rb	37	2.55		3.2 [16][c]	2.55	2.53
88	Sr	38	3.62			3.62	3.58
89	Y	39	4.78	4.75±.30 [16]		4.78	4.76
90	Zr	40			5.88 5.8 [19]	5.88	5.83
91	Zr	40	5.91		5.62±.11 [20]	5.91	5.90
92	Zr	40	6.02			6.02	5.98
93	Zr	40	6.44	6.1±.7 [16]		6.44	6.39
94	Zr	40	6.47			6.47	6.44
95	Mo	42	6.52		6.0±.3 [21]	6.52	6.41
96	Zr	40	6.33			6.33	6.29
97	Mo	42	6.05		5.9±.5 [16][d]	6.05	6.21
98	Mo	42	5.78			5.78	5.86
99	Tc	43		6.14±.16 [16] 6.16±.08 [17]		6.16	6.16
100	Mo	42	6.33			6.33	6.44
101	Ru	44	5.07		5.2±.4 [16]	5.07	5.02
102	Ru	44	4.19		4.1±.3 [16][e]	4.19	4.17
103	Rh	45		2.85±.20 [16]		2.85	3.0
104	Ru	44	1.83			1.83	1.81
105	Pd	46			.83±.20 [16]	0.83	0.90
106	Pd	46	0.39		.38±.05 [16]	0.39	0.39
107	Pd	46		.19±.04 [16]		0.19	0.19
108	Pd	46				0.07[g]	0.07
109	Ag	47		.030 [16]		0.03	0.03
110	Pd	46				0.022[g]	0.018
111	Cd	48		.018 [16]		0.018	0.019
112	Cd	48				0.016[g]	0.010
113	Cd	48				0.014[g]	0.016
114	Cd	48				0.012[g]	0.014
115	In	49		.0104 [16]		0.011	0.0104
116	Cd	48				0.011[g]	0.018
117	Sn	50				0.011[g]	0.011
					Total Yield	99.995	99.8

a Includes long-lived nuclides ($T_{\frac{1}{2}}$ > 100y)
b Recommended values of Croall [16] plus recent measurements
c Cumulative yield ~ 94% of total chain yield [2]
d Cumulative yield ~ 98.5% of total chain yield [2]
e Cumulative yield ~ 99% of total chain yield [2]
f Partial yield of 10.7 y-^{85}Kr
g Interpolated value

The Kr yields of [4] were originally normalized to mass 85 assuming a smooth yield curve through masses 83 to 86. This gives yields at masses 83, 84 and 86 about 4% greater than those of [7]. The assumption of a smooth curve is suspect and the Kr yields of [4] have been used to reduce the uncertainty in the relative Kr yields. To do this $\Sigma(y_i)$ for masses 83, 84 and 86 is set equal to 3.474, obtained using the yields of [7].

3.4 Radiometric Yields. Final Normalization of the Light Mass Peak

To normalize the mass spectrometric relative yields shown in Table I the contribution in the mass ranges below 83 and from 107 to 117, and at masses 99, 103 and 105 is required. Only radio-metric data are available and this has been reviewed up to 1965 by Croall [16]. His recommended values are adopted except for ^{99}Mo where a more recent value of 6.16±0.08% [17] is used. Yields for the remaining nuclides, for which no data are available, are interpolated to give a smooth fit to the measured yields.

The sum of the radiometric and interpolated yields is 11.015% for masses < 83, 99, 103, 105 and 107-117 while the sum of the arbitrarily normalized mass spectrometric yields is 88.41%. An increase of 0.7% in the latter will bring the total light mass peak to 100%.

Table II displays the renormalized mass spectrometric yields, recent radiometric yields, Croall's recommended values [16] and the recommended chain yields of this paper and of Meek and Rider [2]. The yields are displayed as a function of charge displacement from the stable or very long-lived (>100 y) end product of each chain. Yields of nuclides displaced 2 charge units from stability were checked, using the compilation of Meek and Rider [2], to see whether their predicted cumulative yields were significantly less than the total chain yield. Those with fractional yields ≤ 0.99 are indicated by footnotes.

A comparison of mass spectrometric and radiometric yields indicates good agreement for many nuclides and no trend which might indicate that the normalization of the mass spectrometric data is incorrect.

3.5 The Shape of the Heavy Mass Peak

The determination of the shape of the heavy mass peak proceeds in steps in a similar way to that of the light mass peak.

Step 1: All sets of data are normalized so that $\Sigma(y_i)$ = 20.400 for the Nd isotopes of mass 143, 144, 145, 146,

148 and 150. This normalization value should be considered as arbitrary. The normalization applies to all yields linked by isotope dilution [5,6,7] but only to the Nd isotopes of [9]. Yields for masses 145, 146, 148 and 150 agree, but in the case of masses 143 and 144 the data fall into two groups, one with a high 143 yield and low 144 yield, the other with low 143 yield and high 144 yield. Since the sum of the 143 and 144 yields agree for all measurements it is possible that capture in ^{143}Nd has not been taken into account properly, but the pattern is not otherwise consistent with this explanation.

Step 2: The Sm yields determined by isotope dilution [4,5,7] as normalized in step 1 do not agree. For the important fission product, ^{149}Sm, the spread is 14%. The yields, relative to that of ^{149}Sm, are listed below:

	Relative Yields for Sm Isotopes of Mass				
Reference	Sm147	149	151	152	154
[4]	2.13	1.000	0.398	0.251	0.068
[5]	2.04	1.000	0.376	0.242	0.067
[7]	2.11	1.000	0.407	0.211	0.056
[9]	2.12	1.000	0.395*	0.255	0.071

* Corrected for ^{151}Sm half-life (90 y instead of 98 y)

Agreement is better than for the absolute yields but still cannot be considered satisfactory. The choice of ^{149}Sm as reference is suitable in spite of its reactor cross section of ~70 kb because ^{150}Sm, the capture product, is a shielded isotope (negligible fission yield), so that, to the first order, the total of ^{149}Sm and ^{150}Sm atoms gives the ^{149}Sm yield. Further, the second order corrections, ^{147}Pm(n,γ) ^{148}Pm(n,γ) ^{149}Pm(β)^{149}Sm and ^{150}Sm(n,γ)^{151}Sm, are nearly equal and of opposite sign.

The Sm yields adopted here are obtained by normalizing averaged relative yields to the ^{147}Nd yield of [9]. In this work the yield of 11-d ^{147}Nd was measured relative to ^{148}Nd and ^{150}Nd using samples which had such short irradiation and handling times that corrections for ^{147}Nd decay were less than 2%. In addition their normalized yields for other Nd isotopes agree well with the adopted averages.

To obtain relative yield averages some data are omitted. The value of 2.04 [5] is 4% low and is omitted since it contains a large correction for mass 147 hold-up as 2.6-y ^{147}Pm, with no details given on the size of the correction or the half-life used. The ^{152}Sm and ^{154}Sm relative yields of [7]

are also omitted because they are much lower than values obtained by the other experimenters, even though there seems to be no reasonable explanation for the discrepancy.

Step 3: The relative ^{151}Eu and ^{153}Eu yields of [9] have been normalized to 0.41 at mass 151 to obtain a value at mass 153. The latter is in good agreement with the normalized isotope dilution value of [5].

Step 4: The relative Ce yields of [9] at masses 140, 141,142 and 144 are normalized to the adopted value of 5.37 at mass 144. No correction is required for the direct yield of ^{144}Pr. The normalized yields at masses 140, and 142 are in good agreement with those of [5] and [7].

Step 5: The relative Ba yields of [9] at masses 138-140 are normalized to the adopted value of 6.27 at mass 140. No correction is required for the direct yield of ^{138}La.

Step 6: The relative Xe yields of [9] were taken from an earlier paper [22] and normalized to the ^{133}Cs yield using an unpublished measurement of the ratio of ^{133}Xe to ^{136}Xe. The latter is not used here because no details of the decay corrections are available. Instead the relative yields of [22] are normalized to $\Sigma(y_i)$ for masses 130, 132 and 134 using the Xe yields of [7] in step 1. The set of normalized yields is completed using the ^{135}Cs value of [4] and the average of [4], [6] and [7] for ^{133}Cs.

3.6 Radiometric Yields. Final Normalization of the Heavy Mass Peak

Radiochemical yields are displayed in Table IV using a layout identical to that of Table II. For data up to 1965 the evaluated values of [16] are used. To obtain a final normalization for the yields of Table III evaluated yields are required for the mass ranges 118 to 130 and above mass 155. These are obtained by averaging radiochemical values except at mass 128 where the measured yield is assumed to be only 80% of the total chain yield [2]. Where no radiochemical data are available, values are interpolated assuming a smooth curve. The total of radiochemical and interpolated yields in the heavy mass peak outside the range mass 131 to 155 covered in Table III is 3.635% while the arbitrarily normalized yields of Table III add to 95.657. To bring the total heavy mass yield to 100% requires that the values of Table III be increased by 0.7%

A comparison of the mass spectrometric and radiometric yields between masses 131 and 155 agree well within the uncertainties of the radiometric measurements for the important

TABLE III. ANALYSIS FOR SHAPE OF HEAVY MASS PEAK

Mass	Elem	Petruska et al. [4]	Rider et al [6]	Lisman et al. [7]	Chu [5]	Farrar et al. [9]	A[a]	Relative Yields	A[a]	Farrar et al. [9]	A[a]	Farrar et al. [9]	A[a]	Farrar et al. [9]	A[a]	Wanless, Thode [22]	A[a]
		Step 1						Step 2		Step 3		Step 4		Step 5		Step 6	
131	Xe			2.78												2.75[c]	2.77
132	Xe			4.15												4.11[c]	4.13
133	Cs	6.64	6.74	6.71													6.70
134	Xe			7.49												7.56[c]	7.52
135	Cs	6.46															6.46
136	Xe															6.06	6.06
137	Cs	6.20	6.18	6.26										6.20	6.21		
	Ba																
138	Ba			6.78										6.71	6.75		
139	Ba													6.52	6.52		
140	Ba													(6.27)			
	Ce			6.29	6.21							6.32_5	6.27				
141	Ce											5.80	5.80				
142	Ce			5.86	5.91							5.88	5.88				
143	Nd	5.84	5.97	5.88	5.91	5.85	5.89										
144	Nd	5.43	5.28	5.40	5.32	5.42	5.37										
	Ce											(5.37)					
145	Nd	3.89	3.90	3.85	3.90	3.89	3.89										
146	Nd	2.95	2.95	2.94	2.95	2.95	2.95										
147	Nd					2.21			2.21								
	Sm	2.40[b]		2.11	2.24_5			55.25									
148	Nd	1.63	1.67	1.68_5	1.67	1.64	1.66										
149	Sm	1.13		1.00	1.10			26.30	1.05								
150	Nd	0.64	0.63	0.636	0.65	0.64	0.64										
151	Sm	0.45		0.407	0.414			10.35	0.41_4	0.41							
152	Sm	0.285		0.211	0.266			6.55	0.26								
153	Eu				0.163					0.164	0.163						
154	Sm	0.077		0.056	0.074			1.81	0.072_4								
155	Eu				0.032						0.032						

a Adopted relative yields

b +1% correction ^{147}Pm - 2.62y instead of 2.52 y.

c Normalized to [7] using sum of yields for masses 131, 132 and 134.

standards ^{137}Cs and ^{140}Ba. Elsewhere no systematic differences are observed which might indicate an error in the normalization of the mass spectrometric yields from Table III. The recommended values over this mass range are set equal to the mass spectrometric values except for trivial adjustments at masses 137 and 140.

3.7 Discussion of Uncertainties

Relative yields of stable isotopes of a given element can be measured with great precision using a mass spectrometer, with uncertainties typically only a few tenths of one percent. However when fission product measurements from several laboratories are compared the averages at each mass have mean square deviations ranging up to several percent, indicating the presence of systematic errors in the individual measurements. The Zr and Nd yields of Tables I and III are good examples. Systematic errors may be due to the preparation of the source, the conditions of ion production in the mass spectrometer or to the presence of unidentified contaminants.

The determination of absolute yields by isotope dilution, in which the "spike" is one of the isotopes whose abundance is measured, will be subject to the same systematic uncertainties in addition to those arising from the chemical preparation of the "spiked" sample. The procedure used here avoids the main source of uncertainty in absolute yield measurements, namely, the determination of the number of fissions.

It is assumed that the yield at a particular mass has the following components:

(i) The uncertainty in the relative yield. This is mostly systematic and is estimated to be about 0.7% in the individual measurement on the basis of intercomparisons of relative yields, unless differences among experimental values indicate that it should be larger for a particular isotope.

(ii) The uncertainty in the number of atoms of one element relative to the number of atoms of the standard element (Zr or Nd). This is assumed to be predominantly systematic, with 0.7% contributed by each element.

(iii) The uncertainty in the final normalization, including contributions from (ii) above and from the auxiliary radiometric and interpolated yields. A review of the differences between experimentally-determined atom yields for each element gives an uncertainty in the final normalization of 0.7% and 0.9% for the light and heavy mass peaks respectively.

Table V shows the component and overall uncertainties due to yields only for the ten most important fission products. The yields of all of these except ^{103}Rh have been measured mass spectrometrically and included in this evaluation. These are in the heavy mass peak and therefore have a common systematic error due to the uncertainty in the normalization. The overall uncertainty for each fission product is

$$\epsilon = (\epsilon_i^2 + \epsilon_{ii}^2)^{\frac{1}{2}} + \epsilon_{iii}$$

where the subscripts refer to the three components listed above.

TABLE IV. HEAVY MASS YIELDS: MASS SPECTROMETRIC, RADIOMETRIC AND RECOMMENDED

Mass	Stable Fission Product[a]			Yields (%) of Radioactive Fission Products[b]				Recommended	
				Z - 1		Z - 2		This Paper	Meek, Rider
	Elem	Z	Yield (%)						
118	Sn	50						0.011[h]	0.014
119	Sn	50						0.011[h]	0.014
120	Sn	50						0.012[h]	0.014
121	Sb	51		.015 [16]	.0014±.0003 [23] .0012±.0001 [26]			0.014	0.014
122	Sn	50						0.015[h]	0.015
123	Sb	51		.00190±.00003 [23][c]				0.018	0.016
124	Sn	50						0.022[h]	0.018
125	Te	52		.021 [16]	.0291±.0033 [7] .0291±.0007 [23]	.0116±.0001 [23][c]		0.029	0.021
126	Sn	50						0.06[h]	0.032
127	I	53				.135 [16]	.124±.015 [23]	0.13	0.137
128	Te	52				.314±.004 [23][d]		0.39	0.46
129	I	53	0.9 [16]			1.12±.18 [16][e]	.622±.006 [23][e]	0.90	1.0
130	Te	52		2.0±.5 [16]				2.0	2.1
131	Xe	54	2.79	3.1±0.3 [16]				2.79	2.91
132	Xe	54	4.16			4.7 [16]		4.16	4.26
133	Cs	55	6.75			6.5 [16]		6.75	6.69
134	Xe	54	7.57	7.8±1.1 [16]				7.57	7.80
135	Cs	55	6.51			6.1±0.4 [16][f]		6.51	6.43
136	Xe	54	6.10					6.10	6.46
137	Ba	56	6.25	6.23±.07 [28] 6.22±.04 [29]	6.2 [16]			6.24	6.20
138	Ba	56	6.80	7.22±.29 [16]				6.80	6.71
139	La	57		6.57	6.55±.08 [17] 6.55±.35 [16]			6.56	6.48
140	Ce	58	6.32			6.36±.12 [16]	6.35±.15 [27] 6.36±.25 [25]	6.34	6.34
141	Pr	59		5.84	5.50±.34 [7] 6.0 [16]	6.3±.5 [16]		5.84	6.10
142	Ce	58	5.92					5.92	5.90
143	Nd	60	5.93	5.88±.23 [16]		5.67±.12 [27]		5.93	5.91
144	Nd	60	5.41					5.41	5.40
145	Nd	60	3.92					3.92	3.88
146	Nd	60	2.97					2.97	2.95
147	Sm	62				2.23	2.42±.06 [27] 2.24±.12 [16]	2.23	2.19
148	Nd	60	1.67					1.67	1.67
149	Sm	62	1.06	1.1±.2 [16]				1.06	1.04
150	Nd	60	0.64$_5$					0.65	0.65
151	Eu	63	0.42					0.42	0.43
152	Sm	62	0.26					0.26	0.24
153	Eu	63	0.164	.15±.01 [16]	.144±.003 [27]			0.164	0.158
154	Gd	64	0.073					0.073	0.064
155	Gd	64	0.032					0.032	0.031
156	Gd	64		.014 [16]	.0125±.0010 [24]			0.013	0.0134
157	Gd	64		.0061 [16]	.0060±.0007 [24]			0.006	0.0066
158	Gd	64		.002 [16]	.0031±.0006 [24]			0.0025	0.0037
159	Tb	65		.001 [16]		.0011±.0003 [24][g]		0.001	0.0105
*160				.001				0.001	0.0005
							Total Yield	100.00$_4$	100.7

a Includes long-lived nuclided ($T_{\frac{1}{2}}$ > 100 y)
b Recommended values of Croall [16] plus recent measurements
c Partial yield (125-d ^{123}Sn, 9.4-d ^{125}Sn)
d Cumulative yield ~80% of total chain yield [2]
e Cumulative yield ~97% of total chain yield [2]
f Cumulative yield ~97% of total chain yield
g Cumulative yield ~91% of total chain yield [2]
h Interpolated value.

Because the greatest portion of fission product neutron absorption is by nuclides in the heavy mass peak, the total absorption will have a systematic component of about 0.9% plus contributions from uncertainties in relative yields and isotope dilution, which may be added in quadrature. Extrapolating from the uncertainties in barns per fission shown in the last column of Table V, the uncertainty in total fission product absorption is ~ 0.6 barns per fission or ~ 1.4% due to yields alone.

The contribution from cross section uncertainties can be estimated from an earlier survey [30]. At that time the two largest contributors were ^{135}Xe (yield) and ^{147}Pm (cross section). Both the magnitude and uncertainty in the ^{147}Pm cross section have been reduced [12] leaving ^{135}Xe as the dominant source of uncertainty. With the cross section uncertainties included the percent error in fission product absorption is estimated to increase to ~ 0.8 barns. This does not include an estimate of the contribution of unknown cross sections.

A comparison of the recommended yields of this paper and of Meek and Rider [2] listed in Tables II and IV show differences exceeding 1 percent for the isotopes of Kr, Mo, Xe, Sm and mass 141. Except for the last named, these can be attributed to renormalizations and deletions described in sections 3.3 and 3.5. In the case of mass 141, the difference is due to the inclusion of early radiometric data in [2]. For masses where there were no mass spectrometric yields a few quite large differences occur due to the weighting given older radiometric measurements, the inclusion of new data in this paper and differences in interpolation. While the differences are large in absolute terms they do not have an appreciable effect on fission product absorption either through the normalizing procedure used here or directly on the yield of an important fission product except for ^{103}Rh. In the latter case the recommended yields differ by the error listed in Table V.

4. YIELDS OF OTHER FISSILE NUCLIDES

Preliminary evaluations of the yields from the thermal neutron fission of ^{233}U and ^{231}Pu have been completed using the method described here for ^{235}U. In these nuclides there are fewer mass spectrometric measurements so that uncertainties will be greater. When this work is completed it will be published as part II of the fission product evaluation report [12]. The preliminary ^{233}U and ^{239}Pu yield are listed in the report on FISSPROD [1].

TABLE V. UNCERTAINTIES IN YIELDS AND ABSORPTION FOR MOST IMPORTANT ^{235}U FISSION PRODUCTS

Nuclide	$\hat{\sigma}$ (barns)	Absorption[a] (barns/fission)	Percent Uncertainties				ΔA[b] (barns/fission)
			In Relative Yield (ϵ_i)	In Isotope Dilution (ϵ_{ii})	In Normalization (ϵ_{iii})	Overall ϵ	
^{136}Xe	3×10^6	40.3	0.7	0.7	0.9	1.9	0.40
^{143}Nd	330	15.1	0.9	0.9	0.9	1.8	0.20
^{149}Sm	7×10^4	9.5	1.5	1.0	0.9	2.7	0.17
^{147}Pm	350	5.1[c]	0.7	0	0.9	1.6	0.04
^{151}Sm	14×10^3	4.2	3.0	1.0	0.9	4.0	0.14
^{103}Rh	200	3.2	-	-	-	~5 [16]	0.16
^{131}Xe	140	2.5	0.5	0.7	0.9	1.8	0.02
^{133}Cs	50	1.9	0.5	0.5	0.9	1.6	0.01
^{145}Nd	70	1.7	0.3	0	0.9	1.2	~0
^{152}Sm	300	1.2	3.0	1.0	0.9	4.0	0.04

a After an irradiation of 1 n/kb at a flux of 0.5 n/cm^{2}s.

b Uncertainty in absorption due only to the contributions from relative yield and isotope dilution (ΔA = Absorption x $\sqrt{\epsilon_i^2 + \epsilon_{ii}^2}/100$)

c *Including absorption in capture products* ^{148m}Pm *and* ^{148g}Pm.

TABLE VI. COMPARISON OF MEASURED AND CALCULATED FISSION PRODUCT ABSORPTION

Fissile Nuclide	Irradiation n/kb	Quantity[a]	Measured		Calculated (FISSPROD)		
			Original [31]	Revised [33]	New σ, I New Yields	New σ, I Old Yields	Old σ, I Old Yields
			barns per fission				
^{233}U	2.29	σ_o	32.0	37.3±2.8	42.0	44.4	45.3
		$\sigma_o s_o$	235	226±35	163	165	154
^{233}U	2.90	σ_o	29.6	32.9±2.2	39.7	41.9	42.6
		$\sigma_o s_o$	227	200±31	157	159	148
^{235}U	2.03	σ_o	38.2	41.6±2.4	48.9	48.1	48.9
		$\sigma_o s_o$	290	232±34	192	191	179
^{235}U	2.26	σ_o	37.9	40.4±2.2	47.6	46.8	47.6
		$\sigma_o s_o$	250	195±33	190	189	175
^{239}Pu	2.15	σ_o	50.7	54.0±4.2	58.4	56.0	56.8
		$\sigma_o s_o$	242	140±53	277	275	251
^{239}Pu	2.61	σ_o	48.8	50.5±3.9	56.8	54.0	54.8
		$\sigma_o s_o$	199	105±62	268	266	241

a σ_o is the 2200 m/s cross section

$\sigma_o s_o = \frac{2}{\sqrt{\pi}} I$ where I is the reduced resonance integral.

5. COMPARISON WITH EXPERIMENT

The new cross section and yield data have been used to calculate fission product absorption in samples of ^{233}U, ^{235}U, and ^{239}Pu irradiated in NRU at Chalk River and measured by pile oscillator in PTR at Chalk River [31] and in RO at Studsvik, Sweden. The latter comparison is included in the report on the Swedish measurements [32].

FISSPROD calculations based on earlier cross section and yield data were compared with the Chalk River results [31] in a previous paper [30]. Since then the measured values have been revised [33] on the basis of RO measurements of thermal neutron absorption in the calibration samples. Table VI gives the original and revised measured gross fission product cross sections and FISSPROD results. The latter use three sets of data:

(i) new thermal cross section and resonance integral data, the ^{235}U thermal fission yields of this report and the preliminary thermal fission yields of ^{233}U and ^{239}Pu.

(ii) the same cross sections as above, but yield data used in the previous comparison [30] and

(iii) all data from the previous comparison.

It can be seen that the new cross sections decrease the calculated thermal cross section (σ_0) by about 0.7 to 0.9 barns for all fissile nuclides, and that using the new ^{235}U yields causes an increase of the same size. In the case of ^{233}U use of the revised yields produces a further decrease of $\sim$ 2.2 barns. This is due to a decrease in the yields of Nd and Sm isotopes to bring them into agreement with the results of Lisman et al. [7]. The revised ^{239}Pu yield account for a small increase.

The revision in the measured values and input data to FISSPROD has decreased the differences in thermal cross sections and brought the ^{239}Pu value within the sum of the uncertainties but there are still substantial differences for both ^{233}U and ^{235}U. Agreement between measured and calculated resonance integrals ($\sigma_0 s_0$) is not significantly changed for ^{233}U or ^{239}Pu integrals but is now satisfactory for ^{235}U. It is possible that the disagreement in both thermal cross sections and resonance integrals are associated with the interpretation of resonance absorption in pile oscillator measurements.

REFERENCES

[1] LANE, F.E., Atomic Energy of Canada Report No. AECL-3038 (1969).

[2] MEEK, M.E. and RIDER, B.F., U.S. Atomic Energy Commission Report No. APED-5398-A (Revised)(1968).

[3] STEINBERG, E.P. and GLENDENIN, L.E., Proceedings of the First Conference on Peaceful Uses of Atomic Energy 7 3 (Geneva, 1955).
[4] PETRUSKA, J.A., THODE, H.G., and TOMLINSON, R.H., Can. J. Phys. 33 693 (1955).
[5] CHU, Y.Y., Lawrence Radiation Laboratory, University of California, Report No. UCRL-8926.
[6] RIDER, B.F., RUIZ, C.P., PETERSON Jr., J.P., and SMITH, F.R. U.S. Atomic Energy Commission Report No. GEAP-5060 (1965).
[7] LISMAN, F.L., MAECK, W.J., REIN, J.E., FOSTER, Jr., R.E., ABERNATHEY, R.M., DELMORE, Jr., J.E., EMEL, W.A., KUSSY, M.E., McATEE, R.E., WORKMAN, G.D., U.S. Atomic Energy Commission Report No. IN-1277 (1969).
[7a] The Kr yields used in Table I were included in a private communication from Dr. F.L. Lisman of Idaho Nuclear Corp. These are more recent results and are intended to replace the Kr yields in IN-1277.
[8] FARRAR, H., FICKEL, H.R., and TOMLINSON, R.H., Can. J. Phys. 40 1017 (1962).
[9] FARRAR, H., and TOMLINSON, R.H., Nucl. Phys. 34 367 (1962).
[10] INGHRAM, M.G., HAYDEN, R.J., and HESS, D.C., Phys. Rev. 79 271 (1950).
[11] GORSHKOV, V.K., IVANOV, R.N., KUKAVADZE, G.M., and REFORMATSKY, I.A., Atomaya Energiya 3 (1957)(English translation, Sov. J. At. En. 3 729).
[12] WALKER, W.H., Atomic Energy of Canada Report No. AECL-3037, Part I (1969).
[13] AMES, D.P., BUNKER, M.E., LANGER, L.M., and SORENSON, B.M., Phys. Rev. 91 68 (1953).
[14] SOLECKI, J.E., Ames Laboratory Report No. 15-T-234 (1968).
[15] WANLESS, R.K., and THODE, H.G., Can. J. Phys. 33 541 (1955).
[16] CROALL, I.F., U.K. Atomic Energy Establishment Report No. AERE-R5086 (1965).
[17] VON GUNTEN, H.R., and HERMAN, H., Radiochim Acta 8 112 (1967).
[18] KATCOFF, S. and RUBINSON, W., J. Inorg. Nucl. Chem. 27 1447 (1965).
[19] REED, G.W., Phys. Rev. 98 1327 (1955). Original yield for ^{90}Sr, 4.02% assuming $T_{\frac{1}{2}} = 20y$. Value here corrected to $T_{\frac{1}{2}} = 28.9y$.
[20] BAERG, A.P., and BARTHOLOMEW, R.M., Can. J. Chem. 35 980 (1957).
[21] CORYELL, C.D., SAKAKURA, A.Y., ROSS, A.M., Phys. Rev. 77 775 (1950).
[22] WANLESS, R.K., THODE, H.G., Can. J. Phys. 33 541 (1955).
[23] ERDAL, B.R., WILLIAMS, J.C., WAHL, A.C., J. Inorg. Nucl. Chem. 31 2993 (1969).
[24] DANIELS, W.R., and HOFFMAN, D.C., Phys. Rev. 145 911 (1966).
[25] CUIFFOLOTTI, L., En. Nucleare 15 272 (1968).
[26] WEISS, H.V., Phys. Rev. 139B 304 (1965).

[27] BRESESTI, M., BUREI, G., FERRARI, P., MORETTO, L., J. Inorg. Nucl. Chem. 29 1189 (1967). Yields have been renormalized to 5.84% for ^{141}Ce.

[28] MAECK, W.J., REIN, J.E. et al. (Idaho Falls Progress Repts) U.S. Atomic Energy Commission Reports IDO-144660 (1965), IDO-14667 (1965) and IN-1064 (1966)(Average of 3 radiometric measurements).

[29] LARSEN, R.P., and MEYERS, R.J., U.S. Atomic Energy Comm. Report ANL-7225, 252 (1966).

[30] WALKER, W.H., IAEA Conference on Nuclear Data for Reactors (Paris I 521 (1966).

[31] OKAZAKI, A., DURHAM, R.W., LOUNSBURY, M., Atomic Energy of Canada Report No. AECL-2510 (1965).

[32] OKAZAKI, A., and SOKOLOWSKI, E.K., Paper CN26/58 at this conference.

[33] OKAZAKI, A., Private Communication.

REDETERMINATION OF THE THERMAL-NEUTRON ABSORPTION CROSS-SECTIONS OF GROSS FISSION PRODUCTS OF ^{233}U, ^{235}U AND ^{239}Pu

A. OKAZAKI
Atomic Energy of Canada Limited,
Chalk River,
Canada

E.K. SOKOLOWSKI
AB Atomenergi,
Studsvik, Nyköping,
Sweden

Presented by W.H. Walker

Abstract

REDETERMINATION OF THE THERMAL-NEUTRON ABSORPTION CROSS-SECTIONS OF GROSS FISSION PRODUCTS OF ^{233}U, ^{235}U and ^{239}Pu.

The thermal cross-sections of the long-lived gross fission products from ^{233}U, ^{235}U and ^{239}Pu fission have been determined by pile oscillator measurements on highly irradiated samples. The samples, consisting initially of a single fissile nuclide in a matrix of high-purity aluminium, had been irradiated to a depletion of 70-90%, which gave a fission product contribution to the total absorption cross-section of about 10%. Measurements with these samples had previously been performed at AECL, but have now been repeated under more favourable experimental conditions. The fission product cross-sections have been determined with an accuracy of 5%. A comparison with a recent version of the calculational model FISSPROD shows that the calculated cross-sections are consistently about 7% higher than the measured ones.

1. INTRODUCTION

For some reactor types the uncertainty in the gross fission product cross section may contribute substantially to the uncertainty in burn-up predictions: thus, in a heavy-water, natural-uranium reactor, operated on a once-through cycle to a burn-up of 10,000 MWd/t, a 10 % error in the effective fission product cross section will give rise to an error in burn-up of about 650 MWd/t [1]. Consequently much effort has been directed towards improving the basic data and calculational models for the gross fission product cross sections. One such model is the Canadian program FISSPROD [2]. An evaluation of the basic nuclear data used in this program was made by Walker in 1966 [3] and led to an estimation of about 4 % for the uncertainty in the gross fission product cross section. A revision of the data has recently been published [4] and will be discussed at this conference [4a].

There exist few integral experiments of sufficient accuracy to serve as checks of the calculational models. This is due to the fact that in a burnt fuel sample the fission products account only for a small part (usually much less than 10 %)of the total cross section. Attempts to separate the fission products in a controlled way have failed [5]. An alternative approach was chosen by

Okazaki et al. at Chalk River [6], who irradiated samples, initially containing a single uranium or plutonium nuclide (^{233}U, ^{235}U or ^{239}Pu) in a matrix material of low cross section (aluminum). This ensured a maximum fission product contribution to the cross section and a minimum of non-fission transformations, which would complicate the analysis. The total cross sections of the irradiated samples were measured by pile oscillator technique. An essential part of the experiments was the post-irradiation analysis of the samples for remaining heavy nuclides. The estimated accuracy in the measured thermal fission product cross section was 8-10 %. In the case of ^{235}U and ^{233}U the corresponding calculated FISSPROD values were higher by more than the compounded errors. Some systematic error in the pile oscillator measurements was suspected but could not be traced.

The Swedish pile oscillator facility in the R0 reactor offered several advantages over that available to Okazaki et al. [6], and some of its crucial parameters were of different orders of magnitude. Since duplicates of the Canadian samples were available, the measurements were repeated in Sweden.

2. REACTOR CONDITIONS

The Canadian pile oscillator measurements were carried out in the PTR, a light-water pool reactor with MTR-type fuel. It was desirable to perform the measurements in different neutron spectra in order to be able to separate the thermal and resonance components of the fission product cross sections. The only means of changing the spectrum was to vary the material in the sample carrier. In this way two Westcott epithermal-parameter (r) values, 0.029 and 0.047, were obtained. The difference is small, and the uncertainty in the epithermal response of the reactor enters into all the measurements (see below).

The Studsvik measurements were made centrally in the heavy-water reactor R0, fuelled with natural-uranium metal rods in a square lattice, whose geometry can easily be varied. The measurements reported here were made in the "thermal column" obtained by removing the 24 innermost fuel rods from a 13 cm square lattice[1]. The unperturbed spectrum characteristics of the measuring position have been determined to be [7]

$$r = 0.00162 \pm .00005$$

$$T_n = (28 \pm 3)^{\circ}C$$

In order to investigate a possible spectrum hardening effect from the pile oscillator samples themselves, a series of indium and lutetium foil activations were performed. The oscillator samples were simulated with UO_2 rod sections of varying enrichment, and the foils were placed between pellets inside these rods. No increase in the Westcott r values could be detected but an error limit of $\pm$ 0.0015 had to be assigned. The lutetium activations showed a slight increase in the neutron temperature, in accordance with a correlation given in [8] which relates the temperature increase to the sample absorption area. Since the expected temperature increase in the current samples was less than 10 $^{\circ}C$ it was disregarded.

---

1) Measurements were also made in the central cell boundary position in a 13 cm lattice, having an r value of 0.042. However, no conclusive results were obtained due to some ambiguities in the calibration measurements. Details of the measurements will be reported in [9].

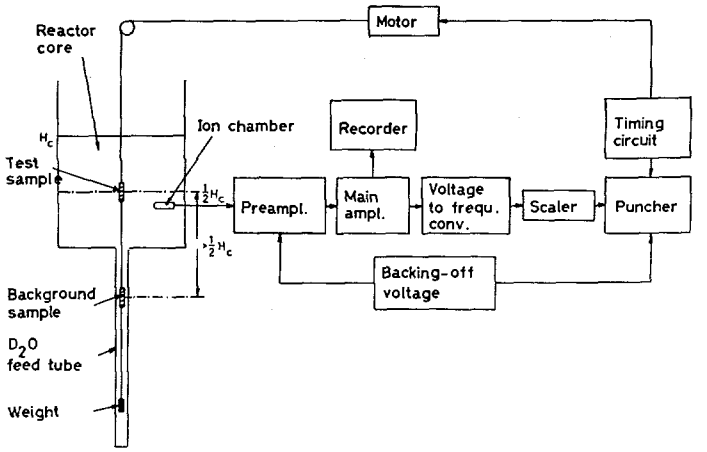

FIG.1. Schematic diagram of the RO pile oscillator equipment.

As was stated in section 1, the dominating part of the reactivity signal from the irradiated samples usually stems from the remaining fissile material and has to be subtracted in the analysis, which therefore becomes very sensitive to errors in the uranium or plutonium content. The contribution from these materials consists of two counteracting components - an absorption part and a production part. The production cross section $\nu\Sigma_f$ is about twice as large as the absorption cross section for the fissile nuclides. To obtain the relative reactivity response for the two types of reactions, $\nu\Sigma_f$ must be weighted with the importance of fission neutrons relative to thermal neutrons. This weighting factor, W, depends on the reactor configuration, and ideally, if W could be made equal to $\Sigma_a/\nu\Sigma_f$, the net reactivity signal from the fissile material would be zero, independent of the amount of material. In the PTR experiments W was found to equal 1.3 and 1.6, while for the RO thermal-column measurements it was 1.0 (section 6.3), thus making the present experiments less sensitive to errors in the fissile materials content.

3. PILE OSCILLATOR EQUIPMENT AND DATA COLLECTION

The pile oscillator equipment for the RO reactor and the data collection system are shown schematically in fig. 1. Two samples (test and background samples) alternated at the center of the reactor core with a period of 60 s. Compared to this period the time of traversal was short, which resulted in a reactivity signal that was approximately a square wave. The distance between the two samples, which equals the stroke length, exceeds half the extrapolated critical core height, so that in the rest positions one sample is always well out of the core. After Fourier analysis of the reactor flux response, carried out with a computer, the ratio between the fundamental-mode flux amplitude, $\Delta\Phi$, and the mean flux level, Φ_o, was obtained. $\Delta\Phi/\Phi_o$ is proportional to the reactivity difference between the test and background samples and can be related to the sample reaction cross sections by calibration (section 6.3). The computer analysis included elimination of reactor power drift up to second-order terms by weighting every four successive half-cycles with a sequence of binomial coefficients [14].

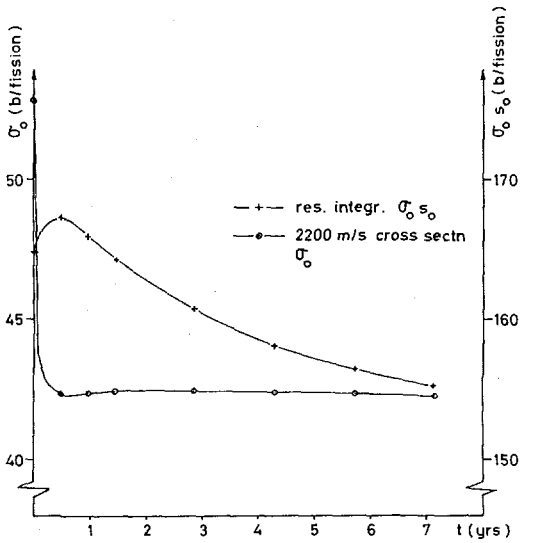

FIG. 2. Calculated variation of fission product cross-sections with time after irradiation (sample A3B^{X}, $\omega = 2.15$ n/kb).

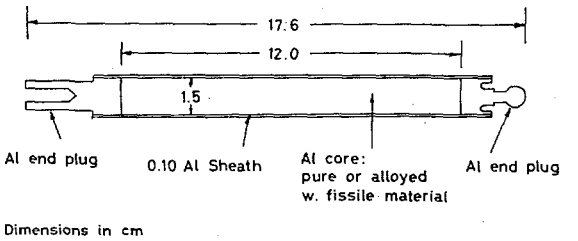

FIG. 3. Sample geometry.

4. IRRADIATED SAMPLES

A detailed description of the sample preparation and analysis has been given in [6]. The samples to be irradiated were made of alloys of the fissile materials with super-pure aluminum in the form of solid cylinders, 1.5 cm in diameter and 15 cm long. Each alloy core was sheathed in aluminum as shown in fig. 3. The initial content of fissile material in a sample was 1.5 g in the case of ^{233}U and ^{235}U, and 1.0 g in the case of ^{239}Pu. Four samples of each fissile material were irradiated; two of each were oscillated and subsequently analyzed destructively at Chalk River. The remaining samples have been oscillated at both Chalk River and Studsvik.

The irradiations took place in the Canadian NRU reactor from April 1960 to May 1961. Hence no short-lived fission products remained at the time of the measurements. However, since a dominating part of the fission products is stable [3], an asymptotic value of the absorption cross section is approached shortly after the irradiation, as shown in fig. 2. - The irradiation position

TABLE Ia: COMPOSITION OF IRRADIATED ^{233}U SAMPLES

Sample		A3B* [2]	A3F*
Initial			
U isotopic content (atom %):	^{233}U	99.787 ±.004	99.787 ±.004
	^{234}U	0.053 ±.002	0.053 ±.002
	^{238}U	0.160 ±.003	0.160 ±.003
^{233}U mass (mg):		1434±3	1433±3
Number of atoms (10^{21})			
	N^o_{23}	3.706 ±.008	3.704 ±.008
	N^o_{24}	0.00196±.00007	0.00196±.00007
	N^o_{28}	0.00593±.00011	0.00593±.00011
Aluminum mass (g).			
in core alloy		56.716	56.617
in sheath and plugs		33.32	33.30
Irradiated			
Number of atoms (10^{21}):			
	N_{23}	1.042 ±.005	0.777 ±.004
	N_{24}	0.2002 ±.0009	0.2113 ±.0009
	N_{25}	0.0191 ±.0002	0.0235 ±.0002
	N_{26}	0.00173±.00004	0.00276±.00004
	N_{28}	0.00582±.00006	0.00578±.00006
$\ln(N^o_{23}/N_{23}) = \sigma_{23}\omega$ [1]:		1.2689	1.5617
ω(n/kb):		2.147	2.642
^{233}U fissions (10^{21}):		2.436	2.676
^{235}U fissions (10^{21}):		0.019	0.030
Total fissions (10^{21}):		2.455	2.706

1) σ_{23} = 591.0 b is the effective absorption cross section of ^{233}U in the irradiation neutron spectrum and ω is the neutron fluence.

2) Asterisks indicate irradiated samples.

was characterized by the Westcott spectral parameters r = 0.022±.004 and T_n = 40± 5 °C . Due to different axial positions for the samples, the fluence and hence the depletion of each type of the fissile nuclide varied somewhat, the latter being 70-80 % for ^{233}U and ^{235}U and around 90 % for ^{239}Pu. Tables Ia-c give the initial and final compositions of the samples investigated here. The post-irradiation data were obtained by interpolation or extrapolation of the compositions for the samples analyzed destructively, on the basis of the reactivity signals measured at Chalk River. The errors in the heavy-nuclide concentrations have been set somewhat higher than the corresponding errors for the nearest analyzed samples.

5. BACKGROUND AND CALIBRATION SAMPLES

In all the measurements the "background" sample (section 3) was a pure aluminum one (denoted by SPD) with the same geometry - i.e. cylindrical core, sheath and end plugs - as the irradiated samples, and of the same quality

TABLE Ib: COMPOSITION OF IRRADIATED ^{235}U SAMPLES

Sample		A5B*	A5F*
Initial			
U isotopic content (atom %):	^{234}U	0.061 ±.002	0.061 ±.002
	^{235}U	99.746 ±.003	99.746 ±.003
	^{236}U	0.066 ±.002	0.066 ±.002
	^{238}U	0.127 ±.001	0.127 ±.001
U mass (mg):		1569±2	1561±2
Number of atoms (10^{21}):			
	N^o_{24}	0.00245±.00008	0.00243±.00008
	N^o_{25}	4.010 ±.005	3.990 ±.005
	N^o_{26}	0.00265±.00008	0.00263±.00008
	N^o_{28}	0.00509±.00004	0.00507±.00004
Aluminum mass (g):			
in core alloy		56.781	56.539
in sheath and plugs		33.575	32.91
Irradiated			
Number of atoms (10^{21}):			
	N_{24}	0.00199±.00001	0.00191±.00001
	N_{25}	1.144 ±.002	0.901 ±.002
	N_{26}	0.421 ±.001	0.452 ±.001
	N_{28}	0.00501±.00001	0.00497±.00001
	^{237}Np	0.00565±.00040	0.00724±.00040
$\ln(N^o_{25}/N_{25}) = \sigma_{25}\omega$ [1]:		1.2542	1.4880
ω(n/kb):		1.888	2.240
^{235}U fissions (10^{21}):		2.439	2.628

1) σ_{25} = 664.4 b is the effective absorption cross section of ^{235}U in the irradiation neutron spectrum and ω is the neutron fluence.

aluminum. Its properties are given in table II. A comparison with tables Ia-c shows that the total aluminum mass in the background sample differed from that in the irradiated samples by only about 1 %. Since the measured reactivity signal is due to the difference between the two samples, any error in the assumed aluminum cross section is thus reduced to a second-order effect.

The calibration samples used for obtaining the reactor response to thermal neutrons were in the form of solution of absorber in heavy water, contained in anodized aluminum cylinders of 1.3 cm inner diameter, and holding 25 cm^3 of solution. B_2O_3 was used as a calibration substance, the concentration being such that the thermal self-shielding correction was small (∿ 1 %). The background samples in the calibration measurements consisted of pure solvent in identical sample holders. Good consistency with the boron calibrations had been obtained using manganese and indium solutions [7]. From geometric considerations it seemed improbable that the solvent (or matrix material) should have any effect on the measured reactivity signals. This was confirmed by repeating the boron solution measurements with light water as the solvent.

TABLE Ic: COMPOSITION OF IRRADIATED ^{239}Pu SAMPLES

Sample	A9A[x]	A9D[x]
Initial		
Pu isotopic content ^{239}Pu	98.150 ±.005	98.150 ±.005
^{240}Pu	1.797 ±.005	1.797 ±.005
^{241}Pu	0.053 ±.001	0.053 ±.001
Pu mass (mg):	949.5±8.0	951.7±8.0
Number of atoms (10^{21}):		
N^o_{49}	2.349 ±.020	2.351 ±.020
N^o_{40}	0.0430 ±.0004	0.0431 ±.0004
N^o_{41}	0.00127±.00003	0.00127±.00003
Aluminum mass (g):		
in core alloy	56.751	56.848
in sheath and plugs	34.92	34.19
Irradiated		
Number of atoms (10^{20}):		
N_{48}	0.0149 ±.0003	0.0125 ±.0003
N_{49}	1.502 ±.023	2.466 ±.037
N_{40} [1)]	3.666 ±.055	4.075 ±.061
N_{41}	0.702 ±.010	0.702 ±.010
N_{42}	0.599 ±.009	0.444 ±.009
^{241}Am [1)]	0.394 ±.008	0.389 ±.008
$\ln(N^o_{49}/N_{49}) = \sigma_{49}\omega$ [2)].	2.750	2.256
ω(n/kb):	2.333	1.915
^{239}Pu fissions (10^{21}):	1.51	1.45
^{241}Pu fissions (10^{21}):	0.19	0.14
Total fissions (10^{21}):	1.70	1.59

1) Corrected to April 1969, the time of the oscillator measurements

2) σ_{49} = 1178.4 b is the effective absorption cross section of ^{239}Pu in the irradiation neutron spectrum and ω is the neutron fluence.

TABLE II. BACKGROUND SAMPLE SPD

Composition data:	
Aluminum mass (g)	
in core	**57.24**
in sheath and plugs	**33.50**
Eff. cross section data[1)]:	
Therm. abs. area A(cm^2)	**0.4717**
Flux depression factor Φ:	**0.9727**

[1)] **See section 6**

TABLE III a: ^{233}U CALIBRATION SAMPLES

Sample	A3J	A3K	B3A	B3C	B3E
Composition data:					
U isotopic content: (atom %)					
^{233}U	99.787±.004	99.787±.004	99.787±.004	99.787±.004	99.787±.004
^{234}U	0.053±.002	0.053±.002	0.053±.002	0.053±.002	0.053±.002
^{238}U	0.160±.003	0.160±.003	0.160±.003	0.160±.003	0.160±.003
^{233}U mass (mg)	465.2±1.0	235.0±.7	293.4±1.2	392.5±1.3	387.1±1.2
Aluminum mass (g):					
in core	56.93	57.06	57.06	57.06	57.01
in sheath and plugs	32.46	33.42	33.77	33.69	33.78
Eff. cross section data, Therm. column:					
Therm. abs. area A(cm^2):					
Uranium	0.6917	0.3494	0.5834	0.5836	0.5755
boron	-	-	0.2849	0.1327	0.0689
aluminum	0.4649	0.4707	0.4725	0.4721	0.4723
total	1.1566	0.8201	1.3408	1.1884	1.1167
Flux depress. factor ϕ:	0.9330	0.9525	0.9224	0.9312	0.9353
Therm. yield area Y(cm^2):	1.5791	0.7977	1.3320	1.3323	1.3140
Res. abs. area R(cm^2):	0.8984	0.4538	0.7578	0.7580	0.7476
Res. yield area F(cm^2):	1.8085	0.9136	1.5254	1.5258	1.5048

TABLE III b: ^{235}U CALIBRATION SAMPLES

Sample	A5I	A5K	B5B	B5C	B5F
Composition data:					
U isotopic content: (atom %)					
^{234}U	0.061±.002	0.061± .002	0.061± .002	0.061± .002	0.061± .002
^{235}U	99.746±.003	99.746±.003	99.746±.003	99.746± .003	99.746±.003
^{236}U	0.066±.002	0.066±.002	0.066±.002	0.066± .002	0.066±.002
^{238}U	0.127±.001	0.127 ±.001	0.127±.001	0.127± .001	0.127±.001
U mass (mg):	520.7±.8	256.2±.7	415.2±.8	417.6± .8	417.9 ±1.0
Boron mass (mg):	-	-	6.26±.06	3.46±.04	1.56 ±.04
Aluminum mass (g):					
in core	57.03	57.04	57.09	57.08	57.03
in sheath and plugs	33.58	33.27	33.185	33.14	33.44
Eff. cross section data, Therm. column:					
Therm. abs. area A(cm^2):					
uranium	0.8780	0.4320	0.7001	0.7041	0.7047
boron	-	-	0.2646	0.1463	0.0659
aluminum	0.4714	0.4698	0.4695	0.4693	0.4706
total	1.3494	0.9018	1.4342	1.3197	1.2412
Flux depress. factor ϕ:	0.9219	0.9478	0.9169	0.9236	0.9281
Therm. yield area Y(cm^2):	1.8150	0.8930	1.4473	1.4556	1.4567
Res. abs. area R(cm^2):	0.1283	0.0631	0.1023	0.1029	0.1038
Res. yield area F(cm^2):	- 0.0713	- 0.0351	- 0.0568	- 0.0572	-0.0572

TABLE IIIc: ^{239}Pu CALIBRATION SAMPLES

Sample	A9J	A9L
Composition data:		
Pu isotopic content (atom %)		
^{239}Pu	98.150±.005	98.150± .005
^{240}Pu	1.797±.005	1.797±.005
^{241}Pu	0.053±.001	0.053±.001
Pu mass (mg):	95.2±.8	23.8±.3
Boron mass (mg):	-	-
Aluminum mass (mg):		
in core	57.20	56.98
in sheath and plugs	33.75	33.46
Eff. cross section data, Therm. column		
Therm. abs. area A(cm^2):		
plutonium	0.2647	0.0662
aluminum	0.4732	0.4705
total	0.7379	0.5367
Flux depress. factor ϕ:	0.9573	0.9689
Therm. yield area Y(cm^2):	0.5394	0.1349
Res. abs. area R(cm^2):	0.7726	0.1931
Res. yield area F(cm^2):	1.1973	0.2993

In addition to the reactor response to thermal neutrons, the relative response to fission neutrons had to be found by calibration. For this purpose a set of aluminum samples, alloyed with the fissile materials of interest, and hence similar to the test samples prior to irradiation, had been manufactured at Chalk River [10]. Two concentrations were available for each fissile nuclide. Furthermore another set of such fissile samples had been borated to various degrees to simulate the irradiated samples containing fission products. In all, 12 fissile calibration samples were available. Their properties are summarized in tables IIIa-c.

6. ANALYSIS OF RESULTS

6.1 Assumed cross sections

The experimental results have been analyzed in terms of the Westcott cross section convention [11]. As already pointed out, the unknown fission product component is a small part of the measured signals - the major part had to be subtracted in the analysis on the basis of the known contents of other sample constituents and their cross sections.

The aluminum was assumed to be a 1/v-absorber. A value of 0.230 b was used for the 2200 m/s absorption cross section of the super-pure aluminum in the sample cores[1]. For the sheaths and end plugs a cross section of 0.238 b was

1) The value recommended for the 2200 m/s aluminum cross section in the latest edition of BNL-325 [12] is 0.235±.005 b.

used. It had been found at Chalk River [6] that a certain burn-up occurred in the aluminum in the course of the irradiations, probably due to high-cross-section impurities. This reduced the absorption area of the irradiated aluminum by about 1 %, which has been taken into account in the analysis. The above assumed aluminum cross sections were checked by measurements on the SPD sample alone (section 6.3).

Boron was treated as a 1/v-absorber with a 2200 m/s cross section of 759 b [12].

For the heavy nuclides the assumed cross sections are summarized in table IV. For the strong resonance absorbers ^{236}U, ^{240}Pu and ^{242}Pu resonance self-shielding was taken into account by means of the self-shielding factors calculated in [6].

6.2 Principles of analysis

The method of analysis used here follows closely that of [6, 10]. Let S be the net reactivity signal, i.e. $\Delta\Phi/\Phi_o$, corrected for zero signal (table V). The basic expression for S is the following:

$$S = a\left[\bar{\phi}_t(WY_t - A_t) + r(WF_t - \beta R_t) + \phi_b A_b\right] \qquad (1)$$

a is the reactor calibration constant for thermal neutrons,

ϕ accounts for the thermal flux perturbation in the sample,

A, the thermal absorption area, $= \sum_i (N\sigma_{oa} g_a)_i$,

Y, the thermal yield area, $= \sum_i (N\sigma_{of} g_f \nu)_i$,

R, the resonance absorption area, $= \sum_i (N\sigma_{oa} s_a)_i$,

F, the resonance yield area, $= \sum_i (N\sigma_{of} s_f \nu)_i$,

W is the importance of fission neutrons relative to thermal neutrons,

β is the importance of epithermal neutrons relative to thermal neutrons (see below),

N_i is the total number of atoms "i" in a sample. The other symbols have their conventional meaning. The subscripts "t" and "b" in equ:n (1) stand for "test" and "background" sample, respectively.

The thermal flux depression factor ϕ was assumed to decrease linearly with the thermal absorption area, viz.

$$\phi = 1 - \alpha A \ .$$

The constant α was determined by activation measurements.

The epithermal weight factor β is generally close to unity in heavy-water systems [7]. Since, in the thermal-column measurements, resonance reactions only constitute a small correction to the total reaction rate, β has been set equal to one exactly.

TABLE IV. HEAVY-NUCLIDE CROSS SECTIONS

	σ_{oa}	σ_{of}	ν	I'_a	g_a	s_a	g_f	s_f
^{233}U*	577.6± 1.8	530.6±1.9	2.4866± 0.0069		0.9961	1.248	0.9959	1.102
^{234}U	95± 3[+]	-	-	600± 60[‡]	1.0	7.22	-	-
^{235}U	678.5± 1.9	580.2± 1.8	2.4229± 0.0066		0.9769	0.1259	0.9754	-0.0475
^{236}U	6± 1**	-	-	400±40**	1.0	76.2	-	-
^{238}U	2.72± 0.02	-	-		1.0019	117.9	-	-
^{237}Np	168± 3[+]	-	-	820±50[‡]	1.0071	5.506	-	-
^{239}Pu*	1012.9± 4.1	741.6± 3.1	2.8799± 0.0090		1.0832	3.000	1.0572	2.324
^{240}Pu	290[++]	-	-	8220±300[‡]	1.0296	32.27	-	-
^{241}Pu*	1375.4±8.6	1007.3±7.2	2.934±0.012		1.0481	1.030	1.0481	1.073
^{242}Pu	20[++]	-	-	1140±100[‡]	1. 007	64.56	-	-
^{241}Am	625± 35**	3.1[‡]	3. 0	1825	1.0199	5.121	1.0163	5.121

*Hanna et al., Atomic Energy Review III, No. 4 (1969)

[+]W. H. Walker, Recommended in private communication

[++]B. R. Leonard, BNWL 1304 (1970)

I'_a is the reduced resonance integral

g_a, s_a, g_f, s_f are based on C. H. Westcott, AECL 1101 (1960) and AECL 3255 (1969)

**BNL 325

TABLE V. MEASURED REACTIVITY SIGNALS $\Delta\Phi/\Phi_0$

Samples, upper / lower	$\Delta\Phi/\Phi_0 \times 10^2$
- / -	0.001±.001
- / SPD	0.956±.007
A3J/SPD	1.876±.003
A3K/SPD	0.963±.002
B3A/SPD	1.043±.002
B3C/SPD	1.293±.002
B3E/SPD	1.416±.002
A5I/SPD	1.984±.003
A5K/SPD	1.015±.002
B5B/SPD	1.086±.002
B5C/SPD	1.340±.002
B5F/SPD	1.471±.002
A9J/SPD	0.592±.002
A9L/SPD	0.1552±.0015
$A3B^x$/SPD	1.421±.004
$A3F^x$/SPD	1.025±.003
$A5B^x$/SPD	1.491±.004
$A5F^x$/SPD	1.140±.004
$A9B^x$/SPD	0.154±.003
$A9D^x$/SPD	0.363±.003

TABLE VI. EFFECTIVE CROSS-SECTION DATA FOR IRRADIATED SAMPLES IN THERMAL COLUMN

Sample	$A3B^x$	$A3F^x$	$A5B^x$	$A5F^x$	$A9A^x$	$A9D^x$
Therm. abs. area A(cm^2):						
heavy nucl.	0.6309	0.4825	0.7619	0.6011	0.4018	0.5191
aluminum	0.4637	0.4631	0.4654	0.4606	0.4721	0.4687
Flux depr. factor ϕ:[1]	0.9301	0.9389	0.9228	0.9324	0.9437	0.9374
Therm. yield area Y(cm^2):	1.3947	1.0528	1.5687	1.2350	0.5570	0.7747
Res. abs. area R(cm^2):						
heavy nucl.	0.865	0.679	0.276	0.268	2.602	2.995
fiss. prod. (calc.)	0.379	0.407	0.444	0.468	0.451	0.434
total	1.244	1.086	0.720	0.736	3.053	3.429
Res. yield area F(cm^2):	1.5130	1.1277	-0.0764	-0.0601	0.9703	1.4488

[1] In calculating ϕ, the fission product contribution to the total thermal absorption area was taken into account by means of the FISSPROD values (section 6.4).

In [10] it was found necessary on purely empirical grounds to add further terms to equ:n (1). This has not been done a priori in the present analysis (see section 6.3).

Table VI gives the known reaction areas (and the flux depression factors according to section 6.3) of the irradiated samples. For the calibration and background samples the corresponding data have been given in tables IIIa-c.

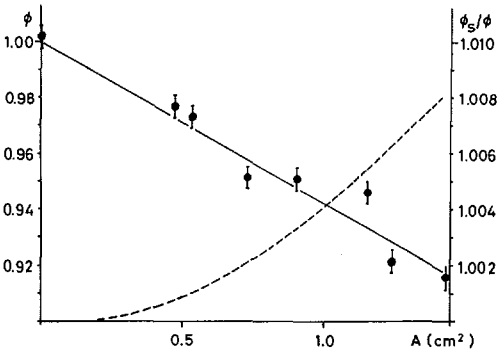

FIG.4. Volume-averaged flux depression factor ϕ versus thermal absorption area A. The solid line is a least-squares fit to the experimental points. Also shown is the surface-to-volume flux ratio ϕ_s/ϕ (dashed curve).

6.3 Calibration measurements

The constant α in the expression $\phi = 1-\alpha A$ was determined from activation measurements on the fissile calibration samples and some additional borated aluminum samples. Thin copper strips were exposed along the surface of the samples, located in the central oscillator position. A normalization foil was irradiated simultaneously at a great distance from the center. From the normalized surface flux thus measured, the volume-average flux was obtained by means of a correction curve (fig. 4) calculated in [10]. The volume-averaged flux was then plotted against the thermal absorption area A as shown in fig. 4 , and α was determined from a least-squares fit to be 0.05791.

The boron solution measurements referred to in section 5 gave for the reactor calibration constant a the value 0.02084±.00009. Applying this value to pile oscillator measurements on the aluminum background sample gave, for the mean 2200 m/s cross section, the value (0.233±.003)b, in excellent agreement with the assumed value of 0.233 b (section 6.1).

The fission neutron weight function W was calculated from pile oscillator measurements of the fissile calibration samples. W must be expected to be rather independent of the origin of the fission neutrons (^{233}U, ^{235}U or ^{239}Pu). However, since the derived W-value may compensate possible errors in the assumed cross sections, it was evaluated separately for the three fissile nuclides. The results are shown in tables VIIa-c. Since only two plutonium calibration samples were available, the W-value for ^{239}Pu must be regarded as rather uncertain. The extraordinarily high value obtained with the sample A9L has been disregarded. - While in the irradiated uranium samples the dominating heavy nuclides are the original ones (^{233}U and ^{235}U), the plutonium samples contain appreciable amounts of heavy nuclides, generated during irradiation (^{240}Pu and ^{241}Pu). For these nuclides the deduced W-value does not compensate possible errors in the assumed cross sections.

TABLE VII a: WEIGHT FUNCTION W FOR ^{233}U FISSION NEUTRONS

Sample	W	$Sx10^2$	
		meas.	fitted
A3J	1.0300± 0.0017	1.875± .003	1.872
A3K	1.0299± 0.0021	0.962± .002	0.961
B3A	1.0383± 0.0047	1.042± .002	1.018
B3C	1.0201± 0.0037	1.292± .002	1.315
B3E	1.0273± 0.0021	1.415± .002	1.420

Average: 1.0291 ± .0030

TABLE VII b: WEIGHT FUNCTION W FOR ^{235}U FISSION NEUTRONS

Sample	W	$Sx10^2$	
		meas.	fitted
A5J	1.0347± 0.0013	1.983± .003	1.987
A5K	1.0391± 0.0019	1.014± .002	1.008
B5B	1.0341± 0.0023	1.085± .002	1.090
B5C	1.0398± 0.0018	1.339± .002	1.328
B5F	1.0311 ± 0.0020	1.470± .002	1.483

Average: 1.0358± .0017

TABLE VII c: WEIGHT FUNCTION W FOR ^{239}Pu FISSION NEUTRONS

Sample	W	$Sx10^2$	
		meas.	fitted
A9J	1.016 ±0.0053	0.591± .002	0.591
A9L	(1.0356±0.0095)	0.1542± .0015	0.1525

Value used: 1.0316±0.0053

6.4 Results

The fission product contribution, δA, to the thermal absorption area A_t was obtained from the measured signals, using equ:n (1). Since the epithermal reaction rate is very low, the fission product component, δR, of the resonance absorption area was taken from FISSPROD calculations. Under the assumption that the fission products are 1/v absorbers in the thermal region ($g = 1$), δA divided by the number of fissions is the mean 2200 m/s fission product cross

section per fission, σ_o . The experimental results, together with the corresponding values calculated with the latest version of FISSPROD [4], are given below:

Sample / σ_o b/fission	A3B*	A3F*	A5B*	A5F*	A9A*	A9D*
exp.	41.9±2.5	38.5±1.8	48.7±2.2	46.5±1.6	62.3±3.3	71.1±3.8
FISSPROD	44.2	42.5	52.0	50.3	66.7	68.2
calc./meas.	1.05	1.10	1.07	1.08	1.07	0.96

7. DISCUSSION

The present measurements have resulted in higher values of σ_o than those reported in [6]. This, together with recent revisions of the nuclear data used in FISSPROD [4] has led to better agreement between the calculated and measured values. The former are now consistently higher by about 7 % except for sample A9D*. For this particular sample the heavy-element concentrations were obtained by a considerable extrapolation from those determined chemically.

The ^{235}U results may be compared to those of Nisle et al. [13], who reported 2200 m/s absorption cross sections of 55 and 47 b/fission for ^{235}U depletions of 64 % and 81 %, respectively. For a sample irradiated in a harder spectrum they obtained 51 b/fission. The precision quoted for their measurements was 7 %, but the possibility of systematic errors could not be excluded, chiefly because the concentrations of remaining heavy nuclides had been calculated rather than measured.

8. ACKNOWLEDGEMENTS

Thanks are due to Mr. Rolf Bladh for assisting with the pile oscillator measurements and the data retrieval.

We also wish to thank Dr. W H Walker for carrying out the FISSPROD calculations.

9. REFERENCES

[1] AHLSTRÖM, P.-E., Investigation of Different Models for Treating Fission Products in Burn-up Calculations, Internal Report, SVV-PM-3626/1 (1966). In Swedish

[2] LANE, F.E., FISSPROD, a G-20 Computer Program. AECL-3038 (1969)

[3] WALKER, W.H., Fission Product Absorption in Thermal Reactors, Proc. IAEA Conf. "Nuclear Data for Thermal Reactors", Paris (1966)

[4] WALKER, W.H., Fission Product Data for Thermal Reactors, Part I - Cross Sections. AECL-3037 (1969)

[4a] WALKER, W.H., The Evaluation of Fission Product Yield Data, Paper at this Conference (1970)

[5] OKAZAKI, A., et al., Absorption Cross Section of Fission Products Separated from Slug 76-11 of NRX Rod 76, AECL-1698 (1963)

[6] OKAZAKI, A., et al., Neutron Absorption Cross Section of Gross Fission Products, AECL-2510 (1965)

[7] SOKOLOWSKI, E.K., BLADH, R., A Determination of the 2200 m/s Absorption Cross Section and Resonance Integral of Arsenic by Pile Oscillator Technique, AE-351 (1969)

[8] SOKOLOWSKI, E.K., JONSSON, A., Epithermal and thermal spectrum indices in heavy-water lattices, J. Nucl. Energy 22 (1968) 27

[9] OKAZAKI, A., SOKOLOWSKI, E.K., AE Report to be published

[10] OKAZAKI, A., et al., Calibration Swing Measurements in PTR, AECL-2506 (1965)

[11] WESTCOTT, C.H., Effective Cross Section Values for Well-moderated Thermal Reactor Spectra, AECL-1101, 3rd corr.edn. (1962)

[12] STEHN, R.J., et al., Neutron Cross Sections, BNL-325, 2nd edn., supplem. 2, 1 (1964)

[13] NISLE, R.G., et al., Fission-product Build-up and Long-term Reactivity Effects, Int. Conf. peaceful Uses atom. Energy (Proc. Conf. Geneva 1964) 28, UN, New York (1964)

[14] PERSSON, R., A Method of Eliminating Aperiodic Variations in Fourier Analysis, e.g. in Pile Oscillator Experiments, Internal Report AEFI-54 (1957). In Swedish. Also to be published as an AE-report

Invited Paper

NEUTRON CROSS-SECTION EVALUATION IN THE THERMAL AND RESONANCE ENERGY RANGE FOR NUCLIDES OF MASS LESS THAN 220

J.S. STORY
UKAEA, Reactor Group,
Atomic Energy Establishment,
Winfrith, Dorchester,
Dorset, United Kingdom

Abstract

NEUTRON CROSS-SECTION EVALUATION IN THE THERMAL AND RESONANCE ENERGY RANGE FOR NUCLIDES OF MASS LESS THAN 220.

Problems of the past and prospects for the near future in evaluation work for the thermal and resonance region in the mass range A less than 220 are discussed. In doing so, thermal-neutron scattering, moderator fast-neutron scattering and neutron age, and resonance cross-sections of other materials are treated.

1. INTRODUCTION

I am supposed to present here a review of the status of evaluation work for the thermal and resonance region in the mass range A less than 220; of its quality and comprehensiveness; of the evaluation methods used; of the principal difficulties encountered; and to comment betimes on the different conclusions and results of evaluations. All this in 30 minutes and a mere 5000 words. Yet this mass range embraces all the moderators, all the structural materials, all the coolants, all the fission products, the shielding materials, the control poisons, and the fundamental reference standards.

Frankly, I do not believe it would be worthwhile to attempt any such task. Rather, I should prefer to discourse briefly on the problems of the past, and on the prospects for the near future, for, indeed, I believe that this Conference occurs at something of a turning point in the field of data evaluation. If the reader of these Proceedings simply wants to know what evaluations have been carried out and what data files exist, for the most part he will find them listed in the CINDA reference index and in annual Newsletters of the CCDN.

To begin with, each of the various groups of evaluators was concerned not with the production of a single data file only, but with scraping together a whole data library covering a good range of materials, fissile and fertile, structural, moderators and coolants. In addition, a range of computer programs was needed for editing and checking purposes, and processing programs to enable users to prepare the derived quantities needed for neutronics calculations. All this very large task had to be completed in some sort merely to get to the starting point.

By now the various data libraries, the American ENDF' B', the KEDAK library, and the UKAEA data library have been brought from the "zero-order" condition up to "first-order". By this I mean that the most horrible defects have been eliminated; a fairly wide range of materials has been covered; and in reactor calculations the results obtained agree reasonably well with representative integral measurements – well enough, at any rate, that very good consistency can be secured through the use of first-order adjustment procedures. The task now, it seems to me, is to try and improve all the most important cross-sections and this is likely to demand more thorough investigation and, more careful testing than has been possible hitherto.

Integral tests are of two kinds: the simple integral parameters such as resonance integrals, fission-spectrum averaged cross-sections, diffusion coefficients and neutron ages have an especial appeal to evaluators, because they are relatively easy to apply in testing a new data file before it is widely released. Testing files against inhomogeneous lattice measurements is generally a much longer and more complex process, and is best recognized as a separate stage in the evolutionary scheme.

2. THERMAL-NEUTRON SCATTERING

So far as moderators are concerned, and I shall confine my remarks to H_2O, D_2O and graphite, the principal properties are the thermal scattering cross-sections and the slowing-down power of which the neutron age is by far the most important characteristic. Both these properties are strongly dependent on the slow neutron free-atom scattering cross-section.

What is the state of thermal scattering law evaluations? It seems to me that this topic has rather dropped out of the news lately. The general procedure nowadays is to compute the moderator scattering law $S(\alpha, \beta)$ from a phonon frequency function $\rho(\omega)$ using the incoherent approximation. Thence are derived the angular moments of the scattering cross-section σ_ℓ $(E \rightarrow E')$. The calculation is usually carried out in two stages inside a computer, and each stage demands quite a long operating time. And what does one have at the end of it? A great matrix of numbers which is practically unsurveyable. A great deal more work is needed to test the validity of such a matrix, and, what is more important from the evaluator's point of view, to learn from it how one can do better next time.

The scattering matrix contains three kinds of error:

i) Errors in the phonon frequency function and associated experimental data. Figure 1 shows the outcome of two series of measurements recently reported for thermal neutron scattering by graphite, and is quite representative of the uncertainties in the phonon spectra for other moderators also.

ii) Computing errors – in particular those which result from hidden complexities in the theory and from the need to keep operating time within reasonable limits.

iii) Errors due to the limitations of the theory – use of the incoherent approximation, for example.

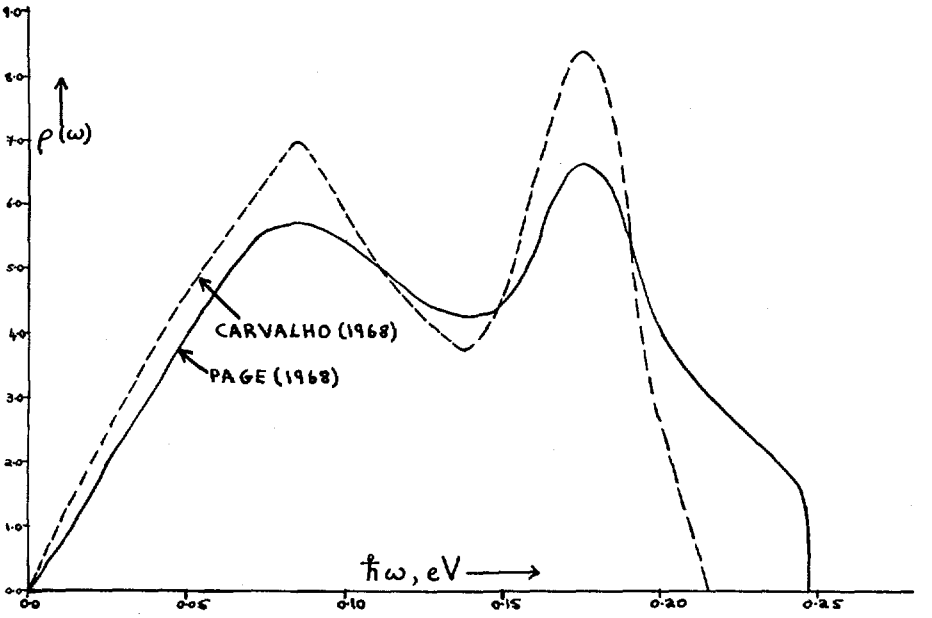

FIG. 1. Graphite phonon frequency functions.

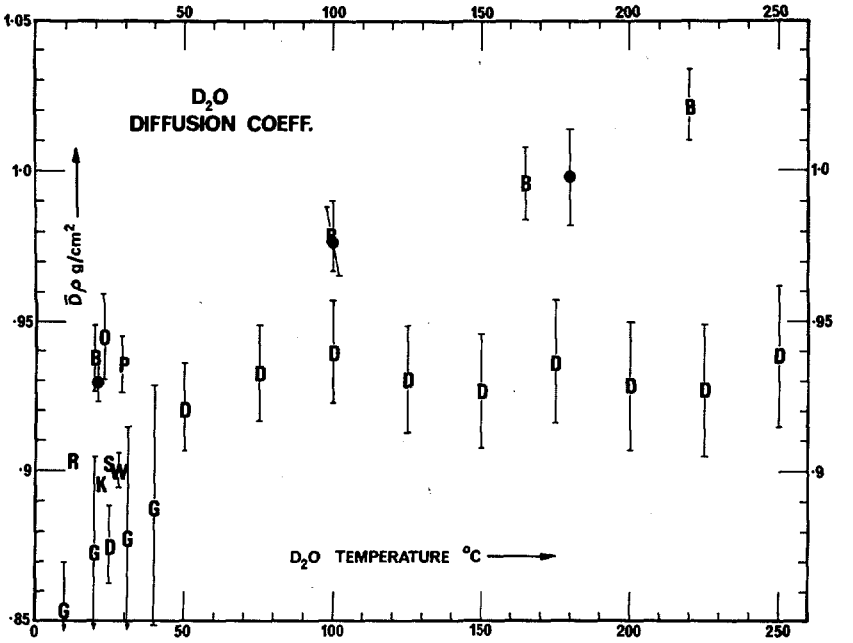

FIG. 2. D_2O diffusion coefficient as a function of the temperature. B – Baumann; D – Daughtry and Waltner; G – Ganguly et al.; K – Kussmaul and Meister (revised to 100% D_2O); P – Parks et al.; R – Raievsky and Horowitz; S – Silk and Wade; W – Westfall and Waltner (corrected to 100% D_2O); O – Kash and Woods; ● – Kornbichler.

There seems to be in the literature very little discussion of the magnitudes of these different sources of error, nor of their effects upon reactor calculations. There has been still less discussion, so far as I am aware, of the important question "what are the principal integral criteria which determine whether or not a given scattering matrix is good enough for its purpose?"

Certainly, the users will not be happy if the scattering matrix does not reproduce the measured neutron diffusion coefficient of the medium, and we should expect to see a reasonable match to the total cross-section also. There are the most precise scattering data in the thermal region. Well, that assertion should be true, but Fig. 2 shows the diffusion coefficient data for D_2O as a function of the moderator temperature. Several measurements at about 20° C have been omitted for the sake of clarity, – measurements of relatively low accuracy which contribute virtually no additional information. The data at the top of the figure, by Baumann (1962) marked with a B, and by Kash and Woods (1953) shown by an open circle, were obtained by measuring static neutron distributions in pure and poisoned D_2O. These results are in excellent agreement with the values calculated by Kornbichler (1965) from differential cross-section data. All the other data were obtained by the pulsed-source method, and with the solitary exception of the measurement by Parks, Baumann et al. (1968) are systematically lower. We have here one of the rare examples where the differential data are called upon to adjudicate between two different classes of integral measurement.

Getting back to the scattering law, we can say that it is not very difficult to adjust the phonon frequency function so that the scattering matrix is consistent with the measured diffusion coefficient for a Maxwellian neutron spectrum at the moderator temperature, but it seems much more difficult to obtain any exact agreement with the total cross-section as a function of energy over the whole thermal range. Deviations of about 5% seem to be the order of the day even for H_2O, for which the incoherent approximation should be nearly exact. Where D_2O and graphite are concerned we expect no such agreement using the incoherent approximation, since the scattering by these materials is predominantly coherent, and we need feel no hesitation in modifying the elastic components of the scattering matrix so as to ensure agreement with the total cross-section; changing the elastic cross-section is not in conflict with the detailed-balance restriction. For an incoherent scatterer, however, such as H_2O, we must note that such a change may conflict with Placzek's zeroth-moment condition:

$$2\int_0^\infty S(\alpha,\beta)\cosh(\beta/2)\,d\beta = 1$$

in Egelstaff's notation, and in this case the change is a justifiable expedient only if it is small.

However, the diffusion coefficient and the total cross-section contain little information on the thermalizing properties of the medium, which are determined by the inelastic part of the scattering matrix: something more is needed to test that. We must return to the computer and may use it to calculate neutron spectra in poisoned moderators; but, of course, we can hardly expect to obtain exact agreement with the measured spectra and the question remains "Is it good enough?". One of the important reactor

requirements is that the moderator temperature coefficient should be correctly reproduced. The $^{239}Pu/^{235}U$ fission ratio is a convenient integral representative of both the neutron spectrum and of the temperature coefficient, – one such representative at any rate.

It is slow work, evolving a scattering matrix in the first instance, then testing it, and then revising the phonon frequency function and re-iterating the whole process. And in mentioning the moderator temperature coefficient I have raised another point of very great significance: it reminds us that the real need is for a consistent set of scattering matrices at a range of temperatures. The phonon frequency spectra of the common moderators are not very precisely determined even at best, and our knowledge of their temperature dependencies is very insecure.

To conclude this outline of the evaluator's problems and black arts in relation to thermal scattering cross-sections it is sufficient to refer briefly to graphite for an illustration. For this moderator we can redress the balance of our ignorance by making use of the integral relationship between the phonon spectrum and the specific heat.

Figure 1 shows the phonon spectra derived recently from experimental measurements by the customary extrapolation technique. Page (1968) concluded from his measurements at 300, 1300 and 1800°K that probably the phonon spectrum can be treated as practically invariant with temperature. Since the experimental data evidently leave considerable doubts as to the shape of $\rho(\omega)$ near its upper limit, and its temperature dependence, we have adopted Page's prescription, but have assumed that the upper cut-off of the phonon spectrum may be determined at each temperature from the specific heat according to the formula

$$2C_V(T)/3R = \int_0^{\omega_{max}(T)} \rho(\omega)\, \beta^2\, (\cosh \beta - 1)^{-1}\, d\omega$$

where R is the gas constant, and $\beta = h\omega/kT$. It is, of course, necessary to renormalize $\rho(\omega)$ over the interval $(0, \omega_{max})$ at each temperature. The scattering matrices determined under these assumptions seem reasonably satisfactory so far as we have been able to test them. However, it has been noticed that for a typical graphite-moderated lattice a 1% change in the specific heat leads to a 0.2% change in the calculated multiplication constant. This implies that one has to be quite careful with the specific heat data to obtain a reasonably smooth form for the moderator temperature coefficient.

3. MODERATOR FAST-NEUTRON SCATTERING AND NEUTRON AGE

The second important characteristic of a moderator is the slowing down age from a fission neutron source. This provides a sensitive test of the validity of the epithermal scattering data especially in the range below 1 or 2 MeV; a systematic error of 1% in the cross-section causes 2% error in the derived neutron age. Current uncertainty about the fission neutron spectrum provokes additional interest in this characteristic – can we learn anything about the fission spectrum by comparing measured and calculated neutron ages? Some re-examination of the cross-section data for these three materials seems very much worth while.

TABLE I. AGE OF FISSION NEUTRONS TO In RESONANCE (~1.46 eV)

		Neutron age (cm^2)		
		H_2O	D_2O	C
Experimental values				
Paschall (1964-6)		26.61 ± 0.32		
Spencer & Williamson (1967)		26.24 ± 0.33		
Olcott (1956)	Extrapolated to 100% purity		112. ±2	
Wade (1958)			110 ±3	
Graves (1962)			112 ±2	
Campbell & Paschall (1964)				307.8 ± 2.0
Calculated values	Data File			
Spanton (1969-70)	DFN-901[a]	26.12 ± 0.08		
Spanton (1969-70)	DFN-68D			302.2
Kemshell (1969)	DFN-218[b]		108.8	
Kemshell (1969)	DFN-256		115.9	
Dunford & Alter (1970)	MAT-1001[c]	26.22 ± 0.13		
Dunford & Alter (1970)	MAT-1003[c]		117.9 ± 0.2	
Dunford & Alter (1970)	MAT-1011			295.7 ± 0.5

[a] DFN-33 used for oxygen
[b] DFN-37 used for oxygen
[c] MAT-1013 used for oxygen

H_2O density 0.9972 g/cm³
D_2O density 1.1046 g/cm³
C density 1.60 g/cm³

All the calculated age values have been revised to agree with the material densities quoted above, and to a fission spectrum with an effective temperature of 1.32 MeV (Watt-Cranberg spectrum). The uncertainty of Olcott's result has been increased to allow for variations of the D_2O purity during the course of the experiments.

In the top half of Table I are given the most recent and reliable of the measured values for fission neutron ages in H_2O, D_2O and graphite, and in the lower half are some values recently calculated using various evaluated data files. Notice that the calculated values for H_2O and for graphite are 1 or 2% too low, whereas two of the 3 values given for D_2O are about 4% too high. So far as H_2O and graphite are concerned the implication of this comparison is that the scattering cross-sections need to be reduced, while for D_2O the scattering cross-section must be increased so that the neutrons will not migrate so quickly away from their source. It is too bad that in each case some of the more recent measurements have tended in exactly the opposite direction! If the fission neutron spectrum is at fault, the results for H_2O and carbon would support some hardening of the spectrum[1].

[1] Traditional values for the effective neutron temperature, of about 1.32 MeV were used in the calculations. Very preliminary estimates suggest that, after revision of the cross-sections, an effective temperature of about 1.35 ± 0.02 MeV would best suit the age data for all three moderators.

TABLE II. SLOW-NEUTRON SCATTERING BY D_2O AND DEUTERIUM

1. Free-atom cross-sections		
	$\sigma[D_2O]$, b	$\sigma[D]$, b
Rainwater et al. (1948)	10.28 ± 0.3	3.275
Fermi & Marshall (1949)	10.50 ± 0.17	3.385
Rayburn & Wollan (1952)	10.43 ± 0.1	3.350
Fluharty (1959)	10.44 ± 0.2	3.355
Weighted mean values	10.44 ± 0.044	3.354 ± 0.030
Free-atom cross-section of oxygen taken as 3.73 ± 0.04 barns		
2. Bound coherent scattering length of D_2O		
		b_{coh}, fm
From above, and bound incoherent cross-section of 4.50 ± 0.08 barns/D_2O molecule, by Gissler (1963)		18.81 ± 0.086
Koester et al. (1969)		19.20 ± 0.08
Bartolini et al. (1968)		18.22 ± 0.063
Nikitin et al. (1955)		19.30 ± 0.15
Wollan et al. (1951)		18.59 ± 0.41
3. s-wave free-atom scattering lengths of D		
From free-atom scattering cross-sections above, and Gissler's result		
a_2 = 0.369 fm,		a_4 = 6.322 fm.
The ratio a_2/a_4 = 0.06203, which is reasonably close to the value 0.119 ± 0.045 measured by Hurst & Alcock (1951).		

Let me now first deal with the recalcitrant results for D_2O. The elderly data file No. 218 leads to a low value for the neutron age because it adopts the old value of 3.4 barns for the free-atom scattering cross-section of deuterium in the 1-eV to 10-keV region. The newer file DFN-256 follows the 1968 evaluation of Horsley and Stewart who adopted a lower value of 3.20 barns, and the ENDF-B file for deuterium is even slightly lower at all energies. This low value for the slow-neutron free-atom cross-section was first suggested by Van Oers and Seagrave (1967) who derived it from measurements by Gissler (1963) of the bound incoherent cross-section of D_2O and by Bartolini et al. (1968) of the bound coherent scattering amplitude.

This is much too selective however: Table II summarizes the slow-neutron scattering data for D_2O and deuterium. In the first section of this table are collected the results of various transmission measurements in the eV-region; the consistency of the data is outstandingly good. Horsley and Stewart suggested that the original values might be rather too large as a result of residual chemical-binding effects reaching out into the eV-region: however, I have made corrections for this, using the first-order term of the Placzek-Wick asymptotic expansion. In stark contrast to the

TABLE III. SLOW-NEUTRON SCATTERING PARAMETERS OF HYDROGEN

1. Free-atom cross-section	
	σ_{free}[H], barns
Melkonian (1949)	20.36 ± 0.10
Simpson et al. (1964)	20.14 ± 0.27[b]
Triftshäuser & Fehsenfeld (1965)	20.464 ± 0.11[a]
Dritsa & Kostikas (1967)	20.14 ± 0.13[b]
Houk & Wilson (1967, 1968)	20.442 ± 0.10[c]
Neill et al. (1968)	20.379 ± 0.076[b]
Weighted mean value	20.364 ± 0.068

[a] Mean of two values;
[b] $\sigma_{fa}|0| = 3.73 \pm 0.04$ barns assumed;
[c] Authors' value for uncertainty only 0.023 barns (0.11%), but no details are given.
Allowing for the small deuterium content of natural hydrogen increases the weighted mean value to 20.366 barns for pure H.

2. Bound-atom coherent scattering length	
Koester et al. (1969)	-3.723 ± 0.003 fm.

3. s-wave free-atom scattering lengths
From the data above
$a_1 = -23.674$ fm
$a_3 = 5.4104$ fm

transmission measurements, the coherent scattering amplitudes listed in the second part of Table II are extremely inconsistent. It seems to me that the weight of the data strongly favours the weighted mean values given in the first part of the table, and the s-wave scattering lengths derived in part 3.

Seagrave has pointed out that his careful measurements of the fast neutron total cross-section of deuterium, from 267 keV upwards, do not extrapolate back smoothly to 3.35 barns at zero-energy. This is shown quite clearly in Fig. 3[2]; if we insist on such a high value at low energy, the total cross-section must flare up quite sharply as the energy falls below 200 keV. Is it reasonable to accept such an anomaly? The figure shows that it is; that some such "anomaly" in this energy region is almost inevitable as a result of the steady decline of the s-wave component and the growth of the p-wave term. The approximate s-wave cross-section shown in this figure was derived using a quite trivial modification to the effective-

[2] The experimental data of Adair et al. (1953) and of Allen et al. (1955) are related, in different ways, to the n-H cross-section: the results shown in Fig. 3 have been revised using up-to-date values for this reference cross-section.

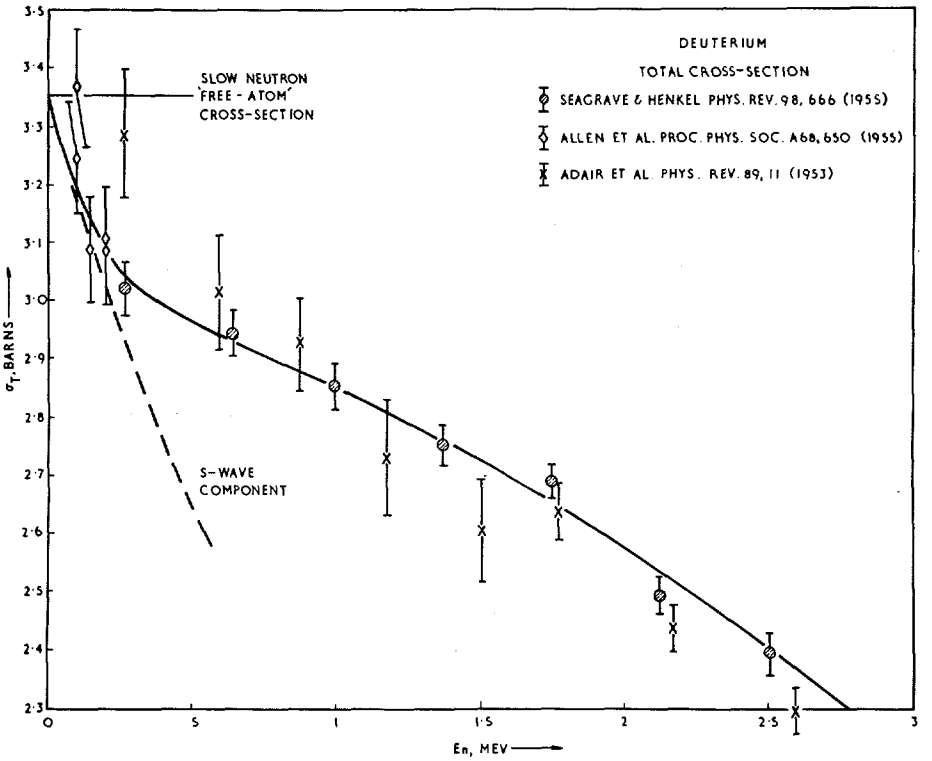

FIG. 3. Deuterium total cross-section.

range analysis of Van Oers and Seagrave and the scattering lengths given at the foot of Table II; in form it may be in error by as much as 10%.

Now that the principal features of this cross-section have been delineated there is a splendid opportunity for experimental confirmation, using time-of-flight spectrometry to fill in the wide open spaces between about 1 keV and 600 keV. A revised phase-shift analysis would also be very valuable.

In compiling the ENDF' B' file for hydrogen Leonard and Stewart (1967) followed for the most part Horsley's evaluation (Horsley, 1966), but for the scattering cross-section they very sensibly preferred to use Gammel's semi-empirical representation. What improvements are now possible? The data on the slow neutron scattering parameters are summarized in Table III. The free-atom cross-sections were all corrected by their authors for any residual chemical-binding effects, mainly by use of the first-order form of the Placzek-Wick asymptotic expansion; the paper by Neill et al. (1968) provides an excellent example of such work. To all appearances the experimental data abundantly confirm the validity of this approximation, despite that we are here dealing with the anomalous case discussed at some length by Wick (1954) in which the mass-ratio of neutron and scattering atom is very nearly unity.

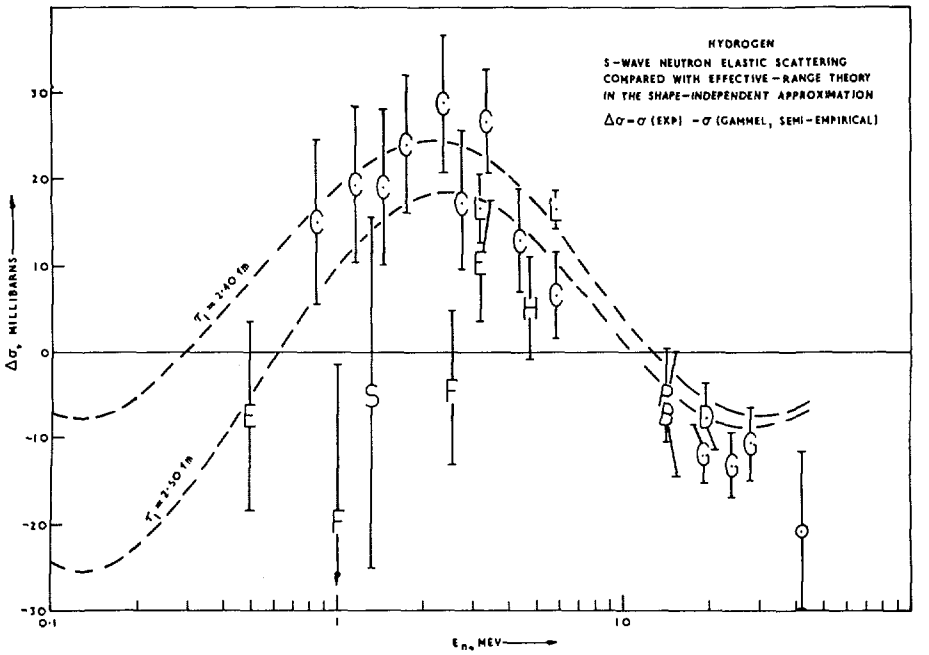

FIG. 4. Hydrogen fast neutron s-wave scattering cross-section compared with the shape-independent form of effective-range theory. The data are shown as deviants from Gammel's semi-empirical fit. B – Coon, Graves and Barschall; C – Clements and Langsford; D – Day et al.; E – Engelke et al.; F – Fields et al.; G – Groce and Sowerby; H – Hafner et al.; L – Lebowitz; O – Hildebrand and Leith; S – Storrs and Frisch.

One other comment must be made about the data in this table – Houk and Wilson have been treated very shabbily. They claimed an uncertainty of only ± 23 millibrans for their result (or ± 0.11%) from transmission measurements in the range 6.5 to 329 eV. Unfortunately, no details of the experiment are yet available, nor of the precautions taken and corrections made, so I thought it best to down-weight their result. In consequence, my weighted mean-value may be too low, perhaps by as much as 61 millibarns.

In Fig. 4 are shown the most precise fast-neutron data on the scattering cross-section. I have presented the data in the form of deviants from Gammel's formula. It is very striking how well the simple effective range formula, shown by the curved lines, describes the deviations from Gammel's semi-empirical fit (the line $\Delta\sigma = 0$). Gammel's formula was fitted to the total scattering cross-section whereas I have presented only the s-wave components of the experimental values; that is why the high energy data fall below the Gammel fit. The contribution of the higher partial waves is very small and is represented sufficiently accurately by the curve in Fig. 5. In Fig. 6, I show again the same set of data as in the earlier slide, with some more sophisticated variants of the effective-range theory. From an evaluator's point of view, the role of the effective-range analysis is simply to ensure a smooth and reasonable fit to the experimental

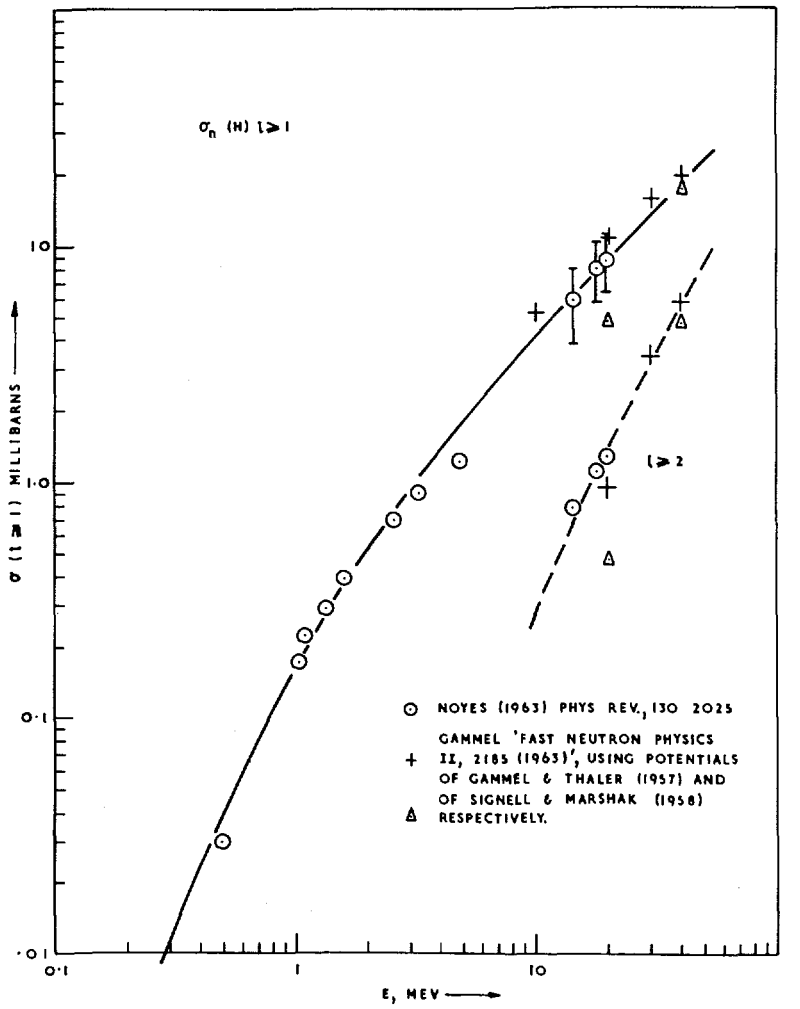

FIG.5. Hydrogen fast neutron scattering cross-sections for partial waves with $\ell \geq 1$.

data, and it is clear that the analysis presented here puts us in a position to produce a very accurate data file for hydrogen. However, charge-conjugate theorists will disapprove of the low values obtained for the singlet-effective-range parameter r_1, and it may be that the theory provides the most cogent argument for thinking the low-energy free-atom cross-section should be increased.

Hopkins and Breit have recently extrapolated the well-known nucleon-nucleon phase-shift analyses to low energies and in this way have re-evaluated the neutron-scattering angular distributions. Of course, the asymmetry is very slight at energies below 40 MeV, since the p-wave scattering contributes less than 10% of the total cross-section of hydrogen even at

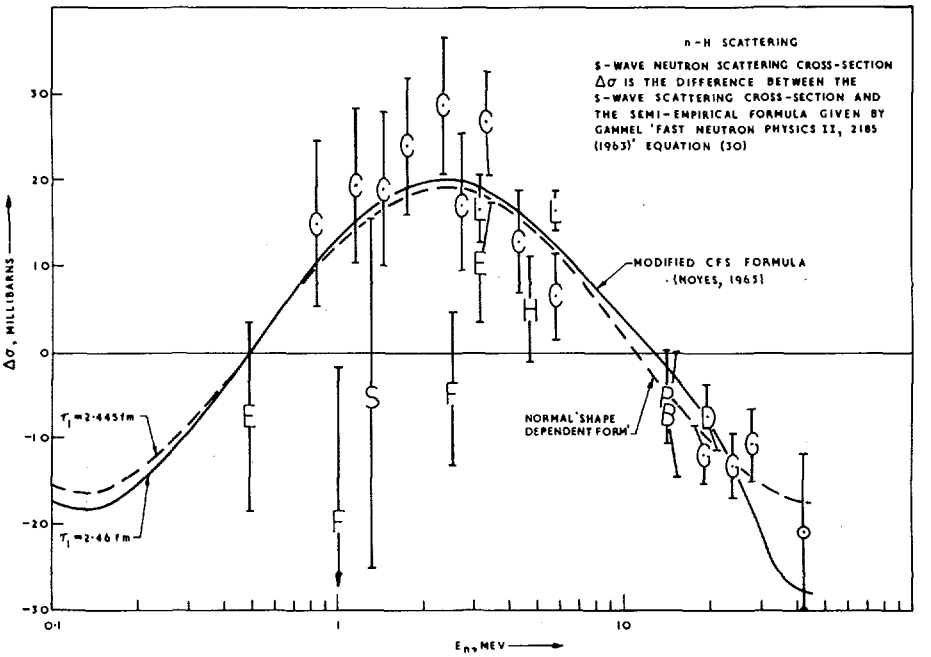

FIG.6. The same as Fig.4 but with two shape dependent variants of the effective range theory.

40 MeV, whereas with deuterium it already exceeds 10% at 750 keV as a consequence of the large size of the loosely bound deuterium nucleus. However, hydrogen and deuterium are alike in that initially the p-wave scattering is preferentially backwards in the centre of mass frame. This results from a pick-up process: with deuterium the incident neutron picks up the proton from the nucleus and carries it off in the forward direction while the other neutron appears as a recoil particle: with hydrogen as target it is simply the proton's charge which is picked up by the incident neutron (though one-pion exchange).

I shall not say much about the scattering cross-sections of carbon, since they are discussed in other papers at this Conference; (Diment and Uttley; Almed et al.). However, in Table IV are listed the experimental data on the slow-neutron free-atom cross-section. Here again Houk and Wilson have claimed extremely high accuracy for their result (better than $\pm 0.1\%$), but it is one of the highest values in the table. It seems not unlikely that their sample, and perhaps some of the others also, had some hydrogen in it, either in a hydrocarbon bond or in the form of adsorbed moisture. Because of this risk I assumed, in deriving a weighted mean value, that none of the data is good to better than $\pm \frac{1}{2}\%$. This weighted mean value is lower than the data in both the UK data file No. 68D and in the ENDF'B' file; a small step in the right direction according to the neutron age comparisons.

The resonance structure of ^{12}C up to 4 or 5 MeV has recently been analysed by Reynolds et al. (1968) using a coupled-channel potential model. While this provides an admirable demonstration of the flexibility and power

TABLE IV. FREE-ATOM TOTAL CROSS-SECTION OF CARBON FOR SLOW NEUTRONS

Reference	σ_T(barn)	
Marshall (1946)	4.84 ±(0.1)	At about 1.46 eV; nominal uncertainty
Jones (1948)	4.7 ±(0.1)	From 3 to 120 eV; nominal uncertainty
Havens et al. (1949)	4.70 ± 0.05	
Egelstaff (1952)	4.56 ±(0.10)	From 4.27 to 83.2 eV; nominal uncertainty
Sailor (1955)	4.74 ± 0.03	At 1.46 eV; BNL crystal spectrometer
Brugger et al. (1956)	(4.71) ± 0.10	Reported average from 14 eV to 10 keV, increased by 0.02 barns to allow for decrease of cross-section for large E
Walton (1961)	4.82 ±(0.10)	From 1.25 to 128 eV; nominal uncertainty
Simpson et al. (1964)	(4.7 ± 0.1)	Read from small graph in the range 5 eV to 1 keV; nominal uncertainty
Rayburn & Wollan (1965)	4.66 ± 0.03	For graphite at about 1.46 eV
	4.74 ± 0.06	For diamond dust at about 1.46 eV
Triftshäuser & Fehsenfeld (1965)	4.743 ± 0.002	At 33.9 eV
	4.7264 ± 0.0024	At 61.1 eV
Koester et al. (1967)	4.727 ± 0.005	Measured with neutron gravity refractometer
Diment & Uttley (1968)	4.744 ±(0.047)	From polynomial fit to data from 85 eV to 1.5 MeV. Nominal uncertainty
Houk & Wilson (1967)	4.7534 ± 0.0045	From 0.3 to 200 eV
Koester et al. (1969)	4.695 ± 0.0042	Measured with neutron gravity refractometer
Preferred value	4.723 ± 0.0125	

of the theory I cannot help feeling that it needlessly complicates the evaluation problem. A great deal of new experimental data of good quality and high resolution have become available in recent years, and it seems to me that the present need is for a much more direct assessment of the experimental data with derivation of best values for the cross-sections and angular distributions and of their accuracy.

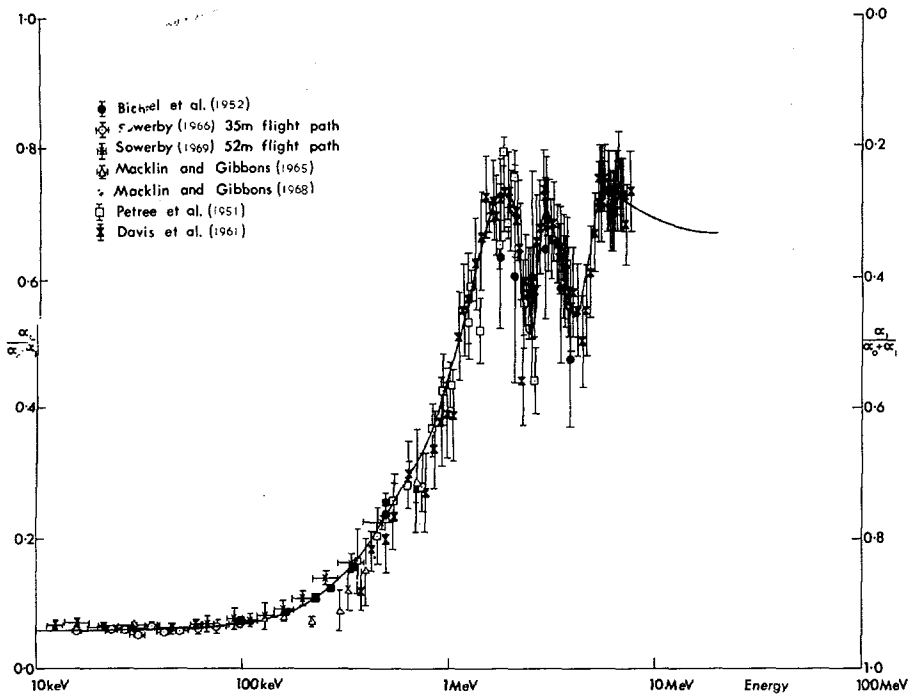

FIG. 7. The branching ratio $\alpha_0/(\alpha_0 + \alpha_1)$ in the exit channel of the ^{10}B (n, alpha) reaction.

4. RESONANCE CROSS-SECTIONS OF OTHER MATERIALS

The neutron cross-sections of ^{6}Li and ^{10}B are the subject of other papers at this Conference, so that despite their importance as reference standards I shall not discuss them here in any detail. It seems that the (n, alpha) cross-section of ^{10}B is now established to within about ± 2% up to about 80 keV; above that energy the spread of the newest experimental data rapidly diverges to ± 20% or more. We are still far short of any adequate picture of the resonance structure of the ^{10}B cross-sections, and even in the low energy range one feature seems to me still very puzzling. Bergman and Shapiro (1961) in their classic study gave reasons for thinking that the low energy cross-section is dominated by a single resonance with $J\pi = 7/2^+$. The constancy and low value of the alpha branching ratio to the ^{7}Li ground state provides further strong confirmation; see Fig. 7. The α_0 and α_1 transitions from the $7/2^+$ state both require $\ell = 3$ in the exit channels so that on energetic grounds alone we should expect an α_0 branch of 70%, as compared with the observed value of about 6%. For reactions through the $5/2^+$ state of the compound nucleus the α_0 branch can have $\ell = 1$, as against $\ell = 3$ for α_1, and in this case the expectation value for the α_0 branch increases to 95%. We need not feel surprised that the branching ratio should have a low value under one single resonance; but it seems at first sight quite surprising that it still

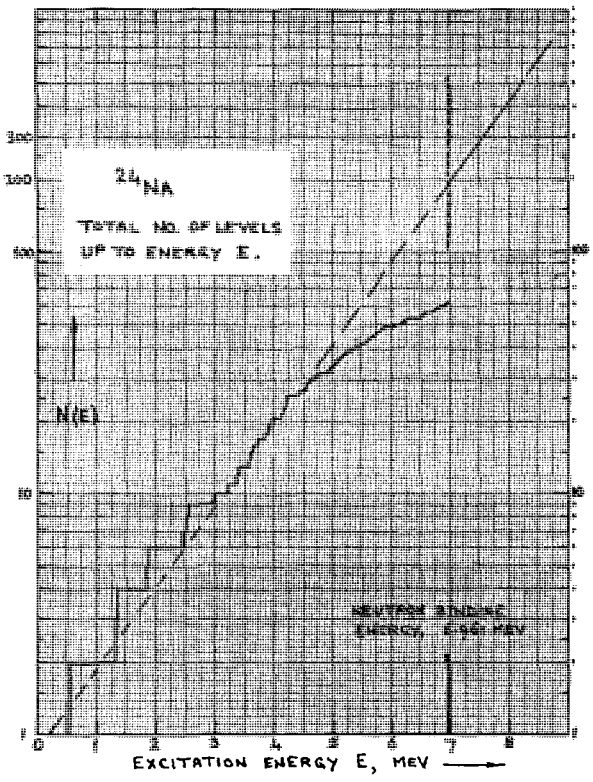

FIG.8. Cumulative plot of the number of levels of ^{24}Na up to excitation energy E.

has not changed very markedly by the time we reach the next resonance at 170 keV.

Since I am supposed to cover the mass range up to A = 219 and have still not got beyond A = 12, it might seem that my own sense of branching ratios is decidedly anomalous, but after all, there are more moderator atoms than anything else in most of our reactors. However, progress with fast reactors is approaching the stage where there is need for better resonance data for sodium and more particularly for the main structural materials. Hitherto, it has been especially the materials from sodium to molybdenum that have presented evaluators the greatest difficulties in the resolved resonance region.

There have been two main problems: the number of missing resonances, and the acute shortage of information on radiation widths. Most of the structural materials have three or more stable isotopes and for these the difficulties are greatly augmented. For sodium until recently one has scarce even had much confidence in the order of magnitude of the resonance spacing. The 1960 supplement to the Barn Book (BNL-325) lists 13 resonances below 860 keV – mostly s- and p-wave resonances, whereas Hibdon (1960, 1961) reported 260 resonances in the same interval, with a rather strange distribution. Using the level density parameters of

Gilbert and Cameron (1965) one estimates that there should be only about 168 levels in this interval, including all spin states: essentially, this is derived from an exponential extrapolation of the known level structure of the compound nucleus in the excitation interval 0 to 4.5 MeV as shown in Fig. 8. From the same formula the mean spacing of (s + p)-wave resonances near the neutron binding energy is expected to be 12 keV, which may be compared with a value of about 20 keV from the recent resonance capture measurements of Hockenbury et al. (1969): the agreement is about as good as can be expected.

If one assumes that the known resonances account for the whole of the thermal capture cross-section an approximate upper limit for the radiation width can be deduced. We are still relying on this argument for what is probably, even now, the best estimate for the radiation width of the 2.8 keV resonance of sodium. If there is a reliable measurement of the resonance capture integral, that can often be used to yield an estimate of the radiation width, though one cannot be sure that the same value is valid in the mean for both s- and p-wave resonances, nor for every isotope if there are more than one.[3] However, in the mass range $A < 100$ the first resonance is usually at quite a high energy and the resonance integral is consequently very small, and difficult to measure reliably unless it can be done by the activation method under cadmium. Measurements with pile oscillators give the resonance capture integral of iron as 1.1 ± 0.2 barns – excluding the 1/v component, whereas the value determined from resonance parameters is only 0.27 barns. The cause of this discrepancy is not yet definitely established, though it may probably be attributed to the presence of some contaminant of higher mass with resonances at eV energies.

A particularly striking feature of recent resonance capture experiments in the mass range 23-60 is the observation and measurement of numbers of narrow p-wave resonances. There is nothing unexpected about this but they make an appreciable contribution to the average capture cross-section in a fast reactor spectrum, and the admixture of strong s-wave resonances and spiky p-wave resonances may result in some unusual self-screening effects, especially at neutron energies below about 100 keV. Certainly, better data are needed than have been available in the past: to see this we need only look at the graph in Schmidt's magnum opus (published only four years ago) for the fast neutron capture cross-section of iron; this shows a factor-4 spread between the highest and lowest data in the range 5-100 keV. Comparison may be made with the up-to-date reappraisal presented by Moxon at this present meeting.

Once we get away from the range of very light nuclides the resolved resonance region acquires a measure of grand simplicity. Resonances are very individualistic and one either has the parametric data or one has not. When the parameters are available it is usually most convenient and realistic to use one or another of the various multi-level formulae for computer derivation of the cross-sections – (see, e.g. James, 1968). But usually, even at best, there are some gaps to fill, some precautions to be taken. With the odd-mass nuclides for example, most of the

---

[3] Pope and Story (1969) report a somewhat more detailed exploration along these lines in an attempt to evaluate radiation widths for the zirconium isotopes.

resonance spin values are undetermined and it is a common practice to assign the average spin value – to set $g = \frac{1}{2}$ – for all these resonances. Now a multi-level formalism necessarily contains (explicitly or implicitly) resonance-resonance interference terms, and if all resonances are given the same spin this interference will be maximized. So it is better practice to assign spin values arbitrarily under the following rules:

i) The relative numbers of resonances of given J should be proportional to 2J + 1 approximately.

ii) Wigner repulsion tends to keep levels of the same spin and parity well separated, so that if there are two spin values for example they will tend to alternate – subject to rule i. In particular, if two resonances are very close together they probably do not both have the same spin and parity.

These rules are very easy to apply and surprisingly effective. A more delicate and mathematical method is to use correlation analysis, as was done for example by Julien et al. (1966) for the resonance parameters of gold.

The effects of distant unresolved resonances should also be allowed for in some way – (see, e.g. James and Story, 1966), because, for example, the interference contributions by distant resonances are coherent and have the effect of increasing the "potential" scattering cross-section at the low-energy end of the resolved range and depressing it at the top end. Procedures for estimating the numbers and distributions of missed resonances within the resolved range are, however, still not well-formalized; so it is fortunate for evaluators that the number and quality of new resonance data are beginning to make headway against the shortages and difficulties which I have just described.

In this review I have tried to give not only an indication of the problems and difficulties of evaluation work in the resolved resonance range, but I hope also a picture of its detail, variety and interest. My acknowledgements go to Messrs A.T.D. Butland and A.L. Pope who have given a great deal of help in preparing this paper.

BIBLIOGRAPHY

ADAIR, R.K., OKAZAKI, A., WALT, M., (Mar.1953), Phys. Rev. 89 1165.

AHMED, N., COPPOLA, M.A., KNITTER, H.H., (June 1970), this conference, paper CN-26/23.

ALLEN, W.D., FERGUSON, A.T.G., ROBERTS, J., (July 1955), Proc. Phys. Soc. A68 650.

BARTOLINI, W., DONALDSON, R.E., GROVES, D.J., (Oct.1968), Phys. Rev. 174 313.

BAUMANN, N.P., (Oct.1962), Nucl. Sci. Engng 14 179. Results revised by HONECK, MICHAEL (1963).

BERGMAN, A.A., SHAPIRO, F.L., (May 1961), Zh. Eksp. Teor. Fiz. 40, 1270; Sov. Phys. JETP 13 895 (Nov.1961).

BRUGGER, R.M., EVANS, J.E., JOKI, E.G., SHANKLAND, R.S., (Nov.1956), Phys. Rev. 104 1054.

CAMPBELL, R.W., PASCHALL, R.K., SWANSON, V.A., (Dec.1964), Nucl. Sci. Engng 20 445. See also NAA-SR-8683, part 1.

CLEMENTS, P.J., LANGSFORD, A., (Aug.1969), AERE PR/NP-16, 39; Phys. Letters 30B, 25 (Sept.1969). Tabular data are listed in Appendix 2 of the minutes of the Oct.1969 meeting of the EANDC, and in EANDC(UK)-120AL, 62 (Apr.1970) = INDC(UK)-10G.

COON, J.H., GRAVES, E.R., BARSCHAL, H.H., (Nov.1952), Phys. Rev. 88, 562.

DAUGHTRY, J.W., WALTNER, A.W., (May 1965), IAEA, Karlsruhe symposium on pulsed neutron research 1 65.

DAVIS, J.C., BARSCHALL, H.H., (Oct.1968), Phys. Letters 27B 636.

DAY, R.B., MILLS, R.L., PERRY, J.E., STAUB, F., (Apr.1959), Phys. Rev. 114, 209.

DIMENT, K.M., UTTLEY, C.A., (Feb.1968), EANDC(UK)-94AL; and this conference, paper CN-26/24 (June 1970).

DRITSA, M., KOSTIKAS, A., (Aug.1967), EANDC(OR)-63L, unpublished.

DUNFORD, C.L., ALTER, H., (Jan.1970), AI-AEC-Memo-12915.

EGELSTAFF, P.A., (Oct.1960), IAEA, Vienna symposium on inelastic scattering of neutrons in liquids and solids, 25.

ENGELKE, C.E., BENENSON, R.E., MELKONIAN, E., LEBOWITZ, J.M., (Jan.1963), Phys. Rev. 129, 324. Energies revised according to DAVIS, BARSCHALL (1968).

FERMI, E., MARSHALL, L., (Feb.1949), Phys. Rev. 75, 578.

FIELDS, R.E., BECKER, R.L., ADAIR, R.K., (Apr.1954), Phys. Rev. 94 389. Energies revised according to DAVIS, BARSCHALL (1968).

FLUHARTY, R.G., (Jan.1959), unpublished; see CCDN-NW/11 5 (Oct.1969). The data were supplied by the CCDN.

GAMMEL, J.L., "Fast Neutron Physics", part 2, (Interscience, 1963) 2220.

GANGULY, N.K., COBB, F.C., WALTNER, A.W., (Oct.1963), Nucl.Sci.Engng 17, 223. Data revised by DAUGHTRY, WALTNER (1965).

GILBERT, A., CAMERON, A.G.W., (Aug.1965), Can. J. Phys. 43 1446.

GISSLER, W., (May 1963), Z. Kristallk. 118, 149.

GRAVES, W.E., (Mar.1962), Nucl. Sci. Engng 12, 439.

GROCE, D.E., SOWERBY, B.D., (July 1966), Nucl. Phys. 83 199.

HAFNER, E.M., HORNYAK, W.F., FALK, C.E., SNOW, G., COOR, T., (Jan.1953), Phys. Rev. 89, 204. Energy revised according to DAVIS, BARSCHALL (1968).

HAVENS, W.W., RAINWATER, L.J., (Apr.1949), Phys. Rev. 75 1296.

HIBDON, C.T., (Oct.1961), Phys. Rev. 124 500.

HILDEBRAND, R., LEITH, C., (Dec.1950), Phys. Rev. 80 842.

HOCKENBURY, R.W., BARTOLOME, Z.M., TATARCZUK, J.R., MOYER, W.R., BLOCK, R.C., (Feb.1969), Phys. Rev. 178 1746.

HONECK, H.C., MICHAEL, P., (May 1963), Nucl. Sci. Engng 16 140.

HOPKINS, J.C., BREIT, G., (May 1970) (to be published).

HORSLEY, A., (Sept.1966), Nuclear Data A2 243.

HORSLEY, A., (July 1968), Nuclear Data A4 321. See also HORSLEY A., STEWART, L., (Jan.1968), LA-3271.

HOUK, T.L., WILSON, R., (July 1967), Revs. Mod. Phys. 39, 546 and erratum, ibid 40 672 (July 1968).

HURST, D.G., ALCOCK, N.Z., (Jan.1951), Can. J. Phys. 29 36.

JAMES, M.F., (Aug.1968), AEEW-R 621.

JAMES, M.F., STORY, J.S., in Nuclear Data for Reactors (Proc. Conf. Paris, 1966), 2, IAEA, Vienna (1967) 359.

JONES, W.B., (Aug.1948), Phys. Rev. 74 364.

JULIEN, J., de BARROS, S., BIANCHI, G., CORGE, G., HUYNH, V.D., le POITTEVIN, G., MORGENSTERN, J. NETTER, F., SAMOUR, C., VASTEL, R., (Feb.1966), Nucl. Phys. 76 391.

KASH, S.W., WOODS, D.C., (May 1953), Phys. Rev. 90 564. Result revised by Honeck, Michael (1963).

KEMSHELL, P.B., (Dec.1969), private communication.

KOESTER, L., (1967), Z. Physik 198 187.

KOESTER, L., NÜCKER, N., NISTLER, W., TRUSTEDT, D., UNGERER, H., (Mar.1969), EANDC(E)-115U, 40; but subsequently see ibid. 127U, 20 (Mar.1970).

KORNBICHLER, S., (July 1965), Nukleonik 7 281.

KUSSMAUL, G., MEISTER, H., (Nov.1963), J. nucl. Energy AB17 411. Result corrected to D_2O purity of 100%.

LEBOWITZ, J., (June 1964), Wash-1048, 21. Energy revised following DAVIS, BARSCHALL (1968).

LEONARD, B.R., STEWART, K., (Oct.1967), ENDF Newsletter 3 No.2.

MARSHALL, J., (July 1946), Phys. Rev. 70 107.

MELKONIAN, E., (Dec.1949), Phys. Rev. 76 1744 and 1750.

MOXON, M.C., (June 1970), these Proceedings, paper CN-26/32.

NEILL, J.M., RUSSELL, J.L., BROWN, J.R., (Aug.1968), Nucl. Sci. Engng 33 265.

NIKITIN, S.J., SMOLYANKIN, W.T., KOLGANOV, W.Z., LEBEDEV, A.W., LOMKAZY, G.S., (Aug.1955), Geneva Conference 2 81.

NOYES, H.P., (June 1963), Phys. Rev. 130 2025.

OLCOTT, R.N., (Aug.1956), Nucl. Sci. Engng 1 327.

PAGE, D.I., (May 1968), in neutron inelastic scattering 1 (Proc. Symp. Copenhagen, 1968), IAEA, Vienna (1968) 325. See also PAGE D.I., HAYWOOD B.C., (May 1968), AERE-R 5778.

PARKS, P.B., PELLARIN, D.J., PROCHNOW, N.H., BAUMANN, N.P., (Aug.1968), Nucl. Sci. Engng 33 209.

PASCHALL, R.K., (Sept.1966), Nucl. Sci. Engng 26 73. See also PASCHALL, R.K., (Dec.1964), Nucl. Sci. Engng 20 436.

PLACZEK, G., (May 1952), Phys. Rev. 86, 377.

POPE, A.L., STORY, J.S., (July 1969), AEEW-M 921.

RAIEVSKY, V., HOROWITZ, J., (May 1954), C. r. 238 1993.

RAINWATER, L.J., HAVENS, W.W., DUNNING, J.R., WU C.S., (Apr.1948), Phys. Rev. 73 733.

RAYBURN, L.A., WOLLAN, E.O., (July 1952), Phys. Rev. 87 174; revised values reported by the same authors in Nucl. Phys. 61 381 (Jan.1965).

REYNOLDS, J.T., SLAVIK, C.J., LUBITZ, C.R., FRANCIS, N.C., (Dec.1968), Phys. Rev. 176 1213.

SAILOR, V., (Apr.1955), unpublished; see CCDN-NW/11, 20 (Oct.1969). The data were supplied by the CCDN.

SCHMIDT, J.J., (Feb.1966), KFK-120, part 1.

SEAGRAVE, J.D., HENKEL, R.L., (May 1955), Phys. Rev. 98 666.

SILK, M.G., WADE, B.O., (May 1968), AERE-M 2034; J. nucl. Energy 23 1 (Mar.1969), and 23 629 (Dec.1969). SILK, M.G., WADE, B.O., WILLIAMS, J.S., (Apr.1969), AERE-R 6059.

SIMPSON, O.D.; FLUHARTY, R.G., MOORE, M.S., MARSHALL, N.H., SIMPSON, F.B., STOKES, G.E., WATANABE, T., YOUNG, T.E., (Nov.1964), Nucl. Instrum. Methods 30 293.

SPANTON, J.H., (Dec.1969) (private communication).

SPENCER, J.D., WILLIAMSON, T.G., (Mar.1967), Nucl. Sci. Engng 27 568.

STORRS, C.L., FRISCH, D.H., (Sept.1954), Phys. Rev. 95 1252. Energy revised according to DAVIS, BARSCHALL (1968).

TRIFTSHÄUSER, W., FEHSENFELD, P., (Feb.1965), EANDC(E)-57U 21.

VAN OERS, W.T.H., SEAGRAVE, J.D., (May 1967), Phys. Letts 24B 562.

WADE, J.W., (July 1958), Nucl. Sci. Eng. 4 12.

WALTON, R.B., (Sept.1961), unpublished; see CCDN-NW/11, 21 (Oct.1969). The data were supplied by the CCDN.

WESTFALL, F.R., WALTNER, A.W., (Nov.1962), Trans. Amer. Phys. Soc. 5 386. Result corrected to D_2O purity of 100%.

WICK, G.C., (June 1954), Phys. Rev. 94 1228.

WOLLAN, E.O., SHULL, C.G., KOEHLER, W.C., (Aug.1951), Phys. Rev. 83 700.

CHAIRMEN OF SESSIONS

Section I	R.F. TASCHEK	United States of America
Section II	F.R. RAE	United Kingdom
Section III	S.I. SUKHORUCHKIN	Union of Soviet Socialist Republics
	R.J. JOLY	France
Section IV	W. HAVENS	United States of America
Section V	W.G. DAVEY	United States of America
Section VI	F.H. FRÖHNER	Federal Republic of Germany
Section VII	B.A. HUTCHINS	United States of America
	Yu.F. CHERNILIN	Union of Soviet Socialist Republics
Section VIII	J.S. STORY	United Kingdom
Section IX	A.I. ABRAMOV	Union of Soviet Socialist Republics

SECRETARIAT

Scientific Secretaries:	V.A. KONSHIN L. HJÄRNE	Division of Research and Laboratories, IAEA
Administrative Secretary:	J.H. STORHAUG	Division of Scientific and Technical Information, IAEA
Editor:	J.W. WEIL	Division of Publications, IAEA
Records Officer:	L.S. LIEBERMANN	Division of Languages, IAEA

IAEA SALES AGENTS AND BOOKSELLERS

Orders for Agency publications can be placed with your bookseller or any of the addresses listed below:

ARGENTINA
Comisión Nacional de
Energía Atómica
Avenida del Libertador 8250
Buenos Aires

AUSTRALIA
Hunter Publications
23 McKillop Street
Melbourne, C.1

AUSTRIA
Publishing Section
International Atomic Energy Agency
Kärntner Ring 11
P.O. Box 590
A-1011 Vienna

BELGIUM
Office International
de Librairie
30, Avenue Marnix
Brussels 5

CANADA
Information Canada
Ottawa, Canada

C.S.S.R.
S.N.T.L.
Spolena 51
Nové Mesto
Prague 1

DENMARK
Ejnar Munksgaard Ltd.
6 Norregade
DK-1165 Copenhagen K

FRANCE
Office International de
Documentation et Librairie
48, Rue Gay-Lussac
F-75 Paris 5e

HUNGARY
Kultura
Hungarian Trading Company
for Books and Newspapers
P.O. Box 149
Budapest 62

INDIA
Oxford Book & Stationery Comp.
17, Park Street
Calcutta 16

ISRAEL
Heiliger & Co.
3, Nathan Strauss Str.
Jerusalem

ITALY
Agenzia Editoriale Commissionaria
A.E.I.O.U.
Via Meravigli 16
I-20123 Milan

JAPAN
Maruzen Company, Ltd.
P.O. Box 5050,
100-31 Tokyo International

MEXICO
Librería Internacional, S.A.
Av. Sonora 206
México 11, D.F.

NETHERLANDS
Martinus Nijhoff N.V.
Lange Voorhout 9
P.O. Box 269
The Hague

PAKISTAN
Mirza Book Agency
65, Shahrah Quaid-E-Azam
P.O. Box 729
Lahore - 3

POLAND
Ars Polona
Centrala Handlu Zagranicznego
Krakowskie Przedmiescie 7
Warsaw

ROMANIA
Cartimex
3-5 13 Decembrie Street
P.O. Box 134-135
Bucarest

SPAIN
Librería Bosch
Ronda Universidad 11
Barcelona - 7

SWEDEN
C.E. Fritzes Kungl. Hovbokhandel
Fredsgatan 2
Stockholm 16

SWITZERLAND
Librairie Payot
Rue Grenus 6
CH-1211 Geneva 11

U.S.S.R.
Mezhdunarodnaya Kniga
Smolenskaya-Sennaya 32-34
Moscow G-200

U.K.
Her Majesty's Stationery Office
P.O. Box 569
London S.E.1

U.S.A.
UNIPUB, Inc.
P.O. Box 433
New York, N.Y. 10016

YUGOSLAVIA
Jugoslovenska Knjiga
Terazije 27
Belgrade

IAEA Publications can also be purchased retail at the United Nations Bookshop at United Nations Headquarters, New York, from the news-stand at the Agency's Headquarters, Vienna, and at most conferences, symposia and seminars organized by the Agency.

In order to facilitate the distribution of its publications, the Agency is prepared to accept payment in UNESCO coupons or in local currencies.

Orders and inquiries from countries not listed above may be sent to:

Publishing Section
International Atomic Energy Agency
Kärntner Ring 11
P.O. Box 590
A-1011 Vienna, Austria

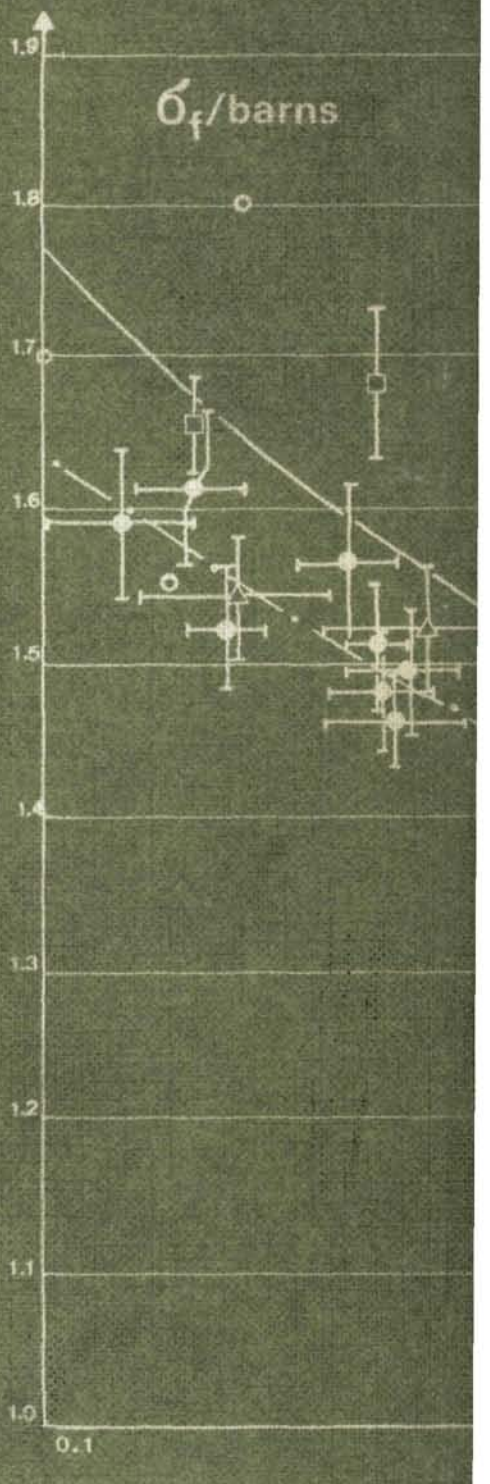

INTERNATIONAL
ATOMIC ENERGY AGENCY
VIENNA, 1970

PRICE: US $21.00
Austrian Schillings 543,-
(£8.15.0 [£8.75]; F.Fr.116,60; DM 76,90)

SUBJECT GROUP: III
Physics/Nuclear Data